



MISSOURI  
**S&T**

# CENTER FOR TRANSPORTATION INFRASTRUCTURE AND SAFETY

## **Self-Consolidating Concrete (SCC) for Infrastructure Elements**

by

**John J. Myers  
Jeffery S. Volz  
Eric Sells  
Krista Porterfield  
Trevor J. Looney  
Brian Tucker  
Kyle Holman**



**NUTC  
R265**

## ***Disclaimer***

The contents of this report reflect the views of the author(s), who are responsible for the facts and the accuracy of information presented herein. This document is disseminated under the sponsorship of the Department of Transportation, University Transportation Centers Program and the Center for Transportation Infrastructure and Safety NUTC program at the Missouri University of Science and Technology, in the interest of information exchange. The U.S. Government and Center for Transportation Infrastructure and Safety assumes no liability for the contents or use thereof.

### Technical Report Documentation Page

1. Report No.  NUTC R265	2. Government Accession No.	3. Recipient's Catalog No.	
4. Title and Subtitle  Self-Consolidating Concrete (SCC) for Infrastructure Elements	5. Report Date  September 2012		6. Performing Organization Code
	7. Author/s  Myers, J.J., Volz, J.S., Sells, E., Porterfield, K., Looney, T., Tucker, B., and Holman, K.		
9. Performing Organization Name and Address  Center for Transportation Infrastructure and Safety/NUTC program Missouri University of Science and Technology 220 Engineering Research Lab Rolla, MO 65409		8. Performing Organization Report No.  00033024	
		10. Work Unit No. (TRAIS)  11. Contract or Grant No.  DTRT06-G-0014	
12. Sponsoring Organization Name and Address  U.S. Department of Transportation Research and Innovative Technology Administration 1200 New Jersey Avenue, SE Washington, DC 20590		13. Type of Report and Period Covered  Final	
		14. Sponsoring Agency Code	
15. Supplementary Notes			
16. Abstract Because of its unique nature, self-consolidating concrete (SCC) has the potential to significantly reduce costs associated with transportation-related infrastructure, benefiting both MoDOT and the residents of Missouri. SCC is a highly flowable, nonsegregating concrete that can be placed without any mechanical consolidation, and thus has the following advantages over conventional concrete: <ul style="list-style-type: none"> <li>•decreased labor and equipment costs during concrete placement,</li> <li>•decreased potential for and costs to repair honeycombing and voids,</li> <li>•increased production rates of precast and cast-in-place elements, and</li> <li>•improved finish and appearance of cast and free concrete surfaces.</li> </ul> However, concerns exist over the structural implications of SCC in cast-in-place and precast elements. Specifically, higher paste contents, higher fines contents, and the use of smaller, rounded aggregates may significantly alter the creep, shrinkage, bond, and shear strength of SCC mixes as compared to traditional concrete mixes with the same compressive strength. These concerns increase for mixtures that use untested aggregate types and various supplementary cementitious materials. Consequently, to achieve the benefits and potential savings with SCC, guidelines are needed for its proper application in bridges, roadways, culverts, retaining walls, and other transportation-related infrastructure components.			
17. Key Words  Self Consolidated Concrete, High Strength Concrete, Shear Strength, Bond Strength, Structural Concrete		18. Distribution Statement  No restrictions. This document is available to the public through the National Technical Information Service, Springfield, Virginia 22161.	
19. Security Classification (of this report)  unclassified	20. Security Classification (of this page) unclassified	21. No. Of Pages  959	22. Price

## EXECUTIVE SUMMARY

This research project entitled, *Self-Consolidating Concrete for Infrastructure Elements*, is separated into seven major task which include Task 1: Literature Review; Task 2: Mix Development; Task 3: Bond and Development of Prestressing Strand and Mild Steel; Task 4: Hardened Properties of SCC Mixes; Task 5: Shear Properties of SCC Mixes; Task 6: Recommendations and Specifications for SCC Implementation; and Task 7: Value to MoDOT and Stakeholders to Implementing SCC. Within these studies, locally available materials were used that were representative of MoDOT produced concrete including benchmark mix designs.

After thorough mechanical property, shear, bond, transfer, and durability testing, it is recommended that SCC be implemented in precast and prestressing applications within the State of Missouri. With SCC showing comparable results for hardened mechanical properties, insignificant variations in shrinkage, creep, abrasion, shear, bond, transfer and development and slightly higher performance for durability, SCC appears to be a viable option to decrease the cost of labor and time consumption during concrete placement. This performance was observed in both normal and high strength SCC, with high strength SCC performing at a slightly higher margin over high strength conventional concrete than SCC performed over conventional concrete. The following advantages over conventional concrete exist:

- *Decreased labor and equipment costs during concrete placement.* Limited “hard” data exists to date in the traditional sense from bid documents involving SCC concrete due to its innovative nature; however, through laboratory experience at Missouri S&T, 40 to 60% less labor was needed to fabricate and place concrete when comparing SCC elements to the conventional concrete elements, which required more personnel to consolidate the conventional concrete elements and produce standard quality control / quality assurance (QC/QA) specimens. As more SCC is implemented, historic cost trends will provide more quantitative financial data. However, it should be noted as SCC involves some new testing standards (i.e. QC/QA tests), there may be a “learning curve” for field and plant engineers / inspectors as they gain experience with new fresh concrete property testing protocols such as Slump Flow ASTM C 1611, J-Ring ASTM C 1621, L-Box (non-ASTM), and Column Segregation ASTM C 161.
- *Improved quality through the decreased potential for and costs to repair honeycombing and voids.* Due to SCC’s flowability, when properly formulated, there holds a great potential to decrease voids, anomalies and other defects that may occur during the placement of conventional concrete. This decreased potential should translate to an increase in the service life of the bridge or structure particularly as high-strength SCC is implemented with its improved durability performance.
- *Increased production rates of precast and cast-in-place elements.* In terms of both precast and cast-in-place elements, SCC offers the unique opportunity to expedite construction due to its unique characteristics. This increased rate of production translates into reduced construction time. This will open infrastructure systems in less time and help the traveling public in Missouri with reduced travel delays and congestion.
- *Improved finish and appearance of cast and free concrete surfaces.* While not a physical cost issue, improved finish and appearance of concrete elements provides an enhanced visual perspective of infrastructure elements for the riding public and will likely translate to a higher perceived level of quality.

# **FINAL SUMMARY REPORT**

TRyy1103

## **Self-Consolidating Concrete (SCC) for Infrastructure Elements**

## TABLE OF CONTENTS

LIST OF TABLES .....	iii
1. REPORT ORGANIZATION .....	1
1.1 Project Acknowledgements .....	1
2. PROJECT WORK PLAN.....	2
2.1 Project Tasks .....	2
2.1.1 Task 1: Literature Review .....	2
2.1.2 Task 2: Mix Development .....	3
2.1.3 Task 3: Bond and Development of Prestressing Strand and Mild Steel.....	3
2.1.4 Task 4: Hardened Properties of SCC Mixes.....	7
2.1.5 Task 5: Shear Properties of SCC Mixes .....	7
2.1.6 Task 6: Recommendations and Specifications for SCC Implementation.....	9
2.1.7 Task 7: Value to MoDOT and Stakeholders to Implementing SCC .....	9
3. TASK SUMMARIES: CONCLUSIONS AND RECOMMENDATIONS.....	11
3.1 Task 1: Literature Review .....	11
3.2 Task 2: Mix Development.....	12
3.3 Task 3: Bond and Development of Prestressing Strand and Mild Steel.....	13
3.4 Task 4: Hardened Properties of SCC Mixes.....	17
3.5 Task 5: Shear Properties of SCC Mixes .....	21
3.6 Task 6: Recommendations and Specifications for SCC Implementation.....	24
3.7 Task 7: Value to MoDOT and Stakeholders to Implementing SCC .....	27
3.8 Overall Project Recommendations .....	28
4. REFERENCES .....	29
5. TESTING STANDARDS .....	29

**LIST OF FIGURES**

Figure 1 Direct Pullout Test Setup.....	6
Figure 2 Beam Splice Test Setup.....	6
Figure 3 Test Fixture for Evaluating Aggregate Interlock .....	9

**LIST OF TABLES**

Table 1 Concrete Test Methods and Protocols.....	4
--------------------------------------------------	---

## 1. REPORT ORGANIZATION

The following report is organized as follows: Section 1 presents the report organization and acknowledgements. The project work plan is presented in Section 2 to familiarize the reader with the overall objectives, project tasks, and scope of the research study. Following the report work plan, the summary findings, conclusions, and recommendations are presented task by task in Section 3. Detailed Technical Reports A through E are attached following this summary report which provides the detailed specifics undertaken in this research investigation. The Summary Report is designed to provide the reader with the project highlights in terms of findings, conclusions, and recommendations, while Reports A through E provide the detailed approach, experimental procedures and processes, results, findings, and recommendations.

### 1.1 PROJECT ACKNOWLEDGEMENTS

The authors wish to acknowledge the leveraged funding to make this extensive study possible; first and foremost from the **Missouri Department of Transportation (MoDOT)**, many thanks for not only the financial support, but also the many insightful comments particularly from the members of the Technical Advisory Group (TAG), namely Ms. Jennifer Harper, Mr. Gregory Sanders, and Mr. Brett Trautman.

In addition, the authors would like to thank the **National University Transportation Center (NUTC): Center for Transportation Infrastructure and Safety (CTIS)** housed at the Missouri University of Science and Technology (Missouri S&T), which provided valuable match funding from the United States Department of Transportation through RITA and the UTC Program.

The researchers would like to thank the **Precast/Prestressed Concrete Institute (PCI)** for providing an extremely valuable Daniel P. Jenny Student Fellowship for Ms. Krista Porterfield. This was the first PCI Fellowship received by Missouri S&T and the project investigators, which allowed for important and more in-depth bond related contributions to the project.

Finally, the project team would like to thank the **Missouri University of Science and Technology** for their valuable contribution in multiple forms: first, in the awarding of five Chancellor's Fellowships to the graduate students working on this project. These individuals represented the very best of the best Missouri S&T graduate students. Secondly, the project team would like to thank the tireless staff of the **Department of Civil, Architectural and Environmental Engineering** and the **Center for Infrastructure Engineering Studies** at Missouri S&T. Their assistance both inside and out of the various laboratories assisted immensely.

## 2. PROJECT WORK PLAN

Because of its unique nature, self-consolidating concrete (SCC) has the potential to significantly reduce costs associated with transportation-related infrastructure, benefiting both MoDOT and the residents of Missouri. SCC is a highly flowable, nonsegregating concrete that can be placed without any mechanical consolidation, and thus has the following advantages over conventional concrete:

- decreased labor and equipment costs during concrete placement,
- decreased potential for and costs to repair honeycombing and voids,
- increased production rates of precast and cast-in-place elements, and
- improved finish and appearance of cast and free concrete surfaces.

However, concerns exist over the structural implications of SCC in cast-in-place and precast elements. Specifically, higher paste contents, higher fines contents, and the use of smaller, rounded aggregates may significantly alter the creep, shrinkage, bond, and shear strength of SCC mixes as compared to traditional concrete mixes with the same compressive strength. These concerns increase for mixtures that use untested aggregate types and various supplementary cementitious materials. Consequently, to achieve the benefits and potential savings with SCC, guidelines are needed for its proper application in bridges, roadways, culverts, retaining walls, and other transportation-related infrastructure components.

### 2.1 PROJECT TASKS

The *objective* of this research was to determine the structural implications of using SCC mixes compared to traditional concrete mixes. This study focused on the hardened properties of SCC mixes containing Missouri aggregates and developed guidelines on its use in infrastructure elements for MoDOT.

The *proposed research plan* included seven (7) tasks necessary to reach this goal, as well as the task durations and level of effort. The research tasks consisted of the following:

#### 2.1.1 Task 1: Literature Review

The purpose of this task was to conduct a comprehensive and critical literature review of past experiences and previous research on SCC, with particular attention to the impact that these findings may have on the research plan. Specifically, the literature review focused on studies involving the hardened properties of SCC that affect structural performance (*e.g.*, bond, shear, prestress losses) and durability (*e.g.*, freeze-thaw resistance, permeability), particularly the role of local aggregates and sensitivity in the mix designs. Sensitivity involves the impact that relatively small changes in the mix design have on the performance of

the material, which is critical for a construction material such as concrete. Furthermore, to establish a solid background for the study, the investigators also reviewed literature on SCC related to fresh properties, workability, stability, admixtures, and mix design methods.

### **2.1.2 Task 2: Mix Development**

The aim of this task was to determine a set number of SCC and non-SCC mix designs to use during the subsequent research. The non-SCC mixes served as controls during the research. Concrete properties, particularly at higher strengths, are very dependent on aggregate type, so comparison mixes are necessary to allow an unbiased assessment of SCC mixes containing Missouri aggregates. This task involved three (3) subtasks.

***Subtask 2a: Survey Missouri Precast Suppliers.*** The investigators surveyed Missouri precast suppliers to obtain representative SCC mix designs currently in use throughout the state, particularly in large metropolitan areas such as St. Louis and Kansas City. All proprietary information on mix designs was treated as confidential and not released to anyone outside the project team.

***Subtask 2b: Survey MoDOT and MoDOT Contractors.*** The investigators surveyed MoDOT and MoDOT contractors on potential SCC mix designs used in infrastructure applications. These sources offered a valuable resource on past experiences with SCC.

***Subtask 2c: Select SCC Mixes for Testing.*** The goal of Subtask 2c was to arrive at four (4) mix designs to form the basis of the subsequent research. These four (4) mix designs, based on the survey results, consisted of SCC and non-SCC versions of both a typical concrete (target compressive strength of 4,000 to 6,000 psi) and a high-strength concrete (target compressive strength of 8,000 to 10,000 psi). The final mix design choices and target strength levels were approved by MoDOT prior to the start of test specimen construction.

### **2.1.3 Task 3: Bond and Development of Prestressing Strand and Mild Steel**

The issue to be addressed under this task was whether SCC enhances or compromises the bond between concrete and reinforcing steel, both prestressing strand and mild steel. Excessive bleeding and lack of stability in SCC can compromise the integrity of the concrete-steel bond, particularly in regard to the top bar effect (greater reduction in bond for upper levels of reinforcement). This task involved two (2) subtasks, with one subtask addressing prestressing strand and the other addressing mild steel. Details regarding the test methods to be investigated are summarized in **Table 1**. Many of the test methods are standard AASHTO/ACI/ASTM/PCI test methods. The reader may be referred to Section 5 of this Summary Report for their affiliated website for additional details on testing and standards on the aforementioned methods.

**TABLE 1: CONCRETE TEST METHODS AND PROTOCOLS**

PROPERTY	TEST METHOD	TEST TITLE/DESCRIPTION	TASK
<b>FRESH CONCRETE PROPERTY TESTS</b>			
Unit Weight	ASTM C 138	Standard Test Method for Density (Unit Weight).	MSTR
Air Content	ASTM C 173	Standard Test Method for Air Content of Freshly Mixed Concrete by the Volumetric Method.	MSTR
Slump	ASTM C 143	Standard Test Method for Slump of Hydraulic-Cement Concrete (non-SCC mixes).	MSTR
Slump Flow	ASTM C 1611	Standard Test Method for Slump Flow of Self-Consolidating Concrete (SCC mixes).	MSTR
J-Ring	ASTM C 1621	Standard Test Method for Passing Ability of Self-Consolidating Concrete by J-Ring (SCC mixes).	MSTR
L-Box	Non-ASTM	Determines the slump flow of the concrete (SCC mixes).	MSTR
Column Segregation	ASTM C 1610	Standard Test Method for Static Segregation of Self-Consolidating Concrete Using Column Technique.	MSTR
<b>HARDENED MECHANICAL PROPERTY TESTS</b>			
Compressive Strength	ASTM C 39	Standard Test Method for Compressive Strength of Cylindrical Concrete Specimens.	4
Splitting Tensile Strength	ASTM C 496	Standard Test Method for Splitting Tensile Strength of Cylindrical Concrete Specimens.	4
Flexural Strength	ASTM C 78	Standard Test Method for Flexural Strength of Concrete.	4
Modulus of Elasticity	ASTM C 469	Standard Test Method for Static Modulus of Elasticity.	4
Creep/Shrinkage	ASTM C 512	Standard Test Method for Creep of Concrete in Compression.	4
<b>DURABILITY TESTS</b>			
Chloride Permeability	ASTM C 1202	Standard Test Method for Electrical Indication of Concrete's Ability to Resist Chloride Ion Penetration.	4
Chloride Permeability	AASHTO T 259	Standard Method of Test for Resistance of Concrete to Chloride Ion Penetration	4
Rapid Freeze Thaw Resistance	ASTM C 666	Standard Test Method for Resistance of Concrete to Rapid Freezing and Thawing.	4
Wear Resistance	ASTM C 944	Standard Test Method for Abrasion Resistance of Concrete or Mortar Surfaces by the Rotating-Cutter Method.	4
<b>PT STRAND BOND TESTS</b>			
Mustafa Pullout Test	Non-ASTM	Current PCI recommended test method.	3
NASP Bond Test	Non-ASTM	Currently undergoing due diligence testing by PCI as new standard.	3
<b>PT STRAND PERFORMANCE (COMPONENT AND FULL-SCALE TESTING)</b>			
Strand End-Slip	Non-ASTM	Property related to both transfer length and development length.	3
Transfer Length	Non-ASTM	Test to determine required length for full prestress transfer.	3
Development Length	Non-ASTM	Test to determine required length for yielding of strand in flexure.	3
<b>MILD STEEL BOND AND DEVELOPMENT</b>			
Direct Pull-out Tests	RILEM 7-II-128	A comparative test that evaluates direct bond strength while minimizing the effect of confining pressures as in previous direct pull-out test methods, see Fig. 1.	3
4-Point Loading Beam Splice Test Specimens	Non-ASTM	See Fig. 2.	3
<b>SHEAR</b>			
Small Scale Beam Tests	Non-ASTM	Small scale tests will be undertaken to examine the components that contribute to the concrete's ability to provide shear resistance. This includes $V_c$ (compression), $V_a$ (aggregate interlock), $V_d$ (dowel action).	5
Full Scale Beam Tests	Non-ASTM	Larger scale tests will examine global behavior in shear including global contribution from the concrete, $V_c$ . Prestressed concrete (PC) members will be studied.	5
<b>Table Notes:</b>			
Non-ASTM – refers to a test method that is not a standard ASTM test. The test is either a generally accepted research practice test or standard undertaken at Missouri S&T for similar studies. Detailed reports A-E provide specifics undertaken.			
MSTR = refers to a Missouri S&T recommended test for this project.			

***Subtask 3a: Prestressing Strand Transfer Length, End Slip, and Development Length.*** This subtask investigated three (3) interrelated issues with regard to prestressing strand performance in concrete, both SCC and non-SCC mixes, namely transfer length, end slip, and development length.

To evaluate bonding characteristics of prestressing strand, there are currently three (3) testing protocols available: the Moustafa Bond Test, the Post-Tensioning Institute (PTI) Bond Test, and the North American Strand Producers (NASP) Bond Test.<sup>1</sup> Based on a review of the literature and the current MoDOT requirements, the investigators performed both the Moustafa (also referred to as the Large Block Pullout Test [LBPT]) and NASP bond tests to evaluate the comparative bond behavior between SCC and non-SCC mixes. The NASP bond test, an updated version of the PCI bond test, is currently undergoing due diligence review by the Precast/Prestressed Concrete Institute (PCI), and will most likely develop into the industry standard.<sup>2,3</sup>

To evaluate strand end slip and transfer length, the investigators constructed and instrumented rectangular beams. The rectangular beams contained either two or four 1/2-inch-diameter strands, with the four-strand beams having two strands at the top and bottom of the section. The four-strand beams were used to evaluate the top bar effect, as top strands are often used to control release stresses for heavily pretensioned sections. The instrumentation included both depth micrometers to measure strand end slip and demountable mechanical strain gauges (DEMEC gauges) to measure changes in concrete surface strains.

To evaluate development length, the investigators constructed and instrumented a series of pretensioned rectangular beams of varying lengths. The beam lengths were based on calculated development lengths from both AASHTO LRFD and ACI 318. Since development length involves adequate stress transfer to insure yielding of the strand, the beams were tested in flexure to failure. Data recorded during the tests included load, deflection, concrete surface strains, strand end slip, and strain in the strands.

***Subtask 3b: Mild Steel Bond and Development.***

This subtask investigated development length of mild steel in both SCC and non-SCC mixes, using both direct pull-out tests and beam splice tests. Although there are a variety of bond and development length testing protocols available, a direct pull-out test offers several advantages, including test specimens that are easy to construct and a testing method that is relatively simple to perform. The downside is a lack of direct comparison with actual structures and the development of compressive and confinement stresses generated due to the reaction plate.

However, modifications suggested in RILEM 7-II-1282 reduce some of these problems and result in a simplified test that offers relative comparisons between concrete or reinforcement types. **Figure 1** is a

schematic of the test specimen based on the RILEM specifications. Bond between the reinforcing bar and the concrete only occurs in the upper half of the concrete block, through the addition of a PVC tube in the lower portion, significantly reducing the effect of any confinement pressure generated as a result of friction between the specimen and the reaction plate.

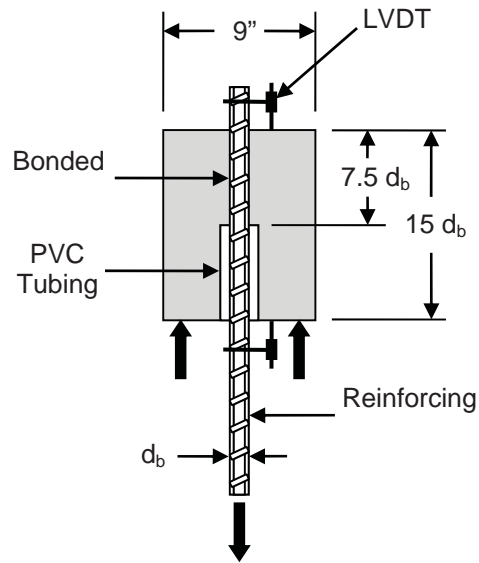


**FIGURE 1: DIRECT PULLOUT TEST SETUP.**

The investigators constructed and instrumented several direct pullout specimens for testing as shown in **Fig. 1**. The variables included bar size and concrete type. Data recorded during the test included load and free end slip at each end of the reinforcing bar.

Although there are a variety of bond and development length testing protocols available, the beam splice specimen shown in **Fig. 2** is generally regarded as the most realistic test method.<sup>1,4</sup> Current AASHTO LRFD and ACI 318 design provisions for development length and splice length are based primarily on data from this type of test setup.<sup>4</sup>

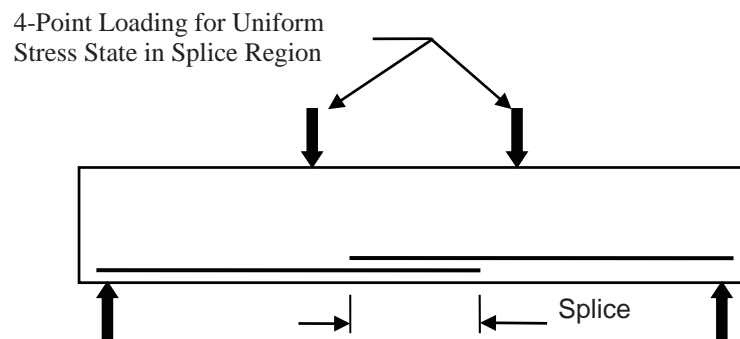


**FIGURE 2: BEAM SPLICE TEST SETUP.**

The investigators constructed and instrumented rectangular beams for splice specimen testing as shown in **Fig. 2**. The variables included lap length and lap position. To evaluate the top bar effect, several beams were cast upside-down with at least 12 inches of concrete below the bars. Specimen instrumentation consisted of strain gauges placed at the start of each lap. Data recorded during the tests included load and deflection of the specimen as it was tested to flexural or bond failure.

#### **2.1.4 Task 4: Hardened Properties of SCC Mixes**

The objective of the proposed research is to determine the structural implications of using SCC mixes compared to traditional concrete mixes. As such, the investigators focused on the hardened properties of SCC mixes as compared to “identical” non-SCC mixes. Task 4 involved three (3) subtasks.

**Subtask 4a: Test Matrix.** **Table 1** represents the test matrix for this research study based on MoDOT’s RFP and the opinions of the investigators. Broadly speaking, the tests are classified into four (4) categories: fresh concrete properties (*e.g.*, slump), hardened mechanical properties (*e.g.*, compressive strength), durability (*e.g.*, freeze-thaw resistance), and structural performance (*e.g.*, bond, shear strength).

**Subtask 4b: Test Results.** This subtask was critical to a successful research program and involved more than simply compiling the test results. In reality, this subtask involved adapting the test matrix as necessary during the course of testing. In other words, if a particular property turned out to be critical to the overall performance of SCC, more or different tests may be warranted, and the testing plan adapted accordingly.

**Subtask 4c: Conclusions & Recommendations.** The investigators developed conclusions and recommendations based on the test results. In addition to evaluating the different SCC mixes for performance, these conclusions and recommendations formed the basis of the draft specifications developed as part of Task 6. The investigators also made recommendations on the design of precast/prestressed girders constructed with SCC, including suggested revisions to Section 700 of MoDOT’s EPG.

#### **2.1.5 Task 5: Shear Properties of SCC Mixes**

The issue to be addressed under this task was to determine whether the current AASHTO *LRFD Bridge Design Specifications* for shear are appropriate for SCC. Higher paste contents, higher fines contents, and the use of smaller, rounded aggregates may significantly alter the shear strength of SCC mixes as compared to traditional concrete mixes with the same compressive strength. As a result, the following three (3) factors were studied based on MoDOT’s RFP and the opinions of the investigators:

1. Shear contribution from aggregate interlock (interface shear transfer), including the influence of concrete strength and aggregate type, size, and shape,
2. Shear contribution from concrete (overall), including moderate to high-strength mix designs, and
3. Shear contribution from steel (stirrups and longitudinal steel).

This task involved two (2) subtasks (see **Table 1**) based on the type of test recommended to study different aspects of each issue, with one subtask based on small scale element and beam tests and the other based on mid-to-full scale beam tests.

**Subtask 5a: Small Scale Element and Beam Tests.** This subtask consisted of small scale element and beam tests. The element tests primarily investigated the complex phenomenon of aggregate interlock (or interface shear transfer). The beam tests, on the other hand, were used to investigate a large variety of variables before moving onto full scale beam tests.

After diagonal cracking and up to the ultimate limit state, aggregate interlock provides a substantial portion of the concrete contribution to shear resistance.<sup>5</sup> In fact, the Modified Compression Field Theory (MCFT) shear design provisions in the current AASHTO *LRFD Bridge Design Specifications* include aggregate interlock as a design parameter to determine the allowable shear stress on the crack plane.<sup>6</sup> The accepted test method to study the effects of aggregate interlock is referred to as a push-off test and is shown in **Figure 3**.<sup>7</sup>

The investigators constructed and instrumented push-off specimens as shown in **Figure 3** to study the impact of SCC mix designs on aggregate interlock. The variables included: concrete strength and aggregate type, size, shape and content level. Aggregate type and proportioning is a significant variable in the design of SCC mixes, which typically use low volumes of coarse aggregate and high paste volumes to maximize flowability. Furthermore, for high-strength concrete, the effect of aggregate interlock is significantly reduced as the aggregate fractures and results in a smoother crack surface. Specimen instrumentation consisted of strain gauges, linear variable displacement transducers (LVDTs) and DEMEC gauges. Data recorded during the tests also included normal and shear forces from the start of loading to failure.

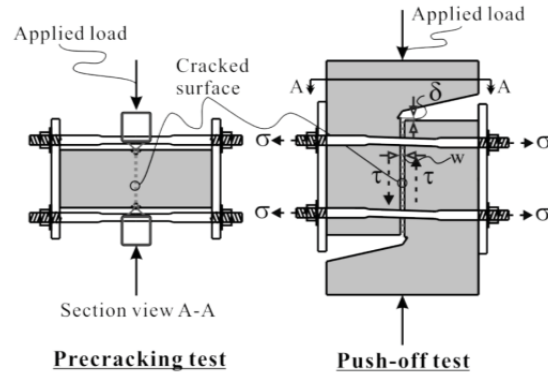


**FIGURE 3: TEST FIXTURE FOR EVALUATING AGGREGATE INTERLOCK.**

The small scale beam tests of this subtask will be used to investigate a large variety of variables before moving onto full scale beam tests. The investigators will construct and instrument a series of rectangular beams to study shear in SCC mixes. The purpose of these tests is to begin to quantify the different contributions to shear strength in an SCC beam. The variables will include: dimensions of the beam cross section, concrete strength, and amount of transverse reinforcement. Specimen instrumentation will consist of strain gauges, DEMEC gauges, and LVDTs. Data recorded during the tests will also include load and deflection of the specimen as it is tested to shear failure.

**Subtask 5b: Mid-to-Full Scale Beam Tests.** This subtask involved mid-to-full scale beam tests to study the global behavior of shear in SCC beams and evaluate the contributions from the concrete and transverse reinforcement. The investigators constructed and instrumented a limited number of rectangular full-scale beams as a final evaluation of the shear behavior of SCC. The results from Subtask 5a were used to determine the variables to study in the full-scale beam tests. Specimen instrumentation consisted of strain gauges, DEMEC gauges, and LVDTs. Data recorded during the tests included load and deflection of the specimen as it was tested to shear failure.

### **2.1.6 Task 6: Recommendations and Specifications for SCC Implementation**

Based on the results of Tasks 1 through 5, the investigators developed recommendations for the use of SCC in infrastructure elements, including suggested revisions to Section 700 of MoDOT's EPG. Based on these recommendations and the results of this research study, the investigators also developed a suggested MoDOT specification for the use of SCC in transportation-related infrastructure.

### **2.1.7 Task 7: Value to MoDOT and Stakeholders to Implementing SCC**

The issue to be addressed under this task was to quantify the value of this research effort. Contained within this "Value to MoDOT" task was both quantitative and qualitative values to MoDOT. Overall, this

task provided a basis for whether or not SCC should be implemented by MoDOT if the technology shows promise based upon the results from Project Tasks 1-5.

### 3. TASK SUMMARIES: CONCLUSIONS AND RECOMMENDATIONS

The following sub-sections summarize the major findings and conclusions as it relates to Project Tasks 1 through 7 as applicable. Prior to the summary, each sub-section refers to the specific Technical Report A through E where the detailed approach, experimental procedures and processes, results, findings, and recommendations may be referenced for much greater detail. Within each finding and conclusion a report designation (i.e. Report “A”) is provided as a reference to the reader such that the detailed report may easily be referenced to gain an improved understanding of how this particular finding or conclusion was established.

#### 3.1 TASK 1: LITERATURE REVIEW

Detailed Technical Reports A through E each provide a thorough literature review related to the topic of study at hand. The reader is referred to the detailed technical reports for the specific literature review on SCC. The more notable general observations include the following:

##### **TECHNICAL REPORT A:**

- National SCC studies have produced guidelines for developing fresh property test programs to develop robust mix designs and reliable QA/QC programs.
- There exist standardized test procedures for testing “fresh” or plastic SCC.
- Research on strand bond in SCC has shown conflicting results, where some mixes have resulted in increased transfer and development lengths compared to conventional concrete while others have shown the opposite effect.
- Research on bond of mild steel in SCC have shown conflicting results, where some mixes have resulted in increased development lengths compared to conventional concrete while others have shown the opposite effect.
- Research on creep and shrinkage of SCC generally indicates increased values due to higher paste and fine contents and lower coarse aggregate contents.
- Research on material properties of SCC generally indicates comparable values compared with conventional concrete.
- Research on durability of SCC generally indicates comparable or improved performance compared with conventional concrete.
- Research on shear strength of SCC has shown conflicting results, where some mixes have resulted in decreased shear strength compared to conventional concrete while others have shown either comparable or increased capacity.

### 3.2 TASK 2: MIX DEVELOPMENT

The aim of this task was to determine a set number of SCC and non-SCC mix designs to use during the subsequent research. The non-SCC mixes served as controls during the research. Concrete properties, particularly at higher strengths, are very dependent on aggregate type, so comparison mixes were necessary to allow an unbiased assessment of SCC mixes containing Missouri aggregates. This task involved three (3) subtasks.

***Subtask 2a: Survey Missouri Precast Suppliers.*** The survey results of Missouri precast suppliers are presented in Section 3 of Technical Report A.

***Subtask 2b: Survey MoDOT and MoDOT Contractors.*** The survey results from MoDOT, MoDOT contractors, and the national level DOT survey is presented in Section 3 of Technical Report A.

***Subtask 2c: Select SCC Mixes for Testing.*** The final selected four (4) mix designs, based on the survey results and MoDOT input are presented in Section 3 and 4 of Technical Report A. This consisted of SCC and non-SCC versions of both a typical concrete (compressive strength of 4,000 to 6,000 psi) and a high-strength concrete (compressive strength of 8,000 to 10,000 psi). The findings and conclusions from this task are as follows:

#### TECHNICAL REPORT A:

- *SCC Precast Producer Survey:* Positive results were gathered from the Missouri precast concrete suppliers; 6 out of the 13 solicited precast suppliers replied with valuable responses, several even provided multiple mix designs in use at their facilities. Results of the survey that are not confidential are reported in Technical Report A, Section 3.1.
- *SCC Ready-Mix Producer Survey:* No ready mix concrete suppliers in Missouri replied to survey solicitations. It is known from the personal experience of the project Principal Investigator that some ready mix producers in Missouri have made SCC, but it remains unknown to what extent or level of sophistication.
- *National DOT Survey:* SCC was used in all applications, not only aesthetic or low stress drainage structures; reportedly, the most common use for SCC is in structural beams and girders.
- *National DOT Survey:* Aggregates used for SCC seem to be as diverse as the local geology; river gravel and limestone are used approximately equally, and other materials such as granite, trap rock, and quartz are used to a lesser extent, as would be typical of conventional concrete.

- *National DOT Survey:* As was reflected in the precast survey responses, the most common nominal maximum aggregate size was 3/4 in. (19 mm) with 1/2 in. (13mm) also commonly reported.
- *National DOT Survey:* The majority of AASHTO survey respondents' reports less than 25% of all projects utilize SCC with first use occurring within the last 7 years; few respondents report a majority of projects using SCC with more than 10 years of experience.

### **3.3 TASK 3: BOND AND DEVELOPMENT OF PRESTRESSING STRAND AND MILD STEEL**

- ***Subtask 3a: Prestressing Strand Transfer Length, End Slip, and Development Length.*** Based on the work undertaken, several conclusions can be drawn regarding the applicability of the NASP test in mortar and LBPT bond tests, the bond performance of SCC compared to conventional concrete, and the feasibility of using concrete strength and pullout test results to predict transfer lengths. The conclusions and recommendations from this subtask are as follows:

#### **TECHNICAL REPORT B, CONCLUSIONS:**

- Based on the linear relationship found between the LBPT and NASP pullout values and the similar coefficients of variation between the two tests for a given strand type, either the LBPT or NASP test are equally valid approaches to evaluating bond performance of prestressing strand. However, the limits set on passing may need some refinement, as two of the strand sources passed the proposed NASP standard but did not pass the LBPT requirements.
- Proportioning for the mortar mixes did appear to have an effect on NASP in mortar pullout values, and it is hypothesized that a decreased amount of sand could detrimentally affect mechanical interlocking and lead to lower pullout values.
- While first slips are not required to be monitored in the NASP test, strands with high 0.1 in. (2.54 mm) pullout loads sometimes had the lowest 0.001 in. (0.025 mm) pullout loads, which could indicate a problem with adhesion of the strand.
- The NASP test in concrete revealed that the high strength concretes had lower first slip values than the normal strength concretes. This could be due to the inclusion of fly ash in the high strength mixes, or the increase in total cementitious content, as these were the only major differences between the normal and high strength mixes.
- SCC and conventional concrete were comparable in terms of bond performance, showing few statistical differences between measured transfer lengths or pullout loads between the two types of concrete.

- Increases in concrete strength generally resulted in shorter, although not always statistically different, transfer lengths, especially if the live end values were removed from the averages. Also, top strands only seemed to show statistically significant increases in transfer length at later ages. The “live end” is the end directly adjacent to where the strand is first released.
- Transfer lengths of bottom strands tended to increase from 1 to 28 days, with most of the increase occurring between 1 and 4 days. Also, the transfer lengths in normal strength mixes appeared to increase more than those in high strength mixes, and transfer lengths in conventional concrete increased more than transfer lengths in SCC. However, no consistent trends were noted for change in top strand transfer lengths over time.
- The AASHTO transfer length equation was generally conservative for all mixes for both top and bottom strands, even when compared to live end transfer lengths. The ACI equations were generally conservative except when compared to live end transfer lengths or the top strands in the normal strength conventional concrete.
- The linear potentiometers were found to be unreliable, and the steel ruler measurements were determined to be imprecise; the transfer lengths determined from the DEMEC readings and 95% Average Mean Strain Method were found to be the most consistent and reliable.
- Due to the fact that increased concrete strength resulted in decreased transfer lengths and increased NASP in concrete pullout loads, concrete strength does have an effect on bond and the equation for transfer length should be a function of concrete strength.
- Transfer length does appear to be related to the square root of concrete compressive strength, as noted by Ramirez and Russell (2008) and others.
- The proposed transfer length equation from Ramirez and Russell (2008) was slightly less conservative than the AASHTO equation, but still mostly conservative when compared to the measured transfer lengths, although the proposed equation was not conservative when compared to the live end transfer lengths.
- Development length specimens tested at embedment lengths of 80% of the development length calculated from the AASHTO and ACI equations still failed in flexure, so the current AASHTO and ACI equations for development length are conservative.
- SCC and conventional concrete appeared to exhibit comparable flexural behavior.
- Ramirez and Russell’s proposed development length equation (2008) appeared to be less conservative than the AASHTO and ACI equation but still conservative in three out of the four cases because in this test program, even the development length tests completed at an embedment length of 58 in. (1,473 mm), which is 80% of the development length calculated from the current AASHTO equation and shorter than any of the development lengths calculated by the proposed

equation, failed in flexure, showing the strand could be fully developed. However, the proposed equation did predict one development length greater than the AASHTO and ACI value for one mix, showing the proposed development length equation may be over-conservative in some cases.

#### **TECHNICAL REPORT B, RECOMMENDATIONS:**

- Because differences in bond quality have been shown to vary greatly depending on the source, a standard bond test should be recommended and performed to ensure strand bond quality before the strand is used in production.
- The NASP test in concrete should not necessarily be a required test for strand bond because the tests showed pullout strength is mostly a function of concrete compressive strength; however the NASP test in concrete still could be useful for identifying possible effects of mix additions or proportioning on bond.
- The pullout limits for both the NASP test in mortar and LBPT need refinement. Additional research should be conducted with NASP and LBPT specimens and corresponding transfer length specimens to see if the NASP minimum value should be raised and the LBPT minimum value should be lowered. Specifically, strands with NASP pullout values between 12,000 and 18,000 lb (53 and 80 kN) and LBPT pullout values between 30.0 and 36.0 kips (133 and 160 kN) should be targeted.
- The pullout value at first slip, or 0.001 in. (0.025 mm) of displacement, should also be reported for the NASP test because low first slip values could indicate problems with adhesion of strand.
- Additional studies should be completed to investigate the effect of mortar mix proportioning on the pullout values from the NASP test in mortar, and limits should be set for proportioning in addition to strength and flow.
- More research should be conducted to determine if the contours of the load vs. displacement curves for the NASP test in mortar specimens can also be indicators of bond quality. Strand types that show plateaus or drop-offs in load at 0.1 in. (2.54 mm) instead of continuing to increase may not have acceptable bond quality, even if they pass a minimum load limit.
- The potentiometer and plate method for measuring end slip should be reinvestigated to see if other plate/potentiometer bonding methods or other less violent release methods could yield useable data. However, the steel ruler method should be abandoned, and end slips should be measured with a more precise means, such as a caliper.
- The current AASHTO and ACI transfer length and development length equations are adequate and conservative for use with conventional concrete as well as SCC.

- The proposed transfer length equation from Ramirez and Russell (2008) should potentially be reinvestigated because the equation was not conservative for live end transfer lengths.
- The proposed development length equation from Ramirez and Russell (2008) should also potentially be reinvestigated because the equation might result in overly conservative values in some cases.

***Subtask 3b: Mild Steel Bond and Development.*** Two test methods were used for bond strength comparisons. The first was a direct pull-out test based on the RILEM 7-II-128 “RC6: Bond test for reinforcing steel. 1. Pull-out test” (RILEM, 1994). Although not directly related to the behavior of a reinforced concrete beam in flexure, the test does provide a realistic comparison of bond between types of concrete. The second test method consisted of a full-scale beam splice test specimen subjected to a four-point loading until failure of the splice. This test method is a non-ASTM test procedure that is generally accepted as the most realistic test method for both development and splice length. The conclusions and recommendations from this subtask are as follows:

**TECHNICAL REPORT C, CONCLUSIONS:**

- Direct Pull-out Testing. Analysis of the test data indicates that the normal strength SCC mix design has higher bond strength and the high strength SCC mix design has lower bond strength than their respective control mix designs for both bar sizes. Statistical analysis indicates that only the #6 (#19) reinforcing bar, high strength SCC mix design specimens did not perform equally with the control.
- Beam Splice Testing. Analysis of the test data indicates that both SCC mix designs exhibited improved bond performance under realistic stress states relative to their respective control mix designs when the splice was cast at the bottom of the specimen. Only the high strength SCC mix design exhibited improved bond performance when the splice was cast at the top of the specimen. However, statistical analysis indicates that all four mix designs performed equally. These findings, along with the findings from the direct pull-out tests, indicate that using SCC is feasible in terms of bond and development of reinforcing steel.

**TECHNICAL REPORT C, RECOMMENDATIONS:**

There have been numerous studies conducted to determine the bond performance of SCC. However, additional studies are needed to establish a database of results that can eventually be used for comparison as well as for future AASHTO/ACI design code changes. Also important for design would be to explore whether or not certain AASHTO/ACI code distinctions, such as confinement, bar size, or bar coating factors, used for conventional concrete designs also apply to SCC, or if they need to be developed

specifically for SCC. Below is a list of recommendations for testable variables related to SCC concrete bond behavior:

- Perform tests with a larger variation in bar sizes based on AASHTO and/or ACI 318 code distinctions for bar size effect on development length.
- Conduct tests determining the effect of different admixtures on the bond performance of SCC.
- Conduct tests determining the effect of various aggregate percentages and types on the bond performance of SCC.
- Perform tests with aggregates from different sources.
- Perform bond test on more specimen types mentioned in ACI 408.

### **3.4 Task 4: Hardened Properties of SCC Mixes**

The objective of the proposed research was to determine the structural implications of using SCC mixes compared to traditional concrete mixes. The mechanical and durability performance of the baseline mixes and the SCC mixes are presented in multiple sections of the technical reports. Section 3 of Technical Report D reports the mechanical property results in terms of shrinkage, creep and abrasion resistance. Section 3 of Technical Report E reports the mechanical property results in terms of compressive strength, modulus of elasticity, modulus of rupture, and splitting tensile strength. Section 5 of Technical Report E reports the durability property results including rapid freezing and thawing, electrical indication to resist chloride penetration, ponding testing performance, and concrete resistivity. Section 5 of Technical Report A reports the mechanical property results as they relate to the various mix designs used for shear related studies. Technical Reports B and C also present hardened property results for their respective testing. The conclusions from this task are as follows:

#### **TECHNICAL REPORT D, CONCLUSIONS:**

- Shrinkage behavior results all indicated shrinkage levels at a microstrain of approximately 780 or lower as would be expected for conventional concrete shrinkage. The higher strength mixes tended to track better to various shrinkage models where the lower strength mixes tended to be over predicted by current models. It should be noted that many of the shrinkage models have not been specifically calibrated for SCC mixes in particular where the mix constituents vary from conventional concrete (i.e. lower coarse aggregate contents).
- Creep behavior results showed that the conventional concrete variation outperformed SCC in terms of creep behavior. This would be expected due to the lower coarse aggregate content in the SCC mixes. For normal strength concrete, these results are supported by every prediction model

that was analyzed. Every model predicts that the normal strength conventional concrete would have a lower creep coefficient than normal strength SCC after 126 days being loaded. The models were not as consistent when predicting the creep behavior of high strength concrete due to their calibration. The overall creep coefficients were approximately at or lower than the values which would be expected for conventional concrete.

- Abrasion resistance results of the locally produced Missouri mixes are very consistent with other national findings. The abrasion resistance of concrete is primarily dependent on compressive strength. For both criteria (mass loss and depth of abrasion), the abrasion resistance of concrete increased as the compressive strength of the specimens increased, with the exception of mass loss properties for the high strength conventional concrete relative to the high strength SCC; where, for the high strength mixes SCC and HSC exhibited similar performance. When comparing the conventional strength concrete mixes with the same design strength, the SCC mix generally showed a lower resistance to wear. This is most likely due to the decreased amount of coarse aggregate in the SCC mixes. Based on observations during and after testing, the majority of mass loss due to abrasion was from the cement paste, as opposed to the aggregate. Generally, for each test, cycle 1 shows the greatest amount of mass loss. The general decrease in measured mass loss for each subsequent cycle indicates that as the depth of wear increases, the aggregate begins to dominate the response. This would explain why the SCC mixes showed a slight decrease in abrasion resistance relative to their conventional concrete equivalents for subsequent cycles.

#### **TECHNICAL REPORT E, CONCLUSIONS:**

- The normal strength SCC mix in this investigation outperformed the conventional normal strength concrete in nearly every aspect tested. This finding is important for determining the plausibility of using SCC instead of conventional concrete. The normal strength SCC mix achieved a higher 28-day compressive strength than the normal strength conventional concrete mix. With the w/cm ratio being equal, as well as the type of aggregate and cement, it is believed that the high amount of HRWR used to provide SCC with its flowable characteristics accounts for the higher strength. The HRWR allows more water to be effective in the hydration process. This characteristic in turn hydrates more of the Portland cement, creating a denser overall microstructure, thus improving the compressive strength of the concrete. The normal strength SCC mix showed a comparable modulus of elasticity to the C6-58L mix. However, both mixes fell below the recommended ACI coefficient used to estimate this property. This was attributed to the aggregate characteristics. The normal strength conventional concrete mix showed a higher modulus of rupture when compared to the SCC mix and exceeded the recommended ACI

coefficient used to estimate the modulus of rupture. However, in regards of the ACI coefficient, the SCC mix only fell slightly below the recommended value of 7.5. Both concrete mixes showed comparable splitting-tensile strength, while both mixes fell below the recommended ACI coefficient used to estimate the splitting-tensile strength.

- The normal strength SCC mix showed very comparable durability behavior and even exceeded the performance of the normal strength conventional concrete mix in some aspects. Both concretes performed poorly for resistance to freeze-thaw. This result is most likely due to the aggregate source incorporated into the specimens. Jefferson City Dolomitic Limestone is known for its poor durability performance, and resistance to freeze-thaw for concrete is very dependent on the aggregate's performance. Both concrete mixes showed very similar performance with the Rapid Chloride Permeability Testing (RCT). This result was further supported by similar performance in the ponding test. While the RCT classified both concrete mixes as moderate permeability, both mixes reached negligible corrosion risk at a relatively shallow depth in the ponding test. Both mixes also performed almost identical in the area of concrete resistivity, indicating a low rate of corrosion.
- The high strength SCC mix outperformed the conventional high strength concrete in nearly every aspect tested. The high strength SCC mix achieved a much higher 28-day compressive strength than the high strength conventional concrete mix. This increase in strength can most likely be attributed to the high dosage of HRWR used to produce the SCC. The HRWR allows more water to be effective in the hydration process. This characteristic in turn hydrates more of the Portland cement, creating a denser overall microstructure, thus improving the compressive strength of the concrete. This was also noted in the normal strength SCC mix but not to the degree observed in the high strength investigation. It could be concluded that the HRWR has a larger effect on strength gain at lower w/cm ratios. The HRWR allows the majority of water to be used in hydration, allowing for a much denser paste. When this aspect is combined with the lower w/cm ratio necessary to achieve high strengths, it appears that SCC will achieve higher compressive strengths than an equivalent conventional concrete mix.
- The high strength SCC mix showed a lower modulus of elasticity (MOE) than the high strength conventional concrete mix. This result was attributed to the decreased amount of coarse aggregate present in the SCC mix. Both of the mixes were considerably lower than the recommended ACI coefficient used to estimate the modulus of elasticity. Both mixes showed comparable modulus of rupture and exceeded the recommended ACI coefficient. Both mixes also showed comparable splitting-tensile strength as well, while both mixes fell short of the recommended ACI coefficient used to estimate this property. As with any HSC project (SCC or non-SCC), particularly those

involving long-span HSC members, a performance-based approach where important design parameters such as MOE should be specified with mix design property characterization before member fabrication for conformance to ensure expected design behavior; for example, in the case of MOE, a required minimum MOE will ensure serviceability requirements will be satisfied. This performance-based approach may be considered even more critical for SCC mix designs since the survey results indicated that the coarse aggregate content will vary more depending on the particular producer.

- The high strength SCC mix significantly outperformed the high strength conventional concrete mix in every durability test except resistance to freezing and thawing. During the freeze-thaw test, the S10-48L showed noticeably poorer performance when compared to the high strength conventional concrete mix. Neither mix contained an air entraining admixture. It is possible that the high strength conventional concrete mix entrapped more air during the mixing process than the high strength SCC mix, improving its performance relative to the SCC mix. In all other durability aspects the high strength SCC mix showed improved performance compared to the high strength conventional concrete mix. In both the RCT and ponding test, the high strength SCC mix showed greater resistance to chloride penetration. The high strength conventional concrete mix was classified as highly permeable by the RCT while the high strength SCC mix was classified as moderate. This classification was further supported by the ponding test. While both mixes performed well, the high strength SCC mix achieved negligible corrosion risk at a third of the depth that the high strength conventional concrete mix achieved negligible corrosion risk. This increase in performance is most likely due to the denser microstructure achieved by SCC. The high strength SCC mix also outperformed the high strength conventional concrete mix in concrete resistivity, most likely due to the denser microstructure.

### **3.5 TASK 5: SHEAR PROPERTIES OF SCC MIXES**

The shear characterization results of locally available SCC and non-SCC mixes are presented in Technical Report A. The conclusions and recommendations from this task are as follows:

#### **TECHNICAL REPORT A, CONCLUSIONS:**

- The increased rate and higher ultimate strength development of SCC compared to CC observed by other researchers was also observed in this investigation.
- The decreased MOE for SCC compared to CC noted by others was not exhibited by the concrete batch proportions tested in this study.

- Researchers have reported conflicting results regarding the relative tensile strength of SCC to CC; this study observed improved tensile strength of SCC with respect to CC.
- The concrete batch proportions containing river gravel exhibited improved hardened mechanical properties of increased compressive strength, increased modulus of elasticity (MOE), and increased splitting tensile strength (STS) despite their decreased surface roughness compared to limestone aggregates tested.
- Vertical push-off specimen fabrication was effective in resembling actual member fabrication and adequately controlled geometrical tolerances for superior stress propagation and improved test results.
- Software imaging of post-failure cross-sections indicate segregation was not a significant issue and that tested specimen closely match calculated material proportions.
- The precrack test result analysis indicated that initial crack widths are highly controllable by increasing the initial clamping force.
- Precrack results exhibited a positive correlation to the concrete compressive strength, tensile strength, and test variations in initial clamping force.
- Push-off test results indicate decreasing aggregate interlock with increasing concrete compressive strength, a trend noted by other researchers and supported by theory.
- For the concrete batch proportions tested, river gravel exhibited superior aggregate interlock capability when compared to the limestone; this was the variable that had the largest effect on shear resistance of the concrete specimen and variables tested within this study.
- Despite other researchers' findings and theoretical conflict, the SCC did not appear to resist shear through aggregate interlock in a distinguishable manner from CC; the effect of coarse aggregate (C.A.) percentage was not detectable for the tests performed in this investigation.
- The E-value that other researchers have proposed and relied on for push-off analysis was discussed and discarded as the highly sensitive analysis tool it has been proposed to be. The E-value does examine shear and normal stress, crack width, and crack opening; however, it effectively averages and smears important incremental information.
- The increased rate of strength gain for SCC relative to CC was also noted for the shear beams; increased SCC strength at the time of release may be important to elastic prestress loss as well as losses over time.
- The tested shear beams exhibited similar flexural stiffness in the elastic range, this is supported by the relative ratio of concrete to steel as well as the consistent MOE of SCC and CC discussed above.

- SCC shear beams demonstrate increased deflections at increased shear strengths over comparable CC beams in this study. Other researchers have seen mixed results when comparing shear strength of SCC and CC beams.
- The beams of this study were tested once on each end. All secondary tests had increased shear strength and deflections over the virgin test indicating increased ductility.
- At failure, the SCC beams displayed crushing in their top fibers, the CC beams failed explosively in a shear plane extending from support to load point, away from developing flexural shear cracks.

#### **TECHNICAL REPORT A, RECOMMENDATIONS:**

- From the investigation undertaken it is evident that it would be advisable to undertake additional research in the subject of SCC shear behavior. There are limited test results for the full range of hardened mechanical and shear tests available to characterize SCC.
- It is recommended that an SCC be designed and developed following the guidelines from the NCHRP report 628 to become familiar with the issues and sensitivities of fresh SCC. Subsequent to SCC batch proportioning, it would be useful to conduct a QA/QC study across numerous Missouri precast and possibly ready-mix suppliers to ensure that adequate control of the material is ensured with the fast and simple fresh tests of slump-flow and J-ring. This process would familiarize all parties involved with the concerns of creating robust SCC, as well as help to establish practical and acceptable limits on the filling capacity and stability of subsequently developed SCC batch proportions.
- No concerns were identified in this investigation with regard to hardened mechanical testing of SCC relative to CC. Strength development and tensile strength was identified to be improved for SCC over similar CC. MOE was consistent between SCC and CC; other researchers have noted decreased MOE for SCC, but have also seen that the lower bound predictive models are still conservative.
- Additional shear testing of SCC would be useful. Push-off tests conducted throughout this investigation proved to be economical and quick, once familiar with the fabrication and testing procedures. Additional push-off testing, with some standardization and improvements to the test suggested by the authors, would be useful in refining the results of this study as well as investigating additional variables. Push-off testing would be most useful for lower strength concrete batch proportions where the impact of aggregate interlock is greater than at higher strengths. Variables that could be investigated could include maximum aggregate size, C.A. gradation, C.A. surface roughness and angularity, C.A. hardness, mineral and chemical

admixtures, as well as the variables tested in this investigation. A broad push-off test program may identify additional or compounding effects that have not been previously identified. It would also be valuable to conduct additional shear beam testing. It was identified that SCC shear beams have been tested in third point loading, but not commonly with distributed loading. Larger scale and more practical geometries of beams and girders should be tested in shear to compare to trends identified in this study. A beam with web-shear cracking may exhibit completely different behavior from the rectangular beams tested in this study that produced flexural-shear cracks and failed in a plane away from these developing cracks. Therefore, a full-scale beam test(s) with complete stress-strain instrumentation is recommended as part of an implementation program.

### **3.6 TASK 6: RECOMMENDATIONS AND SPECIFICATIONS FOR SCC IMPLEMENTATION**

Based on the results of Tasks 1 through 5, the investigators recommend implementation of SCC in the construction of precast/prestressed, transportation-related infrastructure in the State of Missouri. To accomplish this, the following requirements are recommended for incorporation into MoDOT's standard specifications or job specific provisions.

#### **SELF-CONSOLIDATING CONCRETE FOR PRECAST PRODUCTS**

**1.0 Description.** Self-Consolidating Concrete (SCC) is a specially designed concrete that enables the concrete to flow under the influence of its own weight and does not require mechanical vibration for consolidation. All material, proportioning, mixing and transporting of concrete shall be in accordance with Sec 501, except as specified herein.

**2.0 Materials.** All material shall be in accordance with Division 1000, Material Details, except as noted herein.

**2.1 Aggregate.** Fine and coarse aggregate shall be in accordance with Sec 1005, except that the requirements for gradation will not apply.

**2.1.1 Gradation.** The contractor shall submit the target gradation and allowable gradation range of each fraction of each aggregate source used in the mix design. During production, the contractor shall be within the allowable gradation range for each aggregate that was submitted.

**2.1.2 Maximum Coarse Aggregate Size.** Minimum requirement for coarse aggregate passing ¾-inch sieve shall be 100 percent.

**2.1.3 Minimum Coarse Aggregate Content.** Minimum coarse aggregate content shall be 48 percent by weight of total aggregate content.

**2.2 Admixture.** All chemical admixtures shall be in accordance with Sec 1054, except as noted herein.

**2.2.1 High Range Water Reducer.** The polycarboxylate based high range water reducer shall be in accordance with AASHTO M 194, Type F or G.

**2.2.2 Viscosity Modifier.** The viscosity-modifying admixture shall be evaluated according to the test methods and mix design proportions referenced in AASHTO M 194.

**2.2.3 Combination.** The self-consolidating admixture system shall consist of either a polycarboxylate based high range water-reducing admixture or a polycarboxylate based high range water reducer combined with a separate viscosity-modifying admixture.

**3.0 Concrete Mix Design.** At least 120 days prior to using SCC, the contractor shall submit a mix design for approval to Construction and Materials. The SCC mix shall be designed by absolute volume methods or an optimized mix design method such as Shilstone or other recognized optimization method.

**3.1 Required Information.** The mix design shall contain the following information:

- (a) Source, type and specific gravity of Portland cement
- (b) Source, type (class, grade, etc.) and specific gravity of supplementary materials, if used
- (c) Source, name, type and amount of admixture
- (d) Source, type (formation, etc.), ledge number if applicable, and gradation of the aggregate
- (e) Specific gravity and absorption of each fraction in accordance with AASHTO T 85 for coarse aggregate and AASHTO T 84 for fine aggregate, including raw data
- (f) Unit weight of each fraction in accordance with AASHTO T 19
- (h) The design air content and target slump flow (also referred to as slump spread)
- (i) Batch weights of Portland cement and supplemental cementitious materials
- (j) Batch weights of coarse, intermediate and fine aggregates
- (k) Batch weight of water
- (l) Compressive strength at release, 28 days, and 56 days

**3.2 Supplementary Cementitious Materials.** The SCC mix may use fly ash, GGBFS, metakaolin, or silica fume. Ternary mixes will be allowed for SCC. Ternary mixes are mixes that contain a combination of Portland cement and two supplementary cementitious materials. The amount of supplementary cementitious material content shall be limited to the following requirements:

Supplementary Cementitious Material (SCM)	
SCM	Maximum Percent of Total Cementitious Material
Fly Ash (Class C)	25 %
Ground Granulated Blast Furnace Slag (GGBFS)	30 %
Metakaolin	15%
Silica Fume	8 %
Ternary Combinations	40 %

**3.3 Water Amount.** The water/cementitious materials ratio shall meet the following requirements:

Water/Cementitious Materials Ratio	
Minimum	Maximum
0.27	0.37

**3.4 Minimum Cementitious Amount.** The total amount of cementitious materials shall not be below 700 pounds per cubic yard.

**3.5 Slump Flow.** The slump flow (or slump spread) test shall be performed in accordance with ASTM C 1611. The visual stability index rating shall be a maximum of 1. The slump flow shall meet the following requirements:

Slump Flow (inches)	
Minimum	Maximum
20	30

**3.6 Passing Ability.** Passing ability shall be performed in accordance with ASTM C 1621. The test value shall not be less than the slump flow by more than 2 inches.

**3.7 Segregation Resistance.** Resistance to segregation shall be performed in accordance with ASTM C 1610. The test value shall not exceed 10 percent.

**3.8 Air Content.** Air content shall be performed in accordance with AASHTO T 152. The minimum air content shall be as shown on the contract documents.

**3.9 Compressive Strength.** Compressive strength shall be performed in accordance with AASHTO T 22. Concrete shall have tendon release and 28-day minimum compressive strengths as shown on the contract documents.

**4.0 Batching Sequence Plan.** The contractor shall submit a Batching Sequence Plan outlining how the SCC mix will be batched and mixed. The Batching Sequence Plan shall be submitted to the MoDOT Resident Engineer for approval.

**5.0 Trial Batch.** A trial batch shall be done at least 90 days prior to SCC being used to ensure the mix is in accordance with this special provision. The SCC mix design shall not be used until all of the specified criteria have been met. The trial batch shall be at least 3 cubic yards. The MoDOT personnel shall be present during the trial batch. The SCC mix shall be tested for air content, slump flow, visual stability index, passing ability, compressive strength and strand bond (NASP test).

**5.1 Control Mix.** The control mix shall be the Class A-1 concrete mix currently being used by the producer for MoDOT work.

**5.2 Strand Bond.** Strand bond shall be evaluated in accordance with the North American Strand Producers (NASP) test method as prescribed in National Cooperative Highway Research (NCHRP) Report 603: Transfer, Development, and Splice Length in High-Strength Concrete, except as noted herein.

**5.2.1 NASP Test in Mortar.** Minimum acceptance criteria for strand bond in mortar: average of six specimens shall be greater than or equal to 16,000 lb. with no individual test result less than 14,000 lb.

**5.2.2 Additional Testing.** Additional strand bond testing will be required when a different manufacturer or strand configuration is used or if a different manufacturer or type of admixture is used.

**6.0 Production.** SCC mix shall not be used until the concrete mix, the Batching Sequence Plan, and the trial batch have been approved. The SCC mix shall not vary from the mix design submitted for approval. Any changes in material sources, aggregate gradations, or material content shall require a new SCC mix be resubmitted for approval. Changes to the water content and chemical admixture dosages will be allowed to handle changes in environmental conditions.

**6.1 Forms.** SCC mixes generate higher fluid pressures than conventional concrete mixes. Forms shall be mortar-tight and capable of supporting the additional pressure.

**6.2 Reinforcement.** Reinforcement and other critical components shall be tightly secured in the form to prevent these items from shifting during concrete placement.

**7.0 Quality Control.** Because the quality of freshly mixed SCC may fluctuate at the beginning of daily production, the contractor shall conduct air test, slump flow, visual stability index, and passing ability for every truck until consistent and compliant results are obtained. Subsequently, all testing shall be conducted in accordance with MoDOT specifications.

**7.1 Slump Flow Requirement.** During production, the slump flow shall be within +/- 2 inches of the target slump flow designated by the contractor and shall not exceed 30 inches. Sections 3.5 through 3.8 discuss slump flow, passing ability, segregation resistance and air content mix design requirements. Sampling and testing frequency for SCC should conform to current MoDOT requirements for conventional concrete.

### **3.7 TASK 7: VALUE TO MoDOT AND STAKEHOLDERS TO IMPLEMENTING SCC**

The use of self-consolidating concrete provides distinct value to the Missouri Department of Transportation through multiple avenues. Because of its unique nature, self-consolidating concrete (SCC) has the potential to significantly reduce costs associated with transportation-related infrastructure, benefiting both MoDOT and the residents of Missouri. SCC is a highly flowable, nonsegregating concrete that can be placed without any mechanical consolidation, and thus has the following advantages over conventional concrete:

- *Decreased labor and equipment costs during concrete placement.* Limited “hard” data exists to date in the traditional sense from bid documents involving SCC concrete due to its innovative nature; however, through laboratory experience at Missouri S&T, 40 to 60% less labor was needed to fabricate and place concrete when comparing SCC elements to the conventional concrete elements, which required more personnel to consolidate the conventional concrete elements and produce standard quality control / quality assurance (QC/QA) specimens. A similar trend was noted in November 2011 during fabrication of a cast-in-place SCC arch element in a MoDOT Hybrid Composite Beam in Mountain Grove, Missouri. Once concrete placement

started, fabrication times were completed in significantly less time based upon contractor commentary. As more SCC is implemented, historic cost trends will provide more quantitative financial data. However, it should be noted as SCC involves some new testing standards (i.e. QC/QA tests), there may be a “learning curve” for field and plant engineers / inspectors as they gain experience with new fresh concrete property testing protocols such as Slump Flow ASTM C 1611, J-Ring ASTM C 1621, L-Box (non-ASTM), and Column Segregation ASTM C 161.

- *Improved quality through the decreased potential for and costs to repair honeycombing and voids.* Due to SCC’s flowability, when properly formulated, there holds a great potential to decrease voids, anomalies and other defects that may occur during the placement of conventional concrete. This decreased potential should translate to an increase in the service life of the bridge or structure particularly as high-strength SCC is implemented with its improved durability performance.
- *Increased production rates of precast and cast-in-place elements.* In terms of both precast and cast-in-place elements, SCC offers the unique opportunity to expedite construction due to its unique characteristics. This increased rate of production translates into reduced construction time. This will open infrastructure systems in less time and help the traveling public in Missouri with reduced travel delays and congestion.
- *Improved finish and appearance of cast and free concrete surfaces.* While not a physical cost issue, improved finish and appearance of concrete elements provides an enhanced visual perspective of infrastructure elements for the riding public and will likely translate to a higher perceived level of quality.

### **3.8 OVERALL PROJECT RECOMMENDATIONS**

After thorough mechanical property, shear, bond, transfer, and durability testing, it is recommended that SCC be implemented in precast and prestressing applications within the State of Missouri. With SCC showing comparable results for hardened mechanical properties, insignificant variations in shrinkage, creep, abrasion, shear, bond, transfer and development and slightly higher performance for durability, SCC appears to be a viable option to decrease the cost of labor and time consumption during concrete placement. This performance was observed in both normal and high strength SCC, with high strength SCC performing at a slightly higher margin over high strength conventional concrete than SCC performed over conventional concrete.

#### 4. REFERENCES

1. Ramirez, J.A., and Russell, B.W. (2008). *Splice Length for Strand/Reinforcement in High-Strength Concrete*, NCHRP Project 12-60 Report, Transportation Research Board, Washington, D.C.
2. Lorenz, E., and Burgess K.M. (2009). R&D Discusses Research Projects, Committee Report, PCI Journal, Vol. 54, No. 1, Jan.-Feb.
3. ACI-ASCE Joint Committee 423 Prestressed Concrete (2010). Committee Meeting Minutes, March 22, 2010.
4. ACI Committee 408 (2003). "Bond and Development of Straight Reinforcing Bars in Tension (408R-03)," *Technical Documents*, American Concrete Institute, Farmington Hills, MI.
5. Hawkins, N.M., Kuchma, D.A., Mast, R.F., Marsh, M.L., and Reineck, K. (2005). *Simplified Shear Design of Structural Concrete Members*, NCHRP Project 12-61 Report, Transportation Research Board, Washington, D.C.
6. AASHTO (2010). *AASHTO LRFD Bridge Design Specifications*, 5th edition, Washington, D.C.
7. Veechio, F.J. and Collins, M.P. (1986). "The Modified Compression Field Theory for Reinforced Concrete Elements Subjected to Shear," *ACI Journal*, V. 83, No. 2, Mar.-Apr.

#### 5. TESTING STANDARDS

1. AASHTO – American Association of State Highway Transportation Officials: <http://www.transportation.org>
2. ACI – American Concrete Institute: <http://www.concrete.org>
3. ASTM International – American Society of Testing Methods: <http://www.astm.org>
4. PCI – Prestressed/Precast Concrete Institute: <http://www.pci.org>

**FINAL Report A**

TRyy1103

**Project Title: Self-Consolidating Concrete (SCC) for Infrastructure Elements**

**Report A: Self-Consolidating Concrete (SCC) for Infrastructure Elements: Shear Characteristics**

Prepared for  
Missouri Department of Transportation  
Construction and Materials

Missouri University of Science and Technology, Rolla, Missouri

July 2012

The opinions, findings, and conclusions expressed in this publication are those of the principal investigators and the Missouri Department of Transportation. They are not necessarily those of the U.S. Department of Transportation, Federal Highway Administration. This report does not constitute a standard or regulation.



## ABSTRACT

Because of its unique ability to maintain high flow-ability and remain homogeneous, self-consolidating concrete (SCC) has the potential to significantly reduce the costs associated with civil infrastructure; however, the use of higher paste and lower coarse aggregate volumes than non-SCC concretes raises concerns about the structural implications of using SCC. Of particular concern is the effect of concrete compressive strength, and aggregate type, shape, and content level on shear strength of SCC mixes. This research focused on the components that contribute to the concrete's ability to provide shear resistance, in particular, shear provided by aggregate interlock. Variables investigated by push-off tests to determine the shear contribution from aggregate interlock included concrete compressive strength (6 and 10 ksi [41.3 and 68.9 MPa] target), coarse aggregate type (limestone and river gravel), and volumetric content level of the coarse aggregate portion (36%, 48%, 58%, and 60%). Post-failure digital imaging software was used to confirm fresh concrete parameters in the hardened state as well as check for variability and the impact on shear. Additional attention was given to the global contributions of shear by the concrete in larger scaled tests of pre-stressed beam members. The results were used to assess the appropriateness of designing Missouri Infrastructure elements using the current *AASHTO LRFD Bridge Design Specification* for shear and while using typical Missouri SCC batch proportions and materials.

The research suggests that SCC has advanced to the level that robust mix designs can, and have been, utilized for Civil infrastructure. Aggregate interlock results agree with previous researchers that increased concrete compressive strength and the use of river gravel rather than limestone aggregate improves shear resistance. A distinguishable trend was not identifiable for shear resistance with C.A. fraction. Digital imaging confirmed non-segregating mixtures and that the actual C.A. bisecting a shear plane closely matched calculated values. The precrack and push-off testing itself was analyzed and suggestions for future researchers were proposed. Precast prestressed concrete beam tests indicate distinct behavior of SCC relative to control conventional concrete (CC) of similar strengths. The SCC shear beams exhibited increased deflections, higher ultimate loads, and even different failure modes. Given the distinguishable member behavior, additional research is advisable. Future

research should focus on full-scale members with practical geometries and reinforcing configurations.

## TABLE OF CONTENTS

	Page
ABSTRACT .....	iii
TABLE OF CONTENTS .....	v
LIST OF FIGURES .....	ix
LIST OF TABLES.....	xiii
NOTATIONS .....	xv
SECTION 1 .....	1
INTRODUCTION .....	1
1.1 GENERAL.....	1
1.2 OBJECTIVE AND SCOPE .....	2
1.3 ORGANIZATION OF THESIS.....	4
SECTION 2 .....	7
LITERATURE REVIEW .....	7
2.1 GENERAL.....	7
2.2 FRESH CHARACTERISTICS.....	9
2.3 HARDENED CHARACTERISTICS .....	13
2.4 SHEAR CHARACTERISTICS .....	15
2.4.1 General .....	15
2.4.2 Aggregate Interlock .....	17
2.4.3 Push-off Test .....	19
2.4.4 Shear Models .....	21
2.4.5 Shear in Beams .....	28
2.5 SUMMARY .....	35
SECTION 3 .....	37

MIX DESIGN .....	37
3.1 INTRODUCTION .....	37
3.2 SCC PRECAST PRODUCER SURVEY .....	38
3.3 MODOT GUIDENCE AND SPECIFICATIONS .....	43
3.4 SUMMARY .....	45
SECTION 4 .....	48
MATERIAL AND FRESH CONCRETE PROPERTIES .....	48
4.1 GENERAL .....	48
4.2 MATERIAL PROPERTIES .....	50
4.3 FRESH PROPERTIES .....	53
SECTION 5 .....	61
HARDENED PROPERTIES .....	61
5.1 INTRODUCTION .....	61
5.2 TEST SETUP AND PROCEDURE .....	63
5.3 TEST RESULTS .....	67
5.4 DATA ANALYSIS AND CONCLUSIONS .....	70
SECTION 6 .....	82
PUSH-OFF TEST .....	82
6.1 INTRODUCTION .....	82
6.2 TEST SETUP AND PROCEDURE .....	83
6.2.1 Test Setup .....	83
6.2.2 Test Procedure .....	88
6.2.3 ImageJ Analysis Procedure .....	97
6.3 SPECIMEN DESIGN AND FABRICATION .....	103
6.3.1 Initial Design and Fabrication .....	104

6.3.2	Problems Encountered, Proposed Remedies .....	107
6.3.3	Final Design and Fabrication.....	115
6.4	TEST RESULTS AND ANALYSIS .....	119
6.4.1	Precrack Results and Analysis.....	119
6.4.2	Push-Off Results and Analysis.....	129
6.4.3	Cross-Sectional Imaging Results and Analysis.....	149
6.5	CONCLUSIONS.....	154
SECTION 7 .....		158
PRECAST, PRESTRESSED BEAM TESTS.....		158
7.1	INTRODUCTION .....	158
7.2	TEST SETUP AND PROCEDURE .....	158
7.2.1	Test Setup.....	159
7.2.2	Test Procedure .....	162
7.3	MEMBER DESIGN AND FABRICATION .....	166
7.3.1	Member Design .....	166
7.3.2	Member Fabrication .....	169
7.4	TEST RESULTS AND ANALYSIS .....	173
7.5	FINDINGS AND CONCLUSIONS .....	187
SECTION 8 .....		190
SUMMARY, CONCLUSIONS, AND RECOMMENDATIONS .....		190
8.1	SUMMARY.....	190
8.2	FINDINGS AND CONCLUSIONS .....	193
8.3	RECOMMENDATIONS.....	196
REFERENCES .....		199
APPENDIX A: MATERIAL DATA SHEETS .....		205

APPENDIX B: SAMPLE SURVEY QUESTIONNAIRE.....213

APPENDIX C: SAMPLE BATCH WEIGHT AND FRESH PROPERTY RESULT  
SPREADSHEETS ..... 216

APPENDIX D: SHEAR BEAM DESIGN AID ..... 219

## LIST OF FIGURES

	Page
Figure 2.1	Suggested Fresh Property Tests (Mix Design and Quality Control) (NCHRP 2009) .....10
Figure 2.2	Suggested Fresh Consistency by Application (NCHRP 2009) .....12
Figure 2.3	Traditional Shear Resistance Mechanisms (ACI – ASCE 426 1973) ....16
Figure 2.4	Aggregate Interlock (Vecchio and Collins 1986) .....18
Figure 2.5	Push-Off Test Geometry and Orientations.....20
Figure 2.6	Effect of Gradation Variability (Walraven 1981) .....25
Figure 2.7	Determination of Expression for Shear Across Cracks, Equation 2.13 (Vecchio and Collins 1986) .....27
Figure 2.8	Distinguishing Average Versus Local Stresses in Cracked Members (Vecchio and Collins 1986) .....30
Figure 3.1	National DOT Survey Results.....42
Figure 4.1	Designation Key.....48
Figure 4.2	Coarse Aggregate Sieve Analysis.....52
Figure 4.3	6 Cubic Foot Mixing Drum.....53
Figure 4.4	Slump Flow Test.....55
Figure 4.5	J-ring (left) and L-box (Right).....56
Figure 4.6	Segregation Column.....57
Figure 4.7	Pressure Meter and Base Used for Unit Weight and Air Content.....58

Figure 5.1	STS Diagram.....	63
Figure 5.2	MOE and Compressive Strength Test.....	65
Figure 5.3	Splitting Tensile Strength (STS) Test.....	66
Figure 5.4	Compressive Strength Development over Time.....	71
Figure 5.5	“Ultimate” MOE for All Mixtures.....	74
Figure 5.6	“Ultimate” STS for all Mixtures.....	75
Figure 5.7	Normalized “Ultimate” MOE.....	77
Figure 5.8	Normalized “Ultimate” STS.....	78
Figure 6.1	Aggregate Interlock Test Orientations.....	84
Figure 6.2	Precracking Shown to Alleviate Tensile Regions by Barragan.....	85
Figure 6.3	LVDT Placement for Measuring Crack Opening and Slip.....	86
Figure 6.4	Strain Gage Location on External Reinforcement.....	87
Figure 6.5	Aggregate Interlock Specimen Load Blocks.....	88
Figure 6.6	Projected Surface on Apparatus for Positioning.....	89
Figure 6.7	A Properly Positioned Specimen.....	90
Figure 6.8	Properly Anchored LVDTs, Parallel and Perpendicular to Groove.....	91
Figure 6.9	Strain Gages Attached to Data Acquisition System (DAS) .....	92
Figure 6.10	Pre-crack Specimen Positioning.....	94
Figure 6.11	Push-off Test Positioning.....	96
Figure 6.12	Photo Booth Used For Cross-Sectional Imaging.....	98
Figure 6.13	ImageJ Sample Analysis.....	102
Figure 6.14	Initial Specimen Dimensions and Reinforcement.....	105

Figure 6.15	Plan of Initial Specimen Form, Showing Cast Groove and Reinforcement Layout.....	106
Figure 6.16	Complete Initial Formwork, Up To Four Specimen Cast at a Time....	106
Figure 6.17	Unsuccessful Drilled Anchor System.....	108
Figure 6.18	Undesirable Modes of Failure Experienced During Trial Testing.....	111
Figure 6.19	Newly Designed Formwork.....	112
Figure 6.20	Anchor Bolt Formwork.....	113
Figure 6.21	Resultant Cast in Place Anchors.....	114
Figure 6.22	Final Specimen Dimensions and Reinforcement.....	116
Figure 6.23	SCC Placement Technique into New Formwork.....	118
Figure 6.24	Increasing Precrack Load with Increased Compressive Strength.....	123
Figure 6.25	Increasing Precrack Load with Increased STS.....	124
Figure 6.26	Increasing Precrack Load with Increased Initial Normal Stress.....	126
Figure 6.27	Decreasing Crack Opening with Increased Initial Normal Stress.....	127
Figure 6.28	Decreasing Stress Ratio with Increased Initial Normal Stress.....	128
Figure 6.29	Determining “Zero” Crack Opening.....	131
Figure 6.30	Shear Stress Development over Crack Slip Range.....	132
Figure 6.31	Normal Stress Development over Crack Slip Range.....	133
Figure 6.32	E-value over Full Range of Slip Limits.....	134
Figure 6.33	Shear to Normal Stress Ratio vs. Crack Opening.....	137
Figure 6.34	Reduced Compressive Strength Improves Relative Shear Resistance..	138
Figure 6.35	Performance of Specimens Cast at Coreslab Structures, Inc. ....	140
Figure 6.36	E-value across Slip Limit Range.....	142

Figure 6.37	Crack Slip to Opening Relationship.....	144
Figure 6.38	Limestone Mixtures Tested Compared to Previous Researchers.....	145
Figure 6.39	River Gravel Mixtures Tested Compared to Previous Researchers.....	146
Figure 7.1	Initial Three Point Shear Beam Test Setup.....	159
Figure 7.2	Load Actuator used for Shear Beam Tests.....	160
Figure 7.3	Four Point Shear Beam Test Setup.....	161
Figure 7.4	Beam Test Dimensions.....	161
Figure 7.5	Shear Beam Repair Procedure.....	165
Figure 7.6	Shear Beam Details.....	169
Figure 7.7	Reinforcement and Formwork Positioned.....	171
Figure 7.8	Coreslab Structures Inc. Crew Places, Consolidates, and Finishes Concrete for Beams.....	172
Figure 7.9	“Release” of Beams.....	173
Figure 7.10	Beam Strength Development Curves.....	175
Figure 7.11	Beam Load-Deflection Response Curves.....	179
Figure 7.12	Beam Elastic Range Load-Deflection Response.....	180
Figure 7.13	Shear Stress Normalized by the Square Root of Compressive Strength.....	181
Figure 7.14	Crack Development Patterns with Applied Loads.....	184

## LIST OF TABLES

		Page
Table 3.1	Compiled Survey Results from Responding Precast Suppliers.....	39
Table 3.2	Important Averages from Survey Results.....	40
Table 3.3	6 ksi (41.4 MPa) Target Strength CC Batch Proportions.....	43
Table 3.4	6 ksi (41.4 MPa) Target Strength SCC Batch Proportions.....	44
Table 3.5	10 ksi (68.9 MPa) Target Strength CC and SCC Batch Proportions....	45
Table 3.6	Four Basic Mixtures to the SCC Project.....	46
Table 4.1	Concrete Batch Proportions Tested.....	49
Table 4.2	Bulk Specific Gravity (Oven Dry Basis) and Absorption of Aggregate.....	50
Table 4.3	Fresh Property Tests and Results for Limestone Mixtures.....	59
Table 4.4	Fresh Property Tests and Results for River Gravel Mixtures.....	60
Table 5.1	Target Test Ages for Hardened Properties.....	61
Table 5.2	Compressive Strength Test Results for Limestone Mixtures.....	67
Table 5.3	Compressive Strength Test Results for River Gravel Mixtures.....	67
Table 5.4	Compressive Strength Test Results for Coreslab Specimens.....	68
Table 5.5	MOE, STS, and Coefficients Test Results for Limestone Mixtures.....	68
Table 5.6	MOE, STS, and Coefficients Test Results for River Gravel Mixtures..	69
Table 6.1	Mechanical and Pre-Crack Properties.....	120
Table 6.2	ImageJ Segregation Results.....	151
Table 6.3	Calculated and Actual C.A. Volume Fractions.....	153

Table 7.1	Beam Fresh Concrete Properties.....	174
Table 7.2	Tested Beam Companion Compressive Strength Cylinders.....	175
Table 7.3	Extrapolated Beam Strength at Test Age.....	176
Table 7.4	Predicted Shear Beam Behavior.....	185

## NOTATIONS

$a$	Maximum aggregate size
$d_v$	Effective shear depth (per AASHTO)
$f'_c$	Unconfined compressive strength of concrete
$f_{ci}$	Normal stress on the shear plane on the cracked concrete imposed by crack dilation
$f_{ct}$	Tensile strength of concrete, as measured by a splitting tensile strength (STS) test fixed
$f_r$	Modulus of rupture, MOR
$s_x$	Crack spacing parameter, from member and reinforcement geometry
$s_{xe}$	Effective crack spacing parameter
$v_{ci}$	Limiting value of maximum shear stress on the shear plane on the cracked concrete
$\bar{A}_x$	The unit area of contact between the aggregate and paste in the x-direction (in the direction of crack slip)
$\bar{A}_y$	The unit area of contact between the aggregate and paste in the y-direction (in the direction of crack opening).
$E_c$	Young's Modulus (modulus of elasticity) of concrete, MOE
$P$	Pre-crack load
$P_k$	Ratio of aggregate volume to total concrete volume
$R^2$	Coefficient of determination
$V_a$	Shear contribution due to aggregate interlock

$V_c$	Shear strength of concrete
$V_{cy}$	Shear contribution due to concrete in the uncracked compression zone
$V_d$	Shear contribution due to dowel action of longitudinal reinforcement
$V_s$	Shear contribution due to lateral shear reinforcement
$\beta$	Factor of tensile stress in the concrete
$\delta$	Crack slip length
$\delta'$	Crack slip limit
$\epsilon_1$	The principle tensile strain in the concrete
$\epsilon_x$	Longitudinal tensile strain in the web
$\theta$	Angle of principle compressive stress in the web
$\mu$	Friction coefficient
$\sigma$	Normal stress
$\tau$	Shear stress
$w$	Crack opening width
AASHTO	American Association of State Highway and Transportation Officials
ACI	American Concrete Institute
AEA	Air entraining admixture
SCC	Self-consolidating concrete
CC	Conventional concrete
C.A.	Coarse aggregate
CFT	Compression field theory (of shear)
DAS	Data Acquisition System
F.A.	Fine aggregate

FEM	Finite element model
HRWRA	High range water reducing admixture
HSC	High strength concrete
LVDT	Linear voltage displacement transducer
MCFT	Modified compression field theory (of shear)
NCHRP	National Cooperative Highway Research Program
SCOH	Standing Committee on Highways, an AASHTO committee
SOM	Subcommittee on Materials, an AASHTO subcommittee
VMA	Viscosity modifying admixture
W/CM	Water to cementitious material ratio

## 1. INTRODUCTION

### 1.1 GENERAL

Self-consolidating concrete (SCC) is highly flowable, non-segregating concrete that can be placed with no mechanical consolidation. SCC has the potential for numerous advantages over conventional concrete (CC) which include, but are not limited to:

- Reduced labor, equipment, and associated cost
- Is cast with desired mechanical properties, independent of placement crew skill
- Accelerated construction
- Enables filling of complex formwork or members with congested reinforcement
- Decrease employee injuries
- Permits more flexible reinforcement detailing and design
- Creates smooth, aesthetically appealing surfaces

All of the benefits can be accomplished through the use of conventional concrete materials and admixtures. There are, in fact, three recognized mixture-proportioning approaches for making SCC; using high powder content and High Range Water Reducing Admixtures (HRWRA), low powder contents with HRWRA and viscosity modifying admixtures (VMA), and lastly by using moderate amounts of powder content, HRWRA, VMA and controlling stability through other mechanisms such as blending aggregates and lowering water content (ACI 237 2007). This investigation achieved SCC flowability and stability through the first method, by using HRWRA paired with increased ratios of fine aggregate (F.A.) to coarse aggregate (C.A.) and

large cement contents. The first method of achieving SCC was seen to be common practice by Missouri precast concrete providers at the time of this study, and was therefore the method pursued. Details of the batch proportions used will be discussed later, in section 3 of this report.

## **1.2 OBJECTIVE AND SCOPE**

The primary objective of this research was to examine the variables that contribute to aggregate interlock, and their affect on the overall shear behavior of both CC and SCC in a precast, prestressed beam application using locally available materials to reflect current Missouri Precaster practices. The first step was to develop mixtures that were representative of the concrete batch proportions currently being used by Missouri Precasters. Next, plastic properties of the concrete were recorded for an evaluation of behavior and robustness using standard and non-standard test methods. Mechanical properties of compressive strength ( $f'_c$ ), Young's Modulus also known as modulus of elasticity ( $E_c$ ), and splitting tensile strength ( $f_{sp}$ ) were collected for comparison between CC and SCC. To investigate shear, a non-standard, but widely recognized test known as a push-off test was utilized to investigate variables affecting the aggregate interlock component of shear; these results were then compared to test results collected from the testing of precast, prestressed beams.

In the state of Missouri, SCC is not currently permitted by the Missouri Department of Transportation (MoDOT) for use in structural applications without MoDOT oversight, trial batching, and independent laboratory testing, but is used for non-structural precast application because of the many advantages of the material with

respect to CC (MoDOT 2012). This research began with contacting, and collecting survey information from, precast concrete companies in and around the state of Missouri. The intent of the survey was to determine how widespread the use of SCC is in Missouri, establish the sophistication and robustness of the batch proportions used, and to develop a baseline SCC mix design for this research. MoDOT was consulted to establish the CC or control batch proportions. This collected information was then paired with the Principal Investigator's previous work with high strength concrete (HSC) to develop two additional baseline batch proportions for SCC and CC HSC.

The plastic state concrete properties were not the focus of this research; however, standard and non-standard tests were performed in order to develop an understanding of the rheology of the SCC mixes. One important aspect to note would be the achievement of SCC by using HRWRA with an increased F.A. to C.A. ratio for stability as opposed to using a conventional batch proportion with a large HRWRA dosage and VMA for stability. The increase in F.A. volume at the expense of C.A. volume is the explanation some have proposed for why SCC may have reduced aggregate interlock potential as compared to CC.

Mechanical properties of concrete compressive strength, Young's Modulus, and splitting tensile strength were also collected. These mechanical properties are essential to the design and analysis of civil structures. Young's Modulus is used to predict load response of structures, splitting tensile stress can be used to determine cracking behavior and capacity, and strength is used to develop member capacity by several mechanisms as well as being correlated to the other mechanical properties tested. Test results were used to evaluate CC and SCC compared to each other as well as standard prediction equations.

Finally, the main focus of this research is shear capacity and behavior of SCC. Specifically the aggregate interlock component of concrete shear was investigated in detail. The push-off test is a non-standard test, but has been used by researchers since the late 1960's as far as this author could determine, and is widely recognized by concrete shear researchers. A significant benefit of the push-off test is the ability to test many variables at a low cost, given the size of the specimen. Previous research, results, and models will be discussed in section 2 as part of the literature review. The goal with this study was to determine whether current models can be used to predict aggregate interlock while using Missouri aggregates within currently used Missouri precast SCC mixtures. The models were then also compared to the precast prestressed beam test results to determine if predicted behavior was exhibited.

### **1.3 ORGANIZATION OF REPORT**

This report contains eight sections, four appendices, and a list of references. Information regarding each section and appendix is explained below.

Section 1 provides an introduction to this report. A brief background is given as to what self-consolidating concrete is, the potential benefits from using it, and the reason for the reluctance of widespread use. This section also describes the scope of work for this project, and outlines the information contained herein.

The second section conveys detailed information provided by other researchers that is important to this investigation. The literature review was conducted to gather information regarding fresh and hardened concrete properties, as well as shear in hardened concrete. Specific aspects of concrete shear were examined which include

aggregate interlock as a component of shear, the push-off test as an investigation of aggregate interlock, shear models based on aggregate interlock and overall shear behavior, and lastly shear in beams.

Section 3 provides the means by which concrete batch proportions were determined. This section describes the use of a survey that was distributed to Missouri precast concrete plants, Missouri ready mix suppliers, and to American Association of State Highway and Transportation Officials (AASHTO) members across the nation. Section 3 discusses the results of the survey, and how that information was used. MoDOT was also consulted in order to determine the control batch proportions.

The material and fresh concrete properties are presented in section 4. The specific tests and their associated standard for each of the material properties and fresh properties are described, along with the number of each test conducted. The results of the material and fresh concrete properties tests are shown, and briefly discussed.

Section 5 surveys the hardened properties investigated. The test setup and procedures are described. The hardened properties test results are shown and discussed.

The push-off test is presented in section 6. The pre-crack and push-off tests are described in detail. The test setup, procedure, specimen design and fabrication, and all of the difficulties encountered are detailed. Results from the investigation are represented along with a detailed analysis. A forensic investigation of the failed cross-sections of the push-off specimens was also undertaken and is presented in section 6.

Section 7 presents the shear beam test. As in section 6, the test setup, procedure, design, and fabrication are shown, along with difficulties overcome. The member

behavior is evaluated and compared for CC and SCC beams. The analysis and comparison with accepted shear models is also shown.

In section 8, the whole of this report is summarized. Conclusions about this investigation are made when possible, and recommendations are made accordingly.

## 2. LITERATURE REVIEW

### 2.1 GENERAL

The widespread use of SCC has developed from the initial conception in Japan where the material was developed in 1989 to ensure proper consolidation with a small skilled labor workforce in applications where concrete durability and service life were of concern (ACI 237 2007; FHWA 2005). The level of sophistication in relation to SCC has risen substantially in the last twenty years; advanced material proportioning has led to studies investigating the effects of fine-to-coarse aggregate ratio, coarse and fine aggregate characteristics, water-to-cementitious material, binder, and paste ratios, HRWRA, VMA, air entraining admixtures (AEA), mineral admixtures, inert filler fines to replace cement, and more on fresh rheological and hardened mechanical behavior (Khayat and Assaad 2002; Ghezal and Khayat 2002; NCHRP 2009). It can be beneficial to take advantage of the ever-improving material.

Advancements in understanding and chemical admixtures have led to the distinct material behavior that now defines SCC, "...highly flowable, nonsegregating concrete that can spread into place, fill the formwork, and encapsulate the reinforcement without any mechanical consolidation." (ACI 237 2007). The performance of SCC has led to advantages over conventional concrete in many ways including: reduced cost, higher rate of placement, enables filling of highly reinforced sections, provides placement logistics flexibility, reduced noise for urban areas and worker health, decreased laborer injury, and more. SCC in the hardened state can also demonstrate benefits that include the superior surface quality, reduced surface permeability, and more homogeneous mechanical

properties that are developed independent of laborer skill (ACI 237 2007). With all of the advantages of SCC, more and more interested parties are getting involved and encouraging more widespread use.

The material cost of SCC is usually greater than CC because of the large demand of cementitious material and admixtures; however, overall project costs may be reduced because of labor, equipment, and time savings (Ghezal and Khayat 2002; FHWA 2005). It is the multitude of potential advantages that is driving the spreading use of SCC. In the decades since invention, Japan has increasingly used SCC, even on such large-scale projects as the Akashi-Kaikyo bridge (the longest central span suspension bridge in the world) where SCC was used for the anchorages (Nowak et al. 2007). European entities have formed to increase usage of SCC for infrastructure. In 1994, the European Project Group was formed from five organizations dedicated to the promotion of advanced materials and systems for the supply and use of concrete. Since the group was founded, they have developed several state of the art documents (the latest in 2005) addressed to specifiers, designers, purchasers, producers, and users of SCC; they draw their information from the ever burgeoning supply of case studies and research projects from 12 European countries and the UK concrete society. There is, to date, no European Standard (EN) for SCC (EFNARC 2005). The United States is taking similar action to Europe. Interested transportation departments, research universities, societies, and specifying organizations are taking active roles in increasing the U.S. knowledge and use of SCC. Many case studies have been conducted across the country from New York to Virginia, Nebraska, and beyond (FHWA 2005). A project interested in advising the nation in regard to SCC was undertaken and a report was presented that recommended

guidelines for the use of SCC in precast, prestressed concrete bridge elements (NCHRP 2009). The National Cooperative Highway Research Program (NCHRP) report is full of useful information, but has not led to any national specification adoption.

Given the vast number of projects and case studies, there are still no widely accepted specifications for the use of SCC, only guidelines. The complexity of the numerous material interactions that take place in high performance concretes such as SCC make systematic, well designed research essential. Some seemingly contradictory research findings make specifiers and designers reluctant to use this advanced material (FHWA 2005; Kim 2008; Lachemi 2005; Naito et al. 2006; NCHRP 2009). An aspect of concrete that is already not well understood, shear failure, is given even greater scrutiny because of reduced C.A. in SCC.

## **2.2 FRESH CHARACTERISTICS**

The definition of SCC encompasses a great deal of information about the material in the fresh state that may not be readily obvious. The words used to describe SCC; flowable, nonsegregating, and fill are referring to tests with definable quantitative measurements and suggested ranges. Standardized tests have been developed to test filling ability, passing ability, filling capacity, and segregation resistance (static stability); **Figure 2.1** shows a table taken from an NCHRP report that summarizes the fresh property of interest, the associated test methods (standard and non-standard), suggested test result targets, and whether the tests should be conducted as part of an SCC mix design program or for routine quality control (NCHRP 2009). An important feature of the suggested SCC fresh concrete quality control tests is that they can be fulfilled by the

ASTM standardized tests of only slump flow, J-ring flow, and the already utilized air content tests. It is also important to know that the slump flow and J-ring tests are simple, demonstrate repeatability, and fast; the two tests must be conducted within 6 minutes to be in conformance with the standard (ASTM C 1621 2009).

Property	Test Method	Target values	Design	QC
Filling ability	Slump flow T-50 (ASTM C1611)	23.5-29 in. (600-735 mm) 1.5-6 s	√	√
Passing ability	J-Ring flow (ASTM C1621)	21.5-26 in. (545-660 mm)	√	√
	L-Box blocking ratio ( $h_2/h_1$ )	0.5-1.0	√	√
Filling capacity	Filling capacity	70%-100%	√	
	Slump flow and J-Ring flow tests			√
	Slump flow and L-Box tests			√
Static stability	Surface settlement	Rate of settlement, 25-30 min (value can decrease to 10-15 min) -MSA of 3/8 and 1/2 in. (9.5 and 12.5 mm) $\leq 0.27\%/h$ (Max. Settlement $\leq 0.5\%$ ) -MSA of 3/4 in. (19 mm) $\leq 0.12\%/h$ (Max. settlement of 0.3%)	√	
	Column segregation (ASTM C 1610)	Column segregation index (C.O.V.) $\leq 5\%$ Percent static segregation (S) $\leq 15\%$	√	
	VSI (ASTM C 1611)	0-1 (0 for deep elements)	√	√
Air volume	AASHTO T 152	4%-7% depending on exposure conditions, MSA, and type of HRWRA. Ensure stable and uniform distribution of	√	√

**Figure 2.1 – Suggested Fresh Property Tests (Mix Design and Quality Control)**  
(NCHRP 2009)

Because SCC is placed with no external compaction effort, the fresh properties control the quality of placement and the hardened properties; therefore, it is important to develop an SCC with sufficient robustness. Most concrete constituent variability can be equated to water demand, whether it is changes in moisture content, material gradation, or specific surface for example. A well designed SCC should lend acceptable tolerance to daily fluctuations in the materials during production and should withstand a change of 8.5 - 17 lb/yd<sup>3</sup> (5 - 10 L/m<sup>3</sup>) in water content without falling outside performance specifications (EFNARC 2005; NCHRP 2009). Newer VMA chemical admixtures can help to reduce the impact of material variability and enhance the robustness of well designed SCC. However, VMA should not be viewed as a way of avoiding the need for a good mix design, ongoing quality assurance, and careful selection of constituent materials (EFNARC 2006). NCHRP has recommended slump flow and slump flow minus J-ring flow values based on intended use, **Figure 2.2** presents the recommendations which are consistent with other guidelines (EFNARC 2005; NCHRP 2009). It is again worth noting the fresh characteristics are being described by the two simple tests with the benefits described earlier. Also, it has been concluded from other researchers that filling capacity is best described by a combination of passing ability and non-restricted deformability tests such as the two shown below (Hwang, S. et al. 2006).

Relative Values		Slump flow, in.			Slump flow - J-Ring flow, in.		
		23.5-25	25-27.5	27.5-29	3-4	2-3	≤ 2
Low	Reinforce- ment density						
Medium							
High							
Small	Shape intricacy						
Moderate							
Congested							
Shallow	Depth						
Moderate							
Deep							
Short	Length						
Moderate							
Long							
Thin	Thickness						
Moderate							
Thick							
Low	Coarse aggregate content						
Medium							
High							

**Figure 2.2 – Suggested Fresh Consistency by Application (NCHRP 2009)**

It is the need for consistent quality control, the large impact of small material variability, and the more readily controlled environment of the precasting plant that has enabled the more widespread use of SCC by precasters, while leaving the ready mixed concrete industry in its infancy (ACI 237 2007; EFNARC 2006; NDOR 2007). If a good quality SCC mix design is implemented well, superior hardened properties can result. There are also important trade-offs of SCC in the hardened state that should be considered.

### 2.3 HARDENED CHARACTERISTICS

The hardened mechanical properties of compressive strength, tensile strength, and modulus of elasticity will be discussed because of their importance to a designer and/or a specifier. Other hardened characteristics such as creep, shrinkage, durability, and bond are not of interest to this researcher's investigation.

Concrete compressive strength ( $f'_c$ ) is very important to the design of concrete structures as it is a measure of the strength of the construction material. Compressive strength is also highly correlated to elastic stiffness and tensile strength and should be evaluated to predict the structural response to loading. Compressive strength is highly dependent on the water to cementitious material (W/CM) ratio, age, powder content (cement and supplementary cementitious materials), curing conditions, admixtures used, and aggregate gradation and surface texture (Mindess et al. 2003). It has been widely recognized that for a given W/CM, SCC can develop higher compressive strength as compared to CC. The improved compressive strength is a result from the lack of vibration and reduction in bleeding and segregation that promotes a more uniform and improved interfacial transition zone between the aggregate and paste (ACI 237 2007; EFNARC 2005). During a scientific investigation, the impact of the effects of curing conditions, age, powder content, and aggregate gradation and surface texture can be mitigated by controlling these variables.

The tensile strength of concrete is described by two separate tests, but the two are often considered together. The modulus of rupture (MOR,  $f_r$ ) is tested by loading a small concrete beam into flexure and is set equal to the extreme tension fiber stress at failure. The splitting tensile strength (STS,  $f_{ct}$ ) is tested by placing a concrete cylinder on its side

and applying a line load along the length, the splitting tensile strength is then computed from the failure load and geometry of the specimen. There have been mixed results when comparing the tensile strength of SCC to CC. Some report that the tensile strength of SCC is comparable to CC because the volume of paste has no significant effect on tensile strength (EFNARC 2005). Some purport that SCC may have a higher MOR than CC with similar proportions (ACI 237 2007). Lastly, some researchers have found that MOR for SCC may be reduced, while STS for SCC appeared improved; the explanation was that MOR is a more direct test of the SCC's volumetrically increased and weaker paste tension surface, while STS tests a larger cylinder core surface that encompasses the properties of the aggregate, paste, and the interfacial transition zone (Kim 2008). The confusion over the tensile properties of SCC is a potential area for more research to improve estimates.

Modulus of elasticity (MOE,  $E_c$ ) is the linear, elastic straining of a material in response to loading over an area. It is readily agreed by researchers that SCC generally has a decrease in MOE because of the typical practice of removing hard C.A. volumes and replacing them with softer paste volumes. Various reports suggest that SCC can have reduced MOE from 4 - 15%, but SCC has been shown to be well predicted by AASHTO prediction equations and should be adequately covered by the safe assumptions on which the formula are based (ACI 237 2007; EFNARC 2005; Kim 2008, NCHRP 2009). The reduction of MOE for high strength concrete may not be as drastic because the concrete stiffness already relies more on the stiffness of the paste. Because MOE controls the response of concrete members to load as well as the member camber, creep, and shrinkage, the reduction in MOE should be fully understood for the SCC mixtures in use.

For hardened SCC, there appear to be benefits and disadvantages when compared to CC. Compressive strength of SCC can be increased over CC of similar batch proportions. Tensile strength of SCC may be improved relative to CC, but may also exhibit greater variability. Elastic stiffness of SCC is decreased from similar CC, leading to increased camber, shrinkage, creep, and prestress loss potential. The shear characteristics and behavior should also be discussed.

## 2.4 SHEAR CHARACTERISTICS

As already discussed, the constituent material proportions of SCC differ from those traditionally used in CC. With such drastic changes to mixture proportions, an investigation into important failure modes, including shear, should be undertaken.

**2.4.1 General** The shear capacity of concrete can be of great concern, especially in certain shear-critical applications and given the extremely brittle and not well understood mechanisms of failure. The common practice of reducing coarse aggregate volume to increase paste and fine aggregate fractions in SCC mixtures has raised concerns about the possible reduction of shear capacity due to loss of aggregate interlock. The shear strength provided by concrete,  $V_c$ , is taken equal to the failure capacity of a beam without stirrups usually said to be the inclined cracking shear or concrete contribution to shear. **Figure 2.3** shows the relative contributions to inclined cracking shear of the resisting mechanisms of shear in the compression zone,  $V_{cy}$ , the vertical component of shear transferred across the crack by aggregate interlock,  $V_a$ , the dowel action of the longitudinal reinforcement,  $V_d$ , and the shear reinforcing steel,  $V_s$  (ACI – ASCE 426 1973). It can be seen from **Figure 2.3** that aggregate interlock is the primary

mechanism of resistance to shear failure at the time of inclined cracking or member failure without shear reinforcement. So, it can be understood that a significant reduction in aggregate interlock from C.A. replacement can have a significant reduction in total concrete shear resistance.

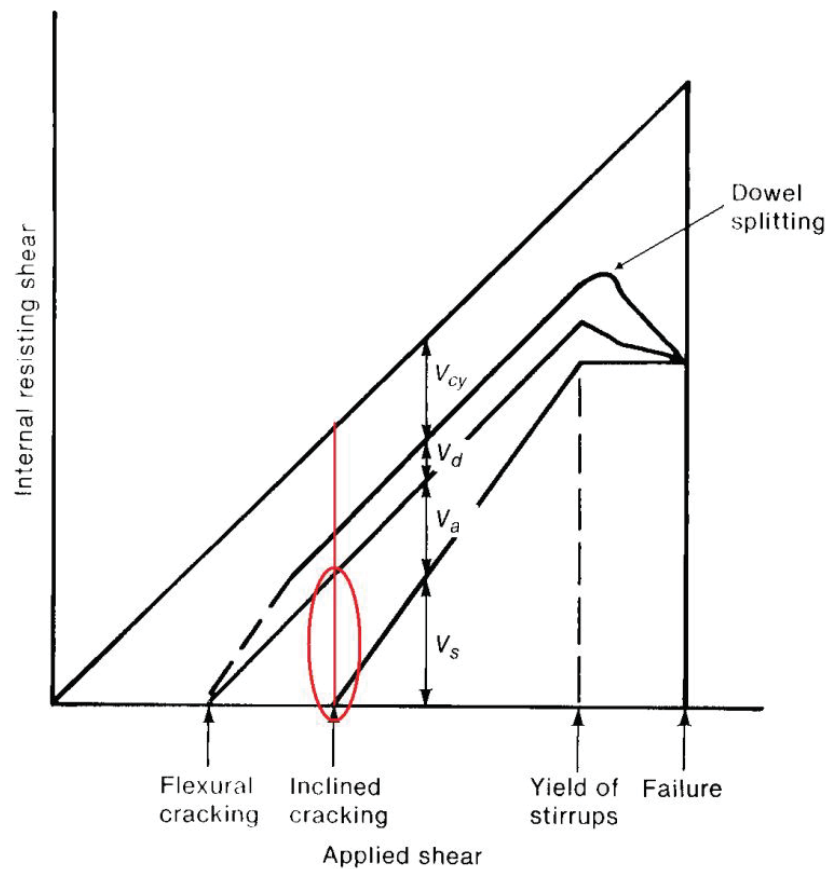


**Figure 2.3 – Traditional Shear Resistance Mechanisms (ACI – ASCE 426 1973)**

To date, there are few studies available that have directly investigated the impact of the reduction of C.A. volume in SCC mixtures on aggregate interlock. One study did look at SCC in particular, and conducted “push-off” tests to directly investigate the impact of concrete compressive strength, aggregate type, and aggregate volume on

aggregate interlock. The results show what would traditionally be shown by theory; aggregate interlock decreases with increased concrete compressive strength, aggregate interlock decreases with reduced C.A. volumes, and that aggregate interlock is affected by the aggregate type (Kim 2008). It is worth continuing to investigate these variables for SCC so that the findings can be verified and models can be more reasonably proposed.

There have been more studies where full scale precast, prestressed SCC and CC beams have been comparatively tested in shear. Some researchers have found that SCC has similar shear capacity to comparison CC beams (FHWA 2005; Kim 2008; Naito et al. 2006). Other projects have found that precast, prestressed SCC girders may fail in shear slightly below comparison CC, but that SCC still exhibited adequate safety margins when compared to predicted capacity from existing design equations (Lachemi 2005; NCHRP 2009). It appears that SCC consistently performs well in full-scale shear members, but additional investigation is warranted given the brittle and unpredictable nature of shear failures.

**2.4.2 Aggregate Interlock** The shear resistance mechanism known as aggregate interlock is developed from the interlocking of aggregate particles on the two faces of a crack in a concrete member. In normal strength concrete, the weak link of the two phase concrete system of aggregate and paste is the interfacial transition zone between, thus, fracture usually develops in the paste, along the surface of the aggregate leaving a roughened crack surface (Walraven 1981). **Figure 2.4** shows the mechanism of aggregate interlock being activated by aggregates of maximum size,  $a$ , along a crack of width,  $\omega$ , and generating shearing and normal stresses of  $v_{ci}$  and  $f_{ci}$  respectively (Vecchio and Collins 1986).

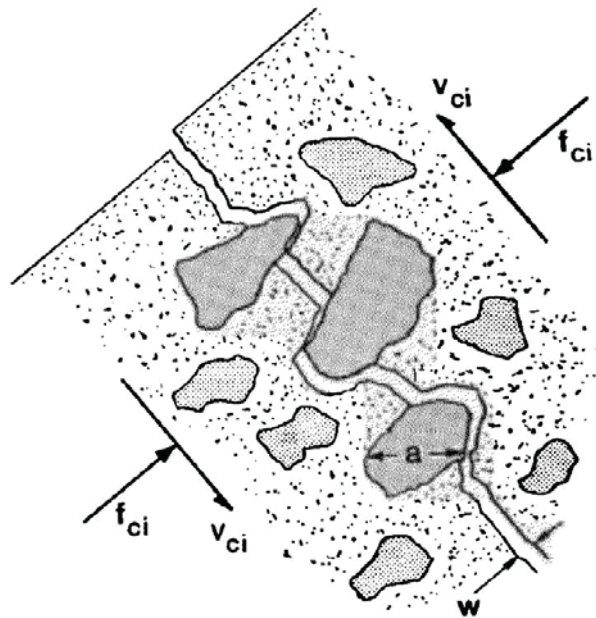


**Figure 2.4 – Aggregate Interlock** (Vecchio and Collins 1986)

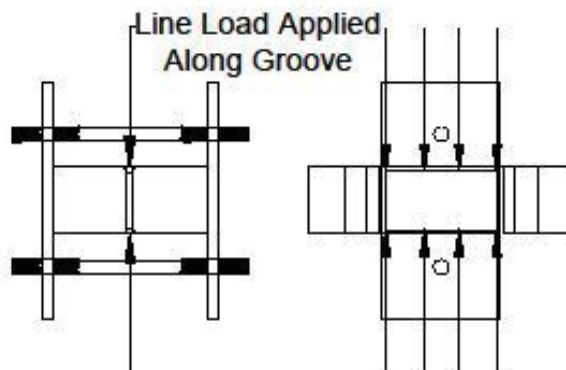
The theoretical aggregate interlock model proposed by Walraven and Reinhardt was confirmed by the push-off tests they performed which also enabled the derivation of the limiting value of  $v_{ci}$ . The model assumes that rigid spherical aggregate protruding from a flat crack interact with rigid, perfectly plastic paste. The aggregate of varying size, based on gradation, contact the deformable paste in a predictable way, this contact area can be computed in the crack opening and sliding directions. The aggregate sliding against the paste causes shearing and normal stresses caused by friction and plastic deformation, and crack dilation respectively (Walraven 1981). It is believed that high strength concrete with higher paste strength causes the crack plane to bisect a number of aggregate particles, effectively reducing aggregate interlock potential; this was confirmed by Walraven, who reported as much as a 65% reduction in aggregate interlock when

testing high strength concretes (Walraven and Stroband 1994). This theory helped to enhance the original compression field theory (CFT) proposed by Collins and Mitchell to form the modified compression field theory (MCFT) from Vecchio and Collins, and the later simplified modified compression field theory (simplified MCFT); that has since been adopted by specifying organizations such as the AASHTO LRFD Bridge Design Specifications and Canadian Standards Association.

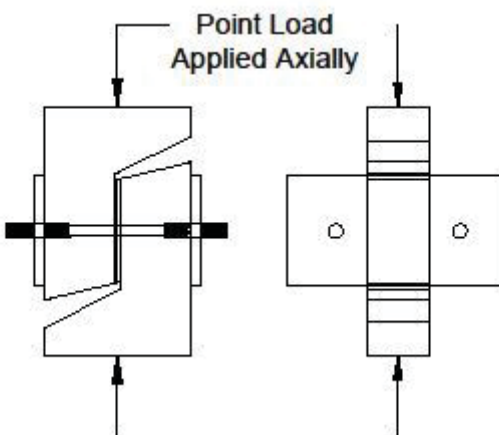
The early push-off testing performed by Walraven was done on normal strength concrete,  $f'_c = 2900 - 8200$  psi (20 – 57 MPa) with river gravel aggregate. The simplified MCFT limits the contribution of aggregate for high strength concrete by taking the aggregate size equal to zero (Wight and MacGregor 2009). A researcher has proposed modification to the current equations for high strength concrete to account for the reduced contribution of aggregate interlock, and for SCC mixtures (Kim 2008). It can be beneficial to investigate the applicability of new proposed equations for normal and high strength SCC for locally available materials.

**2.4.3 Push-off Test** The push-off test has been around in various forms since as early as 1969 (Mattock 1969) as far as this researcher could determine. The test has varied in size, instrumentation, reinforcement detail, and overall restraint. The general test specimen geometry and orientation used in this study can be seen in **Figure 2.5** below, but will be presented in more detail in section 6 below. The size and instrumentation has varied by all researchers, but generally information is collected about the applied load (both ultimate precrack load and the shearing push-off load throughout the test), normal force, and the crack opening and slipping response to load. Internal restraining bars (extending through the shear interface) as well as external restraint

systems, such as the one shown in **Figure 2.5** have been used (Albajar 2008; Barragan et al. 2006; Mattock et al. 1969; Mattock and Hawkins 1972; Walraven and Reinhardt 1981; Walraven and Stroband 1994).



(a) Precrack Test



(b) Push-off Test

**Figure 2.5 – Push-Off Test Geometry and Orientations**

The relationships of interest to this study that were developed by Walraven (1981) resulted from the externally restrained push-off specimen. The results from his investigation, and the analysis of Vecchio and Collins (1986) enabled the prediction of

the maximum shear stress acting on a given crack and formed the foundation of the MCFT.

**2.4.4 Shear Models** According to Walraven (1981), the aggregate sliding against the paste causes shearing and normal stresses from friction and crack dilation respectively; this behavior is developed in a predictable way as described by **Eq. 2.1 – 2.12**.

$$\sigma = \sigma_{pu} (\bar{A}_x - \mu \bar{A}_y) \quad (2.1a)$$

$$\tau = \sigma_{pu} (\bar{A}_y + \mu \bar{A}_x) \quad (2.1b)$$

where  $\sigma$  is stress normal to the direction of the crack,  $\tau$  is shear stress along the direction of the crack,  $\sigma_{pu}$  is the paste strength taken as **Eq. 2.2** by Walraven,  $\mu$  is a friction factor determined as 0.4 by Walraven's study,  $\bar{A}_x$  is the unit area of contact between the aggregate and paste in the x-direction (in the direction of crack slip), and  $\bar{A}_y$  is the unit area of contact between the aggregate and paste in the y-direction (in the direction of crack opening). Basically, the normal stress is reduced by friction resulting from dilation whereas shear stress resistance is enhanced by frictional action developed from crack slipping.

$$\sigma_{pu} = 56.7 f'_c{}^{.56} \text{ (psi)} \quad \text{or} \quad [\sigma_{pu} = 6.39 f'_c{}^{.56}] \text{ (MPa)} \quad (2.2)$$

The unit contact areas can be determined by **Eq. 2.3 – 2.6** which are the result of the full derivation performed by Walraven. It is shown that the contact area of the aggregate with the paste depends upon the crack width  $\omega$ , embedment depth,  $u$ , of the aggregate into the paste, aggregate size,  $a$ , the crack slip length,  $\delta$ , and the ratio of aggregate volume to total concrete volume,  $p_k$ .

$$A_y = \frac{D_{\max}}{\frac{\omega^2 + \delta^2}{\delta}} p_k \cdot \frac{4}{\pi} \cdot F\left(\frac{D}{D_{\max}}\right) \cdot G_1(\delta, \omega, D) \cdot dD \quad (2.3)$$

$$A_x = \frac{D_{\max}}{\frac{\omega^2 + \delta^2}{\delta}} p_k \cdot \frac{4}{\pi} \cdot F\left(\frac{D}{D_{\max}}\right) \cdot G_2(\delta, \omega, D) \cdot dD \quad (2.4)$$

**Eqs. 2.3 and 2.4** where the crack slip,  $\delta$ , is less than the crack opening,  $\omega$  ( $\delta < \omega$ ).

$$A_y = \frac{\omega^2 + \delta^2}{2\omega} p_k \cdot \frac{4}{\pi} \cdot F\left(\frac{D}{D_{\max}}\right) \cdot G_3(\delta, \omega, D) \cdot dD + \frac{D_{\max}}{\frac{\omega^2 + \delta^2}{\omega}} p_k \cdot \frac{4}{\pi} \cdot F\left(\frac{D}{D_{\max}}\right) \cdot G_1(\delta, \omega, D) \cdot dD \quad (2.5)$$

$$\begin{aligned}
A_x = & \frac{\varpi^2 + \delta^2}{2\varpi} \int_{\frac{\varpi^2 + \delta^2}{\varpi}}^{\varpi} p_k \cdot \frac{4}{\pi} \cdot F\left(\frac{D}{D_{\max}}\right) \cdot G_4(\delta, \varpi, D) \cdot dD \\
& + \frac{D_{\max}}{\varpi} \int_{\frac{\varpi^2 + \delta^2}{\varpi}}^{\varpi} p_k \cdot \frac{4}{\pi} \cdot F\left(\frac{D}{D_{\max}}\right) \cdot G_1(\delta, \varpi, D) \cdot dD
\end{aligned} \tag{2.6}$$

**Eqs. 2.5 and 2.6** where the crack slip,  $\delta$ , is more than the crack opening,  $\omega$  ( $\delta > \omega$ ). Where the variables  $G_1$ ,  $G_2$ ,  $G_3$ ,  $G_4$ , and  $F$  are given by **Eq. 2.7 – 2.11**. These variables consider the slip condition of the crack, variability in crack width, aggregate size fractions, and aggregate embedment conditions.

$$G_1(\delta, \varpi, D) = D^{-3} \left( \sqrt{D^2 - (\varpi^2 + \delta^2)} \frac{\delta}{\sqrt{\varpi^2 + \delta^2}} u_{\max} - \varpi \cdot u_{\max} - u_{\max}^2 \right) \tag{2.7}$$

$$\begin{aligned}
G_2(\delta, \varpi, D) = D^{-3} \left\{ \delta - \sqrt{D^2 - (\varpi^2 + \delta^2)} \frac{\varpi}{\sqrt{\varpi^2 + \delta^2}} u_{\max} + (u_{\max} + \varpi) \right. \\
\left. \sqrt{\frac{1}{4} D^2 - (\varpi + u_{\max})^2} - \varpi \sqrt{\frac{1}{4} D^2 - \varpi^2} + \frac{1}{4} D^2 \arcsin \frac{\varpi + u_{\max}}{\frac{1}{2} D} \right. \\
\left. - \frac{D^2}{4} \arcsin \frac{2\varpi}{D} \right\} dD
\end{aligned} \tag{2.8}$$

$$G_3(\delta, \varpi, D) = D^{-3} \left( \frac{1}{2} D - \varpi \right)^2 \tag{2.9}$$

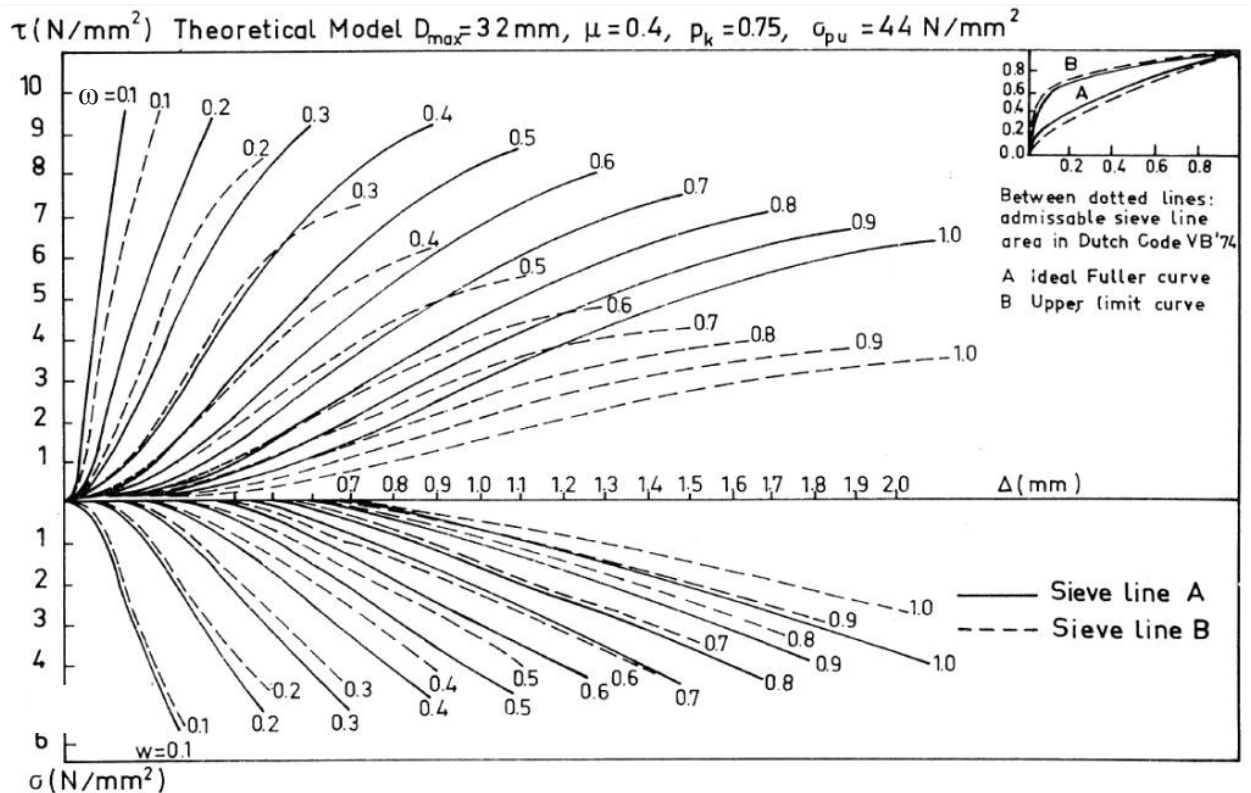
$$G_4(\delta, \varpi, D) = D^{-3} \left( \frac{\pi}{8} D^2 - \varpi \sqrt{\frac{1}{4} D^2 - \varpi^2} - \frac{D^2}{4} \arcsin \frac{2\varpi}{D} \right) \tag{2.10}$$

$$\begin{aligned}
F\left(\frac{D}{D_{\max}}\right) = & 0.532\left(\frac{D}{D_{\max}}\right)^{0.5} - 0.212\left(\frac{D}{D_{\max}}\right)^4 - 0.072\left(\frac{D}{D_{\max}}\right)^6 \\
& - 0.036\left(\frac{D}{D_{\max}}\right)^8 - 0.025\left(\frac{D}{D_{\max}}\right)^{10}
\end{aligned} \tag{2.11}$$

And where  $u_{\max}$ , the maximum aggregate embedment depth for which contact of the paste is still possible, is determined from **Eq. 2.12**.

$$u_{\max} = \frac{-\frac{1}{2}\varpi(\varpi^2 + \delta^2) + \frac{1}{2}\sqrt{\varpi^2(\varpi^2 + \delta^2)^2 - (\varpi^2 + \delta^2)\left\{(\varpi^2 + \delta^2)^2 - \delta^2 D^2\right\}}}{(\varpi^2 + \delta^2)} \tag{2.12}$$

All of these theoretical equations were confirmed from experimental tests performed by Walraven and Reinhardt (1981) where the results were fit to **Eq. 2.1** when setting  $\mu = 0.4$  and  $\sigma_{pu}$  to **Eq. 2.2**. Walraven then continued to demonstrate the effect of various material and aggregate characteristics such as friction factor, cyclic loading, the contribution from various aggregate fractions, maximum aggregate size, and aggregate gradation to evaluate the sensitivity of aggregate interlock to these variables. **Figure 2.6** shows the effect of aggregate gradation; the two gradations are for the same maximum size aggregate, but conform to the upper bound (smaller aggregate) and lower bound (larger aggregate) gradation limits as set by the Netherlands Code of Practice at the time of the evaluation (Walraven 1981).



The effect of the grading curve on the transfer of stresses in a crack for two comparable mixes, confirming to different grading curves ( $D_{max}=32$  mm,  $p_k=0.75$ ,  $\sigma_{pu}=44$  N/mm<sup>2</sup>,  $f_{cc} \approx 32$  N/mm<sup>2</sup>)

Conversion: 1 inch = 25.4 mm  
1 ksi = 6.89 MPa (N/mm<sup>2</sup>)

**Figure 2.6 – Effect of Gradation Variability (Walraven 1981)**

So, the investigation by Walraven and Reinhardt was very useful for understanding the mechanics of aggregate interlock and predicted the behavior closely. It was also made clear from Walraven's study that reducing the maximum aggregate size, reducing the amount of aggregate, or using a sandier gradation as in **Figure 2.6** all had similar effects, which was to reduce shear resistance. As has been discussed, all of these actions are taken either separately or together to achieve stable and robust SCC mixtures;

Walraven's model demonstrates the fundamental concern associated with aggregate interlock and overall shear behavior in SCC.

Vecchio and Collins were then interested in developing a shear model to explain member response to load, and did so in the form of the Modified Compression Field Theory (MCFT). The MCFT had assumptions and models of its own expanding on previous work from Collins and Mitchell to predict stress-strain interaction behavior while also deriving expressions from Walraven and Reinhardt's (1981) experimental work as they presented in **Figure 2.7** to determine **Eq. 2.13 and 2.14** (Vecchio and Collins 1986). The physical tests used to develop stress-strain theory behind the MCFT consisted of flat panels loaded in the x and y direction, at varying ratios. The focus of the panel study was to model concrete as an orthotropic material wherein equilibrium and compatibility are explained in terms of average stresses and strains. The panels were extensively studied in determining the response of cracked concrete to compression and tension, but little attention was given to crack shear behavior. Subsequent to the original panel study, another researcher has reviewed the data for crack shear behavior and determined that existing crack-slip models (such as that described by Walraven) correlate well with the panel data, even though the models were developed from drastically different test setups and mechanistic theories (Vecchio and Lai 2004). Further details of the MCFT will be presented in **Section 2.4.5** below because of the applicability to overall member behavior and the adaptation by specifications such as the AASHTO LRFD Bridge Design Specifications and Canadian Standard Association Design of Concrete Structures (CSA).

$$v_{ci} = 0.18v_{ci,max} + 1.64f_{ci} - 0.82 \frac{f_{ci}^2}{v_{ci}} \quad (2.13)$$

$$v_{ci,max} = \frac{12\sqrt{f'_c}}{.31 + 24\frac{\varpi}{a + .63}} \text{ (psi, in) } \text{ or } \left[ v_{ci,max} = \frac{\sqrt{f'_c}}{.31 + 24\frac{\varpi}{a + 16}} \right] \text{ (MPa, mm) } \quad (2.14)$$

where  $v_{ci}$  is the shear across the crack, limited by  $v_{ci,max}$ , the maximum shear a crack of width,  $\varpi$ , containing aggregate of maximum size,  $a$ , can resist. The compressive stress on the crack surface is  $f_{ci}$  and  $f'_c$  is concrete compressive strength.

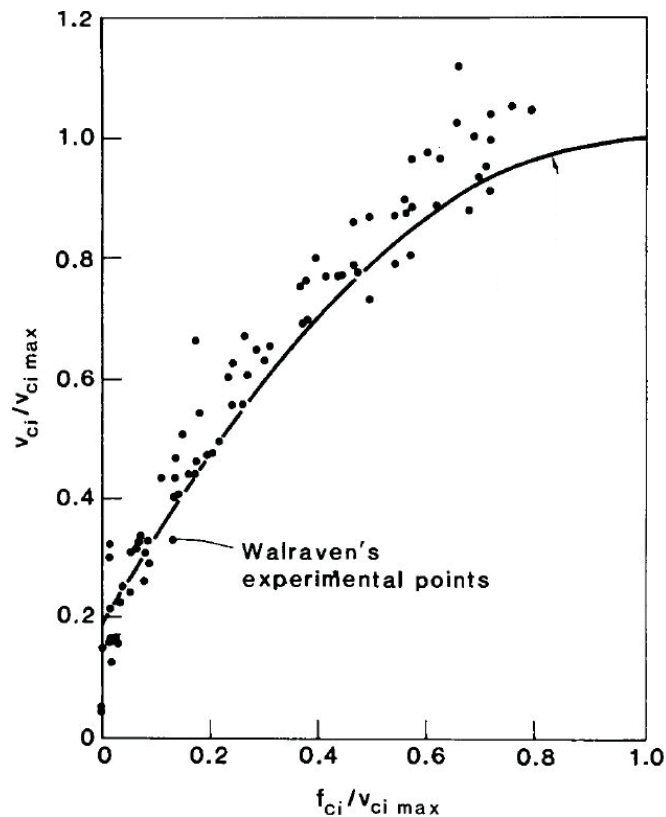


**Figure 2.7 – Determination of Expression for Shear Across Cracks, Equation 2.13**

(Vecchio and Collins 1986)

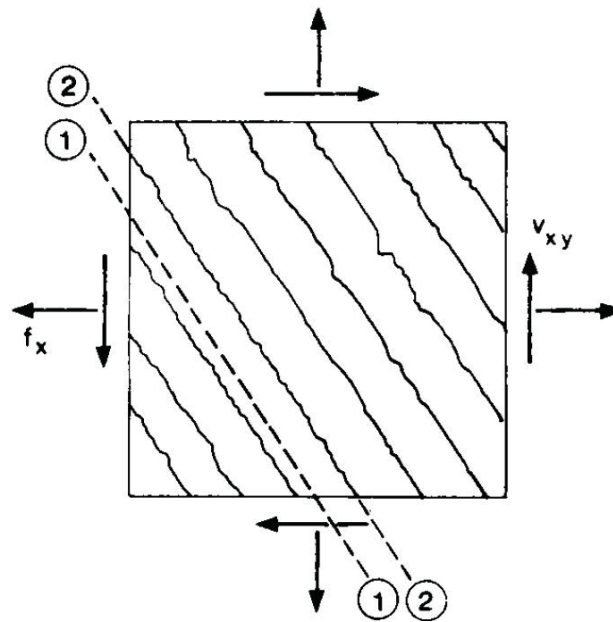
From the models discussed, it can be seen that maximum shear stress development can be predicted as a function of crack widths, aggregate size, and concrete compressive strength. Furthermore, shear can be influenced by normal stresses acting upon cracks as well. It is also worth noting that the most sophisticated models for expressing shear behavior in concrete are determined from both theoretical mechanics as well as empirical fitting of data. Given that the models are fitted for CC of normal strength concrete using river gravel aggregate, additional work with SCC of all strength levels and for high strength concrete in particular is still warranted. Even though researchers have reviewed the models for SCC over a range of strength levels, additional research is justified for SCC using locally available materials because of the increased volatility of SCC behavior with respect to material variability.

**2.4.5 Shear in Beams** To begin, a brief background on the MCFT assumptions and models is worth presenting to provide deeper understanding. Vecchio and Collins (1986) begin with a few simplifying assumptions:

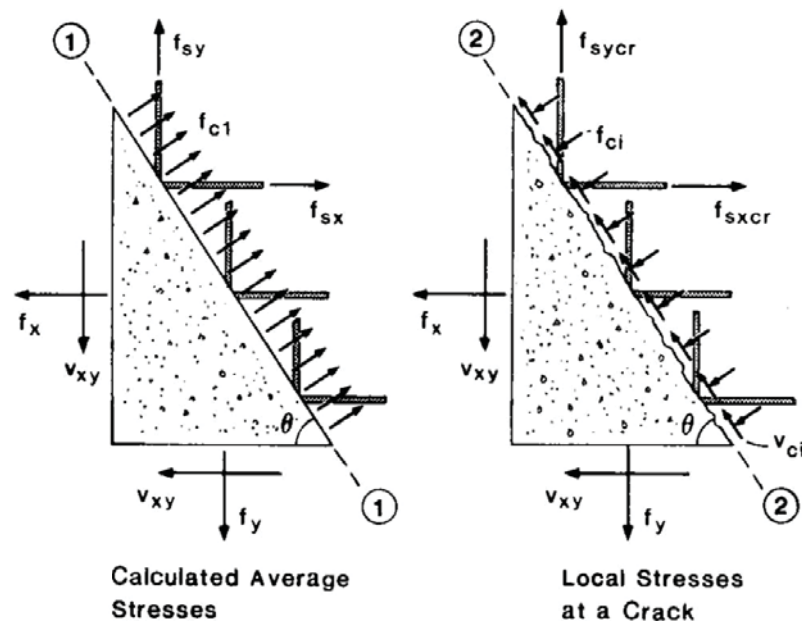
- For each strain state, there corresponds only one stress state
- Stresses and strains can be taken as average when taken over large enough lengths or areas to include several cracks
- There is no overall slip of the reinforcement within the test element
- The reinforcing bars are uniformly distributed

These assumptions are important in defining equilibrium conditions, compatibility equations, and enabling averaging or “smearing” of stresses and strains. Of note was the determination that stress and strain principal axis are roughly equal, meaning cracks

develop in directions orthogonal to principal tensile strains. One important result of the analysis is the understanding of stress transmission across cracks; **Figure 2.8** from Vecchio and Collins demonstrates this concept. The calculated average shear stress of plane 1 is zero, because it is a principle plane; however, there are actually local variations from the average and this is demonstrated at the cracked plane 2 where shear across the crack,  $v_{ci}$ , and the compressive stress on the crack,  $f_{ci}$  act. The evaluation of the local crack stresses has already been shown in **Eq. 2.13** (Vecchio and Collins 1986).



(a) Cracked concrete stress element



(b) Varying ways of viewing stress element

**Figure 2.8 – Distinguishing Average Versus Local Stresses in Cracked Members**

(Vecchio and Collins 1986)

Another important finding from the study was the understanding of cracked concrete response to compressive stress. The maximum compressive stress that concrete can withstand is reduced when the concrete is cracked, and is reduced further if a tensile stress acts orthogonal to the compressive stress. **Eq 2.15** was proposed to describe the diminishing compressive strength of concrete when exposed to increasing tensile stress (Vecchio and Collins 1981).

$$f_{c2} = f_{c2,\max} \left[ 2 \left( \frac{\varepsilon_2}{\varepsilon'_c} \right) - \left( \frac{\varepsilon_2}{\varepsilon'_c} \right)^2 \right] \quad (2.15a)$$

Where

$$\frac{f_{c2,max}}{f'_c} = \frac{1}{.8 - .34 \frac{\varepsilon_1}{\varepsilon'_c}} \leq 1.0 \quad (2.15b)$$

Where  $f_{c2}$  is the principal compressive stress in the concrete,  $\varepsilon_2$  is the principal compressive strain,  $\varepsilon_1$  is the coexisting principal tensile strain, and  $\varepsilon'_c$ , taken as negative, is the concrete strain at peak stress  $f'_c$ . This can explain a host of observed behavior such as reduced shear resistance in high moment regions where large tensile strains may exist, decreased and increased shear resistance with applied tensile and compressive loads respectively, as well as deep beam effects where strains are amplified by the depth of the member and overall shear resistance appears reduced (Sherwood et al. 2006; Vecchio and Collins 1986; Wight and MacGregor 2009). Their analysis formed the foundation of developing strain and size effect components to modern shear models.

Over time, the MCFT has evolved to include new research findings and has attempted to simplify the procedure for finding shear capacity. It has evolved such that shear capacity is computed per **Eq. 2.16 – 2.19** (AASHTO 2007; Sherwood et al. 2006).

$$V = V_c + V_s = 0.0316\beta\sqrt{f'_c}b_vd_v + \frac{A_vf_y}{s}d_v \cot \theta \quad (\text{ksi})$$

$$\left[ V = V_c + V_s = 0.083\beta\sqrt{f'_c}b_vd_v + \frac{A_vf_y}{s}d_v \cot \theta \right] \quad (\text{MPa}) \quad (2.16)$$

Where  $V_c$  and  $V_s$  are the shear contributions from the concrete and shear reinforcement respectively,  $b_v$  is the width of the web of the member,  $d_v$  is the shear depth of the

member,  $f'_c$  is the concrete compressive strength,  $A_v$  is the area of shear reinforcement over a stirrup spacing,  $s$ ,  $f_y$  is the shear reinforcement yield strength,  $\theta$  is the inclination of the crack, and  $\beta$  is the factor for tensile stress in the cracked concrete (AASHTO 2007). The coefficient would be 1 if using psi, and the metric equation then being one twelfth as in **Eq. 2.14**, so the concrete resistance to shear is derived from this equation. The  $\beta$  factor has been expressed by **Eq. 2.17**, slightly modified from the source to account for the way of expressing **Eq. 2.16**, and this closely approximates the values found in the look-up tables available in the AASHTO LRFD (Sherwood et al. 2006). The  $\beta$  factor is comprised of a strain effect term and a size effect term.

$$\beta = \frac{4.82}{(1+1500\varepsilon_x)} * \frac{51}{(39+s_{xe})} \text{ (in.)} \quad \left[ \beta = \frac{4.82}{(1+1500\varepsilon_x)} * \frac{1300}{(1000+s_{xe})} \right] \text{ (mm)} \quad (2.17)$$

Where  $\varepsilon_x$  is the mid-height strain of the member in the longitudinal direction and  $s_{xe}$  is the effective crack spacing parameter occurring at the mid-height of the member. The  $\varepsilon_x$  and  $s_{xe}$  terms are determined from member geometry and loading conditions and from the maximum aggregate size respectively. For the case of not providing adequate lateral reinforcement (as may be done for research to produce shear failures),  $\varepsilon_x$  can be expressed as **Eq. 2.18** and  $s_{xe}$  is always determined from **Eq. 2.19** (AASHTO 2007).

$$\varepsilon_x = \frac{\left( \frac{M_u}{d_v} + 0.5N_u + 0.5(V_u - V_p) \cot \theta - A_{ps}f_{po} \right)}{E_s A_s + E_p A_{ps}} \quad (2.18)$$

$$s_{xe} = \frac{1.38s_x}{a + 0.63} \leq 80 \text{ (in.)} \quad \left[ s_{xe} = \frac{35s_x}{a + 16} \leq 2000 \right] \text{ (mm)} \quad (2.19)$$

Where  $s_x$ , the crack spacing parameter, can be taken as  $d_v$ , as defined above, for beams with concentrated reinforcement in the bottom flange, but is defined differently for members with well distributed longitudinal reinforcement (AASHTO 2007). The form of **Eq. 2.19** should look familiar, as it was derived from the aggregate size effect portion of **Eq. 2.14**. These variables have also been proposed to be used to determine the other objective variable of  $\theta$  as in **Eq. 2.20**, but are found in look-up tables in practice (Sherwood et al. 2007).

$$\theta = (29 + 7000\varepsilon_x)(0.88 + \frac{s_{xe}}{100}) \text{ (in)} \quad \left[ \theta = (29 + 7000\varepsilon_x)(0.88 + \frac{s_{xe}}{2500}) \right] \text{ (mm)} \quad (2.20)$$

The simplifications of determining the objective functions of  $\beta$  and  $\theta$  are helpful for designers, and have been shown to accurately (on a level similar to the un-simplified MCFT) predict member response to loading. So again, the method for determining member shear failure is a blend of theoretical mechanics and empirical test data fitting. Members tested can be monitored to compare observed behavior next to the predictions of the model. SCC and CC batch proportions can be developed to ensure similar mechanical properties and then can be fabricated into members to be tested in shear. The shear behavior of SCC can be compared to that of CC and against the predictive models just described.

As mentioned previously, some researchers have found that SCC behaves similar to CC in shear, while others have found inferior performance of SCC; however, all that this researcher could find concluded that the predictive models were conservative for both SCC and CC. To begin, some of the more harsh conclusions will be presented. A national SCC study found that the two SCC girders tested had similar cracking shears when compared to the two CC girders tested; however, the SCC girders had inferior post-crack behavior with decreased ductility and lower failure loads, likely due to decreased aggregate interlock from C.A. replacement with binder. All tested girders exceeded 2007 AASHTO LRFD predicted nominal shear resistances (NCHRP 2009). Another researcher found very similar behavior; Lachemi found that the prestressed SCC and CC beams in his study showed similar pre-cracking behavior, but the SCC beams had diminishing post-cracking capacity and increased deflections; all beams were conservative by the 1994 CSA model (Lachemi et al. 2005). Other researchers provide more positive results for SCC beams tested in shear. In 2003, VDOT reported that prestressed SCC girders were tested and that shear behavior was “as predicted”, this researcher assumes that to mean relative to shear models used, presumably then modern AASHTO equations (FHWA 2005). Another concludes that prestressed SCC and CC beams exceed nominal strength in all failure modes including shear, that progression of damage was consistent from SCC to CC, and that SCC exhibited increased ductility over CC in all cases (Naito et al. 2006). A different researcher tested his prestressed members in flexure and bond. Upon member failure he measured values of crack opening and shear crack angle for input into the AASHTO LRFD model to predict shear failure loads if the prestressed beams were not constructed to be bond critical. He showed that the AASHTO LRFD

models were conservative overall, but especially for the concrete contribution to shear resistance, even for SCC mixtures (Kim 2008). The numerous researchers found to be investigating SCC seem to be finding the general consensus that SCC may have a slight reduction in shear capacity, but that SCC is still conservatively estimated by prediction equations.

## **2.5 SUMMARY**

SCC has been around for over twenty years, and engineers being an understandably conservative group have not yet written specifications for the widespread use of SCC in the U.S.; however, given the fiscal advantages of the advanced material, it appears to only be gaining in popularity. The rheological characteristics of SCC are well understood today. Fresh property tests have been developed and several have been standardized for testing the unique behavior of plastic SCC. Useful guidelines have been developed for establishing fresh property test result ranges based on the placement application, guidelines for establishing QC/QA testing programs have also been given (**Figures 2.1 and 2.2**). Hardened mechanical properties of SCC are at least partially established. Modulus of elasticity is consistently lower for SCC, but is still conservatively estimated by common models. Concrete compressive strength of SCC is often improved over a CC of a similar batch proportion, while tensile strength is similar. Research has shown SCC as well as high strength concrete to have a diminished shear resistance contribution from aggregate interlock, as demonstrated by studies focused around the push-off test.

Push-off tests can be a useful tool in determining the impact of several variables on the mechanism of aggregate interlock, as it is a small test that can be performed relatively easily and at low cost. Push-off test results have been incorporated into advanced shear models that not only describe shear friction, but also predict compatibility of stresses and strains, and equilibrium conditions. The modern shear models have been shown to accurately predict shear behavior over a wide variety of loading conditions and member geometries. Shear behavior of SCC prestressed beams and girders seems to be similar to CC; at worst, researchers consistently find that SCC shear resistance may be reduced, but is conservatively estimated by current models. Continued research should be undertaken to investigate more fully the variations of SCC and how they affect behavior. More experience with SCC can only lead to increased understanding, improved model fitting, and enhanced use of the benefits that SCC offers.

### 3. MIX DESIGN

#### 3.1 INTRODUCTION

This section describes the process by which the concrete batch proportions were selected to create four basic mixtures: a 6 ksi (41.4 MPa) 28 day target strength CC, a 6 ksi (41.4 MPa) 28 day target strength SCC, a 10 ksi (68.9 MPa) 28 day target strength HSC, and a 10 ksi (68.9 MPa) 28 day target strength HS-SCC. To distinguish between the HSC and HS-SCC, the reporting and naming convention of just CC and SCC were maintained. In this thesis, the difference between CC and SCC refers to the mixture constituents; whereas, the distinction of the target strength will differentiate the normal and high strength concrete batch proportions. The objective of the mix development process was to replicate as closely as possible the kinds of concrete mixtures that would be used by Missouri precast and ready mix concrete suppliers, and toward that end, a survey was created and distributed to numerous Missouri concrete suppliers. The batch proportions were then selected based on the survey results, along with guidance from the project liaison from the Missouri Department of Transportation (MoDOT). The two higher strength (10 ksi [68.9 MPa] 28 day target strength) mixtures were also refined using the knowledge, and previously published work, of the project's Principal Investigator who has worked extensively with high strength concrete (HSC) (Myers and Carrasquillo 1999). This method of mix development was less rigorous than a detailed investigation of several trial batches of varying batch proportions; however, the resultant mixtures should reflect the current state of practice in making SCC from Missouri concrete suppliers using locally available materials. Additionally, material data sheets can

be found for the chemical and mineral admixtures used throughout this investigation in **Appendix A** attached below.

### 3.2 SCC PRECAST PRODUCER SURVEY

A questionnaire was created and distributed to numerous parties so that the research team could have an understanding of the current state of practice regarding SCC use in the state of Missouri and elsewhere. The questionnaire was distributed through email, using online survey software. A Microsoft Word formatted version showing the specific questions asked on the survey can be found below in **Appendix B**. The survey was distributed to 27 Missouri ready mix concrete suppliers, 13 Missouri precast concrete suppliers, and 51 Department of Transportation (DOT) officials who are AASHTO members across the country. Participation in the survey was completely voluntary and contributors were assured that no proprietary mixture information would be disclosed from this investigation.

Unfortunately, no ready mix concrete suppliers replied to our solicitations. It is known from the personal experience of the project Principal Investigator that some ready mix producers in Missouri have made SCC, but it remains unknown to what extent or level of sophistication.

Positive results were gathered from the Missouri precast concrete suppliers; 6 out of 13 solicited precast suppliers replied with valuable responses, several even provided multiple mix designs in use at their facilities. **Table 3.1** details the compiled survey results from the precast suppliers. Due to confidentiality agreements, the actual mix designs from the survey responses cannot be shared. The low, high, and average for each

category are shown. The low and high columns represent the lowest and highest values for a given category and are not representative of a particular concrete batch proportion.

**Table 3.1 – Compiled Survey Results from Responding Precast Suppliers**

Respondent	Low	High	Average
Nominal Max. Agg. Size	1/2"	3/4"	5/8"
Reported Release Strength (psi)	3000	6000	4400
Reported Design Strength (28day unless noted, psi)	5000	10000	7400
Cement (pcy)	580	780	689
Add'l Cementitious Mt'l (pcy)	0	200	54
W/Cm ratio	.28	.46	0.37
Calculated Percent C.A. by weight of Agg. Portion (%)	.30	.53	.48
WR/HRWRA (oz/cy)	8	112	63
Retarder (oz/cy)	0	30	5
VMA (oz/cy)	0	23	3
Air Entrainment (oz/cy)	0	90	20

Indicates Omitted, Presumably Zero Data  
Indicates Calculated Data, not Directly Given

Conversions: 1 inch = 25.4 mm

1 lb/in<sup>2</sup> (psi) = 6.89 kPa

1 oz/yd<sup>3</sup> = 38.7 mL/m<sup>3</sup>

1 lb/yd<sup>3</sup> (pcy) = 0.59 kg/m<sup>3</sup>

Several observations were made from these survey results and key variables in the batch proportions used throughout this study were decided. The survey results were averaged, and the decisions made from these averaged values. Beginning at the top of the average column, the first item of interest is the nominal maximum aggregate size (NMS) of 5/8 inches (16mm), which lies between 1/2 - 3/4 inches (13 - 19 mm) or somewhere between MoDOT's Gradation D and Gradation E. Because some precasters use the larger Gradation D, and because ready mix suppliers would likely use the larger Gradation D,

aggregates used for this study conformed to the gradation requirements of MoDOT Gradation D and will be discussed in full detail in **Section 4.2** below. Next, the average reported design strength was 7400 psi (51.0 MPa) and is near the lower target strength of 6000 psi (41.4 MPa) indicating mixtures that would be of interest to this study. Next, the total average cementitious material of 744lb (337 kg) comprised of 689 lb (313 kg) cement plus 54 lb (24 kg) supplementary cementitious material was used. The average water to cementitious material ratio (W/CM) was calculated at 0.37. The last major point of interest was an average coarse aggregate to total aggregate weight ratio of about 0.48. The specific gravity of these materials is unknown, but typical aggregates have similar densities, so the coarse aggregate was expected to take up about 48% of the aggregate volume. Finally, the average mixture contained water reducers or high range water reducers and air entraining admixtures, but rarely used retarders or viscosity modifying admixtures. **Table 3.2** summarizes the important average variables from the survey below.

**Table 3.2 – Important Averages from Survey Results**

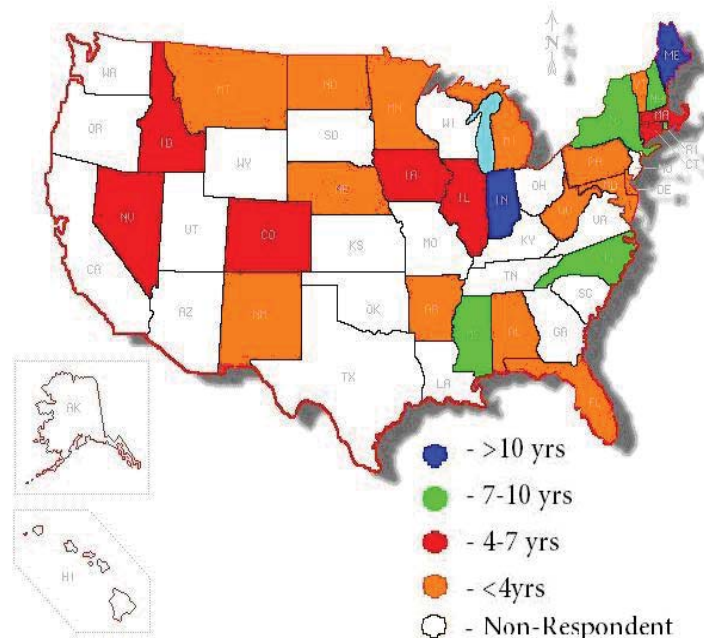
Nominal max. agg. size (inches)	5/8
Compressive strength (lb/in <sup>2</sup> )	7400
Cement (lb/yd <sup>3</sup> )	744
Water to cementitious material (W/CM)	0.37
Coarse aggregate volume fraction (%)	48

Conversion: 1 inch = 25.4 mm

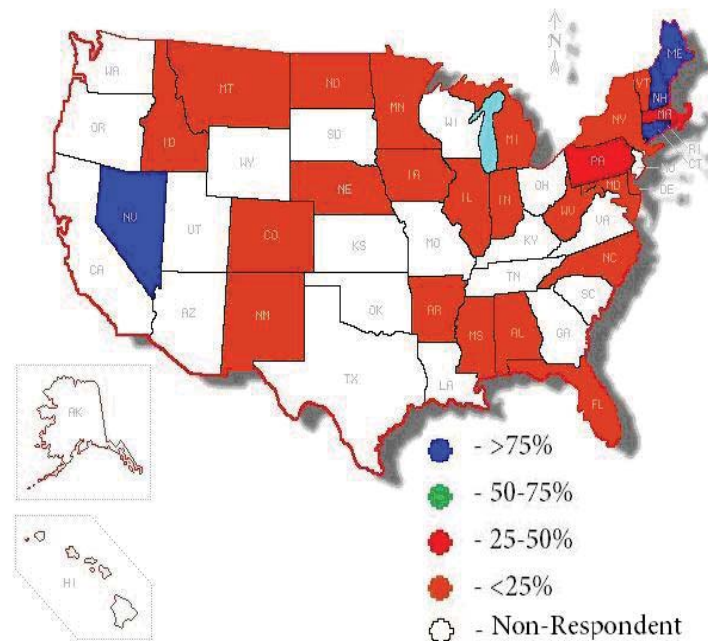
1 lb/in<sup>2</sup> = 6.89 kPa

1 lb/ yd<sup>3</sup> = 0.59 kg/m<sup>3</sup>

The national DOT survey also had good results with 29 replying out of the 51 petitioned. It should also be noted that the national survey participants were selected through the use of the January, 2011 AASHTO online member directory of the Standing Committee on Highways (SCOH) and the Subcommittee on Materials (SOM) by selecting one candidate from each state, with preference for voting members (AASHTO 2011). The purpose of the national survey was to assess the sense of familiarity that industrial leaders have with SCC, to evaluate the relative robustness of their understanding, discover trends, identify potential geographic “hot spots” where use is common, and to recognize where MoDOT’s knowledge base lies relative to others. **Figure 3.1** visually represents some of the insights gained from the national SCC survey using a color coded map from an online source (DIYMAPS 2011).



(a) Years of SCC Use



(b) Estimated Percent of Projects Using SCC

**Figure 3.1 – National DOT Survey Results**

From the responses shown in **Figure 3.1** one can easily see that the North East U.S. generally has more experience with SCC. It can also be seen that as states use SCC for longer periods of time, they generally have a higher percentage of their projects using SCC; this increased usage with time would reflect not only the fiscal advantages of using SCC, but also that positive results are being experienced. It should be noted that the longest reported experience with SCC was 16 years, only now verging on long enough field use durations to have experienced long term durability.

Along with the information conveyed in **Figure 3.1** other trends were identified from the survey responses. Most respondents clearly differentiated the use of SCC between ready mix and precast concrete suppliers; the trend was always a more advanced

knowledge, more common use, and longer use among precasters. SCC was used in all applications, not only aesthetic or low stress drainage structures; reportedly, the most common use for SCC is in structural beams and girders. Aggregates used for SCC seem to be as diverse as the local geology; river gravel and limestone is used approximately equally, and other materials such as granite, trap rock, and quartz are used to a lesser extent, as would be typical of conventional concrete. As was reflected in the precast survey responses, the most common nominal maximum aggregate size was 3/4 inches (19mm) with 1/2 inches (13mm) also being commonly reported. Unlike Missouri precasters, numerous responders reported mix designs used VMA's for stability; this also seemed to be more prevalent among more experienced DOT's.

### 3.3 MoDOT GUIDANCE AND SPECIFICATIONS

The MoDOT concrete materials expert liaison provided this investigation with the baseline batch proportions. The baseline batch proportions were determined by the liaison by examining submitted mix designs used for state projects where CC was used. The CC baseline mixture was expected to develop minimum 28 day strength of 6 ksi (41.4 MPa). The specified batch proportions can be seen in **Table 3.3**.

**Table 3.3 – 6 ksi (41.4 MPa) Target Strength CC Batch Proportions**

Class A-1 Concrete	
Cement (lb/yd <sup>3</sup> )	750
W/CM	0.37
Coarse aggregate volume fraction (%)	58
Design air content (%)	6.0

Conversion: 1 lb/ yd<sup>3</sup> = 0.59 kg/m<sup>3</sup>

Conveniently, the Missouri precast survey responses summarized in **Table 3.2** closely matched the baseline mixture given by MoDOT in **Table 3.3** in two important ways; the cement dosage and water to cement ratio were virtually the same. Because the survey results were so similar to the given MoDOT batch proportions, they were slightly adjusted to match those of **Table 3.3** except the coarse aggregate volume fraction was held down to the 48% resulting from the survey. The adopted 6 ksi (41.4 MPa) target strength SCC mixture is shown in **Table 3.4** below.

**Table 3.4 – 6 ksi (41.4 MPa) Target Strength SCC Batch Proportions**

Cement (lb/yd <sup>3</sup> )	750
W/CM	0.37
Coarse aggregate volume fraction (%)	48
Design air content (%)	6.0

Conversion: 1 lb/ yd<sup>3</sup> = 0.59 kg/m<sup>3</sup>

The next step was to develop the 10 ksi (68.9 MPa) target strength batch proportions. It was decided to increase cementitious material and reduce water to cementitious material ratio in order to increase the compressive strength. A decrease in the design air content to 3% was justified because higher strength concretes result in a disconnected capillary structure due to the lower w/cm ratios used and are therefore less vulnerable to freeze-thaw damage requiring less entrained air content (Myers and Carrasquillo 1999; Mindess 2003). Bridge girders are also inherently protected from critical saturation level to produce freeze-thaw by the deck system coverage. Maintaining the coarse to fine aggregate ratio was done to reflect the survey results and the batch

proportions given by MoDOT. The project Principle Investigator (PI) had worked extensively with high strength concrete throughout his dissertation and so trial batches were made from mixtures familiar to the PI that were used in actual field bridge projects, while maintaining the coarse to fine aggregate ratio, and while attempting to achieve desirable rheology. The resultant batch proportions are shown in **Table 3.5** below.

**Table 3.5 – 10 ksi (68.9MPa) Target Strength CC and SCC Batch Proportions**

	Conventional Concrete	Self-Consolidating Concrete
Cement (lb/yd <sup>3</sup> )	840	840
Class C Fly Ash (lb/yd <sup>3</sup> )	210	210
W/CM	0.30	0.30
Coarse aggregate volume fraction (%)	58	48
Design air content (%)	3.0	3.0

Conversion: 1 lb/ yd<sup>3</sup> = 0.59 kg/m<sup>3</sup>

Increasing the paste volume and using 20% ASTM class C fly ash helped to maintain workability with a water-to-cementitious material ratio as low as 0.30. Again, the fly ash mill certification can be found in **Appendix A** below.

### 3.4 SUMMARY

From reviewing **Tables 3.2 – 3.5** above for the four basic mixtures, the only difference in batch proportions from CC to SCC at each strength level (6 and 10 ksi [41.4 and 68.9 MPa]) is the coarse aggregate volume fraction, with the SCC having decreased amounts of coarse aggregate. **Table 3.6** summarizes the four basic mixtures. The

difference between the strength levels is the paste volume, water to cementitious material ratio, and the air content while maintaining the coarse aggregate volume fraction.

**Table 3.6 – Four Basic Mixtures to the SCC Project**

		Cement, lb	Fly Ash, lb	Water, lb	Fine Aggregate, lb	Coarse Aggregate, lb	MB-AE-90, oz (oz/cwt)	Glenium 7700, oz (oz/cwt)
6ksi	MoDOT A-1 (CC)	750	0	278	1166	1611	11.3 (1.5)	29.3 (3.9)
	SCC	750	0	278	1444	1333	11.3 (1.5)	46.5 (6.2)
10ksi	HSC (CC)	840	210	315	1043	1440	13.7 (1.3)	52.5 (5.0)
	HSC SCC	840	210	315	1291	1192	10.5 (1.0)	75.6 (7.2)

Notes: Aggregate weights based on SSD condition

Cement – Type III

Fly Ash – Class C

HRWRA – BASF Glenium 7700

AEA – BASF MB-AE-90

Conversion: 1 lb = 0.45 kg

1 oz = 29.6 mL

1 oz/cwt = 0.66 mL/kg

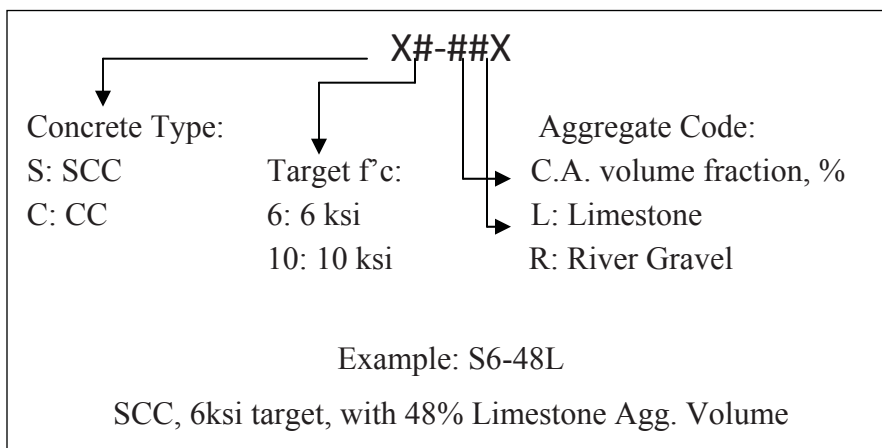
It was also necessary to develop additional SCC batch proportions for testing aggregate interlock. As discussed above, the precaster survey results were used to determine an average 6 ksi (41.4 MPa) SCC mixture for comparison to the 6 ksi (41.4 MPa) CC mixture given by MoDOT; the difference between the SCC and CC mixtures was the coarse aggregate volume fraction. Two additional SCC mixtures were determined from the precaster survey by taking the most outlying coarse aggregate data. The lowest two coarse aggregate volume fractions were most outlying in the data set and averaged to approximately 36%; this was the batch proportion used for the second SCC

mixture. Taking the difference between the baseline and most outlying SCC data, 48% - 36%, of 12% and creating a third SCC mixture equally outlying from the average made a mixture of  $48\% + 12\% = 60\%$ . The high coarse SCC was not reportedly used by any survey respondents, and is more indicative of conventional concrete proportions (58% C.A. was used for the CC mixture) and could be viewed as an upper bound to usable SCC batch proportions. The high coarse SCC can be useful in determining the role of C.A. in aggregate interlock as well as identifying if there is variance in behavior between two similar batch proportions just because one was CC and the other SCC. This was repeated for the 10 ksi (68.9 MPa) target high strength concrete. This entire matrix was then repeated again for a second common type of Missouri aggregate, river gravel. An additional batch proportion was tested from another study being conducted concurrently on the Missouri S&T campus. Lastly, a few additional 4 ksi (27.6 MPa) target strength batch proportions were developed toward the end of the study because all of the mixtures achieved higher than target strengths. A complete test matrix for the aggregate interlock test will be discussed further below and is shown in **Table 4.1**.

## 4. MATERIAL AND FRESH CONCRETE PROPERTIES

### 4.1 GENERAL

This section delineates the actions executed to carry out the material and fresh concrete properties testing for this research investigation. The tasks performed, the information gathered, and the associated testing standards with each task, if any, are reported. To begin with, **Figure 4.1** below defines the way in which the various mixtures were identified, with an example mixture shown. **Table 4.1** below represents a concise resource to see all the concrete batch proportions tested throughout this investigation.



Conversion: 1 ksi = 6.89 MPa

**Figure 4.1 – Designation Key**

**Table 4.1 – Concrete Batch Proportions Tested**

	C.A. Type	Concrete Type	C.A. Volume, %	Designation
4 ksi Target	Limestone	Conventional	58	C4-58L
		Self-Consolidating	36	S4-36L
		Self-Consolidating	60	S4-60L
9 ksi Target*	River Gravel (Pea Gravel)	Self-Consolidating	57	S9-57R
6 ksi Target	Limestone	Conventional	58	C6-58L
		Self-Consolidating	36	S6-36L
		Self-Consolidating	48	S6-48L
		Self-Consolidating	60	S6-60L
	River Gravel	Conventional	58	C6-58R
		Self-Consolidating	36	S6-36R
		Self-Consolidating	48	S6-48R
		Self-Consolidating	60	S6-60R
10 ksi Target	Limestone	Conventional	58	C10-58L
		Self-Consolidating	36	S10-36L
		Self-Consolidating	48	S10-48L
		Self-Consolidating	60	S10-60L
	River Gravel	Conventional	58	C10-58R
		Self-Consolidating	36	S10-36R
		Self-Consolidating	48	S10-48R
		Self-Consolidating	60	S10-60R

\* Actual field mix used in hybrid composite beam bridge field demonstrations project, bridge #B0439 Mountain Grove, MO

Conversion: 1 ksi = 6.89 MPa

The specific tests performed during this study are described. To begin, tests to characterize the materials being used were executed. Properties were then determined for freshly mixed concrete through testing. These actions prepared the investigator to then form hardened concrete specimens and enabled the characterization of the mechanical properties and shear behavior.

## 4.2 MATERIAL PROPERTIES

In order to develop concrete batch proportions that actually match the mix designs determined for use, several tests need to be performed on the materials to be used.

Specific gravity, absorption, and moisture content are all necessary to determine batch weights through the absolute volume method. Additionally, dry sieve gradation tests were also performed on the coarse aggregate samples.

Bulk specific gravity is the link between volume and weight and was tested for the coarse and fine aggregate. Absorption values are measured to determine the change in mass of an aggregate when free water is absorbed into the pore spaces; absorption was determined for the coarse and fine aggregates used. Both the limestone and river gravel coarse aggregates were tested in accordance with ASTM C 127 – 2007, Standard Test Method for Density, Relative Density (Specific Gravity), and Absorption of Coarse Aggregate (ASTM C 127 2007). The fine aggregate was tested in accordance with ASTM C 128 – 2007, Standard Test Method for Density, Relative Density (Specific Gravity), and Absorption of Fine Aggregate (ASTM C 128 2007). **Table 4.2** below summarizes the relative density and absorption values determined for the aggregates used.

**Table 4.2 – Bulk Specific Gravity (Oven Dry Basis) and Absorption of Aggregate**

	Bulk Specific Gravity (Oven-dry, unit-less)	Absorption (%)
Limestone	2.56	3.00
River Gravel	2.59	4.03
Sand	2.60	0.70

Just as absorption of the aggregate material is necessary in determining batch weights, so is moisture content. The total evaporable moisture content measures how much moisture is actually present on the aggregate and should be tracked and measured at the time of use. The total moisture may exceed the aggregate absorption value indicating a saturated aggregate with surface moisture, or total moisture may be below absorption indicating an unsaturated partially dry aggregate particle. Total moisture was determined so that an accurate amount of water could be added to a mixture such that the water to cement ratio was equal to that required of the mix design; total moisture was found by following ASTM C 566 – 2004, Standard Test Method for Total Evaporable Moisture Content of Aggregate by Drying (ASTM C 566 2004).

Next, it should be mentioned that aggregate gradation tests were also performed. Because previous researchers have found that the aggregate interlock mechanism of shear is dependent upon the coarse aggregate nominal maximum size (NMS) as well as gradation (Walraven 1981), it was necessary to find a river gravel and limestone with these properties in common. Additionally, the river gravel was collected and stored in 55 gallon (210 L) drums because of lack of available space to create a stock pile in the lab. Inherent in most methods of transporting aggregate, and the method used in particular, the potential for segregation is high. Gradation testing was performed to help monitor the gradation consistency, and make adjustments if necessary, for the samples used to produce specimens. **Figure 4.2** below shows the gradation curves for the limestone and river gravel coarse aggregates. Observe from **Figure 4.2** that the NMS for both aggregates was 3/4 inch (19mm) and that the relative percent passing for each sieve was fairly consistent between each aggregate type and for each river gravel test. We also

see from the figure that each of these aggregates consistently fall within the boundary lines corresponding to the MoDOT “Gradation D” and ASTM “#67”. The ASTM #67 gradation as well as the procedure performed to sieve the aggregate is found within ASTM C 136 – 2006, Standard Test Method for Sieve Analysis of Fine and Coarse Aggregates (ASTM C 136 2006). Furthermore, coarse aggregates conforming to Gradation D is to be used in structural concrete according to MoDOT (MoDOT 2012).

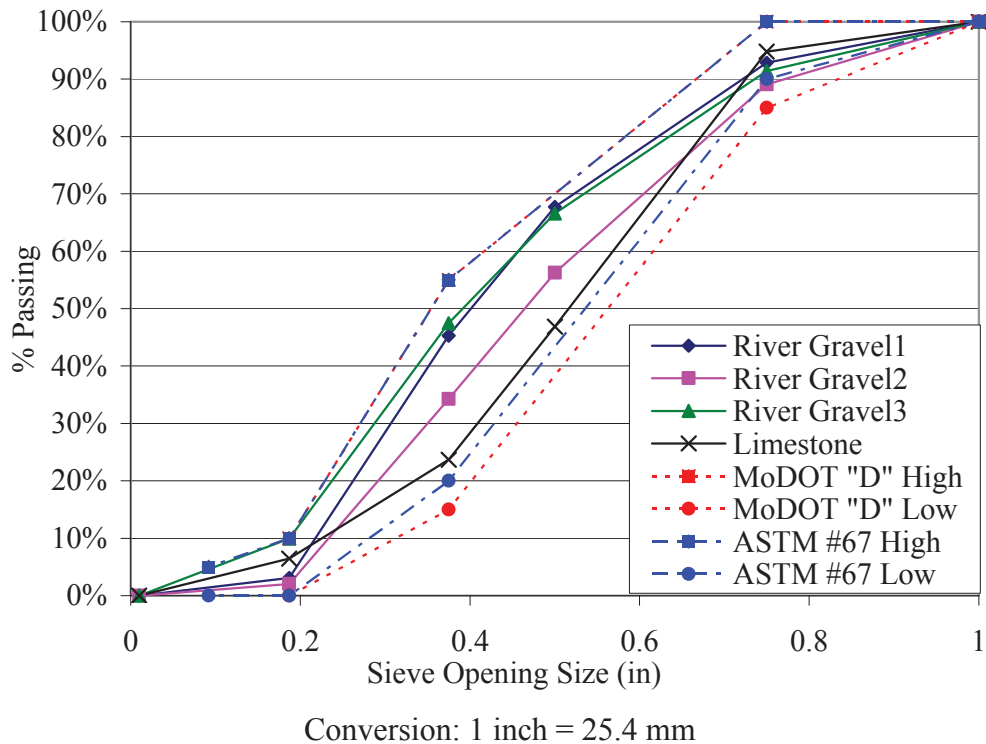


**Figure 4.2 – Coarse Aggregate Sieve Analysis**

All of the collected material parameters were gathered, and consistently tracked over time for variables that may change such as moisture content. The material properties were paired with the batch proportions determined for use in each of the mix designs. A spreadsheet was used to determine the appropriate material batch weights, based on the material absolute volumes. A sample of the batch weight spreadsheet can be found in

**Appendix C** below, along with the spreadsheets used to collect the appropriate fresh concrete properties.

### 4.3 FRESH PROPERTIES

All laboratory mixtures were tested for the same fresh properties, with field mixtures being tested for only part of the test regimen. SCC laboratory mixtures were tested to measure passing ability, consistency and filling ability, stability, unit weight, and air content. SCC field mixtures only measured filling ability, unit weight, and air content. All CC mixtures were measured for consistency (slump), unit weight, and air content. **Figure 4.3** below shows the 6ft<sup>3</sup> (0.17 m<sup>3</sup>) mixer used for all laboratory batching.



**Figure 4.3 – 6 Cubic Foot Mixing Drum**

The slump flow test was used to assess consistency and filling ability of all SCC mixtures following ASTM C 1611 – 2009, Standard Test Method for Slump Flow of Self-Consolidating Concrete (ASTM C 1611 2009). The metrics of slump flow,  $T_{50}$

(Sometimes  $T_{20}$  as in 20 inches rather than 50 centimeters), and VSI are all measured using ASTM C 1611 – 2009. Slump flow is the average of the maximum and perpendicular diameters of the concrete disc resulting from a slump cone being filled with SCC and then lifted; this researcher used the inverted slump cone procedure.  $T_{50}$  is the time required for the slump flow concrete disc to grow to 50 cm (Sometimes called  $T_{20}$  for 20 inches) in the largest diametrical dimension, and indicates viscosity. Finally VSI, or Visual Stability Index, is a subjective visual indication of the stability of the resultant slump flow disc represented as a number from 0-3. A VSI of 0 indicates a stable SCC and 3 is unstable, as evident by a concentration of coarse aggregate in the center of the disc, and a mortar halo around the perimeter of the disc. Guidance is given in the ASTM C 1611 – 2009 document for determining VSI. **Figure 4.4(a) – Figure 4.4(c)** below shows the slump flow test.



(a) Place SCC into inverted slump cone



(b) Lift cone and allow SCC to flow (slump flow of 23.5 inches [595 mm] pictured)



(c) Close-up for Determining VSI (VSI=1; No Mortar Halo, but Surface Sheen)

#### **Figure 4.4 – Slump Flow Test**

Passing ability was evaluated using two test methods. The non-standard, but widely known, “L-box” test was performed, along with the standardized “J-Ring” in the form of ASTM C 1621 – 2009, Standard Test Method for Passing Ability of Self-Consolidating Concrete by J-Ring (ASTM C 1621 2009). The J-ring test is essentially the slump-flow test, with a ring of vertical bars surrounding the inverted slump cone prior to

lifting. The maximum and perpendicular diameters of the concrete disc are averaged, and compared to the slump flow average diameter; passing ability is then determined from the magnitude of the difference. Guidance is given by Table 1 in ASTM C 1621 – 2009 for evaluating passing ability by use of blocking assessment. The L-box test also measures passing ability, but using a different setup. To view the J-ring and L-box setup, see **Figure 4.5** below. The L-box consists of a bottom trough with a vertical box attached, creating an L shape. The vertical box is gated at the bottom, with vertical bars beyond the gate. The vertical box is filled, the gate opened, and the SCC is allowed to flow through the bars and down the trough. The depth of SCC at the end of the trough is measured and divided by the depth of the SCC at the gate; this ratio of depth is used as the parameter to assess passing ability. An L-box test result of 0.85-1.00 can generally be regarded as having adequate passing ability.



**Figure 4.5 – J-ring (left) (J-ring of 22.5 inches [570 mm] pictured) and L-box (Right)**

Next, stability for the laboratory SCC mixture was measured using ASTM C 1610 – 2010, Standard Test Method for Static Segregation of Self-Consolidating Concrete

Using Column Technique (ASTM C 1610 2010). In **Figure 4.6** below, you see the 26 inch (660 mm) tall column used in the segregation column test. The column is filled with SCC and allowed to sit, undisturbed for 15 minutes. The top and bottom fourths are then retained and washed over a #4 (4.75mm) sieve. This researcher then oven-dried the resulting aggregate and performed the calculations prescribed in ASTM C 1610 – 2010 to determine the static segregation of the SCC mixtures, this indicates stability of the mixture.



**Figure 4.6 – Segregation Column**

For all concrete mixtures, except one set of field specimens, the unit weight was determined as in ASTM C 138 – 2010, Standard Test Method for Density (Unit Weight), Yield, and Air Content (Gravimetric) of Concrete (ASTM C 138 2010). The container used to measure unit weight was the base used in measuring air content by the pressure method; **Figure 4.7** below shows the pressure meter and base. For all concrete mixtures,

the air content was measured per the procedure in ASTM C 231 – 2010, Standard Test Method for Air Content of Freshly Mixed Concrete by the Pressure Method (ASTM C 231 2010). Because this standard is for conventional concrete, this researcher should note that no tamping or striking with a mallet was performed for the SCC mixtures during placement into the test apparatus; only the final strike with a mallet while releasing the pressure valve was performed to obtain an accurate reading from the pressure meter.



**Figure 4.7 – Pressure Meter and Base Used for Unit Weight and Air Content**

Lastly for the fresh property tests, for CC mixtures, slump was used to measure consistency and was performed in accordance with ASTM C 143 – 2010, Standard Test Method for Slump of Hydraulic-Cement Concrete (ASTM C 143 2010).

Manual consolidation through tamping was performed for CC mixtures when placing. All specimens were covered for approximately 1 day with plastic sheeting and then transported to a moist cure room. Placement and curing was performed to a standard consistent with ASTM C 192 – 2007, Standard Practice for Making and Curing Concrete

Test Specimens in the Laboratory (ASTM C 192 2007). It should again be noted that SCC mixtures were not manually consolidated, only placed and allowed to self-consolidate.

The fresh concrete properties were measured throughout the execution of this investigation, and therefore will be reported. **Tables 4.3** and **Table 4.4** below concisely organize the experimental program for fresh properties, and their results. The test results were gathered in this study for acceptance of concrete for forming mechanical and shear test specimens; therefore, the results are shown without a thorough analysis.

**Table 4.3 – Fresh Property Tests and Results for Limestone Mixtures**

Name	ASTM (if standard) test method and test description							
	C143 Slump (in)	C138 Unit Weight (lb/ft <sup>3</sup> )	C231 Air Content (%)	C1610 Segregation (%)	C1611 Slump Flow (in)	VSI	C1621 J-Ring (in)	L-box (in/in)
C4-58L	6.5	145.6	5.3	---	---	---	---	---
S4-36L	---	139.2	8.5	---	24.5	1	23.5	---
S4-60L	---	138.8	6.9	---	22.5	1	19.5	---
C6-58L	8.5	144.7	5.5	---	---	---	---	---
S6-36L	---	142.7	7.0	3.5	21.0	0	20	.43
S6-48L	---	139.6	7.3	12.3	25.5	1	25.0	.66
S6-60L	---	144.9	5.0	4.0	26	1	25.5	0
C10-58L	9	148.4	2.8	---	---	---	---	---
S10-36L	---	143.5	3.4	101.7	29	3	30	.96
S10-48L	---	146.4	2.2	31.2	28.5	2	28.5	.94
S10-60L	---	150.0	1.6	**	28.5	1	28	.67
S6-36L*	---	145.6	4.4	---	28.5	1	27	---
S6-60L*	---	143.2	1.6	---	29	2	28.5	---

\* Indicates replicate batch, for supplementing shear test information for bad test results.

\*\* Indicates lost specimen from failure of the segregation column from leaking

Conversion: 1 inch = 25.4 mm

1 lb/ ft<sup>3</sup> = 16.02 kg/m<sup>3</sup>

**Table 4.4 – Fresh Property Tests and Results for River Gravel Mixtures**

Name	ASTM (if standard) test method and test description							
	C143 Slump in	C138 Unit Weight lb/ft <sup>3</sup>	C231 Air Content %	C1610 Segregation %	C1611 Slump Flow in	VSI	C1621 J-Ring in	L-box in/in
C6-58R	6.5	145.5	3.3	---	---	---	---	---
S6-36R	---	141.3	6.5	5.1	25	1	24	.87
S6-48R	---	143.9	3.0	10.4	27	1	26.5	0
S6-60R	---	141.5	5.8	1.6	22.5	1	21.5	0
C10-58R	2	145.6	2.6	---	---	---	---	---
S10-36R	---	144.3	3.0	1.0	29	0	29	.96
S10-48R	---	143.9	2	1.6	27.5	1	27.5	.95
S10-60R	---	145.9	1.5	5.5	27.5	1	26	.82
S9-57R	---	---	2.8	---	27.5	---	---	---

Conversion: 1 inch = 25.4 mm  
1 lb/ ft<sup>3</sup> = 16.02 kg/m<sup>3</sup>

The acceptance criteria for shear testing were broad. With the batch proportions used, the slump of the concrete was approximately 0 to 0.5 inches (0 to 13 mm) before the addition of HRWRA, and the final slump or slump flow was achieved almost entirely through HRWRA addition. While batch proportions were established through surveys and not through trial batches, large fresh property variation was experienced; however, the fresh properties do not affect shear behavior and the large variation is of little concern for this investigation. For the baseline concrete mixtures also used by researchers investigating shrinkage, creep, and durability, additional trial batching was conducted and tighter tolerances were enforced. Overall, the SCC fresh concrete mixtures used exhibited high filling ability with moderate passing ability and therefore moderate filling capacity.

## 5. HARDENED PROPERTIES

### 5.1 INTRODUCTION

Tests were conducted to investigate the hardened concrete mechanical properties of modulus of elasticity (MOE,  $E_c$ ), unconfined compressive strength ( $f'_c$ ), and splitting tensile strength (STS,  $f_{sp}$ ). The tested properties will impact concrete behavior and are therefore important for analyzing companion shear specimens discussed later. These hardened properties were tested for all concrete batch proportions, but not necessarily at all test ages. **Table 5.1** shows the tests performed at various ages of the specimens; there was some variation from **Table 5.1** due to scheduling, particularly for the specimens formed while at Coreslab Structures, Inc. in Marshall, MO.

**Table 5.1 – Target Test Ages for Hardened Properties**

Specimen Age	Compressive Strength	Modulus of Elasticity	Splitting Tensile Stress
1 day	X	---	---
7 day	X	---	---
28 day	X	---	---
56 day*	X	X	X

\* Some specimens were not tested through the full 56 day period, only through 28 days. These would have MOE and STS results at 28 days.

Concrete compressive strength,  $f'_c$ , is used extensively when working with concrete. Numerous models that describe behavior, from those as rudimentary as empirical relationships to the most complex of theories, use concrete compressive strength as a key variable. There are even models correlating concrete compressive

strength to other design variables like those investigated in this study of MOE and STS. Modulus of Elasticity (MOE) is a measure of a material's elastic deformation under load. MOE is used in calculations such as deformations, deflections, and in determining the stiffness of members.

Of interest to this study is also the splitting tensile strength (STS). The STS is an indirect measure of the tensile strength of the concrete. The concept is that a cross-section of a concrete cylinder, when loaded in compression on one diameter, acts as a principally loaded stress element. The loaded concrete cross section results in principal tensile stresses being produced in the perpendicular diameter, which causes cracking when the stress exceed the tensile strength of the concrete. **Figure 5.1** below shows the concept behind the STS test as well as the theoretical stress distribution developed in the cross section of the specimen. The theoretical maximum tensile stress is  $2P/\pi LD$ , where P is the applied compressive load, L the cylinder length, and D the cylinder diameter (Mindess 2003).

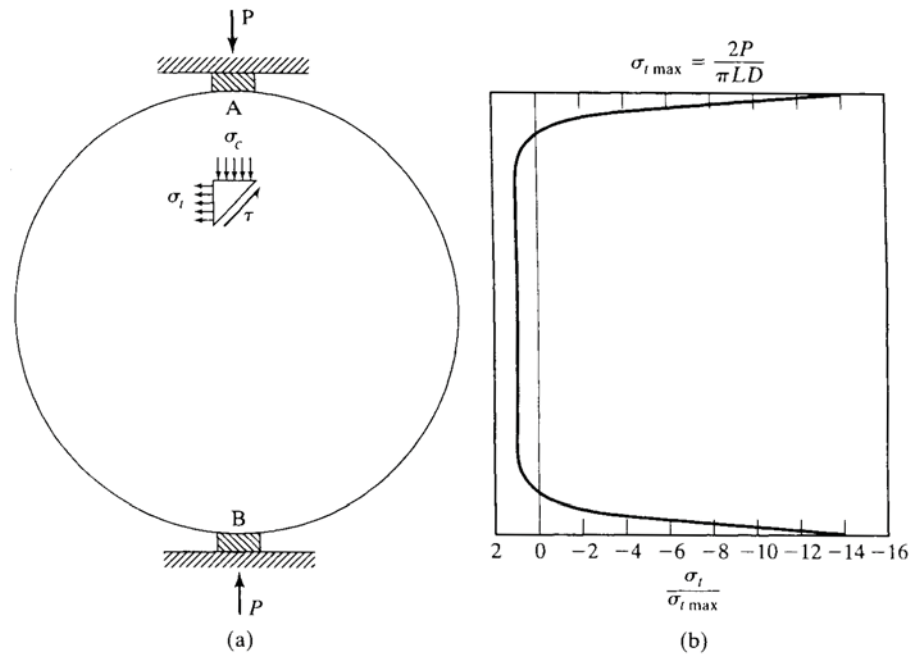


**Figure 5.1 – STS Diagram** (Mindess 2003)

From the figure, it is seen that the majority of the cross-section is loaded in uniform tension; when this tensile stress exceeds the tensile strength of the concrete, the specimen will fail and split along the vertical diameter.

## 5.2 TEST SETUP AND PROCEDURE

With the understanding that concrete compressive strength is an important variable to determine, we must test it accurately, with repeatability. ASTM C 1231 – 2010, Standard Practice for Use of Unbonded Caps in Determination of Compressive Strength of Concrete Cylinders, was used for determining concrete compressive strength (ASTM C 1231 2010). While ASTM C 1231 2010 requires qualification testing for use of neoprene pads with concrete equal to or greater than 12 ksi (82.7 MPa), this action was

not performed. Each specimen was tested on a 600,000 lb (2670 kN.) capacity Forney compression machine until failure. **Figure 5.2** below shows the execution and resultant failure of an unconfined compressive strength test.

MOE was determined using ASTM C 469 – 2010, Standard Test Method for Static Modulus of Elasticity and Poisson's Ratio of Concrete in Compression (ASTM C 469 2010). Several modifications to the standard were made:

- The load was removed abruptly, not at the same rate of loading
- The concrete compressive strengths and MOE were not measured on the same loading
- Companion specimens to determine compressive strength were not used prior to MOE testing, only 1 specimen, then subsequent MOE specimens

To clarify the last deviation, ASTM C 469 2010 requires a set of companion cylinders be used to determine compressive strength such that the 40% stress level can be used for MOE specimen loading; this researcher performed 1 strength test, using the determined value as the compressive strength for the first MOE test. The first MOE specimen was subsequently loaded to failure to make a second determination of compressive strength, which was averaged with the first specimen, and provided the 40% stress level for the second MOE test, and so on. **Figure 5.2** below also shows the MOE test being performed on a cylinder that will then be stressed to failure for testing of compressive strength,  $f'_c$ .



(a) Modulus of elasticity (MOE) test and gage



The same specimen is used for compressive strength:

(b) During test

(c) Test specimen after failure

**Figure 5.2 – MOE and Compressive Strength Test**

The STS investigation followed ASTM C 496 – 2011, Standard Test Method for Splitting Tensile Strength of Cylindrical Concrete Specimens (ASTM C 496 2011). Two modifications to the standard test procedure were made. The specification calls for

supplementary bearing bars when the test specimen exceeds the length of the loading machine's bearing plate, of a thickness equal to the excess length of the specimen. The large thickness of the supplementary bearing bar is intended to ensure uniform loading along the entire length of the specimen. In this study, the excess length of the specimen was about 2 inches (51 mm), while the supplementary bearing bar was only about 1 inch (25 mm) thick, resulting in a modification to the standard test. A small percentage of specimens fractured laterally (through the diameter), directly under the bearing plate, indicating that perhaps the supplementary bearing bar was not thick enough; however, this mode of failure was noted for these specimens. The next modification is in regard to the specified plywood bearing strips. The standard prohibits reuse of plywood bearing strips; however, this researcher used small strips of more durable particle board and continued reuse until imperfections were detected. See **Figure 5.3** for a picture of a STS specimen being tested.



**Figure 5.3 – Splitting Tensile Strength (STS) Test**

### 5.3 TEST RESULTS

The results from the compressive strength, MOE, and STS tests are presented in **Tables 5.2 – 5.6** below. The values listed in the tables are the average of individual test results.

**Table 5.2 – Compressive Strength Test Results for Limestone Mixtures**

Designation	Compressive Strength, $f'_c$ (psi)			
	1 day	7 day	28 day	56 day
C4-58L	2560	5290	6130	---
S4-36L	2790	4910	5850	---
S4-60L	1870	4150	4900	---
C6-58L	4450	6190	7600	---
S6-36L	5530	7350	9460	---
S6-48L	4270	6390	8140	8410
S6-60L	5240	7530	9400	---
C10-58L	5330	8690	10,820	11,210
S10-36L	6390	10,780	13,010	12,580
S10-48L	7380	11,100	13,450	13,740
S10-60L	6850	11,330	13,450	13,880
S6-36L*	6550	9450	10,770	---
S6-60L*	5770	9840	11,050	---

\* Indicates replicate batch, for replacing poor shear test information

Conversion: 1000 psi = 6.89 MPa

**Table 5.3 – Compressive Strength Test Results for River Gravel Mixtures**

Designation	Compressive Strength, $f'_c$ (psi)			
	1 day	7 day	28 day	56 day
C6-58R	6990	10,050	10,180	10,750
S6-36R	6150	9270	10,070	10,640
S6-48R	6410	9860	10,380	10,530
S6-60R	5550	7770	8440	8710
C10-58R	5630	8120	9450	---
S10-36R	8360	12,210	13,940	14,510
S10-48R	7970	12,030	13,650	14,420
S10-60R	7680	11,320	13,570	13,920
*S9-57R	3440	6630	8410	9190

\* Supplementary mixture from another research project on MS&T campus

Conversion: 1000 psi = 6.89 MPa

**Table 5.4 – Compressive Strength Test Results for Coreslab Specimens**

Designation	Compressive Strength, $f'_c$ (psi)				
	1 day	4 day	8 day	14 day	28 day
C6-58L	4810	5110	5620	5630	5730
S6-48L	5660	5840	6690	6910	6950
C10-58L	5670	7890	7950	8360	8480
S10-48L	6330	8300	8600	9100	9250

Conversion: 1000 psi = 6.89 MPa

**Table 5.5 –MOE, STS, and Coefficients Test Results for Limestone Mixtures**

Designation	(psi)		Unit-less Coefficient	
	MOE	STS	MOE	STS
C4-58L	3,837,000	385	54,800	5.5
S4-36L	3,683,000	445	53,600	6.5
S4-60L	3,141,000	380	49,800	6.0
C6-58L	4,614,000	370	52,900	4.3
S6-36L	5,111,000	565	52,600	5.8
S6-48L	4,435,000	460	48,400	5.1
S6-60L	4,855,000	520	50,100	5.4
C10-58L	5,243,000	550	49,500	5.2
S10-36L	5,880,000	580	52,400	5.2
S10-48L	6,046,000	760	51,600	6.5
S10-60L	5,586,000	800	47,400	6.8
S6-36L*	5,188,000	575	54,000	6.1
S6-60L*	5,020,000	570	51,700	5.9

\* Indicates replicate batch, for supplementing shear test information for bad test results.

Conversion: 1000 psi = 6.89 MPa

**Table 5.6 –MOE, STS, and Coefficients Test Results for River Gravel Mixtures**

Designation	(psi)		Unit-less Coefficient	
	MOE	STS	MOE	STS
C6-58R	5,892,000	680	56,800	6.6
S6-36R	5,602,000	725	54,300	7.0
S6-48R	5,812,000	690	56,600	6.7
S6-60R	4,845,000	580	51,900	6.2
C10-58R	5,349,000	550	55,000	5.6
S10-36R	6,767,000	790	56,200	6.5
S10-48R	6,515,000	730	54,300	6.1
S10-60R	6,338,000	745	53,700	6.3
S9-57R	5,009,000	680	52,300	7.1

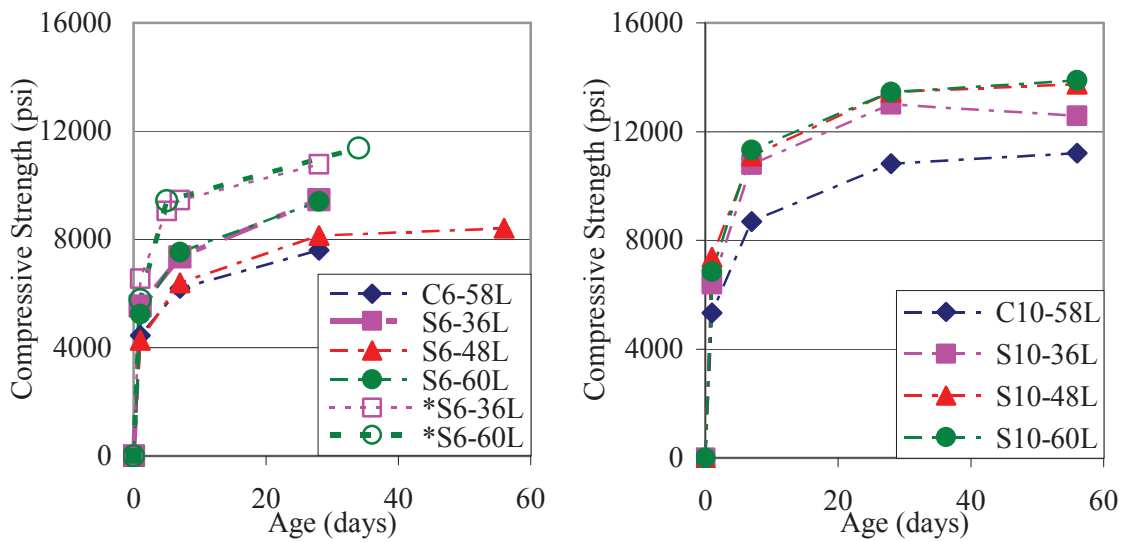
Conversion: 1000 psi = 6.89 MPa

The initial test program intended to test strength only through 28 days and conducting MOE, STS, and the shear tests of precracking and push-off at the “Ultimate” age of 28 days. Some issues arose when performing the shear tests on the first mixtures to reach 28 days, so subsequently cast mixtures were allowed to continue curing through 56 days while the issues were resolved. The shear test results on the mixtures where the issues were noticed were thrown out, and re-batching was conducted to generate new specimens; these subsequent specimens were only cured for 28 days. The testing of shear properties at 28 days as compared to 56 days was not considered to be an issue. Concrete is sufficiently mature, especially concrete made with type III cement, within 28 days, that additional curing to 56 days does not significantly alter the concrete micro structure or pore water distribution.

The following section discusses in more depth the results presented above. Conclusions are presented regarding the hardened concrete properties and why they are important to this study.

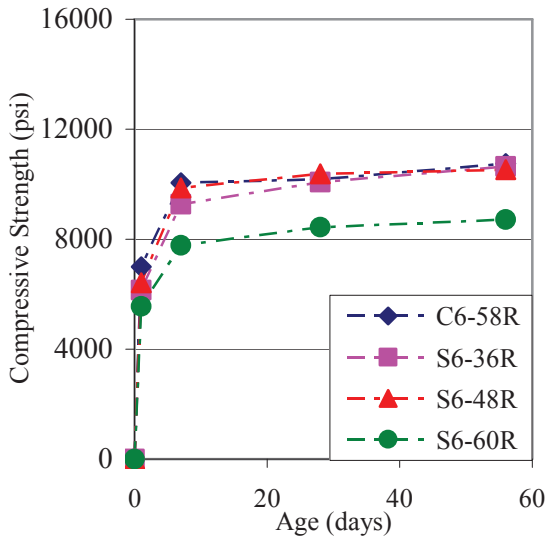
### 5.4 DATA ANALYSIS AND CONCLUSIONS

The results from above are compiled and presented visually in **Figures 5.4 – 5.8**. The strength development of the various mixtures throughout this investigation is plotted in **Figure 5.4**. It is beneficial for both MOE and STS to be normalized with respect to the square root of the compressive strength ( $\sqrt{f'_c}$ ) for comparison to values suggested by the American Concrete Institute (ACI). The MOE, STS, and their coefficients are shown below in **Figure 5.5 – 5.8**.

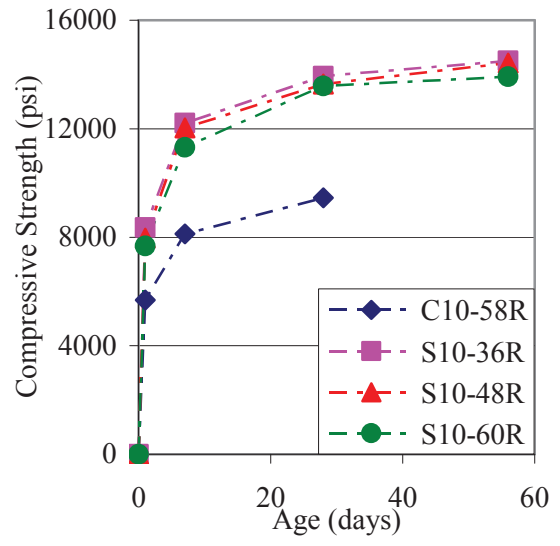


(a) 6ksi target limestone mixtures

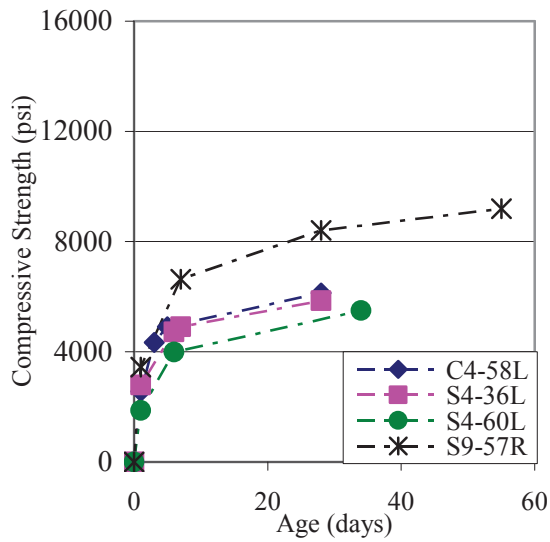
(b) 10ksi target limestone mixtures



(c) 6ksi target river gravel mixtures



(d) 10ksi target river gravel mixtures



(e) Additional mixtures; 4 ksi limestone and 9 ksi pea gravel

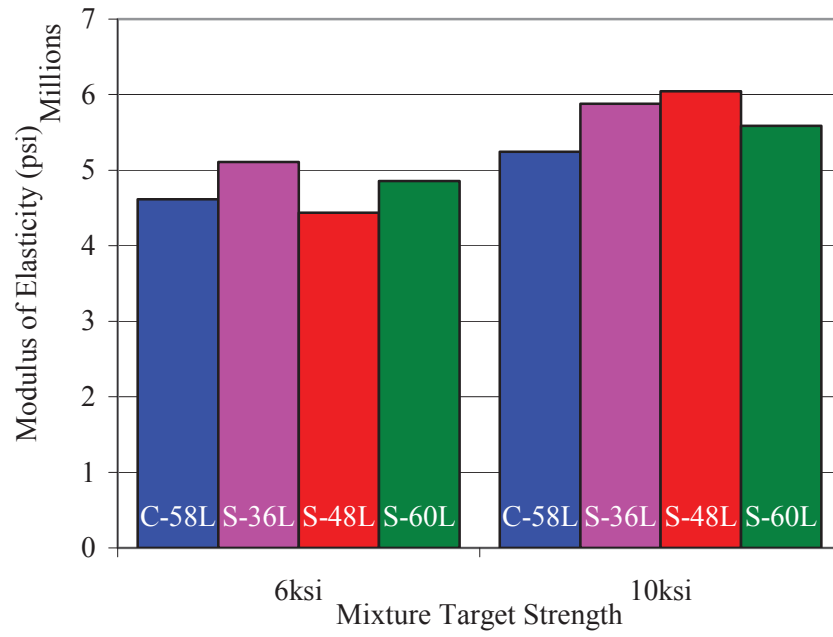
Conversion: 1000 psi = 1 ksi = 6.89 MPa

**Figure 5.4 – Compressive Strength Development over Time**

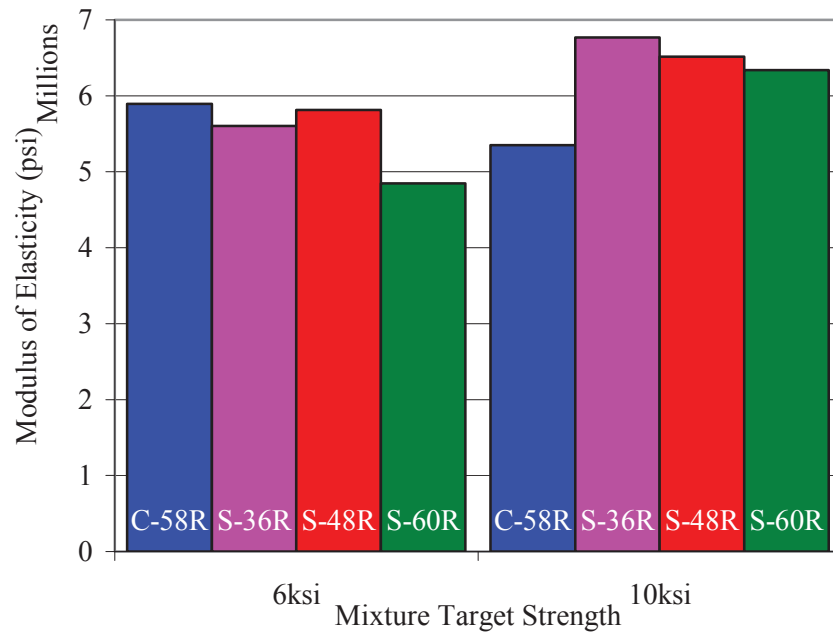
Observe from the strength development curves of **Figure 5.4** a very high rate of strength development at early ages, with a rapid depletion of additional strength gain; this is the type of curve expected for concrete mixtures with type III cement as was used in this investigation, and is also typical of precast concrete suppliers. Some HRWRA's can also contribute to higher early strengths. The manufacturer's product data sheet for the HRWRA used throughout this project (in **Appendix A**), Glenium 7700, indicates potential for higher early strengths (BASF 2010).

Besides the general shape of the strength development curves, the "ultimate" strengths achieved at the time that the shear tests commenced were all higher than the target strengths. The higher-than-target strengths should not be surprising given the mix development process described in **Section 3** where survey results were the primary factors considered in material proportioning. Also observe that the strengths achieved at the time of shear testing are fairly consistent for each group of curves that kept aggregate type and w/c ratio constant.

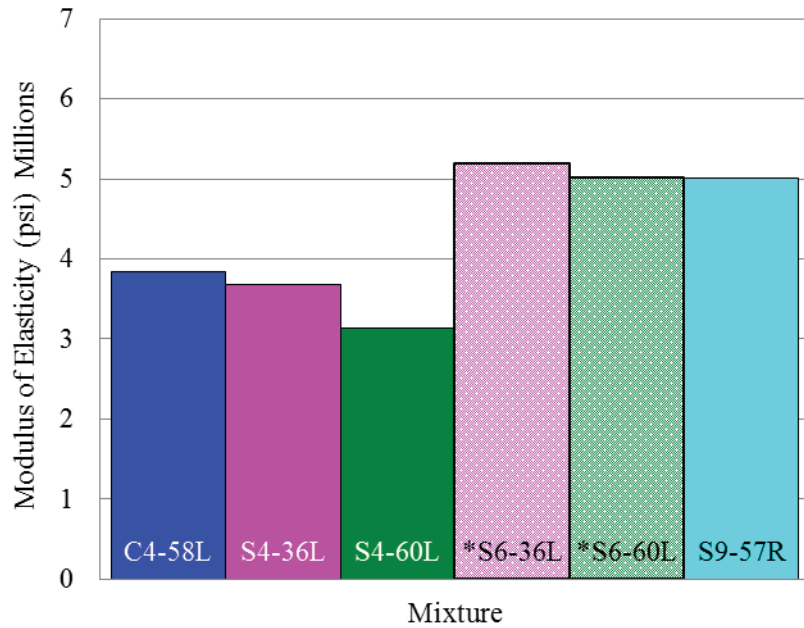
Next, review the results for the MOE and STS tests performed. Note that **Figure 5.5** and **Figure 5.6** show the test results for MOE and STS respectively and that **Figure 5.7** and **Figure 5.8** show the test results normalized with respect to  $\sqrt{f'_c}$  for comparison to typically expected values according to ACI.



(a) Limestone mixtures



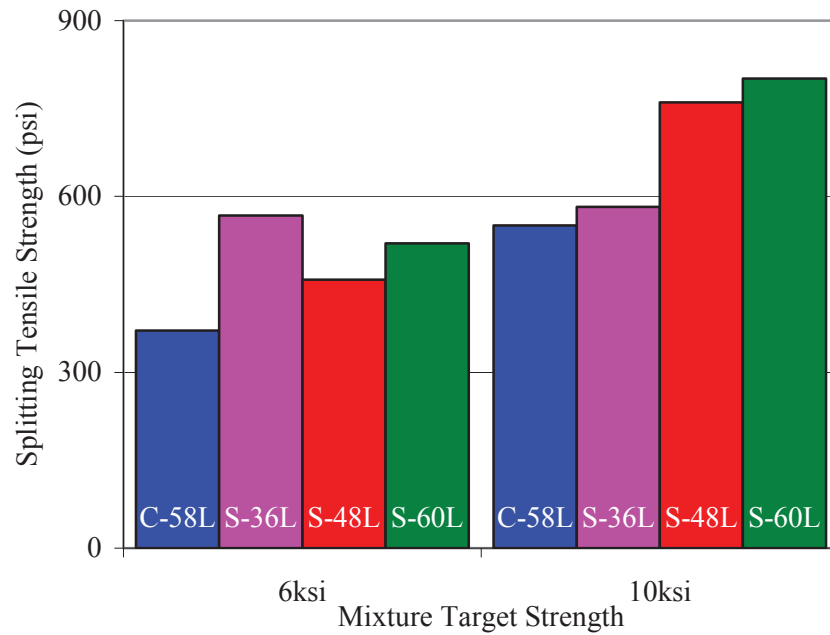
(b) River gravel mixtures



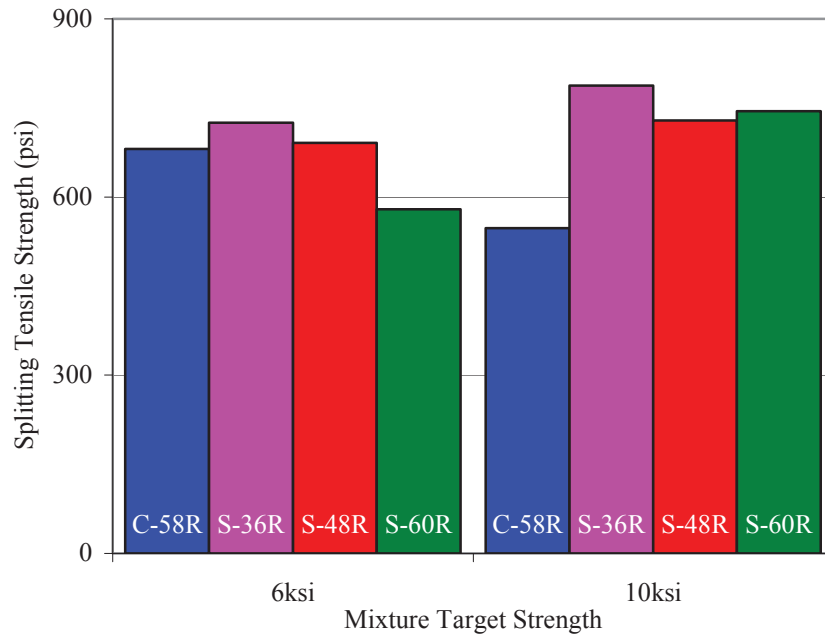
(c) Additional Mixtures; 4 ksi limestone, 6 ksi re-batch, and 9 ksi pea gravel

Conversion: 1 ksi = 6.89 MPa

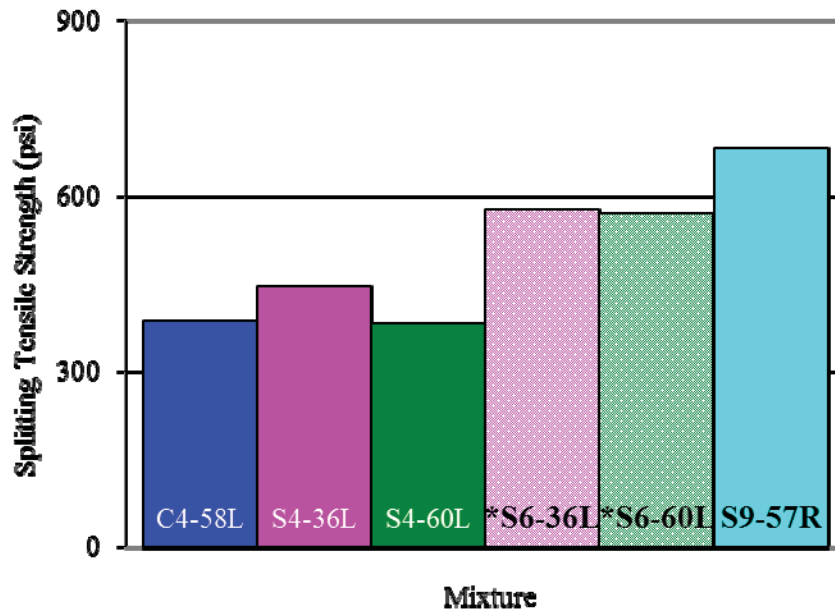
**Figure 5.5 – “Ultimate” MOE for All Mixtures**



(a) Limestone mixtures



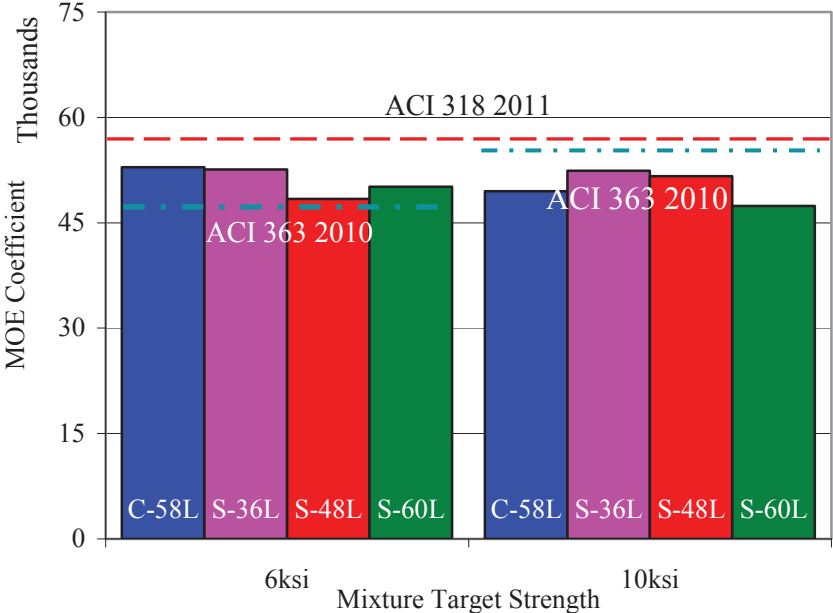
(b) River gravel mixtures



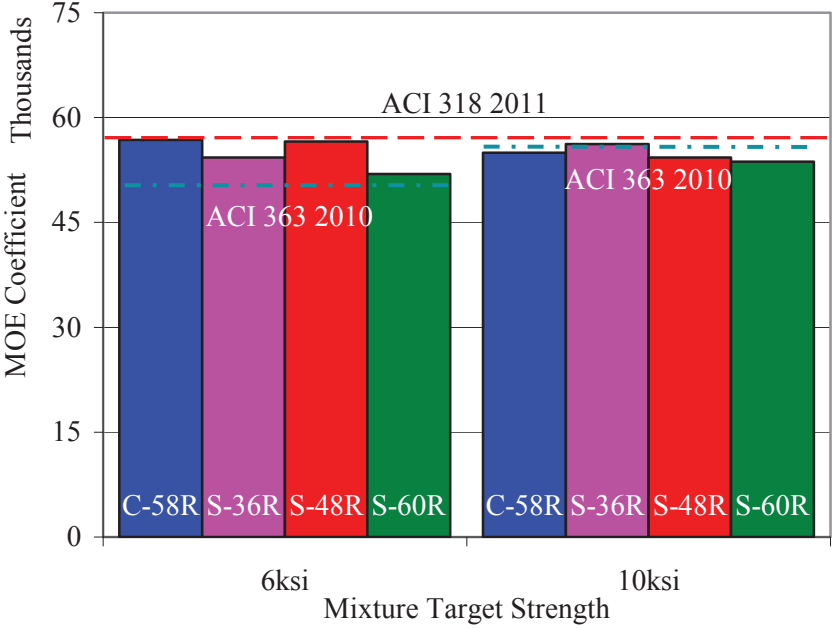
(c) Additional Mixtures; 4 ksi limestone, 6 ksi re-batch, and 9 ksi pea gravel

Conversion: 1000 psi = 1 ksi = 6.89 kPa

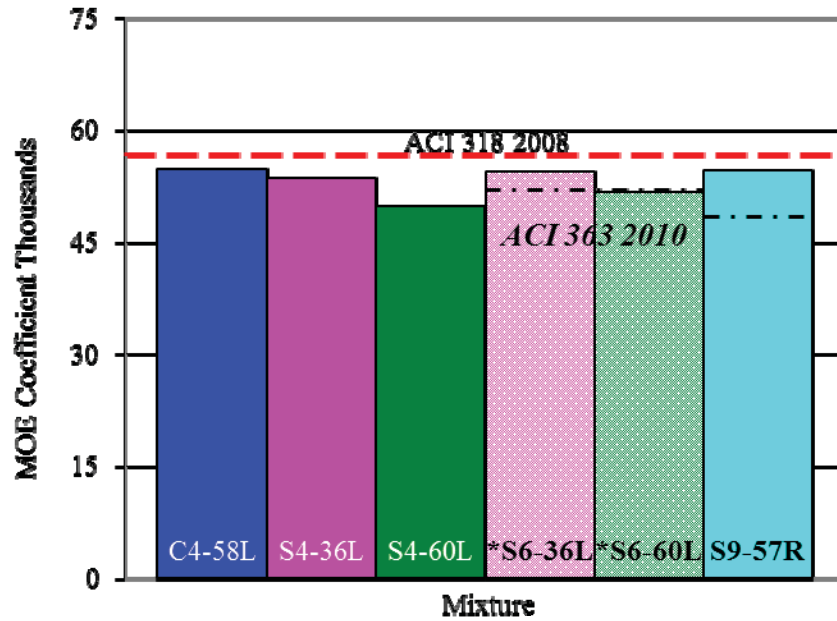
**Figure 5.6 – “Ultimate” STS for all Mixtures**



(a) Limestone mixtures



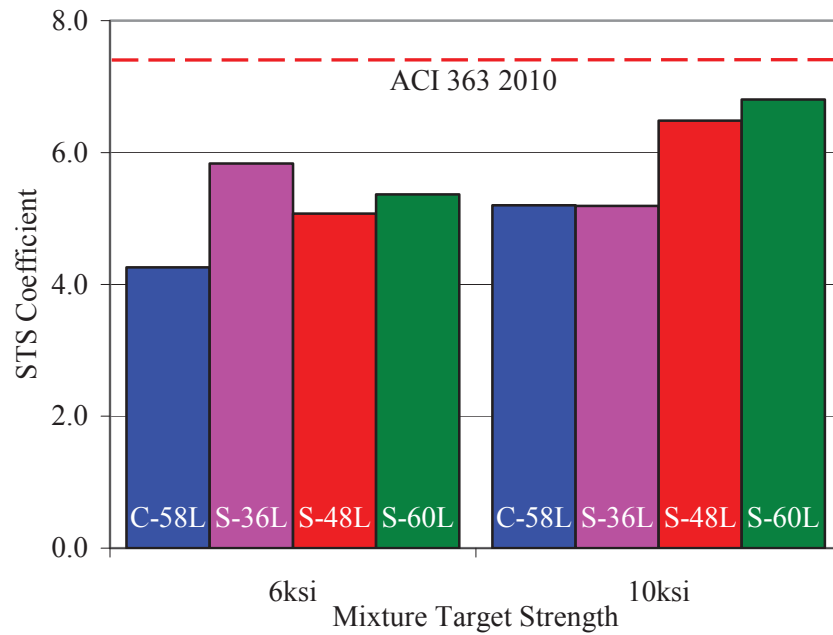
(b) River gravel mixtures



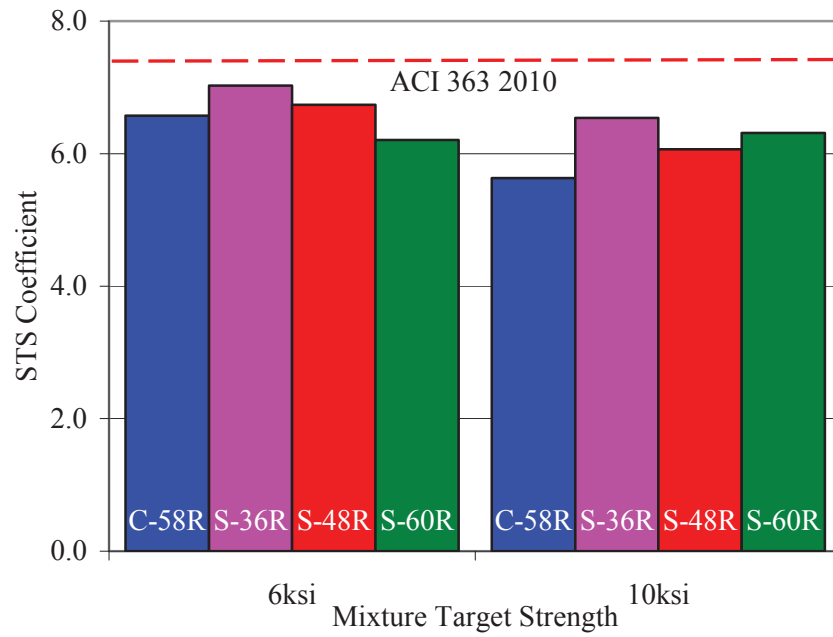
(c) Additional Mixtures; 4 ksi limestone, 6 ksi re-batch, and 9 ksi pea gravel

Conversion: 1 ksi = 6.89 MPa

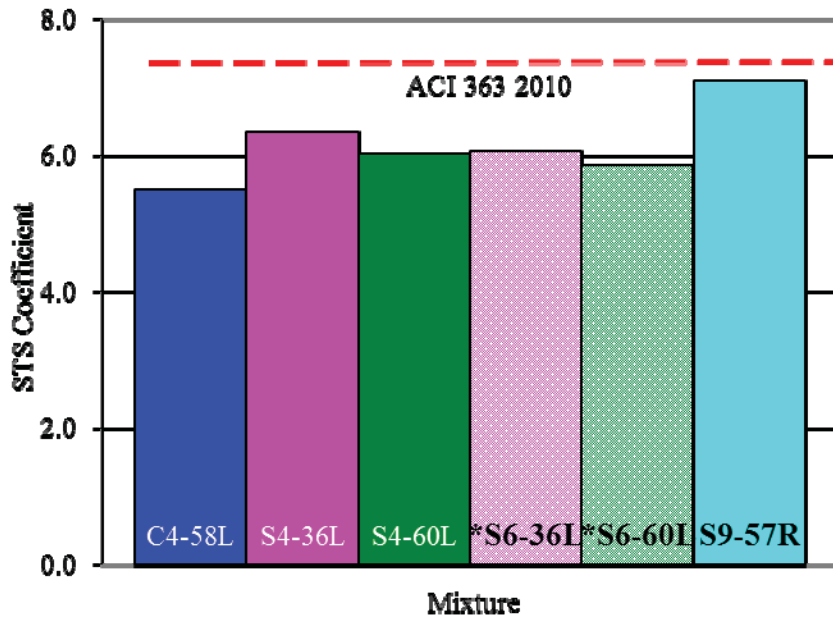
Figure 5.7 – Normalized “Ultimate” MOE



(a) Limestone mixtures



(b) River gravel mixtures



(c) Additional Mixtures; 4 ksi limestone, 6 ksi re-batch, and 9 ksi pea gravel

Conversion: 1 ksi = 6.89 MPa

Figure 5.8 – Normalized "Ultimate" STS

**Figures 5.5** and **5.6** both show that the higher strength mixtures as well as the river gravel mixtures tend to have higher values of MOE and STS compared to the lower strength limestone mixtures. The coefficient for MOE of normal density concrete (90 – 160 lb/ft<sup>3</sup> [1440 – 2560 kg/m<sup>3</sup>]) is permitted to be taken as 57000 (ACI 318 2011). The MOE coefficient for normal density high strength concrete is variable as it consists of a coefficient plus a constant as is shown in **Eq. 5.1** (ACI 363 2010). It should be noted that this empirical model was developed as a lower bound predictor for HSC.

$$E_c = 40000\sqrt{f'_c} + 10^6 \quad (\text{psi}) \quad \left[ E_c = 3320\sqrt{f'_c} + 6900 \right] \quad (\text{MPa}) \quad (5.1)$$

The ACI coefficients for MOE are indicated in **Figure 5.7**. Both the normalweight and normal density high strength MOE coefficient predictors were shown since the target strengths were exceeded for all concrete batch proportions as indicated in **Table 5.2** and **Table 5.3** above; the result is that some mixtures may be better predicted by high strength models, and this is explored. The limestone mixtures were slightly less stiff than predicted by the normalweight concrete approximation, but more closely matched the high strength model. The river gravel mixtures were reasonably estimated by either ACI approximation when normalized for compressive strength, but again even more accurately by the high strength model (ACI 318 2011; ACI 363 2010). The lower MOE coefficient of the limestone mixtures could be due to the weak or soft nature of Missouri limestone aggregates.

ACI 318 does not address STS for anything other than lightweight concrete; therefore, the ACI 363 source is quoted. As all target strengths were exceeded as

mentioned previously, the ACI 363 approximation is likely valid. The ACI coefficient for STS is given by committee 363 as 7.4 and it can be seen in **Figure 5.8** that all mixtures had significantly lower coefficients for all strengths, but especially the 6 ksi (41.4 MPa) target strength limestone series. For each test series, the CC of that series exhibited lower STS than the SCC; this could be due to improved consolidation and homogeneity of SCC during placement. The very low coefficient for STS of the limestone, but only slightly low for the river gravel, could indicate weak transition zones between the aggregate and paste, or more likely, it could be indicative of again having weak Missouri limestone aggregates such that a fracture develops and propagates through the aggregate rather than taking the longer path around the aggregate in the interfacial transition zone (Mindess 2003). The argument for weak limestone aggregates is supported by the recorded STS fracture plane; limestone specimens had much more coarse aggregate fracturing in the failure plane, usually 90-100%, while river gravel specimens consistently had only 65-75%.

From the hardened concrete properties tests there is a clear understanding of concrete compressive strength,  $f'_c$ , modulus of elasticity,  $E_c$  (MOE), and splitting tensile strength,  $f_{sp}$  (STS), of the concrete batch proportions used. The strength development was “high-early” and was consistently higher than targeted or predicted “ultimate” strengths, while maintaining low variability between mixtures that hold the w/c ratio and aggregate type constant. The MOE for each concrete was known; the limestone mixtures were slightly lower than what would be predicted by ACI; this was thought to be due to the soft nature of the Missouri limestone used. The STS for all mixtures were lower than what would be predicted by ACI, especially the 6 ksi (41.4 MPa) target strength

limestone mixtures. The low STS of the limestone mixtures could be caused by poor bond between the mortar and aggregate or, more likely, again because of the weak nature of Missouri limestone aggregates (ACI 318 2011, ACI 363 2010).

## 6. PUSH-OFF TEST

### 6.1 INTRODUCTION

The push-off test is a non-standard, but widely recognized, test used in the testing of shear in concrete. Early researchers include Mattock (1969; 1972), Reinhardt (1981), and Walraven (1981; 1994). Later studies in shear using reinforced panels have refined, but also confirmed, the validity of the models derived from using push-off specimens (Vechio and Lai 2004). The push-off test has the advantage of being relatively small, inexpensive, easy to perform, and not needing any highly specialized pieces of testing equipment; studies using shear panels require the use of a dedicated and expensive test apparatus. The ease with which one can test push-off specimens allows for many variables to be tested, even in relatively small studies. As was done in similar investigations, the specific materials and variables tested were employed to evaluate aggregate interlock shear behavior and evaluate trends. This study investigated varying levels of concrete compressive strength, coarse aggregate type, and coarse aggregate to fine aggregate volume ratios, and cast companion push-off specimens for small prestressed precast beams. The full push-off test matrix is located in **Section 4** and listed in **Table 4.1**. After completion of the push-off test, the tested specimens were retained and images of their cross-sections were made to investigate segregation as well as correlating C.A. volume fraction with shear resistance.

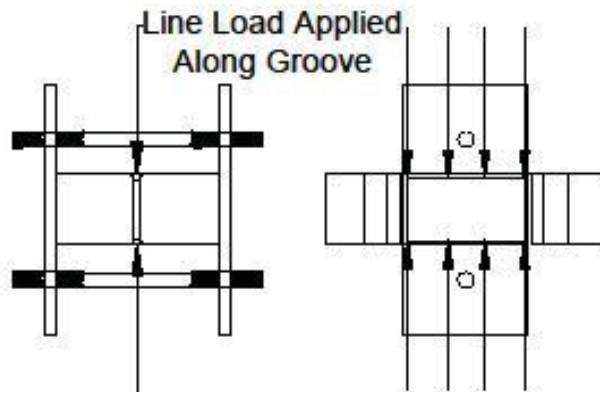
This section will detail the push-off test setup and procedure and the subsequent digital imaging performed. There were several difficulties experienced while performing the push-off tests; these difficulties will be shown, and the actions taken to remedy them

will be explained. The specimen size, geometry, and reinforcement will be detailed. Next, the test results will be presented and an analysis will follow. Lastly, conclusions will be made and summarized.

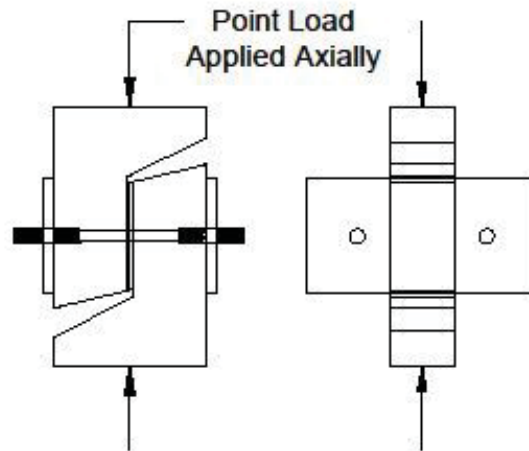
## **6.2 TEST SETUP AND PROCEDURE**

Because the push-off test is non-standard, a detailed description of the test setup and procedure used throughout this study is necessary. Any departures from other researchers, whether done purposefully, or as an oversight, may be important to the resultant findings. The goal of this section would be for future researchers to be able to replicate the tests performed throughout this investigation and to confirm the findings.

**6.2.1 Test Setup** The shear test used in this study consists of two distinct steps; the first step is to “precrack” the specimen, the second is the actual “push-off” test where the bulk of shear behavior information is gathered. See **Figure 6.1** for an elevation view of both the precrack and push-off test. The precrack test is necessary, as it develops the shear crack initial condition. Researchers have also found that precracking is necessary to achieve an actual pure shear interface, otherwise shear along the interface with high concentrated tensile stresses at the ends of the notched insets develop just prior to cracking (Barragan 2006). Barragan developed a finite element model (FEM) representing an uncracked specimen loaded as in a push-off test, the high tension regions can be seen in **Figure 6.2** below, these tensile stresses are alleviated if precracking is performed.

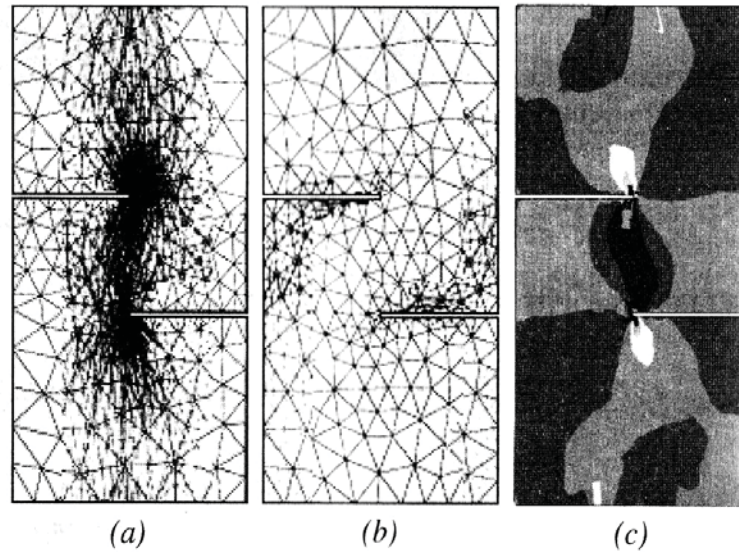


(a) Precrack Test



(b) Push-off Test

**Figure 6.1 – Aggregate Interlock Test Orientations**



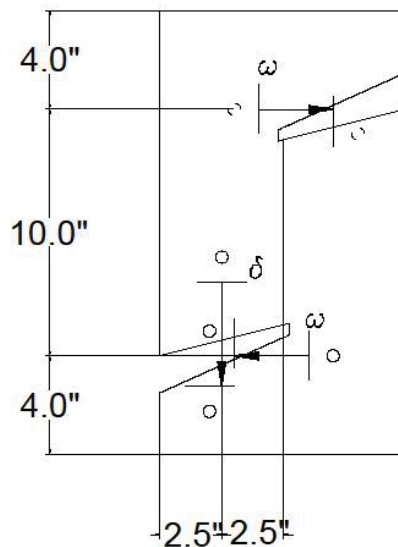
*-Finite element mesh used and distributions of: (a) compressive; (b) tensile; and (c) shear stresses (darker areas indicate higher magnitudes of stress).*

**Figure 6.2 – Precracking Shown to Alleviate Tensile Regions by Barragan**

The externally reinforced test specimen was used as described by Walraven and Reinhardt (1981). Some researchers have used this test setup with internal reinforcement to restrain the two sides, some have used external reinforcement for restraint; this investigation chose to use external reinforcement because of the variables important to the study. The variables of interest in this project were all constituents of the concrete contributing to the mechanism of aggregate interlock; whereas, internally reinforced push-off tests also introduce variables of reinforcement ratio and the mechanism of dowel action contributing to shear.

Data collected from the shear testing includes: the precrack load ( $P$ ), crack opening ( $\omega$ ), crack slipping ( $\delta$ ), normal stresses ( $\sigma$ ), and shear stresses ( $\tau$ ). The crack opening was measured and averaged by two separate point – symmetrically positioned

linear voltage displacement transducers (LVDTs) placed perpendicular to the crack, on opposite ends of the specimen, and on opposite faces as shown in **Figure 6.3**. Crack slippage was also measured with an LVDT as in **Figure 6.3**. The slip LVDT was placed parallel to the crack, across the notch to measure relative displacement of the two sides of the specimen. The load applied by the Tinius Olsen load machine was divided by the interfacial area and results in the applied shear stress. The normal stress was measured using two strain gages applied to each of the two external restraining bars positioned as in **Figure 6.4**. The strain in the bars was taken as the average of the two strain gages applied to each bar. The strain was converted to stress, and then force, with the known Young's modulus and cross-sectional area of the steel bars. The force acting within the restraining bars is thought to act uniformly over the shearing interface of known area and is the resulting normal stress of interest.



Conversion: 1 inch = 25.4 mm

**Figure 6.3 – LVDT Placement for Measuring Crack Opening and Slip**

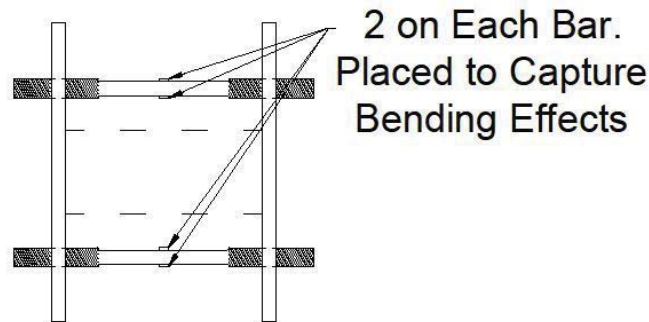


**Figure 6.4 – Strain Gage Location on External Reinforcement**

The size and geometry of the specimens used in this study were unique. The adjusted size was in response to some earlier experienced issues with testing and will be discussed in **Section 6.3** in detail. The resultant dimensions are shown in **Figure 6.22**.

The load blocks used for the precrack and push-off tests also warrant discussion. The load blocks are shown in **Figure 6.5**. The precrack load block consists of a piece of 2 x 2 x 1/4 inch (51 x 51 x 6.4 mm) steel angle welded to a 7.5 x 3 x 3/4 inch (191 x 76 x 19 mm) steel plate with a notch cut out from the center. The angle portion of the block fits into the groove that is cast into the side of the precracked specimen so that a line load is applied along this groove. The notch in the plate exists to allow clearance for the external reinforcing bar that confines the push-off specimens. The push-off blocks are simple 8 x 2 x 1/2 inch (203 x 51 x 13 mm) steel plates. A neoprene pad of durometer 60 hardness was placed between the flat plate and the specimen to mitigate the effects of specimen surface roughness. The push-off blocks were placed on top and bottom of the push-off specimen axially, so that bending moments were not induced.



(a) Pre-crack Load Blocks



(b) Push-off load blocks and pads

**Figure 6.5 – Aggregate Interlock Specimen Load Blocks**

**6.2.2 Test Procedure** This section is meant to delineate the sequence of the precise actions taken in order to perform the aggregate interlock testing which consists of both the precrack and push-off tests so that future researchers may replicate and confirm

the findings. The procedure described assumes that a specimen has already been cast and cured as will be described in **Section 6.3**.

In preparing the specimens, any imperfections on the edges or groove were chiseled and/or sanded away; this permitted full contact of the plates confining the specimens and adequate seating of the precrack load blocks within the cast groove. For positioning of the specimen within the test apparatus, the shear interface surface was projected and drawn on the apparatus as in **Figure 6.6** below. The specimen was slid into place within the apparatus, held to the right height by positioning blocks and metal shims, and then the apparatus was moved until the projected surface on the apparatus aligned with the test surface as determined by use of a carpenter's square. The bolts on the apparatus were tightened until snug and the positioning blocks were removed. A specimen properly positioned within the apparatus with key positions indicated is shown in **Figure 6.7** below.



(a) Projected on Both Surfaces

(b) Accurately Drawn

**Figure 6.6 – Projected Surface on Apparatus for Positioning**



**Figure 6.7 – A Properly Positioned Specimen**

Instrumentation is the next sequence of steps. As will be described later in **Section 6.3**, anchor bolts were cast into the proper position for attaching the necessary LVDTs for measuring crack opening and slip. The LVDT mounts and associated reaction mounts were attached by hand tightening a nut using a wrench over the cast in place anchor bolt; taking care that the mounts were positioned parallel and perpendicular to the crack for the crack opening and crack slip LVDTs respectively. The parallel and perpendicularity of the mounts was again determined through the use of a carpenter's square. Next, the LVDTs themselves were attached and secured by using a double bolt around the mounts. See **Figure 6.8** for properly anchored LVDTs. The strain gages, already attached to the apparatus through common practices, protected from damage by a gummy overlay, and wiring held secure by electrical tape were then attached to the data acquisition system (DAS). **Figure 6.9** shows the strain gages attached to the DAS; each gage was attached by two wires, a positive and a negative. Before each precrack test, the

nuts on the apparatus were tightened such that the strain readouts from the DAS for each bar were averaged to about 110-165 microstrain, resulting in approximately 100 - 150 psi (0.69 – 1.03 MPa) on the shear interface for steel bars of about 3/4 inch (19 mm) diameter and a shear interface of about 3.75 x 7.50 inches (95 x 191 mm). Fortunately, the DAS was capable of zeroing strain readings, so periodically the gages were attached to the DAS with no normal strain applied and re-zeroed; however, the gages maintained their datum consistently and this was done as more of a check than to correct any drifting benchmark.

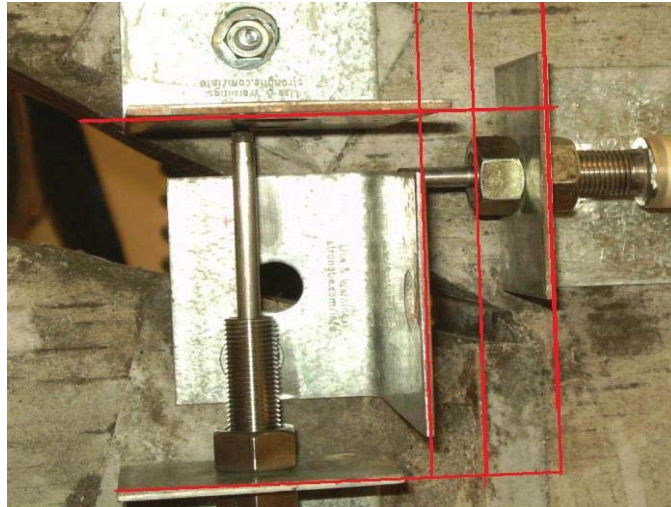


**Figure 6.8 – Properly Anchored LVDTs, Parallel and Perpendicular to Groove**

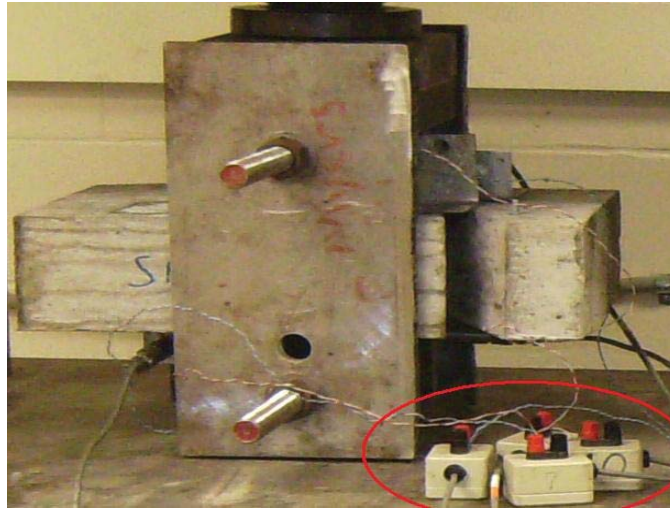


**Figure 6.9 – Strain Gages Attached to Data Acquisition System (DAS)**

Next, the apparatus and specimen were positioned upon the Tinius Olsen loading machine for the precrack test. **Figure 6.9** above actually shows the final position of the precrack test. The specimen was lifted to the height of the Tinius Olsen bottom table by a hand operated fork lift, dragged from the fork lift onto the table, and placed in the horizontal position. Metal shims were placed under the plates that comprise the apparatus so that the specimen was raised to provide adequate clearance for the load block to be placed on the bottom groove of the specimen. The metal shims were removed and the grooved specimen was allowed to settle onto the bottom load block as shown in **Figure 6.10(a)**. The top load block was then placed on the top groove of the specimen and allowed to settle into place as shown in **Figure 6.10(b)**; additional blocks were added as on the bottom to provide adequate spacing between the load applying crosshead of the Tinius Olsen machine and the apparatus. **Figure 6.10(c)** shows the precrack specimen completely positioned and ready for loading; **Figure 6.10(c)** also highlights the gap

between the bottom platen of the Tinius Olsen machine and the test apparatus so that the load is channeled through the load blocks and onto the grooved specimen as intended.



(a) Bottom Load Block Seated into Specimen Groove



(b) Top Load Block Seated into Specimen Groove



(c) Precrack Specimen Ready for Loading, Space Provided Between Apparatus and Load

**Figure 6.10 – Precrack Specimen Positioning**

A preload was applied by a displacement-controlled application at the rate of 0.05 in/sec (1.3 mm/sec) until 100 lb (445 N) of force was applied to the specimen; this helps to settle the load blocks into the specimen and against the Tinius Olsen machine. After the preload was reached, the load was applied by a load-controlled application at the rate of 100 lb/sec (445 N/sec) until the specimen ruptured. The ruptured specimen often had a crack opening in the order of 0.02 – 0.04 inch (0.5 – 1.0 mm) If the ruptured specimen opened less than 0.02 in (0.5 mm), loading was allowed to continue at the rate of 100 lb/sec (445 N/sec) until this minimum was achieved. Upon rupture or attaining the minimum crack opening, loading was stopped, the load platen was returned to the test starting position, and the data acquisition was stopped. The precracking load would be either the load that caused rupture, or the load necessary to attain the minimum crack

opening of 0.02 in (0.5 mm), whichever was greater. The information gathered from this test was the precracking load and the crack opening at the end of the test.

After the precrack test was complete and the Tinius Olsen cross head was raised, the specimen was placed in the vertical position. The push-off loading blocks with their associated neoprene pads were then placed axially concentric with the now cracked shear interface. **Figure 6.11(a) – Figure 6.11(c)** below shows the upright positioning of the push-off specimen along with the neoprene pad and block placement. It should be mentioned that the same attachment to the Tinius Olsen load machine was used for both the precrack and push-off test; the attachment is a spherically seating bearing block of the same type allowed in testing compressive strength cylinders. The spherically seating bearing block allows for some rotation and will help mitigate the generation of moment during the tests. **Figure 6.11(c)** shows the neoprene and bearing block placement as well as the spherically seating bearing block attachment to the Tinius Olsen machine.



(a) Vertical Orientation with Bearing Blocks Axially Located



(b) Bottom Bearing Block with Neoprene Between Specimen



(c) Top Bearing Block with Neoprene and Spherically Seating Attachment Block

**Figure 6.11 – Push-off Test Positioning**

The loading used for the push-off test was the same as the loading used for the precrack test; a 100 lb (445 N) preload achieved at 0.05 in/sec (1.3 mm/sec) and a 100 lb/sec (445 N/sec) load rate thereafter. The loading was then manually halted when the slip LVDT measured a total slip of approximately 0.25 inches (6.4 mm). The load

platen was returned to home, the position before the loading commenced, and the specimen was removed. After the apparatus was loosened from around the specimen, one half was discarded and the other half was retained for dimensional confirmation measurements and for the cross-sectional imaging investigation. The information gathered from the push-off test is much more complex than that gathered from the precrack test and will be discussed in full with the analysis of the results in **Sections 6.4** and **6.5** to follow.

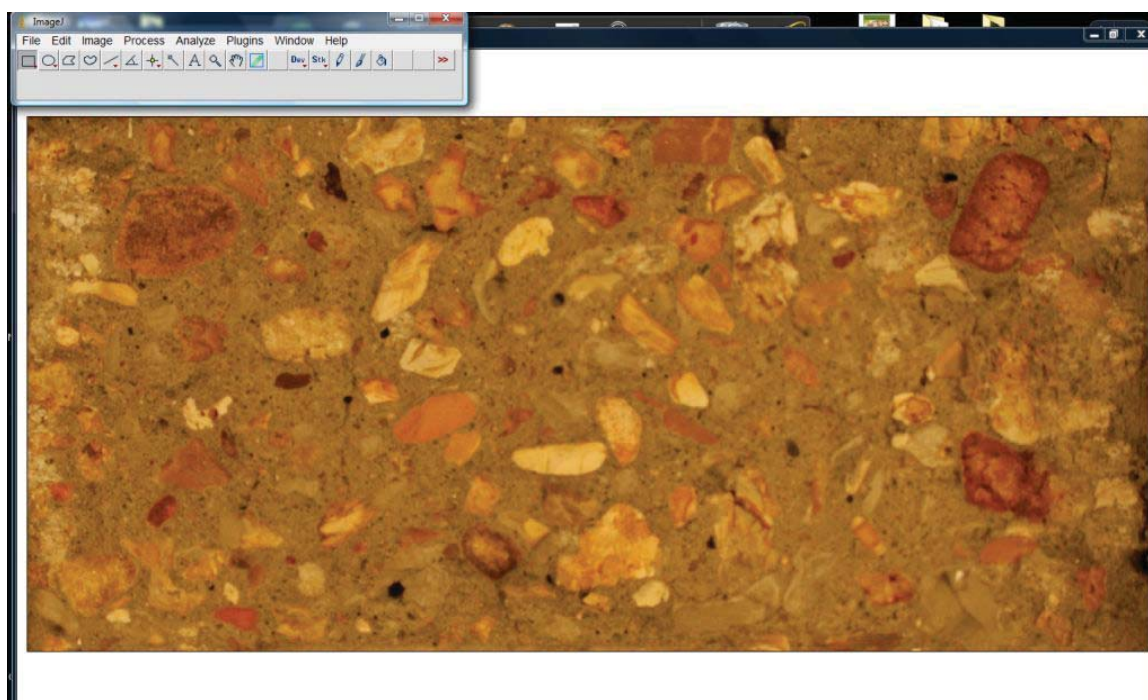
**Section 6.2.3 ImageJ Analysis Procedure** The cross-sectional imaging was aided by several factors. Current work at the Missouri University of Science and Technology campus was undertaken in which very precise and sophisticated imaging was necessary. The researcher constructed a photo booth which addressed all of his various needs specifically, and which more than addressed the needs of this project. **Figure 6.12** below shows the photo booth used in this investigation; it does not look very impressive, but has several features worth mentioning. The four chip cans each hold an LED light bulb, the aluminum interiors act as reflectors with the lids behaving as diffusers. The use of four light sources helps to eliminate shadows on the rough surface being photographed. The LED bulbs were connected to a direct current source so that the photo would not be hindered by the off portion of an alternating current. Secondly, the software used in this investigation, ImageJ, was available for download from the National Institutes of Health website (NIH 2004). The software was developed for the medical field and is much more sophisticated than necessary for this investigation. ImageJ also has numerous users and many contribute to online tutorials and walkthroughs.



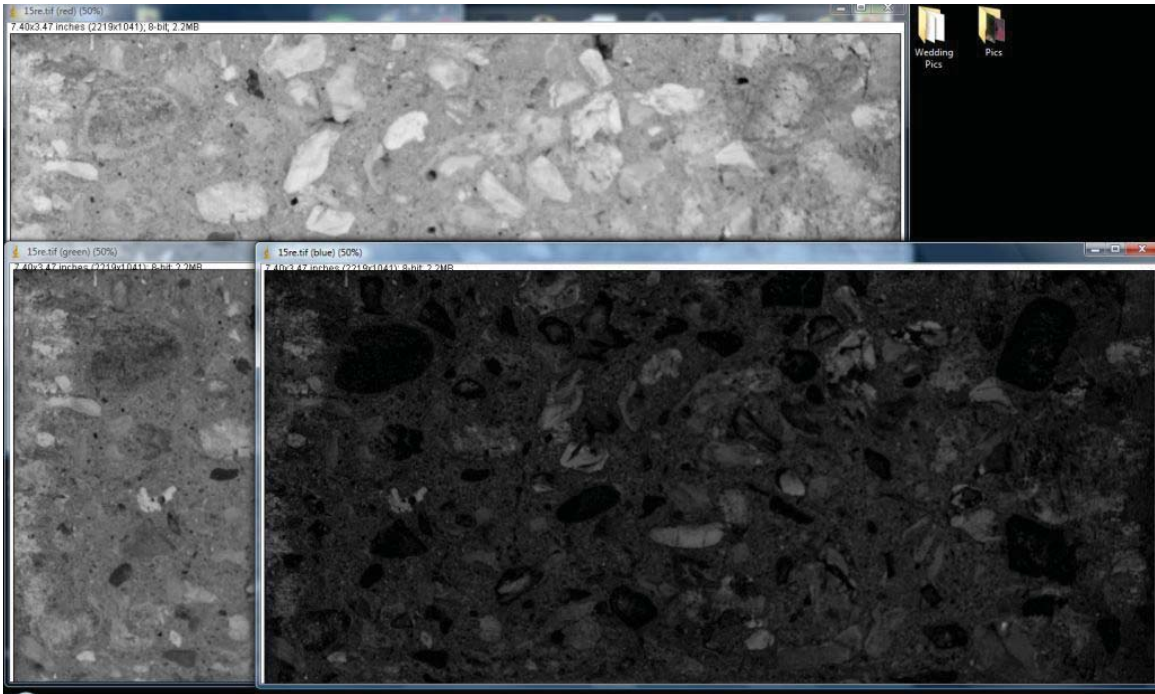
**Figure 6.12 – Photo Booth Used For Cross-Sectional Imaging**

Photographs of the cross-sections of the push-off specimens were taken using the photo booth described and shown above. The digital pictures were cropped down to the size of the push-off specimen cross-section using Microsoft® Office Picture Manager, then imported into ImageJ. The picture was split into the three separate red, green, and blue channels which comprise the original color image. A threshold was then applied to the red and blue channels (the green channel added more “noise” than useful information and was thus deleted) to tell ImageJ which pixels should be included in the analysis based on intensity; these are the coarse aggregate particles of interest to this study. The threshold was set to constant levels between all images. The red and blue channels were then converted to binary images; this separated the pixels of interest (coarse aggregate) from the pixels not of interest (paste matrix). The red and blue channels were then added back together using the image calculator available within ImageJ. A few particles were measured to determine an appropriate particle size to include in the analysis; this eliminated isolated pixels or small clumps of pixels from being counted as coarse

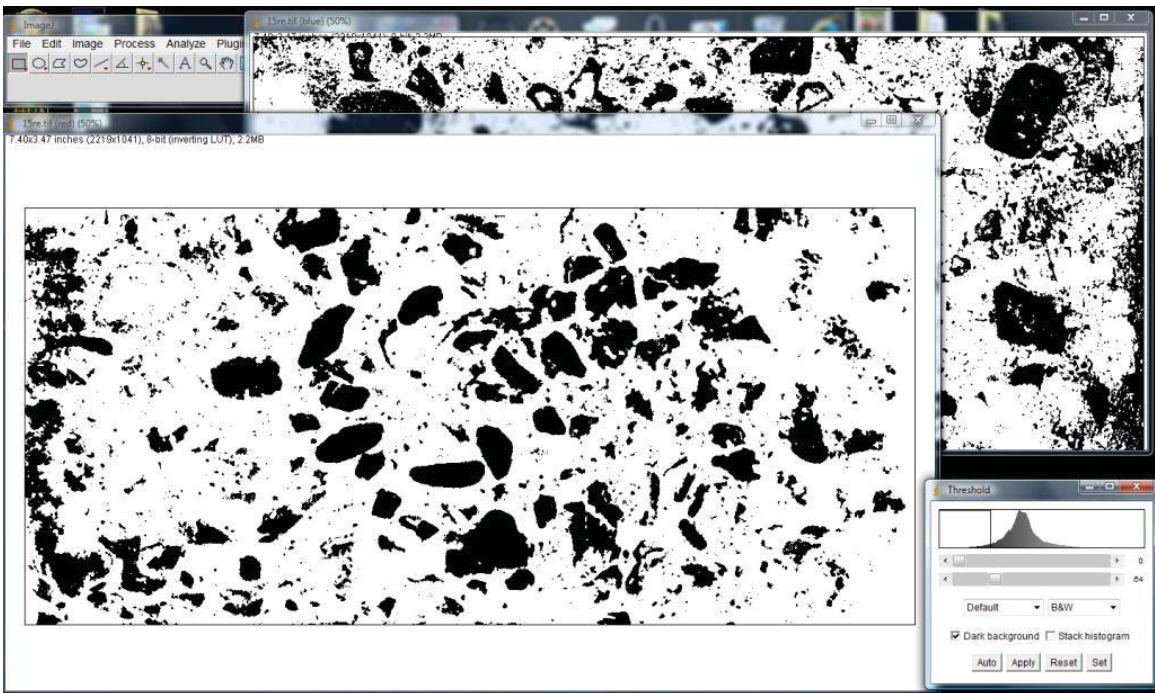
aggregate. The analysis was then performed by ImageJ to determine the number of aggregates counted, the average size, the area fraction, and where the center of mass of the particle was located within the image. A sample cross-section can be found in **Figure 6.13** in which the original cross-section is shown along with the subsequent processes carried out using ImageJ. Large pictures are shown for added visual clarity.



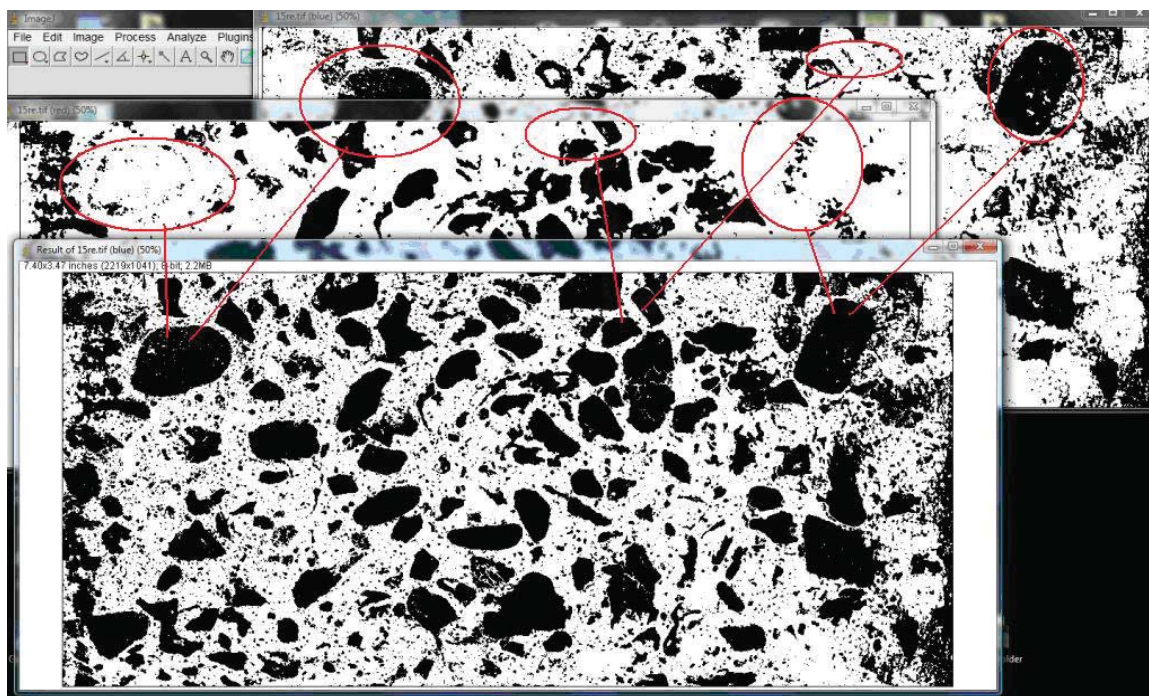
(a) Sample cross-section



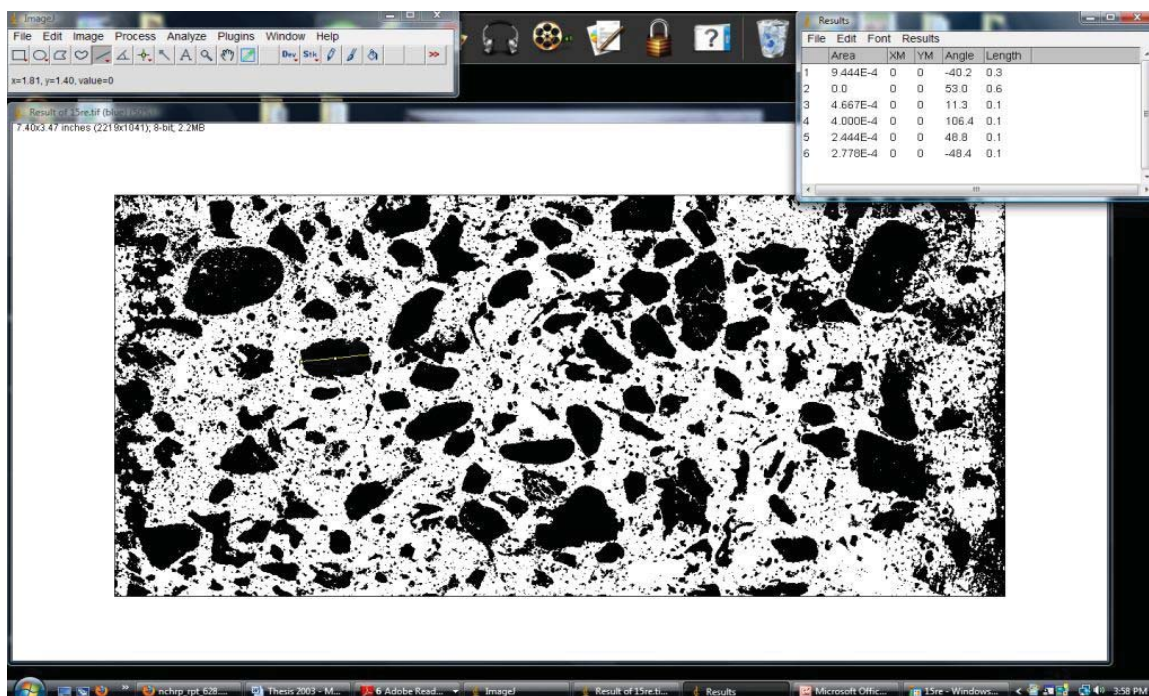
(b) The color image is split into the constituent red, green, and blue channels



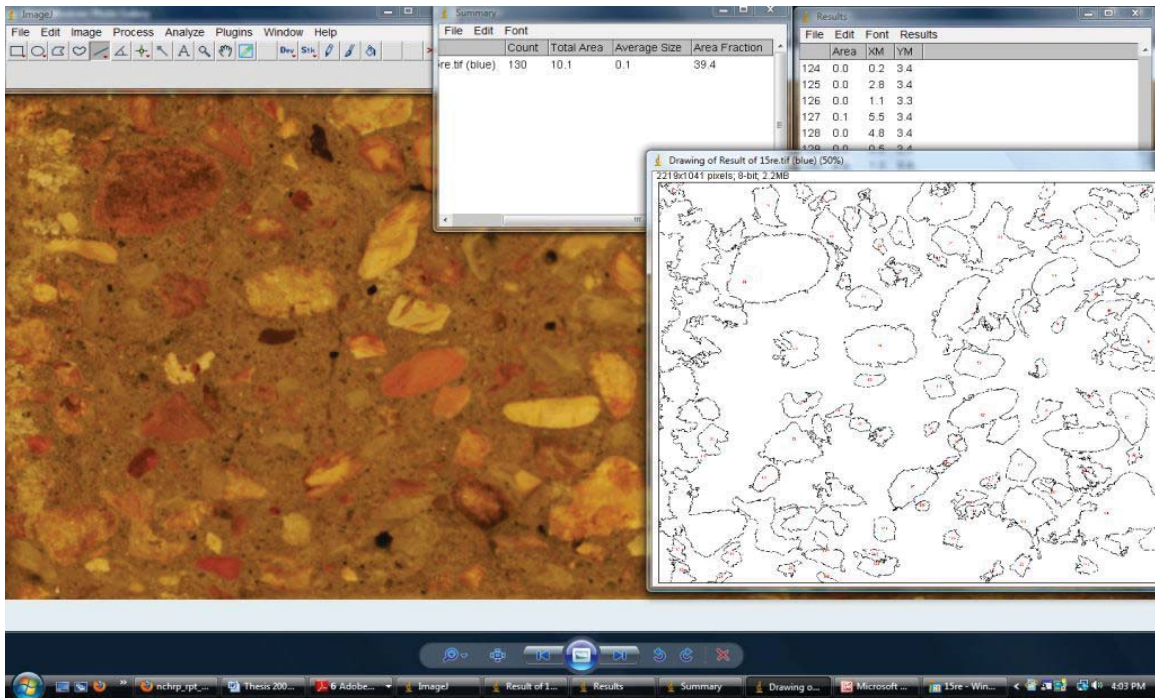
(c) Setting the threshold isolates pixels of interest



(d) The red and blue channels are added, consolidating all detected particles of interest



(e) The particles are measured to count only aggregate and not the surrounding "noise"



(f) Results are summarized and an outline drawing of the counted particles is produced

The screenshot shows a Microsoft Excel spreadsheet with a table of data. The columns are labeled A through J, and the rows are numbered 90 through 107. The data is as follows:

	A	B	C	D	E	F	G	H	I	J
90	89	0.06	2.59	3.64						
91	90	0.01	0.36	3.52						
92	91	0.02	3.28	3.65						
93	92	0.01	1.85	3.65						
94			3.754022							
95										
96										
97			7.48							
98			3.74							
99										
100										
101										
102										
104										
105			0.37%							
106										
107										

(g) The center of mass is determined and segregation is quantified

**Figure 6.13 – ImageJ Sample Analysis**

As a check on the analysis, the area fraction can be compared to the absolute volume of the coarse aggregate in the batch proportions for the mixture under investigation. Segregation can be detected by determining the location of the center of mass for all aggregates counted. Finally, an outline drawing of the particles counted in the analysis was also produced by ImageJ. The results of the forensic image investigation will be presented in **Section 6.4.3** below.

The non-standard precrack and push-off tests have been explained in detail. The exact setup used for this study has been explained. Along with the setup, the precise actions executed during the test procedure for this investigation have been made clear such that a reader could replicate this work. The imaging technique and software used were also shown. Next, the actions taken to fabricate the specimens will be discussed along with the reasoning for the exact specimen and apparatus geometry and detailing used.

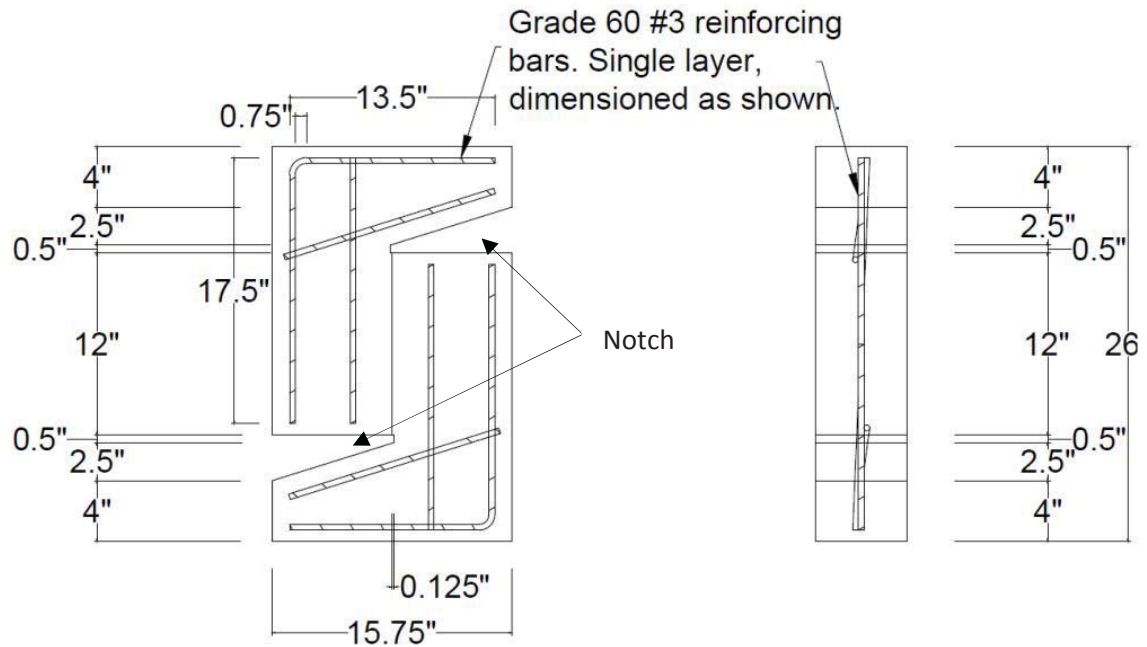
### **6.3 SPECIMEN DESIGN AND FABRICATION**

The use of the push-off test was new to the Missouri University of Science and Technology at the start of this project, and there was therefore no firsthand experience from which to draw any insights into how to fabricate or test the specimens; all of the knowledge was gained from other researcher's published works. Some issues arise when attempting to replicate other's work because even the most thorough author likely has typos, omissions, or may downplay certain issues; on top of these shortcomings, the information is then left to be interpreted by the reader and may be done so erroneously. The point to all of this is that throughout this study, there were several instances where

previous research provided the framework within which to work; however, the details were changed so that the desired outcome could be achieved or enhanced. Several times, the initial design proved inadequate, or the initial procedure was cumbersome or unacceptable. This section attempts to thoroughly discuss the specimen fabrication and design, and the iterations that took place from the beginning of the project to the end.

**6.3.1 Initial Design and Fabrication** Initially, the previous works of Mattock (1969;1972), Walraven and Reinhardt (1981), Albajar (2008), and Kim et al. (2008) were surveyed for dimensions, reinforcement, and external reinforcing apparatus details. The dimensions and exact geometry varied from project to project. The work of Kim et al. (2008) was chosen as the effort most closely resembling the scope of this project; the material used, SCC, the information gathered, and the goal of his study most resembled that of this investigation. With the intention of being able to draw parallels, use similar findings, or simply fill in additional data points, the specimen details were initially based on the work from Kim et al. (2008). So, specimens were cast to conform to the dimensions as shown in **Figure 6.14**. The specimens were cast horizontally, on their sides. The specimens were cast with a groove cast not only along the shear interface, but also through one of the end corbel as shown in **Figure 6.15**. The top of the specimens would then be finished by hand with a groove finished into the surface along the shear interface and the end corbel opposite the end corbel with the groove cast into the bottom surface. The continuation of the groove was to facilitate tight clearance tolerances for the precrack load blocks between the specimens and the test apparatus. Also, the portions of formwork protruding into the interior of the member in **Figure 6.15** formed what are being referred to as notches. The notch forms consisted of thin sheet metal cut and

deformed into shape with expansive foam providing a rigid backing; upon form removal, the foam would be slid out of place, the sheet metal was then easily removed, and the remainder of the formwork was stripped away. **Figure 6.16** shows that up to four specimens could be easily cast at a time on the forms created.



Conversion: 1 inch = 25.4 mm

**Figure 6.14 – Initial Specimen Dimensions and Reinforcement**



**Figure 6.15 – Plan of Initial Specimen Form, Showing Cast Groove and Reinforcement Layout**



**Figure 6.16 – Complete Initial Formwork, Up To Four Specimen Cast at a Time**

The casting of specimens was going fine and no major issues were readily identified. Later, when the first trial batches were tested for precrack and push-off data many issues become apparent and ways to remedy them were subsequently utilized.

**6.3.2 Problems Encountered, Proposed Remedies** The issues that arose while testing will all be discussed in the order encountered. The problems essentially consisted of surface finishing, surface mounting, large specimen size, and premature failures during testing. The actions taken to fix the issues will then be described. The final specimen design will then be discussed in the next section.

Casting of the specimens seemed to be going well, although there were some evident issues. Hand finishing the top surface with a smooth groove proved difficult. Minor errors in finishing the grooves could be corrected by using an electric grinder or sandpaper, but this proved somewhat inconsistent as well as very time consuming.

It was also realized from early trial batches that cast in place anchor bolts would be ideal for attaching the mounts necessary to hold the LVDTs in place during testing as described in **Section 6.2.2** above, and the initial formwork provided no such luxury. The other method of attaching the LVDT mounts was by drilling a pilot hole into the concrete surface using a concrete drill bit on a hammer drill, inserting a small plastic anchor (that was usually too large to fit easily into the hole), and finally securing the LVDT mount with a washer and screw placed into the anchor. This process was time consuming and the anchors, shown in **Figure 6.17**, were difficult to achieve anchorage, sometimes pulled out easily, and would become loose if handled much at all. Additionally, the use of a hammer drill invokes questions regarding damage to the surrounding concrete of the untested specimen.



(a) Concrete Drill Bit and Plastic Anchor



(b) Screw, Washers, Mount, and Anchor Layout



(c) Mount Installed, Anchor Expands

**Figure 6.17 – Unsuccessful Drilled Anchor System**

Notice in **Figure 6.15** that the underside of the notch, the side of the notch facing the shear interface, extended perpendicularly from the shear interface. Also, note the placement of the mounts per **Figure 6.3**. Because the LVDTs were placed around the shear interface, and because the mounts were so narrow, it was difficult to position the mounts such that they provided acceptable clearance for the precrack load block, but also allowed measurement of crack opening.

The size of the specimens also was a bit of an issue. The bulky specimens were too large and heavy to be moved and positioned by one researcher. The size also created tight clearance tolerances for the precrack load blocks to fit between the specimen and the test apparatus. The tight clearance for the load blocks also created the potential to damage the fragile strain gages and their wires attached to the test apparatus.

Next, when all of the anchors were finally successfully placed, the LVDTs and strain gages were attached to the DAS, and the trial specimens were ready to be tested, additional problems were encountered. Premature failure occurred away from the intended shear interface. **Figure 6.18(a) – Figure 6.18(c)** shows the three undesirable modes of failure experienced with the first round of trial batches. It was unfortunate that such difficulties were experienced; yet, the underlying issue to each mode of failure was thought to be understood, and subsequent testing of the changed specimens confirmed this belief. The failure modes shown in **Figure 6.18(a)** and **Figure 6.18(b)** were thought to be the result of insufficient reinforcement and/or insufficient reinforcement anchorage or development length; therefore, these failures could be avoided by increasing the amount of reinforcement and by providing anchorage of the reinforcement. The failure shown in **Figure 6.18(c)** was believed to be caused by the unlevel surface of the end corbel as it contacted the spherically seated load block of the Tinius Olsen machine. The uneven loading caused high compressive stresses on one side of the specimen and

essentially caused failure by crushing on the highly stressed face. Luckily, this mode of failure could also be avoided by improving forming techniques, grinding the ends to level, or by casting some form of a cap on the specimen.



(a) Cracking and Downward Movement of End Corbel



(b) Cracking and Rotation of End Corbel

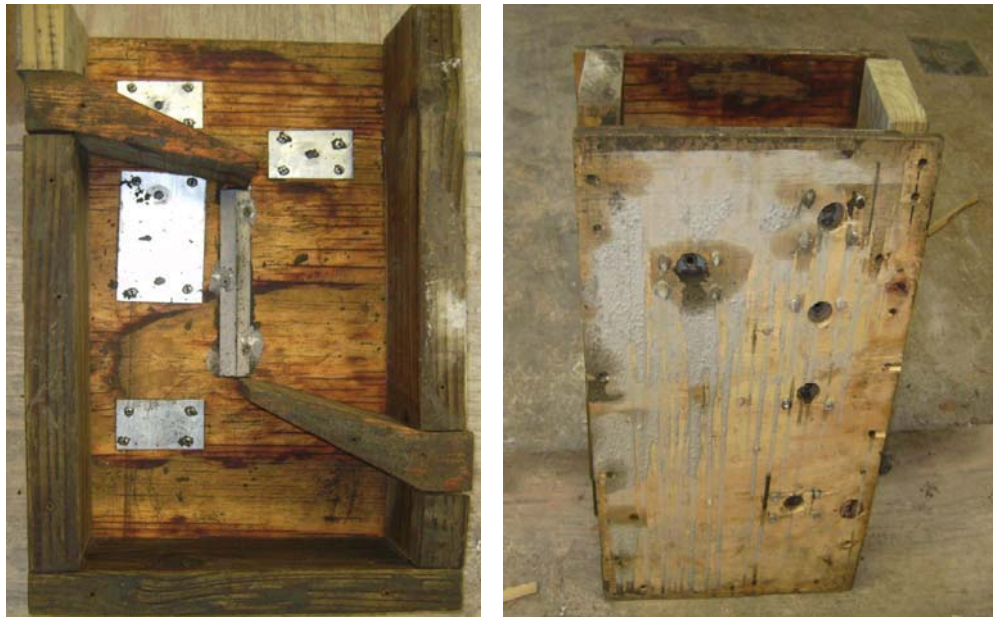


(c) Spalling of Surface on One Side, Followed by Crack Development

**Figure 6.18 – Undesirable Modes of Failure Experienced During Trial Testing**

The difficulties experienced with finishing the specimens, anchoring LVDT mounts, the specimen size, and premature failures have all been discussed. Next, the actions taken to fix the problems are discussed.

Because the list of concerns with the specimen was so long, it was decided that the best thing to do would be to completely redesign the specimens. It was decided to cast the specimens in a vertical fashion so that problems with finishing a grooved surface could be avoided; this fix simultaneously enabled level finishing of the end corbel which would eliminate premature failures during testing of the type shown in **Figure 6.18(c)**. An image of the new form is illustrated in **Figure 6.19**.



(a) Groove, Notch, and Anchor Forms      (b) Cast Upright

**Figure 6.19 – Newly Designed Formwork**

Casting the specimens vertically also corrected an issue which had not been perceived previously; the fidelity between the push-off specimens and beams cast as infrastructure elements. The segregation potential for SCC mixtures is relatively high if batch proportioning and moisture condition measurements of the constituent materials are not properly performed. A beam cast from SCC would be cast in the vertical direction. In a segregating mixture, a disproportionate amount of coarse aggregate would sink below the tension reinforcement, may not contribute as well to aggregate interlock, and would not be included in the area usually used to calculate shear stress,  $b_w \cdot d_v$ , where  $b_w$  is the width of web and  $d_v$  is the shear depth of the member. The vertical casting of the new push-off specimens would allow segregating mixtures to behave as they would for real beams; a disproportionate amount of coarse aggregate could sink below the shear interface and end up in the bottom end corbel. The reduced aggregate in the shear

interface may impact aggregate interlock; the new test specimens would capture this potential.

Since both faces upon which LVDTs were to be mounted were now cast within the new forms, it was possible to include cast in place anchor bolts. **Figure 6.20** shows where a portion of the plywood forms were drilled away, a sheet metal overlay attached, and a hole drilled into the sheet metal so that an anchor bolt could be positioned using a double bolt tightening system. The resulting anchor is shown in **Figure 6.21**. The cast in place anchor bolts not only provided more secure mounting, but also ensured point symmetric positioning of the crack opening LVDTs and consistent mount positioning from test to test.



(a) Inside Forms, Metal Sheet Attached with a Hole Drilled

(b) Outside Forms



(c) Inside Forms, Anchor Attached

(d) Outside Forms

**Figure 6.20 – Anchor Bolt Formwork**

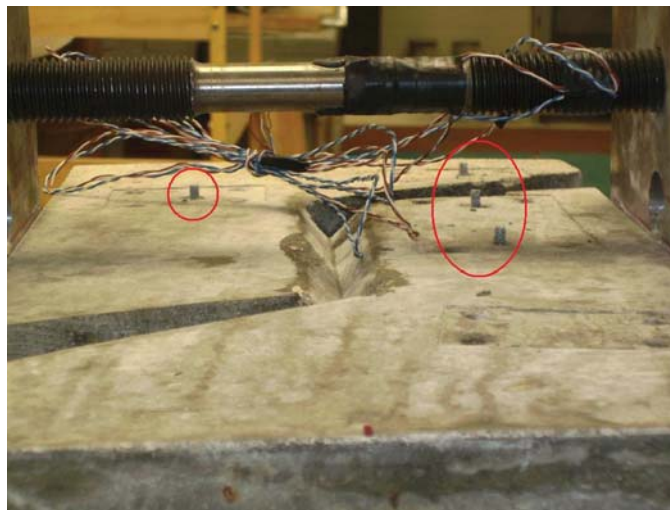


**Figure 6.21 – Resultant Cast in Place Anchors**

It was mentioned above that it was difficult to measure crack opening around the shear interface when the notch protruded perpendicularly from the interface. As can be seen in **Figure 6.19** above, the notches were made to protrude away from the shear interface at an angle; this provided more clear cover for the anchor bolts selected to be put at this position.

Next, it was decided to reduce the size of the specimens. Shrinking the specimens enabled the testing to be performed by one researcher and made the testing much faster. Problems with clearance between the specimen and test apparatus were completely alleviated. The strain gages and wires were damaged less with more tests and the whole test procedure was more resilient. Some readers may raise alarms when changing size. The size effect of shear is a well-documented fact; however, this test results in a comparative assessment of the concrete tested within this study. Because the analysis always consists of comparing one test result from this study to another test result, there is ultimately no concern for size effects. It should also be mentioned that the size of the

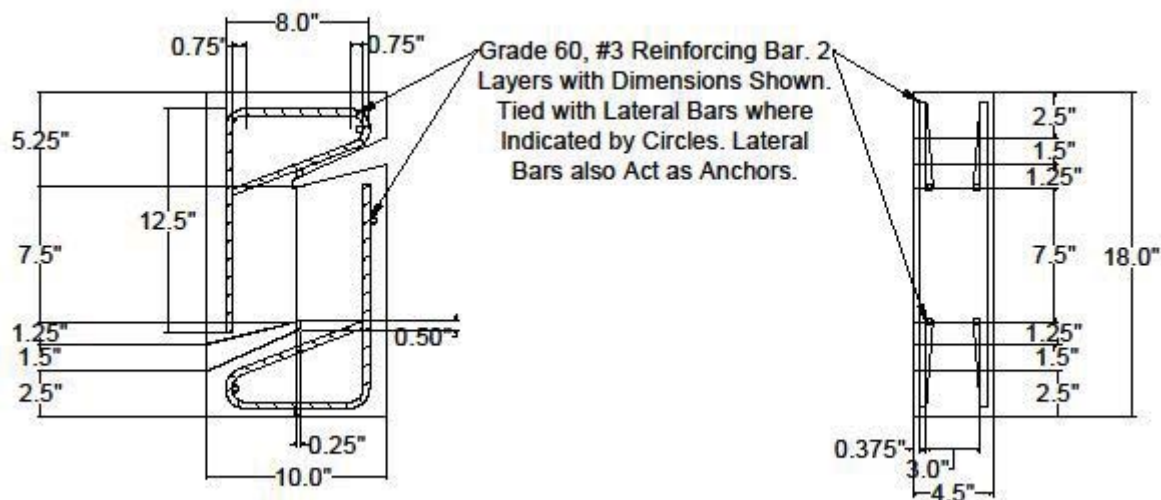
originally designed specimen, and the size of other researcher's push-off tests, may not be very realistically sized when compared to prestressed girders anyway; yet accurate models for shear behavior were determined. So, since this study is essentially comparing conventional concrete aggregate interlock potential to that of varying types of SCC, and because a slightly larger specimen has no more fidelity to beams used in infrastructure, but has proved useful for modeling, it was deemed acceptable to change the size of the test specimens. The new specimen dimensions will be detailed below in **Section 6.3.3**.

Lastly, the reinforcement was increased and the reinforcement was anchored. Reinforcement was doubled over the trial specimens by adding a second bar of the same size. The short corbels did not provide adequate development length, so anchorage was deemed necessary. Improvements in reinforcement detailing eliminated the concern of premature failures of the type shown above in **Figure 6.18(a)** and **Figure 6.18(b)**. The new reinforcement detailing is shown in **Section 6.3.3**.

**6.3.3 Final Design and Fabrication** With all of the previously discussed issues being corrected it is necessary to discuss the resultant test specimens and method of forming them.

The new formwork was shown in **Figure 6.19** above. The exact dimensions of the specimens being created with the new formwork are shown below in **Figure 6.22**. Points are marked and the spacing dimensioned where the cast in place anchor bolts were to be placed. All of the dimensions were selected based on the 3.75 x 7.50 inch (95 x 191 mm) shear interface; all other dimensions were roughly proportioned from the original specimen design so that the various aspect ratios remained similar. The new reinforcement layout is also detailed. Fortunately, the two layers of reinforcement could

be tied together with a lateral piece of reinforcement; this lateral reinforcement acted to consistently space the two layers of rebar as well as acted as an anchor when the rebar was hooked around it.



Conversion: 1 inch = 25.4 mm

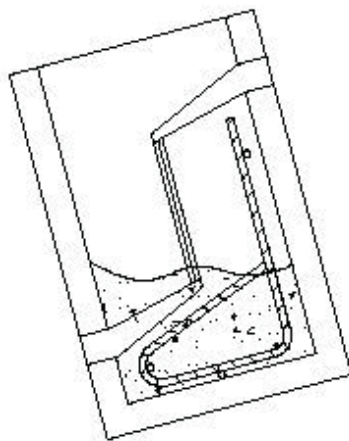
**Figure 6.22 – Final Specimen Dimensions and Reinforcement**

The method of casting the specimens is not as straight forward as for the originally horizontally placed specimens and requires some discussion. The placement technique of the conventional concrete varied from the placement of SCC. Each concrete mixture was placed in three layers; yet, the conventional mixtures were internally vibrated, while the SCC mixtures were not consolidated.

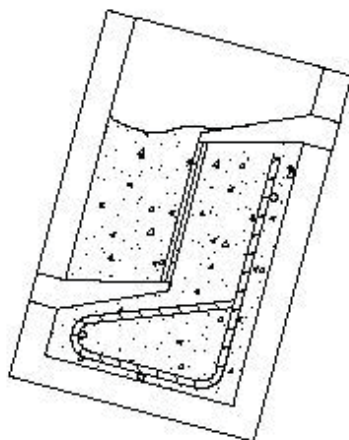
The conventional concrete mixtures were consolidated using vibration because of the inability to properly rod the material. Internal vibration conformed to section 7.4 of ASTM C 192: Standard Practice for Making and Curing Test Specimens in the Laboratory (ASTM C 192 2007). The bottom end corbel was filled and consolidated,

followed by the shear interface, the top rebar cage was inserted, and finally concrete was placed in the top end corbel and consolidated. The top surface was then hand finished with care being taken to ensure a level finish, to avoid the undesirable premature failure during testing shown in **Figure 6.18(c)**.

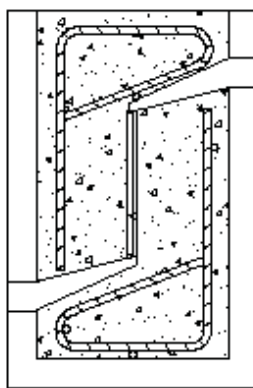
For the SCC mixtures, care was taken not to induce any additional consolidation during placement. **Figure 6.23(a) – Figure 6.23(c)** illustrates the placement technique used for the SCC mixtures. Basically, the bottom end corbel was filled and tilted to allow escape of all entrapped air. The middle, shear interface, section was then filled and tilted the opposite direction to permit entrapped air to escape. The top rebar cage was inserted and SCC was placed into the top end corbel. The top surface was allowed to self-level and was not finished.



(a) Placement in Bottom End Corbel Tilted to Release Entrapped Air



(b) Placement in Middle Section Tilted to Release Entrapped Air



(c) Top Reinforcement and SCC Placement

**Figure 6.23 – SCC Placement Technique into New Formwork**

With this, the specimens have been completely described in their final state. The specimens dimensioned as in **Figure 6.22** and fabricated as in **Figure 6.23** were then ready for testing. The results of the tests performed as described in **Section 6.2** will be presented next, followed by a thorough analysis. The results will be assessed for their import to how SCC behaves in aggregate interlock relative to CC and what this may mean for overall shear behavior of SCC.

## 6.4 TEST RESULTS AND ANALYSIS

The results for the precrack and push-off tests will be shown, discussed, and analyzed. Details of how the data were reduced will be shown for transparency and for the sake of future researchers. The findings and their impact to this and future investigations will be shown. The post-test cross-sectional investigation will also be discussed with the results presented.

**6.4.1 Precrack Results and Analysis** This section presents the results from the precrack tests that precede the push-off shear tests. The section focuses on showing the results, correlating the precrack results to material and test variables, and also on how the results can be used for future researchers.

First, **Tables 6.1(a-f)** show the averaged results for the maximum load and crack opening achieved when precracking the specimens and show the mechanical test results with the associated concrete mixtures. Notice the low coefficient of variation for the compressive strength tests, which is common. Also, note that the crack opening and precrack load variation is of a similar magnitude as the splitting tensile test results.

**Table 6.1 – Mechanical and Pre-Crack Properties**

Conversion: 1000 psi = 6.89 MPa

(a) 6 ksi (41.4 MPa) target strength limestone

		*S6-36L	S6-48L	*S6-60L	C6-58L
Compressive Strength, $f_c$	Avg. (psi)	10,770	8140	9400	7600
	Std. Dev. (psi)	224	159	310	233
	COV (%)	2.1	2.0	3.3	3.1
Splitting Tensile Strength, T	Avg. (psi)	580	460	570	370
	Std. Dev. (psi)	43	112	58	57
	COV (%)	7.4	24.4	10.2	15.4
Precrack Load, P	Avg. (lb)	23,990	26,590	29,190	25,930
	Std. Dev. (lb)	1210	3510	100	3710
	COV (%)	5.0	13.2	0.3	14.3
Crack Opening, w	Avg. (in)	0.028	0.018	0.047	0.019
	Std. Dev. (in)	0.011	0.003	0.007	0.007
	COV (%)	39.3	16.7	14.9	36.8

\*Indicates the re-batch for earlier poor shear test results discussed above and in section 5

(b) 10 ksi (68.9 MPa) target strength limestone

		S10-36L	S10-48L	S10-60L	C10-58L
Compressive Strength, $f_c$	Avg. (psi)	12,580	13,740	13,880	11,210
	Std. Dev. (psi)	936	382	572	180
	COV (%)	7.4	2.8	4.1	1.6
Splitting Tensile Strength, T	Avg. (psi)	580	760	800	540
	Std. Dev. (psi)	144	71	28	62
	COV (%)	24.8	9.3	3.6	11.5
Precrack Load, P	Avg. (lb)	33,430	28,490	34,560	30,970
	Std. Dev. (lb)	6320	3490	11,260	8270
	COV (%)	18.9	12.2	32.6	26.7
Crack Opening, w	Avg. (in)	0.031	0.036	0.022	0.024
	Std. Dev. (in)	0.008	0.009	0.005	0.003
	COV (%)	25.8	25.0	22.7	12.5

(c) 4 and 9 ksi (27.6 and 62.0 MPa) target strength additional mixtures

		S4-36L	S4-60L	C4-58L	S9-57R
Compressive Strength, $f_c$	Avg. (psi)	5850	5490	6130	9190
	Std. Dev. (psi)	328	171	177	116
	COV (%)	5.6	3.1	2.9	1.3
Splitting Tensile Strength, T	Avg. (psi)	440	380	390	680
	Std. Dev. (psi)	40	22	13	71
	COV (%)	9.1	5.8	3.3	10.4
Precrack Load, P	Avg. (lb)	20,940	17,030	31,110	26,590
	Std. Dev. (lb)	1430	2300	2260	6500
	COV (%)	6.8	13.5	7.3	24.4
Crack Opening, w	Avg. (in)	0.021	0.021	0.019	0.016
	Std. Dev. (in)	0.001	0.003	0.001	0.005
	COV (%)	4.8	14.3	5.3	31.3

(d) 6 ksi (41.4 MPa) target strength river gravel

		S6-36R	S6-48R	S6-60R	C6-58R
Compressive Strength, $f_c$	Avg. (psi)	10,640	10,530	8710	10,750
	Std. Dev. (psi)	453	650	508	300
	COV (%)	4.3	6.2	5.8	2.8
Splitting Tensile Strength, T	Avg. (psi)	720	690	580	680
	Std. Dev. (psi)	69	142	40	105
	COV (%)	9.6	20.5	6.9	15.5
Precrack Load, P	Avg. (lb)	30,640	33,280	31,200	30,150
	Std. Dev. (lb)	2930	3780	7160	8090
	COV (%)	9.6	11.4	22.9	26.8
Crack Opening, w	Avg. (in)	0.025	0.022	0.021	0.024
	Std. Dev. (in)	0.006	0.003	0	0.006
	COV (%)	24.0	13.6	0.0	25.0

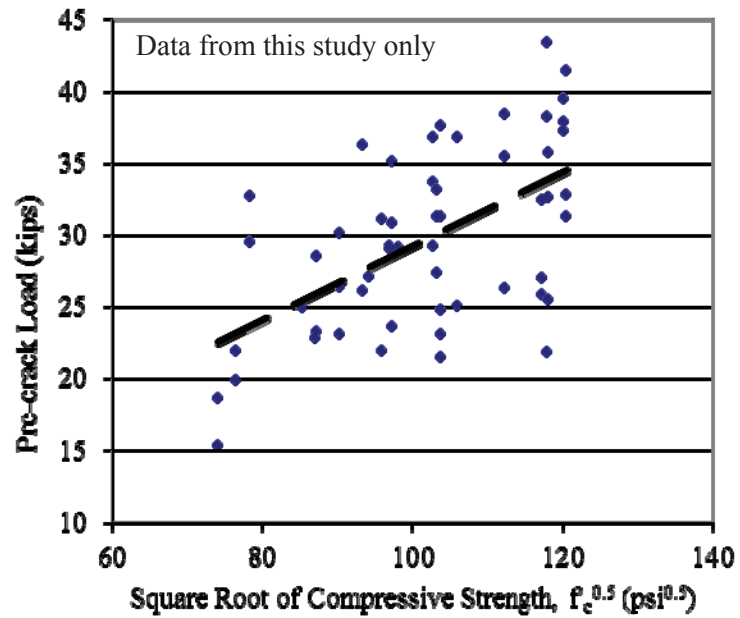
(e) 10 ksi (68.9 MPa) target strength river gravel

		S10-36R	S10-48R	S10-60R	C10-58R
Compressive Strength, $f_c$	Avg. (psi)	14,510	14,420	13,920	9450
	Std. Dev. (psi)	476	386	530	74
	COV (%)	3.3	2.7	3.8	0.8
Splitting Tensile Strength, T	Avg. (psi)	790	730	740	550
	Std. Dev. (psi)	124	68	34	68
	COV (%)	15.7	9.4	4.6	12.4
Precrack Load, P	Avg. (lb)	35,200	38,240	31,320	29,920
	Std. Dev. (lb)	5470	1160	5270	5800
	COV (%)	15.5	3.0	16.8	19.4
Crack Opening, w	Avg. (in)	0.027	0.032	0.021	0.033
	Std. Dev. (in)	0.004	0.008	0.001	0.014
	COV (%)	14.8	25.0	4.8	42.4

(f) Beam companion specimen

		S6-48L	C6-58L	S10-48L	C10-58L
Compressive Strength, $f'_c$	Avg. (psi)	7270	7560	9610	8880
	Std. Dev. (psi)	---	---	---	---
	COV (%)	---	---	---	---
Splitting Tensile Strength, T	Avg. (psi)	---	---	---	---
	Std. Dev. (psi)	---	---	---	---
	COV (%)	---	---	---	---
Precrack Load, P	Avg. (lb)	24,980	22,910	29,170	27,170
	Std. Dev. (lb)	---	---	---	---
	COV (%)	---	---	---	---
Crack Opening, w	Avg. (in)	0.033	0.025	0.020	0.020
	Std. Dev. (in)	---	---	---	---
	COV (%)	---	---	---	---

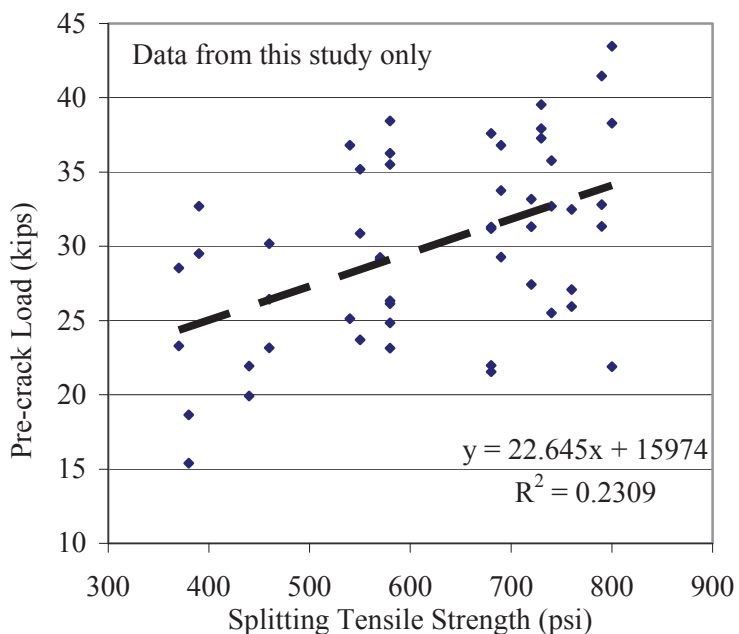
From these test results, several correlations can be shown. As is expected for concrete loaded and failed in all manners of orientation or mode, there is a positive proportionality between the ultimate precrack load achieved and the square root of concrete compressive strength ( $f'_c$ ) as shown in **Figure 6.24**. Notice that the intercept is not set to the origin. A positive y-intercept would imply that a concrete with no strength would still exhibit a precracking load, and this is obviously illogical; yet, a possible explanation exists. By dividing the y-intercept of 3500 lb (15600 N) by the target cross-sectional area of the crack of 3.5 x 7 in. (89 x 178 mm) it is found that the stress resisting cracking with no concrete contribution is about 140 psi (0.96 MPa) which is close to the initial prestressing applied by the confining test apparatus. The average initial prestress was calculated and can be seen in **Figure 6.26** to be close to 140 psi (0.96 MPa).



Conversion: 1000 psi = 6.89 MPa  
 1 lb (force) = 4.45 N

**Figure 6.24 – Increasing Precrack Load with Increased Compressive Strength**

**Figure 6.25** also demonstrates a positive relationship between the ultimate precrack load and the STS of the concrete. Because the precrack specimens are failing due to a similar mechanism as in a STS test, net tension, it makes sense that as a batch proportion improves in STS, it also experiences an increased ultimate precracking load.



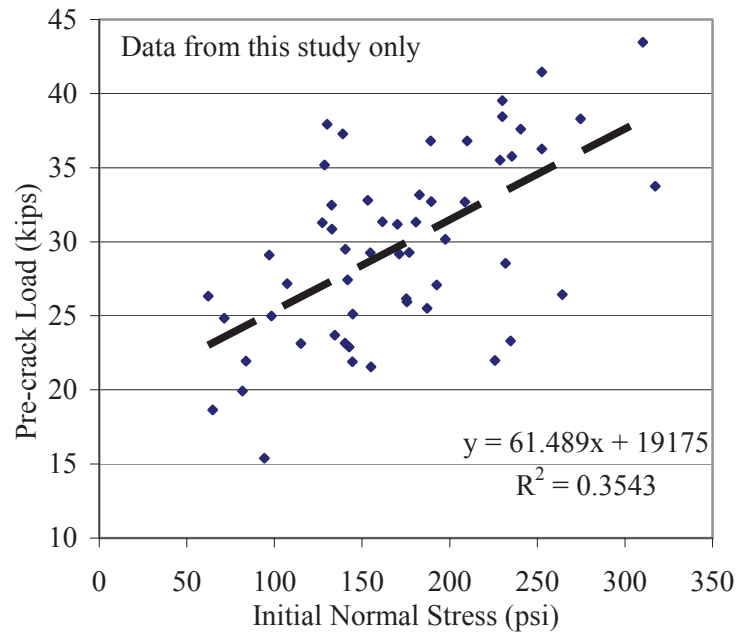
Conversion: 1000 psi = 6.89 MPa  
 1 lb (force) = 4.45 N

**Figure 6.25 – Increasing Precrack Load with Increased STS**

The correlations between maximum precrack load and square root of concrete compressive strength and STS appear relatively weak at a coefficient of determination ( $R^2$ ) of only about 0.33 and 0.23 respectively. The low correlation is typical of all relationships developed from the precrack testing as will be seen. There are numerous and valid reasons for weak relationships in this test. There is an inherent and complex interaction due to the differences associated with the variations in the constituent materials and percentages alone in the test orientation. The material strength inconsistency can be seen in the similarly oriented STS test discussed earlier and which is widely recognized as a reliable test, but with wide variability. Within the precrack and push-off test there is also the added complexity of test variability due to slight changes in

the initial condition from the external restraining frame. These changes in the initial condition will also be reviewed for their impact on the test results.

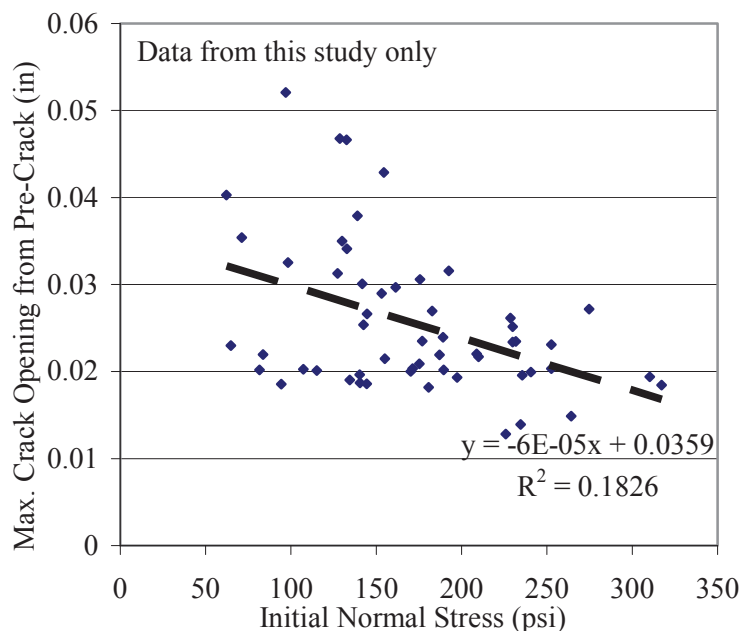
The initial normal stress applied by the externally restraining frame appears to be important in determining both the ultimate precrack load as well as the maximum crack opening, which sets the initial condition for the push-off test to follow. The initial normal stress was controllable to a certain amount of precision by tightening the nuts threaded onto the restraining frame; although, some variability in initial normal stress was inevitable. No previous researchers had advised a target initial normal stress and variation of this stress was examined for test result impact. **Figure 6.26** shows that as the initial normal stress increases, so does the ultimate precrack load; the added confinement acts as a compressive force on the cracking plane that must be overcome before net tension and eventual cracking can occur. Additional insight can also be obtained from this simple plot. Similar to **Figure 6.24** above, there is a positive y-intercept. By eliminating the confinement effect, the average concrete resistance to cracking can be determined. Dividing the y-intercept of **Figure 6.26** by the area yields about 780 psi (5.4 MPa). The average compressive strength was determined to be 10540 psi (72.6 MPa). Normalizing 780 psi (5.4 MPa) by the square root of the average compressive strength yields 7.6, a typical value for the concrete resistance to tensile rupture.



Conversion: 1000 psi = 6.89 MPa  
 1 lb(force) = 4.45 N

**Figure 6.26 – Increasing Precrack Load with Increased Initial Normal Stress**

Increased initial normal stress also acts to decrease the maximum crack width developed from the test as shown in **Figure 6.27**. The specimen engages a stiffer frame when cracking under increased confinement and is thus unable to expand to as large of an opening as when not confined. The level of confinement can be controlled in order to control crack opening.



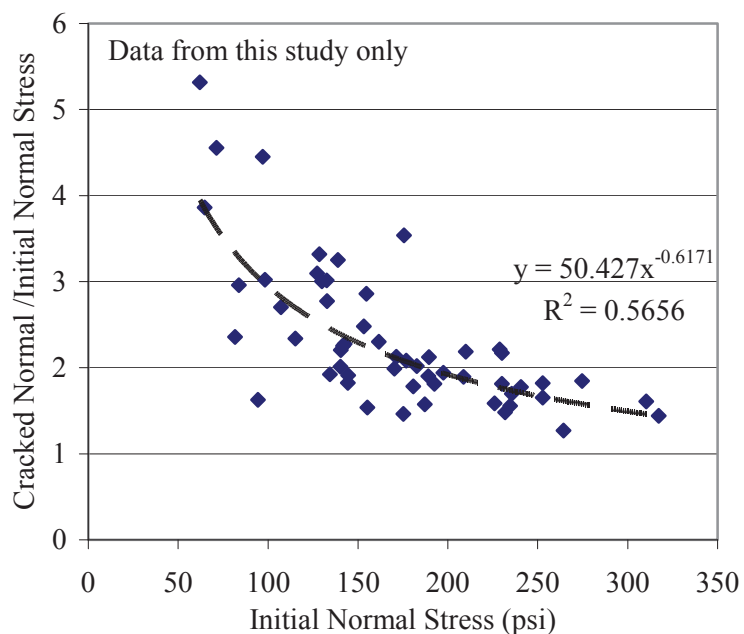
Conversion: 1000 psi = 6.89 MPa  
1 inch = 25.4 mm

**Figure 6.27 – Decreasing Crack Opening with Increased Initial Normal Stress**

So, as discussed earlier, because some of the increase in precrack load can be attributed to increased initial normal stress, as well as increased compressive strength, the coefficients of determination seem falsely low for the direct comparison of only two variables at a time. It is sufficient at this time to assume the relationships shown are valid, and that a multivariable equation could be derived to fully characterize the precracking behavior.

For the use of possible future researchers, another useful relationship is shown.

**Figure 6.28** shows that as the initial normal stress increases, the ratio of the normal stress after the crack develops to the initial normal stress actually decreases.



Conversion: 1000 psi = 6.89 MPa

**Figure 6.28 – Decreasing Stress Ratio with Increased Initial Normal Stress**

The reason researchers could benefit from the relationship shown in **Figure 6.28** is that it shows that increasing the initial normal stress decreases the sudden increase in normal stress caused by cracking of the specimen, and appears to decrease variability of this stress rise. Pairing the results from **Figure 6.27** and **Figure 6.28**, one can conclude that a researcher could achieve smaller crack openings with more consistency by increasing initial confinement; because crack opening sets the initial condition for the push-off test that follows, it is important to control this variable as much as possible.

The precrack test results have been shown for each batch proportion. The precrack results were then correlated to concrete compressive strength, splitting tensile strength, and initial confining normal stress from the test frame, with all showing positive proportionality. The crack opening from the test was then shown to decrease with

increased initial confinement. The specimen was shown to crack more gradually if increased initial confinement was used. The last two relationships can be important for future researchers because together they show that increasing initial normal stress of the test frame decreases crack opening widths and that these smaller crack widths develop more gradually with a greater degree of control. This is important, as other researchers have discussed these tests using small crack widths, some arbitrarily specify smaller than 0.02 inches (0.5 mm), but gave no advice as to what confinement would result in that size of crack width (Kim 2008; Walraven and Reinhardt 1981). One could consistently achieve crack widths smaller than 0.02 in (0.5 mm) using the mixtures and restraining system of this research tightened to an initial normal stress of approximately 300 psi (2.07 MPa) or greater as shown by **Figure 6.27**; this research attained larger crack openings, approximately 0.03 in (0.76 mm) on average. It would be advisable to use increased confinement, and continue the precracking test load until the desired crack opening is achieved, this would produce very consistent crack openings to be used for the initial condition of the push-off test.

**6.4.2 Push-Off Results and Analysis** After the precracking test established the initial crack condition of the shear specimens, the push-off test was performed. The push-off test setup and procedure has been described; although, some discussion of how the raw data collected were formatted and reduced to a consistent and useful form is justified because no previous researchers addressed exactly how their data were analyzed. The data formatting procedure will be detailed. The push-off test results and an analysis of the results will be shown.

As discussed previously, the data collected during push-off testing consisted of the shear loading applied by the testing machine, the normal stress developed in the external test frame bars due to crack dilation and deformation, and the crack slip and opening as measured by LVDTs attached parallel and perpendicular to the cracked plane respectively. All of this data was being collected over each of the roughly five minute push-off tests. The data collection frequency was two points per second; this frequency balanced the collection of too much data with gathering enough data to show high resolution of the results and could have been increased to generate more points during rapid deformation.

The shear load applied by the machine was zeroed before the initialization of load and therefore the applied and effective shear loads are considered equivalent. The strain gages attached to the test frame bars, from which the normal stress was computed, were set to zero strain on the DAS when no stress was applied; therefore, any time the test frame was attached to the specimens (even at the beginning of testing) there was some normal stress, and this was considered the effective normal stress. The crack opening and slip were not considered zero at the beginning of push-off testing. When shear load was applied to the specimen, the crack would actually slip very little (about 0.005 – 0.010 inches [0.127 – 0.254 mm]), and close slightly before dilating; the minimum crack width, or the point at which the crack began to re-open was considered the zero point for crack opening and crack slip. The “zero” crack opening is demonstrated in **Figure 6.29** as the shear stress, and consequently the normal stress, is increased during loading. This “initial” crack condition is important for the remainder of the crack analysis because it normalizes the crack condition between specimens. As shown in the previous section, the

pre-cracks may have been larger for some specimens than for others and the push-off crack closing magnitude would vary in proportion to the pre-crack opening; this can lead to inconsistencies in determining the slip to opening relationship.

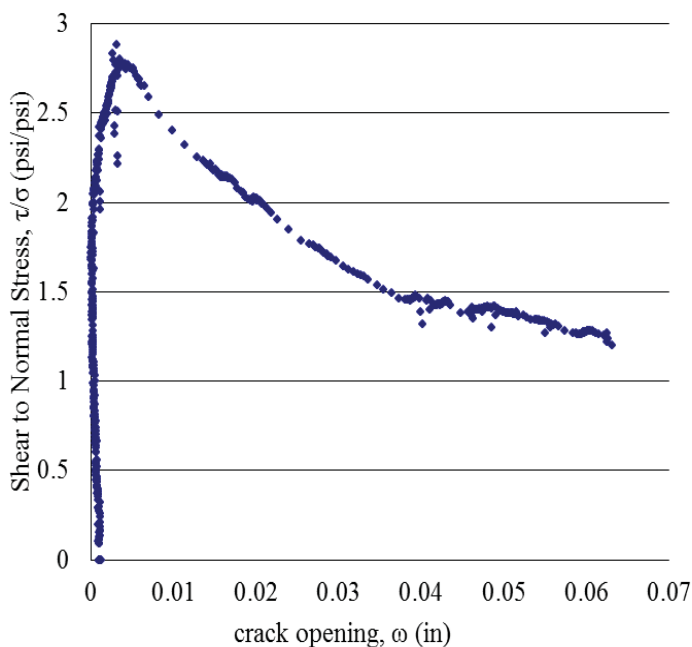


**Figure 6.29 – Determining “Zero” Crack Opening**

Another relationship being demonstrated by **Figure 6.29** is that shear stress is developed at a different rate than normal stress with respect to crack opening (and therefore also crack slip). **Figure 6.30** and **Figure 6.31** demonstrate the difference in shear and normal stress development as the specimen deforms. Notice that there is an initial normal stress, but not an initial shear stress because of the way the test is performed. Notice also that the applied load is in shear and thus the shear stresses develop at a higher rate than the indirectly induced normal stresses caused by crack

dilation and specimen deformation. The normal stresses do not begin to increase until an adequate amount of shear stress is applied to cause crack dilation and deformation, the maximum shear stress to normal stress ratio will indicate the capability of that particular concrete batch proportion to resist shear stress. The shear to normal stress ratio is also dependent upon crack opening as shown in **Figure 6.29**; this was theorized by Walraven (1981) and demonstrated by Walraven and Reinhardt (1981) due to aggregate contact areas. The shear to normal stress ratio will be discussed further below when the test results for each mixture are shown and analyzed.

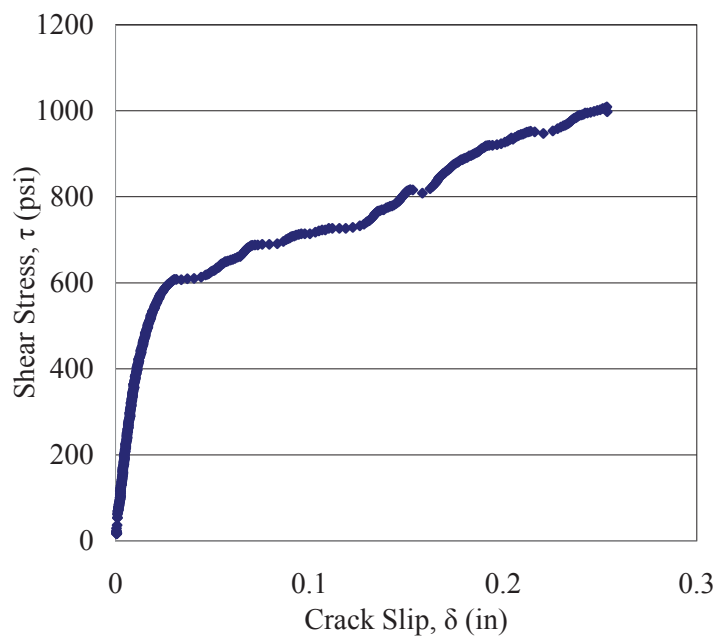


**Figure 6.30 – Shear Stress Development over Crack Slip Range**

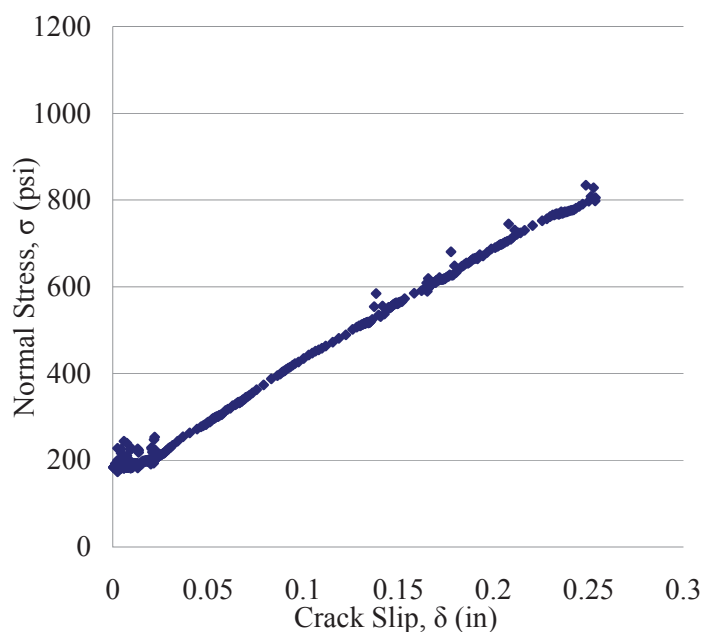


**Figure 6.31 – Normal Stress Development over Crack Slip Range**

As mentioned, the ratio of shear to normal stress indicates a mixture's ability to resist shear, this resistance changes with crack opening; however, a plot such as **Figure 6.29** does not include information about the crack slip. Recent researchers have proposed and used a method of normalizing the shear to normal stress ratio up to a given slip known as the slip limit,  $\delta'$  (Barragan 2006; Kim 2008). The normalized value is known as an E-value and is used to describe the mixture's ability to resist shear in aggregate interlock. The E-value at a given slip limit is found from determining the area under the curves of **Figures 6.30 – 6.31** and dividing the prior by the latter. The equation for E-value would then be given by **Equations 6.1 – 6.3** below. The E-value over the whole range of slip limits for the example data set shown is demonstrated in **Figure 6.32** below.

$$E(\delta') = \frac{V_{Eq}(\delta')}{N_{Eq}(\delta')} \quad (6.1)$$

Where the equivalent shear and normal stresses ( $V_{Eq}$  and  $N_{Eq}$  respectively) are given by:

$$V_{Eq}(\delta') = \frac{\int_0^{\delta'} \tau(\delta) d\delta}{\delta'} \quad (6.2)$$

$$N_{Eq}(\delta') = \frac{\int_0^{\delta'} \sigma(\delta) d\delta}{\delta'} \quad (6.3)$$

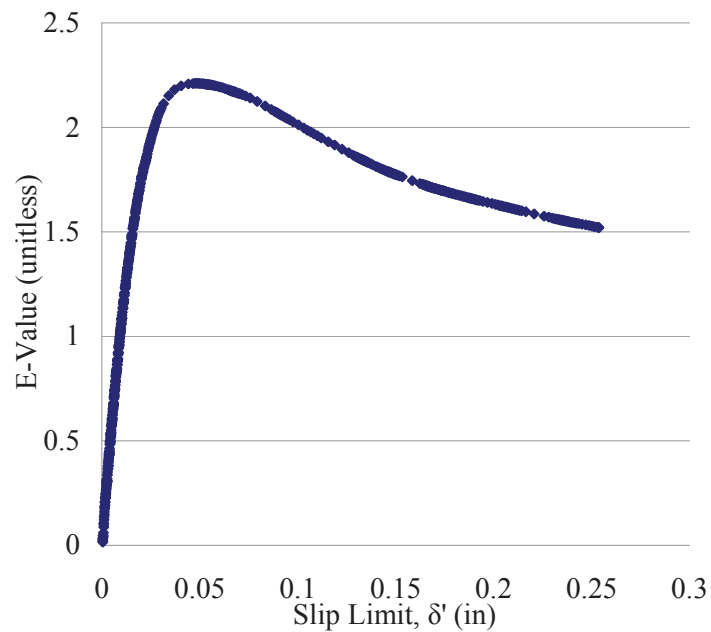


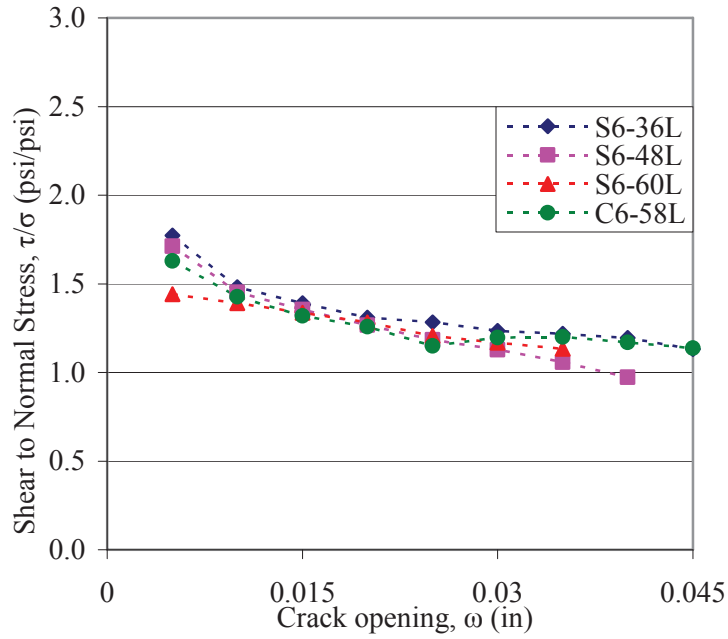
**Figure 6.32 – E-value over Full Range of Slip Limits**

The E-value at a given slip limit is then essentially an averaged shear to normal stress ratio over the entire slip range rather than an instantaneous shear to normal stress at that given slip.

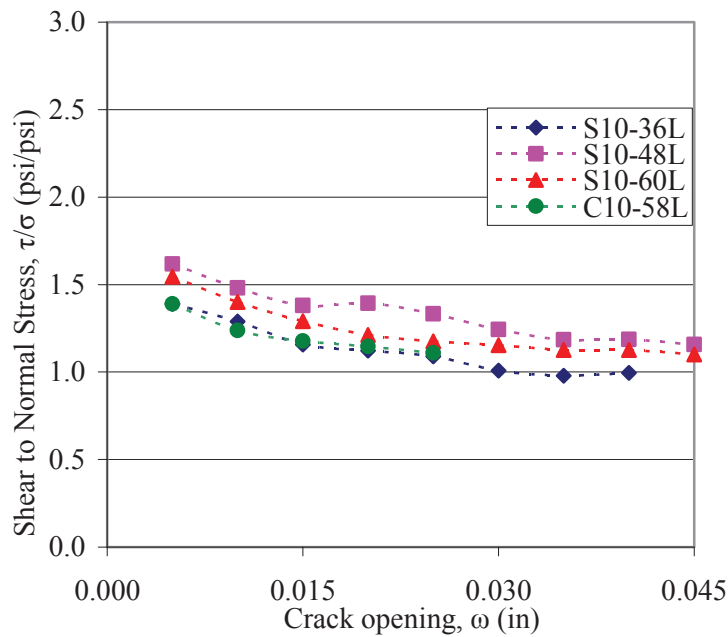
This E-value could be a useful and powerful tool for comparative analysis; still, this should be investigated further. Other researchers have relied heavily on the E-value to perform comparative assessments, but there may be variables, such as the initial normal stress, that may require control to avoid impacting results (Kim 2008). For instance, if **Figure 6.31** had an increased initial normal stress, this researcher suspects it would require greater slips for the curve in **Figure 6.30** to overcome that normal stress, and the peak of **Figure 6.32** would thus be translated to the right. The E-value peak would likely be more rounded and of smaller magnitude. In order for researchers to rely so heavily on the E-value, they should have investigated sensitivity to test variability, and explained that all variables were controlled and to what level; though, this was not done. Because this researcher did not control the initial normal stress at the beginning of push-off test, nor know to what level or extent previous researchers controlled this or similar variables, such a thorough E-value analysis will not be performed. The E-value has been computed, the results will be shown, and trends can be identified; yet, a detailed analysis is unjustified and not shown.

The shear to normal stress ratio ( $\tau/\sigma$ ) across crack opening relationship as demonstrated in **Figure 6.29** was replicated for all tested concrete batch proportions. The point shown for each of the plots in **Figure 6.33** represent the average of at least two test results. For some mixtures tested, the crack did not open the full viewable range of 0.045 inches (1.14 mm). There may be a relatively large stress ratio change or termination of

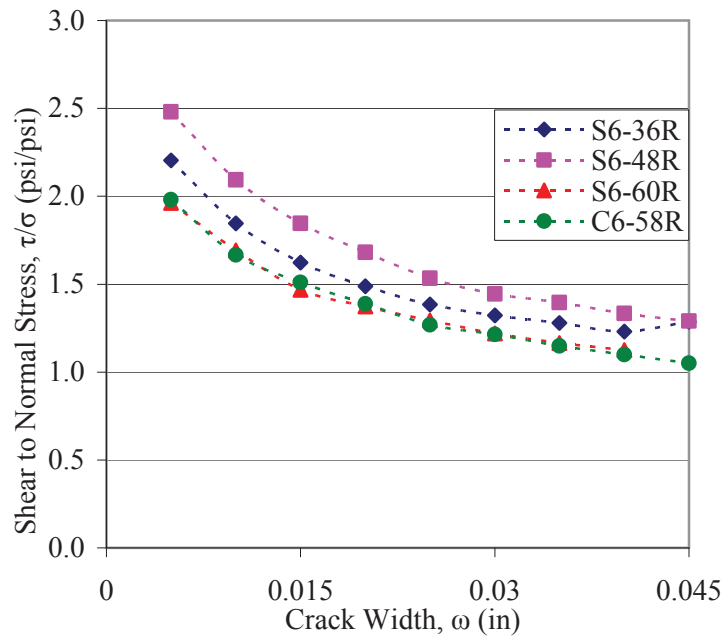
plotted points when one or more tests terminated without reaching large crack openings for a given batch proportion.



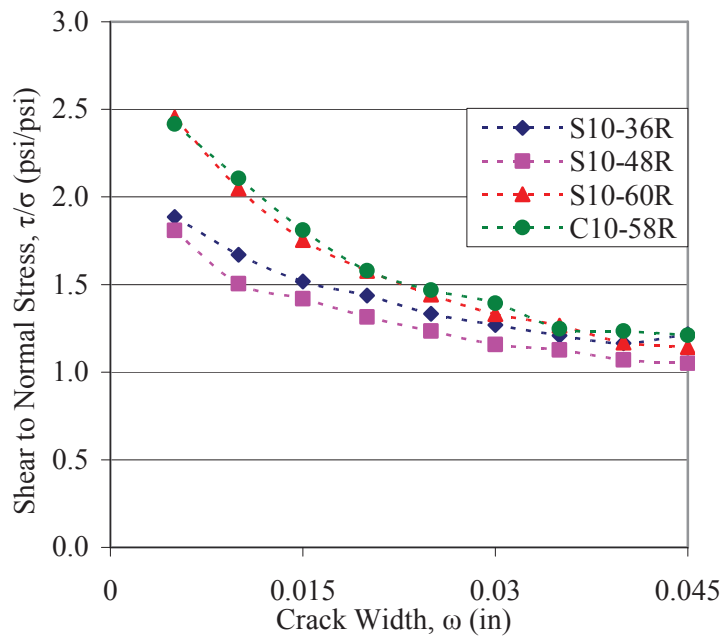
(a) 6 ksi (41.4 MPa) target strength limestone mixtures



(b) 10 ksi (68.9 MPa) target strength limestone mixtures



(c) 6 ksi (41.4 MPa) target strength river gravel mixtures

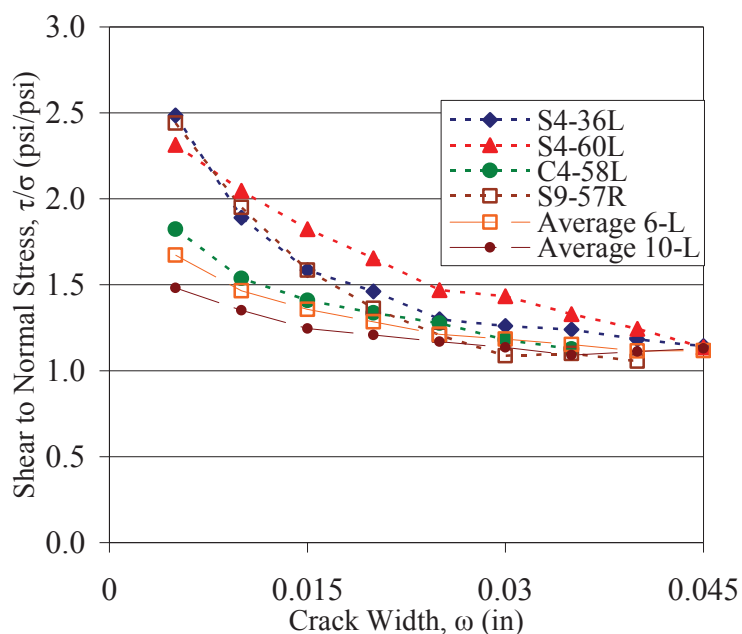


(d) 10 ksi (68.9 MPa) target strength river gravel mixtures

Conversion: 1 inch = 25.4 mm

**Figure 6.33 – Shear to Normal Stress Ratio vs. Crack Opening**

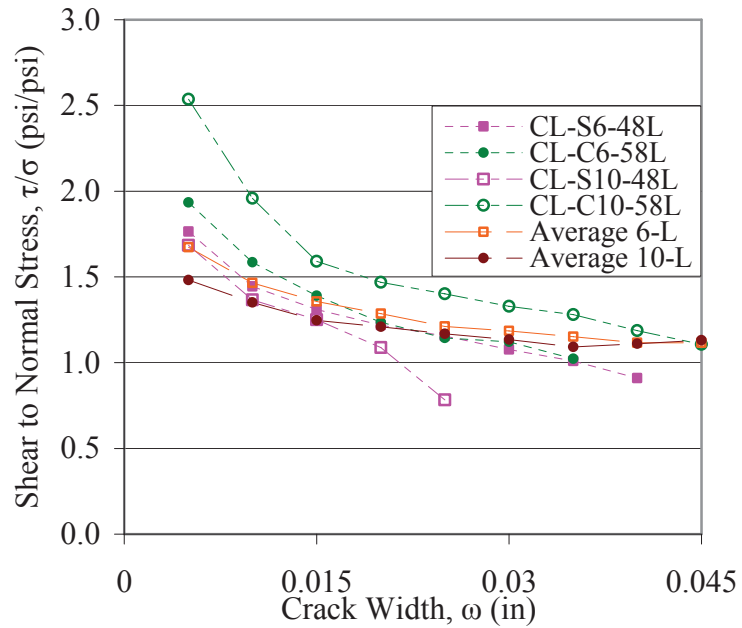
From the four basic strength and aggregate batch proportion groups represented in **Figure 6.33** trends were identified. Between plots (a) to (b) and to a lesser extent between (c) to (d) there seems to be a reduction of shear stress capacity when increasing compressive strength. This appears to be marginal for the batch proportions shown; however, recall that the 6 ksi (41.4 MPa) target strengths were much higher than anticipated, so the strength variation from the “low” to “high” strength mixtures may be slight. **Figure 6.34** shows the additional mixtures tested along with the average limestone batch proportions; because the 4 ksi (27.6 MPa) target strength mixtures actually maintained lower strengths, they really did exhibit a much improved shear to normal stress ratio at small crack widths indicating greater relative shear resistance.



Conversion: 1 inch = 25.4 mm

**Figure 6.34 – Reduced Compressive Strength Improves Relative Shear Resistance**

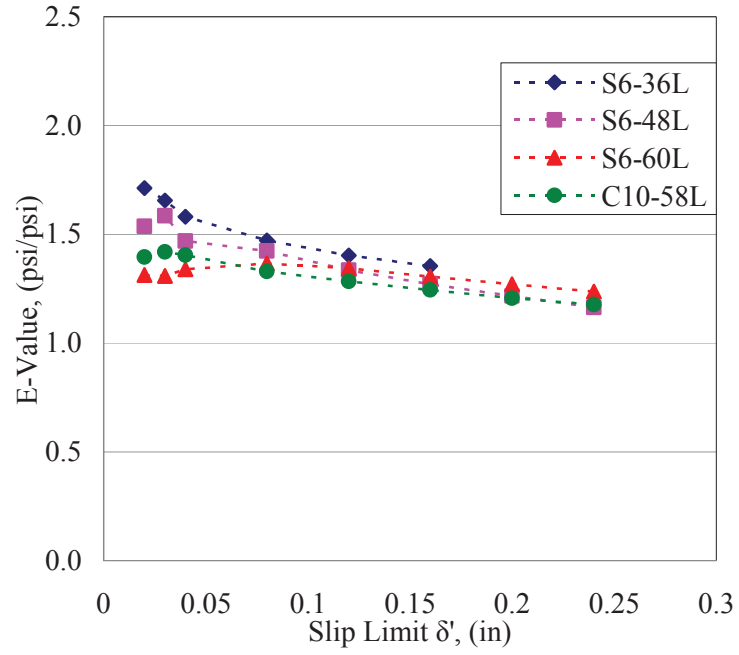
The plots in **Figure 6.33** also show two more trends. When comparing plots (a) and (b) to (c) and (d) there is an obvious improvement in the shear capacity of the river gravel over the limestone mixtures. The improved shear strength of the river gravel mixtures is due to the fact that the aggregate are harder and therefore fractures less along the cracked plane than the limestone. The river gravel mixtures demonstrate the improved shear resistance through openings of about 0.03 in (0.8 mm), with diminishing effects thereafter. Lastly, the final trend identified is that there seems to be no distinction of the shear capacity for CC and SCC mixtures of the same strength and aggregate type investigated within this study. Each of the plots in **Figure 6.33** show tightly bunched data points between all mixtures of the same strength and aggregate type; additionally, the aggregate fraction that appears to resist shear most efficiently for one mixture does not necessarily demonstrate that efficiency for all strength levels or aggregate types. **Figure 6.35** below shows how the shear beam companion specimens cast at Coreslab Structures Inc. compare to the average of all mixtures of the same target strength level tested. Note that there was only one shear beam companion specimen of each batch proportion. From the plot, the average 6 ksi (41.4 MPa) target strength mixtures tested performed very similar to both the 6 ksi (41.4 MPa) CC and SCC companion specimens cast at Coreslab Structures Inc. The 10 ksi (68.9 MPa) CC companion specimen performed better than average; whereas, the SCC companion specimen performed worse than average. The apparently poor performance of the SCC cast at Coreslab Structures, Inc. should not be scrutinized too harshly considering it was produced from a single test specimen.



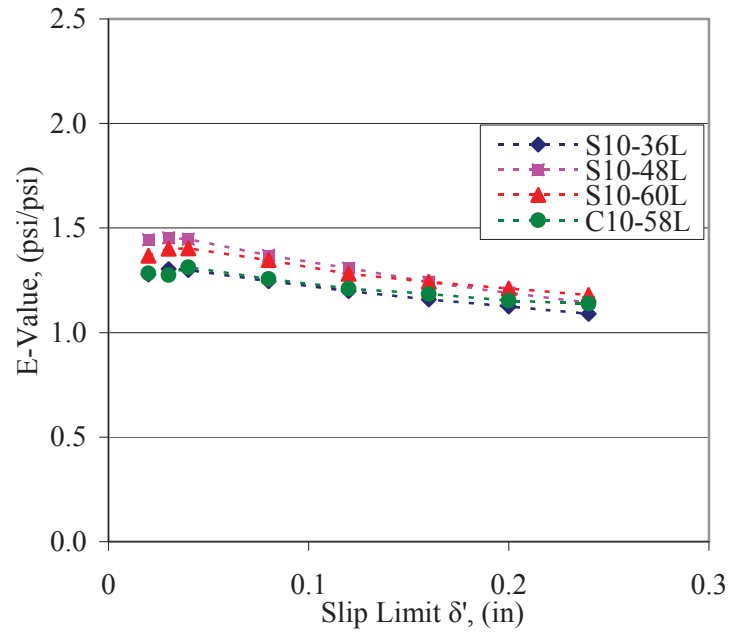
Conversion: 1 inch = 25.4 mm

**Figure 6.35 – Performance of Specimens Cast at Coreslab Structures, Inc.**

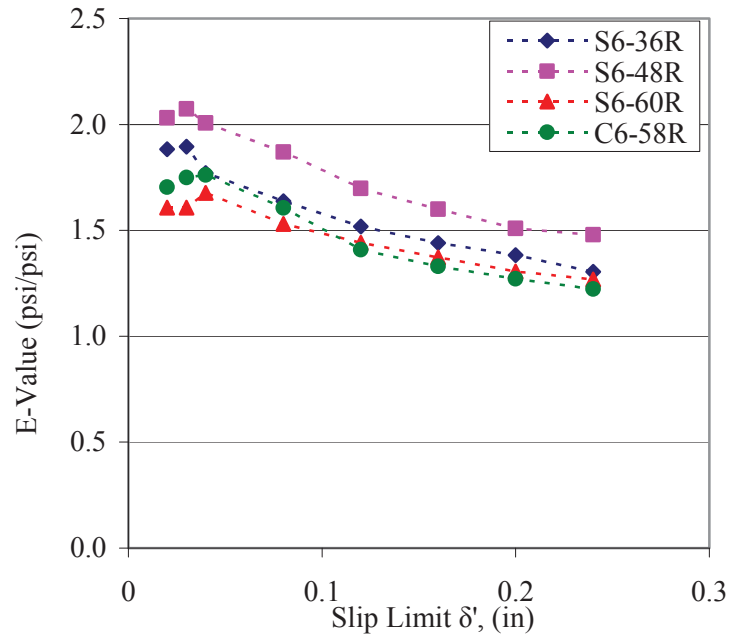
These same relationships can be identified in plots of the E-values over various values of slip limits,  $\delta^*$ . The four basic batch proportion groups can be reviewed in **Figure 6.36**. Recognize that the same trends identified are still present, but over a range of slip limits, not crack width openings. The strength of the mixture seems to have a small impact, the aggregate type appears to have the largest implication, and the C.A. percentage seems to have little influence on the ability of the mixture to resist shear.



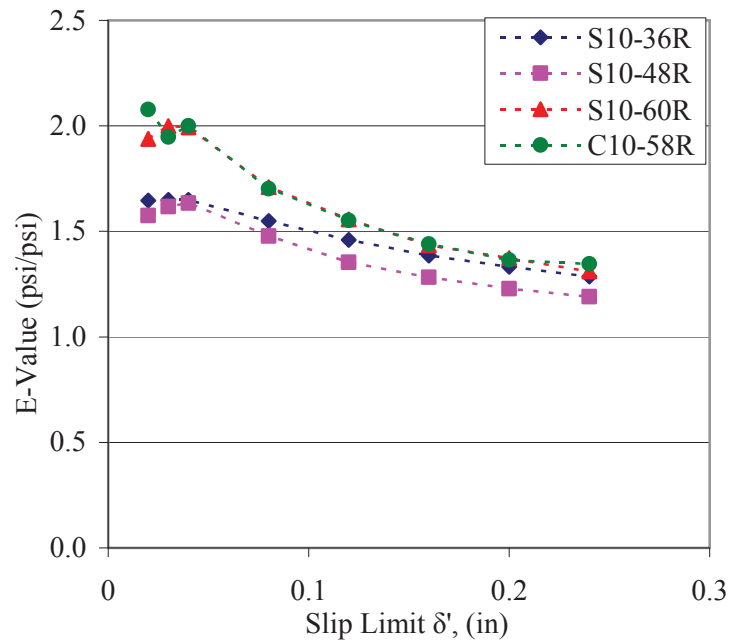
(a) 6 ksi (41.4 MPa) target strength limestone mixtures



(b) 10 ksi (68.9 MPa) target strength limestone mixtures



(c) 6 ksi (41.4 MPa) target strength river gravel mixtures

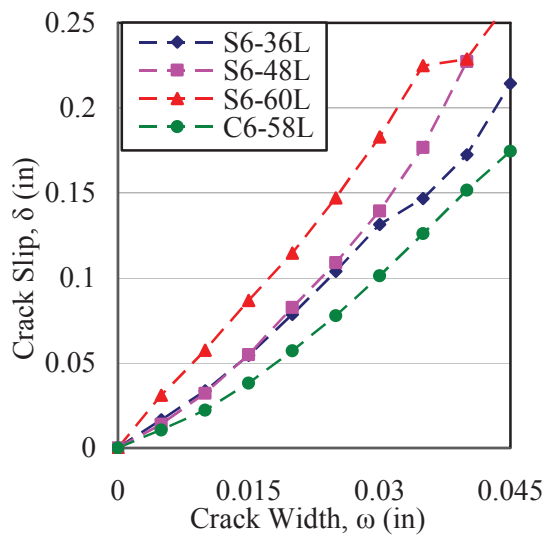


(d) 10 ksi (68.9 MPa) target strength river gravel mixtures

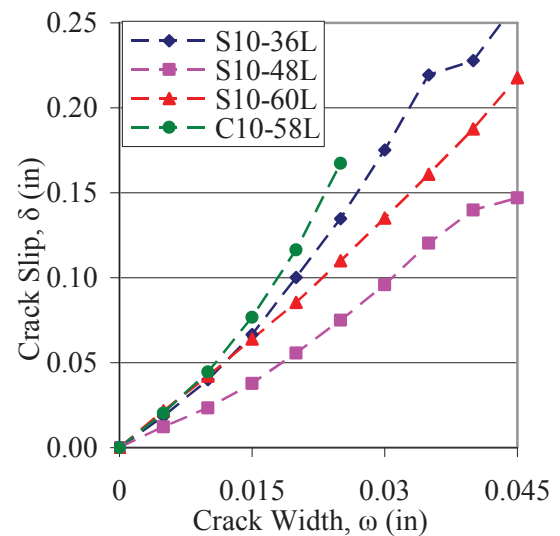
Conversion: 1 inch = 25.4 mm

**Figure 6.36 – E-value across Slip Limit Range**

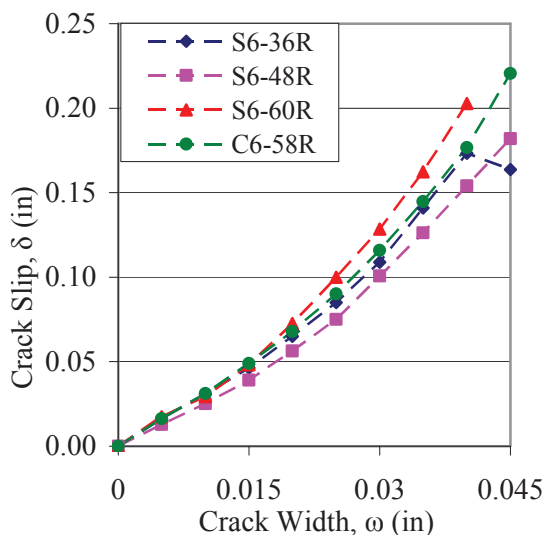
Next, the push-off tests can be used to examine the slip to width relationship. Returning to the theory explained by Walraven, as a crack opens during shear, it also slips. If the roughness of the cracked interface is reduced, there is less resistance to slip for the same amount of crack opening. Thus, if two separate concrete batch proportions are compared and one exhibits increased slip at the same crack opening, it can be concluded that it has a decreased roughness profile. The decreased roughness might be caused by less aggregate, smaller aggregate, more fractures within the aggregate along the crack, or a more finely graded aggregate (Walraven 1981). Because the crack slip to width relationship can convey so much information about the mechanism of aggregate interlock, the test results will be shown and discussed. **Figure 6.37** shows the crack slip to width relationships for the four basic mixtures tested.



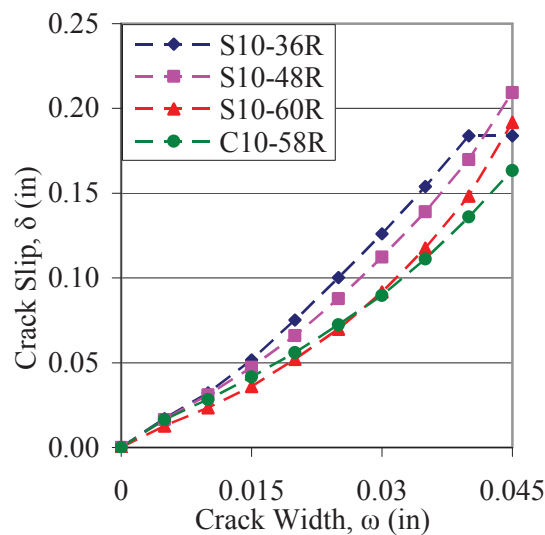
(a) 6 ksi (41.4 MPa) limestone



(b) 10 ksi (68.9 MPa) limestone



(c) 6 ksi (41.4 MPa) river gravel

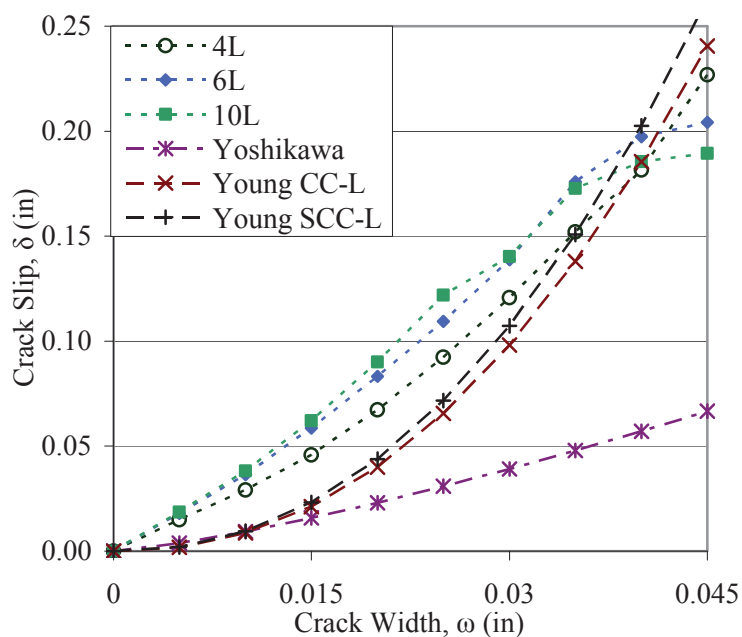


(d) 10 ksi (68.9 MPa) river gravel

Conversion: 1 inch = 25.4 mm

**Figure 6.37 – Crack Slip to Opening Relationship**

From the results shown in **Figure 6.37**, the largest factor governing the slip to width relationship appears to be aggregate type; the crack slip at a crack opening of 0.045 inches (1.14 mm) of limestone mixtures is about 0.25 inches (6.4 mm) as compared to the reduced 0.20 inches (5.1 mm) of the river gravel batch proportions. When comparing all plots, there doesn't seem to be a significant difference between SCC or CC mixtures or between batch proportions of varying C.A. percentage. When comparing the plots of (a) to (b) or (c) to (d) there is little difference between the curves due to strength. **Figure 6.38** shows the averaged results for each strength level of the limestone mixtures and compares them against the averaged limestone results determined by Kim et al. and the river gravel curve developed by Yoshikawa (Kim et al. 2008; Yoshikawa 1989).

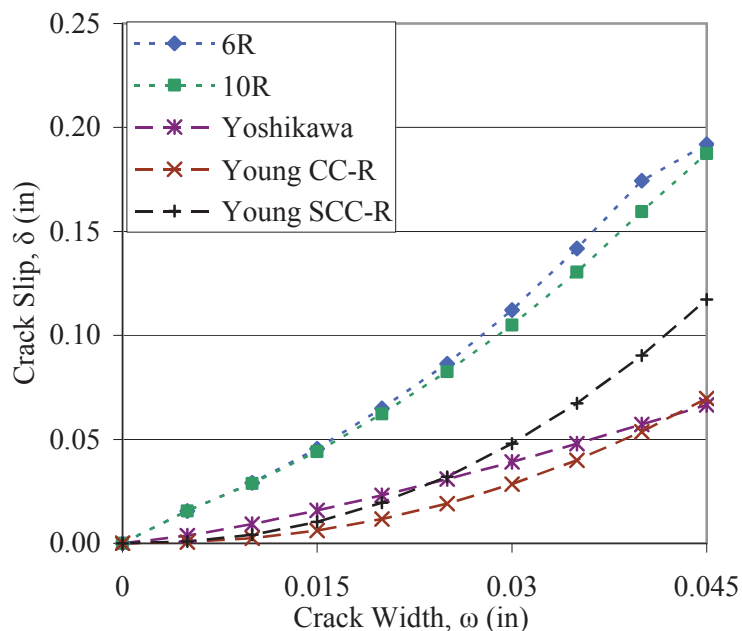


Conversion: 1 inch = 25.4 mm

**Figure 6.38 – Limestone Mixtures Tested Compared to Previous Researchers**

See that the 4 ksi (27.6 MPa) target strength mixture had improved slip resistance at given widths over the higher strength limestone mixtures tested. One can see that the limestone used in this study may have been weaker than that used by Kim et al. because it has more slip at given widths for all strengths tested. See also that all limestone mixtures performed poorly compared to the river gravel mixture tested by Yoshikawa; this is explained by the fact that limestone is generally weaker than river gravel and would therefore have more fractures along the cracked plane and an overall reduced roughness.

**Figure 6.39** shows the averaged results for each strength level of the river gravel mixtures and compares them against the averaged river gravel results determined by Kim et al. (2008) and by Yoshikawa (1989).



Conversion: 1 inch = 25.4 mm

**Figure 6.39 – River Gravel Mixtures Tested Compared to Previous Researchers**

The 6 and 10 ksi (41.4 and 68.9 MPa) target strength river gravel mixtures tested in this project exhibited very similar crack slip to opening behavior. The performance when compared to the river gravel mixtures tested by Kim et al. and Yoshikawa is not as good. The river gravel mixtures tested had a decreased roughness profile and increased rate of progressive aggregate fracture when compared to the other researchers. The inferior performance of the mixtures tested could result from possibly weaker river gravel than what was used by the other researchers, increased concrete compressive strengths which increases aggregate fractures along cracked planes, or both working together. It is still readily evident that the river gravel mixtures performed better than the limestone mixtures of this study.

The push-off test data analysis methodology has been described and thoroughly detailed. It was shown through use of an example specimen how the datum or “zero” point was set for the crack opening and slip from the raw data. Representative shear stress to crack slip and normal stress to crack slip plots were shown. The E-value, used extensively by other researchers was determined for the sample results. The means of determining the E-value by graphical and calculable methods was described. The shear to normal stress ratio was examined over a range of crack openings for all concrete batch proportions tested in this study.

The results demonstrate that concrete type (CC or SCC) and C.A. % makes little difference to the aggregate interlock capability of the concrete batch proportions tested. The strength of the concrete has a noticeable effect, but most dramatically when examining the 4 ksi (27.6 MPa) limestone mixtures in relation to the other higher strength limestone mixtures. Reduced compressive concrete strength improves the relative shear resistance. The strength effect seen in this study is reasonably minimal because the 6 ksi (41.4 MPa) target strength mixtures actually achieved much higher strengths of about 8 - 10 ksi (55.1 – 68.9 MPa). Other researchers have found that the aggregate interlock mechanism of shear resistance diminishes with increased concrete compressive strength, the effect is essentially ignored at strengths above 10 ksi (68.9 MPa) (Bentz et al. 2006; Kim 2008; Walraven and Stroband 1994). This was the whole reason a 4 ksi (27.6 MPa) mixture was developed and tested, so that strength effects could be investigated. Next, the effect of aggregate type appeared to be the most dramatic. The weak nature of Missouri limestone and the improved strength of river gravel led to improved shear resistance of all river gravel mixtures over all limestone concrete batch proportions.

The E-value was discussed in detail. The extensive use of the E-value by other researchers as an analytical tool was called into question. The E-value can be used as a comparative tool and perhaps an analytical one if all variables are controlled and conveyed sufficiently. This researcher examined the E-values and made similar conclusions as from the shear to normal stress over crack opening investigation. No additional analysis was performed as it was considered unjustifiable.

Next, the crack slip to opening relationships were shown and discussed. It was shown that as a mixture exhibited less slip at a given crack width, it demonstrated improved shear resistance. Improved shear resistance results from greater crack profile roughness and reduced propagation of aggregate fracture. An initially rough cracked plane will have less slip than an initially smooth cracked plane. A mixture containing easily fractured aggregate will have increased rates of slip as compared to a mixture containing hard aggregate that resist shear at all crack widths.

The results of the push-off test confirm theoretical relationships between strength and shear capacity, and aggregate strength or fracture along cracks and shear capacity. The effect of concrete type between SCC and CC and the effect of C.A. percentage was not seen. The variation between specimens of a given batch proportion was large enough that the results from other batch proportions of the same strength and aggregate type could not be differentiated. For some combinations of concrete compressive strength and aggregate type, a given SCC would appear to perform the best, but at other strengths and aggregate types another SCC or the CC would appear the most efficient. From the results, no conclusion can be made about the superiority of SCC or CC. Based upon the material

constituents and batch proportions investigated, there does not appear to be significant variations worthy to suggest the SCC mixes studied would yield reduced shear capacity.

After the push-off tests, the cross-sections of the failed specimens were photographed and investigated for segregation and actual C.A. percentage along the cracked plane. The following section discusses the results from the post-testing forensic sectional investigation.

**6.4.3 Cross-Sectional Imaging Results and Analysis** The NIH software ImageJ was used to analyze the post-failure cross-sections of the precrack and push-off tests. The goal was to examine the cross sections for the actual segregation and actual C.A. percentage as the specimens were cast and across the cracked plane. The process by which the cross-sections were analyzed has already been described in **Section 6.2.2**. The results will now be presented with conclusions drawn.

Because the imaging software was used by isolating the different color intensities present in each cross-section, and because some of the mineralogy present in the limestone aggregate was difficult to accurately distinguish from the surrounding paste matrix, the investigation focuses only on the river gravel specimens. The information chosen to be gathered from the analysis consists of the size and location of particles of interest; in this case the particles represent aggregate. The size threshold was set to gather only information about C.A. or, more precisely, particles with an area in excess of 0.008 in<sup>2</sup> (5.16 mm<sup>2</sup>) or a diameter of about 0.10 in (0.25 mm). The area fraction was determined for the C.A. over the entire cross-section. The X and Y coordinate location of each aggregate within the cross section was also determined. The C.A. area fraction could then be determined and compared to the designed C.A. percentage to see if there were

any large discrepancies as to what was actually cast. The coordinate location of each aggregate could be used to determine segregation in both the vertical direction, the segregation due to gravity and placement method, and in the horizontal direction, segregation due to placement method.

The determination of segregation was based on ASTM C 1610 – 2010: Standard Test Method for Static Segregation of Self-Consolidating Concrete Using Column Technique. The equation from ASTM C 1610 – 10 is shown as equation 6.4, the equation used to determine segregation of the hardened specimens is shown as equation 6.5.

$$S = 2 \left[ \frac{(CA_B - CA_T)}{(CA_B + CA_T)} \right] * 100 \quad (6.4)$$

Where S is segregation percentage,  $CA_B$  and  $CA_T$  are the washed and oven dried C.A. masses of the bottom and top sections of the segregation column.

$$S = 2 \left[ \frac{A_p}{A_T} X_i - \frac{X}{2} \right] * 100 \quad (6.5)$$

Where S is the segregation percentage,  $X_i$  and X are the center of the  $i^{\text{th}}$  particle and the total length respectively, and  $A_p$  and  $A_T$  are the area of the  $i^{\text{th}}$  particle and the total area of all particles respectively. The equation used is computing the mass weighted centroid and comparing it to where the centroid should be expected, half of the length. This was then replicated in the Y-direction.

**Table 6.2** summarized the findings from the segregation analysis. The segregation was investigated in both the vertical and horizontal direction. The horizontal position could be considered the segregation just by placement method and the fact that concrete is non-homogeneous and will inevitably exhibit some spatial variation of the constituent materials. Segregation in the vertical direction could be considered the real segregation that is due to the combination of placement method and gravity, just as would be experienced by any concrete placement.

**Table 6.2 – ImageJ Segregation Results**

Mix	Vertical Segregation, %	Horizontal Segregation, %
S10-36R	14.07	15.99
	6.88	1.70
	20.60	4.29
S10-48R	5.54	0.83
	13.98	1.72
	9.21	1.93
S10-60R	5.51	9.92
	12.84	4.59
	3.19	5.27
C10-58R	2.55	14.87
	4.01	25.33
	5.02	4.97
S6-36R	6.16	8.30
	19.46	18.59
	3.20	6.15
S6-48R	7.68	4.36
	25.67	6.26
	11.34	11.58
S6-60R	10.67	2.32
	10.99	5.20
C6-58R	8.01	2.73
	21.45	3.67
	11.70	1.48
CIP	5.61	9.09
	7.17	5.29
<b>Average</b>	10.51	6.49
<b>CC Average</b>	8.79	8.84

From the results, the segregation of all mixtures is reasonable. The placement segregation (horizontal direction) of the SCC was less than that of the CC, which may be reasonable because less effort is actually used to manually place the SCC. More segregation was seen by the SCC in the vertical direction when compared to the average CC segregation. Although there was more segregation for the SCC batch proportions, it was still reasonably low at an average of only 10.51 percent. SCC is considered robust if it can demonstrate a column segregation of 10 percent, so the average SCC mixture tested was very close to this target.

Next, the actual C.A. percentage present was compared to the C.A. calculated based on batch proportions. Throughout this report, the mixtures have been characterized by their C.A. percentage of total aggregate volume; however, this number no longer applies when examining the C.A. percentage of total hardened concrete volume. The latter, C.A. of total volume percentage is calculated from the batch proportions used. It should be noted that neither the volume of air nor the volume of water should be considered in the total hardened volume presented here either. Because the cross-section of a specimen is being viewed, whatever water or air voids that were present at the time of casting are now being looked through, to whatever paste or aggregate happens to be exist behind it on that specific cracked plane. So, the equation for determining C.A. volume fraction of total hardened volume for comparison to the ImageJ results is given as equation 6.6.

$$C.A._{TotalVolume} = \frac{C.A.}{C.A. + F.A. + Cem. + Ash} \quad (6.6)$$

The C.A. volume fraction of the hardened concrete is then the volume of C.A. divided by the total hardened volume given as the sum of C.A., F.A., cement, and fly ash. **Table 6.3** shows the calculated C.A. volume for each river gravel batch proportion tested, and the average C.A. volume determined by the ImageJ analysis.

**Table 6.3 – Calculated and Actual C.A. Volume Fractions**

Mix	Theoretical C.A. Volume, %	Calculated C.A. Volume, %	Percent Variation
S10-36R	26.06	24.44	6.21
S10-48R	34.74	35.30	1.60
S10-60R	43.43	58.71	35.18
C10-58R	41.98	40.37	3.85
S6-36R	29.44	29.03	1.41
S6-48R	39.25	38.90	0.88
S6-60R	49.06	47.87	2.43
C6-58R	47.43	44.12	6.99
CIP	45.29	36.79	18.77

The results of the ImageJ investigation and the calculated theoretical results are in close agreement meaning the ImageJ analysis was accurate in detecting C.A. particles of interest. The small variation also helps to make the findings discussed previously of **Table 6.2** valid. The S10-60R specimen may have needed additional calibration as there were many more aggregate particles counted than there should have been present; although, this could have actually been the case. Perhaps some segregation occurred prior to casting the push-off specimen and a disproportionate amount of C.A. was actually included in the test specimen.

Overall, the ImageJ results were good for the river gravel mixtures. The software was not able to distinguish some of the limestone aggregate from the surrounding paste

matrix; therefore, the forensic analysis of the limestone batch proportions was not performed. Segregation seemed to be minimal for all river gravel mixtures tested, including SCC mixtures. Because the theoretically calculated C.A. volume percentage matched closely to the results of the ImageJ analysis, the analysis appears to have been accurate and justified.

## **6.5 CONCLUSIONS**

The smaller scale experimental shear test program proved valuable. The precrack and push-off tests were thoroughly described in setting up the test, and what steps were necessary to perform the tests. The specimen design was also discussed. There was a preliminary specimen formwork, dimension, and reinforcement that proved inadequate; the problems encountered, the failure mechanism, and the underlying reason were all discussed. The specimen design was re-written and proved much more reliable for testing. The results from the precrack and push-off tests were shown. The post-failure cross-sectional imaging analysis was described and the results presented. The results for all tests were analyzed.

The precrack test was investigated with greater detail than by previous researchers. Prior studies have conveyed no information about what impact the magnitude of the initial normal stress has on the precrack load or the crack opening. It was determined that for the mixtures tested for this project, the initial normal stress leads to increased precrack loads, but more importantly, it leads to reduced crack opening. Higher initial normal stress also appears to reduce the sudden rise in normal stress after crack development, meaning the opening of the crack is less explosive. These findings

are important for researchers seeking to maintain small crack openings (anything less than 0.02 inches [0.5 mm]). From the concrete batch proportions tested, an initial normal stress of about 350 psi (2.41 MPa) should consistently lead to precrack maximum crack widths of less than 0.02 in (0.5 mm). If the crack opening is less than desired, continued loading will gradually open the crack; this process also allows more control over the crack opening size, leading to superior results. Unfortunately these findings were a result of this research and could not be used throughout the testing. Additionally, there was a correlation between increased precracking load to both STS and the square root of concrete compressive strength; this should be expected since the failure mechanism is similar to that of the STS and because increased compressive strength should also improve tensile strength.

The push-off test results demonstrated valuable relationships. The methodology of analyzing the push-off data was described in greater detail than by previous researchers; this improves the repeatability of this research and allows for more transparent findings. The shear to normal stress ratio across crack width relationship was used to determine which concrete batch proportions demonstrated improved resistance to shear. The plots were grouped by target compressive strength and aggregate type. When examining each plot, it showed a CC mixture and three SCC mixtures of varying C.A. percentage; there seemed to be little impact of C.A. fraction or of concrete type. When comparing the plots, trends were identified. There seemed to be a slight effect due to concrete compressive strength; this was very slight and was investigated further by developing three additional low strength concrete batch proportions. The reason for the very slight difference between the 6 – 10 ksi (41.4 – 68.9 MPa) mixtures was likely because the target strengths

were exceeded by almost all mixture; the actual strengths achieved were in the range of about 9 – 12 ksi (62.0 – 82.7 MPa). Researchers have shown that high strength concrete has reduced shear resistance from aggregate interlock because a larger fraction of the aggregate actually fracture along with the paste matrix. The additional low strength (4 ksi [27.6 MPa] target) mixtures proved to a more noticeable degree that this trend was identified in this study. The largest effect on shear resistance appeared to be aggregate type. There was a clear distinction when comparing the limestone results to those produced by the river gravel mixtures. There was benchmarking to previous studies and some discussion about the E-value used by other researchers. The E-value can be a useful comparative tool, just as what was described by the shear to normal stress ratio; yet, this researcher believes it has been used too exhaustively by other researchers and the reasons for this questioning were outlined. The E-value was shown for the mixtures tested, and the conclusions drawn were the same as those just described. Lastly, the push-off test was used to investigate the crack slip to width relationship. The trends identified are given more substance when examined in this way. It is easily seen that mixtures that performed poorly at resisting shear stress exhibited increased slips and increased slip rates at a given crack opening. This is explained by knowing that a surface that is less rough, a smooth crack, will not be engaged by as much aggregate area at a certain crack opening as compared to a very rough crack with protruding aggregates.

The forensic cross-sectional imaging was then discussed. The segregation seen from the imaging software was small. It was interesting to note that SCC exhibited less segregation than CC in the horizontal direction; this is explained by knowing that SCC is allowed to flow into position whereas CC is manually consolidated, this action actually

disturbs the position of aggregate in the side to side direction. SCC did show more segregation in the vertical direction than CC, but the magnitude was still small, suggesting the mixtures tested were robust and resistant to segregation. The C.A. volumetric percentage of the hardened volume was calculated and compared to that counted by the imaging software. The calculated theoretical C.A. volumetric fraction was close to that determined from the analysis; this confirms that the imaging process was accurate and valid.

The smaller scale shear specimen tests have been performed. The results of the tests have been shown. An analysis of the results have been covered and concluded. The next step is to review the large shear specimen tests performed. For this research project, the large shear specimens are precast, prestressed concrete beams.

## **7. PRECAST, PRESTRESSED BEAM TESTS**

### **7.1 INTRODUCTION**

Precast, prestressed beams were fabricated and tested in shear for this investigation. The four baseline mixtures used throughout this project 6 ksi (41.4 MPa) target strength limestone CC and SCC, and 10 ksi (68.9 MPa) target strength limestone CC and SCC) were tested under four point loading. The beams were tested to evaluate the concrete shear strength prediction equations from ACI, AASHTO, and the MCFT. Crack propagation patterns and deflections during beam loading were also recorded.

This section will detail the beam test setup and procedure. There were issues experienced with the initial test setup; the problems encountered and the actions taken to correct them will be discussed. The beam reinforcement detailing and fabrication procedure will be shown. Next, the beam test results will be given. Lastly, the beam shear test results will be analyzed such that conclusions can be drawn about SCC and the conformity of the material behavior to that of CC at similar strength levels.

### **7.2 TEST SETUP AND PROCEDURE**

Numerous researchers have performed beam tests for shear; however, each test setup and procedure may vary slightly from study to study. This section will discuss the details of the shear beam test setup such as the positioning, load and reaction point locations, and the LVDT positioning to capture deflection. The specific procedural actions taken throughout the shear beam testing will also be discussed.

**7.2.1 Test Setup** The shear beam test was developed such that two shear tests could be performed on each beam. Initially, a three point load test was developed that would put the test region into high shear, but leave the remainder of the beam in relatively low shear and moment so as to avoid damaging the beam where it would be subsequently loaded again for the second test. The initial test setup can be seen in **Figure 7.1** below.

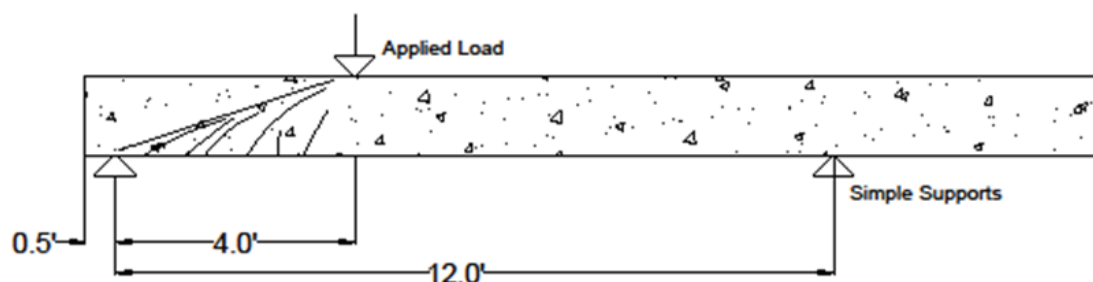


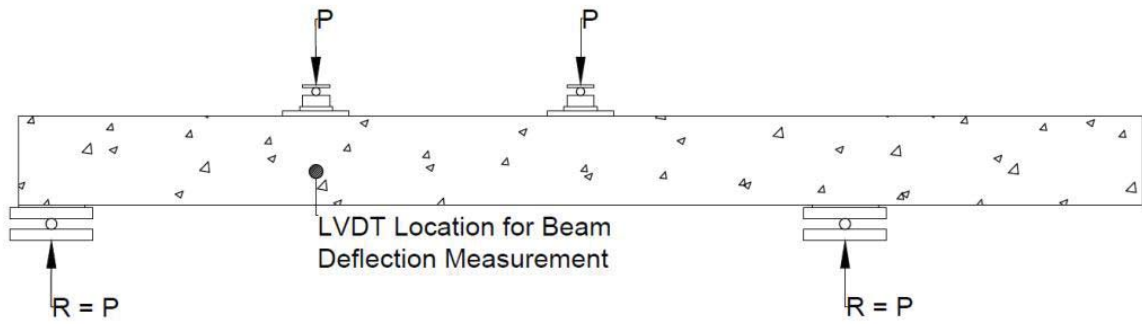
**Figure 7.1 – Initial Three Point Shear Beam Test Setup**

Upon testing of the first beam, it was determined that the three point loading was not effective with the test apparatus in use. **Figure 7.2** shows a picture of the load actuator being used for the testing; it can be seen that with several points of rotation, the load can (and did) become unstable and the apparatus can shift out of position, no longer applying load to the point desired. It should be noted that the beam tested under three point loading did carry enough load initially to develop flexural cracks and even some flexural-shear cracks, but did not fail prior to the apparatus rotating out of position; this disturbed test region was subsequently tested with the new test setup described below.

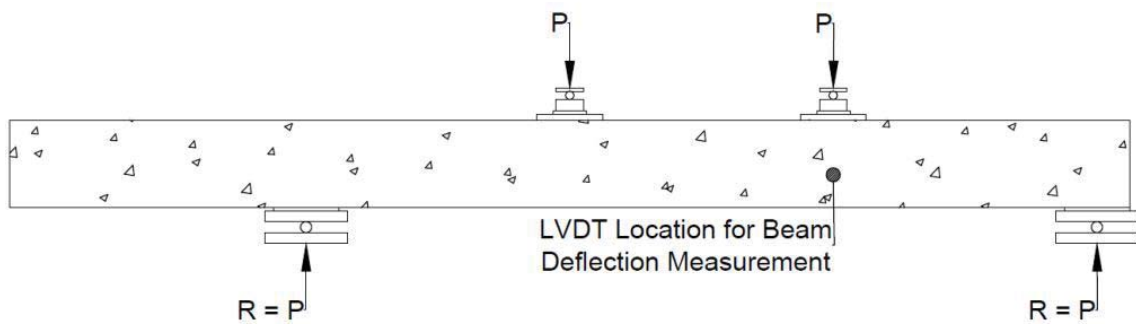


**Figure 7.2 – Load Actuator used for Shear Beam Tests**

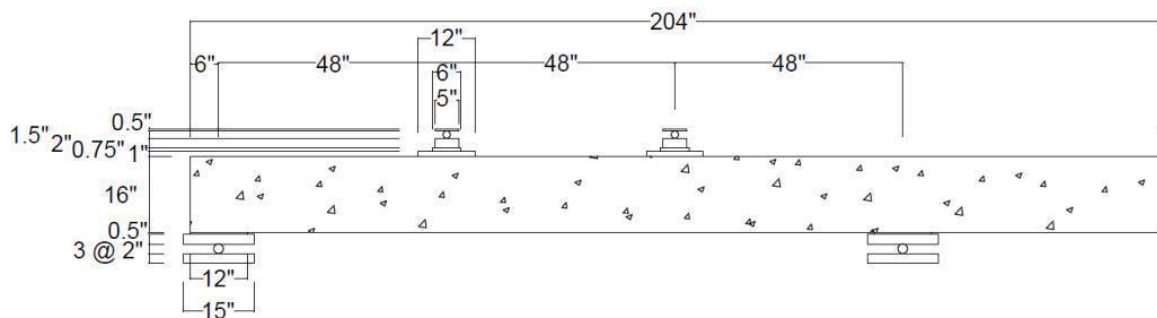
It was determined after the trouble experienced on the first beam tested, to use a four point load test. The shear span on the test region was kept to 4 ft (1.22 m), so the same ultimate load could be expected. The other region of high shear in the first test on a given beam lies outside of the test region of the second test on that beam, so it was determined that each beam could still be used for two tests. There is an influence of the first test on the second, but this will be discussed further below. **Figure 7.3** and **7.4** detail the four point loading test used for all beam tests.



(a) First test on beam



(b) Second test on same beam (moved left 4 ft [1.22 m])

**Figure 7.3 – Four Point Shear Beam Test Setup**

Conversion: 1 inch = 25.4 mm

**Figure 7.4 – Beam Test Dimensions**

An LVDT was attached at the first load point location using a concrete anchor placed well below the compression zone to measure beam deflections during testing; this is also shown in **Figure 7.3**. The LVDT was connected to a data acquisition system where the beam deflection was recorded. The load actuators were also connected to the DAS; actuator deflection and load information was recorded.

The test setup is simple in nature. There were issues with testing the desired three point loading with the test apparatus available; however, four point loading proved to be much more stable and still permitted two tests per beam.

**7.2.2 Test Procedure** The shear beams were tested at varying ages depending on test apparatus availability and when no scheduling conflicts arose; because the lab was busy, the test ages varied widely. Because of the large test age variance, there were also issues with the companion strength cylinders. The strength gain curves and resultant presumed test strength will be shown in **Section 7.4** below.

At the time of testing, each beam was moved into the position detailed above in **Figures 7.3** and **7.4** and the LVDT attached. At the location of the load points, a light dusting of #16 minus sieved sand was leveled below the load blocks so that uniform seating of the load could be accomplished. The load and reaction “points” were positioned into the center of the load and reaction blocks per the ACI 318 – 11 definition of shear span,  $a_v$ , “equal to distance from center of concentrated load to (b) center of support for simply supported members” (ACI 318 2011).

The load actuators were brought into contact with the top of the beam. Each actuator was adjusted such that 100 lb (445 N) of force was detected to seat the load, then the actuators’ displacement datum were set to zero. The test commenced by displacement

control. Each manually initiated displacement step was 0.02 in (0.5 mm) and was reached in 1 minute. Between load steps, propagating cracks were marked to their current terminal lengths and the current load was indicated. At intervals, photographs were taken to help in recording the propagation of cracks. Throughout the test as previously stated, the beam displacement LVDT and actuator displacement and load data were recorded by the DAS. Loading continued in 0.02 in (0.5 mm) intervals until failure was accomplished.

After failure, the actuators were raised to remove the load, the DAS data was saved, and the failure was documented and photographed. The beam was then moved 4 ft (1.22 m) to the west in order to test the second test region on the same beam. After testing the second half of the beam, the beam was removed and discarded. This procedure was repeated for each of the four shear beams.

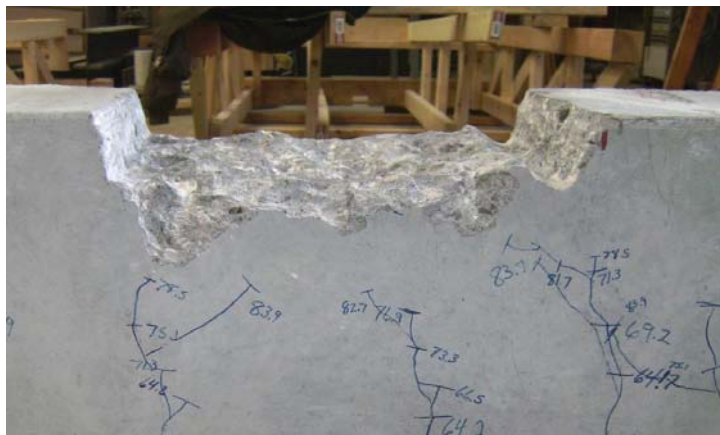
The first beam to be tested (S6-48L) actually failed in flexural crushing during the first four point test performed on that beam. Unfortunately, the crushing occurred near the load point at the midspan of the entire beam; this area would be under high moment in the second test performed on the beam. It was determined that the crushed area should be repaired. This repair was only performed on the S6-48L beam and was positioned away from the second test region such that two test results were still collected.

The procedure for repairing the beam consisted of several steps. The loose concrete cover from the crushed region was removed. The area was chiseled away to ensure that all of the disturbed concrete was removed. The repair area was ground square. It so happened that the repair area lie directly between two lateral ties, so the repair was approximately 12 inches (305 mm) in length and the full 8 inch (203 mm) width of the beam. The surface of the repair area was prepped with a “scrub coat” of Sikatop® 122

plus which achieves an ASTM-C882 modified 28 day bond strength of 2200 psi (15.2 MPa) when used in this fashion, see **Appendix A**. A repair grout was then placed into the repair area, compacted and worked into place, finished, and cured with burlap and plastic sheeting. The repair grout was actually a concrete mixture consisting of the same batch proportions of the beam being prepared (S6-48L), only the coarse aggregate was sieved to include only 0.50 inch (13 mm) minus particles. Twelve 4 x 8 inch (102 x 203 mm) cylinders were also cast and cured in the same fashion next to the repaired beam. The cylinders were used to track strength gain so that beam shear testing could commence when the patch achieved comparable strength to the remainder of the beam. **Figure 7.5** shows the steps taken to repair the previously damaged area of the S6-48L shear beam.



(a) Damaged area chiseled      (b) Hammer drill used to chisel deep into the member



(c) Edges of damaged area were ground square



(d) “Scrub coat” and grout placed, finished (e) Cured under burlap and plastic sheeting

### Figure 7.5 – Shear Beam Repair Procedure

The procedure for testing the shear beams has been described. The precise actions taken throughout the tests were detailed. The unfortunate event of experiencing a crushing failure in the first test region on a beam was described; however, the repair process to enable testing of the second test region on the beam was detailed. Next, the beam reinforcing will be detailed along with the member fabrication process.

### 7.3 MEMBER DESIGN AND FABRICATION

First, the shear beam design methodology will be explained. The difficulty to design a beam to fail in shear, given the constraints imposed by the project funding will be discussed. The resulting member details will be presented. The member fabrication process, which took place at Coreslab Structures, Inc. in Marshall, MO will also be shown.

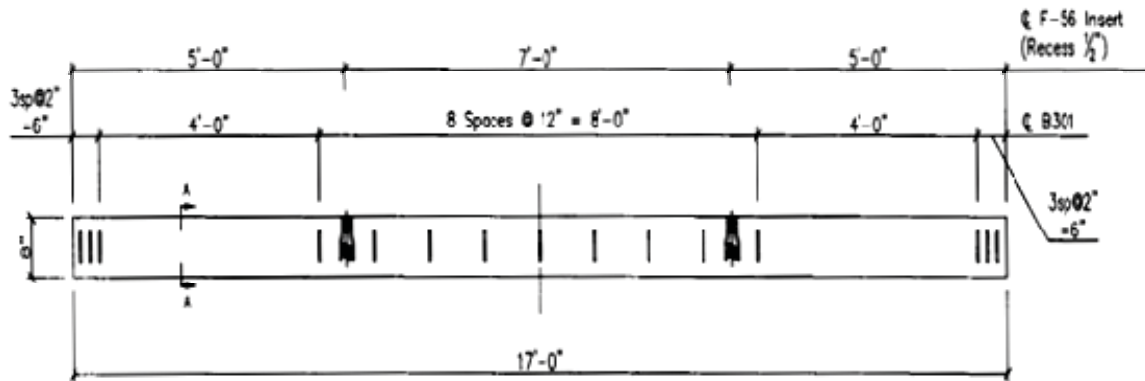
**7.3.1 Member Design** The first and most difficult constraint to overcome when designing the prestressed shear beams was that the cross-section was to be rectangular due to fabrication cost. Next, the beams had to be small enough that the prestressed concrete producer that fabricated the beams for the project could manufacture them for a reasonable cost to the project. The beams were designed against the simple calculations of ACI 318 2011. By using rectangular cross-section beams, the most typically experienced shear failure mode of prestressed beams or girders, what ACI denotes  $V_{cw}$ , is eliminated because the web stresses are not excessively high relative to the rest of the section (ACI 318 2011). The remaining shear failure mode is  $V_{ci}$ , the “nominal shear strength provided by concrete when diagonal cracking results from combined shear and moment” (ACI 318 2011). One can then imagine that it may be difficult to design a beam to fail in shear, when the beam is inherently experiencing simultaneous high moment and given the classically wide variability of shear capacity; that is exactly what was attempted.

In order to develop a reinforcement detail, a Microsoft Excel spreadsheet was developed such that numerous cross-sections with varying concrete dimensions and longitudinal reinforcing patterns could be checked rapidly. A sample spreadsheet beam

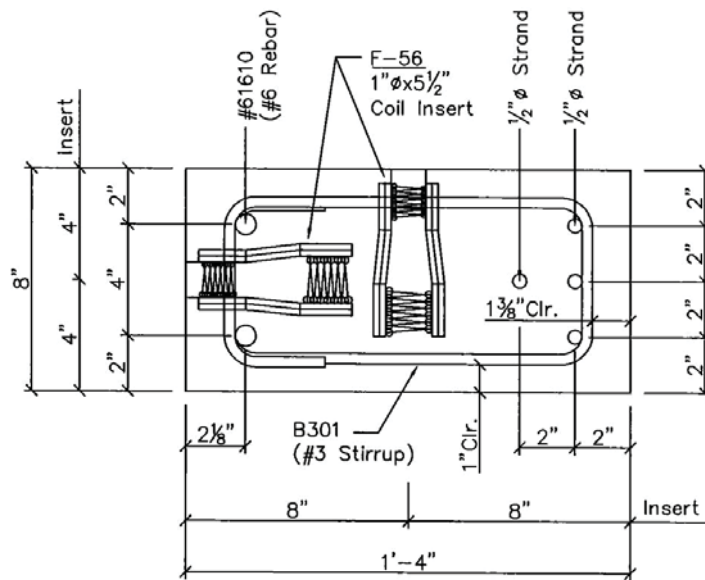
design aid can be viewed in **Appendix D** below. The input equations came from the ACI 318 2011 building code. The fiber stresses were computed in accordance with the “Basic Concept Method” as described by Nawy (Nawy 2010). The computed fiber stresses were checked against transfer stress limits of section 18.4.1 of ACI, top fibers in excess of the stress limit were reinforced with mild rebar (ACI 318 2011). The steel tendons were jacked to 70% of the specified tensile strength ( $f_{pu} = 270 \text{ ksi [1860 MPa]}$ ) to accomplish the fiber stresses desired. The stress in prestressing steel at nominal flexural strength,  $f_{ps}$ , was then computed by equation 18-3 of section 18.7.2 of ACI; this was important in computing the predicted nominal moment (ACI 318 2011). Using basic static equations, the shear that would be present at the predicted nominal moment was determined. Next, the basic shear equation 11-9 of section 11.3.2 ACI was used to predict nominal shear strength provided by concrete. Lastly, the predicted nominal shear strength was compared to the shear present at the predicted nominal moment; this ratio should be less than one to enable a shear mode of failure. It should be noted that a ratio less than one would predict a shear failure occurring before a flexural failure; however, each limit state prediction was made from equations developed empirically with their own ingrained variability, and a ratio below one does not ensure a shear failure. A lower ratio will more likely result in shear failure, so the goal of the analysis is to reduce the ratio while remaining within the constraints set by the code and by the cost of the project.

The resultant member design for the shear beams can be seen in **Figure 7.6** below and was used for all shear beams; the figure comes from the final shop drawings produced by Coreslab Structures, Inc. of Marshal, MO, the precast concrete producer aiding in fabricating the prestressed members for this research project. As shown in

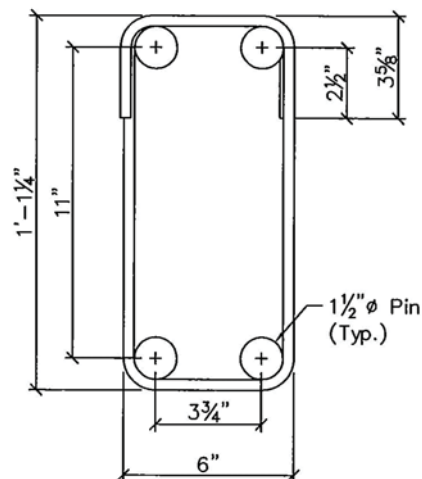
**Figure 7.6**, the beams were actually cast on their side because it was easier for Coreslab Structures, Inc. to produce the formwork for this orientation.



(a) Beam Elevation



(b) Section A-A



(c) Stirrup Detail

Conversion: 1 inch = 25.4 mm  
1 foot = 305 mm

**Figure 7.6 – Shear Beam Details**

The final member design achieved a shear strength capacity to flexural strength capacity ratio of approximately 65-70% with the ACI equations used. The ratio achieved was presumed sufficient to produce shear failure of the test beams; the results are discussed below in **Section 7.4** where it will be seen that this presumption was not entirely accurate.

**7.3.2 Member Fabrication** The precast, prestressed shear beams were fabricated at Coreslab Structures, Inc. in Marshall, MO. The employees at Coreslab Structures, Inc. were very accommodating throughout the entirety of this research project. Coreslab Structures, Inc. participated in the SCC survey discussed in **Section 2**, lent one of their prestressing beds to this research project for four business days and a weekend, and helped fabricate the prestressed members investigated.

Fabricating the precast, prestressed shear beams was accomplished rapidly with the experienced crew at Coreslab. The mild reinforcing ties were placed around the prestressing steel tendons. The steel tendons were then placed in the desired configuration and prestressed to the initial jacking force specified. The formwork was placed and welded. The longitudinal mild reinforcing bars were placed within the lateral ties and suspended from rebar placed across the top of the formwork. The ties were spaced according to **Figure 7.6(a)** above, and tied to the prestressed tendons and the longitudinal mild reinforcement. All of these actions are represented in **Figure 7.7** and were accomplished by the Coreslab Structures, Inc. employees before the research team's arrival at 8:00am.



(a) “Dead end” steel tendons anchored into position



(b) Shear beam end



(c) Shear beam middle section



(d) Full prestressing bed with bond and shear beams in place

### **Figure 7.7 – Reinforcement and Formwork Positioned**

Next, the concrete was batched at the on-site central batching plant. The batch proportions used for forming the beams were the four baseline mixtures described in **Table 3.6**. The concrete was then transported across the worksite in Coreslab's Tuckerbilt T630 off-road concrete hauler. A sample was taken from the Tuckerbilt® for fresh concrete properties testing by the research team. Meanwhile, the Coreslab Structures, Inc. crew placed, consolidated, and finished the bond and shear beams. **Figure 7.8** shows the crew placing the concrete.



**Figure 7.8 – Coreslab Structures, Inc. Crew Places, Consolidates, and Finishes Concrete for Beams**

The following morning, the Coreslab Structures crew stripped the forms. The research team had to then take several hours to instrument the precast bond beams. After instrumentation, the tendons were cut simultaneously. The beams were then stored outside, on site, until it was convenient for the Missouri S&T staff to haul them back to Rolla, MO for final testing. **Figure 7.9** shows the stripped forms and tendons being cut at the time of release.



(a) Forms are stripped



(b) Tendons are cut

**Figure 7.9 – “Release” of Beams**

At this stage, the beams had been designed for shear failure, the reinforcement detailed, the reinforcement placed and tied, the concrete cast, and the members returned to Rolla, MO for testing. The test setup and procedure have been detailed. The actual results of the precast, prestressed shear beams will be presented next.

#### **7.4 TEST RESULTS AND ANALYSIS**

The shear beam results must be presented and discussed. Data was collected for fresh concrete properties, mechanical properties, as well as shear properties for the concrete mixtures used to cast the shear beams.

The fresh concrete properties assessed were consistency, filling ability, passing ability, unit weight, and air content; these properties have been discussed in greater detail in **Section 4.3** above. The fresh concrete property test results are summarized in **Table 7.1** below. The consistency, filling ability, and passing ability were appreciably low for the 10 ksi (68.9 MPa) target strength mixtures; this could be the result of trial batches

being performed on a smaller mixer with presumably tighter quality control. The air content on the 10 ksi (68.9 MPa) target strength mixtures was much higher than the 3% target. The variation of the tested fresh properties from the targets did not impact the results of the shear tests; the high air content will hinder strength gain for the 10 ksi (68.9 MPa) target mixtures, but the effect of strength is conventionally normalized anyway.

**Table 7.1 – Beam Fresh Concrete Properties**

Date of Pour	Mixture	Slump/ Slump Flow (inches)	J-Ring (inches)	Unit Weight (lb/ft <sup>3</sup> )	Air Content
7/21/2011	C6-58L	8.5	---	137.6	6.0%
	S6-48L	28	28	139.2	7.5%
7/25/2011	C10-58L	4.5	---	142.4	6.5%
	S10-48L	22	18	141.6	7.0%

Conversion: 1 inch = 25.4 mm

1 lb/ft<sup>3</sup> = 16.02 kg/m<sup>3</sup>

Compressive strength companion specimens were formed at the time of shear beam fabrication. The compressive strength test results are presented in **Table 7.2** below; the strength development curves for each concrete batch proportion used for beam fabrication are also shown in **Figure 7.10** below. The beams were cast at the same time as the precast, prestressed bond beams tested by another researcher on this project. The other researcher tested the bond beams previous to the shear beams, and broke all strength cylinders before the test date of the shear beams. There were several data points for strength gain, so a good strength development curve was created for each batch proportion; however, no actual strength cylinders remained at the time of shear beam testing. The shortage of test cylinders resulted from bad breaks necessitating additional

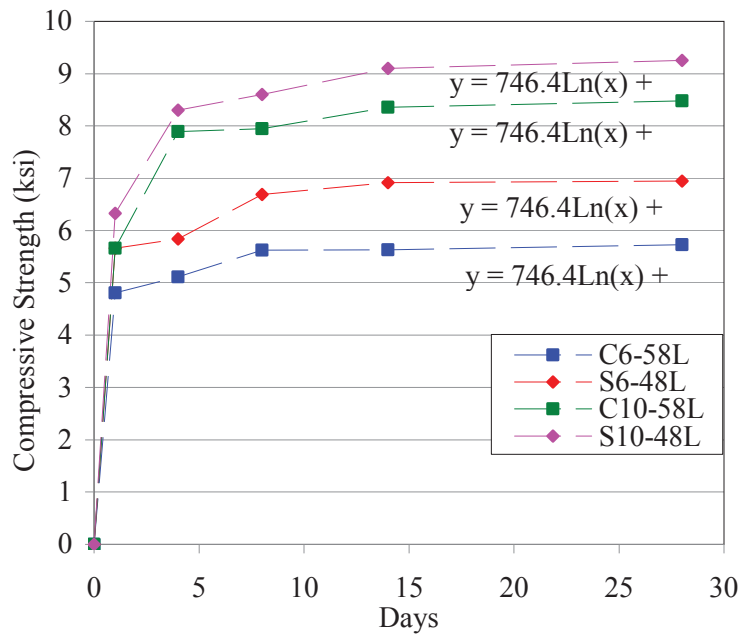
specimen testing at planned ages, as well as the addition of an unplanned 14 day break.

Better coordination with the bond beam researcher would have been desirable.

**Table 7.2 – Tested Beam Companion Compressive Strength Cylinders**

		Test Age (days)				
		1	4	8	14	28
Compressive Strength (psi)	C6-58L	4810	5110	5620	5630	5730
	S6-48L	5660	5840	6690	6910	6950
	C10-58L	5670	7890	7950	8360	8480
	S10-48L	6330	8300	8600	9100	9250

Conversion: 1 lb/in<sup>2</sup> = 6.89 kPa



Conversion: 1000 psi = 1 ksi = 6.89 MPa

**Figure 7.10 – Beam Strength Development Curves**

The logarithmically fitted strength development curves of **Figure 7.10** were extrapolated to determine the compressive strength of each shear beam on the test date. The presumed compressive strength for each beam test is listed below in **Table 7.3**.

**Table 7.3 – Extrapolated Beam Strength at Test Age**

Mixture	Test Age Strength (psi)	
	South End	North End
C6-58L	7560	7570
S6-48L	7270	7490
C10-58L	8880	8880
S10-48L	9610	9620

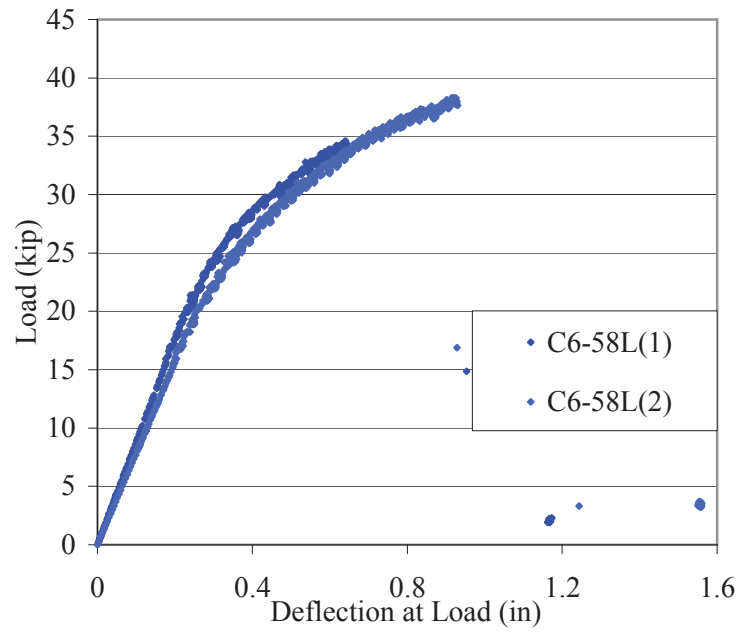
Conversion: 1 lb/in<sup>2</sup> = 6.89 kPa

Next, the shear beam test results can be discussed. **Figure 7.11** below shows the load-deformation curves generated from each of the shear beam tests. Some differences and similarities between the CC and SCC curves are noticed immediately. First, at a given target strength level, the SCC beams tend to have higher ultimate loads paired with increased ultimate deflections over the CC beams. The increase deflections occur past the failure point of the comparison CC beams, similar member stiffness is experienced by all beams up to the point of companion CC beam failure; thus, the similar crack propagation behavior leads to similar member cracked moment of inertia and flexural resistance behavior. Similar behavioral trends such as SCC having increased deflections and increases in failure moment were identified by Kim et. al. (2008).

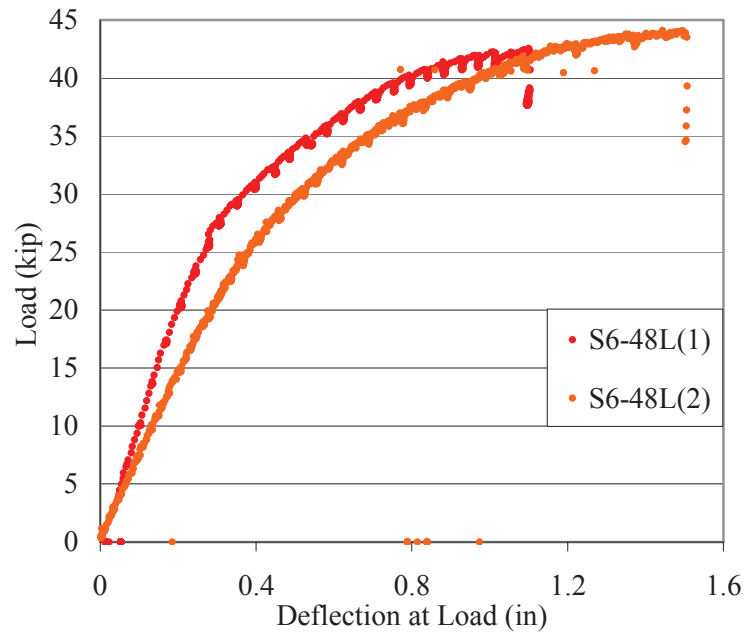
For all beams, the second shear test achieves a higher ultimate load and increased deflection; this is likely due to the effects of the overlapping previously tested region. The shape of the load-deflection curves indicates yielding of the prestressing tendons,

and would cause strain-hardening to develop in the tendons allowing for increase moment carrying capacity. The effects of cracking in the overlapping previously tested region would decrease the effective moment of inertia of the beam, decreasing stiffness, and increasing ductility when compared to an uncracked beam at low stress. The effect of cracking at high moments could increase the effective moment of inertia as compared to a “virgin” specimen due to previous strain hardening effects, or could decrease the stiffness due to increased cracks. Under each situation, the ductility of the secondary test will improve and maximum deflections will increase. The effect of increased ductility is believed to be the cause in the two separate failure modes and drastically different behavior in the two tests performed on the C10-58L beam. Although there is an obvious difference in the behavior of each “virgin” and secondary shear beam tests, both tests provide useful information and should be considered valid. As mentioned, the shape of the load-deflection curves indicates yielding of the prestressing tendons. Shear failures are typically brittle in nature with an elastic rise in load with sudden failure. For the test configuration and member geometry utilized, high moments and flexural stresses were imposed near the point of shear failure. These large bending moments likely lead to yielding of the reinforcement prior to failure. Information such as load-deflection shape, load at first cracking, failure mode, and failure load was collected from all shear beam tests.

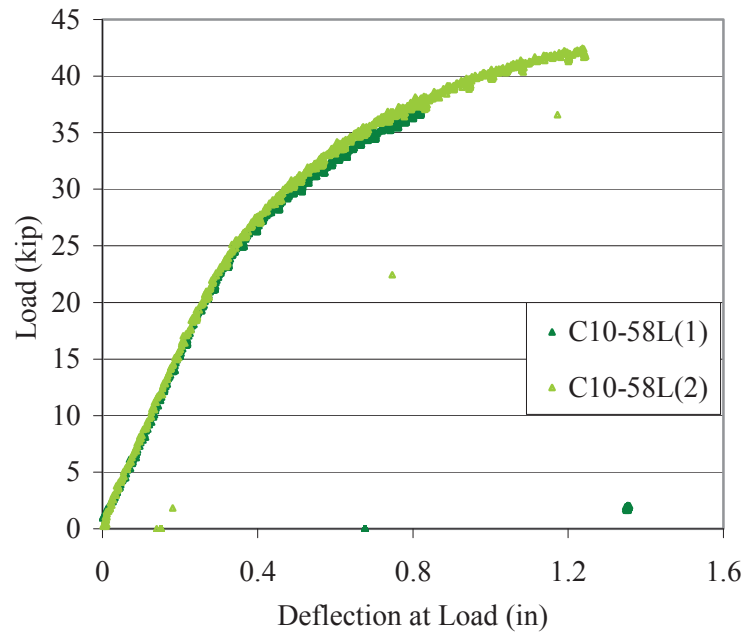
The slight divergence in the slope of the S6-48L beam is thought to be resulting from the repair previously described. The repair was done on the top fibers of the beam near the point load for the first test of this beam. If the patch had higher stiffness than the virgin beam, this would result in a steeper initial slope-deflection as is seen in **Figure 7.11 (b)** below.



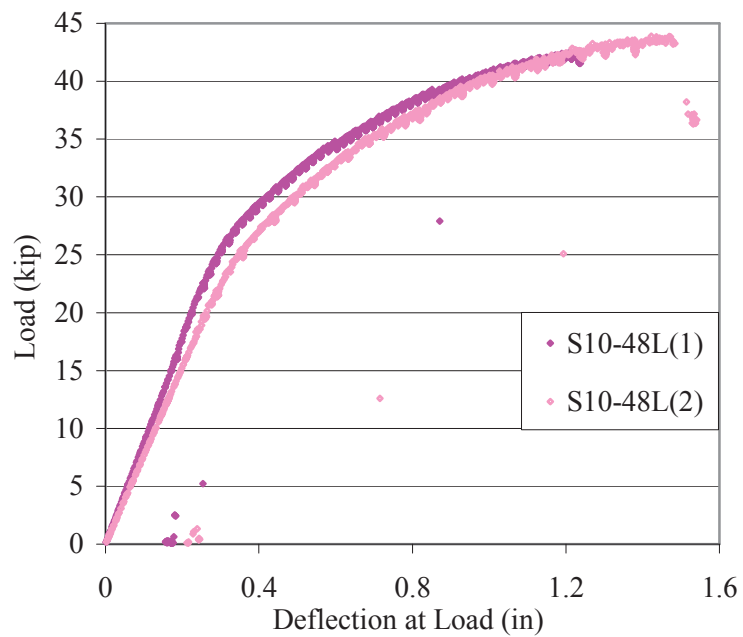
(a) 6 ksi (41.4 MPa) target strength CC beam



(b) 6 ksi (41.4 MPa) target strength SCC beam



(c) 10 ksi (68.9 MPa) target strength CC beam



(d) 10 ksi (68.9 MPa) target strength SCC beam

**Figure 7.11 – Beam Load-Deflection Response Curves**

Although the load-deflection curves for CC and SCC mixtures have numerous differences, there is also some similarity between the curves. All of the beams tested resulted in load-deformation curves with distinct elastically and plastically behaving regions. **Figure 7.12** below compares the elastic region for all beams; it is clear that the CC and SCC mixtures tested have similar stiffness in the elastic range. The similar elastic range can be supported by the fact that the flexural stiffness is primarily driven by the concrete stiffness due to relative area of concrete to steel. From the testing of MOE shown in **Section 5**, specifically **Figure 5.7(a)**, the limestone SCC and CC batch proportions tested exhibited similar normalized MOE; therefore, similar flexural stiffness can be expected.

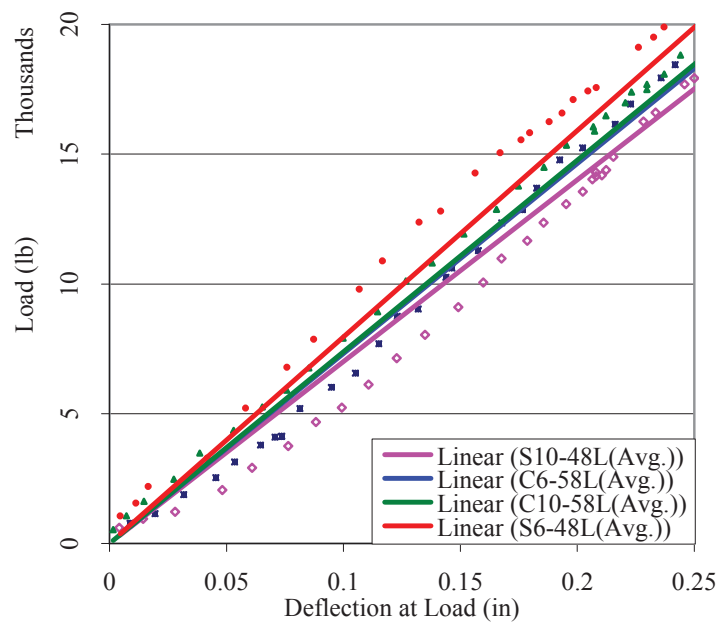


**Figure 7.12 – Beam Elastic Range Load-Deflection Response**

In order to more precisely examine how the SCC and CC compare in ultimate failure shear, each beam was normalized by the cross-sectional dimensions (constant for all beams) and the square root of the concrete compressive strength. The normalized graph is seen next in **Figure 7.13**. This re-iterates that the SCC did fail at higher shear stresses than the comparable CC batch proportions; yet, this trend diminished for the higher strength batch proportions.

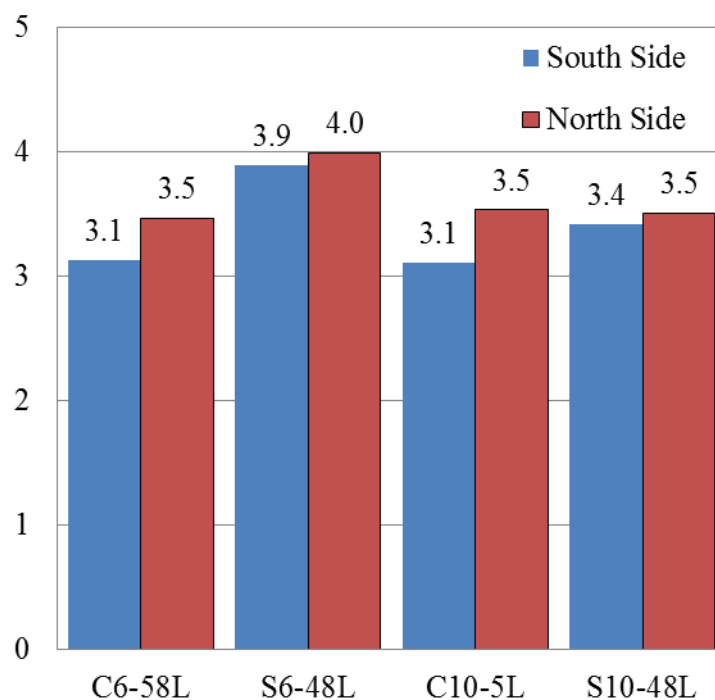
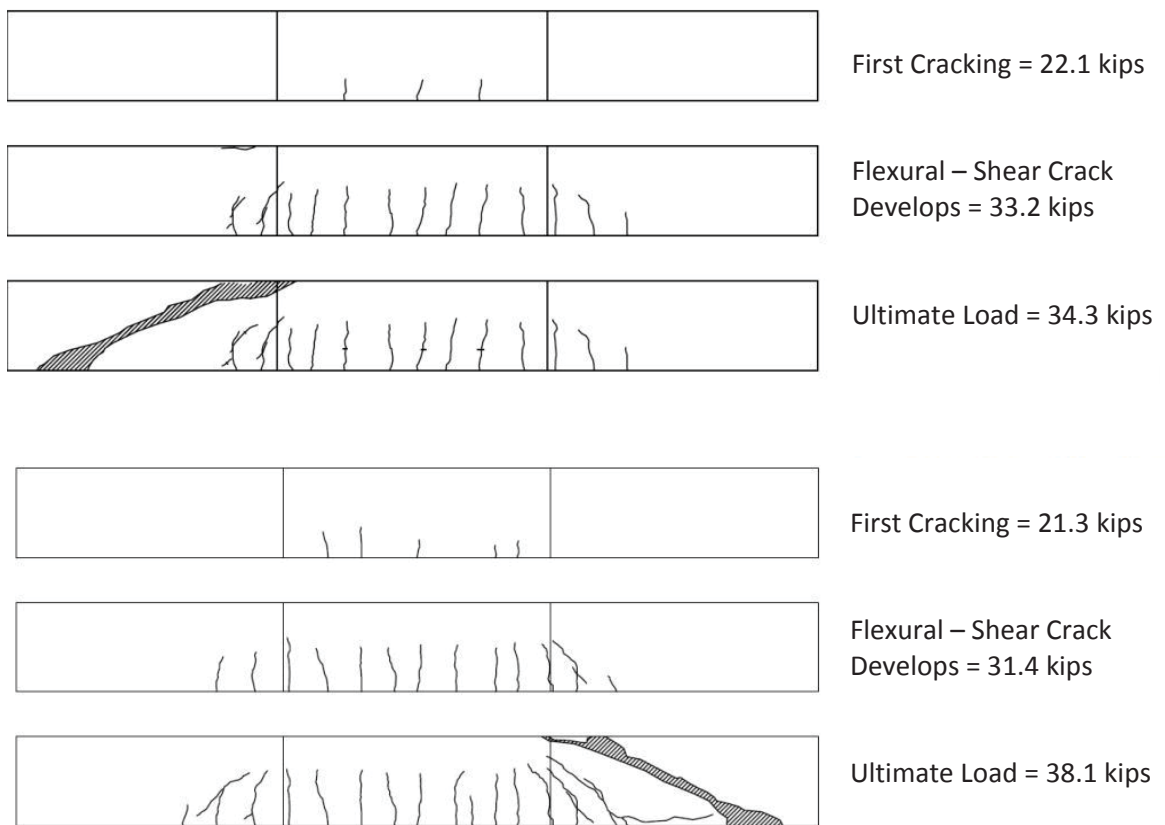


**Figure 7.13 – Shear Stress Normalized by the Square Root of Compressive Strength**

There was also a distinction between the CC and SCC mixtures with respect to how the specimens behaved and ultimately failed. The CC beams failed in shear while the SCC beams failed in concrete crushing of the top fiber. The CC beams would develop flexural cracking from which a flexural-shear crack would develop; yet, once the ultimate

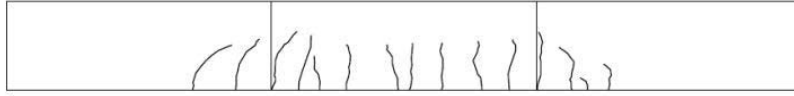
load was achieved, an explosive shear failure would occur that did not align or interact with the flexural-shear crack. The SCC beams would develop flexural cracks, flexural shear cracks, and eventually concrete crushing would occur in the top fiber of the beam. The progression of cracks and the final failure have been documented and are shown graphically in **Figure 7.13** below.



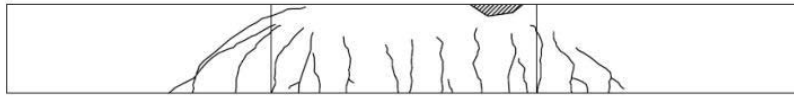
(a) C6-58L South / North Ends



First Cracking = 23.4 kips



Flexural – Shear Crack Develops = 34.6 kips



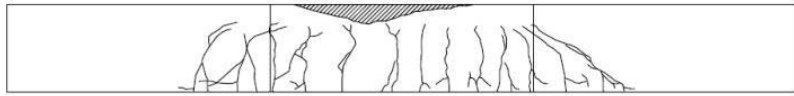
Ultimate Load = 42.0 kips



First Cracking = 24.4 kips



Flexural – Shear Crack Develops = 37.7 kips



Ultimate Load = 43.7 kips

(b) S6-48L South / North Ends



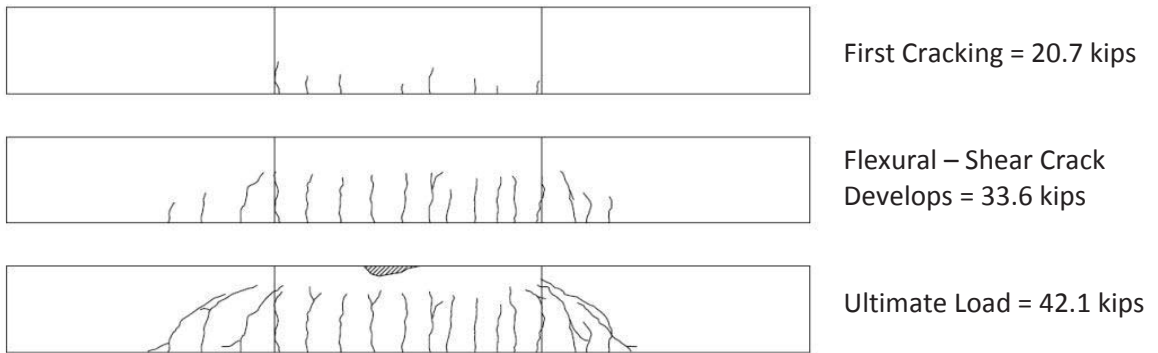
First Cracking = 21.5 kips



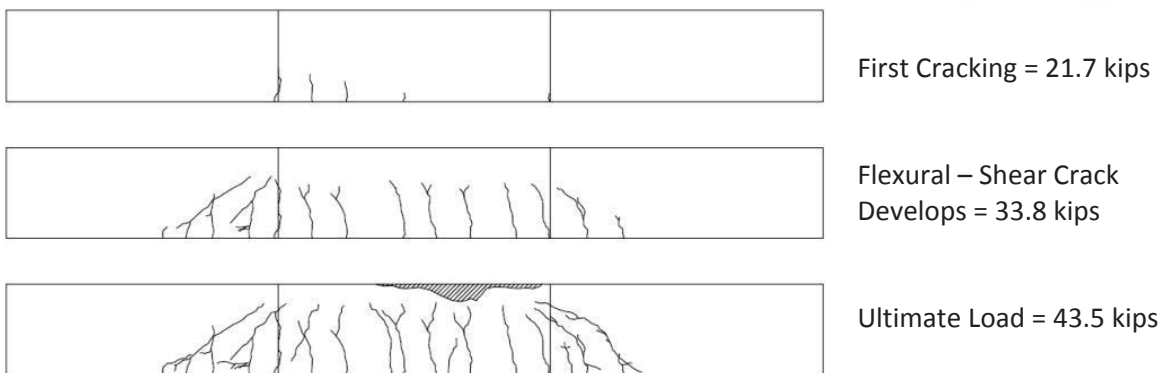
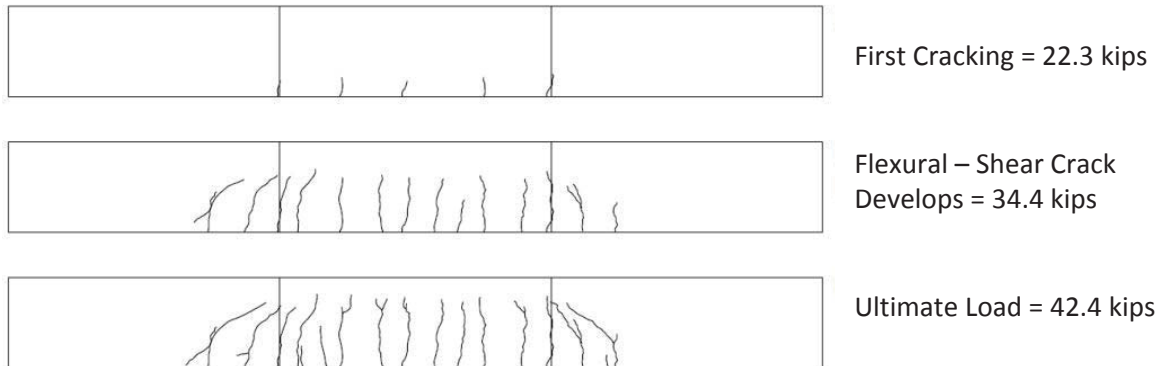
Flexural – Shear Crack Develops = 34.9 kips



Ultimate Load = 37.0 kips



(c) C10-58L South / North Ends



(d) S10-48L South / North Ends

Conversion: 1 kip = 6.89 MPa

**Figure 7.14 – Crack Development Patterns with Applied Loads**

The cracking, flexural-cracking, and failure loads and failure mode for each shear beam test has been shown. **Table 7.4** summarizes the findings against the predicted response of the various beams according to ACI, AASHTO, and the MCFT through use of Response 2000 created by Bentz and Collins while at the University of Toronto.

**Table 7.4 – Predicted Shear Beam Behavior**

	Predicted Failure (kips)			Average Actual (measured, self weight, and preload; kips)
	ACI	AASHTO	MCFT	
C6-58L	25.80	25.33	35.90	36.69
S6-48L	25.77	25.15	35.80	43.34
C10-58L	26.58	26.44	36.20	40.04
S10-48L	26.99	27.01	36.60	43.44

Conversion: 1 kip = 4.45 kN

**Table 7.4** provides the predicted and actual shear that exists at  $d_v$ , the effective shear depth, or 12 inches (305 mm) from the edge of the support. It is seen from **Table 7.4** that the actual failure shears are substantially higher than the predicted failure shears. The underestimation of the models is good, it means they are conservative estimates. It is seen that the predicted failure load by ACI and AASHTO are very similar and are more conservative than the MCFT. This observation makes sense because the ACI and AASHTO predictive models are design models and are therefore lower bound solutions. The MCFT is a limit state model that is derived mechanistically, and then fitted to empirical failure data. Notice that none of the models predicted the trend of significantly increased shear resistance by the SCC; the models do not consider the SCC and CC differently since they have the same material constituents.

It has already been shown that the SCC beams failed at higher loads and therefore it is peculiar why they did not fail explosively in shear as the CC beams had. Because the SCC beams exhibited increased deflections, the shear test regions were evidently allowed to rotate more freely, relieving the shearing stresses enough that shear failure was not actually achieved. The question is then what allowed increased deflection of the SCC beams with respect to the CC beams.

This researcher proposes some possible mechanisms to consider when rectifying the improved performance of the SCC beams with respect to the companion CC beams. These are hypotheses, and unfortunately limited measurements were taken to confirm or deny these suppositions. First, the SCC beams at each strength level achieved higher strengths at the time of release. Improved strength at release will result in less camber, and more importantly, less elastic shortening of the steel tendon; this in turn provides increased clamping forces through the life of the beam. The improved clamping force in the SCC beams may be the reason that higher initial cracking loads were exhibited relative to the CC beams which can be seen in **Figure 7.13**. Decreased elastic shortening of the steel at release may also lead to reduced damage to the relatively “green” concrete beams; more strain energy from the steel tendon is released into a low strength beam, which will also be more susceptible to damage and micro-cracking. Next, improved clamping forces in the uncracked shear test region of the SCC beams relative to the CC beams may be the reason the CC beams failed in shear whereas the SCC beams failed in concrete crushing.

The effectively clamped SCC shear region, not subject to moments high enough to cause flexural cracking, could effectively rotate between the simple support and the test load

point. The companion CC beams, which were not as effectively clamped within the shear region, failed explosively in shear when the tensile strains reached concrete capacity. This same effect may be the reason why the C10-58L beam exhibited two separate behaviors. The virgin test side failed in shear; however, the secondary test was conducted on a cracked member that was more ductile and the shear test region was allowed to more freely rotate between the support and load point. Although the beams were not thoroughly instrumented to numerically support these mechanistic hypotheses, there is supporting evidence of their validity when examining cracking behavior, cracking loads, failure loads, and failure modes.

## **7.5 FINDINGS AND CONCLUSIONS**

Precast, prestressed beams were fabricated and tested in shear for this investigation. The four baseline mixtures used throughout this project 6 ksi (41.4 MPa) target strength limestone CC and SCC, and 10 ksi (68.9 MPa) target strength limestone CC and SCC) were tested in four point loading. The beams were tested to evaluate the concrete shear strength prediction equations by ACI, AASHTO, and the MCFT. Crack propagation patterns and deflections during beam loading were also recorded.

The beam test setup and procedure were detailed. The problems experienced with the S6-48L beam were described and the method of repairing the damaged area was explained. The beams were fabricated at Coreslab Structures, Inc. in Marshall, MO.

The shear test results were shown. It was seen that the second test region of each beam experienced increased shear load and deflection over the first test region; this was explained by the reduced effective moment of inertia of a larger length of beam as well as

the strain hardening effect in the prestressing strand. These effects lead to increased ductility. It was also seen that all beams exhibited similar elastic stiffness prior to the first flexural crack development. The elastic stiffness is driven by the large area of concrete relative to steel, it was seen that the CC and SCC limestone batch proportions tested and described in **Section 5** exhibited similar stiffnesses. Also in **Section 5**, it was shown that SCC may exhibit improved tensile strength over CC, this may also help to explain improved resistance to initial cracking of the SCC. It was also shown that the SCC beams experienced increased deflections and failure loads over the CC beams. The improved deflection and load carrying capacity of the SCC is hypothesized to be explained by differences in prestress losses at time of release, and subsequently through concrete compressive strength development. The hypothetically decreased prestress losses of the SCC were believed to improve initial cracking resistance, mitigated damage of the concrete at release, and lead to improved failure behavior and loads. Finally, the failure modes differed from the SCC to CC. The SCC experienced flexure cracking, flexural-shear cracking, and finally concrete crushing; however, the CC experienced flexure cracking, flexural-shear cracking, then explosive shear failure which occurred at a location away from the developing flexural-shear crack. There was also improved shear resistance when comparing the higher strength CC or SCC to the lower strength CC or SCC respectively, as would be expected. The trend of increased release strength for improved shear resistance holds true when comparing the higher to lower strength batch proportions also.

The tests performed on the limestone batch proportions of this research project indicate improved performance of SCC when compared to CC. Improved SCC shear

resistance was unexpected. The expectation of SCC to have decreased shear capacity comes primarily from the effect of decreased C.A. fraction. The results from this investigation have shown that reduced C.A. fraction is not enough to conclude reduced shear capacity. The C.A. fraction may have a real impact on shear capacity at a given crack due to aggregate interlock; yet, it may be more important to know how that crack got there, and what stresses are acting on and around it. The beams of this investigation, when shear failure was observed, failed away from flexural cracked regions. This research has given valuable insight into SCC behavior, and shown that SCC should not be readily discarded as a construction material. Because of the limited practicality of rectangular cross-sections for prestressed concrete beams and girders, additional research of SCC tested in differing geometrical and scalar cross-sections should be carried out.

## **8. SUMMARY, CONCLUSIONS, AND RECOMMENDATIONS**

### **8.1 SUMMARY**

The purpose of this report was to investigate the ability of SCC to resist shear forces relative to CC at normal and high strengths. That objective was accomplished by performing a sequence of activities that were believed to contribute to the whole picture of how SCC behaves in shear as compared to CC.

First, a literature review was undertaken. The literature review surveyed relevant and necessary information available that would contribute to understanding SCC and how it behaves in the plastic and hardened state, with emphasis on shear behavior. Plastic concrete behavior and mechanics, current industry recognized guidelines and recommended practices for achieving robust SCC, and plastic concrete test procedures were identified. Hardened concrete behavior and predictive models were reviewed along with hardened concrete standardized mechanical test procedures. Fundamental shear theory, specifics about the aggregate interlock shear mechanism, and widely recognized shear predictive models were reviewed and analyzed. Small scale concrete shear tests were surveyed, and one, the push-off test, was selected for use in investigating the aggregate interlock mechanism of shear resistance for this study. Precast prestressed beam studies were also reviewed for behavior in shear; researchers that had investigated beam shear with SCC were also found.

Next, before any physical work could be accomplished, the concrete batch proportions to be tested had to be determined. The determination of concrete mixtures to test was achieved by the aid of MoDOT and Missouri precast concrete suppliers through

responses to a survey inquiring about SCC batch proportions in use at the time of this study. It should be noted that precast concrete suppliers in Missouri are using SCC for structural and non-structural applications for building construction; yet only non-structural members are permitted to be cast using SCC for MoDOT infrastructure. MoDOT gave guidelines for determining the control (normal density conventional concrete), and the survey responses gave typical Missouri precast SCC. The survey was also sent to Missouri ready-mix suppliers as well as AASHTO members from each of the fifty states; no responses were received from the ready-mix suppliers, but useful information was gathered about the prevalence and robustness of SCC across the US.

The constituent materials used throughout this study were investigated. There are limitations on the physical properties of the materials used in concrete; these properties were measured and were confirmed to be acceptable for use. The tested properties included absorption, bulk specific gravity, moisture content, and gradation. The measurement of the physical properties also enables proportioning of materials according to the standard volumetric method. Once the constituent materials were characterized and the batch proportions to be tested were obtained as described above, fresh concrete was mixed. The fresh concrete behavior was also measured using standard and non-standard methodologies. The L-box and other, newly developed or narrowly used SCC test procedures have not yet been accepted by standards associations. The tested fresh properties include slump, slump-flow,  $T_{20}$ , VSI, J-ring, L-box, segregation column, unit weight, and air percentage by the pressure method.

Next, hardened concrete behavior was tested. Hardened properties tests included the concrete compressive strength, Young's Modulus, and splitting tensile strength.

These hardened properties are very important for correlation to member behavior under load. These properties have real impacts on concrete performance, and are all commonly present in mechanistic failure models of all kinds, including the failure mode of interest to this investigator – shear.

Shear behavior was monitored by two major test regiments. First, the small scale push-off test was used to investigate the aggregate interlock mechanism contribution to shear resistance. The test schedule consisted of testing CC and SCC at two separate strength levels, with two distinct C.A. types, and the SCC had three variations of C.A. volumetric fraction of the aggregate portion. Additional mixtures were tested because the test was relatively simple and low cost. The additional batch proportions tested included a companion push-off specimen of the shear beams tested (to be discussed shortly), specimens for a third strength level of limestone aggregate mixtures, and two specimens from concrete produced by another active researcher at Missouri S&T. Post-failure imaging of the cross-section was performed to give added insight into segregation and aggregate contribution. Next, shear behavior was also explored through testing precast prestressed concrete beams. The beams were selected to be precast prestressed because of increased compatibility with real-world applications; however, the beams were not full-scale and were of simple rectangular geometry. The beams could not comprise the entire cost of this research; therefore, four economical beams were constructed that permitted testing on both ends resulting in eight shear beam test results.

With the details of the materials, tests, and theory gathered, work commenced. Batch proportions were determined from a practical means and reflect current industry practice. Fresh and hardened concrete properties were tested and recorded for correlation

to shear test results. Shear was investigated through two avenues; one looked at the specifics of relative behavior of SCC and CC when subject to aggregate interlock, the other looked at the macroscopic behavior of a shear beam. All of these tasks, results, and analyses contribute to the ability to compare and contrast CC and SCC. The investigation was able to accomplish the objective of characterizing SCC relative to CC and enabled the statement of the following conclusions.

## **8.2 FINDINGS AND CONCLUSIONS**

The following findings and conclusions are supported by the review of literature and the observed behavior and test results from this investigation:

- National SCC studies have produced guidelines for developing fresh property test programs to develop robust mix designs and reliable QA/QC programs.
- There exist standardized test procedures for testing “fresh” or plastic SCC.
- The majority of AASHTO survey respondents report less than 25% of all projects utilizing SCC with first use occurring within the last 7 years; few respondents report a majority of projects using SCC with more than 10 years of experience.
- The increased rate and higher ultimate strength development of SCC compared to CC observed by other researchers was also observed in this investigation.
- The decreased MOE for SCC compared to CC noted by others was not exhibited by the concrete batch proportions tested in this study.

- Researchers have reported conflicting results regarding the relative tensile strength of SCC to CC; this researcher witnessed improved tensile strength of SCC with respect to CC.
- The concrete batch proportions containing river gravel exhibited improved hardened mechanical properties of increased compressive strength, increased MOE, and increased STS despite their decreased surface roughness compared to limestone aggregates tested.
- Vertical push-off specimen fabrication was effective in resembling actual member fabrication and adequately controlled geometrical tolerances for superior stress propagation and improved test results.
- Software imaging of post-failure cross-sections indicate segregation was not a significant issue and that tested specimens closely match calculated material proportions.
- The precrack test result analysis indicates that initial crack widths are highly controllable by increasing the initial clamping force.
- Precrack load was found to be proportional to concrete compressive strength, tensile strength, and initial clamping force.
- Push-off test results indicate decreasing aggregate interlock with increasing concrete compressive strength, a trend noted by other researchers and supported by theory.
- For the concrete batch proportions tested, river gravel exhibited superior aggregate interlock capability when compared to the limestone; this was the

variable that had the largest effect on shear resistance of the concrete specimens and variables tested within this study.

- Despite other researchers findings and theoretical conflict, the SCC did not appear to resist shear through aggregate interlock in a manner distinguishable from CC; the effect of C.A. percentage was not detectable for the tests performed in this investigation.
- The E-value that other researchers have proposed and relied on for push-off analysis was discussed and discarded as the highly sensitive analysis tool it has been proposed to be. The E-value does examine shear and normal stress, crack width, and crack opening; however, it effectively averages and smears important incremental information.
- The increased rate of strength gain for SCC relative to CC was also noted for the shear beams; increased SCC strength at the time of release may be important to elastic prestress loss as well as losses over time.
- The tested shear beams exhibited similar flexural stiffness in the elastic range, this is supported by the consistent MOE of SCC and CC discussed above.
- SCC shear beams demonstrate increased deflections at increased shear strengths over comparable CC beams in this study. Other researchers have seen mixed results when comparing shear strength of SCC and CC beams.
- The beams of this study were tested once on each end. All secondary tests had increased shear strength and deflections over the virgin test indicating increased ductility.

- At failure, the SCC beams displayed crushing in their top fibers, the CC beams failed explosively in a shear plane extending from support to load point, away from developing flexural shear cracks.

These conclusions are drawn from the testing performed throughout this investigation. Other researcher's findings were incorporated into the conclusions when possible, their findings either support or deviate from the findings of this study.

### **8.3 RECOMMENDATIONS**

It is recommended that an SCC be designed and developed following the guidelines from the NCHRP report 628 to become familiar with the issues and sensitivities of fresh SCC. Subsequent to SCC batch proportioning, it would be useful to conduct a QA/QC study across numerous Missouri precast and possibly ready-mix suppliers to ensure that adequate control of the material is ensured with the fast and simple fresh tests of slump-flow and J-ring. This process would familiarize all parties involved with the concerns of creating robust SCC, as well as help to establish practical and acceptable limits on the filling capacity and stability of subsequently developed SCC batch proportions.

No concerns were identified in this investigation with regard to hardened mechanical testing of SCC relative to CC. Strength development and tensile strength was identified to be improved for SCC over similar CC. MOE was consistent between SCC and CC; other researchers have noted decreased MOE for SCC, but have also seen that the lower bound predictive models are still conservative.

Additional shear testing of SCC would be useful. Push-off tests conducted throughout this investigation proved to be economical and quick, once familiar with the fabrication and testing procedures. Additional push-off testing, with some standardization and improvements to the test suggested by this researcher, would be useful in refining the results of this study as well as investigating additional variables. Push-off testing would be most useful for lower strength concrete batch proportions where the impact of aggregate interlock is greater than at higher strengths. Variables that could be investigated could include maximum aggregate size, C.A. gradation, C.A. surface roughness and angularity, C.A. hardness, mineral and chemical admixtures, as well as the variables tested in this investigation. A broad push-off test program may identify additional or compounding effects that have not been previously identified. It would also be valuable to conduct additional shear beam testing. As with CC, it was identified that SCC shear beams have been tested in third point loading, but not commonly with distributed loading. Larger scale and more practical geometries of beams and girders should be tested in shear to compare to trends identified in this study. A beam with web-shear cracking may exhibit completely different behavior from the rectangular beams tested in this study that produced flexural-shear cracks and failed in a plane away from these developing cracks. Full-scale beam testing with complete stress-strain instrumentation should be undertaken. Given that SCC has already seen consistent public use, ongoing monitoring of a conservatively designed SCC beam used by the public may also be deemed acceptable.

(This Page Intentionally Left Blank)

## REFERENCES

- American Association of State Highway and Transportation Officials (AASHTO) Load and Resistance Factor Design (LRFD) (2004). Bridge design specifications and commentary, AASHTO, Washington, D.C.
- AASHTO “Subcommittee on Materials.” <<http://www.materials.transportation.org>> (Jan. 16. 2011).
- American Concrete Institute (ACI) Committee 237 (2007). “Self-consolidating concrete.” American Concrete Institute, Farmington Hills, Michigan.
- ACI Committee 318 (2011). “Building Code Requirements for Structural Concrete (ACI 318-08) and Commentary.” American Concrete Institute, Farmington Hills, Michigan.
- ACI Committee 363 (2010). “Report on High-Strength Concrete.” American Concrete Institute, Farmington Hills, Michigan.
- ACI – ASCE Committee 426 (1973). “The Shear Strength of Reinforced Concrete Members – Chapters 1 to 4,” Proceeds ASCE, J. of the Structural Division, 99 (6), 1091-1187.
- American Society for Testing and Materials (ASTM) C127 (2007). “Standard Test Method for Density, Relative Density (Specific Gravity), and Absorption of Coarse Aggregate.” Annual book of ASTM standards, ASTM, West Conshohocken, Pennsylvania.

- ASTM C128 (2007). “Standard Test Method for Density, Relative Density (Specific Gravity), and Absorption of Fine Aggregate.” Annual book of ASTM standards, ASTM, West Conshohocken, Pennsylvania.
- ASTM C136 (2006). “Standard Test Method for Sieve Analysis of Fine and Coarse Aggregates.” Annual book of ASTM standards, ASTM, West Conshohocken, Pennsylvania.
- ASTM C138 (2010). “Standard Test Method for Density (Unit Weight), Yield, and Air Content (Gravimetric) of Concrete.” Annual book of ASTM standards, ASTM, West Conshohocken, Pennsylvania.
- ASTM C143 (2010). “Standard Test Method for Slump of Hydraulic-Cement Concrete.” Annual book of ASTM standards, ASTM, West Conshohocken, Pennsylvania.
- ASTM C192 (2007). “Standard Practice for Making and Curing Concrete Test Specimens in the Laboratory.” Annual book of ASTM standards, ASTM, West Conshohocken, Pennsylvania.
- ASTM C231 (2010). “Standard Test Method for Air Content of Freshly Mixed Concrete by the Pressure Method.” Annual book of ASTM standards, ASTM, West Conshohocken, Pennsylvania.
- ASTM C469 (2010). “Standard Test Method for Static Modulus of Elasticity and Poisson’s Ratio of Concrete in Compression.” Annual book of ASTM standards, ASTM, West Conshohocken, Pennsylvania.
- ASTM C496 (2011). “Standard Test Method for Splitting Tensile Strength of Cylindrical Concrete Specimens.” Annual book of ASTM standards, ASTM, West Conshohocken, Pennsylvania.

- ASTM C566 (2004). "Standard Test Method for Total Evaporable Moisture Content of Aggregate by Drying." Annual book of ASTM standards, ASTM, West Conshohocken, Pennsylvania.
- ASTM C1231 (2010). "Standard Practice for Use of Unbonded Caps in Determination of Compressive Strength of Concrete Cylinders." Annual book of ASTM standards, ASTM, West Conshohocken, Pennsylvania.
- ASTM C1611 (2009). "Standard Test Method for Slump Flow of Self-Consolidating Concrete." Annual book of ASTM standards, ASTM, West Conshohocken, Pennsylvania.
- ASTM C1621 (2009). "Standard Test Method for Passing Ability of Self-Consolidating Concrete by J-Ring." Annual book of ASTM standards, ASTM, West Conshohocken, Pennsylvania.
- Albajar, J. S. (2008). "The Influence of Aggregate Fracture on the Shear Strength of Reinforced Concrete Beams." Doctoral Thesis, Imperial College London, London, United Kingdom.
- Barragan, B., Gettu, R., Agullo, L. and Zerbino, R. (2006). "Shear failure of steel fiber-reinforced concrete based on push-off tests." *ACI Mater. J.*, 103 (4), 251-257.
- BASF (2010). "Glenium 7700 Data Sheet." <<http://www.basf-admixtures.com>> (March 15, 2011).
- BASF (2011). "MB-AE-90 Data Sheet." <<http://www.basf-admixtures.com>> (March 15, 2011).

- Bentz, E. C., Vecchio, F. J., and Collins, M. P. (2006). "Simplified Modified Compression Field Theory for Calculating Shear of Reinforced Concrete Elements." *ACI Struct. J.*, 103(4), 614-624.
- DIYMAPS (2011). "Do It Yourself Color-Coded State, US, Canada and Mexico Maps." <<http://diymaps.net>> (Aug. 19. 2011).
- EFNARC (2005). "The European Guidelines for Self-compacting Concrete." <<http://www.efnarc.org>> (Jan. 21. 2012).
- EFNARC (2006). "Guidelines for Viscosity Modifying Admixtures for Concrete." <<http://www.efnarc.org>> (Jan. 28. 2012).
- FHWA (2005). "Advances in Self-consolidating Concrete." Focus, <<http://www.fhwa.dot.gov>> (Dec. 15. 2011).
- Ghezal, A., and Khayat, K. H. (2002). "Optimizing self-consolidating concrete with limestone filler by using statistical factorial design methods." *ACI Mater. J.*, 99(3), 264-272.
- Hwang, S., Khayat, K. H., and Bonneau, O. (2006). "Performance-Based Specifications of Self-Consolidating Concrete use in Structural Applications." *ACI Mater. J.*, 103(2), 121-129.
- Khayat, K. H., and Assaad, J. (2002). "Air-Void Stability in Self-Consolidating Concrete." *ACI Mater. J.*, 99(4), 408-416.
- Kim, Y. H. (2008). "Characterization of Self-Consolidating Concrete for the Design of Precast, Pretensioned Bridge Superstructure Elements." Doctoral Dissertation, Texas A&M University, College Station, Texas.

- Mattock, A. H., Hawkins, N. M. (1972). "Shear Transfer in Reinforced Concrete – Recent Research." *PCI J.*, 17(2), 55-75.
- Mattock, A. H., Hofbeck, J. A., and Ibrahim, I. O. (1969). "Shear Transfer in Reinforced Concrete." *ACI J.*, 66(2), 119-128.
- Mindess, S., Young, J. F., Darwin, D. (2003). "Concrete – Second Edition." Prentice Hall, Upper Saddle River, New Jersey.
- Missouri Department of Transportation (MoDOT) (2012). "Missouri Standard Specifications for Highway Construction." MoDOT, Jefferson City, MO.
- Myers, J. J., Carrasquillo, R. L. (1999). "The Production and Quality Control of High Performance Concrete in Texas Bridge Structures." Center for Transportation Researcher, Research Report 580/589-1, The University of Texas at Austin.
- Naito, C.J., Parent, G., and Brunn, G. (2006). "Performance of Bulb-T Girders Made with Self-Consolidating Concrete." *PCI J.*, 51(6), 72-85.
- National Cooperative Highway Research Program (NCHRP) (2009). "Report 628 – Self-Consolidating Concrete for Precast, Prestressed Concrete Bridge Elements." Transportation Research Board, Washington, D.C.
- National Institute of Health (NIH) (2004). "ImageJ." Image Processing and Analysis in Java, <<http://rsbweb.nih.gov/ij/>> (Nov. 6, 2011).
- Nawy, E. G. (2010). "Prestressed Concrete - A Fundamental Approach - Fifth Edition Update." Prentice Hall, Upper Saddle River, New Jersey.
- Nowak, A., Morcous, G., Kaszynska, M., Tuan, C., Paczkowski, P., Akhnoukh, A., Lutomirski, T., and Kozikowski, M. (2007). "Development of a Guide for Cast-

in-Place Applications of Self-Consolidating Concrete.” Nebraska Department of Roads (NDOR), Lincoln, Nebraska.

Sika (2003). “Sikatop® 122 Plus – Product Data Sheet.” Products and Solutions – Concrete Restoration, <<http://usa.sika.com/en/group.html>> (Jan. 20, 2012).

Vecchio, F. J., and Collins, M. P. (1986). “The Modified Compression Field Theory for Reinforced Concrete Elements Subjected to Shear.” *ACI Struct. J.*, 83(2), 219-231.

Vecchio, F. J., and Lai, D. (2004). “Crack Shear-Slip in Reinforced Concrete Elements.” *J. of Advanced Concrete Technology*, 2(3), 289-300.

Walraven, J. C. (1981). “Fundamental analysis of aggregate interlock.” *J. Struct. Div.*, ASCE, 107(11), 2245-2270.

Walraven, J. C., and Reinhardt, H. W. (1981). “Theory and Experiments on Mechanical Behavior of Cracks in Plain and Reinforced Concrete Subjected to Shear Loading.” *Heron*, 26(1A), 68.

Walraven, J. C., and Stroband, J. (1994). “Shear Friction in High-Strength Concrete.” SP-149, Proc., American Concrete Institute Int. Conf., Singapore, 311-330.

**APPENDIX A**  
**MATERIAL DATA SHEETS**



3	05 50 00	Product Data Cast-in-Place Concrete Precast Concrete
	05 40 00	

### Description

Glenium 7700 ready-to-use high-range water-reducing admixture is based on the next generation of polycarboxylate technology found in all of the Glenium 7000 series products. This technology combines state-of-the-art molecular design with a precise understanding of regional cements to provide specific and exceptional value to all phases of the concrete construction process.

Glenium 7700 is particularly effective in improving the day to day consistency of concrete mixtures. This is accomplished by providing unparalleled slump retention without compromising early compressive strength development and setting time. Workability retention helps to maintain more consistent performance from batch to batch, thereby improving operational efficiencies. Glenium 7700 meets ASTM C 494 compliance requirements for Type A, water-reducing, and Type F, high-range water-reducing, admixtures.

### Applications

Recommended for use in:

- Concrete requiring high-early compressive strength development
- Applications requiring workability retention without retardation
- Concrete where high flowability, increased stability and durability are needed
- Production of Self-Consolidating Concrete (SCC) mixtures
- Concrete with varying water reduction requirements (5-40%)

## Glenium® 7700

### High-Range Water-Reducing Admixture

#### Features

- Superior slump retention
- Excellent early strength development
- High ultimate strengths
- Optimum setting time
- Consistent air entrainment
- Dosage flexibility

#### Benefits

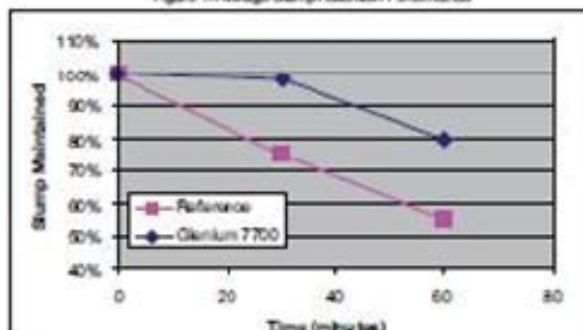
- Consistency in placement operations
- Optimized mixture costs
- Reduction in patching costs
- Ability to attain difficult combinations of high-early and late-age compressive strengths
- Increased productivity
- Improved operational efficiencies
- Less QC support
- Fewer rejected loads
- Faster form turnover
- Workability retention without retardation

#### Performance Characteristics

**Slump Retention:** Concrete produced with Glenium 7700 admixture maintains slump significantly longer than concrete mixtures containing naphthalene, melamine, and first generation polycarboxylate high-range water-reducing admixtures. This slump retention is achieved without affecting rate of hardening or early age compressive strength development.

**Mixture Data:** Figure 1 represents average slump retention performance across multiple field trials throughout North America. Figure 2 represents average compressive strength results from these same field trials. Materials were all different as were starting consistencies. The reference admixture in this graph represents the first generation of high-early strength polycarboxylate technology.

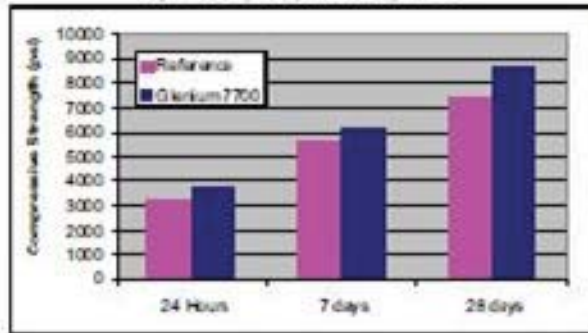
Figure 1. Average Slump Retention Performance



Master  
Builders

## Product Data: Glenium® 7700

Figure 2. Average Compressive Strength Results



### Guidelines for Use

**Dosage:** Glenium 7700 has a recommended dosage range of 2-15 fl oz/cwt (130-975 mL/100 kg) of cementitious materials. For most applications, dosages in the range of 2-12 fl oz/cwt (130-780 mL/100 kg) will provide excellent performance. For very high performance and Rheodynamic® Self-Consolidating concrete mixtures, up to 15 fl oz/cwt (975 mL/100 kg) of cementitious materials can be utilized. Because of variations in concrete materials, job site conditions and/or applications, dosages outside of the recommended range may be required. In such cases, contact your local sales representative.

**Mixing:** Glenium 7700 admixture can be added with the initial batch water or as a delayed addition. However, optimum water reduction is generally obtained with a delayed addition.

### Product Notes

**Corrosivity - Non-Chloride, Non-Corrosive:** Glenium 7700 admixture will neither initiate nor promote corrosion of reinforcing steel embedded in concrete, prestressing steel or of galvanized steel floor and roof systems. Neither calcium chloride nor other chloride-based ingredients are used in the manufacture of Glenium 7700 admixture.

**Compatibility:** Glenium 7700 admixture is compatible with most admixtures used in the production of quality concrete, including normal, mid-range and high-range water-reducing admixtures, accelerators, retarders, extended set control admixtures, air-entrainers, corrosion inhibitors, and shrinkage reducers.

**Do not use Glenium 7700 admixture with admixtures containing beta-naphtholene sulfonate. Erratic behaviors in slump, workability retention and pumpability may be experienced.**

### Storage and Handling

**Storage Temperature:** Glenium 7700 admixture must be stored at temperatures above 40 °F (5 °C). If Glenium 7700 admixture freezes, thaw and reconstitute by mechanical agitation. Do not use pressurized air for agitation without consulting technical support.

**Shelf Life:** Glenium 7700 admixture has a minimum shelf life of 6 months. Depending on storage conditions, the shelf life may be greater than stated. To ensure the longest shelf life potential, recirculation is recommended. Please contact your local sales representative regarding suitability for use and dosage recommendations if the shelf life of Glenium 7700 admixture has been exceeded.

### Packaging

Glenium 7700 admixture is supplied in 55 gal (208 L) drums, 275 gal (1040 L) totes and by bulk delivery.

### Related Documents

Material Safety Data Sheets: Glenium 7700 admixture

### Additional Information

For additional information on Glenium 7700 admixture or its use in developing concrete mixtures with special performance characteristics, contact your local sales representative.

*The Admixture Systems business of BASF's Construction Chemicals division is a leading provider of innovative admixtures for specialty concrete used in the ready-mixed, precast, manufactured concrete products, underground construction and paving markets throughout the North American region. The Company's respected Master Builders brand products are used to improve the placing, pumping, finishing, appearance and performance characteristics of concrete.*

**LIMITED WARRANTY NOTICE:** We warrant our products to be of good quality and will replace or, at our discretion, refund the purchase price of any products proved defective. Satisfactory results depend not only upon quality products, but also upon many factors beyond our control. Therefore, except for such replacement or refund, BASF MAKES NO WARRANTY OR GUARANTEE, EXPRESS OR IMPLIED, INCLUDING WARRANTIES OF FITNESS FOR A PARTICULAR PURPOSE OR MERCHANTABILITY, RESPECTING ITS PRODUCTS, and BASF shall have no other liability with respect thereto. Any claims regarding product defect must be received in writing within one (1) year from the date of shipment. User shall determine the suitability of the products for the intended use and assume all risks and liability in connection therewith. Any authorized change in the printed recommendations concerning the use of our products must bear the signature of the BASF technical manager.

This information and all further technical advice are based on BASF's present knowledge and experience. However, BASF assumes no liability for providing such information and advice including the extent to which such information and advice may relate to existing third party intellectual property rights, especially patent rights. BASF SHALL NOT BE RESPONSIBLE FOR CONSEQUENTIAL, INDIRECT OR INCIDENTAL DAMAGES (INCLUDING LOSS OF PROFITS) OF ANY KIND. BASF reserves the right to make any changes according to technological progress or further developments.

For Professional use only. Not for sale to or use by the general public.

BASF Corporation  
Admixture Systems

[www.masterbuilders.com](http://www.masterbuilders.com)

United States: 23700 Chagrin Boulevard, Cleveland, Ohio 44122-5544 • Tel: 800 628-9990 • Fax: 216 833-8821  
Canada: 1800 Clark Boulevard, Brampton, Ontario L6T 4M7 • Tel: 800 387-5862 • Fax: 905 792-0651

© Construction Research & Technology GmbH

© BASF Corporation, 2010 • Printed in USA • 06/10 • LIT # 3000032



Master  
Builders



3	03 30 00	Product Data Cast-in-Place Concrete Precast Concrete Mass Concrete
	03 40 00	
	03 70 00	

### Description

MB-AE 90 air-entraining admixture is for use in concrete mixtures. It meets the requirements of ASTM C 260, AASHTO M 154 and CRD-C 13.

### Applications

Recommended for use in:

- Concrete exposed to cyclic freezing and thawing
- Production of high-quality normal or lightweight concrete (heavyweight concrete normally does not contain entrained air)
- All paving-related concrete exposed to freezing and thawing cycles

## MB-AE™ 90

### Air-Entraining Admixture

#### Features

- Ready-to-use in the proper concentration for rapid, accurate dispensing

#### Benefits

- Improved resistance to damage from cyclic freezing and thawing
- Improved resistance to scaling from deicing salts
- Improved plasticity and workability
- Reduced permeability – increased watertightness
- Reduced segregation and bleeding

#### Performance Characteristics

Concrete durability research has established that the best protection for concrete from the adverse effects of freezing and thawing cycles and deicing salts results from: proper air content in the hardened concrete, a suitable air-void system in terms of bubble size and spacing, and adequate concrete strength, assuming the use of sound aggregates and proper mixing, transporting, placing, consolidation, finishing and curing techniques. MB-AE 90 admixture can be used to obtain adequate freeze-thaw durability in a properly proportioned concrete mixture, if standard industry practices are followed.

**Air Content Determination:** The total air content of normal weight concrete should be measured in strict accordance with ASTM C 231, "Standard Test Method for Air Content of Freshly Mixed Concrete by the Pressure Method" or ASTM C 173/C 173M, "Standard Test Method for Air Content of Freshly Mixed Concrete by the Volumetric Method."

The air content of lightweight concrete should only be determined using the Volumetric Method. The air content should be verified by calculating the gravimetric air content in accordance with ASTM C 138/C 138M, "Standard Test Method for Density (Unit Weight), Yield, and Air Content (Gravimetric) of Concrete." If the total air content, as measured by the Pressure Method or Volumetric Method and as verified by the Gravimetric Method, deviates by more than 1-1/2%, the cause should be determined and corrected through equipment calibration or by whatever process is deemed necessary.

#### Guidelines for Use

**Dosage:** There is no standard dosage for MB-AE 90 admixture. The exact quantity of air-entraining admixture needed for a given air content of concrete varies because of differences in concrete-making materials and ambient conditions. Typical factors that might influence the amount of air entrained include: temperature, cementitious materials, sand gradation, sand-aggregate ratio, mixture proportions, slump, means of conveying and placement, consolidation and finishing technique. The amount of MB-AE 90 admixture used will depend upon the amount of entrained air required under actual job conditions. In a trial mixture, use 1/4 to 4 fl oz/cwt (16-260 mL/100 kg) of cementitious material. Measure the air content of the trial mixture, and, if needed, either increase or decrease the quantity of MB-AE 90 admixture to obtain the desired air content.

In mixtures containing water-reducing or set-control admixtures, the amount of MB-AE 90 admixture needed may be somewhat less than the amount required in plain concrete.

**Master  
Builders**

## Product Data: MB-AE™ 90

Due to possible changes in the factors that can affect the dosage of MB-AE 90 admixture, frequent air content checks should be made during the course of the work. Adjustments to the dosage should be based on the amount of entrained air required in the mixture at the point of placement.

If an unusually high or low dosage of MB-AE 90 admixture is required to obtain the desired air content, consult your Local sales representative. In such cases, it may be necessary to determine that, in addition to a proper air content in the fresh concrete, a suitable air-void system is achieved in the hardened concrete.

**Dispensing and Mixing:** Add MB-AE 90 admixture to the concrete mixture using a dispenser designed for air-entraining admixtures, or add manually using a suitable measuring device that ensures accuracy within plus or minus 3% of the required amount.

For optimum, consistent performance, the air-entraining admixture should be dispensed on damp, fine aggregate. If the concrete mixture contains fine lightweight aggregate, field evaluations should be conducted to determine the best method to dispense the air-entraining admixture.

### Precaution

In a 2005 publication from the Portland Cement Association (PCA R&D Serial No. 2789), it was reported that problematic air-void clustering that can potentially lead to above normal decreases in strength was found to coincide with late additions of water to air-entrained concretes. Late additions of water include the conventional practice of holding back water during batching for addition at the jobsite. Therefore, caution should be exercised with delayed additions of water to air-entrained concrete. Furthermore, an air content check should be performed after any post-batching addition to an air-entrained concrete mixture.

### Product Notes

**Corrosivity – Non-Chloride, Non-Corrosive:** MB-AE 90 admixture will neither initiate nor promote corrosion of reinforcing and prestressing steel embedded in concrete, or of galvanized floor and roof systems. No calcium chloride or other chloride-based ingredients are used in the manufacture of this admixture.

**Compatibility:** MB-AE 90 admixture may be used in combination with any BASF admixture, unless stated otherwise on the data sheet for the other product. When used in conjunction with other admixtures, each admixture must be dispensed separately into the concrete mixture.

### Storage and Handling

**Storage Temperature:** MB-AE 90 admixture should be stored and dispensed at 31 °F (-0.5 °C) or higher. Although freezing does not harm this product, precautions should be taken to protect it from freezing. If MB-AE 90 admixture freezes, thaw at 35 °F (2 °C) or above and completely reconstitute by mild mechanical agitation. **Do not use pressurized air for agitation.**

**Shelf Life:** MB-AE 90 admixture has a minimum shelf life of 18 months. Depending on storage conditions, the shelf life may be greater than stated. Please contact your Local sales representative regarding suitability for use and dosage recommendations if the shelf life of MB-AE 90 admixture has been exceeded.

**Safety:** Chemical goggles and gloves are recommended when transferring or handling this material.

### Packaging

MB-AE 90 admixture is supplied in 55 gal (208 L) drums, 275 gal (1040 L) totes and by bulk delivery.

### Related Documents

Material Safety Data Sheets: MB-AE 90 admixture.

### Additional Information

For additional information on MB-AE 90 admixture, or its use in developing a concrete mixture with special performance characteristics, contact your Local sales representative.

*The Admixture Systems business of BASF's Construction Chemicals division is a leading provider of innovative admixtures for specialty concrete used in the ready-mixed, precast, manufactured concrete products, underground construction and paving markets throughout the North American region. The Company's respected Master Builders brand products are used to improve the placing, pumping, finishing, appearance and performance characteristics of concrete.*

**LIMITED WARRANTY NOTICE.** We warrant our products to be of good quality and will replace or, at our discretion, refund the purchase price of any products proved defective. Satisfactory results depend not only upon quality products, but also upon many factors beyond our control. Therefore, except for such replacement or refund, BASF MAKES NO WARRANTY OR GUARANTEE, EXPRESS OR IMPLIED, INCLUDING WARRANTIES OF FITNESS FOR A PARTICULAR PURPOSE OR MERCHANTABILITY, RESPECTING ITS PRODUCTS, and BASF shall have no other liability with respect thereto. Any claims regarding product defect must be received in writing within one (1) year from the date of shipment. User shall determine the suitability of the products for the intended use and assume all risks and liability in connection therewith. Any authorized change in the printed recommendations concerning the use of our products must bear the signature of the BASF Technical Manager.

This information and all further technical advice are based on BASF's present knowledge and experience. However, BASF assumes no liability for providing such information and advice including the extent to which such information and advice may relate to existing third party intellectual property rights, especially patent rights. BASF SHALL NOT BE RESPONSIBLE FOR CONSEQUENTIAL, INDIRECT OR INCIDENTAL DAMAGES (INCLUDING LOSS OF PROFITS) OF ANY KIND. BASF reserves the right to make any changes according to technological progress or further developments.

For Professional use only. Not for sale to or use by the general public.

**BASF Corporation**  
Admixture Systems

[www.masterbuilders.com](http://www.masterbuilders.com)

United States: 23700 Chagrin Boulevard, Cleveland, Ohio 44122-8544 • Tel: 800 629-0990 • Fax: 216 839-8821

Canada: 1800 Clark Boulevard, Brampton, Ontario L6T 4M7 • Tel: 800 387-5882 • Fax: 905 792-0851

© BASF Corporation

© BASF Corporation 2011 • Printed in USA • 04/11 • LIT # 1017027



**Master  
Builders**

# SIKATOP® 122 PLUS

Two-component, polymer-modified, cementitious, trowel-grade mortar plus FerroGard 901 penetrating corrosion inhibitor



## Description

Sika Top 122 PLUS is a two-component, polymer-modified, portland-cement, fast-setting, trowel-grade mortar. It is a high performance repair mortar for horizontal and vertical surfaces and offers the additional benefit of FerroGard 901, a penetrating corrosion inhibitor.

## Where to Use

- On grade, above, and below grade on concrete and mortar.
- On horizontal surfaces.
- As a structural repair material for parking structures, industrial plants, walkways, bridges, tunnels, dams, and ramps.
- To level concrete surfaces.
- As an overlay system for topping/resurfacing concrete.
- Overlay in cathodic protection systems.

## Advantages

- High compressive and flexural strengths.
- High early strengths. Opens to traffic fast: foot in 4-6 hours, pneumatic tire in 8-12 hours.
- High abrasion resistance.
- Increased freeze/thaw durability and resistance to deicing salts.
- Compatible with coefficient of thermal expansion of concrete - Passes ASTM C-884 (modified).
- Increased density - improved carbon dioxide resistance (carbonation) without adversely affecting water vapor transmission (not a vapor barrier).
- Enhanced with FerroGard 901, a penetrating corrosion inhibitor - reduces corrosion even in the adjacent concrete.
- Not flammable, non-toxic.
- Conforms to ECA/USPHS standards for surface contact with potable water.
- USDA approved for food industry.
- ANSI/NSF Standard 61 potable water approved.

## Yield

0.51 cu. ft./ unit mortar; 0.75 cu. ft./unit concrete; (Sika Top 122 + 42 lbs. 3/8 pea gravel)

## Packaging

Component 'A' - 1-gal. plastic jug; 4/carton.  
Component 'B' - 61.5-lb. multi-wall bag.

## Typical Data

(Material and curing conditions @ 73°F (23°C) and 50% R.H.)

## Shelf Life

One year in original, unopened packaging.

## Storage Conditions

Store dry at 40°-95°F (4°-35°C). Condition material to 65°-75°F before using. Protect Component 'A' from freezing; if frozen, discard.

## Color

Concrete gray when mixed.

## Mixing Ratio

Plant-proportioned kit. Mix entire unit.

## Application

Approximately 30 minutes.

## Time

Application time is dependent on temperature and relative humidity.

## Finishing Time

50-120 minutes (**Note:** All times start after adding Component 'B' to Component 'A' and are highly affected by temperature, relative humidity, substrate temperature, wind, sun and other job site conditions.)

## Density (wet mix)

136 lbs./cu. ft. (2.18 kg./l)

## Flexural Strength (ASTM C-293)

28 days 2,000 psi (13.8 MPa)

## Splitting Tensile strength (ASTM C-496)

28 days 750 psi (5.2 MPa)

## Bond Strength\* (ASTM C-882 modified)

28 days 2,200 psi (15.2 MPa)

## Bond Strength Pull-Out Test

## Compressive Strength (ASTM C-109)

1 day 1,250 psi (8.6 MPa)

7 days 5,000 psi (34.5 MPa)

28 days 6,000 psi (41.4 MPa)

## Permeability (AASHTO T-277)

28 days Approximately 500 Coulombs

## Freeze/Thaw Resistance (ASTM C-666)

300 cycles 98%

## Corrosion Testing for ferrogard 901

## Cracked Beam Corrosion Tests:

Reduced corrosion rates 63% versus control specimens.  
ASTM G109 modified after 400 days.

\* Mortar scrubbed into substrate.

## How to Use

### Substrate

Concrete, mortar, and masonry products.

**Surface Preparation:** Concrete/Mortar: Remove all deteriorated concrete, dirt, oil, grease, and all bond-inhibiting materials from surface. Be sure repair area is not less than 1/8 inch in depth. Preparation work should be done by high pressure water blast, scabber, or other appropriate mechanical means to obtain an exposed aggregate surface with a minimum surface profile of  $\pm 1/16$  inch (CSP-5). Saturate surface with clean water. Substrate should be saturated surface dry (SSD) with no standing water during application.

# SIKATOP® 122 PLUS

Two-component, polymer-modified, cementitious, trowel-grade mortar plus FerroGard 901 penetrating corrosion inhibitor



**Reinforcing Steel:** Steel reinforcement should be thoroughly prepared by mechanical cleaning to remove all traces of rust. Where corrosion has occurred due to the presence of chlorides, the steel should be high-pressure washed with clean water after mechanical cleaning. For priming of reinforcing steel use Sika Armatec 110 EpoCem (consult Technical Data Sheet).

## Priming

**Concrete Substrate:** Prime the prepared substrate with a brush or sprayed applied coat of Sika Armatec 110 EpoCem (consult Technical Data Sheet). Alternately, a scrub coat of SikaTop 122 Plus can be applied prior to placement of the mortar. The repair mortar has to be applied into the wet scrub coat before it dries.

## Mixing

Pour approximately 7/8 of Component 'A' into the mixing container. Add Component 'B' (powder) while mixing continuously. Mix mechanically with a low-speed drill (400-600 rpm) and mixing paddle or mortar mixer. Add remaining Component 'A' (liquid) to mix if a more loose consistency is desired. Mix to a uniform consistency, maximum 3 minutes. Thorough mixing and proper proportioning of the two components is necessary. For SikaTop 122 PLUS concrete: Pour all of Component 'A' into mixing container. Add all of Component 'B' while mixing, then introduce 3/8 inch coarse aggregate at desired quantity. Mix to uniform consistency, maximum 3 minutes. Addition rate is 42 lbs. per bag (approx. 3.0 to 3.5 gal. by loose volume). The aggregate must be non-reactive (reference ASTM C1260, C227 and C289), clean, wellgraded, saturated surface dry, have low absorption and high density, and comply with ASTM C 33 size number 8 per Table 2. Note: Variances in the quality of the aggregate will affect the physical properties of SikaTop 122 PLUS. The yield is increased to 0.75 cu. ft./unit with the addition of the aggregate (42 lbs.). Do not use limestone aggregate.

## Application & Finish

SikaTop 122 PLUS must be scrubbed into the substrate, filling all pores and voids. Force material against edge of repair, working toward center. After filling repair, consolidate, then screed. Allow mortar or concrete to set to desired stiffness, then finish with wood or sponge float for a smooth surface, or broom or burlap-drag for a rough finish.

## Curing

As per ACI recommendations for portland cement concrete, curing is required. Moist cure with wet burlap and polyethylene, a fine mist of water or a water based\* compatible curing compound. Curing compounds adversely affect the adhesion of following layers of mortar, leveling mortar or protective coatings. Moist curing should commence immediately after finishing. Protect newly applied material from direct sunlight, wind, rain and frost. \*Pretesting of curing compound is recommended.

Sika warrants this product for one year from date of installation to be free from manufacturing defects and to meet the technical properties on the current technical data sheet if used as directed within shelf life. User determines suitability of product for intended use and assumes all risks. Buyer's sole remedy shall be limited to the purchase price or replacement of product exclusive of labor or cost of labor. NO OTHER WARRANTIES EXPRESSED OR IMPLIED SHALL APPLY INCLUDING ANY WARRANTY OF MERCHANTABILITY OR FITNESS FOR A PARTICULAR PURPOSE. SIKA SHALL NOT BE LIABLE UNDER ANY LEGAL THEORY FOR SPECIAL OR CONSEQUENTIAL DAMAGES.

## Limitations

Application thickness:	Min.	Max. in one lift
Neat	1/8 inch (3 mm)	1 inch (25 mm)
Extended	1 inch (25 mm)	4 inches (100 mm)

- Minimum ambient and surface temperatures 45°F (7°C) and rising at time of application.
- Addition of coarse aggregates may result in variations of the physical properties of the mortar.
- Do not use solvent-based curing compound.
- Size, shape and depth of repair must be carefully considered and consistent with practices recommended by ACI. For additional information, contact Technical Service.
- For additional information on substrate preparation, refer to ICRI Guideline No.03732 Coatings, and Polymer Overlays.
- If aggressive means of substrate preparation is employed, substrate strength should be tested in accordance with ACI 503 Appendix A prior to the repair application.
- As with all cement based materials, avoid contact with aluminum to prevent adverse chemical reaction and possible product failure. Insulate potential areas of contact by coating aluminum bars, rails, posts etc. with an appropriate epoxy such as Sikadur Hi-Mod 32.

## Caution

**Component 'A'** - Irritant - May cause skin/eye/respiratory irritation. Avoid breathing vapors. Use with adequate ventilation. Avoid skin and eye contact. Safety goggles and rubber gloves are recommended.

**Component 'B'** - Irritant; suspect carcinogen - Contains portland cement and sand (crystalline silica). Skin and eye irritant. Avoid contact. Dust may cause respiratory tract irritation. Avoid breathing dust. Use only with adequate ventilation. May cause delayed lung injury (silicosis). IARC lists crystalline silica as having sufficient evidence of carcinogenicity in laboratory animals and limited evidence of carcinogenicity in humans. NTP also lists crystalline silica as a suspect carcinogen. Use of safety goggles and chemical resistant gloves is recommended. If PELs are exceeded, an appropriate, NIOSH approved respirator is required. Remove contaminated clothing.

## First Aid

In case of skin contact, wash thoroughly with soap and water. For eye contact, flush immediately with plenty of water for at least 15 minutes, and contact a physician. For respiratory problems, remove person to fresh air.

## Clean Up

In case of spillage, scoop or vacuum into appropriate container, and dispose of in accordance with current, applicable local, state and federal regulations. Keep container tightly closed and in an upright position to prevent spillage and leakage. Mixed components: Uncured material can be removed with water. Cured material can only be removed mechanically.

Chemical analysis, MRT Labadie, Silo C, sample date 3/4/11, sample ID # 11MRSM037

	<u>Class C</u>	<u>Method</u>	<u>Analysis:</u>			
<b>Silicon Dioxide</b>	33.46	ICP	Sam Marshall			
<b>Aluminum Oxide</b>	19.53	ICP				
<b>Ferric Oxide</b>	6.28	ICP				
<b>Calcium Oxide</b>	26.28	ICP				
<b>Magnesium Oxide</b>	5.54	ICP				
<b>Sulfur Trioxide</b>	2.40	LECO				
<b>Loss on Ignition</b>	0.34	C311				
<b>Moisture</b>	0.15	C311				
<b>Potassium Oxide</b>	0.45	ICP				
<b>Phosphorus Pentoxide</b>	1.30	ICP				
<b>Titanium Dioxide</b>	1.48	ICP				
<b>Sodium Oxide</b>	1.728	ICP				
<b>Manganic Oxide</b>	0.041	ICP				
<b>Zinc Oxide</b>	0.019	ICP				
<b>Chromium Oxide</b>	0.011	ICP				
<b>Barium Oxide</b>	0.841	ICP				
<b>Strontium Oxide</b>	0.397	ICP				
<b>Sum Oxides (Si+Al+Fe)</b>	59.270	C618				
<b>Available alkalis</b>						
<b>TOTALS</b>	<b>98.86</b>			<b>0.00</b>		<b>0.00</b>

**APPENDIX B**  
**SAMPLE SURVEY QUESTIONNAIRE**

Dear Valued Partner,

The Missouri University of Science and Technology (Missouri S&T), in association with the Missouri Department of Transportation (MoDOT), is conducting research in the use of Self-Consolidating Concrete (SCC) for bridge structural elements. The research is focused on testing mixes and aggregates likely to be used in Missouri, because previous research has shown SCC to be sensitive to the materials used.

Dr. John Myers and Graduate Research Assistant Eric Sells with Missouri S&T has developed a SCC survey, and we would appreciate valuable input from industry leading companies such as your own. We understand your business is built upon the quality mix designs your company has developed; therefore, all survey responses will be kept strictly confidential and only seen by the research team and limited technical contacts within MoDOT. With these safeguards in place, we respectfully request that you complete the SCC survey.

We appreciate your valuable input. If you have any questions regarding the integrity of this research please contact Jen Harper at (573)526-3636 or Jennifer.harper@modot.gov. If you experience any problems with the survey itself, please contact Eric Sells at (417)298-4932 or ebsn87@mail.mst.edu

1. What is your Contact information?

- (a) What is your name? \_\_\_\_\_
- (b) What is your position? \_\_\_\_\_
- (c) How long have you had this position? \_\_\_\_\_
- (d) What is your Phone number? \_\_\_\_\_
- (e) What is your email address? \_\_\_\_\_

2. Does your company use Self-Consolidating Concrete (SCC)? (highlight one)      Yes      No

- (a) If Not, Why: \_\_\_\_\_  
\_\_\_\_\_
- (b) If So, When did you first begin producing SCC mixes? \_\_\_\_\_

3. About what percentage of your current projects use SCC? \_\_\_\_\_ %

4. For what Applications have you used SCC mixes? (highlight)

- |                      |                 |                          |                  |
|----------------------|-----------------|--------------------------|------------------|
| Architectural Panels | Shear Walls     | Structural Beams/Girders | Reinforced Slabs |
| Pipes/Culverts       | Retaining Walls | Bridge Deck Panels       | Columns          |

Other: \_\_\_\_\_

5. What has been the range of strengths achieved?

- (a) At time of release: \_\_\_\_\_
- (b) Design Strength (28 day): \_\_\_\_\_

6. What types of coarse aggregates have been used? (highlight)

River Gravel                      Dolomitic Limestone      Calcitic Limestone                      Quartz

Blast Furnace Slag              Chert                                      Expanded Shale or Slate

Other: \_\_\_\_\_

7. What maximum aggregate size was used? \_\_\_\_\_

8. What fraction (by weight) of coarse aggregate was used? \_\_\_\_\_ %

9. What has been typical mix designs used? (Please list specific mixes used, ranges of typically used mixes, or both)

- Cement Type (I-V) \_\_\_\_\_.
- Cement Dosage (lb/cy) \_\_\_\_\_.
- Coarse Agg. Type \_\_\_\_\_.
- Coarse Dosage (lb/cy) \_\_\_\_\_.
- Fine Agg. Type \_\_\_\_\_.
- Fine Agg. Dosage (lb/cy) \_\_\_\_\_.
- Mineral Admixtures Type \_\_\_\_\_.
- Mineral Admix. Dosage (lb/cy) \_\_\_\_\_.
- Chemical Admix. Type (air) \_\_\_\_\_.
- Dosage (oz/cwt) \_\_\_\_\_.
- Chem. Admix. Type (WR/HRWRA) \_\_\_\_\_.
- Dosage (oz/cwt) \_\_\_\_\_.
- Chem. Admix. Type (VMA) \_\_\_\_\_.
- Dosage (oz/cwt) \_\_\_\_\_.

10. Who is/are your aggregate/materials supplier(s)? \_\_\_\_\_

(This will be used to determine index properties of the raw materials)

11. Who is/are your chemical admixture supplier(s)? \_\_\_\_\_

(This will be used to determine admixture alternatives and market base for these types of chemicals)

12. May we contact you for additional information if a trend is realized through the survey responses, research results, or for clarifying information? (highlight one)              Yes              No

13. Preferred Contact Method? (highlight)              Phone              E-mail

**APPENDIX C**  
**SAMPLE BATCH WEIGHT AND FRESH PROPERTY RESULT**  
**SPREADSHEETS**

w/Cm	0.37
Batch (ft <sup>3</sup> )	3.35
F.A. % (of Agg. Portion)	42%
Air Dosage (oz/cwt)	0.7
HRWRA Dosage (oz/cwt)	3.1

Batch ID	C6-58L (8/3/2011)	
Addmixtures (mL)		
Air	MB-AE-90	19
HRWRA	Glenium 7700	85

Material	Weight ,W (lb)	Specific Gravity, G (lb/ft <sup>3</sup> )	Unit Weight Water, $\gamma_w$ (lb/ft <sup>3</sup> )	Abs. Volume (ft <sup>3</sup> )	Agg. Water Correction (lb)	Agg. Batch Correction	Final Batch Weights
Cement	750.00	3.15	62.4	3.82	---	---	93.1
Water	277.50	1.00	62.4	4.45	---	---	39.8
Air	0.06	0.00		1.62	---	---	0.0
C.A.	1610.7	2.60	62.4	9.93	-44.4	1614.6	200.3
F.A.	1166.3	2.60	62.4	7.19	1.5	1176.1	145.9

TMC <sub>C.A.</sub>	0.243	Absorption <sub>C.A.</sub>	3	SM <sub>C.A.</sub>	-2.757
TMC <sub>F.A.</sub>	0.831	Absorption <sub>F.A.</sub>	0.7	SM <sub>F.A.</sub>	0.131

Record:

Batch Time	Before HRWRA	After HRWRA	Measured Air Content	Temp.	Unit Weight

Note Any Abnormalities:

**Yellow Cells** – Input cells which may vary from batch proportion to batch proportion  
**Blue Cells** – Output cells which vary depending upon input cells

Figure C.1 – Sample Batch Weight Spreadsheet

Static Segregation		ASTM C1610		Batch ID		S1-36L (8/1/2011)	
		(Less than A + 2 min)	(B + 15min +/- 1 min)	To nearest .1 lb		(Less than C + 20 min)	2(E-D)/(E+D) in %
	A	B	C	D	E	F	G
Batch ID	Time Begin	Time finished	Time after Standing	OD #4 sieve of top	OD #4 sieve of bottom	Time finished	Static Seg.
S1-36L							
S1-36L							

Slump Flow and T <sub>50</sub>		ASTM C1611				
		Largest dia.	Perp. Dia. (nearest .25in)	(A+B)/2 (nearest .5in)	Time to 20 in (nearest .2sec)	See Appendix of ASTM for guidance
		A	B	C	D	E
Batch ID	d <sub>1</sub>	d <sub>2</sub>	Slump Flow	T <sub>50</sub>	VSI	
S1-36L						
S1-36L						

J-Ring		ASTM C1621			
		Largest dia.	Perp. Dia. (.25in)	(A+B)/2 (.5in)	See Tbl 1 of ASTM for guidance
		A	B	C	D
Batch ID	j <sub>1</sub>	j <sub>2</sub>	J-Ring Flow	Blocking Assessment	
S1-36L					
S1-36L					

L-Box		Non-standard		
		Height Gate	Height End	(B/A)
		A	B	D
Batch ID	h1	h2	Filling Ability	
S1-36L				
S1-36L				

Note: some brief instruction to ensure consistency with associated ASTM test standards.

**Figure C.2 – Sample Fresh Property Spreadsheet (Unpopulated)**

**APPENDIX D**  
**SHEAR BEAM DESIGN AID**

X-Section Details		
h	16	in
yt	8	in
yb	8	in
b	8	in
A	128	in <sup>2</sup>
I	2731	in <sup>4</sup>
L	17	ft
f'ci	4000	psi

Tendon Details							
Line	# Tendons	g (in)			Area (in <sup>2</sup> )		
		North End	Mid	South End			
1	2	2	2	2	0.153	fpu	270000
2	2	4	4	4	0.153	fpi	189000
3	0	6	6	6	0.153	fse	170100
Tot	4						
	e	5	5	5			

-----> 0.63 fpu

Fiber Stresses						
	End			Mid		
	Calc.	Limit	Accept?	Calc.	Limit	Accept?
f <sup>t</sup>	711.6293	379.4733	N.G.	542.2934	189.7367	N.G.
f <sub>b</sub>	-2338.21	-2800	OK	-2168.87	-2400	OK

-----> Can Reinforce

6ksi	
<b>Flexural Capacity</b>	
fps	251.8
a	3.78
Mn	1712.5
<b>Shear Capacity</b>	
Pu	53.5
Vu	35.7
Vc	24.6
	69%

10ksi	
<b>Flexural Capacity</b>	
fps	257.4
a	2.32
Mn	1865.6
<b>Shear Capacity</b>	
Pu	58.3
Vu	38.9
Vc	26.0
	67%

**Yellow** – Indicates percentage of predicted concrete shear capacity relative to ultimate shear produced at the predicted flexural capacity

**Figure D.1 – Shear Beam Design Aid Spreadsheet**

**FINAL Report B**

TRyy1103

**Project Title: Self-Consolidating Concrete (SCC) for Infrastructure Elements**

**Report B: Self-Consolidating Concrete (SCC) for Infrastructure Elements: Bond, Transfer Length, and Development Length of Prestressing Strand in SCC**

Prepared for  
Missouri Department of Transportation  
Construction and Materials

Missouri University of Science and Technology, Rolla, Missouri

July 2012

The opinions, findings, and conclusions expressed in this publication are those of the principal investigators and the Missouri Department of Transportation. They are not necessarily those of the U.S. Department of Transportation, Federal Highway Administration. This report does not constitute a standard or regulation



## ABSTRACT

Due to its economic advantages, the use of self-consolidating concrete (SCC) has increased rapidly in recent years. However, because SCC mixes typically have decreased amounts of coarse aggregate and high amounts of admixtures, industry members have expressed concerns that the bond of prestressing strand in SCC may be compromised. While the bond performance of prestressing strand in a new material such as SCC is an important topic requiring investigation, the results are only applicable if the research is completed on strands with similar bond quality as the strands used in the field. Therefore, the objectives of this research program were to investigate the transfer and development lengths of prestressing strand in SCC and also evaluate the effectiveness of two proposed bond tests in determining acceptable bond quality of strand.

Transfer and development lengths of 0.5-in. diameter (12.5 mm), Grade 270 prestressing strand were evaluated using rectangular beams constructed from normal and high strength conventional concrete and SCC mixes. End slips at release and strain readings over 28 days were used to calculate transfer lengths, and development lengths were evaluated through four-point loading at varying embedment lengths. Additionally, the NASP bond test and Large Block Pullout Tests (LBPT) were evaluated with strand from three different sources to determine if one test could be considered more reliable at predicting acceptable bond.

Results indicated that bond performance of SCC and conventional concrete were comparable, and that AASHTO and ACI equations for transfer and development length were generally conservative. The NASP bond test and LBPT were found to be equally valid, but the acceptance limits for both tests appear to require revisions.

## TABLE OF CONTENTS

	Page
ABSTRACT .....	iii
LIST OF ILLUSTRATIONS .....	viii
LIST OF TABLES .....	xiii
NOMENCLATURE .....	xvi
1. INTRODUCTION .....	1
1.1. BACKGROUND .....	1
1.2. OBJECTIVES .....	2
1.3. SCOPE .....	3
1.4. OUTLINE .....	4
2. LITERATURE REVIEW .....	6
2.1. INTRODUCTION .....	6
2.2. EXPLANATION OF TRANSFER LENGTH, FLEXURAL BOND LENGTH, AND DEVELOPMENT LENGTH .....	6
2.3. BOND THEORY .....	7
2.3.1. Adhesion .....	8
2.3.2. Hoyer Effect .....	8
2.3.3. Mechanical Interlock .....	9
2.4. FACTORS AFFECTING TRANSFER AND DEVELOPMENT LENGTHS ..	9
2.4.1. Strand Size .....	10
2.4.2. Steel Stress Level .....	10
2.4.3. Concrete Strength .....	10
2.4.4. Time Dependent Losses .....	11
2.4.5. Type of Release .....	12
2.4.6. Consolidation and Consistency of Concrete around Strand .....	12
2.5. ACI AND AASHTO CODE EQUATIONS .....	13
2.5.1. AASHTO LRFD Bridge Design Specifications .....	13
2.5.2. ACI 318-11 .....	15
2.5.3. Background of the AASHTO and ACI Development Length	

Equations .....	16
<b>2.6. RESEARCH REGARDING ACCEPTANCE OF A STANDARD BOND TEST .....</b>	<b>19</b>
2.6.1. Logan (1997) .....	19
2.6.2. Rose and Russell (1997).....	21
2.6.3. NASP Bond Testing Rounds I-IV .....	22
2.6.4. Ramirez and Russell (2008).. .....	26
2.6.5. Current Status and Recent Developments .....	27
<b>2.7. RESEARCH REGARDING BOND OF PRESTRESSING STRAND IN SCC .....</b>	<b>28</b>
2.7.1. Girgis and Tuan (2005) .....	28
2.7.2. Larson, Peterman, and Esmaeily (2007) .....	29
2.7.3. Pozolo and Andrawes (2011) .....	31
2.7.4. Staton, Do, Ruiz, and Hale (2009) .....	32
2.7.5. Floyd, Ruiz, Do, Staton, and Hale (2011) .....	33
2.7.6. Boehm, Barnes, and Schindler (2010).....	34
2.7.7. Burgueño and Haq (2007) .....	35
<b>3. BOND TEST PROGRAM AND RESULTS .....</b>	<b>36</b>
3.1. INTRODUCTION .....	36
3.2. TENSILE PROPERTIES OF PRESTRESSING STRANDS.....	38
3.2.1. Tension Test Setup and Procedure .....	38
3.2.2. Tension Test Results .....	40
3.3. NASP BOND TEST .....	42
3.3.1. NASP Test Specimen Design.....	42
3.3.2. NASP Test Specimen Fabrication.....	45
3.3.3. NASP Test Setup and Procedure.....	49
3.3.4. NASP Test Results .....	53
3.3.4.1 Results from Standard NASP Test in Mortar .....	53
3.3.4.2 Results from Modified NASP Test in Concrete .....	57
3.4. LARGE BLOCK PULLOUT TEST.....	61
3.4.1. LBPT Specimen Design .....	61

3.4.2. LBPT Specimen Fabrication .....	63
3.4.3. LBPT Test Setup and Procedure .....	66
3.4.4. LBPT Results .....	69
4. TRANSFER LENGTH AND DEVELOPMENT LENGTH TEST PROGRAM AND RESULTS.....	76
4.1. INTRODUCTION .....	76
4.2. TRANSFER AND DEVELOPMENT LENGTH BEAM DESIGN.....	76
4.2.1. Mix/Specimen Identifications and Mix Designs .....	76
4.2.2. Fresh and Hardened Properties of Concrete Mixtures .....	78
4.2.3. Strand and Mild Reinforcement Design.....	80
4.3. TRANSFER AND DEVELOPMENT LENGTH BEAM FABRICATION ....	83
4.4. TRANSFER LENGTH TEST SETUPS, PROCEDURES, AND RESULTS ..	86
4.4.1. 95% Average Mean Strain Method .....	87
4.4.1.1 DEMEC Instrumentation .....	87
4.4.1.2 95% Average Mean Strain Procedure.....	91
4.4.1.3 95% Average Mean Strain Transfer Lengths.....	93
4.4.2. End Slip Method of Determining Initial Transfer Length.....	97
4.4.2.1 Linear Potentiometer Setup and Procedure.....	98
4.4.2.2 Steel Ruler Setup and Procedure.....	105
4.4.2.3 Transfer Length Determination from End Slip Data .....	107
4.5. DEVELOPMENT LENGTH TEST SETUP, PROCEDURE, AND RESULTS .....	110
4.5.1. Four-Point Loading Setup and Instrumentation .....	111
4.5.2. Four-Point Loading Procedure .....	115
4.5.3. Four-Point Loading Results.....	116
5. DISCUSSION AND COMPARISON OF RESULTS .....	120
5.1. INTRODUCTION .....	120
5.2. BOND TEST RESULTS .....	120
5.2.1. Discussion of NASP Test in Mortar Results .....	121
5.2.2. Discussion of NASP Test in Concrete Results.....	128
5.2.3. Discussion of LBPT Results.....	135

5.2.4. Comparison of NASP Test in Mortar Results to LBPT Results .....	136
5.3. TRANSFER LENGTH TEST RESULTS .....	140
5.3.1. Discussion of 95% Average Mean Strain Transfer Length Results.....	140
5.3.1.1 Comparison of SCC to Conventional Concrete .....	146
5.3.1.2 Comparison of Normal Strength to High Strength .....	153
5.3.1.3 Comparison of Bottom Strand to Top Strand .....	159
5.3.1.4 Change in Transfer Length over Time.....	164
5.3.1.5 Comparison to AASHTO and ACI Equations for Transfer Length. ....	166
5.3.2. Discussion of Initial End Slip Transfer Length Results .....	171
5.3.3. Correlation of NASP Test in Concrete Results to 95% Average Mean Strain Transfer Lengths .....	175
5.4. DEVELOPMENT LENGTH TEST RESULTS .....	185
6. FINDINGS, CONCLUSIONS, AND RECOMMENDATIONS .....	191
6.1. FINDINGS.....	191
6.1.1. Bond Test Results.....	191
6.1.2. Transfer Length Test Results .....	192
6.1.3. Development Length Test Results .....	194
6.2. CONCLUSIONS .....	195
6.3. RECOMMENDATIONS.....	197

## LIST OF ILLUSTRATIONS

Figure	Page
2.1 – Variation of Stress in a Strand Along the Length of a Beam (Adapted from ACI 318-11) .....	7
2.2 – Hoyer Effect (Adapted from Russell and Burns 1993).....	8
2.3 – Original Representation of Flexural Bond Length (adapted from Tabatabai and Dickson, 1993) .....	18
3.1 – Bond Test Identification Code .....	37
3.2 – Tension Test Specimens .....	39
3.3 – Tension Test Setup.....	40
3.4 – Fractured Tension Test Specimen.....	41
3.5 – NASP Specimen Mold .....	43
3.6 – Strands with Bond Breakers.....	43
3.7 – Mortar Mix in Drum Mixer.....	46
3.8 – Flow Test .....	47
3.9 – Mortar Cubes .....	47
3.10 – NASP Mold and Strand Setup .....	48
3.11 – Filling Specimens for NASP Test in Concrete .....	49
3.12 – Capped NASP in Concrete Specimens and Cylinders.....	49
3.13 – NASP Test Frame .....	51
3.14 – NASP Test Setup .....	52
3.15 – NASP Test Setup Details .....	52
3.16 – NASP Test LVDT Setup.....	53
3.17 – Typical Load vs. Slip Plot for NASP Test in Mortar (N-101-A).....	54
3.18 – Typical Load vs. Slip Plot for Concrete NASP Test (N-101-S6).....	58
3.19 – Cross-Section of LBPT Specimen .....	62
3.20 – Profile of LBPT Specimen.....	62
3.21 – Strand Layout Pattern .....	63
3.22 – LBPT Specimen Before Casting.....	64
3.23 – Casting the LBPT Specimen.....	65

3.24 – Finished LBPT Specimen .....	66
3.25 – LBPT Hydraulic Jack and Load Cell Setup.....	67
3.26 – Steel Table for LBPT .....	68
3.27 – Full LBPT Setup .....	69
3.28 – Visual Comparison of Strands .....	72
3.29 – Towel Wipe Results for Strand Type 101.....	73
3.30 – Towel Wipe Results for Strand Type 102.....	73
3.31 – Towel Wipe Results for Strand Type 103.....	73
4.1 – Mix and Specimen Identification Code .....	77
4.2 - Two-Strand Beam Cross-Section .....	81
4.3 – Four-Strand Beam Cross-Section .....	81
4.4 – Profile of Two-Strand Beams .....	82
4.5 – Profile of Four-Strand Beams .....	82
4.6 – C6 and S6 Prestressing Bed Layout.....	84
4.7 – C10 and S10 Prestressing Bed Layout.....	84
4.8 – Beam Fabrication at Coreslab Structures in Marshall, MO.....	85
4.9 – Beams After Form Removal and Before Instrumentation .....	85
4.10 – Bolt Cutting Strands at Release .....	86
4.11 – Setting DEMEC Points with Setting Bar .....	88
4.12 – Honeycombing Preventing DEMEC Placement at Point 4 on C10-4-1_SW .....	89
4.13 – Taking DEMEC Readings .....	90
4.14 – C6 and S6 Beams in Storage Yard at Coreslab.....	90
4.15 – Mean Strains .....	91
4.16 – Typical 95% Average Mean Strain Smoothed Curve for Determining Transfer Lengths – S-10-2-2-NE and S10-2-2_SE.....	92
4.17 – Typical 95% Average Mean Strain Smoothed Curves for Determining Transfer Lengths from 1 to 28 Days – S10-2-2-NE and S10-2-2_SE.....	93
4.18 – Relationship Between Steel Stress and Strain and Transfer Length (adapted from Russell and Burns, 1993).....	98
4.19 – Linear Potentiometer Setup.....	99
4.20 – Synergy Data Acquisition Computer Setup.....	99

4.21 – Improved Potentiometer-FRP Assemblies with Zip Ties and Plastic Epoxy (Top) and Gorilla Glue Expanding Foam (Bottom).....	102
4.22 – Typical End Slip Plot: C6 Two-Strand Beams Potentiometer Reading vs. Time Elapsed Plot from Synergy.....	104
4.23 – Electrical Tape on Strands for Steel Ruler Measurements of End Slip.....	106
4.24 – Four-Point Loading Test Setup for Evaluating 58-in. (1,473 mm) Embedment Length .....	112
4.25 – 58 in. (1,473 mm) Embedment Length Test Setup.....	113
4.26 – 73 in. (1,854 mm) Embedment Length Test Setup.....	113
4.27 – LVDT Setup for Measuring Deflection at Midspan .....	114
4.28 – Linear Potentiometer Setup on Four-Point Loading Tests .....	115
4.29 – Cracks Marked with Permanent Marker during Development Length Test.....	116
4.30 – Typical Moment vs. Deflection and Strand End Slip vs. Deflection Plot from Four-Point Loading Data.....	117
4.31 – Typical Concrete Crushing Failure for Development Length Tests.....	118
5.1 – NASP in Mortar Pullout Values .....	121
5.2 – N-101-B Load vs. Slip .....	123
5.3 – N-102-B Load vs. Slip.....	124
5.4 – N-103-B Load vs. Slip.....	124
5.5 – Comparison of N-101-A and N-101-B Pullout Loads.....	128
5.6 – NASP in Concrete Pullout Loads – 1 Day.....	129
5.7 – NASP in Concrete Pullout Loads – 8 Day.....	130
5.8 – NASP in Concrete Pullout Loads $\sqrt{f'_c}$ – 1 Day.....	134
5.9 – NASP in Concrete Pullout Loads $\sqrt{f'_c}$ – 8 Day.....	134
5.10 – LBPT Average First Slip and Peak Pullout Loads .....	136
5.11 – LBPT Pullout Loads vs. NASP Pullout Loads .....	139
5.12 – C6 and S6 Transfer Length Locations .....	142
5.13 – C10 and S10 Transfer Length Locations .....	142
5.14 – Release of C10-2 Beams.....	144
5.15 – C6-2 and S6-2 Transfer Lengths with 90% Confidence Intervals.....	148
5.16 – C10-2 and S10-2 Transfer Lengths with 90% Confidence Intervals.....	148

5.17 – C10-2 (D) and S10-2 Transfer Lengths with 90% Confidence Intervals .....	149
5.18 – C6-4 and S6-4 Transfer Lengths with 90% Confidence Intervals.....	151
5.19 – C10-4 and S10-4 Transfer Lengths with 90% Confidence Intervals.....	151
5.20 – C10-4 and S10-4 (D) Transfer Lengths and 90% Confidence Intervals.....	152
5.21 – C6-2 and C10-2 Transfer Lengths and 90% Confidence Intervals.....	154
5.22 – C6-2 and C10-2 (D) Transfer Lengths and 90% Confidence Intervals .....	155
5.23 – S6-2 and S10-2 Transfer Lengths and 90% Confidence Intervals.....	155
5.24 – C6-4 and C10-4 Transfer Lengths and 90% Confidence Intervals.....	157
5.25 – S6-4 and S10-4 Transfer Lengths and 90% Confidence Intervals.....	158
5.26 – S6-4 and S10-4 (D) Transfer Lengths and 90% Confidence Intervals .....	158
5.27 – C6-2 and C6-4 Transfer Lengths and 90% Confidence Intervals.....	160
5.28 – C10-2 and C10-4 Transfer Lengths and 90% Confidence Intervals.....	161
5.29 – C10-2 (D) and C10-4 Transfer Lengths and 90% Confidence Intervals .....	161
5.30 – S6-2 and S6-4 Transfer Lengths and 90% Confidence Intervals.....	162
5.31 – S10-2 and S10-4 Transfer Lengths and 90% Confidence Intervals.....	163
5.32 – S10-2 and S10-4 (D) Transfer Lengths and 90% Confidence Intervals .....	163
5.33 – Average Transfer Lengths Compared to AASHTO and ACI Equations (Bottom Strands) .....	169
5.34 – Average Transfer Lengths Compared to AASHTO and ACI Equations (Top Strands) .....	170
5.35 – NCHRP Normalized NASP Pull-out Values vs. Concrete Strength (Ramirez and Russell 2008).....	177
5.36 – NCHRP Normalized NASP Pull-out Values vs. $\sqrt{f'_c}$ (Ramirez and Russell 2008).....	177
5.37 – NCHRP Transfer Lengths vs. Normalized NASP Bond Values (Ramirez and Russell 2008).....	178
5.38 – Normalized NASP in Concrete Pullout Values vs. Concrete Strength (NCHRP and Missouri S&T).....	181
5.39 – Normalized NASP in Concrete Pullout Values vs. Square Root of Concrete Strength (NCHRP and Missouri S&T) .....	182
5.40 – Normalized NASP Value vs. Transfer Length at Release .....	183

5.41 – NCHRP Distribution of Bond and Flexural Failures for Strands A/B (Ramirez and Russell 2008)..... 187

5.42 – NCHRP and Missouri S&T Concrete Strength vs. Embedment Length Development Test Results..... 188

## LIST OF TABLES

Table	Page
2.1 – NASP Round II R2 Values Comparing Moustafa, PTI, and NASP Pullout Results Between Sites (Russell and Paulsgrove 1999b) .....	23
2.2 – Round III Coefficient of Variation ( $R^2$ ) Values Relating 28 Day Transfer Lengths to Bond Test Pullout Values (adapted from Hawkins and Ramirez 2010) .....	24
2.3 – Round III NASP Pullout Values and Failure Modes from Flexural Testing of Single Strand Beams (Hawkins and Ramirez 2010) .....	25
2.4 – Round III NASP Pullout Values and Failure Modes from Flexural Testing of Double Strand Beams (Hawkins and Ramirez 2010) .....	25
2.5 – Girgis and Tuan Results .....	29
2.6 – Concrete Strength at Testing and Development Length Ranges .....	33
3.1 – Direct Tension Test Results .....	41
3.2 – Mortar Mix Design for NASP Tests .....	45
3.3 – NASP Test in Mortar Test Matrix .....	45
3.4 – NASP in Mortar Results for Strand 101 Mix A .....	55
3.5 – NASP in Mortar Results for Strand 101 Mix B .....	55
3.6 – NASP in Mortar Results for Strand 102 Mix B .....	56
3.7 – NASP in Mortar Results for Strand 103 Mix B .....	56
3.8 – Summary of NASP Test in Mortar Pullout Values and Mortar Properties .....	57
3.9 – Concrete NASP Results – C6 and S6 .....	59
3.10 – Concrete NASP Results – C10 and S10 .....	60
3.11 – Missouri S&T's and Logan's LBPT Mix Designs .....	64
3.12 – Fresh and Hardened Properties of LBPT Concrete Mix .....	66
3.13 – LBPT Results .....	70
3.13 Continued – LBPT Results .....	71
3.14 – Summary of LBPT Pullout Loads .....	75
4.1 – Mix Designs .....	78
4.2 – Fresh Concrete Properties .....	79
4.3 – Concrete Strengths and 28 Day Moduli of Elasticity .....	80

4.4 – Transfer Lengths for Top Strands of Four-Strand Beams (1-28 Days) .....	94
4.5 – Transfer Lengths for Bottom Strands of Two-Strand Beams (1-28 Days) .....	95
4.6 – Average Transfer Lengths for Top Strands of Four-Strand Beams .....	96
4.7 – Average Transfer Lengths for Bottom Strands of Two-Strand Beams .....	96
4.8 – Measured End Slips from Linear Potentiometers .....	105
4.9 – Measured End Slips from Steel Ruler .....	107
4.10 – Initial Transfer Lengths from Steel Ruler End Slips, Synergy End Slips, and DEMEC Data for Bottom Strands on C6 and S6 Beams .....	108
4.11 – Initial Transfer Lengths from Steel Ruler End Slips, Synergy End Slips, and DEMEC Data for Bottom Strands on C10 and S10 Beams .....	109
4.12 – Initial Transfer Lengths from Steel Ruler End Slips, Synergy End Slips, and DEMEC Data for Top Strands on C6, S6, C10, and S10 Beams .....	110
4.13. Nominal and Actual Moment Capacities .....	118
4.14 – Summary of Average Nominal and Actual Moment Capacities .....	119
5.1 – Average Pullout 0.1-in. (2.54 mm) Pullout Values from Missouri S&T and NCHRP 10-62 for Strands 102 and 103 .....	125
5.2 – N-101-A and N-101-B Pullout Loads .....	127
5.3 – NASP in Concrete Results for C6 and S6 Normalized to $\sqrt{f'_c}$ .....	132
5.4 – NASP in Concrete Results for C10 and S10 Normalized to $\sqrt{f'_c}$ .....	133
5.5 – LBPT Results Statistical Summary .....	135
5.6 – NASP in Mortar and LBPT Pullout Loads .....	138
5.7 – Pass/Fail Results for NASP in Mortar and LBPT .....	139
5.8 – Standard and Modified Transfer Length Averages (Bottom Strands) .....	145
5.9 – Standard and Modified Length Averages (Top Strands) .....	146
5.10 – Conventional Concrete vs. SCC: Summary of Statistical Differences Between Bottom Strand Transfer Lengths .....	149
5.11 – Conventional Concrete vs. SCC: Summary of Statistical Differences Between Top Strand Transfer Lengths .....	152
5.12 – Normal Strength vs. High Strength: Summary of Statistical Differences Between Bottom Strand Transfer Lengths .....	156

5.13 – Normal Strength vs. High Strength: Summary of Statistical Differences Between Top Strand Transfer Lengths .....	159
5.14 – Top Strand vs. Bottom Strand: Summary of Statistical Differences Between Transfer Lengths .....	165
5.15 – Summary of Increases in Transfer Lengths .....	165
5.16 – Ratio of Average Transfer Lengths to AASHTO and ACI Values (Bottom Strands) .....	169
5.17 – Ratio of Average Transfer Lengths to AASHTO and ACI Values (Top Strands) .....	170
5.18 – Comparison of Synergy-DEMEC and Ruler-DEMEC Transfer Lengths (Bottom Strands) .....	174
5.19 – Comparison of Synergy-DEMEC and Ruler-DEMEC Transfer Lengths (Top Strands) .....	175
5.20 – Summary of Data for Comparison with NCHRP Results.....	179
5.21 – Summary of Trend line Equations and R2 Values for NCHRP and Missouri S&T Data .....	184
5.22 – Comparison of Measured Transfer Lengths to Values Calculated by Current and Proposed AASHTO Equations.....	185
5.23 – Comparison of Experimental and Calculated Moment Capacities .....	186
5.24 – Comparison of Development Lengths Calculated by Current and Proposed AASHTO Equations.....	189

## NOMENCLATURE

Symbol	Description
$A_{ps}$	Area of prestressing strand, in <sup>2</sup>
$d_b$	Nominal diameter of strand, in. (ACI 318-11 and AASHTO LRFD-07)
$D$	Nominal diameter of strand, in. (Tabatabai and Dickson 1993)
$E_{ps}$	Modulus of elasticity of prestressing strand, psi or ksi
$f_c$	Concrete compressive strength at 28 days or otherwise specified, psi
$f_{ci}$	Concrete compressive strength at release, psi
$f_{ce}$	Stress in concrete outside transfer zone due to stress in strand immediately after release, psi or ksi
$f_{pe}$	Effective stress in the strand after losses, psi (AASHTO LRFD-07)
$f_{ps}$	Stress in prestressing steel at nominal flexural strength, psi (ACI 318-11)
$f_{pu}$	Specified tensile strength of prestressing steel, psi (ACI 318-11)
$f_{sb}$	Average stress in the steel at general bond slip, psi or ksi (Tabatabai and Dickson 1993)
$f_{si}$	Stress in strand immediately after release, instead of after all losses, psi or ksi (Buckner 1995)
$f_{si}$	Stress in strand immediately before release, psi or ksi (Anderson and Anderson 1976)
$f_{se}$	Effective stress in prestressing strand after allowance for all prestress losses, psi or ksi (ACI 318-11 and Tabatabai and Dickson 1993)
$f_{se}$	Effective stress in prestressing strand immediately after release, psi or ksi (Anderson and Anderson 1976)
$f_{su}$	Stress developed in the strand at ultimate strength of a member, ksi (Tabatabai and Dickson 1993)
$f_{su}^*$	Average stress in the prestressing steel at ultimate load, ksi (Tabatabai and Dickson 1993)
$f_u$	Ultimate tensile strength of prestressing strand as determined through a tension test in this research, ksi

$l_e$	Embedment length, in.
$l_d$	Development length, in. (AASHTO LRFD-07 and ACI 318-11)
$l_{fb}$	Flexural bond length, in.
$l_t$	Transfer length, in.
$L$	Embedment length, in. (Tabatabai and Dickson 1993)
$L_T$	Transfer length, in. (Tabatabai and Dickson 1993 and Anderson and Anderson 1976)
$M_{cr}$	Moment at which cracking first occurred in four-point load tests, k-in.
$M_n$	Calculated nominal moment capacity for four-point loading specimens, k-in.
$M_u$	Ultimate applied moment for four-point loading specimens, k-in.
$U_t$	Average bond stress, taken to be 0.4 ksi (Tabatabai and Dickson 1993)
$\Delta$	Measured end slip of strand at release, in.
$\epsilon_{ce}$	Strain in prestressing strand immediately after release, in./in.
$\epsilon_{se}$	Strain in prestressing strand immediately after release, in./in.
$\epsilon_{si}$	Strain in prestressing strand immediately before release, in./in.
$\Sigma_0$	Circumference of prestressing strand, in. (Tabatabai and Dickson 1993)
$\kappa$	Bond reduction factor of 1.6 for members greater than 24 in. deep (AASHTO LRFD-07)

## 1. INTRODUCTION

### 1.1. BACKGROUND

Self-consolidating concrete (SCC) is a material that is on the forefront of construction technology. The flowable nature of SCC eliminates the needs for mechanical vibration and finishing, which are typically required during placement of conventional concrete, saving costs in the form of labor, time, and equipment as well as increasing production rates at precast plants. In addition, the ability of SCC to securely fill formwork and congested areas of reinforcement under its own weight leads to a decrease in the potential for honeycombing and voids, resulting in better aesthetic appearance and structural quality. Despite the flowability of SCC, the concrete is still non-segregating due to the addition of certain admixtures and proper proportioning of the mix. The cost saving attributes, combined with the improved appearance and comparable structural quality compared to conventional concrete, make SCC especially of interest to precasters.

Although the economic and performance benefits make SCC desirable for use in construction, the addition of admixtures and adjustments to mix proportions that give SCC its unique qualities can alter structural properties when compared to conventional concrete, especially in terms of transfer and development lengths of prestressing strand. Because SCC mixes typically have decreased amounts of coarse aggregate and high amounts of admixtures, industry members have expressed concerns that the bond of prestressing strand in SCC may be compromised. In response to these concerns, some research programs have recently been implemented, especially by state Departments of Transportation, to investigate the effects of SCC on prestressing strand and determine if SCC is acceptable for precast plants to use in the construction of prestressed members, such as infrastructure elements (Boehm et al. 2010, Larson et al. 2007).

While the bond of prestressing strand in SCC has been a current research subject, the bond quality of prestressing strand in general has also been a topic of interest in recent years. Only in the past few decades have concerns regarding excessive end slips of strands and measured transfer lengths significantly longer than those predicted by the AASHTO LRFD and ACI 318 equations begun to surface (Cousins et al. 1990). Research has since indicated that bond quality is an inherent property of the strand and can vary

from source to source. These recent issues with bond quality are most likely due to the current production process of prestressing strand compared to the original production processes. Today's strands are typically heated through induction, while the original process employed convection heating. The convection process heated the strands to much higher temperatures, and it is hypothesized that the higher temperatures burned off more of the residues from the wire drawing process and combusted the organic impurities on the surfaces (Rose and Russell 1997). It is believed that the lower temperatures from induction heating result in more residues left on the strands, which could affect bond; however, a direct correlation has not yet been established.

While the exact relationship between production process and bond quality has yet to be determined, differences in bond quality of strands have still been proven to exist, and as a result, several tests for assessing the bond quality of strands have been proposed. These pullout tests consist of sections of strand cast in concrete or mortar, and acceptable bond quality is determined by comparing the average pullout load to a minimum value. The different pullout tests and the standard limits for the tests have been investigated since the mid 1990's, but a standard test and limit have still not been accepted.

Bond of prestressing strand has become an important topic in recent years, especially as new materials are being developed and put into use. While the bond of prestressing strand in a new material such as SCC is an important topic that deserves investigation, the results are only valid and applicable if the research tests are completed on strands with similar bond quality as the type of strand being used in the field. Therefore, it is important to develop a test that can pre-qualify strand based on bond so researchers as well as industry members can use similar strand types, so trends seen in test results will be accurately reflected in the field.

## **1.2. OBJECTIVES**

In order to investigate the possibility of implementing specifications that would allow precasters to use SCC for the construction of infrastructure elements for Missouri projects, the Missouri Department of Transportation (MoDOT) funded a research project examining the effect of SCC on various structural properties, including shear, durability, creep and shrinkage, bond with mild steel reinforcement, and bond with prestressing

strand. The portion of the research program related to the bond of prestressing strand is presented in this report, and the main objectives of this portion of the research were to 1) investigate the transfer and development lengths of 0.5-in.-diameter (12.7 mm), Grade 270 prestressing strand in normal strength and high strength conventional and SCC mixes similar to those used by precast plants in Missouri, and 2) evaluate two pullout tests proposed for the acceptance or rejection of strand based on bond quality.

In terms of evaluating the transfer and development lengths, the goals were to 1) compare SCC results to conventional concrete results to determine if SCC compromises, enhances, or has no effect on bond performance of prestressing strand, 2) compare SCC and conventional concrete results to values predicted by AASHTO LRFD-07 and ACI 318 code equations to determine if the design equations are conservative, 3) compare the normal strength concrete results to high strength concrete results to determine the effect of concrete strength on bond, and 4) compare results from top-cast strands and bottom-cast strands to evaluate the top-bar effect on prestressing strand.

Regarding the investigation of pullout tests, the goals were to 1) compare bond quality of prestressing strand from three different sources using two proposed pullout test methods and 2) correlate pullout results to measured transfer lengths.

The ultimate goal was to analyze the results from the transfer and development length and bond portions of this research program and make recommendations to MoDOT for guidelines regarding the use of SCC by precast plants for infrastructure elements and the acceptance of prestressing strand based on bond.

### **1.3. SCOPE**

In order to evaluate the bond of prestressing strand, first, a literature review that included studies examining the transfer and development lengths of prestressing strand in SCC as well as previous research related to pullout tests and strand bond quality was conducted. Based on the literature review, a research plan was developed.

The transfer and development lengths of 0.5-in.-diameter (12.7 mm), Grade 270 prestressing strand were evaluated and compared in four concrete mixes. The four mixes included a normal strength and high strength conventional concrete and a normal strength and high strength SCC. Three 17-ft.-long (5.18 m) beams were cast from each mix for a

total of 12 full-scale specimens. For each mix, two beams were cast with two strands, both on the bottom, and one beam was cast with four strands, two on the bottom and two on the top. The four-strand beams were constructed to evaluate the effect of casting position on transfer length. All beams were first used to measure transfer lengths periodically from release to 28 days after casting. Once all transfer length data was collected, the development lengths of the two-strand beams were evaluated through four-point loading.

In the bond testing portion of this research program, 0.5-in.-diameter (12.7 mm), Grade 270 strand from three different sources was evaluated through two different proposed bond tests, and the pullout loads were compared to each other and to the recommended minimum limit specified by each test. The strands were also then cast in a modified bond test using the four concrete mixes used to construct the transfer and development length beam specimens with the goal of determining if the pullout loads from the tests performed in concrete could be correlated to the measured transfer lengths and be an indicator of bond performance.

#### **1.4. OUTLINE**

This report is composed of six sections and six appendices. Section 1 gives a brief introduction to the subject area and explains why this research was done. The first section also presents the objectives and scope of work of the research covered in this report.

Section 2 contains the Literature Review conducted on the topics of bond and specifically bond of prestressing strand in SCC. First, relevant terms and the mechanisms of bond theory are defined and discussed. Next the AASHTO LRFD-07 and ACI 318-11 code equations for transfer and development length are presented along with a brief background of the development of the equations. Finally, summaries of previous research regarding general bond acceptance tests of prestressing strands and also bond, transfer length, and development length of prestressing strands in SCC are explained.

Section 3 presents the bond test program portion of this research. The design and fabrication of pullout specimens as well as the setup, procedure, and results for each test are discussed. Setup and procedure for tension testing performed on samples of the

prestressing strands and the resulting mechanical properties are also included in this section.

The transfer length and development length test program is explained in Section 4. This section outlines the design and fabrication of the prestressed beams used for this research as well as the set-up, procedure, and results for the transfer length and development length tests.

Section 5 contains the discussion of all results, including evaluation of bond performance of prestressing strand in conventional concrete versus SCC and comparison of results to AASHTO and ACI code provisions. A comparison and discussion of the two bond tests evaluated in this program are also included in this section, along with discussion of the correlation between results of the pullout tests and measured transfer lengths.

Finally, the findings obtained from each section of the study along with the conclusions that were drawn based on the findings are presented in Section 6. This section also includes recommendations for proposed specifications and future research.

There are also six appendices included in this report. Appendix A includes the summary of concrete compressive strengths from 1 to 28 days for the four concrete mixes. Appendix B contains the load vs. deflection plots for the NASP in concrete tests, while the load vs. time curves from the LBPT specimens are presented in Appendix C. The 95% Average Mean Strain plots for transfer length determination are included in Appendix D, and the end slip plots from the linear potentiometers connected to the Synergy data acquisition system can be found in Appendix E. Finally, Appendix F includes photos, moment and end slip vs. deflection plots, and descriptions of all four-point load tests.

## 2. LITERATURE REVIEW

### 2.1. INTRODUCTION

This Literature Review first explains the relevant terms related to bond of prestressing strand and then discusses theory of bond mechanisms and the factors that affect transfer and development lengths. Next, the current AASHTO and ACI provisions for transfer length and development length of prestressing strand are presented along with information on the background of the development of the equations. Finally, previous research regarding bond acceptance tests for prestressing strand and the bond of prestressing strand in SCC are discussed.

### 2.2. EXPLANATION OF TRANSFER LENGTH, FLEXURAL BOND LENGTH, AND DEVELOPMENT LENGTH

Transfer length,  $l_t$ , is defined as the length from the free end of the member to the point along the length of the beam where the effective prestress in the strand is fully transferred to the concrete. The stress in the strand along the length of the transfer length is assumed to vary linearly from zero at the free end to  $f_{pe}$ , the effective prestress after losses, at the end of the transfer length.

Flexural bond length,  $l_{fb}$ , is defined as the length of fully bonded strand beyond the transfer length that is required to fully develop the stress in the strand to  $f_{ps}$ , the ultimate stress at nominal flexural capacity, when load is applied to the member.

Development length,  $l_d$ , is the sum of the transfer length and flexural bond length. The transfer length, flexural bond length, and development length are illustrated in **Figure 2.1**.

Additionally, the term embedment length,  $l_e$ , is discussed frequently in this report. Embedment length is the distance from the free end of the beam to the point along the strand where the cross-section of the member is being assessed for strength. This is often the closest point from the end of the strand to where the critical cross-section is, or where the maximum moment is in the member, and the point where the strand would need to be fully developed to maximum nominal flexural resistance. To investigate development length, a beam is typically loaded with a point load, and the embedment length is the

distance from the free end of the beam to the point load. If the beam fails in flexure, the strand is fully developed and the embedment length is greater than the development length, but if the beam fails in bond, the embedment length is shorter than what is needed to fully develop the strand.

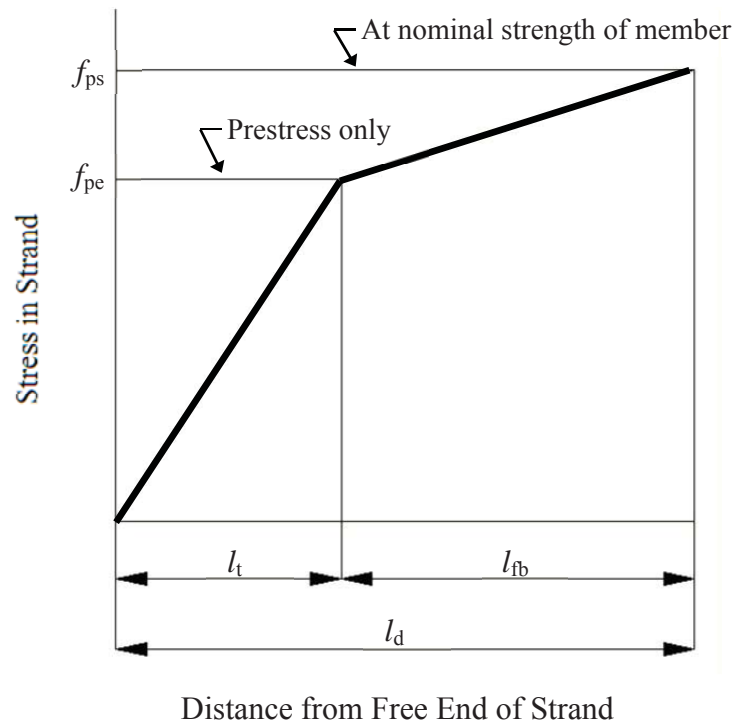


**Figure 2.1 – Variation of Stress in a Strand Along the Length of a Beam  
(Adapted from ACI 318-11)**

### 2.3. BOND THEORY

Combinations of several factors have been shown to contribute to bond of prestressing strand to concrete. Depending on the circumstances, adhesion, Hoyer effect, and mechanical interlocking can act singly or in combinations to resist slippage of the strand in concrete (Russell and Burns 1993). Research completed by Janney (1953) regarding bond of plain wires and strand in concrete led him to conclude that friction is a

major contributor to bond. While friction is not individually discussed in this section, friction plays a large role in both the Hoyer effect and mechanical interlocking.

**2.3.1. Adhesion.** Adhesion is the thin layer of glue that chemically forms between the strand and the concrete. As soon as the strand slips, adhesion is lost, and the bond stress that had been contributed by adhesion goes to zero and is transferred to other bond mechanisms. Since the transfer zone is characterized by the strand moving relative to the concrete, adhesion does not contribute to the bond in the transfer zone (Russell and Burns 1993).

**2.3.2. Hoyer Effect.** In the transfer zone, a major contributor to bond is a factor known as the Hoyer effect. As a strand is stressed, the strand becomes longer, but also thinner due to Poisson's effect. When the strand is cut, the release of the stress causes the wires in the strand to expand back to their original forms, but this expansion is resisted by the concrete. As a result, wedging action occurs between the strand and concrete as the strand produces a normal force on the concrete from radial expansion, and the resulting friction resists the movement of the strand into the concrete (**Figure 2.2**).

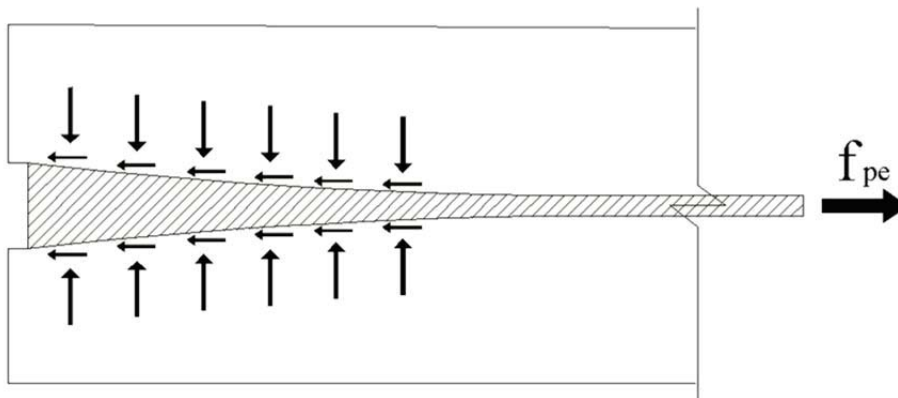


**Figure 2.2 – Hoyer Effect (Adapted from Russell and Burns 1993)**

The Hoyer effect is only applicable in the transfer zones because the radial expansion only occurs at the ends where the strand slips relative to the concrete. Once an outside load is applied, as the wave of stress that starts at the maximum moment zone gets pushed into the transfer zone, the stress in the strand increases and the strand

becomes thinner again. The frictional forces from Hoyer effect decrease and mechanical interlock is then the only force resisting bond.

**2.3.3. Mechanical Interlock.** When concrete is cast around prestressing strand, the concrete molds around the strand and between the grooves of the wires. When the strand tries to move through the concrete and untwist due to release of stress, the concrete ridges formed between the wires resist the movement. This effect is known as mechanical interlock. While some of this friction helps bond the strand in the transfer zone, mechanical interlock is the main form of resistance in flexural bond (Russell and Burns 1993).

#### **2.4. FACTORS AFFECTING TRANSFER AND DEVELOPMENT LENGTHS**

Over the years, many studies have been completed regarding transfer length and development length of prestressing strands, and although the current equations are functions of only stress in the strand after losses and at ultimate as well as nominal strand diameter, many other factors have also been proven to affect bond. Zia and Mostafa (1977) conducted an extensive literature review on previous testing regarding development length and attempted to pinpoint the many factors that affect bond. Based on their findings, some of the factors that have been found to influence transfer length and development length include:

1. Strand size (diameter)
2. Strand stress level
3. Concrete strength
4. Time dependent effects (losses)
5. Type of release (gradual or sudden)
6. Consolidation and consistency of concrete around strand
7. Surface condition of strand (clean, rusted, epoxy-coated)
8. Confinement
9. Cover and spacing
10. Type of strand (stress relieved, low relaxation)
11. Type of loading (static, repeated, impact)

The effects of the first six factors are briefly discussed below.

**2.4.1. Strand Size.** It is commonly accepted that an increase in strand diameter results in an increase in transfer and development lengths. Kaar, LaFraugh, and Mass (1963) were some of the first researchers to document this aspect. Based on transfer length testing of 0.25-in., 0.375-in., 0.5-in., and 0.6-in.-diameter (6.35 mm, 9.53 mm, 12.7 mm, and 15.2 mm) strands, it was noted that larger diameter strands yielded longer transfer lengths, and the relationship between strand diameter and transfer length at release was approximately linear (Kaar, et al. 1963). Based on this research, the direct relationship between strand diameter and transfer length was adopted into current code equations for transfer length and development length.

**2.4.2. Steel Stress Level.** With an increase of initial stress in the strand, the surface area that is required to transfer the stress to the concrete also increases, resulting in longer transfer lengths. The current equations for transfer and development lengths are based on  $f_{se}$ , or effective stress after all losses. While this is reasonable for flexural bond length, it has been noted that the use of  $f_{se}$  does not necessarily seem applicable to transfer length at release, and that  $f_{si}$ , or the stress in the strand immediately after release instead of after all losses, should instead be applied to the calculation of transfer length (Buckner 1995). This approach would result in longer, more conservative transfer length calculations. As discussed, the equation for transfer length was developed based on research performed in the 1950's and 60's using Grade 250 strands which were also stressed to lower levels than what is commonly used today theoretically rendering the equation unconservative for today's use. Some researchers have proposed equations for transfer length expressed as a function of  $f_{si}$  instead of  $f_{se}$  (Zia and Mostafa 1977, Buckner 1995), but research has not consistently shown that the current equation is, in fact, unconservative, so no changes have yet been made to the current AASHTO and ACI equations.

**2.4.3. Concrete Strength.** Although the study performed by Kaar, LaFraugh, and Mass in 1963 indicated that concrete strength had little effect on transfer length, many studies since have proven the correlation between high concrete strengths and decreased transfer lengths. The bond over the transfer length is primarily due to friction between the strand and the concrete caused by radial expansion of the strand at release that occurs due

to Poisson's effect. According to Barnes et al. (2003), this friction depends on how well the concrete surrounding the strand reacts to the pressure caused by the increasing circumference. The release results in radial cracking in the concrete surrounding the strand, which softens the concrete. Therefore, a higher tensile strength and stiffness means the concrete can respond better to the radial expansion, resulting in better friction and shorter transfer lengths. Since the ACI 318-11 Sections 8.5.1 and 9.5.3.2 show that modulus of elasticity and modulus of rupture are directly related to the square root of concrete strength, it follows that transfer length should also be related to the square root of concrete strength at release (Barnes et al. 2003).

While Kaar, LaFraugh, and Mass only studied concrete release strengths up to 5,000 psi (34.5 MPa), today's release strengths can range to over 10,000 psi (68.9 MPa). Many researchers, including Mitchell et al. (1993), Lane (1998), and Ramirez and Russell (2008), have since published studies relating increased concrete strengths to decreased transfer lengths. The studies have also resulted in a number of proposed, revised equations for transfer length and development length (Zia and Mostafa 1977, Mitchell et al. 1993, Lane 1998, Ramirez and Russell 2008), almost all of which relate transfer length to the square root of concrete compressive strength. However, much debate still exists over the exact effect of concrete strength on transfer and development lengths, and since the current equation is considered conservative for high concrete strengths, there is no immediate rush to update the equation.

**2.4.4. Time Dependent Losses.** Research has shown that transfer lengths tend to increase over time. Barnes et al. (2003) suggested although stress in the strand decreases over time due to losses, transfer lengths still do not decrease over time because of the inelasticity of the concrete immediately surrounding the strand. The increases in transfer lengths are most likely due to propagation of the radial cracking and the resulting softening of the concrete grip (Barnes et al. 2003). Transfer lengths measured by Kaar, LaFraugh, and Mass showed average increase in transfer lengths of 6% over one year, with the maximum increase being 19% (1963). In FHWA research, transfer lengths of 32 AASHTO Type II beams increased 30% in 28 days and then an additional 7% between 28 and 185 days (Lane 1998). Research by Barnes et al. (2003) showed 28 day average transfer lengths increases of 10-20%, with some individual increases as high as 50%.

Also, Boehm et al. (2010) reported 0.5-in.-diameter (12.7 mm) strands in conventional concrete had a 38% increase in transfer length over three months.

**2.4.5. Type of Release.** Sudden release methods, such as flame cutting, have been proven to result in longer transfer lengths than more gradual release methods, such as detensioning. In their review of data from previous studies for the establishment of a new development length equation, Zia and Mostafa separately plotted transfer lengths vs. the ratio of the initial stress in the strand at release to concrete strength at release ( $f_{si}/f'_{ci}$ ) for ends exposed to sudden release and ends exposed to gradual release and found that for a given  $f_{si}/f'_{ci}$  value, the transfer lengths from sudden release were longer than transfer lengths from gradual release (1977).

Similarly, transfer lengths have also been shown to be longer at live ends, or locations where the strand is first cut to relieve tension, as opposed to dead ends, or ends not directly adjacent to the first release point in the strand. Kaar, LaFraugh, and Mass found that for strands up to 0.5-in. (12.7 mm) in diameter, live end transfer lengths averaged 20% longer than dead end transfer lengths, while 0.6-in.-diameter (15.2 mm) strands showed a 30% increase from dead to live ends (1963). For uncoated strands, Cousins et al. (1990) found that transfer lengths at live ends for 0.5-in. and 0.6-in.-diameter (12.7 mm and 15.2 mm) strands averaged 8% higher than dead ends, while 0.375-in.-diameter (9.53 mm) strands actually had live end transfer lengths 6% shorter than the dead ends. Additionally, Russell and Burns (1997) reported live end transfer lengths to be 34% longer than dead end transfer lengths.

**2.4.6. Consolidation and Consistency of Concrete around Strand.** As the use of new types of concrete, such as SCC, becomes more prevalent, the properties of the concrete surrounding the strand is becoming an increasingly important topic. Since SCC is not mechanically vibrated, it is still being debated whether the flowable nature of SCC results in adequate consolidation around the strand, or if it could actually improve the condition of consolidation around the strand compared to vibrated conventional concrete (Larson et al. 2007). Several studies reporting conflicting results on the effect of SCC on bond of prestressing strand are discussed in Section 2.7 of this report.

Related to the aspect of condition of concrete surrounding the strand is the subject of strand locations in members. ACI-318-11 and the AASHTO LRFD-07 code account

for the “top bar effect” for mild deformed reinforcing bars, which implies that bars located in the top of a member during casting have longer development lengths than bars located at the bottom. This phenomenon has been attributed to various reasons, including bleed water and air getting trapped on the bottom surfaces of the top bars (Peterman 2007) and the idea that concrete-bar friction results mainly from concrete consolidated above bars than immediately below (Wan et al. 2002). In a research study by Petrou and Joiner (2000), end slips of strands in prestressed piles from five plants were analyzed, and top strands were found to have end slips an average of 2.3 times longer than bottom strands, with some instances showing end slips of top strands up to 4-5 times longer. In a subsequent research program, Wan measured end slips of strands in 32 18-in.-square (457 mm) concrete piles and noted that top-cast strands had average end slips of 0.140 in. (3.56 mm), while bottom-cast strands had end slips of only 0.058 in. (1.47 mm) (2002). However, ACI and AASHTO currently have no provision for increasing development lengths of prestressing strands located in the top of a member. A 1.3 multiplier was suggested by Buckner (1995) and Lane (1998) and incorporated to Section 5.11.4.2 of the AASHTO code shortly after, but the provision has since been removed (Peterman 2007).

## **2.5. ACI AND AASHTO CODE EQUATIONS**

The *AASHTO LRFD Bridge Design Specifications* (2007), which shall hereby be referred to as the AASHTO code, is the governing document for the design of prestressed bridge girders used by the Missouri Department of Transportation, so the AASHTO equations for transfer length and development length were used as the basis for the analyses in this program. Additionally, results were compared to values determined by equations in ACI’s *Building Code Requirements for Structural Concrete*, or ACI 318-11. This subsection identifies the relevant code equations and discusses the backgrounds behind the equations.

**2.5.1. AASHTO LRFD Bridge Design Specifications.** The guidelines for the development of prestressing strand can be found in Section 5.11.4 of the AASHTO code. Although there is no specific equation for transfer length in the AASHTO code, Section 5.11.4.1 states that “the transfer length may be taken as 60 strand diameters.” Therefore,

the AASHTO equation for transfer length in inches,  $l_t$ , can be represented by **Eq. 2.1**, where  $d_b$  is the nominal diameter of the strand in inches.

$$l_t = 60d_b \quad (2.1)$$

In terms of development length, Section 5.11.4.2 of AASHTO then defines the minimum development length in Eq. 5.11.4.2-1, which is shown here as **Eq. 2.2**, where  $l_d$  is the development length in inches,  $\kappa$  is a multiplier of 1.0 for members with depth less than or equal to 24 in. (610 mm) and 1.6 for members deeper than 24 in. (610 mm),  $f_{ps}$  is the average stress in the prestressing steel at the time for which the nominal resistance of the member is required in ksi,  $f_{pe}$  is the effective stress in the prestressing steel after losses in ksi, and  $d_b$  is the nominal strand diameter in inches.

$$l_d = \kappa \left( f_{ps} - \frac{2}{3} f_{pe} \right) d_b \quad (2.2)$$

The 1.6 multiplier for deep members is based on research performed by Shahawy (2001), which indicated a relationship between shear and bond. Three-point load tests were performed on 83 prestressed pile specimens with six different cross-sections and 12 AASHTO Type II girders at varying embedment lengths and shear spans, and the slippage of strands, applied moments, and final failure modes were noted. These tests indicated that members with depths greater than 24 in. (610 mm) needed development lengths up to 50% longer than those predicted by the original AASHTO equation, or **Eq. 2.2** without the  $\kappa$  factor. Shahawy came to the conclusion that for deep members, the shear-flexural interaction has a significant effect on development length, and he proposed a new development length equation with factors to take into account the effect of shear on strand slippage before failure. AASHTO did not adopt the proposed equation, but based on the research, added a 1.6 multiplier for members with a depth greater than 24 in. (610 mm) to the development length equation, which when applied to Shahawy's research results, proved to give mostly conservative results.

The AASHTO equation for and provisions regarding development length has undergone many revisions and will likely continue to be adjusted. In 1988, the FHWA administered a memorandum that imposed a 1.6 multiplier on the AASHTO development length equation, increased strand spacing requirements, and banned the use of 0.6-in.-diameter (15.2 mm) strand (Lane 1998). This memorandum, and specifically the clause regarding the 1.6 multiplier, was issued mostly in response to research completed in the mid 1980's by Cousins, Johnston, and Zia, which indicated development lengths much longer than those predicted by the AASHTO equation (Lane 1998). The research covered transfer and development length of epoxy coated and uncoated strands and tested square and rectangular members with one strand, but the research program is mainly known for showing the measured transfer and development length results of the uncoated strands to be 48-67% longer, depending on the strand size, than the lengths predicted by the AASHTO and ACI equations (Cousins et al. 1990).

Based on the alarming results, FHWA initiated a test program focusing on development length, and more research has since shown that the ban on 0.6-in.-diameter (15.2 mm) strand and limits on spacing requirements could be repealed, and the restrictions were lifted in 1996 (Lane 1998). Shortly after, the 1.6 safety factor was proven over-conservative in most cases, and that safety factor was lifted as well. However, as discussed, now the 1.6 multiplier is applied in certain cases to account for shear effects on bond of strand in deep members. Also, based on the surge in development length research spawned by the FHWA memorandums, many new development length equations have been proposed (Zia and Mostafa 1977, Mitchell 1993, Buckner 1995, Lane 1998, Ramirez and Russell 2008), a number of which take into account the effect of concrete strength, which has proven to affect bond. However, much debate still exists, and none of these equations have yet been adopted.

**2.5.2. ACI 318-11.** In the ACI 318-11 code, the provisions for the development of prestressing strand are presented in Section 12.9. The equation for development length is shown in the ACI 318-11 code as Eq. 12-4, and consists of two terms, where the first term is equal to the transfer length and the second term represents the flexural development length, as noted by the commentary in R12-9. The ACI 318-11 equations for transfer and development length are shown here as **Eqs. 2.3** and **2.4**,

respectively, where  $l_t$  is the transfer length in inches,  $l_d$  is the development length in inches,  $f_{se}$  is the effective stress in the prestressing steel after losses in psi,  $f_{ps}$  is the stress in the prestressing steel at the nominal flexural strength in psi, and  $d_b$  is the nominal diameter of the strand in inches.

$$l_t = \left( \frac{f_{se}}{3000} \right) d_b \quad (2.3)$$

$$l_d = \left( \frac{f_{se}}{3000} \right) d_b + \left( \frac{f_{ps} - f_{se}}{1000} \right) d_b \quad (2.4)$$

It should be noted that the ACI equation for development length (**Eq. 2.4**) is equal to the AASHTO equation for development length (**Eq. 2.2**) when the depth of the member is less than or equal to 24 in. (610 mm).

ACI 318-11 also provides an additional equation for transfer length for the shear design of prestressed members. In Section 11.3.4, ACI 318-11 requires that shear designs of prestressed members be based on a reduced stress in the strand for sections of a member that are closer to the support than the transfer length. For this design, the transfer length is to be taken as 50 times the nominal diameter of the strand. This additional ACI transfer length equation is presented here as **Eq. 2.5**, where  $l_t$  is the transfer length in inches and  $d_b$  is the nominal diameter of the strand in inches.

$$l_t = 50d_b \quad (2.5)$$

### 2.5.3. Background of the AASHTO and ACI Development Length Equations.

As discussed, although the AASHTO and ACI equations for development length (**Eq. 2.2** and **Eq. 2.4**, respectively) are formatted differently, they are essentially the same equation (when  $\kappa = 1.0$  for **Eq. 2.2**). The equation was first incorporated into ACI-318 in 1963, and AASHTO also adopted it 10 years later. According to an extensive study conducted by Tabatabai and Dickson (1993) on the origins of the equation, the basis of the equation stems from research conducted by Hanson and Kaar and Kaar, LaFraugh, and Mass for the Portland Cement Association (PCA) in the 1950's and 1960's. The

studies were conducted with 250 ksi (1.72 GPa), stress relieved strands, which were stressed to 60%-70% of capacity and cast in concrete strengths up to 5,500 psi (34.5 MPa). Majority of today's prestressed members are constructed with 270 ksi (1.86 GPa), low relaxation strands that are often subjected to higher initial stresses and cast in concrete with higher strengths. These differences between practices today vs. practices decades ago could be cause for concern as to whether the design equations derived on outdated construction methods can still adequately apply to members today.

Hanson and Kaar tested 0.25-in., 0.375-in., and 0.5-in.-diameter (6.4 mm, 9.5 mm, and 12.7 mm) Grade 250 prestressing strands in members at varying embedment lengths. Although Hanson and Kaar recommended minimum embedment lengths based on their research, the current transfer length and development length equations were actually developed by Alan H. Mattock. The values calculated from Mattock's equations, which are based on Hanson and Kaar's data and findings, are actually less conservative than Hanson and Kaar's recommendations (Tabatabai and Dickson 1993).

Based on the assumption that the force in the steel must equal the transfer bond force, Mattock used **Eq. 2.6** to solve for transfer length in inches,  $L_t$ , where  $U_t$  is the average bond stress in ksi,  $\Sigma_0$  is the circumference of the prestressing strand in inches,  $A_{ps}$  is the area of prestressing strand in ksi, and  $f_{se}$  is the effective stress in the strand after losses in ksi.

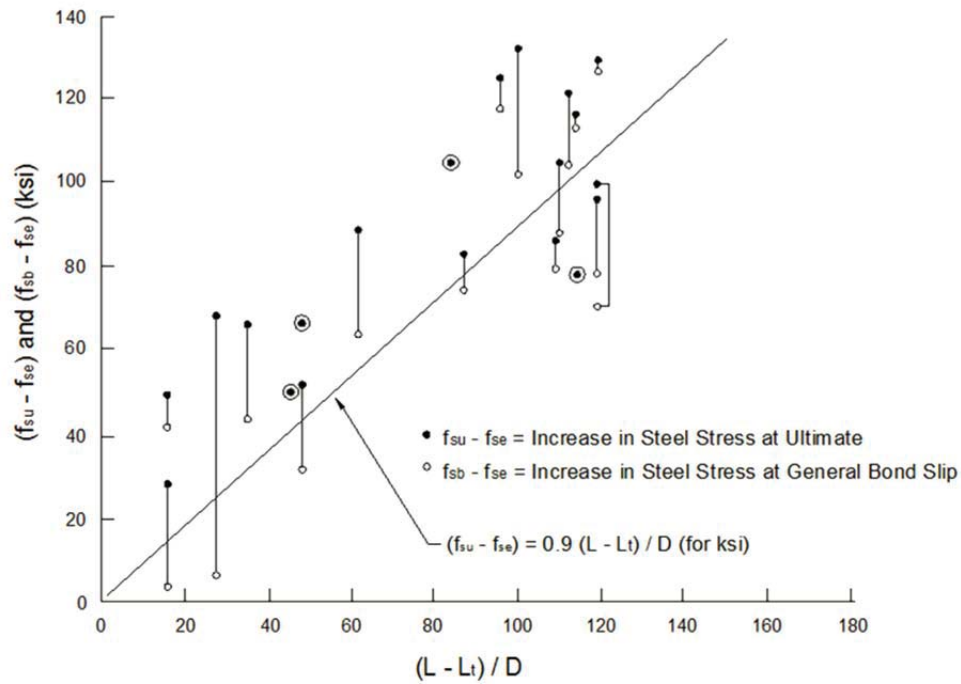
$$U_t \Sigma_0 L_t = A_{ps} f_{se} \quad (2.6)$$

$U_t$  was assumed to be 0.4 ksi (2.76 MPa) based on the data from Hanson and Kaar, and  $\Sigma_0$  and  $A_{ps}$  were taken to be  $4/3\pi D$  and  $0.725\pi D^2/4$ , respectively, where  $D$  is the nominal diameter of the strand in inches, to account for the actual circumference and area of the prestressing strand. Substituting these values into **Eq. 2.6** yielded **Eq. 2.7**, which is equal to the current transfer length equation specified by ACI.

$$L_t \approx \frac{f_{se} D}{3} \quad (2.7)$$

It should be noted that the basis for the transfer length equation is an average of the results from Hanson and Kaar, and is not meant to be conservative. The same is true of the equation derived for flexural development length. When evaluating flexural bond length, for each specimen, Mattock plotted the increase in steel stress from the effective prestress at the point of general bond slip ( $f_{sb} - f_{se}$ ) and the increase in steel stress from the effective prestress at ultimate failure ( $f_{su} - f_{se}$ ) vs. the embedment length minus the transfer length divided by the nominal diameter, as seen in **Figure 2.3**. The trend line is presented in **Eq. 2.8**, and as shown in **Figure 2.3**, in many cases the line runs above the point of general bond slip but below ultimate failure. According to Mattock, the line is “a reasonable mean line for general bond slip” (Tabatabai and Dickson 1993).

$$f_{su}^* - f_{se} = 0.9 \left( \frac{L - L_t}{D} \right) \quad (2.8)$$



Conversion: 1 ksi = 6.89 MPa  
 1 in. = 25.4 mm

**Figure 2.3 – Original Representation of Flexural Bond Length  
 (adapted from Tabatabai and Dickson, 1993)**

**Eq. 2.8** was later revised to **Eq. 2.9**, and substituting in  $L_t/D = f_{se}/3$  from **Eq. 2.7** and rearranging the equation yields **Eq. 2.10**. **Eq. 2.10** is equivalent to **Eq. 2.2**, or the current AASHTO development length equation without the  $\kappa$  factor, and functionally equivalent to the ACI development length equation in **Eq. 2.4** as well.

$$f_{su}^* - f_{se} = \frac{L - L_t}{D} \quad (2.9)$$

$$L = \left( f_{su}^* - \frac{2}{3} f_{se} \right) D \quad (2.10)$$

In conclusion, the current transfer length and development equations are based on research completed almost 60 years ago involving 250 ksi (1.72 GPa), stress-relieved strands stressed to 60%-70% capacity in lower strength concretes, while today's practices commonly use 270 ksi (1.86 GPa), low-relaxation strands stressed to 75% capacity in higher strength concretes. Additionally, the equations were not developed to be conservative, but rather, they were derived based on averages. Many researchers wonder how applicable these equations are to today's prestressed concrete, and although many new transfer length and development length equations based on recent research have been proposed in the past two decades to update the equations and include the effect of concrete strength, a revised equation has yet to be agreed upon.

## 2.6. RESEARCH REGARDING ACCEPTANCE OF A STANDARD BOND TEST

Since the mid 1990's, several test programs have been completed in order to investigate the potential of different bond tests to produce consistent results from test to test and site to site. The ultimate goal of the research programs has been to develop a standardized test that would be able to pre-qualify strand in terms of having acceptable bond performance.

**2.6.1. Logan (1997).** The main purpose of Logan's test program was to see if bond quality of strand could be assessed through simple untensioned pullout tests by correlating the pullout values to results from end slip monitoring and flexural testing on prestressed beams. In order to obtain a wide representation of the prestressing strand used

in the western hemisphere, Logan collected samples of strand from six sources from across the country.

First, pullout tests based on the method created by Saad Moustafa were run on each strand source. Six strands from each source were cast vertically with an 18 in. (457 mm) embedment length in a block of standard structural concrete. The blocks were cured overnight, and then a jack was used to pull out each strand until the peak load could no longer be sustained. Four of the six samples had average maximum pullout loads ranging from 36.8 kips to 41.6 kips (164 kN to 185 kN), while the other two sources had average values of 11.2 (49.8 kN) and 10.7 kips (47.6 kN). When these results were compared to the performance of the strands in the end slip and flexural testing of the beams, the beams with the four strands with high pullout values had transfer and development lengths less than predicted by ACI 318-95, while the beams with the strands with low pullout capacities failed in bond, meaning the transfer length and development lengths predicted by ACI 318-95 were unconservative for those strands. Based on these results, Logan proposed lowering the minimum pullout value from 38.2 kips (170 kN), as determined by Moustafa, to 36 kips (160 kN) because the strands with pullout values of 37.7 kips (168 kN) and 36.8 kips (164 kN) performed well in the beam testing. Logan suggested that this minimum pullout limit could be even further reduced, but further testing would have to be done on strands with pullout capacities between 11.2 kips (49.8 kN) and 36.8 kips (164 kN).

In order to test the transfer length and development length of the strands, 17-ft.-long (5.18 m) beams with 6.5 in. x 12 in. (165 mm x 305 mm) cross-sections and one strand located at 2 in. (50.8 mm) from the bottom were constructed. The end slips of the strands into the concrete at release were measured, and then the end slip values were used in conjunction with Mast's strand slip theory to calculate transfer lengths. The calculated transfer lengths were then compared to transfer lengths calculated by the equation in ACI 318-95. Each end of the beam was then tested in flexure at a different embedment length, and it was noted whether each test resulted in either a flexural or bond failure. By comparing the transfer lengths calculated by end slip to the calculated and actual moment capacities, it was found that Mast's strand slip theory accurately predicted which beams failed in bond and which failed in flexure.

Logan also investigated whether factors such as color, noticeable residue, rust, and pitch of the outer strands could be used to predict bond quality. Before each of the pullout tests, Logan noted the color and rust of the strands, wiped a clean towel over each strand to visually quantify the amount of residue on each, and measured the pitch of the outside wires, or the distance for one wire to make a complete revolution around the strand. Overall, Logan found no strong correlation between any of the factors and the pullout capacities of the strands, so it was concluded that neither color, residue, rust, nor pitch can be considered a reliable predictor of bond.

**2.6.2. Rose and Russell (1997).** The research program was designed to evaluate the effectiveness of three test methods that could be used to assess the bond of prestressing strand. Data from simple untensioned direct tension pullout tests, pretensioned direct pullout tests, and measured end slips and transfer lengths on beams were used to determine the relative bond performance of Grade 270 0.5-in.-diameter (12.7 mm) strands from different manufacturers and having different surface conditions of as-received, cleaned, silane treated, and weathered. The ultimate goal was to see if one test could be considered superior.

The simple untensioned pullout tests were based on Logan's method (1997) and consisted of strands cast vertically with 18 in. (457 mm) of embedment length in 2 ft. x 3 ft. x 4 ft. (610 mm x 914 mm x 1,219 mm) blocks of concrete. The tensioned pullout tests had 5.5 in. (127 mm) square cross-sections and were 12 in. (305 mm) in length with 12 in. (305 mm) embedment. It was thought that the tensioned pullout tests would more closely represent the bond in prestressed members because these tests would include the Hoyer effect resulting from the release of tension. The beams used for end slip and transfer length measurements had 6 in. x 12 in. (152 mm x 305 mm) cross-sections and were 17 ft. (5.18 m) in length, except for the beams with the silane-treated strand, which were 24 ft. (7.32 m) long. Each beam contained two strands, and the beams were instrumented so that strain readings could be taken with a detachable mechanical strain gage (DEMEC gage). The 95% Average Mean Strain Method was then used to analyze the transfer lengths.

Ultimately, it was concluded that the end slip measurements consistently gave the most accurate assessment of bond. The greater the end slip, the longer the transfer length,

and the typical equation was found to be adequate. In terms of the pullout tests, the simple untensioned test was found to be better than the tensioned pullout test, but no strong correlation existed between the simple pullout results and the transfer lengths. The tensioned pullout test was found to be difficult to set up and run and also yielded inconsistent results. Except for the silane treated strand, the simple tension test showed that the lower the maximum pullout value, the higher the transfer length. The silane-treated strand showed adequate bond performance in the simple pullout test, but had the largest measured transfer lengths. Therefore, it was concluded that simple untensioned pullout test mirroring Logan's method is still not an overly reliable predictor of bond.

**2.6.3. NASP Bond Testing Rounds I-IV.** In the late 1990's, the North American Strand Producers (NASP) funded a research project to compare tests designed to assess strand bond and ultimately determine a test suitable for strand bond acceptance. This project consisted of several rounds of testing and was based out of the University of Oklahoma (OU).

The first round of testing compared the Moustafa test, the PTI bond test, and the friction bond test (Russell and Paulsgrove 1999a). From the results, it was determined the friction bond test gave inconclusive and inconsistent results, so in Rounds II and III, researchers continued to investigate the Moustafa Test and the PTI test, but in these rounds, the friction bond test was discarded and the NASP bond test was added. The NASP bond test was similar to the PTI test, but a mortar with Type III cement, sand, and water was used in place of the grout of Type I cement and water that was specified by the PTI test. The addition of sand made the mix stiffer and minimized shrinkage (Russell and Paulsgrove 1999b).

In Round II, in order to determine the repeatability and reproducibility of the three tests, several series of the three tests were completed at different locations. The Moustafa test was run at Stresscon in Colorado, the Florida Wire and Cable Company (FWC), and OU, while the PTI and NASP tests were only completed at FWC and OU.

One conclusion that was reached from the Round II of testing was that results indicated that the Moustafa test was a good predictor of relative bond but was not a good absolute predictor of bond; the rank of strands was always the same at each site, but the specific pullout values did not correlate well between sites. This conclusion was further

confirmed in Round III of testing. In terms of the NASP bond test vs. the PTI test, the NASP test showed slightly more consistent results. For both tests, it was noted that the pullout values had the least variation at a slip of 0.1 in. (2.54 mm). For this slip, plotting results comparing NASP test series from OU and FWC resulted in coefficients of determination ( $R^2$  values) of 0.97 and 0.98, indicating a strong correlation of test results between tests at the same site as well as between sites, as seen in **Table 2.1**. These coefficients of determination were significantly higher than  $R^2$  values derived from comparing results from different sites for either the Moustafa or PTI test (**Table 2.1**). Therefore, a main conclusion from this round of testing was that the NASP bond test was standing out as the most replicable of the three (Russell and Paulsgrove 1999b).

**Table 2.1 – NASP Round II R2 Values Comparing Moustafa, PTI, and NASP Pullout Results Between Sites (Russell and Paulsgrove 1999b)**

Data Comparison	Moustafa	PTI Pull-Out			NASP Pull-Out		
	Maximum Strand Force	Maximum Strand Force	Force at 0.10 in. SLIP	Force at 0.01 in. SLIP	Maximum Strand Force	Force at 0.10 in. SLIP	Force at 0.01 in. SLIP
	$r^2$	$r^2$	$r^2$	$r^2$	$r^2$	$r^2$	$r^2$
Series 1 vs. Series 1							
OU vs. FWC	0.88	0.87	0.90	0.73	0.97	0.98	0.90
OU vs. STRESSCON	0.92						
STRESSCON vs. FWC	0.94						
OU Series 1 vs. OU Series 2					0.97	0.97	0.71
OU Series 1 vs. FWC Series 2					0.87	0.97	0.72
<b><math>r^2</math> (coefficient of determination)</b> regression about "best fit" line							

Round III of the testing included flexural beam specimens, and one of the main goals was to see if transfer lengths and development lengths could be correlated to pullout values from the three tests to determine if absolute limits of pullout values could be set for any of the tests. Single strand beams and double strand beams were constructed at OU and FWC with strand from four different sources. Transfer lengths were computed

by measuring the strand draw-in at release and at 28 days. **Table 2.2** shows the  $R^2$  values correlating 28 day transfer length to pullout values for the three tests. The Moustafa test had generally low correlations across the board, while the PTI test had low correlations at one site but high correlations at the other. The NASP test had consistently reasonable correlations at both sites for both beam types. Comparing the pullout values to 28 day transfer lengths further strengthened the argument for focusing further research on developing the NASP bond test (Hawkins and Ramirez 2010).

**Table 2.2 – Round III Coefficient of Variation ( $R^2$ ) Values Relating 28 Day Transfer Lengths to Bond Test Pullout Values (adapted from Hawkins and Ramirez 2010)**

Test	OU		FWC	
	Single Strand Transfer Lengths	Double Strand Transfer Lengths	Single Strand Transfer Lengths	Double Strand Transfer Lengths
Moustafa Pullout Values	0.50	0.50	0.73	0.87
PTI Pullout Values	0.52	0.29	0.95	0.84
NASP Pullout Values	0.83	0.73	0.98	0.76

In order to evaluate development length, each end of each beam was tested in four-point loading at an embedment length of either 73 in. (1,854 mm) or 58 in. (1,473 mm) and the mode of failure was noted. The results are summarized in **Table 2.3** for the single strand beams and **Table 2.4** for the double strand beams. N corresponds to tests completed at 73 in. (1,854 mm) embedment, and S represents tests completed at 58 in. (1,473 mm) embedment. Bond failures indicated that the embedment length was not sufficient to develop sufficient stress in the strand, and the results from the development length testing were used to help set 10,500 lb. (46.7 kN) average pullout value and 9,000 lb. (40.0 kN) individual pullout value minimum limits for bond acceptance for the NASP test (Hawkins and Ramirez 2010).

**Table 2.3 – Round III NASP Pullout Values and Failure Modes from Flexural Testing of Single Strand Beams (Hawkins and Ramirez 2010)**

Single Strand Beams: NASP P.O. Values vs. Failure Mode							
Strand	Lt @ 28 Days (in.)	NASP P.O. Value (lbs.)		Failure Mode			
		Average	Low	1N	2N	1S	2S
AA	16.2	14950	11500	F	F	F	F
FF	31.2	7300	5500	F	F	V	B
HH	30.2	10700	8900	F	F	F	B
II	39.2	4140	2620	F	B	B	B

- F = Flexural Failure  
 - V = Shear Failure  
 - B = Bond Failure

**Table 2.4 – Round III NASP Pullout Values and Failure Modes from Flexural Testing of Double Strand Beams (Hawkins and Ramirez 2010)**

Double Strand Beams: NASP P.O. Values vs. Failure Mode							
Strand	Lt @ 28 Days (in.)	NASP P.O. Value (lbs.)		Failure Mode			
		Average	Low	1N	2N	1S	2S
AA	17.4	14950	11500	F	F	F	F
FF	24.2	7300	5500	F	F	F	F
HH	26.3	10700	8900	F	F	F	F
II	42.7	4140	2620	F	B	B	B

- F = Flexural Failure  
 - V = Shear Failure  
 - B = Bond Failure

From Rounds II and III of testing, it was determined that the NASP test showed the most promise for becoming a test that could accurately and consistently assess strand bond. Therefore, Round IV of testing focused on taking steps to standardize the NASP bond test. First, a parametric study was run at OU to study the effects of mortar strength, mortar flow, temperature and curing conditions, load vs. displacement control, and loading rate on the NASP test results. From this study, current limits for each variable as seen in the proposed standard were determined. After the testing at OU established the

more specific standard limits and procedures, round robin testing was completed on several strand samples at OU, Purdue University, and University of Arkansas to see how well the test would replicate between sites using various cement and sand sources. Plotting the NASP results from Purdue and University of Arkansas to results from OU resulted in  $R^2$  values of 0.92 and 0.89, respectively, and trends from both comparisons were very close to the “perfect fit” line, or the same pullout load from both sites. From these observations, it was concluded that the NASP test is reproducible and can be replicated from site to site with acceptably consistent results (Russell 2006).

**2.6.4. Ramirez and Russell (2008).** As part of the testing done for the National Cooperative Research Program (NCHRP) Report 603, Ramirez and Russell investigated bond and corresponding transfer and development lengths of 0.5-in. and 0.6-in.-diameter (12.7mm and 15.2mm) prestressing strand in high strength concretes. Due to the recent increase in use of high strength concrete, the main purpose of this program was to investigate the effect of concrete strength on bond of prestressing strands and propose revised transfer and development length equations to AASHTO.

Eight I-shaped beams and 43 rectangular beams were constructed using four strand sources and concretes with one day target strengths ranging from 4 to 10 ksi (27.5 to 68.9 MPa) to monitor transfer lengths through DEMEC readings and end slips and to evaluate development lengths through four-point flexural testing at varying embedment lengths. Another goal of the research program was to refine and standardize the NASP test, and Rounds III and IV of NASP round-robin testing were completed as a part of this test program. Additionally, a modified NASP test in concrete was also implemented to determine how concrete strength directly affects bond.

From their research, Ramirez and Russell concluded that increasing concrete strength results in improved bond performance. Pullout values for the modified NASP in concrete test increased as concrete strength increased, and members with high concrete strength displayed shorter transfer lengths. In terms of bond, the results from this program showed the NASP test in mortar to be a good indicator of bond performance. The pullout results from the standard NASP test in mortar correlated well with transfer and development length results; strands with high NASP pullout values consistently had shorter transfer and development lengths.

Ultimately, based on their results, the research team made recommendations to AASHTO for updates to the bond, transfer, and development provisions in the code. First, the report proposed new transfer and development length equations, which take into account the effect of concrete strength. Additionally, the researchers recommended that the NASP test be accepted as the Standard Test for Strand Bond and implemented to control bond quality of strands. However, to date, no official revisions have yet been made to the AASHTO code.

**2.6.5. Current Status and Recent Developments.** Currently, Logan's modified Moustafa test, now known as the Large Block Pullout Test (LBPT), is required to be conducted in PCI member plants to assure the bond quality of strand (Precast/Prestressed Concrete Institute 2003). However, as the current research has shown, LBPT results are difficult to reproduce from site to site, and the NASP test is proving to be more reliable than the LBPT. Although the NASP test shows promise for becoming the "Standard Test Method to Assess the Bond of 0.5-in. (12.7 mm) and 0.6-in. (15.2 mm) Seven Wire Strand with Cementitious Material," a due diligence report conducted on the four rounds of testing came to several conclusions that show more testing is required before the test is accepted as a standard (Hawkins and Ramirez 2010).

First, since Round IV testing exposed the NASP test's sensitivity to mortar flow and strength, it can be assumed that sand angularity can also have a significant effect on results. Hawkins and Ramirez suggest that a range of angularity be specified since angularity greatly affects workability. Also, although the goal of Round IV round robin testing was to prove that the test was reproducible between sites, Hawkins and Ramirez deemed the results as not "statistically defensible," and suggested that more testing be done at between four to six independent sites. They also recommend that more development length testing be done to identify pullout limits (Hawkins and Ramirez 2010). A research program funded by PCI addressing these issues about the NASP test is currently beginning to get underway at the time of this report.

Although the NASP test appears to be the front runner for becoming the standard bond test, recent developments with the LBPT have shown that the test may still be potentially viable as a reproducible test. Based on a recent, unpublished study, Logan has discovered a correlation between soft limestone coarse aggregates and low pullout values,

and test results have suggested that using a coarse aggregate with a Mohs hardness value of 6.0 or higher will improve the consistency of results (Logan, personal communication, October 20, 2011). Further testing needs to be completed in order to determine if the standardization of the hardness of the coarse aggregate will truly improve reproducibility of the LBPT from site to site.

## **2.7. RESEARCH REGARDING BOND OF PRESTRESSING STRAND IN SCC**

As the use of SCC has become more and more popular, an increasing number of studies have been completed in order to investigate the bond of prestressing strand in SCC. In these studies, transfer and development lengths of prestressing strand in SCC were compared to the lengths measured in conventional concrete to determine if bond behavior between the two concretes is comparable. Experimentally determined transfer and development lengths were also compared to values calculated by the AASHTO and ACI equations. The findings of these studies are presented in this section.

**2.7.1. Girgis and Tuan (2005).** Three mixes were investigated in this study: two SCC mixes (Mix 1 and Mix 2) and one conventional mix (Mix 3). The SCC mixes had partial replacement of cement with Class C fly ash and also contained a viscosity modifying admixture (VMA). One full scale NU bridge girder was cast per mix and each girder contained 0.6-in.-diameter (15.2 mm) strand, which was pre-qualified through the Moustafa test, now known as the Large Block Pullout Test, using Logan's concrete mix. The bridge girders, which were parts of three different projects around Nebraska, were instrumented with DEMEC points, and readings were taken at 1, 3, 7, 14, and 28 days after casting. Transfer lengths were calculated using the 95% Average Mean Strain Method. Moustafa pullout tests were also completed on the 0.6-in.-diameter (15.2 mm) strands with the three concrete mixes to determine if pullout values in the concrete mix could be correlated to transfer lengths. Smaller pullout tests were also performed on #4, #6, and #8 deformed bars and 0.6-in.-diameter (15.2 mm) strand.

The SCC mixes had much longer initial transfer lengths than the conventional mix; Mix 1 had an average initial transfer length 80% higher than Mix 3, and Mix 2 had an average initial transfer length over two times that of Mix 3. However, the Moustafa pullout values from the tests completed in the concrete mixes did not predict the longer

transfer lengths in the SCC. It would be assumed that higher pullout values would correspond to shorter transfer lengths, but, in fact, Mix 2 had the highest average pullout load, yet had the longest initial transfer length. The Moustafa pullout values from the concrete mixes and initial transfer lengths from this study are presented in **Table 2.5**.

**Table 2.5 – Girgis and Tuan Results**

Mix	Concrete Type	Girder Type	Average Pullout Load (kip)	Average Initial Transfer Length (in.)
Mix 1	SCC	NU1100	43.4	36
Mix 2	SCC	NU900	54.2	43
Mix 3	Conventional	NU1350	48.0	20

Conversion: 1 kip = 4.45 kN

1 in. = 25.4 mm

**2.7.2. Larson, Peterman, and Esmaily (2007).** Larson, Peterman, and Esmaily undertook a project funded by the Kansas Department of Transportation (KDOT) to investigate the bond performance of prestressing strand in SCC. The main goal was to determine if ACI and AASHTO equations would still be conservative when applied to SCC so Kansas precasters would be permitted to use the material to construct bridge girders.

First, Large Block Pullout Tests were run on strand that was to be used in the project. Pullout tests were performed using Logan's specified mix in order to qualify the strand based on pullout values determined by Logan, and strands were also cast in blocks of SCC to compare pullout values in SCC to those of the standard mix. The strands in Logan's mix passed the bond acceptance criteria, but in terms of comparing pullout values from the two concretes, the pullout values for the SCC tests were significantly lower than the pullout values from the conventional concrete; the average SCC pullout value was 22.5 kips (100 kN) while the average pullout value from Logan's concrete mix was 39.5 kips (176 kN).

Several types of beams were then constructed with 0.5-in.-diameter (12.7 mm), Grade 270 prestressing strand to measure transfer lengths due to end slip and then to evaluate development length through four-point load testing. The same SCC mix, which contained no VMA or supplemental cementitious materials, was used for all specimens. Six single strand beams (SSB) with 8 in. x 12 in. (203 mm x 305 mm) cross-sections were cast with one strand located 2 in. (50.8 mm) from the bottom, and six top strand beams (TSB) with 8 in. x 24 in. (203 mm x 610 mm) cross-sections were cast with one strand located at 22 in. (559 mm) from the bottom in order to study the top strand effect. The depth of the TSB's was decreased to 12 in. (305 mm) at the maximum moment range so the SSB and TSB results could be compared. Finally, four T-beams (TB) were cast with strands at a depth of 19 in. (483 mm).

The transfer lengths were determined by measuring strand end slips with a caliper at release and at 21 days and using the values to calculate transfer lengths according to Mast's slip theory. The 21 day average transfer lengths were found to be 21 in. (533 mm) for the SSB specimens, 30 in. (762 mm) for the TSB specimens, and 29 in. (737 mm) for the TB specimens. Additionally, the specimens with bottom strands (TB and SSB) showed increases in transfer length ranging from 10-20%, while the top strands (TSB specimens) had increases of 40-45%.

All development length tests failed in flexure due to strand rupture. The actual maximum moments surpassed the calculated nominal moment capacities by 10-20% for the beams tested at 100% of the calculated development length and 25-30% for the beams tested at 80% of the calculated development length.

Overall, several conclusions were made based on the results of this test program. First, the "top strand effect" theory appeared to be supported; average measured 21 day transfer lengths for the TSB specimens were approximately 50% longer than measured bottom strand transfer lengths, and top strand transfer lengths also showed a much higher increase over 21 days than the bottom strands. Top strands in the study also had on average over 60% longer transfer lengths than the current ACI provision of  $50d_b$ . Another main conclusion that was drawn was that the ACI and AASHTO code equations for transfer length and development length of bottom strands are conservative and adequate for SCC. Finally, even though the SCC pullout values were low, the results from the

transfer and development length tests for the strand in SCC were acceptable, so therefore, Logan's pullout acceptance limits should not be applied to pullouts performed in SCC.

**2.7.3. Pozolo and Andrawes (2011).** In order to study the effect of SCC on the bond and transfer lengths of 0.5-in.-diameter (12.7 mm), Grade 270 prestressing strand in Illinois bridge girders, SCC and conventional concrete mixture designs conforming to standards set by the Illinois Department of Transportation (IDOT) were used to cast modified Moustafa pullout test blocks, and hollow box girders and I-girders were constructed out of SCC. The modified Moustafa pullout tests were first run to determine if the bond of strand in SCC was comparable to the bond of strand in conventional concrete, and then transfer lengths were measured on the SCC girders.

In order to compare bond properties of SCC versus conventional concrete, one SCC mix and one conventional concrete (CC) mix were used to cast modified Moustafa pullout test blocks. The SCC mix contained no VMA or supplementary cementitious materials. For each mix, two 2 ft. x 2 ft. x 5.5 ft. (610 mm x 610 mm x 1,676 mm) blocks were cast with 14 strands each, and pullout tests were then completed at 1, 3, 7, and 28 days. Tests were completed using a hollow core hydraulic jack applying load at 0.4 in./min. (10.2 mm/min.). The non-linear slip load and maximum pullout load were recorded. The normalized pullout values for both concrete types at the different days showed the nonlinear slip loads and peak pullout loads were comparable for SCC and CC; in fact, except for an anomaly in the 7 day testing, the SCC peak pullout loads were higher than the CC peak pullout loads. From these results, it was concluded that strands exhibited acceptable bond in SCC, and the project could be continued to test the strand in SCC girders.

The next phase of the project involved casting two I-girders (I-1 and I-2) and two hollow box girders (Box-1 and Box-2) with the SCC mix and monitoring the change in transfer lengths over time by using DEMEC points attached to the concrete surface at the level of the prestressing strand. Strain measurements were taken at 1, 3, 7, 14, and 28 days, and the 95% Average Mean Strain Method was employed to determine transfer lengths. The measured transfer lengths were then compared to transfer lengths calculated by ACI-318-08 and AASHTO equations for transfer length, and it was found that every measured transfer length except for one end were shorter than the ACI and AASHTO

limits. The one end that did not meet the ACI and AASHTO criteria had low concrete strength and was the end that was first released. Overall, the measured lengths averaged 86% below  $50d_b$ , 72% below  $60d_b$ , and 69% below  $f_{pe}d_b/3$ , so it was determined that strands would exhibit acceptable bond in SCC girders in Illinois.

**2.7.4. Staton, Do, Ruiz, and Hale (2009).** For this program, the researchers evaluated the transfer lengths of 0.6-in-diameter (15.2 mm), Grade 270 prestressing strand in two different SCC mixtures and a high strength conventional concrete. The mixes included an SCC with Type I cement (SCC-I), an SCC with Type III cement and Class C fly ash (SCC-III), and a high-strength conventional concrete (HSC). The strand was first prequalified through the NASP bond test, and then beams were constructed and instrumented with DEMEC points to measure the transfer lengths of the strands over time.

In order to evaluate transfer lengths, 18-ft.-long (5.49 m) beams with 6.5 in. x 12 in. (165 mm x 305 mm) cross-sections, two strands at 2 in. (50.8 mm) from the bottom, and stirrups at 6 in. (152 mm) on center were constructed from three different mixes. Eight beams were cast with the SCC-I, and the SCC-III and HSC were used to cast 6 beams each for a total of 20 beams. The beams were instrumented with DEMEC points, and readings were taken at 1, 3, 7, 14, and 28 days. The 95% Average Mean Strain Method was then used to determine transfer lengths.

The transfer lengths at all ages were compared for all mixes using 90% confidence intervals. Overall, it was found that there was no statistical difference between the HSC and SCC-I transfer lengths, but transfer lengths at 28 days were 3.5 in. (88.9 mm) shorter for the SCC-III beams than for the HSC beams. In terms of transfer length growth, both the SCC-I and SCC-III beams averaged about 8% growth, while the HSC transfer lengths averaged around 12% growth. Also, all measured transfer lengths were shorter than lengths calculated by the ACI and AASHTO equations. For SCC, the measured transfer lengths averaged about 60% below the transfer length predicted by the ACI equation. However, it should be noted that the strands in this research were released by detensioning, and a harsher release method might have resulted in longer transfer lengths.

**2.7.5. Floyd, Ruiz, Do, Staton, and Hale (2011).** This research program was a continuation of the study of transfer lengths of 0.6-in.-diameter (15.2 mm) strand in SCC by Staton, Do, Ruiz, and Hale. The same beams that were used to measure transfer lengths were also then tested to evaluate the effects of SCC on development length. One end of each beam was tested by applying a single point load to a simple span at a predetermined embedment length. For each test, the failure moment and first slip moment were noted and compared to the calculated nominal moment capacity, and from these observations, it was determined whether the beam failed in bond or flexure. The embedment length for each test was varied based on whether the embedment length of the previous test resulted in a bond or flexural failure. Ultimately, the development length for each concrete type was narrowed down to a range based on failure modes resulting from the different embedment lengths (**Table 2.6**). For instance, based on results, the development length for 0.6-in.-diameter (15.2 mm) strand in SCC-I is most likely longer than 35 in. (889 mm) but shorter than 37.5 in (953 mm).

**Table 2.6 – Concrete Strength at Testing and Development Length Ranges**

Concrete Type	$f'_{c,test}$ (psi)	Development Lengths	
		Low End (in)	High End (in)
SCC-I	14,770	35	37.5
SCC-III	13,190	30	32.5
HSC	14,510	30	35

Conversion: 1 psi = 6.89 kPa

1 in. = 25.4 mm

In conclusion, it was determined that the HSC and SCC specimens had comparable development lengths, although SCC-I appeared to have development lengths slightly greater than the HSC. Still, all experimentally determined development lengths were much shorter than lengths calculated by the ACI/AASHTO equation; SCC-I and HSC development lengths were 60-66% shorter, and SCC-III lengths were 64-67% shorter.

**2.7.6. Boehm, Barnes, and Schindler (2010).** The Alabama Department of Transportation funded a study dedicated to determining if the use of SCC is feasible for bridge girder construction in Alabama. Six AASHTO Type I girders with 0.5-in.-diameter (12.7 mm) “special” Grade 270 prestressing strand composite decks were used to evaluate transfer lengths and development lengths. A moderate strength conventional concrete (STD-M), a moderate strength SCC (SCC-MS), and a high strength (SCC-HS) were used for comparison, and two beams were constructed per mix. All three mixes contained Type III cement, and the two SCC mixes also contained ground granulated blast furnace slag (GGBFS). Also, for the SCC mixes, SCC-MS contained a VMA, while SCC-HS did not. The moderate strength conventional concrete and SCC had target release strengths of 5,000 psi (34.5 MPa), while the high strength SCC had a target release strength of 10,000 psi (68.9 MPa). DEMEC points and the 95% Average Mean Strain Method were used to monitor transfer lengths over three months, and strand draw-in was measured at release with a steel ruler. Flexural bond length was evaluated using four-point loading, and for each mix, one test was completed at an embedment length of 135 in. (3,429 mm), one at 85 in. (2,159 mm), and two at 65 in. (1,651 mm). The development length calculated by AASHTO was 124 in. (3,150 mm).

Through the transfer lengths determined by the 95% Average Mean Strain Method, the study concluded that there was no significant difference between transfer lengths of strands in conventional concrete or SCC for full size girders. Additionally, the ACI and AASHTO equations for transfer length were found to be generally conservative, especially for high strength concretes. Also, SCC transfer lengths were found to increase an average of 28% over three months, while transfer lengths in conventional concrete increased 38%. In terms of the transfer lengths determined from the draw-in measurements, the study found little correlation between these values and the transfer lengths determined by the 95% Average Mean Strain Method.

All four-point load tests failed in flexure, even at the embedment lengths significantly shorter than the value recommended by AASHTO. Therefore, the AASHTO equation was deemed conservative. Results also showed that SCC performed comparably to conventional concrete, exceeding calculated nominal moment capacities by similar amounts.

Overall, SCC was determined to be comparable to conventional concrete in terms of bond. Additionally, the AASHTO and ACI equations for transfer length and development length were found to be conservative for both SCC and conventional concrete. Ultimately, this study approved the potential use of SCC in bridge girders in Alabama.

**2.7.7. Burgueño and Haq (2007).** Burgueño and Haq investigated the effect of how the different methods and admixtures used in making SCC can affect bond of prestressing strand. The study included three SCC mixes (SCC1, SCC2, and SCC3) and one conventional mix (NCC). SCC1 had a 0.35 water to cement ratio with decreased coarse aggregate, increased fines, and a significant amount of high range water reducer (HRWR), while SCC3 had a 0.45 water to cement ratio, proportions of aggregate similar to those of conventional concrete, and additions of a HRWR and a viscosity modifying admixture (VMA) to produce the fluidity and stability. SCC2 had a 0.40 water to cement ratio and admixture and aggregate proportions between those of SCC1 and SCC3. The three SCC mixes were also compared to a conventional concrete (NCC). Large Block Pullout Tests were completed using the four mixes, and 38-ft. long T-beams using 0.5-in.-diameter (12.7 mm), Grade 270 prestressing strand were cast from each mix to monitor transfer length using DEMEC points and the 95% Average Mean Strain Method and evaluate development length through three-point flexural tests.

Overall, the NCC was found to have slightly better bond than the SCC mixes. The SCC mixes on average had 12% lower pullout values, 36% longer transfer lengths, and 3% longer development lengths. Although transfer lengths were longer for SCC than NCC, the transfer lengths in all SCC mixes were still shorter than the transfer lengths predicted by the ACI code. In terms of comparing the three SCC mixes to determine effects of mix proportioning on bond, it appeared that SCC1 (high fines mix) had the lowest bond capacity of the three, and SCC3 (conventional mix with HRWR and VMA) showed the highest bond capacity of the three.

### 3. BOND TEST PROGRAM AND RESULTS

#### 3.1. INTRODUCTION

The bond test program involved two types of pullout tests: the North American Strand Producers (NASP) Pullout Test and the Large Block Pullout Test (LBPT). The NASP test consists of six pullout specimens, where each specimen is composed of a section of strand cast concentrically in a cylinder of specified mortar. The LBPT is comprised of six strands cast in a block of concrete having a specific mix design. Both the NASP test and LBPT specify that the pullout tests are to be performed 24 hours after casting. Because there is currently no accepted standard for the testing of bond of prestressing strand, the main purpose of the bond test program was to compare the NASP test in mortar and the LBPT to see if one test could be deemed more reliable than the other in terms of qualifying strand based on bond. In order to compare the two tests, prestressing strand from three different sources was obtained, and the standard NASP test in mortar and the LBPT were performed on strand from each source.

Additionally, the NASP test was also performed using the four concrete mixes that were developed for the transfer length and development length portions of the project, instead of the specified mortar. The NASP tests in concrete were performed only on strands from the same source as the beams, and the purpose of the testing was to see if any correlation could be made between the pullout values and transfer lengths. For each mixture, six total NASP specimens were made and three specimens were tested at 1 day and the remaining three were tested at 8 days. While the standard NASP test in mortar assesses only the bond quality of the strand itself, the NASP test in concrete gives an idea of the actual bond behavior of the strand in a specific concrete and concrete strength.

Prestressing strand from three different sources was used for comparing the standard NASP test in mortar and the LBPT. In this report, the strands will be identified as 101, 102, or 103 to designate the source. Strand type 101 was the strand type that was used in the beams, and strands 102 and 103 were samples of strand remaining from previous bond testing completed during NCHRP 10-62. Samples 102 and 103 were used to provide a comparison between different strand manufacturers. Because three different

sources of strand were used for multiple pullout tests, an identification code was developed to distinguish the specific bond test and strand combinations (**Figure 3.1**).

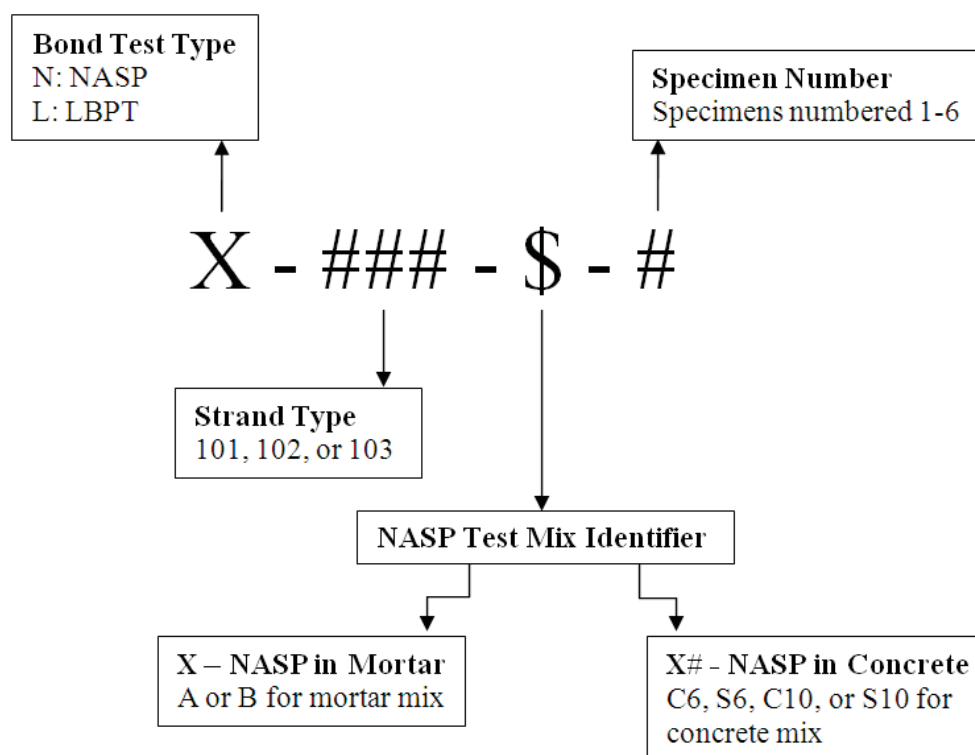


**Figure 3.1 – Bond Test Identification Code**

For instance, N-101-A-1 designates the first specimen in the group of six NASP tests using strand type 101 in mortar Mix A, while N-101-C6-1 designates the first specimen in a group of six NASP tests using strand type 101 in the conventional concrete, 6,000 psi (41.4 MPa) target strength mix.

A few notes should be made concerning the NASP test in concrete specimens. First, the concrete mix designs used for the beams, and consequently the NASP tests in concrete, are discussed in **Section 4.2**. Also, all NASP in concrete tests were completed with strand type 101 because this was the strand type used in the beams. Finally, the NASP tests in concrete were run with three specimens tested at 1 day and three specimens tested at 8 days; therefore, it should be noted that for the NASP tests in

concrete, specimens numbered 1-3 were tested at 1 day, and specimens numbered 4-6 were tested at 8 days. Consequently, N-101-C6-1 indicates a C6 NASP specimen tested at 1 day, while N-101-C6-4 indicates a C6 NASP specimen tested at 8 days.

Finally, L-101-1 designates the first specimen in the group of the six type 101 strands cast for the LBPT. Since one concrete mix was used for the LBPT, the mix identification label was dropped for the LBPT identifiers.

This chapter first describes program used to determine the strands' tensile properties in **Section 3.2**. **Section 3.2** also summarizes ultimate tensile strength,  $f_u$ , and modulus of elasticity,  $E_{ps}$ , of each source. Next, **Section 3.3** presents the set-up, instrumentation, procedure, and results for the standard NASP tests in mortar as well as the NASP tests in concrete. Finally, the set-up, instrumentation, procedure, and results for the LBPT are reported in **Section 3.4**.

### **3.2. TENSILE PROPERTIES OF PRESTRESSING STRANDS**

The tensile properties of the three strand types used were found in order to aid in the evaluation of the pullout tests and to determine the ultimate moment capacities of the full-scale prestressed beams. Tensile tests were completed on strand types 101, 102, and 103, and the average ultimate strength and modulus of elasticity were found for each source.

**3.2.1. Tension Test Setup and Procedure.** Three tension specimens were tested for each strand source. The strands were cut into 18-in.-long (457 mm) sections and 3-in.-long (76.2 mm) aluminum tube sleeves were placed on each end of each test specimen to protect the strand from the grip serrations and facilitate gripping, as suggested in ASTM A1061/A1061M-09: Standard Test Methods for Testing Multi-Wire Steel Strand. The aluminum sleeves consisted of 6061 aluminum tubing with a 0.625 in. (15.9 mm) outside diameter, 0.527 in. (13.4 mm) inside diameter, and 0.049 in. (1.24 mm) wall thickness. Two sleeves were slid onto each specimen, and then small welds were placed on each end of the strand to ensure the wires would be loaded uniformly and also to keep the aluminum sleeves from sliding off the specimen. A set of three tension test specimens can be seen in **Figure 3.2**.

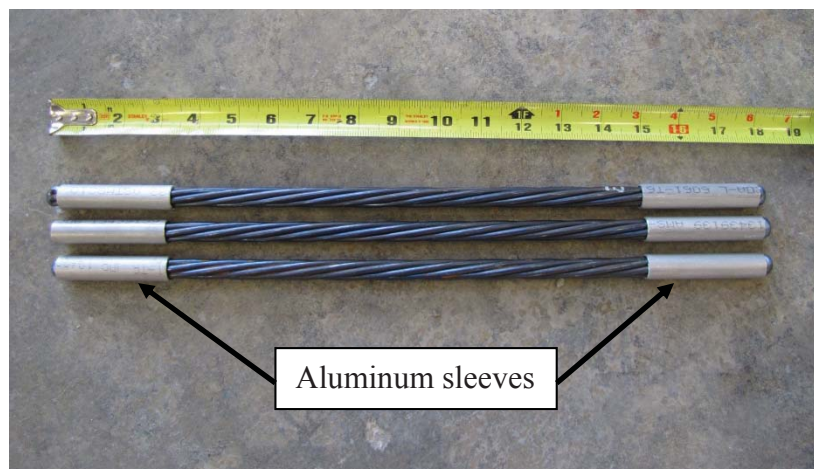


**Figure 3.2 – Tension Test Specimens**

An MTS 880 Universal Testing Machine was used to apply tension to each specimen until fracture. Each strand was centered and clamped into the grips. The gripping strength was initially set at 3.5 ksi (24.1 MPa), but the first set of tests exhibited slippage. As a result, after the first set of tests, the gripping strength was increased to 7.5 ksi (51.2 MPa), and no further slippage was experienced. The initial set that showed slippage in the grips was discarded, and an additional three specimens of the same strand type were tested using the 7.5 ksi (51.2 MPa) gripping strength to determine the final properties.

After setting the specimen in the grips, an initial load of 4,130 lb. (18.3 kN), which corresponds to 10% of the minimum specified fracture load, was applied based on ASTM A416/A416M-10: Standard Specification for Steel Strand, Uncoated Seven-Wire for Prestressed Concrete. Then, a 2-in.-long (50.8 mm) extensometer was attached near the middle of the section between the grips. The tension test setup with the extensometer is shown in **Figure 3.3**. Each specimen was then loaded at a rate of 3,235 lb./min. (14.4 kN/min.) until fracture. The load rate was chosen based on the limitations in ASTM A370-11a: Standard Test Methods and Definitions for Mechanical Testing of Steel Products, the limitations of the MTS equipment, and previous strand tensile testing performed on the MTS test machine. The majority of specimens fractured in the grips, but all specimens failed above the minimum fracture load of 41,300 lb (184 kN), so the

tests were considered valid according to ASTM A1061. A fractured specimen that failed away from the grips is pictured in **Figure 3.4**.

The data acquisition system recorded load, strain, and stroke and was set to record four readings per second. For each tension specimen, the extensometer was removed after a strain reading of approximately 0.008 in./in. was reached, and then the specimen continued to be loaded until failure. The extensometer was able to record sufficient data for the determination of the modulus of elasticity but was removed at a safe margin before fracture so the extensometer would not be damaged. Yield strength, which would have corresponded to a strain of 0.01 in./in., was not determined.

**3.2.2. Tension Test Results.** The collected load and extensometer data was used to determine the ultimate tensile strength ( $f_u$ ) and the modulus of elasticity ( $E_{ps}$ ) for each strand source. The average, standard deviation, and coefficient of variation (COV) results for  $f_u$  and  $E_{ps}$  presented in **Table 3.1** are based on three tension test specimens per strand type.

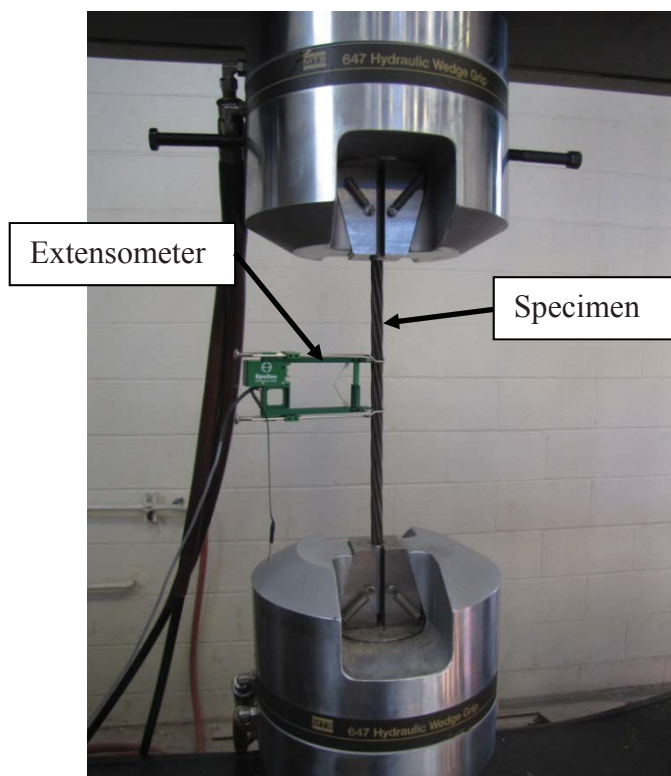


**Figure 3.3 – Tension Test Setup**



**Figure 3.4 – Fractured Tension Test Specimen**

**Table 3.1 – Direct Tension Test Results**

Strand Type	Statistic	$f_u$ (ksi)	$E_{ps}$ (ksi)
101	Average	287.5	29,400
	Std. Dev.	1.8	1,131.4
	COV	0.63%	3.85%
102	Average	285.0	27,500
	Std. Dev.	0.2	193.0
	COV	0.06%	0.70%
103	Average	287.7	28,500
	Std. Dev.	0.3	71.6
	COV	0.12%	0.25%

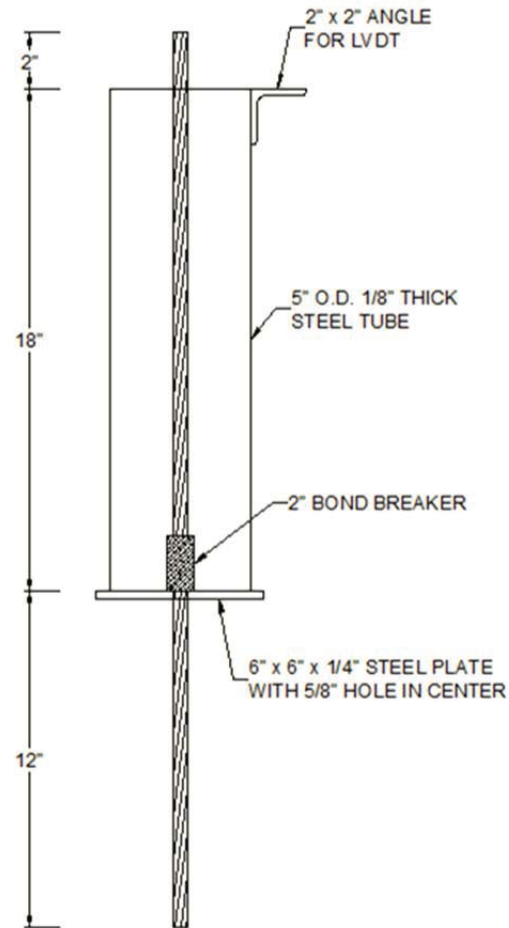
Conversion: 1 ksi = 6.89 MPa

### 3.3. NASP BOND TEST

The NASP Bond Test was performed in both the specified mortar, so results could be compared to the LBPT results, and the four concrete mixes, so pullout results could be correlated to transfer lengths. Aside from the mortar vs. concrete mixes, the specimen design and testing methods were virtually identical for both types of NASP tests.

**3.3.1. NASP Test Specimen Design.** The NASP specimen molds were identical for both the mortar and concrete NASP tests. The molds were constructed from 18-in.-long (457 mm) sections of 5 in. (127 mm) outside diameter,  $\frac{1}{8}$ -in.-thick (3.18 mm) steel tubing. The sections of tube were welded to 6 in. x 6 in. x  $\frac{1}{4}$  in. (152 mm x 152 mm x 6.35 mm) steel plates with a  $\frac{5}{8}$ -in.-diameter (15.9 mm) hole in the center. A 1  $\frac{3}{4}$  in. (44.5 mm) section of inverted 2 in. x 2 in. (50.8 mm x 50.8 mm) angle was welded onto the side of the tube at the open end to allow for the attachment of an LVDT during testing. Before testing, the angle piece on each specimen mold was checked with a level to ensure a horizontal surface and adjusted as necessary. A diagram of the steel mold is shown in **Figure 3.5**.

The strands were cut into 32-in.-long (813 mm) segments and were positioned so that 2 in. (50.8 mm) of strand would protrude from the top in order for the LVDT to measure slip, and 12 in. (305 mm) would extend from the bottom so the chuck would have sufficient strand to grip. A grinder was used to shape the top end of each strand, so that the outer wires were tapered upwards to the center wire, which had a level surface for the LVDT. Additionally, a 2-in.-long (50.8 mm) bond breaker constructed from foam insulation was wrapped around the strand and secured with duct tape. As shown in **Figure 3.5**, the bond breaker was positioned immediately above the hole in the bottom plate, and extended upward 2 in. (50.8 mm) into the mortar or concrete. The bond breakers are depicted in **Figure 3.6**.



Conversion: 1 in. = 25.4 mm

**Figure 3.5 – NASP Specimen Mold**



**Figure 3.6 – Strands with Bond Breakers**

For the NASP test in mortar, a significant number of trial batches of mortar were required in order to develop a mortar mix design that would meet the specific requirements set forth by the proposed standard in Appendix H of NCHRP 603 (Ramirez and Russell 2008). The proposed standard requires a mortar flow greater than or equal to 100 but less than or equal to 125 as measured in accordance with the procedure in ASTM C1437-07: Standard Test Method for Flow of Hydraulic Cement Mortar. Furthermore, the 24-hour average compressive strength of three mortar cubes was required to fall within the range of 4,500 psi (31.0 MPa) to 5,000 psi (34.5 MPa). The mortar consisted of Type III cement, fine aggregate, and water. The fine aggregate gradation conformed to ASTM C33/C33M-11a: Standard Specification for Concrete Aggregates. For the first few trial batches, the moisture content of the fine aggregate was measured and factored into the mix design; however because of the variability of results obtained, all fine aggregate for the remaining trial and final batches was oven dried to maintain more precise control of the water-cement ratio.

The initial NASP test for strand type 101 was completed during the summer of 2011, but the NASP tests for strand types 102 and 103 were completed over six months later in February of 2012. The mix design that was developed during the summer, Mix A, for strand type 101 did not meet the requirements of the proposed standard when used for testing strand types 102 and 103. When trial batches of Mix A were produced in February, the batches gave comparable 24 hour strengths to the trial batches of Mix A that were produced the previous summer, but the flow values were consistently lower than the previous batches and did not meet the criteria of the standard. Therefore, a revised mix design, Mix B, meeting the flow and strength criteria was developed for testing of strand types 102 and 103. Mix B was significantly different from Mix A in terms of proportioning, and because extra samples of strand type 101 were still available during the testing of types 102 and 103, the NASP test was performed again on strand type 101 in March 2012 with the new mix design, Mix B. The final mortar mix designs can be found in **Table 3.2**, and the test matrix for the NASP test in mortar is shown in **Table 3.3**.

For the NASP tests in concrete, the NASP specimens were poured at Coreslab Structures in Marshall, Missouri from the same batches that were used for the beams and

using strand type 101, which was the same strand type used in the beams. The mix designs for the C6, S6, C10, and S10 concretes can be found in **Table 4.1** in **Section 4.2**.

**Table 3.2 – Mortar Mix Design for NASP Tests**

Mix ID	Water/Cement Ratio	Sand/Cement Ratio	Oven Dried Sand (lb/ft <sup>3</sup> )	Type III Cement (lb/ft <sup>3</sup> )	Water (lb/ft <sup>3</sup> )
A	0.38	1.2 : 1	64.3	53.4	20.7
B	0.395	0.9 : 1	52.7	58.6	23.5

Conversion: 1 lb/ft<sup>3</sup> = 16.0 kg/m<sup>3</sup>

**Table 3.3 – NASP Test in Mortar Test Matrix**

Strand Type	Mix A	Mix B
101	X	X
102		X
103		X

**3.3.2. NASP Test Specimen Fabrication.** For the mortar specimens, the mortar was mixed in a 2 ft<sup>3</sup> (0.056 m<sup>3</sup>) drum mixer according to a procedure based on ASTM C192/C192M-07: Standard Practice for Making and Curing Concrete Test Specimens in the Laboratory. The mixer was started and all of the sand and enough water to produce a slurry were added. After the sand and water had thoroughly mixed, the cement and remaining water were then added in approximately three equal increments, allowing time for mixing between each increment. Once all the components were in the mixer, the mortar was mixed for three minutes. Then, the mixer was stopped for approximately two minutes while the blades were scraped with a spatula. Finally, the mortar was mixed for an additional two minutes. **Figure 3.7** shows the mortar in the drum mixer.



**Figure 3.7 – Mortar Mix in Drum Mixer**

The flow test was performed according to ASTM C1437-07: Standard Test Method for Flow of Hydraulic Cement Mortar immediately after mixing. After conducting the flow test, the mortar cube molds and NASP steel casings were filled. Three sets of three 2 in. x 2 in. x 2 in. (50.8 mm x 50.8 mm x 50.8 mm) mortar cubes were made according to ASTM C109/C109M-11a: Standard Test Method for Compressive Strength of Hydraulic Cement Mortars (Using 2 in. or 50 mm cube specimens). Three sets of cubes were made so that the mortar strength could be monitored before, during, and after testing. During the casting process, cube molds were also weighed before and after being filled in order to determine fresh unit weight. The flow test and cube-making process are depicted in **Figures 3.8** and **3.9**, respectively.

In order to fill the NASP molds, the six molds were placed on a custom wooden platform with two rows of three  $\frac{5}{8}$ -in.-diameter (15.9 mm) holes on the top and bottom sections of plywood so that the strands could be placed vertically in the molds and rest at the correct height, as seen in **Figure 3.10**. The steel tubes were filled in three equal layers, and each layer was vibrated with a handheld 1 in<sup>2</sup> (645 mm<sup>2</sup>) battery powered vibrator. Once the specimen molds were filled and vibrated, wooden caps designed to fit securely around the mold and with  $\frac{5}{8}$ -in.-diameter (15.9 mm) holes in the center of each

were placed on the top of each specimen to ensure the strands would remain plumb and concentric within the mold. The cube molds and table holding the six specimens were placed in the moist cure room for 24 hours.



**Figure 3.8 – Flow Test**



**Figure 3.9 – Mortar Cubes**



**Figure 3.10 – NASP Mold and Strand Setup**

For the NASP tests in concrete, the only difference is the steel molds were filled with the appropriate concrete mix instead of mortar. Once again, the molds were filled in three equal layers, and each layer was vibrated with the 1 in<sup>2</sup> (645 mm<sup>2</sup>) handheld vibrator. Filling of the molds for one of the concrete mixes can be seen in **Figure 3.11**. The caps were placed on the molds to keep the strands plum and concentric, and the outside of the molds were vibrated once more to ensure consolidation. The specimens were match cured with the beams. Six specimens were made for each mix, and for each mix, three specimens were tested at 24 hours and three specimens were tested at 8 days. Concrete cylinders measuring 4 in. x 8 in. (102 mm x 203 mm) were used to determine the compressive strength of the concrete at the times of testing. The final capped NASP specimens and cylinders for one of the concrete mixes can be seen in **Figure 3.12**.



**Figure 3.11 – Filling Specimens for NASP Test in Concrete**



**Figure 3.12 – Capped NASP in Concrete Specimens and Cylinders**

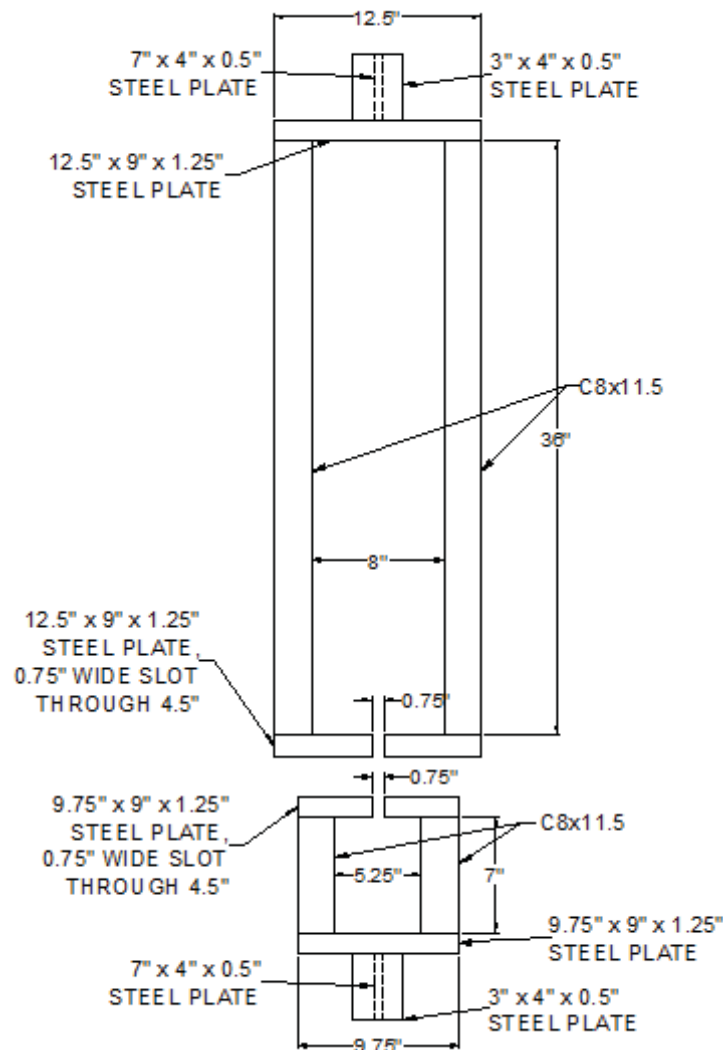
**3.3.3. NASP Test Setup and Procedure.** On the day after casting, cubes or cylinders were first tested to determine compressive strength. For the mortar, one set of three cubes was tested between 22 and 23 hours to ensure the compressive strength of the

mortar was at or near 4,500 psi (31.0 MPa). The second set of cubes was tested at around 24 hours, which corresponded to the beginning of NASP testing, and the third set was tested after the NASP testing was complete, or at around 25 or 26 hours. The average compressive strengths from immediately before and immediately after testing were averaged to determine the reported mortar compressive strength during testing. For the concrete NASP tests, a target compressive strength range was not required, so one set of three cylinders was tested at around 24 hours to determine compressive strength.

For the mortar NASP tests, all six specimens were tested at approximately 24 hours, while three specimens were tested at 24 hours and three specimens were tested at 8 days for each concrete mix. The specimens were tested using an MTS 880 Universal Testing Machine and steel frames that had been constructed specifically for the test. The frames, which are illustrated and dimensioned in **Figure 3.13**, were subsequently secured within the grips of the MTS via vertical plates welded to the top and bottom. The top frame held the cylindrical NASP specimen, and a chuck gripped the strand and bore against the top plate of the bottom frame, securing the specimen at approximately 6 in. (152 mm) from the bottom plate of the specimen, as show in **Figure 3.14**. Additionally, a steel plate was placed between the chuck and the bottom frame, and a steel plate and neoprene pad were placed under the specimen on the top frame, as seen in **Figure 3.15**. The bottom crosshead remained stationary, while the top crosshead moved upwards, applying load to the strand. The test method specifies that the load be applied at a rate of 0.1 in./min. (2.54 mm/min.), but the rate also must not exceed 8,000 lb./min. (35.6 kN/min.). The specimen was loaded at 0.1 in./min. (2.54 mm/min.) but a calculation was performed later using **Eq. 3.1**, which was also used by researchers in Round IV of the NASP testing (Russell 2006) to ensure the load rate was under 8,000 lb./min. (35.6 kN/min.). In **Eq. 3.1**,  $T_{6000}$  is the time elapsed in seconds when the pullout load was 6,000 lb. (26.7 kN) and  $T_{4000}$  is the time elapsed in seconds when the pullout load was 4,000 lb. (17.8 kN). Time and load values were interpolated from the data.

$$Load\ Rate = \frac{(6,000lb - 4,000lb)}{(T_{6000} - T_{4000})(60)} \quad (3.1)$$

An LVDT was secured in a specially constructed steel apparatus that was designed to be clamped to the specimen and would position the LVDT onto the center wire of the portion of strand protruding from the top, as seen in **Figure 3.16**. The data acquisition system collected the MTS stroke and load data and the LVDT readings at a rate of two readings per second. The load rate was applied to the specimen until a slip of 0.1 in. (2.54 mm) was observed.



Conversion: 1 lb = 4.45 N  
1 in. = 25.4 mm

**Figure 3.13 – NASP Test Frame**

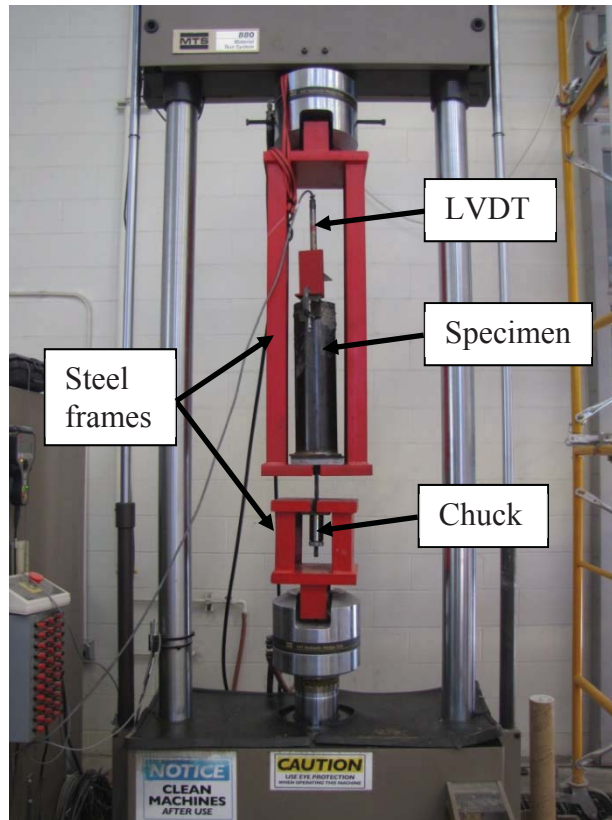
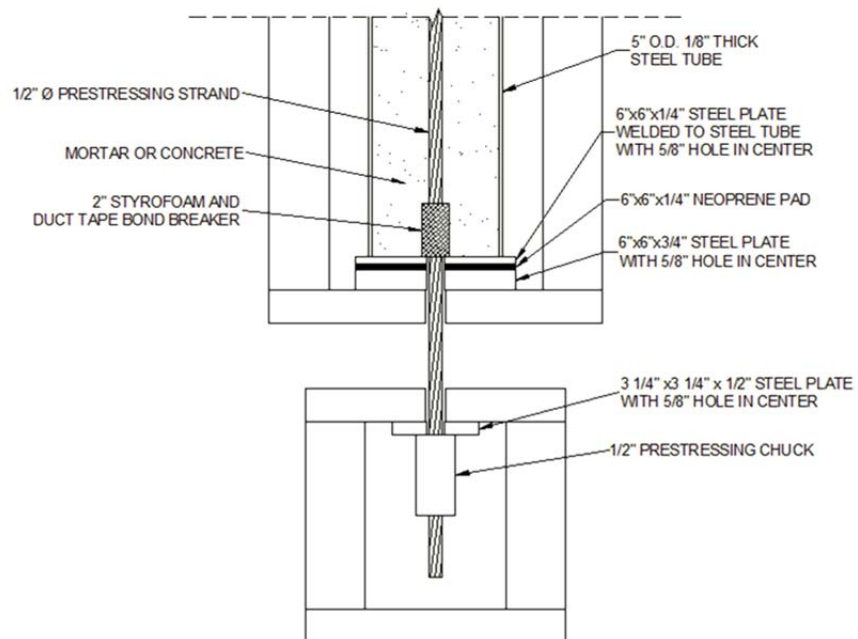
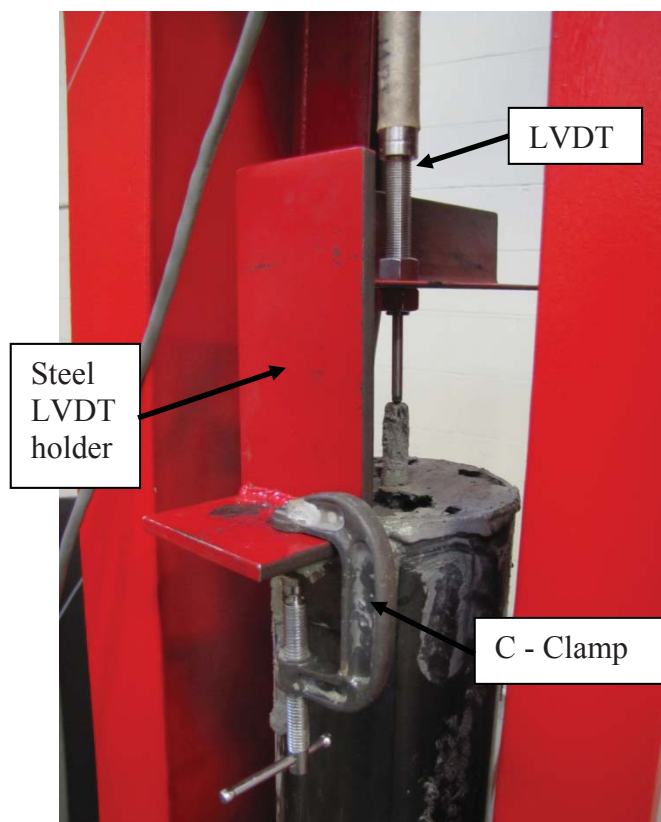


Figure 3.14 – NASP Test Setup



Conversion: 1 in. = 25.4 mm

Figure 3.15 – NASP Test Setup Details



**Figure 3.16 – NASP Test LVDT Setup**

**3.3.4. NASP Test Results.** In this section, the NASP test results have been divided into the results for the tests in mortar and the tests in concrete. The results are presented in load vs. slip plots, and the loads at 0.001 in. (0.025 mm) and 0.1 in. (2.54 mm) of slip for each specimen are presented in tables.

**3.3.4.1 Results from Standard NASP Test in Mortar.** The results from the NASP tests in mortar performed on the samples of strand from three different sources are presented in this subsection. First, the load data from the MTS and the slip data from the LVDT were organized into load vs. slip plots. An example load vs. slip plot can be found in **Figure 3.17**. The plot shows the load vs. slip curves for all six specimens of the same strand type, and the average minimum pullout load for acceptable bond quality as suggested by the proposed standard is also marked on each plot. For 0.5-in.-diameter (12.7 mm) strand, the average minimum pullout value is 10,500 lb (46.7 kN). All plots

for the mortar NASP tests for strand types 101, 102, and 103 can be found in the discussion of the NASP test results in **Section 5.2.1**.

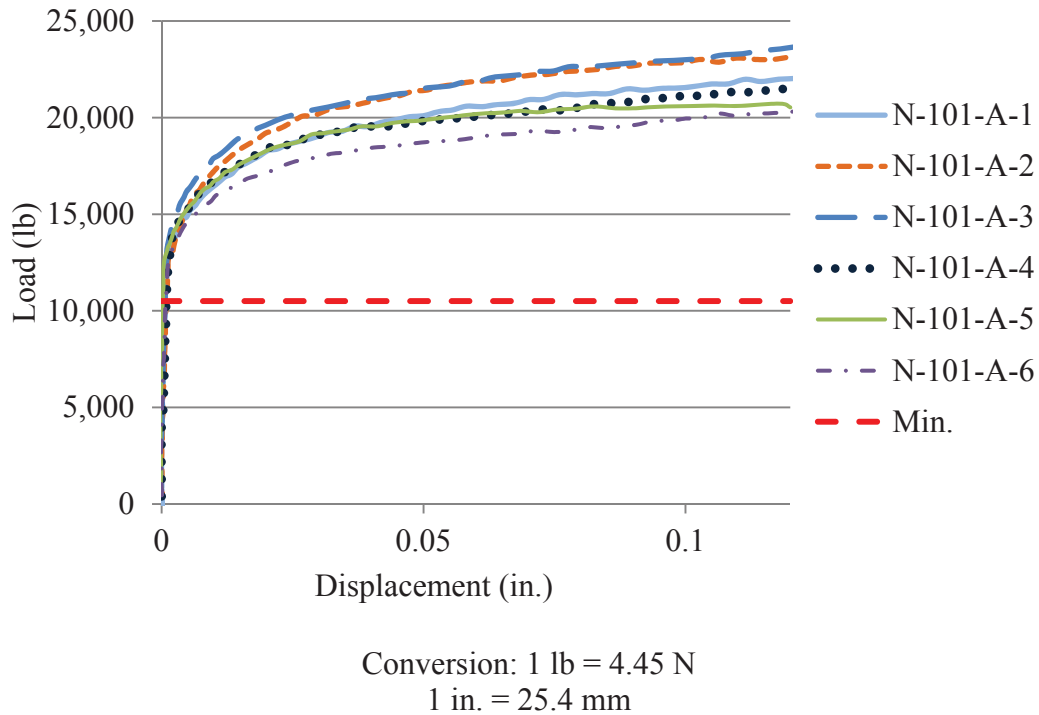


**Figure 3.17 – Typical Load vs. Slip Plot for NASP Test in Mortar (N-101-A)**

**Tables 3.4, 3.5, 3.6, and 3.7** present the loads at slip values of 0.001 in. (0.025 mm) and 0.1 in. (2.54 mm) for the NASP tests performed on strand and mortar mix combinations of 101-A, 101-B, 102-B, and 103-B, respectively. The mortar strength, mortar flow, and average loading rate for each set of tests are also reported in each table. **Table 3.8** summarizes the average loads at 0.001 in. (0.025 mm) and 0.1 in. (2.54 mm) slip, as well as fresh and hardened properties of the mortar used for each test so the results from the different tests can be compared side by side.

**Table 3.4 – NASP in Mortar Results for Strand 101 Mix A**

<b>Specimen ID</b>	<b>Load at 0.001 in. Slip (lb)</b>	<b>Load at 0.1 in. Slip (lb)</b>
N-101-A-1	12,500	22,100
N-101-A-2	10,600	22,900
N-101-A-3	12,600	23,000
N-101-A-4	11,100	21,100
N-101-A-5	13,100	20,600
N-101-A-6	11,500	20,000
<b>Average</b>	<b>11,900</b>	<b>21,600</b>
<b>Std. Dev.</b>	<b>965</b>	<b>1,249</b>
<b>COV</b>	<b>8.1%</b>	<b>5.8%</b>
$f'_c = 4,980$ psi		
Flow = 112.1		
Average Load Rate = 6,539 lb./min.		

Conversion: 1 lb. = 4.45 N

1 psi = 6.89 kPa

1 in. = 25.4 mm

**Table 3.5 – NASP in Mortar Results for Strand 101 Mix B**

<b>Specimen ID</b>	<b>Load at 0.001 in. Slip (lb)</b>	<b>Load at 0.1 in. Slip (lb)</b>
N-101-B-1	8,100	19,100
N-101-B-2	6,500	17,300
N-101-B-3	7,800	17,800
N-101-B-4	7,200	19,100
N-101-B-5	8,900	18,200
N-101-B-6	5,200	17,800
<b>Average</b>	<b>7,300</b>	<b>18,200</b>
<b>Std. Dev.</b>	<b>1,311</b>	<b>751</b>
<b>COV</b>	<b>18.0%</b>	<b>4.1%</b>
$f'_c = 5,000$ psi		
Flow = 100.2		
Average Load Rate = 6,933 lb./min.		

Conversion: 1 lb. = 4.45 N

1 psi = 6.89 kPa

1 in. = 25.4 mm

**Table 3.6 – NASP in Mortar Results for Strand 102 Mix B**

<b>Specimen ID</b>	<b>Load at 0.001 in. Slip (lb)</b>	<b>Load at 0.1 in. Slip (lb)</b>
N-102-B-1	3,200	11,000
N-102-B-2	3,300	12,400
N-102-B-3	4,200	12,600
N-102-B-4	1,900	9,300
N-102-B-5	3,800	12,400
N-102-B-6	2,400	12,300
<b>Average</b>	<b>3,100</b>	<b>11,700</b>
<b>Std. Dev.</b>	<b>860</b>	<b>1,289</b>
<b>COV</b>	<b>27.4%</b>	<b>11.0%</b>
$f'_c = 4,820$ psi		
Flow = 116.0		
Average Load Rate = 6,420 lb./min.		

Conversion: 1 lb. = 4.45 N,  
 1 psi = 6.89 kPa  
 1 in. = 25.4 mm

**Table 3.7 – NASP in Mortar Results for Strand 103 Mix B**

<b>Specimen ID</b>	<b>Load at 0.001 in. Slip (lb)</b>	<b>Load at 0.1 in. Slip (lb)</b>
N-103-B-1	3,500	15,800
N-103-B-2	2,600	20,500
N-103-B-3	1,800	18,600
N-103-B-4	700	16,000
N-103-B-5	8,700*	19,700
N-103-B-6	1,200	21,300
<b>Average</b>	<b>2,000</b>	<b>18,700</b>
<b>Std. Dev.</b>	<b>1,091</b>	<b>2,295</b>
<b>COV</b>	<b>55.6%</b>	<b>12.3%</b>
$f'_c = 4,770$ psi		
Flow = 111.6		
Average Load Rate = 6,590 lb./min.		

\* - Value was statistically removed from average and std. dev.

Conversion: 1 lb. = 4.45 N  
 1 psi = 6.89 kPa  
 1 in. = 25.4 mm

**Table 3.8 – Summary of NASP Test in Mortar Pullout Values and Mortar Properties**

Strand/Mix ID	Avg. Load at 0.001 in. (lb.)	Avg. Load at 0.1 in. (lb.)	$f'_c$ (psi)	Flow	Unit Weight (lb/ft <sup>3</sup> )	Average Load Rate (lb/min.)
N-101-A	11,900	21,600	4,980	112.1	142.9	6,539
N-101-B	7,300	18,200	5,000	100.2	136.5	6,933
N-102-B	3,100	11,700	4,820	116.0	134.2	6,420
N-103-B	1,960	18,700	4,770	111.6	134.9	6,590

Conversion: 1 lb. = 4.45 N

1 psi = 6.89 kPa

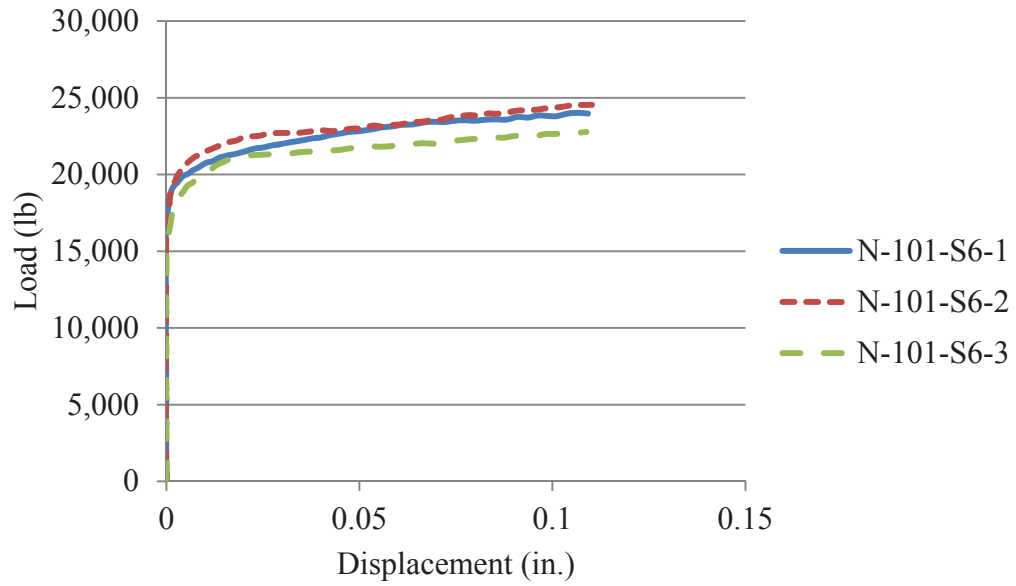
1 lb/ft<sup>3</sup> = 16.0 kg/m<sup>3</sup>

1 in. = 25.4 mm

**3.3.4.2 Results from Modified NASP Test in Concrete.** The results from the 24-hour and 8 day NASP tests run on the concrete NASP specimens are presented here. First, the load data from the MTS and the slip data from the LVDT were organized into load vs. slip plots. An example load vs. slip plot can be found in **Figure 3.18**. Each plot shows the curves for the three specimens of the same concrete mix tested at either 1 day or 8 days. All plots for the concrete NASP tests can be found in Appendix B.

The written procedure specifies that the pullout load is defined as the load at 0.1 in. (2.54 mm) of strand slip, but the pullout load at 0.001 in. (0.025 mm) of slip was also recorded. **Table 3.9** contains the individual and average loads corresponding to 0.001 in. (0.025 mm) and 0.1 in. (2.54 mm) of slip for concrete mixes C6 and S6 tested at 1 day and 8 days, as well the standard deviation and coefficient of variation for each set of three loads. **Table 3.10** contains the same data for the C10 and S10 mixes.

In **Table 3.9**, specimen N-101-C10-1 does not have a 0.1 in. (2.54 mm) pullout load value because this was the first test completed, and the test reached the maximum stroke of the MTS before the slip reached 0.1 in. (2.54 mm). The allowable stroke distance was increased after this test, so this problem was not encountered again.



Conversion: 1 lb = 4.45 N  
1 in. = 2.54 mm

**Figure 3.18 – Typical Load vs. Slip Plot for Concrete NASP Test (N-101-S6)**

Table 3.9 – Concrete NASP Results – C6 and S6

Mix	Day	Specimen ID	f <sup>c</sup> (psi)	Load at Slip of 0.001 in.			Load at Slip of 0.1 in.				
				Load (lb.)	Average (lb.)	Std. Dev. (lb.)	COV	Load (lb.)	Average (lb.)	Std. Dev. (lb.)	COV
C6	1 Day	N-101-C6-1	4,810	16,900	17,700	971	5.49%	20,900	21,100	529	2.51%
		N-101-C6-2		17,500				20,700			
		N-101-C6-3		18,800				21,700			
	8 Day	N-101-C6-4	5,620	18,200	18,900	2,676	14.16%	24,900	24,200	907	3.75%
		N-101-C6-5		16,700				24,600			
		N-101-C6-6		21,900				23,200			
S6	1 Day	N-101-S6-1	5,660	18,700	18,000	1,127	6.26%	23,900	23,700	874	3.69%
		N-101-S6-2		18,600				24,400			
		N-101-S6-3		16,700				22,700			
	8 Day	N-101-S6-4	6,690	18,100	19,000	1,137	5.99%	24,700	26,200	1,375	5.25%
		N-101-S6-5		18,700				26,500			
		N-101-S6-6		20,300				27,400			

Conversion: 1 lb. = 4.45 N  
1 in. = 25.4 mm

Table 3.10 – Concrete NASP Results – C10 and S10

Mix	Day	Specimen ID	f <sub>c</sub> (psi)	Load at Slip of 0.001 in.			Load at Slip of 0.1 in.				
				Load (lb.)	Average (lb.)	Std. Dev. (lb.)	COV	Load (lb.)	Average (lb.)	Std. Dev. (lb.)	COV
C10	1 Day	N-101-C10-1	5,670	14,000	15,000	850		N/A	26,700	1,202	4.51%
		N-101-C10-2		15,300				27,500			
		N-101-C10-3		15,600				25,800			
	8 Day	N-101-C10-4	7,950	15,500	17,100	2,600	15.20%	24,400	28,600	3,707	12.96%
		N-101-C10-5		15,700				30,200			
		N-101-C10-6		20,100				31,300			
S10	1 Day	N-101-S10-1	6,330	13,600	12,900	1,358	10.52%	29,000	27,300	9,420	34.51%
		N-101-S10-2		11,300				17,100			
		N-101-S10-3		13,700				35,700			
	8 Day	N-101-S10-4	8,600	18,500	16,900	1,550	9.17%	39,600	36,700	3,799	10.35%
		N-101-S10-5		15,400				38,100			
		N-101-S10-6		16,900				32,400			

Conversion: 1 lb. = 4.45 N  
1 in. = 25.4 mm

### 3.4. LARGE BLOCK PULLOUT TEST

The large block pullout test was performed on all three strand sources to compare results to those of the standard NASP test in mortar. Samples of strand 101 were received four months before samples of 102 and 103, so the samples of strand type 101 were wrapped in plastic, secured with duct tape, and stored in a closed container until testing to keep the strands in as-received condition. A single block was cast with six strands from each source, and the pullout tests to determine load at first slip and peak load were performed approximately 24 hours after casting.

**3.4.1. LBPT Specimen Design.** The LBPT specimen was designed based on Logan's study completed in 1997. The 2 ft. x 2 ft. x 6 ft.-8 in. (610 mm x 610 mm x 203 mm) block of concrete was designed to hold 18 strand samples, six samples from each of the three strand sources. Strands were cut to 52 in. (1321 mm) lengths, so each strand could have 18 in. (457 mm) of bonded length, a 2 in. (50.8 mm) bond breaker made from foam insulation and duct tape, and 32 in. (813 mm) of strand protruding from the concrete surface to accommodate the test setup. The strands were spaced in two rows 12 in. (305 mm) apart, and each row contained nine strands spaced at 8 in. (203 mm) on center. The mild reinforcing and strand layout are shown in **Figures 3.19** and **3.20**. All mild reinforcing conformed to ASTM A615, Grade 60. Steel chairs measuring 5 in. (127 mm) high were used to support the mild steel cage, which in turn provided attachment points and support for the strand samples.

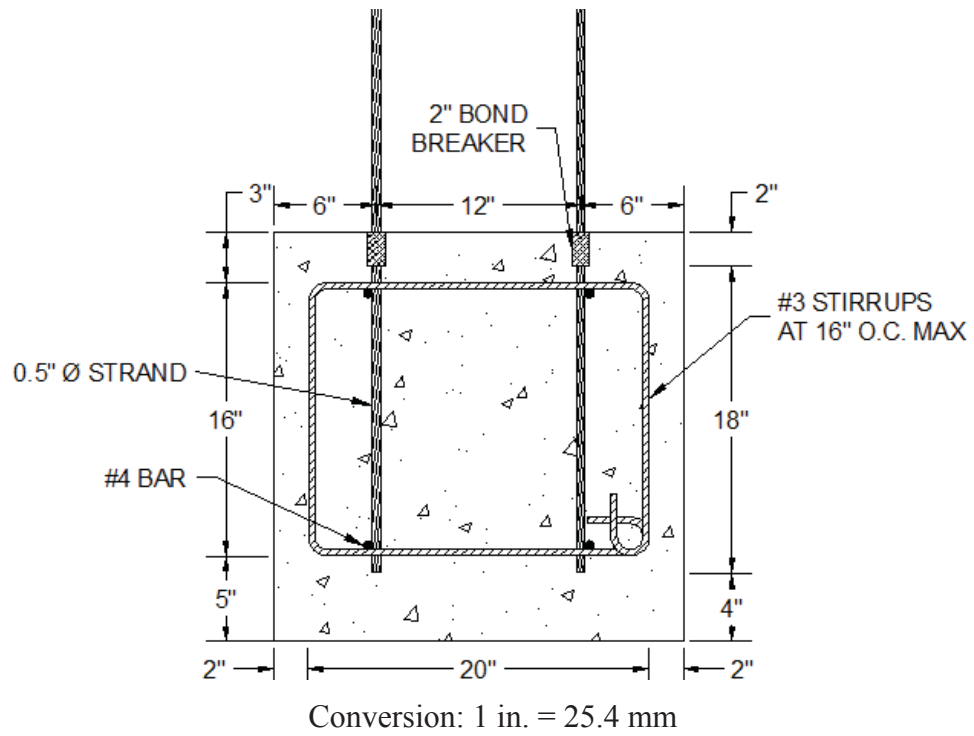


Figure 3.19 – Cross-Section of LBPT Specimen

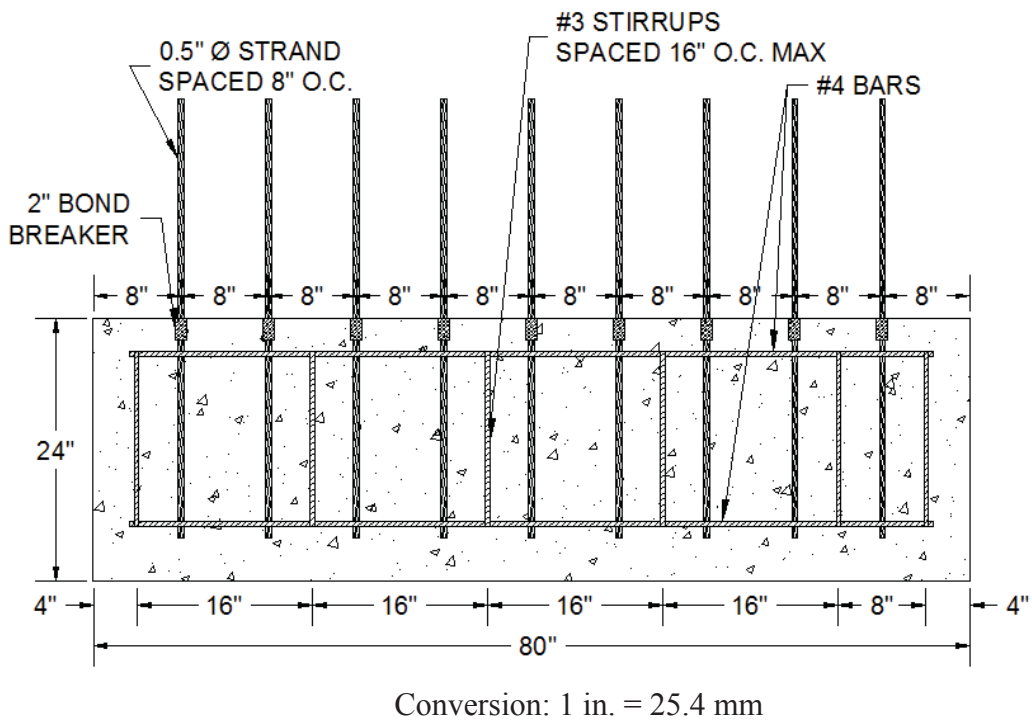
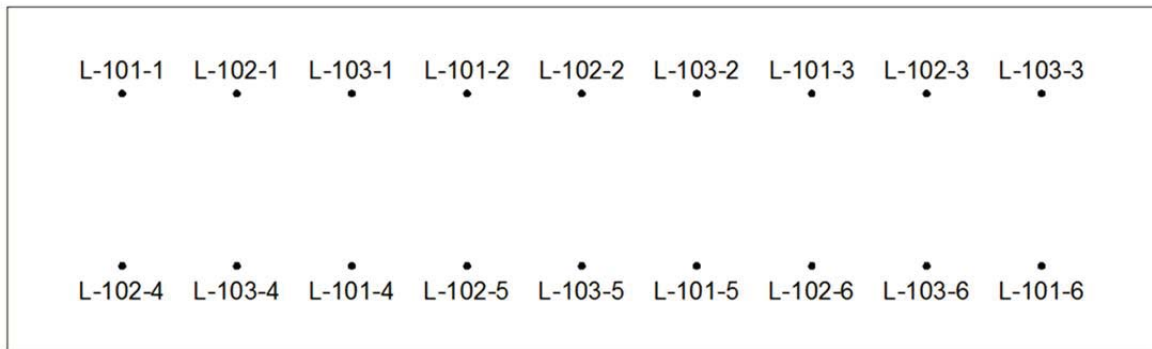


Figure 3.20 – Profile of LBPT Specimen

**3.4.2. LBPT Specimen Fabrication.** Due to the large volume of concrete required, the LBPT specimen was cast at a precast plant, and the test was performed on site the day after casting. The form was constructed out of three 8 ft. x 2 ft. (2438 mm x 610 mm) standard formwork panels, which made up the sides and bottom of the form. Standard formwork panels measuring 2 ft. x 3 ft. (610 mm x 914 mm) were secured on each end, but an end block made of a plywood panel and 2x4's was placed at one end of the form to shorten the standard form to the required length of 6 ft.-8 in. (2032 mm). The formwork and reinforcing cage were constructed at the Missouri S&T High Bay Structures Laboratory, and then for casting, the formwork and cage were transported by truck to Prestressed Casting Company, a precast plant located in Springfield, Missouri.

Upon arrival at the plant, the formwork and mild steel cage were placed on top of a precasting bed, and the strands were tied to the designated locations on the longitudinal bars of the reinforcing cage using wire ties. The strands were labeled with duct tape flags and were arranged so that the different strand sources were mixed throughout locations on the specimen to randomize the test in case any inconsistencies in the concrete existed. The strand layout pattern was the same pattern used by Logan (1997) and is shown in **Figure 3.21**. A picture of the LBPT specimen before casting can be seen in **Figure 3.22**.



**Figure 3.21 – Strand Layout Pattern**



**Figure 3.22 – LBPT Specimen Before Casting**

The specimen was fabricated from structural concrete with no admixtures. The mix design was extremely similar to Logan's (1997), and both mix designs are shown in **Table 3.11**. Also, it is important to note that Granite-Iron Mountain Trap Rock with an average Mohs Hardness of approximately 6.5 was used for the coarse aggregate. Recent unpublished research by Logan indicates that the Mohs Hardness of the coarse aggregate can affect the test results, and softer aggregates lead to lower pullout values. Therefore, Logan has recently recommended that when conducting the LBPT, the coarse aggregate should have a Mohs Hardness of 6.0 or greater to achieve consistency among testing (D. Logan, personal communication, October 20, 2011).

**Table 3.11 – Missouri S&T's and Logan's LBPT Mix Designs**

Material	Weight (lb/yd <sup>3</sup> )	
	Missouri S&T	Logan
Type III Cement	660	660
<sup>3</sup> / <sub>4</sub> " Coarse Aggregate	1785	1900
Fine Aggregate	1033	1100
Water	290	290

Conversion: 1 lb/yd<sup>3</sup> = 0.593 kg/m<sup>3</sup>

The concrete was mixed at the batch plant on site and delivered by a sidewinder to the specimen form. Before the concrete was placed, a slump test was run according to ASTM C143/C143M–10a: Standard Test Method for Slump of Hydraulic Cement Concrete to ensure the slump was close to the 3 in. (76.2 mm) target slump. Once the slump was deemed acceptable, the LBPT form was filled. Due to the low slump, the concrete was heavily vibrated, but great care was taken during placement and vibration to avoid jostling the strands. The concrete placement process is illustrated in **Figure 3.23**. During placement, 6 in. x 12 in. (152 mm x 305 mm) cylinders were also cast to determine unit weight and monitor compressive strength, and air content was determined in the field as well. The fresh and hardened concrete properties are presented in **Table 3.12**.

After casting, the surface of the LBPT specimen was finished, and then the specimen was cured overnight by means of wet burlap, plastic sheeting, and the heated prestressing bed. The burlap was placed on the surface of the concrete around the strands, and the plastic sheeting was tented over the entire specimen and supported by a frame of 2x4's so the plastic would not touch the strands. The finished specimen and part of the wooden frame for the plastic sheeting is shown in **Figure 3.24**.



**Figure 3.23 – Casting the LBPT Specimen**

**Table 3.12 – Fresh and Hardened Properties of LBPT Concrete Mix**

<b>Fresh or Hardened Concrete Property</b>	<b>Value</b>
$f'_c$ at Test (psi)	4,250
Slump (in.)	4
Unit Weight (lb./ft <sup>3</sup> )	143.3
Air Content	2.5%

Conversion: 1 psi = 6.89 kPa

1 in. = 25.4 mm

1 lb./ft<sup>3</sup> = 16.0 kg/m<sup>3</sup>

**Figure 3.24 – Finished LBPT Specimen**

**3.4.3. LBPT Test Setup and Procedure.** On the night before the day of casting, all strands were labeled with duct tape flags and then subjected to a visual inspection and towel wipe test, as prescribed by Logan (1997). The strands were first visually observed for color, rust spots, and rust coatings, and then a clean, white rag was wiped down the length of the strand, and the amount of residue on the rag was noted. The results of the visual observations and towel wipe tests are presented in **Section 3.4.4**. After completing the visual observations and towel wipe tests, the strands were packed in a shipping box for transportation to the precast plant for casting the next day.

The strands were cast in the LBPT specimen as described in **Section 3.4.2**, and then the research team returned to the precast plant approximately 24 hours after casting to perform the pullout tests. The average strength of the concrete at the time of testing was 4,250 psi (29.3 MPa). Logan maintains that LBPT can be performed in concrete strengths ranging from 3,500 psi (24.1 MPa) to 5,900 psi (40.7 MPa) and still give consistent results, so the compressive strength of the concrete at the time of testing was deemed acceptable. Also, it should be noted that no honeycombing or voids were observed in the concrete, indicating adequate consolidation.

Upon arrival at the plant, the form was removed, and then the data acquisition system, 100 kip (4.45 kN) load cell, and 30 ton (8.90 kN) hollow core hydraulic jack were set up. For each strand, first, a steel table was placed over the strand, and then the jack was placed on the strand, followed by a steel plate, the load cell, another steel plate, and a prestressing chuck. The setup is illustrated in **Figure 3.25**.

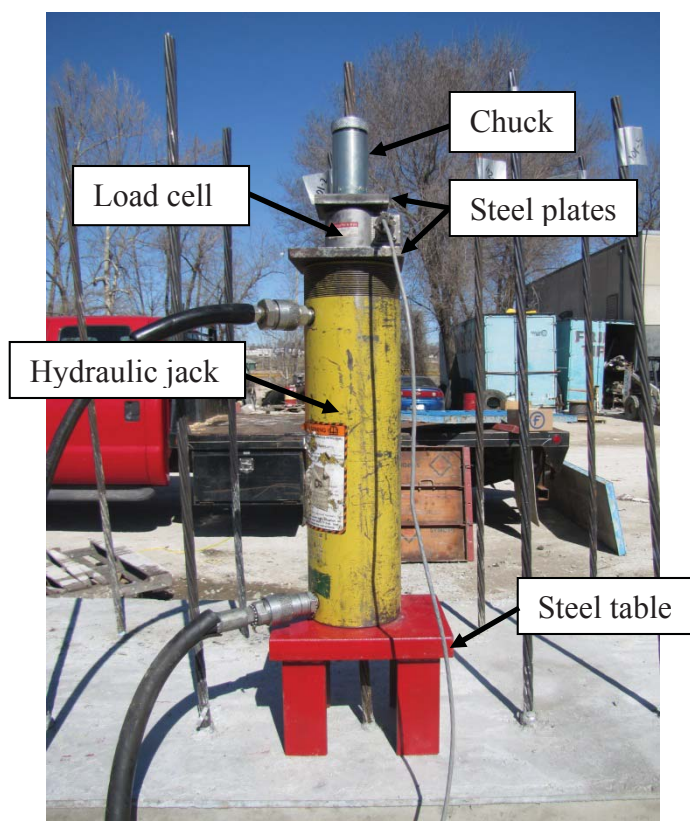


**Figure 3.25 – LBPT Hydraulic Jack and Load Cell Setup**

The 8 in. x 6 in. x 6-in. (203 mm x 152 mm x 152 mm) steel table, which is pictured in **Figure 3.26**, was constructed from a 1-in.-thick (25.4 mm) steel plate with a  $\frac{5}{8}$ -in.-diameter (15.9 mm) hole in the center and four 2 in. x 2 in. (50.8 mm x 50.8 mm) sections of angle. The table was designed based on the one used by Logan, and the purpose of the table was to give the jack a flat surface to contact and help distribute the load to the concrete.



**Figure 3.26 – Steel Table for LBPT**

Once the jack and load cell were positioned on the strand, a three-person team was used to run the test, as shown in **Figure 3.27**. One person operated the pump to apply load to the strand, one person observed the strand and reported first slip, and one person monitored the data acquisition system to record the load at first slip and peak load. According to Logan, load is supposed to be applied at approximately 20 kips/min. (89.0 kN/min.). Since the load was applied via a manual pump, there was no direct way to monitor the load rate, so the individual at the data acquisition system used a stopwatch and monitored the load. Based on the load cell and stopwatch, the individual instructed the pump operator to either increase or decrease the loading rate. Additionally, a sample

test block with two strands was cast at the same time as the LBPT specimen, and the test block was used to refine the test procedure prior to performing the actual strand pullout tests.

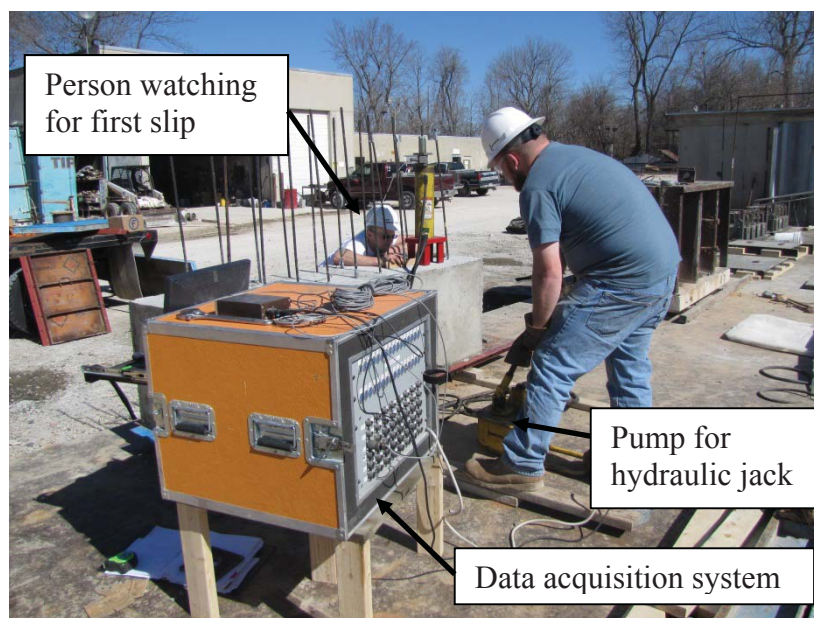


**Figure 3.27 – Full LBPT Setup**

Load was applied until the data acquisition system indicated a distinct drop off in load or until there was a loud noise and a sudden drop off in load. The load noise was determined to be the chuck slipping as the strand stretched and tried to untwist, but then suddenly snapped back into its twisted state. The load at first slip was determined through coordination between the individual watching the strand and the individual monitoring the data acquisition system. At first noticeable movement, the person watching the strand called out “Slip!”, and the person monitoring the data acquisition system recorded the load value at that moment. Peak load was estimated in the field and then refined through analysis of the collected load data.

**3.4.4. LBPT Results.** The results from the visual observations, towel wipe tests, and the actual pullout tests are summarized for each strand in **Table 3.13** and then discussed in the following paragraphs.

Table 3.13 – LBPT Results

Specimen ID	First Slip Load (kips)	Peak Load (kips)	Surface Condition (Visual and Towel Wipe)	Test Description
L-101-1	15.9	34.3	No rust Light/moderate residue	Gradual slip to loud noise abrupt drop off in load 2” pullout
L-101-2	17.9	34.2	No rust Light/moderate residue	Gradual slip to peak load, test stopped 1” pullout
L-101-3	20.2	35.9	Light rust Moderate residue	Gradual slip to clear peak load, then load noise and abrupt drop off in load 3” pullout
L-101-4	31.2	38.8	Moderate rust spots in bonded area Moderate residue	Gradual slip to loud noise and abrupt drop off in load 1.5” pullout
L-101-5	19.2	38.5	Moderate/heavy rust spots in bonded area Moderate residue	Gradual slip to loud noise and abrupt drop off in load 2.75” pullout
L-101-6	22.1	38.1	No rust Light residue	Gradual slip to loud noise and abrupt drop off in load 3” pullout
L-102-1	9.7	27.1	Dull, light rust layer Heavy Residue	Gradual slip to loud noise and abrupt drop off in load 2.5” pullout
L-102-2	12.3	27.1	Dull, light rust layer Moderate residue	Gradual slip to peak load, test stopped 2” pullout
L-102-3	13.8	31.0*	Dull, light rust layer Moderate residue	Gradual slip to peak load, test stopped 2” pullout Data recording accidentally stopped at slip

\* - Data collection was accidentally stopped midway through the test, and this is the estimated value from the field.

Table 3.13 Continued – LBPT Results

Specimen ID	First Slip Load (kips)	Peak Load (kips)	Surface Condition (Visual and Towel Wipe)	Test Description
L-102-4	13.9	40.1	Dull, light rust layer and many heavy rust spots in bonded area Heavy orange residue	Gradual slip, strand broke in concrete 4.5" pullout
L-102-5	12.1	25.1	Dull, light rust layer and some rust spots in bonded area Moderate/heavy residue	Gradual slip to loud noise and abrupt drop off in load 2" pullout
L102-6	14.3	31.9	Dull, light rust layer Moderate/heavy residue	Gradual slip to loud noise and abrupt drop off in load 2.25" pullout
L-103-1	19.7	33.5	Blue tinge, some rust spots at bottom of bonded area Light residue	Gradual slip to loud noise and abrupt drop off in load 2" pullout
L-103-2	21.3	33.5	Blue tinge, little rust specks Moderate residue	Gradual slip to loud noise and abrupt drop off in load 3" pullout
L-103-3	15.9	38.7	Blue tinge, light rust spots in bonded area Moderate residue	Gradual slip to loud noise and abrupt drop off in load 4" pullout, but wedge marks show chuck slipped
L-103-4	17.3	35.6	Blue tinge, light rust spots in bonded area Moderate residue	Gradual slip to loud noise and abrupt drop off in load 3.5" pullout
L-103-5	16.7	26.6	Blue tinge, light rust spots in bonded area Light residue	Gradual slip to loud noise and abrupt drop off in load 2.25" pullout
L-103-6	24.6	39.2	Blue tinge, light rust spots in bonded area Light residue	Gradual slip to loud noise and abrupt drop off in load 3.5" pullout

Conversion: 1 kip = 4.45 kN  
1 in. = 25.4 mm

In terms of the visual observations, a comparison of the strands can be seen in **Figure 3.28**. Strand type 102 showed the largest number of rust spots and also appeared to have a dull, light rust over all surfaces. Strand types 101 and 103 appeared to be similar in terms of very little noticeable rust, but strand type 103 actually had a slightly shiny, almost blue tinge to the wires. A written description of the visual observations for each strand can be found in **Table 3.11**.



**Figure 3.28 – Visual Comparison of Strands**

The results of the towel wipe test for strand types 101, 102, and 103 are displayed in **Figures 3.29, 3.30, and 3.31**, respectively. Compared to the other strand types, type 102 had a noticeable moderate to heavy brown/orange residue on almost all strands (**Figure 3.30**). Strand type 103 showed very light residue (**Figure 3.31**), and strand type 101 exhibited light to moderate amounts of residue (**Figure 3.29**). A written description of the results of the towel wipe test for each strand can be found in **Table 3.13**.



**Figure 3.29 – Towel Wipe Results for Strand Type 101**



**Figure 3.30 – Towel Wipe Results for Strand Type 102**



**Figure 3.31 – Towel Wipe Results for Strand Type 103**

Time and load were collected by the data acquisition system at a sampling rate of two points per second, and the data was converted into excel files to plot load vs. time and determine the maximum applied load. The load vs. time plots can be found in Appendix C. The estimated first slip load and peak load determined from the collected data are summarized for each strand in **Table 3.13**. A summary of just the first slip and peak pullout loads, along with the averages, standard deviations, and coefficients of

variation for each strand type are presented in **Table 3.14**. For comparison, it should be noted that Logan's limits for first slip and peak load are 16 kips (71.2 kN) and 36 kips (160 kN), respectively.

As the footnote on **Tables 3.13** and **3.14** indicate, the peak load for L-102-3 is load from field observations because the data was not collected electronically. However, this value is still considered valid because during analysis, it was noted that estimated values were very close to the values determined through analysis of the electronically collected data. Additionally, as noted in the footnote in **Table 3.14**, the peak load for L-102-4 and the first slip load for L-101-4 were not included in their respective averages or standard deviations. For L-102-4, because the peak load exceeded 40 kips and it was observed that the strand became untwisted above the concrete at failure, it was determined that this specimen actually ruptured in the concrete. This was seen as an anomaly, especially since this was the strand type with the worst bond overall, so the peak load value was not used in the analysis. Additionally, the first slip load of L-101-4 was deemed high, so the value was not included in the first slip average for that specimen.

Table 3.14 – Summary of LBPT Pullout Loads

Strand Type	Specimen ID	First Slip Load			Peak Load				
		Load (kips)	Avg. (kips)	Std. Dev. (kips)	COV	Load (kips)	Avg. (kips)	Std. Dev. (kips)	COV
101	L-101-1	15.9	19.1	2.3	12.27%	34.3	36.6	2.1	5.76%
	L-101-2	17.9				34.2			
	L-101-3	20.2				35.9			
	L-101-4	31.2**				38.8			
	L-101-5	19.2				38.5			
	L-101-6	22.1				38.1			
102	L-102-1	9.7	12.7	1.7	13.53%	27.1	27.8	2.9	10.40%
	L-102-2	12.3				27.1			
	L-102-3	13.8				31.0*			
	L-102-4	13.9				40.1**			
	L-102-5	12.1				25.1			
	L-102-6	14.3				31.9			
103	L-103-1	19.7	19.3	3.3	17.16%	33.5	34.5	4.6	13.30%
	L-103-2	21.3				33.5			
	L-103-3	15.9				38.7			
	L-103-4	17.3				35.6			
	L-103-5	16.7				26.6			
	L-103-6	24.6				39.2			

Conversion: 1 kip = 4.4 kN

\* - Data collection was accidentally stopped midway through the test, and this is the estimated value from the field.

\*\* - Load was removed from average and std. dev.

## 4. TRANSFER LENGTH AND DEVELOPMENT LENGTH TEST PROGRAM AND RESULTS

### 4.1. INTRODUCTION

In order to study the effect that different concrete mixes have on transfer length and development length, twelve 17-foot long (5,182 mm) rectangular prestressed beams with either two or four strands were constructed. The beams were first used to measure transfer lengths at release and then periodically over two months. After all transfer length measurements had been taken, each end of each beam was tested in flexure at different span lengths to determine if development lengths calculated from AASHTO and ACI codes are conservative for the concrete mixes tested. The design and fabrication of the beams are presented in **Sections 4.2** and **4.3**, respectively. **Section 4.4** covers the setup, procedure, and result for each transfer length test, and the setup, procedure, and results from the development length test program are presented in **Section 4.5**.

### 4.2. TRANSFER AND DEVELOPMENT LENGTH BEAM DESIGN

In terms of specimen design, the concrete mixes were based on typical mix designs produced around Missouri, and the dimensions and reinforcement layouts of the specimens were based on previous research done by Ramirez and Russell (2008). The details of the mix designs and specimen designs are discussed in this subsection.

**4.2.1. Mix/Specimen Identifications and Mix Designs.** The goal of the research was to evaluate the effects of type of concrete and concrete strength on strand bond performance. As a result, four mix designs were developed: a normal and high strength conventional concrete and a normal and high strength self-consolidating concrete (SCC). The target strengths for the normal strength and high strength mixes were 6,000 psi (41.4 MPa) and 10,000 psi (69.0 MPa), respectively. An identification code was developed to distinguish the mixes and specimens, as shown in **Figure 4.1**.

For example, C6 simply refers to the conventional concrete, 6,000 psi (41.4 MPa) target strength mix, while C6-2-1 refers to the beam fabricated with the conventional concrete, 6,000 psi (41.4 MPa) target strength mix, having two strands, and being the first of two beams constructed with the specific mix and strand layout. Since the two-strand

beams were used for testing both transfer length and development length, an additional code was added to distinguish between the tests. For instance, C6-2-1\_NE indicates the transfer length testing on the north end of the strand on the east side of the beam previously described, while C6-2-1\_58 indicates the testing of the 58 in. (1,473 mm) embedment length on the same beam. All directions for transfer length designation are relative to the cardinal position of casting.

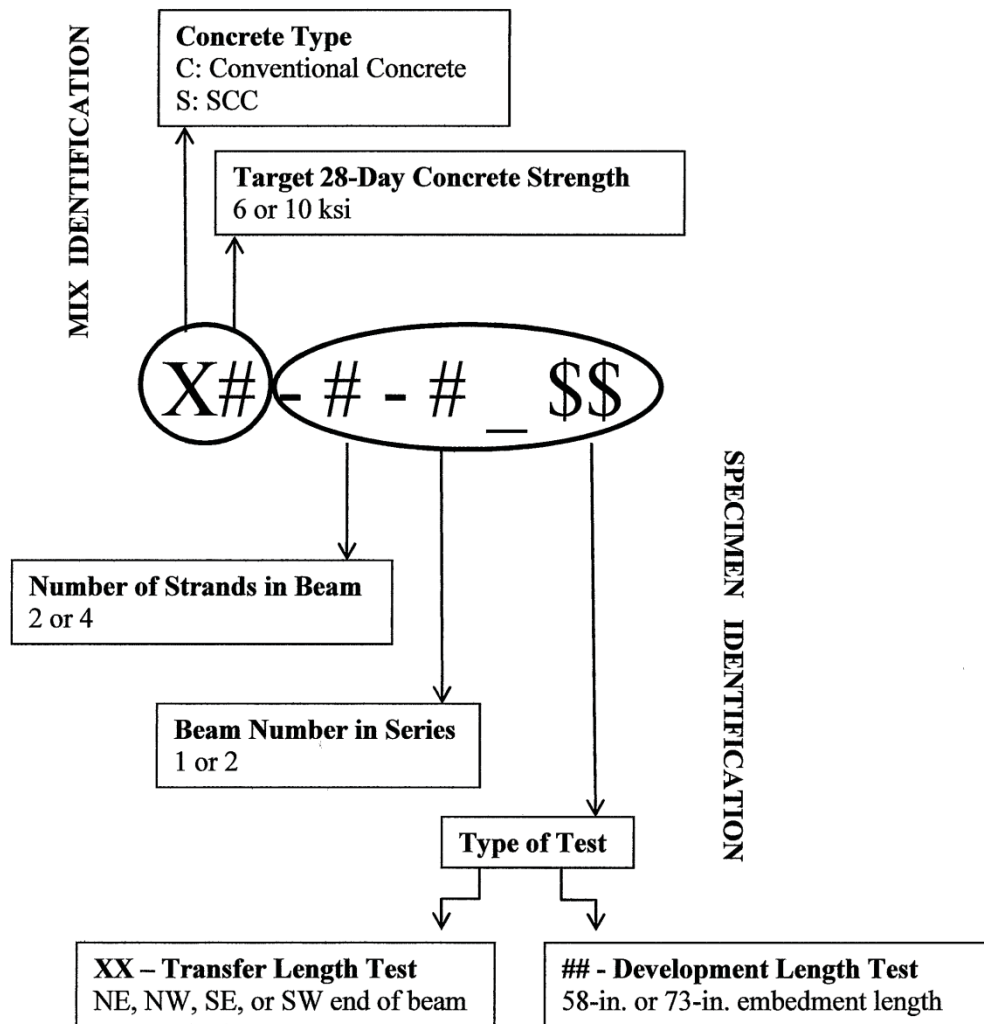


Figure 4.1 – Mix and Specimen Identification Code

The normal strength conventional mix (C6) is MoDOT's A-1 precast/prestressed mix, and the remaining mix designs were developed based on results from surveys that were sent to precast plants around Missouri and previous research performed at Missouri S&T. This step ensured that the concrete used in the research would be comparable to the concrete that is being used in the field. The mix designs are broken down in **Table 4.1**.

**Table 4.1 – Mix Designs**

Material	Concrete Mix ID			
	C6	S6	C10	S10
Type III Cement (lb/yd <sup>3</sup> )	750	750	840	840
Class C Fly Ash (lb/yd <sup>3</sup> )	0	0	210	210
Water (lb/yd <sup>3</sup> )	278	278	315	315
Fine Aggregate (lb/yd <sup>3</sup> )	1166	1444	1043	1291
Coarse Aggregate (lb/yd <sup>3</sup> )	1611	1333	1440	1192
MB-AE-90 (oz/yd <sup>3</sup> ) [oz/cwt]	11.3 [1.5]	11.3 [1.5]	13.7 [1.3]	10.5 [1.0]
Glenium 7700 (oz/yd <sup>3</sup> ) [oz/cwt]	29.3 [3.9]	46.5 [6.2]	52.5 [5.0]	75.6 [7.2]

Conversion: 1 lb/yd<sup>3</sup> = 0.593 kg/m<sup>3</sup>  
 1 oz/yd<sup>3</sup> = 38.7 mL/m<sup>3</sup>

**4.2.2. Fresh and Hardened Properties of Concrete Mixtures.** All mixes were first tested in trial batches in the Materials Lab at Missouri S&T in order to work out the correct mix proportions to obtain the target fresh and hardened properties before the final specimens were constructed at Coreslab Structures, Inc. (Coreslab) in Marshall, MO. Final fresh and hardened properties of all four concrete mixtures were measured and recorded.

In terms of fresh properties, slump, slump flow, and J-ring were performed on the appropriate mixes, and unit weight and air content were found for all mixes. The standard slump test was run on the conventional concrete mixes according to ASTM C143/C143M-10a: Standard Test Method for Slump of Hydraulic Cement Concrete.

Slump flow for the SCC mixes was measured according to ASTM C1611/C116M-09 Standard Test Method for Slump Flow of Self-Consolidating Concrete using Filling Procedure B in Section 8.2.2 with the inverted slump mold. Additionally, passing ability of the SCC mixes was evaluated using ASTM C1621/C1621M-09b: Standard Test Method for Passing Ability of Self-Consolidating Concrete by J-Ring. Air content for all mixes was determined using a Type B pressure meter and following ASTM C231/C231M-10: Standard Test Method for Air Content of Freshly Mixed Concrete by the Pressure Method. Finally, unit weight of each mix was determined through the rodding procedure specified in Section 6.3 of ASTM C138/C138M-10b: Standard Test Method for Density (Unit Weight), Yield, and Air Content (Gravimetric) of Concrete. The fresh properties of all four mixtures are shown in **Table 4.2**.

**Table 4.2 – Fresh Concrete Properties**

Property	Concrete Mix ID			
	C6	S6	C10	S10
Slump (in.)	8.5	N/A	4.5	N/A
Slump Flow (in.)	N/A	28	N/A	22
J-Ring (in.)	N/A	28	N/A	18
Unit Weight (lb/ft <sup>3</sup> )	137.6	139.2	142.4	141.6
Air Content (%)	6	7.5	6.5	7

Conversion: 1 in. = 25.4 mm

1 lb/ft<sup>3</sup> = 16.0 kg/m<sup>3</sup>

In terms of hardened concrete properties, compressive strength was measured at 1, 4, 8, 14, and 28 days, and the modulus of elasticity was determined at 28 days. The normal strength mixes had target one day strengths of 4,000 psi (27.6 MPa) and target 28 day strengths of 6,000 psi (41.4 MPa), while the high strength mixes were designed to reach 6,000 psi (41.4 MPa) and 10,000 psi (69.0 MPa) at one day and 28 days, respectively. All compressive strengths were determined by testing 4 in. x 8 in. (102 mm x 203 mm) cylinders on the Forney compressive testing machine and following ASTM

C39/C39M-11a: Standard Test Method for Compressive Strength of Cylindrical Concrete Specimens.

In addition to testing compressive strength, the modulus of elasticity of each concrete mix was tested and recorded at 28 days. To determine modulus of elasticity of each mix, a two-ring modulus test frame was used in accordance with the procedure specified by ASTM C469/C469M-10: Standard Test Method for Static Modulus of Elasticity and Poisson's Ratio of Concrete in Compression.

**Table 4.3** summarizes the initial and 28 day compressive strengths and the 28-day moduli of elasticity for the four mixes. The C10 mix was the only mix that did not reach the one day target strength, and three of the four mixes did not reach the target 28 day strengths. C6 was just slightly under the goal of 6,000 psi (41.4 MPa), while the two high strength mixes fell short of the 10,000 psi (69.0 MPa) target strength. However, the 28 day strengths of C10 and S10 were still high enough to be significantly different than the 28 day C6 and S6 strengths. A full 28 day strength curve can be found in Appendix A.

**Table 4.3 – Concrete Strengths and 28 Day Moduli of Elasticity**

Property	C6	S6	C10	S10
$f_{ci}$ (psi)	4810	5660	5670	6330
$f_c$ (psi)	5730	6950	8480	9250
Modulus of Elasticity (psi)	4,126,500	4,820,500	4,806,800	4,736,900

Conversion: 1 psi = 6.89 kPa

**4.2.3. Strand and Mild Reinforcement Design.** The beams used for measuring transfer length and testing development length were designed based on the specimens constructed for similar research completed by Ramirez and Russell (2008). The beams were designed to be 17 ft. (5,182 mm) in length with 6.5 in.-wide (165 mm) by 12 in.-high (305 mm) cross-sections. The prestressing strand for all beams consisted of 0.5 in.-diameter (12.7 mm), Grade 270, low relaxation seven wire strand from the same roll. As illustrated in **Figure 4.2**, the two-strand beams were constructed with two strands placed

2 in. (50.8 mm) from the bottom and spaced 2.5 in. (63.5 mm) on center. The four strand beams were constructed with two strands at 2 in. (50.8 mm) from the bottom and two strands at 2 in. (50.8 mm) from the top, with both sets again spaced at 2.5 in. (63.5 mm) on center, as shown in **Figure 4.3**. The four-strand beams were included in the research program in order to study the top-bar effect on transfer length.

The mild reinforcement consisted of closed stirrups constructed out of ASTM A615, Grade 60, #3 mild reinforcing steel. The stirrups were placed at 2 in. (50.8 mm) on center at the ends of the beams to conservatively meet AASHTO requirements for cracking at release and spaced 6 in. (152 mm) on center elsewhere to ensure the beams would not fail in shear when undergoing flexural testing for development length. Two ASTM A615, Grade 60, #6 bars were placed in the top of each beam to control stresses during release. The profiles and strand and reinforcement layouts of the two-strand and four-strand beams are illustrated in **Figure 4.4** and **Figure 4.5**, respectively.

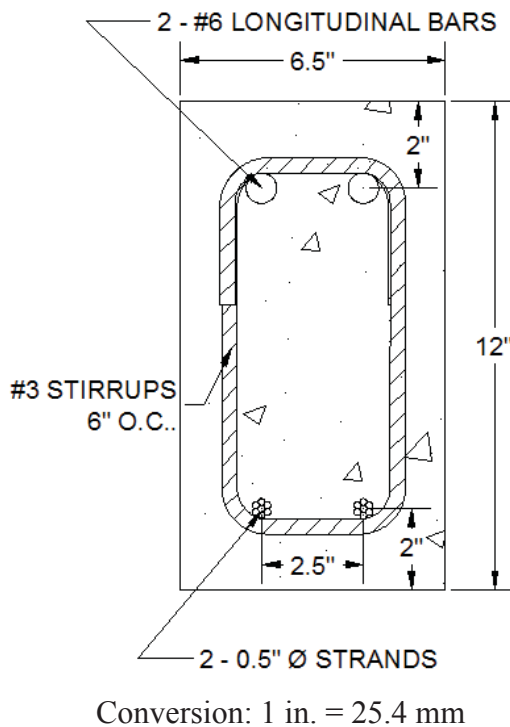


**Figure 4.2 - Two-Strand Beam  
Cross-Section**

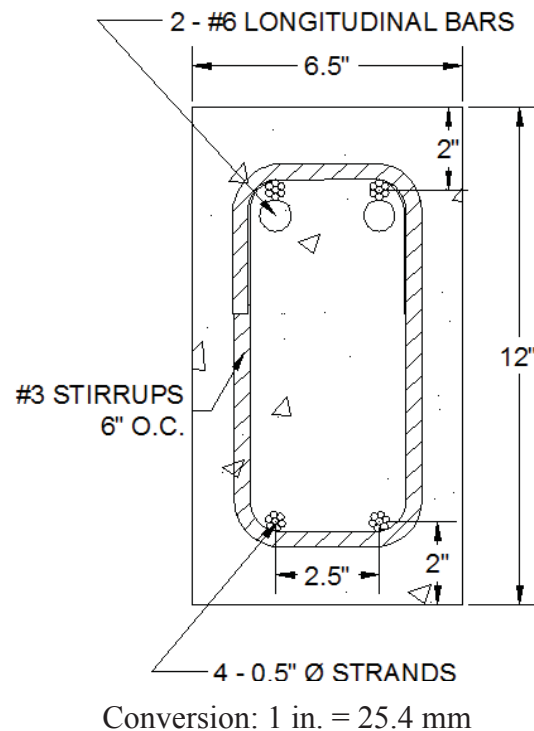
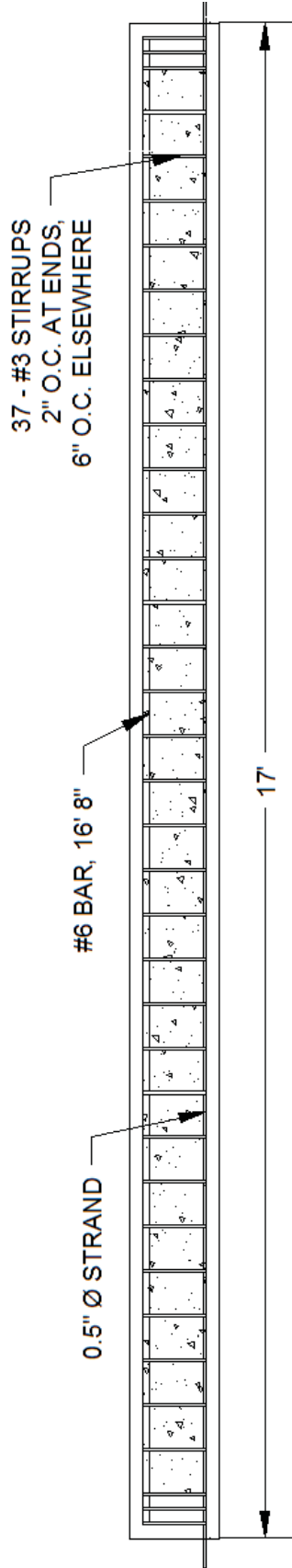
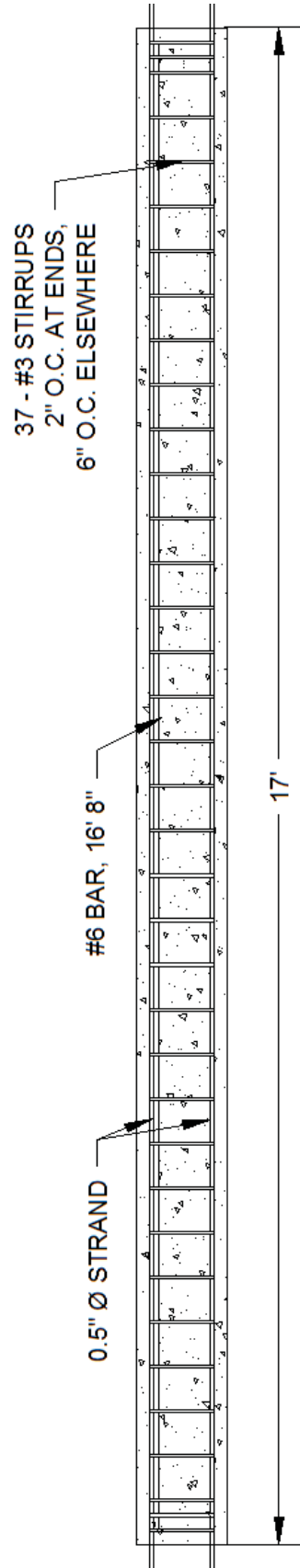


**Figure 4.3 - Four-Strand Beam  
Cross-Section**



Conversion: 1 in. = 25.4 mm  
1 ft. = 305 mm

Figure 4.4 – Profile of Two-Strand Beams



Conversion: 1 in. = 25.4 mm  
1 ft. = 305 mm

Figure 4.5 – Profile of Four-Strand Beams

### 4.3. TRANSFER AND DEVELOPMENT LENGTH BEAM FABRICATION

The beams were cast at Coreslab, a precast plant in Marshall, Missouri. Three beams designed to measure transfer length and development length were cast per mix: two two-strand beams and one four-strand beam. Additionally, one beam designed for shear testing was fabricated from each mix. While the shear beams are shown in the prestressing bed layout (**Figures 4.6 and 4.7**), the testing of these beams is not covered in this report.

The C6 and S6 beams were cast on July 21, 2011, while the C10 and S10 beams were cast on July 25, 2011. All sets of beams were released at approximately 24-26 hours after casting. The beams were cast in a 100-ft.-long (30.48 m) prestressing bed with the two-strand beams cast in one line, the four-strand beams cast in another line, and the shear beams cast in a third line. The prestressing bed layout for the C6 and S6 beams is depicted in **Figure 4.6**, while the layout for the C10 and S10 beams is shown in **Figure 4.7**.

For each mix, the concrete was mixed at the on-site batch plant and then delivered to the bed by a sidewinder. Fresh properties were measured and recorded, and once the batch was deemed acceptable, the sidewinder proceeded to fill the four beam molds (two two-strand beams, one four-strand beam, and one shear beam). One batch in the sidewinder was sufficient to complete all four beams, so the mix was kept consistent from beam to beam. The beams constructed with the conventional concretes were heavily vibrated, and the SCC beams were also lightly vibrated to ensure full consolidation. The sidewinder and beam fabrication process is illustrated in **Figure 4.8**.

Casting for both the normal strength and high strength mixes took place between late morning and early afternoon on the days of casting. The beams were cured with wet burlap and plastic overnight, and then the forms were removed early the next morning so the instrumentation could be applied before releasing the strands. **Figure 4.9** shows the transfer length and the development length beams after removal of the forms and before instrumentation. Strands were released between 24-26 hours after casting, and bolt cutters were used to release the strands one at a time. Since transfer length is affected by method of release, and the harsher the release method, the longer the transfer length, cutting the strands abruptly with bolt cutters was a conservative, or worst-case, method of release. In

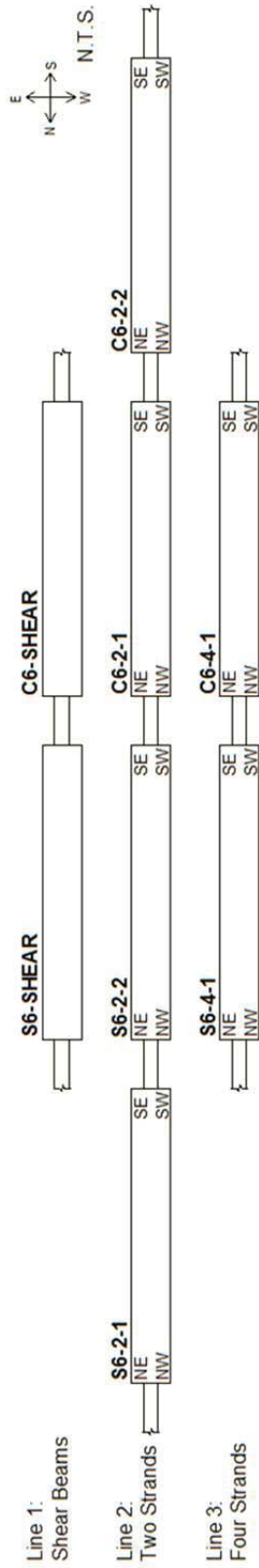


Figure 4.6 – C6 and S6 Prestressing Bed Layout

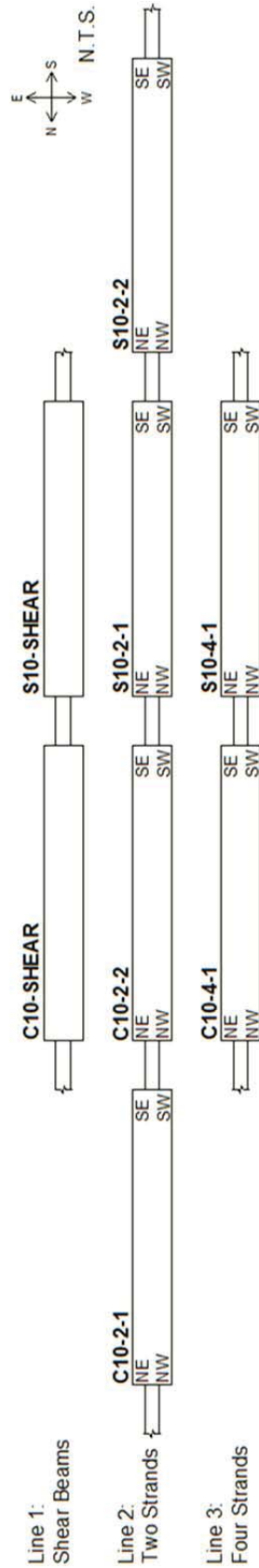


Figure 4.7 – C10 and S10 Prestressing Bed Layout



**Figure 4.8 – Beam Fabrication at Coreslab Structures in Marshall, MO**



**Figure 4.9 – Beams After Form Removal and Before Instrumentation**

order to try and release each strand all at once, one person lined up at each location where the strand would need to be cut to separate all the beams, and then the strands were ordered to be cut at the same time on cue. **Figure 4.10** demonstrates how bolt cutters

were used to release the strands. It should be noted that often, not all strands were cut on the first try at all locations. Consequences of the sequence of strand release will be discussed in Section 5.3.1.



**Figure 4.10 – Bolt Cutting Strands at Release**

#### **4.4. TRANSFER LENGTH TEST SETUPS, PROCEDURES, AND RESULTS**

Tests were done to determine transfer length at release as well as monitor the change in transfer length over time. The 95% Average Mean Strain Method, which depended on readings from demountable mechanical (DEMEC) points and a DEMEC strain gauge, was the main method employed to determine transfer lengths periodically from release to approximately 56 days after casting. Additionally, transfer lengths at release were also determined by the end slip method, which involves calculating an initial transfer length based on how much the strand slips into the concrete upon cutting. End slip of the strands was measured by linear potentiometers as well as by hand with a steel tape measure.

**4.4.1. 95% Average Mean Strain Method.** The 95% Average Mean Strain Method relies on the theory of strain compatibility between the strand and concrete. When a pretensioned strand is released, the strand loses some stress due to elastic shortening. In the transfer zone, the stress and strain in the steel and concrete are equal to zero at the unrestrained end of the beam and increase linearly as the strand transfers its stress to the concrete through bond. Beyond the transfer zone in the fully bonded area, the change in strain of the strand from the initial strain to the strain after release is equal to the strain in the concrete. By measuring concrete surface strain with DEMEC points and a DEMEC gauge, the point where the concrete strain, or the change in strain of the strand, becomes constant can be determined, and this point is the transfer length. Russell and Burns (1993) explained the use of DEMEC points and the 95% Average Mean Strain Method in depth, and many researchers have since used this process to successfully determine transfer lengths.

The following subsections explain the process of affixing the DEMEC points, taking DEMEC readings, converting the readings into strains, plotting the strains, and determining transfer lengths based on the plots. The final transfer lengths at 1, 4, 8, 14, 28, and approximately 56 days as determined by the 95% Average Mean Strain Method are presented in **subsection 4.4.1.3**.

**4.4.1.1 DEMEC Instrumentation.** On the morning after casting, the forms were removed, and a permanent marker was used to mark each beam with the correct beam identification code and to mark each end with cardinal points of NE, NW, SE, or SW based on casting position. Since each beam contained two strands of interest (the top two strands on the four strand beams), and each strand had two ends once the beam was released, the direction labels identified the four distinct transfer lengths per beam.

The DEMEC points were to be applied on the concrete surface at each transfer length location at the level of the prestressing strand. Therefore, after identifying the beams, a 5-ft.-long (1.52 m) line was marked starting from the end of the beam at each of the four transfer length locations on each beam at 2 in. (50.8 mm) from the bottom on the two strand beams and 2 in. (50.8 mm) from the top on the four-strand beams. A plexiglass template with nine 1/8-in.-diameter (3.18 mm) holes was then used to mark where the DEMEC points should be applied. The holes in the template began 0.98 in. (25

mm) from each end, and the holes were spaced 3.94 in. (100 mm) apart. The template was lined up with the closest end of the beam, and the first nine holes were marked along the line that had been drawn. Then the template was repositioned such that the first hole in the template lined up with the last hole that was marked, and an additional eight points were marked for a total of 17 points per transfer length location.

Once all the points were marked, a three-person team worked to apply a dab of 5-minute, concrete-metal epoxy to each marking, affix a DEMEC point, and set the points with the 7.87 in. (200 mm) setting bar. **Figure 4.11** depicts setting the DEMEC points. A few points could not be set due to surface honeycombing over the area where the point was supposed to be located. In these cases, the point was simply skipped. An example of this can be seen in **Figure 4.12**, where point 4 on C10-4-1\_SW could not be placed due to honeycombing.



**Figure 4.11 – Setting DEMEC Points with Setting Bar**

After all the points were set, initial readings were taken with the DEMEC gauge before the strands were cut. **Figure 4.13** shows an example of how the DEMEC readings were taken. Since the DEMEC gauge is designed to measure points set with the 7.87 in.

(200 mm) setting bar, and the points were spaced 3.94 in. (100 mm) apart, overlapping readings were taken. If points were missing due to honeycombing or set incorrectly and unreadable, the readings involving that point were simply skipped. After the initial reading, subsequent readings were taken immediately after release (1 day), and then at 4, 8, 14, and 28 days, and then at the time of development length testing, or around 56 days. All subsequent readings were compared back to the initial reading to determine the change from the initial point prior to strand release.

The beams were stored in the storage yard at Coreslab through 28 days so that the DEMEC points would not be disturbed by travel from the plant to the university. **Figure 4.14** shows the storage conditions for the beams. Although the beams were subject to temperature and humidity changes from being stored outdoors, the DEMEC reference bar was not needed for corrections. For this research, the absolute change from the initial reading did not matter, only the relative change. The 95% Average Mean Strain Method is not based on the strain readings themselves, but simply where the strain readings along the length of the beam become constant.



**Figure 4.12 – Honeycombing Preventing DEMEC Placement at Point 4 on C10-4-1\_SW**



**Figure 4.13 – Taking DEMEC Readings**



**Figure 4.14 – C6 and S6 Beams in Storage Yard at Coreslab**

**4.4.1.2 95% Average Mean Strain Procedure.** The first step in the 95% Average Mean Strain Procedure was determining the strains. The initial readings were subtracted from the final DEMEC readings on a given day, and the change in DEMEC reading was multiplied by the calibration factor provided by the manufacturer to convert the DEMEC number into microstrain. Consecutive sets of three readings were then averaged so the final plot would have a “smoothed curve.” The first point consisted of the mean of the first two readings, and the mean of every three readings was taken after that. An illustration of how the readings were averaged can be found in **Figure 4.15**, and the pattern shown would continue for all points. If readings were missing due to missing or faulty points, the other two readings in the set of three were averaged to obtain the mean strain for that point.

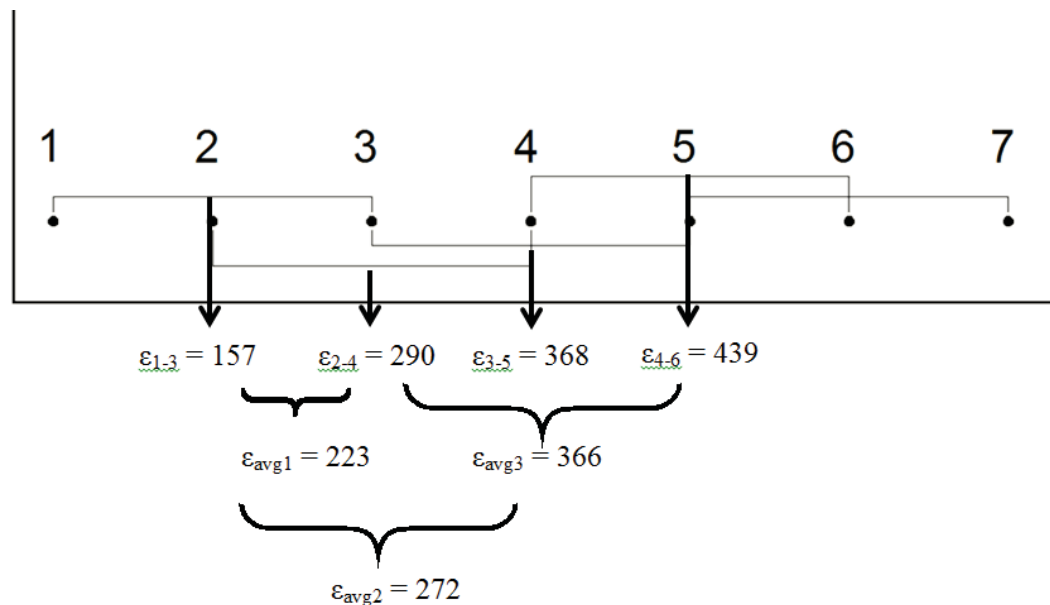


**Figure 4.15 – Mean Strains**

Once the mean strains and the values' corresponding distances from the end of the beam were determined, a plot of microstrain vs. distance from the end of the beam was created for each strand. A typical smoothed mean strain plot for one strand with readings from immediately after release is illustrated in **Figure 4.16**. In this particular case, the

plot shows the strains along the north and south ends of the east strand of beam S10-2-2. The plateaus on each of the curves indicate where the strain became constant, which indicates that the prestressing force had been fully transferred to the beam.

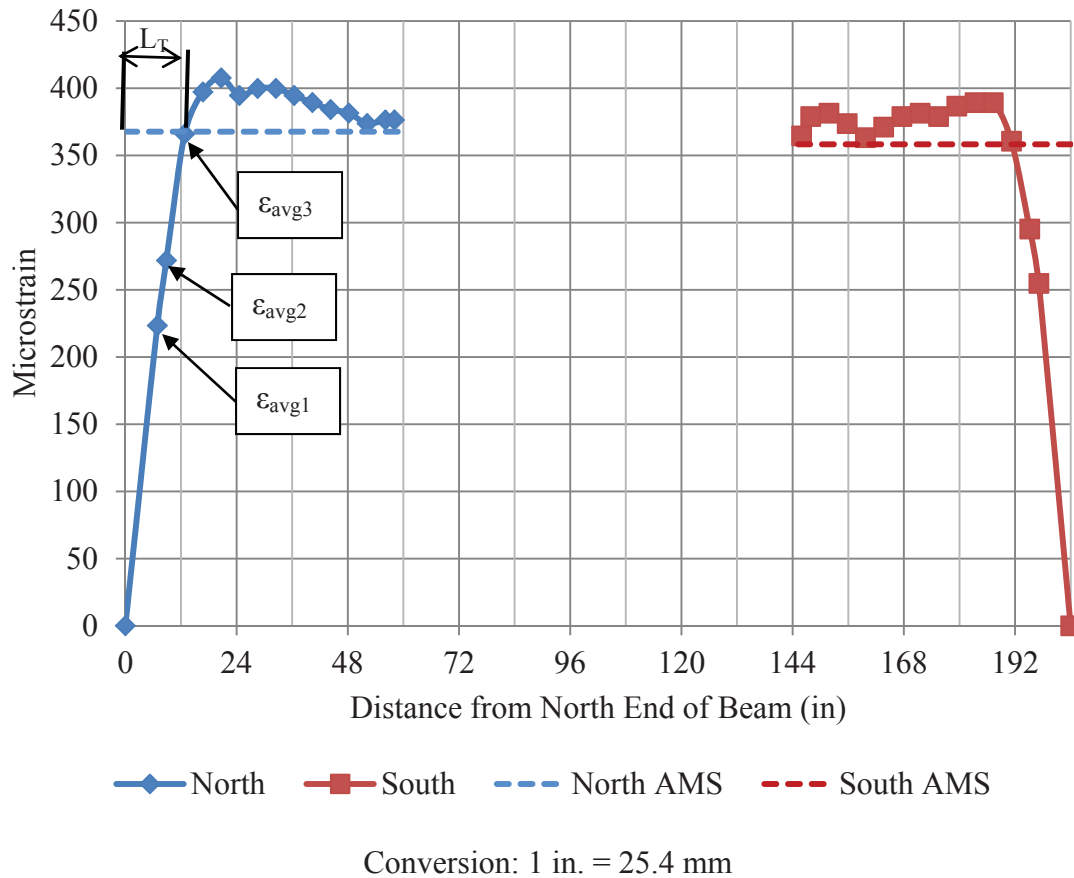


**Figure 4.16 – Typical 95% Average Mean Strain Smoothed Curve for Determining Transfer Lengths – S-10-2-2-NE and S10-2-2\_SE**

In order to apply the 95% Average Mean Strain Method, the points on each plateau were averaged to come up with an average mean strain value. Determining which points should be included in the plateau is subjective, but the method is designed so that subtle fluctuations in including or not including a point one way or the other has a negligible effect on the transfer length (Russell and Burns 1993). After an average value of the plateau was determined, a line was drawn on the plot at 95% of the average mean

strain value. The intersection of the 95% average mean strain line and the smoothed curve on each plot indicates the transfer length for that strand end. This intersection calculation was done by linearly interpolating between the two curve points where the 95% average mean strain line met the curve.

**4.4.1.3 95% Average Mean Strain Transfer Lengths.** Four transfer lengths were determined per beam for a total of eight bottom transfer lengths and four top transfer lengths per day, per mix. A typical strain plot for one strand is shown in **Figure 4.17**. The plot contains the strain profiles for DEMEC readings taken at 1, 4, 8, 14, 28, and approximately 56 days. All strain plots, like the typical plot shown in **Figure 4.17**, are included in Appendix D.

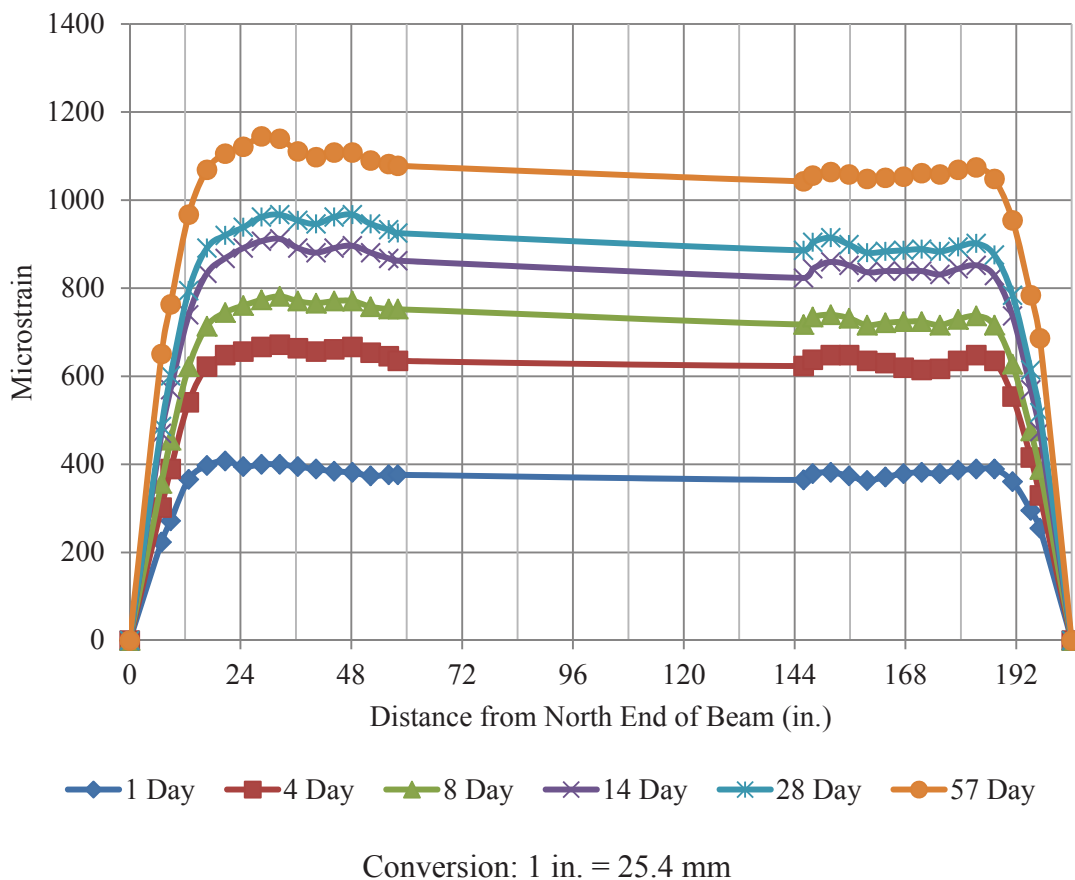


**Figure 4.17 – Typical 95% Average Mean Strain Smoothed Curves for Determining Transfer Lengths from 1 to 28 Days – S10-2-2-NE and S10-2-2\_SE**

**Tables 4.4 and 4.5** list transfer lengths for all specimens for 1, 4, 8, 14, 28 and approximately 56 days as determined by the 95% Average Mean Strain Method. **Table 4.4** reports transfer lengths of the top strands of the four-strand beams, while **Table 4.5** reports the transfer lengths of the bottom strands of the two-strand beams. **Table 4.6** summarizes the average transfer lengths, standard deviations, and coefficients of variation (COV) for the top strands for each mix at each day. **Table 4.7** contains the same average value, standard deviation, and COV summary for the bottom strands. N/A indicates that a transfer length reading could not be obtained because the DEMEC readings did not result in a plot where a conclusive transfer length could be determined.

**Table 4.4 – Transfer Lengths for Top Strands of Four-Strand Beams (1-28 Days)**

Transfer Length ID		1 Day (in.)	4 Day (in.)	8 Day (in.)	14 Day (in.)	28 Day (in.)	~56 Day (in.)
C6-4-1	NE	N/A	N/A	N/A	N/A	N/A	N/A
	NW	N/A	N/A	N/A	N/A	N/A	N/A
	SE	31.3	N/A	30.0	31.2	31.8	N/A
	SW	18.2	N/A	24.9	24.1	25.9	26.3
S6-4-1	NE	20.5	24.7	22.6	22.2	20.9	22.8
	NW	N/A	N/A	N/A	N/A	N/A	N/A
	SE	N/A	N/A	N/A	N/A	N/A	N/A
	SW	15.9	18.9	21.9	20.1	19.2	22.0
C10-4-1	NE	18.8	19.7	19.4	19.8	23.9	22.3
	NW	15.3	16.5	17.6	16.6	17.0	18.8
	SE	15.1	13.3	14.7	14.8	15.8	N/A
	SW	18.9	19.2	19.2	18.8	19.2	19.7
S10-4-1	NE	18.0	15.5	14.2	14.7	14.7	15.2
	NW	17.6	18.4	17.1	17.5	16.6	18.2
	SE	27.7	21.2	28.1	27.9	28.0	29.0
	SW	14.0	12.8	14.8	15.9	14.0	15.6

Conversion: 1 in. = 25.4 mm

Table 4.5 – Transfer Lengths for Bottom Strands of Two-Strand Beams (1-28 Days)

Transfer Length ID		1 Day (in.)	4 Day (in.)	8 Day (in.)	14 Day (in.)	28 Day (in.)	~56 Day (in.)
C6-2-1	NE	19.6	20.1	27.7	29.2	31.9	28.6
	NW	20.3	22.0	22.0	23.5	24.4	23.9
	SE	19.8	22.3	30.4	30.4	30.6	N/A
	SW	15.5	20.0	21.2	24.1	26.0	23.6
C6-2-2	NE	17.0	27.3	19.7	22.1	20.6	25.6
	NW	13.8	16.1	16.6	17.0	17.6	18.7
	SE	14.2	15.2	17.0	16.5	16.4	15.9
	SW	N/A	N/A	23.6	26.5	21.3	23.0
S6-2-1	NE	10.6	19.2	20.2	20.3	20.4	22.5
	NW	14.2	16.7	16.7	15.3	18.9	19.9
	SE	N/A	N/A	N/A	N/A	N/A	N/A
	SW	19.1	21.4	21.5	22.1	22.8	20.2
S6-2-2	NE	15.9	23.9	16.4	18.1	16.5	19.2
	NW	13.4	15.5	17.8	17.6	19.2	19.9
	SE	13.4	16.2	17.1	16.6	16.7	16.5
	SW	14.3	16.1	17.8	19.9	19.5	16.1
C10-2-1	NE	14.9	18.2	18.5	18.9	18.6	18.7
	NW	15.4	18.5	18.8	17.7	18.5	16.4
	SE	30.1	31.2	31.0	29.6	30.1	31.4
	SW	31.4	33.9	34.5	34.4	33.7	34.8
C10-2-2	NE	22.0	25.3	24.1	24.2	27.1	26.2
	NW	22.3	25.8	29.0	29.7	30.4	30.1
	SE	11.9	13.7	13.8	14.4	14.9	14.0
	SW	12.8	14.8	17.8	16.6	16.6	16.4
S10-2-1	NE	13.7	17.7	15.6	15.9	16.0	15.2
	NW	14.2	15.8	15.6	16.0	15.9	15.8
	SE	12.3	12.4	12.9	13.2	13.1	13.8
	SW	13.5	15.9	16.1	15.9	16.1	15.8
S10-2-2	NE	13.0	17.1	18.5	17.9	18.3	16.1
	NW	17.9	21.0	19.6	20.6	20.1	19.7
	SE	12.7	15.0	15.5	15.5	15.5	14.9
	SW	12.9	16.3	16.7	17.2	17.5	16.4

Conversion: 1 in. = 25.4 mm

**Table 4.6 – Average Transfer Lengths for Top Strands of Four-Strand Beams**

Transfer Length ID		1 Day (in.)	4 Day (in.)	8 Day (in.)	14 Day (in.)	28 Day (in.)	~56 Day (in.)
C6-4	Avg.	24.8	N/A	27.5	27.6	28.9	26.3
	Std. Dev.	9.25	N/A	3.63	4.98	4.15	N/A
	COV	37.4%	N/A	13.2%	18.0%	14.4%	N/A
S6-4	Avg.	18.2	21.8	22.2	21.1	20.1	22.4
	Std. Dev.	3.26	4.15	0.55	1.50	1.20	0.58
	COV	17.9%	19.0%	2.5%	7.1%	6.0%	2.6%
C10-4	Avg.	17.0	17.2	17.7	17.5	19.0	20.3
	Std. Dev.	2.08	2.95	2.19	2.22	3.59	1.80
	COV	12.2%	17.1%	12.3%	12.7%	18.9%	8.9%
S10-4	Avg.	19.3	17.0	18.6	19.0	18.3	19.5
	Std. Dev.	5.86	3.63	6.50	6.02	6.52	6.46
	COV	30.3%	21.4%	35.0%	31.7%	35.6%	33.1%

Conversion: 1 in. = 25.4 mm

**Table 4.7 – Average Transfer Lengths for Bottom Strands of Two-Strand Beams**

Transfer Length ID		1 Day (in.)	4 Day (in.)	8 Day (in.)	14 Day (in.)	28 Day (in.)	~56 Day (in.)
C6-2	Avg.	17.2	20.4	22.3	23.7	23.6	24.2
	Std. Dev.	2.76	4.07	4.85	5.09	5.69	5.55
	COV	16.1%	19.9%	21.8%	21.5%	24.1%	24.4%
S6-2	Avg.	14.4	18.4	18.2	18.6	19.2	19.2
	Std. Dev.	2.61	3.20	1.90	2.35	2.17	2.21
	COV	18.1%	17.4%	10.5%	12.7%	11.3%	11.5%
C10-2	Avg.	20.1	22.7	23.4	23.2	23.7	23.5
	Std. Dev.	7.63	7.53	7.38	7.38	7.35	8.06
	COV	37.9%	33.2%	31.5%	31.8%	31.0%	34.3%
S10-2	Avg.	13.8	16.4	16.3	16.5	16.6	15.9
	Std. Dev.	1.76	2.44	2.04	2.15	2.09	1.71
	COV	12.8%	14.9%	12.5%	13.0%	12.6%	10.7%

Conversion: 1 in. = 25.4 mm

**4.4.2. End Slip Method of Determining Initial Transfer Length.** While the 95% Average Mean Strain Method was the main method used for determining both the transfer lengths at release and the transfer lengths over time, the end slip method was also used to determine initial transfer lengths. The end slip method computes the initial transfer length,  $L_T$ , based on the amount the strand slips into the concrete upon release. The relationship between the end slip and transfer length can be seen in **Eq. 4.1**, where  $E_{ps}$  is the modulus of elasticity of the steel strand in ksi,  $f_{si}$  is the stress in the strand immediately before release in ksi, and  $\Delta$  is the measured end-slip of the strand in inches.

$$L_T = \frac{2E_{ps}\Delta}{f_{si}} \quad (4.1)$$

The theory of the relationship between end slip and transfer length was first thoroughly explained by Anderson and Anderson (1976), and has since been explained and successfully used by other researchers. When a tensioned strand is cut, the prestressing force is transferred to the member, shortening the member as well as the strand. The strand loses some of its prestress, and this loss in stress is known as elastic shortening. This is shown in **Figure 4.18**, where  $f_{si}$  is the stress in the strand immediately before release, and  $f_{se}$  is stress in strand after elastic shortening immediately after release. The stress in the strand varies linearly from zero at the end of the member to  $f_{se}$  at a certain distance from the end of the member, or the transfer length,  $L_T$ . Because of the linear relationship between stress and strain, it can also be said that the strain varies linearly in the transfer zone, from zero at the end to  $\epsilon_{se} = f_{se}/E_{ps}$  at the transfer length. Due to strain compatibility, it is assumed that in the fully bonded area, the strain in the concrete,  $\epsilon_{ce}$ , equals the change in strain of the steel,  $(f_{si}-f_{se})/E_{ps}$ . The strain in the concrete therefore varies linearly from zero at the end to  $(f_{si}-f_{se})/E_{ps}$  at the transfer length. As a result, in the transfer zone, there is a differential strain that varies from  $\epsilon_{si} = f_{si}/E_{ps}$  at the end of the member, where both the strain in the concrete and steel are zero, to zero at the transfer length, where the strain in the concrete equals the change in strain of the steel. This differential strain is represented by the shaded area in **Figure 4.18**, and the area is equal to the slip of the strand relative to the concrete. The area is represented by the

integral in **Eq. 4.2**, but because the variations in concrete and steel strains in the transfer zone are linear, the integral can be simplified to **Eq. 4.1**.

$$L_T = \int_0^{L_T} [\epsilon_{si} - \epsilon_s(x)] dx - \int_0^{L_T} \epsilon_c(x) dx \quad (4.2)$$

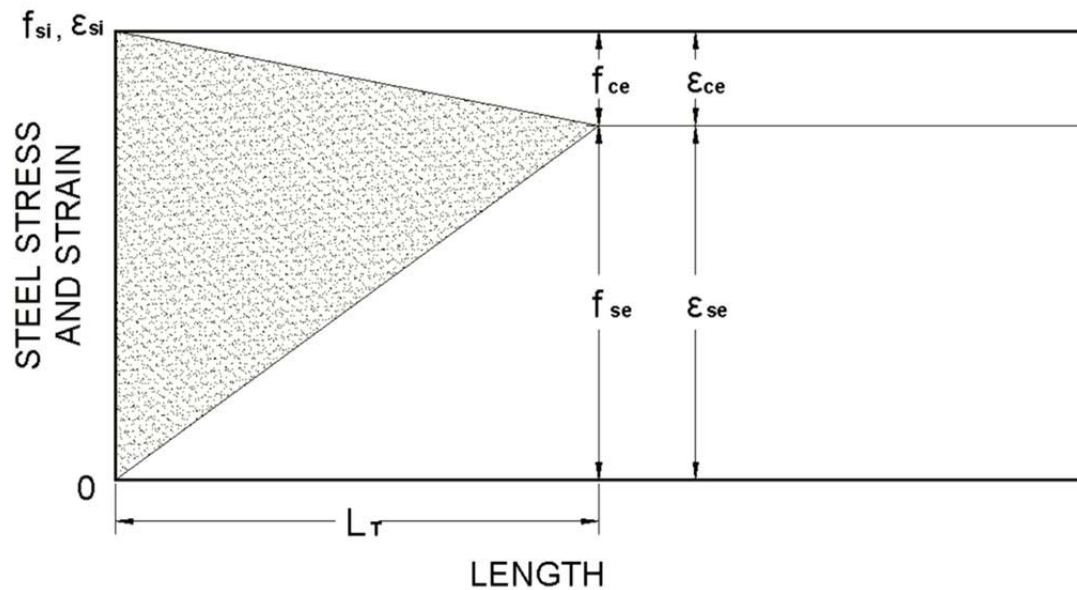


**Figure 4.18 – Relationship Between Steel Stress and Strain and Transfer Length (adapted from Russell and Burns, 1993)**

In this test program, the end slips of the strands were measured in two ways: by computer with electronic linear potentiometers and by hand with a steel ruler. The end slips measured by each method were then used in conjunction with **Eq. 4.1** to determine transfer lengths.

**4.4.2.1 Linear Potentiometer Setup and Procedure.** The first method of end slip determination involved securing linear potentiometers to the ends of the strands before they were cut and attaching the potentiometers to a Synergy data acquisition computer (Synergy). The linear potentiometer setup on the strands of a two strand beam

is depicted in **Figure 4.19**, while the Synergy data acquisition computer is shown in **Figure 4.20**.

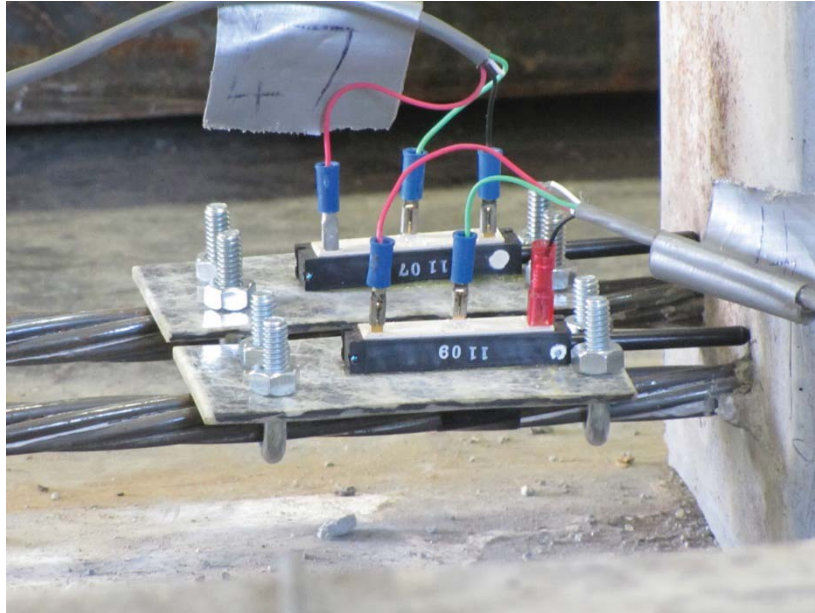


**Figure 4.19 – Linear Potentiometer Setup**

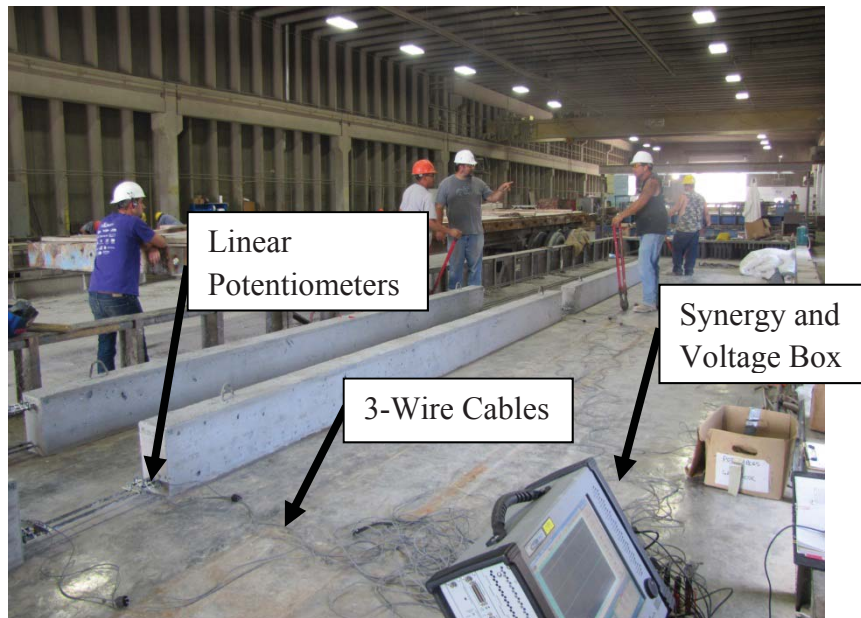


**Figure 4.20 – Synergy Data Acquisition Computer Setup**

The linear potentiometers, which could measure displacements up to 1.5 in. (38.1 mm), were epoxied on to 2 in. x 4 in. (50.8 mm x 102 mm) sections of FRP, which were then bolted to the strands. The initial epoxy that was used to bond the potentiometers to the FRP did not perform well on the first set of beams and resulted in numerous failures between the potentiometer and FRP, so different epoxies and methods of securing the potentiometers to the sections of FRP were experimented with when the potentiometers were used on the next release day. The methods of securing the potentiometers to the FRP bases are described later in this subsection. Two sets of holes were drilled through the FRP bases, and the potentiometer-FRP assemblies were bolted to the strands with two 0.5-in.-diameter (12.7 mm) U-bolts, as seen in **Figure 4.19**. Each potentiometer-FRP assembly was rotated about its strand until the free end was lined up with a smooth portion of the beam end. Once the potentiometers were lined up in a suitable position, the U-bolts were securely tightened with a wrench. The potentiometers were attached to the strands so that initial readings of approximately 0.1 in. (2.54 mm) to 0.5 in. (12.7 mm) could be read on the Synergy, meaning that the potentiometers were slightly depressed and making solid contact with the beam. The initial readings were subtracted from the final slip readings to determine the amount of strand slip. The potentiometers were attached to a power box with 3-wire cables, and the power box was hooked up to the Synergy via banana jack cables. The sample rate on the Synergy was set to record data at 1000 samples per second.

The Synergy could record up to 16 data sets at one time. The beams were cut one line at a time, so the potentiometers were first attached to the line of two-strand beams, and after all the two-strand beams had been released, the potentiometers were then attached to the strands of the four-strand beams. Although there were 16 transfer length locations on the line of the four two-strand beams, only 12 readings could be taken on each day because the cables could not reach the far north and south ends of the line of beams. In regards to the four-strand beams, on the first day (C6 and S6 beams), only two readings could be taken because only two potentiometer-FRP assemblies remained intact after the release of the two-strand beams. On the second release day (C10 and S10 beams), significantly more potentiometer-FRP assemblies survived the release of the two-strand beams due to improved bonding methods, so potentiometers were attached to

all 16 transfer length locations on the two four-strand beams. Although the eight transfer length locations on the top strands were the only locations of importance on the four-strand beams, the potentiometers were attached to the bottom strands as well in order to collect as much data as possible and also determine if any relationship existed between the bottom strand readings from the two-strand beams and the four-strand beams.

As mentioned, the bonding of the potentiometers to the FRP bases proved to be problematic. Initially, the surfaces of the FRP sections were roughened with sandpaper, and an 8-minute multi-use epoxy was used to attach the potentiometers to the FRP plates. On the first day of use, almost all potentiometers detached or loosened from their FRP bases due to the sudden release of the strands. It was noted that the epoxy on the broken bonds had a slightly tacky texture, and because the testing was completed in an open shed during the summer, one hypothesis was that the heat affected the epoxy's bonding ability.

Before the potentiometers were used on the next set of beams, several methods were used to try to improve the bond of the potentiometers to the FRP plates. First, the surfaces of the FRP plates were roughened to a greater degree by using a very small grinding wheel attached to a Dremmel. Then, several different epoxies were tested with the intent of determining which one performed the best. The three epoxies tested included a 5-minute plastic bonder epoxy, gorilla glue epoxy, and gorilla glue expanding foam. Additionally, two plastic zip ties were added to each potentiometer-FRP assembly to facilitate bonding as the epoxy dried as well as add an extra securing measure to the assembly. A picture of the improved potentiometer-FRP assemblies with zip ties, plastic epoxy, and gorilla glue expanding foam can be seen in **Figure 4.21**. Although significantly more assemblies remained intact on the second release day, there was no improvement in the acquisition of readable results.

In order to determine the end slips from the data collected on the Synergy, the files were first downloaded from the Synergy to a personal computer and saved as Microsoft Excel files. Data was then organized into potentiometer reading vs. time plots. Since the potentiometers were attached to one line of beams at a time during the release process, plots were organized to include data from the same line of beams so the same amount of elapsed time could be shown. Each data series from each potentiometer shows

readings from a few seconds before the first strand in the line was cut to a few seconds after the last cut had been made on the line of beams.

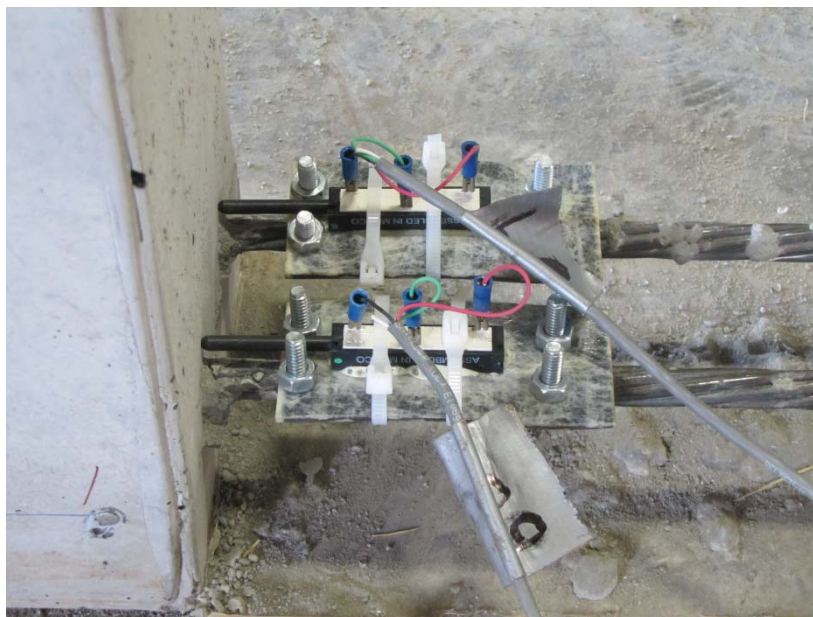


**Figure 4.21 – Improved Potentiometer-FRP Assemblies with Zip Ties and Plastic Epoxy (Top) and Gorilla Glue Expanding Foam (Bottom)**

An example potentiometer vs. time plot is shown in **Figure 4.22**, which illustrates the end slips for the C6 line of two-strand beams (C6-2-1 and C6-2-2). The plot shows the plateau of initial readings for each location where a potentiometer was applied and then shows the gradual change in the potentiometer readings over time as the strands were cut. End slip values were determined by averaging the values on the initial and final plateaus and then subtracting the average initial reading from the average final reading. However, very few potentiometers actually showed changes in readings that could be accepted as valid data.

The potentiometer readings vs. time plots show that there were several standard ways that the potentiometer readings changed as the strands were cut. Sudden jumps to zero, such as 2-1\_NE in **Figure 4.22**, indicate that the white or red wires in the three wire cable became disconnected from the potentiometer, or the assembly broke or slipped off

the strand. Sudden jumps to readings of 1.5 in. (38.1 mm) indicate only the black wire became disconnected from the potentiometer. Although 1.5-in. (38.1 mm) is not shown on the y-axis of the plots because the majority of readings were within the range of 0 in. to 0.5 in. (12.7 mm), it can be assumed that any data series that exits the top of the plot, such as 2-1\_SW in **Figure 4.22**, goes to 1.5 in. (38.1 mm).

Of the data series that show jumps not immediately going to 0 in. or 1.5 in. (38.1 mm), many of these are negative jumps. In the case of a negative jump, this means the potentiometer moved out from its initial position and slipped backwards, resulting in an invalid reading. A positive jump indicates a potentially good reading, where the strand slipped into the concrete, and the potentiometer was pushed in. However, there is still no guarantee that a positive jump is a valid end slip. After seeing how sensitive the potentiometers ended up being in terms of bond to the plate, disconnected wires, and slippage on the strand, there is a strong possibility that outside stimuli other than the slipping of the stand, such as accidentally bumping the strand or potentiometer, could have affected the readings. Despite this possibility, it was determined that all positive jumps greater than 0.01 in (0.25 mm), which still only corresponds to a transfer length of approximately 3 in. (76.2 mm), were deemed reasonable to report as valid end slips.

Several other special situations also had to be considered when evaluating the end slip data. A few of the potentiometers registered a valid positive jump, but after a while the readings went to 0 in. or 1.5 in. (38.1 mm). For example, 2-1\_SE, 2-1\_NE, and 2-2\_NW in **Figure 4.22** all seemed to register a slight positive slip, but then the readings abruptly went to 0 in. after 10 to 35 seconds. In these cases, it was determined that the plateau of the final potentiometer reading was held long enough to be considered valid. The other type of special case involved series that showed a significant amount of noise in the data, such as 2-1\_NW in **Figure 4.22**. Noise most likely indicates that the strand or potentiometer was bumped or somehow affected by outside stimuli. In these cases, if the potentiometer registered a stable reading after the noise, the ultimate change from initial to final reading was still considered valid if the change was positive and significant. In the specific case of C6-2-1\_NW, it was decided that even though there was a stable plateau after the noise, the data should be rendered invalid. The fact that the reading first

dropped to 0 in. and then increased back up again put the stability and validity of the potentiometer into question.

In conclusion, the interpretation of end slip data was highly subjective at times, and a lot of assumptions had to be made about which data could be considered valid. All potentiometer reading vs. time plots can be found in Appendix E.

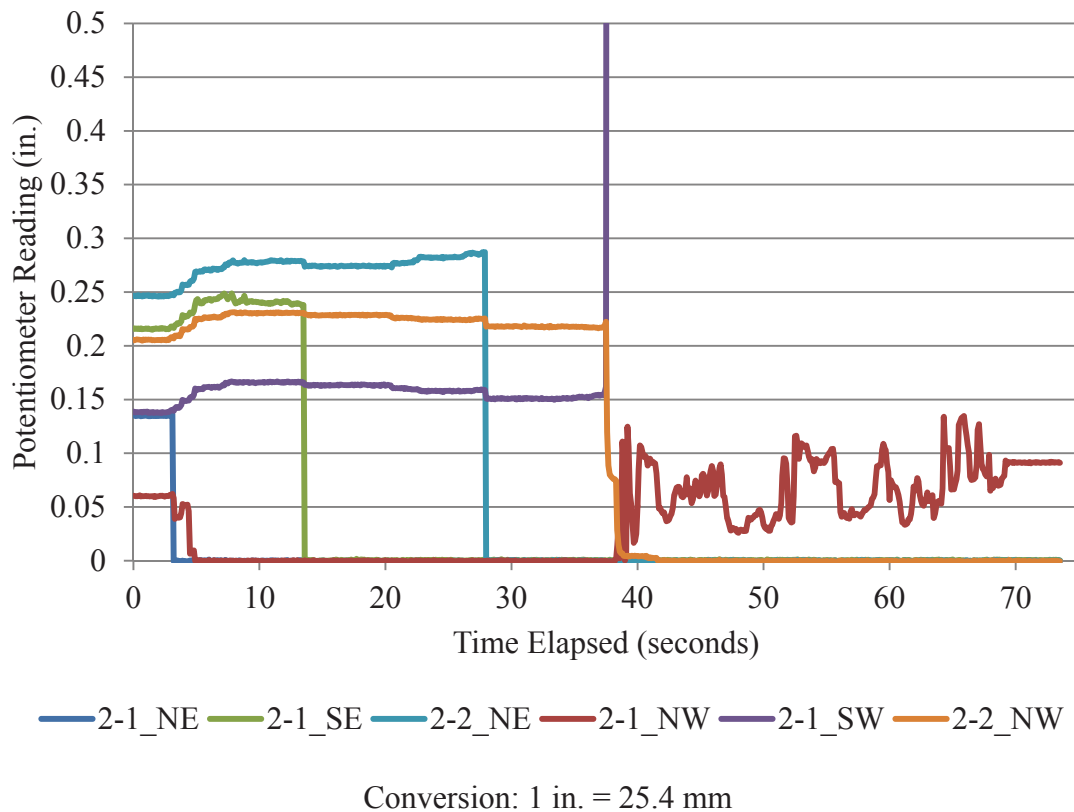


**Figure 4.22 – Typical End Slip Plot: C6 Two-Strand Beams Potentiometer Reading vs. Time Elapsed Plot from Synergy**

**Table 4.8** shows the end slips measured from the data acquisition system. Each two-strand beam had four possible locations (bottom), while each four strand beam had eight possible locations (bottom and top). A dash indicates a potentiometer was not applied at that location due to either the cables being unable to reach the end of the beam line or a lack of a sufficient number of potentiometers. “N/A” indicates that no

reasonable data could be obtained from the readings, while a number in the cell is the measured end slip in inches.

**Table 4.8 – Measured End Slips from Linear Potentiometers**

Specimen ID	Bottom				Top			
	NE (in.)	NW (in.)	SE (in.)	SW (in.)	NE (in.)	NW (in.)	SE (in.)	SW (in.)
C6-2-1	N/A	N/A	0.025	0.028				
C6-2-2	0.033	0.025	-	-				
C6-4-1	-	-	-	-	N/A	-	-	-
S6-2-1	-	-	N/A	N/A				
S6-2-2	N/A	0.050	N/A	0.051				
S6-4-1	-	-	-	-	-	-	-	N/A
C10-2-1	-	-	N/A	N/A				
C10-2-2	N/A	N/A	0.041	0.036				
C10-4-1	N/A	N/A	0.066	N/A	N/A	N/A	N/A	N/A
S10-2-1	0.029	0.083	0.025	0.016				
S10-2-2	0.031	0.016	-	-				
S10-4-1	N/A	N/A	N/A	0.050	N/A	N/A	N/A	N/A

Conversion: 1 in. = 25.4 mm

**4.4.2.2 Steel Ruler Setup and Procedure.** In addition to electronic collection of end slip data, a steel ruler was also used to measure end slip by hand. First, black electrical tape was wrapped around the strand with approximately 2 in. (50.8 mm) of strand showing between the end of the beam and the beginning of the tape. The taped strands can be seen in **Figure 4.23**. Next, a steel ruler was used to measure the initial distance from the surface of the beam to the beginning of the tape. The measurements were taken to the nearest  $\frac{1}{32}$  in. (0.79 mm). In order to keep the measurements as consistent as possible, initial and final measurements were taken by the same individual. Additionally, for each measurement, a permanent marker was used to mark a line on the concrete surface, indicating where the steel ruler had been placed to take the initial measurement. This way, the ruler could be lined up in the same place to take the final

measurement. Measurements were taken at all possible transfer length locations on all beams.

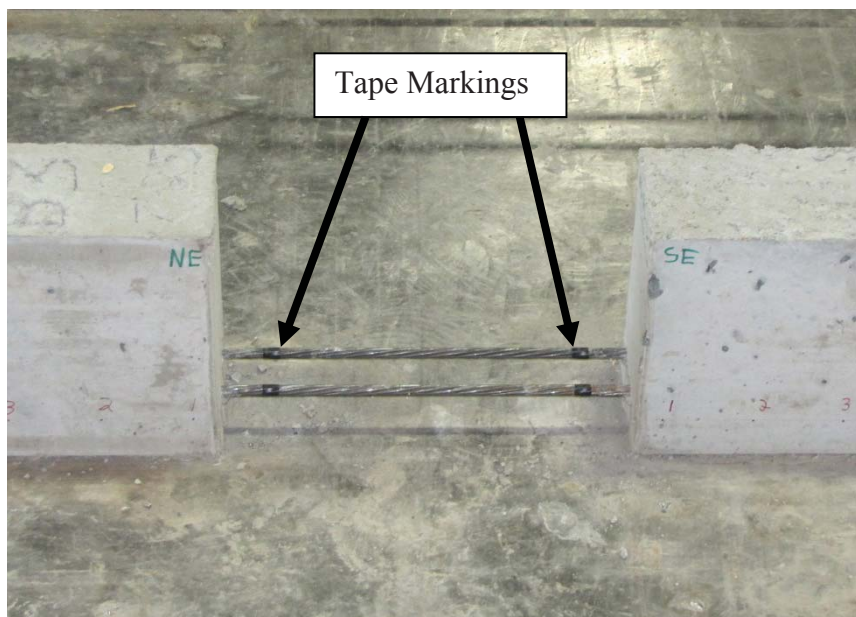


**Figure 4.23 – Electrical Tape on Strands for Steel Ruler Measurements of End Slip**

The end slip measurements in inches as measured by hand with the steel ruler are presented in **Table 4.9**. C10-2-1\_SW and S10-4-1\_NW (bottom) did not have final readings because on each beam, the portion of concrete with the mark where the ruler had been lined up to take the initial reading had broken off when the beam was released. Additionally, C6-4-1\_NE (bottom), S6-4-1\_SE (bottom), C10-2-2\_NW, and S10-4-1\_NE (bottom) showed increases in end slip, which is contrary to what was expected.

**Table 4.9 – Measured End Slips from Steel Ruler**

Specimen ID	Bottom				Top			
	NE (in.)	NW (in.)	SE (in.)	SW (in.)	NE (in.)	NW (in.)	SE (in.)	SW (in.)
C6-2-1	0.125	0.031	0.031	0.063				
C6-2-2	0.063	0.063	0.031	0.063				
C6-4-1	-0.156	0.063	0.094	0.063	0.094	0.063	0.094	0.063
S6-2-1	0.063	0.031	0.031	0.094				
S6-2-2	0.063	0.063	0.063	0.000				
S6-4-1	0.031	0.063	-0.094	0.031	0.031	0.094	0.063	0.063
C10-2-1	0.000	0.063	0.000	N/A				
C10-2-2	0.047	-0.125	0.063	0.063				
C10-4-1	0.000	0.047	0.000	0.031	0.031	0.016	0.031	0.047
S10-2-1	0.063	0.047	0.047	0.063				
S10-2-2	0.047	0.063	0.078	0.094				
S10-4-1	-0.016	N/A	0.047	0.031	0.016	0.000	0.031	0.063

Conversion: 1 in. = 25.4 mm

**4.4.2.3 Transfer Length Determination from End Slip Data.** Once all of the end slip values were determined, the values were used to calculate initial transfer lengths, using **Eq. 4.1**, as discussed in **Section 4.3.2**.  $E_{ps}$  was taken to be the experimentally determined modulus of elasticity of the prestressing strand, or 29400 ksi (203 GPa), and  $f_{si}$ , or the stress in the strand before release, was taken to be 75% of 270 ksi (1,862 MPa). The measured end slips in inches were inserted into the equation to calculate a transfer length at each applicable location.

$$L_T = \frac{2E_{ps}\Delta}{f_{si}} \quad (4.1)$$

**Tables 4.10 – 4.12** summarize the transfer lengths in inches calculated from the measured end slips from both the linear potentiometers (Synergy) and the steel ruler. The last column in each table also includes the transfer lengths determined by the 95% Average Mean Strain Method from the 1 Day DEMEC data for comparison. **Table 4.10** reports the transfer lengths for the bottom strands of the C6 and S6 beams, while **Table**

**4.11** reports the transfer lengths for the bottom strands of the C10 and S10 beams. **Table 4.12** reports the transfer lengths for all of the top strands.

**Table 4.10 – Initial Transfer Lengths from Steel Ruler End Slips, Synergy End Slips, and DEMEC Data for Bottom Strands on C6 and S6 Beams**

Transfer Length Location		Steel Ruler End Slip $L_T$ (in.)	Synergy End Slip $L_T$ (in.)	DEMEC 1 Day $L_T$ (in.)
C6-2-1	NE	35.8	N/A	19.6
	NW	9.0	N/A	20.3
	SE	9.0	7.2	19.8
	SW	17.9	8.0	15.5
C6-2-2	NE	17.9	9.5	17.0
	NW	17.9	7.2	13.8
	SE	9.0	-	14.2
	SW	17.9	-	N/A
C6-4-1	NE	N/A	-	-
	NW	17.9	-	-
	SE	26.9	-	-
	SW	17.9	-	-
S6-2-1	NE	17.9	-	10.6
	NW	9.0	-	14.2
	SE	9.0	N/A	N/A
	SW	26.9	N/A	19.1
S6-2-2	NE	17.9	N/A	15.9
	NW	17.9	14.3	13.4
	SE	17.9	N/A	13.4
	SW	0.0	14.6	14.3
S6-4-1	NE	9.0	-	-
	NW	17.9	-	-
	SE	N/A	-	-
	SW	9.0	-	-

Conversion: 1 in. = 25.4 mm

**Table 4.11 – Initial Transfer Lengths from Steel Ruler End Slips, Synergy End Slips, and DEMEC Data for Bottom Strands on C10 and S10 Beams**

Transfer Length Location		Steel Ruler End Slip $L_T$ (in.)	Synergy End Slip $L_T$ (in.)	DEMEC 1 Day $L_T$ (in.)
C10-2-1	NE	0.0	-	14.9
	NW	17.9	-	15.4
	SE	0.0	N/A	30.1
	SW	N/A	N/A	31.4
C10-2-2	NE	13.4	N/A	22.0
	NW	N/A	N/A	22.3
	SE	17.9	11.7	11.9
	SW	17.9	10.3	12.8
C10-4-1	NE	0.0	N/A	-
	NW	13.4	N/A	-
	SE	13.4	18.9	-
	SW	17.9	N/A	-
S10-2-1	NE	13.4	8.3	13.7
	NW	17.9	23.8	14.2
	SE	13.4	7.2	12.3
	SW	17.9	4.6	13.5
S10-2-2	NE	13.4	8.9	13.0
	NW	17.9	4.6	17.9
	SE	22.4	-	12.7
	SW	26.9	-	12.9
S10-4-1	NE	N/A	N/A	-
	NW	N/A	N/A	-
	SE	13.4	N/A	-
	SW	9.0	14.3	-

Conversion: 1 in. = 25.4 mm

**Table 4.12 – Initial Transfer Lengths from Steel Ruler End Slips, Synergy End Slips, and DEMEC Data for Top Strands on C6, S6, C10, and S10 Beams**

Transfer Length Location		Steel Ruler End Slip $L_T$ (in.)	Synergy End Slip $L_T$ (in.)	DEMEC 1 Day $L_T$ (in.)
C6-4-1	NE	26.9	N/A	N/A
	NW	17.9	-	N/A
	SE	26.9	-	31.3
	SW	17.9	-	18.2
S6-4-1	NE	9.0	-	20.5
	NW	26.9	-	N/A
	SE	17.9	-	N/A
	SW	17.9	N/A	15.9
C10-4-1	NE	9.0	N/A	18.8
	NW	4.5	N/A	15.3
	SE	9.0	N/A	15.1
	SW	13.4	N/A	18.9
S10-4-1	NE	4.5	N/A	18.0
	NW	0.0	N/A	17.6
	SE	9.0	N/A	27.7
	SW	17.9	N/A	14.0

Conversion: 1 in. = 25.4 mm

#### 4.5. DEVELOPMENT LENGTH TEST SETUP, PROCEDURE, AND RESULTS

A four-point loading test setup was used to test each end of the beams in flexure at different embedment lengths, where the embedment length is the distance from the end of the beam to the first load point, and then determine if the beam failed in flexure or bond. There is no direct way to test development length, but iterative testing of different embedment lengths can indicate a range in which the development length falls.

Theoretically, if the embedment length at testing was exactly equal to the development length, the member would fail in bond and flexure at the same time. A bond failure indicates the strand could not be fully developed, so the development length is longer than the tested embedment length, while a flexural failure indicates that the strand was able to be fully developed, so the embedment length was longer than the actual development length.

For each beam, one end was first tested at an embedment length of 58-in. (1,473 mm), and then the other end was tested at an embedment length of 73-in. (1,854 mm). The shorter length corresponds to approximately 80% of the ACI/AASHTO recommended development length, and the longer length is approximately equal to the calculated ACI/AASHTO development length. As noted in **Section 2.5**, the ACI and AASHTO equations for development length are equal when the member is less than or equal to 24-in. (610 mm) deep. The mode of failure was determined through a combination of noting the crack pattern, determining if the applied moment at failure fell below or exceeded the calculated nominal moment capacity, and noting if the strands on the tested end experienced any significant slip. A flexural failure, which would be indicated by strand yielding or concrete crushing, a failure moment at or above the nominal moment, and negligible end slips in the strands, would imply that the strand had enough effective, bonded length to fully develop the moment capacity.

**4.5.1. Four-Point Loading Setup and Instrumentation.** The four-point load tests were completed on a steel frame designed for flexural beam testing at the Missouri S&T Structural Engineering High Bay Research Laboratory (SERL). The beams were supported on two steel plates on top of rollers, and two hydraulic actuators were used to apply two point loads at 24 in. (610 mm) apart using spreader beams (**Figure 4.24**). Since the beams were tested one end at a time, the supports were positioned so the end of the beam could be tested at the correct embedment length, and the two point loads would be positioned in the middle of the simply supported span. The end not being tested was cantilevered over one of the supports.

For each beam, the 58 in. (1,473 mm) embedment length was tested first, and then the beam was shifted to test the 73 in. (1,854 mm) embedment length on the other end. The beam test setups for the 58 in. (1,473 mm) and 73 in. (1,854 mm) embedment length tests are illustrated in **Figures 4.25** and **4.26**, respectively. **Figures 4.25** and **4.26** also show how portions of the beam overlapped during each test. The shaded portion of the beam in **Figure 4.25** indicates where the maximum moment region would be during the 73 in. (1,854 mm) test. This shows that the 73 in. (1,854 mm) embedment length was largely unaffected by the 58 in. (1,473 mm) test because the majority of the end tested in the 73-in. (1,854 mm) test was cantilevered over one support during the 58 in. (1,473

mm) test, and therefore unaffected by the loading. **Figure 4.26** shows cracks indicating approximately where the failed portion from the 58 in. (1,473 mm) test would have been located on the beam during the 73 in. (1,854 mm) test. Although the failed portion of the beam from the 58 in. (1,473 mm) test fell partly within the span of the 73 in. (1,854 mm) test, the failed portion did not fall within the maximum moment zone of the 73 in. (1,854 mm) test. Furthermore, additional development length was available on the side of the beam containing the failed portion from the 58 in (1,473 mm) test due to the cantilevered portion extending beyond the support.



**Figure 4.24 – Four-Point Loading Test Setup for Evaluating 58-in. (1,473 mm) Embedment Length**

From these observations, several assumptions were made regarding the effect the first flexural test would have on the second. First, it was assumed that the bond of 73 in. (1,854 mm) embedment length would have been negligibly affected by the 58 in. (1,473

mm) test because 68 in. (1,727 mm) of the 73 in. (1,854 mm) was cantilevered. It was also assumed that the zone experiencing maximum moment during the 73 in. (1,854 mm) test would still be able to develop full moment capacity because the area was assumed to be fully bonded to begin with, and the area also should not have seen a moment close to the nominal capacity during the 58 in. (1,473 mm) test. **Figure 4.26** corroborates this by showing that while cracks did form and extend outside the region between the two point loads, the failed portion from the 58 in. (1,473 mm) test still did not affect the maximum moment zone of the 73 in. (1,854 mm) test. Based on these assumptions, the 73 in. (1,854 mm) test on each beam was assumed to be valid. Furthermore, this test setup has been successfully used in previous research (Ramirez and Russell 2008).

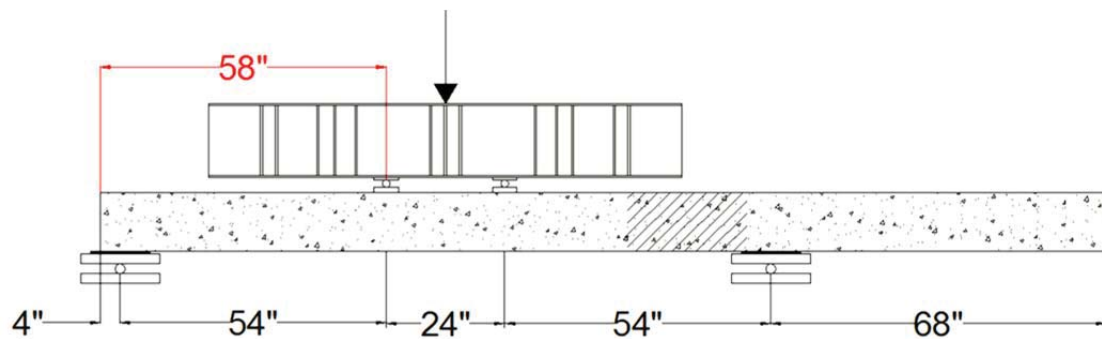


**Figure 4.25 – 58 in. (1,473 mm) Embedment Length Test Setup**

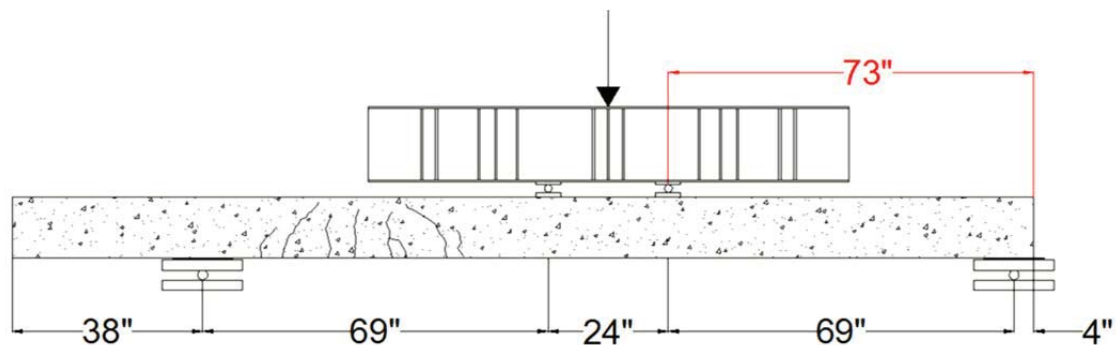


**Figure 4.26 – 73 in. (1,854 mm) Embedment Length Test Setup**

Instrumentation was installed to measure deflection of the beam and slip in the strands. In order to measure deflection, a Linear Voltage Differential Transformer (LVDT) was placed on a level section of angle bolted at midspan of the span (**Figure 4.27**). Also, the linear potentiometers that were used to measure initial end slip of the strands at release were attached to the strands on the end of the beam to monitor slipping of the strands (**Figure 4.28**). In order to keep the slip measurements consistent, the free end of the potentiometer was lined up at the top of the strands. On some beams, the area of contact was uneven, so in these cases, 1 in. x 1 in. (25.4 mm x 25.4 mm) sections of plexiglass were attached to the contact areas with an epoxy, which is also shown in **Figure 4.28**. A description of the linear potentiometers can be found in **Section 4.3.2.1**. A data acquisition system was used to record the load applied by each actuator, deflection as measured by the LVDT, and slip in the strands as measured by the linear potentiometer on each strand.



**Figure 4.27 – LVDT Setup for Measuring Deflection at Midspan**



**Figure 4.28 – Linear Potentiometer Setup on Four-Point Loading Tests**

**4.5.2. Four-Point Loading Procedure.** Once the beam was positioned at the correct tested embedment length and the instrumentation was installed, the beam was loaded in a displacement controlled method until failure. Most of the beams were loaded at increments of 0.05 in. (1.27 mm) of deflection until the total deflection reached 1.0 in. (25.4 mm). After 1.0 in. (25.4 mm) of total deflection, the beam continued to be loaded at increments of 0.05 in. (1.27 mm), but the beam was only checked and marked for cracks at increments of 0.1 in. (2.54 mm) of deflection until failure. Failure was determined to be when the beam would no longer support any additional load.

At each deflection step, the beam was checked for cracks, and any crack or continuation of a crack were marked with permanent marker, and the maximum load for that step was written next to the end of the crack (**Figure 4.29**). The load that corresponded to initial flexural cracking and the ultimate failure mode were visually noted. The loads applied by the hydraulic actuators, end slips as measured by the potentiometers, and deflection at midspan as measured by the LVDT were monitored throughout the test by the data acquisition systems. From the recorded data, moment vs. deflection and end-slip vs. deflection were plotted for each test, and a typical plot of both relationships can be found in **Figure 4.30**. The applied moments include the moment

from the self-weight of the beam. Additionally, the load cells were located above the spreader beam, so moment resulting from the dead load of the spreader beam was also added into the final applied moment.



**Figure 4.29 – Cracks Marked with Permanent Marker during Development Length Test**

**4.5.3. Four-Point Loading Results.** In **Figure 4.30**, the dashed line on the plot indicates the calculated nominal moment capacity for the beam. The experimentally determined ultimate strength and modulus of elasticity of the strand as well as the actual strength of the concrete were used in the calculations of the nominal moment capacities. In **Figure 4.30**, the peak of the moment curve exceeds the calculated nominal moment capacity, and the end slip remained negligible throughout the test. The combination of these results indicates C10-2-1\_58 failed in flexure. Plots, photographs, and a summary of the loading method and results of each test can be found in Appendix F.

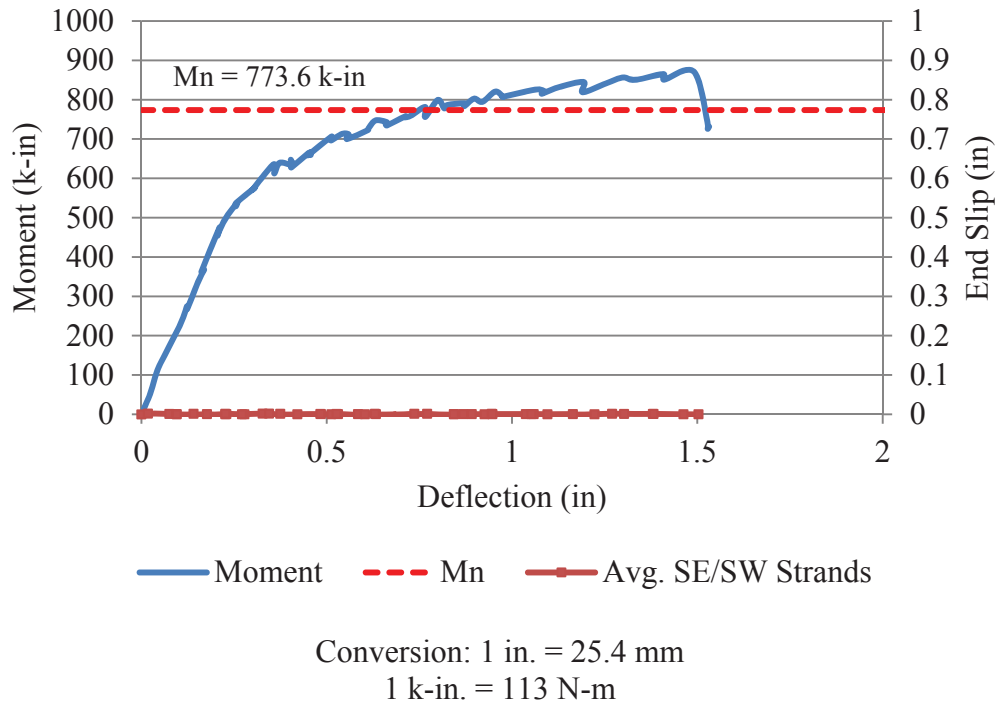


**Figure 4.30 – Typical Moment vs. Deflection and Strand End Slip vs. Deflection Plot from Four-Point Loading Data**

**Table 4.12** identifies the observed cracking moment ( $M_{cr}$ ), ultimate applied moment ( $M_u$ ), and calculated nominal moment ( $M_n$ ) for each test as well as the ratio of the ultimate applied moment to the calculated nominal moment, average strand end slip, visual observations regarding failure, and the final failure mode. In terms of the  $M_u/M_n$  ratio, a ratio greater than one indicates the beam had a greater moment capacity than predicted, and therefore, the embedment length was conservative. The final failure mode was determined through analysis of a combination of the  $M_u/M_n$  ratio, average strand end slip, and visual observations. Since all beams had a  $M_u/M_n$  ratio greater than one, showed virtually no end slip in the strands, and largely exhibited concrete crushing in the maximum moment zone (**Figure 4.31**), all tests were determined to have failed in flexure. **Table 4.13** summarizes the average moment capacities and average  $M_u/M_n$  ratios for each mix at each embedment length.

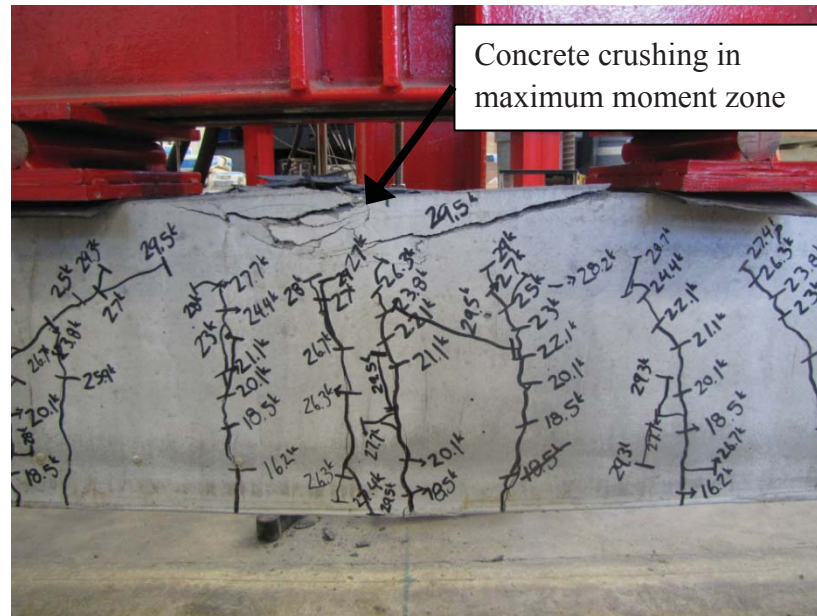


Figure 4.31 – Typical Concrete Crushing Failure for Development Length Tests

Table 4.12. Nominal and Actual Moment Capacities

Test ID	$M_{cr}$ (k-in)	$M_u$ (k-in)	$M_n$ (k-in)	$M_u/M_n$	Average End Slip (in.)	Visual Observations	Failure Mode
C6-2-1_58	469.2	811.8	742.7	1.093	0.000	Concrete Crushing	Flexural
C6-2-1_73	529.5	834.8	742.7	1.124	0.000	Concrete Crushing	Flexural
C6-2-2_58	482.7	836.6	742.7	1.126	0.000	Concrete Crushing	Flexural
C6-2-2_73	498.4	837.6	742.7	1.128	0.000	Concrete Crushing	Flexural
S6-2-1_58	523.3	867.7	757.9	1.145	0.000	Concrete Crushing	Flexural
S6-2-1_73	505.5	878.4	757.9	1.159	0.000	Concrete Crushing*	Flexural
S6-2-2_58	501.7	889.9	757.9	1.174	0.000	Concrete Crushing	Flexural
S6-2-2_73	460.7	843.1	757.9	1.112	0.000	Concrete Crushing	Flexural

\* Concrete crushing occurred outside the maximum moment zone

**Table 4.12 Continued – Nominal and Actual Moment Capacities**

Test ID	$M_{cr}$ (k-in)	$M_u$ (k-in)	$M_n$ (k-in)	$M_u/M_n$	Average End Slip (in.)	Visual Observations	Failure Mode
C10-2-1_58	534.2	880.3	773.6	1.138	0.000	Concrete Crushing	Flexural
C10-2-1_73	495.6	880.7	773.6	1.138	0.000	Concrete Crushing	Flexural
C10-2-2_58	466.7	875.3	773.6	1.132	0.001	Concrete Crushing	Flexural
C10-2-2_73	492.1	885.8	773.6	1.145	0.000	Concrete Crushing	Flexural
S10-2-1_58	499.1	883.3	790.7	1.117	0.000	Concrete Crushing	Flexural
S10-2-1_73	519.7	904.2	790.7	1.144	0.000	Concrete Crushing	Flexural
S10-2-2_58	553.1	901.1	790.7	1.140	0.000	Concrete Crushing	Flexural
S10-2-2_73	530.1	871.7	790.7	1.102	0.000	Concrete Crushing	Flexural

Conversion: 1 in. = 25.4 mm

1 k-in. = 113 N-m

**Table 4.13 – Summary of Average Nominal and Actual Moment Capacities**

Mix ID	$M_n$ (k-in)	58 in. (1,473 mm)		73 in. (1,854 mm)	
		$M_u$ (k-in)	$M_u/M_n$	$M_u$ (k-in)	$M_u/M_n$
C6	742.7	824.2	1.110	836.2	1.126
S6	757.9	878.8	1.160	860.8	1.136
C10	773.6	877.8	1.135	883.3	1.142
S10	790.7	892.2	1.128	888.0	1.123

Conversion: 1 k-in. = 113 N-m

## **5. DISCUSSION AND COMPARISON OF RESULTS**

### **5.1. INTRODUCTION**

The two main objectives of this research program were to 1) evaluate two different bond tests and 2) compare bond performance of SCC vs. conventional concrete through a test program investigating transfer and development lengths of 0.5-in.-diameter (12.7 mm), Grade 270 prestressing strand.

In terms of analysis of the bond tests, the main goals were to 1) compare and evaluate the consistency of two types of pullout tests designed to assess bond-ability of prestressing strand, and 2) determine if pullout test values can be correlated to measured transfer lengths.

For the transfer and development length testing portion of the study, the goals were to 1) determine if a significant difference was seen between bond performance of prestressing strand in SCC vs. conventional concrete, 2) compare experimental transfer and development length results to values calculated from equations in the AASHTO and ACI codes to determine if the equations that are being used in design are conservative for both conventional concrete and SCC, 3) evaluate the effect of concrete strength on bond performance, and 4) determine if casting position has a significant effect on transfer length of prestressing strand.

The analyses of results in relation to these research goals are discussed in this section.

### **5.2. BOND TEST RESULTS**

Several different analyses were performed on the results from the NASP tests in mortar and concrete and the LBPT. First, the three strand types were analyzed based on bond acceptance limits of the NASP test in mortar and the LBPT, and then the overall pass/fail and relative rankings from each test were compared to each other to see if both tests produced similar results. The results from the NASP tests in concrete were then analyzed to determine if any differences could be seen between the pullout tests done in conventional concrete versus SCC and also compared to equations based on concrete compressive strength determined by previous research.

**5.2.1. Discussion of NASP Test in Mortar Results.** The pullout values for 0.1 in. (2.54 mm) and 0.001 in. (0.025 mm) for strand types 101, 102, and 103 are presented in **Table 3.8** but are also displayed graphically in **Figure 5.1** for ease of comparison and discussion. In **Figure 5.1**, the error bars represent one standard deviation above and below the average. For reasons discussed in Section 3.3.1, N-101-A and N-101-B were completed with the same strand source but two different mix designs. N-101-B, N-102-B, and N-103-B were directly compared to evaluate relative bond quality of the three sources, and N-101-A was compared to N-101-B to determine the effect of mortar mix design on pullout values.

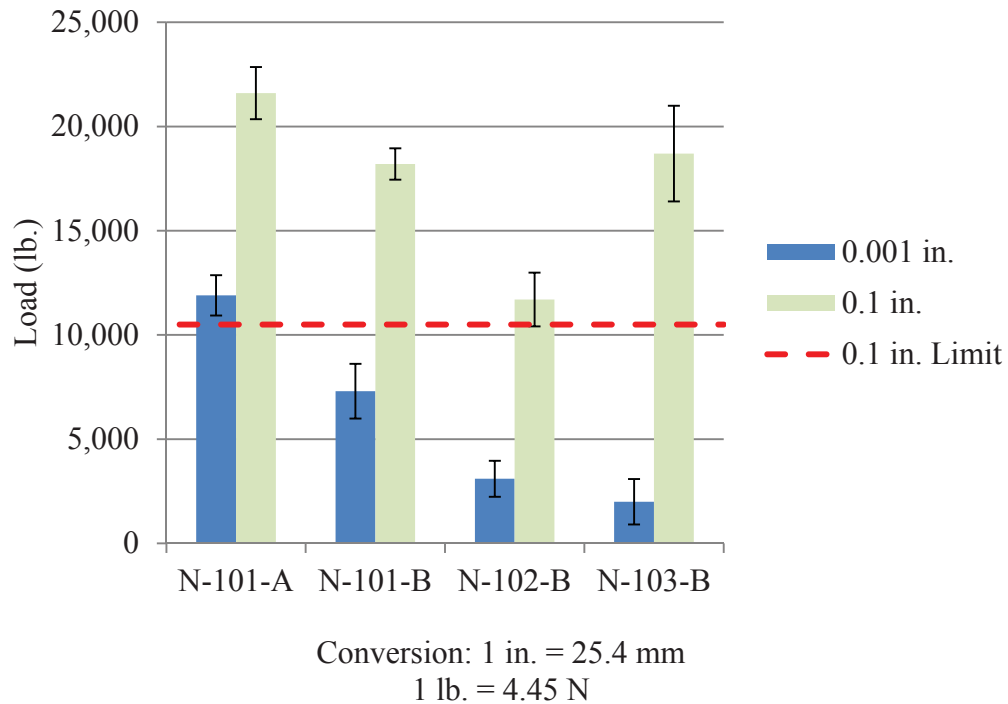


**Figure 5.1 – NASP in Mortar Pullout Values**

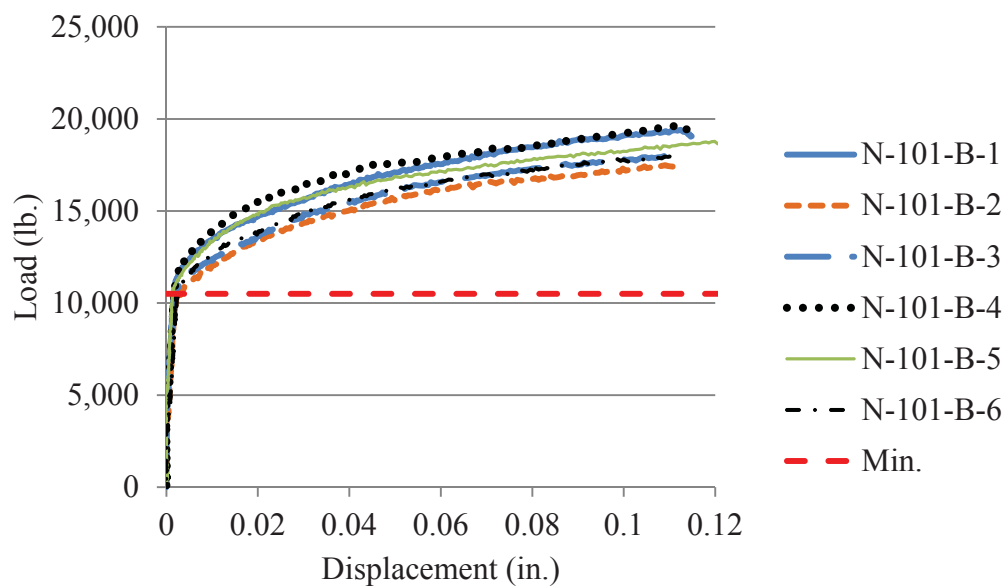
The NASP test specifies that for 0.5-in.-diameter (12.7 mm) strand, the minimum average pullout value at a strand slip of 0.1 in. (2.54 mm) is 10,500 lb (46.7 kN), and no individual test should have a result falling below 9,000 lb (40.0 kN). Strand types 101 and 103 were comparable and showed the best bond quality by exceeding the specified

average minimum pullout value by 73% and 75%, respectively. Strand type 102 also passed, but exceeded the minimum required value by only 11%. Strand type 102 also came close to failing the individual requirement with N-102-B-4 having a 0.1 in. (2.54 mm) pullout value of 9,300 lb (41.4 kN) (**Table 3.6**). Still, all three strand types exceeded the minimum bond acceptance criteria as specified by the NASP test, and as a result, all sources were deemed to have acceptable bond quality based on the proposed standard.

Although all strands passed strictly based on the criteria, several other observations were noted that could possibly affect analysis of bond quality. First, although the bond acceptance criteria in the proposed standard is based on the load at 0.1 in. (2.54 mm) slip, in this research, the loads at 0.001 in. (0.025 mm) slip were also recorded so the strands could also be analyzed and compared based on “first slip.” Interestingly, in the analysis of the results, it was discovered that N-103-B had the highest average pullout value at 0.1 in. (2.54 mm) but the lowest average pullout value at 0.001 in. (0.025 mm), as shown in **Figure 5.1**. Although strand 103 appeared to have the best bond quality based on the 0.1 in. (2.54 mm) slip load, initial slip was caused by an extremely low load compared to the other two strand types. First slip is caused by the sudden loss of adhesion, or the chemical bond that forms between the strand and mortar or concrete. Currently, the proposed standard bases acceptance only on the 0.1 in. (2.54 mm) pullout load, but the low 0.001 in. (0.025 mm) pullout load could possibly indicate a problem with adhesion, which could affect bond performance, or at least warrant more investigation.

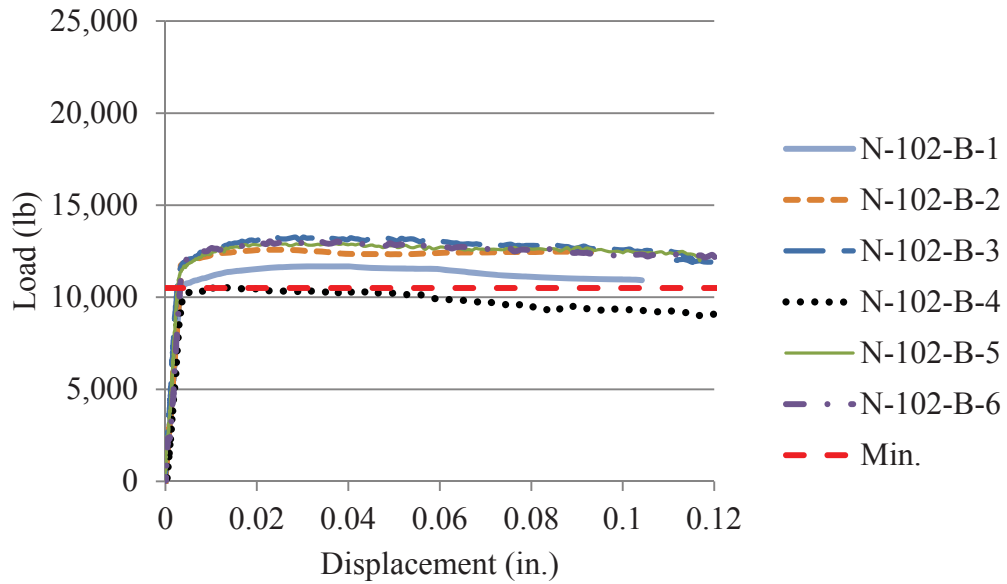
Additionally, analysis of the load vs. slip plots of the three strand types showed a trend that could help distinguish acceptable from poor bond quality. The load vs. slip plots for N-101-B, N-102-B, and N-103-B are presented in **Figures 5.2, 5.3, and 5.4**, respectively. Strand types 101 and 103 both had average pullout values that exceeded the minimum required average by over 70%, and both load vs. slip plots, shown in **Figures 5.2 and 5.4**, indicate that for each specimen, the loads were still increasing at a slip of 0.1 in. (0.025 mm). However, strand type 102, which only exceeded the minimum average by 11%, shows a distinct plateau, or softening, and eventually a gradual decrease in load as slip continues to increase (**Figure 5.3**). The plateaus in loads for strand type 102, which were not seen in the load vs. slip plots for types 101 and 103, which clearly had high

bond quality, is a sign that strand type 102 may still have questionable bond quality even though the strand type passed based on the threshold values. This concern was also noted by Hawkins and Ramirez in their due diligence study performed on the four rounds of NASP testing (2010).



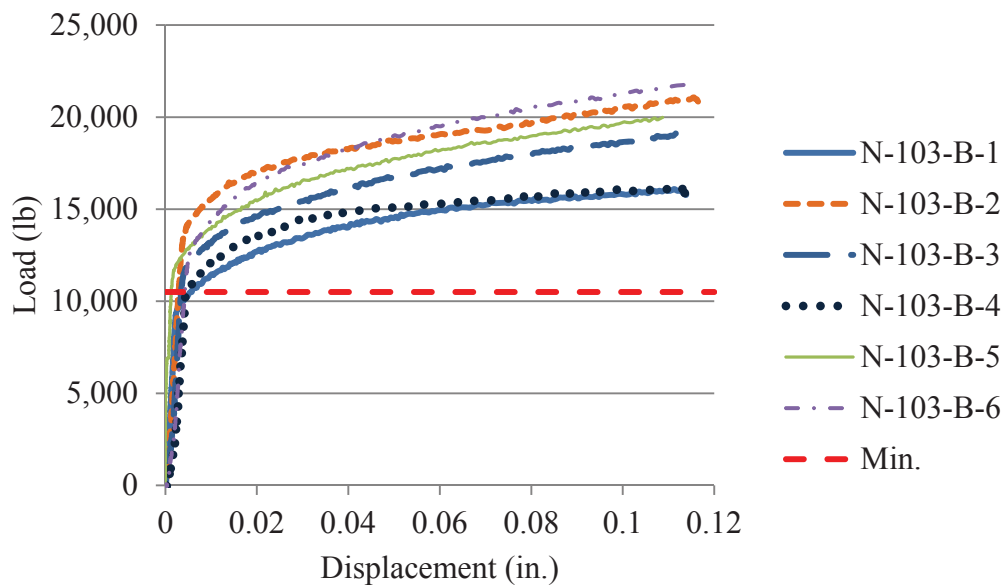
Conversion: 1 in. = 25.4 mm  
1 lb = 4.45 N

**Figure 5.2 – N-101-B Load vs. Slip**



Conversion: 1 in. = 25.4 mm  
 1 lb = 4.45 N

**Figure 5.3 – N-102-B Load vs. Slip**



Conversion: 1-in. = 25.4 mm  
 1 lb = 4.45 N

**Figure 5.4 – N-103-B Load vs. Slip**

While no known previous bond testing had been done on strand type 101, NASP tests had been completed on strand types 102 and 103 during NCHRP 10-62, and samples of the two strand types were sent to Missouri S&T to be blindly tested to see if similar NASP test results could be obtained. After testing was completed at Missouri S&T, the previous results from NCHRP 10-62 were acquired and compared to the results from this test program. The 0.1 in. (2.54 mm) average pullout value results from NCHRP 10-62 and Missouri S&T for strands 102 and 103 and the percent differences are displayed in **Table 5.1**.

**Table 5.1 – Average Pullout 0.1-in. (2.54 mm) Pullout Values from Missouri S&T and NCHRP 10-62 for Strands 102 and 103**

<b>Strand ID</b>	<b>NCHRP 10-62 Pullout Load (lb)</b>	<b>Missouri S&amp;T Pullout Load (lb)</b>	<b>Percent Difference</b>
102	10,600	11,700	9.9%
103	13,300	18,700	33.8%

Conversion: 1 lb = 4.45 N

The results from Missouri S&T were higher than the results from NCHRP 10-62, and the values from strand type 102 had a difference of 9.9% while there was a 33.8% difference between the pullout values for strand type 103. The differences between the average pullout values from NCHRP 10-62 and Missouri S&T could be explained by several factors. First, the strands were sent to Missouri S&T months after the initial testing, and that time could have allowed the strand surface quality to degrade. Also, the mix designs and compressive strength and flow properties of the mixes used for the tests conducted for NCHRP 10-62 were unknown. Even if the compressive strengths and flow values for the tests done by NCHRP 10-62 were within the acceptable ranges, as were the mixes used by Missouri S&T, differences in mix designs, such as the water/cement ratio or amount and angularity of the sand could have affected the pullout loads.

While the proposed standard only specifies compressive strength and flow ranges and has no restrictions on mix proportioning, the round robin testing completed for the development of the NASP test indicated that the desired mix properties can usually be

obtained by using a mix design with a 0.45 water/cement ratio and a sand/cement ratio of around 2:1 (Hawkins and Ramirez 2010). Most literature from other research where the NASP test was completed indicates the use of mix designs similar to this. However, with the materials available, Missouri S&T was unable to create a mix with the desired properties using the conventional mix proportions and instead used a mix with a water/cement ratio of 0.395 and a sand/cement ratio of 0.9:1, which is drastically different than the proposed typical proportions. There are many unknowns regarding the treatment of the strands between tests and the mix designs, but on the surface, the noticeable differences appear to indicate that in this case, the test did not seem to be reproducible between sites.

The effect of differences in mix proportioning was tested to an extent through comparing pullout values from strand type 101 in mortar Mix A and mortar Mix B. Strand type 101 was initially tested months before types 102 and 103, and the mix design that had originally been used for type 101, mortar Mix A, did not give the same flow properties when tested in trial batches again before testing 102 and 103, most likely due to changes in the sand. A new mix design, mortar Mix B, which also met the strength and flow properties was developed. The mix designs for Mix A and Mix B were discussed in **Section 3.3.1** and can be found in **Table 3.2**. Mix B had a slightly higher water/cement ratio and a much lower sand/cement ratio compared to Mix A. After testing was completed on types 102 and 103 with Mix B, it was decided that remaining samples of type 101 should be tested in Mix B as well, so all pullout values could be directly compared. The samples of strand 101 were wrapped in plastic and stored in a closed container for the six months between the initial and final testing.

The pullout values for strand type 101 in mortar mixes A and B are shown in **Table 5.2**. Both the 0.001 in. (0.025 mm) and 0.1 in. (2.54 mm) pullout loads were consistently lower in Mix B compared to Mix A. The 0.1 in. (2.54 mm) average pullout value for Mix B was 15.7% lower than Mix A, and the 0.001 in. (0.025 mm) average pullout value for Mix B was 38.7% lower. The 0.001 in. (0.025 mm) and 0.1 in. (2.54 mm) average pullout loads are presented graphically in **Figure 5.5**, with error bars representing 95% confidence intervals for each set. When comparing the 0.001 in. (0.025 mm) and 0.1 in. (2.54 mm) pullout loads between the two mixes, the 95% confidence

interval error bars do not overlap at either slip value. Therefore, both the pullout values at 0.001 in. (0.025 mm) and the pullout values at 0.1 in. (2.54 mm) were found to be statistically different between the NASP test completed in Mix A and the NASP test completed in Mix B. As **Table 3.8** shows, both mixes had strengths and flows falling within the required ranges, so it is proposed that the differences in mix proportioning was the reason behind the difference in pullout values. One hypothesis is that the significant decrease in sand content in Mix B could have decreased the effects of mechanical interlock and friction on the strand, causing the lower pullout values.

Since the different mix proportioning between Mix A and Mix B seemed to affect the pullout values, it would follow that the NASP tests completed at other sites with the more conventional mix designs should also produce different pullout values from the values determined at Missouri S&T. However, based on previous tests in literature, the mixes used for NCHRP 10-62 most likely had more sand than Mix B used by Missouri S&T, which should increase the pullout values according to the conclusion drawn from the results of strand 101 in Mix A and Mix B. However, this was not the case, as shown in **Table 5.1**.

**Table 5.2 – N-101-A and N-101-B Pullout Loads**

Specimen No.	N-101-A (lb)		N-101-B (lb)	
	0.001 in.	0.1 in	0.001 in.	0.1 in
1	12,500	22,100	8,100	19,100
2	10,600	22,900	6,500	17,300
3	12,600	23,000	7,800	17,800
4	11,100	21,100	7,200	19,100
5	13,100	20,600	8,900	18,200
6	11,500	20,000	5,200	17,800
<b>Avg.</b>	<b>11,900</b>	<b>21,600</b>	<b>7,300</b>	<b>18,200</b>
<b>Std. Dev.</b>	<b>978</b>	<b>1,242</b>	<b>1,304</b>	<b>741</b>
<b>COV</b>	<b>8.2%</b>	<b>5.8%</b>	<b>17.9%</b>	<b>4.1%</b>

Conversion: 1 in. = 25.4 mm  
1 lb = 4.45 N

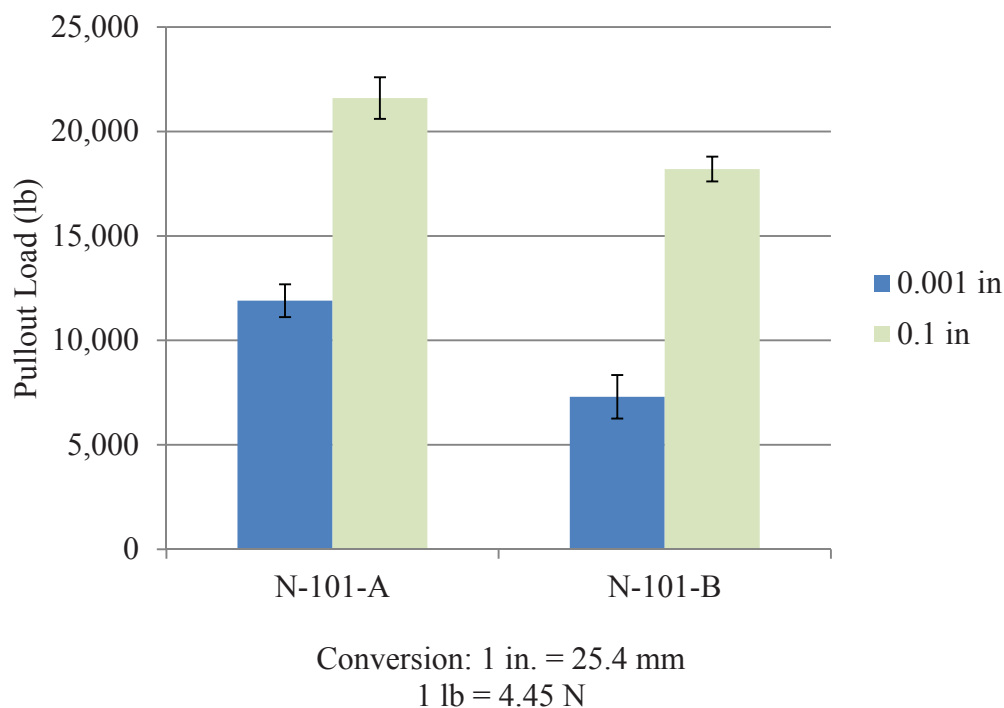


**Figure 5.5 – Comparison of N-101-A and N-101-B Pullout Loads**

**5.2.2. Discussion of NASP Test in Concrete Results.** The results from the NASP tests in concrete are presented in **Tables 3.9** and **3.10** and are also presented graphically in **Figures 5.6** and **5.7** with error bars representing one standard deviation above and below the average. **Figure 5.6** displays the 0.001 in. (0.025 mm) and 0.1 in. (2.54 mm) pullout results for C6, S6, C10, and S10 at 1 day, while **Figure 5.7** shows the 0.001 in. (0.025 mm) and 0.1 in. (2.54 mm) pullout results for the four concrete mixes at 8 days.

As discussed in **Section 2.4.3**, concrete strength has been shown to increase bond performance. **Figures 5.6** and **5.7** appear to support this conclusion. At both 1 and 8 days, the high strength conventional concrete 0.1 in. (2.54 mm) average pullout load (N-101-C10) was statistically higher than the normal strength conventional concrete 0.1 in. (2.54 mm) pullout load (N-101-C6). In terms of comparing normal strength to high strength SCC, the 1 day pullout loads showed no statistical difference because the standard deviation of N-101-S10 is so high. However, **Figure 5.7** shows that at 8 days, the high strength SCC (N-101-S10) clearly had a higher pullout load than the normal strength

SCC (N-101-S6). The data presented in **Figures 5.6** and **5.7** generally show that for a given type of concrete, an increase in concrete strength resulted in a higher pullout value, leading to the conclusion that increasing concrete strength improves bond. This supports the trend that has been noted by previous researchers, specifically, Ramirez and Russell (2008), who also conducted NASP tests in concretes at different strengths. They reported that increasing concrete strength resulted in increased NASP pullout loads, and the pullout loads showed a relatively strong correlation to the square root of the concrete compressive strength (Ramirez and Russell 2008).

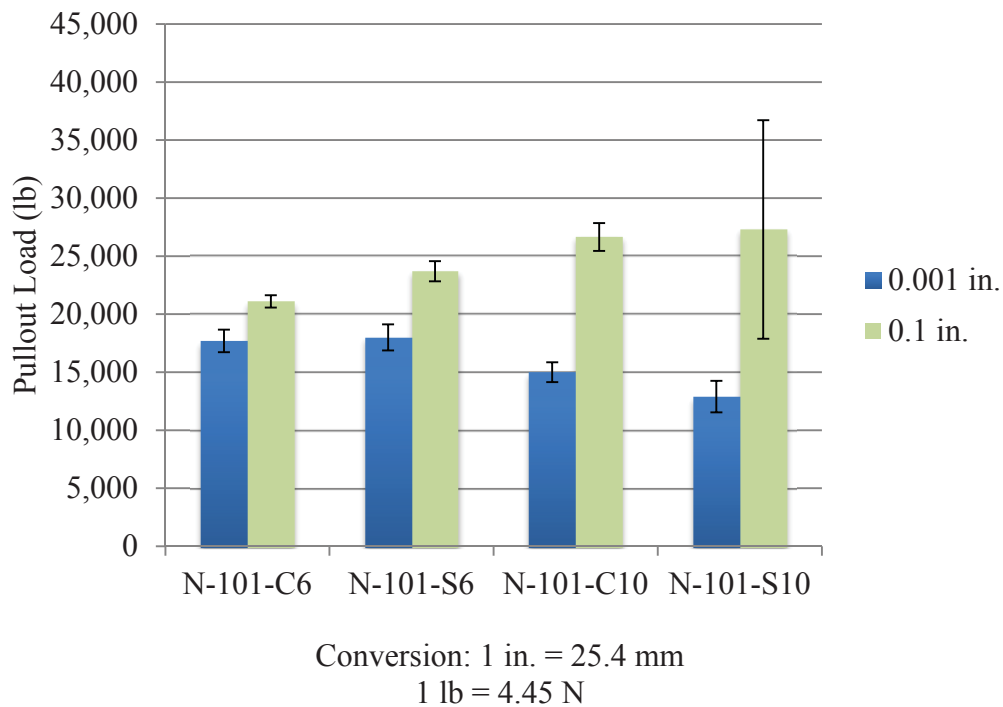


**Figure 5.6 – NASP in Concrete Pullout Loads – 1 Day**

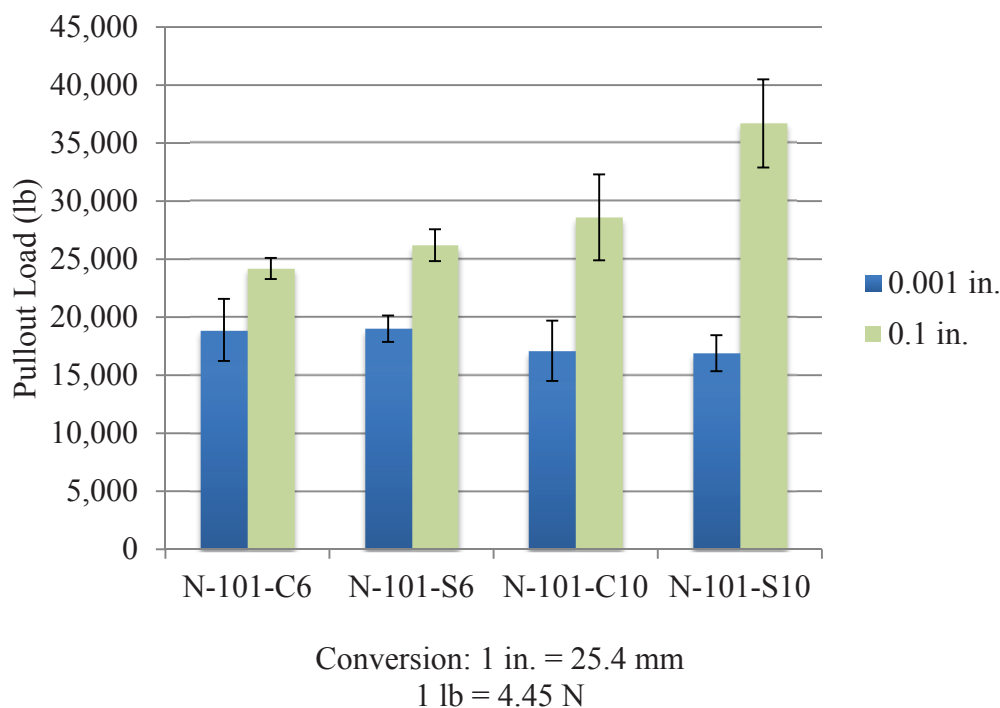


**Figure 5.7 – NASP in Concrete Pullout Loads – 8 Day**

In addition to a comparison based on concrete strength, the results from the NASP tests in concrete were also evaluated to determine if the type of concrete affected the pullout loads. In order to directly compare the bond performance of conventional concrete to SCC, the pullout loads were normalized by dividing the pullout value for each mix at each day by the square root of the compressive strength at the time of testing. As discussed, research by Ramirez and Russell (2008) suggested that the NASP pullout loads can be correlated to the square root of concrete strength, so dividing the pullout loads by the square root of the compressive strength negated the effect of the compressive strength on the pullout loads so that the loads could be compared based solely on concrete type. The normalized pullout loads for C6 and S6 are presented in **Table 5.3**, and the normalized pullout loads for mixes C10 and S10 are shown in **Table 5.4**. The pullout loads divided by the square roots of the concrete compressive strengths with the standard deviation error bars are graphed in **Figures 5.8** and **5.9**. **Figure 5.8** shows the values for the 1 day tests, and **Figure 5.9** contains the results for the 8 day tests.

According to **Figure 5.8**, at 1 day, there was virtually no difference between bond performance of the normal strength conventional concrete and SCC (C6 and S6) at either 0.001 in. (0.025 mm) or 0.1 in. (2.54 mm) of slip. However, in terms of the high strength mixes, the conventional concrete mix (C10) appeared to have slightly better bond in terms of first slip, but there was no difference at 0.1-in. (2.54 mm) pullout loads, mostly due to the high standard deviation in the results from the S10 mix.

Regarding the 8 day results, **Figure 5.9** shows that once again, there was no difference in bond performance between the normal strength conventional concrete and SCC (C6 and S6) at either 0.001 in. (0.025 mm) or 0.1 in. (2.54 mm) of strand slip. According to **Figure 5.9**, at 8 days, there was also no difference in bond performance between the high strength conventional and SCC mixes (C10 and S10). Based on the averages, the S10 mix did appear to somewhat out-perform the C10 mix at the 0.1-in. (2.54 mm) slip benchmark, but error bars overlapped slightly, so that conclusion could not be definitively drawn.

In conclusion, for the NASP test performed with concrete instead of mortar, generally no difference was noted between the bond performance of SCC vs. conventional concrete. However, one conclusion that could be drawn from analysis of **Figures 5.8** and **5.9** is that the high strength mixes (C10 and S10) consistently had lower pullout loads at 0.001 in. (0.025 mm) of slip than the conventional strength mixes (C6 and S6), and since the loads had been normalized with respect to concrete strength, this observation is most likely due to other factors affecting the concrete, such as mix design. Based on previous discussion, the low first slip load is likely due to a change in the adhesion between the strand and the concrete, indicating that the high strength mixes had lower adhesion with the strand than the normal strength mixes. The only major differences that was noted between the high strength and normal strength mix designs was that the high strength mixes contained some fly ash replacement and higher cementitious content, while the normal strength mixes did not, and this could be a possible factor affecting the adhesion.

Table 5.3 – NASP in Concrete Results for C6 and S6 Normalized to  $\sqrt{f'_c}$ 

Mix	Day	Specimen ID	$\sqrt{f'_c}$ (psi)	Load/ $\sqrt{f'_c}$ at Slip of 0.001 in.			Load/ $\sqrt{f'_c}$ at Slip of 0.1 in.				
				Load/ $\sqrt{f'_c}$ (lb/ $\sqrt{\text{psi}}$ )	Avg. Load/ $\sqrt{f'_c}$ (lb/ $\sqrt{\text{psi}}$ )	Std. Dev. (lb.)	COV	Load/ $\sqrt{f'_c}$ (lb/ $\sqrt{\text{psi}}$ )	Avg. Load/ $\sqrt{f'_c}$ (lb/ $\sqrt{\text{psi}}$ )	Std. Dev. (lb.)	COV
C6	1 Day	N-C6-1	69.35	243.7	255.7	14.0	5.48%	301.4	304.2	7.6	2.51%
		N-C6-2		252.3				298.5			
		N-C6-3		271.1				312.9			
	8 Day	N-C6-4	74.97	242.8	252.6	35.7	14.14%	332.1	323.3	12.1	3.74%
		N-C6-5		222.8				328.1			
		N-C6-6		292.1				309.5			
S6	1 Day	N-S6-1	75.23	248.6	239.3	15.0	6.26%	317.7	314.6	11.6	3.69%
		N-S6-2		247.2				324.3			
		N-S6-3		222.0				301.7			
	8 Day	N-S6-4	81.79	221.3	232.7	13.9	5.98%	302.0	320.3	16.8	5.25%
		N-S6-5		228.6				324.0			
		N-S6-6		248.2				335.0			

Conversion: 1 in. = 25.4 mm

1 lb = 4.45 N

1 psi = 6.89 kPa

Table 5.4 – NASP in Concrete Results for C10 and S10 Normalized to  $\sqrt{f'_c}$ 

Mix	Day	Specimen ID	$\sqrt{f'_c}$ (psi)	Load/ $\sqrt{f'_c}$ at Slip of 0.001 in.			Load/ $\sqrt{f'_c}$ at Slip of 0.1 in.				
				Load/ $\sqrt{f'_c}$ (lb/ $\sqrt{\text{psi}}$ )	Avg. Load/ $\sqrt{f'_c}$ (lb/ $\sqrt{\text{psi}}$ )	Std. Dev. (lb.)	COV	Load/ $\sqrt{f'_c}$ (lb/ $\sqrt{\text{psi}}$ )	Avg. Load/ $\sqrt{f'_c}$ (lb/ $\sqrt{\text{psi}}$ )	Std. Dev. (lb.)	COV
C10	1 Day	N-C10-1	75.30	185.9	198.8	11.3	5.68%	N/A	353.9	16.0	4.51%
		N-C10-2		203.2				365.2			
		N-C10-3		207.2				342.6			
	8 Day	N-C10-4	89.16	173.8	191.8	29.2	15.20%	273.7	321.1	41.6	12.95%
		N-C10-5		176.1				338.7			
		N-C10-6		225.4				351.0			
S10	1 Day	N-C10-1	79.56	170.9	161.7	17.1	10.55%	364.5	342.7	118.4	34.55%
		N-S10-2		142.0				214.9			
		N-S10-3		172.2				448.7			
	8 Day	N-S10-4	92.74	199.5	182.6	16.7	9.16%	427.0	395.7	41.0	10.35%
		N-S10-5		166.1				410.8			
		N-S10-6		182.2				349.4			

Conversion: 1 in. = 25.4 mm

1 lb = 4.45 N

1 psi = 6.89 kPa

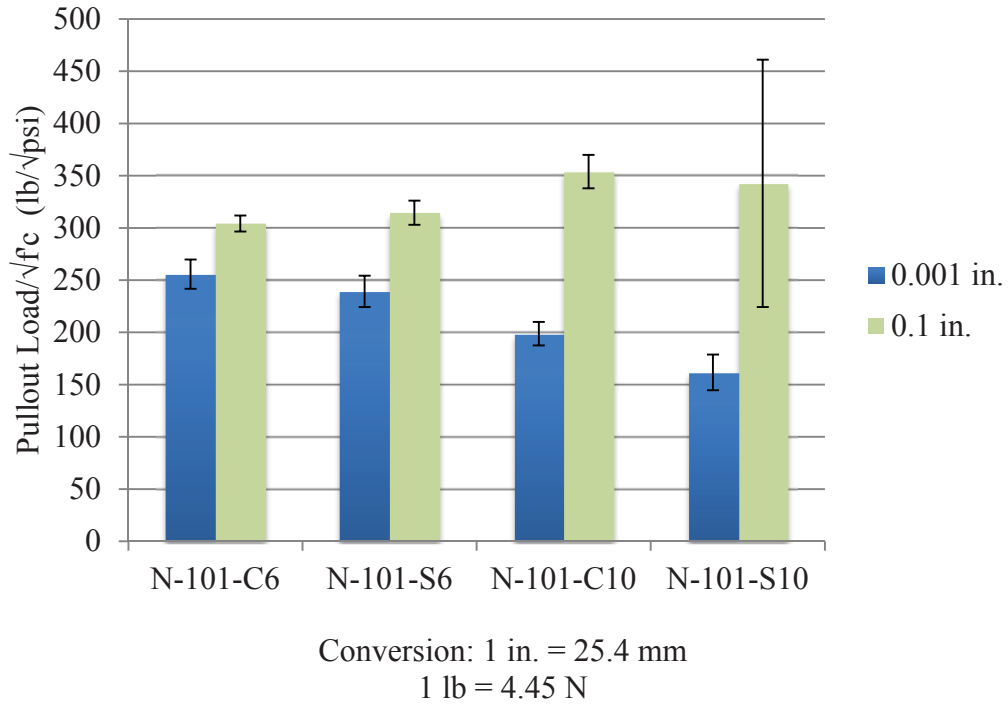


**Figure 5.8 – NASP in Concrete Pullout Loads  $\sqrt{f'_c}$  – 1 Day**

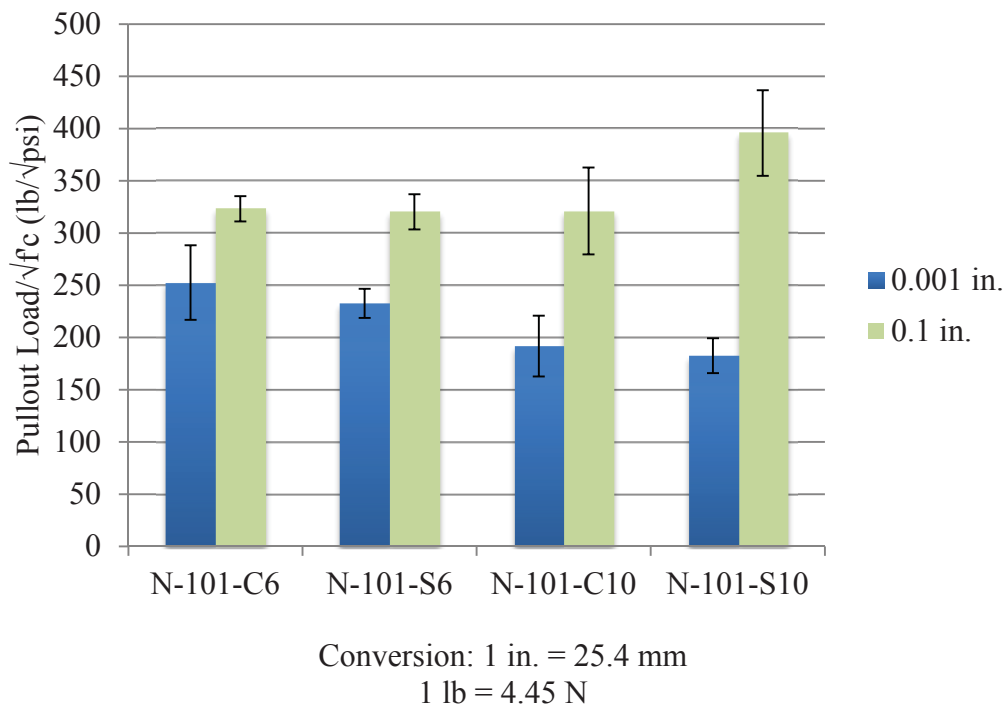


**Figure 5.9 – NASP in Concrete Pullout Loads  $\sqrt{f'_c}$  – 8 Day**

**5.2.3. Discussion of LBPT Results.** The LBPT procedure is described in **Section 3.4**, and the results for all specimens can be found in **Table 3.13**. The average first slip load and peak load results, along with the standard deviation and coefficient of variation (COV), for each strand type are presented in this section in **Table 5.5**.

**Table 5.5 – LBPT Results Statistical Summary**

Strand ID	First Slip Load			Peak Load		
	Avg. Load (k)	Std. Dev. (k)	COV	Avg. Load (k)	Std. Dev. (k)	COV
101	19.1	2.3	12.27%	36.6	2.1	5.76%
102	12.7	1.7	13.53%	27.8	2.9	10.40%
103	19.3	3.3	17.16%	34.5	4.6	13.30%

Conversion: 1 kip = 4.45 kN

The average load values were compared to the limits set forth by Logan (Logan, personal communication, October 20, 2011). Logan recommends that in order for a strand to have acceptable bond quality, the average first slip load must exceed 16 kips (71.1 kN), and the average peak load value must be greater than 36 kips (160.1 kN). Additionally, Logan set the maximum allowable coefficient of variation for the peak loads at 10%. The average first slip load and peak load for each strand type as well as the first slip and peak minimum limits are presented graphically in **Figure 5.10**. The error bars represent one standard deviation from either side of the mean.

As seen in **Figure 5.10**, strand type 101 was the only strand type that passed the LBPT with the requirements proposed by Logan. The average first slip load and average peak load exceeded the limits by 19.1% and 1.76%, respectively, and the coefficient of variation for the peak load values was 5.76%, falling well below the 10% coefficient of variation limit. Meanwhile, strand type 103 passed the load at first slip limit, but the average peak load fell short of the 36 kip (160.1 kN) minimum limit. Strand type 102 did not pass either limit. Strand types 102 and 103 also had coefficient of variation values for the peak loads exceeding 10%.

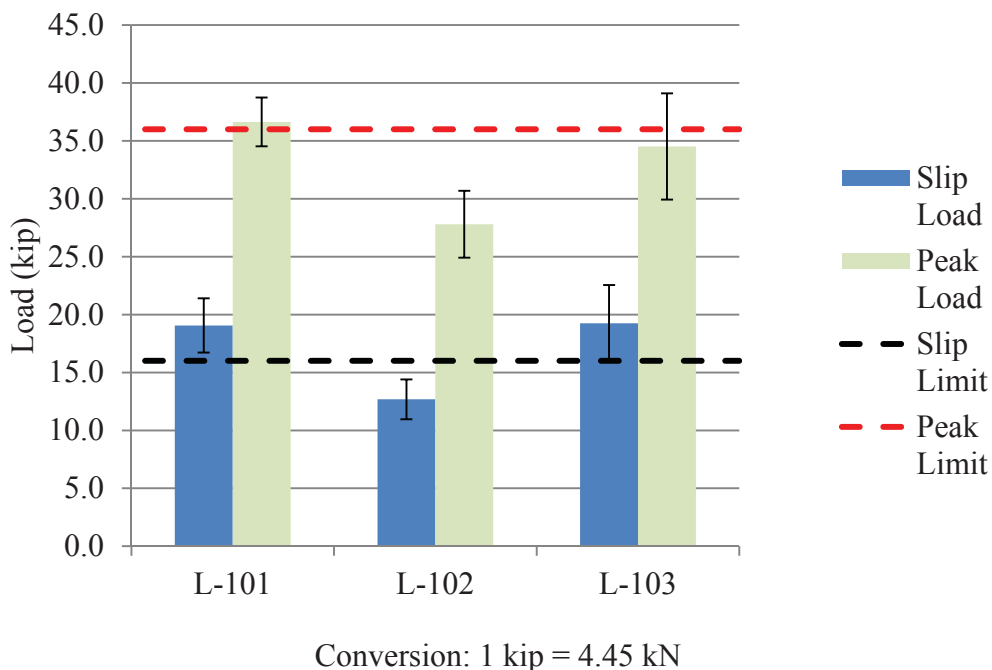


**Figure 5.10 – LBPT Average First Slip and Peak Pullout Loads**

Visual observations and results from the towel wipe test, which were presented in **Table 3.13**, were also compared to the final results to determine if qualitative data could be any indication of the bond performance of the strand. Some researchers have found that rust improves bond quality, yet strand type 102 had the most observed rust and the heaviest residue, but also the lowest average pullout values. However, strand L-102-4 was the only strand that ruptured in the concrete, and this strand was noted to have the highest number of rust spots and heaviest residue out of all the strand samples. Strand types 101 and 103 had very comparable pullout values, and both strands were noted to have light to moderate residue and very little rust. In this project, it appeared that lighter residue led to higher pullout values, but only three strand samples were tested, and due to limited data and the subjective nature of the visual tests, it was determined that no clear correlation existed between amount of rust and residue and strand bond performance.

**5.2.4. Comparison of NASP Test in Mortar Results to LBPT Results.** One of the purposes of this research program was to compare the NASP test in mortar to the LBPT to determine if one test can be deemed as better or more consistent than the other.

The results from both tests were evaluated to see if the overall results from the different strand types were consistent from test to test.

The pullout results from the NASP in mortar and the LBPT are presented for comparison in **Table 5.6**. The values presented from the NASP tests are the loads at 0.1 in (2.54 mm) slip from the tests completed in mortar Mix B, while the values presented from the LBPT are the peak pullout loads. **Table 5.6** displays the six individual results for each strand and each test as well as the average value, standard deviation, and coefficient of variation for each strand and test.

One observation that can be made from examination of **Table 5.6** is that for a given strand type, the coefficient of variation determined from the NASP test and LBPT was remarkably similar (within 1-2%). This would indicate that both the NASP test and LBPT seem to be more or less equal in terms of consistency of results.

In order to determine if a correlation existed between the LBPT and NASP test in mortar performed in this study, the LBPT peak pullout loads and NASP pullout loads at 0.1 in (2.54 mm) slip were plotted against each other. The data was manipulated so that for the results for each strand type, the six NASP pullout loads and six LBPT pullout loads were sorted from lowest to highest within their respective tests. Then, within each strand type, the lowest NASP pullout value was plotted against the lowest LBPT pullout value, and the second lowest values from each test were plotted against each other, and so on. The plot of LBPT pullout loads vs. NASP in mortar pullout loads is presented in **Figure 5.11**.

The linear trend line through the points in **Figure 5.11** yielded an  $R^2$  value of 0.77, which shows there was a somewhat strong correlation between the NASP in mortar pullout loads and LBPT pullout loads in this study. Based on this comparison as well as the previous observation with respect to comparing coefficients of variation for each test method, it appears that either the LBPT or NASP test are equally valid approaches to evaluating bond performance of prestressing strand. However, the limits set on passing may need some refinement, as two of the strand sources passed the proposed NASP standard but did not pass the LBPT requirements.

Table 5.6 – NASP in Mortar and LBPT Pullout Loads

Strand Type	Specimen No. or Statistic	NASP (Mix B) 0.1 in Pullout Load (lb)	LBPT Peak Pullout Load (k)
101	1	19,100	34.3
	2	17,300	34.2
	3	17,800	35.9
	4	19,100	38.8
	5	18,200	38.5
	6	17,800	38.1
	<b>Avg.</b>	<b>18,200</b>	<b>36.6</b>
	<b>Std. Dev.</b>	<b>741</b>	<b>2.1</b>
	<b>COV</b>	<b>4.07%</b>	<b>5.76%</b>
102	1	11,000	27.1
	2	12,400	27.1
	3	12,600	31.0*
	4	9,300	40.1**
	5	12,400	25.1
	6	12,300	31.9
	<b>Avg.</b>	<b>11,700</b>	<b>27.8</b>
	<b>Std. Dev.</b>	<b>1,296</b>	<b>2.9</b>
	<b>COV</b>	<b>11.07%</b>	<b>10.40%</b>
103	1	15,800	33.5
	2	20,500	33.5
	3	18,600	38.7
	4	16,000	35.6
	5	19,700	26.6
	6	21,300	39.2
	<b>Avg.</b>	<b>18,700</b>	<b>34.5</b>
	<b>Std. Dev.</b>	<b>2,311</b>	<b>4.6</b>
	<b>COV</b>	<b>12.36%</b>	<b>13.30%</b>

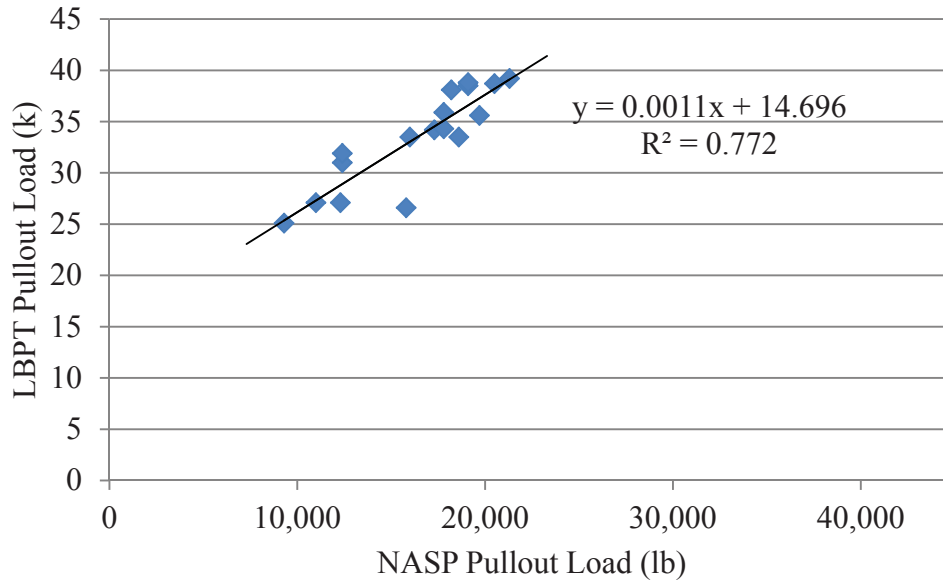
\* - Data collection accidentally stopped early, so value determined by observation.

\*\* - Strand fractured, value not included in average or standard deviation.

Conversion: 1 in. = 25.4 mm

1 lb = 4.45 N

1 kip = 4.45 kN



Conversion: 1 lb = 4.45 N  
1 kip = 4.45 kN

**Figure 5.11 – LBPT Pullout Loads vs. NASP Pullout Loads**

As discussed in **Sections 5.2.1** and **5.2.3**, the NASP test and LBPT results were compared to their respective acceptance limits to determine if each strand passed or failed. The pass/fail results as well as the overall ranking of the strands in terms of bond from each test are presented in **Table 5.7**. The ranks were based on the load at 0.1 in. (2.54 mm) slip for the NASP test in mortar and the peak pullout load for the LBPT.

**Table 5.7 – Pass/Fail Results for NASP in Mortar and LBPT**

Strand ID	NASP in Mortar		LBPT	
	Rank	Pass/Fail	Rank	Pass/Fail
101	2	PASS	1	PASS
102	3	PASS	3	FAIL
103	1	PASS	2	FAIL

The correlation between tests was not consistent. As seen in **Table 5.7**, strand type 101 was the only type that was considered to have acceptable bond performance by both tests. Strand types 102 and 103 both passed the NASP test in mortar but failed the LBPT. The relative bond between strands was also not the same between tests. Strand type 102 had the worst bond performance in both the NASP and LBPT, but strand type 103 had the best performance in the NASP test, while strand type 101 had the best performance in the LBPT. However, strand types 101 and 103 were extremely comparable, and average pullout values between the two types were within 2.7% for the NASP test and 6.0% for the LBPT. Also, error bars show the standard deviations for the two types overlapped significantly for the NASP Test (**Figure 5.1**) as well as the LBPT (**Figure 5.10**). Therefore, the differences in rank are not statistically significant for types 101 and 103. The two test methods can be considered fairly accurate with respect to relative bond between strands, but in terms of absolute bond and rejecting or accepting strand based on set limits, the NASP test passed all three types while the LBPT only passed one out of the three.

### **5.3. TRANSFER LENGTH TEST RESULTS**

The transfer lengths determined from DEMEC data and the 95% Average Mean Strain Method, as well as values determined from the end slip values measured by the Synergy data acquisition and steel ruler, are evaluated and discussed in this subsection.

**5.3.1. Discussion of 95% Average Mean Strain Transfer Length Results.** The primary method used for determining transfer lengths was the 95% Average Mean Strain Method. The process of developing strain profiles based on DEMEC readings and determining the transfer lengths is described in **Section 4.4.1**. The final individual transfer lengths at 1, 4, 8, 14, 28, and approximately 56 days as determined by the 95% Average Mean Strain Method are presented in **Tables 4.3** and **4.4**, and the average transfer lengths and the standard deviations for each mix for the top and bottom strands are summarized in **Tables 4.5** and **4.6**. The averages and standard deviations are based on all of the individual results from each mix, but additional analysis in this section revealed individual measurements that could potentially be removed when comparing averages to

each other to determine if differences between measured transfer lengths from mix to mix are statistically significant.

As discussed in **Section 2.4.5**, previous research has indicated that a transfer length at a “live end,” or end directly adjacent to where the strand is first released, is typically longer than a transfer length at a “dead end,” or end not adjacent to the place where the strand is first cut. In this research, the live and dead ends of the strands were not directly monitored. In this research program, for release of each strand, one person was positioned at each location where the strand would need to be cut to separate all the beams in the line, and all locations were attempted to be cut at the same time using bolt cutters, as described in **Section 4.3**. However, it was very hard for the workers to sever all locations at exactly the same time, and typically one or two locations on one strand were severed before others. It was not noted at the site which location on each strand was cut first, but it was surmised that the linear potentiometer data would be able to indicate which ends were severed first. However, due to the proven unreliability of the potentiometers, the electronically collected data could not reliably indicate the sequence of strand release.

Although there is no hard evidence as to the sequence of release, analysis of the transfer length data does potentially indicate where some of the live ends could have occurred. **Figures 5.12** and **5.13** show the casting layouts and initial (1 day) transfer lengths determined by the 95% Average Mean Strain Method at each individual location. The circles indicate locations that have comparatively higher measured transfer lengths, which could possibly indicate the live end locations.

In **Figure 5.12**, C6-4-1\_SE is the only location that appears unusually high, but no definite conclusion could be made regarding a live end because only two transfer lengths out of four were able to be determined for the top strands in the C6 mix. The transfer lengths at C6-4-1\_NE and C6-4-1\_NW were not established because there were no defined plateaus on the strain profiles. This could be due to faulty DEMEC readings, or the strains were in fact still increasing, which could indicate that those locations were live ends. However, there was no way to come to definite conclusions, so averages were not adjusted for either of the normal strength mixes for two strands or four strands.

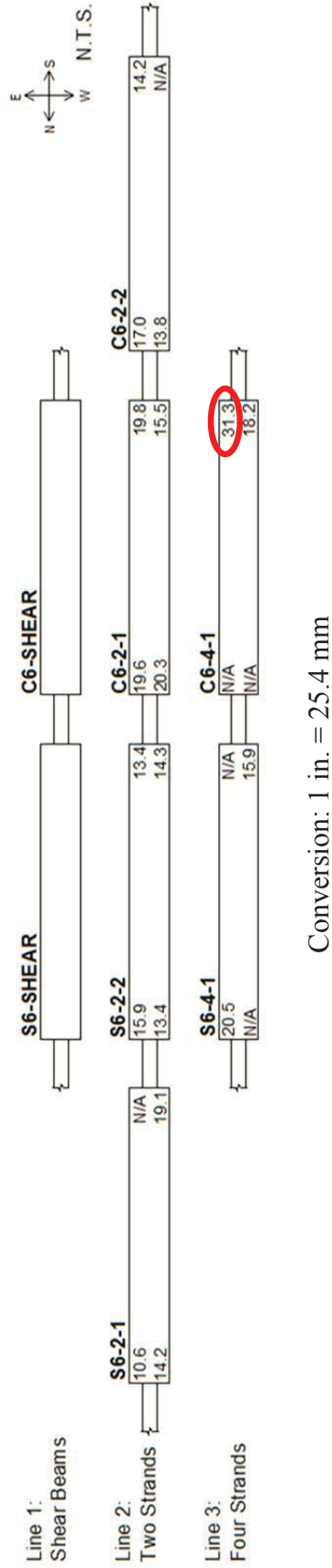


Figure 5.12 – C6 and S6 Transfer Length Locations

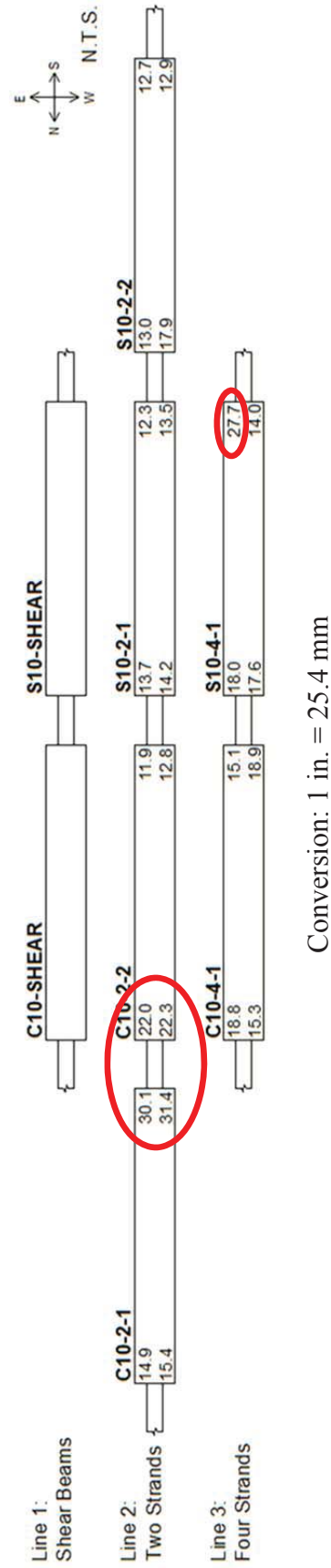
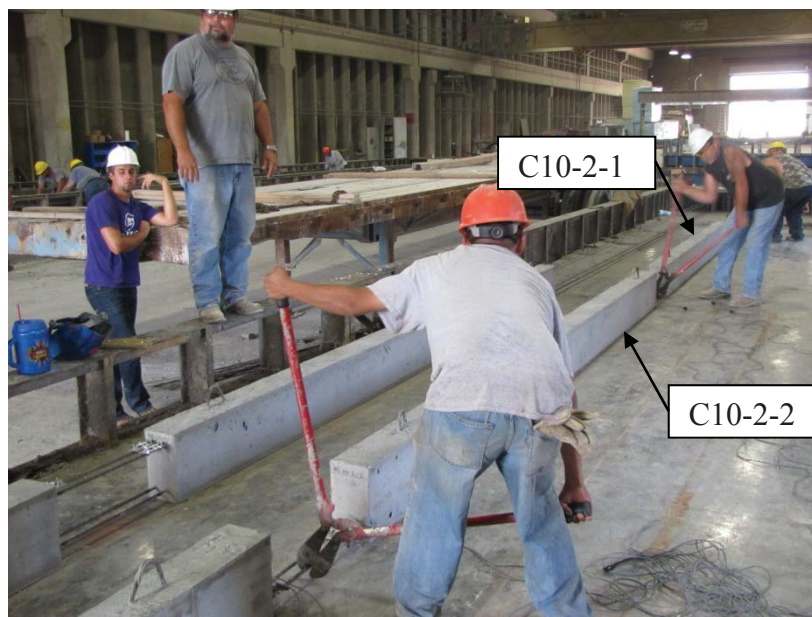


Figure 5.13 – C10 and S10 Transfer Length Locations

Some more refined conclusions could be made regarding the high strength mixes, based on observations of **Figure 5.13**. Although S10-4-1\_SE was not statistically an outlier, the value was still comparatively high, and several different transfer length averages were calculated for comparison. The standard average transfer length, S10-4, was taken with all four values, and then the potential dead end transfer length average, S10-4 (D), was calculated with the NE, NW, and SW values while the SE value was taken as the live end transfer length, S10-4 (L).

According to **Figure 5.13**, the four locations that seem to definitively indicate live ends are C10-2-1\_SE, C10-2-1\_SW, C10-2-2\_NE, and C10-2-2\_NW. Due to significant and consistent differences in transfer lengths, it appears that the east strand in the two-strand line of high strength beams was first severed between C10-2-1\_SE and C10-2-2\_NE, and the first cut on the west strand was made between C10-2-1\_SW and C10-2-2\_NW. Photographic evidence taken at the time of release seems to confirm this determination. **Figure 5.14** was taken during release of the east strand of the line of the high strength two-strand beams, and the worker cutting the location between beams C10-2-1 and C10-2-2 is clearly in motion, while the worker between C10-2-2 and S10-2-1 has not started to cut the strand. The person who cut the east strand between C10-2-1 and C10-2-2 also cut the west strand between the two beams, and if he was early on the first strand, chances are reasonable that he was early on the second strand as well. Although the remaining workers cannot be seen, the fact that evidence shows the location between C10-2-1 and C10-2-2 was cut before at least one other location combined with the high transfer length results leads to the assumption that ends C10-2-1\_SE, C10-2-1\_SW, C10-2-2\_NE, and C10-2-2\_NW could reasonably be considered the live ends for that line. Therefore, in addition to the standard full C10-2 average for each day, the adjusted average C10-2 (D) was taken for the dead ends, and the adjusted average C10-2 (L) was calculated for the live ends. The different transfer length averages for C10-2 at 1, 4, 8, 14, and 28 days were compared to transfer lengths in the S10 mix.



**Figure 5.14 – Release of C10-2 Beams**

The standard and modified dead and live end averages, standard deviations, and coefficients of variation for each mix for the bottom and top strands are shown in **Tables 5.8** and **5.9**, respectively. The “standard” values are the averages and standard deviations calculated based on all reported transfer lengths, and the “modified” values are the live end or dead end averages and standard deviations taken when applicable. C10-2 (L) values in **Table 5.8** are the averages at each day for the possible live ends for the bottom strands and include C10-2-1\_SE, C10-2-1\_SW, C10-2-2\_NE, and C10-2-2\_NW, while C10-2 (D) values are the dead end averages, which include the remaining ends in the C10-2 beams. S10-4 (L) for the top strands in **Table 5.9** is only the S10-4-1\_SE value at each day, and S10-4 (D) values are the averages of the remaining three ends. The different averages were compared to determine if there was any statistical difference between transfer lengths measured in the conventional concrete and SCC and then compared to values calculated by AASHTO and ACI equations. Throughout the remainder of this report, it should be noted that a mix identification with a “2” suffix indicates bottom strand average, while a mix identification with a “4” suffix indicates a top strand average.

**Table 5.8 – Standard and Modified Transfer Length Averages (Bottom Strands)**

<b>Bottom Strands</b>		<b>1 Day (in.)</b>	<b>4 Day (in.)</b>	<b>8 Day (in.)</b>	<b>14 Day (in.)</b>	<b>28 Day (in.)</b>	<b>~56 Day (in.)</b>
C6-2	Avg.	17.2	20.4	22.3	23.7	23.6	22.8
	Std. Dev.	2.76	4.07	4.85	5.09	5.69	4.22
	COV	16.1%	19.9%	21.8%	21.5%	24.1%	18.5%
S6-2	Avg.	14.4	18.4	18.2	18.6	19.2	19.2
	Std. Dev.	2.61	3.20	1.90	2.35	2.17	2.21
	COV	18.1%	17.4%	10.5%	12.7%	11.3%	11.5%
C10-2	Avg.	20.1	22.7	23.4	23.2	23.7	23.5
	Std. Dev.	7.63	7.53	7.38	7.38	7.35	8.06
	COV	37.9%	33.2%	31.5%	31.8%	31.0%	34.3%
C10-2 (D)*	Avg.	13.7	16.3	17.2	16.9	17.2	16.4
	Std. Dev.	1.70	2.41	2.31	1.92	1.78	1.90
	COV	12.3%	14.8%	13.4%	11.4%	10.4%	11.6%
C10-2 (L)*	Avg.	26.5	29.1	29.7	29.5	30.3	30.6
	Std. Dev.	4.99	4.22	4.33	4.17	2.69	3.55
	COV	18.9%	14.5%	14.6%	14.1%	8.9%	11.6%
S10-2	Avg.	13.8	16.4	16.3	16.5	16.6	15.9
	Std. Dev.	1.76	2.44	2.04	2.15	2.09	1.71
	COV	12.8%	14.9%	12.5%	13.0%	12.6%	10.7%

\* = Modified averages, which include only the assumed dead end (D) or assumed live end (L) transfer length values

Conversion: 1 in. = 25.4 mm

**Table 5.9 – Standard and Modified Length Averages (Top Strands)**

Top Strands		1 Day (in.)	4 Day (in.)	8 Day (in.)	14 Day (in.)	28 Day (in.)	~56 Day (in.)
C6-4	Avg.	24.8	N/A	27.5	27.6	28.9	26.3
	Std. Dev.	9.25	N/A	3.63	4.98	4.15	N/A
	COV	37.4%	N/A	13.2%	18.0%	14.4%	N/A
S6-4	Avg.	18.2	21.8	22.2	21.1	20.1	22.4
	Std. Dev.	3.26	4.15	0.55	1.50	1.20	0.58
	COV	17.9%	19.0%	2.5%	7.1%	6.0%	2.6%
C10-4	Avg.	17.0	17.2	17.7	17.5	19.0	20.3
	Std. Dev.	2.08	2.95	2.19	2.22	3.59	1.80
	COV	12.2%	17.1%	12.3%	12.7%	18.9%	8.9%
S10-4	Avg.	19.3	17.0	18.6	19.0	18.3	19.5
	Std. Dev.	5.86	3.63	6.50	6.02	6.52	6.46
	COV	30.3%	21.4%	35.0%	31.7%	35.6%	33.1%
S10-4 (D)*	Avg.	16.5	15.6	15.4	16.0	15.1	16.3
	Std. Dev.	2.22	2.80	1.54	1.39	1.35	1.63
	COV	13.4%	18.0%	10.0%	8.6%	8.9%	10.0%
S10-4 (L)*	Avg.	27.7	21.2	28.1	27.9	28.0	29.0
	Std. Dev.	-	-	-	-	-	-
	COV	-	-	-	-	-	-

\* = Modified averages, which include only the assumed dead end (D) or assumed live end (L) transfer length values

Conversion: 1 in. = 25.4 mm

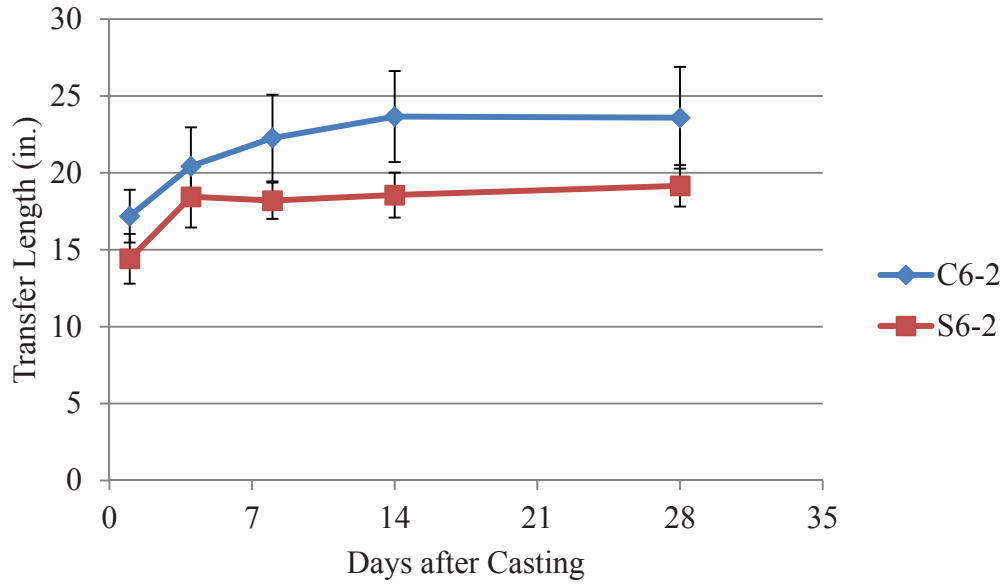
**5.3.1.1 Comparison of SCC to Conventional Concrete.** In order to determine if the average transfer lengths were statistically different between conventional concrete and SCC, the 90% confidence interval for each mix at each day from 1-28 days was calculated, and then average transfer lengths of mixes were plotted against each other with error bars at each point representing the 90% confidence intervals. Points with overlapping error bars showed the average transfer lengths for those two mixes at a given time after casting were not statistically different. This process of determining statistical significance is based on the data analysis performed by Staton, Do, Ruiz, and Hale in a similar study on transfer length (2009). It should be noted that in the following comparisons, the transfer length averages at approximately 56 days were not included in

the evaluation because the transfer lengths were determined between 48 and 57 days after casting depending on when the four-point flexural testing was completed, so averages were not directly comparable.

The bottom strands in normal strength conventional concrete and SCC mixes (C6-2 and S6-2) are compared in **Figure 5.15**, and the high strength conventional and SCC mixes (C10-2 and C10-2 (D) and S10) are compared in **Figure 5.16** and **5.17**. In **Figure 5.15**, although C6-2 appears to have had higher average transfer lengths, the 90% confidence interval error bars overlap in all cases except at 14 days, meaning that there was really no difference in bottom transfer lengths in normal strength conventional concrete versus SCC. Although there is no overlap at 14 days, the gap is so narrow, that it can be assumed there was no statistical difference at 14 days as well.

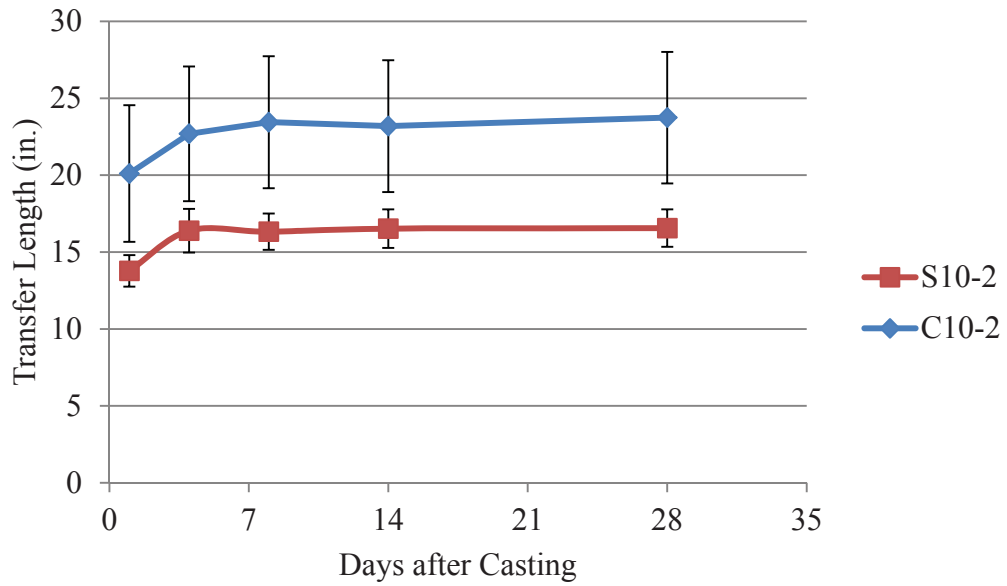
On the other hand, **Figure 5.16** appears to show there was a statistical difference between the high strength conventional concrete and SCC bottom strand transfer lengths, with C10-2 having the longer transfer lengths. However, the 90% confidence intervals for the C10 mix are very large due to the inclusion of the possible live end transfer lengths. C10-2 (D) is the average of the four possible dead end transfer lengths, and when C10-2 (D) average transfer lengths are compared to the S10-2 average transfer lengths in **Figure 5.17**, the values are almost identical and there is no statistical difference. S10-2 average transfer lengths were not compared to the C10-2 (L) because it can be assumed that the S10-2 averages are based on dead end transfer lengths, so comparing the S10-2 averages to the live end C10-2 averages would not be a valid comparison.

Overall, the statistical analysis shows that for bottom strands, there was no statistical difference between transfer lengths in conventional concrete and SCC at both normal strength and high strength levels up to 28 days after casting. However, this was only true when the perceived live end transfer lengths were removed from the averages. A summary of the bottom strand transfer lengths from this research for each conventional concrete vs. SCC comparison is presented in **Table 5.10**. Shaded pairs indicate a statistical difference between the averages.



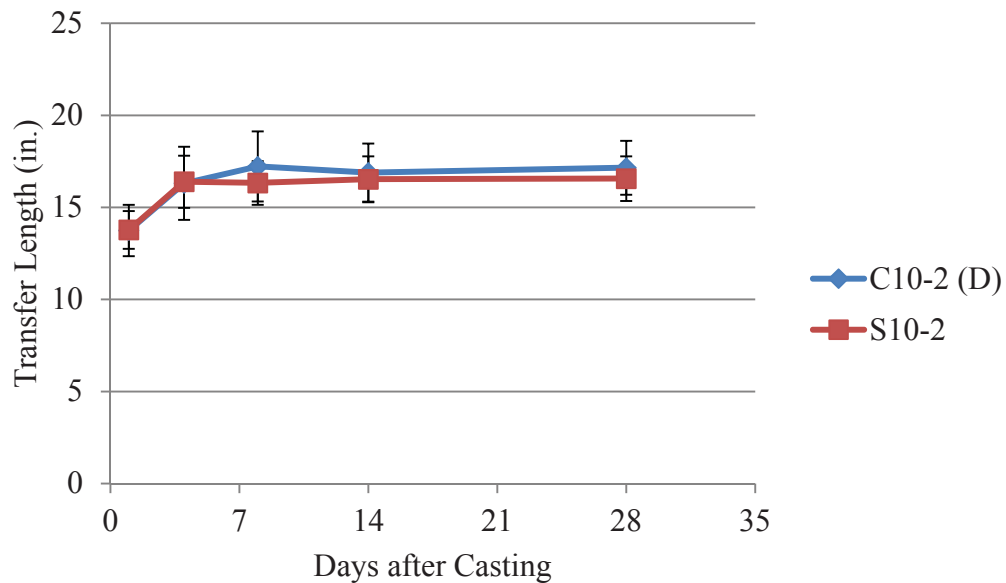
Conversion: 1 in. = 25.4 mm

**Figure 5.15 – C6-2 and S6-2 Transfer Lengths with 90% Confidence Intervals**



Conversion: 1 in. = 25.4 mm

**Figure 5.16 – C10-2 and S10-2 Transfer Lengths with 90% Confidence Intervals**



Conversion: 1 in. = 25.4 mm

**Figure 5.17 – C10-2 (D) and S10-2 Transfer Lengths with 90% Confidence Intervals**

**Table 5.10 – Conventional Concrete vs. SCC: Summary of Statistical Differences Between Bottom Strand Transfer Lengths**

Combination	1 Day (in.)	4 Day (in.)	8 Day (in.)	14 Day (in.)	28 Day (in.)
C6-2	17.2	20.4	22.3	23.7	23.6
S6-2	14.4	18.4	18.2	18.6	19.2
C10-2	20.1	22.7	23.4	23.2	23.7
S10-2	13.8	16.4	16.3	16.5	16.6
C10-2 (D)	13.7	16.3	17.2	16.9	17.2
S10-2	13.8	16.4	16.3	16.5	16.6

\*Shaded pairs indicate statistical difference between values (90% CI)

Conversion: 1 in. = 25.4 mm

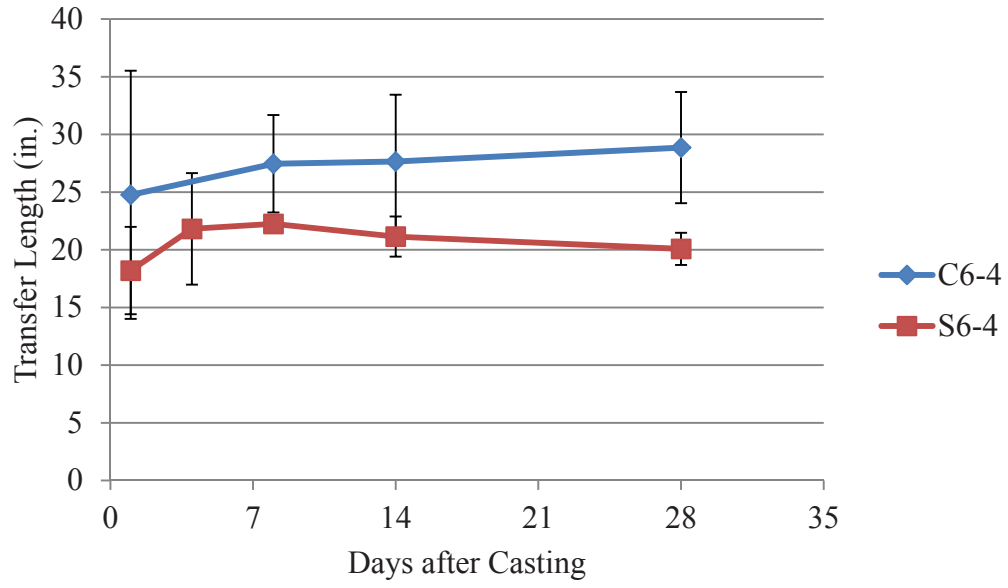
The same statistical analysis between transfer lengths in conventional concrete and SCC at the normal and high compressive strength levels was completed for the top strands as well. However, since only one four strand beam was constructed per mix,

averages for top strand transfer lengths were based on only four readings, and in many instances, the DEMEC readings resulted in unreasonable plots where transfer lengths could not be determined. In the cases of the C6-4 and S6-4 beams, the average top strand transfer lengths and standard deviations were only based on two readings each. The top strands in normal strength conventional concrete and SCC mixes (C6-4 and S6-4) are compared in **Figure 5.18**, and the high strength conventional and SCC mixes [C10-4 and S10-4 and S10-4 (D)] are compared in **Figures 5.19** and **5.20**.

**Figure 5.18** shows overlap of the 90% confidence interval error bars for all days except 28 days for the C6 and S6 mixes. However, these averages and standard deviations for the top strand for these mixes were only based on two readings each, so although the plot indicates that top strand transfer lengths in the normal strength conventional and SCC mixes were generally not statistically different, this conclusion is based on limited data.

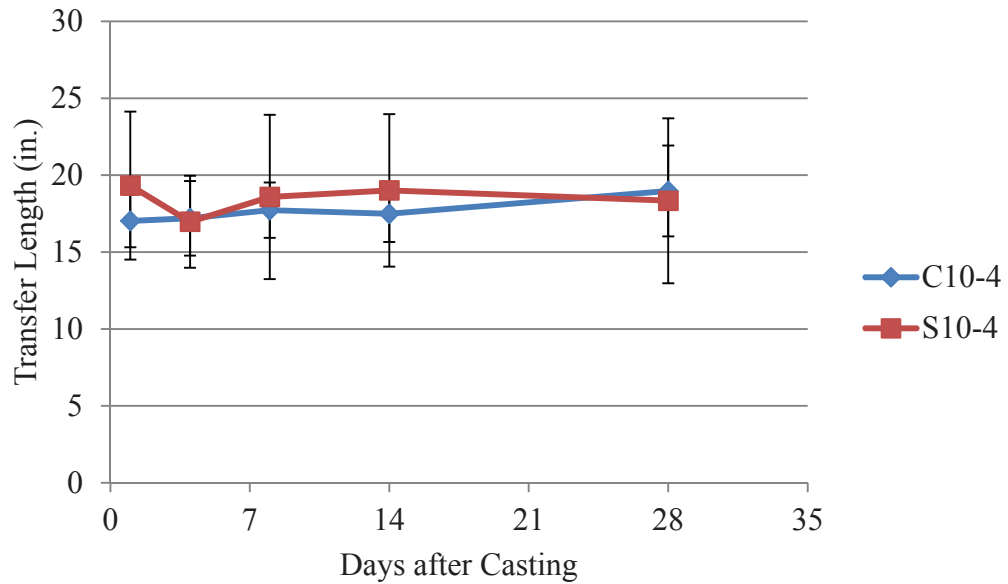
In terms of the transfer lengths of top strands in the high strength mixes, the C10-4 transfer lengths are compared to the full S10-4 averages in **Figure 5.19** and then compared to the S10-4 (D) averages in **Figure 5.20**. The 90% confidence intervals overlap in both cases, indicating that there was no difference in top strand transfer lengths in high strength conventional concrete or high strength SCC.

SCC top strand transfer lengths were generally shorter than the conventional concrete top strand transfer lengths, but only a few statistical differences were seen between transfer lengths in the normal strength mixes, and none were seen between either combination of the high strength conventional concrete and SCC averages. A summary of the top strand transfer lengths for each conventional concrete vs. SCC comparison is presented in **Table 5.11**. Shaded pairs indicate a statistical difference between the averages.



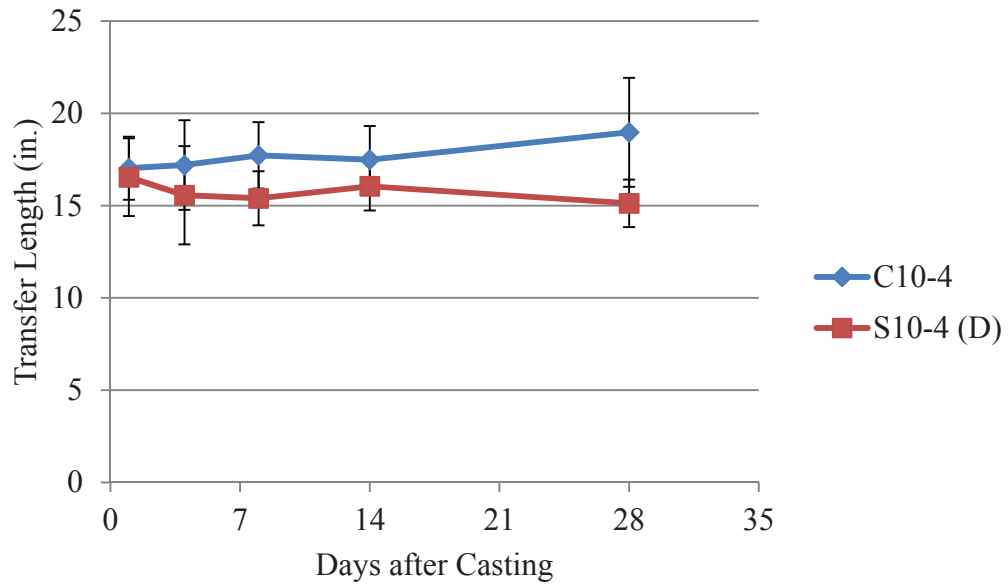
Conversion: 1 in. = 25.4 mm

**Figure 5.18 – C6-4 and S6-4 Transfer Lengths with 90% Confidence Intervals**



Conversion: 1 in. = 25.4 mm

**Figure 5.19 – C10-4 and S10-4 Transfer Lengths with 90% Confidence Intervals**



Conversion: 1 in. = 25.4 mm

**Figure 5.20 – C10-4 and S10-4 (D) Transfer Lengths and 90% Confidence Intervals**

**Table 5.11 – Conventional Concrete vs. SCC: Summary of Statistical Differences Between Top Strand Transfer Lengths**

Combination	1 Day (in.)	4 Day (in.)	8 Day (in.)	14 Day (in.)	28 Day (in.)
C6-4	24.8	N/A	27.5	27.6	28.9
S6-4	18.2	21.8	22.2	21.1	20.1
C10-4	17.0	17.2	17.7	17.5	19.0
S10-4	19.3	17.0	18.6	19.0	18.3
C10-4	17.0	17.2	17.7	17.5	19.0
S10-4 (D)	16.5	15.6	15.4	16.0	15.1

\*Shaded pairs indicate statistical difference between values (90% CI)

Conversion: 1 in. = 25.4 mm

Overall, the results show that there was no significant difference between transfer lengths measured in conventional concrete and SCC of the same strength level from one to 28 days after casting. The plots compare C6 to S6 transfer lengths and C10 to S10 transfer lengths for both top and bottom strands and with the full and modified averages

that include or do not include the possible live end transfer lengths, and although the plots generally show the SCC average transfer lengths were shorter than conventional concrete average transfer lengths, the 90% confidence interval error bars overlap in almost all cases, rendering the differences in transfer lengths statistically insignificant.

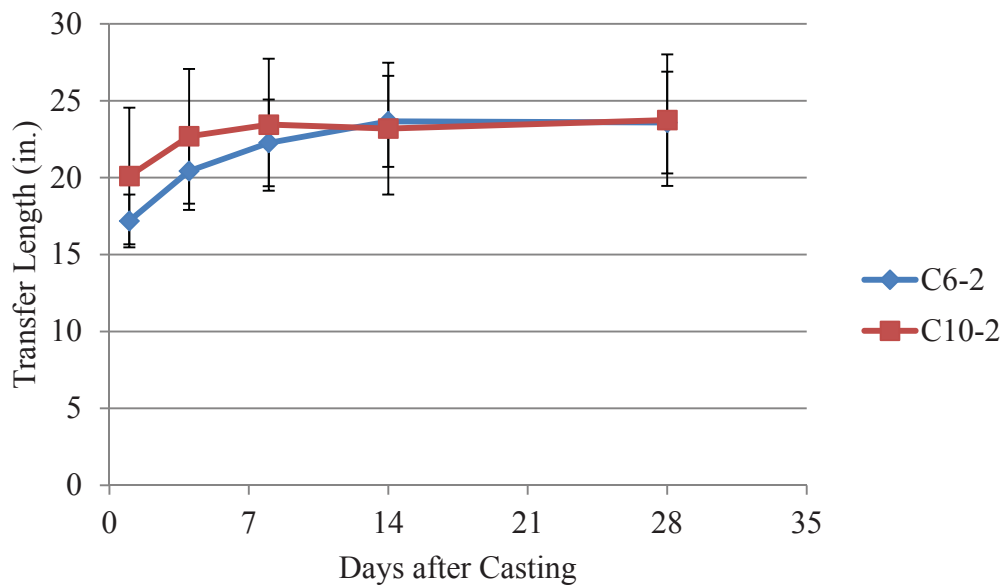
Although some previous studies have shown SCC transfer lengths being longer than those in conventional concrete (Girgis and Tuan 2005 and Burgueño 2007), the results from this research matched findings from Staton et al. (2009) and Boehm et al. (2010), who both reported no overall significant difference between SCC and conventional concrete. It should be noted that these previous studies only evaluated bottom strand.

**5.3.1.2 Comparison of Normal Strength to High Strength.** The top and bottom transfer length values were also analyzed to determine the degree to which concrete strength affects transfer length. The bottom strands in normal strength conventional concrete and high strength conventional concrete [C6-2 and C10-2 and C10-2 (D)] are compared in **Figure 5.21** and **5.22**, and the normal and high strength SCC mixes (S6-2 and S10-2) are compared in **Figure 5.23**.

**Figure 5.21** shows that there is significant overlap of the 90% confidence interval error bars at all days, so it appears there was no difference between the normal strength and high strength conventional concrete mixes (C6-2 and C10-2). However, when C6-2 average transfer lengths were compared to the averages of the dead end transfer lengths of the high strength conventional concrete [C10-2 (D)] transfer lengths, the transfer lengths in the higher strength concrete were notably shorter than the transfer lengths in the normal strength concrete. **Figure 5.22** shows that the 90% error bars do not overlap for the C6-2 and C10-2 (D), so this implies when the live end transfer lengths were removed, there was a statistical difference between the transfer lengths in normal and high strength conventional concretes.

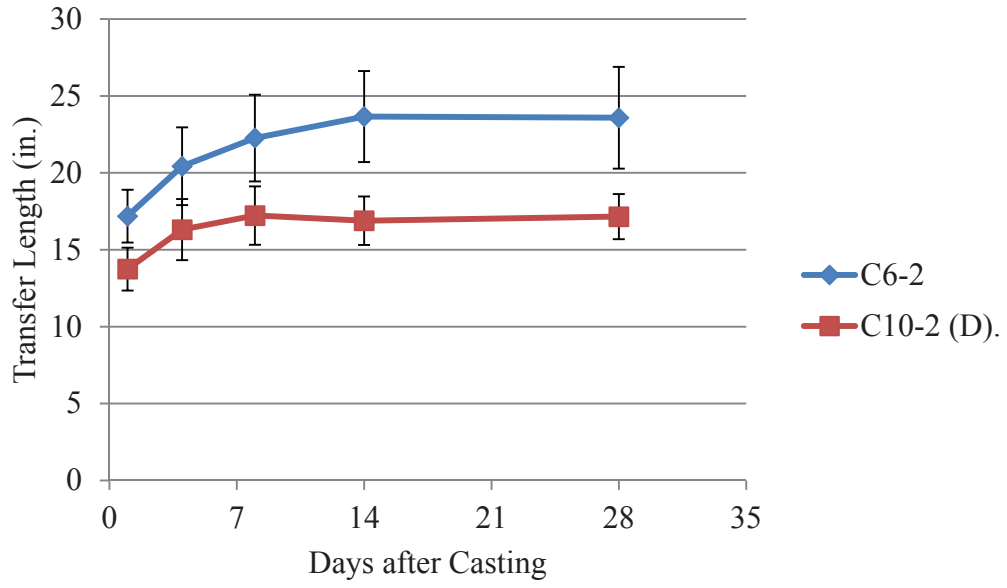
**Figure 5.23** shows that the S10-2 transfer lengths appear to be slightly shorter than the S6-2 transfer lengths, but the 90% confidence interval error bars overlap, so according to the data, there was no statistical difference between bottom strand transfer lengths in normal strength and high strength SCC.

Overall, the statistical analysis shows that for bottom strands, an increase in compressive strength resulted in shorter transfer lengths for conventional concrete, especially when the live end transfer lengths were removed from the averages. However, concrete strength did not appear to significantly influence transfer lengths in SCC. A summary of the bottom strand transfer lengths for each normal strength to high strength comparison is presented in **Table 5.12**. Shaded pairs indicate a statistical difference between the averages.



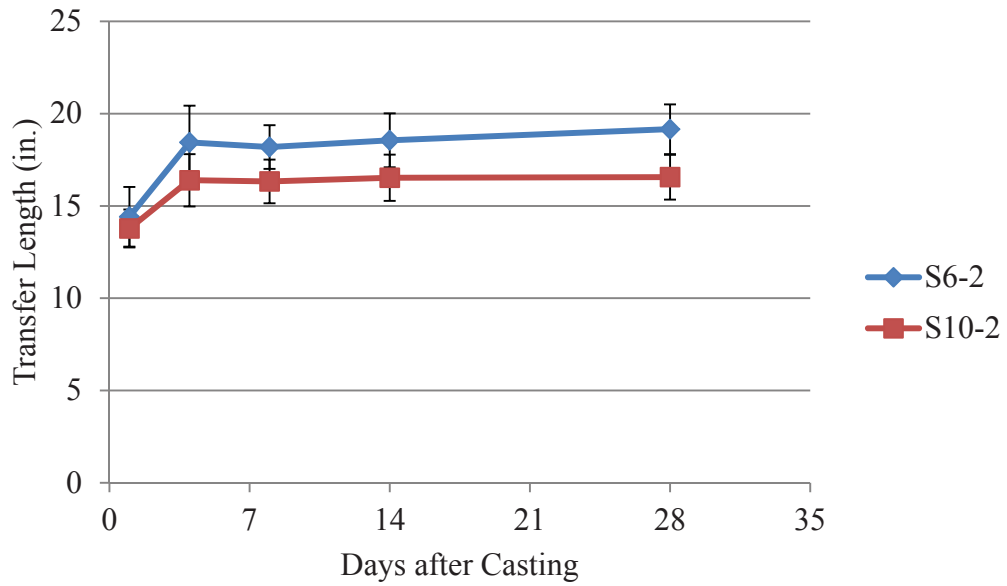
Conversion: 1 in. = 25.4 mm

**Figure 5.21 – C6-2 and C10-2 Transfer Lengths and 90% Confidence Intervals**



Conversion: 1 in. = 25.4 mm

**Figure 5.22 – C6-2 and C10-2 (D) Transfer Lengths and 90% Confidence Intervals**



Conversion: 1 in. = 25.4 mm

**Figure 5.23 – S6-2 and S10-2 Transfer Lengths and 90% Confidence Intervals**

**Table 5.12 – Normal Strength vs. High Strength: Summary of Statistical Differences Between Bottom Strand Transfer Lengths**

Combination	1 Day (in.)	4 Day (in.)	8 Day (in.)	14 Day (in.)	28 Day (in.)
C6-2	17.2	20.4	22.3	23.7	23.6
C10-2	20.1	22.7	23.4	23.2	23.7
C6-2	17.2	20.4	22.3	23.7	23.6
C10-2 (D)	13.7	16.3	17.2	16.9	17.2
S6-2	14.4	18.4	18.2	18.6	19.2
S10-2	13.8	16.4	16.3	16.5	16.6

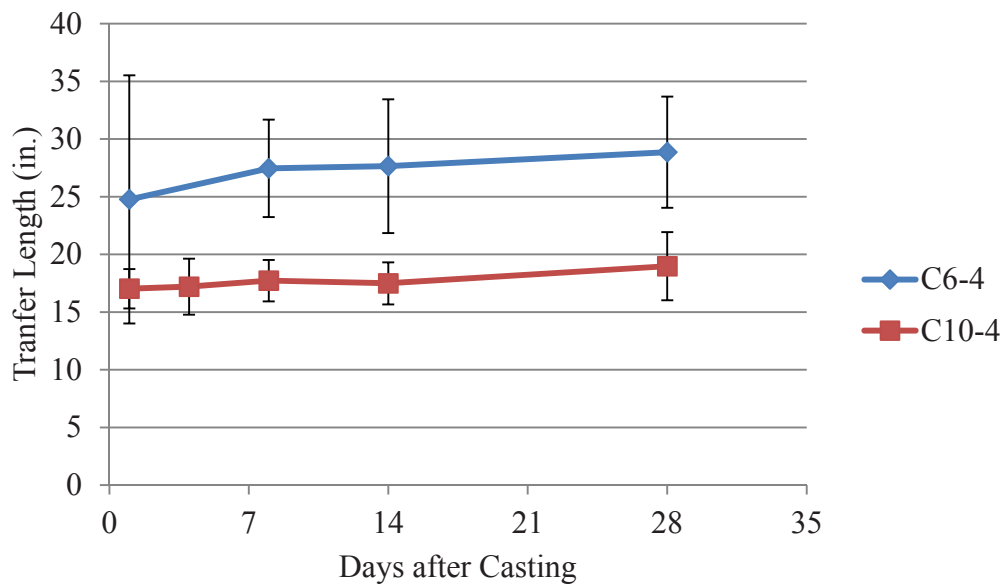
\*Shaded pairs indicate statistical difference between values (90% CI)  
Conversion: 1 in. = 25.4 mm

In terms of the effect of concrete strength on top strand transfer lengths, the 90% confidence interval error bars in **Figure 5.24** show that the top strand transfer lengths in the high strength conventional concrete were generally shorter than the top strand transfer lengths in the normal strength conventional concrete. There does not appear to be a statistical difference between the one day transfer lengths, but the 90% confidence interval for C6-4 was fairly large, measuring 10.7 in. (272 mm) above and below the average. Also, the C6-4 average transfer lengths were only based on two values for each day. The transfer lengths in the normal strength conventional concrete did appear to be consistently longer than the transfer lengths in the high strength conventional concrete; however it should be noted that this conclusion is based on limited data.

The top strand transfer lengths in the normal strength and high strength SCC mixes are compared in **Figure 5.25** and **5.26**. **Figure 5.25** shows no statistical difference between the S6-4 and full average of S10-4 transfer lengths. However, when the normal strength SCC transfer lengths are compared to the average dead end high strength SCC transfer lengths in **Figure 5.26**, this plot indicates that there was no statistical difference at 1 and 4 days, but the S10-4 (D) transfer lengths seemed to be generally shorter than the S6-4 transfer lengths at later ages.

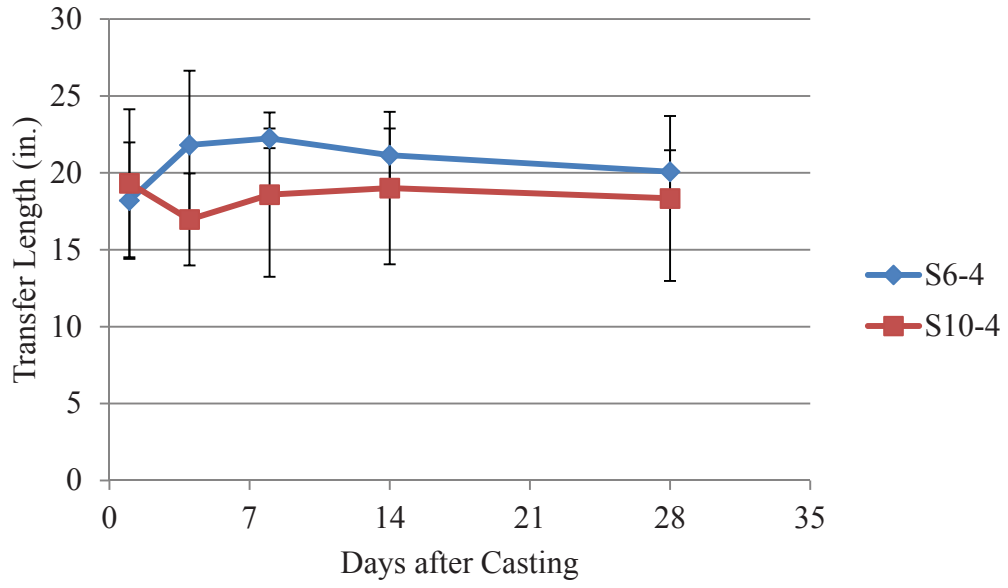
For the top strands in this research program, the increase in concrete strength in conventional concrete generally resulted in shorter transfer lengths, although it should be

noted that the C6-4 average values were only based on two readings. In SCC, when the possible live end was removed from the S10-4 data, the increase in concrete strength also appeared to shorten top strand transfer lengths, specifically at later ages. A summary of the top strand transfer lengths for each normal strength to high strength comparison is presented in **Table 5.13**. Shaded pairs indicate a statistical difference between the averages.



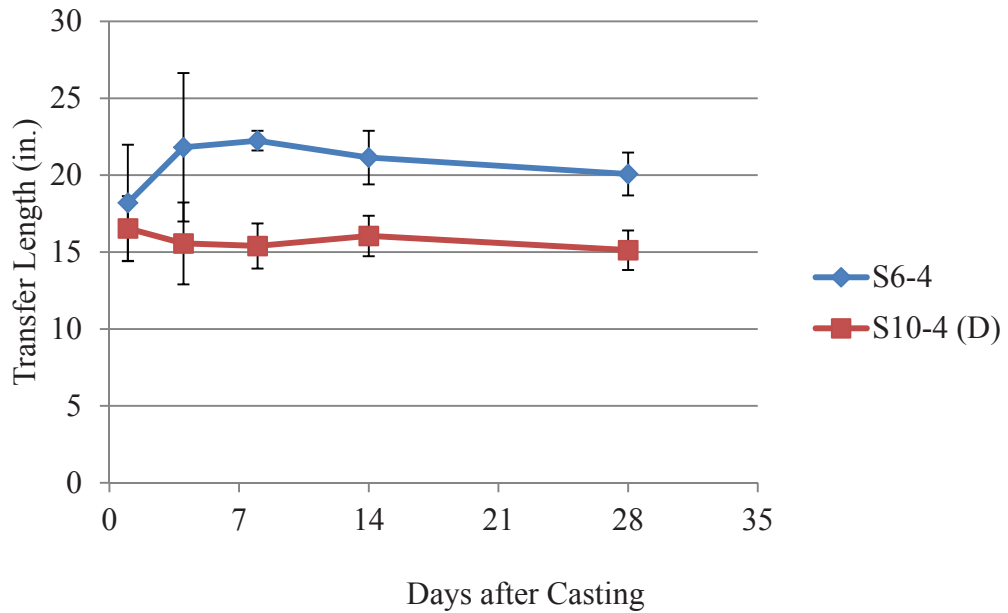
Conversion: 1 in. = 25.4 mm

**Figure 5.24 – C6-4 and C10-4 Transfer Lengths and 90% Confidence Intervals**



Conversion: 1 in. = 25.4 mm

**Figure 5.25 – S6-4 and S10-4 Transfer Lengths and 90% Confidence Intervals**



Conversion: 1 in. = 25.4 mm

**Figure 5.26 – S6-4 and S10-4 (D) Transfer Lengths and 90% Confidence Intervals**

**Table 5.13 – Normal Strength vs. High Strength: Summary of Statistical Differences Between Top Strand Transfer Lengths**

Combination	1 Day (in.)	4 Day (in.)	8 Day (in.)	14 Day (in.)	28 Day (in.)
C6-4	24.8	N/A	27.5	27.6	28.9
C10-4	17.0	17.2	17.7	17.5	19.0
S6-4	18.2	21.8	22.2	21.1	20.1
S10-4	19.3	17.0	18.6	19.0	18.3
S6-4	18.2	21.8	22.2	21.1	20.1
S10-4 (D)	16.5	15.6	15.4	16.0	15.1

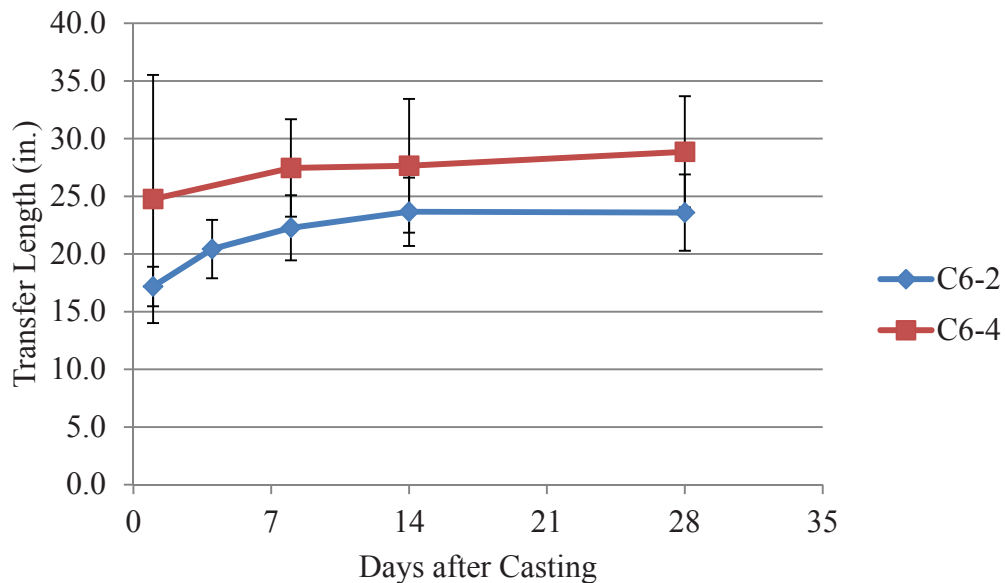
\*Shaded pairs indicate statistical difference between values (90% CI)  
Conversion: 1 in. = 25.4 mm

Except for the bottom strands in SCC, all comparisons of normal to high strength concretes showed decreased transfer lengths at higher strengths when the live end values were removed from the averages. For the top strands, this was especially true for 8 to 28 days.

As discussed in **Section 2.4.3**, the idea of transfer length being inversely proportional to concrete strength has been shown by many previous researchers. Mitchell et al. (1993), Lane (1998), Ramirez and Russell (2008), and others have all noted the effect of concrete strength, and except for the bottom strands in SCC, this research mostly upheld the previous findings.

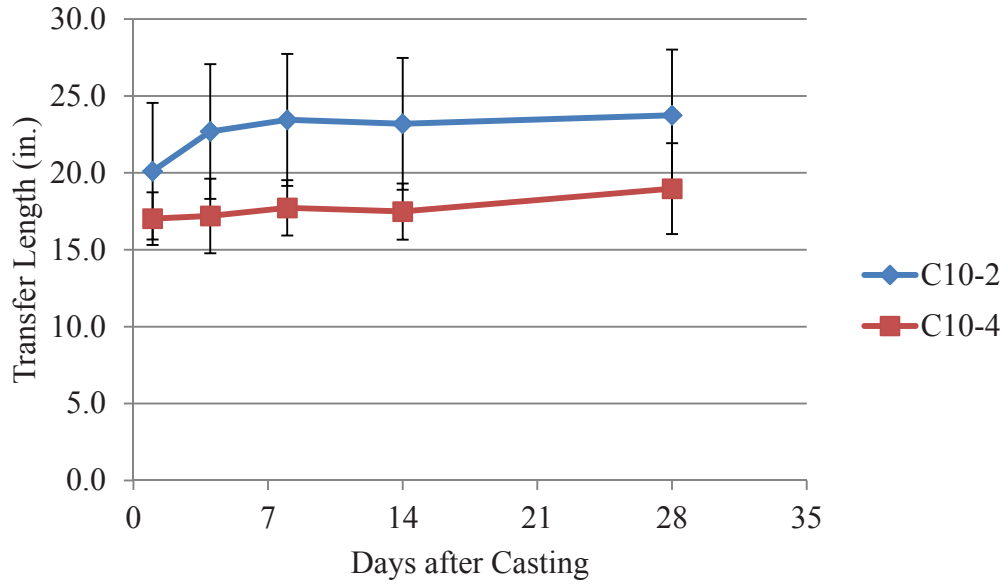
**5.3.1.3 Comparison of Bottom Strand to Top Strand.** For each mix, bottom strand transfer lengths were compared to top strand transfer lengths to determine if significant differences existed. Previous research has indicated that top strands have the potential for longer transfer lengths than bottom strands due to bleed water and air collecting under the top strands and reduced consolidation at the top of a member, thus reducing bond (Peterman 2007, Wan et al. 2002). The same 90% confidence interval approach that was used to compare conventional concrete to SCC and normal strength to high strength was used to evaluate statistically significant differences between top and bottom strand transfer lengths. Top and bottom strand transfer lengths for each mix from 1 to 28 days are plotted in **Figures 5.27-5.32**.

**Figures 5.27-5.29** examine the top and bottom strands in conventional concrete. **Figure 5.27** compares the top and bottom strand transfer lengths in the normal strength conventional concrete, while **Figures 5.28** and **5.29** compare the high strength full and dead end bottom strand averages to the top strand averages. **Figures 5.27** and **5.29** show that the top strand transfer length averages were higher than the bottom strand averages, but the 90% confidence interval error bars overlap in all cases except when comparing C10-2 (D) to C10-4 at one day (**Figure 5.29**). Although the error bars overlap in **Figure 5.28** as well, **Figure 5.28** actually indicates in high strength conventional concrete, the average bottom strand transfer lengths (C10-2) were actually longer than the average top strand transfer lengths (C10-4); however, the C10-2 averages include the possible live ends, which would make the averages much higher. Aside from this one anomaly, the comparison of top strand transfer lengths to bottom strand transfer lengths did not appear to show any statistically significant differences in either normal or high strength conventional concrete.



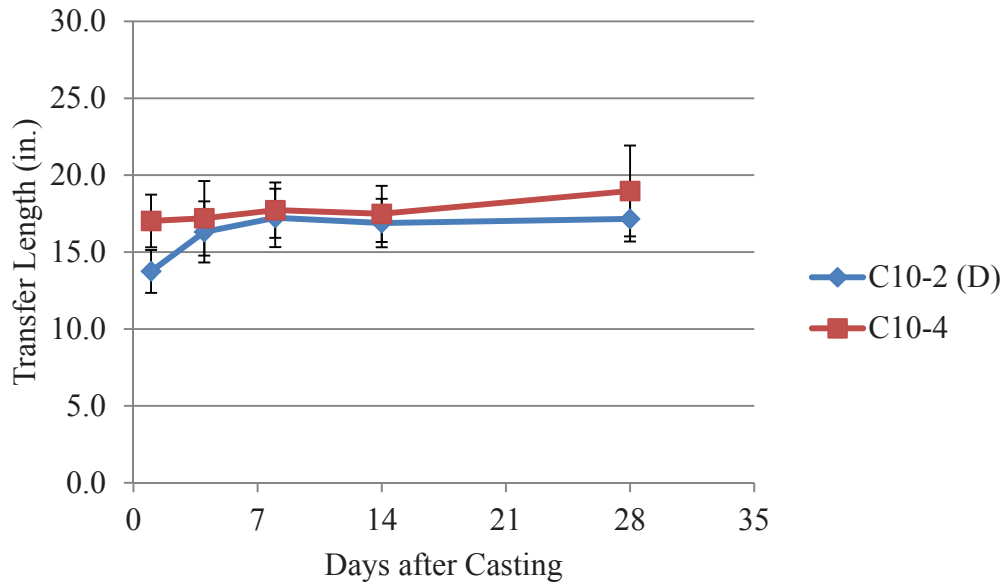
Conversion: 1 in. = 25.4 mm

**Figure 5.27 – C6-2 and C6-4 Transfer Lengths and 90% Confidence Intervals**



Conversion: 1 in. = 25.4 mm

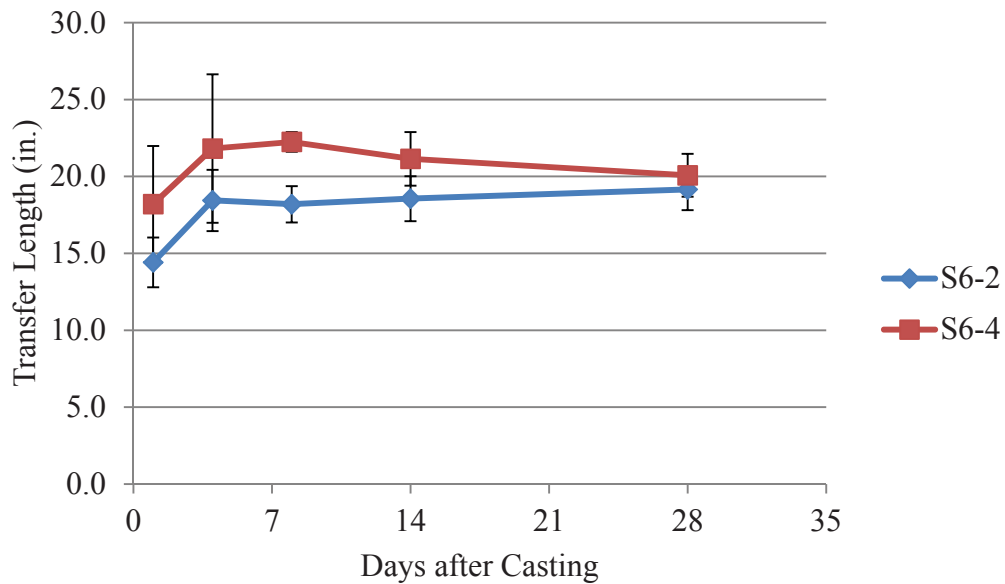
**Figure 5.28 – C10-2 and C10-4 Transfer Lengths and 90% Confidence Intervals**



Conversion: 1 in. = 25.4 mm

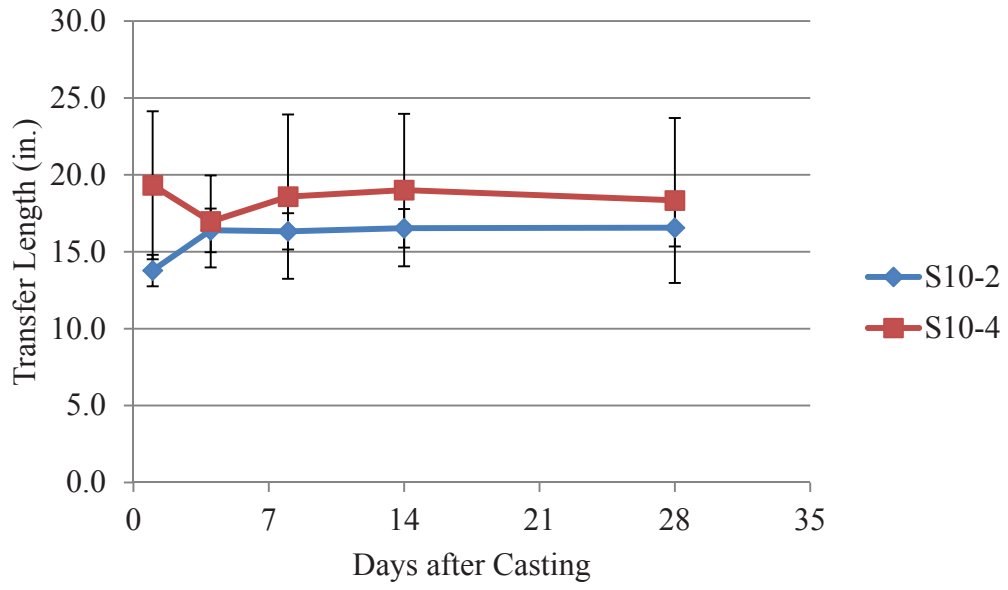
**Figure 5.29 – C10-2 (D) and C10-4 Transfer Lengths and 90% Confidence Intervals**

**Figures 5.30-5.32** examine the top and bottom strands in SCC. **Figure 5.30** compares the top and bottom strand transfer lengths in the normal strength SCC, while **Figure 5.31** and **5.32** compare the high strength SCC bottom strand averages to the full and dead end top strand averages. **Figures 5.30** and **5.31** show the top strand transfer length averages were higher than the bottom strand averages, but the 90% confidence interval error bars overlap in all cases except when comparing S6-2 to S6-4 at 8 days. For the high strength SCC, when the possible live end was removed from the average top strand transfer length, the transfer lengths appear to be almost identical (**Figure 5.32**). As was seen with the conventional concrete, aside from one anomaly, almost no statistically significant differences were seen between top and bottom strands in either normal or high strength SCC.



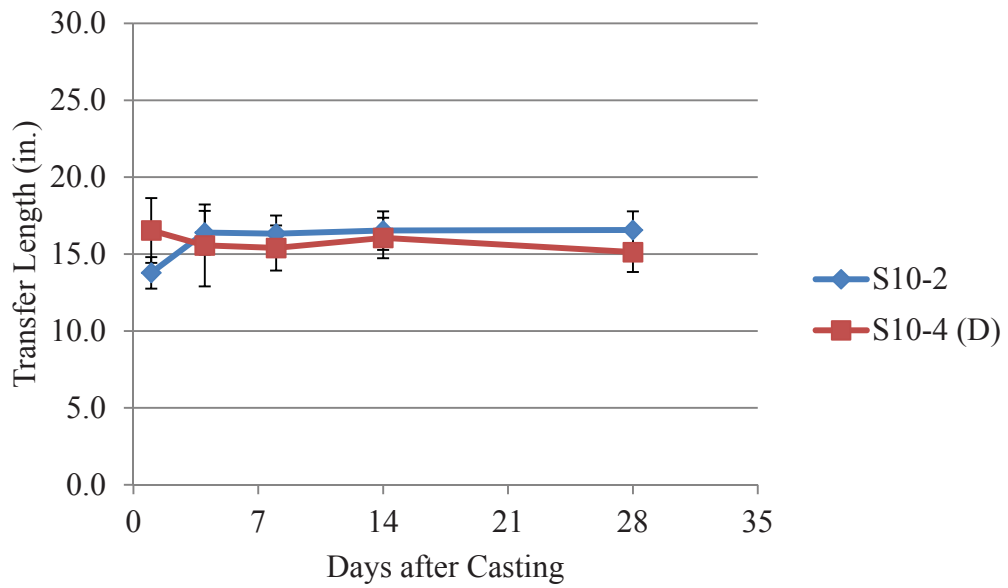
Conversion: 1 in. = 25.4 mm

**Figure 5.30 – S6-2 and S6-4 Transfer Lengths and 90% Confidence Intervals**



Conversion: 1 in. = 25.4 mm

**Figure 5.31 – S10-2 and S10-4 Transfer Lengths and 90% Confidence Intervals**



Conversion: 1 in. = 25.4 mm

**Figure 5.32 – S10-2 and S10-4 (D) Transfer Lengths and 90% Confidence Intervals**

Overall, the top strands generally had longer transfer lengths based on straight averages, but analysis indicated that there were no trends showing statistically significant differences between transfer lengths in top and bottom strands in the same concrete mix. This does not follow previous research findings. As discussed in **Section 2.4.6**, Wan et al. (2002) and Petrou et al. (2000) both found significantly more slip in top-cast strands compared to bottom-cast strands in piles constructed from conventional concrete. Specifically in terms of SCC, Larson et al. (2007) reported top strand transfer lengths to be 50% longer than bottom strand transfer lengths. However, the top strand transfer lengths in the current study were often longer than those for the bottom strands, especially when live end values were removed from the averages for C10-2, on average 9 to 26% although still within recognized limits of statistical variability.

For this study, a summary of the transfer lengths for each top strand vs. bottom strand comparison for all concrete mixes is presented in **Table 5.14**. Shaded pairs indicate a statistical difference between the averages, and the lack of shaded pairs indicates that in this research, there was no trend indicating top strand transfer lengths were longer than bottom strand transfer lengths.

**5.3.1.4 Change in Transfer Length over Time.** As discussed in **Section 2.4.4**, numerous previous research studies dating back to Kaar, LaFraugh, and Mass (1963) have shown transfer lengths increasing over time, so the data from this study was analyzed to see if the same trend was observed. The percent increases in transfer lengths for top and bottom strands in each mix are presented in **Table 5.15**. The increases are broken down into initial increases, or the percent increases from 1 to 4 days, and additional increases, or the percent increases from 4 to 28 days, and total increases, or the full percent increases from 1 to 28 days. Negative percent increases indicate the transfer lengths actually decreased.

**Table 5.14 – Top Strand vs. Bottom Strand: Summary of Statistical Differences  
Between Transfer Lengths**

Combination	1 Day (in.)	4 Day (in.)	8 Day (in.)	14 Day (in.)	28 Day (in.)
C6-2	17.2	20.4	22.3	23.7	23.6
C6-4	24.8	N/A	27.5	27.6	28.9
C10-2	20.1	22.7	23.4	23.2	23.7
C10-4	17.0	17.2	17.7	17.5	19.0
C10-2 (D)	13.7	16.3	17.2	16.9	17.2
C10-4	17.0	17.2	17.7	17.5	19.0
S6-2	14.4	18.4	18.2	18.6	19.2
S6-4	18.2	21.8	22.2	21.1	20.1
S10-2	13.8	16.4	16.3	16.5	16.6
S10-4	19.3	17.0	18.6	19.0	18.3
S10-2	13.8	16.4	16.3	16.5	16.6
S10-4 (D)	16.5	15.6	15.4	16.0	15.1

\*Shaded pairs indicate statistical difference between values (90% CI)  
Conversion: 1 in. = 25.4 mm

**Table 5.15 – Summary of Increases in Transfer Lengths**

Mix ID	Initial Increase (1 Day to 4 Days)	Additional Increase (4 Days to 28 Days)	Total Increase (1 Day to 28 Days)
C6-2	18.9%	15.4%	37.3%
S6-2	28.0%	3.9%	32.9%
C10-2	12.8%	4.6%	18.1%
C10-2 (D)	18.7%	5.2%	24.8%
C10-2 (L)	9.8%	4.3%	14.5%
S10-2	19.0%	1.0%	20.2%
C6-4	N/A	N/A	16.5%
S6-4	19.9%	-8.0%	10.3%
C10-4	1.0%	10.3%	11.5%
S10-4	-12.2%	8.0%	-5.1%
S10-4 (D)	-5.9%	-2.8%	-8.6%
S10-4 (L)	-23.4%	31.9%	1.1%

The bottom strands did show increases in transfer length over time between 1 and 28 days after casting, with total increases ranging from a minimum of 14.5% for C10-2 (L) to a maximum of 37.3% for C6-2. Generally, most of the increase occurred within the first four days, and then the rate of increase appeared to slow significantly from 4 to 28 days. The normal strength mixes appeared to show higher percent increases than the high strength mixes, but no definitive conclusion could be established regarding the performance of conventional concrete to SCC.

The top strands were much more inconsistent. The SCC mixes actually showed decreases in some cases. S6-4 had a decrease from 4 to 28 days, while all combinations of S10-4 transfer length averages showed an initial decrease, and S10-4 and S10-4 (D) also had overall decreases in averages. C6-4 did not have a 4-day average, so the total increase could not be broken down into initial and additional increases. C10-4 had very little initial increase and saw most of the increase occur between 4 and 28 days, which is opposite of what was generally seen in the bottom strands. In conclusion, the top strand transfer lengths did not always increase, and the increases that were seen were generally not as large as the increases that were observed in the bottom strand transfer lengths.

When the increases in bottom strand transfer lengths from this study are compared to results found by recent studies, the 14.5%-37.3% increases are consistent with what has been observed by other researchers. Over 28 days, Staton et al. (2009) observed 8% growth for SCC transfer lengths and 12% growth for high strength conventional concrete transfer lengths. Also, Boehm et al. (2010) reported 28% increases in SCC transfer lengths over 3 months with 38% increases in conventional concrete transfer lengths for the same period. Finally, increases of 10-20% were seen in the bottom strands of SCC beams 21 days after casting in the study conducted by Larson et al. (2007). The only study that assessed increases in top strand transfer lengths was Larson et al. (2007). In that study, increases of 40-45% were seen in the top strand transfer lengths, but the results regarding increases in top strand transfer lengths reported in this report were inconclusive.

#### **5.3.1.5 Comparison to AASHTO and ACI Equations for Transfer Length.**

After the transfer length averages were compared to each other to determine the effects of concrete type, concrete strength, and strand location, the averages were then compared

to values determined by the AASHTO and ACI equations to ensure the measured values did not exceed the calculated design values. The AASHTO and ACI transfer length equations were presented and discussed in **Section 2.5** of this report; however, they are repeated here for clarity and convenience.

The AASHTO equation for transfer length is given by **Eq. 5.1**, where  $l_t$  is the transfer length in inches and  $d_b$  is the nominal diameter of the strand in inches. For a 0.5-in.-diameter (12.7 mm) strand,  $l_t$  as calculated by the AASHTO equation is equal to 30 in. (762 mm).

$$l_t = 60d_b \quad (5.1)$$

ACI 318-11 presents two equations for transfer length: a general equation and an equation that is used when determining whether a reduced stress in the strand needs to be accounted for when designing for shear near the end of a member. The general ACI transfer length equation that is given in Section 12.9 of the ACI 318-11 code is shown here as equation **Eq. 5.2**, where  $l_t$  is the transfer length in inches,  $f_{se}$  is the effective stress in the prestressing strand after losses in psi and  $d_b$  is the nominal diameter of the strand in inches. Typical values for  $f_{se}$  range from 60 – 65% of  $f_{pu}$  depending on the conditions of stressing and losses. In terms of comparison, it was determined that a lower  $f_{se}$  value ( $0.6f_{pu}$ ) should be used, so the calculated transfer length would be shorter and more conservative for comparison. Assuming 20% final losses, the 28-day transfer length calculated by **Eq. 5.2** would equal 27 in. (686 mm).

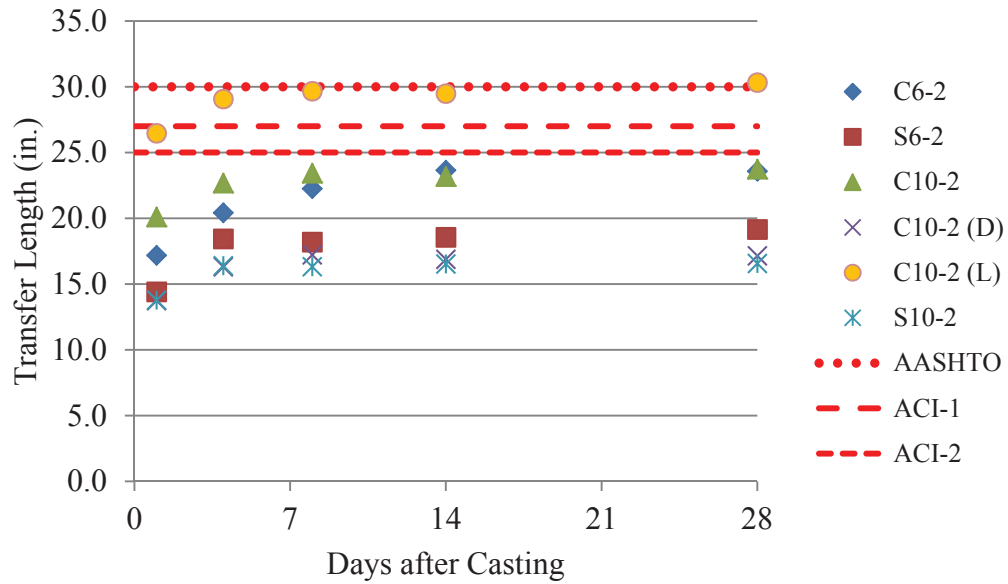
$$l_t = \left( \frac{f_{se}}{3000} \right) d_b \quad (5.2)$$

The transfer length equation for shear design from Section 11.3.4 of ACI 318-11 is presented in **Eq. 5.3**, where  $l_t$  is the transfer length in inches and  $d_b$  is the nominal strand diameter in inches. For a 0.5-in.-diameter (12.7 mm) strand, this transfer length would equal 25 in. (635 mm).

$$l_t = 50d_b \quad (5.3)$$

The full average transfer lengths as well as the possible live and dead end averages for each mix are plotted and compared to the values calculated from the AASHTO and two ACI equations for transfer length in **Figures 5.33** and **5.34**. **Figure 5.33** contains the average values for the bottom strands while **Figure 5.34** displays the results for the top strands. Each plot contains horizontal lines indicating the transfer length value calculated by each code equation, and the legend labels the values as AASHTO, ACI-1, and ACI-2. AASHTO corresponds to the 30 in. (762 mm) value calculated by **Eq. 5.1**, ACI-1 represents the 27 in. (686 mm) value determined from **Eq. 5.2**, and ACI-2 is equal to 25 in. (635 mm), as calculated from **Eq. 5.3**. Additionally, **Tables 5.16** and **5.17** compare the ratios of the calculated AASHTO and ACI values to the average transfer length 28 days after casting for each mix for the bottom and top strands, respectively. In **Tables 5.16** and **5.17**, a value greater than one indicates that the transfer length calculated from the code equation exceeded the average measured transfer length.

As seen in **Figure 5.33**, the bottom strands in almost all mixes had average transfer lengths falling below values calculated from all equations. The exception was the possible average live end transfer lengths measured in the C10 mix. The average C10-2 (L) transfer lengths were greater than the transfer lengths predicted by the shear ACI equation (**Eq. 5.3**) at one day and both ACI equations at 4, 8 and 14 days. The average transfer length at 28 days for C10-2 (L) was 11% greater than the value calculated by ACI-1 and 18% greater than ACI-2 (**Table 5.16**). The AASHTO equation was conservative for the C10-2 (L) average transfer lengths up to 28 days, where the measured transfer length, which barely exceeded the limit. The code equations applied to the SCC mixes appeared to be more conservative than when applied to the conventional concrete mixes, but as discussed, statistical analysis showed the differences between averages were not statistically significant.



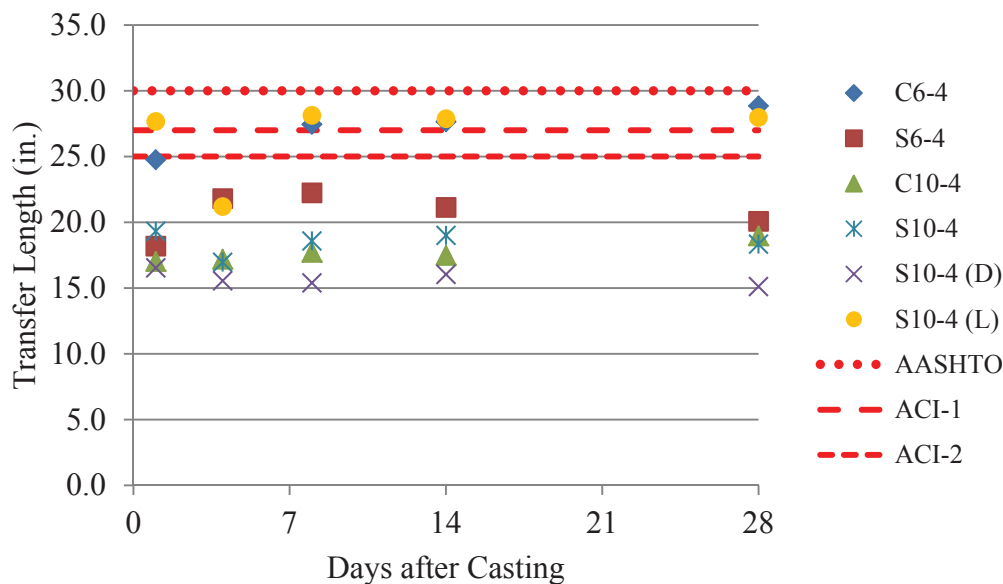
Conversion: 1 in. = 25.4 mm

**Figure 5.33 – Average Transfer Lengths Compared to AASHTO and ACI Equations (Bottom Strands)**

**Table 5.16 – Ratio of Average Transfer Lengths to AASHTO and ACI Values (Bottom Strands)**

	28 Day Avg. (in.)	AASHTO/Avg. (AASHTO = 30 in.)	ACI-1/Avg. (ACI-1 = 27 in.)	ACI-2/Avg. (ACI-2 = 25 in.)
C6-2	23.6	1.27	1.14	1.06
CS6-2	19.2	1.57	1.41	1.31
C10-2	23.7	1.26	1.14	1.05
C10-2 (D)	17.2	1.75	1.57	1.46
C10-2 (L)	30.3	0.99	0.89	0.82
S10-2	16.6	1.81	1.63	1.51

Conversion: 1 in. = 25.4 mm



Conversion: 1 in. = 25.4 mm

**Figure 5.34 – Average Transfer Lengths Compared to AASHTO and ACI Equations (Top Strands)**

**Table 5.17 – Ratio of Average Transfer Lengths to AASHTO and ACI Values (Top Strands)**

	28 Day Avg. (in.)	AASHTO/Avg. (AASHTO = 30 in.)	ACI-1/Avg. (ACI-1 = 27 in.)	ACI-2/Avg. (ACI-2 = 25 in.)
C6-4	28.9	1.04	0.94	0.87
S6-4	20.1	1.49	1.34	1.25
C10-4	19.0	1.58	1.42	1.32
S10-4	18.3	1.64	1.47	1.36
S10-4 (D)	15.1	1.98	1.79	1.65
S10-4 (L)	28.0	1.07	0.97	0.89

Conversion: 1 in. = 25.4 mm

In terms of the average top strand transfer lengths, **Figure 5.34** shows a similar trend, with the equations being conservative in most cases. One exception was again the possible live end transfer length, which was greater than the values computed by both ACI equations at all days except day 4. However, the normal strength conventional

concrete also had average transfer lengths exceeding both ACI limits at 8, 14, and 28 days. The 28-day average for C6-4 exceeded the ACI-1 and ACI-2 limits by 3% and 11%, respectively (**Table 5.17**). The AASHTO equation once again proved to be conservative for all mixes.

Other studies have also found the AASHTO and ACI transfer length equations to be largely conservative for SCC as well as conventional concrete. Pozolo and Andrawes (2011) found SCC bottom transfer lengths to be on average 86% below  $50d_b$ , 72% lower than  $60d_b$ , and 69% under  $f_{pe}d_b/3$ , while Staton et al. (2009) found SCC transfer lengths to be 60% below  $f_{pe}d_b/3$  as well. Larson et al. (2007) and Boehm et al. (2010) also found the equations to be conservative for bottom strands and adequate to use with SCC and conventional concrete. However, in terms of top strands, Larson et al. (2007) found top strand transfer lengths in SCC to be 60% longer than predicted by  $50d_b$ . Here, C6-4 averages were the only top strand averages to exceed the ACI code limit.

**5.3.2. Discussion of Initial End Slip Transfer Length Results.** Initial transfer lengths were determined by measuring end slips of the strands at release through both electronic and manual means, as discussed in **Sections 4.4.2.1** and **4.4.2.2**. The transfer lengths determined from the end slips measured by both methods are discussed in this subsection, but overall, the transfer lengths determined by the initial end slips were abandoned because they were deemed unreliable and imprecise compared to the 1 day results determined from the DEMEC readings and the 95% Average Mean Strain Method.

In terms of the end slips measured by the Synergy data acquisition, the gauges that were used in this research program proved to be highly unreliable. The release method appeared to be too violent, and the potentiometers consistently separated from the base plates or slipped on the strands, as discussed in **Section 4.4.2.1**. The potentiometers were attached to 32 bottom transfer length locations, and only 16 potentiometers yielded what were deemed valid end slips, for a success rate of 50%. The potentiometers were also attached to 10 top transfer length locations, and the potentiometers were unable to yield any readable data from any of these locations. Therefore, for the 42 locations where the potentiometers were installed to collect data, the potentiometers only registered a valid reading 16 times, for a total success rate of only 38%. Also, for the steel rulers, the

measurements could only be taken to the nearest  $1/32$ -in. (0.79 mm), so precision was a limiting factor.

In light of the unreliability of the potentiometers and the imprecision of the steel ruler measurements, the transfer lengths determined from the 95% Average Mean Strain Method were deemed to be the most consistent and were the transfer lengths that were used for all comparisons of the transfer lengths in the different mixes as well as all comparisons to AASHTO and ACI predicted values. Still, for the sake of comparison, the transfer lengths determined from the Synergy data and steel ruler end slip measurements are compared to the transfer lengths determined from the 95% Average Mean Strain Method in **Tables 5.18** and **5.19**. The tables show the average, standard deviation and the number of readings the average and standard deviation were based on for each method as well as the percent difference between the transfer length from the Synergy or steel ruler data to the transfer length determined from the DEMEC points and 95% Average Mean Strain Method. **Table 5.18** contains the comparisons for all bottom strand data, and **Table 5.19** contains the comparisons for the top strand data. Although the mixes are labeled with “2” to denote the two strand beams, and consequently the bottom strands, ruler and Synergy data were also taken on bottom strands of the four-strand beams and are included in the averages and standard deviations for the bottom strands.

**Table 5.18** shows that for the bottom strands, some of the average Synergy transfer lengths were actually very similar to the DEMEC transfer lengths. The S6 transfer lengths have only a 0.36% difference between averages, but it should be noted that the Synergy average is based on only two values. The Synergy and DEMEC transfer lengths for C10-2 (D) were also very close for this comparison, with only 0.66% difference. Generally all of the Synergy transfer lengths were less than the DEMEC transfer lengths.

The percent differences between the ruler and DEMEC transfer lengths ranged from slightly over 4% to over 76%. The precision for the method was low, which meant that the standard deviations for the transfer lengths for all mixes was high, ranging from around 5 in. (127 mm) to 8.5 in. (216 mm). Overall, correlation between the transfer lengths determined by the steel ruler end slip measurements to the DEMEC transfer lengths was very low, and although there were some isolated instances of steel ruler

transfer lengths matching up well to the DEMEC transfer lengths, large differences generally existed between transfer lengths determined by these two methods as well.

Several studies have also measured transfer length through end slips as well as DEMEC readings in conjunction with the 95% Average Mean Strain Method. These studies, including Rose and Russell (1997), Ramirez and Russell (2008), and Boehm et al. (2010), found the transfer lengths calculated from end slips to match fairly well with the transfer lengths determined from DEMEC readings. Unlike these studies, the results in this report did not show a correlation between transfer lengths calculated with the two methods, but this can most likely be attributed to the shortcomings of the methods of end slip data collection in this research program.

All transfer lengths determined by both end slip methods are reported in this report, but all values were essentially disregarded in terms of analysis. Only the transfer lengths determined by the 95% Average Mean Strain Method were used for comparative analyses.

**Table 5.18 – Comparison of Synergy-DEMEC and Ruler-DEMEC Transfer Lengths (Bottom Strands)**

Bottom Strands		Synergy-DEMEC Comparison			Ruler-DEMEC Comparison		
		Synergy (in.)	DEMEC (in.)	% Diff.	Ruler (in.)	DEMEC (in.)	% Diff.
C6-2	Avg.	7.9	17.2	73.48%	17.9	17.2	4.10%
	Std. Dev.	1.08	2.76		8.01	2.76	
	n	4	7		11	7	
S6-2	Avg.	14.5	14.4	0.36%	13.8	14.4	4.10%
	Std. Dev.	0.20	2.61		7.34	2.61	
	n	2	7		11	7	
C10-2	Avg.	13.7	20.1	38.24%	9.0	20.1	76.79%
	Std. Dev.	4.60	7.63		8.17	7.63	
	n	3	8		10	8	
C10-2 (D)	Avg.	13.7	13.7	0.66%	9.5	13.7	36.40%
	Std. Dev.	4.60	1.70		8.44	1.70	
	n	3	4		8	4	
C10-2 (L)	Avg.	N/A	26.5	N/A	6.7	26.5	119.3%
	Std. Dev.	N/A	4.99		9.49	4.99	
	n	0	4		2	4	
S10-2	Avg.	10.2	13.8	29.57%	16.6	13.8	18.33%
	Std. Dev.	6.82	1.76		5.19	1.76	
	n	7	8		10	8	

Conversion: 1 in. = 25.4 mm

**Table 5.19 – Comparison of Synergy-DEMEC and Ruler-DEMEC Transfer Lengths (Top Strands)**

Top Strands		Synergy-DEMEC Comparison			Ruler-DEMEC Comparison		
		Synergy (in.)	DEMEC (in.)	% Diff.	Ruler (in.)	DEMEC (in.)	% Diff.
C6-4	Avg.	N/A	24.8	N/A	22.4	24.8	10.11%
	Std. Dev.	N/A	9.25		5.17	9.25	
	n	0	2		4	2	
S6-4	Avg.	N/A	18.2	N/A	17.9	18.2	1.63%
	Std. Dev.	N/A	3.26		7.31	3.26	
	n	0	2		4	2	
C10-4	Avg.	N/A	17.0	N/A	9.0	17.0	62.16%
	Std. Dev.	N/A	2.08		3.65	2.08	
	n	0	4		4	4	
S10-4	Avg.	N/A	19.3	N/A	7.8	19.3	84.63%
	Std. Dev.	N/A	5.86		7.64	5.86	
	n	0	4		4	4	
S10-4 (D)	Avg.	N/A	16.5	N/A	7.5	16.5	75.67%
	Std. Dev.	N/A	2.22		9.32	2.22	
	n	0	3		3	3	
S10-4 (L)	Avg.	N/A	27.7	N/A	9.0	27.7	-
	Std. Dev.	N/A	-		-	-	
	n	0	1		1	1	

Conversion: 1 in. = 25.4 mm

**5.3.3. Correlation of NASP Test in Concrete Results to 95% Average Mean Strain Transfer Lengths.** While results from this study indicated that concrete type (conventional concrete vs. SCC) did not appear to affect transfer lengths, concrete strength did seem to have an effect. The results from this study generally indicated that an increase in concrete strength resulted in lower transfer lengths, which follows the trends of previous research, as discussed in **Section 2.4.3**. Specifically, Ramirez and Russell (2008) studied the effect of concrete strength on transfer length in an NCHRP study, and based on the results, they proposed new equations for transfer length and development

length, which both incorporate concrete strength as a parameter. The data from this current independent study were compared to the results presented in NCHRP Report 603.

Ramirez and Russell (2008) analyzed pullout loads from the standard NASP test in mortar and modified NASP test in concrete and transfer lengths measured in rectangular and I-beams for three strand types, A, B, and D. The modified NASP in concrete specimens and the beam specimens used for measuring transfer lengths were constructed from conventional concrete with a range of compressive strengths. From the NASP in concrete results, they noted that for each strand type, the pullout load increased as concrete strength increased, and the pullout load increase was proportional to the square root of the concrete compressive strength. The NASP in concrete values were normalized by dividing the NASP in concrete pullout load by the appropriate standard NASP in mortar pullout load for each strand, and then the ratios were plotted against the concrete compressive strength (ksi), as seen in **Figure 5.35**. The NASP in concrete normalized by NASP in mortar value vs.  $f'_c$  confirmed the observation that the bond performance is related to the square root of  $f'_c$ , yielding a power trend line equation with an exponent of close to 0.5 (**Eq. 5.4**).

$$\frac{NASP_{concrete}}{NASP} = 0.49139x^{0.51702} \quad (5.4)$$

Based on this result, NASP in concrete pullout load normalized by the NASP in mortar pullout load ( $NASP_{conc}/NASP$ ) was then plotted against the square root of the compressive strength at one day (ksi), as seen in **Figure 5.36**. This relationship showed a rather strong linear correlation, with an  $R^2$  value of 0.79. From this plot, a relationship between bond performance and concrete compressive strength was derived and is shown in **Eq. 5.5**.

$$\frac{NASP_{concrete}}{NASP} = 0.51\sqrt{f'_{ci}} \quad (5.5)$$

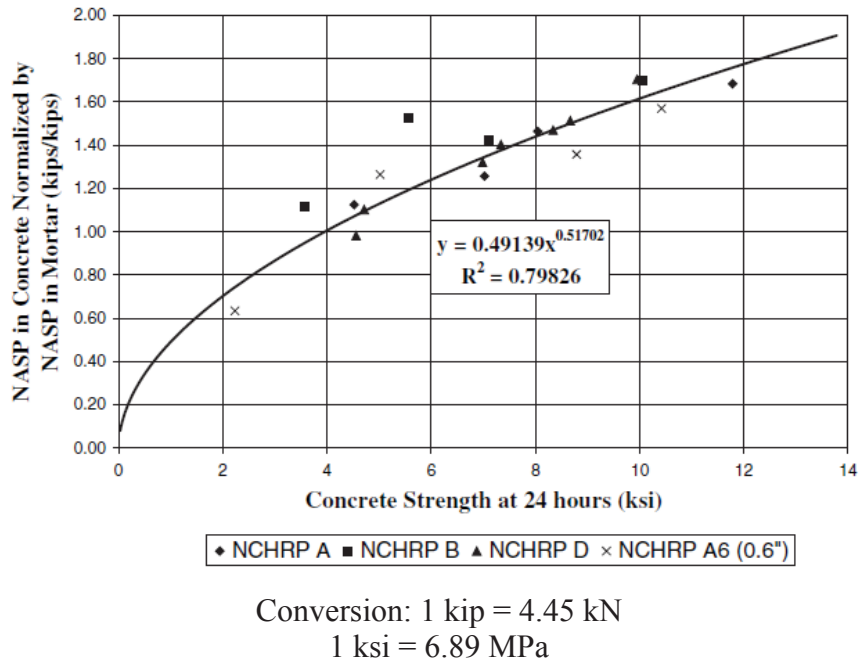


**Figure 5.35 – NCHRP Normalized NASP Pull-out Values vs. Concrete Strength (Ramirez and Russell 2008)**

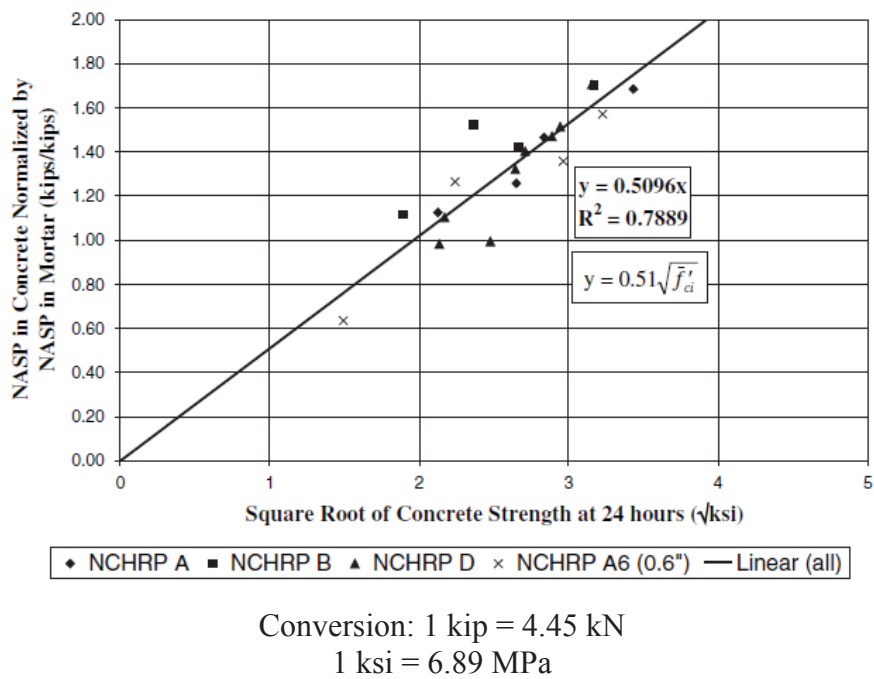
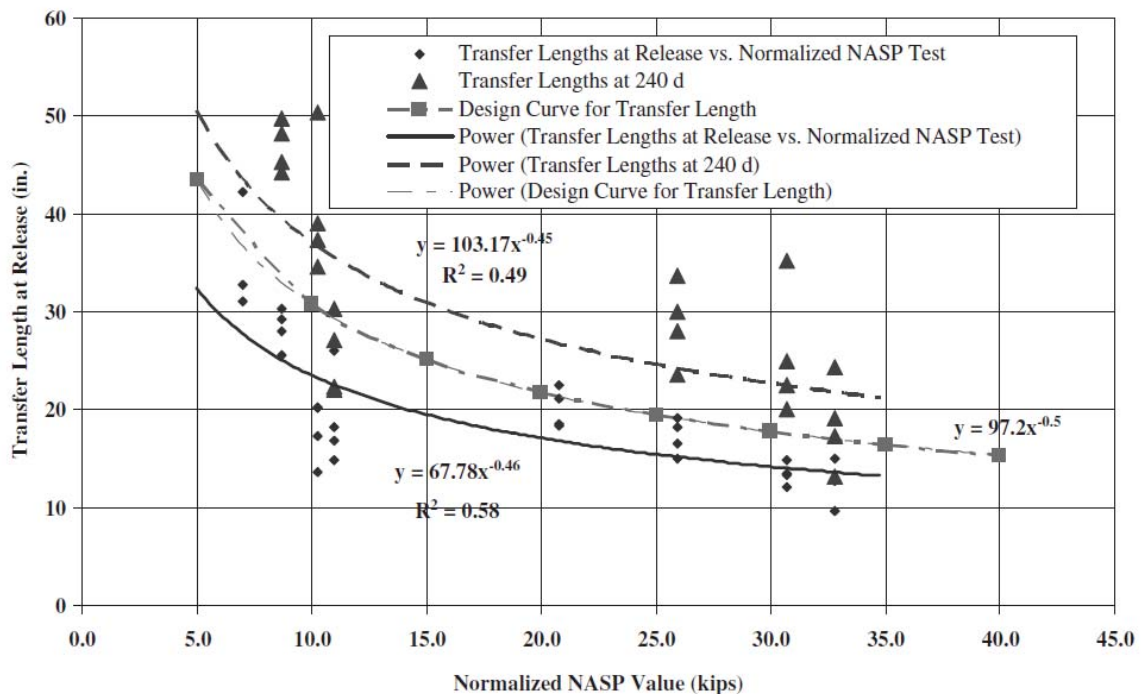


**Figure 5.36 – NCHRP Normalized NASP Pull-out Values vs.  $\sqrt{f'_c}$  (Ramirez and Russell 2008)**

From this relationship, it can be said that the ratio of the NASP in concrete pullout value to the NASP in mortar value is approximately equal to one half the square root of the concrete compressive strength at 1 day in ksi. Thus, the equation was rearranged, and the normalized NASP value was calculated using **Eq. 5.6**, where  $f'_{ci}$  is the one day compressive strength (ksi) and NASP is the average pullout load determined from the standard NASP in mortar test (k).

$$\text{Normalized NASP Value} = 0.5 \sqrt{f'_{ci}} (\text{NASP}) \quad (5.6)$$

Transfer length was then plotted against the normalized NASP value. This relationship is displayed in **Figure 5.37**, effectively relating concrete strength, standard NASP test in mortar pullout value, and transfer length.



Conversion: 1 kip = 4.45 kN

1 in. = 25.4 mm

**Figure 5.37 – NCHRP Transfer Lengths vs. Normalized NASP Bond Values (Ramirez and Russell 2008)**

The results produced by the Missouri S&T research program were compared to the results from the NCHRP study to see if these results followed the same trends that were discovered during the NCHRP program. In this study, only one strand type was used for the construction of the transfer length beams (strand type 101), but two standard NASP tests in mortar were run on this strand type, resulting in two different NASP pullout values. Therefore, results from this program were determined using the NASP pullout loads from tests completed with both mortar mixes, N-101-A (NASP<sub>A</sub>) and N-101-B (NASP<sub>B</sub>), and both sets of results were presented and compared to the NCHRP results.

The applicable data from this research program that is used for the comparison of Missouri S&T's results to the NCHRP research is summarized in **Table 5.20**. The one day compressive strength, square root of the one day compressive strength, and pullout value from the modified NASP in concrete tests are presented for each mix. Also, the standard NASP in mortar values for both the tests completed in mortar Mix A (NASP<sub>A</sub>) and Mix B (NASP<sub>B</sub>) are presented along with the ratios of the NASP in concrete and NASP in mortar pullout loads.

**Table 5.20 – Summary of Data for Comparison with NCHRP Results**

Mix	$f'_{ci}$ (ksi)	$\sqrt{f'_{ci}}$ ( $\sqrt{\text{ksi}}$ )	NASP <sub>conc</sub> (k)	NASP <sub>A</sub> [N-101-A] (k)	NASP <sub>B</sub> [N-101-B] (k)	NASP <sub>conc</sub> / NASP <sub>A</sub>	NASP <sub>conc</sub> / NASP <sub>B</sub>
C6	4.81	2.19	21.1	21.6	18.2	0.977	1.159
S6	5.66	2.38	23.7	21.6	18.2	1.097	1.302
C10	5.67	2.38	26.7	21.6	18.2	1.234	1.464
S10	6.33	2.52	27.3	21.6	18.2	1.264	1.500

Conversion: 1 kip = 4.45 kN

1 ksi = 6.89 MPa

In order to compare the data from the two research programs, **Figures 5.35, 5.36, and 5.37** were recreated in order for the data from the Missouri S&T research program to be plotted along with the NCHRP data, and these recreated plots are presented in **Figures 5.38, 5.39, and 5.40**. The results from this research are presented with values calculated

using the NASP in mortar pullout load from N-101-A ( $NASP_A$ ) and also using the NASP in mortar pullout load from N-101-B ( $NASP_B$ ). Although all data is included on each figure, it should be noted that the equations and  $R^2$  values displayed on **Figures 5.38-5.40** are calculated based solely on the NCHRP data. **Figure 5.38** plots the relationship of  $NASP_{conc}/NASP$  vs.  $f'_c$ , while **Figure 5.39** shows the relationship of the  $NASP_{conc}/NASP$  ratios and  $\sqrt{f'_c}$ . **Figure 5.40** finally relates concrete compressive strength and NASP pullout loads to transfer length by plotting transfer lengths at release vs. normalized NASP values, as calculated by **Eq. 5.6**. While the original figure in NCHRP Report 603 includes transfer lengths at release and at 240 days, only the data from release as well as the trend line from release is plotted here to have a direct comparison to the transfer lengths measured at release in this research program. This program did not include measuring transfer lengths at 240 days.

For all figures, the trend line equations and  $R^2$  values for just the NCHRP data, the NCHRP data plus the Missouri S&T data with  $NASP_A$ , and the NCHRP data plus the Missouri S&T data with  $NASP_B$  are summarized in **Table 5.21**. This summary shows how close the results from this research program are to the results of the NCHRP research by showing how little the inclusion of different results change the trend line equations and  $R^2$  values.

**Figure 5.38** shows the data from this program appeared to follow the relationship between the  $NASP_{conc}/NASP$  ratios and concrete compressive strength that was established in the NCHRP research. The  $NASP_{conc}/NASP$  ratios calculated with the  $NASP_A$  values appear to match up well with the NCHRP data ( $R^2 = 0.79$ ), and even though the  $NASP_{conc}/NASP$  ratios with  $NASP_B$  values are on the high end of the scatter, the  $R^2$  value for this data combined with the NCHRP data is still 0.74 (**Table 5.21**). This is lower than 0.80, which corresponds to the  $R^2$  value for just the NCHRP results, but 0.74 still indicates a fair correlation. Therefore, it can be concluded that for results calculated with  $NASP_A$  and  $NASP_B$  both fall reasonably within the scatter of the NCHRP results.

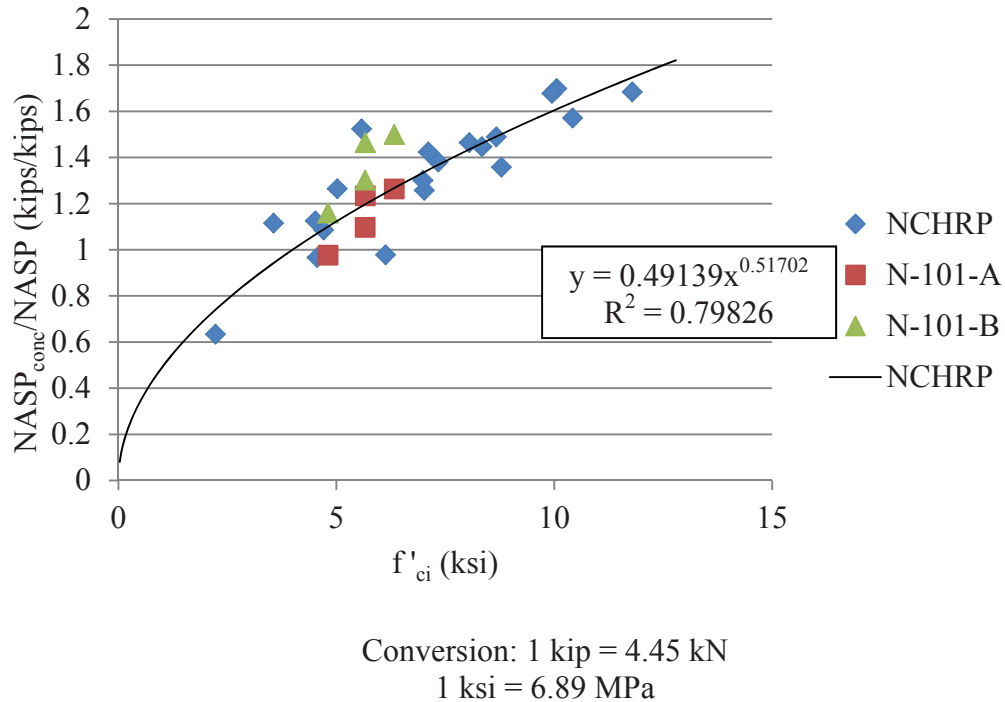


**Figure 5.38 – Normalized NASP in Concrete Pullout Values vs. Concrete Strength (NCHRP and Missouri S&T)**

Plotting the  $NASP_{conc}/NASP$  vs.  $\sqrt{f'_c}$  results from this research program along with the results from the NCHRP program also indicated the results from this program seemed to follow the trend previously established by the NCHRP results (**Figure 5.39**). The NCHRP data alone had an  $R^2$  value of 0.79, and the NCHRP data combined with the  $NASP_A$  Missouri S&T data resulted in an  $R^2$  value of 0.79 as well, while the NCHRP data combined with the  $NASP_B$  Missouri S&T data resulted in an  $R^2$  value of 0.72 (**Table 5.21**). The  $NASP_{conc}/NASP$  results with the  $NASP_A$  value appeared to more closely fit the data from the NCHRP study, but the  $NASP_{conc}/NASP$  ratios with the  $NASP_B$  value were still reasonable, even though they were on the high side of the scatter.

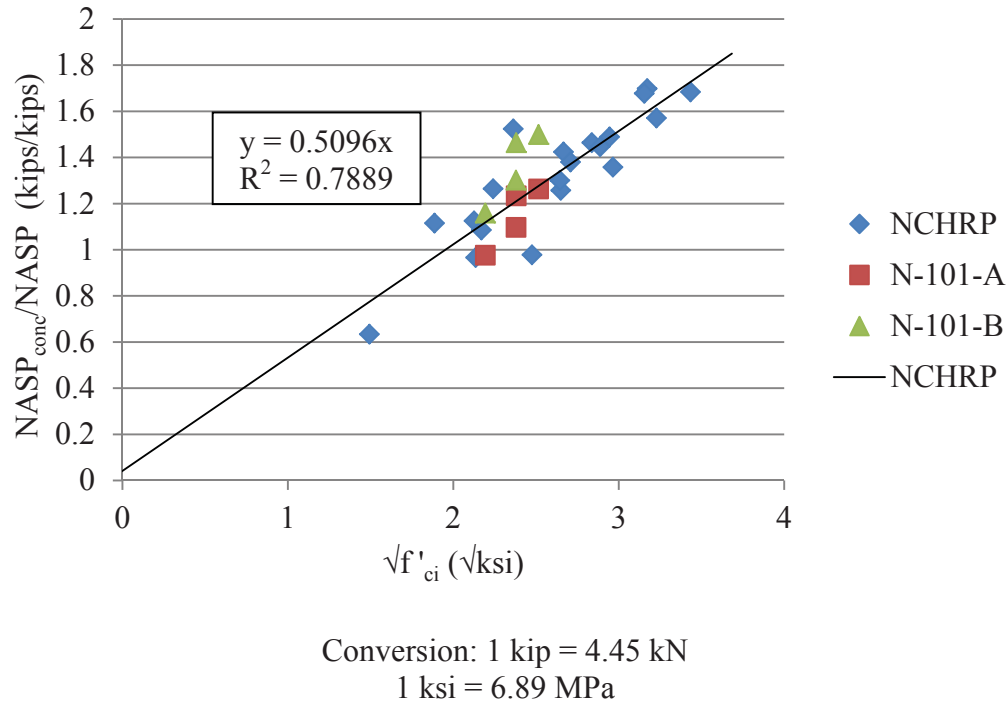


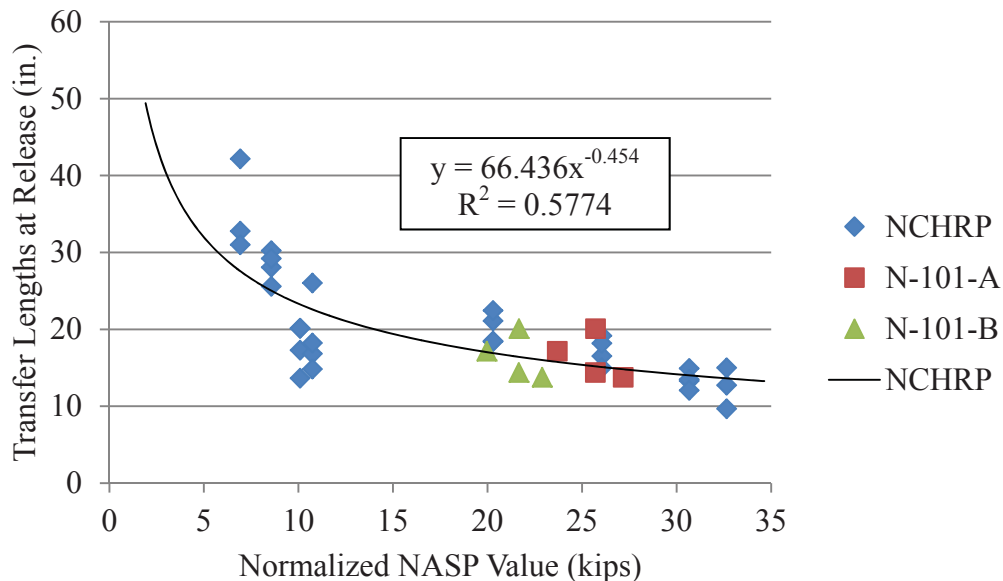
**Figure 5.39 – Normalized NASP in Concrete Pullout Values vs. Square Root of Concrete Strength (NCHRP and Missouri S&T)**

The relationship between bond behavior and the square root of compressive strength that was established by the NCHRP research was supported by the results from this research program. **Figures 5.38** and **5.39** visually indicate that the results from this research project generally fall within the scatter from the NCHRP research, and Table 5.21 shows that the  $R^2$  values from the NCHRP data alone compared to  $R^2$  values from the NCHRP data combined with results from Missouri S&T are relatively close. Because the relationship was validated, it was deemed acceptable to apply the relationship found in **Eq. 5.6** to the Missouri S&T results to calculate a normalized NASP value based on concrete strength and the NASP in mortar values and plot the transfer lengths at release vs. the normalized NASP values from this study along with the values from the NCHRP research (**Figure 5.40**). The NCHRP data did not have an overly strong correlation to begin with, having an  $R^2$  value of 0.58, but the inclusion of the Missouri S&T data based on the  $NASP_A$  or  $NASP_B$  values did not seem to significantly alter the trend line equation or  $R^2$  value, showing the results with either NASP test in mortar pullout load follow the

NCHRP trend. Based on the results, transfer length at release could possibly be predicted by the trend line in **Figure 5.40**, where  $x$  is the value corresponding to one-half of the square root of the concrete strength at release in ksi multiplied by the NASP in mortar pullout load in kips.

Based on the results from the NCHRP study, those researchers proposed a new equation for transfer length for the AASHTO code that incorporates the relationship between concrete compressive strength and transfer length (Ramirez and Russell 2008). The proposed transfer length equation is presented here as **Eq. 5.7**, where  $f'_{ci}$  is the concrete compressive strength at release in ksi and  $d_b$  is the nominal diameter of the strand in inches. The equation results in a transfer length of  $60d_b$  at a concrete strength of 4 ksi (27.6 MPa) and sets a minimum limit of  $40d_b$ .

$$l_t = \frac{120}{\sqrt{f'_{ci}}} d_b \geq 40d_b \quad (5.7)$$



Conversion: 1 kip = 4.45 kN  
1 in = 25.4 mm

**Figure 5.40 – Normalized NASP Value vs. Transfer Length at Release**

**Table 5.21 – Summary of Trend line Equations and R2 Values for NCHRP and Missouri S&T Data**

	$\frac{NASP_{conc}}{NASP}$ vs. $f'_{ci}$ (Figure 5.35)	$\frac{NASP_{conc}}{NASP}$ vs. $\sqrt{f'_{ci}}$ (Figure 5.36)	Transfer Length at Release vs. Normalized NASP (Figure 5.37)
NCHRP	$y=0.4914x^{0.5170}$ $R^2 = 0.798$	$y=0.5096x$ $R^2 = 0.789$	$y=66.436x^{-0.454}$ $R^2 = 0.577$
NCHRP and Missouri S&T Results with $NASP_A$	$y=0.4753x^{0.5275}$ $R^2 = 0.790$	$y=0.5052x$ $R^2 = 0.786$	$y=65.202x^{-0.445}$ $R^2 = 0.574$
NCHRP and Missouri S&T Results with $NASP_B$	$y=0.5142x^{0.5004}$ $R^2 = 0.740$	$y=0.4722x$ $R^2 = 0.723$	$y = 66.849x^{-0.457}$ $R^2 = 0.577$

**Table 5.22** compares the measured transfer lengths for the top and bottom strands in each mix from the current study to the transfer lengths calculated by the current AASHTO code equation and the equation proposed in the NCHRP report. As **Table 5.22** indicates, the transfer lengths calculated by the proposed equation are less than the current 30 in. (762 mm), and most of the measured transfer lengths at 1 and 28 days were still less than the values calculated by the proposed equation. The only measured transfer lengths that exceeded the transfer lengths calculated from the proposed equation were the C10-2 (L) and S10-4 (L) averages. The C10-2 (L) 1 and 28 day transfer lengths exceeded the calculated value from the proposed equation by 4.8% and 20.2%, respectively, while the S10-4 (L) 1 and 28 day transfer lengths were 16.4% and 17.6% higher than the value from the proposed equation. However, it should be noted that the S10-4 (L) value is only based on a single value. The transfer length value calculated from the current AASHTO equation was conservative for all measured transfer lengths. In conclusion, while the proposed equation was lower than the values calculated by the current AASHTO equation but still adequately conservative for most of the measured transfer lengths, the proposed equation was not conservative when compared to the live end transfer lengths.

**Table 5.22 – Comparison of Measured Transfer Lengths to Values Calculated by Current and Proposed AASHTO Equations**

	Measured Transfer Length at 1 day (in.)	Measured Transfer Length at 28 Days (in.)	Current AASHTO $l_t = 60d_b$	Proposed AASHTO $l_t = \frac{120}{\sqrt{f'_{ci}}} d_b$
C6-2	17.2	23.6	30	27.3
S6-2	14.4	19.2	30	25.2
C10-2	20.1	23.7	30	25.2
C10-2 (D)	13.7	17.2	30	25.2
C10-2 (L)	26.4	30.3	30	25.2
S10-2	13.7	16.6	30	23.8
C6-4	24.8	28.9	30	27.3
S6-4	18.2	20.1	30	25.2
C10-4	17.0	19.0	30	25.2
S10-4	19.3	18.3	30	23.8
S10-4 (D)	16.5	15.1	30	23.8
S10-4 (L)	27.7	28.0	30	23.8

Conversion: 1 in. = 25.4 mm

#### 5.4. DEVELOPMENT LENGTH TEST RESULTS

Development length was also evaluated to determine if differences existed in SCC and conventional concrete behavior and also to see if the AASHTO and ACI equations are conservative. The method and procedure for the four-point loading with varying embedment lengths that were used to investigate development length is described in **Section 4.5**, and the results for each development length test, including visual observations of failure, experimental moment capacity, and average strand slip are presented in **Table 4.12**. Only bottom strand development length was evaluated, so only the two-strand beams were tested. In each case, the specimen failed due to concrete crushing, reached an experimental moment capacity that exceeded the calculated nominal moment capacity, and showed negligible end slip in the strands. From these results, it was determined that bond failure was not an issue and the strands were fully developed at embedment lengths of both 73 in. (1,854 mm) and 58 in. (1,473 mm), or 100% and 80% of the calculated development length, respectively. Therefore, in this research, the

AASHTO and ACI design equations for development length are conservative because flexural failures occurred even at 80% of the calculated development length.

The calculated and experimental moment capacities are summarized in **Table 5.23** and analyzed to see if SCC or conventional concrete resulted in higher increases in actual moment capacities compared to calculated capacities. Overall, all experimental moment capacities were 11-16% above the calculated capacities. The largest discrepancy between SCC and conventional concrete was between C6 and S6 at 58 in. (1473 mm), where S6 had an average moment capacity 16% higher than the calculated value, while C6 only had an average capacity 11% higher. Otherwise, all other comparisons were within approximately 2%.

**Table 5.23 – Comparison of Experimental and Calculated Moment Capacities**

Mix ID	$M_n$ (k-in)	58 in. (1,473 mm)		73 in. (1,854 mm)	
		$M_u$ (k-in)	$M_u/M_n$	$M_u$ (k-in)	$M_u/M_n$
C6	742.7	824.2	1.110	836.2	1.126
S6	757.9	878.8	1.160	860.8	1.136
C10	773.6	877.8	1.135	883.3	1.142
S10	790.7	892.2	1.128	888.0	1.123

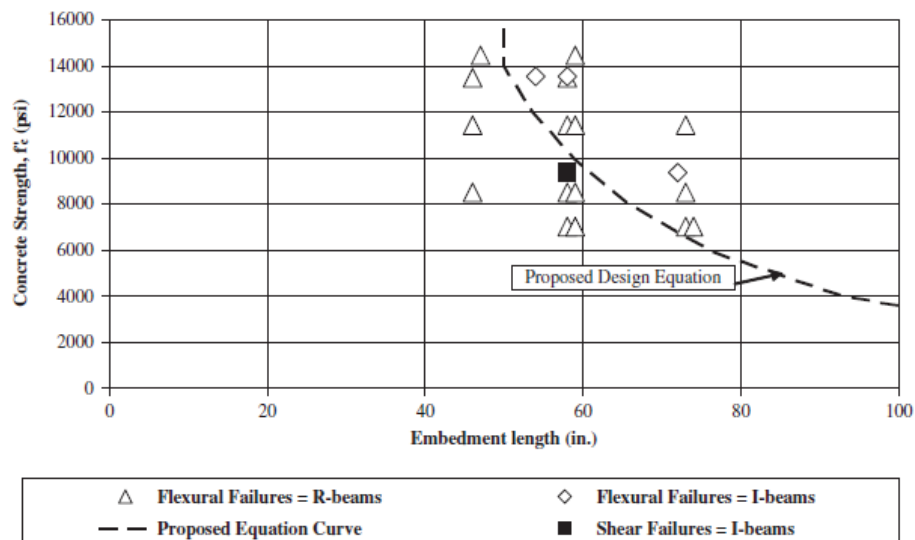
Conversion: 1 in. = 25.4 mm

1 k-in. = 113 N-m

As discussed in **Section 5.3.3**, the results of the NCHRP report showed a correlation between increasing concrete strength and decreasing transfer length. In addition to proposing a new transfer length equation for the AASHTO code, the NCHRP researchers also proposed a new development length equation, which takes into account the effect of concrete strength on development length (Ramirez and Russell 2008). The equation is presented here as **Eq. 5.8**, where  $f'_{ci}$  is the concrete compressive strength at one day in ksi,  $f'_c$  is the concrete compressive strength at 28 days in ksi, and  $d_b$  is the nominal strand diameter in inches. If the  $d_b$  variable is multiplied through, the first term in the equation becomes the proposed transfer length equation, while the second term represents the flexural bond length.

$$l_d = \left[ \frac{120}{\sqrt{f'_{ci}}} + \frac{225}{\sqrt{f'_c}} \right] d_b \geq 100d_b \quad (5.8)$$

The NCHRP researchers graphically displayed the results of the four-point load test by plotting concrete strength at the time of test vs. embedment length, and each point indicated whether the given test resulted in a flexural, shear, or bond failure (Ramirez and Russell 2008). **Figure 5.41** is the NCHRP plot of concrete strength vs. embedment length plot for strands A and B, the strands with high quality bond, in both the rectangular and I-beams. The proposed design equation, **Eq. 5.8**, was also plotted with the data. For plotting the equation,  $f'_{ci}$  was taken as 66.7% of  $f'_c$ , which according to the NCHRP report is a reasonable assumption based on general, past experience (Ramirez and Russell 2008). The plot shows that for a given concrete strength, embedment lengths to the right of the line would be conservative and likely result in a flexural failure, while embedment lengths to the left of the line may not be conservative and may result in a bond failure.



Conversion: 1 psi = 6.89 kPa  
1 in. = 25.4 mm

**Figure 5.41 – NCHRP Distribution of Bond and Flexural Failures for Strands A/B (Ramirez and Russell 2008)**

**Figure 5.41** was recreated so that the results from the Missouri S&T research could be plotted with the NCHRP results. This recreated plot of concrete strength vs. embedment length is shown in **Figure 5.42**. For the NCHRP data presented in **Figure 5.42**, only the data points from the tests on the rectangular beams were plotted so that the data would be directly comparable to the Missouri S&T data, which was also for rectangular beam sections. Also, points were not designed to differentiate between flexural, bond, or shear failures, because for both the NCHRP and Missouri S&T data shown, all tests failed in flexure. It was chosen to compare the data from this test to the data from the test with strands A and B because strands A and B exhibited high bond quality, as did strand type 101 used in the Missouri S&T research. **Figure 5.42** shows that the equation is conservative for strands with high bond quality because even tests with embedment lengths less than the length predicted by the design equation, or points to the left of the curve, resulted in flexural failures.

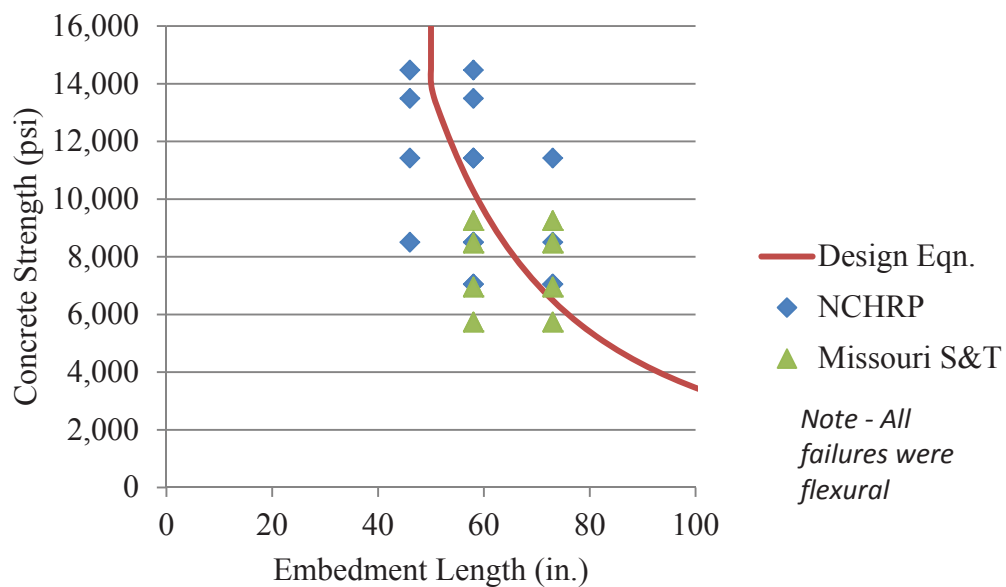


**Figure 5.42 – NCHRP and Missouri S&T Concrete Strength vs. Embedment Length Development Test Results**

The development lengths for each concrete mix calculated by the current AASHTO equation and the proposed AASHTO equation are presented in **Table 5.24**. The development length calculated by the proposed AASHTO equation for the C6 mix is actually 102% of the value from the current AASHTO equation, but the other development lengths calculated from the proposed equation range from 83% to 93% of the value calculated by the current AASHTO equation. According to this research, the proposed development length equation appears to be conservative because in this test program, even the development length tests run at an embedment length of 58 in (1,473 mm), which is 80% of the development length calculated from the current AASHTO equation and less than any of the development lengths calculated by the proposed equation, failed in flexure, showing the strand was fully bonded.

**Table 5.24 – Comparison of Development Lengths Calculated by Current and Proposed AASHTO Equations**

Mix ID	Current AASHTO (in.) $l_d = \left( f_{ps} - \frac{2}{3} f_{pe} \right) d_b$	Proposed AASHTO (in.) $l_d = \left[ \frac{120}{\sqrt{f'_{ci}}} + \frac{225}{\sqrt{f'_c}} \right] d_b$
C6	73	74.4
S6	73	67.9
C10	73	63.8
S10	73	60.8

Conversion: 1 in. = 25.4

Overall, it was found that SCC and conventional concrete performed equally well in terms of adequately bonding with prestressing strand to fully develop the stress in the strand. Additionally, the AASHTO and ACI equations were determined to be conservative. The proposed AASHTO development length equation also appeared to be conservative, except when applied to the live end transfer length averages. Also, while the equations proved to be mostly conservative, it should be noted that the strand used in these specimens was shown to have exceptional bond quality through the NASP test and

LBPT, and using strand with lesser bond quality could result in less conservative, or failing, results.

## 6. FINDINGS, CONCLUSIONS, AND RECOMMENDATIONS

### 6.1. FINDINGS

The findings from the bond testing portion of the research as well as the transfer length and development length testing are discussed below.

**6.1.1. Bond Test Results.** The findings from the NASP test in mortar, modified NASP test in concrete, and LBPT are as follows:

- All three strand types were deemed to have acceptable bond based on the NASP test minimum pullout load requirements.
- The rank of bond performance of strands based on pullout loads at 0.001 in. (0.025 mm) slip was not always the same as the rank determined based on the loads at 0.1 in. (2.54 mm) slip.
- Although strand type 102 passed the NASP test acceptance criteria, the load vs. slip plot displayed a plateau and drop off in load at 0.1 in. (2.54 mm) slip, while strand types 101 and 103, which had much higher pullout values, were still showing increases in load at 0.1 in. (2.54 mm) slip.
- For strand types 102 and 103, the NASP pullout loads from the Missouri S&T testing were significantly higher than the NASP pullout loads determined during the NCHRP testing.
- The two different mortar mixes used to test strand type 101 resulted in a statistically significant difference in average pullout loads.
- Compared to the normal strength concretes, high strength concretes generally had higher 0.1 in. (2.54 mm) pullout loads, but lower 0.001 in. (2.54 mm) pullout loads.
- When normalized to the square root of concrete compressive strength, no statistical difference was observed between the SCC and conventional concrete pullout loads.
- Only strand type 101 passed the first slip and peak load limits of the LBPT. Strand type 102 failed both LBPT limits, while strand type 103 passed the first slip limit but failed the peak load limit.

- No correlation was found between the visual observations and residues on the strands and the final pullout results from the LBPT.
- All three strand types passed the NASP test, while strand type 101 was the only type to pass the LBPT.
- For a given strand type, the coefficient of variation values determined from both tests were very similar.
- Plotting LBPT results vs. NASP test results indicated a linear trend line with an  $R^2$  value of 0.77, meaning there was a fair correlation between the two tests and each one could be an equally valid test.
- Both tests predicted strand type 102 to be the worst, but the NASP test indicated that 103 was the top performer, while the LBPT indicated strand type 101 was the best. However the results for types 101 and 103 were extremely close for both tests.

**6.1.2. Transfer Length Test Results.** The findings from the transfer lengths determined through the 95% Average Mean Strain Method and the transfer lengths at release calculated by initial end slips are as follows:

- Live and dead ends were not noted at the time of release, but measured transfer lengths indicated some locations where transfer lengths were significantly longer and live ends could be reasonably assumed.
- No significant differences were seen between transfer lengths in SCC and those in conventional concrete for either top or bottom strands from 1 to 28 days when possible live end values were removed from averages.
- In terms of the effect of concrete strength on transfer length, higher strength concrete resulted in shorter transfer lengths for bottom strands in conventional concrete when the possible live end values were removed from the average, but no differences were seen between the transfer lengths in normal and high strength SCC for bottom strands. For top strands, the high strength mixes for both the SCC and conventional concrete had shorter transfer lengths, but only from 8 to 28 days.
- For all concrete mixes at all ages, no statistically significant differences were observed between the transfer lengths of top strands vs. bottom strands.

- For bottom strands, transfer lengths in normal strength concretes increased 33 to 37% over 28 days, while transfer lengths in high strength mixes increased 14 to 24%, and higher increases were observed in transfer lengths in conventional concrete compared to SCC for a given strength level.
- For top strands, no consistent increases were seen over 28 days for any mix or strength, and the high strength SCC mix actually showed decreases in transfer lengths over time.
- For both top and bottom strands, except for the possible live end averages of both the top and bottom strands and top strands in the normal strength conventional concrete, measured transfer lengths were shorter than the values predicted by the two ACI equations. All measured top and bottom transfer lengths, even the possible live end averages, were shorter than the value predicted by AASHTO equation.
- Due to the violent release method, many of the potentiometers did not register valid end slips because the potentiometers either became separated from the plate attached to the strand or the wires connecting the potentiometers to the Synergy data acquisition became disconnected. Only 38% of all potentiometers that were installed registered what could be considered valid end slips.
- The steel ruler measurements had a precision of only  $\frac{1}{32}$  in. (0.79 mm) and the same measurements were consistently reported, rendering the steel ruler method of determining end slips imprecise.
- The percent differences between the average DEMEC and Synergy transfer lengths for each mix ranged from 0.36 to 73%. The transfer lengths calculated from the end slips measured by the potentiometers were generally less than the transfer lengths determined from the DEMEC readings.
- The percent differences between the average DEMEC and ruler transfer lengths ranged from 4 to 119%. The transfer lengths calculated from the end slips measured by the steel ruler were generally less than the transfer lengths determined from the DEMEC readings.
- When plotted with results from a similar program by Ramirez and Russell (2008), NASP in concrete pullout loads normalized by NASP in mortar pullout

loads were shown to follow the same correlation to the square root of concrete compressive strength, as was found by Ramirez and Russell. The correlation was not significantly changed whether the results from the NASP test in mortar Mix A or the results from the NASP test in mortar Mix B were used.

- When NASP values normalized to the square root of concrete compressive strength were plotted against transfer lengths at release, the scatter was found to fall within the scatter reported in the NCHRP report, confirming the relationship between the NASP in mortar pullout values, concrete compressive strength, and initial transfer lengths, found by Ramirez and Russell (2008).
- When Ramirez and Russell's proposed transfer length equation was applied to the data from this study, the equation was found to give values shorter than the current AASHTO equation, but the calculated values were still found to generally be conservative, except when compared to the possible live end averages.

**6.1.3. Development Length Test Results.** The findings from the four-point loading tests performed to evaluate development lengths are as follows:

- All development length test specimens failed in flexure due to concrete crushing.
- All development length test specimens sustained an applied moment that exceeded the calculated nominal moment.
- All development length test specimens showed negligible strand end slip during testing.
- SCC and conventional concrete specimens exceeded the calculated nominal moment capacities by similar amounts and exhibited similar flexural bond behavior.
- When Ramirez and Russell's proposed development length equation was applied to the data from this study, the equation was found to produce development lengths shorter than the AASHTO equation for three of the four mixes. For the normal strength conventional concrete mix, the proposed equation actually resulted in a transfer length longer than the length predicted by the AASHTO equation.

## 6.2. CONCLUSIONS

Based on the previously stated findings, several conclusions can be drawn regarding the applicability of NASP test in mortar and LBPT bond tests, the bond performance of SCC compared to conventional concrete, and the feasibility of using concrete strength and pullout test results to predict transfer lengths.

1. Based on the linear relationship found between the LBPT and NASP pullout values and the similar coefficients of variation between the two tests for a given strand type, either the LBPT or NASP test are equally valid approaches to evaluating bond performance of prestressing strand. However, the limits set on passing may need some refinement, as two of the strand sources passed the proposed NASP standard but did not pass the LBPT requirements.
2. Proportioning for the mortar mixes did appear to have an effect on NASP in mortar pullout values, and it is hypothesized that a decreased amount of sand could detrimentally affect mechanical interlocking and lead to lower pullout values.
3. While first slips are not required to be monitored in the NASP test, strands with high 0.1 in. (2.54 mm) pullout loads sometimes had the lowest 0.001 in. (0.025 mm) pullout loads, which could indicate a problem with adhesion of the strand.
4. The NASP test in concrete revealed that the high strength concretes had lower first slip values than the normal strength concretes. Compared to their normal strength counterparts, the high strength mixes generally had a lower water/cement ratio, a decrease in coarse and fine aggregate content, an increase in total cementitious material, and an increase in high range water reducer.
5. SCC and conventional concrete were comparable in terms of bond performance, showing few statistical differences between measured transfer lengths or pullout loads between the two types of concrete.
6. Increases in concrete strength generally resulted in shorter, although not always statistically different, transfer lengths, especially if the possible live end values were removed from the averages. Also, top strands only seemed to show statistically significant increases in transfer length at later ages.

7. Transfer lengths of bottom strands tended to increase from 1 to 28 days, with most of the increase occurring between 1 and 4 days. Also, the transfer lengths in normal strength mixes appeared to increase more than those in high strength mixes, and transfer lengths in conventional concrete increased more than transfer lengths in SCC. However, no consistent trends were noted for change in top strand transfer lengths over time.
8. The AASHTO transfer length equation was generally conservative for all mixes for both top and bottom strands, even when compared to possible live end transfer lengths. The ACI equations were generally conservative except when compared to live end transfer lengths or the top strands in the normal strength conventional concrete.
9. The linear potentiometers used in this study were found to be unreliable, and the steel ruler measurements were determined to be imprecise; the transfer lengths determined from the DEMEC readings and 95% Average Mean Strain Method were found to be the most consistent and reliable.
10. Due to the fact that increased concrete strength resulted in decreased transfer lengths and increased NASP in concrete pullout loads, concrete strength does have an effect on bond and the equation for transfer length should be a function of concrete strength.
11. In this study, transfer length did appear to be related to the square root of concrete compressive strength, which follows the trend noted by Ramirez and Russell (2008) and others.
12. The proposed transfer length equation from Ramirez and Russell (2008) was slightly less conservative than the AASHTO equation, but still mostly conservative when compared to the measured transfer lengths, although the proposed equation was not conservative when compared to the live end transfer lengths.
13. Development length specimens tested at embedment lengths of 80% of the development length calculated from the AASHTO and ACI equations still failed in flexure, so the current AASHTO and ACI equations for development length are conservative.

14. SCC and conventional concrete appeared to exhibit comparable flexural behavior.
15. Ramirez and Russell's proposed development length equation (2008) appeared to be less conservative than the AASHTO and ACI equation, but still conservative in three out of the four cases. In this test program, even the development length tests completed at an embedment length of 58 in (1,473 mm), which is 80% of the development length calculated from the current AASHTO equation and shorter than any of the development lengths calculated by the proposed equation, failed in flexure, showing the strand stress could be fully developed. However, the proposed equation did predict one development length greater than the AASHTO and ACI value for one mix, showing the proposed development length equation may be over-conservative in some cases.

### **6.3. RECOMMENDATIONS**

From the conclusions, the following recommendations for future work and for implementation of tests are listed below:

1. Because differences in bond quality have been shown to vary greatly depending on the source of strand, a standard bond test should be recommended and implemented by MoDOT to ensure strand bond quality before the strand is used in production. Missouri S&T recommends that the NASP Bond test as described in NCHRP Report 603 be prescribed; however, the minimum acceptance criteria loads should be increased to 16,000 lb (71.2 kN) for the average of six specimens and 14,000 lb (62.3 kN) for an individual specimen.
2. The NASP test in concrete should not necessarily be a required test for strand bond because the tests showed pullout strength is mostly a function of concrete compressive strength; however the NASP test in concrete still could be useful for identifying possible effects of mix additions or proportioning on bond.
3. The pullout limits for both the NASP test in mortar and LBPT need refinement. Additional research should be conducted with NASP and LBPT specimens and corresponding transfer length specimens to see if the NASP minimum value should be raised and the LBPT minimum value should be lowered. Specifically, strands with NASP pullout values between 12,000 and 18,000 lb (53 and 80 kN)

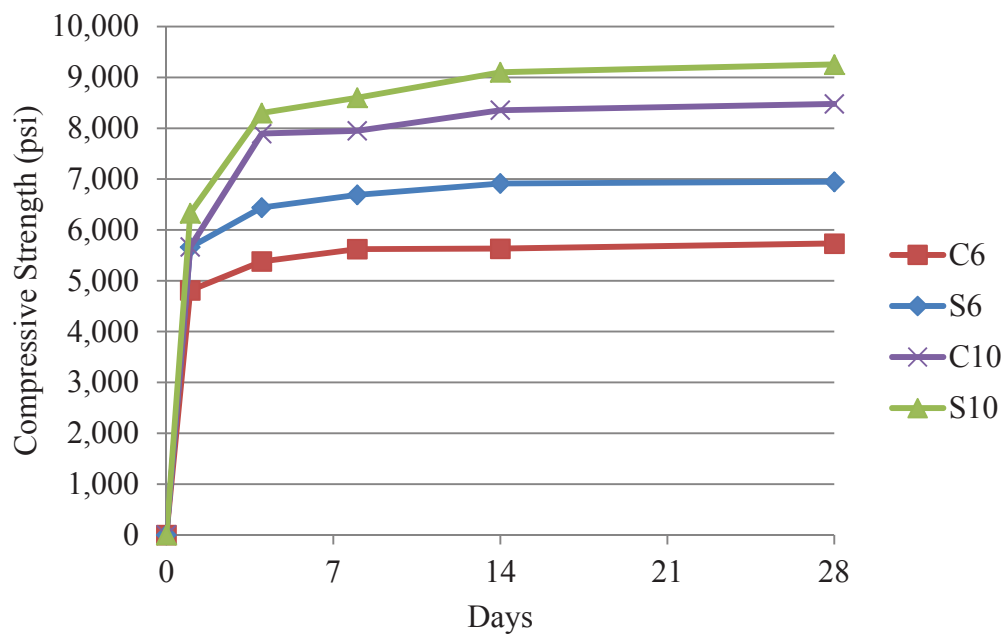
and LBPT pullout values between 30.0 and 36.0 kips (133 and 160 kN) should be targeted.

4. The pullout value at first slip, or 0.001 in. (0.025 mm) of slip, should also be reported for the NASP test because low first slip values could indicate problems with adhesion of strand.
5. Additional studies should be completed to investigate the effect of mortar mix proportioning on the pullout values from the NASP test in mortar, and limits should be set for proportioning in addition to strength and flow.
6. More research should be conducted to determine if the contours of the load vs. slip curves for the NASP test in mortar specimens can also be indicators of bond quality. Strand types that show plateaus or drop-offs in load at 0.1 in. (2.54 mm) instead of continuing to increase may not have acceptable bond quality, even if they pass a minimum load limit.
7. The potentiometer and plate method for measuring end slip should be reinvestigated to see if other plate/potentiometer bonding methods or other less violent release methods could yield useable data. However, the steel ruler method should be abandoned, and end slips should be measured with a more precise means, such as a caliper.
8. The current AASHTO and ACI transfer length and development length equations are adequate and conservative for use with conventional concrete as well as SCC.
9. The proposed transfer length equation from Ramirez and Russell (2008) should potentially be reinvestigated because the equation was not conservative for live end transfer lengths.
10. The proposed development length equation from Ramirez and Russell (2008) should also potentially be reinvestigated because the equation might result in overly conservative values in some cases.

**APPENDIX A**  
**Concrete Compressive Strength Summary**

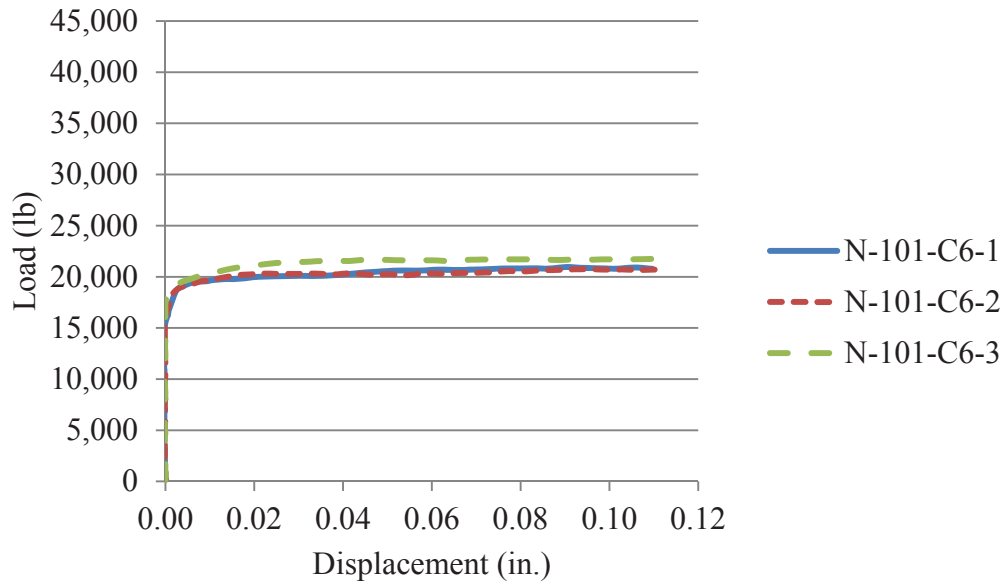
**Table A.1 – Summary of Concrete Compressive Strengths**

Mix ID	Concrete Compressive Strength				
	1 Day (psi)	4 Day (psi)	8 Day (psi)	14 Day (psi)	28 Day (psi)
C6	4,810	5,380	5,620	5,630	5,730
S6	5,660	6,440	6,690	6,910	6,950
C10	5,670	7,890	7,950	8,350	8,480
S10	6,330	8,300	8,600	9,100	9,250

**Figure A.1 – Concrete Compressive Strength over Time**

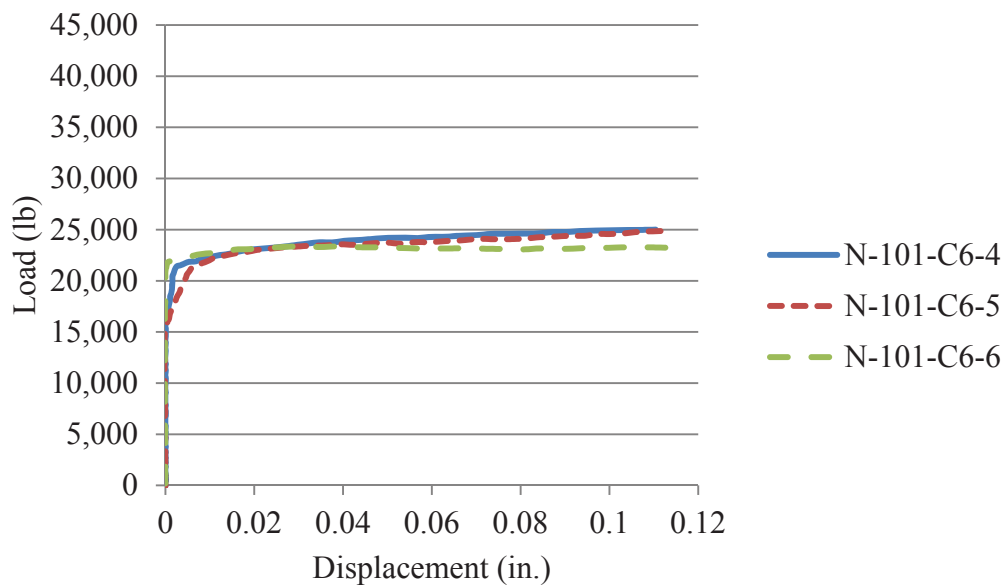
## **APPENDIX B**

### **NASP in Concrete Load vs. Slip Plots**



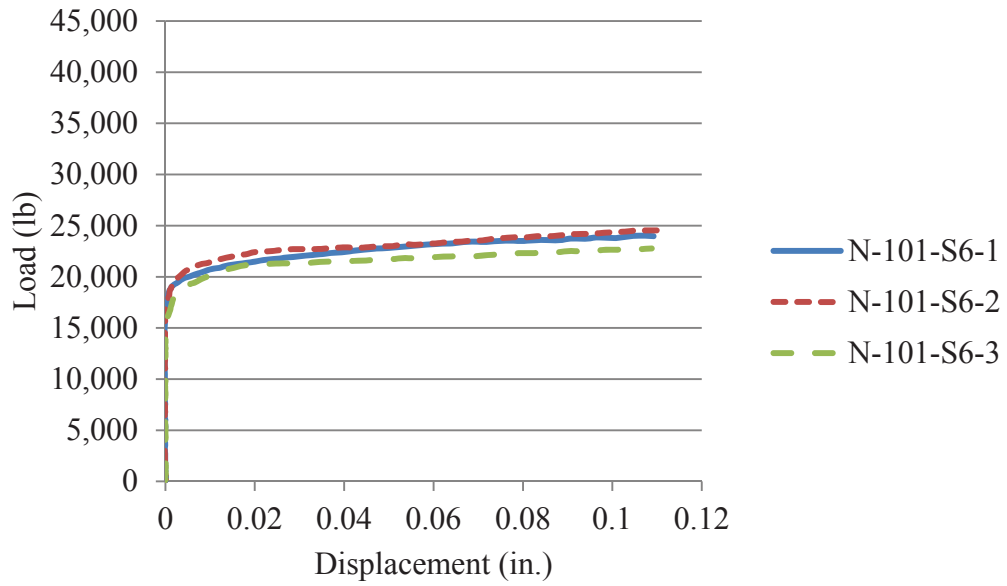
Conversion: 1 in. = 25.4 mm  
 1 lb = 4.45 N

**Figure B.1 – C6 NASP in Concrete – 1 Day**



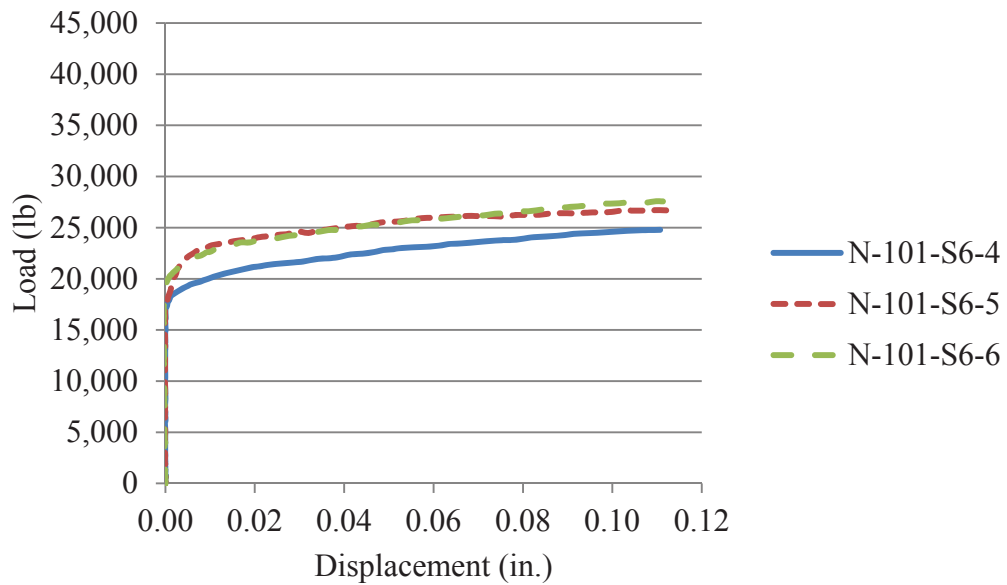
Conversion: 1 in. = 25.4 mm  
 1 lb = 4.45 N

**Figure B.2 – C6 NASP in Concrete – 8 Day**



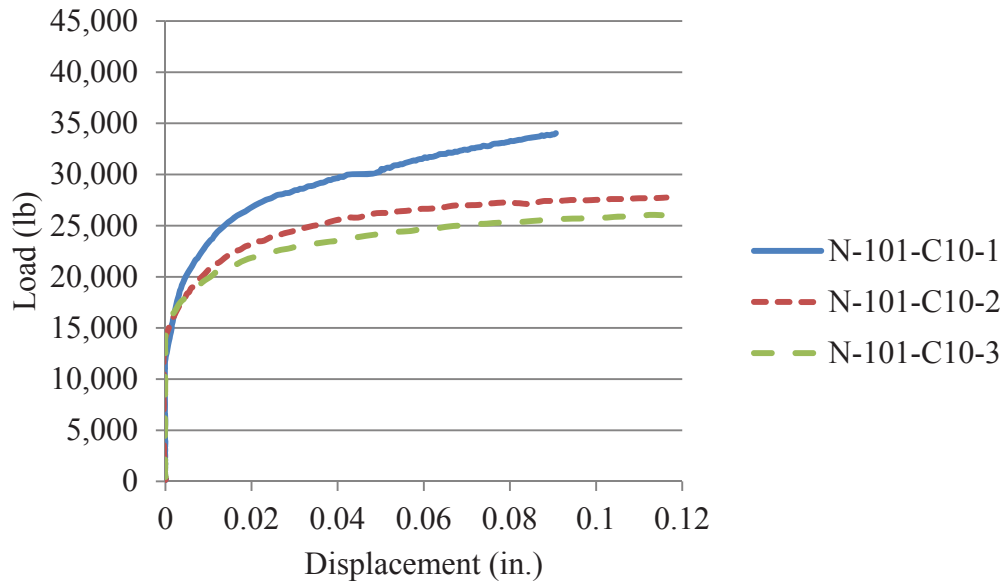
Conversion: 1 in. = 25.4 mm  
 1 lb = 4.45 N

**Figure B.3 – S6 NASP in Concrete – 1 Day**



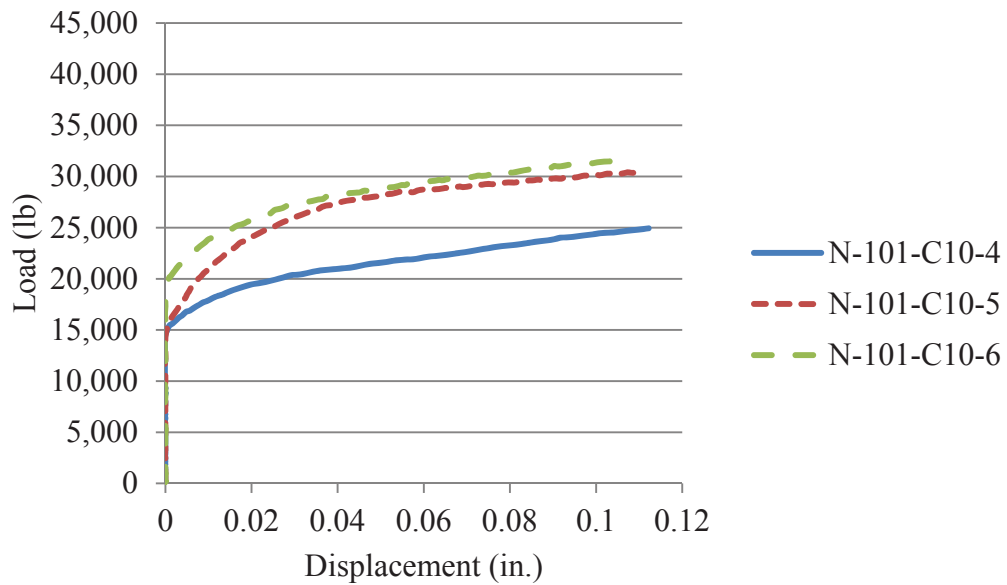
Conversion: 1 in. = 25.4 mm  
 1 lb = 4.45 N

**Figure B.4 – S6 NASP in Concrete – 8 Day**



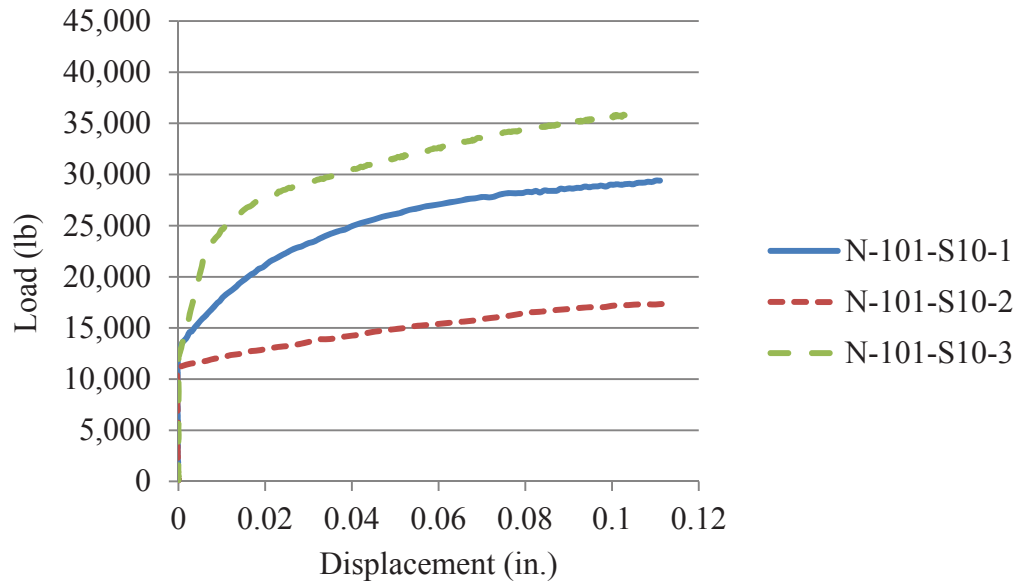
Conversion: 1 in. = 25.4 mm  
1 lb = 4.45 N

**Figure B.5 – C10 NASP in Concrete – 1 Day**



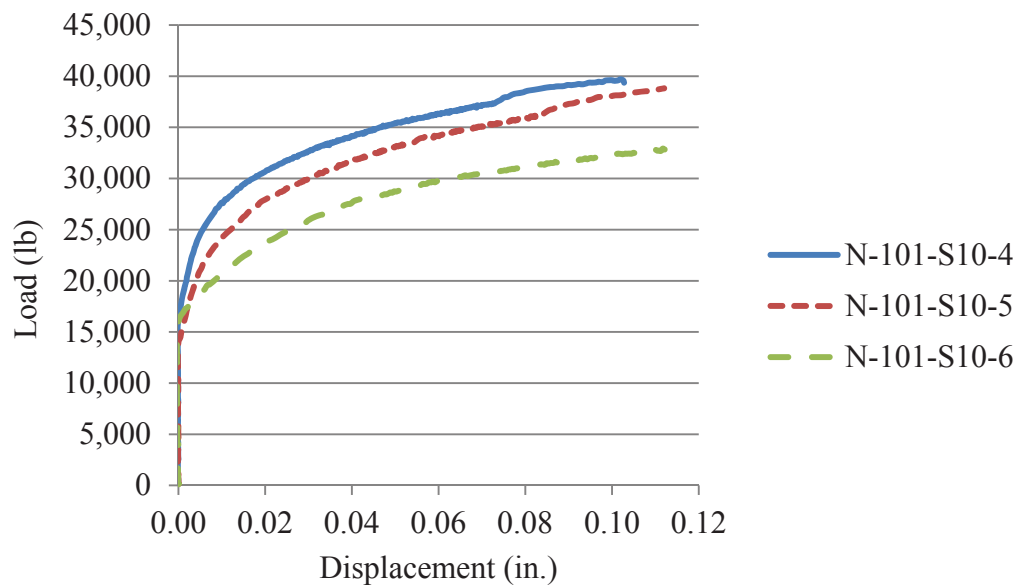
Conversion: 1 in. = 25.4 mm  
1 lb = 4.45 N

**Figure B.6 – C10 NASP in Concrete – 8 Day**



Conversion: 1 in. = 25.4 mm  
1 lb = 4.45 N

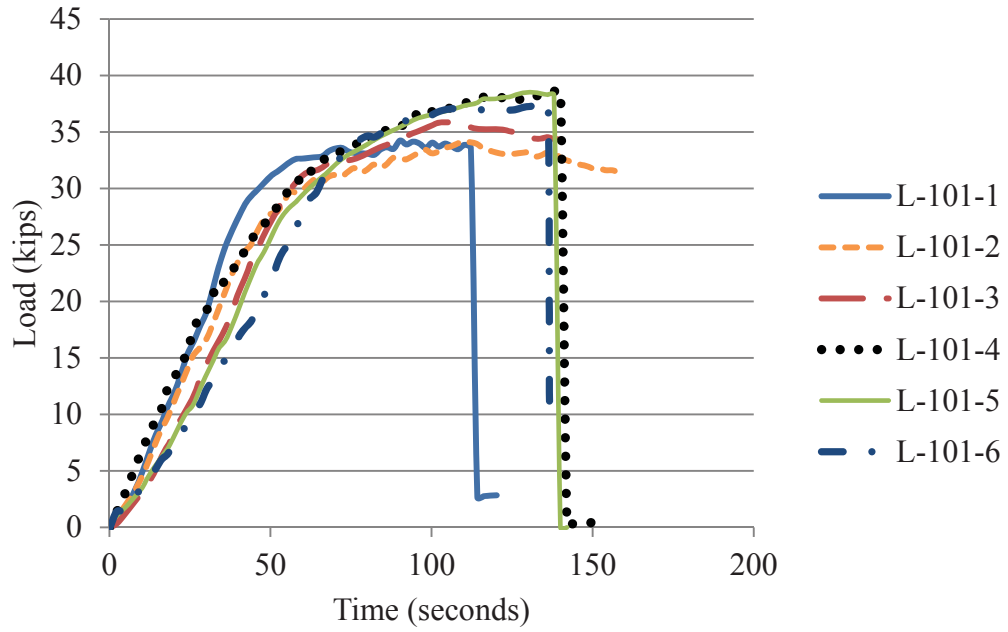
**Figure B.7 – S10 NASP in Concrete – 1 Day**



Conversion: 1 in. = 25.4 mm  
1 lb = 4.45 N

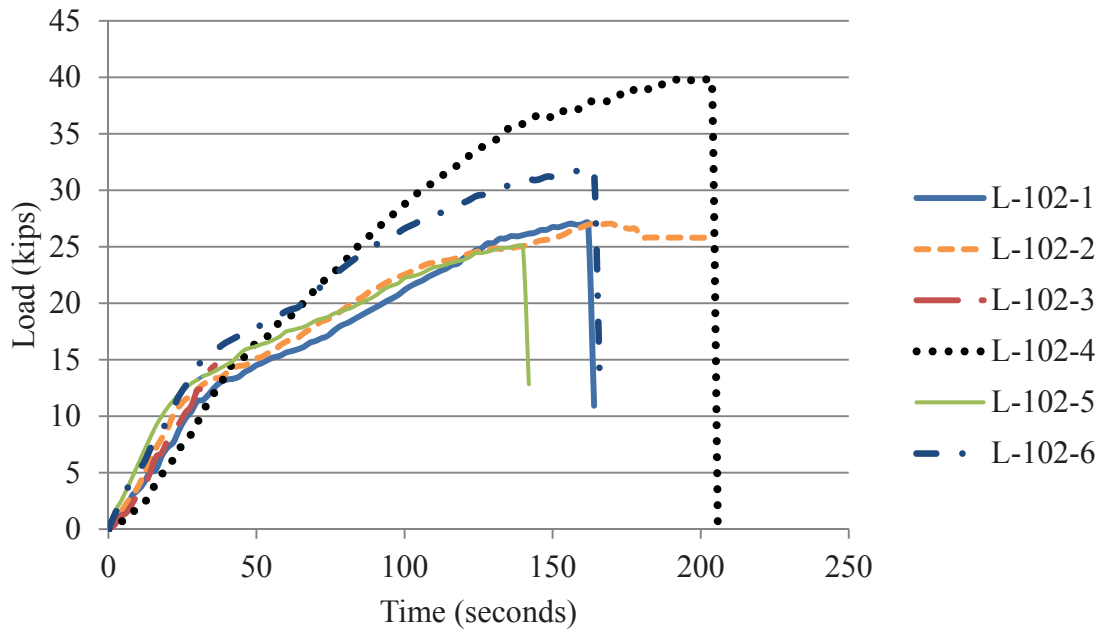
**Figure B.8 – S10 NASP in Concrete – 8 Day**

**APPENDIX C**  
**LBPT Load vs. Time Plots**



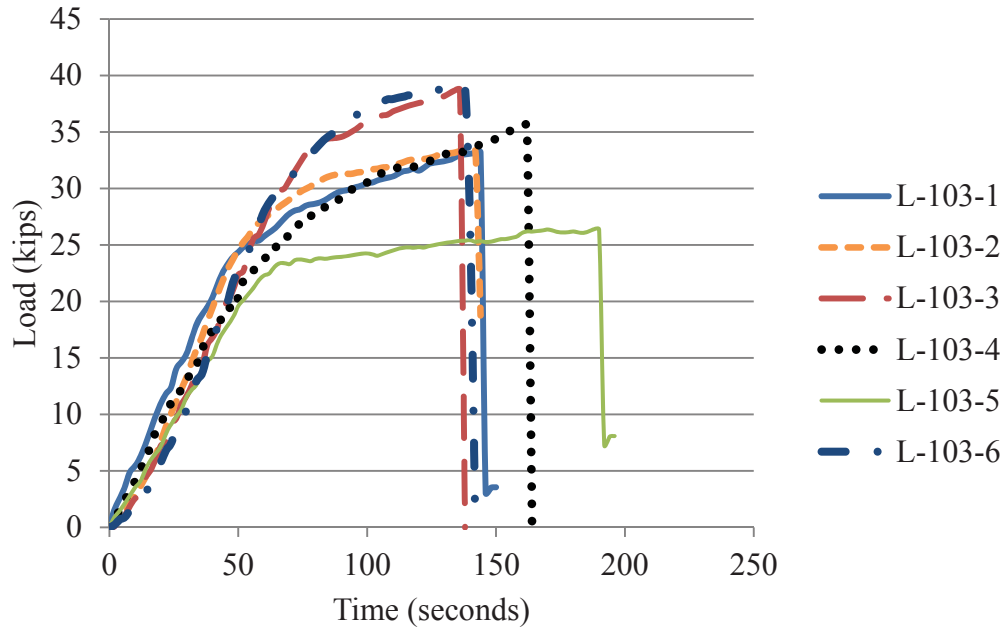
Conversion: 1 kip = 4.45 kN

**Figure C.1 – LBPT Results for Strand Type 101**



Conversion: 1 kip = 4.45 kN

**Figure C.2 – LBPT Results for Strand Type 102**



Conversion: 1 kip = 4.45 kN

**Figure C.3 – LBPT Results for Strand Type 103**

**APPENDIX D**  
**95% Average Mean Strain Plots**

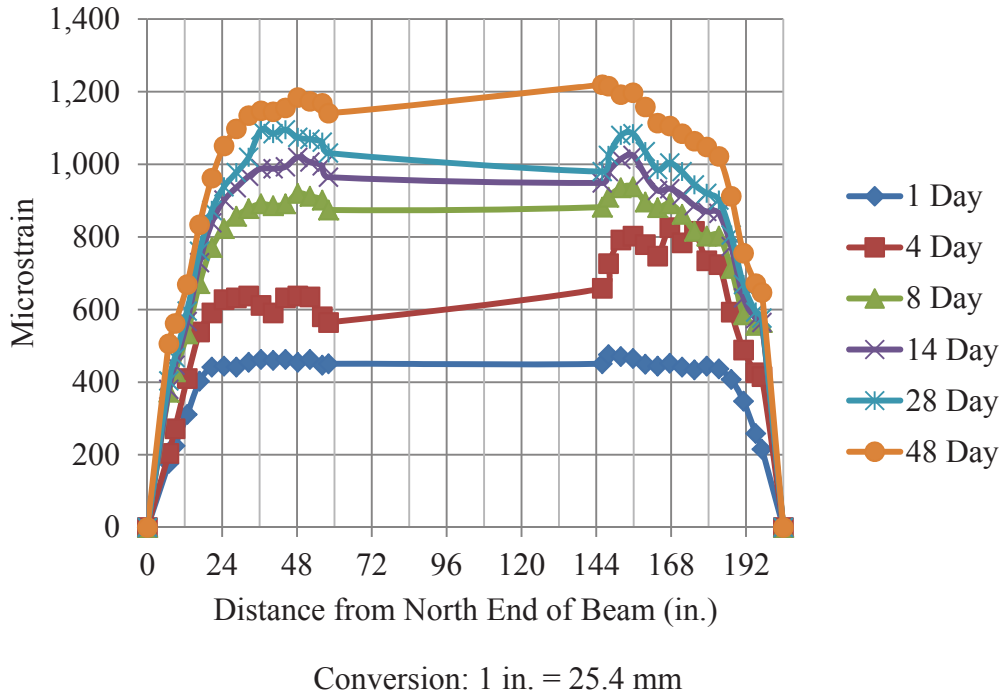


Figure D.1 – C6-2-1\_NE and C6-2-1\_SE Average Mean Strains

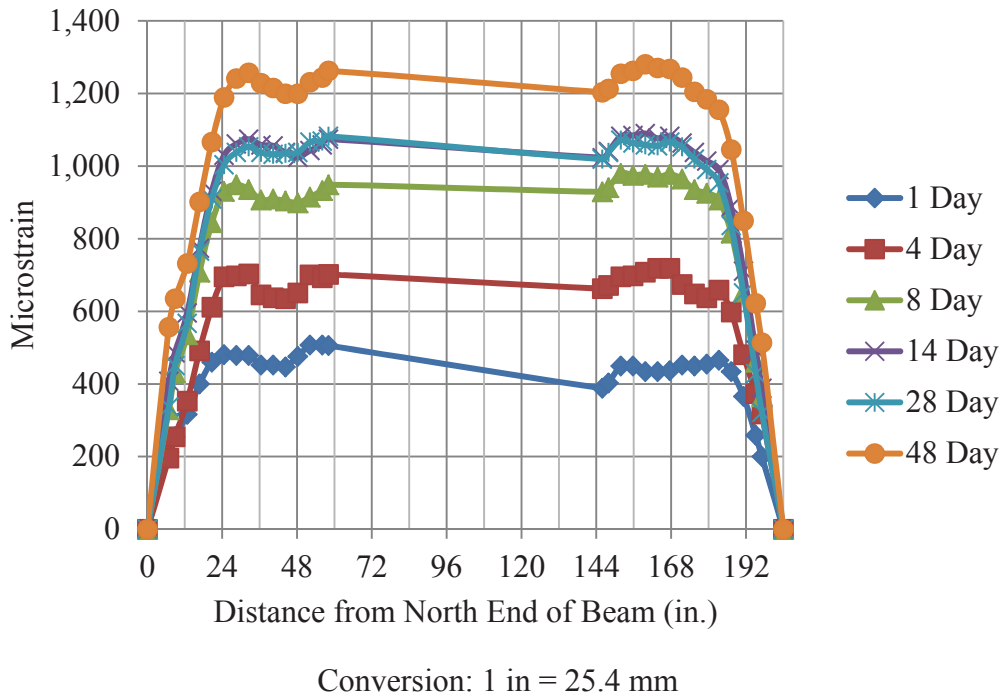


Figure D.2 – C6-2-1\_NW and C6-2-1\_SW Average Mean Strains

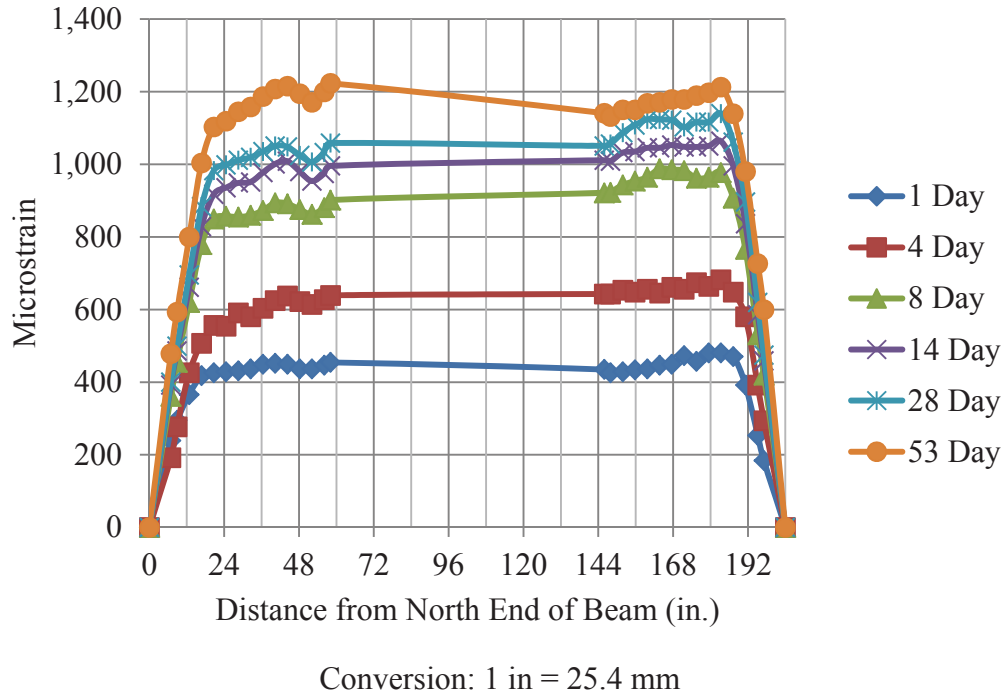


Figure D.3 – C6-2-2\_NE and C6-2-2\_SE Average Mean Strains

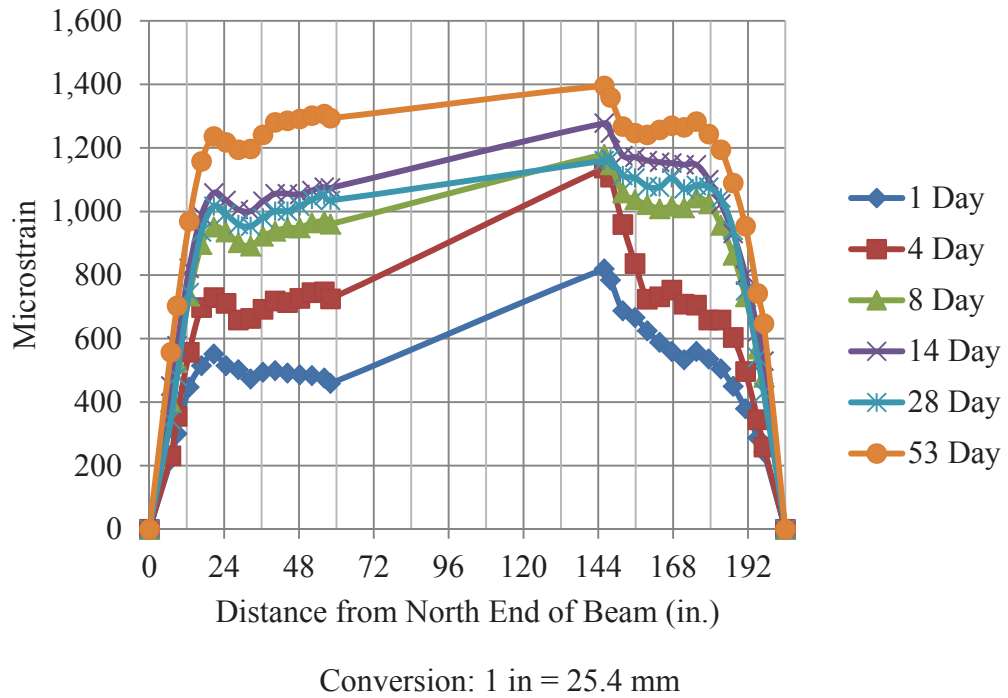


Figure D.4 – C6-2-2\_NW and C6-2-2\_SW Average Mean Strains

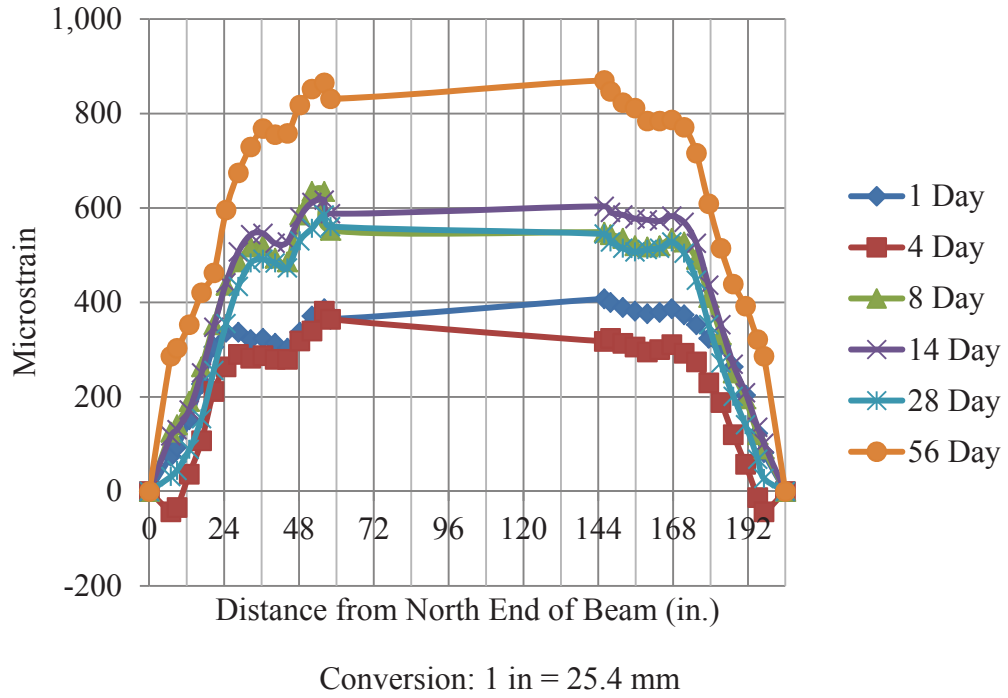


Figure D.5 – C6-4-1\_NE and C6-2-1\_SE Average Mean Strains

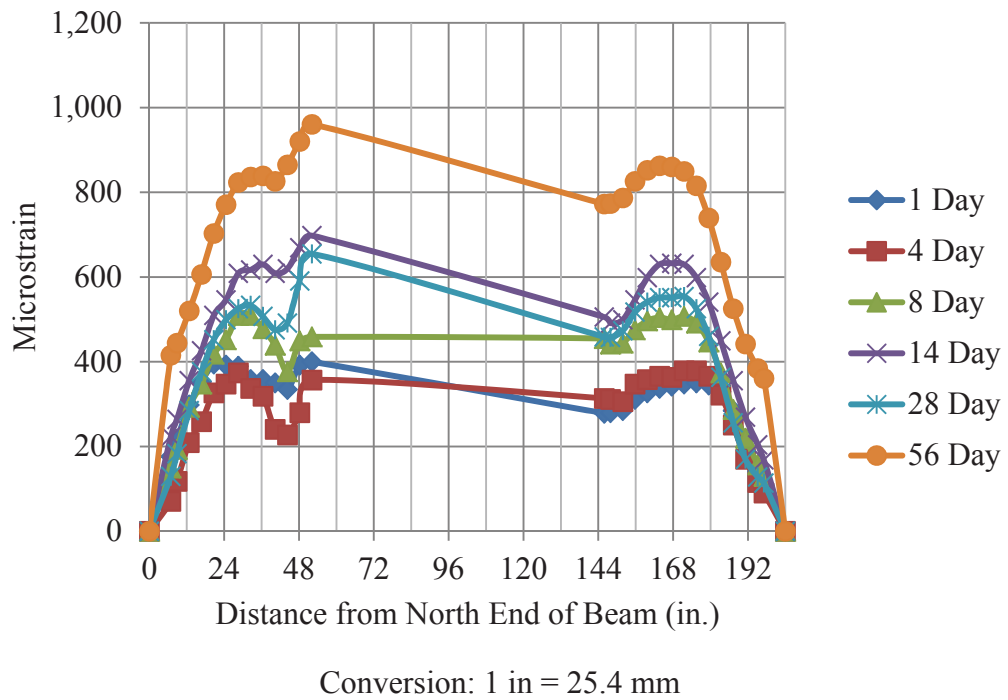


Figure D.6 – C6-4-1\_NW and C6-4-1\_SW Average Mean Strains

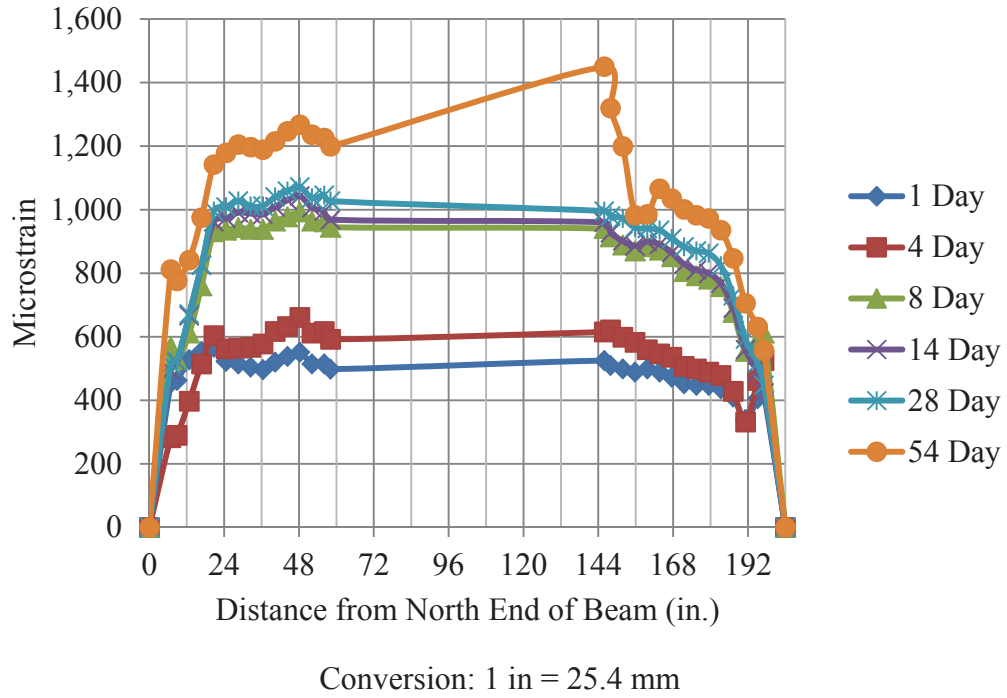


Figure D.7 – S6-2-1\_NE and S6-2-1\_SE Average Mean Strains

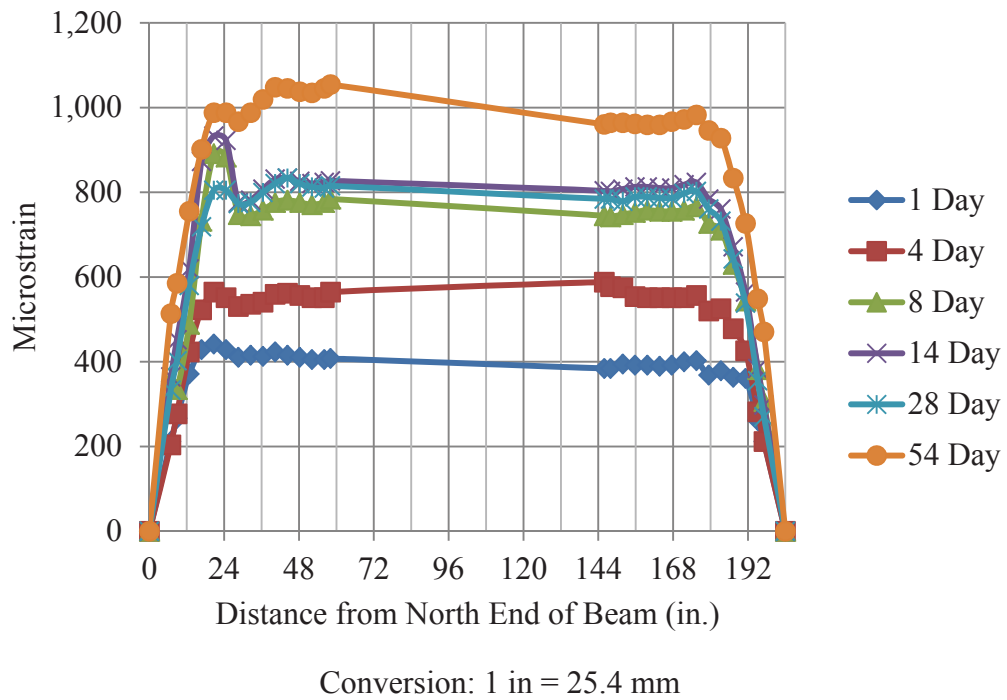
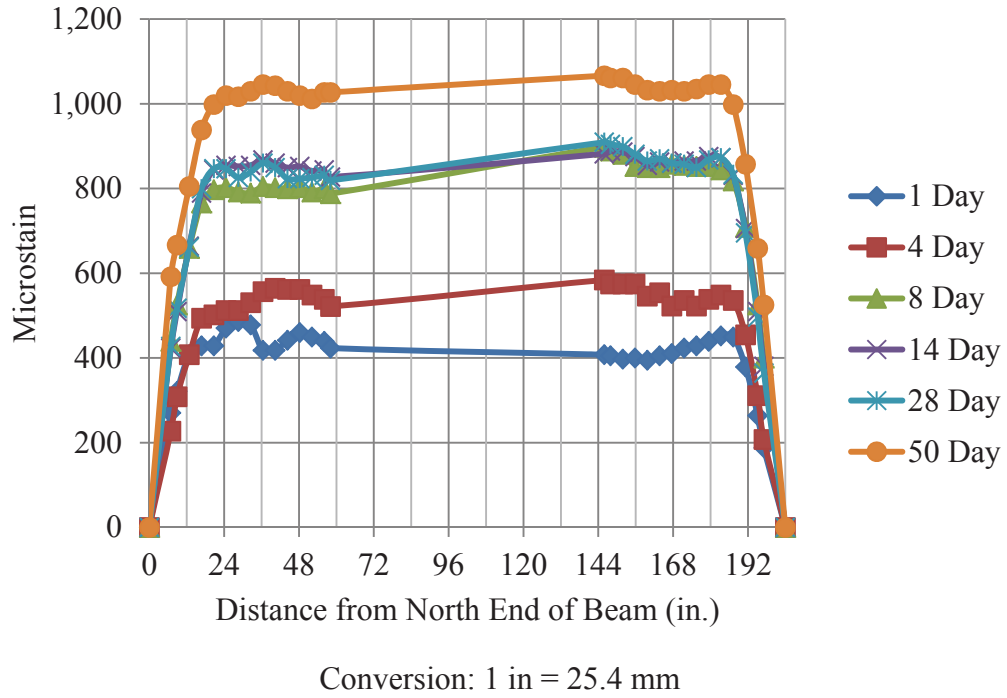
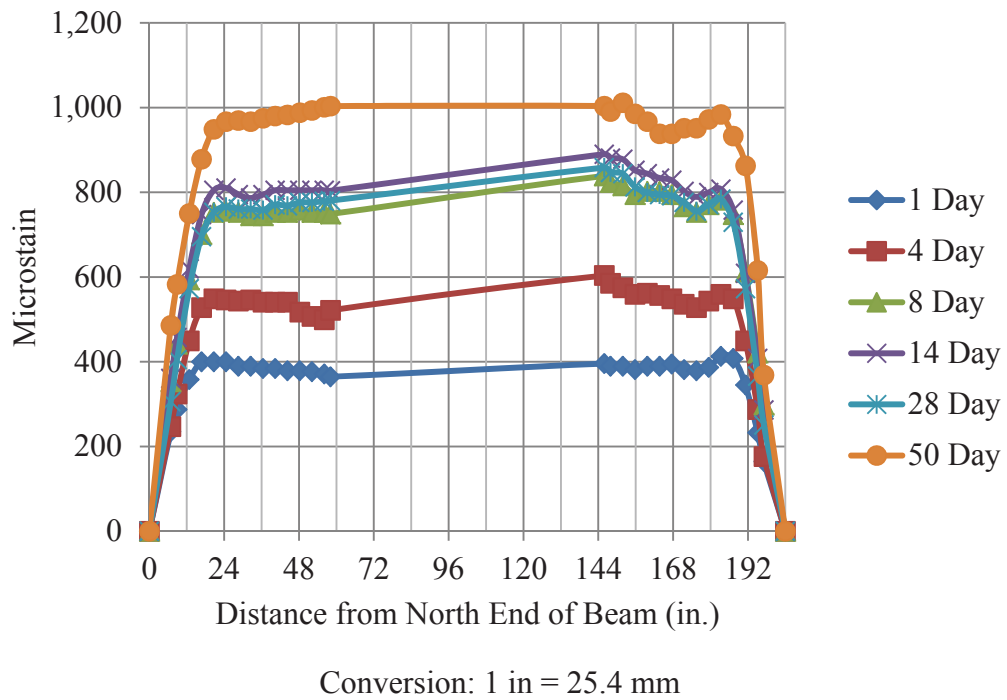


Figure D.8 – S6-2-1\_NW and S6-2-1\_SW Average Mean Strains



**Figure D.9 – S6-2-2\_NE and S6-2-2\_SE Average Mean Strains**



**Figure D.10 – S6-2-2\_NW and S6-2-2\_SW Average Mean Strains**

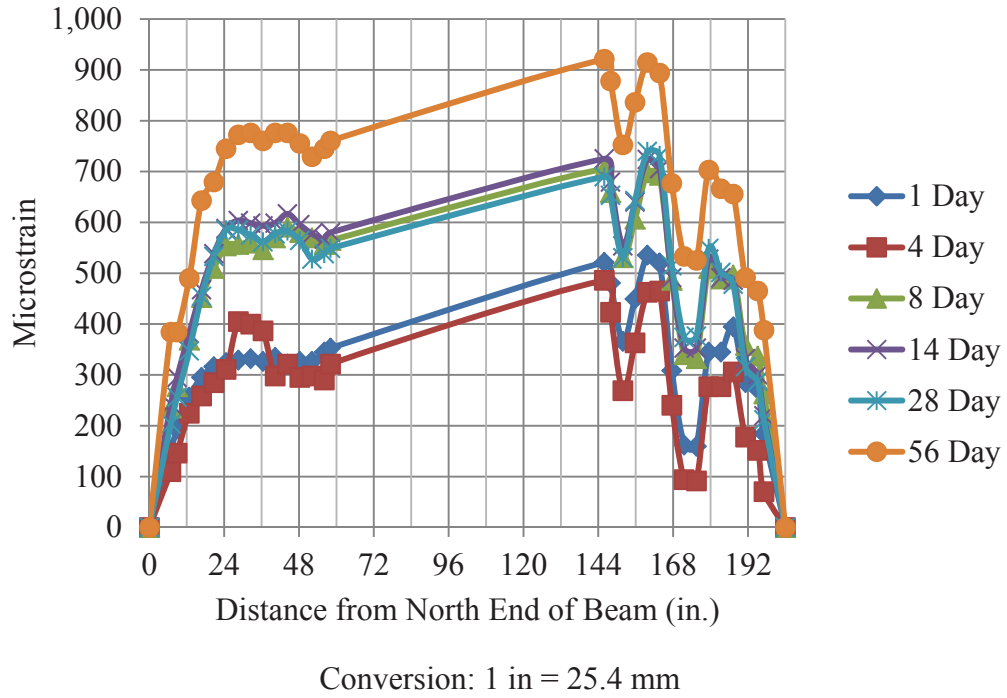


**Figure D.11 – S6-4-1\_NE and S6-4-1\_SE Average Mean Strains**

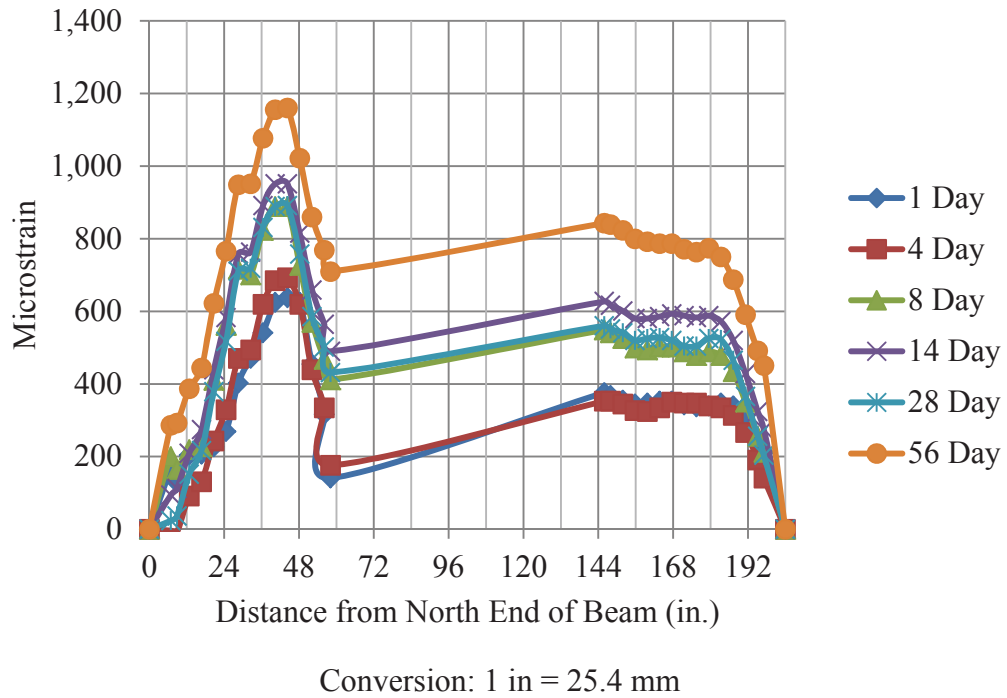


**Figure D.12 – S6-4-1\_NW and S6-4-1\_SW Average Mean Strains**

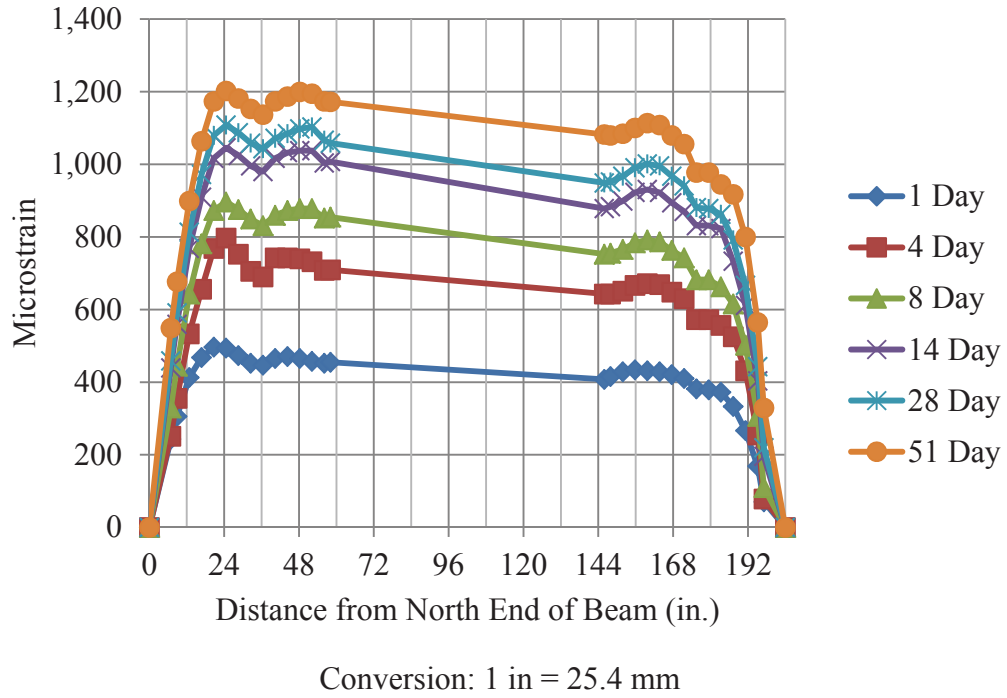


Figure D.13 – C10-2-1\_NE and C10-2-1\_SE Average Mean Strains

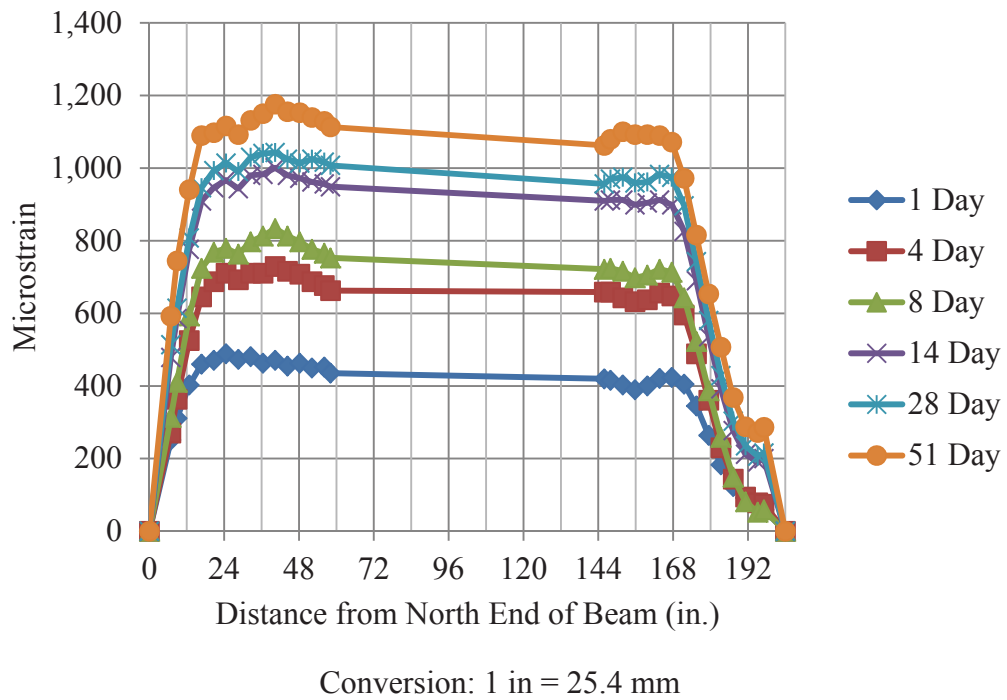


Figure D.14 – C10-2-1\_NW and C10-2-1\_SW Average Mean Strains

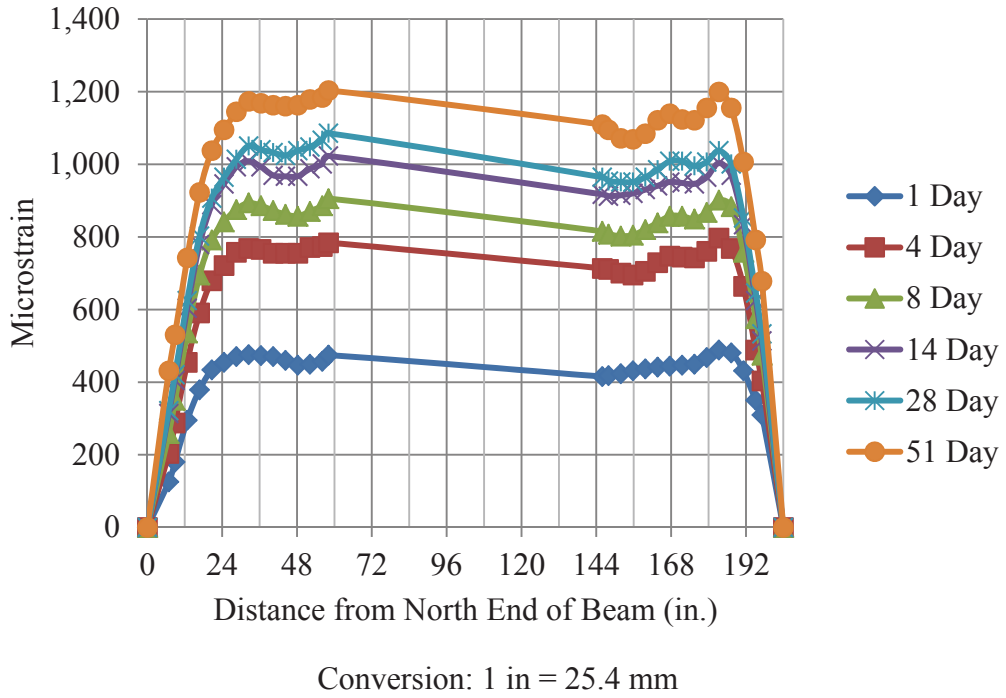


Figure D.15 – C10-2-2\_NE and C10-2-2\_SE Average Mean Strains

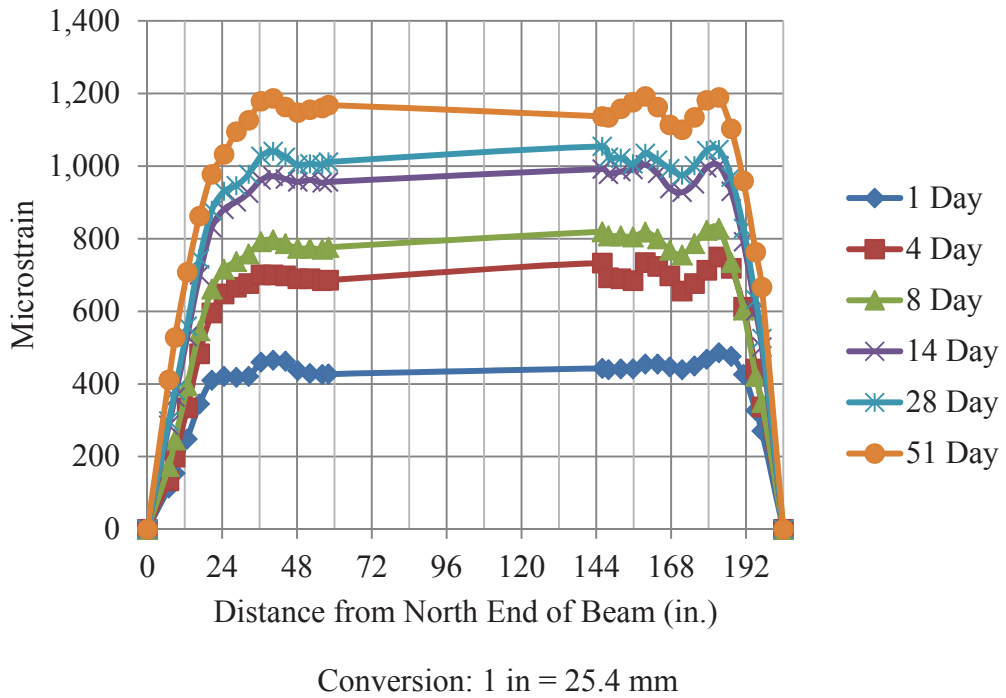


Figure D.16 – C10-2-2\_NW and C10-2-2\_SW Average Mean Strains

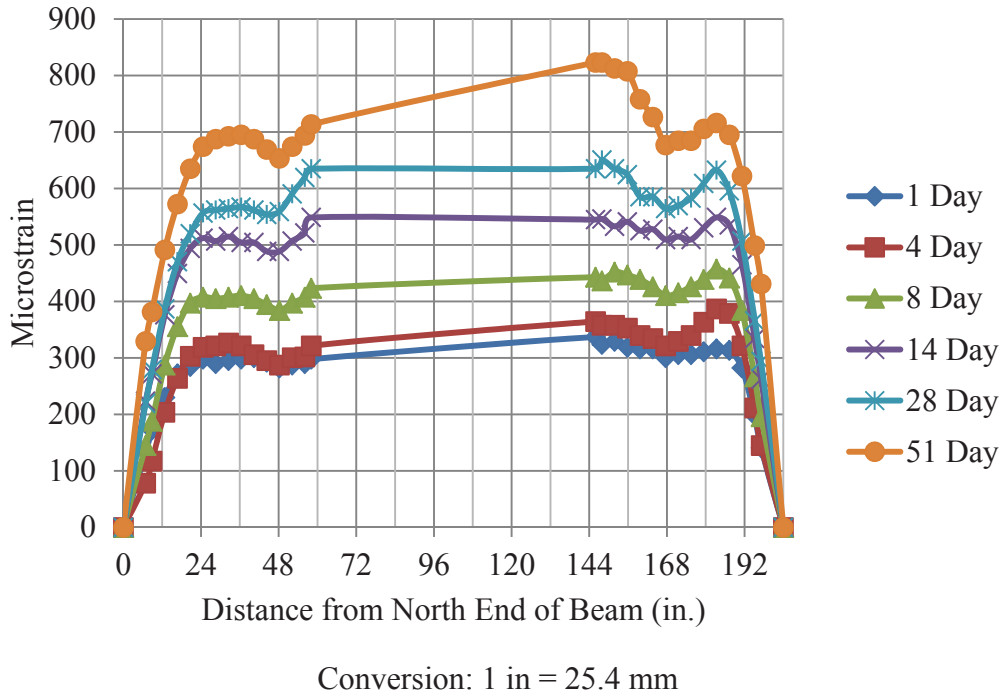


Figure D.17 – C10-4-1\_NE and C10-4-1\_SE Average Mean Strains

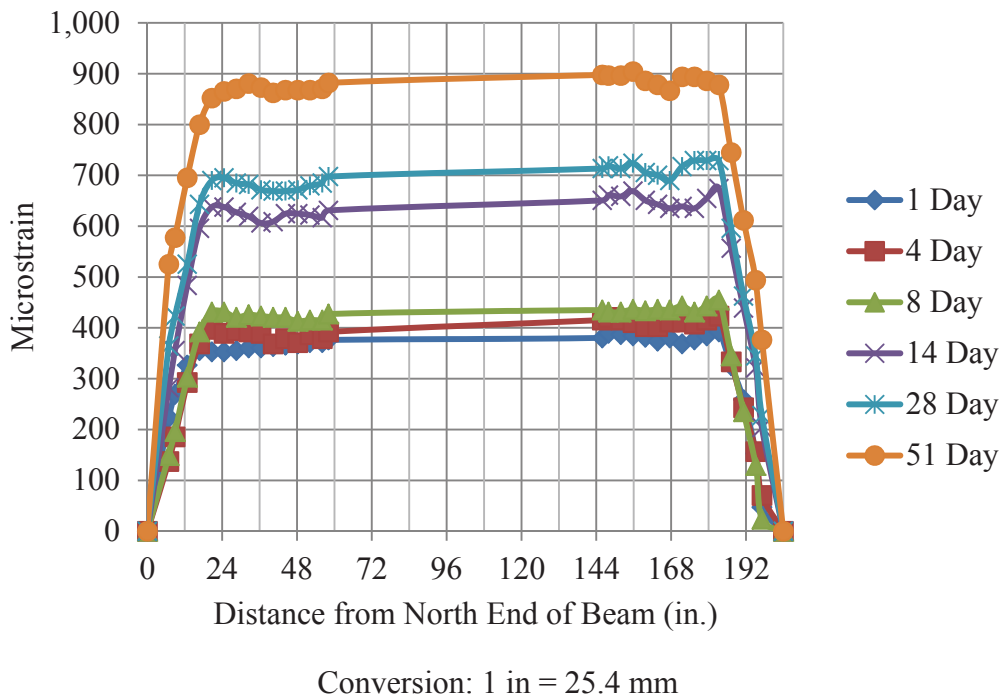


Figure D.18 – C10-4-1\_NW and C10-4-1\_SW Average Mean Strains

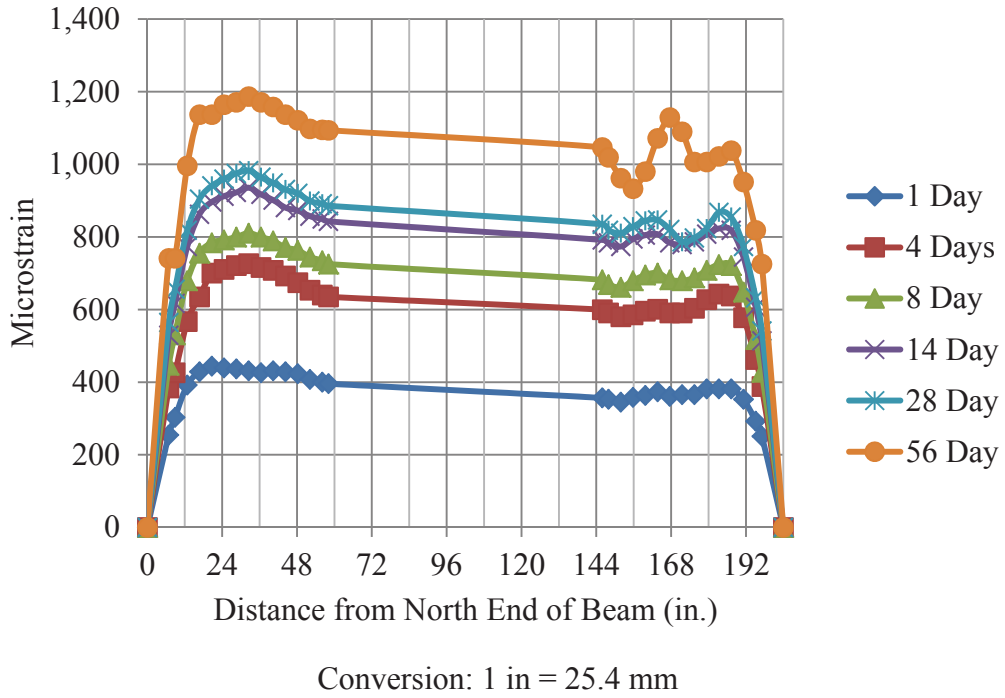


Figure D.19 – S10-2-1\_NE and S10-2-1\_SE Average Mean Strains

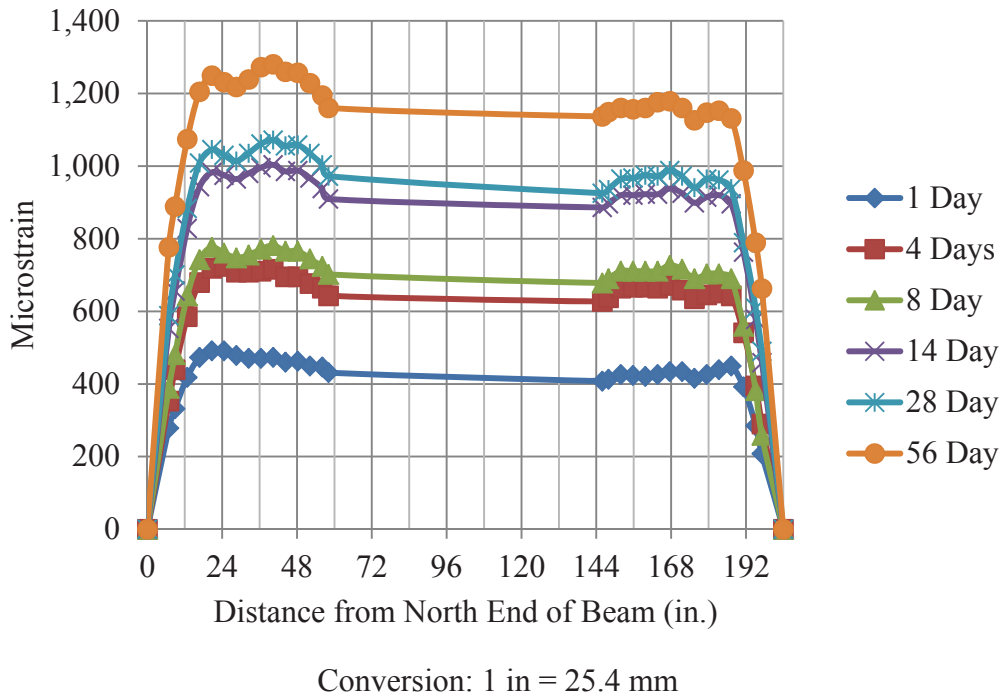


Figure D.20 – S10-2-1\_NW and S10-2-1\_SW Average Mean Strains

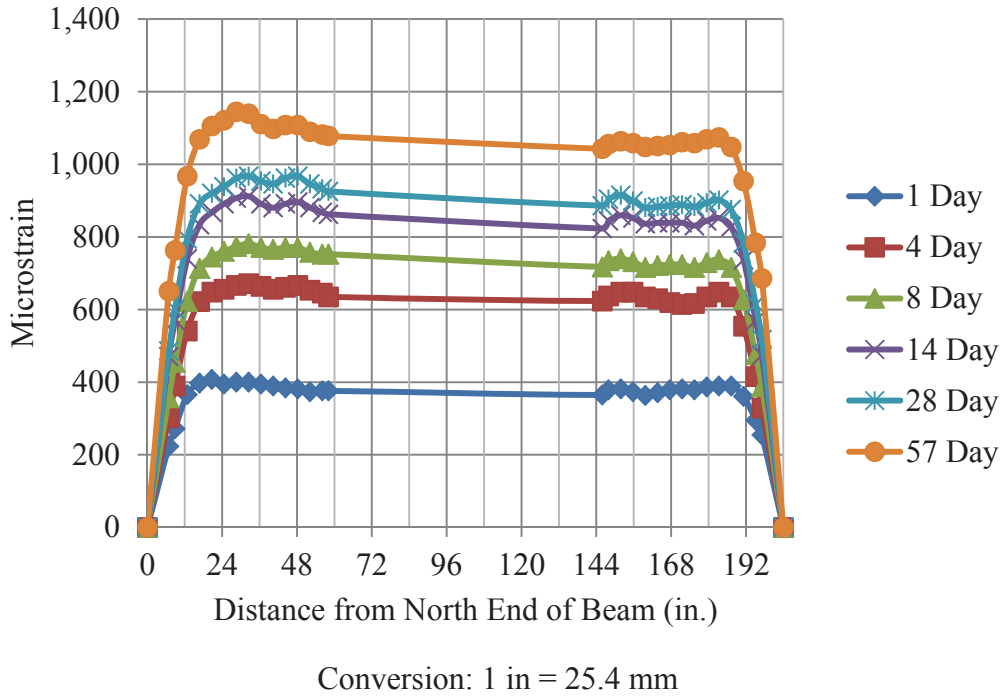


Figure D.21 – S10-2-2\_NE and S10-2-2\_SE Average Mean Strains

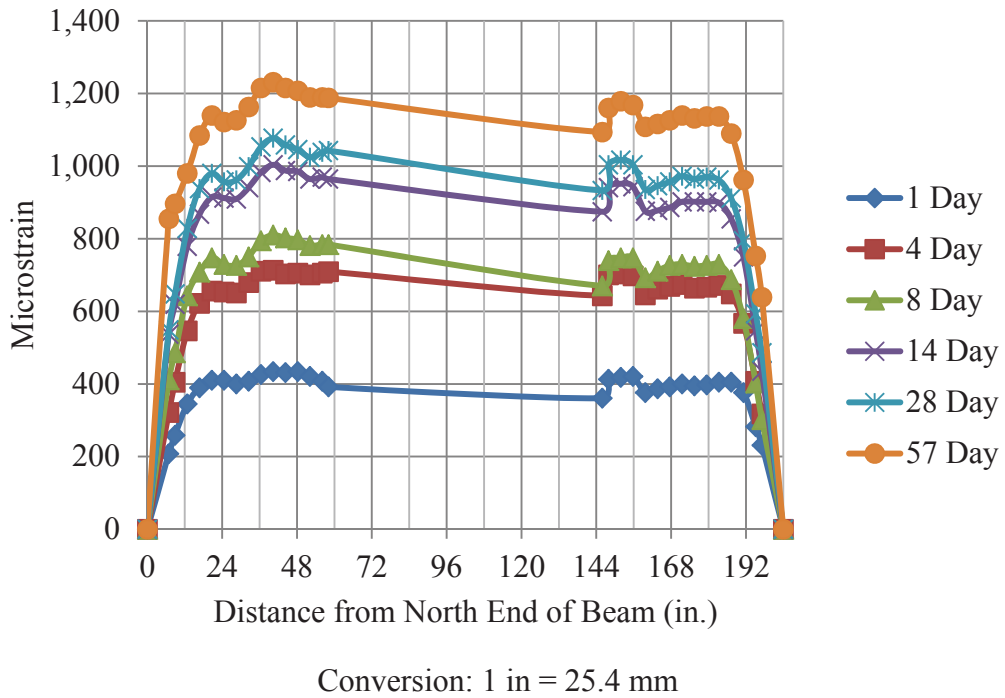


Figure D.22 – S10-2-2\_NW and S10-2-2\_SW Average Mean Strains

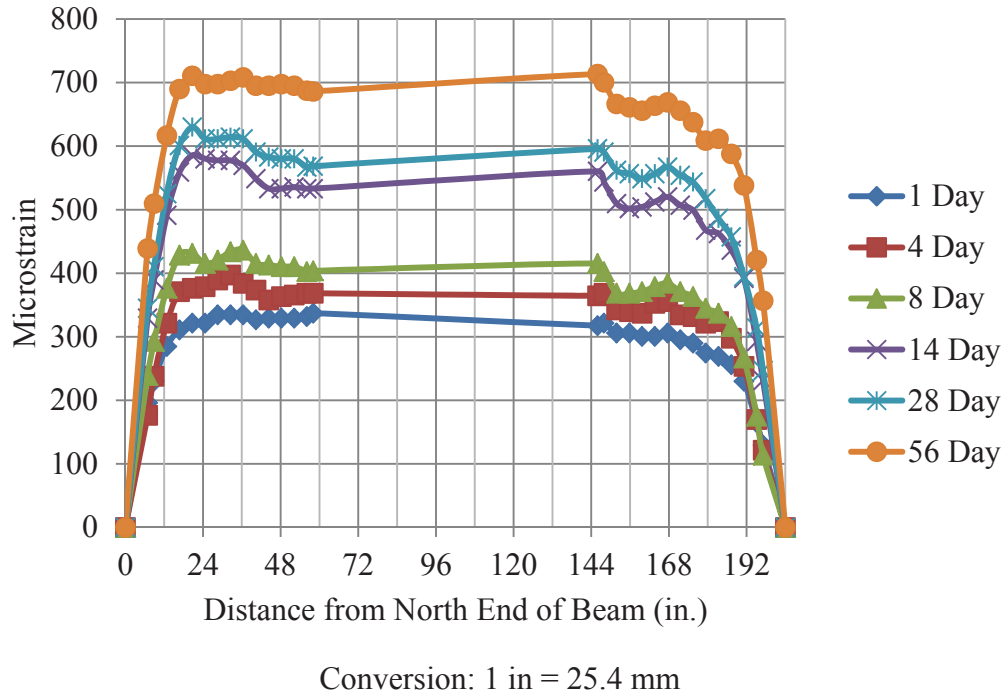


Figure D.23 – S10-4-1\_NE and S10-4-1\_SE Average Mean Strains

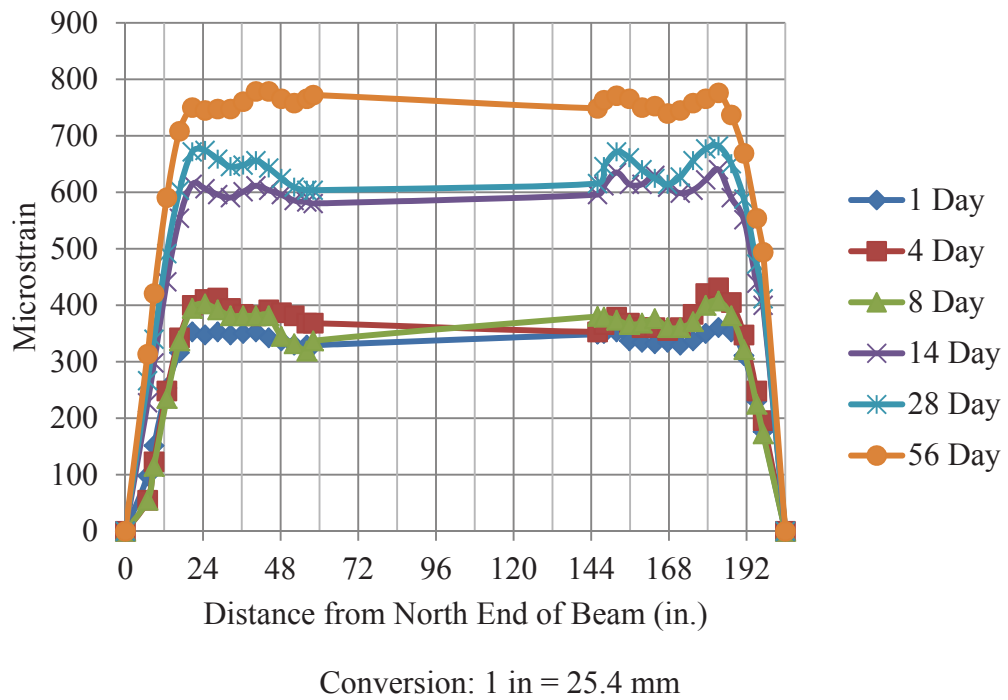
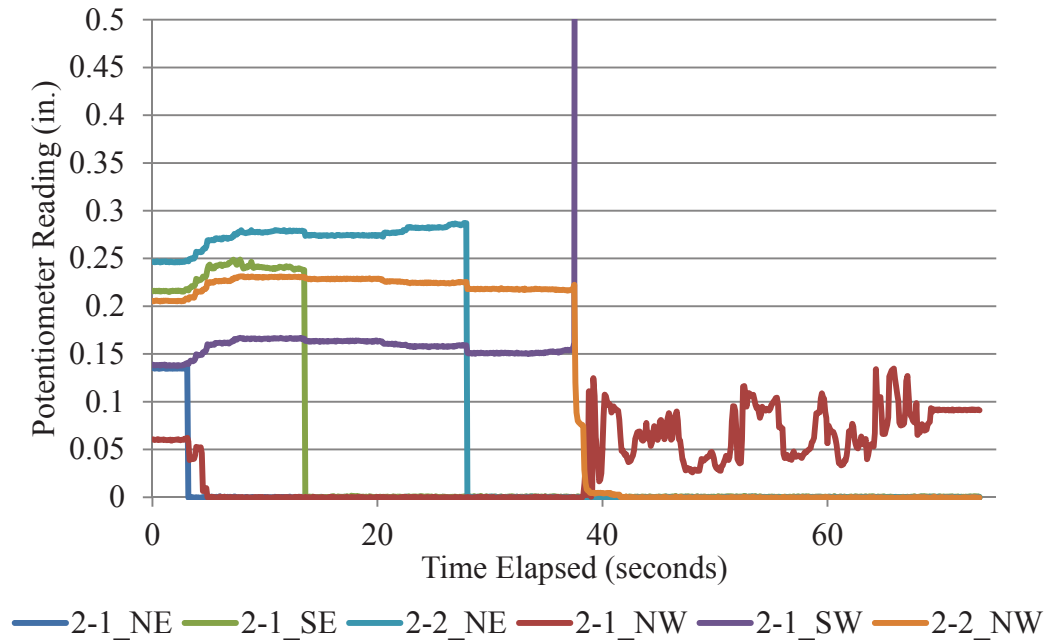


Figure D.24 – S10-4-1\_NW and S10-4-1\_SW Average Mean Strains

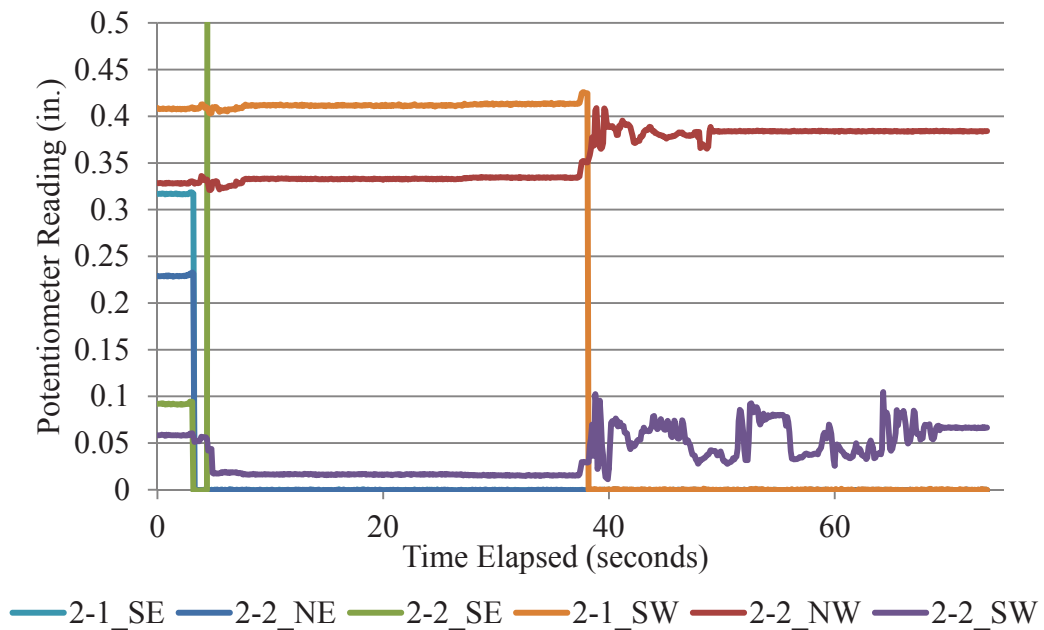
## **APPENDIX E**

### **Linear Potentiometer End Slip Plots**



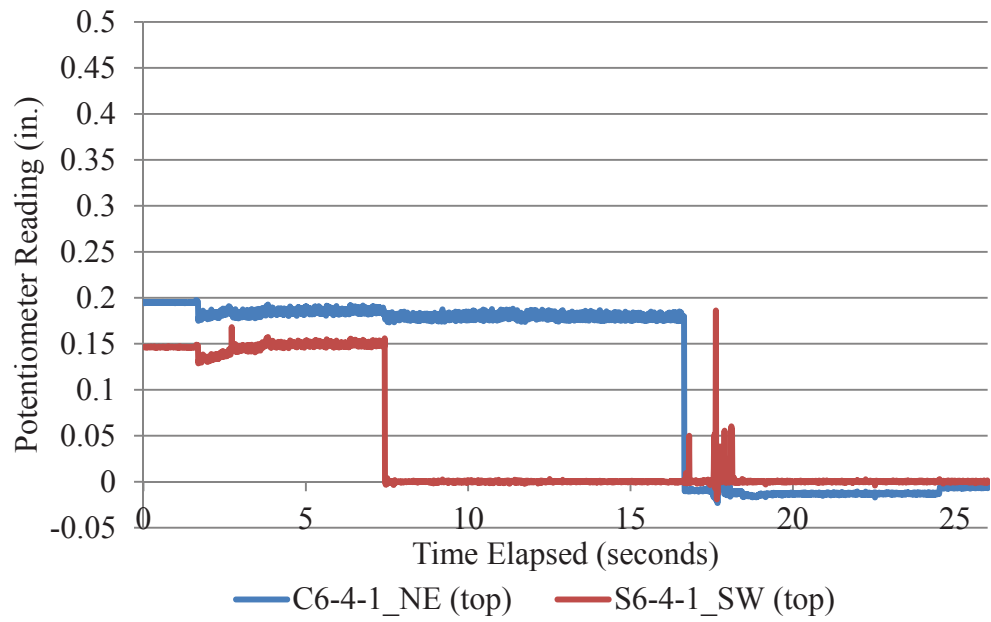
Conversion: 1 in. = 25.4 mm

**Figure E.1 – C6-2-1 and C6-2-2 Strands**



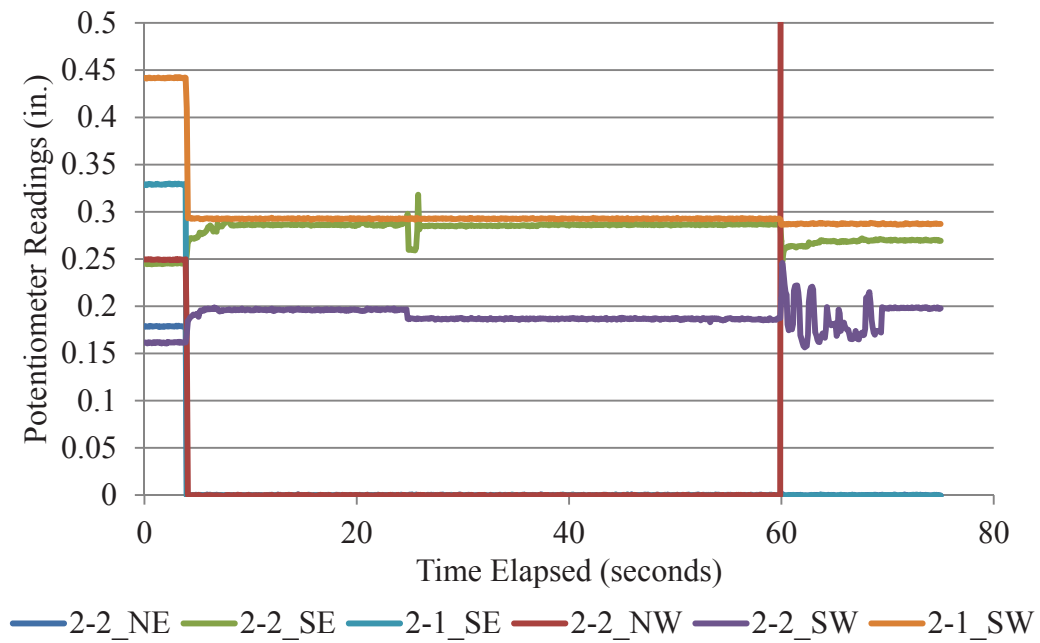
Conversion: 1 in. = 25.4 mm

**Figure E.2 – S6-2-1 and S6-2-2 Strands**



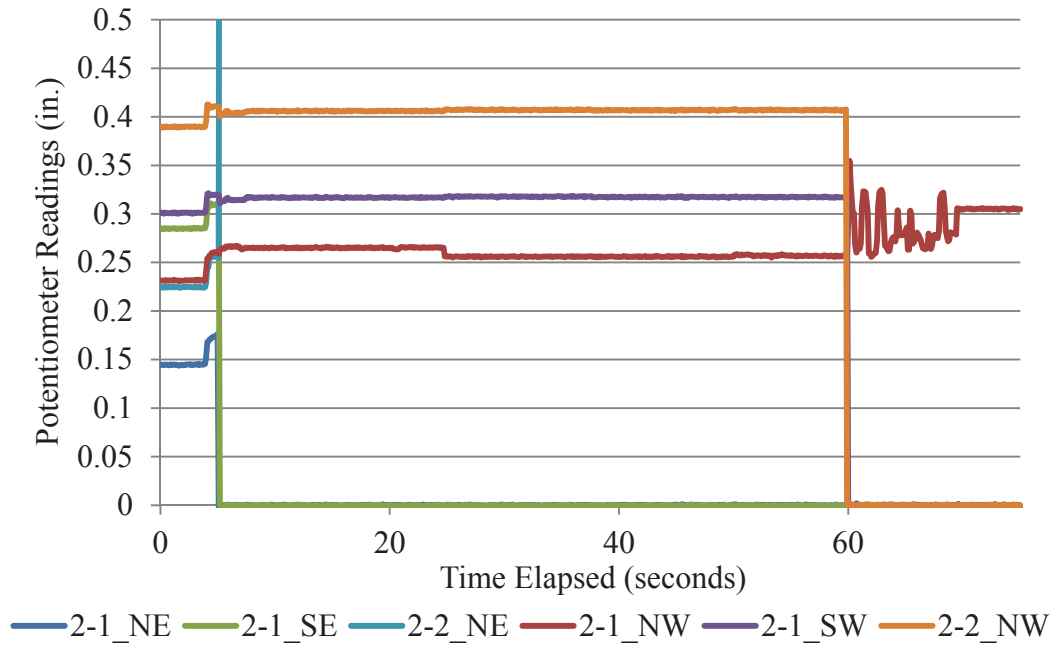
Conversion: 1 in. = 25.4 mm

**Figure E.3 – C6-4-1 and S6-4-1 Top Strands**



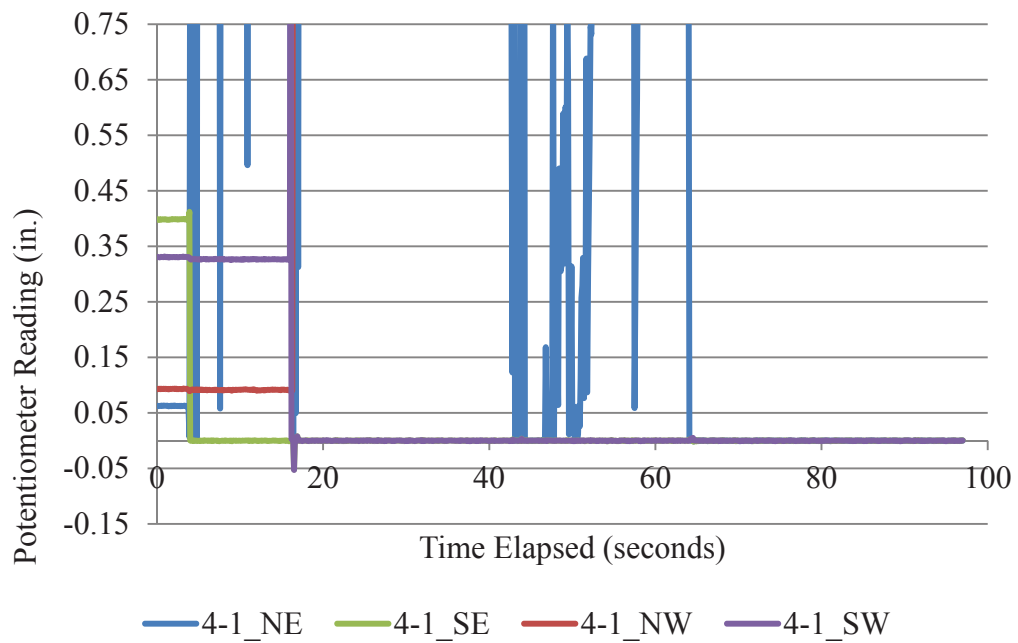
Conversion: 1 in. = 25.4 mm

**Figure E.4 – C10-2-1 and C10-2-2 Strands**



Conversion: 1 in. = 25.4 mm

**Figure E.5 – S10-2-1 and S10-2-2 Strands**



Conversion: 1 in. = 25.4 mm

**Figure E.6 – C10-4-1 Top Strands**

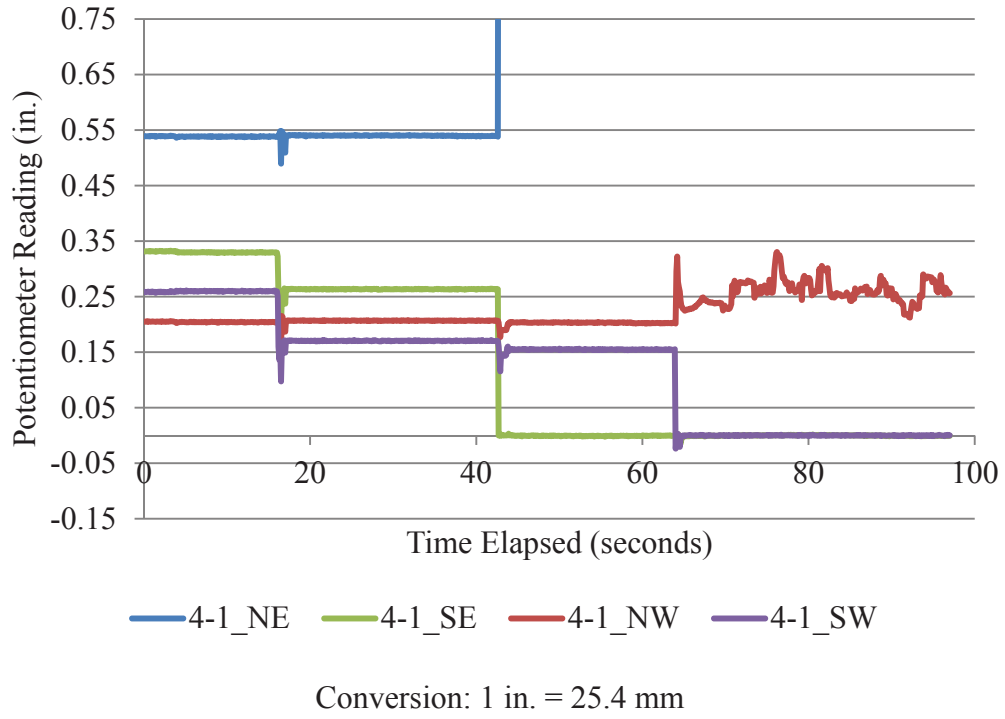


**Figure E.7 – C10-4-1 Bottom strands**

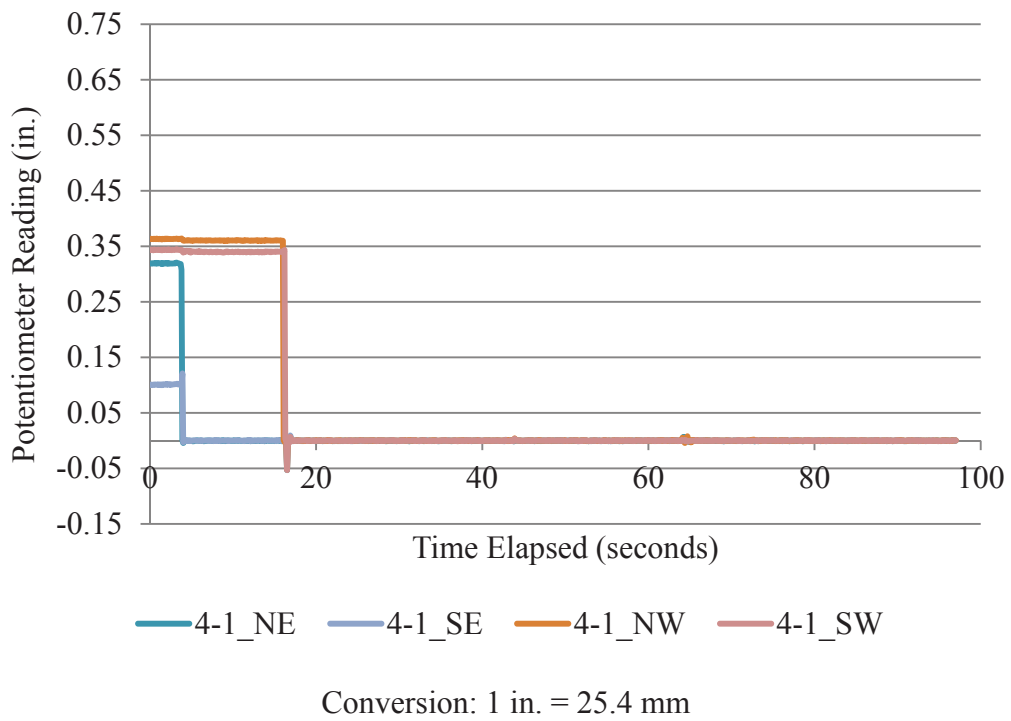
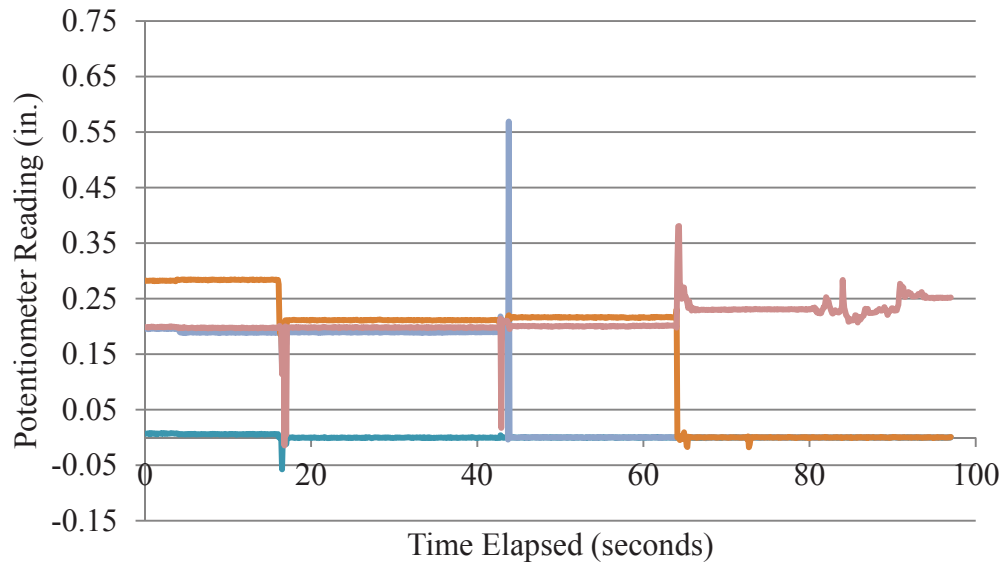


**Figure E.8 – S10-4-1 Top Strands**



— 4-1\_NE — 4-1\_SE — 4-1\_NW — 4-1\_SW

Conversion: 1 in. = 25.4 mm

**Figure E.9 – S10-4-1 Bottom Strands**

**APPENDIX F**  
**Development Length Test Summaries**

**BEAM ID:** C6-2-1\_58**DATE OF TESTING:** 9/7/2011**DAYS AFTER CASTING:** 48

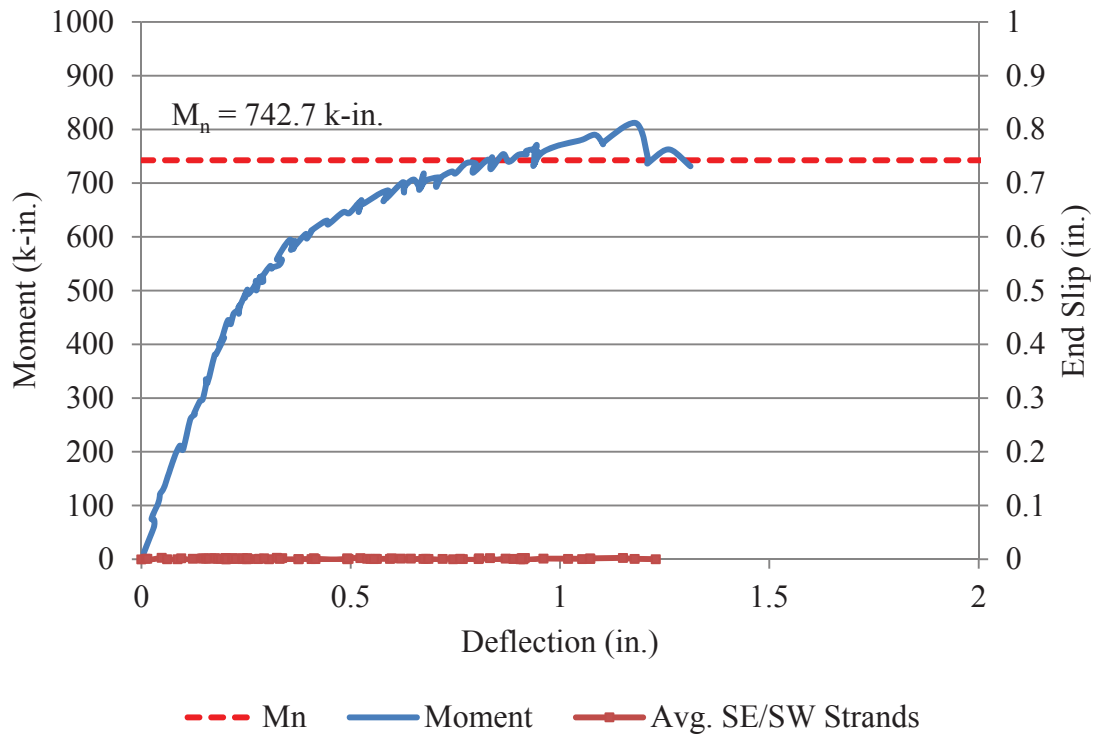
Test Summary		
Embedment Length	58 in.	
Failure Mode (Flexural or Bond)	Flexural	
Beam End	SE/SW	
Span Length	132 in.	
Deflection at Failure	1.2 in.	
Concrete Compressive Strength	5730 psi	
Maximum Moment Capacity	Expected	742.7 k-in.
	Actual	811.8 k-in.
Average Transfer Length	At Release	17.2 in.
	At Time of Testing	24.2 in.
Average 0.1 in. NASP Load for Strand 101		
Standard NASP(Mix B)		18200 lb
NASP in Concrete (1 Day)		21100 lb

The test was set up as deflection-controlled, and the beam was initially deflected in increments of 0.02 in. (0.508 mm). Once deflection reached 1.00 in. (2.54 mm), the increments were increased to 0.05 in. (1.27 mm) until failure because at this point, the beam was taking on increasingly less load per deflection increment. At each deflection increment, the load was noted and then the beam was checked for cracks, which were marked with permanent marker.

The first flexural crack was observed directly under the right support at a deflection of 0.30 in. (7.62 mm) and load of about 15.1 kips (67.2 kN). Subsequent flexural cracks in the middle and under the left support appeared at a deflection of 0.32 in. (8.13 mm) and load of 15.9 kips (70.7 kN). These cracks as well as subsequent cracks propagated vertically and then began angling towards the supports. The beam failed due to concrete crushing within the compression zone at a load of 27.8 kips (124 kN) and reached a deflection of 1.2 in. (30.5 mm) at failure. Negligible end slip was observed on both the SE and SW strands.



Figure F.1 – C6-2-1\_58 at Failure with Detail of Concrete Crushing



Conversion: 1 in. = 25.4 mm  
 1 k-in. = 113 N-m

Figure F.2 – C6-2-1\_58 Moment vs. Deflection and Strand End Slip vs. Deflection

**BEAM ID:** C6-2-1\_73

**DATE OF TESTING:** 9/7/2011

**DAYS AFTER CASTING:** 48

<b>Test Summary</b>		
Embedment Length	73 in.	
Failure Mode (Flexural or Bond)	Flexural	
Beam End	NE/NW	
Span Length	162 in.	
Deflection at Failure	1.9 in.	
Concrete Compressive Strength	5730 psi	
Maximum Moment Capacity	Expected	742.7 k-in.
	Actual	834.8 k-in.
Average Transfer Length (DEMEC)	At Release	17.2 in.
	At Time of Testing	24.2 in.
Average 0.1 in. NASP Load for Strand 101		
Standard NASP (Mix B)		18200 lb
NASP in Concrete (1 Day)		21100 lb

Conversion: 1 in. = 25.4 mm

1 lb = 4.45 N

1 psi = 6.89 kPa

The test was set up as deflection-controlled, and the beam was initially deflected in increments of 0.02 in. (0.508 mm). Once deflection reached 1.00 in. (25.4 mm), the increments were increased to 0.05 in. (1.27 mm) until failure because at this point, the beam was taking on increasingly less load per deflection increment. At each deflection increment, the load was noted and then the beam was checked for cracks, which were marked with permanent marker.

The first flexural cracks were observed under the right support and middle at a deflection of 0.48 in. (12.2 mm) and load of about 12.8 kips (56.9 kN). Subsequent cracks propagated vertically inside and outside the maximum moment zone and then began angling towards the supports. The beam failed due to concrete crushing within the compression zone at a load of 21.6 kips (96.1 kN) and reached a deflection of 1.9 in. (48.3 mm) at failure. Negligible end slip was observed on both the NE and NW strands.



**BEAM ID:** C6-2-2\_58

**DATE OF TESTING:** 9/12/2011

**DAYS AFTER CASTING:** 53

Test Summary		
Embedment Length	58 in.	
Failure Mode (Flexural or Bond)	Flexural	
Beam End	SE/SW	
Span Length	132 in.	
Deflection at Failure	1.2 in.	
Concrete Compressive Strength	5730 psi	
Maximum Moment Capacity	Expected	742.7 k-in.
	Actual	836.6 k-in.
Average Transfer Length	At Release	17.2 in.
	At Time of Testing	24.2 in.
Average 0.1 in. NASP Load for Strand 101		
Standard NASP (Mix B)		18200 lb
NASP in Concrete (1 Day)		21100 lb

Conversion: 1 in. = 25.4 mm

1 lb = 4.45 N

1 psi = 6.89 kPa

The test was set up as deflection-controlled, and the beam was deflected in increments of 0.05 in. (1.27 mm) until failure. The deflection increment was increased to 0.05 in. (1.27 mm) from 0.02 in. (0.508 mm) because it was deemed that 0.02 in (0.508 mm). increments was too slow. At each deflection increment, the load was noted and then the beam was checked for cracks, which were marked with permanent marker.

The first flexural cracks were observed under the supports and middle at a deflection of 0.25 in. (6.35 mm) and load of about 15.6 kips (69.4 kN). Subsequent cracks propagated vertically inside and outside the maximum moment zone and then began angling towards the supports. The beam failed due to concrete crushing within the compression zone at a load of 28.7 kips (128 kN) and reached a deflection of 1.21 in. (30.7 mm) at failure. Negligible end slip was observed on both the SE and SW strands.

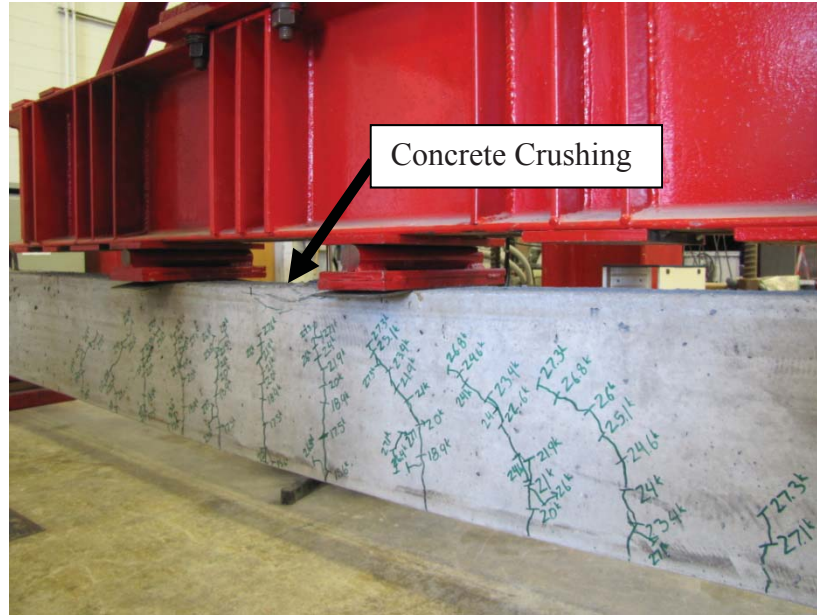
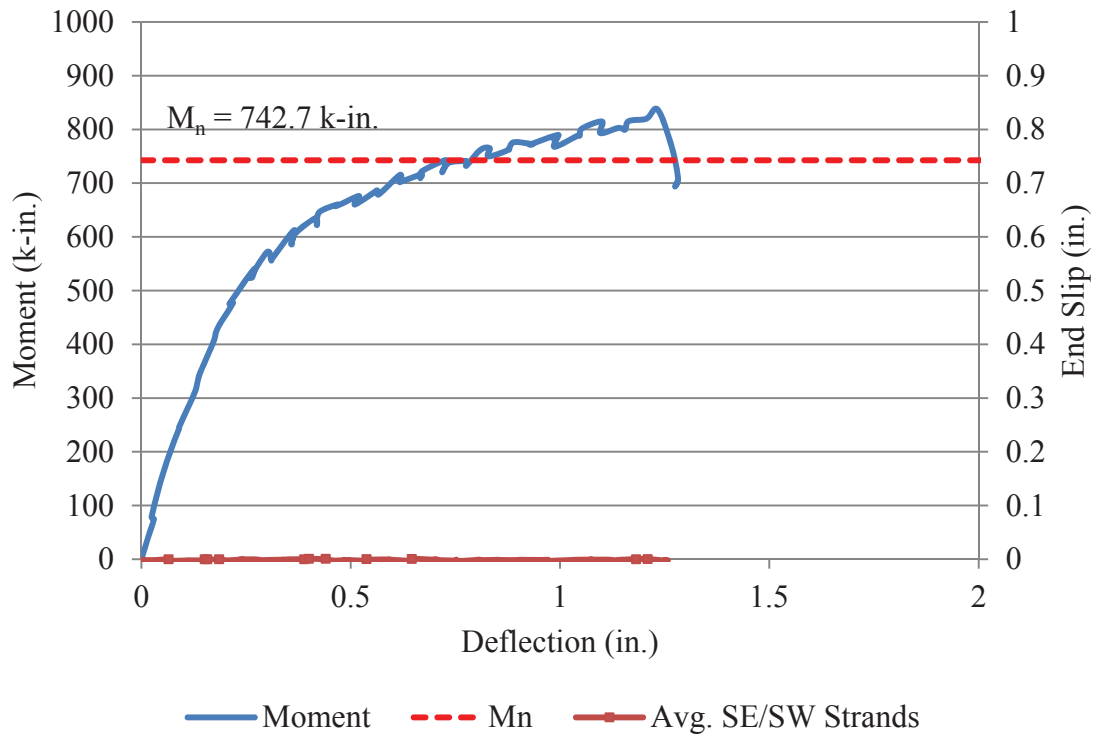


Figure F.5 – C6-2-2\_58 at Failure



Conversion: 1 in. = 25.4 mm  
 1 k-in. = 113 N-m

Figure F.6 – C6-2-2\_58 Moment vs. Deflection and Strand End Slip vs. Deflection

**BEAM ID:** C6-2-2\_73**DATE OF TESTING:** 9/13/2011**DAYS AFTER CASTING:** 54

Test Summary		
Embedment Length	73 in.	
Failure Mode (Flexural or Bond)	Flexural	
Beam End	NE/NW	
Span Length	162 in.	
Deflection at Failure	1.7 in.	
Concrete Compressive Strength	5730 psi	
Maximum Moment Capacity	Expected	742.7 k-in.
	Actual	837.6 k-in.
Average Transfer Length	At Release	17.2 in.
	At Time of Testing	24.2 in.
Average 0.1 in. NASP Load for Strand 101		
Standard NASP (Mix B)		18200 lb
NASP in Concrete (1 Day)		21100 lb

Conversion: 1 in. = 25.4 mm

1 lb = 4.45 N

1 psi = 6.89 kPa

The test was set up as deflection-controlled, and the beam was deflected in increments of 0.05 in. (1.27 mm) until failure. The deflection increment was increased to 0.05 in. (1.27 mm) from 0.02 in. (0.508 mm) because it was deemed that 0.02 in. (0.508 mm) increments were too slow. At each deflection increment, the load was noted and then the beam was checked for cracks, which were marked with permanent marker.

The first flexural crack was observed under the right support at a deflection of 0.40 in. (10.2 mm) and load of about 11.9 kips (52.9 kN). Subsequent cracks propagated vertically inside and outside the maximum moment zone and then began angling towards the supports. The beam failed due to concrete crushing within the compression zone at a load of 21.7 kips (96.5 kN) and reached a deflection of 1.73 in. (43.9 mm) at failure. Negligible end slip was observed on both the NE and NW strands.

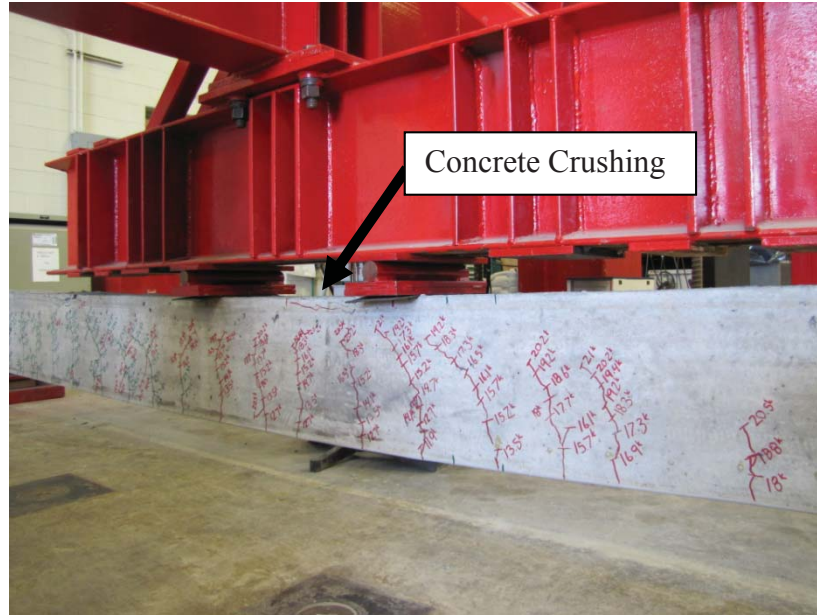
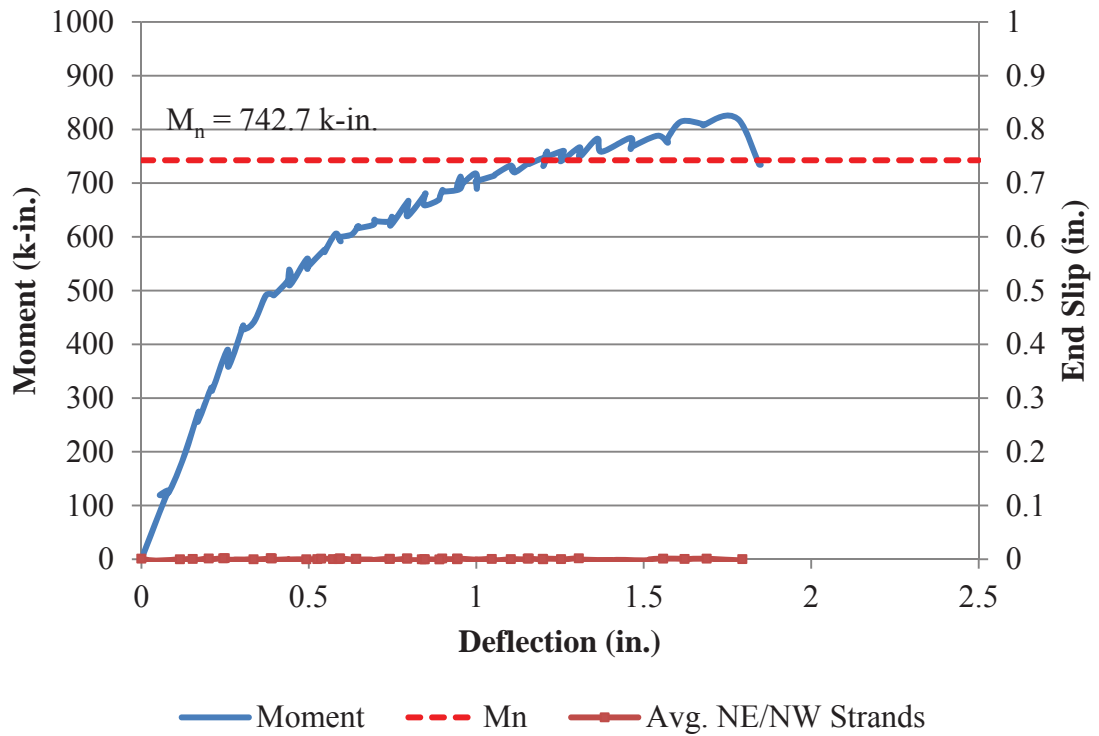


Figure F.7 – C6-2-2\_73 at Failure



Conversion: 1 in. = 25.4 mm  
 1 k-in. = 113 N-m

Figure F.8 – C6-2-2\_73 Moment vs. Deflection and Strand End Slip vs. Deflection

**BEAM ID:** S6-2-1\_58**DATE OF TESTING:** 9/14/2011**DAYS AFTER CASTING:** 55

Test Summary		
Embedment Length	58 in.	
Failure Mode (Flexural or Bond)	Flexural	
Beam End	SE/SW	
Span Length	132 in.	
Deflection at Failure	1.5 in.	
Concrete Compressive Strength	6950 psi	
Maximum Moment Capacity	Expected	757.9 k-in.
	Actual	867.7 k-in.
Average Transfer Length	At Release	14.4 in.
	At Time of Testing	19.2 in.
Average 0.1 in. NASP Load for Strand 101		
Standard NASP (Mix B)		18200 lb
NASP in Concrete (1 Day)		23700 lb

Conversion: 1 in. = 25.4 mm

1 lb = 4.45 N

1 psi = 6.89 kPa

The test was set up as deflection-controlled, and the beam was deflected in increments of 0.05 in. (1.27 mm) until failure. The deflection increment was increased to 0.05 in. (1.27 mm) from 0.02 in. (0.508 mm) because it was deemed that 0.02 in. (0.508 mm) increments were too slow. At each deflection increment, the load was noted and then the beam was checked for cracks, which were marked with permanent marker.

The first flexural crack was observed under the right support at a deflection of 0.25 in. (6.35 mm) and load of about 17.1 kips (76.1 kN). Subsequent cracks propagated vertically inside and outside the maximum moment zone and then began angling towards the supports. The beam failed due to concrete crushing within the compression zone at a load of 29.9 kips (133 kN) and reached a deflection of 1.49 in. (37.8 mm) at failure. Negligible end slip was observed on both the SE and SW strands.



**BEAM ID:** S6-2-1\_73

**DATE OF TESTING:** 9/14/2011

**DAYS AFTER CASTING:** 55

<b>Test Summary</b>		
Embedment Length	73 in.	
Failure Mode (Flexural or Bond)	Flexural	
Beam End	NE/NW	
Span Length	162 in.	
Deflection at Failure	2.2 in.	
Concrete Compressive Strength	6950 psi	
Maximum Moment Capacity	Expected	757.9 k-in.
	Actual	878.4 k-in.
Average Transfer Length	At Release	14.4 in.
	At Time of Testing	19.2 in.
Average 0.1 in. NASP Load for Strand 101		
Standard NASP (Mix B)		18200 lb
NASP in Concrete (1 Day)		23700 lb

Conversion: 1 in. = 25.4 mm

1 lb = 4.45 N

1 psi = 6.89 kPa

The test was set up as deflection-controlled, and the beam was deflected in increments of 0.05 in. (1.27 mm) until failure. The deflection increment was increased to 0.05 in. (1.27 mm) from 0.02 in. (0.508 mm) because it was deemed that 0.02 in. (0.508 mm) increments were too slow. At each deflection increment, the load was noted and then the beam was checked for cracks, which were marked with permanent marker.

The first flexural crack was observed under the midspan and right support at a deflection of 0.45 in. (11.4 mm) and load of about 12.1 kips (53.8 kN). Subsequent cracks propagated vertically inside and outside the maximum moment zone and then began angling towards the supports. Horizontal cracks near midspan at the level of prestressing strand were noted at a deflection of 1.30 in. (33.0 mm) and a load of 19.8 kips (88.1 kN). The beam failed due to concrete crushing within the compression zone at a load of 22.9 kips (102 kN) and reached a deflection of 2.20 in. (55.9 mm) at failure. Negligible end slip was observed on both the NE and NW strands.

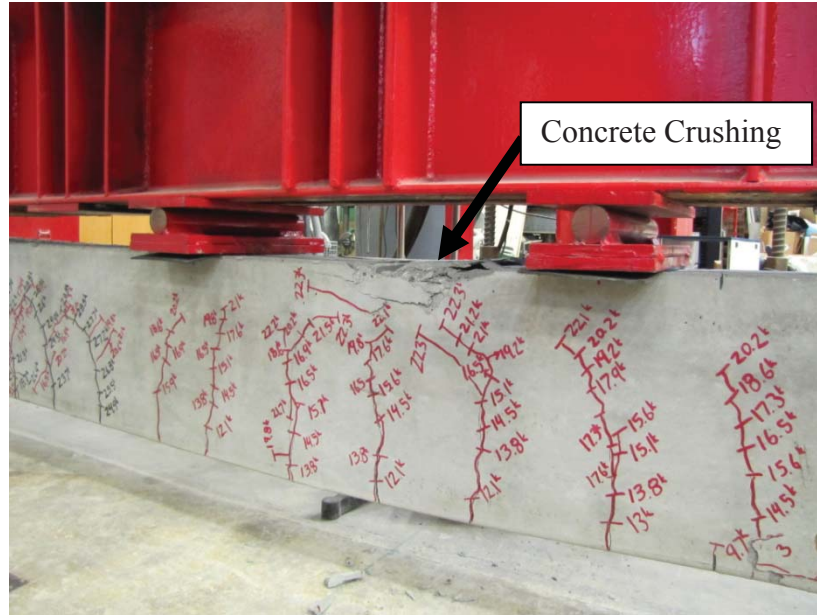
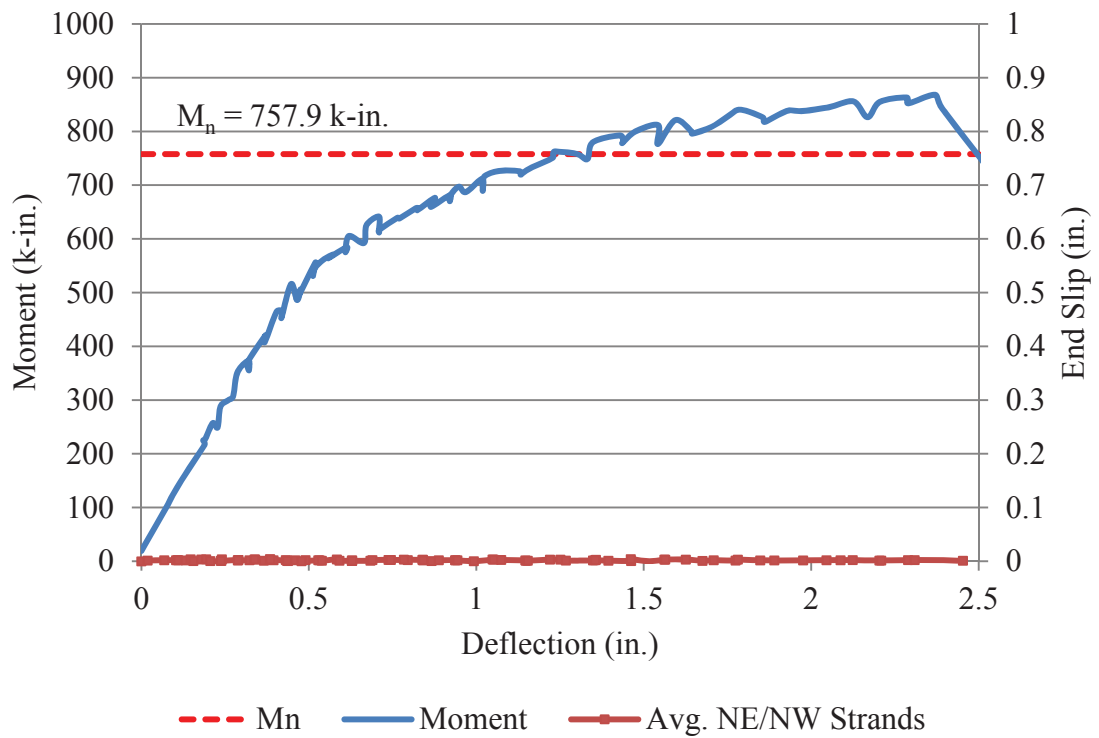


Figure F.11 – S6-2-1\_73 at Failure



Conversion: 1 in. = 25.4 mm  
 1 k-in. = 113 N-m

Figure F.12 – S6-2-1\_73 Moment vs. Deflection and Strand End Slip vs. Deflection

**BEAM ID:** S6-2-2\_58

**DATE OF TESTING:** 9/9/2011

**DAYS AFTER CASTING:** 50

<b>Test Summary</b>		
Embedment Length	58 in.	
Failure Mode (Flexural or Bond)	Flexural	
Beam End	SE/SW	
Span Length	132 in.	
Deflection at Failure	1.5 in.	
Concrete Compressive Strength	6950 psi	
Maximum Moment Capacity	Expected	757.9 k-in.
	Actual	889.9 k-in.
Average Transfer Length	At Release	14.4 in.
	At Time of Testing	19.2 in.
Average 0.1 in. NASP Load for Strand 101		
Standard NASP (Mix B)		18200 lb
NASP in Concrete (1 Day)		23700 lb

Conversion: 1 in. = 25.4 mm

1 lb = 4.45 N

1 psi = 6.89 kPa

The test was set up as deflection-controlled, and the beam was deflected in increments of 0.05 in. (1.27 mm) until failure. The deflection increment was increased to 0.05 in. (1.27 mm) from 0.02 in. (0.508 mm) because it was deemed that 0.02 in. (0.508 mm) increments were too slow. At each deflection increment, the load was noted and then the beam was checked for cracks, which were marked with permanent marker.

The first flexural crack was observed under the right support at a deflection of 0.25 in. (6.35 mm) and load of about 16.3 kips (72.5 kN). Subsequent cracks propagated vertically inside and outside the maximum moment zone and then began angling towards the supports. Horizontal cracks near midspan at the level of prestressing strand were noted at a deflection of 0.75 in. (19.1 mm) and a load of 25.9 kips (115 kN). The beam failed due to concrete crushing within the compression zone at a load of 30.7 kips (137 kN) and reached a deflection of 1.52 in. (38.6 mm) at failure. Negligible end slip was observed on both the SE and SW strands.



**BEAM ID:** S6-2-2\_73

**DATE OF TESTING:** 9/9/2011

**DAYS AFTER CASTING:** 50

<b>Test Summary</b>		
Embedment Length	73 in.	
Failure Mode (Flexural or Bond)	Flexural	
Beam End	NE/NW	
Span Length	162 in.	
Deflection at Failure	1.8 in.	
Concrete Compressive Strength	6950 psi	
Maximum Moment Capacity	Expected	757.9 k-in.
	Actual	843.1 k-in.
Average Transfer Length	At Release	14.4 in.
	At Time of Testing	19.2 in.
Average 0.1 in. NASP Load for Strand 101		
Standard NASP (Mix B)		18200 lb
NASP in Concrete (1 Day)		23700 lb

Conversion: 1 in. = 25.4 mm

1 lb = 4.45 N

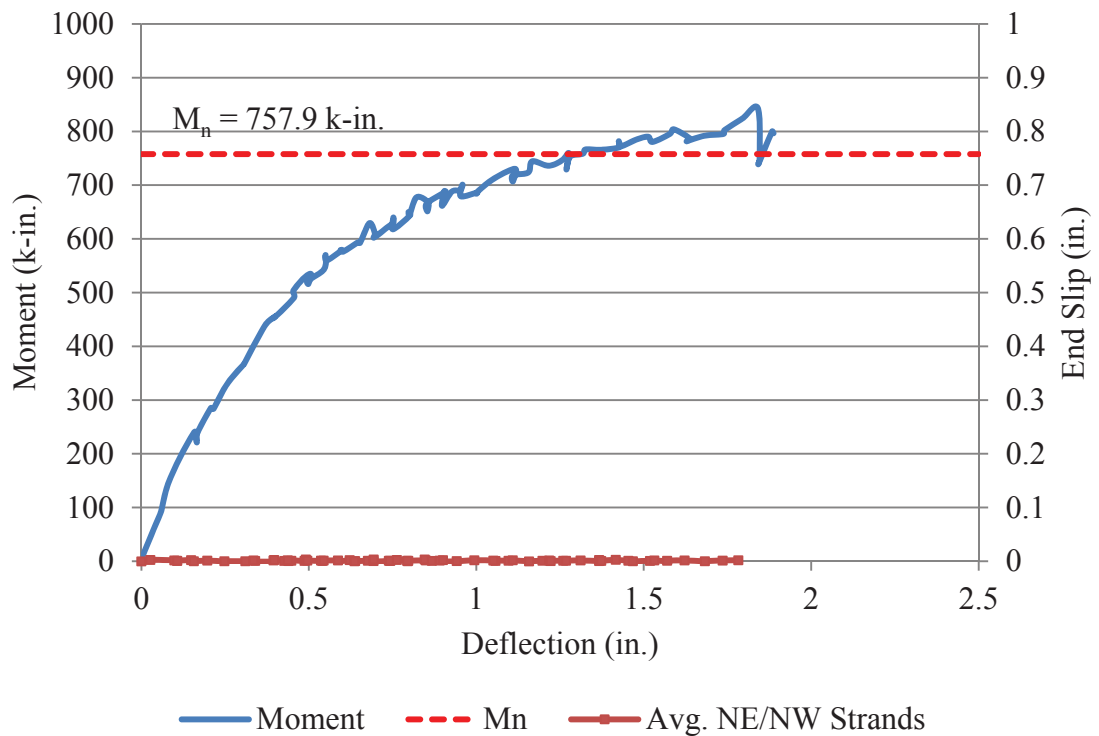
1 psi = 6.89 kPa

The test was set up as deflection-controlled, and the beam was deflected in increments of 0.05 in. (1.27 mm) until failure. The deflection increment was increased to 0.05 in. (1.27 mm) from 0.02 in. (0.508 mm) because it was deemed that 0.02 in. (0.508 mm) increments were too slow. At each deflection increment, the load was noted and then the beam was checked for cracks, which were marked with permanent marker.

The first flexural crack was observed under the left support at a deflection of 0.40 in. (10.2 mm) and load of about 10.8 kips (48.0 kN). Subsequent cracks propagated vertically inside and outside the maximum moment zone and then began angling towards the supports. The beam failed due to concrete crushing outside the compression zone at a load of 21.9 kips (97.4 kN) and reached a deflection of 1.78 in. (45.2 mm) at failure. The failure occurred in the area that had already failed during the 58 in. (1,473 mm) embedment length test, however, it was still deemed a flexural failure by concrete crushing. Negligible end slip was observed on both the NE and NW strands.



Figure F.15 – S6-2-2\_73 at Failure



Conversion: 1 in. = 25.4 mm  
 1 k-in. = 113 N-m

Figure F.16 – S6-2-2\_73 Moment vs. Deflection and Strand End Slip vs. Deflection

**BEAM ID:** C10-2-1\_58

**DATE OF TESTING:** 9/15/2011

**DAYS AFTER CASTING:** 52

<b>Test Summary</b>		
Embedment Length	58 in.	
Failure Mode (Flexural or Bond)	Flexural	
Beam End	SE/SW	
Span Length	132 in.	
Deflection at Failure	1.5 in.	
Concrete Compressive Strength	8480 psi	
Maximum Moment Capacity	Expected	773.6 k-in.
	Actual	880.3 k-in.
Average Transfer Length	At Release	20.1 in.
	At Time of Testing	23.5 in.
Average 0.1 in. NASP Load for Strand 101		
Standard NASP (Mix B)		18200 lb
NASP in Concrete (1 Day)		26700 lb

Conversion: 1 in. = 25.4 mm

1 lb = 4.45 N

1 psi = 6.89 kPa

The test was set up as deflection-controlled, and the beam was deflected in increments of 0.05 in. (1.27 mm) until failure. The deflection increment was increased to 0.05 in. (1.27 mm) from 0.02 in. (0.508 mm) because it was deemed that 0.02 in. (0.508 mm) increments were too slow. At each deflection increment, the load was noted and then the beam was checked for cracks, which were marked with permanent marker.

The first flexural crack was observed under the midspan and right support at a deflection of 0.30 in. (7.62 mm) and load of about 17.5 kips (77.8 kN). Subsequent cracks propagated vertically inside and outside the maximum moment zone and then began angling towards the supports. Horizontal cracks near midspan at the level of prestressing strand were noted at a deflection of 0.65 in. (16.5 mm) and a load of 24.8 kips (110 kN). The beam failed due to concrete crushing within the compression zone at a load of 30.3 kips (135 kN) and reached a deflection of 1.48 in. (37.6 mm) at failure. Negligible end slip was observed on both the SE and SW strands.

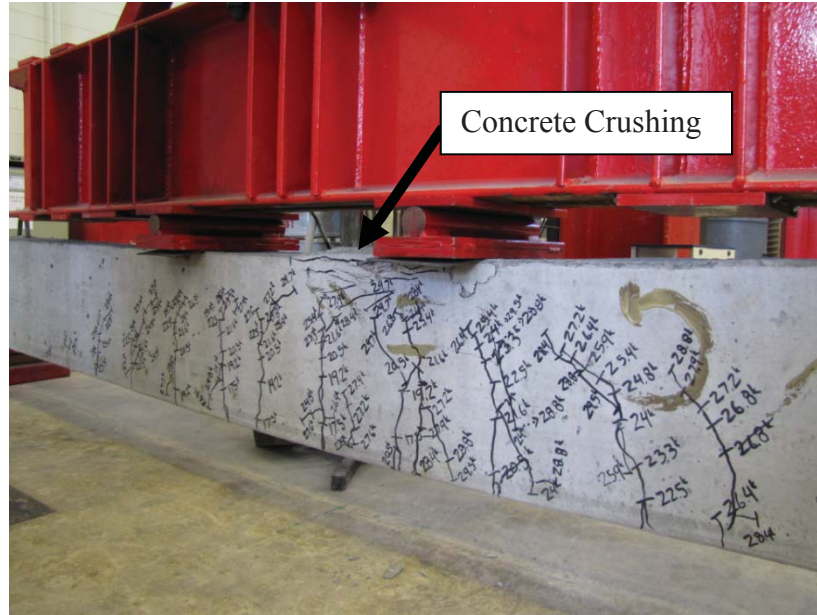
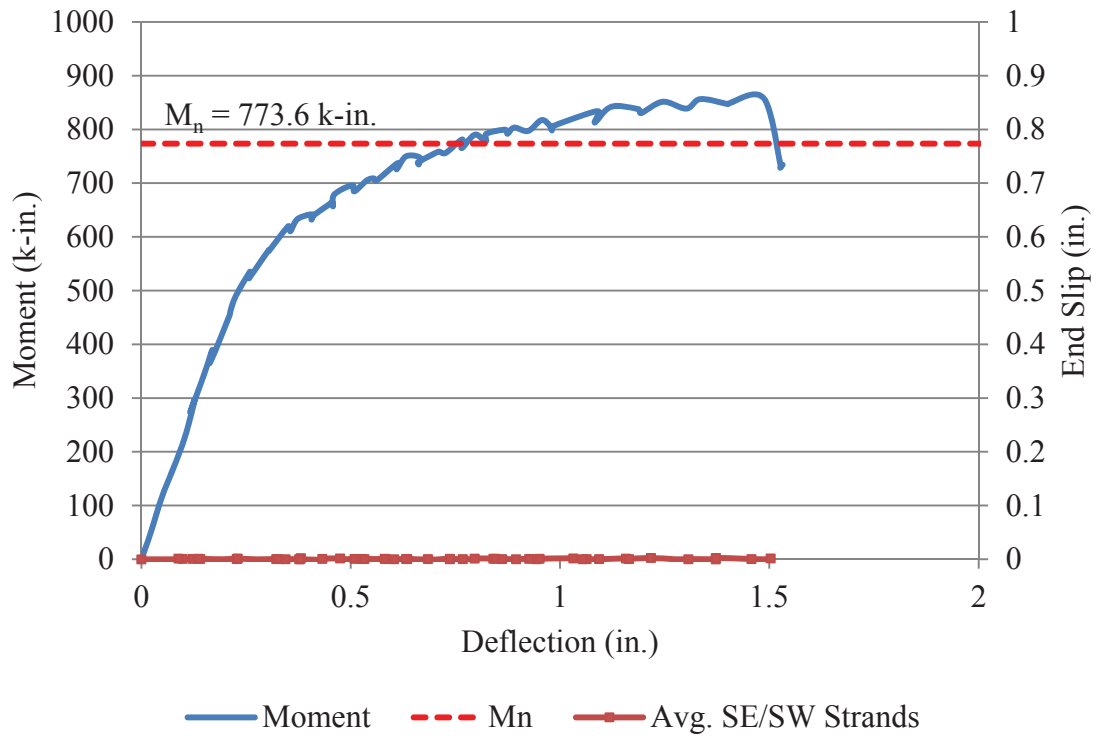


Figure F.17 – C10-2-1\_58 at Failure



Conversion: 1 in. = 25.4 mm  
 1 k-in. = 113 N-m

Figure F.18 – C10-2-1\_58 Moment vs. Deflection and Strand End Slip vs. Deflection

**BEAM ID:** C10-2-1\_73

**DATE OF TESTING:** 9/16/2011

**DAYS AFTER CASTING:** 53

<b>Test Summary</b>		
Embedment Length	73 in.	
Failure Mode (Flexural or Bond)	Flexural	
Beam End	NE/NW	
Span Length	162 in.	
Deflection at Failure	2.0 in.	
Concrete Compressive Strength	8480 psi	
Maximum Moment Capacity	Expected	773.6 k-in.
	Actual	880.7 k-in.
Average Transfer Length	At Release	20.1 in.
	At Time of Testing	23.5 in.
Average 0.1 in. NASP Load for Strand 101		
Standard NASP (Mix B)		18200 lb
NASP in Concrete (1 Day)		26700 lb

Conversion: 1 in. = 25.4 mm

1 lb = 4.45 N

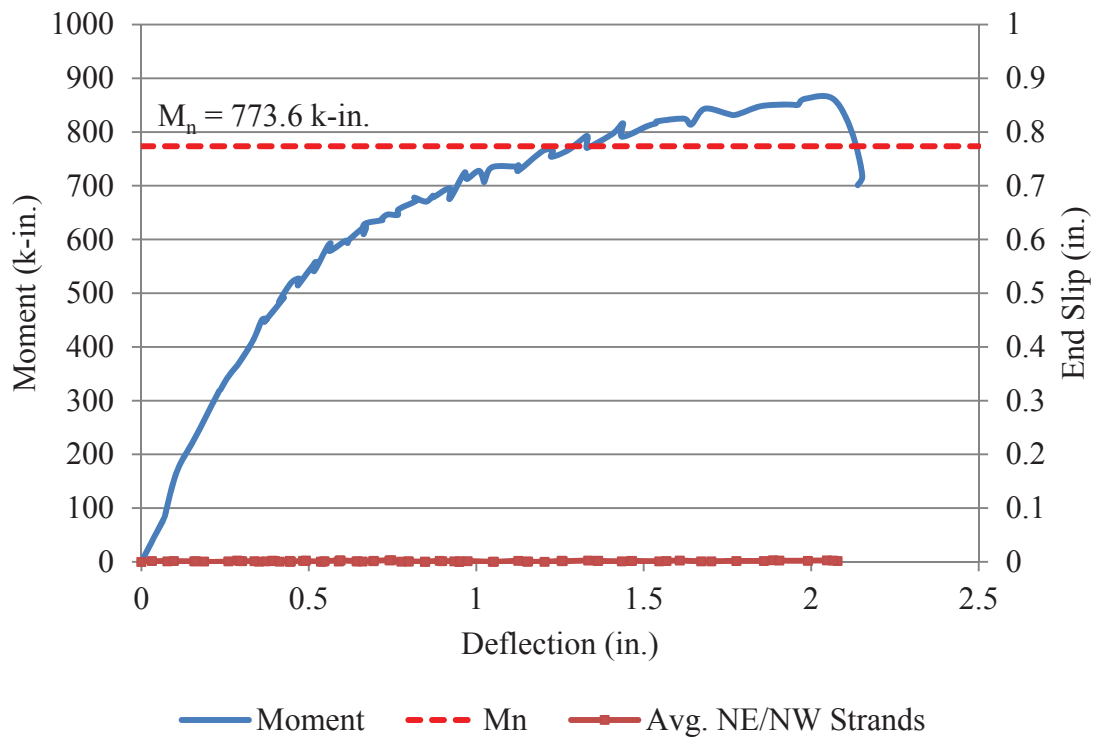
1 psi = 6.89 kPa

The test was set up as deflection-controlled, and the beam was deflected in increments of 0.05 in. (1.27 mm) until failure. The deflection increment was increased to 0.05 in. (1.27 mm) from 0.02 in. (0.508 mm) because it was deemed that 0.02 in. (0.508 mm) increments were too slow. At each deflection increment, the load was noted and then the beam was checked for cracks, which were marked with permanent marker.

The first flexural crack was observed under the midspan and right support at a deflection of 0.40 in. (10.2 mm) and load of about 11.8 kips (52.5 kN). Subsequent cracks propagated vertically inside and outside the maximum moment zone and then began angling towards the supports. Horizontal cracks near midspan at the level of prestressing strand were noted at a deflection of 1.20 in. (30.5 mm) and a load of 19.5 kips (86.7 kN). The beam failed due to concrete crushing within the compression zone at a load of 23.0 kips (102 kN) and reached a deflection of 1.97 in. (50.0 mm) at failure. Negligible end slip was observed on both the NE and NW strands.



Figure F.19 – C10-2-1\_73 at Failure



Conversion: 1 in. = 25.4 mm  
 1 k-in. = 113 N-m

Figure F.20 – C10-2-1\_73 Moment vs. Deflection and Strand End Slip vs. Deflection

**BEAM ID:** C10-2-2\_58

**DATE OF TESTING:** 9/16/2011

**DAYS AFTER CASTING:** 53

Test Summary	
Embedment Length	58 in.
Failure Mode (Flexural or Bond)	Flexural
Beam End	SE/SW
Span Length	132 in.
Deflection at Failure	1.5 in.
Concrete Compressive Strength	8480 psi
Maximum Moment Capacity	Expected 875.3 k-in.
	Actual 813.6 k-in.
Average Transfer Length	At Release 20.1 in.
	At Time of Testing 23.5 in.
Average 0.1 in. NASP Load for Strand 101	
Standard NASP (Mix B)	18200 lb
NASP in Concrete (1 Day)	26700 lb

Conversion: 1 in. = 25.4 mm

1 lb = 4.45 N

1 psi = 6.89 kPa

The test was set up as deflection-controlled, and the beam was deflected in increments of 0.05 in. (1.27 mm) until failure. The deflection increment was increased to 0.05 in. (1.27 mm) from 0.02 in. (0.508 mm) because it was deemed that 0.02 in. (0.508 mm) increments were too slow. At each deflection increment, the load was noted and then the beam was checked for cracks, which were marked with permanent marker.

The first flexural crack was observed under midspan at a deflection of 0.25 in. (6.35 mm) and load of about 15.0 kips (66.7 kN). Subsequent cracks propagated vertically inside and outside the maximum moment zone and then began angling towards the supports. Horizontal cracks near midspan at the level of prestressing strand were noted at a deflection of 0.85 in. (21.6 mm) and a load of 26.5 kips (118 kN). The beam failed due to concrete crushing within the compression zone at a load of 30.1 kips (134 kN) and reached a deflection of 1.51 in. (38.4 mm) at failure. Negligible end slip was observed on both the SE and SW strands.



**BEAM ID:** C10-2-2\_73

**DATE OF TESTING:** 9/16/2011

**DAYS AFTER CASTING:** 53

Test Summary		
Embedment Length	73 in.	
Failure Mode (Flexural or Bond)	Flexural	
Beam End	NE/NW	
Span Length	162 in.	
Deflection at Failure	2.0 in.	
Concrete Compressive Strength	8480 psi	
Maximum Moment Capacity	Expected	773.6 k-in.
	Actual	885.8 k-in.
Average Transfer Length	At Release	20.1 in.
	At Time of Testing	23.5 in.
Average 0.1 in. NASP Load for Strand 101		
Standard NASP(Mix B)		18200 lb
NASP in Concrete (1 Day)		26700 lb

Conversion: 1 in. = 25.4 mm

1 lb = 4.45 N

1 psi = 6.89 kPa

The test was set up as deflection-controlled, and the beam was deflected in increments of 0.05 in. (1.27 mm) until failure. The deflection increment was increased to 0.05 in. (1.27 mm) from 0.02 in. (0.508 mm) because it was deemed that 0.02 in. (0.508 mm) increments were too slow. At each deflection increment, the load was noted and then the beam was checked for cracks, which were marked with permanent marker.

The first flexural crack was observed under the midspan at a deflection of 0.45 in. (11.4 mm) and load of about 11.7 kips (52.0 kN). Subsequent cracks propagated vertically inside and outside the maximum moment zone and then began angling towards the supports. Horizontal cracks near midspan at the level of prestressing strand were noted at a deflection of 1.20 in. (30.5 mm) and a load of 18.8 kips (83.6 kN). The beam failed due to concrete crushing within the compression zone at a load of 23.1 kips (103 kN) and reached a deflection of 1.97 in. (50.0 mm) at failure. Negligible end slip was observed on both the NE and NW strands.

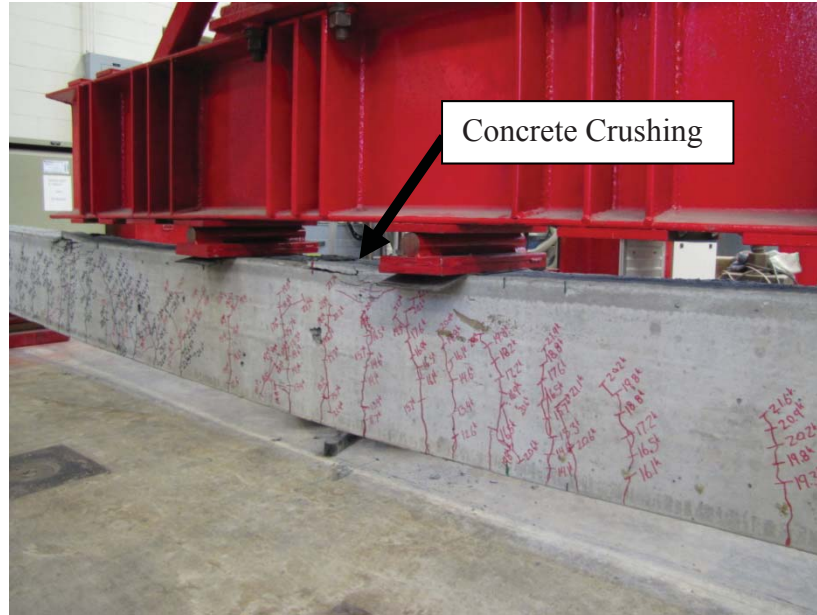
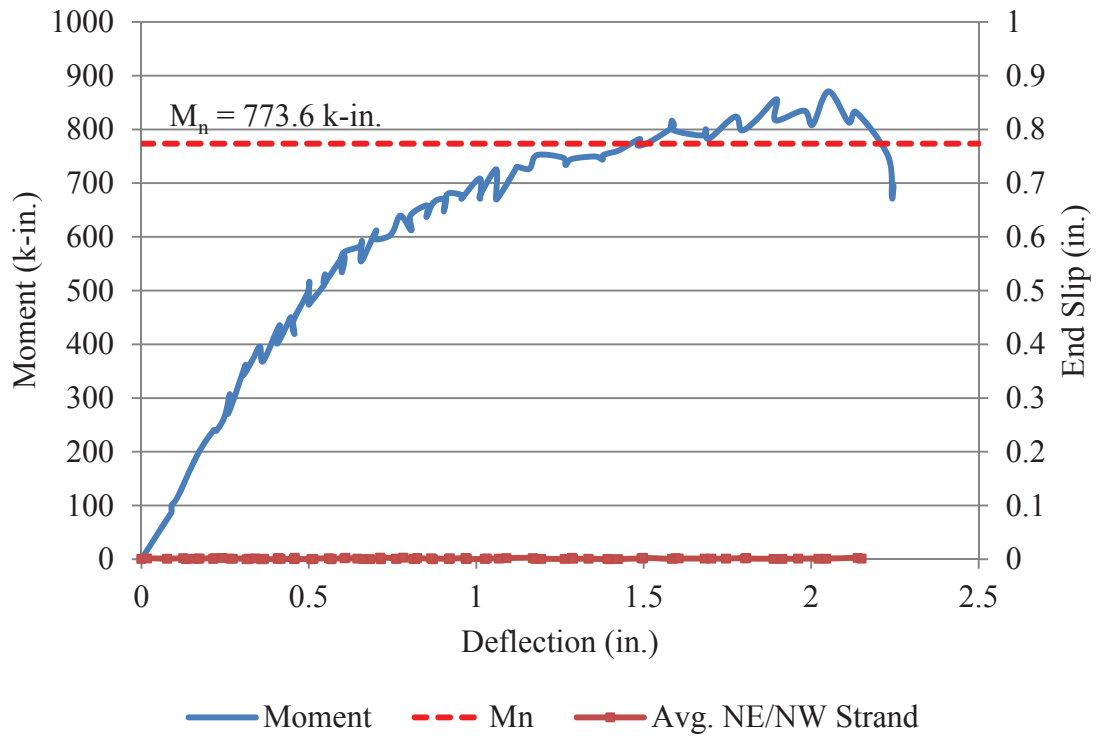


Figure F.23 – C10-2-2\_73 at Failure



Conversion: 1 in. = 25.4 mm  
 1 k-in. = 113 N-m

Figure F.24 – C10-2-2\_73 Moment vs. Deflection and Strand End Slip vs. Deflection

**BEAM ID:** S10-2-1\_58

**DATE OF TESTING:** 9/20/2011

**DAYS AFTER CASTING:** 57

<b>Test Summary</b>		
Embedment Length	58 in.	
Failure Mode (Flexural or Bond)	Flexural	
Beam End	SE/SW	
Span Length	132 in.	
Deflection at Failure	1.5 in.	
Concrete Compressive Strength	9250 psi	
Maximum Moment Capacity	Expected	790.7 k-in.
	Actual	883.3 k-in.
Average Transfer Length	At Release	13.8 in.
	At Time of Testing	15.9 in.
Average 0.1 in. NASP Load for Strand 101		
Standard NASP (Mix B)		18200 lb
NASP in Concrete (1 Day)		27300 lb

Conversion: 1 in. = 25.4 mm

1 lb = 4.45 N

1 psi = 6.89 kPa

The test was set up as deflection-controlled, and the beam was deflected in increments of 0.05 in. (1.27 mm) until failure. The deflection increment was increased to 0.05 in. (1.27 mm) from 0.02 in. (0.508mm) because it was deemed that 0.02 in. (0.508 mm) increments were too slow. At each deflection increment, the load was noted and then the beam was checked for cracks, which were marked with permanent marker.

The first flexural cracks were observed under the midspan and right support at a deflection of 0.25 in. (6.35 mm) and load of about 16.2 kips (72.1 kN). Subsequent cracks propagated vertically inside and outside the maximum moment zone and then began angling towards the supports. Horizontal cracks near midspan at the level of prestressing strand were noted at a deflection of 0.75 in. (19.0 mm) and a load of 25.9 kips (115 kN). The beam failed due to concrete crushing within the compression zone at a load of 30.4 kips (135 kN) and reached a deflection of 1.47 in. (37.3 mm) at failure. Negligible end slip was observed on both the SE and SW strands.

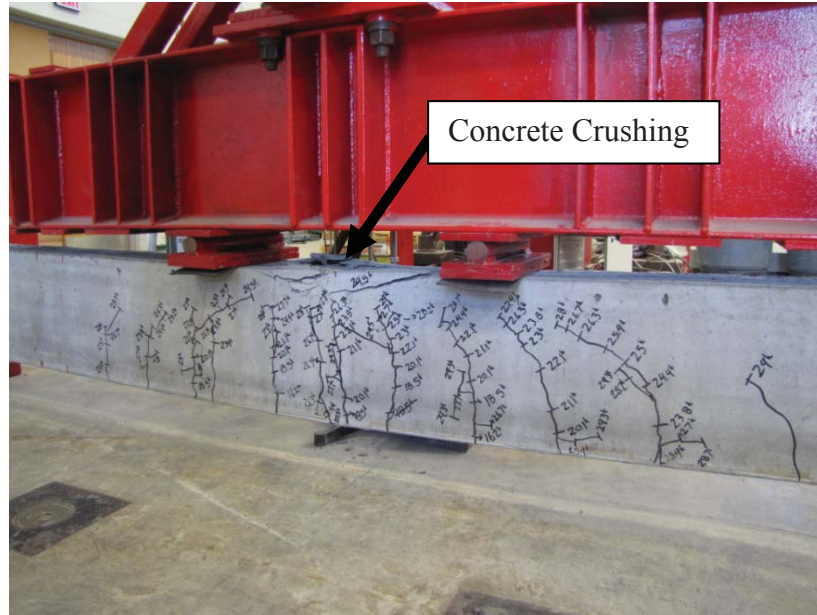
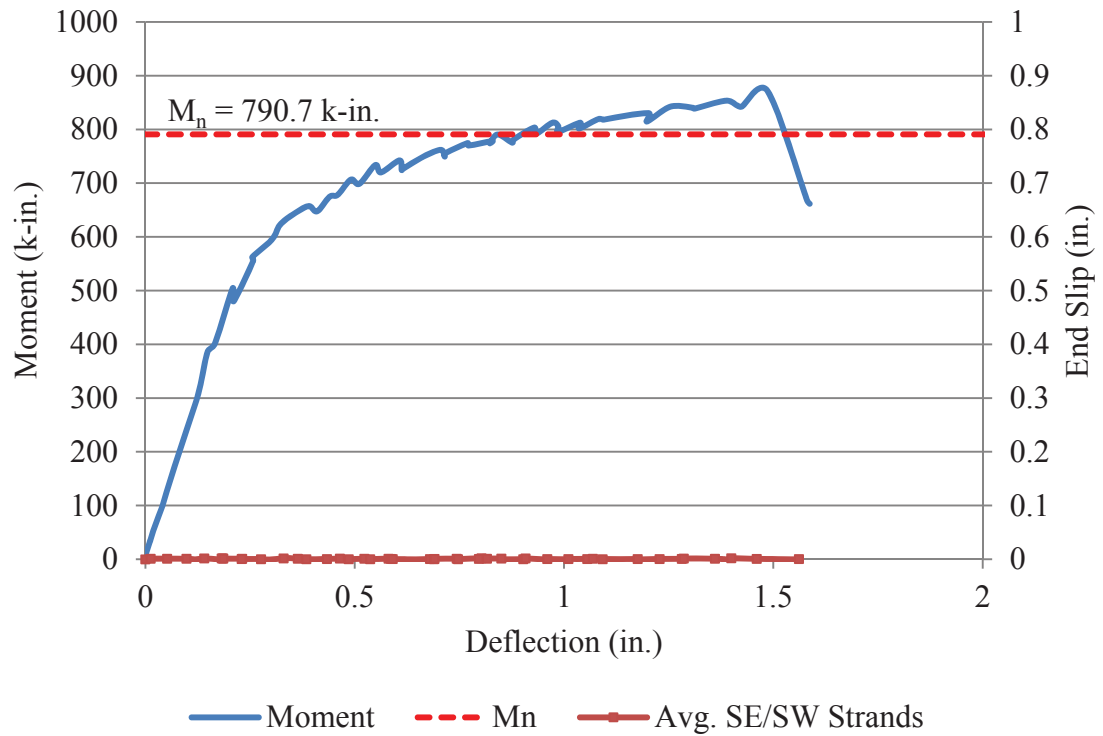


Figure F.25 – S10-2-1\_58 at Failure



Conversion: 1 in. = 25.4 mm  
 1 k-in. = 113 N-m

Figure F.26 – S10-2-1\_58 Moment vs. Deflection and Strand End Slip vs. Deflection

**BEAM ID:** S10-2-1\_73

**DATE OF TESTING:** 9/21/2011

**DAYS AFTER CASTING:** 58

Test Summary		
Embedment Length	73 in.	
Failure Mode (Flexural or Bond)	Flexural	
Beam End	NE/NW	
Span Length	162 in.	
Deflection at Failure	2.3 in.	
Concrete Compressive Strength	9250 psi	
Maximum Moment Capacity	Expected	790.7 k-in.
	Actual	904.2 k-in.
Average Transfer Length	At Release	13.8 in.
	At Time of Testing	15.9 in.
Average 0.1 in. NASP Load for Strand 101		
Standard NASP (Mix B)		18200 lb
NASP in Concrete (1 Day)		27300 lb

Conversion: 1 in. = 25.4 mm

1 lb = 4.45 N

1 psi = 6.89 kPa

The test was set up as deflection-controlled, and the beam was deflected in increments of 0.05 in. (1.27 mm) until failure. The deflection increment was increased to 0.05 in. (1.27 mm) from 0.02 in. (0.508 mm) because it was deemed that 0.02 in. (0.508 mm) increments were too slow. At each deflection increment, the load was noted and then the beam was checked for cracks, which were marked with permanent marker.

The first flexural crack was observed under the midspan at a deflection of 0.40 in. (10.2 mm) and load of about 12.5 kips (55.6 kN). Subsequent cracks propagated vertically inside and outside the maximum moment zone and then began angling towards the supports. Horizontal cracks near midspan at the level of prestressing strand were noted at a deflection of 1.00 in. (25.4 mm) and a load of 18.7 kips (83.2 kN). The beam failed due to concrete crushing within the compression zone at a load of 23.6 kips (105 kN) and reached a deflection of 2.29 in. (58.2 mm) at failure. Negligible end slip was observed on both the NE and NW strands.

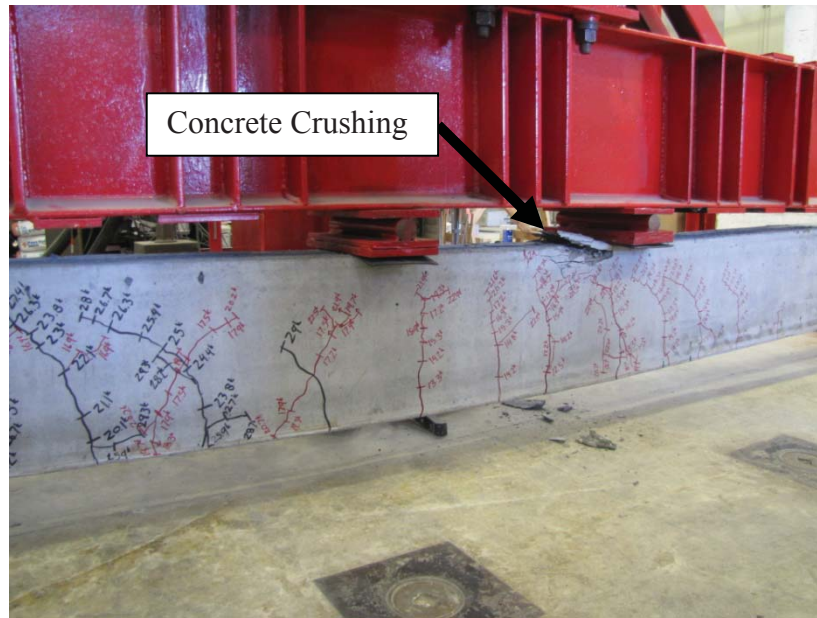
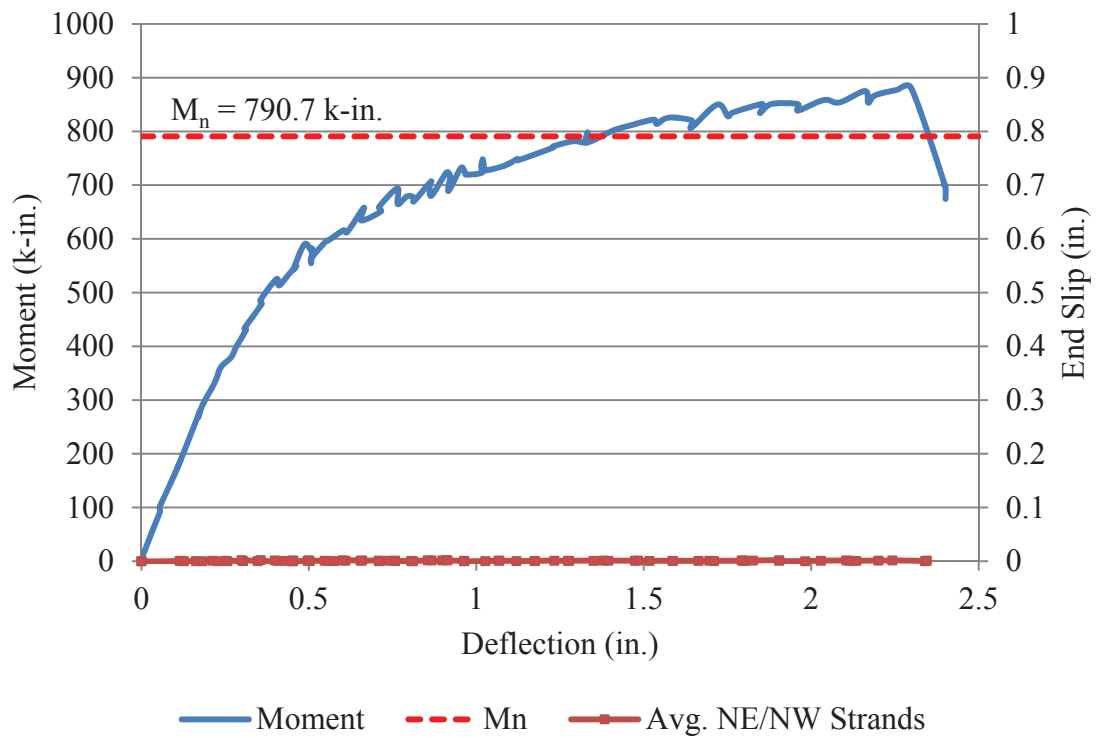


Figure F.27 – S10-2-1\_73 at Failure



Conversion: 1 in. = 25.4 mm  
 1 k-in. = 113 N-m

Figure F.28 – S10-2-1\_73 Moment vs. Deflection and Strand End Slip vs. Deflection

**BEAM ID:** S10-2-2\_58

**DATE OF TESTING:** 9/21/2011

**DAYS AFTER CASTING:** 58

<b>Test Summary</b>		
Embedment Length	58 in.	
Failure Mode (Flexural or Bond)	Flexural	
Beam End	SE/SW	
Span Length	132 in.	
Deflection at Failure	1.2 in.	
Concrete Compressive Strength	9250 psi	
Maximum Moment Capacity	Expected	790.7 k-in.
	Actual	901.2 k-in.
Average Transfer Length	At Release	13.8 in.
	At Time of Testing	15.9 in.
Average 0.1 in. NASP Load for Strand 101		
Standard NASP (Mix B)		18200 lb
NASP in Concrete (1 Day)		27300 lb

Conversion: 1 in. = 25.4 mm

1 lb = 4.45 N

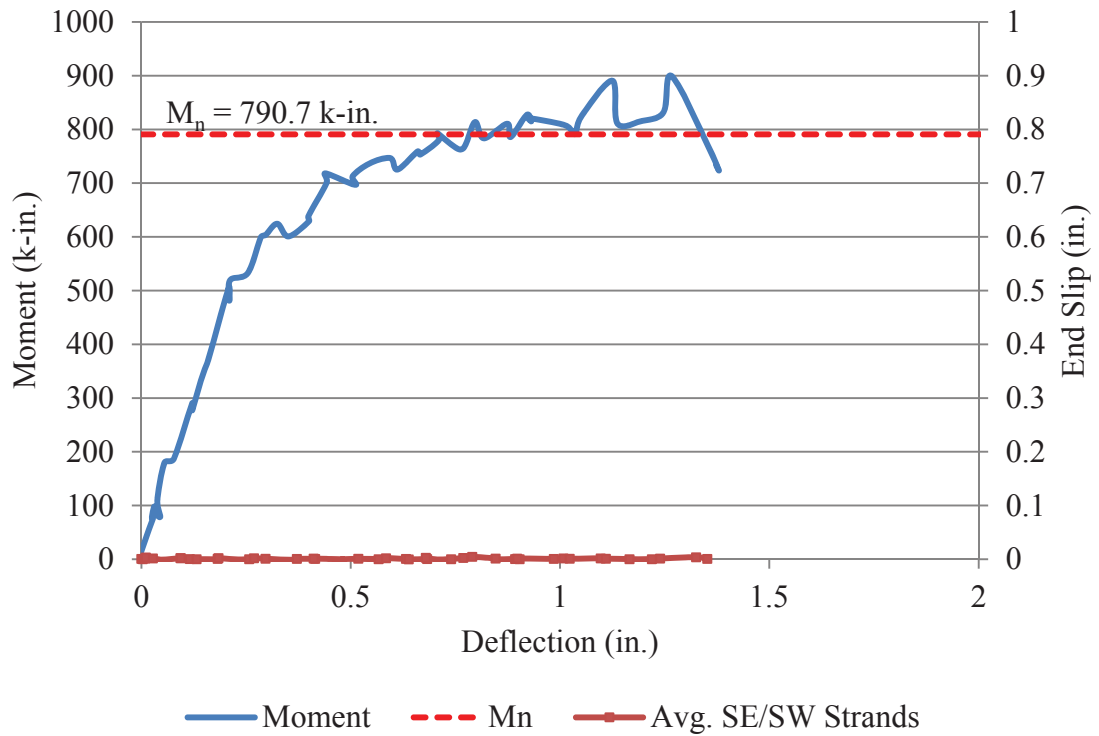
1 psi = 6.89 kPa

The test was set up as deflection-controlled, and the beam was deflected in increments of 0.05 in. (1.27 mm) until failure. The deflection increment was increased to 0.05 in. (1.27 mm) from 0.02 in. (0.508 mm) because it was deemed that 0.02 in. (0.508 mm) increments were too slow. At each deflection increment, the load was noted and then the beam was checked for cracks, which were marked with permanent marker.

The first flexural cracks were observed under the midspan and both supports at a deflection of 0.35 in. (8.89 mm) and load of about 18.2 kips (81.0 kN). Subsequent cracks propagated vertically inside and outside the maximum moment zone and then began angling towards the supports. Horizontal cracks near midspan at the level of prestressing strand were noted at a deflection of 0.80 in. (20.3 mm) and a load of 26.3 kips (117 kN). The beam failed due to concrete crushing within the compression zone at a load of 31.1 kips (138 kN) and reached a deflection of 1.20 in. (30.5 mm) at failure. Negligible end slip was observed on both the SE and SW strands.



Figure F.29 – S10-2-2\_58 at Failure



Conversion: 1 in. = 25.4 mm  
 1 k-in. = 113 N-m

Figure F.30 – S10-2-2\_58 Moment vs. Deflection and Strand End Slip vs. Deflection

**BEAM ID:** S10-2-2\_73

**DATE:** 9/22/2011

**DAYS AFTER CASTING:** 59

Test Summary		
Embedment Length	73 in.	
Failure Mode (Flexural or Bond)	Flexural	
Beam End	NE/NW	
Span Length	162 in.	
Deflection at Failure	2.0 in.	
Concrete Compressive Strength	9250 psi	
Maximum Moment Capacity	Expected	790.7 k-in.
	Actual	871.7 k-in.
Average Transfer Length	At Release	13.8 in.
	At Time of Testing	15.9 in.
Average 0.1 in. NASP Load for Strand 101		
Standard NASP (Mix B)		18200 lb
NASP in Concrete (1 Day)		27300 lb

Conversion: 1 in. = 25.4 mm

1 lb = 4.45 N

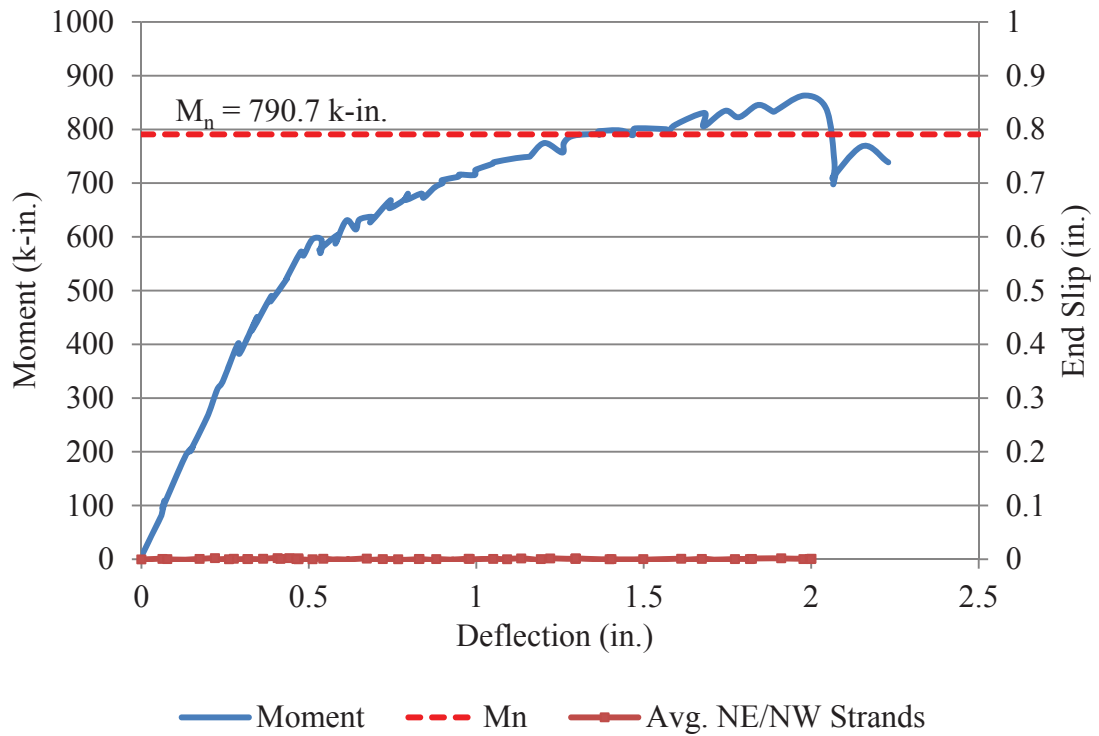
1 psi = 6.89 kPa

The test was set up as deflection-controlled, and the beam was deflected in increments of 0.05 in. (1.27 mm) until failure. The deflection increment was increased to 0.05 in. (1.27 mm) from 0.02 in. (0.508 mm) because it was deemed that 0.02 in. (0.508 mm) increments were too slow. At each deflection increment, the load was noted and then the beam was checked for cracks, which were marked with permanent marker.

The first flexural crack was observed under the midspan at a deflection of 0.40 in. (10.2 mm) and load of about 12.8 kips (56.9 kN). Subsequent cracks propagated vertically inside and outside the maximum moment zone and then began angling towards the supports. Horizontal cracks near midspan at the level of prestressing strand were noted at a deflection of 0.65 in. (16.5 mm) and a load of 16.2 kips (72.1 kN). The beam failed due to concrete crushing within the compression zone at a load of 22.7 kips (101 kN) and reached a deflection of 1.97 in. (50.0 mm) at failure. Negligible end slip was observed on both the NE and NW strands.



Figure F.31 – S10-2-2\_73 at Failure



Conversion: 1 in. = 25.4 mm  
 1 k-in. = 113 N-m

Figure F.32 – S10-2-2\_73 Moment vs. Deflection and Strand End Slip vs. Deflection

## BIBLIOGRAPHY

- AASHTO (2008). *AASHTO LRFD Bridge Design Specifications: Customary U.S. Units*. 4<sup>th</sup> ed. Washington D.C.: American Association of State Highway Transportation Officials (AASHTO).
- ACI 318 (2011). “Building Code Requirements for Structural Concrete (ACI 318-11) and Commentary (ACI 318R-11).” Farmington Hills, Michigan: American Concrete Institute (ACI).
- Anderson, A. R. and Anderson, R. G. (1976). An Assurance Criterion for Flexural Bond in Pretensioned Hollow Core Units.” *ACI Journal*, 73 (8), 457-464.
- ASTM A 370 (2011). “Standard Test Methods and Definitions for Mechanical Testing of Steel Products.” *American Society of Testing and Materials*, West Conshohocken, PA.
- ASTM A 416 (2010). “Standard Specification for Steel Strand, Uncoated Seven-Wire for Prestressed Concrete.” *American Society of Testing and Materials*, West Conshohocken, PA.
- ASTM A 1061 (2009). “Standard Test Methods for Testing Multi-Wire Steel Strand.” *American Society of Testing and Materials*, West Conshohocken, PA.
- ASTM C 33 (2011). “Standard Specification for Concrete Aggregates.” *American Society of Testing and Materials*, West Conshohocken, PA.
- ASTM C 39 (2011). “Standard Test Method for Compressive Strength of Cylindrical Concrete Specimens.” *American Society of Testing and Materials*, West Conshohocken, PA.
- ASTM C 109 (2011). “Standard Test Method for Compressive Strength of Hydraulic Cement Mortars (Using 2-in. or [50 mm] Cube Specimens).” *American Society of Testing and Materials*, West Conshohocken, PA.
- ASTM C 138 (2010). “Standard Test Method for Density (Unit Weight), Yield, and Air Content (Gravimetric) of Concrete.” *American Society of Testing and Materials*, West Conshohocken, PA.
- ASTM C 143 (2010). “Standard Test Method for Slump of Hydraulic Cement Concrete.” *American Society of Testing and Materials*, West Conshohocken, PA.
- ASTM C 192 (2007). “Standard Practice for Making and Curing Concrete Test Specimens in the Laboratory.” *American Society of Testing and Materials*, West Conshohocken, PA.

- ASTM C 231 (2010). "Standard Test Method for Air Content of Freshly Mixed Concrete by the Pressure Method." *American Society of Testing and Materials*, West Conshohocken, PA.
- ASTM C 469 (2010). "Standard Test Method for Static Modulus of Elasticity and Poisson's Ratio of Concrete in Compression." *American Society of Testing and Materials*, West Conshohocken, PA.
- ASTM C 1437 (2007). "Standard Test Method for Flow of Hydraulic Cement Mortar." *American Society of Testing and Materials*, West Conshohocken, PA.
- ASTM C 1611 (2009). "Standard Test Method for Slump Flow of Self-Consolidating Concrete." *American Society of Testing and Materials*, West Conshohocken, PA.
- ASTM C 1621 (2009). "Standard Test Method for Passing Ability of Self-Consolidating Concrete by J-Ring." *American Society of Testing and Materials*, West Conshohocken, PA.
- Barnes, R. W., Grove, J. W., and Burns, N. H. (2003). "Experimental Assessment of Factors Affecting Transfer Length." *ACI Structural Journal*, 100 (6), 740-748.
- Boehm, K. M., Barnes, R. W., and Schindler, A. K. (2010). *Performance of Self-Consolidating Concrete in Prestressed Girders*. Auburn University, AL: Highway Research Center and Department of Civil Engineering at Auburn University.
- Buckner, C. D. (1995). "A Review of Strand Development Length of Pretensioned Concrete Members." *PCI Journal*, 40 (2), 84-105.
- Burgueño, R. and Haq, M. (2007). "Effect of SCC Mixture Proportioning on Transfer and Development Length of Prestressing Strand." *ACI Special Publication*, 247, 105-116.
- Cousins, T. E., Johnston, D. W., and Zia, P. (1990). "Transfer Length of Epoxy-Coated Prestressing Strand." *ACI Materials Journal*, 87 (3), 193-203.
- Floyd, R. W., Ruiz, E. D., Do, N. H., Staton, B. W., and Hale, W. M. (2011). "Development Lengths of High-Strength Self-Consolidating Concrete Beams." *PCI Journal*, 56 (1), 36-53.
- Girgis, A. F. M. and Tuan, C. Y. (2005). "Bond Strength and Transfer Length of Pretensioned Bridge Girders Cast with Self-Consolidating Concrete." *PCI Journal*, 50 (6), 72-87.
- Hawkins, N. M. and Ramirez, J. A. (2010). *Due Diligence Review of NASP Strand Bond Test Method*. Champaign, IL: University of Illinois at Urbana-Champaign, and West Lafayette, IN: Purdue University.

- Janney, J. R. (1954). "Nature of Bond in Pre-Tensioned Prestressed Concrete." *Journal of the American Concrete Institute*, 25 (9), 717-736.
- Kaar, P. H., LaFraugh, R. W., and Mass, M. A. (1963). "Influence of Concrete Strength on Strand Transfer Length." *PCI Journal*, 8 (5), 47-67.
- Lane, S.N. (1998). *A New Development Length Equation for Pretensioned Strands in Bridge Beams and Piles*. McLean, Virginia: Federal Highway Administration (FHWA).
- Larson, K. H., Peterman, R. J., and Esmaeily, A. (2007). "Bond Characteristics of Self-Consolidating Concrete for Prestressed Bridge Girders." *PCI Journal*, 52 (4), 44-57.
- Levy, K. (2007). "Bond Behavior of Prestressed Reinforcement in Beams Constructed with Self-Consolidating Concrete." M.S. Report, Auburn University, Auburn, AL.
- Logan, D. R. (1997). "Acceptance Criteria for Bond Quality of Strand for Pretensioned Prestressed Concrete Applications." *PCI Journal*, 42 (2), 52-90.
- Mitchell, D., Cook, W. D., Khan, A. A., and Tham, T. (1993). "Influence of High Strength Concrete on Transfer and Development Length of Pretensioning Strand." *PCI Journal*, 38 (3), 52-66.
- Peterman, R. J. (2007). "The Effects of As-Cast Depth and Concrete Fluidity on Strand Bond." *PCI Journal*, 52 (3), 72-101.
- Petrou, M. F., Wan, B., Joiner, W. S., Trezos, C. G., and Harries, K. A. (2000). "Excessive Strand End Slip in Prestressed Piles." *ACI Structural Journal*, 97 (5), 774-782.
- Pozolo, A. M. and Andrawes, B. (2011). "Transfer Length in Prestressed Self-Consolidating Concrete Box and I-Girders." *ACI Structural Journal*, 108 (3), 341-349.
- Precast/Prestressed Concrete Institute (PCI). (2003). *Interim Guidelines for the Use of Self-Consolidating Concrete in Precast/Prestressed Concrete Institute Member Plants*. 1<sup>st</sup>. Ed. Chicago, IL: Precast/Prestressed Concrete Institute (PCI).
- Ramirez, J. A. and Russell, B. W. (2008). *Transfer, Development, and Splice Length for Strand/Reinforcement in High-Strength Concrete*. Washington D.C.: Transportation Research Board.
- Rose, D. R. and Russell, B. W. (1997). "Investigation of Standardized Tests to Measure the Bond Performance of Prestressing Strand." *PCI Journal*, 42 (4), 56-80.
- Russell, B.W. (2006). *Final Report NASP Round IV Strand Bond Testing*. Stillwater, OK: Oklahoma State University.

- Russell, B.W. and Burns, N.H. (1993). *Design Guidelines for Transfer, Development and Debonding of Large Diameter Seven Wire Strands in Pretensioned Concrete Girders*. Austin, TX: Center for Transportation Research at the University of Texas at Austin.
- Russell, B. W. and Burns, N. H. (1997). "Measurement of Transfer Lengths in Pretensioned Concrete Elements." *Journal of Structural Engineering*, 123 (5), 541-549.
- Russell, B. W. and Paulsgrove, G. A. (1999a). *NASP Strand Bond Testing Round One Pull-out Tests and Friction Bond Tests of Untensioned Strand*. Norman, OK: Fears Structural Engineering Laboratory at the University of Oklahoma.
- Russell, B. W. and Paulsgrove, G. A. (1999b). *NASP Strand Bond Testing Round Two Assessing Repeatability and Reproducibility of the Moustafa Test, the PTI Bond Test, and the NASP Bond Test*. Norman, OK: Fears Structural Engineering Laboratory at the University of Oklahoma.
- Shahawy, M. (2001). "A Critical Evaluation of the AASHTO Provisions for Strand Development Length of Prestressed Concrete Members." *PCI Journal*, 46 (4), 94-117.
- Staton, B. W., Do, N. H., Ruiz, E. D., and Hale, W. M. (2009). "Transfer Lengths of Prestressed Beams Cast with Self-Consolidating Concrete." *PCI Journal*, 54 (2), 64-83.
- Tabatabai, H. and Dickson, T. J. (1993). "The History of the Prestressing Strand Development Length Equation." *PCI Journal*, 38 (6), 64-75.
- Wan, B., Petrou, M. F., Harries, K. A., and Hussein, A. A. (2002). "Top Bar Effects in Prestressed Concrete Piles." *ACI Structural Journal*, 99 (2), 208-214.

**FINAL Report C**

TRyy1103

**Project Title: Self-Consolidating Concrete (SCC) for Infrastructure Elements**

**Report C: Self-Consolidating Concrete (SCC) for Infrastructure Elements: Bond Behavior of Mild Reinforcing Steel in SCC**

Prepared for  
Missouri Department of Transportation  
Construction and Materials

Missouri University of Science and Technology, Rolla, Missouri

July 2012

The opinions, findings, and conclusions expressed in this publication are those of the principal investigators and the Missouri Department of Transportation. They are not necessarily those of the U.S. Department of Transportation, Federal Highway Administration. This report does not constitute a standard or regulation



## ABSTRACT

The main objective of this study was to determine the effect on bond performance of mild reinforcing steel in self-consolidating concrete (SCC). The SCC test program consisted of comparing the bond performance of normal and high strength SCC with their respective MoDOT standard mix designs.

Two test methods were used for bond strength comparisons. The first was a direct pull-out test based on the RILEM 7-II-128 “RC6: Bond test for reinforcing steel. 1. Pull-out test” (RILEM, 1994). The direct pull-out tests were performed on specimens with #4 (#13) and #6 (#19) deformed reinforcing bars.

The second test method consisted of a full-scale beam splice test specimen subjected to a four-point loading until failure of the splice. This test method is a non-ASTM test procedure that is generally accepted as the most realistic test method for both development and splice length. The beam splice tests were performed on beams with #6 (#19) reinforcing bars spliced at midspan at a specific length to ensure bond failure occurs prior to shear or flexural failure.

Analysis of the SCC data indicates that using SCC does not result in any increase in the required development length of mild reinforcing.

## TABLE OF CONTENTS

	Page
ABSTRACT.....	iii
LIST OF ILLUSTRATIONS.....	vii
LIST OF TABLES.....	xi
SECTION	
1. INTRODUCTION.....	1
1.1. BACKGROUND AND JUSTIFICATION FOR SELF-CONSOLIDATING CONCRETE RESEARCH.....	1
1.1.1. General.....	1
1.1.2. Benefits of SCC.....	1
1.1.3. Concerns with SCC.....	2
1.2. OBJECTIVES & SCOPE OF WORK.....	2
1.3. RESEARCH PLAN.....	3
1.4. OUTLINE.....	3
2. LITERATURE REVIEW.....	5
2.1. BOND CHARACTERISTICS.....	5
2.2. COMMON BOND TESTS.....	8
2.3. SELF-CONSOLIDATING CONCRETE BOND RESEARCH.....	11
3. MIX DESIGNS AND CONCRETE PROPERTIES.....	19
3.1. INTRODUCTION.....	19
3.2. CONCRETE PROPERTIES.....	19
3.2.1. Fresh Concrete Properties.....	19
3.2.2. Compressive Strength of Concrete.....	23
3.2.3. Modulus of Rupture of Concrete.....	25
3.2.4. Splitting Tensile Strength of Concrete.....	27
3.3. SELF-CONSOLIDATING CONCRETE (SCC) MIX DESIGNS.....	28
3.3.1. Normal Strength Control Mix Design.....	28
3.3.2. SCC Normal Strength Mix Design.....	31

3.3.3. High Strength Control Mix Design .....	33
3.3.4. SCC High Strength Mix Design .....	36
4. EXPERIMENTAL PROGRAM.....	40
4.1. INTRODUCTION .....	40
4.2. DIRECT PULL-OUT TEST .....	40
4.2.1. Direct Pull-out Specimen Design .....	40
4.2.2. Direct Pull-out Specimen Fabrication .....	43
4.2.3. Direct Pull-out Test Setup .....	45
4.2.4. Direct Pull-out Test Procedure .....	46
4.3. BEAM SPLICE TEST .....	47
4.3.1. Beam Splice Specimen Design.....	47
4.3.2. Beam Splice Specimen Fabrication.....	49
4.3.3. Beam Splice Specimen Test Setup.....	55
4.3.4. Beam Splice Test Procedure.....	57
5. SCC TEST RESULTS AND EVALUATION.....	58
5.1. DIRECT PULL-OUT TEST RESULTS.....	58
5.2. BEAM SPLICE TEST RESULTS.....	63
5.3. REINFORCING BAR TENSION TEST.....	70
5.4. ANALYSIS OF RESULTS .....	71
5.4.1. Methodology .....	71
5.4.2. Analysis and Interpretation – Direct Pull-out Test Results .....	74
5.4.3. Analysis and Interpretation – Beam Splice Test Results .....	80
5.5. FINDINGS AND CONCLUSIONS .....	88
6. FINDINGS, CONCLUSIONS, AND RECOMMENDATIONS.....	90
6.1. FINDINGS.....	90
6.1.1. Direct Pull-out Testing.....	90
6.1.2. Beam Splice Testing.....	91
6.2. CONCLUSIONS.....	91
6.2.1. Direct Pull-out Testing.....	91
6.2.2. Beam Splice Testing.....	92
6.3. RECOMMENDATIONS.....	92

APPENDICES

A. SCC TEST PROGRAM BEAM SPLICE FAILURE PHOTOGRAPHS .....	94
B. SCC TEST PROGRAM TEST DATA PLOTS.....	107
C. SCC TEST PROGRAM STATISTICAL ANALYSIS .....	118
BIBLIOGRAPHY.....	122

## LIST OF ILLUSTRATIONS

Figure	Page
2.1. Stress transfer between steel and surrounding concrete (ACI 408R, 2003) .....	6
2.2. Direct pull-out test specimen (ACI 408R, 2003) .....	9
2.3. Beam-end pull-out test specimen (ACI 408R, 2003).....	10
2.4. Beam anchorage test specimen (ACI 408R, 2003).....	11
2.5. Beam splice test specimen (ACI 408R, 2003).....	11
3.1. Slump test.....	20
3.2. Slump flow test .....	21
3.3. J-ring test.....	22
3.4. Casting compressive strength cylinders.....	24
3.5. Compressive strength test setup.....	24
3.6. Modulus of rupture test specimens .....	26
3.7. Modulus of rupture test setup .....	26
3.8. Splitting tensile strength test setup .....	27
3.9. Plot of C6-58L compressive strength .....	30
3.10. Plot of S6-48L compressive strength.....	32
3.11. Plot of C10-58L compressive strength .....	35
3.12. Plot of S10-48L compressive strength.....	38
4.1. Pull-out specimen with dimensions for #4 (#13) reinforcing bars .....	42
4.2. Pull-out specimen with dimensions for #6 (#19) reinforcing bars .....	42
4.3. Pull-out specimen construction.....	44
4.4. Completed specimens .....	45
4.5. Direct pull-out test setup.....	46
4.6. LVDT installation to measure bar slip.....	46
4.7. Beam splice specimen reinforcing layout.....	49
4.8. Beam splice specimen cross section .....	49
4.9. Finished reinforcing bar cage.....	51
4.10. Spliced longitudinal bars for normal strength concrete .....	52
4.11. Reinforcing bar cages in beam forms .....	52

4.12. Concrete bucket being filled with fresh concrete .....	53
4.13. Placement of concrete into beam forms.....	54
4.14. Finished beams in forms .....	54
4.15. Beam loading schematic .....	55
4.16. Beam positioned within load frame .....	56
4.17. LVDT installation .....	57
5.1. C6-58L pull-out test results .....	61
5.2. S6-48L pull-out test results.....	61
5.3. C10-58L pull-out test results .....	62
5.4. S10-48L pull-out test results.....	62
5.5. Example SCC applied load vs. slip plot.....	63
5.6. C6-58L peak load data plot.....	65
5.7. S6-48L peak load data plot .....	66
5.8. C10-58L peak load data plot.....	66
5.9. S10-48L peak load data plot .....	67
5.10. Typical load vs. displacement plot.....	68
5.11. Typical load vs. strain plot.....	68
5.12. Failed splice region of C6-58LBB1 .....	69
5.13. Bottom of splice region of C6-58LBB1.....	69
5.14. Bottom of splice region of C10-58LTB with splice revealed.....	70
5.15. Plot of peak load for each normal strength mix design .....	77
5.16. Plot of peak load for each high strength mix design.....	77
5.17. Normal strength normalized load vs. slip plot for #4 (#13) bars .....	78
5.18. Normal strength normalized load vs. slip plot for #6 (#19) bars .....	79
5.19. High strength normalized load vs. slip plot for #4 (#13) bars .....	79
5.20. High strength normalized load vs. slip plot for #6 (#19) bars .....	80
5.21. Normalized peak load plot for the normal strength mix design.....	83
5.22. Normalized peak load plot for the high strength mix design.....	83
5.23. Normalized steel stress at failure load for normal strength mix designs .....	86
5.24. Normalized steel stress at failure load for normal strength mix designs .....	86
5.25. Typical normalized load vs. strain plot for the normal strength specimens .....	87

5.26. Typical normalized load vs. strain plot for the high strength specimens.....	88
A.1. C6-58LBB1 .....	95
A.2. C6-58LBB2.....	96
A.3. C6-58LTB .....	97
A.4. S6-48LBB1 .....	98
A.5. S6-48LBB2 .....	99
A.6. S6-48LTB side view .....	100
A.7. C10-58LBB1 .....	101
A.8. C10-58LBB2.....	102
A.9. C10-58LTB.....	103
A.10.S10-48LBB1 .....	104
A.11.S10-48LBB2 .....	105
A.12.S10-48LTB .....	106
B.1 Normal strength direct pull-out applied load comparisons .....	108
B.2.High strength direct pull-out applied load comparisons .....	108
B.3.Applied load vs. slip plot for #4 (#13) C6-58L.....	109
B.4.Applied load vs. slip plot for #4 (#13) S6-48L .....	109
B.5.Applied load vs. slip plot for #4 (#13) C10-58L.....	110
B.6.Applied load vs. slip plot for #4 (#13) S10-48L .....	110
B.7.Applied load vs. slip plot for #6 (#19) C6-58L.....	111
B.8.Applied load vs. slip plot for #6 (#19) S6-48L .....	111
B.9.Applied load vs. slip plot for #6 (#19) C10-58L.....	112
B.10. Applied load vs. slip plot for #6 (#19) S10-48L.....	112
B.11. Normal strength beam splice applied load comparisons.....	113
B.12. High strength beam splice applied load comparisons.....	113
B.13. Applied load vs. strain (average of all gages per specimen) for C6-58L .....	114
B.14. Applied load vs. strain (average of all gages per specimen) for S6-48L.....	114
B.15. Applied load vs. strain (average of all gages per specimen) for C10-58L .....	115
B.16. Applied load vs. strain (average of all gages per specimen) for S10-48L.....	115
B.17. Applied load vs. displacement for C6-58L.....	116
B.18. Applied load vs. displacement for S6-48L .....	116

B.19. Applied load vs. displacement for C10-58L ..... 117

B.20. Applied load vs. displacement for S10-48L ..... 117

## LIST OF TABLES

Table	Page
3.1. C6-58L mix proportions .....	28
3.2. Compressive strength data of C6-58L .....	29
3.3. Splitting tensile strength test results for C6-58L .....	30
3.4. Modulus of rupture test results for C6-58L .....	31
3.5. S6-48L mix proportions .....	31
3.6. Compressive strength data of S6-48L .....	32
3.7. Splitting tensile strength test results for S6-48L .....	33
3.8. Modulus of rupture test results for S6-48L .....	33
3.9. C10-58L mix proportions .....	34
3.10. Compressive strength data of C10-58L .....	35
3.11. Splitting tensile strength test results for C10-58L .....	36
3.12. Modulus of rupture test results for C10-58L .....	36
3.13. S10-48L mix proportions .....	37
3.14. Compressive strength data of S10-48L .....	38
3.15. Splitting tensile strength test results for S10-48L .....	39
3.16. Modulus of rupture test results for S10-48L .....	39
5.1. SCC direct pull-out test matrix .....	58
5.2. SCC pull-out test results .....	60
5.3. SCC beam splice test matrix .....	64
5.4. Peak load and reinforcing bar stress .....	65
5.5. #6 (#19) reinforcing bar tension test results .....	71
5.6. Test day compressive strengths for test specimens .....	73
5.7. SCC normal strength normalized pull-out test results .....	75
5.8. SCC high strength normalized pull-out test results .....	76
5.9. Normalized peak loads for each specimen .....	82
5.10. Normalized steel stress at failure for each specimen .....	84
5.11. Normalized steel stress compared to theoretical steel stress at failure .....	85

# 1. INTRODUCTION

## 1.1. BACKGROUND AND JUSTIFICATION FOR SELF-CONSOLIDATING CONCRETE RESEARCH

**1.1.1. General.** The key difference between self-consolidating concrete (SCC) and conventional concrete is workability. SCC is characterized by its fluidity and its ability to eliminate the need for mechanical consolidation through the use of vibrators. Typically, three different methods are used for producing an SCC mix design. The first method is by the addition of a viscosity modifying admixture (VMA), along with a water reducer to a conventional concrete mix design. The VMA reduces the likelihood of segregation of the coarse aggregate by increasing the viscosity of the water. The water reducer increases the flowability of the paste. The second method is through increasing the fine-to-coarse aggregate ratio and the addition of a water reducer. The lower coarse aggregate content increases the flowability and lowers the potential for segregation. The third method is essentially a combination of the first two methods.

**1.1.2. Benefits of SCC.** Because of its unique nature, self-consolidating concrete (SCC) has the potential to significantly reduce costs associated with concrete construction. SCC is a highly flowable, nonsegregating concrete that can be placed without any mechanical consolidation, and thus has the following advantages over conventional concrete:

- decreased labor and equipment costs during concrete placement,
- decreased potential for and costs to repair honeycombing and voids,
- increased production rates of precast and cast-in-place elements, and

- improved finish and appearance of cast and free concrete surfaces (Myers and Volz, 2011).

**1.1.3. Concerns with SCC.** Concerns exist over the structural implications of SCC in cast-in-place and precast elements. Specifically, higher paste contents, higher fines contents, and the use of smaller, rounded aggregates may significantly alter the bond strength of SCC mixes as compared to traditional concrete mixes with the same compressive strength. These concerns increase for mixtures that use untested aggregate types and various supplementary cementitious materials. Consequently, to achieve the benefits and potential savings with SCC, guidelines are needed for its proper application in bridges, roadways, culverts, retaining walls, and other transportation-related infrastructure components (Myers and Volz, 2011)..

## **1.2. OBJECTIVES & SCOPE OF WORK**

The main objective of this study was to determine the effect on bond performance of SCC. The SCC test program consisted of comparing the bond performance of normal and high strength SCC with their respective MoDOT standard mix designs.

The following scope of work was implemented in an effort to attain these objectives: (1) review applicable literature; (2) develop a research plan; (3) design and construct test fixtures; (4) design and construct test specimens; (5) test specimens to failure and record applicable data; (6) analyze results and conduct comparisons between experimental and control mix designs; (7) develop conclusions and recommendations; (8) prepare this report in order to document the information obtained during this study.

### **1.3. RESEARCH PLAN**

The research plan entailed determining the bond performance of SCC relative to MoDOT standard mix designs. For the SCC test program, two SCC mix designs were determined from a survey of precast suppliers, one normal strength and one high strength, and used for comparison.

Two test methods were used for bond strength comparisons. The first was a direct pull-out test based on the RILEM 7-II-128 “RC6: Bond test for reinforcing steel. 1. Pull-out test” (RILEM, 1994). Although not directly related to the behavior of a reinforced concrete beam in flexure, the test does provide a realistic comparison of bond between types of concrete. A total of 24 direct pull-out test specimens were constructed and tested to bond failure using this test method. The second test method consisted of a full-scale beam splice test specimen subjected to a four-point loading until failure of the splice. This test method is a non-ASTM test procedure that is generally accepted as the most realistic test method for both development and splice length. A total of 12 full-scale beam splice test specimens were constructed and tested to failure.

### **1.4. OUTLINE**

This report consists of six sections and three appendices. Section 1 briefly explains the characteristics, benefits, and concerns of SCC, as well as the study’s objective and the manner in which the objective was attained.

Section 2 explains the mechanisms behind bond strength of deformed reinforcing bars embedded in concrete, common methods for testing bond strength, and past bond research conducted on SCC.

Section 3 details the mix designs used in this study and their associated fresh concrete properties as well as the mechanical and strength properties determined at the time of bond testing.

Section 4 details the direct pull-out and beam splice test specimen design, fabrication, and testing setup and procedure.

Section 5 presents the test result normalization process, the recorded test program results, normalized test results, and the comparisons of SCC results to their control mix designs.

Section 6 restates the findings that were established during the course of this study and presents conclusions and recommendations based on the test results obtained.

## 2. LITERATURE REVIEW

### 2.1. BOND CHARACTERISTICS

Due to its very low tensile strength, concrete, by itself, would be a poor structural material to use in members resisting anything but a concentric axial compressive load. The tensile strength of concrete is generally only 10% of its compressive strength. However, the addition of steel reinforcing bars in the areas of the cross section of the member experiencing tensile stresses has proven to be a suitable solution to overcoming the poor tensile strength of concrete. The high tensile strength of steel is able to withstand the tensile stresses upon failure of the concrete. In order to obtain complete composite behavior between the reinforcing steel and the concrete, the tensile stresses must be fully transferred to the steel from the concrete. This transfer of stresses is facilitated by an adequate bond between the steel reinforcing bars and concrete.

The three modes of stress transfer from concrete to deformed steel reinforcement are through chemical adhesion, friction along the steel-concrete interface, and bearing resistance of the ribs on the steel against the surrounding concrete, as shown in **Figure 2.1**. Chemical adhesion refers to the bonding of the steel to the concrete through chemical reactions between the two surfaces. Upon initial loading, the resistance through chemical adhesion is the first stress transfer mechanism to fail. Upon failure of the chemical adhesion, the slipping action of the bar initiates the transfer of stresses from friction and rib anchorage. Frictional forces developed along the smooth faces of the reinforcing bar are relatively small compared to the forces transferred through the ribs. As the bar slip

increases, stress transfer through friction decreases, to a point where most of the tensile stresses are transferred through anchorage of the ribs.

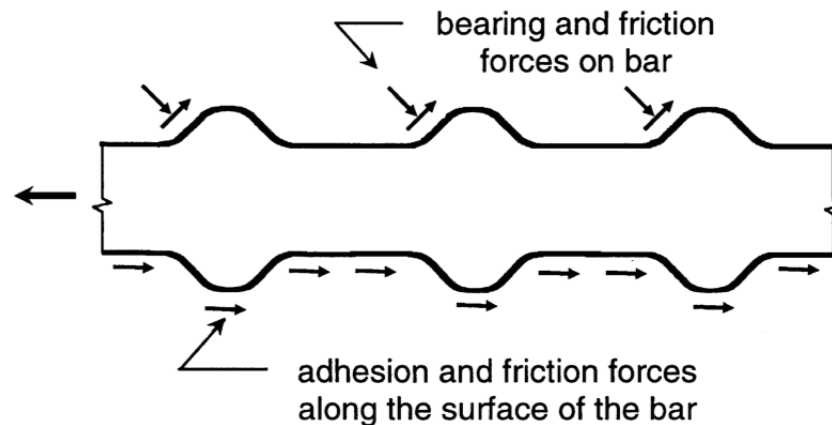


**Figure 2.1 – Stress transfer between steel and surrounding concrete (ACI 408R, 2003)**

As the load is increased, complete failure of the bond will occur by the concrete crushing against the ribs. One type of bond failure results when the bar is pulled directly out of the concrete, creating a shear plane along the outer edges of the steel ribs. This occurs when there is sufficient concrete cover and clear spacing between the reinforcing bars. Another type of bond failure is a splitting failure of the concrete cover. This occurs when there is insufficient concrete cover or insufficient clear spacing between the reinforcing bars (ACI 408R, 2003).

With adequate bond, tensile stresses can be transferred from the concrete to the reinforcing bar such that the bar will fail through yielding, and eventually fracture. The shortest length required to increase the stress of the bar from zero to the yield stress is called the development length of the bar. The development length of reinforcing steel is

dependent on the bar diameter and yield stress, as well as the coefficient of friction on the steel/concrete interface. The need for reinforcement splices is common in monolithic construction of large members, such as columns extending multiple levels of a structure. The allowable types of tension splices are lapped splices, mechanical splices, and welded splices. Lap splices are the transfer of tensile stresses from one bar to the concrete, then from the concrete to another bar by overlapping the two reinforcing bars. The overlapping distance must be at least the development length of the bar. Mechanical splices are achieved through the use of various steel devices that connect the ends of the two bars being spliced. Welded splices consist of welding the two bars being spliced together (Wight and MacGregor, 2009).

The factors affecting the bond strength between reinforcing steel bars and concrete are a function of the structural characteristics of the member, as well as characteristics of the bar and concrete. One structural characteristic that plays a large role in affecting the bond strength of steel and concrete is the concrete cover and spacing between bars. As the concrete cover and bar spacing increase, the bond strength will also increase. The increase in bond strength is attributed to the decreasing likelihood of splitting failures with large spacing and cover. Another structural characteristic affecting bond strength is the presence of transverse reinforcement. The presence of transverse reinforcement surrounding the embedded bar slows the progressions of splitting cracks, which effectively increases bond strength. Also, the location of the bar during casting of the member affects the bond strength between the steel and concrete. Bars with a large volume of concrete cast below them have lower bond strengths than bars cast at the

bottom of a member. This lower bond strength is caused by concrete settlement and the presences of excess bleed water around top-cast bars (ACI 408R, 2003).

Reinforcing bar and concrete properties also play a role in affecting the bond strength of steel and concrete. Bar size and geometry can greatly alter bond strength. Larger bars with higher relative rib areas achieve higher total bond forces than small bars. Bar surface condition, such as cleanliness and coating, significantly affect bond strength. While bars with rust and mill scale do not adversely affect bond strength, surface contaminants such as mud, oil, and other nonmetallic coatings will decrease bond strength. Also, epoxy coated bars have a tendency to reduce bond strength. Concrete properties such as compressive and tensile strength, and fracture energy will also affect bond strength. Increasing compressive and tensile strengths, and fracture energy will subsequently increase bond strength. The addition of transverse reinforcement also increases the extent that the concrete compressive strength affects bond strength. Also, increasing the aggregate percentage in a concrete mix, as well as aggregate strength, will increase bond strength (ACI 408R, 2003).

## **2.2. COMMON BOND TESTS**

There have been numerous test methods created to determine the bond strength between concrete and steel reinforcing bars. There are four common methods of bond testing. Two small-scale test methods are the direct pull-out test and the beam-end pullout test. Two large-scale test methods are the beam anchorage test and the beam splice test. The direct pull-out test specimen, shown in **Figure 2.2**, is the most common of the four tests listed above due to the ease of fabricating the test specimens and performing the test.

This test is run by supporting the concrete and applying tension to the reinforcing bar until failure, as shown in **Figure 2.2**. This bond test is the least accurate test for defining the actual bond strength and is best used for comparison purposes only.

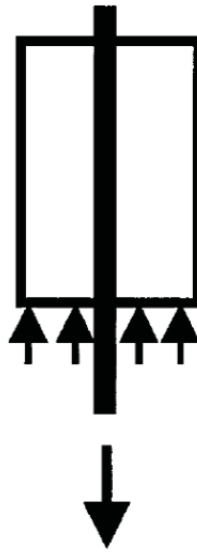


**Figure 2.2 – Direct pull-out test specimen** (ACI 408R, 2003)

The beam-end pull-out, also called the modified cantilever beam, test specimen is shown in **Figure 2.3**. This test is relatively easy to construct and perform and gives an accurate representation of how embedded reinforcing bars would behave in a full-scale beam. The compressive force applied must be located at least the same distance as the embedded length away from the end of the reinforcing bar. A length of reinforcing bar at the contact surface is left unbounded in order to prevent a conical failure surface from forming.

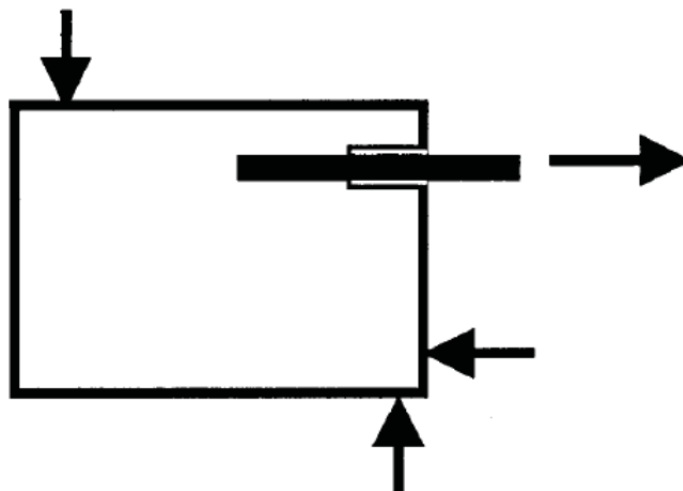


**Figure 2.3 – Beam-end pull-out test specimen (ACI 408R, 2003)**

The beam anchorage test specimen is shown in **Figure 2.4**. This test specimen is meant to represent a full-scale beam with two cracked sections and a known length of bonded area. This test specimen is designed to measure development length of the reinforcing bar. **Figure 2.5** shows the beam splice test specimen. This test specimen is designed to measure the splice length of the reinforcing bar. The reinforcing bar splice placement and loading configuration is developed to subject the spliced region to a constant moment along the length of the splice. Current ACI 318-08 (ACI 318-08, 2008) design provisions for development length and splice length are based primarily on data from this type of test. Bond strengths determined from both test specimens are generally similar.

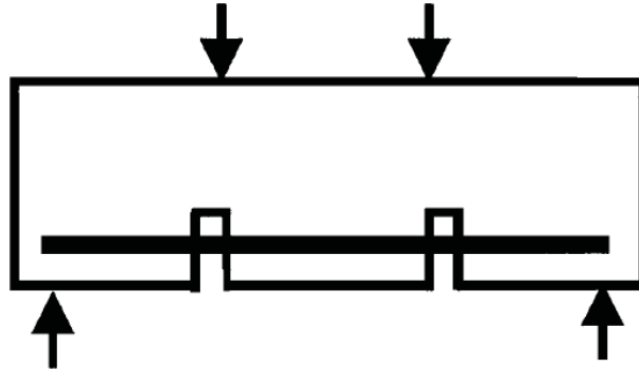


**Figure 2.4 – Beam anchorage test specimen (ACI 408R, 2003)**

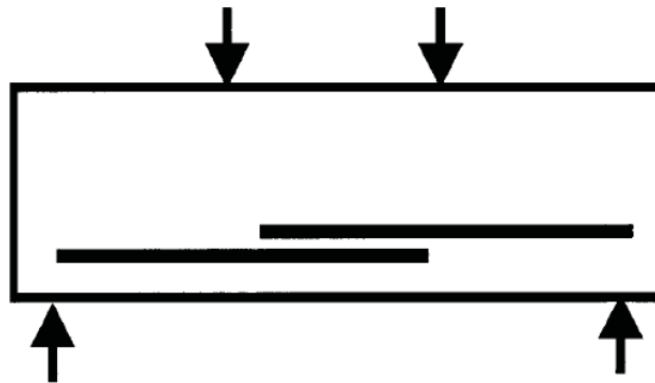


**Figure 2.5 – Beam splice test specimen (ACI 408R, 2003)**

### **2.3. SELF-CONSOLIDATING CONCRETE BOND RESEARCH**

The key difference between SCC and conventional concrete is workability. SCC is characterized by its fluidity and its ability to eliminate the need for mechanical consolidation via the use of vibrators. Typically, three different methods are used for producing an SCC mix design. The first method is by the addition of a viscosity modifying admixture (VMA), along with a water reducer to a conventional concrete mix design. The VMA reduces the likelihood of segregation of the coarse aggregate by increasing the viscosity of the water. The water reducer increases the flowability of the

paste. The second method is through increasing the fine-to-coarse aggregate ratio and the addition of a water reducer. The lower coarse aggregate content increases the flowability and lowers the potential for segregation. The third method is essentially a combination of the first two methods.

There have been numerous studies conducted to determine the bond performance of SCC relative to conventional concrete. One such study was conducted at Ryerson University entitled “Bond Strength of Deformed Bars in Large Reinforced Concrete Members Cast with Industrial Self-Consolidating Concrete Mixture” (Hassan *et al*, 2009). This study focused on comparing the bond performance of deformed bars embedded in large, heavily reinforced direct pull-out specimens made with conventional and self-consolidating concrete. The pull-out specimens were 13 ft. (4000 mm) long, 4 ft. tall (1200 mm), and 1 ft. wide (300 mm). Thirty #6 (#20) deformed bars were bonded 6 in. (150 mm) and a plastic sleeve was used to debond the other half of the embedded bar. The bars were placed 6, 20, and 34 in. (150, 510, and 870 mm) from the bottom of the specimen in order to examine the effect of the depth of cast concrete beneath the bar (top bar effect). Longitudinal reinforcement of nine #11 (#36) bars at the top, three #8 (#25) bars at the bottom, and eight #5 (#16) bars spaced evenly between the top and bottom bars. Closed stirrups spaced 6.3 in. (160 mm) on center and consisting of #3 (#11) bars were used for transverse reinforcement. The embedded bars were divided into 5 groups that were tested at 1, 3, 7, 14, and 28 days to track bond strength development. All embedded bars were tested to failure. The authors concluded that no significant differences were seen between SCC and conventional concrete in terms of bond strength development. Also, the normalized bond stress at failure was slightly higher for SCC than

conventional concrete for 3, 7, 14, and 28 days (Hassan *et al.*, 2009). However, only pull-out specimens were tested.

Another study focusing on comparing bond strengths of SCC with conventional concrete through direct pull-out specimens was conducted in Iran entitled “Bond Strength of Reinforcing Steel in Self-Compacting Concrete” (Foroughi-Asl *et al.*, 2008). The direct pull-out specimens were based on the RILEM 7-II-128 “RC6: Bond test for reinforcing steel. 1. Pull-out test” (RILEM, 1994). The specimens consisted of embedding #3 (#10), #5 (#16), and #6 (#20) ribbed reinforcing bars in a 6 in. (150 mm) concrete cube. A plastic sleeve was used to debond a 2 in. (50 mm) length of bar at the base of the specimen, leaving 4 in. (100 mm) of bonded length. All direct pull-out specimens were tested to failure. The test results of this study indicate that SCC performs at the same level as conventional concrete in terms of bond strength. However, it was noted that due to the retarding effect of the water reducing admixture used in this study, the bond strength of SCC developed slower than that of conventional concrete (Foroughi-Asl *et al.*, 2008).

Researchers at Université de Toulouse in France conducted a study entitled “Bond and Cracking Properties of Self-Consolidating Concrete” (Castel *et al.*, 2008). The focus of this program was to determine the bond strength and cracking behavior of SCC and conventional concrete by conducting tension member and beam flexure tests. The tension member test was performed on a 19.7-in-long (500 mm) concrete block with a square, 3.94-in.-wide (100 mm) cross section. A length of deformed, #4 (#13) reinforcing bar was embedded in the center of the concrete section. Two tension member tests were performed for each type of concrete. The full-scale beam specimens were 6.6 ft. (2000

mm) long, with a cross section of 6 in. x 7.9 in. (150 mm x 200 mm). The longitudinal reinforcement consisted of two #3 (#10) and two #2 (#6) deformed reinforcing bars on the bottom and top of the cross section, respectively. Transverse reinforcement consisted of #2 (#6) closed stirrups spaced at 7.8 in. (198 mm) on center along the entire length of the beam. Cracks along the beam were evaluated at service and ultimate loads. One beam test was conducted for each concrete type and both beams failed by crushing of the concrete in the compression zone. The tension member test results indicated that there was no difference in transfer length between SCC and conventional concrete. The transfer lengths for each concrete decreased slightly as the concrete compressive strength increased. The beam test results indicated that there was no significant difference in cracking moment between SCC and conventional concrete. The moment capacity and bending stiffness at service level loads were also similar (Castel *et al.*, 2008).

A study comparing bond strength between SCC and conventional concrete through testing full-scale beam specimens was also conducted in Turkey entitled “Strength of Tension Lap-Splices in Full Scale Self-Compacting Concrete Beams” (Turk *et al.*, 2009). Full-scale beam specimens were constructed with two lap splices of longitudinal bars in the tension region of the beam cross section. The beams were then subjected to a 4-point-loading until failure. Twelve beam specimens were cast in this study; six beams for each mix design. The beams were 6.6 ft. (2000 mm) in length, with a cross section of 7.9 in. x 12 in. (200 mm x 300 mm). Three of the six beams were constructed with #5 (#16) longitudinal reinforcing bars and the other three contained #6 (#20) longitudinal bars. The longitudinal bars were spliced 12.2 in. (310 mm) at midspan of the beam and subjected to a constant moment. The splice length was chosen to ensure

no yielding of the bars occurred. Transverse reinforcement consisted of #3 (#10) bars spaced at 3.1 in. (80 mm) on center along the entire length of the beam, effectively confining the spliced region. The clear cover in each beam was 1.2 in. (30 mm). All beams were loaded to failure. The normalized bond strengths of the SCC beam specimens were 4% higher than the control specimens for both bar diameters. It was also noted that the SCC beam specimens produced longer cracks than the control specimens, giving evidence that the paste in the SCC more thoroughly coated the reinforcing bar (Turk *et al.*, 2009).

Another study was conducted in Spain comparing the bond strength of SCC and conventional concrete entitled “Bond Behaviour of Reinforcement in Self-Compacting Concretes” (Valcuende and Parra, 2008). Comparison of bond strengths was accomplished through the use of direct pull-out tests. The specimens tested in this study included 7.9 in. (200 mm) cube specimens and square cross-section, 4.9-ft.-tall (1500 mm) columns. One length of #5 (#16) diameter reinforcing bars was embedded into each cube specimen, with a bonded length of 3.15 in. (80 mm). Twelve cube specimens were constructed for each mix design. Of the twelve cubes constructed, six specimens were tested at 28 days and the other six specimens were tested at 90 days. Six lengths of #5 (#12) bars were embedded into each column, with a bonded length of 2.36 in. (60 mm). Four columns were constructed for each mix design. At 28 days, six 5.9 in. (150 mm) cube specimens were cut from the column and tested to bond failure. Rubber sleeves were used to ensure the specified length of bar remained unboned from the surrounding concrete. The bars in each column were located 2.95 in. (75 mm), 10.83 in. (275 mm), 18.7 in. (475 mm), 26.57 in. (675 mm), 41.34 in. (1050 mm), and 56.1 in. (1425 mm)

from the bottom of the specimen. The columns were constructed to evaluate top-bar effect. The test results obtained indicate that the SCC specimens exhibited higher bond strength than that of the conventional concrete specimens. The authors noted that SCC behaved more homogeneously than the conventional concrete mixes in the column test specimens. This indicates that top-bar effect is less pronounced in SCC than in conventional concrete (Valcuende and Parra, 2008).

SCC bond strength relative to conventional concrete was also studied and detailed in a report entitled “Effect of Reinforcing Bar Orientation and Location on Bond with Self-Consolidating Concrete” (Castel *et al.*, 2006). Direct pull-out tests were constructed to compare bond strengths. Also, reinforcing bars were cast vertically and horizontally in the concrete to determine the effect of bar orientation on bond strength. The pull-out specimens were 4.73 in. (120 mm) long, with a cross section of 4 in. x 4 in. (100 mm x 100 mm). The reinforcing bars embedded in the concrete were #5 (#12) plain and ribbed bars. The bonded length was 2.36 in. (60 mm) for each specimen. The specimens were cast in 19.7 in. (500 mm) lengths and sawn into three parts at 28 days. Two pull-out specimens were tested for each configuration. The effect of bar location was also tested through the use of large specimens. The same reinforcing bars were used for the large test specimens. The specimens were 59.1 in. (1100 mm) tall and the reinforcing bars were spaced 4 in. (100 mm) apart, evenly along the height of the specimen. At 28 days, the large specimen was cut to create smaller specimens the same size as the small pull-out specimens. The test results indicated that the orientation of the deformed bars had a similar influence on bond strength for both 3,625 psi (25 MPa) SCC and conventional concrete. Bond strengths for the 5,800 psi (40 MPa) concrete mixes were not affected by

bar orientation. Reduction in bond strength was seen for each concrete type as the amount of concrete cast below the bar increased in the large specimen tests. Similar reductions were seen for both SCC and conventional concrete. Overall, SCC exhibited higher bond strength than conventional concrete for both concrete strengths (Castel *et al.*, 2006).

Another study evaluating the bond behavior of SCC was entitled “Self-Compacting Concrete (SCC) Time Development of the Materials and the Bond Behaviour” (Dehn *et al.*, 2000). This study focused on evaluating the bond strength increase over time in SCC by testing direct pull-out specimens at 1, 3, 7, and 28 days. The direct pull-out test specimens consisted of a cylinder of concrete that was 4 in. (100 mm) in diameter and 4 in (100 mm) long. Reinforcing consisted of #3 (#10) bars embedded 2 in. (50 mm) in the concrete, with an unbonded length of 2 in. (50 mm). A plastic sleeve was used to ensure the appropriate length of bar remained unbonded during casting. A total of twelve specimens were cast and three specimens at each specified day to evaluate the bond strength gain over time. The tested specimens were then compared to the bond law of conventional concrete developed by König and Tue. The test results indicated that the bond behavior of SCC was superior to that of conventional concrete (Dehn *et al.*, 2000).

Another test comparing bond strengths of SCC and conventional concrete was entitled “Development of Bond Strength of Reinforcement Steel in Self-Consolidating Concrete” (Chan *et al.*, 2003). This study compares bond strengths of SCC and conventional concrete by testing direct pull-out specimens. Full-scale walls were constructed with reinforcing bars embedded parallel to the depth of the wall. The specimen was 47.24 in. x 35.43 in. x 169.29 in. (1200 mm x 900 mm x 4300 mm). Three

rows of deformed reinforcing bars were embedded horizontally at 7.87, 19.7, and 31.5 in. (200, 500, and 800 mm) from the bottom of the specimen. A length of 4 in. (100 mm) was bonded and lengths of polyvinyl chloride (PVC) were used as bond breakers at both ends of the embedded reinforcing bars. The test results collected indicated that the extent of differing bond strengths with respect to elevation at casting was less significant with SCC than with conventional concrete. Also, SCC exhibited significantly higher bond strength and less top-bar effect than the conventional concrete (Chan *et al.*, 2003).

### 3. MIX DESIGNS AND CONCRETE PROPERTIES

#### 3.1. INTRODUCTION

The following chapter contains the mix designs for both the self-consolidating concrete (SCC) mix designs and their respective controls. Also included in this chapter are the methods and results of the testing done to determine the fresh and hardened properties of each mix.

#### 3.2. CONCRETE PROPERTIES

**3.2.1. Fresh Concrete Properties.** Various tests were conducted on the fresh concrete prior to casting the test specimens. The type of fresh concrete test was dependent on the type of concrete being tested. A slump test was performed on all the conventional concrete mixes upon arrival of the concrete mixing truck in accordance with ASTM C143/C143M “Standard Test Method for Slump of Hydraulic-Cement Concrete” (ASTM C143/C143M, 2010). A standard mold for the slump test was dampened and placed on a metal slump pan. Then the mold was filled to one-third of its volume with the fresh concrete. The concrete was then rodded 25 times uniformly over the cross section with a standard tamping rod. This process was repeated for the subsequent two layers. Upon finishing the last layer, the top of the concrete was smoothed using the tamping rod and any excess concrete was removed from around the base of the mold. The mold was then lifted vertically slowly in accordance with the ASTM established method noted above. The length that the top of the fresh concrete slumped upon removal of the mold was recorded as the slump of the concrete. The slump test is shown in **Figure 3.1**.



**Figure 3.1 – Slump test**

Two unique test methods were conducted on the SCC to determine workability. The first was the slump flow test in accordance with ASTM C1611/C1611M “Standard Test Method for Slump Flow of Self-Consolidating Concrete” (ASTM C1611/C1611M, 2009). The same mold used for the slump test was also used for the slump flow test. The inside of the mold was dampened and placed upside down (large opening facing upward) on a metal slump pan. The mold was then filled in a continuous manner until the mold was slightly overfilled above its top. The surface was then leveled with a strike-off bar, and then the mold was raised vertically slowly in accordance with the ASTM. When the concrete had stopped flowing, the diameter of the concrete was measured along perpendicular axes and averaged to determine the slump flow. The slump flow test is shown in **Figure 3.2**.



**Figure 3.2 – Slump flow test**

The second unique test for SCC was the J-ring test conducted in accordance with ASTM C1621/C1621M “Standard Test Method for Passing Ability of Self-Consolidating Concrete by J-Ring” (ASTM C1621/C1621M, 2009). The procedure for the J-ring test is the same as for the slump flow. However, after dampening the mold, it is placed on the slump pan in the center of a standard J-ring. The same filling, finishing, and mold removal procedures as those used for the slump flow are then conducted for the J-ring test. The diameter of the concrete ring was then measured in two perpendicular locations and averaged. The J-ring test is shown in **Figure 3.3**.



**Figure 3.3 – J-ring test**

The unit weight and air content were also determined. The unit weight of the fresh concrete was determined in accordance with ASTM C138/C138M “Standard Test Method for Density (Unit Weight), Yield, and Air Content (Gravimetric) of Concrete” (ASTM C138/C138M, 2010). A steel cylindrical container was used as the measure for this test. The inside of the measure was first dampened, and then it was weighed and measured to determine its empty weight and volume, respectively. Then fresh concrete was added to the measure to one-third of its volume. The concrete was then rodded 25 times with a standard tamping rod and the measure was struck with a rubber mallet 15 times around its outside perimeter. This step was repeated for the second and third level of concrete. Upon filling the measure, the concrete was finished with a strike-off plate and any excess concrete was removed from the rim of the measure using a sponge. The measure was then weighed to determine its weight and the weight of the concrete it contained. The weight of the measure was then subtracted from the combined weight of

the measure and the concrete to determine the weight of the concrete. The weight of the concrete was then divided by the volume of the measure to determine the unit weight of the concrete.

The air content of the concrete was determined in accordance with ASTM C231/C231M “Standard Test Method for Air Content of Freshly Mixed Concrete by the Pressure Method” (ASTM C231/C231M, 2010). A standard type-B meter was used for this test. The same steel container and filling procedure used for determining the unit weight were used for the air content test. After completing the filling process, the flange of the cover assembly was thoroughly cleaned and clamped onto the steel container. Both petcocks were opened and water was added to one petcock until the water emerged from the other petcock to remove any excess air in the steel container. The air bleeder valve was then closed and air was pumped into the container until the gauge hand was on the initial pressure line. Both petcocks were then closed and the main air valve was opened while simultaneously tapping the container smartly with a rubber mallet. The air content shown on the gauge was then recorded as the air content of the concrete.

**3.2.2. Compressive Strength of Concrete.** The concrete compressive strength was determined in accordance with ASTM C39/39M “Standard Test Method for Compressive Strength of Cylindrical Concrete Specimens” (ASTM C39/C39M, 2011). The specimens consisted of 4 in. (102 mm) diameter, 8 in. (203 mm) tall cylinders for each mix design. **Figure 3.4** displays the cylinders being cast. Prior to testing, the cylinders were capped in order to eliminate the effect of point stresses caused by an uneven surface. The capped cylinders were then subjected to a compressive axial load across their entire circular cross section until failure, applied at a rate appropriate for the

testing apparatus and in conformance with ASTM C39/C39M. The test setup is shown in **Figure 3.5**.



**Figure 3.4 – Casting compressive strength cylinders**



**Figure 3.5 – Compressive strength test setup**

**3.2.3. Modulus of Rupture of Concrete.** The modulus of rupture was determined in accordance with ASTM C78/C78M “Standard Test Method for Flexural Strength of Concrete (Using Simple Beam Third-Point Loading) (ASTM C78/C78M, 2010). The test consists of subjecting a 6 in. x 6 in. x 24 in. (152 mm x 152 mm x 610 mm) concrete beam to a four-point load until failure. **Eq. 3.1** was used to determine the modulus of rupture from each beam test result.

$$R = \frac{PL}{bd^2} \quad (3.1)$$

Where R is the modulus of rupture, P is the maximum applied load, L is the span length, b is the average width of the specimens at the fractured surface, and d is the average depth of the specimen at the fractured surface. The test specimens are shown in **Figure 3.6** and the test setup is shown in **Figure 3.7**.



**Figure 3.6 – Modulus of rupture test specimens**



**Figure 3.7 – Modulus of rupture test setup**

**3.2.4. Splitting Tensile Strength of Concrete.** The splitting tensile strength was determined in accordance with ASTM C496/C496M “Standard Test Method for Splitting Tensile Strength of Cylindrical Concrete Specimens” (ASTM C496/C496M, 2011). The specimens consisted of 6 in. (152 mm) diameter, 12 in. (305 mm) tall cylinders for each mix design, which were tested upon reaching the appropriate concrete compressive strength. **Eq. 3.2** was used to determine the splitting tensile strength of each cylinder test result.

$$T = \frac{2P}{\pi ld} \quad (3.2)$$

Where T is the splitting tensile strength, P is the maximum applied load, l is the length of the specimen, and d is the diameter of the specimen. The splitting tensile strength test setup is shown in **Figure 3.8**.



**Figure 3.8 – Splitting tensile strength test setup**

### 3.3. SELF-CONSOLIDATING CONCRETE (SCC) MIX DESIGNS

A survey of Missouri precast suppliers was conducted in order to obtain representative SCC mix designs currently in use throughout the state, particularly in large metropolitan areas such as St. Louis and Kansas City. The results of this survey were then used to develop a normal strength and a high strength SCC mix design, with specified compressive strengths of 6,000 psi (41.4 MPa) and 10,000 psi (69 MPa), respectively. The target air content was 6% and the target slump flow was 23 to 28 in. (584 to 711 mm) for both SCC mix designs. Two standard MoDOT mix designs with the same specified compressive strengths as their respective SCC mix designs were chosen as the controls. The target air content was 6% and the target slump was 4 to 5 in. (102 to 127 mm) for both control mix designs. The air entraining admixture MB-AE-90 and the water reducing admixture Glenium 7700 were used to obtain the necessary properties.

**3.3.1. Normal Strength Control Mix Design.** The normal strength control mix design was designated C6-58L and is shown in **Table 3.1**.

**Table 3.1 – C6-58L mix proportions**

<b>Ingredient</b>	<b>Weight (lb./yd<sup>3</sup>)</b>
w/cm	0.37
Cement (Type 1)	750
Coarse Aggregate	1,611
Fine Aggregate	1,166
MB-AE-90	1.5 oz./cwt.
Glenium 7500	4.7 oz./cwt.

Conversion: 1 lb./ yd<sup>3</sup> = 0.59 kg/m<sup>3</sup>

1 oz. = 29.6 ml

1 lb. = 0.45 kg

The slump, air content, and unit weight of the concrete used for the fabrication of test specimens was determined upon arrival of the concrete mixing truck. The slump measured 8 in. (203 mm), the air content measured 9.0%, and the unit weight measured 139.6 lb./ft<sup>3</sup> (2240 kg/m<sup>3</sup>).

Test specimens for determining the compressive strength, splitting tensile strength, and modulus of rupture of the concrete were fabricated along with the bond test specimens. The concrete compressive strength test results are shown in **Table 3.2** and plotted in **Figure 3.9**. The splitting tensile strength results are shown in **Table 3.3**. The modulus of rupture test results are shown in **Table 3.4**.

**Table 3.2 – Compressive strength data of C6-58L**

<b>Day</b>	<b>Average Strength (psi)</b>
<b>1</b>	3,695
<b>3</b>	5,115
<b>7</b>	5,330
<b>14</b>	5,910
<b>16</b>	5,720

Conversion: 1 psi = 6.9 kPa

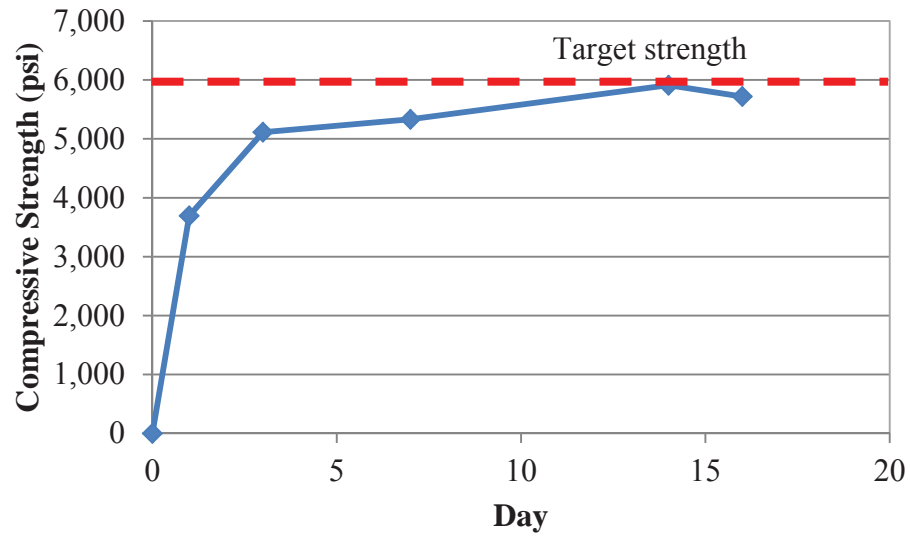


**Figure 3.9 – Plot of C6-58L compressive strength**  
Conversion: 1 psi = 6.9 kPa

**Table 3.3 – Splitting tensile strength test results for C6-58L**

Specimen	Peak Load (lb.)	Splitting Tensile Strength (psi)
<b>C6-58L-1</b>	43,155	380
<b>C6-58L-2</b>	51,870	460
<b>C6-58L-3</b>	50,250	445
<b>Average:</b>		430

Conversion: 1 lb. = 4.45 N  
1 psi = 6.9 kPa

**Table 3.4 – Modulus of rupture test results for C6-58L**

Specimen	Peak Load (lb.)	Modulus of Rupture (psi)
C6-58L-1	6,255	520
C6-58L-2	6,310	530
C6-58L-3	5,670	480
C6-58L-4	5,375	440
<b>Average:</b>		490

Conversion: 1 lb. = 4.45 N

1 psi = 6.9 kPa

**3.3.2. SCC Normal Strength Mix Design.** The SCC normal strength mix design was designated S6-48L and is shown in **Table 3.5**.

The slump flow, J-ring, air content, and unit weight of the concrete used for the fabrication of test specimens was determined upon arrival of the concrete mixing truck. The slump flow measured 24 in. (610 mm), the J-ring measured 20.75 in. (527 mm), the air content measured 6%, and the unit weight measured 145.7 lb./ft<sup>3</sup> (2330 kg/m<sup>3</sup>).

**Table 3.5 – S6-48L mix proportions**

Ingredient	Weight (lb./yd <sup>3</sup> )
w/cm	0.37
Cement (Type 1)	750
Coarse Aggregate	1,333
Fine Aggregate	1,444
MB-AE-90	1.5 oz./cwt.
Glenium 7500	6.2 oz./cwt.

Conversion: 1 lb./ yd<sup>3</sup> = 0.59 kg/m<sup>3</sup>

1 oz. = 29.6 ml

1 lb. = 0.45 kg

Test specimens for determining the compressive strength, splitting tensile strength, and modulus of rupture of the concrete were fabricated along with the bond test

specimens. The concrete compressive strength test results are shown in **Table 3.6** and plotted in **Figure 3.10**. The splitting tensile strength results are shown in **Table 3.7**. The modulus of rupture test results are shown in **Table 3.8**.

**Table 3.6 – Compressive strength data of S6-48L**

Day	Average Strength (psi)
1	5,320
3	6,990
5	6,840

Conversion: 1 psi = 6.9 kPa

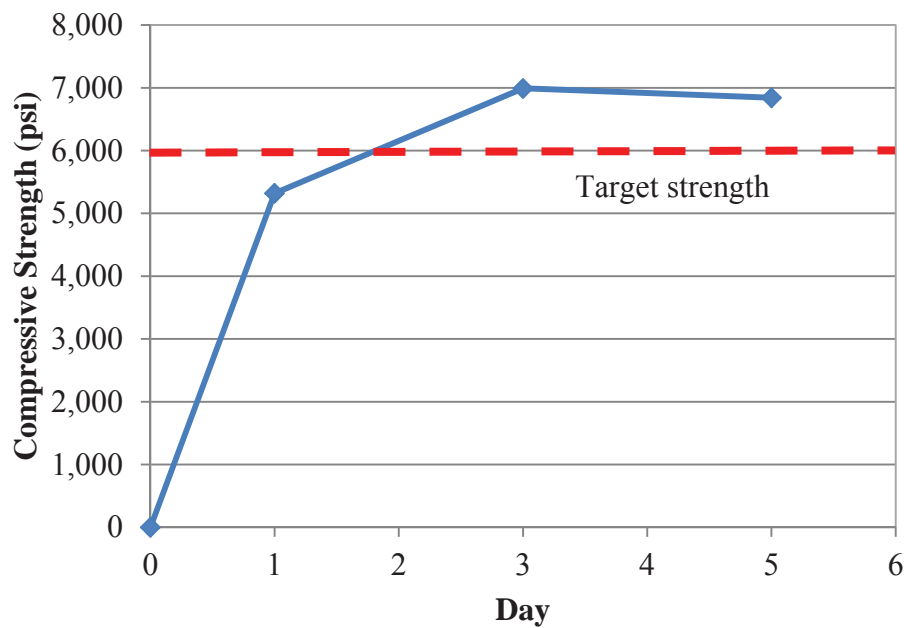


**Figure 3.10 – Plot of S6-48L compressive strength**

Conversion: 1 psi = 6.9 kPa

**Table 3.7 – Splitting tensile strength test results for S6-48L**

<b>Specimen</b>	<b>Peak Load (lb.)</b>	<b>Splitting Tensile Strength (psi)</b>
<b>S6-48L-1</b>	53,760	475
<b>S6-48L-2</b>	62,580	555
<b>S6-48L-3</b>	62,790	555
<b>Average:</b>		530

Conversion: 1 lb. = 4.45 N

1 psi = 6.9 kPa

**Table 3.8 – Modulus of rupture test results for S6-48L**

<b>Specimen</b>	<b>Peak Load (lb.)</b>	<b>Modulus of Rupture (psi)</b>
<b>S6-48L-1</b>	5,155	430
<b>S6-48L-2</b>	5,680	470
<b>S6-48L-3</b>	6,980	570
<b>S6-48L-4</b>	6,210	520
<b>Average:</b>		495

Conversion: 1 lb. = 4.45 N

1 psi = 6.9 kPa

**3.3.3. High Strength Control Mix Design.** The high strength control mix design was designated C10-58L and is shown in **Table 3.9**.

**Table 3.9 – C10-58L mix proportions**

<b>Ingredient</b>	<b>Weight (lb./yd<sup>3</sup>)</b>
w/cm	0.30
Cement (Type 1)	840
Fly Ash (Class C)	210
Coarse Aggregate	1,440
Fine Aggregate	1,043
MB-AE-90	1.3 oz./cwt.
Glenium 7500	5 oz./cwt.

Conversion: 1 lb./ yd<sup>3</sup> = 0.59 kg/m<sup>3</sup>

1 oz. = 29.6 ml

1 lb. = 0.45 kg

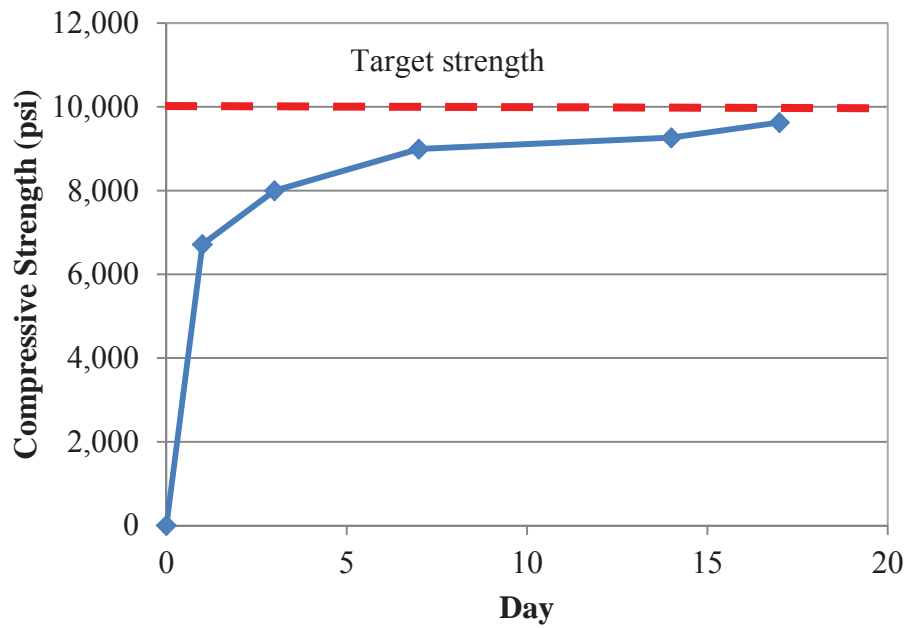
The slump, air content, and unit weight of the concrete used for the fabrication of test specimens was determined upon arrival of the concrete mixing truck. The slump measured 2 in. (51 mm), the air content measured 2.5%, and the unit weight measured 152.2 lb./ft<sup>3</sup> (2440 kg/m<sup>3</sup>).

Test specimens for determining the compressive strength, splitting tensile strength, and modulus of rupture of the concrete were fabricated along with the bond test specimens. The concrete compressive strength test results are shown in **Table 3.10** and plotted in **Figure 3.11**. The splitting tensile strength results are shown in **Table 3.11**. The modulus of rupture test results are shown in **Table 3.12**.

**Table 3.10 – Compressive strength data of C10-58L**

Day	Average Strength (psi)
1	6,715
3	8,000
7	8,995
14	9,265
17	9,625

Conversion: 1 psi = 6.9 kPa

**Figure 3.11 – Plot of C10-58L compressive strength**

Conversion: 1 psi = 6.9 kPa

**Table 3.11 – Splitting tensile strength test results for C10-58L**

<b>Specimen</b>	<b>Peak Load (lb.)</b>	<b>Splitting Tensile Strength (psi)</b>
<b>C10-58L-1</b>	67,380	600
<b>C10-58L-2</b>	62,595	555
<b>C10-58L-3</b>	62,685	555
<b>Average:</b>		570

Conversion: 1 lb. = 4.45 N

1 psi = 6.9 kPa

**Table 3.12 – Modulus of rupture test results for C10-58L**

<b>Specimen</b>	<b>Peak Load (lb.)</b>	<b>Modulus of Rupture (psi)</b>
<b>C10-58L-1</b>	8,585	705
<b>C10-58L-2</b>	7,925	645
<b>C10-58L-3</b>	8,345	680
<b>C10-58L-4</b>	9,220	730
<b>Average:</b>		690

Conversion: 1 lb. = 4.45 N

1 psi = 6.9 kPa

**3.3.4. SCC High Strength Mix Design.** The SCC high strength mix design was designated S10-48L and is shown in **Table 3.13**.

**Table 3.13 – S10-48L mix proportions**

<b>Ingredient</b>	<b>Weight (lb./yd<sup>3</sup>)</b>
w/cm	0.30
Cement (Type 1)	840
Fly Ash (Class C)	210
Coarse Aggregate	1,192
Fine Aggregate	1,291
MB-AE-90	1 oz./cwt.
Glenium 7500	7.2 oz./cwt.

Conversion: 1 lb./ yd<sup>3</sup> = 0.59 kg/m<sup>3</sup>

1 oz. = 29.6 ml

1 lb. = 0.45 kg

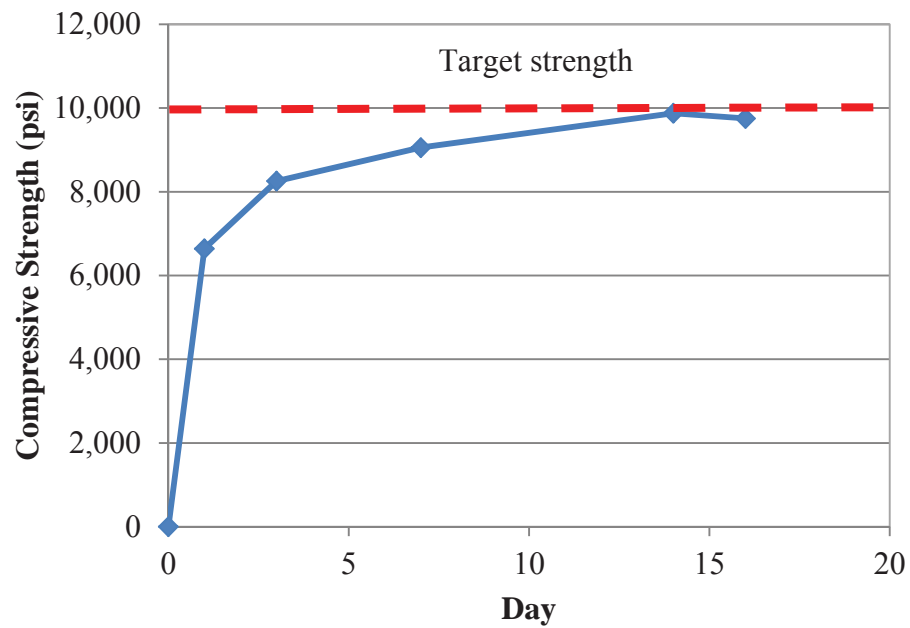
The slump flow, J-ring, air content, and unit weight of the concrete used for the fabrication of test specimens was determined upon arrival of the concrete mixing truck. The slump flow measured 23.5 in. (597 mm), the J-ring measured 21.5 in. (546 mm), the air content measured 3.0%, and the unit weight measured 149.4 lb./ft<sup>3</sup> (2400 kg/m<sup>3</sup>).

Test specimens for determining the compressive strength, splitting tensile strength, and modulus of rupture of the concrete were fabricated along with the bond test specimens. The concrete compressive strength test results are shown in **Table 3.14** and plotted in **Figure 3.12**. The splitting tensile strength results are shown in **Table 3.15**. The modulus of rupture test results are shown in **Table 3.16**.

**Table 3.14 – Compressive strength data of S10-48L**

Day	Average Strength (psi)
1	6,640
3	8,255
7	9,055
14	9,880
16	9,755

Conversion: 1 psi = 6.9 kPa

**Figure 3.12 – Plot of S10-48L compressive strength**

Conversion: 1 psi = 6.9 kPa

**Table 3.15 – Splitting tensile strength test results for S10-48L**

<b>Specimen</b>	<b>Peak Load (lb.)</b>	<b>Splitting Tensile Strength (psi)</b>
<b>S10-48L-1</b>	70,770	625
<b>S10-48L-2</b>	59,925	530
<b>S10-48L-3</b>	61,215	540
<b>Average:</b>		565

Conversion: 1 lb. = 4.45 N

1 psi = 6.9 kPa

**Table 3.16 – Modulus of rupture test results for S10-48L**

<b>Specimen</b>	<b>Peak Load (lb.)</b>	<b>Modulus of Rupture (psi)</b>
<b>S10-48L-1</b>	5,925	480
<b>S10-48L-2</b>	7,400	605
<b>S10-48L-3</b>	6,670	550
<b>S10-48L-4</b>	6,465	535
<b>Average:</b>		540

Conversion: 1 lb. = 4.45 N

1 psi = 6.9 kPa

## 4. EXPERIMENTAL PROGRAM

### 4.1. INTRODUCTION

The experimental program included both direct pull-out tests, as well as full-scale beam splice specimen tests. The direct pull-out specimens were based on RILEM 7-II-128 “RC6: Bond test for reinforcing steel. 1. Pull-out test” (RILEM, 1994). The beam splice specimen tests were based on recommendations in ACI 408R-03 “Bond and Development of Straight Reinforcing Bars in Tension” (ACI 408R-03, 2003). The following is a discussion of the design, setup, instrumentation, and procedures for both testing methods.

### 4.2. DIRECT PULL-OUT TEST

**4.2.1. Direct Pull-out Specimen Design.** The direct pull-out specimen tests were based on the RILEM 7-II-128 “RC6: Bond test for reinforcing steel. 1. Pull-out test” (RILEM, 1994). Several changes were made to the recommended test specimen based on results from previous research (Wolfe, 2011). The test involves casting a length of reinforcing bar within a concrete cylinder and applying a direct tension force on the bar until the bonded length fails. Although not directly related to the behavior of a reinforced concrete beam in flexure, the test does provide a realistic comparison of bond between types of concrete.

The RILEM standard states that the reinforcing bar will be embedded in the concrete a total length of 15 times the bar diameter to be tested. A bond breaker a length of 7.5 times the bar diameter is to be placed so that the bar is unbonded from the bottom

surface to halfway in the concrete, leaving a bonded length of 7.5 times the bar diameter. The unbounded length at the bottom of the concrete segment is to reduce restraint stresses caused by friction with the loading head. Previous testing showed this bonded length to be too long and yielding of the bar occurred prior to failure in some instances (Wolfe, 2011). To ensure the bond failed before the bar yielded, the total concrete depth was reduced to 10 times the bar diameter with a bonded length of 5 times the bar diameter.

The RILEM standard specifies a square concrete cross section with sides having a length of 8.75 in. (222 mm). For this test program, a circular concrete cross section with a diameter of 12 in. (305 mm) was used instead. This change eliminated the potential for a splitting failure (side cover failure) and also maintained a constant cover for the reinforcing bar.

The protocol for the direct pull-out tests included two bar sizes – #4 (#13) and #6 (#19) – in order to evaluate the bond performance over a range of reinforcing sizes. The total length of each bar was 40 in (1016 mm). A length of 3/8 in. (10 mm) was left exposed at the top of the specimen to measure bar slip using a Linear Voltage Differential Transformer (LVDT). **Figures 4.1** and **4.2** are schematic diagrams of the specimen dimensions for the #4 (#13) and #6 (#19) bars, respectively.

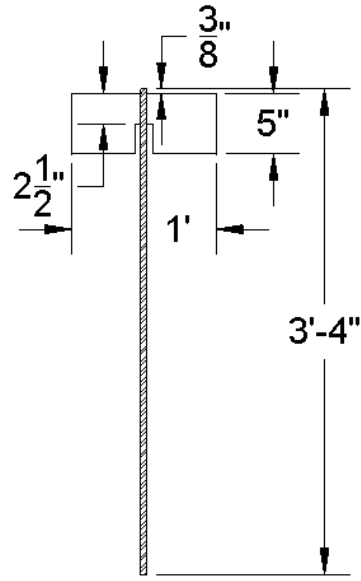


**Figure 4.1 – Pull-out specimen with dimensions for #4 (#13) reinforcing bars**  
 Conversion: 1 in. = 25.4 mm

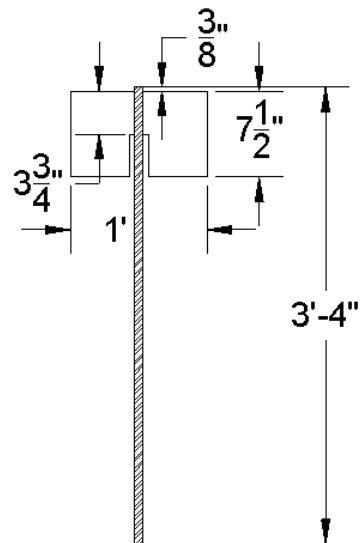


**Figure 4.2 – Pull-out specimen with dimensions for #6 (#19) reinforcing bars**  
 Conversion: 1 in. = 25.4 mm

**4.2.2. Direct Pull-out Specimen Fabrication.** The formwork base for the direct pull-out test specimen was constructed with a 14-in.-square (356 mm), 3/8-in.-thick (10 mm) section of plywood. A hole that was 1/16 in. (0.16 mm) larger than the bar diameter being tested was drilled through the center of the plywood squares. Cardboard tubing (Quick-Tube) was then cut to the required length, depending on the bar size being tested. Waterproof silicone adhesive caulk was then used to bind the cardboard tubing to the plywood squares.

The reinforcing bar for each specimen was sectioned into 40 in. (1016 mm) lengths. Polyvinyl chloride (PVC) tubing was used to form the bond breaker. For the #4 (#13) bar, the PVC had an inside diameter of 3/4 in. (19 mm) and was sectioned into lengths of 2.5 in. (64 mm). For the #6 (#19) bar, the PVC had an inside diameter of 1 in. (25 mm) and was sectioned into 3.75 in. (95 mm) lengths. A mark was made on each bar to facilitate the placement of the PVC bond breaker. The PVC was slid onto the reinforcing bar and shims of cardboard were used to center the bar in the PVC. The PVC was then adhered to the reinforcing bar using waterproof silicone adhesive caulk and was carefully finished to ensure there were no gaps in the caulk for the concrete paste to get between the bar and the PVC.

The top of the formwork was also a 14-in.-square (356 mm) of 3/8-in.-thick (10 mm) plywood with a hole drilled through its center. To ensure that the bars were plumb within the concrete encasement, prior to constructing the specimens, the reinforcing bars were placed in the completed forms and leveled. Upon leveling the bars, an outline of the cylindrical form was drawn on the underside of the top plywood square. Wood spacers were then screwed into the plywood square along the outline of the cardboard tubing.

The specimens were cast by first placing the reinforcing bar through the hole in the base of the formwork. Concrete was then placed in the cylindrical formwork and consolidated as necessary. After proper placement of the concrete, the exposed surface was finished. The top of the formwork was then carefully slid down the reinforcing bar and the wood spacers were fit snugly over the cylindrical forms. The reinforcing bar was checked to ensure it was plumb and then the sides of the cylindrical forms were lightly vibrated. The pull-out and companion material property specimens were allowed to cure until the concrete reached its specified strength prior to testing. The cardboard tubing was removed on the day of testing. Construction of the pull-out specimens is shown in **Figure 4.3**, with complete specimens shown in **Figure 4.4**.



**Figure 4.3 – Pull-out specimen construction**



**Figure 4.4 – Completed specimens**

**4.2.3. Direct Pull-out Test Setup.** Testing of the direct pull-out specimens was completed using a 200,000-lb-capacity (890 kN) testing machine manufactured by Tinius Olson. The test setup is shown in **Figures 4.5** and **4.6**. The cylindrical forms were removed immediately prior to testing. A neoprene pad with a hole in its center was placed on the top platform of the test machine to ensure uniform bearing of the concrete. The specimens were flipped upside down and the reinforcing bar was then threaded through the hole in the neoprene pad on the top platform and placed between the grips installed on the middle platform. An LVDT was then clamped to a stand, and the stand was placed on top of the concrete section of the specimen. The needle of the LVDT was placed on top of the 3/8 in. (10 mm) length of exposed reinforcing bar to measure slip.

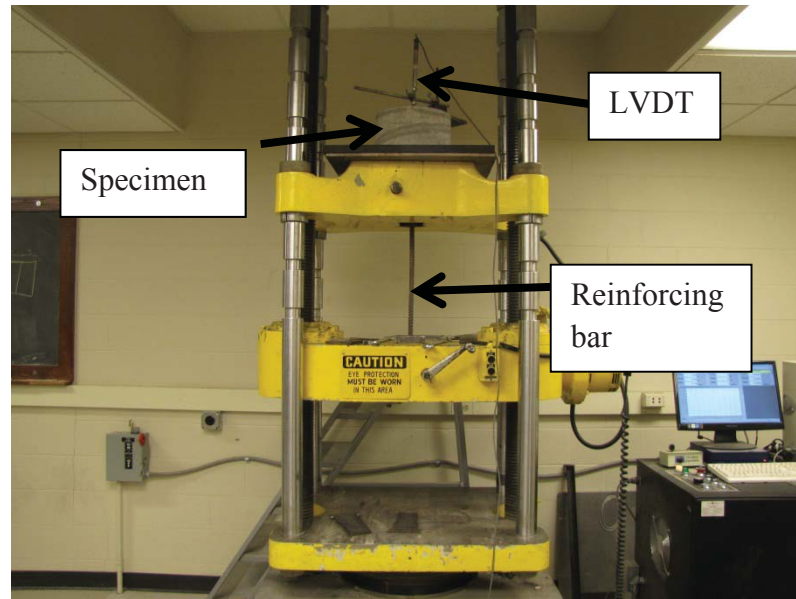


**Figure 4.5 – Direct pull-out test setup**

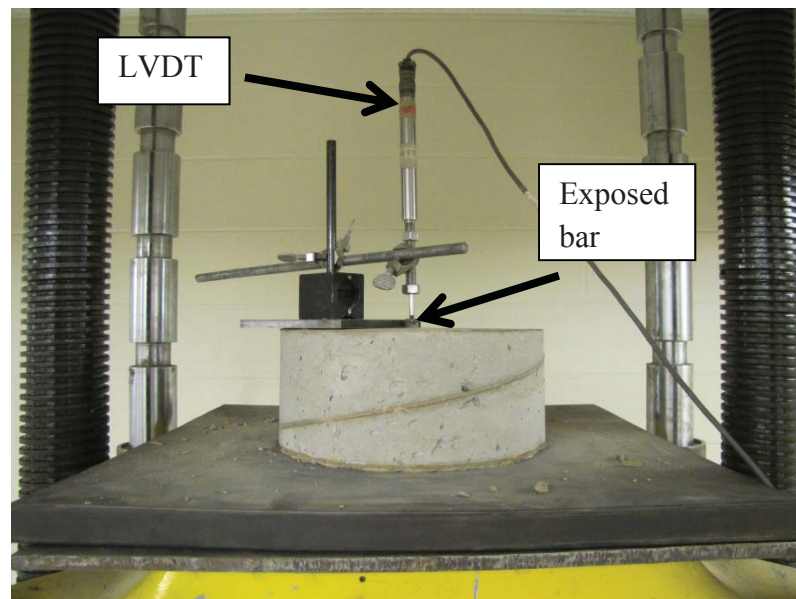


**Figure 4.6 – LVDT installation to measure bar slip**

**4.2.4. Direct Pull-out Test Procedure.** The middle platform was manually positioned to allow for the reinforcing bar to be clamped. The equipment controlling the

Tinius Olson was programmed to apply a displacement controlled load rate of 0.1 in. (3 mm) per minute. Upon initiating a new test, the LVDT data collection platform was started and the clamps were closed around the reinforcing bar while the middle platform was simultaneously lowered. This step was done to seat the test specimen and apply an initial load sufficient to maintain a proper grip on the reinforcing bar during testing. The test program was then initiated and allowed to run until a distinct peak was observed in the applied load vs. bar slip plot. This step was done to ensure there was no residual load carrying capacity in the bonded region and that the proper failure load was determined. At that point, the test program and LVDT data collection platform were both stopped and the test specimen was removed.

### **4.3. BEAM SPLICE TEST**

**4.3.1. Beam Splice Specimen Design.** The beam splice test specimens were designed following a non-ASTM test procedure that is generally accepted as the most realistic test method for both development and splice length. This test consists of applying a full-scale beam specimen to a four-point loading until failure of the splice occurs. The splice is located in the region of the beam subjected to a constant moment, and thus constant stress. The realistic stress-state in the area of the reinforcing bars makes for an accurate representation of the bond strength of the tested member (ACI 408R-03, 2003).

Details of the beam splice specimens used in this current study are shown in **Figures 4.7** and **4.8**. The beams measured 10 ft. (3050 mm) in length, with a cross section of 12 in. x 18 in. (305 mm x 457 mm) and contained a splice centered at midspan.

Transverse steel consisting of #3 (#10), ASTM A615-09, Grade 60, U-shaped stirrups were used for shear reinforcement. A stirrup spacing less than the ACI 318-08 maximum stirrup spacing was used to ensure that bond failure occurred prior to shear failure. The stirrups were terminated at approximately 5 in. (127 mm) from each end of the splice to eliminate the effects of confinement within the splice region. The longitudinal reinforcement consisted of three, ASTM A615-09, Grade 60, #6 (#19) bars spliced at midspan of the beam. The splice length was based on a percentage of the development length of the longitudinal reinforcing bars calculated in accordance with ACI 318-08 “Building Code Requirements for Structural Concrete” (ACI 318-08, 2008) (**Eq. 4.1**).

$$l_d = \left( \frac{3}{40} \frac{f_y}{\lambda \sqrt{f'_c}} \frac{\Psi_t \Psi_e \Psi_s}{\left( \frac{c_b + K_{tr}}{d_b} \right)} \right) d_b \quad (4.1)$$

Where  $l_d$  is the development length,  $f_y$  is the specified yield strength of reinforcement,  $\lambda$  is the lightweight concrete modification factor,  $f'_c$  is the specified compressive strength of concrete,  $\Psi_t$  is the reinforcement location modification factor,  $\Psi_e$  is the reinforcement coating modification factor,  $\Psi_s$  is the reinforcement size modification factor,  $c_b$  is the smaller of the distance from center of a bar to nearest concrete surface and one-half the center-to-center spacing of bars being developed,  $K_{tr}$  is the transverse reinforcement index, and  $d_b$  is the nominal diameter of the reinforcing bar.

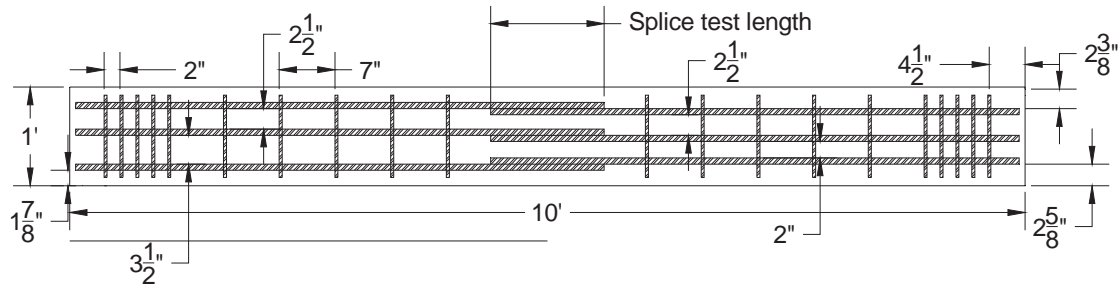


**Figure 4.7 – Beam splice specimen reinforcing layout**

Conversion: 1 in. = 25.4 mm

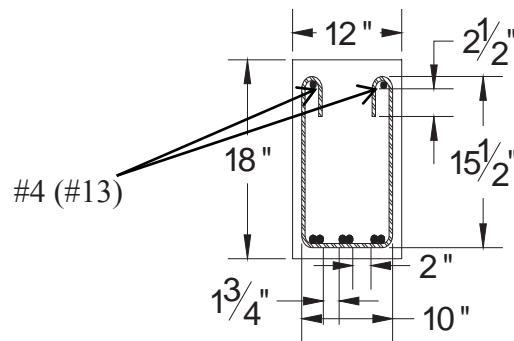


**Figure 4.8 – Beam splice specimen cross section**

Conversion: 1 in. = 25.4 mm

To ensure bond failure before yielding of the reinforcing bar, a splice length less than the code required development length was used in the test specimen. Prior researchers used one-half of a Class B splice as the lap length (Wolfe, 2011). However, several test specimens in that study exhibited signs of yielding in the reinforcement prior to bond failure. Therefore, for this current study, the splice length was limited to 70% of the development length.

**4.3.2. Beam Splice Specimen Fabrication.** The concrete formwork consisted of five removable and reusable pieces constructed from steel and wood. The pieces were connected through the use of steel keys and wire ties were used to hold the keys in place. The original beam forms were 14 ft. (4267 mm) in length. Consequently, 4 ft. (1219 mm)

wooden bulkheads were constructed to reduce the length of the beam forms to 10 ft. (3048 mm).

The #3 (#10) reinforcing bars were then sectioned to the appropriate length and bent to form the U-stirrups. The longitudinal reinforcement was sectioned to the appropriate length to obtain the proper splice length, as well as create a standard hook at the opposite end for proper development. All rust and mill scale was removed from the spliced region of each bar using a wire brush cup attached to an electric grinder. This step was done to ensure the bond strength was not affected in any way by the existence of rust and mill scale, thus maintaining conformity between the splice in each specimen. The longitudinal bars were then placed on saw-horses, aligned to obtain the appropriate splice length, and the stirrups were secured to the longitudinal bars using steel wire ties. A strain gauge was attached to the longitudinal bars at one end of each splice to monitor the strain during testing. Then, to ensure the stirrups stayed aligned vertically within the forms, two #4 (#13) bars were tied to the top bend of the stirrups and the end stirrups were tied to the hooked ends of the longitudinal bars. A finished reinforcing bar cage is shown in **Figure 4.9**.



**Figure 4.9 – Finished reinforcing bar cage**

Two of the cages were then lowered into the beam forms using 1 in. (25 mm) steel chairs on the bottom and sides to maintain 1 in. (25 mm) of clear cover to the outside edge of the stirrups. The third cage was turned upside down and 1.5 in. (38 mm) chairs were attached to the bottom of the cage to maintain clear cover to the splice at the top of the beam. Then, 1 in. (25 mm) chairs were also attached to the side of the stirrups to maintain 1 in. (25 mm) clear cover to the stirrups. Steel crossties were attached to the tops of the beam forms to maintain the proper beam width along the depth of the beam. Hooks were then tied to the crossties to facilitate transportation of the specimen after curing. **Figure 4.10** shows a picture of the spliced region in the beam forms, and **Figure 4.11** displays the three cages in their respective forms.

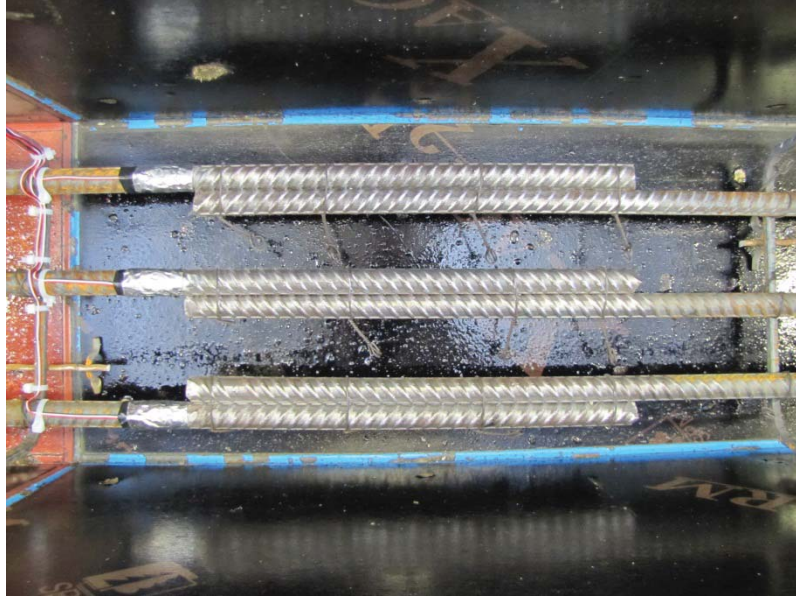


**Figure 4.10 – Spliced longitudinal bars for normal strength concrete**



**Figure 4.11 – Reinforcing bar cages in beam forms**

The concrete used to construct the specimens was delivered from a local ready-mix facility, Rolla Ready Mix (RRM). The mix design was supplied to RRM although

some of the water was held in abeyance in order to adjust the water content at the lab. Once the concrete truck arrived at the lab, the slump was measured and the reserve water was added as necessary to arrive at the required water-to-cementitious material ratio. At that point, all necessary activators and admixtures were added to the concrete truck, which was then mixed at high speed for 10 minutes to obtain the final material. At this point, the fresh concrete was loaded into a concrete bucket as shown in **Figure 4.12**. The bucket was then positioned with the overhead crane to facilitate placement of the concrete into the formwork as shown in **Figure 4.13**. The concrete was then consolidated as required for the particular concrete mix. This process was repeated until the beam forms were filled. The tops of the beams were then finished using trowels as shown in **Figure 4.14**.

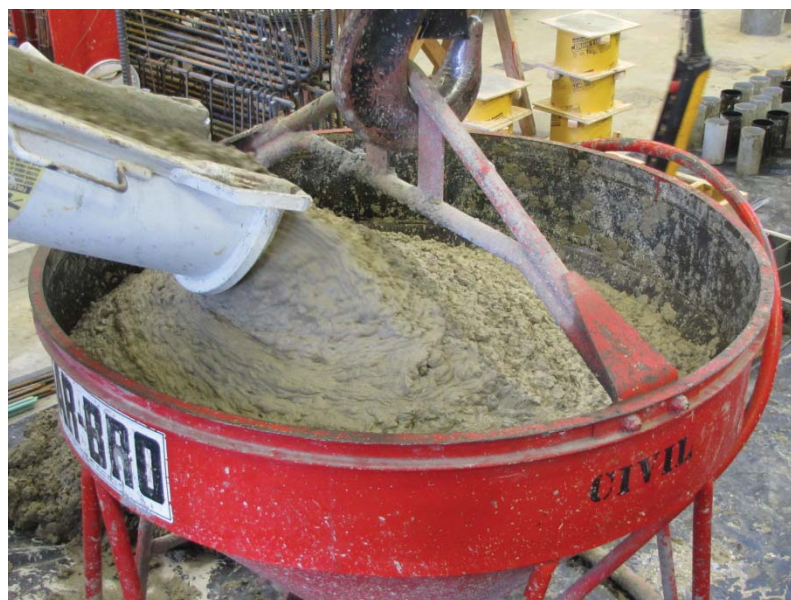


**Figure 4.12 – Concrete bucket being filled with fresh concrete**



**Figure 4.13 – Placement of concrete into beam forms**



**Figure 4.14 – Finished beams in forms**

Once the concrete reached initial set, the beam specimens and companion material property specimens were covered with wet burlap and plastic. The specimens were

allowed to cure until the concrete compressive strength reached a minimum of 1500 psi (10.3 MPa), at which point they were removed from the forms and remained within the temperature-controlled High Bay Lab. The beams were then tested upon reaching their respective design compressive strengths.

**4.3.3. Beam Splice Specimen Test Setup.** A schematic and photograph of the test setup are shown in **Figures 4.15** and **4.16**, respectively. The test consists of subjecting the beam splice specimen to four-point loading, ensuring that the region containing the splice is located in a constant moment region. The beam was then placed onto the supports. Two steel rollers were placed on the top surface of the beam specimen and steel spreader beams were used to transfer the applied load from two 140-kip-capacity (623 kN) hydraulic actuators.

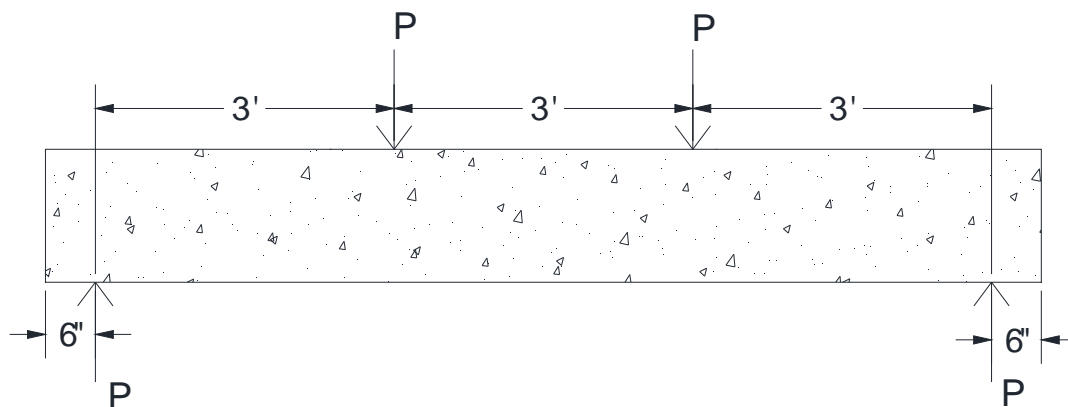


**Figure 4.15 – Beam loading schematic**

Conversion: 1 in. = 25.4 mm

The process of installing the beams into the test setup started with marking the center point, load points, and spreader beam outline onto each specimen. The strain gauge wires were then attached to a strain gauge converter box for subsequent attachment to the data acquisition system. At this point, the overhead crane was used to transport the beams

to a location adjacent to the test setup. The beams were then lowered onto steel rollers to facilitate placement into the test setup. The beam was then rolled into a position where the center point mark was directly below the center web stiffener on the spreader beam. One end was lined up with the spreader beam, lifted off of the steel roller with a hydraulic jack, and then lowered onto the support. This process was then repeated for the other support to line the beam up properly in the test frame. Once the beam was positioned within the test frame, metal plates were installed at the load point marks and the transfer beam was lowered into place. **Figure 4.16** shows the beam in the load frame located at the Missouri S&T High-Bay Structures Laboratory. A segment of aluminum angle was attached to the midpoint of the beam and an LVDT was placed on the aluminum to measure the deflection at midspan during testing as shown in **Figure 4.17**. The strain gauge wire converter box was then attached to the data acquisition system.



**Figure 4.16 – Beam positioned within load frame**

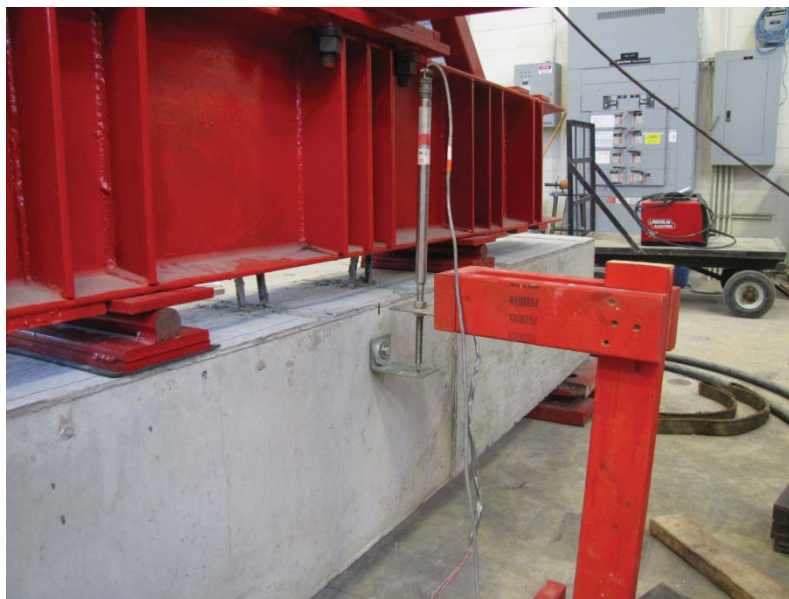


**Figure 4.17 – LVDT installation**

**4.3.4. Beam Splice Test Procedure.** Prior to beginning the test, the data acquisition system was initiated to record applied load, LVDT data, and strain gauge data. The load was then applied by the two 140-kip-capacity (623 kN) hydraulic actuators acting through the spreader beams. Each test was performed under displacement control, and the load was applied in a series of loading steps of 0.02 in. (0.5 mm), which corresponded to a load of approximately 3 kips (13 kN), until failure. Electronic measurements of strain and deformation were recorded throughout the entire loading history of the specimens. The crack patterns in the concrete were marked at every other load step to track propagation as the load was increased. Loading of the beams continued until a very prominent failure occurred, which was usually signaled both audibly and by a significant drop in the load-deflection behavior of the specimen.

## 5. SCC TEST RESULTS AND EVALUATION

### 5.1. DIRECT PULL-OUT TEST RESULTS

The direct pull-out specimens were constructed to evaluate the bond performance of SCC. The MoDOT standard mix design was used as a baseline for test result comparisons. A total of 24 direct pull-out test specimens were constructed for the SCC test program. There were six test specimens constructed for each of the four mix designs, which consisted of two SCC mixes and two control mixes. Of the six specimens constructed for each mix design, three specimens contained a #4 (#13) reinforcing bar and three specimens contained a #6 (#19) reinforcing bar. The test matrix for the SCC direct pull-out test program is shown in **Table 5.1**.

**Table 5.1 – SCC direct pull-out test matrix**

Mix I.D.	Bar Size	No. of Specimens
<b>C6-58L</b>	#4 (#13)	3
	#6 (#19)	3
<b>S6-48L</b>	#4 (#13)	3
	#6 (#19)	3
<b>C10-58L</b>	#4 (#13)	3
	#6 (#19)	3
<b>S10-48L</b>	#4 (#13)	3
	#6 (#19)	3

The applied load and corresponding slip of each reinforcing bar through the surrounding concrete were recorded for each test. Once compiled, the maximum applied load (peak load) for each test specimen was determined and used for bond strength comparison. **Table 5.2** displays the peak load for each of the test specimens in the SCC

test program, as well as average and coefficient of variation (COV) for each group of data. The first number in the specimen name represents the bar size, the following PO designates that specimen as a pull-out specimen, and the final number is the number of the specimen. Plots of the peak load for the C6-58L, S6-48L, C10-58L, and S10-48L specimens are shown in **Figures 5.1, 5.2, 5.3, and 5.4**, respectively. The plots indicate that results from tests having the same parameters are relatively similar. This fact is also demonstrated by the relatively small COV within a group of test specimens, with the highest being 5%. The consistent results between tests with the same parameters lend confidence in the ability of this test to accurately compare the bond strength between mix designs.

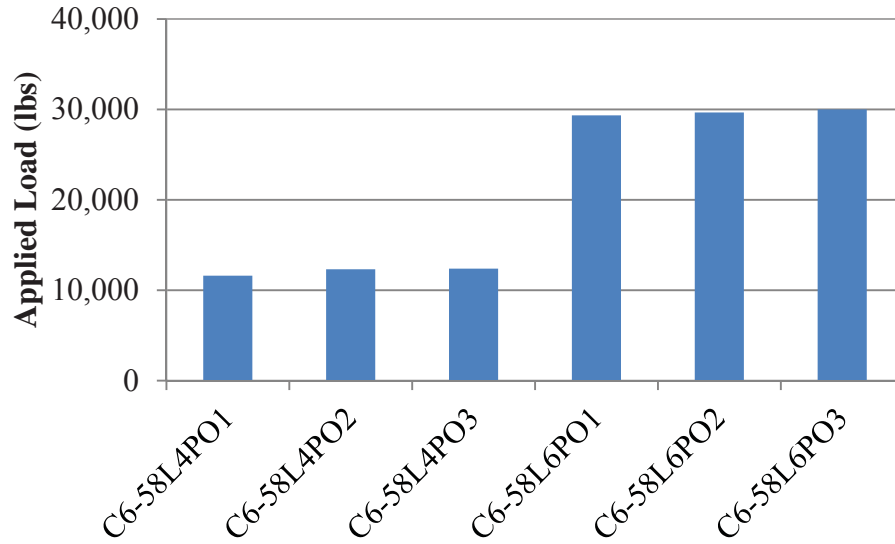
The load and slip data were also plotted for comparison of test results. An example of a load vs. slip plot is shown in **Figure 5.5**. All other load vs. slip plots have a similar shape and only differ in the magnitude of the values plotted. The mode of failure of all the pull-out test specimens consisted of the reinforcing bar slipping through the concrete section. Appendix E contains the load vs. slip plots for all 24 pull-out specimens.

Table 5.2 – SCC pull-out test results

Mix	Bar Size	Specimen	Max Applied Load (lb.)	Average Applied Load (lb.)	COV (%)
C6-58L	#4 (#13)	4PO1	12,320	12,109	3.6
		4PO2	12,394		
		4PO3	11,612		
	#6 (#19)	6PO1	29,997	29,665	1.1
		6PO2	29,659		
		6PO3	29,340		
S6-48L	#4 (#13)	4PO1	15,395	15,214	1.8
		4PO2	14,893		
		4PO3	15,354		
	#6 (#19)	6PO1	36,129	36,022	2.9
		6PO2	34,941		
		6PO3	36,996		
C10-58L	#4 (#13)	4PO1	18,527	18,926	5.2
		4PO2	18,210		
		4PO3	20,042		
	#6 (#19)	6PO1	43,347	43,682	0.8
		6PO2	43,997		
		6PO3	43,701		
S10-48L	#4 (#13)	4PO1	17,713	17,948	1.3
		4PO2	17,939		
		4PO3	18,191		
	#6 (#19)	6PO1	40,805	40,154	1.6
		6PO2	40,114		
		6PO3	39,542		

Conversion: 1 in. = 25.4 mm

1 lb. = 4.45 N



**Figure 5.1 –C6-58L pull-out test results**  
Conversion: 1 lb. = 4.45 N

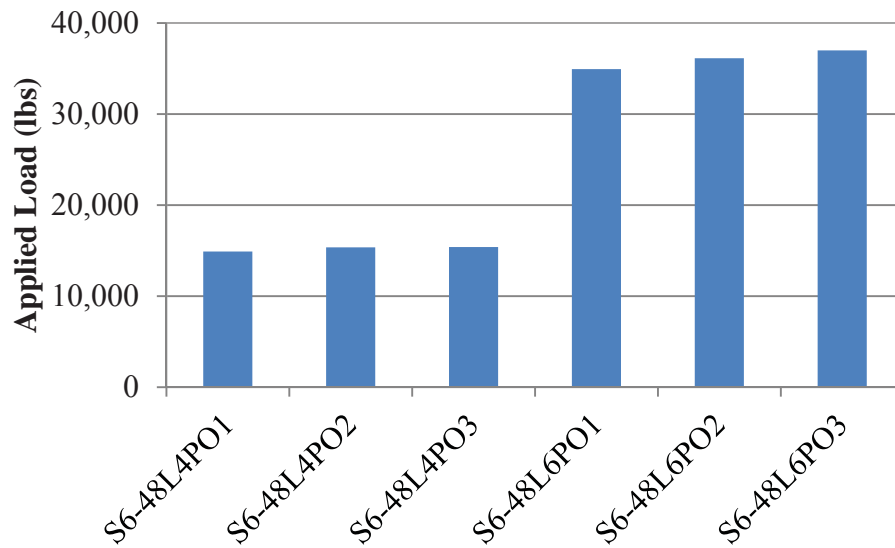


**Figure 5.2 – S6-48L pull-out test results**  
Conversion: 1 lb. = 4.45 N

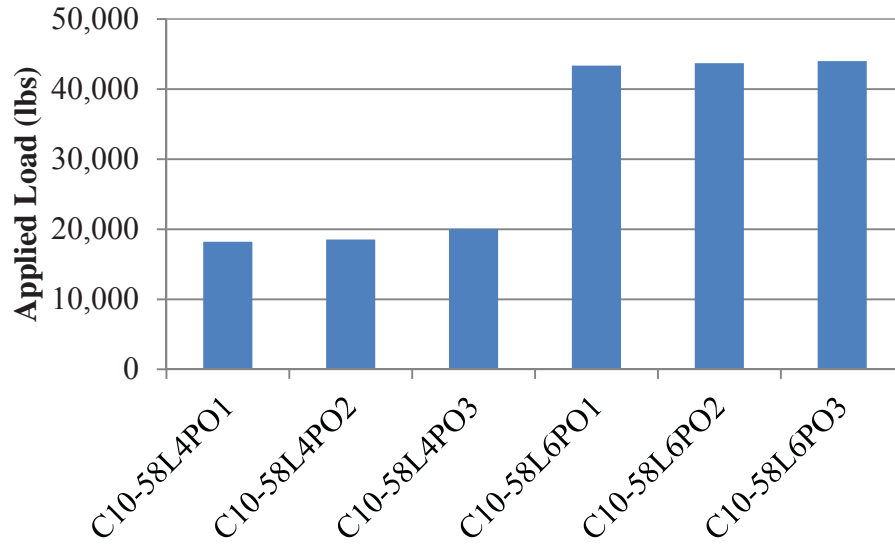


**Figure 5.3 – C10-58L pull-out test results**  
Conversion: 1 lb. = 4.45 N

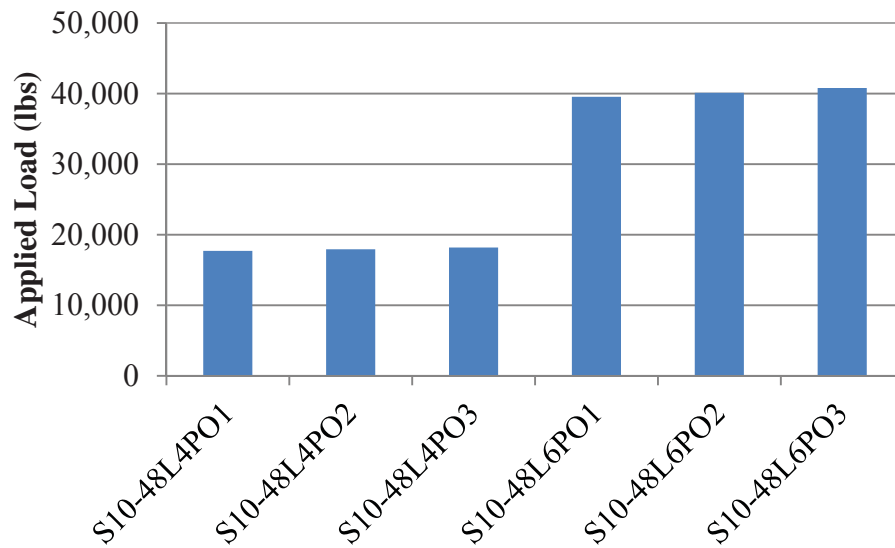


**Figure 5.4 – S10-48L pull-out test results**  
Conversion: 1 lb. = 4.45 N

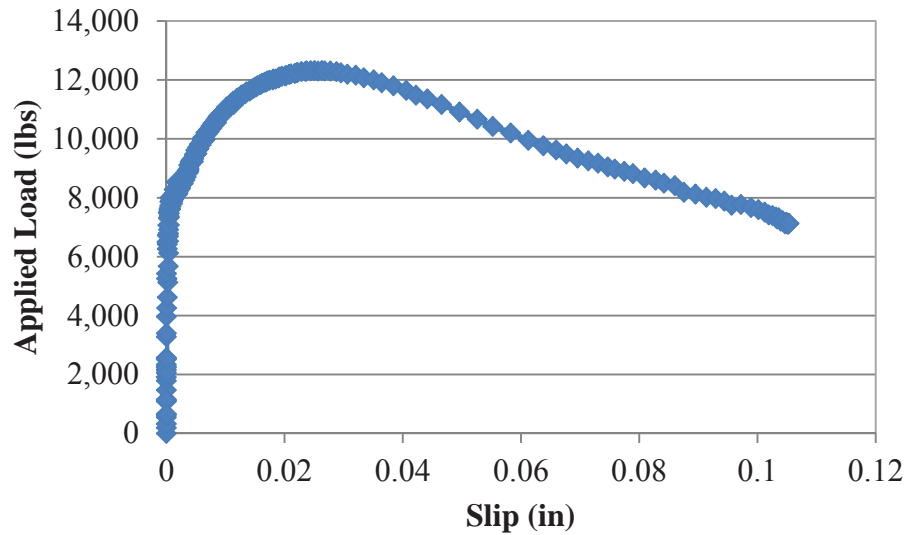


**Figure 5.5 – Example SCC applied load vs. slip plot**

Conversion: 1 lb. = 4.45 N

1 in. = 25.4 mm

## 5.2. BEAM SPLICE TEST RESULTS

The beam splice test specimens were constructed to evaluate the bond performance of SCC under more realistic loading conditions. The MoDOT standard mix design was used as a baseline for test result comparisons. A total of 12 test specimens with 3#6 (#19) longitudinal reinforcing bars spliced at midspan were constructed for the SCC test program. There were three specimens constructed for each of the four concrete mix designs to be evaluated. Of the three test specimens, two specimens were constructed with the spliced reinforcing bars located at the bottom of the beam cross section and one specimen was constructed with the splice at the top of the beam cross section to evaluate top-bar effect. The test matrix for the SCC beam splice test program is shown in **Table 5.3**. A splice length of 11.71 in. (297 mm) with three splices was used for each normal strength test specimen and 14.18 in. (360 mm) with four splices was used for each high strength test specimen. An extra splice was added to the high strength test specimens

because 70% of the calculated development length for the high strength mix design with three splices was relatively small (much less than the ACI 318-08 minimum). To obtain a higher splice length, four splices were used in the high strength mix design specimens. By decreasing the clear spacing between the bars being developed, the calculated development length was increased.

**Table 5.3 – SCC beam splice test matrix**

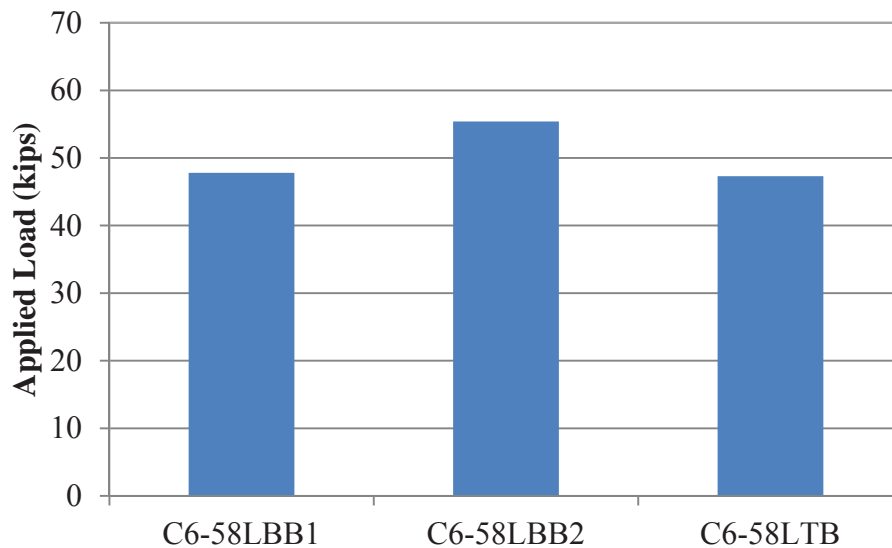
<b>Mix I.D.</b>	<b>Bar Size</b>	<b>Splice Location</b>	<b>No. of Specimens</b>
<b>C6-58L</b>	#6 (#19)	Bottom	2
		Top	1
<b>S6-48L</b>	#6 (#19)	Bottom	2
		Top	1
<b>C6-58L</b>	#6 (#19)	Bottom	2
		Top	1
<b>S6-48L</b>	#6 (#19)	Bottom	2
		Top	1

The applied load, corresponding midspan deflection, and corresponding strain at the end of each bar splice was recorded for each test. The peak load and peak stress were collected for each test specimen and are shown in **Table 5.4**. The bottom splice specimens are denoted with the abbreviation BB and the top splice specimens are denoted with the abbreviation TB. Steel stress recorded at failure of the specimen was determined by averaging the strain readings from each strain gage in a member and finding the peak strain that occurred during loading. This peak strain was then multiplied by the modulus of elasticity of the steel determined from the tension test to determine peak stress. The peak loads for the C6-58L, S6-48L, C10-58L, and S10-48L specimens are plotted in **Figures 5.6, 5.7, 5.8, and 5.9**, respectively.

**Table 5.4 – Peak load and reinforcing bar stress**

Mix	Specimen	Steel Stress Recorded at Failure (ksi)	Peak Load (kips)
<b>C6-58L</b>	<b>BB1</b>	49.5	47.8
	<b>BB2</b>	50.8	55.4
	<b>TB</b>	54.7	47.3
<b>S6-48L</b>	<b>BB1</b>	63.2	60.8
	<b>BB2</b>	59.7	58.2
	<b>TB</b>	50.6	53.4
<b>C10-58L</b>	<b>BB1</b>	62.0	85.4
	<b>BB2</b>	57.9	76.1
	<b>TB</b>	73.8	87.7
<b>S10-48L</b>	<b>BB1</b>	54.9	78.3
	<b>BB2</b>	65.5	83.3
	<b>TB</b>	79.2	96.9

Conversion: 1 ksi = 6.9 MPa

**Figure 5.6 – C6-58L peak load data plot**

Conversion: 1 kip = 4.45 kN

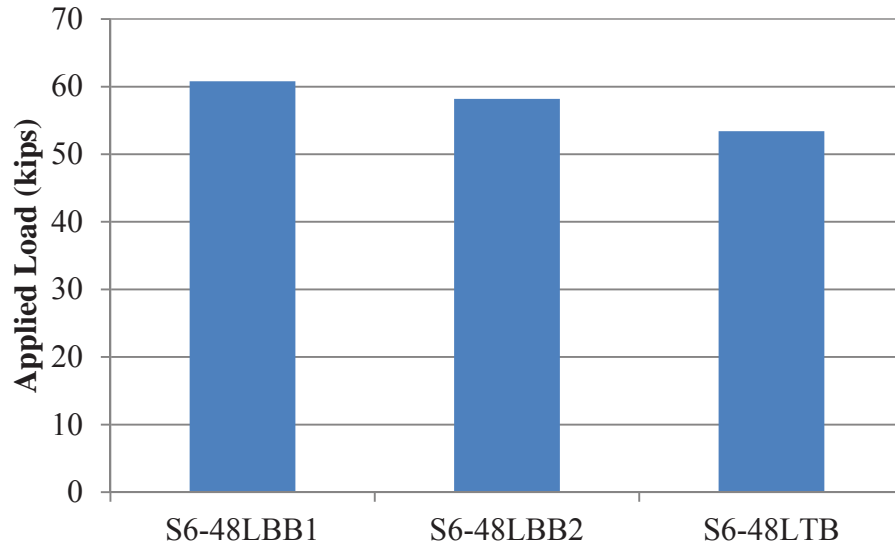


**Figure 5.7 – S6-48L peak load data plot**  
Conversion: 1 kip = 4.45 kN

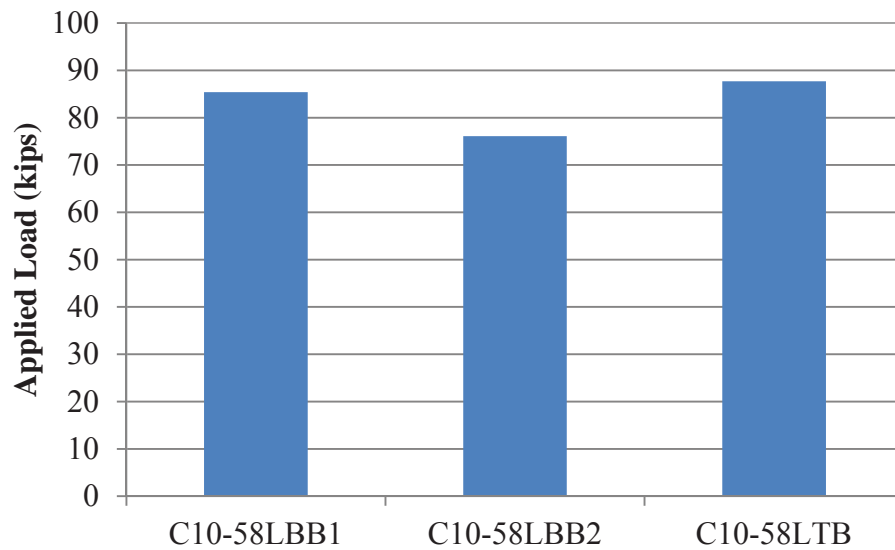


**Figure 5.8 – C10-58L peak load data plot**  
Conversion: 1 kip = 4.45 kN

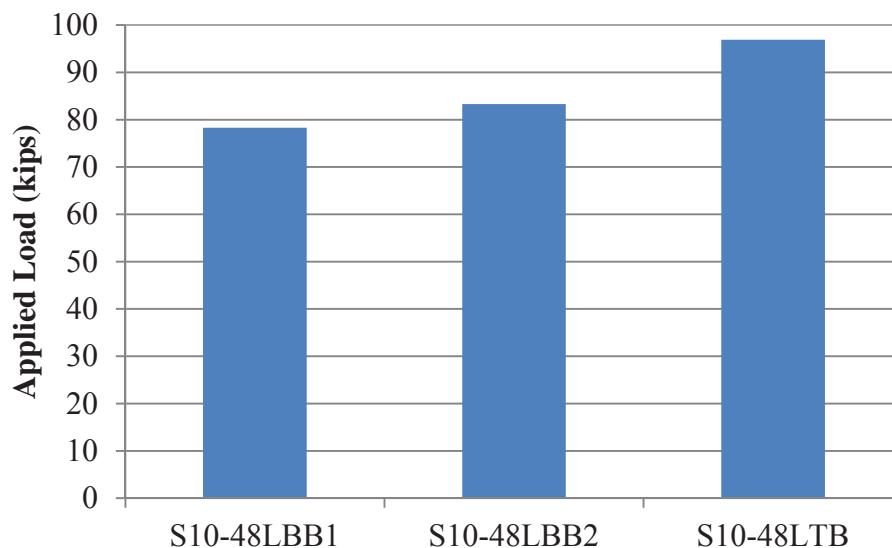


**Figure 5.9 – S10-48L peak load data plot**

Conversion: 1 kip = 4.45 kN

The deflection and strain data were also plotted with the load data to observe the response of the specimens during testing. A typical load vs. displacement at midspan plot is shown in **Figure 5.10**. A typical load vs. strain plot is shown in **Figure 5.11**. The plots shown are from the S10-48LBB1 specimen. Both plots show that the beam began to develop flexural crack at a load of approximately 20 kips (89 kN). At the failure load, all specimens exhibited visible and audible signs of complete bond failure, having never yielded the reinforcing bars. Evidence of this is shown in the linear behavior indicated in both the load vs. deflection plot and the load vs. strain plot. Appendix E contains the load vs. slip plots for all 12 beam splice specimens.

The cracking patterns in the beam splice specimens also revealed a bond failure. For example, **Figures 5.12** and **5.13** display the failed beam specimen designated C6-58LBB1. Both figures display longitudinal cracking along the bars within the splice zone, which is indicative of a bond-splitting failure. **Figure 5.14** displays a splice revealed due

to spalling of the concrete along the entire splice region. Appendix D contains photographs of the 12 beam splice specimens after failure.

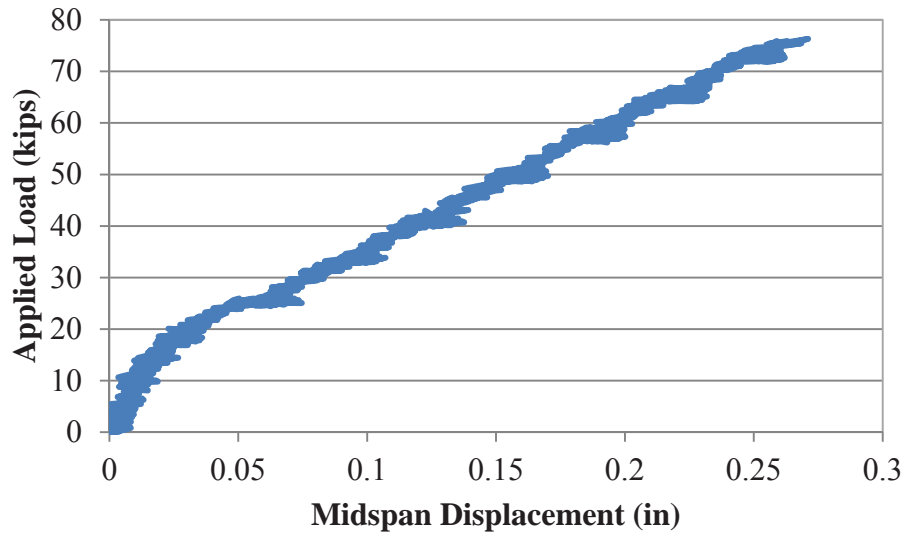


**Figure 5.10 – Typical load vs. displacement plot**

Conversion: 1 in. = 25.4 mm

1 kip = 4.45 kN

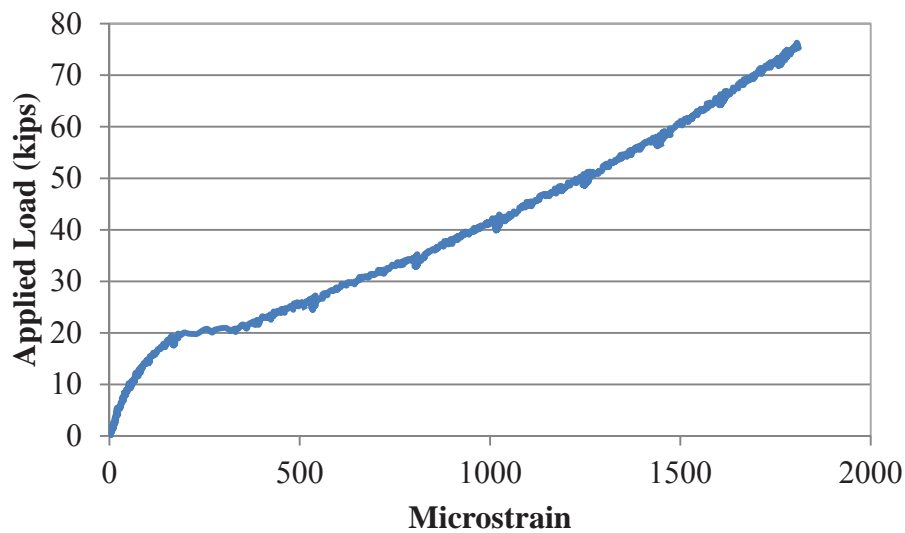


**Figure 5.11 – Typical load vs. strain plot**

Conversion: 1 kip = 4.45 kN



**Figure 5.12 – Failed splice region of C6-58LBB1**



**Figure 5.13 – Bottom of splice region of C6-58LBB1**



**Figure 5.14 – Bottom of splice region of C10-58LTB with splice revealed**

### **5.3. REINFORCING BAR TENSION TEST**

A tension test was performed on the #6 (#19) longitudinal reinforcing bars used in each beam specimen following ASTM E8-09, “Standard Test Methods for Tension Testing of Metallic Materials” (ASTM E9-09). Three 30 in. (762 mm) lengths of reinforcing bar were clamped at each end in a 200,000 pound (890 kN) Tinius Olson testing machine and load was applied until the bar fractured. The strain and applied load were recorded during testing. The strain with a 0.5% offset was recorded and used to determine the yield strength of each bar. The modulus of elasticity was also determined for each bar. The average yield stress of the test was used as a comparison tool to check that the reinforcing bars within the splice region in each beam specimen did not reach yield. **Table 5.5** displays the results of the tension test performed.

**Table 5.5 – #6 (#19) reinforcing bar tension test results**

Specimen	Yield Stress (ksi)	Average Yield Stress (ksi)	Initial Tangent Modulus (ksi)	Average Modulus (ksi)
1	81.1	81.1	33,130	30,310
2	81.3		26,510	
3	81		31,295	

Conversion: 1 ksi = 6.9 MPa

## 5.4. ANALYSIS OF RESULTS

**5.4.1. Methodology.** Direct comparison between test results is not possible due to the fact that the test day concrete strength varies for each mix. Therefore, normalization of the value of interest was completed to facilitate direct comparison of test results. Two separate normalization formulas were used in this study. The first normalization formula is based on the development length equations in ACI 318-08 (ACI 318-08, 2008) and AASHTO LRFD-07 (AASHTO, 2007), shown as **Eqs. 5.1** and **5.2**, respectively. Both equations express the development length of a reinforcing bar in tension as a function of the inverse square root of the compressive strength. Therefore, the first normalization of the test results was based on multiplying values by the square root of the ratio of the specified design strength and the test day compressive strength, shown in **Eq. 5.3**.

$$l_d = \left( \frac{3}{40} \frac{f_y}{\lambda \sqrt{f'_c}} \frac{\psi_t \psi_e \psi_s}{\left( \frac{c_b + K_{tr}}{d_b} \right)} \right) d_b \quad (5.1)$$

Where  $l_d$  is the development length,  $f_y$  is the specified yield strength of reinforcement,  $\lambda$  is the lightweight concrete modification factor,  $f'_c$  is the specified compressive strength

of concrete,  $\Psi_t$  is the reinforcement location modification factor,  $\Psi_e$  is the reinforcement coating modification factor,  $\Psi_s$  is the reinforcement size modification factor,  $c_b$  is the smaller of the distance from center of a bar to nearest concrete surface or one-half the center-to-center spacing of bars being developed,  $K_{tr}$  is the transverse reinforcement index, and  $d_b$  is the nominal diameter of reinforcing bar.

$$l_{db} = \frac{1.25 A_b f_y}{\sqrt{f'_c}} \geq 0.4 d_b f_y \quad (5.2)$$

Where  $l_{db}$  is the tension development length,  $f_y$  is the specified yield strength of reinforcement,  $A_b$  is the area of reinforcing bar,  $f'_c$  is the specified compressive strength of concrete, and  $d_b$  is the reinforcing bar diameter.

$$\text{Normalized Load} = \text{Failure load} \sqrt{\frac{\text{Design strength}}{\text{Strength at testing}}} \quad (5.3)$$

The second normalization formula is based on the development length equation in ACI 408R-03 (2003), as shown in **Eq. 5.4**. The development length of a reinforcing bar in tension in this equation is a function of the inverse fourth root of the compressive strength. Therefore, the normalization of the test results was based on the fourth root of the ratio of the specified design strength and the test day compressive strength, as shown in **Eq. 5.5**.

$$l_d = \left( \frac{\left( \frac{f_y}{f'_c} \right)^{1/4} - 1970 \omega}{62 \left( \frac{c \omega + K_{tr}}{d_b} \right)} \alpha \beta \lambda \right) d_b \quad (5.4)$$

Where  $l_d$  is the development length,  $f_y$  is the specified yield strength of reinforcement,  $\lambda$  is the lightweight concrete modification factor,  $f'_c$  is the specified compressive strength of concrete,  $\alpha$  is the reinforcement location modification factor,  $\beta$  is the reinforcement coating modification factor,  $\omega$  is equal to  $0.1 (c_{\max}/c_{\min}) + 0.9 \leq 1.25$ ,  $c$  is the spacing or cover dimension,  $d_b$  is the nominal diameter of reinforcing bar, and  $K_{tr}$  is the transverse reinforcement index.

$$\text{Normalized Load} = \text{Failure load} \left( \frac{\text{Design strength}}{\text{Strength at testing}} \right)^{1/4} \quad (5.5)$$

The design strength for the normal and high strength mix design were 6,000 psi (41.4 MPa) and 10,000 psi (69 MPa), respectively. The strengths at testing for each mix design can be seen in **Table 5.6**.

**Table 5.6 - Test day compressive strengths for test specimens**

	Test Day Strength (psi)				
	Cylinder 1	Cylinder 2	Cylinder 3	Average	COV (%)
<b>C6-58L</b>	5794	5557	5806	5719	2.5
<b>S6-48L</b>	6805	6703	7015	6841	2.3
<b>C10-58L</b>	9403	9832	9639	9625	2.2
<b>S10-48L</b>	9589	9951	9720	9753	1.9

Note: 1 psi = 6.9 kPa

#### 5.4.2. Analysis and Interpretation – Direct Pull-out Test Results. Table 5.7

contains the peak load, concrete strength at time of testing, and normalized peak load for each normal strength test specimen. **Table 5.8** contains the same results for the high strength specimens. **Figure 5.15** is a plot of the average square root normalized peak load for each normal strength mix design and bar size. **Figure 5.16** displays the plot of the average square root normalized peak load for each high strength mix design and bar size. The error bars indicate the range of test data collected. The SCC specimens exhibited similar bond strength relative to the control mix design for both bar sizes. The average of the #4 (#13) S6-48L specimens failed at a load 1,870 lb. (8.3 kN) higher than the control, and the average of the #6 (#19) S6-48L specimens failed at a load 3,416 lb. (15.2 kN) higher than the control, which represents differences of 15.2 and 11.3%, respectively. The average of the #4 (#13) S10-48L specimens failed at a load 1,176 lb. (5.2 kN) lower than the control, and the average of the #6 (#19) S10-48L specimens failed at a load 3,994 lb. (17.8 kN) lower than the control, which represents differences of 6.1 and 9.0%, respectively. However, paired t-tests indicate that there is no statistically significant difference between the results for each mix design, indicating that the SCC has essentially the same bond strength as conventional concrete.

Table 5.7 – SCC normal strength normalized pull-out test results

Mix	Bar Size	Specimen	Peak Load (lb.)	Concrete Compressive Strength (psi)	Normalized Load (lb.)				COV (%)				
					Square Root Adjustment	Fourth Root Adjustment	Average of Square Root Adjustment	Average of Fourth Root Adjustment					
C6-58L	#4 (#13)	4PO1	12,320	5,814	12,516	12,417	12,301	12,204	3.6				
		4PO2	12,394		12,591	12,492							
		4PO3	11,612		11,796	11,704							
	#6 (#19)	6PO1	29,997		30,473	30,234	30,136	29,900		1.1			
		6PO2	29,659		30,130	29,893							
		6PO3	29,340		29,806	29,572							
	S6-48L	#4 (#13)	4PO1		15,395	6,916	14,339	14,858			14,171	14,683	1.8
			4PO2		14,893		13,872	14,373					
			4PO3		15,354		14,301	14,818					
#6 (#19)		6PO1	36,129	33,651	34,868		33,552	34,765	2.9				
		6PO2	34,941	32,545	33,722								
		6PO3	36,996	34,459	35,705								

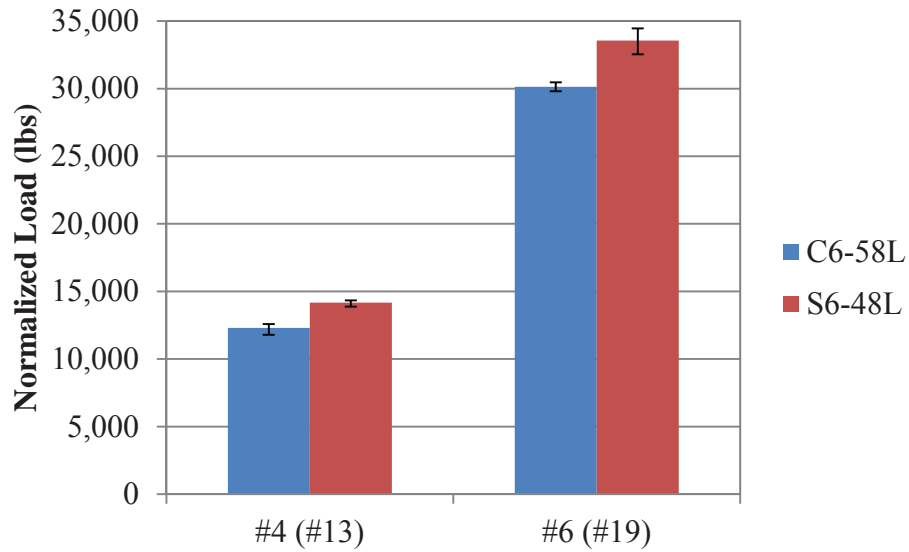
Conversion: 1 lb. = 4.45 N  
1 psi = 6.9 kPa

Table 5.8 – SCC high strength normalized pull-out test results

Mix	Bar Size	Specimen	Peak Load (lb.)	Concrete Compressive Strength (psi)	Normalized Load (lb.)				COV (%)	
					Square Root Adjustment	Fourth Root Adjustment	Average of Square Root Adjustment	Average of Fourth Root Adjustment		
<b>C10-58L</b>	<b>#4 (#13)</b>	<b>4PO1</b>	18,527	9,625	18,884	18,705	19,292	19,108	5.2	
		<b>4PO2</b>	18,210		18,561	18,385				
		<b>4PO3</b>	20,042		20,429	20,234				
	<b>#6 (#19)</b>	<b>6PO1</b>	43,347		44,183	43,763	44,524	44,101		0.8
		<b>6PO2</b>	43,997		44,846	44,419				
		<b>6PO3</b>	43,701		44,544	44,121				
<b>S10-48L</b>	<b>#4 (#13)</b>	<b>4PO1</b>	17,713	9,815	17,879	17,796	18,116	18,032	1.3	
		<b>4PO2</b>	17,939		18,107	18,023				
		<b>4PO3</b>	18,191		18,362	18,276				
	<b>#6 (#19)</b>	<b>6PO1</b>	40,805		41,188	40,996	40,530	40,342		1.6
		<b>6PO2</b>	40,114		40,490	40,302				
		<b>6PO3</b>	39,542		39,913	39,727				

Conversion: 1 lb. = 4.45 N

1 psi = 6.9 kPa



**Figure 5.15 – Plot of peak load for each normal strength mix design**  
Conversion: 1 lb. = 4.45 N

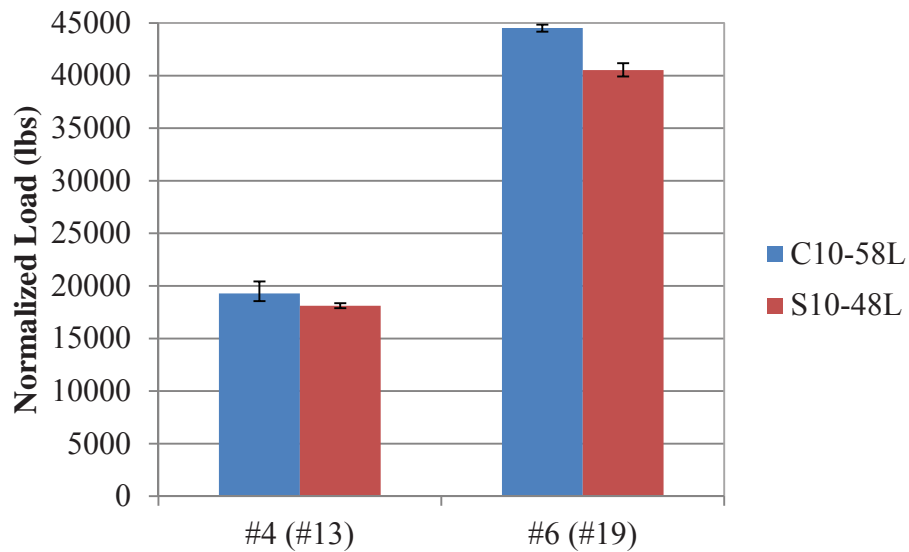


**Figure 5.16 – Plot of peak load for each high strength mix design**  
Conversion:  
1 lb. = 4.45 N

Figures 5.17 and 5.18 display a typical plot of the normalized load vs. slip of the #4 (#13) and #6 (#19) pull-out specimens for the normal strength mix designs,

respectively. **Figures 5.19** and **5.20** displays a typical normalized load vs. slip of the #4 (#13) and #6 (#19) pull-out specimens for the high strength mix designs, respectively. The plots indicate that bar slip occurred around the same load for each normal strength test specimen and #4 (#13) high strength specimens. However, bar slip in the #6 (#19) high strength SCC test specimens occurred at a lower load than that of the control specimens. More importantly, the overall behavior was very similar between all four mix designs. This behavior, combined with a forensic investigation of the failed specimens, indicates that the concrete surrounding the bar crushed around the same load for all the normal strength specimens and the #4 (#13) high strength specimens, but at a lower load for the #6 (#19) high strength SCC specimens than that of the control specimens.

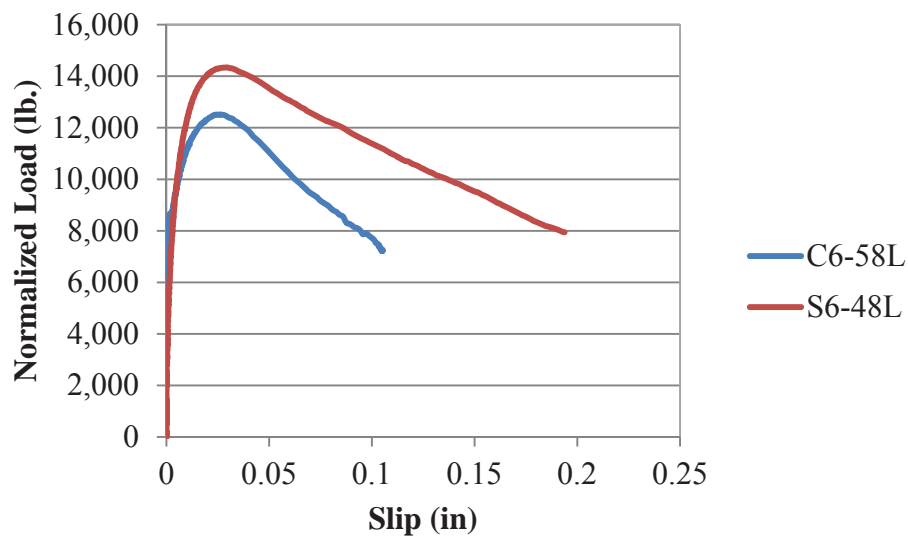


**Figure 5.17 – Normal strength normalized load vs. slip plot for #4 (#13) bars**

Conversion: 1 in. = 25.4 mm

1 lb. = 4.45 N

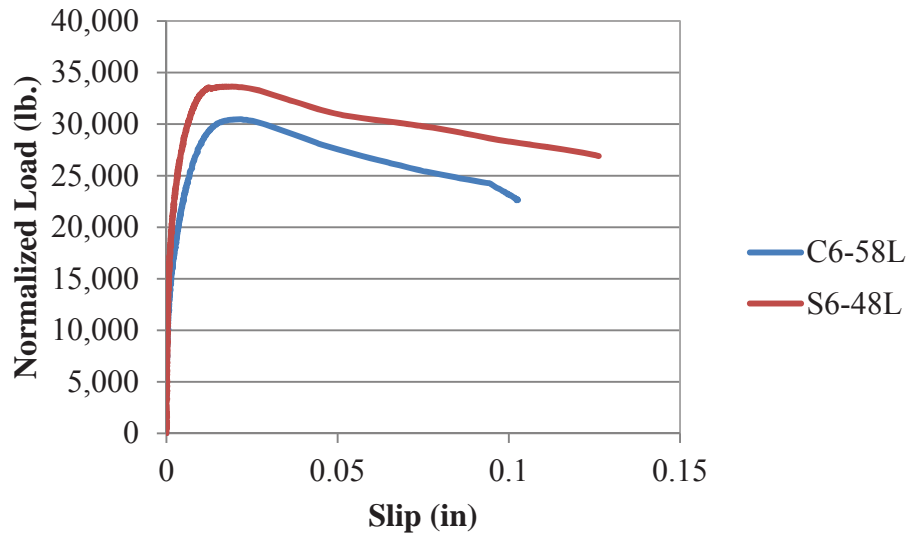


**Figure 5.18 – Normal strength normalized load vs. slip plot for #6 (#19) bars**  
 Conversion: 1 in. = 25.4 mm  
 1 lb. = 4.45 N

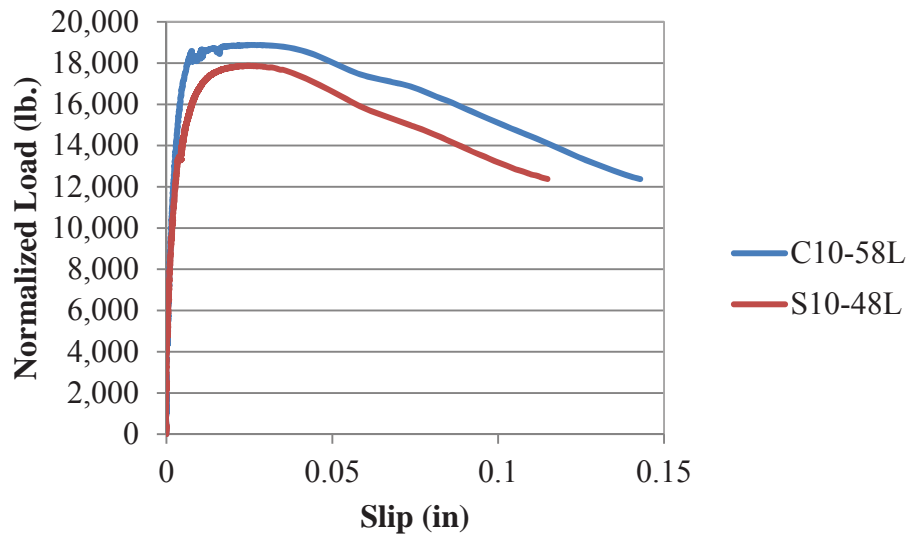


**Figure 5.19 – High strength normalized load vs. slip plot for #4 (#13) bars**  
 Conversion: 1 in. = 25.4 mm  
 1 lb. = 4.45 N

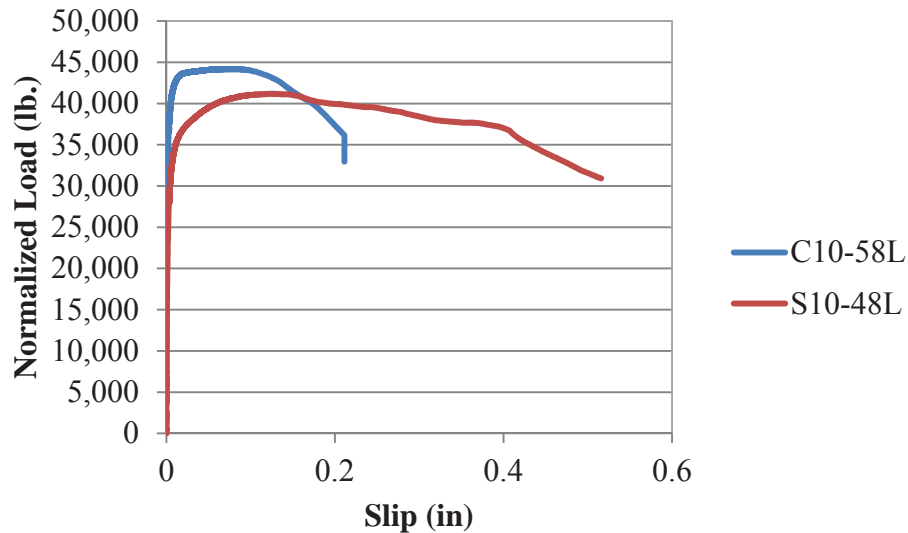


**Figure 5.20 – High strength normalized load vs. slip plot for #6 (#19) bars**  
 Conversion: 1 in. = 25.4 mm  
 1 lb. = 4.45 N

#### 5.4.3. Analysis and Interpretation – Beam Splice Test Results. Table 5.9

contains the peak load, concrete strength at time of testing, and normalized peak load of each specimen tested. The square root normalized peak loads are plotted in **Figures 5.21** and **5.22** for the normal strength and high strength mix designs, respectively. **Table 5.10** contains the measured steel stress at failure, concrete strength at time of testing, and normalized measured steel stress at failure. The square root normalized steel stresses are shown plotted in **Figures 5.23** and **5.24** for the normal strength and high strength mix designs, respectively. The error bars indicate the range of test data collected. The normalized steel stresses were compared to the theoretical stress calculated using the moment-curvature program Response-2000 (Bentz, 2000) and are shown in **Table 5.11**. The moment at midspan of the specimen used when calculating the theoretical stress was a combination of both applied load moment and dead load moment. The applied load moment includes the weight of the spreader beams used to distribute the load from the

actuators. The design concrete strengths of 6,000 psi (41.4 MPa) and 10,000 psi (69 MPa) were used when calculating the theoretical steel stress for the normal and high strength mix designs, respectively.

The average longitudinal bar stress for the S6-48L bottom splice specimens was 6.3 ksi (43.4 MPa) higher than that of the control bottom splice specimens, which represents a difference of 12.4%. The average peak stress for the S10-48L bottom splice specimens was 0.3 ksi (2.1 MPa) higher than that of the control bottom splice specimens, which represents a difference of 0.5%. The peak stress for the S6-48L mix design top splice specimen mix design was 4.4 ksi (30.3 MPa) lower than that of the control specimen, which represents a difference of 7.9%. The peak stress for the S10-48L top splice specimen was 4.7 ksi (32.4 MPa) higher than that of the control specimen, which represents a difference of 6.2%. This data indicates that with the bottom splice specimens, the SCC mix designs performed at the same level as the control mix design. The opposite trend was seen for the normal strength top bar splice specimen. This could be attributed to an issue with segregation in SCC mix designs, as well as the existence of excess bleed water. The coarse aggregate was not evenly distributed along the depth of the member. The loss of coarse aggregate at the top of the member caused the S6-48LTB specimen to fail at a lower stress. The peak stress for the S10-48LTB specimen was higher than that of the control specimen. This indicates segregation was not as much of an issue with the high strength SCC mix design. However, the differences were not statistically significant to justify any definitive conclusions of the top-bar effect for SCC.

Table 5.9 – Normalized peak loads for each specimen

Mix	Specimen	Max Applied Load (kips)	Concrete Compressive Strength (psi)	Normalized Load (kips)		
				Square Root Adjustment	Fourth Root Adjustment	Average of Square Root Adjustment
C6-58L	BB1	47.8	5814	48.6	48.2	52.4
	BB2	55.4		56.3	55.8	
	TB	47.3		48.1	47.7	
S6-48L	BB1	60.8	6916	56.6	58.7	55.4
	BB2	58.2		54.2	56.2	
	TB	53.4		49.7	51.5	
C10-58L	BB1	85.4	9625	87.0	86.2	82.3
	BB2	76.1		77.6	76.8	
	TB	87.7		89.4	88.5	
S10-48L	BB1	78.3	9815	79.0	78.7	81.6
	BB2	83.3		84.1	83.7	
	TB	96.9		97.8	97.4	

Conversion: 1 ksi = 6.9 MPa

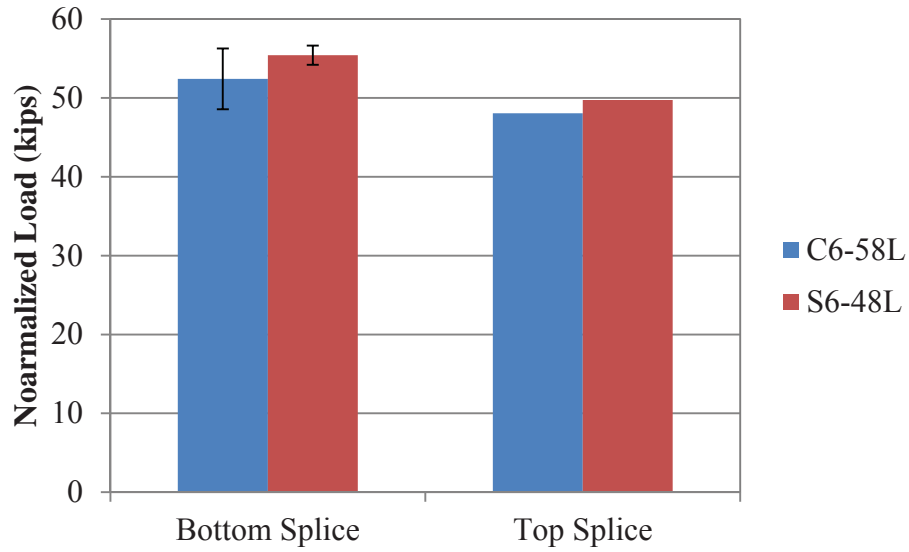


**Figure 5.21 – Normalized peak load plot for the normal strength mix design**  
Conversion: 1 kip = 4.45 kN

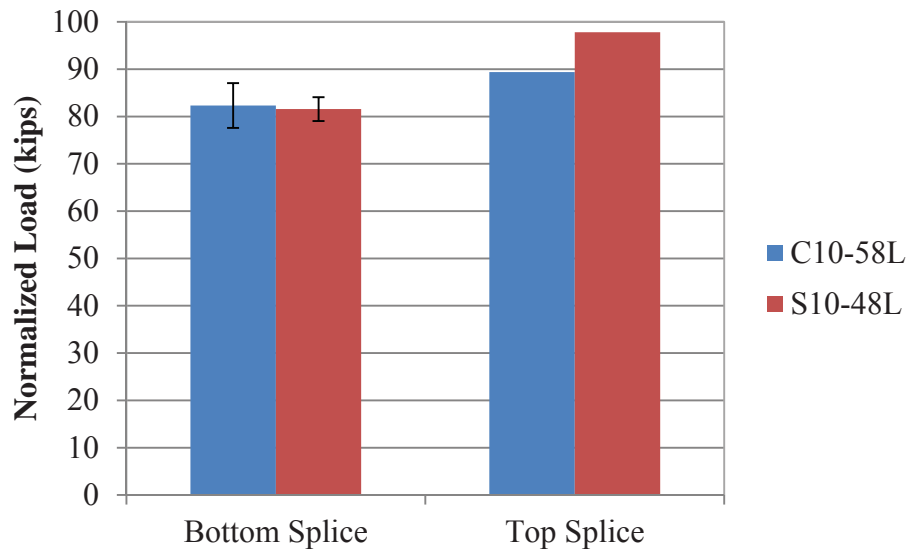


**Figure 5.22 – Normalized peak load plot for the high strength mix design**  
Conversion: 1 kip = 4.45 kN

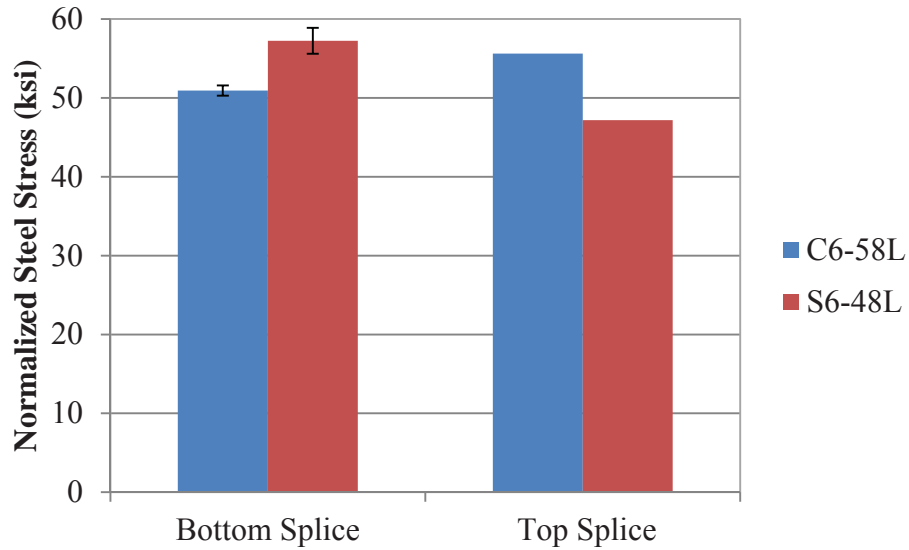
Table 5.10 – Normalized steel stress at failure for each specimen

Mix	Specimen	Steel Stress Recorded at Failure (ksi)	Concrete Compressive Strength (psi)	Normalized Steel Stress (ksi)	
				Square Root Adjustment	Fourth Root Adjustment
C6-58L	BB1	49.5	5814	50.3	49.9
	BB2	50.8		51.6	51.2
	TB	54.7		55.6	55.2
S6-48L	BB1	63.2	6916	58.9	61.0
	BB2	59.7		55.6	57.6
	TB	50.6		47.2	48.9
C10-58L	BB1	62.0	9625	63.2	62.6
	BB2	57.9		59.0	58.5
	TB	73.8		75.3	74.5
S10-48L	BB1	54.9	9815	55.4	55.2
	BB2	65.5		66.1	65.8
	TB	79.2		80.0	79.6

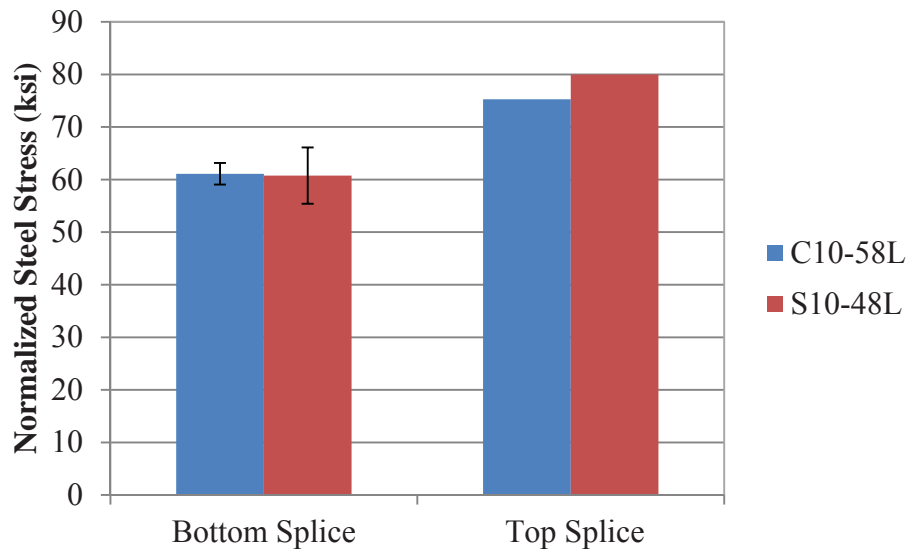
Conversion: 1 kip = 4.45 kN

Table 5.11 – Normalized steel stress compared to theoretical steel stress at failure

Mix	Specimen	Normalized Steel Stress (ksi)		Calculated Stress at Failure Load (ksi)	Measured/Calculated Stress	
		Square Root Adjustment	Fourth Root Adjustment		Square Root Adjustment	Fourth Root Adjustment
C6-58L	BB1	50.3	49.9	45.5	0.90	1.10
	BB2	51.6	51.2	52.5	1.02	0.97
	TB	55.6	55.2	45.0	0.81	1.23
S6-48L	BB1	58.9	61.0	57.5	0.98	1.06
	BB2	55.6	57.6	55.1	0.99	1.05
	TB	47.2	48.9	50.6	1.07	0.97
C10-58L	BB1	63.2	62.6	79.5	1.26	0.79
	BB2	59.0	58.5	71.0	1.20	0.82
	TB	75.3	74.5	81.6	1.08	0.91
S10-48L	BB1	55.4	55.2	73.0	1.32	0.76
	BB2	66.1	65.8	77.6	1.17	0.85
	TB	80.0	79.6	90.0	1.13	0.88



**Figure 5.23 – Normalized steel stress at failure load for normal strength mix designs**  
Conversion: 1 ksi = 6.9 MPa



**Figure 5.24 – Normalized steel stress at failure load for normal strength mix designs**  
Conversion: 1 ksi = 6.9 MPa

Normalized load vs. strain of the longitudinal reinforcing bar was also plotted for comparison. A typical plot of the average bottom splice strain for a specimen of each mix

design is shown in **Figures 5.25** and **5.26**. As seen in the plots, all four specimens have two distinct linear sections. The first represents pre-flexural cracking behavior and the second represents post-flexural cracking behavior. Both plots show that, regardless of strength, the SCC mix designs cracked at a higher load than the control mix designs. Most importantly, all load-strain plots indicated linear behavior up to failure. In other words, the reinforcing bars failed in bond, having never reached yield.

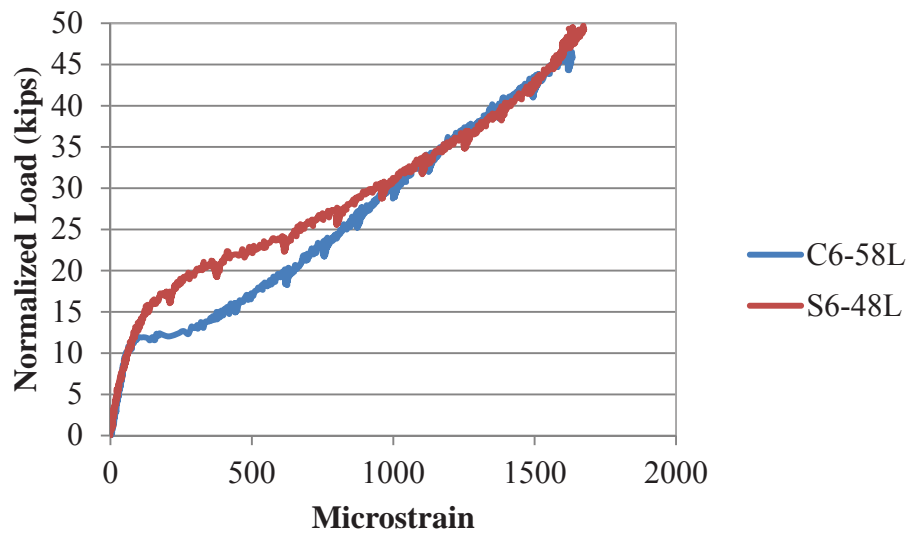


**Figure 5.25 – Typical normalized load vs. strain plot for the normal strength specimens**

Conversion: 1 kip = 4.45 kN

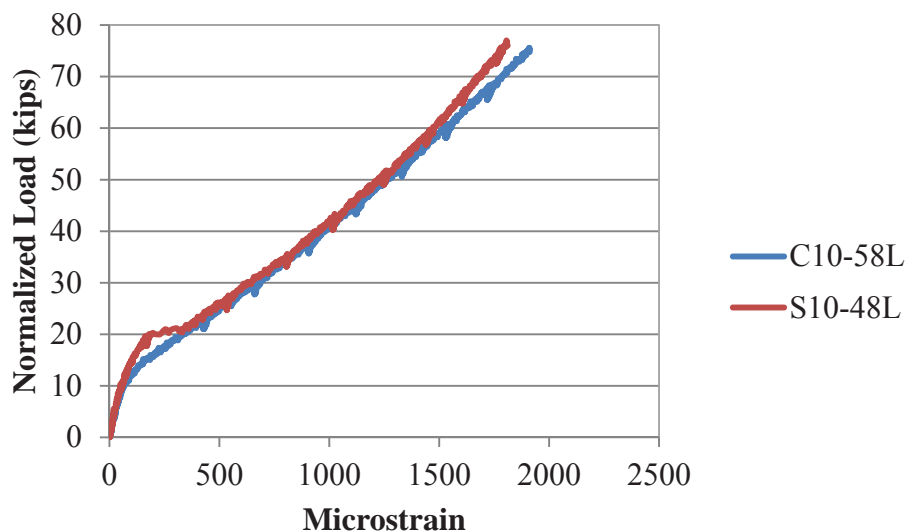


**Figure 5.26 – Typical normalized load vs. strain plot for the high strength specimens**  
Conversion: 1 kip = 4.45 kN

## 5.5. FINDINGS AND CONCLUSIONS

Based on analysis of the test results, the following conclusions are presented:

1. The average peak load for the #4 (#13), S6-48L and S10-48L pull-out specimens was 15.2% higher and 6.1% lower than that of the control, respectively. The average peak load for the #6 (#19), S6-48L and S10-48L pull-out specimens was 11.3% higher and 9.0% lower than that of the control, respectively. This data indicates that the normal strength SCC mix design has higher bond strength and the high strength SCC has lower bond strength than their respective control mix designs with both bar sizes. Statistical analysis indicates that only the #6 (#19) reinforcing bar, high strength SCC mix design specimens did not perform equally with the control.
2. The average peak bar stress for the S6-48L and S10-48L bottom splice beam specimens was 12.4% higher and 0.5% lower than that of the control

specimens, respectively. The peak bar stress for the S6-48L and S10-48L top splice beam specimens was 7.4% lower and 6.2% higher than that of the control specimens, respectively. This data indicates that both SCC mix designs exhibited improved bond performance under realistic stress states relative to their respective control mix designs when the splice was cast at the bottom of the specimen. Only the high strength SCC mix design exhibited improved bond performance when the splice was cast at the top of the specimen. However, statistical analysis indicates that all four mix designs performed comparably.

## 6. FINDINGS, CONCLUSIONS, AND RECOMMENDATIONS

The main objective of this study was to determine the effect on bond performance of self-consolidating concrete (SCC). The SCC test program consisted of comparing the bond performance of normal and high strength SCC with their respective MoDOT standard mix designs.

Two test methods were used for bond strength comparisons. The first was a direct pull-out test based on the RILEM 7-II-128 “RC6: Bond test for reinforcing steel. 1. Pull-out test” (RILEM, 1994). Although not directly related to the behavior of a reinforced concrete beam in flexure, the test does provide a realistic comparison of bond between types of concrete. The second test method consisted of a full-scale beam splice test specimen subjected to a four-point loading until failure of the splice. This test method is a non-ASTM test procedure that is generally accepted as the most realistic test method for both development and splice length.

This section contains the findings of the test program, as well as conclusions based on these findings and recommendations for future research.

### 6.1. FINDINGS

**6.1.1. Direct Pull-out Testing.** A total of 24 direct pull-out test specimens were constructed for the SCC test program. There were six test specimens constructed for each of the four mix designs, which consisted of two SCC mixes and two control mixes. Of the six specimens constructed for each mix design, three specimens contained a #4 (#13) reinforcing bar and three specimens contained a #6 (#19) reinforcing bar. Each specimen

was tested to failure. The average peak load for the #4 (#13), S6-48L and S10-48L pull-out specimens was 15.2% higher and 6.1% lower than that of the control, respectively. The average peak load for the #6 (#19), S6-48L and S10-48L pull-out specimens was 11.3% higher and 9.0% lower than that of the control, respectively.

**6.1.2. Beam Splice Testing.** A total of 12 test specimens were constructed with 3#6 (#19) longitudinal reinforcing bars spliced at midspan for the SCC test program. There were three specimens constructed for each of the four concrete mix designs to be evaluated. Of the three test specimens, two specimens were constructed with the spliced reinforcing bars located at the bottom of the beam cross section and one specimen was constructed with the splice at the top of the beam cross section to evaluate top-bar effect. Each specimen was tested to bond failure. The average peak bar stress for the S6-48L and S10-48L bottom splice beam specimens was 12.4% and 0.5% higher than that of the control specimens, respectively. The peak bar stress for the S6-48L and S10-48L top splice beam specimens was 7.4% lower and 6.2% higher than that of the control specimens, respectively.

## **6.2. CONCLUSIONS**

**6.2.1. Direct Pull-out Testing.** Analysis of the test data indicates that the normal strength SCC mix design has higher bond strength and the high strength SCC mix design has lower bond strength than their respective control mix designs for both bar sizes. Statistical analysis indicates that only the #6 (#19) reinforcing bar, high strength SCC mix design specimens did not perform comparably with the control.

**6.2.2. Beam Splice Testing.** Analysis of the test data indicates that both SCC mix designs exhibited improved bond performance under realistic stress states relative to their respective control mix designs when the splice was cast at the bottom of the specimen. Only the high strength SCC mix design exhibited improved bond performance when the splice was cast at the top of the specimen. However, statistical analysis indicates that all four mix designs performed comparably. These findings, along with the findings from the direct pull-out tests, indicate that using SCC is feasible in terms of bond and development of reinforcing steel.

### **6.3. RECOMMENDATIONS**

There have been numerous studies conducted to determine the bond performance of SCC. However, additional studies are needed to establish a database of results that can eventually be used for comparison as well as for future ACI design code changes. Also important for design would be to explore whether or not certain ACI code distinctions, such as confinement, bar size, or bar coating factors, used for conventional concrete designs also apply to SCC, or if they need to be developed specifically for SCC. Below is a list of recommendations for testable variables related to SCC concrete bond behavior:

- Perform tests with a larger variation in bar sizes based on ACI 318 code distinctions for bar size effect on development length,
- Conduct tests determining the effect of different admixtures on the bond performance of SCC,
- Conduct tests determining the effect of various aggregate percentages and types on the bond performance of SCC,

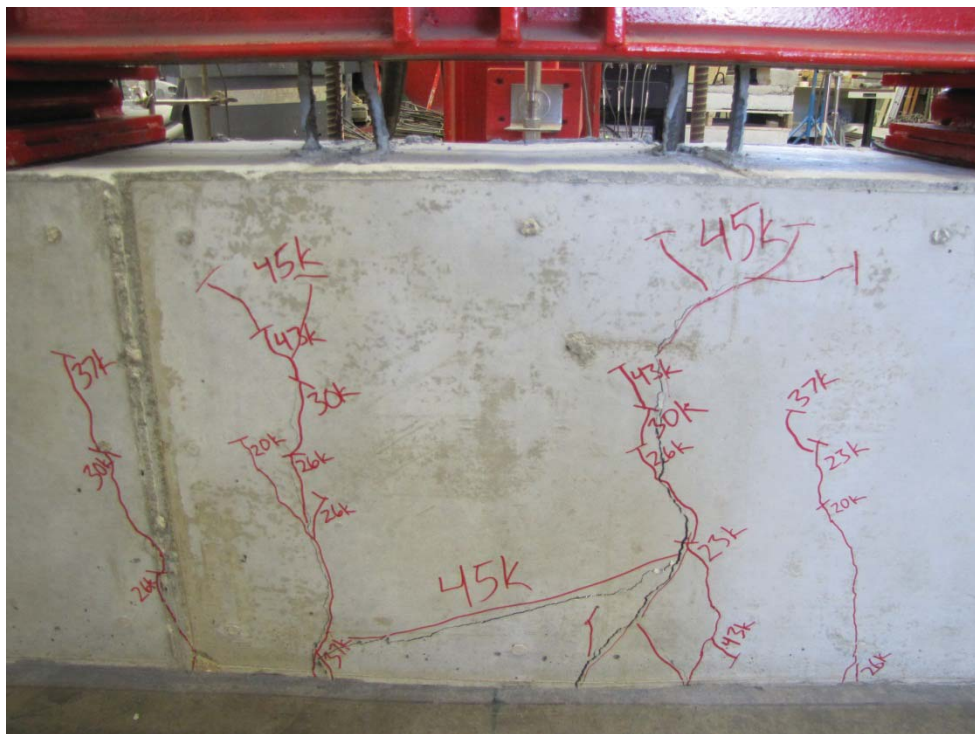
- Perform tests with aggregates from different sources, and
- Perform bond tests on more specimen types mentioned in ACI 408.

**APPENDIX A**

**SCC TEST PROGRAM BEAM SPLICE FAILURE PHOTOGRAPHS**



(a) Bottom View

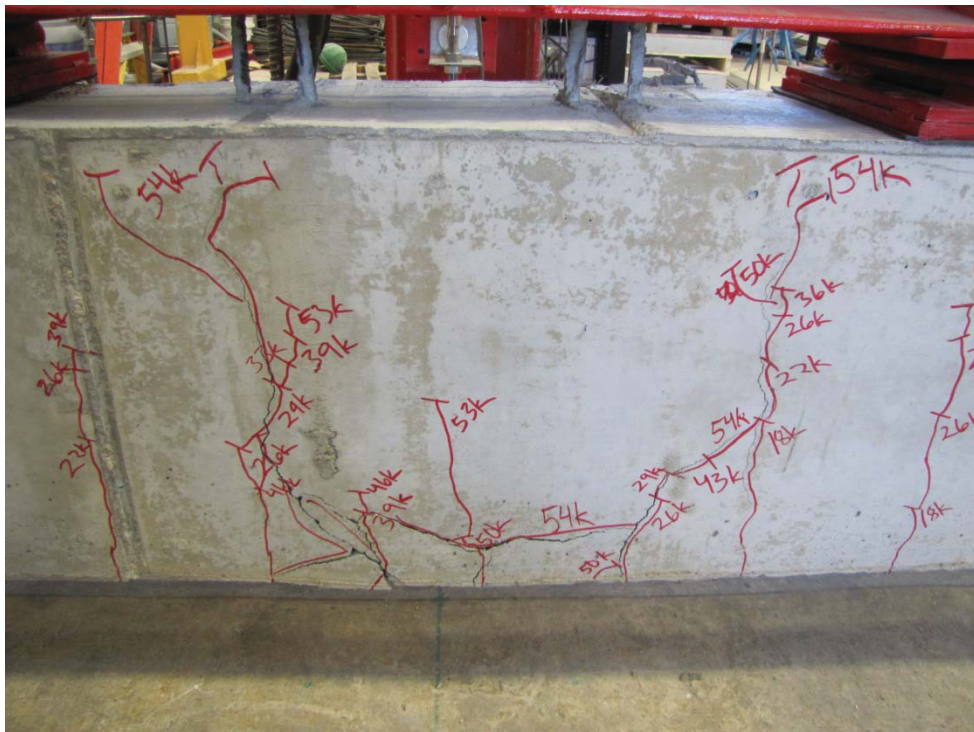


(b) Side View

**Figure A.1 – C6-58LBB1**



(a) Bottom View



(b) Side View

Figure A.2 – C6-58LBB2



(a) Bottom View



(b) Side View

**Figure A.3 – C6-58LTB**







(a) Full crack pattern

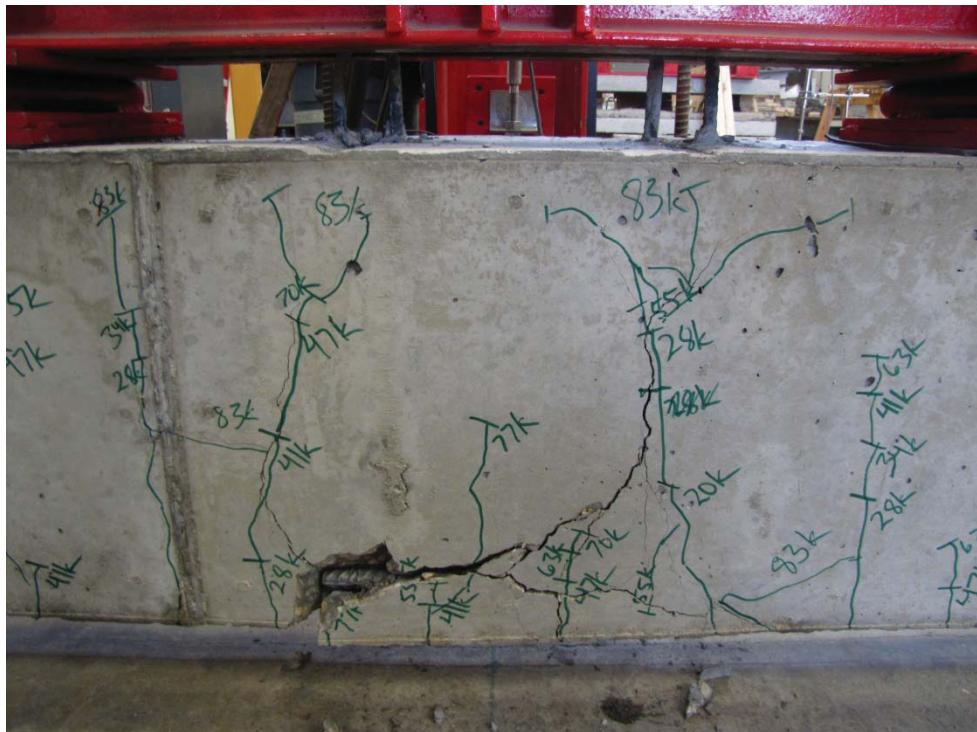


(b) Side View

**Figure A.6 – S6-48LTB side view**



(a) Bottom View

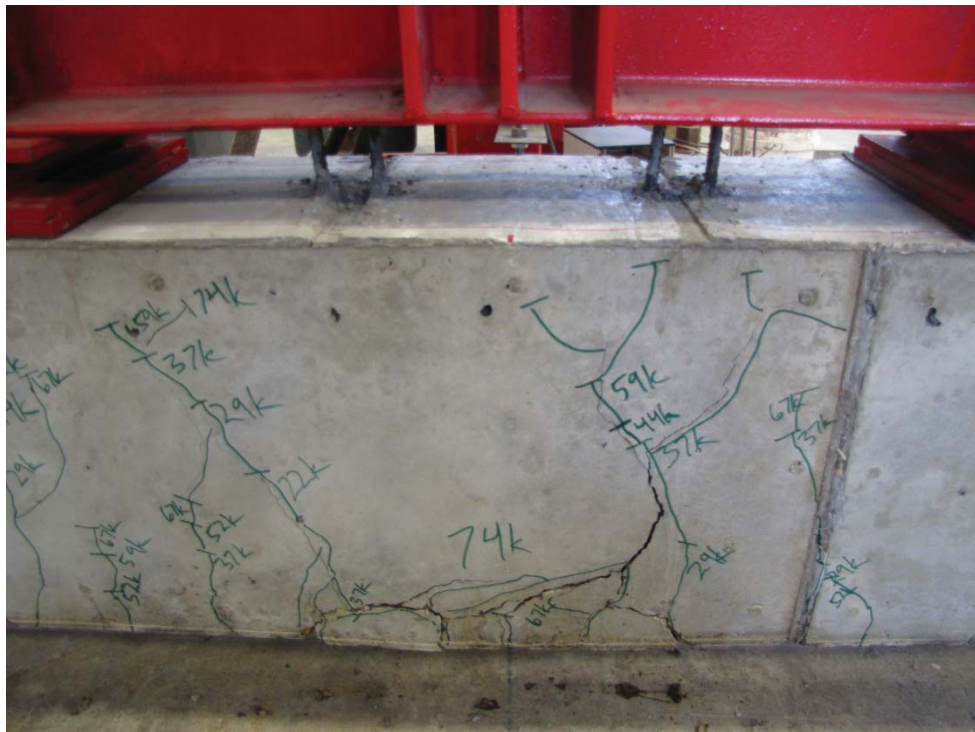


(b) Side View

**Figure A.7 – C10-58LBB1**



(a) Bottom View



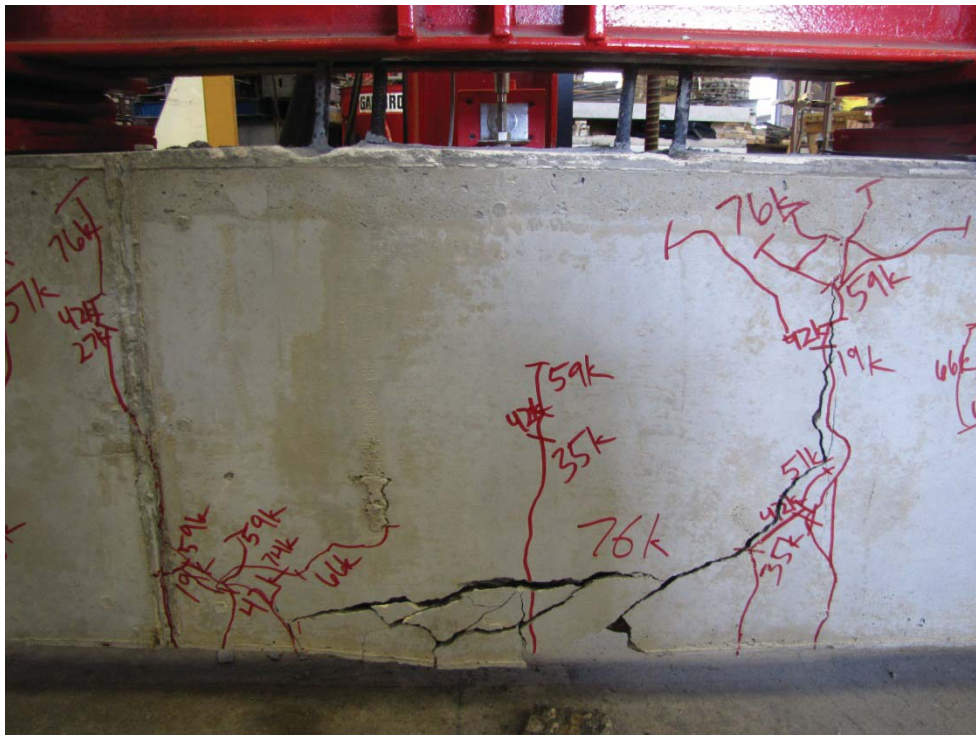
(b) Side View

**Figure A.8 – C10-58LBB2**





(a) Bottom View



(b) Side View

**Figure A.10 – S10-48LBB1**



(a) Bottom View

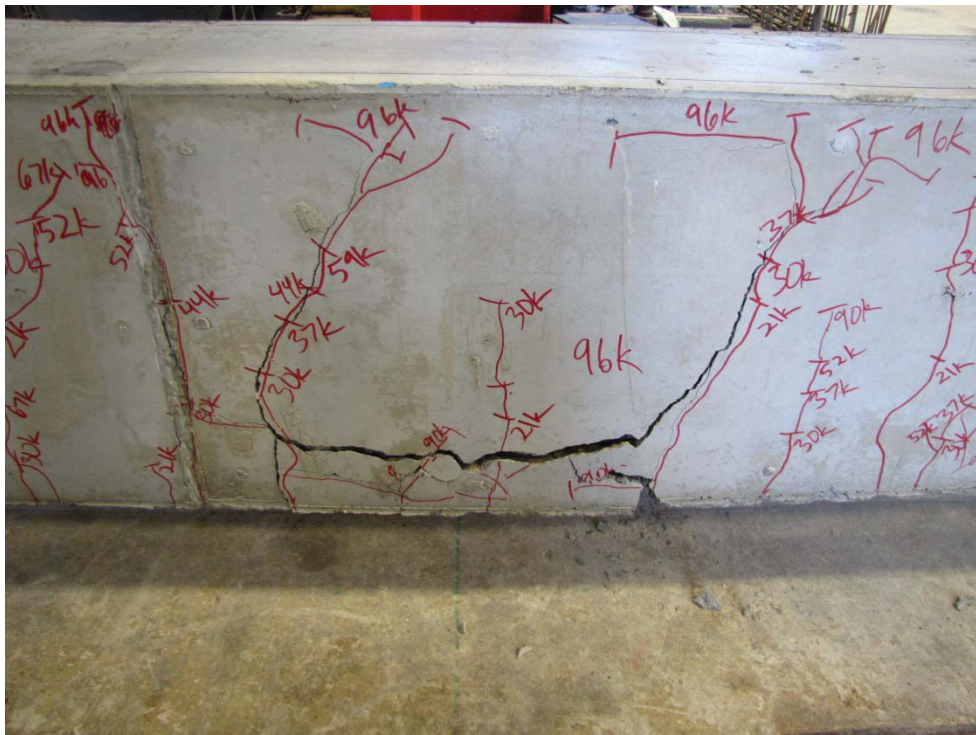


(b) Side View

Figure A.11 – S10-48LBB2



(a) Bottom View



(b) Side View

**Figure A.12 – S10-48LTB**

**APPENDIX B**

**SCC TEST PROGRAM TEST DATA PLOTS**

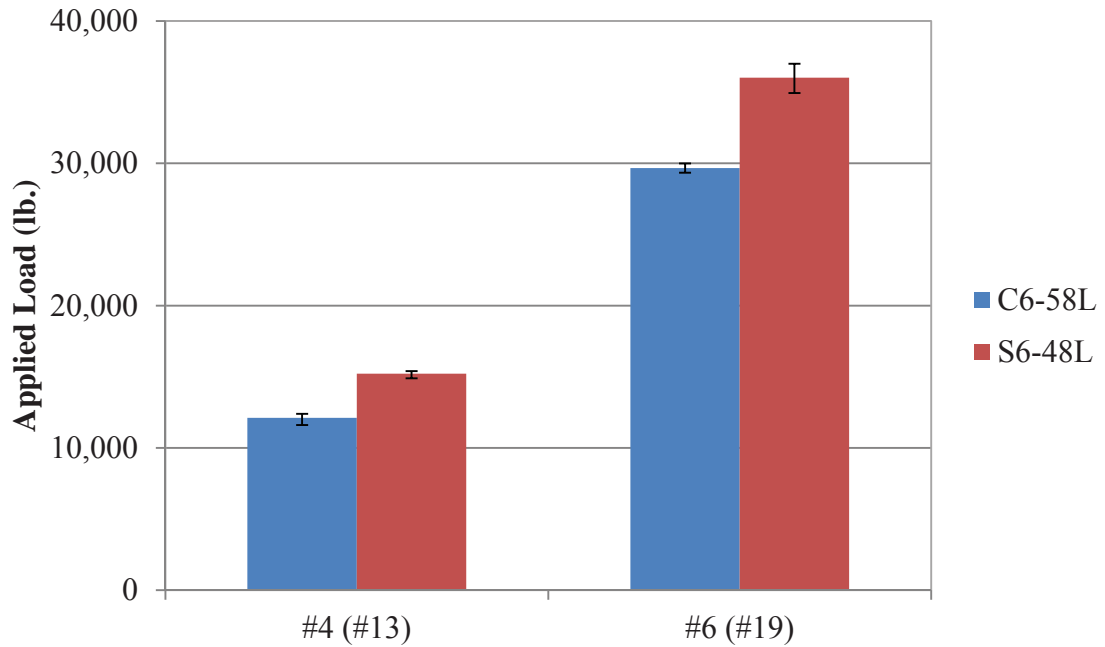


**Figure B.1 – Normal strength direct pull-out applied load comparisons**

Conversion: 1 lb. = 4.45 N

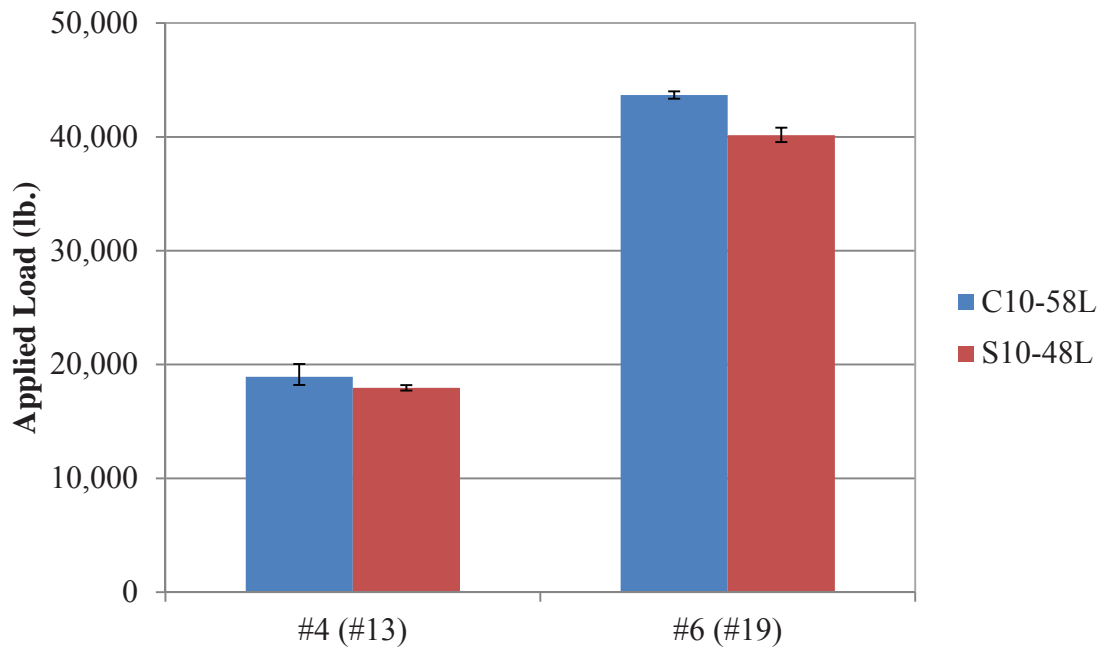


**Figure B.2 – High strength direct pull-out applied load comparisons**

Conversion: 1 lb. = 4.45 N

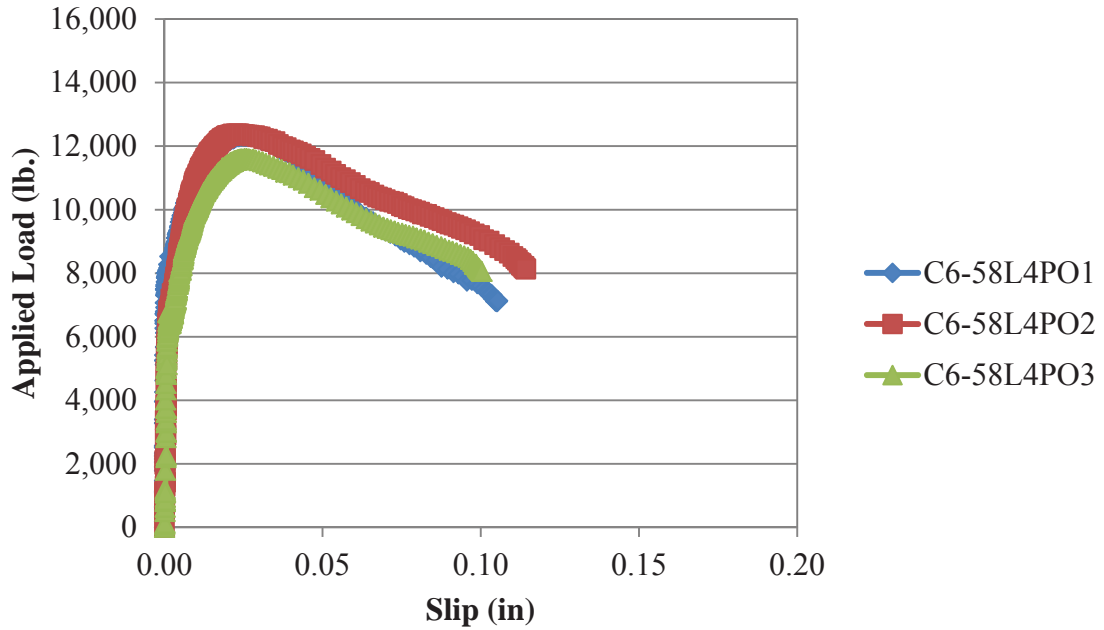


**Figure B.3 – Applied load vs. slip plot for #4 (#13) C6-58L**

Conversion: 1 in. = 25.4 mm

1 lb. = 4.45 N

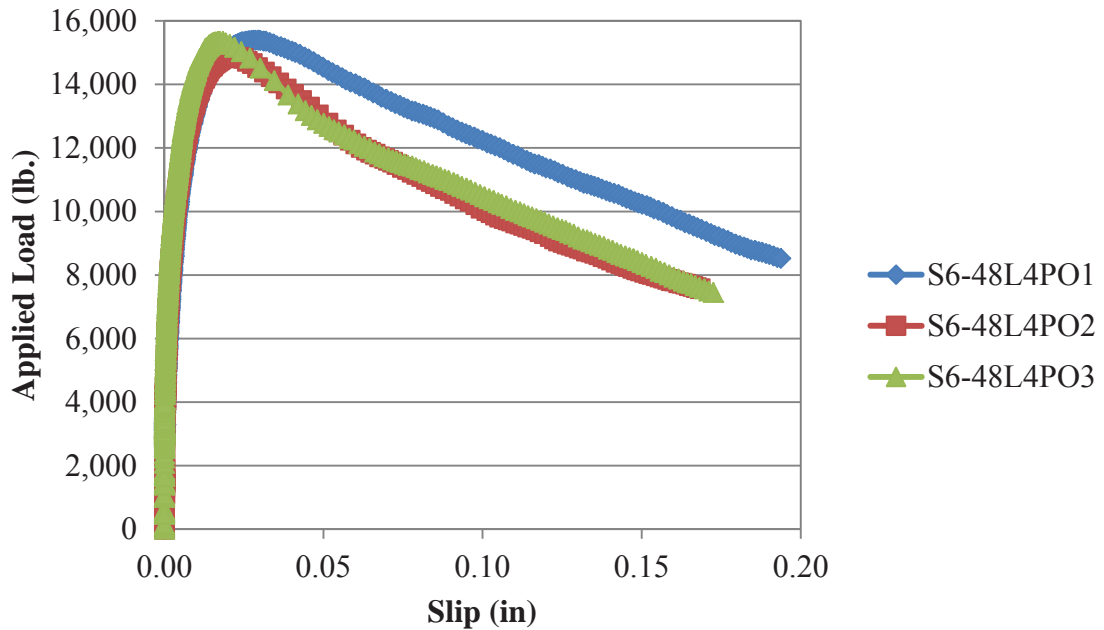


**Figure B.4 – Applied load vs. slip plot for #4 (#13) S6-48L**

Conversion: 1 in. = 25.4 mm

1 lb. = 4.45 N

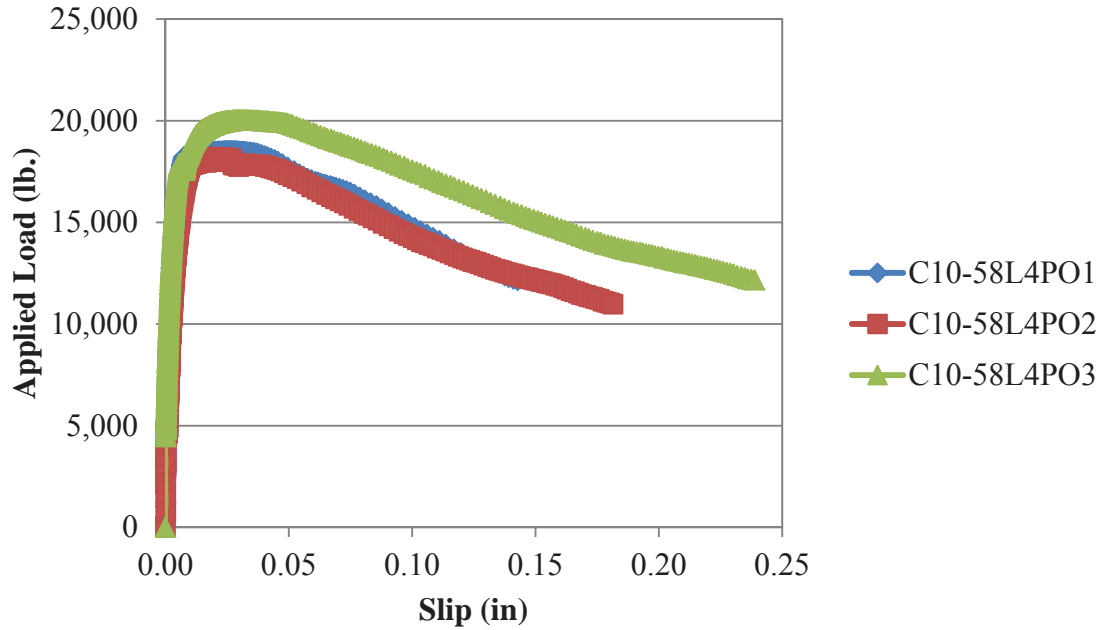


**Figure B.5 – Applied load vs. slip plot for #4 (#13) C10-58L**

Conversion: 1 in. = 25.4 mm

1 lb. = 4.45 N

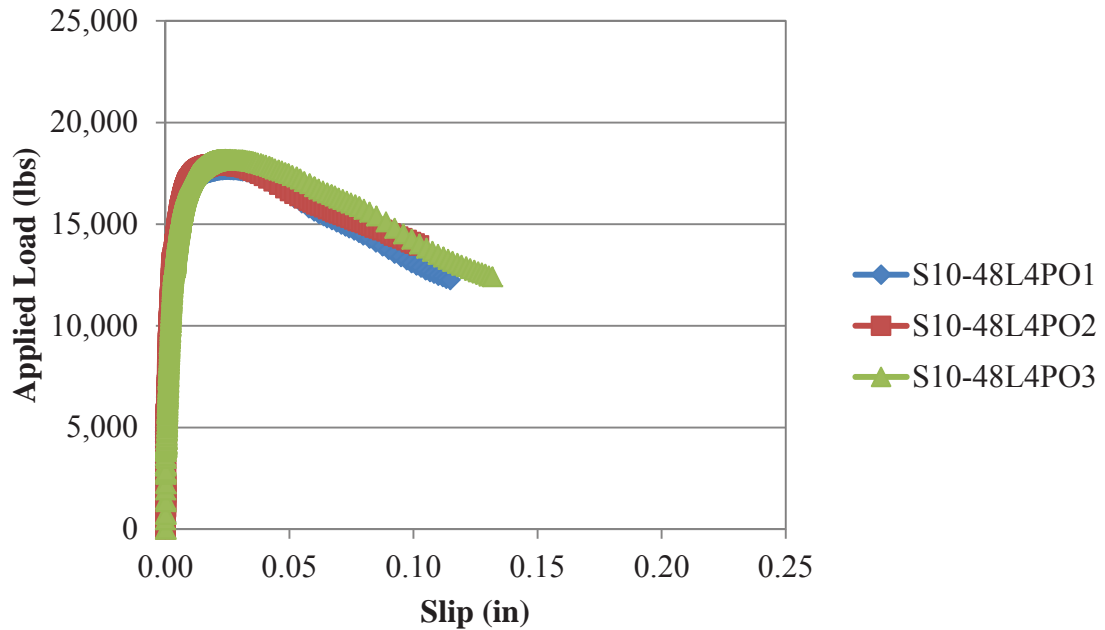


**Figure B.6 – Applied load vs. slip plot for #4 (#13) S10-48L**

Conversion: 1 in. = 25.4 mm

1 lb. = 4.45 N

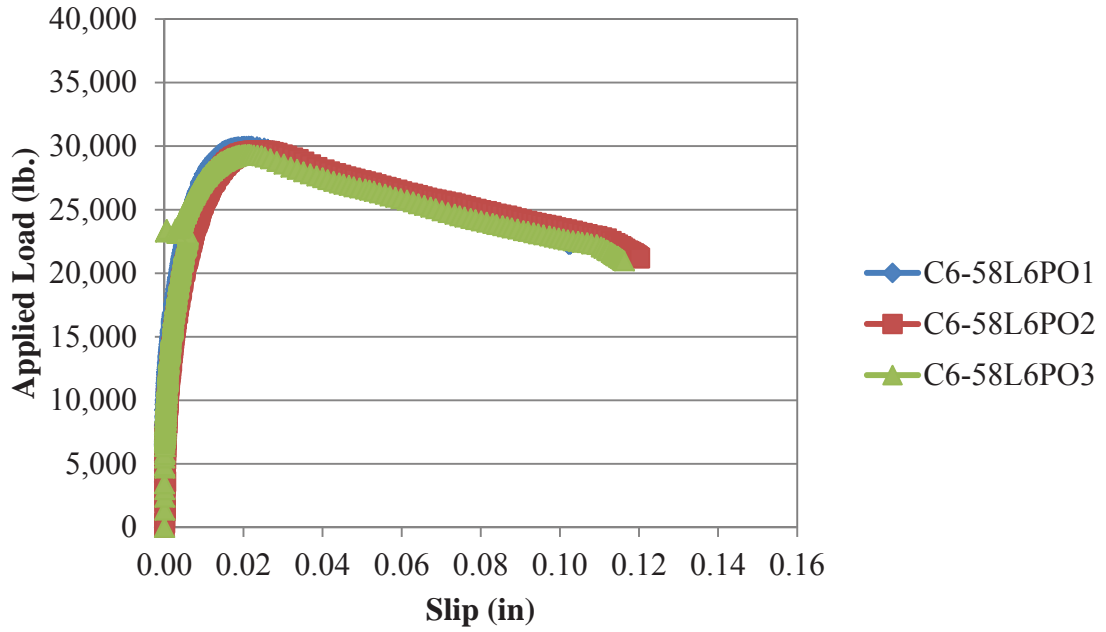


**Figure B.7 – Applied load vs. slip plot for #6 (#19) C6-58L**

Conversion: 1 in. = 25.4 mm

1 lb. = 4.45 N

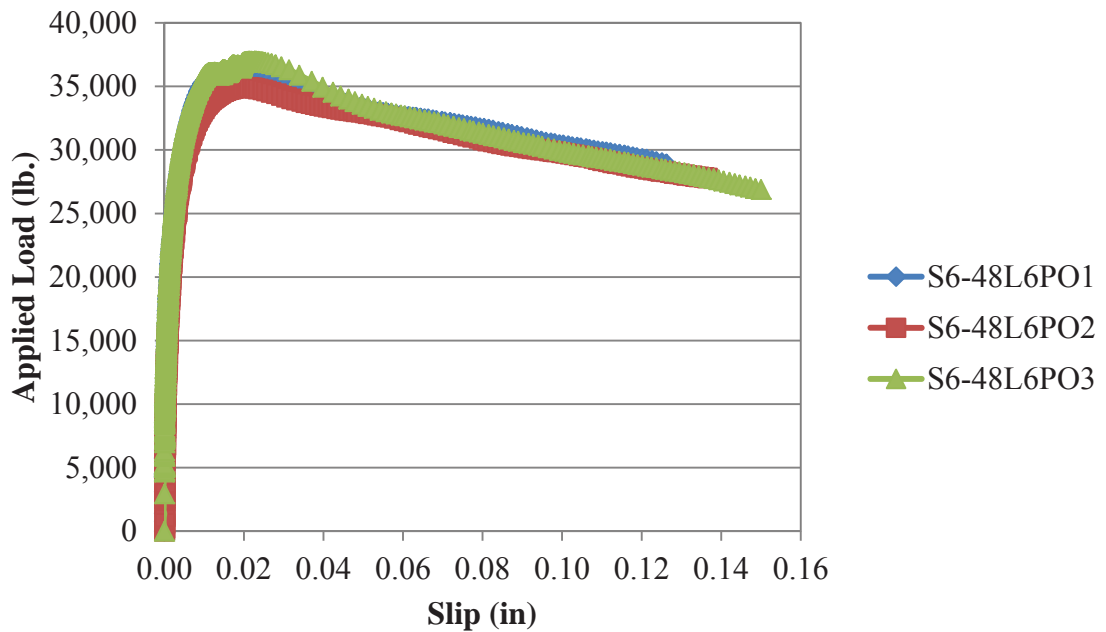


**Figure B.8 – Applied load vs. slip plot for #6 (#19) S6-48L**

Conversion: 1 in. = 25.4 mm

1 lb. = 4.45 N

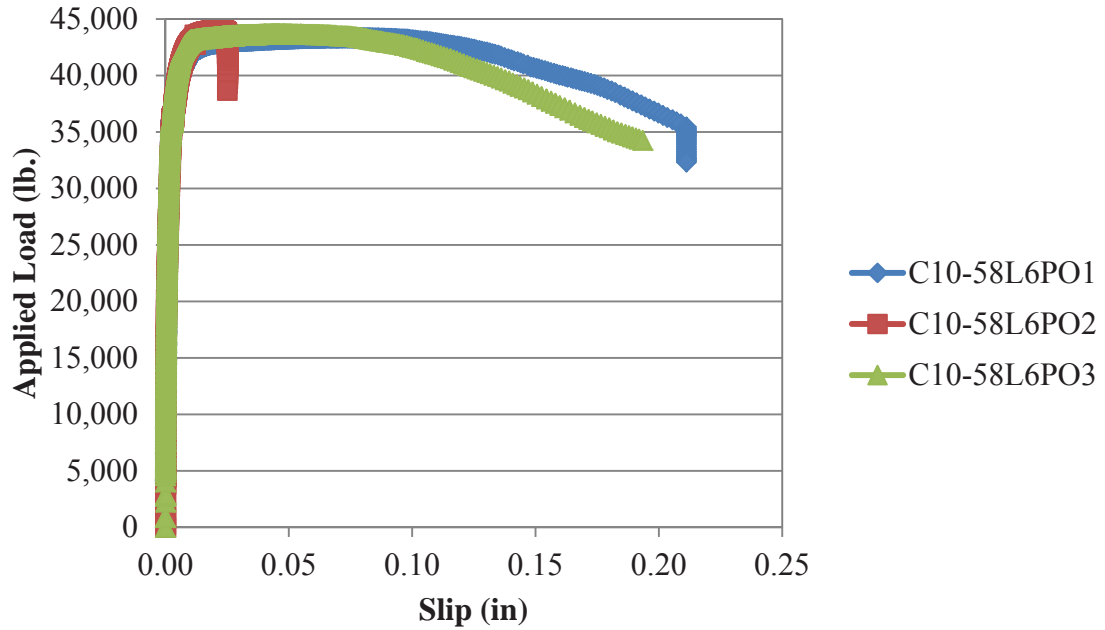


**Figure B.9 – Applied load vs. slip plot for #6 (#19) C10-58L**

Conversion: 1 in. = 25.4 mm

1 lb. = 4.45 N

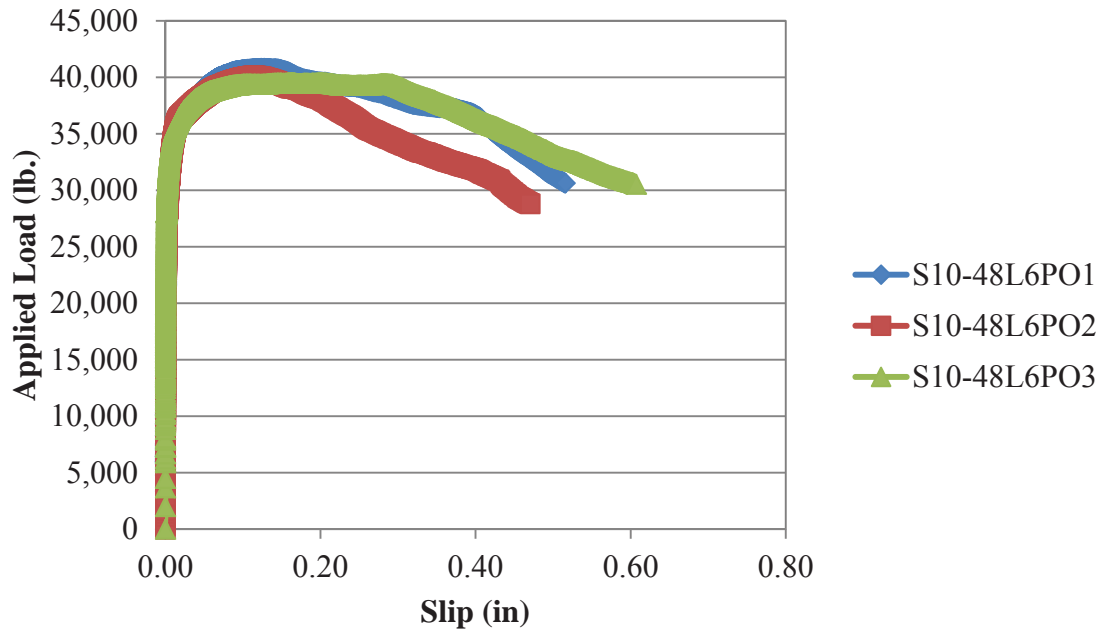


**Figure B.10 – Applied load vs. slip plot for #6 (#19) S10-48L**

Conversion: 1 in. = 25.4 mm

1 lb. = 4.45 N

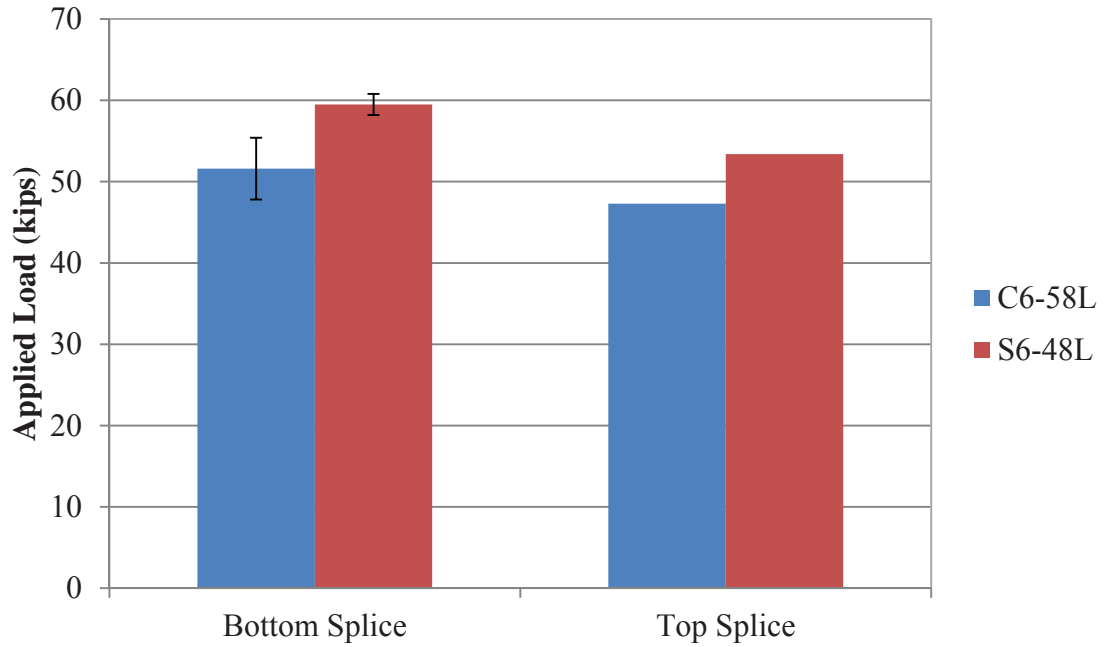


**Figure B.11 – Normal strength beam splice applied load comparisons**  
Conversion: 1 kip = 4.45 kN

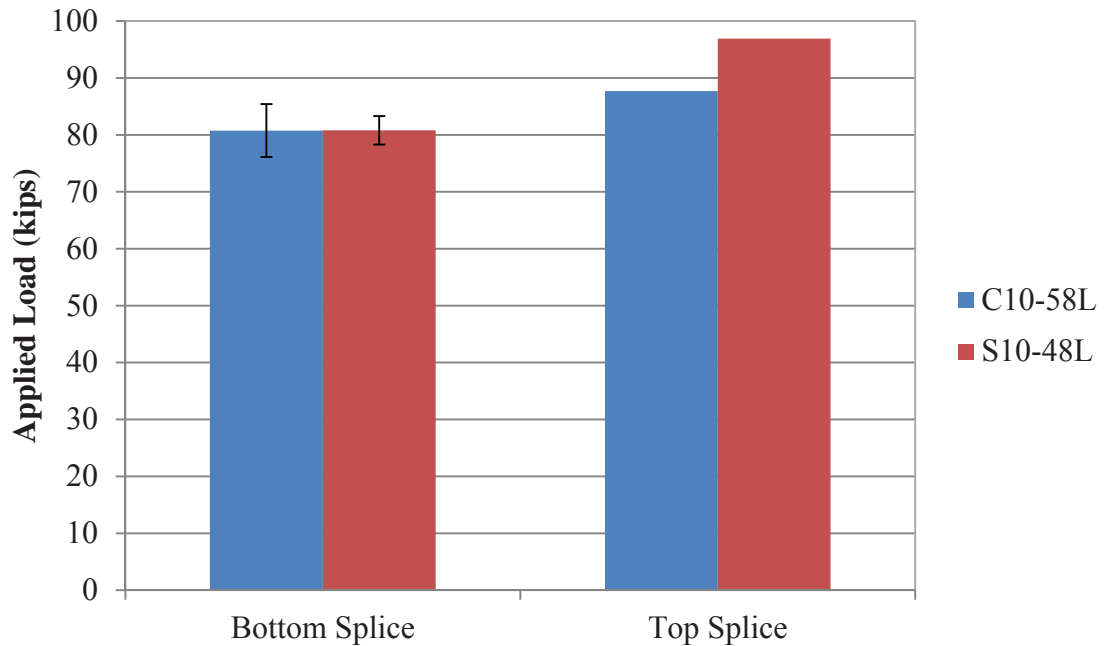


**Figure B.12 – High strength beam splice applied load comparisons**  
Conversion: 1 kip = 4.45 kN

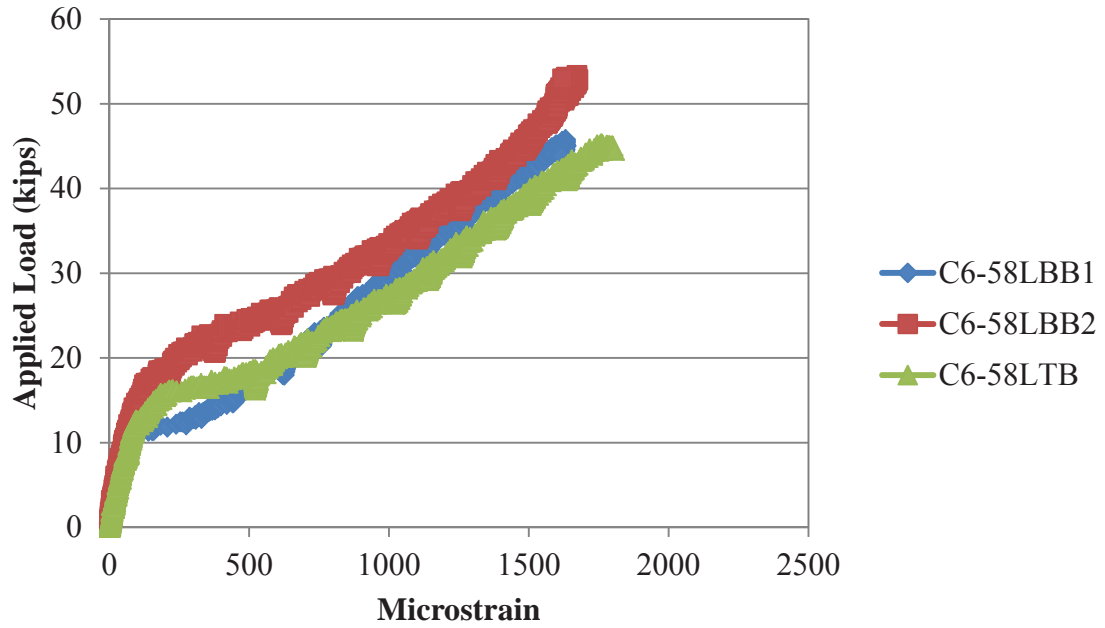


**Figure B.13 – Applied load vs. strain (average of all gages per specimen)  
for C6-58L**

Conversion: 1 kip = 4.45 kN

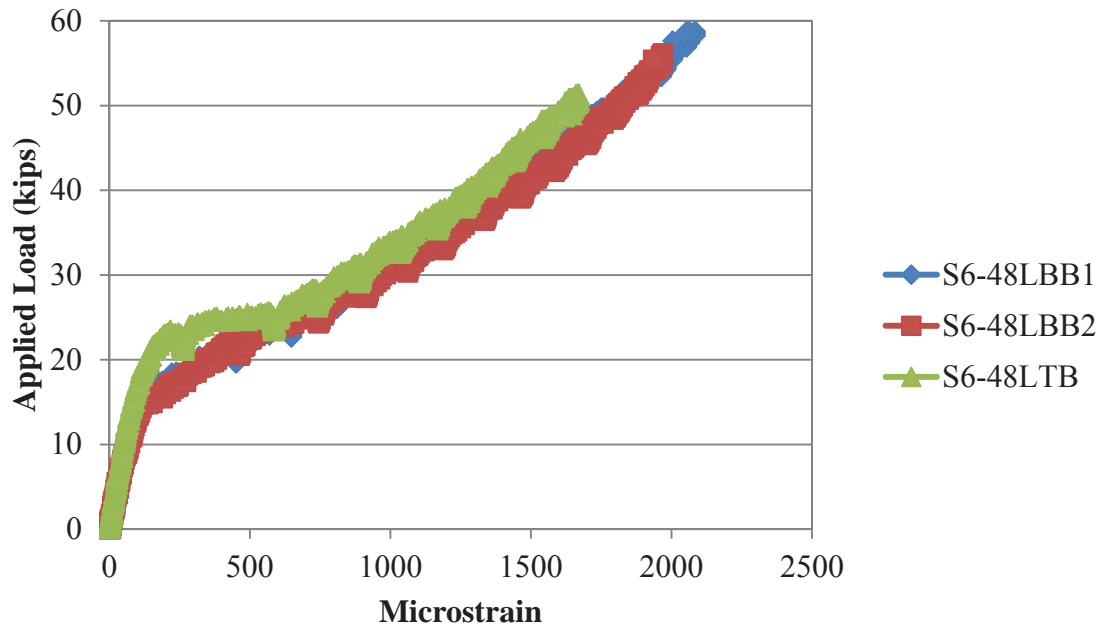


**Figure B.14 – Applied load vs. strain (average of all gages per specimen)  
for S6-48L**

Conversion: 1 kip = 4.45 kN

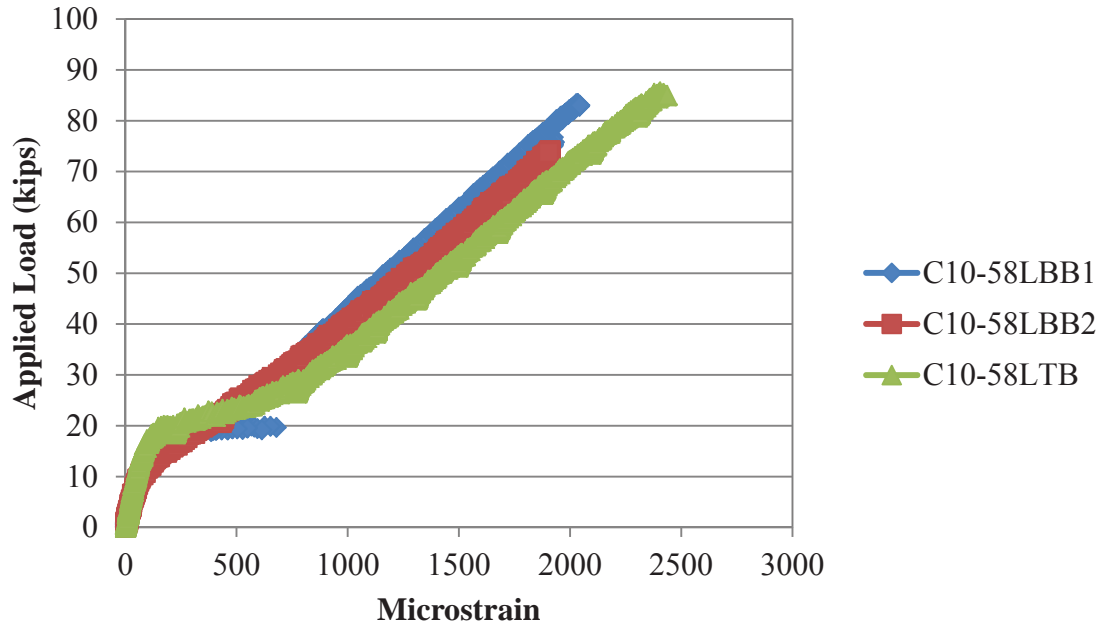


**Figure B.15 – Applied load vs. strain (average of all gages per specimen)  
for C10-58L**

Conversion: 1 kip = 4.45 kN

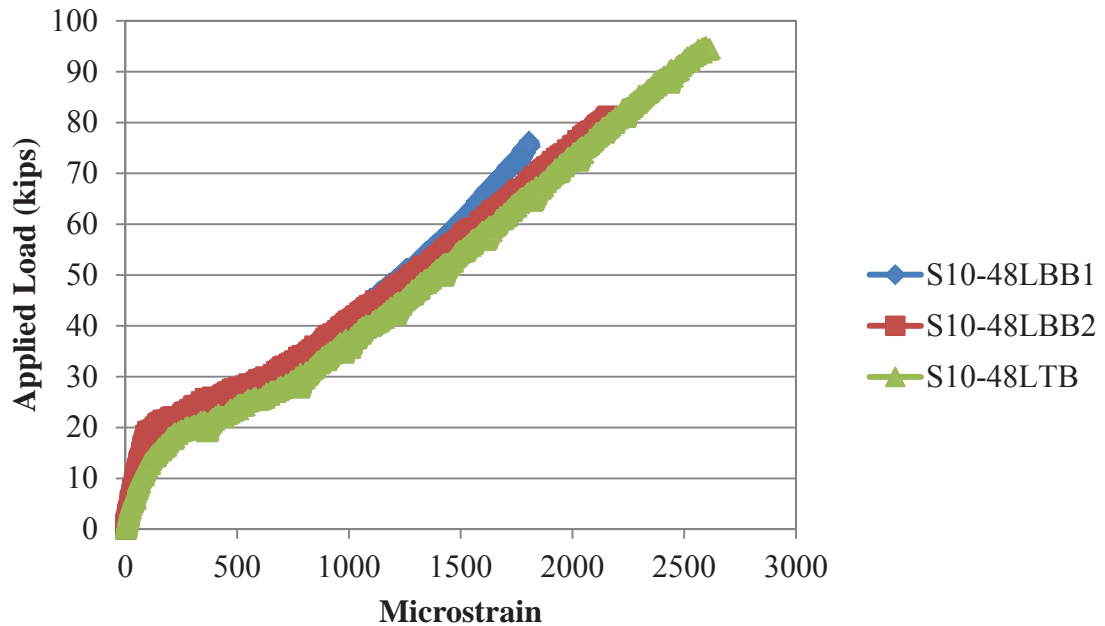


**Figure B.16 – Applied load vs. strain (average of all gages per specimen)  
for S10-48L**

Conversion: 1 kip = 4.45 kN

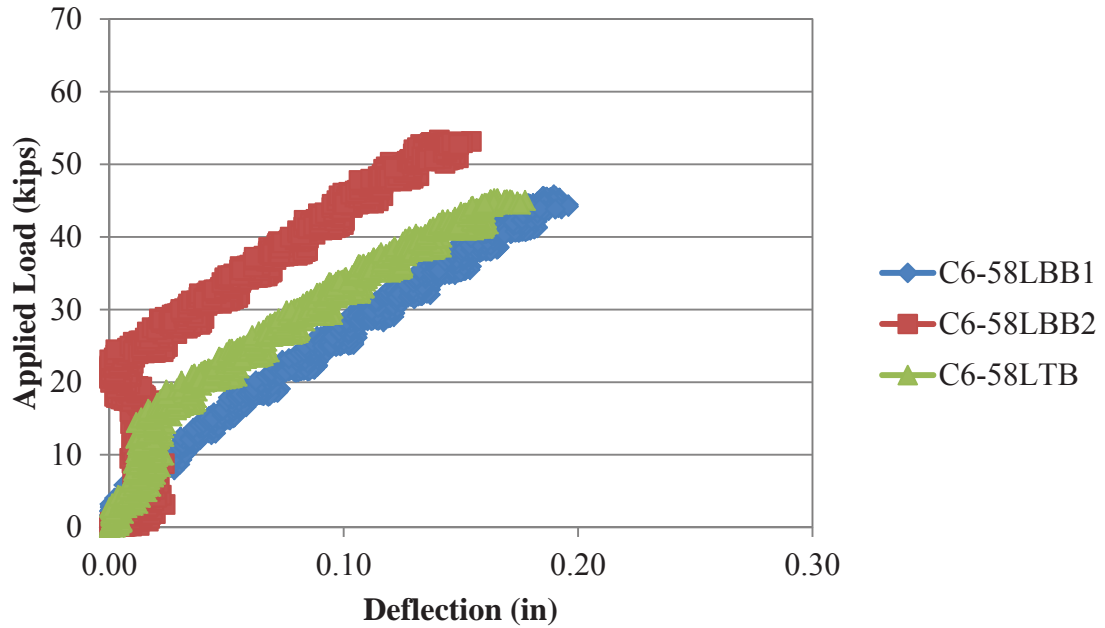


**Figure B.17 – Applied load vs. displacement for C6-58L**

Conversion: 1 in. = 25.4 mm

1 kip. = 4.45 kN

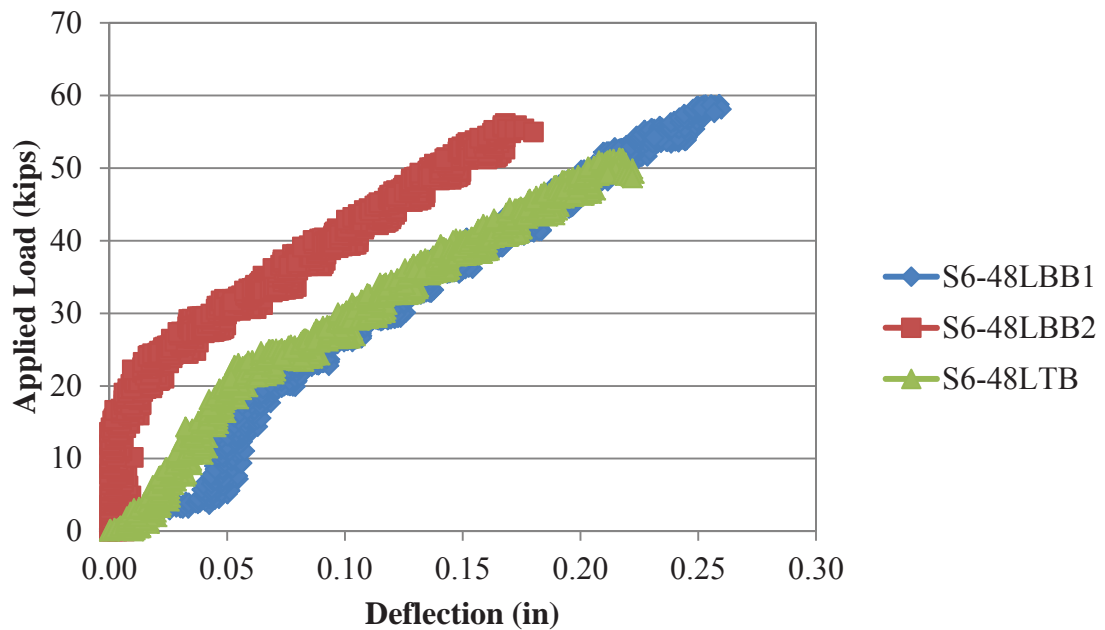


**Figure B.18 – Applied load vs. displacement for S6-48L**

Conversion: 1 in. = 25.4 mm

1 kip. = 4.45 kN

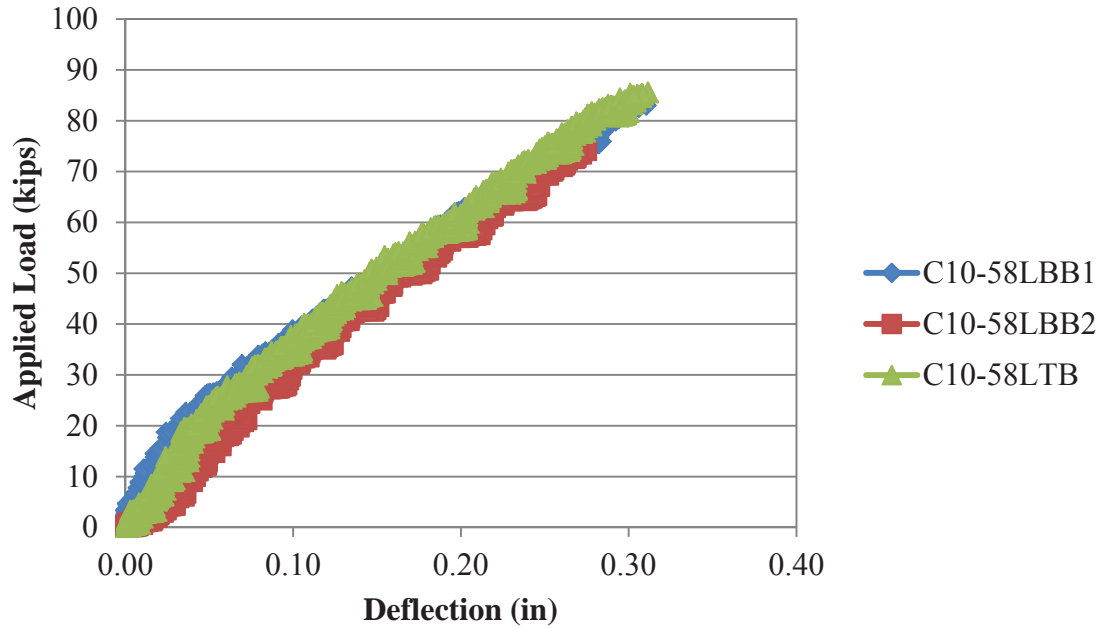


**Figure B.19 – Applied load vs. displacement for C10-58L**

Conversion: 1 in. = 25.4 mm

1 kip. = 4.45 kN

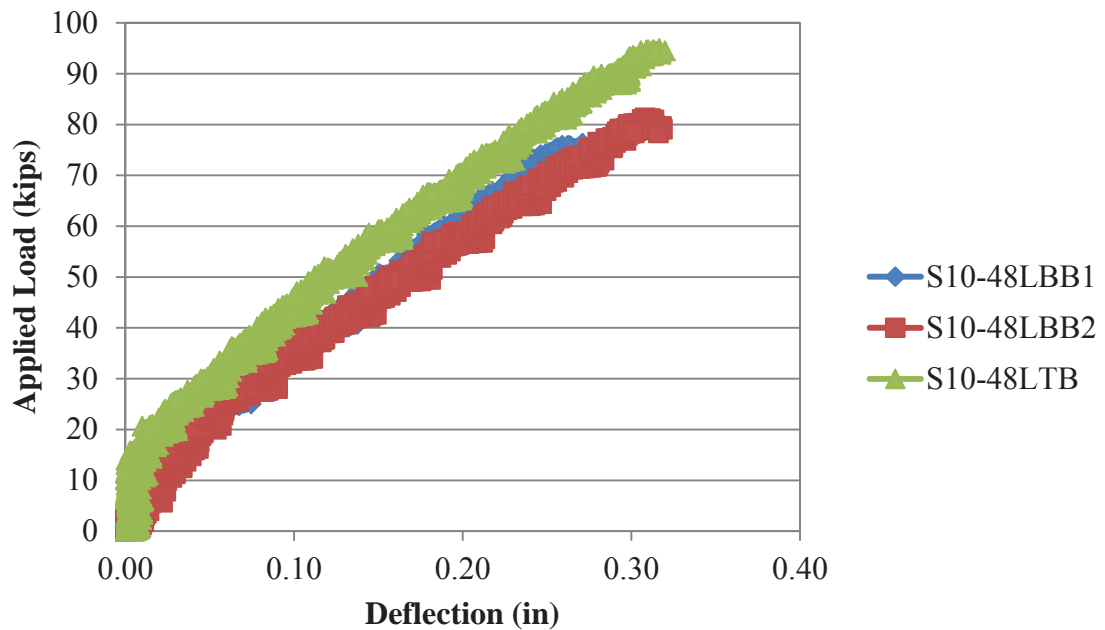


**Figure B.20 – Applied load vs. displacement for S10-48L**

Conversion: 1 in. = 25.4 mm

1 kip. = 4.45 kN

**APPENDIX C**

**SCC TEST PROGRAM STATISTICAL ANALYSIS**

**Table C.1 – t-test for #4 (#13) C6-58L and S6-48L  
direct pull-out specimen average comparison**

	<i>Variable 1</i>	<i>Variable 2</i>
Mean	12299.77281	14170.70786
Variance	192306.7928	67409.77444
Observations	3	3
Pearson Correlation	0.999925572	
Hypothesized Mean Difference	0	
df	2	
	-	
t Stat	18.10958303	
P(T<=t) one-tail	0.001517652	
t Critical one-tail	2.91998558	
P(T<=t) two-tail	0.003035304	
t Critical two-tail	4.30265273	

**Table C.2 – t-test for #4 (#13) C10-58L and S10-48L  
direct pull-out specimen average comparison**

	<i>Variable 1</i>	<i>Variable 2</i>
Mean	19291.505	18116.022
Variance	996006.58	58255.052
Observations	3	3
Pearson Correlation	0.9461693	
Hypothesized Mean Difference	0	
df	2	
t Stat	2.631888	
P(T<=t) one-tail	0.0595581	
t Critical one-tail	2.9199856	
P(T<=t) two-tail	0.1191161	
t Critical two-tail	4.3026527	

**Table C.3 – t-test for #6 (#19) C6-58L and S6-48L  
direct pull-out specimen average comparison**

	<i>Variable 1</i>	<i>Variable 2</i>
Mean	30133.52917	33551.81008
Variance	111376.4402	923374.4939
Observations	3	3
Pearson Correlation	0.994319729	
Hypothesized Mean Difference	0	
df	2	
	-	
t Stat	9.396487376	
P(T<=t) one-tail	0.005568476	
t Critical one-tail	2.91998558	
P(T<=t) two-tail	0.011136952	
t Critical two-tail	4.30265273	

**Table C.4 – t-test for #6 (#19) C10-58L and S10-48L  
direct pull-out specimen average comparison**

	<i>Variable 1</i>	<i>Variable 2</i>
Mean	44524.47747	40530.32231
Variance	110031.5152	407511.2922
Observations	3	3
Pearson Correlation	0.994406672	
Hypothesized Mean Difference	0	
df	2	
t Stat	22.28085073	
P(T<=t) one-tail	0.001004146	
t Critical one-tail	2.91998558	
P(T<=t) two-tail	0.002008291	
t Critical two-tail	4.30265273	

**Table C.5 – t-test for C6-58L and S6-48L beam splice average comparison**

	<i>Variable 1</i>	<i>Variable 2</i>
Mean	52.49015377	53.88631511
Variance	7.720148065	36.49494056
Observations	3	3
	-	-
Pearson Correlation	0.999116478	
Hypothesized Mean Difference	0	
df	2	
	-	-
t Stat	0.274238986	
P(T<=t) one-tail	0.404815006	
t Critical one-tail	2.91998558	
P(T<=t) two-tail	0.809630013	
t Critical two-tail	4.30265273	

**Table C.6 – t-test for C10-58L and S10-48L beam splice average comparison**

	<i>Variable 1</i>	<i>Variable 2</i>
Mean	65.81842085	67.16694327
Variance	71.11065656	151.7248173
Observations	3	3
Pearson Correlation	0.767542424	
Hypothesized Mean Difference	0	
df	2	
	-	-
t Stat	0.293378545	
P(T<=t) one-tail	0.398437399	
t Critical one-tail	2.91998558	
P(T<=t) two-tail	0.796874798	
t Critical two-tail	4.30265273	

## BIBLIOGRAPHY

- AASHTO (2007). AASHTO LRFD Bridge Design Specification. Fourth Edition, Washington, D.C.
- ACI 318 (2008). Building Code Requirements for Structural Concrete (ACI 318-08) and Commentary. American Concrete Institute, Farmington Hills, MI.
- ACI 408R (2003). Bond and Development of Straight Reinforcing Bars in Tension. American Concrete Institute, Farmington Hills, MI.
- ASTM C 39 (2011). Standard Test Method for Compressive Strength of Cylindrical Concrete Specimens. *American Society for Testing and Materials*. West Conshohocken, PA.
- ASTM C 78 (2010). Standard Test Method for Flexural Strength of Concrete (Using Simple Beam with Third-Point Loading). *American Society for Testing and Materials*. West Conshohocken, PA.
- ASTM C 138 (2010). Standard Test Method for Density (Unit Weight), Yield, and Air Content (Gravimetric) of Concrete. *American Society for Testing and Materials*. West Conshohocken, PA.
- ASTM C 143 (2010). Standard Test Methods for Slump of Hydraulic Cement Concrete. *American Society for Testing and Materials*. West Conshohocken, PA.
- ASTM C 231 (2010). Standard Test Method for Air Content of Freshly Mixed Concrete by the Pressure Method. *American Society for Testing and Materials*. West Conshohocken, PA.
- ASTM C 496 (2011). Standard Test Method for Splitting Tensile Strength of Cylindrical Concrete Specimens. *American Society for Testing and Materials*. West Conshohocken, PA.
- ASTM C 1611 (2009). Standard Test Method for Slump Flow of Self-Consolidating Concrete. *American Society for Testing and Materials*. West Conshohocken, PA.
- ASTM C 1621 (2009). Standard Test Method for Passing Ability of Self-Consolidating Concrete by J-Ring. *American Society for Testing and Materials*. West Conshohocken, PA.
- ASTM E 8 (2009). Standard Test Methods for Tension Testing of Metallic Materials. *American Society for Testing and Materials*. West Conshohocken, PA.

- Bentz, E., Collins, M. (2000). Response-2000 Reinforced Concrete Sectional Analysis. Version 1.0.5. Toronto, Canada.
- Castel, A., Thierry, V., Kriengkai, V., Raoul, F. (2006). Effect of Reinforcing Bar Orientation and Location on Bond with Self-Consolidating Concrete. *ACI Structural Journal*, 100-S59.
- Castel, A., Vidal, T., Francois, R. (2010). "Bond and Cracking Properties of Self-Consolidating Concrete." Université de Toulouse, France.
- Chan, Y., Chen, Y., Liu, Y.(2003). Development of Bond Strength of Reinforcement Steel in Self-Consolidating Concrete. *ACI Structural Journal*, 100-S52.
- Dehn, F., Holschemacher, K., Weibe, D. (2000). "Self-Compacting Concrete (SCC) Time Development of the Material Properties and the Bond Behavior." Universität Leipzig.
- Foroughi-Asl, A., Dilmaghani, S., Famili, H. (2008). "Bond Strength of Reinforcement Steel in Self-Compacting Concrete." University of Tabriz, Iran.
- Hassan,, A., Hossain, K., Lachemi, M. (2009). "Bond Strength of Deformed Bars in Large Reinforced Concrete Members Cast with Industrial Self-Consolidating Concrete Mixture." Ryerson University, Toronto, Canada.
- RILEM 7-II-28. (1994). "Bond Test for Reinforcing Steel. 2. Pull-out test." E & FN Spon, London.
- Turk, K., Benli, A., Calayir, Y. (2009). "Bond Strength of Tension Lap-Splices in Full Scale Self-Consolidating Concrete Beams." Harran University, Sanliurfa, Turkey.
- Valcuende, M., Parra, C. (2008). "Bond Behavior of Reinforcement in Self-Compacting Concrete." Polytechnic University of Valencia, Spain.
- Wight, J., MacGregor, J. (2009). "Reinforced Concrete Mechanics and Design." Fifth Edition. Upper Saddle River, NJ: Pearson Education, Inc., 360-406.
- Wolfe, M. (2011). "Bond Strength of High-Volume Fly Ash Concrete." M.S. Thesis, Missouri University of Science and Technology, Rolla, MO.

**FINAL Report D**

TRyy1103

**Project Title: Self-Consolidating Concrete (SCC) for Infrastructure Elements**

**Report D: Self-Consolidating Concrete (SCC) for Infrastructure Elements: Creep, Shrinkage and Abrasion Resistance**

Prepared for  
Missouri Department of Transportation  
Construction and Materials

Missouri University of Science and Technology, Rolla, Missouri

July 2012

The opinions, findings, and conclusions expressed in this publication are those of the principal investigators and the Missouri Department of Transportation. They are not necessarily those of the U.S. Department of Transportation, Federal Highway Administration. This report does not constitute a standard or regulation



## **ABSTRACT**

Concrete specimens were fabricated for shrinkage, creep, and abrasion resistance testing. Variations of self-consolidating concrete (SCC) and conventional concrete were all tested. The results were compared to previous similar testing programs and used to determine the adequacy of the materials for use in practice.

The testing program consisted of normal strength (6000 psi) and high strength (10,000 psi) variations of SCC and conventional concrete.

All specimens were tested for compressive strength, modulus of elasticity, shrinkage strain, creep strain, and abrasion resistance. All tests were performed according to their respective ASTM standard methods. In general, SCC performed well relative to conventional concrete at high strengths, but not as well at normal strengths for shrinkage and creep.

## TABLE OF CONTENTS

	Page
ABSTRACT .....	iii
LIST OF ILLUSTRATIONS .....	vii
LIST OF TABLES .....	ix
NOMENCLATURE .....	x
1. LITERATURE REVIEW .....	1
SECTION	
1.1. SELF-CONSOLIDATING CONCRETE (SCC).....	1
1.1.1. Definition of SCC.....	1
1.1.2. Advantages of SCC .....	1
1.2. SHRINKAGE OF CONCRETE .....	1
1.2.1. Definition of Shrinkage .....	1
1.2.2. Factors Affecting Shrinkage.....	2
1.3. SHRINKAGE MODELS.....	4
1.3.1. ACI 209R-92 .....	4
1.3.2. NCHRP Report 496 (2003) .....	8
1.3.3. Model B3 .....	10
1.3.4. CEB-FIP 90 .....	11
1.3.5. GL 2000.....	12
1.4. SCC SHRINKAGE RESEARCH.....	13
1.4.1. NCHRP Report 628 (2009) .....	14
1.4.2. Shindler, et. al.....	14
1.4.3. Fernandez-Gomez and Landsberger.....	15
1.4.4. Long, et. al.....	15
1.5. CREEP OF CONCRETE.....	16
1.5.1. Definition of Creep.....	16
1.5.2. Factors Affecting Creep .....	17
1.6. CREEP MODELS.....	18
1.6.1. ACI 209R-92 .....	18

1.6.2. NCHRP Report 496.....	20
1.6.3. CEB-FIP 90 .....	21
1.6.4. GL 2000.....	22
1.7. SCC CREEP RESEARCH.....	23
1.7.1. NCHRP Report 628.....	23
1.7.2. Long and Khayat .....	24
1.7.3. Long, et. el.....	24
1.8. Application of Shrinkage and Creep.....	24
1.8.1. Prestress Loss .....	24
1.8.2. Load Effects .....	26
1.8.3. Beam Deflection.....	26
1.9. CONCRETE ABRASION .....	27
1.9.1. Definition of Concrete Abrasion .....	27
1.9.2. Factors Affecting Concrete Abrasion.....	27
1.10. SCC ABRASION RESEARCH.....	27
2. RESEARCH PROGRAM .....	28
2.1. MIX DESIGNS.....	28
2.1.1. SCC.. .....	28
2.2. SHRINKAGE AND CREEP SPECIMEN CONSTRUCTION.....	29
2.2.1. Shrinkage and Creep Specimens .....	29
2.2.2. Shrinkage and Creep Molds .....	30
2.2.3. Shrinkage and Creep Specimen Casting .....	31
2.2.4. Shrinkage and Creep De-Molding and Preparation .....	31
2.2.5. Shrinkage and Creep Data Acquisition .....	31
2.3. ABRASION SPECIMEN CONSTRUCTION .....	32
2.4. TESTING PROCEDURES.....	33
2.4.1. Shrinkage Testing Procedures .....	33
2.4.2. Creep Testing Procedures.....	36
2.4.3. Abrasion Resistance Testing Procedures .....	39
3. SCC RESULTS AND DISCUSSION.....	43
3.1. SHRINKAGE .....	43

3.1.1. Results .....	43
3.1.2. Discussion and Conclusions .....	43
3.2. CREEP .....	52
3.2.1. Results .....	52
3.2.2. Discussion and Conclusions .....	53
3.3. ABRASION RESISTANCE .....	57
3.3.1. Results .....	57
3.3.2. Discussion and Conclusions .....	60
APPENDICES	
A. SHRINKAGE WITH RELATIVE HUMIDITY DATA .....	62
B. EXAMPLE STRAIN CALCULATIONS .....	67
C. COEFFICIENT OF VARIATION DATA .....	70
BIBLIOGRAPHY .....	73

## LIST OF ILLUSTRATIONS

Figure	Page
Figure 1.1 - Relationship Between Moist Cure Time and Shrinkage Strain .....	3
Figure 1.2 - Stress vs. Time for Prestressed Bridge Girder (Tadros et. al. 2003).....	25
Figure 2.1 - Shrinkage and Creep Form.....	30
Figure 2.2 – Shrinkage and Creep Specimens and DEMEC Point Arrangement (Myers and Yang, 2005).....	32
Figure 2.3 – DEMEC Reading Taken on Specimen.....	34
Figure 2.4 - Reference Bar.....	34
Figure 2.5 - Reading Taken on Reference Bar .....	35
Figure 2.6 - Gauge Factor Used for Shrinkage and Creep Calculations.....	35
Figure 2.7 - Example DEMEC Gauge Reading.....	35
Figure 2.8 - Schematic of Creep Loading Frame (Myers and Yang, 2005) .....	36
Figure 2.9 - Creep Loading Frame with Specimen.....	37
Figure 2.10 - Reading Taken on Creep Specimen .....	38
Figure 2.11 - Schematic of Abrasion Rotating Cutter (ASTM C944).....	40
Figure 2.12 - Rotating Cutter .....	40
Figure 2.13 - Abrasion Resistance Test In Progress.....	41
Figure 2.14 - Depth of Wear Measurement Points .....	41
Figure 2.15 - Abrasion Resistance Specimen After Testing.....	42
Figure 3.1 - C6-58L Shrinkage Results and Prediction Models .....	46
Figure 3.2 - S6-48L Shrinkage Results and Prediction Models.....	47
Figure 3.3 - C10-58L Shrinkage Results and Prediction Models .....	48
Figure 3.4 - S10-58L Shrinkage Results and Prediction Models.....	49
Figure 3.5 - SCC Shrinkage Results (Best fit Logarithmic).....	50
Figure 3.6 – SCC Results with Shrinkage Databases (Fernandez-Gomez, Shindler et. al., and Holshemacher).....	51
Figure 3.7 – SCC Coefficient of Creep Results.....	54
Figure 3.8 – S6-48L Plotted Against Results from Long and Khayat (2011) .....	55
Figure 3.9 – S10-48L Plotted Against Results from Long and Khayat (2011) .....	56

Figure 3.10 - C6-58L Mass Loss Results.....	57
Figure 3.11 - S6-48L Mass Loss Results .....	58
Figure 3.12 - C10-58L Mass Loss Results.....	58
Figure 3.13 - S10-48L Mass Loss Results .....	59
Figure 3.14 - SCC Mass Loss Results .....	59
Figure 3.15 - SCC Depth of Wear Results.....	60
Figure A.1 – C6-58L shrinkage data shown with recorded relative humidity.....	63
Figure A.2 - S6-48L shrinkage data shown with recorded relative humidity.....	64
Figure A.3 – C10-58L shrinkage data shown with recorded relative humidity.....	65
Figure A.4 – S10-48L shrinkage data shown with recorded relative humidity .....	66
Figure B.1 – Example shrinkage and creep strain calculation.....	68
Figure B.2 – Example shrinkage and creep strain calculations with equations shown ....	69
Figure C.1 – C6-58L and S6-48L COV Data .....	71
Figure C.2 – C10-58L and S10-48L COV Data .....	72

**LIST OF TABLES**

Table	Page
Table 1.1 - Standard Conditions as Defined by ACI 209R-92 .....	6
Table 1.2 – Coded Values for Eqs. 1.48 – 1.49 .....	16
Table 2.1 - SCC Test Program Mix Designs and mechanical properties .....	29
Table 3.1 – SCC results compared to Eqs. 2.48 – 2.49 by Long et. al. ....	52
Table 3.2 - Summary of SCC Creep Results .....	52
Table 3.3 - Summary of Results Shown with 28 Day Measured Compressive Strength .	60

## NOMENCLATURE

Symbol	Description
A	Cement type correction factor (NCHRP 628)
$A_c$	Cross-section area ( $\text{mm}^2$ ) (CEB-FIP 90)
c	Cement content ( $\text{lb}/\text{yd}^3$ ) (ACI 209R-92)
D	Effective cross-section thickness (Model B3)
$D_0$	Datum reading on the reference bar
$D_i$	Subsequent reading on the reference bar
f	Size effects factor (ACI 209R-92)
$f'_c$	Tested compressive strength of concrete (psi, ksi, MPa)
$f'_{ci}$	Specified compressive strength of concrete (ksi) (NCHRP 496)
$f_{cm}$	Tested compressive strength of concrete at 28 days age (psi, ksi, MPa) (CEB-FIP 90)
G	Gauge factor
H	Relative humidity (% or decimal)
K	Cement type correction factor (GL 2000)
$k_f$	Concrete strength factor (NCHRP 496)
$k_{hc}$	Humidity factor (NCHRP 496)
$k_{hs}$	Humidity factor (NCHRP 496 and NCHRP 628)
$k_{la}$	Loading factor (NCHRP 496)
$k_s$	Size factor (NCHRP 496 and NCHRP 628) or Cross-section shape factor (Model B3)
$k_{td}$	Time development factor (NCHRP 496)

$R_0$	Datum reading on tested material
RH	Relative humidity (%) (CEB-FIP 90)
$R_i$	Subsequent reading on tested material
s	Slump of fresh concrete (in)
S(t)	Time dependence factor (Model B3)
t	Age of concrete (days)
$t_0$	Age of concrete when drying begins (days) (Model B3) or Age at which creep specimen is loaded (days) (ACI 209R-92 and CEB FIP 90)
$t_c$	Age of concrete when drying begins (days) (ACI 209R-92 and GL 2000)
$t_i$	Age at which creep specimen is loaded (days) (NCHRP 496)
$t_s$	Age of concrete at the beginning of shrinkage (days) (CEB-FIP 90)
u	Perimeter in contact with the atmosphere (mm) (CEB-FIP 90)
V/S	Volume to Surface area ratio (in or mm)
w	Water content of concrete (lb/ft <sup>3</sup> )
$\alpha$	Concrete air content (%)
$\alpha_1$	Cement type correction factor (Model B3)
$\alpha_2$	Curing condition correction factor
$\beta(h)$	Humidity correction factor (GL 2000)
$\beta(t)$	Time effect correction factor (GL 2000)
$\beta_c$	Coefficient to describe the development of creep with time after loading (CEB FIP 90)

$\beta_{RH}$	Relative humidity correction factor (CEB-FIP 90)
$\beta_s$	Coefficient to describe the development of shrinkage with time (CEB-FIP 90)
$\beta_{sc}$	Concrete type correction factor (CEB-FIP 90)
$\gamma_{c,RH}$	Humidity correction factor (ACI 209R-92)
$\gamma_{c,s}$	Slump correction factor (ACI 209R-92)
$\gamma_{c,t0}$	Curing condition correction factor (ACI 209R-92)
$\gamma_{c,vs}$	Size correction factor (ACI 209R-92)
$\gamma_{c,\alpha}$	Air content correction factor (ACI 209R-92)
$\gamma_{c,\psi}$	Fine aggregate correction factor (ACI 209R-92)
$\gamma_{sh,c}$	Cement content correction factor (ACI 209R-92)
$\gamma_{sh,RH}$	Relative humidity correction factor (ACI 209R-92)
$\gamma_{sh,s}$	Slump correction factor (ACI 209R-92)
$\gamma_{sh,tc}$	Initial moist cure duration correction factor (ACI 209R-92)
$sh_{,vs}$	Volume/surface area correction factor (ACI 209R-92)
$\gamma_{sh,\alpha}$	Air content correction factor (ACI 209R-92)
$\gamma_{sh,\psi}$	Fine aggregate correction factor (ACI 209R-92)
$\Delta_{\epsilon c}$	Change in creep strain from one reading to the next
$\Delta_{\epsilon s}$	Change in shrinkage strain from one reading to the next
$\epsilon_{cso}$	Notional shrinkage coefficient (CEB-FIP 90)
$\epsilon_{es(t,ts)}$	Calculated ultimate shrinkage strain ( $\mu\epsilon$ ) (CEB-FIP 90)
$\epsilon_i$	Measured strain due to initial loading of creep specimen
$\epsilon_{es(t,t0)}$	Calculated shrinkage strain at a given age ( $\mu\epsilon$ ) (Model B3)

$\epsilon_{sh}$	Calculated shrinkage strain at a given age ( $\mu\epsilon$ ) (NCHRP 496, GL 2000, and NCHRP 628)
$\epsilon_{sh(t,tc)}$	Calculated shrinkage strain at a given age ( $\mu\epsilon$ ) (ACI 209R-92)
$\epsilon_{shu}$	Calculated ultimate shrinkage strain ( $\mu\epsilon$ ) (ACI 209R-92) or Notional ultimate shrinkage strain (GL 2000)
$\epsilon_{sh\infty}$	Calculated ultimate shrinkage strain ( $\mu\epsilon$ ) (Model B3)
$\epsilon_t$	Measured creep strain at a given age
$\lambda_{\Delta}$	Multiplier for additional deflection due to long-term effects (ACI 318-08)
$\xi$	Time dependant factor for sustained load (ACI 318-08)
$\rho'$	Compression reinforcement ratio (ACI 318-08)
$\tau_{sh}$	Size dependence factor (Model B3)
$\Phi_{(t,t_0)}$	Calculated creep coefficient at a given age (ACI 209R-92 and CEB FIP 90) or Measured creep coefficient at a given age
$\Phi_0$	Notional creep coefficient (CEB FIP 90)
$\Phi_{28}$	Calculated creep coefficient at a given age (GL 2000)
$\Phi_{(tc)}$	Factor that takes into account drying before loading (GL 2000)
$\Phi_u$	Calculated ultimate creep coefficient (ACI 209R-92)
$\Psi$	Ratio of fine aggregate to total aggregate by weight (%)
$\Psi_{(t,t_i)}$	Calculated creep coefficient at a given age (NCHRP 496 and NCHRP 628)

## 1. LITERATURE REVIEW

### 1.1. SELF-CONSOLIDATING CONCRETE (SCC)

**1.1.1. Definition of SCC.** ACI 237R-07 defines self-consolidating concrete as “highly flowable, nonsegregating concrete that can spread into place, fill the formwork, and encapsulate the reinforcement without any mechanical consolidation.” In order to achieve the necessary fluidity, a high range water reducer (HRWR) is often utilized.

**1.1.2. Advantages of SCC.** The choice of SCC over conventional concrete results in both economical and material performance benefits. The use of SCC eliminates the necessity of manual compaction, typically achieved by vibration. The self-leveling properties of SCC additionally reduce or eliminate the need for screeding operations to achieve a flat surface. This reduction in jobsite labor and equipment forces, along with the time saved by not having to perform these labor intensive operations, lead to significant savings. Because of its fluidity, SCC has the ability to effectively flow into areas that conventional concrete cannot. SCC is therefore ideal for construction of members with significant reinforcement congestion or unusually shaped members. This allows for greater freedom in member design and reinforcement detailing. Finally, the reduction in honeycombing is beneficial both structurally and aesthetically (ACI 237R-07).

### 1.2. SHRINKAGE OF CONCRETE

**1.2.1. Definition of Shrinkage.** Shrinkage of concrete is the decrease in volume of hardened concrete with time. Shrinkage is expressed as the strain measured on a load-free specimen, most often as the dimensionless unit microstrain (strain  $\times 10^{-6}$ ).

Concrete experiences shrinkage in three ways, drying shrinkage, autogenous (chemical) shrinkage, and carbonation shrinkage. Autogenous shrinkage is due strictly to the hydration reactions of the cement. Drying shrinkage is the strain imposed on a specimen exposed to the atmosphere and allowed to dry. Carbonation shrinkage is caused by the reaction of calcium hydroxide with cement with carbon dioxide in the atmosphere. The magnitude and rate of shrinkage is dependent on a number of factors. These factors are accounted for and described in the various industry models and research projects in the following sections.

**1.2.2. Factors Affecting Shrinkage (ACI 209.1R-05).** Shrinkage of concrete is closely related to shrinkage of paste. Therefore the amount of paste in the mix significantly affects the level of concrete shrinkage. Paste volume is determined by the quantity, size, and gradation of aggregate. Because paste volume is largely dependent on aggregate properties, the most important factor in determining a concrete's shrinkage level is the aggregate used in the mix. Similarly, the water content, cement content, and slump will affect the shrinkage of concrete. These three factors are indications of the paste volume and therefore can be used to determine the shrinkage potential of a mix. Aggregate acts as a restraining force to shrinkage, therefore an aggregate with a higher modulus of elasticity (MOE) will better restrain against shrinkage than an aggregate with a lower MOE. The characteristics of the cement itself are other significant indicators of shrinkage potential. Research has shown cements with low sulfate content, high alumina content, and cements that are finely ground exhibit increased shrinkage.

The environment which the concrete is exposed to can also influence shrinkage. The biggest environmental factor is the relative humidity of the surrounding air. As

shown by **Eq. 1.1**, as relative humidity increases, shrinkage decreases due to the decrease in potential moisture loss. It has also been shown that an increase in temperature increases the ultimate shrinkage of concrete.

$$\text{shrinkage} \propto 1 - \left(\frac{h}{100}\right)^b \quad (1.1)$$

Where: h is relative humidity in percent, and b is a constant that ranges from 1 to 4.

Finally, the design and construction of concrete specimens can influence shrinkage. The curing conditions experienced by the concrete have a significant effect on shrinkage.

Generally, the longer the specimen is allowed to moist cure, the less it will shrink.

However, research conducted by Perenchio (1997), **Figure 1.1**, shows that there may not be a simple relationship between moist cure time and shrinkage.

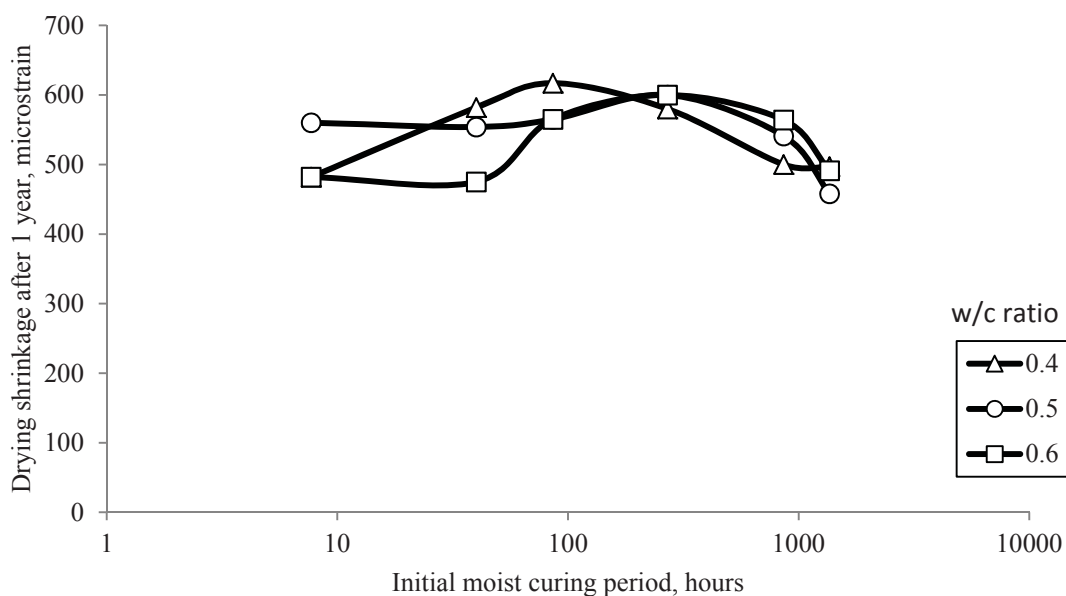


**Figure 1.1 - Relationship Between Moist Cure Time and Shrinkage Strain**

(adapted from Perenchio 1997)

Larger members tend to dry slower, so the ratio of volume to surface area is a significant factor in shrinkage of concrete.

$$\text{shrinkage} \propto \frac{1}{\left(\frac{V}{S}\right)^2} \quad (1.2)$$

Where: V/S is the volume to surface area ratio in inches.

### **1.3. SHRINKAGE MODELS.**

The ability to accurately predict the shrinkage of a concrete structure is extremely important. An accurate model for shrinkage will allow the engineer to predict long term serviceability, durability, and stability of a given structure. As mentioned above, there are many different factors that affect a concrete's susceptibility to shrinkage. Because of these factors, accurate prediction of shrinkage is very difficult. The models described below take into account many of the factors described above in their attempt to predict concrete shrinkage (Bazant and Baweja, 2000).

**1.3.1. ACI 209R-92.** This model, developed by Branson and Christiason (1971) and modified by ACI committee 209, predicts shrinkage strain of concrete at a given age under standard conditions. The original model by Branson and Christiason was developed based on a best fit from a sample of 95 shrinkage specimens and using an ultimate shrinkage strain of  $800 \times 10^{-6}$  in./in. (mm/mm). However, subsequent research by Branson and Chen, based on a sample of 356 shrinkage data points, concluded that the

ultimate shrinkage strain should be  $780 \times 10^{-6}$  in./in. (mm/mm). The prediction model, **Eq. 1.3 – 1.5**, apply only to the standard conditions as shown in **Table 1.1**.

$$\epsilon_{sh}(t, t_c) = \frac{(t-t_c)^\alpha}{f+(t-t_c)^\alpha} \epsilon_{shu} \quad (\mu\epsilon) \quad (1.3)$$

$$\epsilon_{shu} = 780 \times 10^{-6} \quad (\mu\epsilon) \quad (1.4)$$

$$f = 26.0e^{\{0.36(V/S)\}} \quad (1.5)$$

Where:  $f$  is 35 (moist cure) or 55 (steam cure), or by **Eq. 1.5** if size effects are to be considered,  $\alpha$  is assumed to be 1,  $t$  is the age of concrete in days, and  $t_c$  is the age of concrete when drying begins in days.

**Table 1.1 - Standard Conditions as Defined by ACI 209R-92**

Factors		Variables		Standard	
Concrete	Concrete Composition	Cement Paste Content	Type of Cement	Type I or III	
		W/C	Slump	2.7 in (70mm)	
		Mix Proportions	Air Content	≤ 6%	
		Aggregate Characteristics	Fine Aggregate %	50%	
		Degree of Compaction	Cement Content	470 to 752 lb/yd <sup>3</sup> (279 to 446 kg/m <sup>3</sup> )	
	Initial Curing	Length of Initial Curing	Moist Cured		7 days
			Steam Cured		1 - 3 days
		Curing Temperature	Moist Cured		73.4 ± 4°F (23 ± 2°C)
			Steam Cured		≤ 212°F (≤ 100°C)
		Curing Humidity	Relative Humidity		≥ 95%
Member Geometry & Environment	Environment	Concrete Temperature	Concrete Temperature	73.4°F ± 4°F (23 ± 2°C)	
		Concrete Water Content	Ambient Relative Humidity	40%	
	Geometry	Size and Shape	Volume-Surface Ratio (V/S)		V/S = 1.5 in (38mm)
			Minimum Thickness		6 in (150mm)

When concrete is not subject to any or all of the standard conditions, correction factors shall be applied, as shown in **Eq. 1.6 – 1.16**.

$$\epsilon_{sh}(t, t_c) = \frac{(t-t_c)^\alpha}{f+(t-t_c)^\alpha} \times \epsilon_{shu} \quad (\mu\epsilon) \quad (1.6)$$

$$f = 26.0e^{\{0.36(V/S)\}} \quad (1.7)$$

$$\epsilon_{shu} = 780\gamma_{sh} \times 10^{-6} \quad (\mu\epsilon) \quad (1.8)$$

$$\gamma_{sh} = \gamma_{sh,tc} \gamma_{sh,RH} \gamma_{sh,vs} \gamma_{sh,s} \gamma_{sh,\psi} \gamma_{sh,c} \gamma_{sh,\alpha} \quad (1.9)$$

$$\gamma_{sh,tc} = 1.202 - .2337 \log(t_c) \quad (1.10)$$

$$\gamma_{sh,RH} = \begin{cases} 1.40 - 1.02h & \text{for } 0.40 \leq h \leq 0.80 \\ 3.00 - 3.0h & \text{for } 0.80 \leq h \leq 1 \end{cases} \quad (1.11)$$

$$\gamma_{sh,vs} = 1.2e^{\{-0.12(V/S)\}} \quad (1.12)$$

$$\gamma_{sh,s} = 0.89 + 0.041s \quad (1.13)$$

$$\gamma_{sh,\psi} = \begin{cases} 0.30 + 0.014\psi & \text{for } \psi \leq 50\% \\ 0.90 + 0.002\psi & \text{for } \psi > 50\% \end{cases} \quad (1.14)$$

$$\gamma_{sh,c} = 0.75 + 0.00036c \quad (1.15)$$

$$\gamma_{sh,\alpha} = 0.95 + 0.008\alpha \geq 1 \quad (1.16)$$

Where:  $\epsilon_{sh}(t, t_c)$  is the calculated shrinkage strain at a given age,  $\epsilon_{shu}$  is the calculated ultimate shrinkage strain,  $\gamma_{sh,tc}$  is the initial moist cure duration correction factor,  $t$  is the age of concrete in days,  $t_c$  is the age of concrete when drying starts in days,  $\gamma_{sh,RH}$  is the

relative humidity correction factor,  $h$  is humidity in decimals,  $\gamma_{sh,vs}$  is the volume/surface area correction factor, where  $V/S$  is the volume to surface area ratio in inches,  $\gamma_{sh,s}$  is the slump correction factor,  $s$  is slump in inches,  $\gamma_{sh,\psi}$  is the fine aggregate correction factor,  $\psi$  is the ratio of fine aggregate to total aggregate by weight expressed as percentage,  $\gamma_{sh,c}$  is the cement content correction factor,  $c$  is the cement content in  $\text{lb}/\text{yd}^3$ ,  $\gamma_{sh,\alpha}$  is the air content correction factor, and  $\alpha$  is the air content in percent. In **Eq 1.6**, the value of  $\alpha$  can be assumed to be equal to 1, with  $f$  assumed to be equal to 35 for concrete that is moist cured for seven days or 55 for concrete subject to 1-3 days of steam curing. In order to totally consider shape and size effects,  $\alpha$  is still assumed to be equal to 1, with  $f$  given by **Eq. 1.7**.

**1.3.2. NCHRP Report 496 (2003).** The National Cooperative Highway Research Program (NCHRP) conducted research on shrinkage of high strength concrete in the states of Nebraska, New Hampshire, Texas, and Washington. This research project was sponsored by the American Association of State Highway and Transportation Officials (AASHTO) and the results adopted into the 2007 AASHTO LRFD Bridge Design Specifications. Laboratory shrinkage data was obtained from three 4 in. (101.6 mm) by 4 in. (101.6 mm) by 24 in. (609.6 mm) specimens per mix, with a total of 48 specimens tested including both normal and high strength concrete. Field specimens were also made and cured in the same condition as corresponding bridge girders in each of the four participating states. The field program consisted of a set of three 4 in. (101.6 mm) by 4 in. (101.6 mm) by 24 in. (609.6 mm) shrinkage specimens at each location with measurements taken for 3 months. The data showed that an ultimate shrinkage strain of  $480 \times 10^{-6}$  in./in. (mm/mm) should be assumed. The modification factors in the model

account for the effects of high strength concrete. **Eq. 1.17 – 1.22** present the proposed shrinkage formula as proposed in this study.

$$\varepsilon_{sh} = 480 \times 10^{-6} \gamma_{sh} \quad (\mu\varepsilon) \quad (1.17)$$

$$\gamma_{sh} = k_{td} k_s k_{hs} k_f \quad (1.18)$$

$$k_{td} = \frac{t}{61 - 4f'_{ci} + t} \quad (1.19)$$

$$k_{hs} = 2.00 - 0.0143H \quad (1.20)$$

$$k_s = \frac{1064 - 94V/S}{735} \quad (1.21)$$

$$k_f = \frac{5}{1 + f'_{ci}} \quad (1.22)$$

Where:  $\varepsilon_{sh}$  is the calculated shrinkage strain at a given age,  $k_{td}$  is the time development factor,  $t$  is the age of the concrete in days,  $k_{hs}$  is the humidity factor,  $H$  is the average ambient relative humidity in percent,  $k_s$  is the size factor,  $V/S$  is the volume to surface area ratio in inches,  $k_f$  is the concrete strength factor, and  $f'_{ci}$  is the specified compressive strength of concrete in ksi.

**1.3.3. Model B3.** Model B3 (Bazant and Baweja) is the third update of shrinkage predictions developed at Northwestern University, based on BP model  $\beta_3$  and BP-KX model  $\beta_4$ . This model is simpler than previous versions and is validated by a larger set of test data. **Eq. 1.23 – 1.32** present the B3 shrinkage prediction model.

$$\varepsilon_{sh}(t, t_0) = -\varepsilon_{sh\infty} k_h S(t) \quad (\mu\varepsilon) \quad (1.23)$$

$$S(t) = \tanh \sqrt{\frac{t-t_0}{\tau_{sh}}} \quad (1.24)$$

$$k_h = \begin{cases} 1 - h^3 & \text{for } h \leq 0.98 \\ -0.2 & \text{for } h = 1 \text{ (swelling in water)} \\ \text{linear} & \\ \text{interpolation} & \text{for } 0.98 \leq h \leq 1 \end{cases} \quad (1.25)$$

$$\tau_{sh} = k_t (k_s D)^2 \quad (1.26)$$

$$k_t = 190.8 t_0^{-0.08} f'_c{}^{-1/4} \quad (1.27)$$

$$D = 2V/S \text{ (in.)} \quad (1.28)$$

$$k_s = \begin{cases} 1.00 & \text{for an infinite slab} \\ 1.15 & \text{for an infinite cylinder} \\ 1.25 & \text{for an infinite square prism} \\ 1.30 & \text{for a sphere} \\ 1.55 & \text{for a cube} \end{cases} \quad (1.29)$$

$$\varepsilon_{sh\infty} = -\alpha_1\alpha_2[26w^{2.1}f'_c{}^{-0.28} + 270] \quad (\mu\varepsilon) \quad (1.30)$$

$$\alpha_1 = \begin{array}{ll} 1.0 & \text{for type I cement} \\ 0.85 & \text{for type II cement} \\ 1.1 & \text{for type III cement} \end{array} \quad (1.31)$$

$$\alpha_2 = \begin{array}{ll} 0.75 & \text{for steam – curing} \\ 1.2 & \text{for sealed or normal curing in air} \\ & \text{with initial protection against drying} \\ 1.0 & \text{for curing in water or at 100\% relative humidity} \end{array} \quad (1.32)$$

Where:  $\varepsilon_{shu}(t, t_0)$  is the calculated shrinkage strain at a given age,  $S(t)$  is the time dependence factor,  $t$  is the age of concrete in days,  $t_0$  is the age of concrete at which drying begins,  $\tau_{sh}$  is the size dependence factor,  $f'_c$  is the cylinder compressive strength in psi,  $D$  is the effective cross-section thickness,  $V/S$  is the volume to surface area ratio in inches,  $k_s$  is the cross-section shape factor,  $\varepsilon_{sh\infty}$  is the calculated ultimate shrinkage strain,  $\alpha_1$  is the cement type correction factor,  $\alpha_2$  is the curing condition correction factor, and  $w$  is the water content of the concrete in  $\text{lb/ft}^3$ .

**1.3.4. CEB-FIP 90.** This model, developed jointly by Euro-International Concrete Committee (CEB – Comité Euro-International du Béton) and the International Federation for Prestressing (FIP – Fédération Internationale de la Précontrainte) is found in the CEB-FIP Model Code 1990. It is stated that due to its international character, the code is more general than most and does not apply to any particular structure type. **Eq. 1.33 – 1.38** present this model for calculating shrinkage strain.

$$\varepsilon_{es}(t, t_s) = \varepsilon_{cso}\beta_s(t - t_s) \quad (\mu\varepsilon) \quad (1.33)$$

$$\varepsilon_{\text{cso}} = \varepsilon_s(f_{\text{cm}})(\beta_{\text{RH}}) \quad (1.34)$$

$$\beta_s(t - t_s) = \sqrt{\frac{(t - t_s)}{350 \left( \frac{2A_c}{100u} \right)^2 + (t - t_s)}} \quad (1.35)$$

$$\varepsilon_s(f_{\text{cm}}) = [160 + 10\beta_{\text{sc}}(9 - 0.1f_{\text{cm}})] \times 10^{-6} \quad (1.36)$$

$$\beta_{\text{RH}} = -1.55 \left[ 1 - \left( \frac{\text{RH}}{100} \right)^3 \right] \quad (1.37)$$

$$\beta_{\text{sc}} = \begin{cases} 4 & \text{for slowly hardening cements} \\ 5 & \text{for normal or rapid hardening cements} \\ 8 & \text{for rapid hardening high strength cements} \end{cases} \quad (1.38)$$

Where:  $\varepsilon_{\text{es}}(t, t_s)$  is the calculated ultimate shrinkage strain,  $\varepsilon_{\text{cso}}$  is the notional shrinkage coefficient,  $\beta_s$  is the coefficient to describe the development of shrinkage with time,  $t$  is the age of concrete in days,  $t_s$  is the age of concrete at the beginning of shrinkage in days,  $A_c$  is the cross section area in  $\text{mm}^2$ ,  $u$  is the perimeter in contact with the atmosphere in mm,  $f_{\text{cm}}$  is the compressive strength of concrete at age of 28 days in MPa,  $\beta_{\text{RH}}$  is the relative humidity correction factor, RH is the relative humidity in percent, and  $\beta_{\text{sc}}$  is the concrete type correction factor.

**1.3.5. GL 2000.** This model, developed by Gardener and Lockman was published in the ACI materials journal under the title “Design provisions for drying shrinkage and Creep of Normal-Strength Concrete.” The model developed is shown in **Eq. 1.39 – 1.43.**

$$\varepsilon_{sh} = \varepsilon_{shu}\beta(h)\beta(t) \quad (\mu\varepsilon) \quad (1.39)$$

$$\varepsilon_{shu} = 1000K\sqrt{\frac{30}{f'_c}} \times 10^{-6} \quad (\mu\varepsilon) \quad (1.40)$$

$$\beta(h) = 1 - 1.18h^4 \quad (1.41)$$

$$\beta(t) = \sqrt{\frac{t-t_c}{t-t_c+0.15(V/S)^2}} \quad (1.42)$$

$$K = \begin{array}{ll} 1 & \text{for type I cement} \\ 0.75 & \text{for type II cement} \\ 1.15 & \text{for type III cement} \end{array} \quad (1.43)$$

Where:  $\varepsilon_{sh}$  is the calculated shrinkage strain at a given age,  $\varepsilon_{shu}$  is the notional ultimate shrinkage strain,  $\beta(h)$  is the humidity correction factor,  $h$  is humidity in decimals,  $\beta(t)$  is the correction factor for the effect of time on shrinkage,  $t_c$  is the age that drying has commenced in days,  $t$  is age of concrete in days,  $V/S$  is the volume to surface area ratio, and  $K$  is the cement type correction factor.

#### 1.4. SCC SHRINKAGE RESEARCH

A number of shrinkage models have been developed which are formulated specifically for self consolidating concrete. The sections to follow present some shrinkage models that apply to SCC.

**1.4.1. NCHRP Report 628 (2009).** The study undertaken as part of NCHRP Report 628 concluded that the most accurate current prediction model for shrinkage of SCC was the CEB-FIP 90 at the time of investigation. Following the comparison of test data to available models, the NCHRP study also proposed a shrinkage model for SCC. This model, shown in **Eq. 1.44 – 1.47**, is simply the AASHTO 2004 prediction model with an added calibration factor, A, which accounts for effects of SCC.

$$\epsilon_{sh} = -k_s k_{hs} \left( \frac{t}{55+t} \right) 0.56 \times 10^{-3} \times A \quad (\mu\epsilon) \quad (1.44)$$

$$k_{hs} = 2.00 - 0.0143H \quad (1.45)$$

$$k_s = \left[ \frac{\frac{t}{26e^{0.0142(V/S)+t}}}{\frac{t}{45+t}} \right] \left[ \frac{1064-3.70(V/S)}{923} \right] \quad (1.46)$$

$$A = \begin{array}{ll} 0.918 & \text{for Type I/II cement} \\ 1.065 & \text{for Type III cement} \end{array} \quad (1.47)$$

Where:  $\epsilon_{sh}$  is the calculated shrinkage strain at a given age,  $k_s$  is the size factor,  $k_{hs}$  is the humidity factor, H is relative humidity in percent, t is drying time in days, V/S is the volume to surface area ratio, and A is the cement type correction factor.

**1.4.2. Shindler, et. al.** The goal of this project was to investigate the shrinkage potential of typical mixes used in precast/prestressed concrete construction. Twenty-one SCC mixes were tested along with two conventional mixes. The specimens tested were 3 in. (76.2 mm) by 3 in. (76.2 mm) by 11.25 in. (285.75 mm) prisms. They

were cured in a lime bath for seven days prior to drying. The results suggest very little difference in 28 day shrinkage between the SCC and conventional mixes. At 112 days, the SCC mixes performed better on average than the conventional mixes.

**1.4.3. Fernandez-Gomez and Landsberger.** Experimental shrinkage results were gathered from 25 published investigations. The database compiled included results from 93 SCC mixes and 30 conventional concrete (CC) mixes. The results were analyzed in order to determine which shrinkage model best fit the data. The models analyzed were CEB-FIP 90, ACI 209, B3, GL 2000, and the Spanish EHE model. The Spanish EHE model is based on the CEB-FIP 90 model; however, it doesn't include the factor accounting for cement type. The data was also analyzed to determine which material or mix parameters most influenced shrinkage strain. It was concluded that, based on three statistical models (best-fit line, residual analysis, and coefficient of variation), the B3 and ACI 209 models best predicted shrinkage results for both SCC and CC.

**1.4.4. Long, et. al.** The goal of this study was to develop equations to predict mechanical properties, workability, and visco-elastic properties of SCC. This was accomplished by evaluating 16 different SCC mixes and determining the key parameters which effect the desired properties. The parameters evaluated were the binder content, binder type, w/c, viscosity modifying admixture (VMA) content, and sand to aggregate ratio (S/A). Using statistical analysis of the data obtained, the following equations were developed. The variables in the equations are defined according to **Table 1.2**.

**Table 1.2 – Coded Values for Eqs. 1.48 – 1.49**

Absolute	Coded		
	-1	0	+1
Binder content (BC) (kg/m <sup>3</sup> )	440	470	500
Binder type (BT)	Type MS	Type MS + HE	Type HE + 20% FA
w/cm	0.34	0.37	0.40
VMA content (mL/100 kg CM)	0	50	100
Sand-to-aggregate ratio (S/A) By volume	0.46	0.50	0.54

Conversion: 1 kg/m<sup>3</sup> = 1.686 lb/yd<sup>3</sup>  
 1 mL/100kg = 1.707 fl. oz./100 lb.

56 day autogenous shrinkage:

$$\begin{aligned} \mu\varepsilon = & +201 + 67.1 \text{ BT} - 40.6 \text{ w/cm} - 18.8 (\text{BC} \cdot \text{w/cm}) \\ & +17.8 (\text{BC} \cdot \text{S/A}) \quad (\mu\varepsilon) \end{aligned} \quad (1.48)$$

112 day drying shrinkage:

$$\begin{aligned} \mu\varepsilon = & +554 - 58.1 \text{ w/cm} + 48.4 \text{ BC} + 46.2 (\text{w/cm} \cdot \text{VMA}) \\ & +41.9 (\text{w/cm} \cdot \text{BT}) - 40.6 (\text{BC} \cdot \text{VMA}) + 37.4 \text{ S/A} \\ & +30.8 (\text{VMA} \cdot \text{BT}) \quad (\mu\varepsilon) \end{aligned} \quad (1.49)$$

## 1.5. CREEP OF CONCRETE

**1.5.1. Definition of Creep.** Creep of concrete is defined as “the time-dependent increase in strain under sustained constant load taking place after the initial strain at loading.” (ACI 209.1R-05). Initial strain is the short term strain at the moment of loading. Initial strain is difficult to determine as it is very dependent on the duration and rate of initial load and there is no clear distinction between initial strain and creep strain. Creep strain can be broken up into two parts, basic creep and drying creep. Basic creep is

“the increase in strain under sustained constant load of a concrete specimen in which moisture losses or gains are prevented.” Even after 30 years of measurement on sealed concrete specimens, it had yet to be determined if basic creep approaches an ultimate value. Drying creep is the additional creep occurring in a specimen exposed to the environment and allowed to dry. The effects of creep can be expressed in three ways. The first is similar to that of shrinkage, where creep strain is simply expressed in terms of microstrain (strain  $\times 10^{-6}$ ). The second way is called the creep coefficient. The creep coefficient is the ratio of creep strain to the initial strain at loading. The third is specific creep. Specific creep is the ratio of microstrain to applied load (psi).

**1.5.2. Factors Affecting Creep.** Like shrinkage, creep is affected by numerous material, mix design, environmental, and construction related factors. Similar to shrinkage, the amount, size, gradation, and properties of the aggregate are very influential on creep of concrete. An increase in aggregate volume will decrease creep. Aggregate gradation is believed to influence creep of concrete because of its relation to changes in overall aggregate volume. The size of aggregate affects bond between paste and aggregate, which controls stress concentration and microcracking. Unlike shrinkage, which is primarily affected by properties of the paste, creep is very dependent on the elastic properties of the aggregate. Concretes with aggregate that have a lower modulus of elasticity generally have higher creep. The primary environmental factor in creep is relative humidity. As relative humidity increases, drying creep significantly decreases. Specimens in environments where drying cannot occur may have only one quarter of the creep of concrete which is allowed to dry. The effects of construction and design on creep are slightly different than shrinkage. One similarity is that increased curing time

will decrease creep strain. Unlike shrinkage, basic creep is not affected by the size and shape of the member. The factor that most affects creep is the load applied to the specimen. The magnitude of the load, and the age at which the load is first applied are very important. Loads up to  $0.40f'_c$  are considered to be linearly related to creep. Finally, concrete loaded at later ages has lower creep.

## 1.6. CREEP MODELS

As with shrinkage, considerable research has been done and models developed to predict the creep potential of concrete. The following sections will present various models for calculating creep. This includes industry models developed for use with conventional concrete as well as models developed specifically for self-consolidating concrete.

**1.6.1. ACI 209R-92.** This model is based on the same research as the ACI 209 shrinkage model. The standard conditions as shown in **Table 1.1** apply to creep as well. **Eq. 1.50 – 1.52** represent the general model for concrete meeting the standard conditions. If standard conditions are met,  $\gamma_c$  is taken to be equal to 1. Like the shrinkage model, if any or all of the standard conditions are not met, the model modification factors must be used as shown in **Eq. 1.50 – 1.59**.

$$\Phi(t, t_0) = \frac{(t-t_0)^\psi}{d+(t-t_0)^\psi} \Phi_u \quad (1.50)$$

$$\Phi_u = 2.35\gamma_c \quad (1.51)$$

$$d = 26.0e^{\{0.36(V/S)\}} \quad (1.52)$$

$$\gamma_c = \gamma_{c,t_0} \gamma_{c,RH} \gamma_{c,vs} \gamma_{c,s} \gamma_{c,\psi} \gamma_{c,\alpha} \quad (1.53)$$

$$\gamma_{c,t_0} = \begin{cases} 1.25t_0^{-0.118} & \text{for moist curing} \\ 1.13t_0^{-0.094} & \text{for steam curing} \end{cases} \quad (1.54)$$

$$\gamma_{c,RH} = 1.27 - 0.67h \quad (1.55)$$

$$\gamma_{c,vs} = \frac{2}{3} (1 + 1.13e^{\{-0.54(V/S)\}}) \quad (1.56)$$

$$\gamma_{c,s} = 0.82 + 0.067s \quad (1.57)$$

$$\gamma_{c,\psi} = 0.88 + 0.0024\psi \quad (1.58)$$

$$\gamma_{c,\alpha} = 0.46 + 0.09\alpha \geq 1 \quad (1.59)$$

Where:  $\Phi(t,t_0)$  is the calculated creep coefficient at a given age,  $\Phi_u$  is the calculated ultimate creep coefficient,  $t$  is the age of the specimen in days,  $\gamma_{c,t_0}$  is the curing condition correction factor,  $t_0$  is the age at which the specimen is loaded in days,  $\gamma_{c,RH}$  is the humidity correction factor,  $h$  is relative humidity in decimals,  $\gamma_{c,vs}$  is the size correction factor,  $V/S$  is the volume to surface area ratio,  $\gamma_{c,s}$  is the slump correction factor,  $s$  is slump in inches,  $\gamma_{c,\psi}$  is the fine aggregate correction factor,  $\psi$  is the ratio of fine aggregate to total aggregate by weight expressed as percentage,  $\gamma_{c,\alpha}$  is the air content correction factor, and  $\alpha$  is the air content in percent. For shape and size effects to be totally

considered,  $d$  is to be determined using **Eq. 1.52** and  $\psi$  assumed to be equal to 1.0. Otherwise, average values of  $d=10$  and  $\psi=0.6$  are to be assumed.

**1.6.2. NCHRP Report 496.** This proposed creep model was developed in a similar manner to that of the NCHRP Report 496 shrinkage model. The correction factors that are identical to those used in the corresponding shrinkage model have already been defined in Section 1.3.2. The model is shown in **Eq. 1.60 – 1.66**.

$$\psi(t, t_i) = 1.90\gamma_{cr} \quad (1.60)$$

$$\gamma_{cr} = k_{td}k_{la}k_s k_{hc}k_f \quad (1.61)$$

$$k_{td} = \frac{t}{61-4f'_{ci}+t} \quad (1.62)$$

$$k_{la} = t_i^{-0.118} \quad (1.63)$$

$$k_s = \frac{1064-94V/S}{735} \quad (1.64)$$

$$k_{hc} = 1.56 - 0.008H \quad (1.65)$$

$$k_f = \frac{5}{1+f'_{ci}} \quad (1.66)$$

Where:  $\psi(t, t_i)$  is the calculated creep coefficient at a given age,  $k_{td}$  is the time development factor,  $t$  is the age of the concrete in days,  $k_{ta}$  is the loading factor,  $t_i$  is the age at which creep specimen is loaded in days,  $k_s$  is the size factor,  $V/S$  is the volume to surface area ratio,  $k_{hc}$  is the humidity factor,  $H$  is the average ambient relative humidity in percent,  $k_f$  is the concrete strength factor, and  $f'_{ci}$  is the specified compressive strength of concrete in ksi.

**1.6.3. CEB-FIP 90.** The following equations apply to the creep model as developed jointly by CEB and FIP as presented in the CEB-FIP Model Code 1990.

$$\Phi(t, t_0) = \Phi_0 \beta_c(t - t_0) \quad (1.67)$$

$$\Phi_0 = \Phi_{RH} \beta(f_{cm}) \beta(t_0) \quad (1.68)$$

$$\Phi_{RH} = 1 + \frac{1 - RH}{0.46 \left( \frac{2A_c}{100u} \right)^{1/3}} \quad (1.69)$$

$$\beta(f_{cm}) = \frac{5.3}{(f_{cm}/10)^{0.5}} \quad (1.70)$$

$$\beta(t_0) = \frac{1}{0.1 + t_0^{0.2}} \quad (1.71)$$

$$\beta_c(t - t_0) = \left[ \frac{(t - t_0)}{\beta_H + (t - t_0)} \right]^{0.3} \quad (1.72)$$

$$\beta_H = 150 \{ 1 + (1.2RH)^{18} \} \left( \frac{2A_c}{100u} \right) + 250 \leq 1500 \quad (1.73)$$

Where:  $\Phi(t, t_0)$  is the calculated creep coefficient at a given age,  $\Phi_0$  is the notional creep coefficient,  $\beta_c$  is the coefficient to describe the development of creep with time after loading,  $t$  is the age of concrete in days,  $t_0$  is the age of concrete at loading in days, RH is the relative humidity in decimals,  $A_c$  is the cross section area in  $\text{mm}^2$ ,  $u$  is the perimeter in contact with the atmosphere in mm, and  $f_{cm}$  is the mean compressive strength of concrete at the age of 28 days in MPa.

**1.6.4. GL 2000.** As with the GL 2000 shrinkage model, the following creep model was published in the ACI materials journal under the title “Design Provisions for Drying Shrinkage and Creep of Normal-Strength Concrete”.

$$\Phi_{28} = \Phi(t_c) \left[ 2 \left( \frac{(t-t_c)^{0.3}}{(t-t_c)^{0.3}+14} \right) + \left( \frac{7}{t_0} \right)^{0.5} \left( \frac{t-t_c}{t-t_c+7} \right)^{0.5} + 2.5(1 - 1.086h^2) \left( \frac{t-t_0}{t-t_0+97(V/S)^2} \right)^{0.5} \right] \quad (1.74)$$

$$\Phi(t_c) = \left[ 1 - \left( \frac{t-t_c}{t-t_c+97(V/S)^2} \right)^{0.5} \right]^{0.5} \quad (1.75)$$

Where:  $\Phi_{28}$  is the calculated creep coefficient at a given age,  $\Phi(t_c)$  is a factor that takes into account drying before loading,  $t$  is age of concrete in days,  $t_c$  is the age of concrete when drying begins,  $t_0$  is the age the concrete was loaded,  $h$  is humidity in decimals, and  $V/S$  is the volume to surface area ratio in mm.

## 1.7. SCC CREEP RESEARCH

**1.7.1. NCHRP Report 628.** As with shrinkage, NCHRP 628 presents an SCC specific creep prediction model which is a modified version of the AASHTO 2004 model. **Eq. 1.76 – 1.81** are used to calculate creep of SCC using the proposed modification factor.

$$\psi(t, t_i) = 1.9k_{vs}k_{hc}k_fk_{td}k_i^{-0.118} \times A \quad (1.76)$$

$$k_{vs} = 1.45 - 0.0051(V/S) \geq 0 \quad (1.77)$$

$$k_{hc} = 1.56 - 0.08H \quad (1.78)$$

$$k_f = \frac{35}{7+f'_{ci}} \quad (1.79)$$

$$k_{td} = \left( \frac{t}{61 - 0.58f'_{ci} + t} \right) \quad (1.80)$$

$$A = \begin{cases} 1.19 & \text{for Type I/II cement} \\ 1.35 & \text{for Type III cement} \end{cases} \quad (1.81)$$

Where:  $\psi(t, t_i)$  is the calculated creep coefficient,  $k_{vs}$  is the volume to surface area factor,  $V/S$  is the volume to surface area ratio,  $k_{hc}$  is the humidity correction factor,  $H$  is relative humidity in percent,  $k_f$  is the concrete strength factor,  $f'_{ci}$  is the concrete compressive strength at time of loading in MPa,  $k_{td}$  is the time development factor,  $t$  is age of concrete since loading in days, and  $A$  is the cement type correction factor.

**1.7.2. Long and Khayat.** A total of 16 SCC mixes were tested for creep. The purpose of this experimental program was to determine the key mixture design and material selection parameters that most affect creep of SCC. Additionally, conclusions were made on which current creep prediction model best estimates creep of SCC. It was found that the binder type (i.e. cementitious materials) was most influential on creep of SCC, followed by binder content. The model that best predicts creep of SCC was found to be CEB-FIP 90. The modified AASHTO model described in Section 1.7.1. was also determined to successfully predict creep of SCC.

**1.7.3. Long, et. al.** The same study as described in Section 1.4.4 was also done to develop a prediction equation for creep strain of SCC. The following equation was developed to predict creep of SCC, with the same variable definitions as shown in **Table 1.2.**

112 day creep strain ( $\mu\epsilon$ ):

$$\begin{aligned}
 &+1036 + 73.6 BT + 40.7 (VMA \cdot BT) + 38.8 BC \\
 &+34.9 (w/cm \cdot BT) - 32.9 (BC \cdot S/A)
 \end{aligned}
 \tag{1.82}$$

## **1.8. Application of Shrinkage and Creep**

**1.8.1. Prestress Loss.** Prestress loss is “the loss of compressive force acting on the concrete component of a prestressed concrete section.” (NCHRP 426) The ability to accurately predict the prestress loss in beams is very dependent on the ability to predict the beam’s shortening due to shrinkage and creep. Shortening of the beam reduces the tensile force in the prestressed reinforcement and must be accounted for in design.

NCHRP 426 names three components which significantly affect the prestress loss in pretensioned concrete members which directly relate to shrinkage and creep. These components are:

1. Instantaneous prestress loss due to elastic shortening at transfer of force from prestressed reinforcement to concrete.
2. Long-term prestress loss due to shrinkage and creep of concrete and relaxation of prestressing strands between the time of transfer and deck placement.
3. Long-term prestress loss between the time of deck placement to the final service life of the structure due to shrinkage and creep of the girder.

**Figure 1.2** shows the prestress loss over the life cycle of a pretensioned concrete girder. The loss between points D and E represent the loss due to creep, shrinkage, and relaxation of prestressing strands.

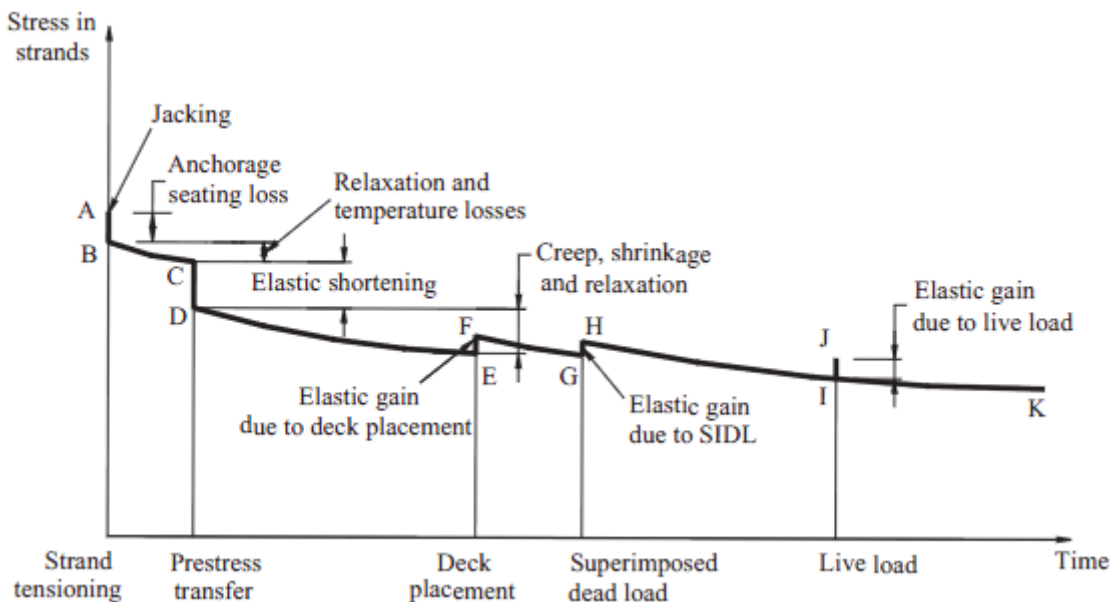


**Figure 1.2 - Stress vs. Time for Prestressed Bridge Girder (Tadros et. al. 2003)**

**1.8.2. Load Effects.** The procedures in “Design of Continuous Highway Bridges with Precast, Prestressed Concrete Girders” published by the Portland Cement Association (PCA) take into account additional moments due to shrinkage and creep when determining loads for design. In this method, fixed end moments due to creep and end driving moments due to shrinkage are calculated. These applied moments result from a continuity connection being made at supports by the placement of the bridge deck. The placement restricts free rotation of the beams and therefore produces moment in the connection. The moments calculated by this method are then added to all other load effects at all sections for determination of the ultimate design load. The shrinkage driving moment calculation is done by first calculating theoretical ultimate shrinkage values for the beam and the slab. The differential shrinkage between the beam and slab are then used to determine an applied moment due to shrinkage. The applied moment due to creep results from prestressed creep and dead load creep. Theoretical creep coefficients are calculated for the time before and after deck placement. The creep that occurs after deck placement is what contributes to the applied moment.

**1.8.3. Beam Deflection.** Shrinkage and creep must also be accounted for when calculating long term deflection of flexural members. Eq. 9-11 of ACI 318-08, shown here as **Eq. 1.83**, accounts for long term sustained loads. This factor is multiplied by the immediate deflection caused by the load considered.

$$\lambda_{\Delta} = \frac{\xi}{1+50\rho'} \quad (1.83)$$

Where:  $\lambda_{\Delta}$  is the multiplier for additional deflection due to long-term effects,  $\xi$  is the time dependent factor for sustained load, and  $\rho'$  is compression reinforcement ratio.

## **1.9. CONCRETE ABRASION**

**1.9.1. Definition of Concrete Abrasion.** Abrasion is the physical wearing down of a material. The most common sources of abrasion of concrete structures are by the friction between vehicle tires and concrete pavement road surfaces, and by water flows over exposed dam or bridge footings. Concrete abrasion leads to a decrease in member thickness which can lead to cracking or failure of the structure (Atis).

**1.9.2. Factors Affecting Concrete Abrasion.** Several material properties and construction factors can affect the abrasion resistance of concrete. The concrete strength is the most influential property in regards to abrasion resistance. The properties of the aggregate are also very important in a concrete's resistance to abrasion. The surface finish and whether or not a hardener or topping is used effects abrasion resistance as well (Naik et. al.).

## **1.10. SCC ABRASION RESEARCH**

Little research has been done on self-consolidating concrete's abrasion resistance relative to conventional concrete. This is most likely due to the fact that the use of SCC is not motivated primarily by its hardened properties but by its fresh concrete properties. Also SCC members are less likely to be exposed to abrasive action as SCC is normally reserved for use in pre-stressed members such as girders which are typically not exposed to vehicles or water.

## 2. RESEARCH PROGRAM

### 2.1. MIX DESIGNS

**2.1.1. SCC.** The SCC testing program consisted of four mixes, two being SCC with two as conventional concrete equivalents to the SCC mixes. The naming convention used in the SCC testing program begins with either C (conventional concrete) or S (SCC). The next number indicates the target 28 day compressive strength, in ksi. Following the dash is a number indicating the ratio of fine aggregate to total aggregate by weight. It finishes with L, indicating the type of coarse aggregate used, dolomitic limestone. The baseline normal strength concrete tested was MoDOT A-1 (C6-58L). The A-1 mix was used as the comparative mix to the normal strength SCC mix (S6-48L). Both mixes had identical w/c and air content, with the aggregate ratio and HRWR dosage adjusted. The S6-28L mix design was based on the average of survey responses from regional precast plants. The baseline high strength concrete (C10-58L) mix design was based on research done by Myers and Carrasquillo (2000) at the University of Texas at Austin. The high strength SCC mix (S10-48L) was designed based on the C10-58L mix design and finalized after trial batches were made and adjusted. The designs of the mixes tested can be found in **Table 2.1** along with measured 28 day compressive strength ( $f'_c$ ) and modulus of elasticity (MOE). All mixes and specimens were batched and cast in the Missouri University of Science and Technology (Missouri S&T) concrete lab located in Butler-Carlton Hall. All testing was done in the High Bay Structures Engineering Laboratory (SERL) also located in Butler-Carlton Hall on the campus of Missouri S&T. Due to the large volume of concrete produced for various studies associated with this overall research program (i.e. Reports A, B, C, D, and E) some concrete production was

done in separate batches on different days resulting in some minor variations in concrete properties between various reports.

**Table 2.1 - SCC Test Program Mix Designs and mechanical properties**

Material	Amount (per cubic yard)			
	C6-58L	S6-48L	C10-58L	S10-48L
Water	277.5 lb.	277.5 lb.	315 lb.	315 lb.
Cement	750 lb. (Type I)	750 lb. (Type I)	840 lb. (Type III)	840 lb. (Type III)
Coarse Aggregate	1610 lb.	1333 lb.	1440 lb.	1192 lb.
Fine Aggregate	1444 lb.	1444 lb.	1043 lb.	1291 lb.
Fly Ash	N/A	N/A	210 lb.	210 lb.
BASF MB-AE-90 (air entrainment)	2.3 fl oz/cwt	1.2 fl oz/cwt	1.25 fl oz/cwt	1.0 fl oz/cwt
BASF Glenium (HRWR)	4.7 fl oz/cwt	6.2 fl oz/cwt	4.9 fl oz/cwt	6.0 fl oz/cwt
f'c (psi)	7,000	5,500	11,000	13,500
MOE (psi)	3,450,000	3,130,000	3,900,000	4,200,000

Conversion:  $1 \text{ kg/m}^3 = 1.686 \text{ lb/yd}^3$

1 fl oz = 26.57 mL

1 psi = 6.89 kPa

## 2.2. SHRINKAGE AND CREEP SPECIMEN CONSTRUCTION

**2.2.1. Shrinkage and Creep Specimens.** Both shrinkage and creep testing were done using identical specimens. Although only four specimens per mix were necessary for testing (two each for shrinkage and creep), six specimens per mix were cast in case any specimens were damaged during de-molding. These specimens were fabricated and prepared as described below.

**2.2.2. Shrinkage and Creep Molds.** The molds for the shrinkage and creep specimens were 4 in. diameter PVC pipe adhered to a plywood base. The PVC was cut into 24 in. sections with care being taken to ensure all cuts were made so that the mold would sit flush and orthogonal to the base. The PVC was also notched on opposite sides. The notches made de-molding much easier and significantly reduced the possibility of damaging the specimens during de-molding. Once prepared the PVC was adhered to a 1 ft. (304.8 mm) by 1 ft. (304.8 mm) plywood base using a waterproof silicon sealant. The completed molds were allowed to sit for at least 24 hours before use to allow for the sealant to fully set up. **Figure 2.1** shows a completed shrinkage and creep mold.



**Figure 2.1 - Shrinkage and Creep Form**

**2.2.3. Shrinkage and Creep Specimen Casting.** Specimens were consolidated in a manner similar to that prescribed in ASTM C31 “Standard Practice for Making and Curing Concrete Test Specimens in the Field” for a 6 in. diameter cylinder.

Consolidation and vibration were performed when necessary. The specimens were cast in three layers of approximately equal depth and were rodded 25 times per layer for all mixes. External vibration was also performed after each layer was rodded using an electric handheld concrete vibrator as needed. Specimens were moist cured until de-molded and prepared.

**2.2.4. Shrinkage and Creep De-Molding and Preparation.** All specimens were de-molded within 24 hours of their initial set time. De-molding was done by first cutting through the notched section with a utility knife. A hammer and chisel were then used to split the mold and remove it from the concrete. Creep specimens were sulfur capped on both ends in preparation for loading at 28 days. Shrinkage specimens were sulfur capped on only the bottom end, allowing for stability and more accurate readings.

**2.2.5. Shrinkage and Creep Data Acquisition.** A demountable mechanical strain gauge (DEMEC) was used to measure strain in the concrete. DEMEC points, small pre-drilled stainless steel discs, were adhered to the surface of the specimen. They were arranged in three vertical lines of five points, 120° apart, as shown in **Fig. 2.2**. This arrangement allowed for 9 readings to be taken per specimen. The average of all readings taken per specimen was taken as the value to be used for strain calculation. The points in one line per specimen were adhered using gel control super glue. The instant hardening allowed for initial readings to be made on each specimen as soon as possible.

The remaining points were adhered using concrete/metal epoxy, which took up to 24 hours to fully harden for accurate reading to be taken. The points adhered with super glue were later protected using the epoxy.

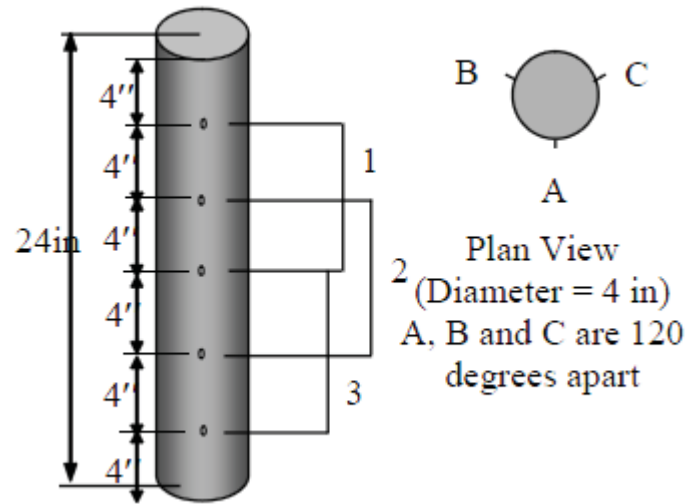


**Figure 2.2 – Shrinkage and Creep Specimens and DEMEC Point Arrangement (Myers and Yang, 2005)**

### 2.3. ABRASION SPECIMEN CONSTRUCTION

One specimen per mix was cast for abrasion test. Each specimen was large enough so that three replicate abrasion tests could be done for each mix. Abrasion specimens measured 6 in. (152.4 mm) by 16 in. (406.4 mm) by 3.5 in. (88.9 mm) and were cast in a mold made from wooden 2x4 sections and attached to a plywood base. The baseline mixes were consolidated similar to that prescribed in ASTM C31 “Standard Practice for Making and Curing Concrete Test Specimens in the Field” for a 6 in. (152.4 mm) wide beam. External vibration was used as necessary. To ensure that abrasion tests on all specimens were consistent, every specimen tested was finished by the same individual using a hand trowel. Specimens were moist cured until tested. All testing was performed on the top finished surface of the specimen.

## 2.4. TESTING PROCEDURES

**2.4.1. Shrinkage Testing Procedures.** A modified version of ASTM C157 “Standard Test Method for Length Change of Hardened Hydraulic-Cement Mortar and Concrete” was used to determine the shrinkage of the concrete specimens. Until the age of loading for creep, four specimens were used for shrinkage determination. At 28 days, two of these specimens were transferred to creep frames, leaving two remaining specimens to be tested for long term shrinkage. Nine strain readings could be taken per specimen, with the average of all readings taken as the value to be used for shrinkage calculation. Strain was determined using the DEMEC readings and calculated by **Eq. 2.1** as found in “Simplified Instructions for Using a Digital DEMEC Gauge”. An example of a DEMEC reading being taken on a specimen is shown in **Figure 2.3**. Readings were normalized by taking a reading on the reference bar (see **Figure 2.4**) as shown in **Figure 2.5**. Shrinkage strain experienced during the first day after demolding was estimated based on linear interpolation of subsequent strain values, as calculated by **Eq. 2.1**

$$\Delta\varepsilon_s = G((R_i - R_0) - (D_i - D_0)) \quad (\mu\varepsilon) \quad (2.1)$$

Where:  $\Delta\varepsilon_s$  is the change in strain from one reading to the next, G is the gauge factor shown in **Figure 2.6**,  $0.400 \times 10^{-5}$  strain per division (4 microstrain),  $D_0$  is the datum reading on the reference bar,  $D_i$  is the subsequent reading on the reference bar,  $R_0$  is the datum reading on the tested material, and  $R_i$  is the subsequent reading on the tested material. Gauge units are the digital gauge reading without the decimal point. For example, **Figure 2.7** shows a reading of 2.523 which equates to 2523 gauge units.



**Figure 2.3 – DEMEC Reading Taken on Specimen**



**Figure 2.4 - Reference Bar**



Figure 2.5 - Reading Taken on Reference Bar



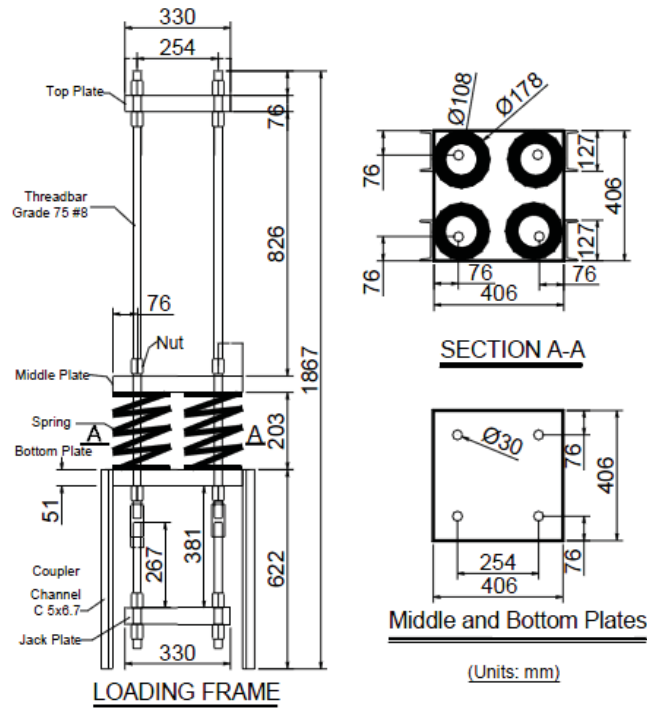
Figure 2.6 - Gauge Factor Used for Shrinkage and Creep Calculations



Figure 2.7 - Example DEMEC Gauge Reading

**2.4.2. Creep Testing Procedures.** A modified version of ASTM C512 “Standard Test Method for Creep of Concrete in Compression” was used to determine the creep of the concrete specimens tested. Until the age of loading, creep specimens acted as shrinkage specimens. This is a modification of ASTM C512, as the specimens were not moist cured beyond the time of de-molding. Additionally, humidity was not controlled however it was recorded.

At 28 days, representative specimens were tested according to ASTM C39 “Standard Test Method for Compressive Strength of Cylindrical Concrete Specimens” and ASTM C469 “Standard Test Method for Static Modulus of Elasticity and Poisson’s Ratio of Concrete in Compression.” Creep specimens were then loaded to 40% of their measured 28 day compressive strength in the creep frames shown in **Figures 2.8 – 2.9**. The design of the creep frames was based on research done by Myers and Yang (2005).



**Figure 2.8 - Schematic of Creep Loading Frame (Myers and Yang, 2004)**  
(1 in = 25.4 mm)



**Figure 2.9 - Creep Loading Frame with Specimen**

Measurements taken on creep specimens were done in the exact way as with the shrinkage specimens. **Eq. 2.2** was used to determine the change in strain between one creep reading to the next. Using the calculated creep strain, the coefficient of creep could be determined by **Eq. 2.3**. Creep and shrinkage readings for like specimens were taken at the same interval. Readings were also taken immediately before and after loading to determine initial elastic strain due to loading. **Figure 2.10** shows a reading being taken on a creep specimen.

$$\Delta\varepsilon_c = G((R_i - R_0) - (D_i - D_0)) - \Delta\varepsilon_s \quad (\mu\varepsilon) \quad (2.2)$$

Where:  $\Delta\varepsilon_c$  is the change in creep strain between readings.

$$\Phi(t, t_0) = \varepsilon_t / \varepsilon_i \quad (2.3)$$

Where:  $\Phi(t, t_0)$  is the measured creep coefficient at a given age,  $\varepsilon_i$  is the measured strain due to initial loading of the specimen,  $\varepsilon_t$  is the measured creep strain at a given age.

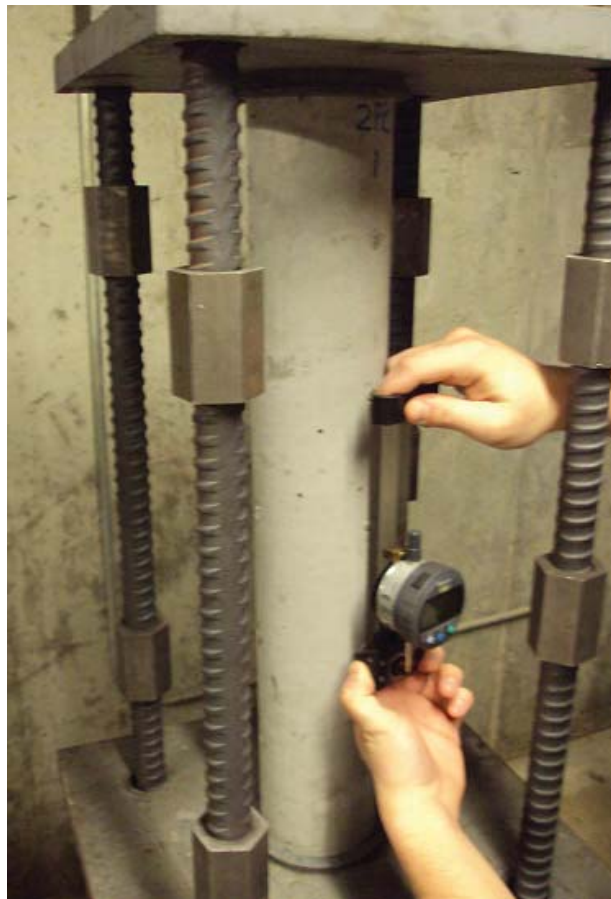


**Figure 2.10 - Reading Taken on Creep Specimen**

**2.4.3. Abrasion Resistance Testing Procedures.** ASTM C944 “Standard Test Method for Abrasion Resistance of Concrete or Mortar Surfaces by the Rotating-Cutter Method” was used to determine abrasion resistance. A schematic of the rotating cutter used is shown in **Figure 2.11**, which is taken from ASTM C944. The actual rotating cutter is shown in **Figure 2.12**. Abrasion specimens were moist cured until testing at 28 days age. One specimen per mix was constructed, which allowed for three abrasion tests. One abrasion test consisted of three abrasion cycles. Each cycle lasted two minutes. A load of 44lb, defined as a double load in ASTM C944, was applied at a rate of 300 rpm using a drill press as shown in **Figure 2.13**. After each cycle, mass loss (mg) was recorded by subtracting the final weight from the initial weight. Each cycle per test was done on the same spot. After completion of each abrasion test, the average depth of wear (mm) was measured using digital calipers. The average depth of wear was calculated from a total of eight depth measurements relative to the adjacent untested surface, four taken on the outer perimeter of the tested surface and four taken around the inner perimeter, at the points indicated in **Figure 2.14**. The measurements were made using a digital caliper. On the day of testing, the specimen was removed from moist cure and surface dried by blotting with paper towels. This was done to avoid any mass loss due to moisture loss. A completed specimen after all three abrasion tests is shown in **Figure 2.15**.

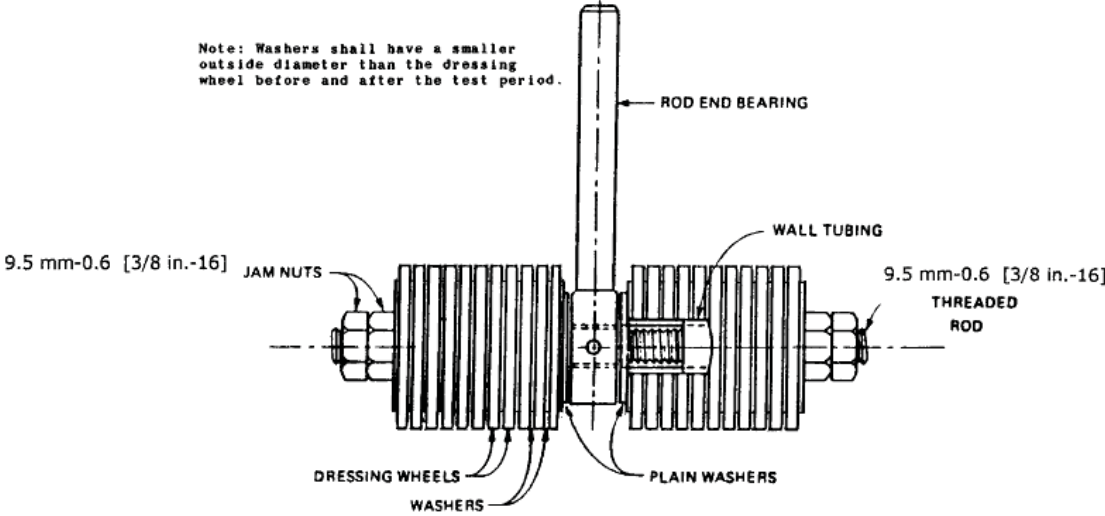


Figure 2.11 - Schematic of Abrasion Rotating Cutter (ASTM C944)  
(1 in = 25.4 mm)



Figure 2.12 - Rotating Cutter



Figure 2.13 - Abrasion Resistance Test In Progress

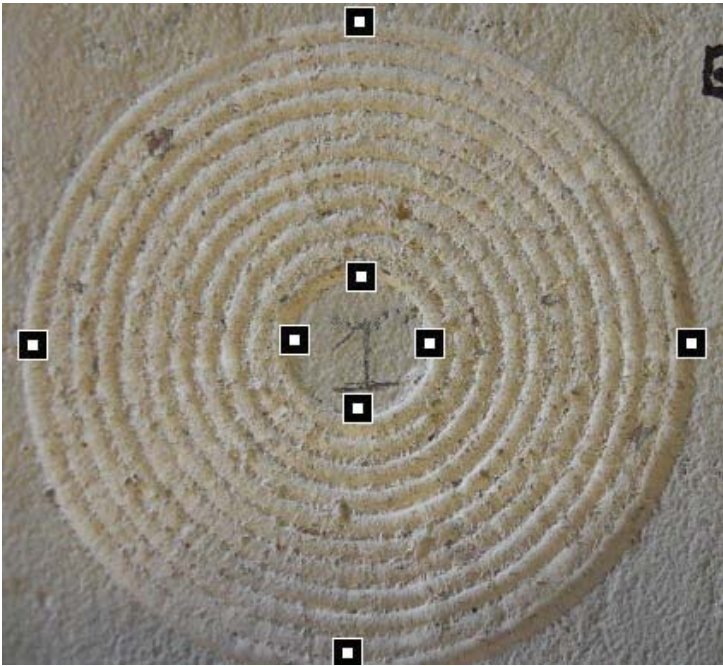


Figure 2.14 - Depth of Wear Measurement Points



**Figure 2.15 - Abrasion Resistance Specimen After Testing**

### 3. SCC RESULTS AND DISCUSSION

#### 3.1. SHRINKAGE

**3.1.1. Results.** Figures 3.1 – 3.4 show the experimental data obtained from shrinkage tests of SCC plotted with the various prediction models discussed in Section 1. Figure 3.5 shows the experimental results of all four mixes plotted with one another. In figures where different data sources are together, the source of the data can be found in parentheses after the data label in the legend of its respective figure. All data obtained in this study was gathered at Missouri S&T.

**3.1.2. Discussion and Conclusions.** For the lower strength variations, C6-58L and S6-48L, the relative shrinkage strains are not consistent with the SCC prediction model found in NCHRP Report 628. This model was a modification of the AASHTO prediction model, with an added factor to account for the effects of SCC. In the NCHRP Report 628 model, SCC made using Type I/II cement should show a reduction in shrinkage strain. The reduction factor in NCHRP Report 628 for SCC with Type I/II cement is 0.918, therefore it is expected that S6-48L would have a reduction in shrinkage strain. The reason for this inconsistency with previous data could be the difference in mix designs used in this project compared to others. Since shrinkage of concrete is most related to shrinkage of paste, it would be expected that mixes with higher paste volumes would experience more shrinkage. Relative to all mixes tested by Schindler, et. al., S6-48L had a greater cement content, fine aggregate content, and FA/CA ratio. In a similar study done by Long, Khayat and Xing, it was concluded that shrinkage is highly affected by binder content. The relatively high binder content and low coarse aggregate content of S6-48L could be the reason for the large shrinkage strains.

For high strength variations, C10-58L and S10-48L, the experimental results are very consistent with previous findings. Schindler, et. al. reported that high strength SCC mixes show a reduction in shrinkage relative to high strength conventional concrete. Therefore it can be expected that, in terms of shrinkage, high strength SCC is an adequate alternative to conventional high strength concrete.

Besides the mix designs themselves, the environment the specimens were exposed to seemed to have a significant effect on shrinkage. As seen in Appendix A, there is a correlation between shrinkage and relative humidity. The unexpected decreases in shrinkage that were measured tend to correspond to days with unusually high relative humidity. This confirms the relationship given by **Eq. 1.1** from ACI 209.1R-05 which states that shrinkage is inversely related to relative humidity.

Comparing the results to previous studies, both SCC mixes perform adequately. **Table 3.1** and **Figure 3.6** show the shrinkage data of S6-48L and S10-48L relative to the database compiled in Fernandez-Gomez and Landsberger, Shindler et. al., and Holshemacher and the equations developed by Long, et.al. The 112 day shrinkage strains calculated from Long et. al. are the 56 day autogenous shrinkage (**Eq. 1.48**) added to the 112 day drying shrinkage (**Eq. 1.49**). This is acceptable as it has been shown that autogenous shrinkage reaches stable values after 56 days (Long, Khayat, and Xing). Results from this study are consistent with the database compiled by Fernandez-Gomez and Landsberger, which includes 93 SCC mixes. At all ages that were tested in this study the results for both S6-48L and S10-48L fall within the limits of the database. When comparing to the shrinkage prediction equations developed by Long et. al., however, S6-48L doesn't seem to perform quite as well. Again, when comparing S10-48L to this

previous SCC shrinkage study, it performs very well. Below is a summary figure showing the SCC mixes tested in this program shown with the databases compiled by Fernandez-Gomez and Landsberger, Schindler et. al., and Holschemacher. The shrinkage from Schindler et. al. is likely lower due to the specimens being submerged in a lime bath for the first 7 days.

Finally, results for the normal strength variations are consistent with the observation made by Holschemacher (2004) that “In the majority of the evaluated data the shrinkage of SCC is 10 to 50% higher than the one of conventional concrete.” At 150 days, S6-48L had experienced 24% greater shrinkage than C10-58L. This trend, however, does not hold true for the high strength variations.

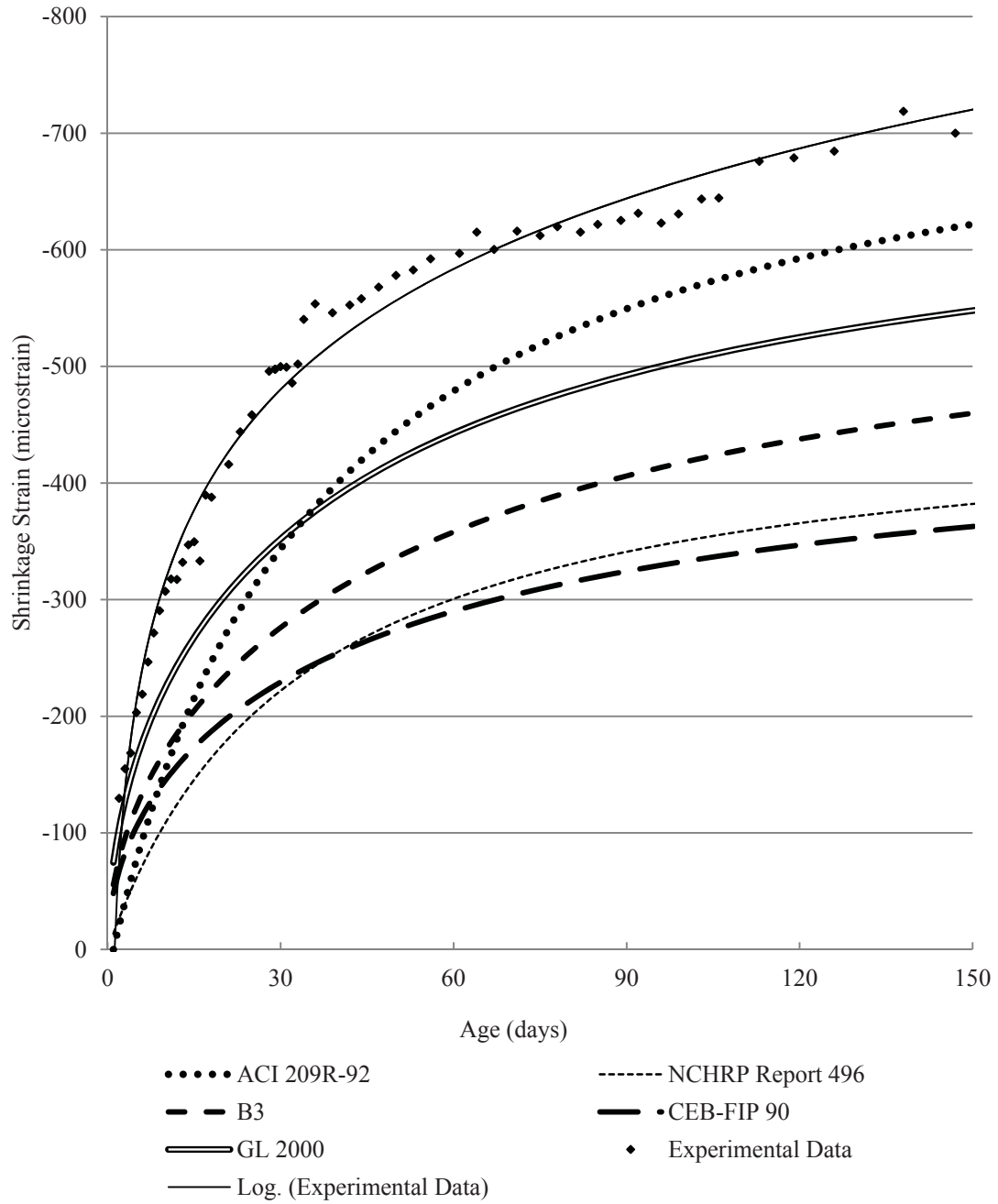


**Figure 3.1 - C6-58L Shrinkage Results and Prediction Models**

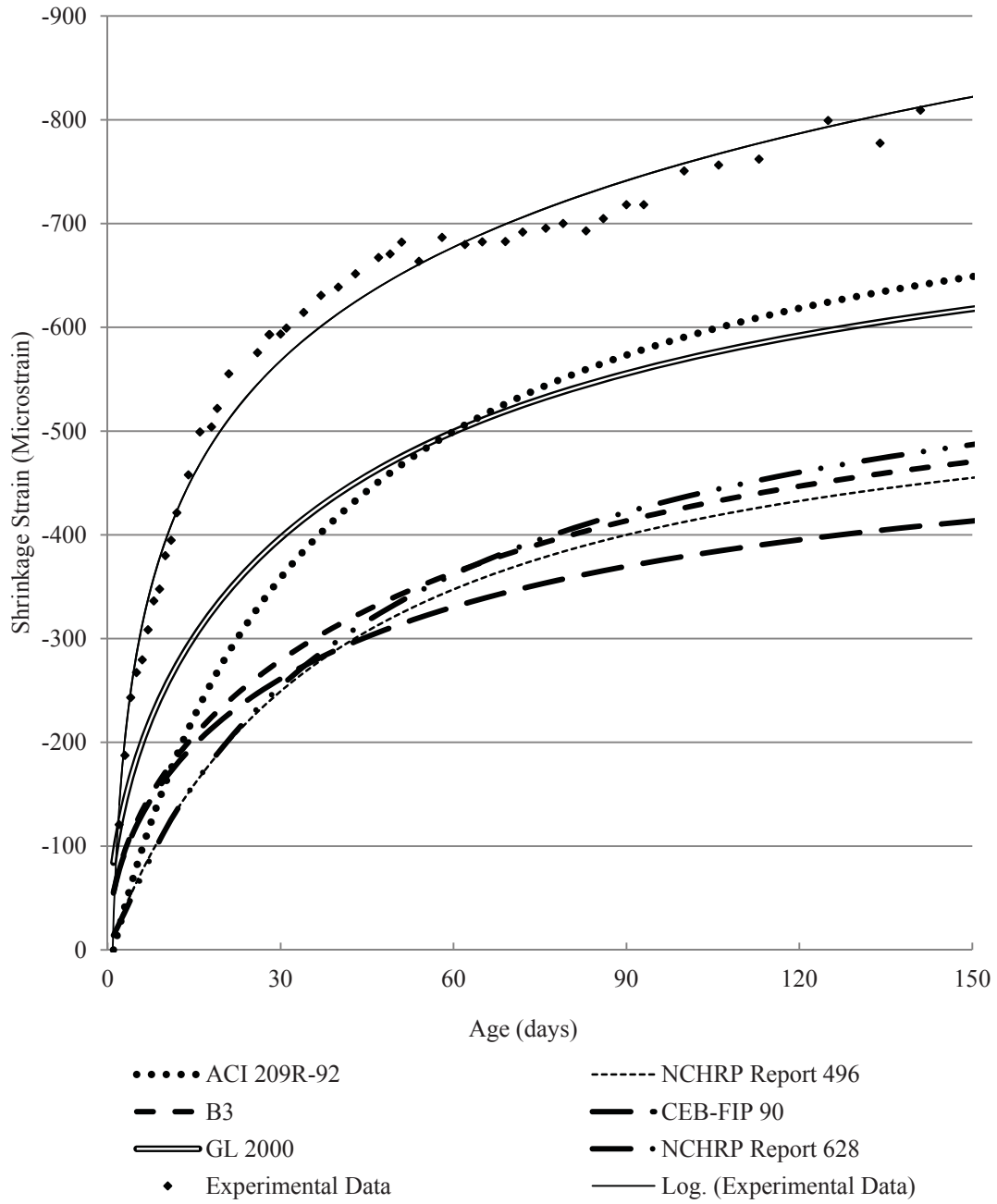


**Figure 3.2 - S6-48L Shrinkage Results and Prediction Models**

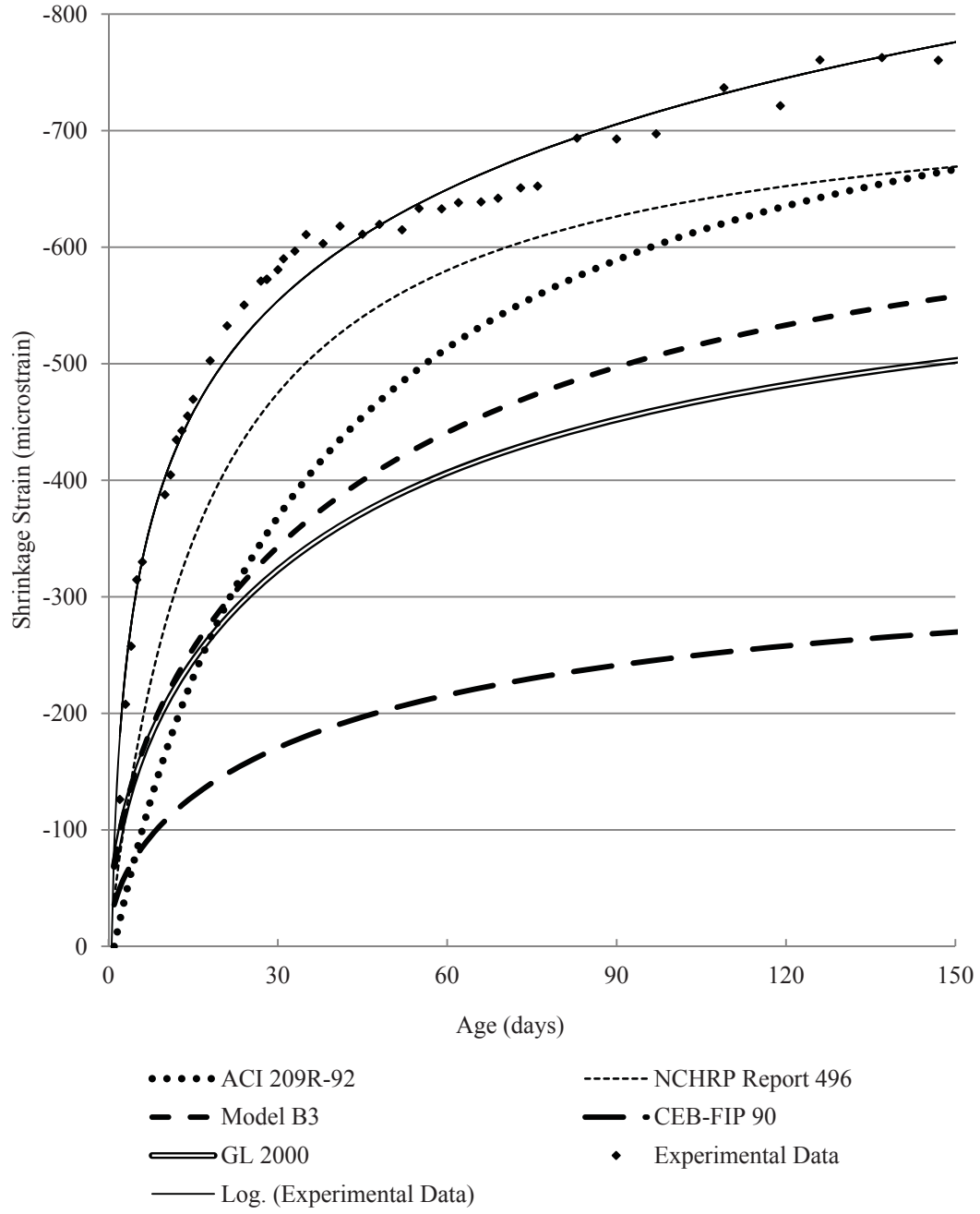


**Figure 3.3 - C10-58L Shrinkage Results and Prediction Models**

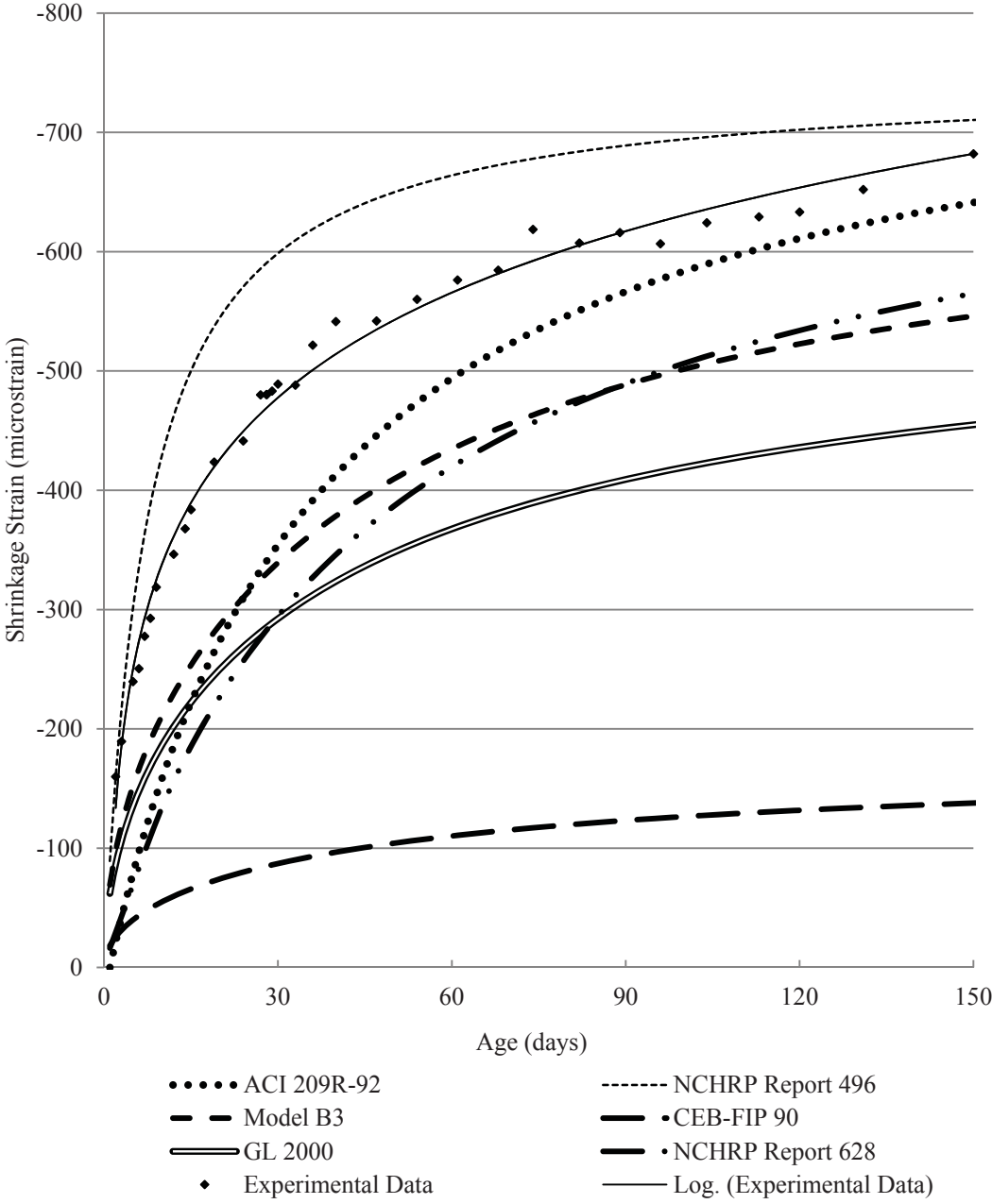
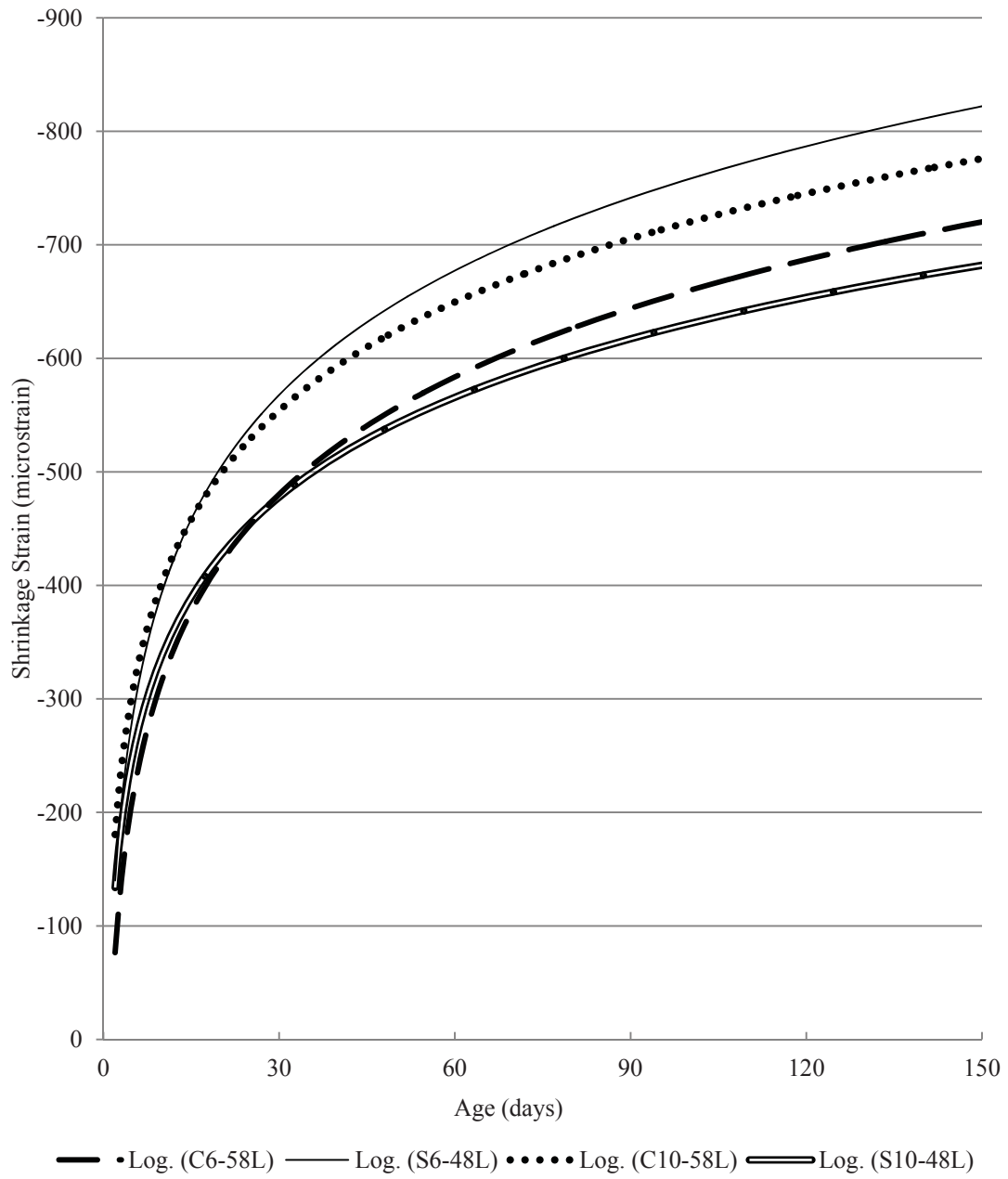
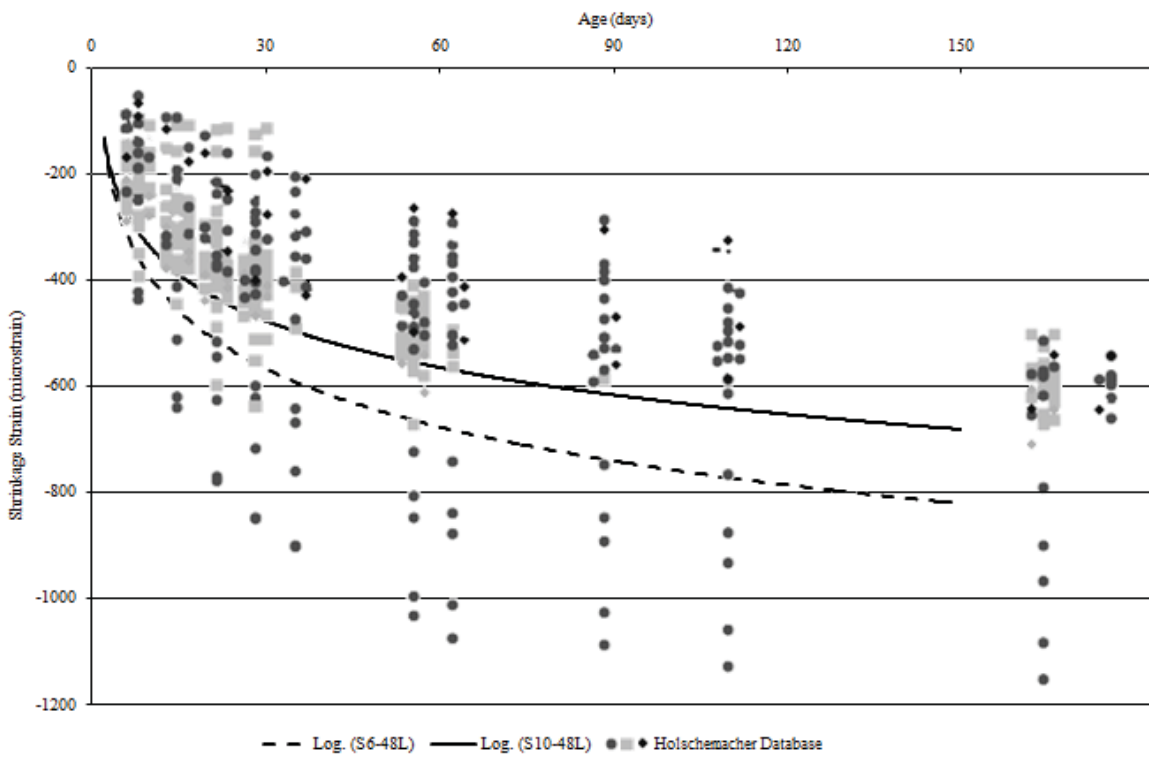
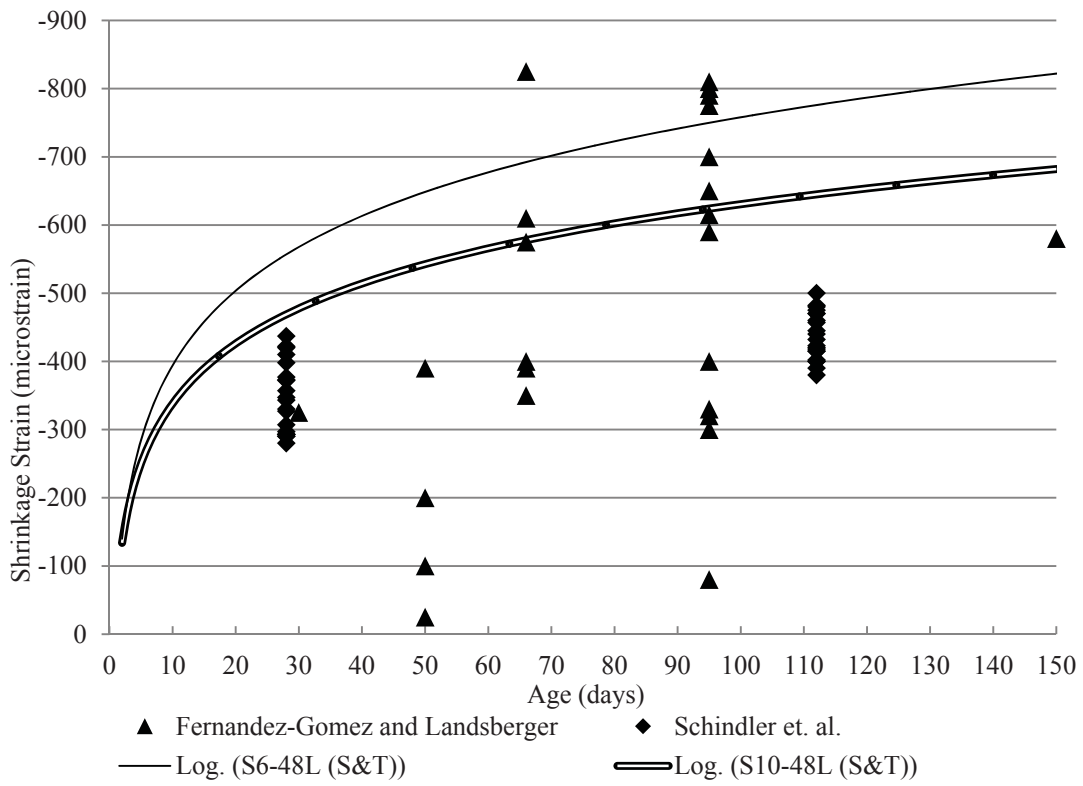


Figure 3.4 - S10-58L Shrinkage Results and Prediction Models



**Figure 3.5 - SCC Shrinkage Results (Best fit Logarithmic)**



**Figure 3.6 – SCC Results with Shrinkage Databases (Fernandez-Gomez, Shindler et. al., and Holschemacher)**

**Table 3.1 – SCC results compared to Eqs. 2.48 – 2.49 by Long et. al.**

Specimen	112 Day Measured Shrinkage Strain (microstrain)	112 Day Theoretical Shrinkage Strain (microstrain)
S6-48L	-761	-659
S10-48L	-628	-1029

### 3.2. CREEP

**3.2.1. Results.** Creep Results are shown in **Table 3.2** and **Figure 3.7**. In figures where different data sources are together, the source of the data can be found in parentheses after the data label in the legend of its respective figure. For all specimens tested for this study, the notation (S&T) will be used.

**Table 3.2 - Summary of SCC Creep Results**

Creep Strain (microstrain)				
Specimen	Days After Loading			
	7	14	56	126
C6-58L	282	329	608	862
S6-48L	196	272	592	928
C10-58L	371	452	949	1326
S10-48L	441	557	874	1005
Percentage of 126 Day Creep				
C6-58L	33	38	71	100
S6-48L	21	29	64	100
C10-58L	28	34	72	100
S10-48L	44	55	87	100
Measured Creep Coefficient				
C6-58L	0.387	0.451	0.834	1.18
S6-48L	0.477	0.660	1.44	2.25
C10-58L	0.423	0.516	1.08	1.51
S10-48L	0.388	0.489	0.768	0.883
Specific Creep ( $\mu\epsilon/\text{psi}$ )				
C6-58L	0.101	0.118	0.217	0.308
S6-48L	0.089	0.124	0.269	0.422
C10-58L	0.085	0.103	0.216	0.302
S10-48L	0.082	0.104	0.163	0.188

Conversion: 1 MPa = 145.04 psi

**3.2.2. Discussion and Conclusions.** Like the shrinkage results, for normal strength specimens, the conventional concrete variation outperformed SCC. Also like the shrinkage results, for the high strength specimens, SCC outperformed conventional concrete.

For normal strength concrete, these results are supported by every prediction model that was analyzed. Every model predicts that C6-58L would have a lower creep coefficient than S6-48L after 126 days being loaded. The models were not as consistent when predicting the creep behavior of high strength concrete. The model identified by Long and Khayat (2011) as best predicting SCC creep behavior, CEB-FIP 90, does predict the behavior of specimens in this study. CEB-FIP 90 predicts that, like the results, S10-48L would have a lower creep coefficient than C10-58L after 126 days being loaded. Additionally, NCHRP Report 628 (2009), the model which is specifically for SCC, also predicts the same relationship.

In terms of comparing the results to previous research, both specimens performed very well. Long and Khayat (2011) investigated the creep strain on 16 SCC mixes. Eight of these mixes Nos. 1-8, were all very similar to S6-48L in terms of compressive strength, with Nos. 1-4 having a w/c of .34 and Nos. 5-8 with a w/c of .40. When plotted against these mixes, as shown in **Figure 3.8**, S6-48L performs very well. The same relationship exists between S10-48L and Nos. 9-12 from Long and Khayat (2011). These mixes have a similar amount of cement, however did not achieve the compressive strength of S10-48L. Creep results from S10-48L are shown with mix Nos. 9-12 in **Figure 3.9**. All specimens tested in Long and Khayat (2011) were loaded to 40% of their measured compressive strength, but at 18 hours age. The lower creep strain experienced

by the specimens in this study relative to Long and Khayat are possibly due to the concrete in the study being loaded at a later age when the strength and stiffness has increased relative to that of 18 hour old concrete.

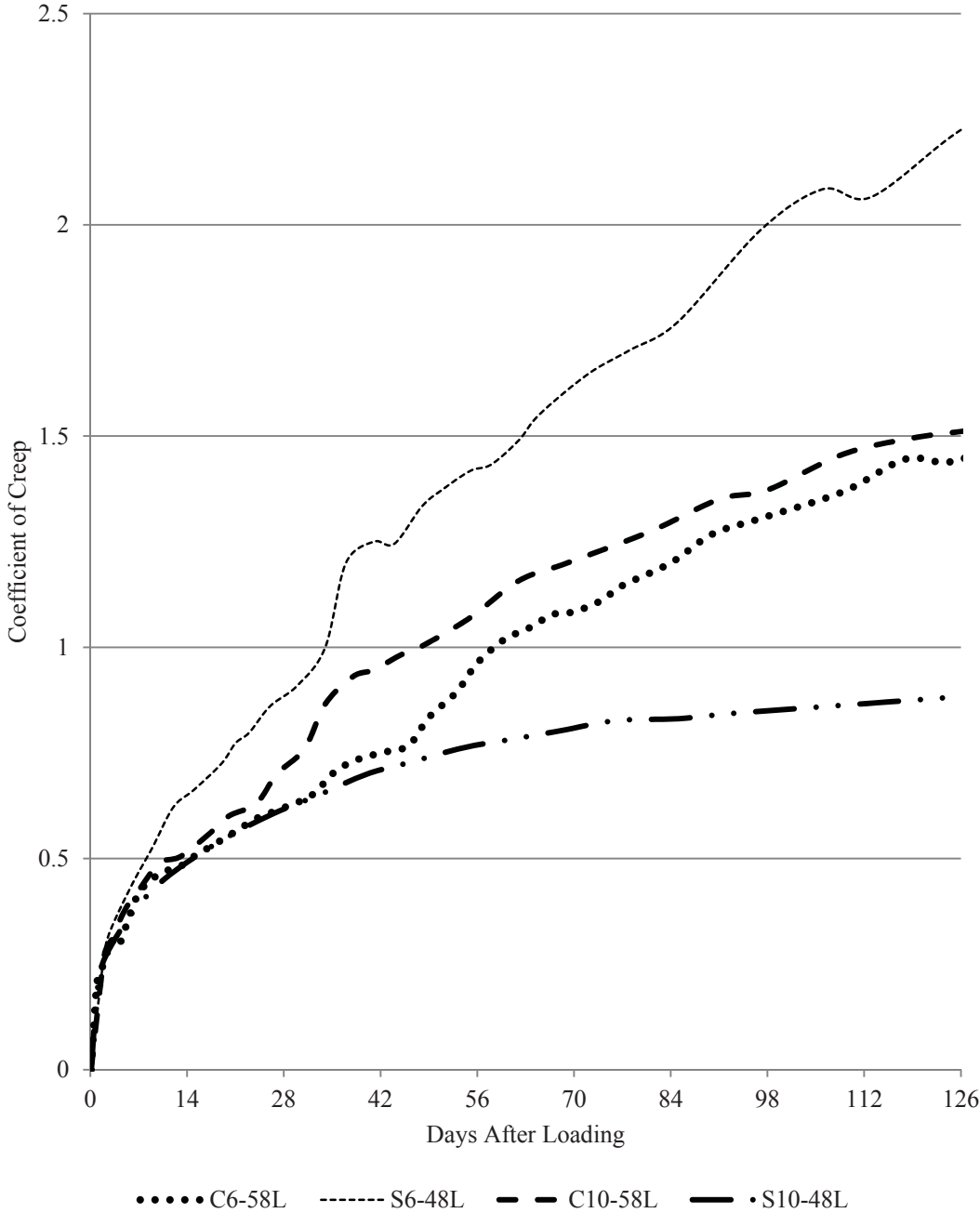


Figure 3.7 – SCC Coefficient of Creep Results

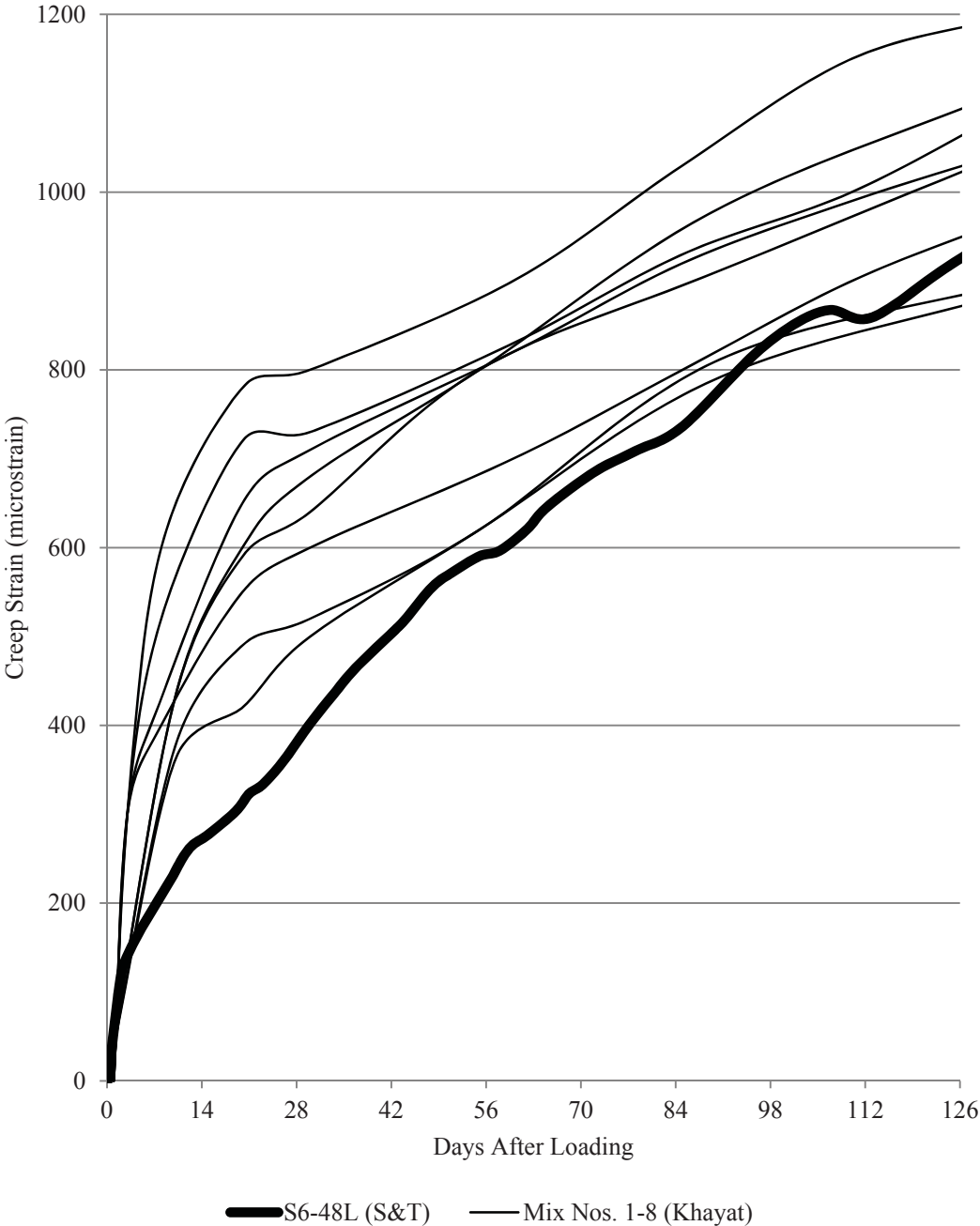
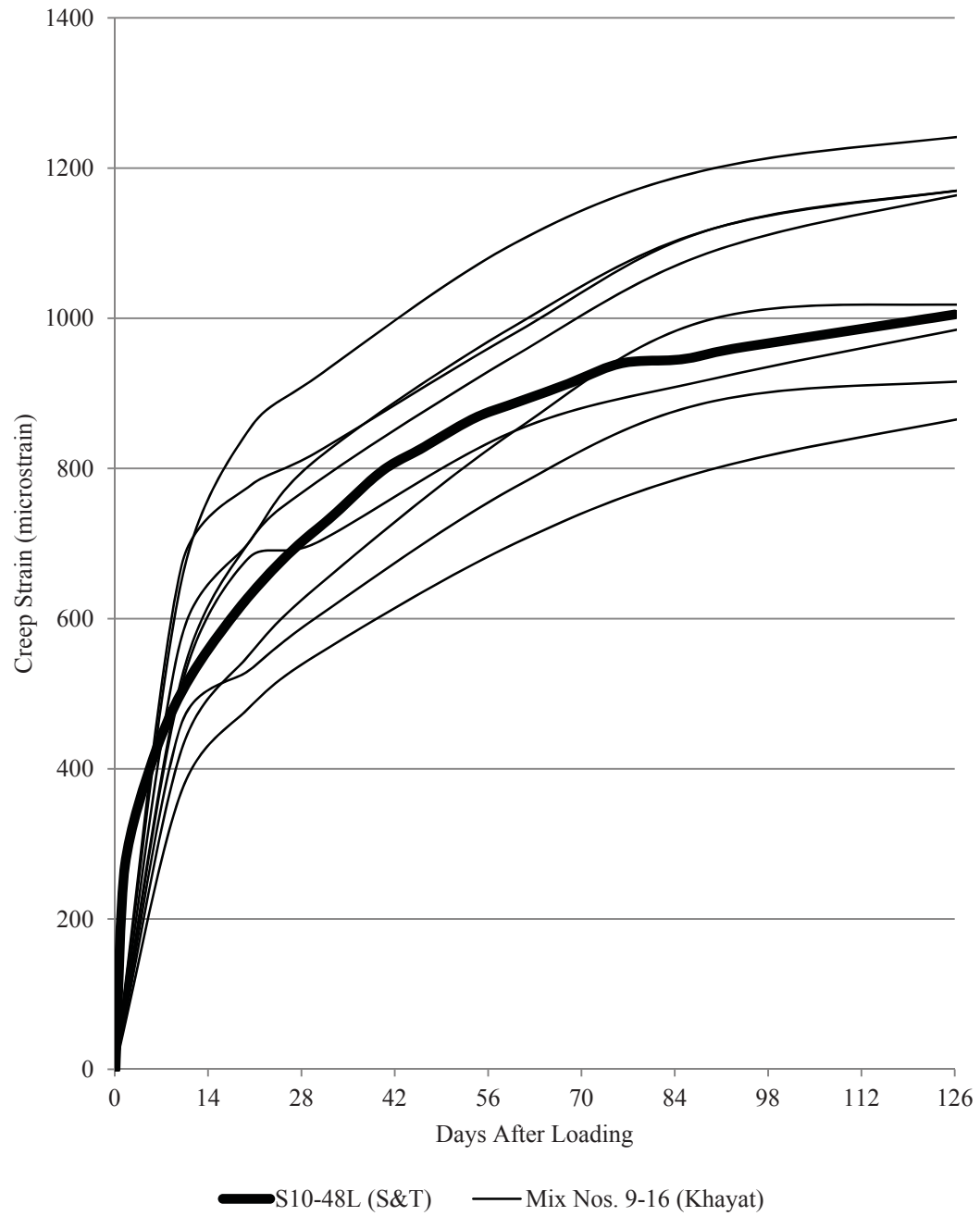


Figure 3.8 – S6-48L Plotted Against Results from Long and Khayat (2011)



**Figure 3.9 – S10-48L Plotted Against Results from Long and Khayat (2011)**

### 3.3. ABRASION RESISTANCE

**3.3.1. Results.** Figures 3.10 – 3.13 show the mass losses recorded after each two minute abrasion cycle for each mix tested. Figure 3.14 shows the cumulative mass loss comparison between the four mixes. Figure 3.15 shows the depth of wear results from abrasion testing. Table 3.3 shows a summary of all results along with measured 28 day compressive strength. One test consisted of three cycles.

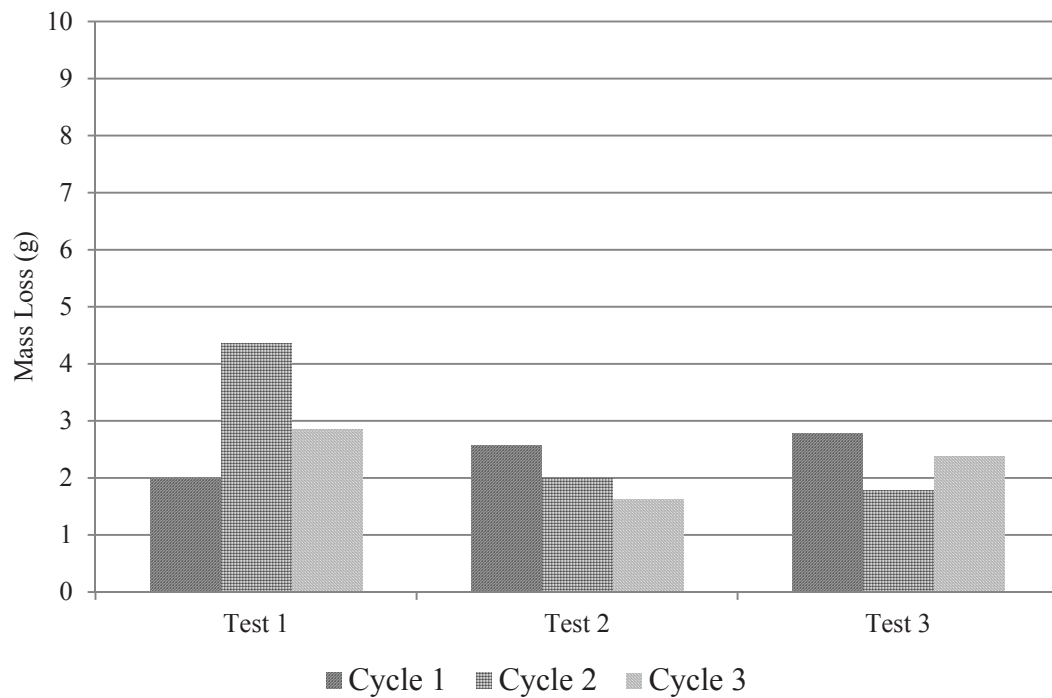


**Figure 3.10 - C6-58L Mass Loss Results**

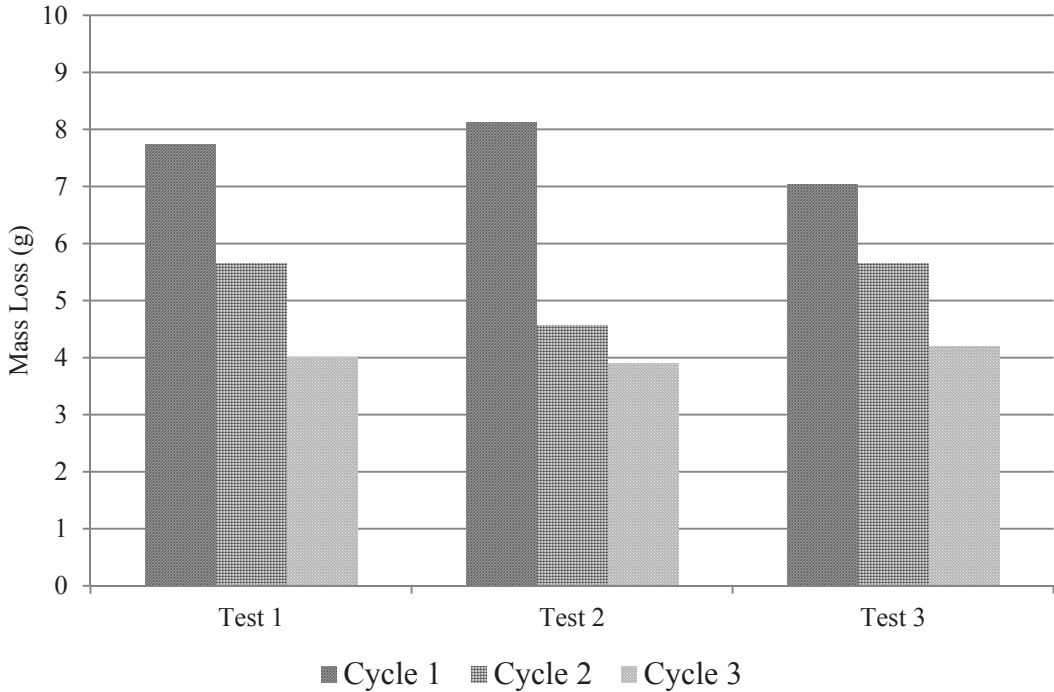


**Figure 3.11 - S6-48L Mass Loss Results**

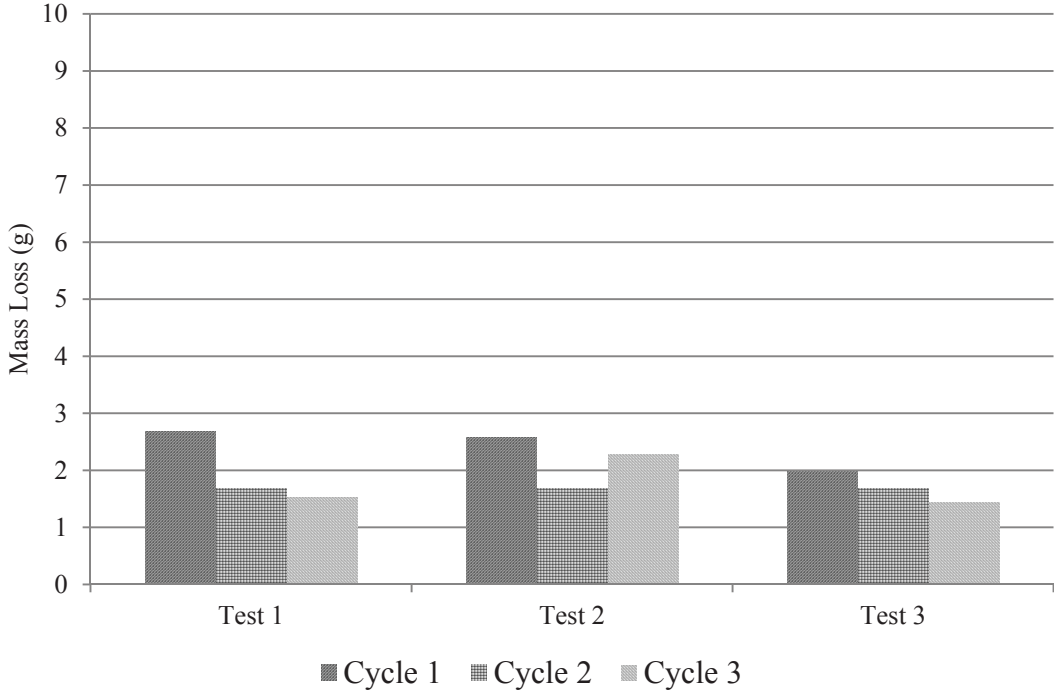


**Figure 3.12 - C10-58L Mass Loss Results**

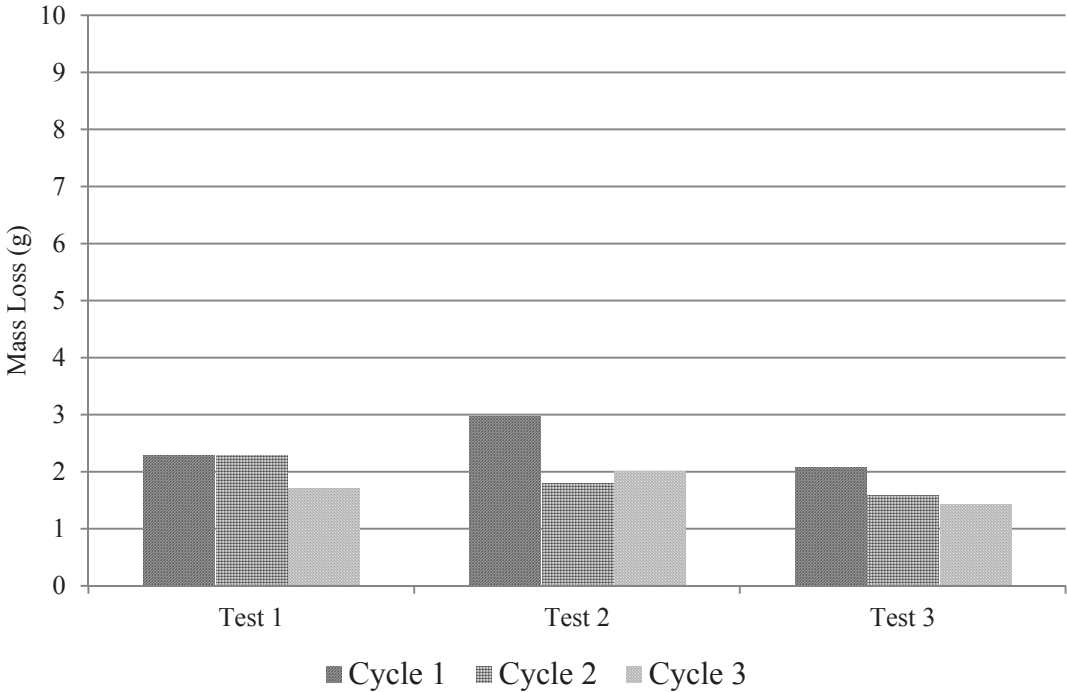


Figure 3.13 - S10-48L Mass Loss Results

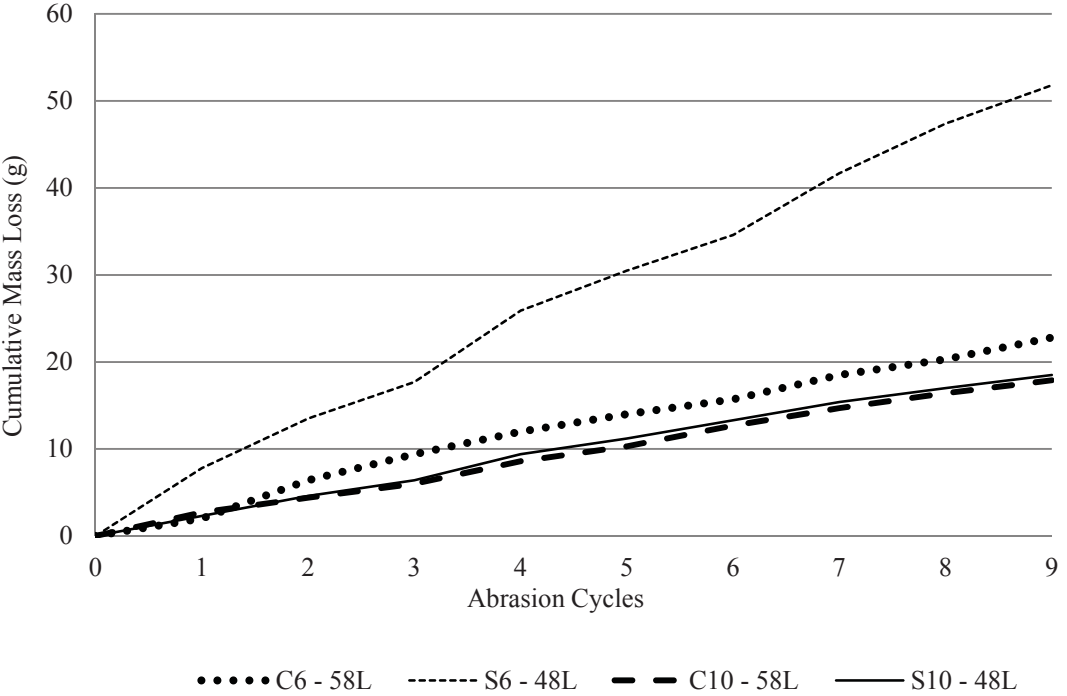
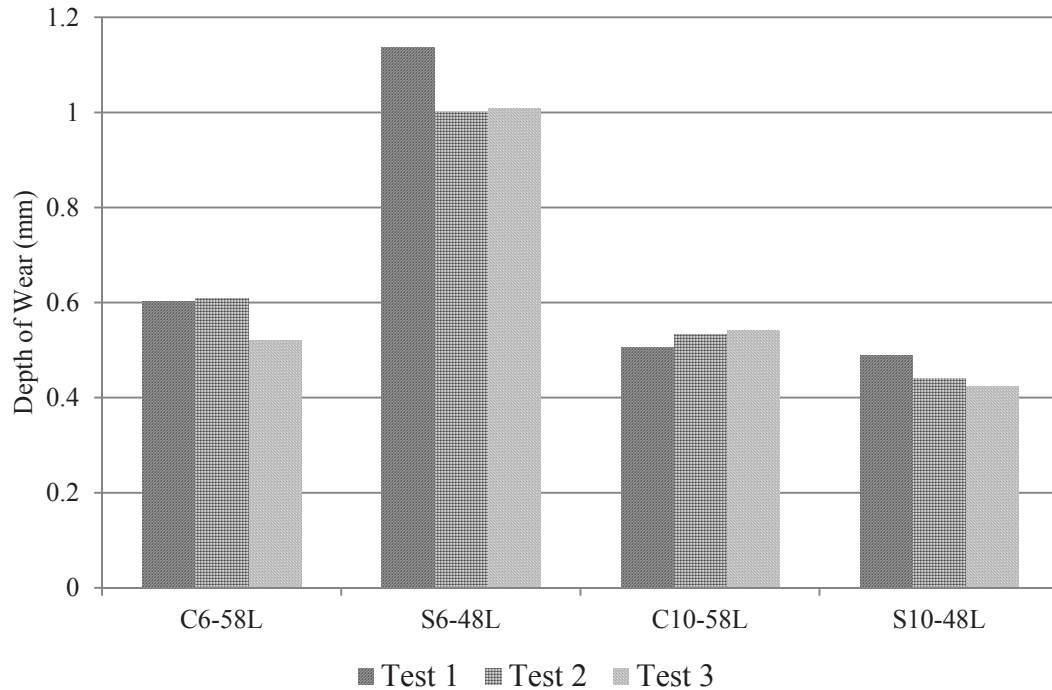


Figure 3.14 - SCC Mass Loss Results



**Figure 3.15 - SCC Depth of Wear Results**

**Table 3.3 - Summary of Results Shown with 28 Day Measured Compressive Strength**

	C6-58L	S6-48L	C10-58L	S10-48L
28 Day Compressive Strength (psi)	7,000	5,500	11,000	13,500
Avg. Mass loss (g)	2.53	5.76	1.99	2.06
Avg. Depth of Wear (mm)	0.59	1.07	0.54	0.47

Conversion: 1 MPa = 145.04 psi

1 lb. = 453.59 g

1 in. = 25.4 mm

**3.3.2. Discussion and Conclusions.** The results obtained are very consistent with trends found in previous studies. As was concluded in both Atis and Naik, the abrasion resistance of concrete is primarily dependent on compressive strength. For both

criteria (mass loss and depth of abrasion), the abrasion resistance of concrete increased as the compressive strength of the specimens increased, except for the mass loss of S10-48L relative to C10-58L. Additionally, when comparing concrete mixes with the same design strength, the SCC mix generally showed a lower resistance to wear. This is most likely due to the decreased amount of coarse aggregate in the SCC mixes. Based on observations during and after testing, the majority of mass loss due to abrasion was from the cement paste, as opposed to the aggregate. Generally, for each test, cycle 1 shows the greatest amount of mass loss. The general decrease in measured mass loss for each subsequent cycle indicates that as the depth of wear gets larger, the presence of aggregate begins to take effect. This would explain why the SCC mixes showed a decrease in abrasion resistance relative to their conventional concrete equivalents.

APPENDIX A.  
SHRINKAGE DATA WITH RELATIVE HUMIDITY DATA

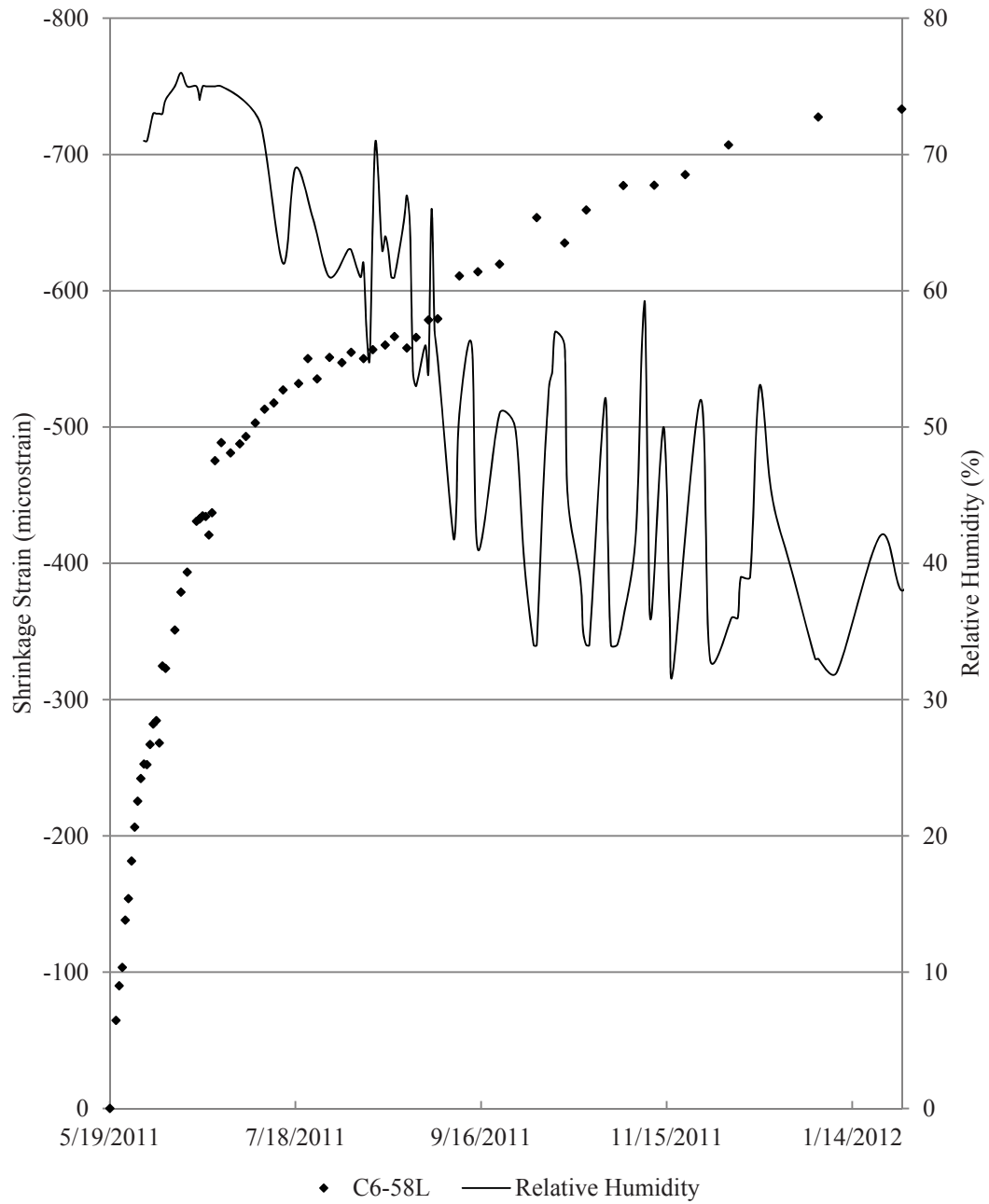


**Figure A.1 – C6-58L shrinkage data shown with recorded relative humidity**

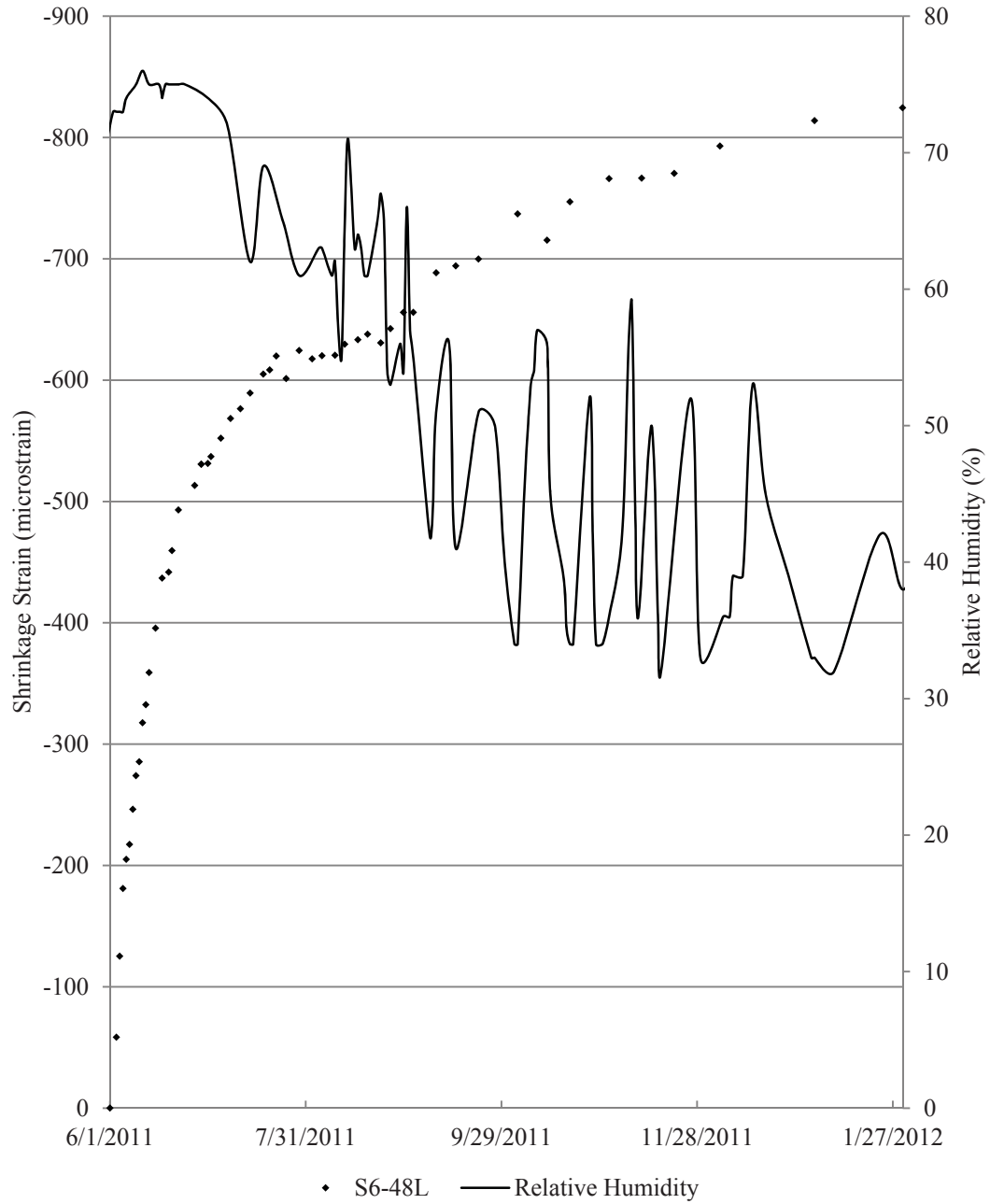


**Figure A.2 - S6-48L shrinkage data shown with recorded relative humidity**

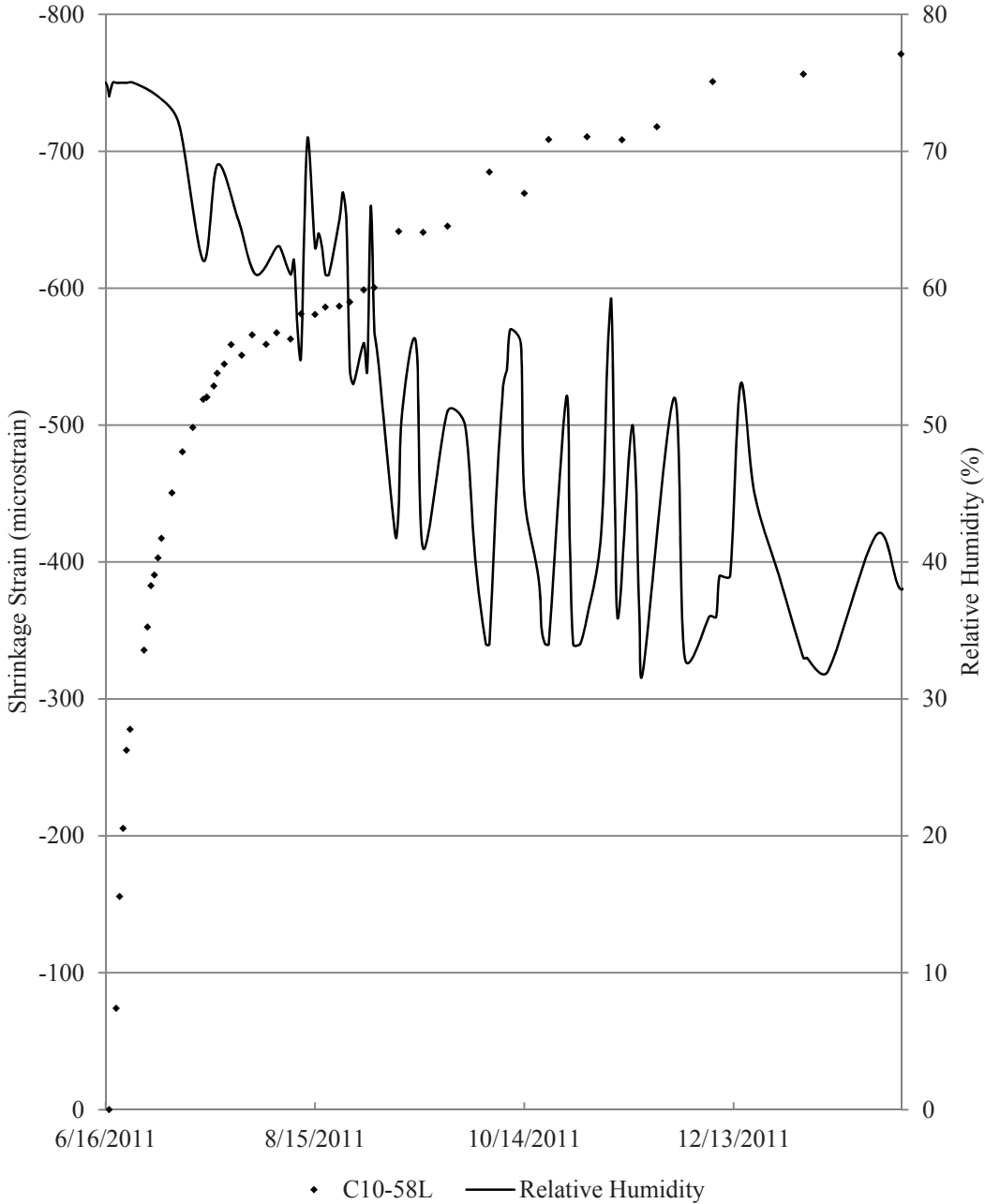
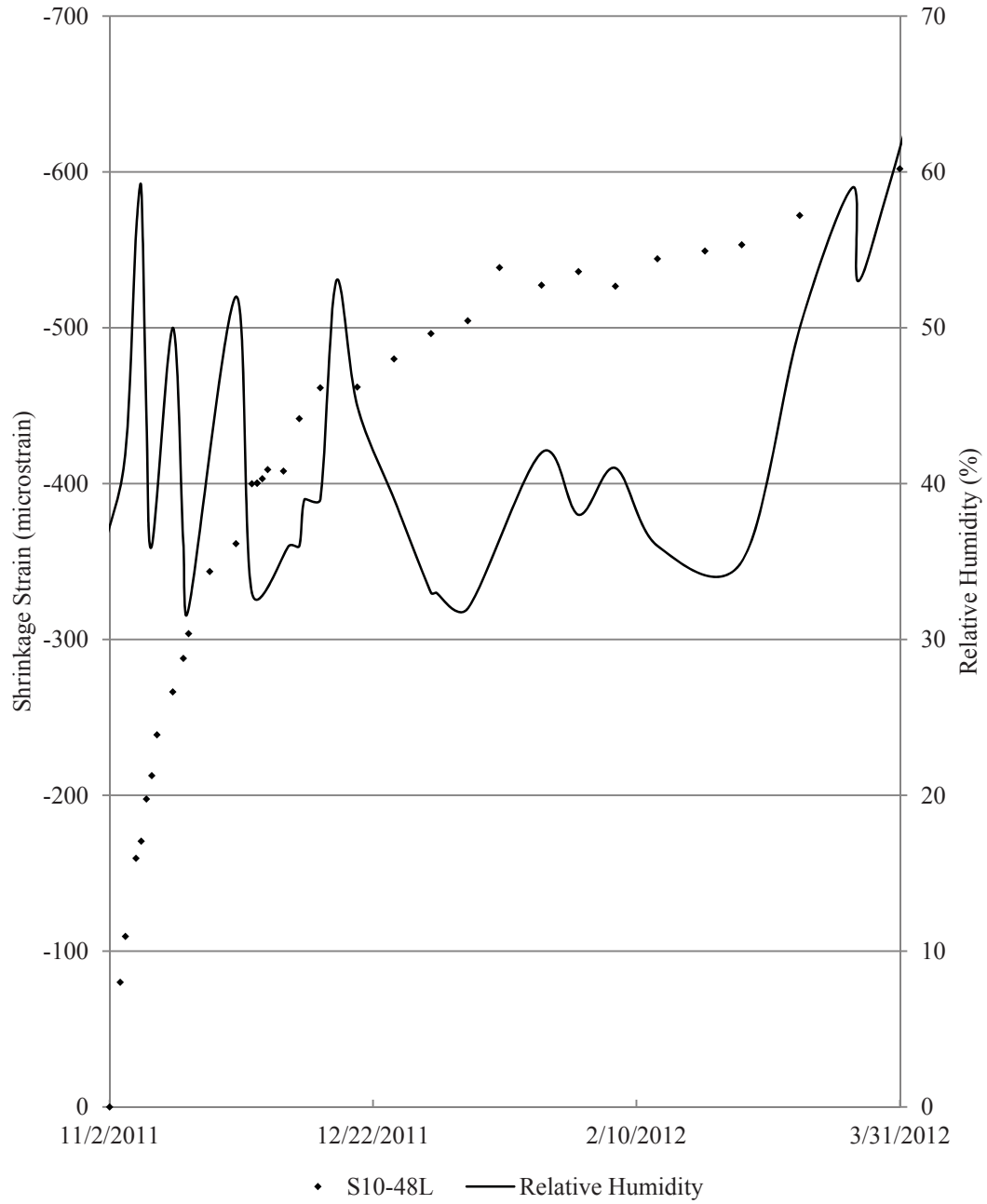


Figure A.3 – C10-58L shrinkage data shown with recorded relative humidity



**Figure A.4 – S10-48L shrinkage data shown with recorded relative humidity**

APPENDIX B.  
EXAMPLE STRAIN CALCULATIONS

	A	B	C	D	E	F	G
1			Example Shrinkage and Creep Calculation				
2							
3			G= 0.40 x 10 <sup>-5</sup> (mm/mm)				
4			G= 4.00 x 10 <sup>-6</sup> (mm/mm)				
5							
6					Measured Data		
7			Specimen	Reading			
8			Refer Bar		2525	2524	2525
9			C6-58L SH1	1--1	2130	2111	2106
10			C6-58L SH1	1--2	3633	3615	3611
11			C6-58L SH1	1--3	4018	4002	3998
12			C6-58L SH1	2--1	2549	2531	2529
13			C6-58L SH1	2--2	3179	3162	3162
14			C6-58L SH1	2--3	3230	3213	3210
15			C6-58L SH1	3--1	5867	5846	5846
16			C6-58L SH1	3--2	1980	1962	1960
17			C6-58L SH1	3--3	2182	2166	2165
18							
19							
20					Calculated Strain		
21							
22			C6-58L SH1	1--1		-72	-24
23			C6-58L SH1	1--2		-68	-20
24			C6-58L SH1	1--3		-60	-20
25			C6-58L SH1	2--1		-68	-12
26			C6-58L SH1	2--2		-64	-4
27			C6-58L SH1	2--3		-64	-16
28			C6-58L SH1	3--1		-80	-4
29			C6-58L SH1	3--2		-68	-12
30			C6-58L SH1	3--3		-60	-8
31							
32			Average Shrinkage			-67.1	-13.3
33			Cumulative Shrinkage			-67.1	-80.4
34							

Figure B.1 – Example shrinkage and creep strain calculation

	A	B	C	D	E	F	G
1			Example Shrinkage and Creep Calculation				
2							
3			G= 0.4 x 10 <sup>-5</sup> (mm/mm)				
4			G= 4 x 10 <sup>-6</sup> (mm/mm)				
5							
6						Measured Data	
7			Specimen	Reading			
8			Refer Bar		2525	2524	2525
9			C6-58L SH1	1--1	2130	2111	2106
10			C6-58L SH1	1--2	3633	3615	3611
11			C6-58L SH1	1--3	4018	4002	3998
12			C6-58L SH1	2--1	2549	2531	2529
13			C6-58L SH1	2--2	3179	3162	3162
14			C6-58L SH1	2--3	3230	3213	3210
15			C6-58L SH1	3--1	5867	5846	5846
16			C6-58L SH1	3--2	1980	1962	1960
17			C6-58L SH1	3--3	2182	2166	2165
18							
19							
20						Calculated Strain	
21							
22			C6-58L SH1	1--1		=B54*((F9-E9)-(F58-E58))	=B54*((G9-F9)-(G58-F58))
23			C6-58L SH1	1--2		=B54*((F10-E10)-(F58-E58))	=B54*((G10-F10)-(G58-F58))
24			C6-58L SH1	1--3		=B54*((F11-E11)-(F58-E58))	=B54*((G11-F11)-(G58-F58))
25			C6-58L SH1	2--1		=B54*((F12-E12)-(F58-E58))	=B54*((G12-F12)-(G58-F58))
26			C6-58L SH1	2--2		=B54*((F13-E13)-(F58-E58))	=B54*((G13-F13)-(G58-F58))
27			C6-58L SH1	2--3		=B54*((F14-E14)-(F58-E58))	=B54*((G14-F14)-(G58-F58))
28			C6-58L SH1	3--1		=B54*((F15-E15)-(F58-E58))	=B54*((G15-F15)-(G58-F58))
29			C6-58L SH1	3--2		=B54*((F16-E16)-(F58-E58))	=B54*((G16-F16)-(G58-F58))
30			C6-58L SH1	3--3		=B54*((F17-E17)-(F58-E58))	=B54*((G17-F17)-(G58-F58))
31							
32			Average Shrinkage			=AVERAGE(F22:F30)	=AVERAGE(G22:G30)
33			Cumulative Shrinkage			=F32	=F33+G32
34							
35							

Figure B.2 – Example shrinkage and creep strain calculations with equations shown

APPENDIX C.  
COEFFICIENT OF VARIATION DATA

C6-58L		Shrinkage														
Age (days)		2	3	4	5	6	7	8	9	10	11	12	13	14	15	16
COV		0.20	0.62	0.46	0.25	0.74	0.41	0.25	0.62	0.42	0.45	9.57	0.28	0.25	7.83	1.21
		17	18	21	23	25	28	29	30	31	32	33	34	36	39	42
		0.25	6.75	0.27	0.19	0.36	0.17	1.94	1.11	5.25	0.82	0.72	0.18	0.53	1.38	0.58
		44	47	50	53	56	61	64	67	71	75	78	82	85	89	92
		0.51	0.59	0.28	0.53	0.38	0.61	0.17	0.22	0.20	0.57	0.31	0.53	0.41	0.62	0.55
		96	99	103	106	113	119	126	138	147	154					
		0.28	0.37	0.25	2.91	0.18	0.94	0.56	0.16	0.43	0.38					
		Creep														
Age (days after loading)					1	2	3	4	5	7	10	13	15	18	21	24
COV					0.60	0.55	0.89	0.87	0.21	0.48	1.04	0.46	0.43	0.40	0.39	0.43
		27	32	35	38	42	46	49	53	56	60	63	67	70	74	77
		0.32	0.45	0.22	3.68	1.22	3.35	0.33	1.37	0.63	0.62	0.46	1.02	0.45	0.34	0.54
		84	90	97	109	118	125									
		0.35	0.51	0.48	0.34	3.29	0.37									
		S6-48L														
		Shrinkage														
Age (days)		2	3	4	5	6	7	8	9	10	11	12	14	16	18	19
COV		0.50	0.45	0.31	0.48	0.74	0.21	0.16	0.65	0.24	0.24	0.13	0.16	0.10	0.51	0.37
		21	26	28	30	31	34	37	40	43	47	49	51	54	58	62
		0.26	0.31	0.21	3.74	0.36	0.18	0.18	0.48	0.18	0.21	1.01	0.27	0.20	0.14	0.42
		65	69	72	76	79	83	86	90	93	100	106	113	125	134	141
		0.77	6.64	0.40	0.66	0.58	0.32	0.31	0.19	0.00	0.17	0.53	0.90	0.17	0.16	0.16
		153														
		0.17														
		Creep														
Age (days after loading)					2	3	6	9	12	15	19	21	23	26	30	34
COV					0.92	0.21	0.18	0.17	0.22	0.15	0.13	0.43	0.62	2.29	0.11	1.66
		37	41	44	48	51	55	58	62	65	72	78	85	97	106	113
		0.41	0.42	1.56	1.03	0.89	2.71	0.47	0.54	0.85	0.42	0.56	0.52	0.95	3.30	0.35
		125														
		0.31														

Figure C.1 – C6-58L and S6-48L COV Data

C10-58L		Shrinkage														
Age (days)		2	3	4	5	6	10	11	12	13	14	15	18	21	24	27
COV		0.08	0.16	0.26	0.18	0.42	0.13	0.18	0.12	0.87	0.56	0.19	0.12	0.12	0.17	0.15
		28	30	31	33	35	38	41	45	48	52	55	59	62	66	69
		1.41	0.39	0.33	0.46	0.22	0.65	0.20	0.27	0.32	0.53	0.15	5.25	0.36	3.09	1.13
		73	76	83	90	97	109	119	126	137	147	157				
		0.40	1.56	0.16	3.09	0.61	0.11	0.21	0.10	1.24	0.92	0.25				
		Creep														
Age (days after loading)					2	3	5	7	10	13	17	20	24	27	31	34
COV					1.73	0.34	0.34	0.38	0.55	0.42	0.40	0.20	0.34	0.16	0.70	9.37
		38	41	45	48	55	62	69	81	91	98	109	119	129		
		1.89	0.49	0.21	0.62	0.17	0.29	0.21	0.17	0.58	0.14	0.27	0.20	0.14		
		S10-48L														
		Shrinkage														
Age (days)		2	3	5	6	7	8	9	12	14	15	19	24	27	28	29
COV		0.10	0.18	0.08	0.26	0.15	0.27	0.15	0.14	0.20	0.28	0.10	0.18	0.11	8.19	1.30
		30	33	36	40	47	54	61	68	74	82	89	96	104	113	120
		0.42	18.62	0.48	0.13	5.92	0.16	0.20	0.32	0.11	0.26	0.33	0.40	0.30	0.46	0.35
		131														
		0.87														
		Creep														
Age (days after loading)					1	2	5	8	12	19	26	33	40	46	54	61
COV					0.27	0.19	0.16	0.15	0.16	0.17	0.13	0.15	0.14	0.15	0.29	0.18
		68	76	85	92	103	126									
		0.4	0.18	9.27	0.22	0.13	0.45									

Figure C.2 – C10-58L and S10-48L COV Data

## BIBLIOGRAPHY

- American Concrete Institute (ACI 116R-00) (2000), "Cement and Concrete Terminology." American Concrete Institute, Detroit, Michigan.
- American Concrete Institute (ACI 209R-92) (1997), "Prediction of Creep, Shrinkage, and Temperature Effects in Concrete Structures." American Concrete Institute, Detroit, Michigan.
- American Concrete Institute (ACI 209.1R-05) (2005), "Report on Factors Affecting Shrinkage and Creep of Hardened Concrete." American Concrete Institute, Detroit, Michigan.
- American Concrete Institute (ACI 237R-07) (2007), "Self-Consolidating Concrete." American Concrete Institute, Detroit, Michigan.
- American Concrete Institute (ACI 318-08) (2008), "Building Code Requirements for Structural Concrete and Commentary." American Concrete Institute, Detroit, Michigan.
- ASTM C31/C31 M-09 (2009). "Standard Practice for Making and Curing Concrete Test Specimens in the Field." American Society for Testing and Materials, West Conshohocken, Pennsylvania.
- ASTM C39/C39 M-05 (2005). "Standard Test Method for Compressive Strength of Cylindrical Concrete Specimens." American Society for Testing and Materials, West Conshohocken, Pennsylvania.
- ASTM C157/C157 M-08 (2008). "Standard Practice for Length Change of Hardened Hydraulic-Cement Mortar and Concrete." American Society for Testing and Materials, West Conshohocken, Pennsylvania.
- ASTM C3512/C512 M-10 (2010). "Standard Practice for Creep of Concrete in Compression." American Society for Testing and Materials, West Conshohocken, Pennsylvania.
- ASTM C944/C944 M-99 (2005). "Standard Practice for Abrasion Resistance of Concrete of Mortar Surfaces by the Rotating-Cutter Method." American Society for Testing and Materials, West Conshohocken, Pennsylvania.

- Bazant, Z. P. and Baweja, S. (2000). "Creep and Shrinkage Prediction Model for Analysis and Design of Concrete Structures: Model B3" Adam Neville Symposium: Creep and Shrinkage—Structural Design Effects, ACI SP-194, A. Al-Manaseer, ed., Am. Concrete Institute, Farmington Hills, Michigan, 2000, 1–83.
- Branson, D. E., and Christiason, M. L. (1971) "Time-Dependent Concrete Properties Related to Design-Strength and Elastic Properties," Designing for Effects of Creep, Shrinkage, Temperature in Concrete Structures, SP-27, American Concrete Institute, Detroit, MI, pp. 257-277.
- Comite Euro – International Du Beton (CEB) (1990), "CEB-FIP Model Code 1990" Thomas Telford, 1990-1993, 53-58.
- Fernandez-Gomez, J. and Landsberger, G.A. (2007). "Evaluation of Shrinkage Prediction Models for Self-Consolidating Concrete." ACI Materials Journal, October 2007, 464-473.
- Freyermuth, C.L. (1969). "Design of Continuous Highway Bridges with Precast, Prestressed Concrete Girders." Journal of the Prestressed Concrete Institute, Vol. 14, No. 2, 14-39.
- Gardner, N.J., and Lockman, M.J. (2001), "Design Provisions for Drying Shrinkage and Creep of Normal-Strength Concrete" ACI Materials Journal, 159-167.
- Holschemacher, K (2004). "Hardened Material Properties of Self-Compacting Concrete" Journal of Civil Engineering and Management, Vol X, No 4, 261-266.
- Khayat, K.H., and Mitchell, D. (2009). "Self-Consolidating Concrete for Precast, Prestressed Concrete Bridge Elements." National Cooperative Highway Research Program Report 628, Transportation Research Board, Washington, D.C.
- Long, W., Khayat, K.H., and Xing, F. (2011). "Autogenous Shrinkage of Prestressed Self-Consolidating Concrete." The Open Civil Engineering Journal, 2011, 5, 116-123.
- Long, et. al. (2011). "Statistical Models to Predict Fresh and Hardened Properties of Self-Consolidating Concrete." RILEM Materials and Structures, 2001.
- Myers, J.J., Carrasquillo, R.L. (1999). "The Production and Quality Control of High Performance Concrete in Texas Bridge Structures," Center for Transportation Research, Report Number 580-589-1, November 1999, pp 564.
- Myers, J.J. and Yang, Y. (2004). "High Performance Concrete for Bridge A6130-Route 412 Pemiscot County, MO," Missouri Department of Transportation, Report RDT 04-016, June 2004.

- Perenchio, W.F., (1997). "The Drying Shrinkage Dilemma-Some Observations and Questions About Drying Shrinkage and its Consequence," *Concrete Construction*, V. 42, No. 4, pp. 379-383.
- Schindler, A.K., et. al. (2007). "Properties of Self-Consolidating Concrete for Prestressed Members." *ACI Materials Journal*, January-February 2007, 53-61.
- Tadros, M.K., Al-Omaishi, N., Seguirant, S.J., and Gallt, J.G. (2003). "Prestress Losses in Pretensioned High-Strength Concrete Bridge Girders." National Cooperative Highway Research Program Report 496, Transportation Research Board, National Research Council, Washington, D.C.

**FINAL Report E**

TRyy1103

**Project Title: Self-Consolidating Concrete (SCC) for Infrastructure Elements**

**Report E: Self-Consolidating Concrete (SCC) for Infrastructure Elements: Hardened Mechanical Properties and Durability Performance**

Prepared for  
Missouri Department of Transportation  
Construction and Materials

Missouri University of Science and Technology, Rolla, Missouri

July 2012

The opinions, findings, and conclusions expressed in this publication are those of the principal investigators and the Missouri Department of Transportation. They are not necessarily those of the U.S. Department of Transportation, Federal Highway Administration. This report does not constitute a standard or regulation.



## **ABSTRACT**

Concrete is one of the most produced and utilized materials in the world. Due to the labor intensive and time consuming nature of concrete construction, new and innovative concrete mixes are being explored. Self-consolidating concrete (SCC) is one such method of improving the overall cost and time efficiency of concrete production. SCC is a highly flowable form of concrete. This characteristic drastically reduces the amount of labor and time needed to place the concrete. The highly flowable nature also allows for much easier placement in applications of highly congested reinforcement.

In order to test this new and innovative concrete mix, SCC was tested for both hardened material properties and durability in this investigation. The results indicated that SCC was superior to the baseline conventional concrete.

## TABLE OF CONTENTS

	Page
LIST OF ILLUSTRATIONS .....	viii
LIST OF TABLES .....	xi
1. INTRODUCTION .....	1
1.1. BACKGROUND, PROBLEM, & JUSTIFICATION .....	1
1.1.1. Self-Consolidating Concrete .....	1
1.2. OBJECTIVES & SCOPE OF WORK .....	2
1.2.1. Self-Consolidating Concrete .....	2
1.3. RESEARCH PLAN .....	3
1.3.1. Self-Consolidating Concrete .....	3
1.4. OUTLINE .....	3
1.4.1. Self-Consolidating Concrete .....	3
2. LITERATURE REVIEW .....	5
2.1. SELF-CONSOLIDATING CONCRETE .....	5
2.2. MECHANICAL PROPERTY TESTING METHODS .....	11
2.2.1. Compressive Strength.....	11
2.2.2. Modulus of Elasticity .....	12
2.2.3. Modulus of Rupture.....	13
2.2.4. Splitting Tensile Strength.....	14
2.3. DURABILITY OF CONCRETE .....	15
2.3.1. Freezing and Thawing .....	15
2.3.2. Chloride Attack .....	17
2.4. DURABILITY TESTING METHODS .....	20
2.4.1. Resistance to Freezing and Thawing.....	20
2.4.2. Rapid Chloride Penetration .....	21
2.4.3. Chloride Content Analysis .....	23
2.4.4. Concrete Resistivity .....	25
2.4.5. Scaling Resistance .....	28
2.5. SELF-CONSOLIDATING CONCRETE .....	29

2.5.1. Mechanical Properties .....	29
2.5.2. Durability Performance .....	30
3. MECHANICAL PROPERTY TESTS .....	31
3.1. INTRODUCTION .....	31
3.2. MIX DESIGN .....	32
3.2.1. Self-Consolidating Concrete Mix Design .....	32
3.3. COMPRESSIVE STRENGTH TEST.....	37
3.3.1. Introduction .....	37
3.3.2. Fabrication.....	38
3.3.3. Testing & Procedure.....	39
3.4. MODULUS OF ELASTICITY TEST .....	42
3.4.1. Introduction .....	42
3.4.2. Fabrication.....	42
3.4.3. Testing & Procedure.....	43
3.5. MODULUS OF RUPTURE TEST.....	45
3.5.1. Introduction .....	45
3.5.2. Fabrication.....	45
3.5.3. Testing & Procedure.....	45
3.6. SPLITTING TENSILE TEST.....	48
3.6.1. Introduction .....	48
3.6.2. Fabrication.....	48
3.6.3. Testing & Procedure.....	49
4. DURABILITY TESTS.....	51
4.1. INTRODUCTION .....	51
4.2. RAPID FREEZING & THAWING TEST .....	52
4.2.1. Introduction .....	52
4.2.2. Fabrication.....	52
4.2.3. Testing & Procedure.....	55
4.3. ELECTRICAL INDICATION TO RESIST CHLORIDE ION PENETRATION TEST .....	56
4.3.1. Introduction .....	56

4.3.2. Fabrication.....	57
4.3.3. Testing & Procedure.....	57
4.4. PONDING TEST .....	60
4.4.1. Introduction .....	60
4.4.2. Fabrication.....	60
4.4.3. Testing & Procedure.....	61
4.5. CONCRETE RESISTIVITY TEST.....	65
4.5.1. Introduction .....	65
4.5.2. Fabrication.....	67
4.5.3. Testing & Procedure.....	67
5. SELF-CONSOLIDATING CONCRETE HARDENED PROPERTY AND DURABILITY RESULTS .....	69
5.1. COMPRESSIVE STRENGTH.....	69
5.2. MODULUS OF ELASTICITY.....	73
5.3. MODULUS OF RUPTURE .....	77
5.4. SPLITTING TENSILE.....	81
5.5. RAPID FREEZING & THAWING.....	84
5.6. ELECTRICAL INDICATION TO RESIST CHLORIDE PENETRATION ...	86
5.7. PONDING TEST .....	89
5.8. CONCRETE RESISTIVITY .....	92
6. EVALUATION OF SELF-CONSOLIDATING CONCRETE .....	98
6.1. NORMAL STRENGTH SCC.....	98
6.1.1. Mechanical Properties .....	99
6.1.2. Durability Performance .....	104
6.2. HIGH STRENGTH SCC .....	106
6.2.1. Mechanical Properties of High Strength Mixes .....	107
6.2.2. Durability Performance of High Strength Mixes .....	114
7. FINDINGS, CONCLUSIONS, AND RECOMMENDATIONS .....	117
7.1. FINDINGS AND CONCLUSIONS .....	117
7.1.1. Normal Strength SCC.....	117
7.1.2. High Strength SCC.....	118

7.2. RECOMMENDATIONS.....	120
7.2.1. SCC.....	120
SCC DURABILITY TEST RESULTS DATA .....	121
REFERENCES .....	165

## LIST OF ILLUSTRATIONS

Figure	Page
Figure 2.1 – Slump Flow Test.....	7
Figure 2.2 – J-Ring Test.....	8
Figure 2.3 – Typical L-box Test Set-Up with Gate Removed.....	9
Figure 2.4 – Typical Segregation Column.....	10
Figure 2.7 – Typical Stress-Strain Diagram for Concrete .....	
Showing the Different Elastic Moduli [Mindess et al., 2002].....	12
Figure 2.8 - Typical Modulus of Rupture Testing Setup [ASTM C 78–10].....	14
Figure 2.9 - The Relative Volumes of Various Iron Oxides.....	
from Mansfield [1981], Corrosion 37(5), 301-307. ....	18
Figure 2.10 - Typical RCT Setup.....	22
Figure 2.11 - Schematic Representation of the Four-Probe Resistivity Method [Broomfield, 2007].....	27
Figure 3.1 - Compressive Strength Testing Setup .....	41
Figure 3.2 - High Strength Compressive Strength Specimens Post-Test .....	42
Figure 3.3 – 4 in. (102 mm) x 8 in. (203 mm) Cylinder Mold .....	
Compared to 6 in. (152 mm) x 12 in. (305 mm) Cylinder Mold.....	43
Figure 3.4 - Typical Compressometer .....	44
Figure 3.5 - Prepared Modulus of Rupture Specimen .....	46
Figure 3.6 - Modulus of Rupture Testing Setup .....	47
Figure 3.7 - Modulus of Rupture Specimen Post-Test .....	47
Figure 3.8 - Typical Splitting Tensile Test Setup.....	49
Figure 3.9 - Splitting Tensile Specimens Post-Test.....	50
Figure 4.1 - Freezing and Thawing Specimen Molds.....	53
Figure 4.2 - Freezing and Thawing Specimen with Protruding Bolt.....	54
Figure 4.3 - Setting Coating Being Applied to Concrete Specimens .....	58
Figure 4.4 - Typical Completed Specimen .....	59
Figure 4.5 – Typical RCT Setup.....	59
Figure 4.6 - Typical Ponding Specimen .....	62

Figure 4.7 - Concrete Core and Resulting Void in the Concrete Specimen .....	62
Figure 4.8 - Depths at which Powder Samples Were Collected.....	63
Figure 4.9 - Canin <sup>+</sup> Wenner Probe.....	66
Figure 4.10 - Wenner Probe Grid .....	68
Figure 5.1 - Compressive Strength Profile for Normal Strength Mixes.....	70
Figure 5.2 - Compressive Strength Profile for High Strength Concrete Mixes.....	72
Figure 5.3 – Example of RCT Results .....	87
Figure 5.4 – Average Chloride Content vs. Depth of Conventional Mixes.....	91
Figure 5.5 – Average Chloride Content vs. Depth of High Strength Mixes.....	92
Figure 5.6 - Individual Specimen Results for Concrete Resistivity for C6-58L Mix.....	93
Figure 5.7 - Individual Specimen Results for Concrete Resistivity for S6-48L Mix .....	94
Figure 5.8 – Averaged Results for Concrete Resistivity for Normal Strength Mixes .....	95
Figure 5.9 - Individual Specimen Results for Concrete Resistivity for C10-58L Mix.....	96
Figure 5.10 - Individual Specimen Results for Concrete Resistivity for S10-48L Mix ...	96
Figure 5.11 – Averaged Results for Concrete Resistivity for High Strength Mixes .....	97
Figure 6.1 – Compressive Strength vs. Modulus of Elasticity .....	101
Figure 6.2 – Compressive Strength vs. Modulus of Rupture.....	102
Figure 6.3 – Compressive Strength vs. Splitting-Tensile Strength.....	103
Figure 6.4 – Average Chloride Content vs. Depth of Conventional Mixes.....	105
Figure 6.5 – Average Resistivity of Normal Strength Concrete Mixes.....	106
Figure 6.6 - Compressive Strength vs. Modulus of Elasticity .....	110
Figure 6.7 – High Strength Mixes Compared to ACI-363 Equations.....	111
Figure 6.8 – Compressive Strength vs. Modulus of Rupture.....	112
Figure 6.9 – Compressive Strength vs. Splitting-Tensile Strength.....	113
Figure 6.10 – Average Chloride Content vs. Depth of High Strength Mixes.....	115
Figure 6.11 – Average Resistivity of High Strength Concrete Mixes .....	116
Figure A.1 – C6-58L-EC1TOP RCT Data .....	137
Figure A.2 – C6-58L-EC1MIDDLE RCT Data .....	138
Figure A.3 – C6-58L-EC2TOP RCT Data .....	139
Figure A.4 – C6-58L-EC2MIDDLE RCT Data .....	140
Figure A.5 – S6-48L-EC1TOP RCT Data.....	141

Figure A.6 – S6-48L-EC1MIDDLE RCT Data .....	142
Figure A.7 – S6-48L-EC2TOP RCT Data .....	143
Figure A.8 – S6-48L-EC2MIDDLE RCT Data .....	144
Figure A.9 – C10-58L-EC1TOP RCT Data .....	145
Figure A.10 – C10-58L-EC1MIDDLE RCT Data .....	146
Figure A.11 – C10-58L-EC2TOP RCT Data .....	147
Figure A.12 – C10-58L-EC2MIDDLE RCT Data .....	148
Figure A.13 – S10-48L-EC1TOP RCT Data .....	149
Figure A.14 – S10-48L-EC1MIDDLE RCT Data .....	150
Figure A.15 – C6-58L-FT1 Data .....	153
Figure A.16 – C6-58L-FT2 Data .....	154
Figure A.17 – C6-58L-FT3 Data .....	155
Figure A.18 – S6-48L-FT1 Data .....	156
Figure A.19 – S6-48L-FT2 Data .....	157
Figure A.20 – S6-48L-FT3 Data .....	158
Figure A.21 – C10-58L-FT1 Data .....	159
Figure A.22 – C10-58L-FT2 Data .....	160
Figure A.23 – C10-58L-FT3 Data .....	161
Figure A.24 – S10-48L-FT1 Data .....	162
Figure A.25 – S10-48L-FT2 Data .....	163
Figure A.26 – S10-48L-FT3 Data .....	164

## LIST OF TABLES

Table	Page
Table 2.1 Effect of w/cm Ratio on the Air Void System in Concrete .....	17
Table 2.2 Chloride Ion Penetrability Based On Charge Passed [ASTM C1202–10] .....	22
Table 2.3 Chloride Limits for New Construction in % Chloride by Mass of Cement [ACI, 2001] .....	24
Table 2.4 Correlation Between Percent Water Soluble Chloride .....	24
by Mass of Concrete and Corrosion Risk [Broomfield, 2007] .....	24
Table 2.5 Correlation Between Concrete Resistivity and the Rate of Corrosion for a Depassivated Steel Bar Embedded within the Concrete [Broomfield, 2007] .....	28
Table 2.6 Rating Scale for Scaling Resistance [MoDOT] .....	29
Table 3.1 Test Matrix for Mechanical Properties .....	32
Table 3.2 Mix Design per Cubic Yard for SCC Investigation .....	33
Table 3.3 Typical Fresh Concrete Properties for Conventional Concrete Mixes .....	36
Table 3.4 Typical Fresh Concrete Properties for Self-Consolidating Concrete Mixes ....	37
Table 4.1 Test Matrix for Durability Performance .....	52
Table 5.1 Individual Compressive Strength Results for Normal Strength Mixes .....	69
Table 5.2 Averaged Compressive Strength Results for Normal Strength Mixes .....	70
Table 5.3 Individual Compressive Strength Results for High Strength Concrete Mixes ..	71
Table 5.4 Averaged Compressive Strength Results for High Strength Concrete Mixes ..	71
Table 5.5 Individual Modulus of Elasticity Results for Normal Strength Mixes .....	73
Table 5.6 Average Modulus of Elasticity Results for Normal Strength Mixes .....	74
Table 5.7 Normalized Modulus of Elasticity for Conventional Concrete Mixes .....	75
Table 5.8 Normalized AASHTO Modulus of Elasticity for Conventional Concrete Mixes .....	75
Table 5.9 Individual Modulus of Elasticity Results for High Strength Concrete Mixes ..	76
Table 5.10 Average Modulus of Elasticity Results for High Strength Concrete Mixes ...	76
Table 5.11 Normalized Modulus of Elasticity for High Strength Concrete Mixes .....	76
Table 5.12 Normalized AASHTO Modulus of Elasticity for High Strength Concrete Mixes .....	77

Table 5.13 Individual Modulus of Rupture Results for Normal Strength Mixes .....	77
Table 5.14 Averaged Modulus of Rupture for Normal Strength Mixes .....	78
Table 5.15 Normalized Modulus of Rupture for Normal Strength Mixes.....	78
Table 5.16 Normalized AASHTO Modulus of Rupture for Normal Strength Mixes .....	79
Table 5.17 Individual Modulus of Rupture Results for High Strength Concrete Mixes ..	80
Table 5.18 Average Modulus of Rupture Results for High Strength Concrete Mixes .....	80
Table 5.19 Normalized Modulus of Rupture Results for High Strength Concrete Mixes	80
Table 5.20 Normalized AASHTO Modulus of Rupture for High Strength Mixes.....	81
Table 5.21 Individual Splitting-Tensile Test Results for Normal Strength Concrete Mixes .....	82
Table 5.22 Averaged Splitting-Tensile Test Results for Normal Strength Concrete Mixes .....	82
Table 5.23 Normalized Splitting-Tensile Results for Normal Strength Concrete Mixes .	83
Table 5.24 Individual Splitting-Tensile Test Results for High Strength Concrete Mixes	83
Table 5.25 Averaged Splitting-Tensile Test Results for High Strength Concrete Mixes.	84
Table 5.26 Normalized Splitting-Tensile Results for High Strength Concrete Mixes .....	84
Table 5.27 Individual Results of Rapid Freezing and Thawing Test for Normal Strength Mixes .....	85
Table 5.28 Averaged Durability Factors for Normal Strength Mixes .....	85
Table 5.29 Individual Results of Freezing and Thawing Test for High Strength Mixes..	86
Table 5.30 Averaged Durability Factors for High Strength Mixes .....	86
Table 5.31 Individual RCT Results for Normal Strength Mixes .....	88
Table 5.32 Averaged Results of RCT and Permeability Class of Conventional Mixes ...	88
Table 5.33 Individual Results of RCT for High Strength Mixes .....	89
Table 5.34 Averaged Results of RCT and Permeability Class for High Strength Mixes.	89
Table 5.35 Correlation Between Percent Chloride by .....	90
Mass of Concrete and Corrosion Risk [Broomfield, 2007] .....	90
Table 5.36 Average Chloride Content at Specified Depths of Normal Strength Mixes...	90
Table 5.37 Average Chloride Content at Specified Depths of High Strength Mixes .....	91
Table 5.38 Final Resistivity of Normal Strength Concrete Mixes.....	95
Table 5.39 Final Resistivity of High Strength Concrete Mixes.....	97

Table 6.1 Outline of Results of Normal Strength Concrete Mixes.....	99
Table 6.2 Normalized Mechanical Properties Compared to Respective ACI Coefficients .....	100
Table 6.3 Normalized Mechanical Properties Compared to Respective AASHTO Coefficients .....	104
Table 6.4 Outline of Results of High Strength Concrete Mixes.....	107
Table 6.5 Normalized Mechanical Properties Compared to Respective ACI Coefficients .....	108
Table 6.6 Normalized Mechanical Properties Compared to Respective AASHTO Coefficients .....	113
Table A.1 C6-58L-1R (Weeks 1-7) .....	122
Table A.2 C6-58L-1R (Weeks 8-14) .....	122
Table A.3 C6-58L-1R (Weeks 15-21) .....	122
Table A.4 C6-58L-1R (Weeks 22-24) .....	123
Table A.5 C6-58L-2R (Weeks 1-7) .....	123
Table A.6 C6-58L-2R (Weeks 8-14) .....	123
Table A.7 C6-58L-2R (Weeks 15-21) .....	124
Table A.8 C6-58L-2R (Weeks 22-24) .....	124
Table A.9 C6-58L-3R (Weeks 1-7) .....	124
Table A.10 C6-58L-3R (Weeks 8-14) .....	125
Table A.11 C6-58L-3R (Weeks 15-21) .....	125
Table A.12 C6-58L-3R (Weeks 22-24) .....	125
Table A.13 S6-48L-1R (Weeks 1-7).....	126
Table A.14 S6-48L-1R (Weeks 8-14).....	126
Table A.15 S6-48L-1R (Weeks 15-21).....	126
Table A.16 S6-48L-1R (Weeks 22-24).....	127
Table A.17 S6-48L-2R (Weeks 1-7).....	127
Table A.18 S6-48L-2R (Weeks 8-14).....	127
Table A.19 S6-48L-2R (Weeks 15-21).....	128
Table A.20 S6-48L-2R (Weeks 22-24).....	128
Table A.21 C10-58L-1R (Weeks 1-7) .....	128

Table A.22 C10-58L-1R (Weeks 8-14) .....	129
Table A.23 C10-58L-1R (Weeks 15-21) .....	129
Table A.24 C10-58L-1R (Weeks 22-24) .....	129
Table A.25 C10-58L-2R (Weeks 1-7) .....	130
Table A.26 C10-58L-2R (Weeks 8-14) .....	130
Table A.27 C10-58L-2R (Weeks 15-21) .....	130
Table A.28 C10-58L-2R (Weeks 22-24) .....	131
Table A.29 C10-58L-3R (Weeks 1-7) .....	131
Table A.30 C10-58L-3R (Weeks 8-14) .....	131
Table A.31 C10-58L-3R (Weeks 15-21) .....	132
Table A.32 C10-58L-3R (Weeks 22-24) .....	132
Table A.33 S10-48L-1R (Weeks 1-7).....	132
Table A.34 S10-48L-1R (Weeks 8-14).....	133
Table A.35 S10-48L-1R (Weeks 15-21).....	133
Table A.36 S10-48L-1R (Weeks 22-24).....	133
Table A.37 S10-48L-2R (Weeks 1-7).....	134
Table A.38 S10-48L-2R (Weeks 8-14).....	134
Table A.39 S10-48L-2R (Weeks 15-21).....	134
Table A.40 S10-48L-2R (Weeks 22-24).....	135
Table A.41 S10-48L-3R (Weeks 1-7).....	135
Table A.42 S10-48L-3R (Weeks 8-14).....	135
Table A.43 S10-48L-3R (Weeks 15-21).....	136
Table A.44 S10-48L-3R (Weeks 22-24).....	136
Table A.45 C6-58L Chloride Content Data .....	151
Table A.46 S6-48L Chloride Content Data .....	151
Table A.47 C10-58L Chloride Content Data .....	151
Table A.48 S10-48L Chloride Content Data .....	152

## 1. INTRODUCTION

### 1.1. BACKGROUND, PROBLEM, & JUSTIFICATION

**1.1.1. Self-Consolidating Concrete.** Self-consolidating concrete (SCC) was developed in Japan in the late 1980's to solve the problem of a growing shortage of concrete laborers. Concrete, by its very nature, can be a challenging material to construct properly, particularly with very complex geometrical shapes or within elements containing very congested reinforcement. Placement and finishing of conventional concrete requires a significant amount of labor and is very time consuming. SCC was developed in an attempt to solve these problems. SCC is defined as a concrete that spreads easily under its own weight while still resisting segregation. The benefits of SCC include decreased labor and equipment cost during concrete placement, decreased potential for honeycombing and voids, increased production rates of precast and cast-in-place elements, and improved finish and appearance of cast and free concrete surfaces. However, concerns exist over the structural implications of SCC in cast-in-place and precast elements. Specifically, higher paste contents, higher fine contents, and the use of smaller, rounded aggregates may significantly alter the behavior of SCC compared to traditional concrete mixes with similar water to cementitious ratio (w/cm).

Consequently, to achieve the benefits and potential savings with SCC, the behavior of the material needs to be evaluated relative to conventional concrete. One necessary step required to make SCC so workable is to increase the fine aggregate content while decreasing the coarse aggregate content. However, increasing the fine aggregate content is believed to reduce the modulus of elasticity, as well as the tensile strength of concrete. This decrease in coarse aggregate content could also have negative

side effects on the durability performance of SCC. Resistance to freeze-thaw is largely impacted by the type and content of the coarse aggregate used in the concrete. This change to the coarse aggregate may alter the durability performance of the material. However, some research has shown that the increased density of the paste is thought to improve durability performance with a decrease in overall porosity. As a result, a systematic evaluation of the hardened material properties and durability performance of SCC is required prior to implementing its use in transportation-related infrastructure.

## **1.2. OBJECTIVES & SCOPE OF WORK**

**1.2.1. Self-Consolidating Concrete.** The main objective of this study is to investigate the mechanical properties and the durability performance of SCC in comparison to conventional concrete.

The following scope of work was implemented in an effort to attain this objective: (1) review applicable and relevant literature; (2) develop a research plan; (3) evaluate the mechanical and durability properties of both normal strength and high strength SCC mixes; (4) compare the SCC mixes with conventional concrete mixes; (5) verify the validity of using current hardened property tests on SCC; (6) analyze the information gathered throughout the testing to develop findings, conclusions, and recommendations; and (7) prepare this thesis in order to document the information obtained during this investigation.

### **1.3. RESEARCH PLAN**

**1.3.1. Self-Consolidating Concrete.** The research plan entailed developing SCC mix designs based on current Missouri precast plant applications. The mix designs are described in Section 3. Several standard hardened property tests were selected to evaluate the performance of the SCC mixes in comparison to conventional concrete, including compressive strength, modulus of elasticity, modulus of rupture, and splitting-tensile strength. These tests were also used to determine their validity in predicting the performance of SCC.

Specimens were also fabricated in order to evaluate the durability performance of SCC. The tests performed on the mixes consisted of chloride penetration by electrical indication and ponding methods, freeze-thaw resistance, and concrete resistivity. Both the conventional and SCC mixes were subjected to these durability tests in order to compare their performance.

### **1.4. OUTLINE**

**1.4.1. Self-Consolidating Concrete.** This report consists of seven sections and one appendix. Section 1 briefly explains the history and benefits of using SCC. Also within Section 1 are the objectives, scope of work, and research plan.

Section 2 summarizes how SCC is produced and new test methods used to evaluate the fresh properties of SCC. The mechanical property tests are also discussed in further detail. Lastly, the durability tests as well as the mechanisms behind the durability issues are discussed.

Section 3 explains the development of the SCC mix designs including the selection of chemical admixtures. This section includes typical fresh properties measured

during this investigation. Also, the mechanical property tests are discussed in more detail as well as equations used to estimate the behavior of concrete.

Section 4 consists of discussing the tests used to evaluate the durability performance in further detail.

Section 5 presents the results of both the mechanical property tests as well as the durability tests. Also presented in this section are the normalized results of the mechanical property tests in comparison to traditional relationships used to estimate the behavior of concrete.

Section 6 outlines the results of the investigation and evaluates the data based on a statistical analysis. Also, the results of the investigation are discussed to propose a theory on the outcome of the tests in order to recommend how to successfully implement SCC.

Section 7 consists of the conclusion of the investigation as well as any recommendations based on the findings from the mechanical tests as well as the durability performance of the SCC mixes in comparison to conventional concrete.

There is one appendix contained in this thesis. Appendix A contains additional test data associated with the durability tests of the SCC mixes.

## 2. LITERATURE REVIEW

### 2.1. SELF-CONSOLIDATING CONCRETE

Self-consolidating concrete (SCC) is a relatively new mix of concrete which is characterized by its high degree of workability. SCC is very flowable and doesn't require any vibration when placing in the formwork. SCC also finishes very smoothly, leaving a glassy finish after curing. SCC originated in Japan in the 1980's due to Japan's decreasing labor force [Khayat, 1999]. In order to achieve the high workability of SCC while maintaining cohesiveness, the composition of SCC has to be altered. This can be done one of three ways: chemically, materially, or a combination of the two. To produce SCC chemically, two admixtures are used, High Range Water Reducers (HRWR) and Viscosity Modifying Admixtures (VMA). In concrete, the cement particles typically carry either positive or negative charges. The attraction between particles causes them to agglomerate. Water is trapped inside these particles and is not able to add to the workability of the fresh concrete. HRWRs place a like charge on the cement particles causing them to repel each other. This frees the water in the paste to add to the workability of the concrete. VMAs are used to increase the viscosity of the water, which prevents the highly flowable mix from segregating. These two admixtures allow for SCC to have the high flowability necessary to be beneficial while maintaining cohesiveness. This can also be achieved through purely physical means. To achieve the flowability of SCC, the water to cementitious material ratio (w/cm) must be increased. In order to maintain cohesiveness in such a relatively wet mix, the fine aggregate content must be increased. It is typical to see SCC mixes that contain more fine aggregate than coarse aggregate, which is completely opposite of conventional concrete. Most SCC mixes

today are produced using the third technique, which is a combination of altering the physical composition of the mix as well as the addition of chemical admixtures. These SCC mixtures maintain the high fine aggregate content while using a low w/cm ratio. The highly flowable behavior is achieved through the addition of a HRWR. This creates SCC that is both flowable and doesn't need vibration while maintaining a low w/cm, which can yield stronger and more durable concrete.

Due to the highly flowable nature of SCC, most of the conventional fresh property tests are not applicable to SCC. For this reason, several new property tests were derived in order to test the fresh properties of SCC, which included tests to evaluate properties specific to SCC. These new properties include flowability, passability, and resistance to segregation. In order to test the flowability, which is comparable to the slump of conventional concrete, the slump flow test was created. This test is outlined in ASTM C 1611-09, "Standard Test Method for Slump Flow of Self-Consolidating Concrete." Using a standard Abram's cone, either in the upright or inverted position, the SCC is placed into the cone in a single lift with no tamping or vibration. The cone is then lifted from the slump flow plate and the diameter of the spread is measured. The slump flow test is also used to note the resistance of SCC to segregation. If an SCC mix has segregation problems, most of the coarse aggregate will stay towards the center of the circle. The time it takes for the SCC spread to reach a diameter of 20 in. (50 cm) is also recorded. This reading indicates the ability of the SCC to fill molds and remain stable. The typical target value for the spread of SCC ranges from 22 in. (56 cm) to 29 in. (74 cm). A typical SCC slump flow spread can be seen in **Figure 2.1**.



**Figure 2.1 – Slump Flow Test**

Another test used in correlation with the slump flow test is the J-Ring test. This test is outlined in ASTM C 1621-09, “Standard Test Method for Passing Ability of Self-Consolidating Concrete by J-Ring.” In this test, the slump flow test is performed but a circular ring with vertical bars is placed on the slump flow plate. The concrete is allowed to spread into a circle but must pass through the J-Ring. This test is to simulate reinforcing bars, altering the flow of the SCC. A poor performing SCC mix will maintain a noticeable amount of the coarse aggregate within the J-Ring, allowing only the mortar fraction (cement, sand, and water) to pass through. This behavior indicates a lack of cohesiveness, which would prove detrimental if used in the field. The diameter of the spread using the J-Ring is also measured, and in addition to the behavior of the coarse aggregate during the test, a successful test typically requires the J-Ring diameter to measure no more than 2 in. (51 mm) less than the value recorded for the corresponding slump flow. A typical J-Ring spread can be seen in **Figure 2.2**.



**Figure 2.2 – J-Ring Test**

Other fresh property tests include the L-box test and the segregation column to measure passability and stability, respectively. The L-box is a non-ASTM test outlined in ACI 237-07 which is used to determine the passing and filling ability of an SCC mix. The vertical column of the L-box is first filled with SCC in a single lift, without vibration or tamping. A gate is then lifted allowing the SCC to flow out of the vertical column and into the horizontal trough of the L-box. At the gate there are three bars simulating reinforcing steel that the SCC must pass through. The SCC must reach the end of the horizontal section of the L-box in order for it to pass. Additionally the ratio of the height of the SCC at the end of the trough over the height of the SCC at the gate is measured. This is referred to as the “blocking ratio”. A SCC mix must have a minimum blocking ratio of 0.8 to be considered acceptable. The closer the blocking ratio is to 1.0 the better performance a SCC mix can be expected to show. A typical L-box is shown in **Figure 2.3**.

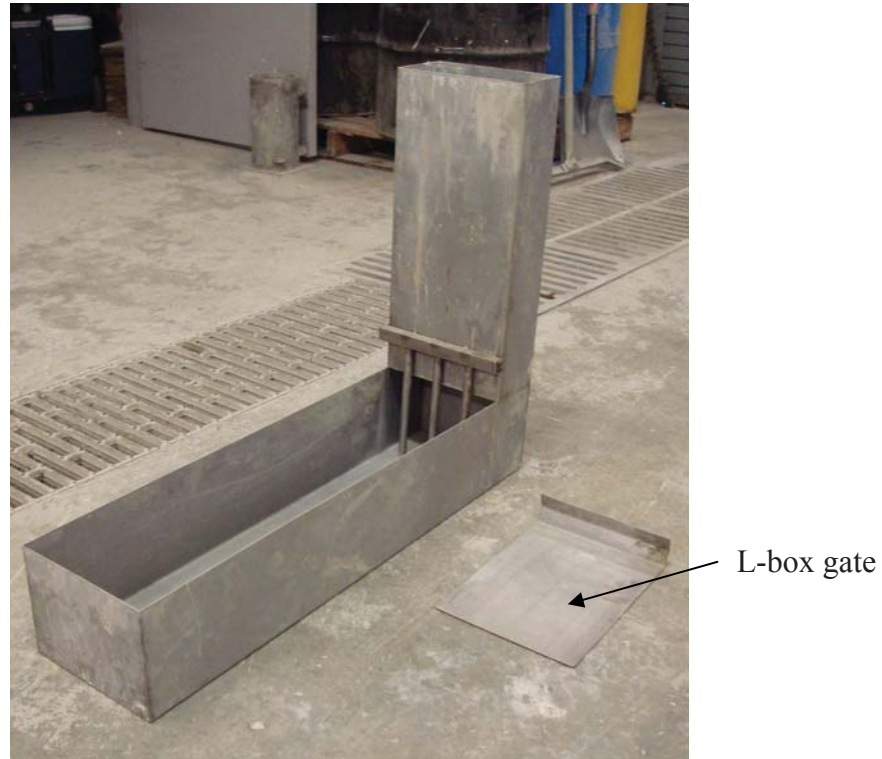


**Figure 2.3 – Typical L-box Test Set-Up with Gate Removed**

The segregation column is used to determine the ability of the SCC mix to resist static segregation. This test is outline in ASTM C 1610-10, “Standard Test Method for Static Segregation of Self-Consolidating Concrete Using Column Technique.” A column measuring 26 in. (660 mm) in height and 8 in. (200 mm) in diameter is filled in one lift with SCC. This column is made up of three separate sections, the top and bottom sections measuring 6.5 in. (165 mm) in height and the middle section measuring 13 in. (330 mm) in height. The segregation column can be seen in **Figure 2.4**. Once the column is filled, the SCC is then allowed to sit for 15 minutes. The SCC from the top and bottom sections of the column is then collected separately and rinsed over a No. 4 sieve in order to separate the paste from the aggregate. The aggregate from the top and bottom column

sections is then dried and weighed. Using these weights the static segregation is calculated in accordance with **Eq. 2.1**.

$$S = 2 \left[ \frac{(CA_B - CA_T)}{(CA_B + CA_T)} \right] \times 100, \text{ if } CA_B > CA_T \quad (2.1)$$

$$S = 0, \text{ if } CA_b \leq CA_T$$

Where S is the static segregation in percent,  $CA_T$  is the mass of coarse aggregate in the top section of the column, and  $CA_B$  is the mass of coarse aggregate in the bottom section of the column. Although an acceptable standard for static segregation has not yet been established, an SCC mix is generally considered acceptable if the static segregation is less than 10%.



**Figure 2.4 – Typical Segregation Column**

## 2.2. MECHANICAL PROPERTY TESTING METHODS

**2.2.1. Compressive Strength.** The compressive strength of concrete is the most important of all the mechanical properties. Measuring compressive strength is influenced by many factors including specimen size, curing conditions, load rate, etc. In order to control variations in testing and consequently variations in results, a standard test method was developed by ASTM International. The standard for determining the compressive strength of concrete is outlined in ASTM C 39–11, “Standard Test Method for Compressive Strength of Cylindrical Concrete Specimens.” This standard requires cylindrical specimens for testing. The specimens used in laboratory testing measure either 4 in. (102 mm) in diameter x 8 in. (203 mm) in height or 6 in. (152 mm) in diameter x 12 in. (305 mm) in height. The specimens are prepared by filling the molds in equal lifts and rodding each lift a specified number of times. The numbers of lifts and extent of rodding depends on the diameter and cross sectional area, which is specified in ASTM C 192-07 “Standard Practice for Making and Curing Concrete Test Specimens in the Laboratory.” After each lift, the mold is also struck with a mallet to ensure consolidation. After 24 hours in a moist curing chamber, the specimens are de-molded and returned to the moist curing chamber until the proper test date. Common testing dates for measuring a concrete’s strength gain profile are 1, 7, and 28 days after batching. The cylindrical specimens are ground flat or capped before testing. This flat surface reduces localized stress on the specimen. Capping can be done with sulfur capping compound or neoprene pads. Dimensions of the specimens are taken before being loaded at a constant rate until

failure. The load recorded at failure is divided by the cross-sectional area to find the compressive strength of the concrete.

**2.2.2. Modulus of Elasticity.** Due to the nonlinear inelastic behavior of concrete, the modulus of elasticity (MOE) can be different depending on how it is measured. The MOE is the slope of the stress–strain curve between two designated points. An example of the different moduli of elasticity that can be measured can be seen in **Figure 2.7**.

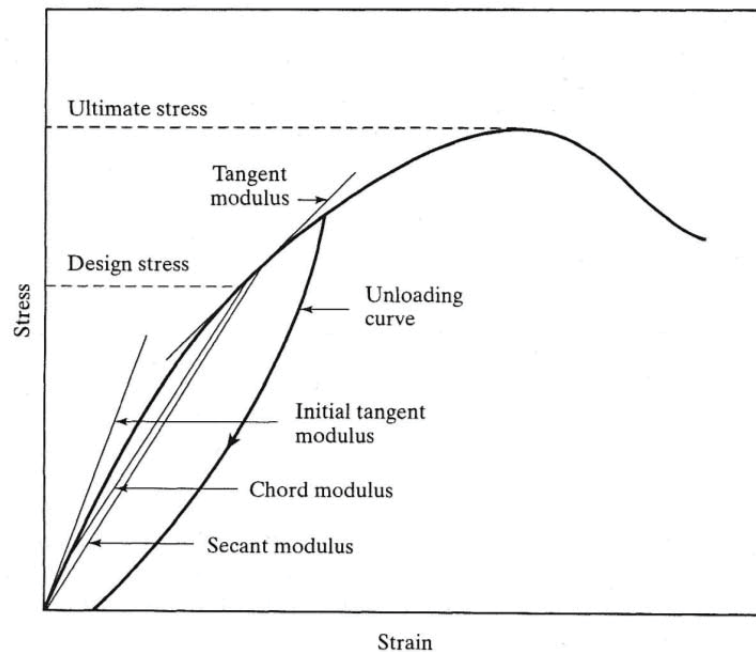


**Figure 2.7 – Typical Stress-Strain Diagram for Concrete, Showing the Different Elastic Moduli [Mindess et al., 2002]**

In order to standardize the measured modulus of elasticity, ASTM International developed a standard test method ASTM C 469-10, “Standard Test Method for Static Modulus of Elasticity and Poisson’s Ratio of Concrete in Compression.” This test method measures what is known as the chord modulus of elasticity. The specimens used in this

test are the same type used in the compressive strength test. Either the 4 in. (102 mm) or 6 in. (152 mm) diameter cylindrical specimens can be used. Specimens are fabricated and cured in the same manner as the compressive strength specimens. After 28 days of moist curing, specimens are prepared for testing. Using a Compressometer, the strain produced at 40% of the ultimate load is recorded. Also, the stress that produces a measured strain of 0.00005 in./in. is recorded. Using these values, the chord modulus of elasticity can be calculated in accordance with **Eq. 2.2**.

$$E_c = \frac{(S_2 - S_1)}{(\epsilon_2 - 0.00005)} \quad (2.2)$$

**2.2.3. Modulus of Rupture.** The modulus of rupture is an important property in the calculation of the cracking moment of concrete and thus determining how a concrete member will behave post-cracking. ASTM International has created a standard for testing the modulus of rupture known as ASTM C 78-10, “Standard Test Method for Flexural Strength of Concrete (Using Simple Beam with Third-Point Loading).” This approach is an indirect way to measure the tensile strength of concrete. The specimen has to have an overall depth of a third of the span length. The span length shall be such that it measures three times the distance in between the load points of the testing apparatus. Also, the specimen shall overhang the supports by at least 1 in. (25 mm). The schematic diagram in **Figure 2.8** summarizes these requirements.

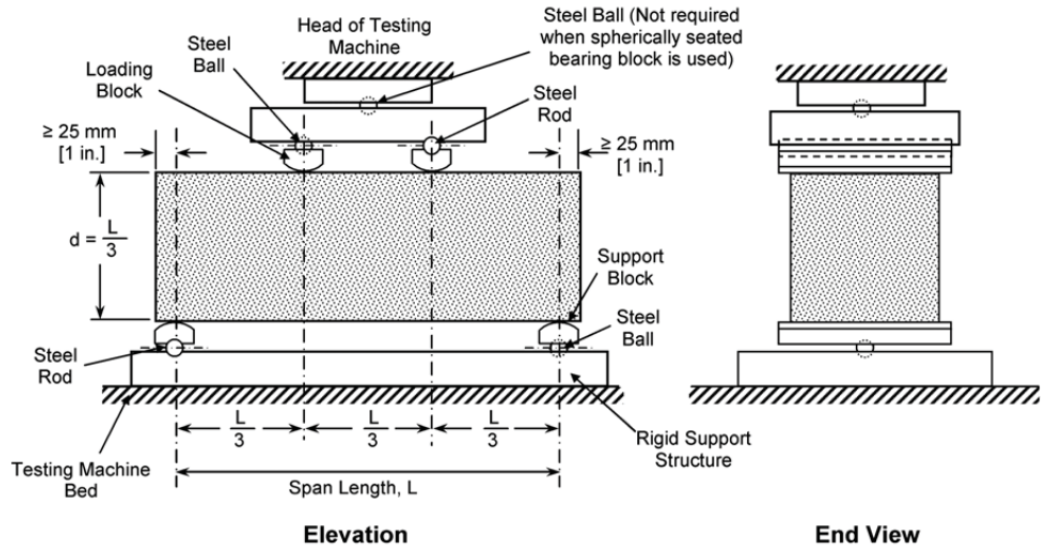


**Figure 2.8 - Typical Modulus of Rupture Testing Setup [ASTM C 78–10]**

The specimen is then loaded until failure. After testing, the dimensions are recorded and the modulus of rupture is computed in accordance with **Eq. 2.3**. While this test method overestimates the “true” tensile strength of concrete, the test does simulate the most common way concrete is placed into tension, through flexure.

$$R = \frac{PL}{bd^2} \quad (2.3)$$

**2.2.4. Splitting Tensile Strength.** While the modulus of rupture test described in Section 2.3.3 tests for the tensile strength of concrete indirectly, the splitting tensile test uses a much more direct manner. This test is outlined in ASTM C 496–11, “Splitting Tensile Strength of Cylindrical Concrete Specimens.” The cylindrical specimens measure either 4 in. (102 mm) in diameter by 8 in. (203 mm) in height or 6 in. (152 mm) in diameter and 12 in. (305 mm) in height. The method for preparing the specimens used in the splitting-tensile test is outline in ASTM C 192. Specimens are

stored in a moist curing chamber and tested after 28 days. Diametral lines are drawn on the specimens to ensure that they are in the same axial plane. The dimensions of the specimens are then taken. The specimens are then placed on top of a 1 in. (25 mm) wide x 3/8 in. (10 mm) thick plywood strip within the testing apparatus. A second plywood strip is then placed on top of the specimen so the two strips align with the diametral lines. This ensures that the load is distributed in one plane of the specimen. The peak load is recorded and the tensile strength is then calculated in accordance with **Eq. 2.4**.

$$T = \frac{2P}{\pi LD} \quad (2.4)$$

## **2.3. DURABILITY OF CONCRETE**

**2.3.1. Freezing and Thawing.** Concrete is a porous material which allows water to permeate into its microstructure. When concrete containing moisture is subjected to repeated cycles of freezing and thawing, severe deterioration can occur. Initially researchers believed that this damage was caused by the expansion of water when it transitioned into ice. The trapped water would freeze and expand in the capillary pores and exert hydraulic pressure on the hardened paste. This theory of hydraulic pressure was proposed by T.C Powers [Mindess et al., 2002]. Later, Powers developed a new theory based on osmotic pressure [Powers, 1956]. He proposed this theory after observing that concrete paste, when frozen, shrank first than expanded. He also observed that air entrained cement paste would shrink indefinitely and the same deterioration is observed when liquids that do not expand when frozen were used to saturate the concrete. Investigators developed two possible explanations for these observations. The first is

osmotic pressure. As water is drawn to the freezing sites through osmosis, osmotic pressure is built up. This eventually would cause the concrete to crack. Another possible explanation is vapor pressure. The ice that begins to form in the pores has less chemical potential than the supercooled water in the unfrozen pores. This creates a lower vapor pressure. This condition causes the relative humidity at the freezing pores to lower, which draws water towards them to maintain equilibrium. This pressure would also cause the concrete to begin to crack.

The introduction of air entraining admixtures has had a positive effect on the resistance of concrete to freezing and thawing deterioration. The air bubbles in the concrete allow for excess space for the water to move and freeze without damaging the concrete. These bubbles must be spaced at certain intervals to be effective in protecting the concrete. If the bubbles are too far apart, the water cannot move to these “safety valves” and the pressure cannot be relieved. The air-entraining system becomes ineffective in fully saturated concrete due to all the pores and air bubbles containing water. Many other factors influence a concrete’s resistance to freezing and thawing attack, the most important of which is the permeability of the concrete. With concretes having a low water/cement ratio and usually a low permeability, freeze/thaw resistance generally increases [Mindess et al., 2002]. This relationship can be seen in **Table 2.1**.

**Table 2.1 Effect of w/cm Ratio on the Air Void System in Concrete**

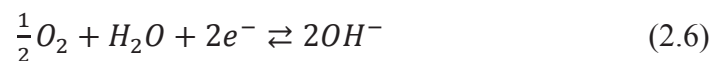
w/c ratio	Air content (%)	Spacing factor mm (in.)	Liner expansion per freeze – thaw cycle
0.35	4.8	0.11 (0.0043)	0.00004
0.45	4.7	0.14 (0.0055)	0.00014
0.55	5.2	0.15 (0.0059)	0.00021
0.65	4.9	0.18 (0.0071)	0.00026
0.75	5.3	0.23 (0.0091)	0.00036

1 in. = 2.54 cm.

**2.3.2. Chloride Attack.** Chloride ions attack the passive layer that forms on reinforcing steel placed within a high pH environment, such as concrete. Chloride ions are most commonly introduced into concrete through deicing salts. These salts can remain on bridge decks for days or even weeks, penetrating into the concrete structure and eventually destroying the passive layer of the reinforcing steel. Corrosion in steel begins with the iron being oxidized at an anode as shown in **Eq. 2.5**.



At the cathode, water is reduced into hydroxyl ( $OH^{-}$ ) ions as shown in **Eq. 2.6**.



These hydroxyl ions then flow from the cathode to the anode. At the anode, the ferrous ions and the hydroxyl ions react to form ferrous hydroxide as shown in **Eq. 2.7**.



When oxygen and water are introduced the ferrous hydroxide will spontaneously oxidize into hydrated ferric oxide (rust) as shown in **Eq. 2.8**.



This hydrated ferric oxide, or red rust that is commonly seen, is known to have six times the volume of the original iron [Broomfield, 2007]. The increased volume induces expansive stresses in the concrete, eventually leading to cracking and progressive deterioration. The volume of iron and various forms of oxidized irons can be seen in

**Figure 2.9.**

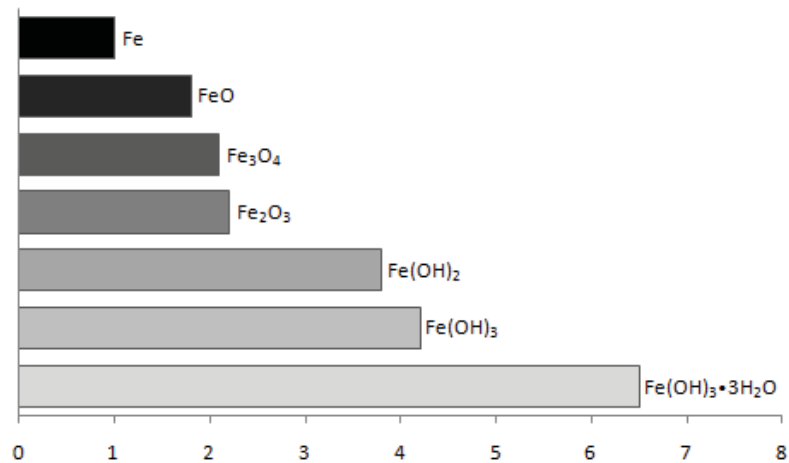


**Figure 2.9 - The Relative Volumes of Various Iron Oxides from Mansfield [1981], Corrosion 37(5), 301-307.**

This reaction can be largely avoided in concrete structures. Conventional concrete is highly alkaline which allows for the formation of a passive oxide film (FeOOH) on the reinforcement. The Fe(OH)<sub>2</sub> is oxidized to create this film as shown in **Eq. 2.9**.



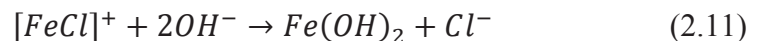
Chlorides effectively destroy this passive layer allowing for the reinforcement to corrode.

Chlorides react with ferrous ions to create a soluble iron-chloride complex as shown in

**Eq. 2.10**.



This complex in turn reacts with the hydroxyl to form the ferrous hydroxide which oxidizes into expansive rust as shown in **Eq. 2.11**.



The largest factor influencing the effect of chlorides in concrete is the permeability of the concrete. The permeability relates to the amount and rate of oxygen, moisture, and chloride penetration into the microstructure of the concrete over time. Permeability is most influenced by the water to cementitious material ratio (w/cm). The lower the w/cm ratio of the concrete, the lower the porosity [Powers et al., 1954]. Decreasing the permeability of concrete will improve its durability. Water can carry harmful chemicals,

such as chlorides, into the concrete's pores. The diffusion of chemicals into hardened concrete is described by *Fick's Second Law* as shown in **Eq. 2.12**.

$$\frac{\partial C}{\partial t} = K_d \frac{\partial^2 C}{\partial x^2} \quad (2.12)$$

Where C is the concentration, t is the time,  $K_d$  is the diffusion coefficient, and x is the depth. The solution of this equation is shown in **Eq. 2.13** [Broomfield 2007].

$$\frac{C_{max}-C_d}{C_{max}-C_{min}} = erf\left(\frac{x}{\sqrt{4D_c t}}\right) \quad (2.13)$$

Where  $C_d$  is the chloride concentration at depth (x), x is the specified depth, t is the time,  $D_c$  is the diffusion coefficient of concrete,  $C_{max}$  is the maximum chloride content of the concrete,  $C_{min}$  is the baseline chloride content of the concrete, and erf is the error function. Using this function the chloride penetration over time can be estimated. This equation has proved to estimate chloride contents extremely accurately when compared to field results [Berke and Hicks, 1996].

## 2.4. DURABILITY TESTING METHODS

**2.4.1. Resistance to Freezing and Thawing.** In order to evaluate the potentially devastating effects of freezing and thawing cycles, ASTM International developed a standardized test to simulate these conditions in the lab. This test is outlined in ASTM C 666–03 “Standard Test Method for Resistance of Concrete to Rapid Freezing and Thawing.” Specimens used in this test are prisms that are made and cured in

accordance with ASTM C 192. The dimension requirements of these specimens are specified in ASTM C 666. The specimens are cured for 14 days before testing unless otherwise specified. This test subjects the specimens to 300 freezing and thawing cycles. Every 36 cycles, the specimens are removed and properties of the concrete are measured. These properties include the transverse frequency, total length change, and total weight change. These specimens can be tested using two different procedures, A or B. Procedure A specifies that the specimens be surrounded by water during the freezing and thawing cycles, while Procedure B specifies that the specimens be surrounded by air during freezing and water during thawing. Between the testing intervals, both the relative dynamic modulus of elasticity and the durability factor are calculated. Using these values, the concrete can be evaluated for its durability performance. The test calls for the cycles to be stopped when the measured durability factor falls below 50. Every Department of Transportation has its own criteria for acceptable durability factor and sets a minimum for acceptance. The acceptability criteria for the state of Missouri and for this investigation will be discussed in Sections 6.1.2 and 6.2.2.

**2.4.2. Rapid Chloride Penetration.** The diffusion of chlorides can be extremely damaging, as stated previously. However the process is very slow, and testing the chloride penetration accurately can take years. In order to test a concrete's ability to resist chloride penetration, ASTM International developed a testing method that could be performed much more quickly. This testing method is outlined in ASTM C 1202-10, "Standard Test Method for Electrical Indication of Concrete's Ability to Resist Chloride Ion Penetration." This test is also known as the Rapid Chloride Test (RCT). The test specimens consist of concrete disks subjected to a constant voltage to determine their

resistance to chloride penetration. The disks are cut from concrete cylinders that are fabricated and cured according to ASTM C 192. The disks, measuring 4 in. (102 mm) in diameter and 2 in. (51 mm) thick, are prepared according to ASTM C 1202 and subjected to 60 V for 6 hours as shown in **Figure 2.10**.

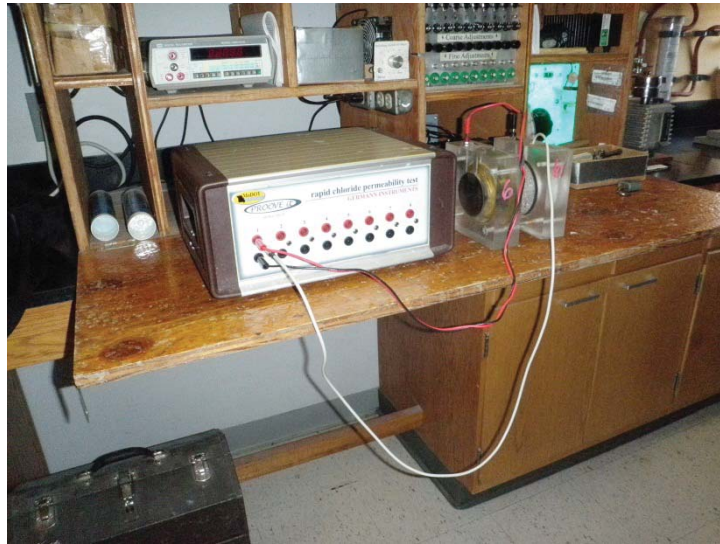


**Figure 2.10 - Typical RCT Setup**

During the test, the current is recorded every 30 minutes. Using a plot of current versus time, the total charge passed is calculated and used to determine the permeability class of the concrete. There is a correlation between the amount of charge passed and the chloride ion penetrability of concrete. This correlation can be seen in **Table 2.2**.

**Table 2.2 Chloride Ion Penetrability Based On Charge Passed [ASTM C1202–10]**

Charge Passed (coulombs)	Chloride Ion Penetrability
>4000	High
2000-4000	Moderate
1000-2000	Low
100-1000	Very Low
<100	Negligible

**2.4.3. Chloride Content Analysis.** While the test outlined in ASTM C 1202 is an adequate test when the results are required quickly, it does not subject the concrete to realistic conditions. ASTM C 1202 is only suitable for research and development. One study has indicated that ASTM C 1202 gives false indications for concretes made with supplementary cementitious materials, such as fly ash, slag, silica fume, and slag [Shi, 2002]. This study showed that cement containing supplementary cementitious material would yield falsely high results than what was observed in the field. Researchers found that the change in chemical composition due to the addition of supplementary cementitious material affected the results of the Rapid Chloride Test. In order to properly evaluate a concrete's ability to resist chloride penetration, it should be tested directly using ASTM C 1543-10, "Standard Test Method for Determining the Penetration of Chloride Ion into Concrete by Ponding." This test method involves subjecting concrete specimens to a 5% by weight sodium chloride solution for 120 days. The specimens are then cored and powder samples are collected to determine the chloride content at multiple levels. According to Broomfield [2007], it is recommended that a minimum of four data points be used in developing a chloride profile in order to obtain an accurate representation of the chloride distribution. A chloride content analysis is then performed on the powder samples in order to determine the chloride profile of the concrete. Two types of chloride analyses can be performed on the concrete powder; acid-soluble and water-soluble. Acid-soluble tests will determine the total chloride content, including those chlorides trapped in the aggregate and paste ( $C_3A$ ). Water-soluble tests will only determine those chlorides free to deteriorate the passive layer of the concrete, thus promoting corrosion. In some

cases, the acid-soluble test will overestimate the corrosion potential of a concrete and in others provide a reasonable evaluation. ACI has developed limits on chloride content for new construction for varying applications of concrete. These limitations can be seen in **Table 2.3**.

**Table 2.3 Chloride Limits for New Construction in % Chloride by Mass of Cement [ACI, 2001]**

	Test method	
	Acid Soluble	Water Soluble
Concrete Application	ASTM C1152	ASTM C1218
Pre-stressed concrete	0.08	0.06
Reinforced concrete in wet conditions	0.10	0.08
Reinforced concrete in dry conditions	0.20	0.15

For in place structures, classifications were developed based on chloride contents and the corrosion risk. These classifications can be seen in **Table 2.4**. [Broomfield, 2007]

**Table 2.4 Correlation Between Percent Water Soluble Chloride by Mass of Concrete and Corrosion Risk [Broomfield, 2007]**

% Chloride by mass of concrete	Corrosion Risk
<0.03	Negligible
0.03-0.06	Low
0.06-0.14	Moderate
>0.14	High

The chloride profile determined from this test method indicates the concentration of the chloride ions in the concrete as a function of depth from the surface. As stated in Section 2.4.2, chlorides will destroy the passive layer on the reinforcement in the concrete, exposing the steel to elements that will initiate corrosion. The chloride profile determined from this test method will indicate the amount of ions at specified depth to determine a concrete's ability to resist diffusion and therefore chloride ingress. In general, this test is a comparative test and does not necessarily indicate the response of a structure in service.

**2.4.4. Concrete Resistivity.** Electrical resistance also plays an important role in the ability of concrete to resist corrosion. When hydroxyl ions (OH<sup>-</sup>) are created at the cathode, they must move to the anode to cause the oxidation process to begin. The slower these ions are transported, the slower the corrosion process. This ionic current is similar to electrical current. Therefore, the rate of corrosion of the reinforcement can be estimated by the electrical resistance of the concrete [Whiting and Nagi, 2003].

Three methods have been developed to analyze the electrical resistance of concrete: single-electrode method, two-probe method, and the four probe method. Of the three methods the two-probe method is the most labor intensive and least accurate [Broomfield, 2007]. The two-probe method works by measuring the potential between two electrodes by passing an alternating current between them. If aggregates are located near the electrodes this can cause a false reading. Aggregates have a higher resistivity than concrete paste and will therefore cause a reading to be much higher than the actual resistivity. In order to counteract this problem, shallow holes can be drilled to place the electrodes into. However this is what makes the two probe method labor intensive.

The single-electrode method is a more advanced method to determine a concrete's resistivity. This method uses a disk placed on the concrete's surface as an electrode and the embedded steel reinforcement as the second electrode. The resistivity of the concrete is measured using **Eq. 2.14**.

$$\text{Resistivity } (\Omega\text{cm}) = 2RD \quad (2.14)$$

Where R is the resistance drop between the embedded reinforcement and the surface electrode, and D is the diameter of the surface electrode.

The third method is the four-probe method developed by Frank Wenner. This method was developed in 1916 and was designed for geophysical studies. This method has become widely accepted by the industry and is known as the Wenner method. The probe used in this method has four equally spaced electrodes on a single rod. The two outer electrodes send an alternating current through the concrete while the middle two electrodes measure the change in potential. The resistivity is then calculated using **Eq. 2.15**.

$$\rho = \frac{2\pi sV}{I} \quad (2.15)$$

Where  $\rho$  is the resistivity ( $\Omega\text{cm}$ ),  $s$  is the spacing between the electrodes (cm),  $V$  is the voltage (V), and  $I$  is the applied current (A). When the current is applied through the concrete it travels in a hemispherical pattern. This can be seen in **Figure 2.11**. This

allows for a greater area of concrete to be measured and thus avoids the influence of highly resistive aggregates.

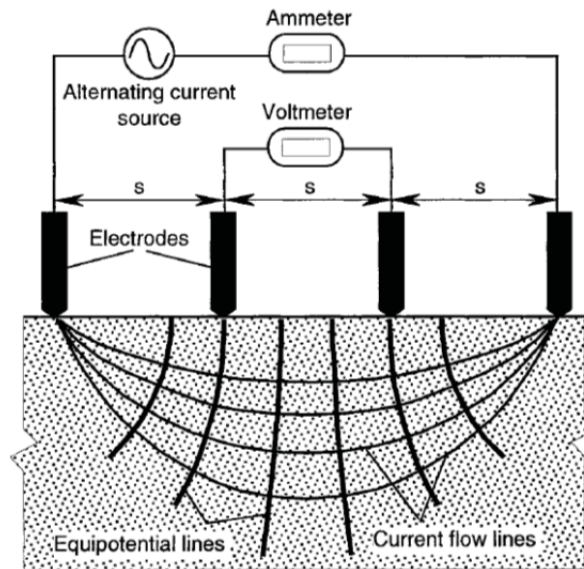


**Figure 2.11 - Schematic Representation of the Four-Probe Resistivity Method [Broomfield, 2007]**

The four-probe method is based on the theory that the resistivity values measured by the equation above are accurate if the current and potential fields exist in a semi-infinite volume of material [Whiting and Nagi, 2003]. This assumption indicates that larger concrete specimens will yield more accurate results. This condition has been found to be true. Measuring relatively thin concrete members or near edges produces noticeable errors. It is recommended that the spacing between the electrodes of the probe do not exceed  $\frac{1}{4}$  of the smallest concrete section dimension. Another source of error is the non-homogeneous composition of concrete. While the assumption of the Wenner method is that the material will have a consistent resistivity, this is not the case for concrete. Highly resistive aggregates are surrounded by low-resistivity paste which affects the

measurements. According to research, this source of error can be avoided by using a probe where the spacing between electrodes is greater than 1.5 times the aggregate maximum size. This approach will maintain a coefficient of variation less than 5% [Whiting and Nagi, 2003]. A correlation was developed between measured concrete resistivity and the corrosion rate of embedded reinforcement. This classification can be seen in **Table 2.5**. This relationship was developed by Langford and Broomfield in 1987 and is widely used in the field.

**Table 2.5 Correlation Between Concrete Resistivity and the Rate of Corrosion for a Depassivated Steel Bar Embedded within the Concrete [Broomfield, 2007]**

Concrete Resistivity	Rate of Corrosion
>20 kΩcm	Low
10-20 kΩcm	Low to Moderate
5-10 kΩcm	High
<5 kΩcm	Very High

**2.4.5. Scaling Resistance.** The presence of salt solutions on concrete can cause additional damage besides corrosion of the reinforcing steel. The surface of the concrete can become pitted and roughened by a mechanism called scaling. In addition to leaving the surface scarred and rough, it can also increase the permeability of the concrete. To evaluate a concrete's resistance to scaling ASTM has created a test method ASTM C 672-03, "Standard Test Method for Scaling Resistance of Concrete Surfaces Exposed to Deicing Chemicals." This test method requires specimens to have at least 72 in<sup>2</sup> (46,452 mm<sup>2</sup>) of surface area and be at least 3 in. (76 mm) deep. The specimens are broom finished and a dike is built up around the perimeter of the specimen. This dike

must be at least 0.75 in. (19 mm) tall and approximately 1 in. (25 mm) wide. The specimen is then moist cured for 14 days and then air cured for 14 days. When the curing duration is over the surface of the specimen is covered with a solution having a concentration of 5.34 oz /gal (0.04 g/mL) of anhydrous calcium chloride. The specimen is then subjected to 50 cycles of freezing and thawing. After every 5 cycles, the solution is completely replaced and the condition of the surface is evaluated. After 50 cycles the surface of the concrete is evaluated and given a rating based on the scaling resistance. The rating scale can be seen in **Table 2.6**.

**Table 2.6 Rating Scale for Scaling Resistance [MoDOT]**

Rating	Condition of Surface
1	No scaling
2	Very slight scaling
3	Slight to moderate scaling
4	Moderate scaling
5	Moderate to severe scaling

## 2.5. SELF-CONSOLIDATING CONCRETE

**2.5.1. Mechanical Properties.** Through several investigations ACI has released report ACI 237R-07, “Self-Consolidating Concrete” outlining SCC and the properties that can be expected. The document outlines both fresh properties as well as performance requirements SCC should meet to be used in the field. In the area of compressive strength, SCC tends to perform very well. In order to achieve the flowable behavior of SCC, the w/cm ratio must be lowered through the use of a HRWR. This combination can yield higher 28-day compressive strengths than conventional concrete at the same w/cm ratio. The use of a HRWR allows for more Portland cement to be

hydrated creating a denser microstructure which in turn creates a concrete stronger in compression. In the area of modulus of rupture SCC should perform better than conventional concrete. This is due to the above mentioned denser microstructure [Sonebi and Bartos, 2001]. In the area of modulus of elasticity investigations have reported conflicting conclusions. According to Bennenck [2002], SCC mixes of equal compressive strengths to conventional concrete showed a lower modulus of elasticity by as much as 15%. This result is most likely due to the high fine aggregate content that it takes to maintain cohesiveness in SCC. However, Persson [1999] as well as Mortsell and Rodum [2001] found that the modulus of elasticity of SCC was very similar to conventional concrete of equal compressive strengths.

**2.5.2. Durability Performance.** With a denser microstructure created by the very nature of the concrete, SCC is believed to have better durability performance than conventional concrete. Khayat [2002] found that with a proper air-void system SCC shows excellent freeze-thaw resistance when subject to 300 cycles. It has been seen that SCC tends to have lower chloride diffusion than conventional concrete [Audenaert, 2003]. This result indicates that SCC should perform well in the area of the electrical indication of chloride penetration test as well as the ponding test. This reduction in chloride penetration is due to the denser microstructure found in SCC as mentioned previously. This denser microstructure should also lead to better resistivity than conventional concrete when measured with the Wenner probe.

### 3. MECHANICAL PROPERTY TESTS

#### 3.1. INTRODUCTION

This section discusses the mechanical property tests used to evaluate the performance of the specialized concrete – self-consolidating concrete (SCC). The mechanical property comparison was important because these properties are essential to estimating the behavior of concrete in the field. These also serve as a good indicator of the quality of the concrete. The following mechanical property tests were included in the scope of work of this investigation:

- Compressive Strength of Cylindrical Concrete Specimens (ASTM C 39-11a)
- Static Modulus of Elasticity and Poisson’s Ratio of Concrete in Compression (ASTM C 469-10)
- Flexural Strength of Concrete (Using Simple Beam with Third-Point Loading) (ASTM C 78-10)
- Splitting Tensile Strength of Cylindrical Concrete Specimens (ASTM C 496-11)

These are standard tests that are used to investigate the most commonly used mechanical properties of concrete. Running these tests on both the conventional concrete and the specialized concretes will not only assure the quality of the conventional concrete but also will serve as a baseline of comparison for the specialized concretes. These mechanical properties are used in many aspects of design, and the results of these tests will allow investigators to determine how applicable existing formulas are in estimating these properties.

An outline for all the mechanical tests performed on all experimental mixes is shown in **Table 3.1**. The outline identifies the number of test specimens fabricated for

each test for each concrete mix. All of the concrete specimens were moist cured until the designated testing date. The date tested is listed as number of days after batching of the concrete.

**Table 3.1 Test Matrix for Mechanical Properties**

Material Property	Number of Specimens	Moist Curing Duration, days	Testing Date(s), days
Compressive Strength	9, (3/date)	1, 7, 28	1, 7, 28
Modulus of Elasticity	3	28	28
Flexural Strength	3	28	28
Splitting Tensile Strength	3	28	28

### 3.2. MIX DESIGN

**3.2.1. Self-Consolidating Concrete Mix Design.** One of the most essential parts of the investigation was the determination of the mix designs to be tested. Mix designs had to adequately represent mixes used by various contractors throughout the state of Missouri. Several contractors were already using SCC in some projects. It was important to establish an idea of what was commonly being used in the state to make the results from the investigation as applicable and relevant as possible. A survey was sent to several major concrete contractors and precasters throughout Missouri asking questions with regard to their use of SCC, including details such as cement content, admixture type and dosages, and aggregate content, type, and gradation. The responses were collected and together with mixes previously used in research at Missouri University of Science and Technology, mix designs that were relevant to contractors in the state of Missouri were then created. The admixture additions to the concrete mixes were given in dosage ranges. In order to find the appropriate admixture dosages, trial batches were mixed and

admixtures were added. If the admixtures had too great of an effect, the mix was re-batched and a smaller dosage was used. If the dosage did not have the desired effect, the same was done with a greater dosage. This process was repeated until the desired plastic properties were achieved.

The final mix designs are shown in **Table 3.2**. The mix design ID is based on characteristics of each mix. The first letter of the name designates the type of concrete, C for conventional concrete, S for self-consolidating concrete. The first number designates the target strength of the mix, 6 for 6,000 psi (41.3 MPa) and 10 for 10,000 psi (68.9 MPa). The second number designates the coarse aggregate percentage as a function of the total amount of aggregate, 58 for 58% coarse aggregate content, 48 for 48% coarse aggregate content. The last letter designates the type of coarse aggregate used, with L for limestone and R for river gravel; although only limestone was considered for material property testing reported in this thesis (Another aspect of this investigation not covered in this thesis studied the effects of different types of coarse aggregates on the shear behavior of SCC.)

**Table 3.2 Mix Design per Cubic Yard for SCC Investigation**

	Mix Design ID			
	C6-58L	S6-48L	C10-58L	S10-48L
Cement (Type III) (lb)	750	750	840	840
Fly Ash (lb)	0	0	210	210
w/cm ratio	0.37	0.37	0.3	0.3
Coarse Aggregate, SSD (lb)	1611	1333	1440	1192
Fine Aggregate, SSD (lb)	1166	1444	1043	1291
HRWR dosage (fl. oz)	29.25	46.5	52.5	63
Air Entrainment (fl. oz)	11.25	11.25	0	0

1 lb = 0.45 kg  
1 fl. oz. = 29.57 mL

For example, C6-58L stands for conventional concrete with a target strength of 6,000 psi (41.3 MPa) and a coarse aggregate content of 58% limestone. The abbreviation HRWR in the table stands for high range water reducer, which was Glenium 7700 manufactured by the BASF Corporation (BASF). The air entraining admixture used was MB-AE-90, also manufactured by BASF. The reasons these admixtures were used is explained later in this section.

For the mix designs shown in Table 3.2 a Type III cement was chosen for high early strength. The coarse aggregate was dolomitic limestone with a nominal maximum aggregate size of  $\frac{3}{4}$  in. (19.05 mm) from Capital City Quarry located in Rolla, Missouri. The fine aggregate was river sand from the Missouri River. The SCC mixes contained a lower percentage of coarse aggregate and a higher percentage of fine aggregate to provide the necessary filling, passing, and flowability characteristics. It should be noted that the batch water was adjusted to account for any moisture that was present in the aggregate. The total moisture content was found by taking a representative sample of the aggregate and weighing it. The sample was then placed into an oven and dried over night. The dried sample was then re-weighed and the difference was taken as the total moisture content.

Two types of admixtures were also used in the mix design, a high range water reducer (HRWR) and an air-entraining admixture. A HRWR was added to the mix in order to achieve the high flowability of the self-consolidating concrete without increasing the water to cementitious material ratio (w/cm). This allowed the concrete to maintain a comparable strength to its conventional counterpart but have the flowable plastic behavior that makes the concrete self-consolidating. In concrete, the cement particles

typically carry either positive or negative charges. The attraction between particles causes them to agglomerate. Water is trapped inside these particles and is not able to add to the workability of the fresh concrete. HRWRs place a like charge on the cement particles causing them to repel each other. This frees the water in the paste to add to the workability of the concrete. This apparent increase in water content allows the workability to increase while maintaining the low w/cm that is necessary for high strength concrete.

To provide the necessary durability of concrete, an air-entraining admixture was also used. Concrete that is exposed to freezing and thawing temperatures is at risk of serious deterioration. One of the most effective ways to protect against that is using an air-entraining admixture. This admixture creates an air void system in the concrete paste that is composed of millions of tiny bubbles. This air void system allows for the pressure that builds up due to the freezing of water to be released into these tiny bubbles. The normal strength concrete mixes (C6-58L and S6-48L) had a target total air content of 6%, (entrapped and entrained), while the high strength concretes did not use any air entraining admixture. This number was based on ACI recommendation for air content based on the  $\frac{3}{4}$ " nominal maximum size of the coarse aggregate for optimal frost resistance. These admixtures were added at trial dosages until the desired behavior and air contents were achieved. The admixtures were added to the concrete during the mixing process by adding the dosages into the batch water. This allowed the admixtures to be dispersed in the fresh concrete. The proper dosages were established using 3 ft<sup>3</sup> (0.08 m<sup>3</sup>) mixes. When the proper dosages were found for the trial batches, the measurements were calculated for the larger pours.

Fresh concrete properties were measured during each batching operation, either within the Butler Carlton Civil Engineering Hall (BCH) Materials Lab for mixes prepared on site or within the BCH Structural Engineering High-Bay Research Laboratory (SERL), at Missouri S&T for mixes delivered by a local ready-mix supplier. These tests were performed to ensure that certain properties were achieved such as workability and air content. The following fresh property tests were performed on the conventional concrete mixes:

- Slump of Hydraulic-Cement Concrete (ASTM C 143)
- Unit of Weight of Concrete (ASTM C 138)
- Air Content of Freshly Mixed Concrete by the Pressure Method (ASTM C 173)

Typical fresh properties of the conventional concrete mixes are shown in **Table 3.3**.

**Table 3.3 Typical Fresh Concrete Properties for Conventional Concrete Mixes**

Property	Mix Design ID	
	C6-58L	C10-58L
Slump (in)	5.0	4.5
Air Content (%)	5.5	2.8
Unit Weight (lb/ft <sup>3</sup> )	144.7	148.4

$$1 \text{ in} = 2.54 \text{ cm}$$

$$1 \text{ lb/ft}^3 = 16.02 \text{ kg/m}^3$$

Due to its unique nature, SCC requires several additional fresh property tests. These tests were done to ensure both adequate flowability and resistance to segregation. The following fresh property tests were performed on the self-consolidating concrete mixes:

- Slump Flow of Self-Consolidating Concrete (ASTM C 1611)
- Passing Ability of Self-Consolidating Concrete by J-Ring (ASTM C 1621)

- Static Segregation of Self-Consolidating Concrete Using Column Technique (ASTM C 1610)
- Unit Weight of Concrete (ASTM C 138M)
- Air Content of Freshly Mixed Concrete by the Pressure Method (ASTM C 173M)

Typical fresh properties of the SCC mixes are shown in **Table 3.4**.

**Table 3.4 Typical Fresh Concrete Properties for Self-Consolidating Concrete Mixes**

	Mix Design ID	
	S6-48L	S10-48L
Slump flow (in)	25.5	28.5
J Ring (in)	25.0	28.5
Segregation Column (%)	12.3	31.2
Unit Weight (lb/ft <sup>3</sup> )	139.6	146.4
Air Content (%)	5.5	2.2

$$1 \text{ in.} = 2.54 \text{ cm.}$$

$$1 \text{ lb/ft}^3 = 16.02 \text{ kg/m}^3$$

The unit weight and air content tests were modified for the SCC mixes. Both ASTM tests call for the air pot to be filled in three equal lifts, with each lift rodded 24 times. The sides of the air pot were also to be struck smartly 12 to 15 times per lift. Due to the unique nature of SCC, the air pot was filled in a single lift and was neither rodded nor struck with a rubber mallet. A similar modification was used for fabrication of the compressive strength cylinders.

### 3.3. COMPRESSIVE STRENGTH TEST

**3.3.1. Introduction.** The compressive strength test was used in several different aspects of the research project. It was used as a quality control and quality assurance, (QC/QA) tool. The compressive strength results from the experimental mixes

were compared to target values to assure the strengths were within the desired limits. These values can also be compared to other strengths of similar mixes to evaluate behavior. The compressive strength was also used to assure the quality of the concrete by observing any drastic differences between the target and actual strengths. The compressive strength of concrete is also an important factor in many tests that were used in this investigation, such as shear, bond, and creep.

**3.3.2. Fabrication.** A minimum of 9 compressive strength cylinders were cast for each mix design. All specimens were prepared in accordance with ASTM C 192-07, “Standard Practice for Making and Curing Concrete Test Specimens in the Laboratory” using 4 in. (102 mm) diameter by 8 in. (203 mm) long plastic cylinder molds. The molds were lubricated using form release oil prior to the placement of concrete. The concrete was rodded in order to reduce air voids and to assure the concrete would be sufficiently consolidated. The sides of the mold were also struck smartly for each lift with a rubber mallet in order to consolidate the concrete. It should be noted that the compressive strength specimens made with the self-consolidating mixes were not rodded or struck due to the plastic highly flowable behavior of the concrete. Instead these mixes were placed in one continuous lift. Immediately after casting, plastic lids were placed over the molds and the specimens were covered with plastic. After allowing for 16 to 24 hours of setting time, the concrete specimens were removed from the molds using compressed air and placed inside a temperature-controlled moist curing room until the designated testing date.

**3.3.3. Testing & Procedure.** The testing of the compressive strength of the experimental mixes was performed in accordance with ASTM C 39-11, “Standard Test Method for Compressive Strength of Cylindrical Concrete Specimens.” A minimum of 3 compressive strength cylinders were used at each test age. Testing occurred at 1, 7, and 28 days after batching. These are typical testing dates for compressive strength tests. Prior to testing, the specimens had to be capped in order to provide a flat surface for testing. The two methods used to cap specimens in this project were sulfur capping and neoprene pad capping.

Neoprene pads were used to cap any specimens constructed with a high strength concrete mix. Any specimens that were constructed with normal strength concrete were sulfur capped. Prior to using the neoprene pads, the concrete specimens were ground smooth using a concrete grinding machine. Once the ends were removed off all rough spots, the cylinders were placed into steel retaining rings with a neoprene pad between the specimen and the steel. With the steel retaining rings and neoprene pads on both the top and bottom of the concrete specimen, it was loaded into the compressive strength testing machine. Specimens that were sulfur capped were placed into liquid sulfur capping compound to create a smooth liquid cap that hardened within seconds and could be tested in a few hours. At least two hours before the compressive strength test was to occur, the concrete specimens were removed from the moist curing chamber and the moisture was removed from the ends. When the specimens were ready to be capped, an ample amount of sulfur capping compound was poured into the capping mold. The specimen was quickly held against the mold to ensure it was level and it was gently but quickly lowered in the capping compound. The capping compound hardened very

quickly, so capping the cylinders needed to be done in a swift manner. Once the capping compound hardened around the concrete specimen, it was removed and the process was repeated on the other end. Once the specimen was capped on both ends, it was returned to the moist curing chamber. In order for the capping compound to reach its maximum strength, the capped specimens had to sit in the moist curing chamber for a minimum of two hours. After this time, the concrete specimens could be tested for compressive strength.

Before the compressive strength tests were run, the dimensions of the specimens were measured. The diameter was measured three times and the average was used to compute the compressive strength. From the measured diameter, the cross sectional area was calculated. The height was also measured. The specimens were then loosely wrapped in a canvas wrap (not shown) and placed in the testing apparatus, as shown in **Figure 3.1**. A Forney 600 kip (2,669 kN) compression testing machine was used. Steel plates were placed on the load deck in order to minimize the distance traveled. The specimen was then placed in the apparatus, centered, and brought to just below the upper plate.



**Figure 3.1 - Compressive Strength Testing Setup**

When the setup was complete, the specimen was loaded at a load rate specified for 4 in. (102 mm) diameter specimens. The target load rate was 525 lb/sec. (238 kg/sec.). The specimen was loaded at the specified rate until it could no longer sustain a load and the load rate dropped to a negative value. The machine was turned off and the peak load was recorded. Completed test specimens are show in **Figure 3.2**.



**Figure 3.2 - High Strength Compressive Strength Specimens Post-Test**

The load was then divided by the cross sectional area to get the measured compressive strength in pounds per square inch. A minimum of three specimens were tested at a given test age and the results were averaged to get the final measured compressive strength.

### **3.4. MODULUS OF ELASTICITY TEST**

**3.4.1. Introduction.** The modulus of elasticity is an important property to investigate as it is used to determine the anticipated amount of deflection in design. This is important in designing for serviceability of a structure. The modulus of elasticity of concrete is determined by testing specimens in the linear elastic range. Specimens are loaded to a specified stress while the strain is measured. The slope of the stress–strain curve is taken as the modulus of elasticity.

**3.4.2. Fabrication.** Specimens used to measure the modulus of elasticity were fabricated according to ASTM C 192–07. These are the same type of specimens that were used for compressive strength testing. A minimum of three specimens were created for each mix design. For the modulus of elasticity test, the specimens could be fabricated

either using 4 in. (102 mm) diameter by 8 in. (203 mm) long cylinders or 6 in.(152 mm) diameter by 12 in.(305 mm) long cylinders. The two types of cylinder molds can be seen in **Figure 3.3**. It should be noted that for the SCC mixes, 4 in. (102 mm) x 8 in. (203 mm) specimens were used.



**Figure 3.3 – 4 in. (102 mm) x 8 in. (203 mm) Cylinder Mold Compared to 6 in. (152 mm) x 12 in. (305 mm) Cylinder Mold**

Specimens were de-molded after 24 hours and placed in the moist curing chamber for 28 days before testing. Before the test was conducted, all test specimens were sulfur capped in the same manner as the compressive strength cylinders.

**3.4.3. Testing & Procedure.** After the specimens were allowed to cure for 28 days, the specimens were tested in accordance with ASTM C 469–10, “Standard Test Method for Static Modulus of Elasticity and Poisson’s Ratio of Concrete in Compression.” The dimensions of the specimens were measured, and before loading, the specimen was fitted with a compressometer in order to measure the deflection of the cylinder during loading. A typical compressometer can be seen in **Figure 3.4**.



**Figure 3.4 - Typical Compressometer**

The specimen was then placed into a compression loading apparatus and loaded at a constant rate. The load was recorded when the deflection of the specimen reached 0.0004 in. (0.01 mm). The specimen was continually loaded until the load reached 40% of the ultimate strength of the concrete. The value of the ultimate strength was determined from compressive strength tests of companion specimens. When the load on the specimen reached 40% of the measured ultimate load, the deflection was recorded. This test was then performed three additional times on the same specimen. The data recorded during the first test run on each specimen was disregarded and only the following three tests were used for averaging. Using these deflections, the strains were calculated and the corresponding stresses were used to calculate the modulus of elasticity using Eq. 3.1.

$$E_c = \frac{(S_2 - S_1)}{(\varepsilon_2 - 0.00005)} \quad (3.1)$$

Where  $S_2$  is the stress measured at 40% of the ultimate load and  $S_1$  is the stress measured when the deflection of the specimen reached 0.0004 in. (0.01 mm) and  $\epsilon_2$  is the strain produced by  $S_2$ . The results from the individual tests were then averaged and the averages from the three tests were then averaged to obtain the measured modulus of elasticity.

### **3.5. MODULUS OF RUPTURE TEST**

**3.5.1. Introduction.** The modulus of rupture test is used to determine the flexural strength or tensile strength of the concrete. This is an important mechanical property to investigate. The modulus of rupture is important in design for estimating the cracking moment of the concrete when subjected to flexure.

**3.5.2. Fabrication.** The specimens used for the modulus of rupture test were fabricated in accordance with ASTM C 78–10, “Standard Test Method for Flexural Strength of Concrete (Using Simple Beam with Third-Point Loading).” Three specimens were fabricated for every concrete mix. The specimens measured 6 in. (152 mm) x 6 in. (152 mm) in cross section with a length of 24 in. (610 mm). The specimens were filled with two lifts, each lift being rodded 72 times. It should be noted that the SCC was not rodded when specimens were cast. The specimens were cast in one single lift. The specimens were de-molded after 24 hours and stored in a moist curing chamber for 28 days. After 28 days they were prepared for testing.

**3.5.3. Testing & Procedure.** After 28 days, the specimens were removed from the moist curing chamber. The supports on the testing apparatus were 18 in. (457 mm) apart. In order to align the specimen on the supports, it had to be divided into thirds. The

first 3 in. (76 mm) of either end of the specimen were not included in the measuring. This caused the 18 in. (457 mm) span to be divided into 3, 6 in. spans. The load points would be placed on the 6 in. mark and the 12 in. mark, creating the third-point loading. The prepared specimen can be seen in **Figure 3.5**.

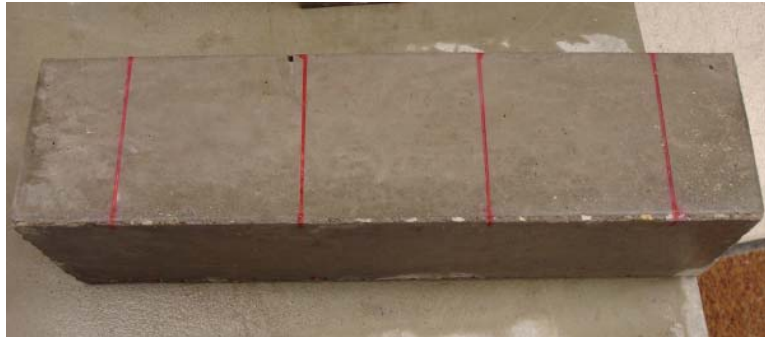


**Figure 3.5 - Prepared Modulus of Rupture Specimen**

The specimen was rotated and loaded into the testing machine on a formed side to provide the smoothest surface and thus prevent localized forces on the beam. The load was applied at the aforementioned points. A leather pad was placed in between the concrete specimen and the load points in order to help distribute the load. The test setup can be seen in **Figure 3.6**. It is important to note that during the set-up, the specimen was kept moist in order to prevent any internal stresses from developing.



**Figure 3.6 - Modulus of Rupture Testing Setup**

The load head was then lowered until it made contact with the leather pads. The beam was then loaded at a constant rate until failure. If the beam failed within the middle third, the test was accepted. It should be noted that all beams tested in this investigation failed in the middle third of the beam. A post failure specimen can be seen in **Figure 3.7**. The failure load was recorded and subsequently used to calculate the modulus of rupture using **Eq. 3.2**.



**Figure 3.7 - Modulus of Rupture Specimen Post-Test**

The beam was removed from the testing apparatus and its dimensions were measured. The width and depth of the beam were measured three times and averaged. The modulus of rupture was then calculated using **Eq. 3.2**.

$$R = \frac{PL}{bd^2} \quad (3.2)$$

Where P is the peak load, L is the distance between supports, b is the average width of the beam after testing, and d is the average depth of the beam after testing.

### **3.6. SPLITTING TENSILE TEST**

**3.6.1. Introduction.** ASTM has not yet specified a standardized test to find the direct tensile strength of concrete. There is a standardized test for an indirect tension test known as the splitting tensile test. This test involves loading a cylindrical specimen along its longitudinal axis until failure. This test is thought to measure a greater tensile strength than a direct tensile strength. However it is usually lower than a measured strength from a modulus of rupture test. The splitting tensile test is a good indication of a concrete's tensile strength but should be performed alongside other tests such as the modulus of rupture test.

**3.6.2. Fabrication.** The specimens used for the splitting tensile test were fabricated in accordance with ASTM C 496–11, “Standard Test Method for Splitting Tensile Strength of Cylindrical Concrete Specimens.” A minimum of three specimens were made for each concrete mix. The specimens were made using 4 in. (102 mm) diameter by 8 in. (203 mm) long cylindrical molds. The specimens used for the splitting

tensile test were the same types of specimens used for the compressive strength test. The specimens were fabricated according to ASTM C 192. After 24 hours, the specimens were de-molded and placed in a moist curing chamber for 28 days, at which time they were then tested.

**3.6.3. Testing & Procedure.** After the specimens were allowed to cure for 28 days, the specimens were removed from the curing chamber for testing. The diameter and height of the specimens were recorded. The diameter of the specimen was marked on the top of the specimen. Two lines were then drawn down the long side of the specimen from the previously drawn line. This was done to assist in lining up the specimen in the testing apparatus. The specimen was then loaded into the testing apparatus on the line drawn down its vertical axis. The specimen was placed on a piece of plywood. Another plywood strip was placed on the top of the specimen between it and the load platen. These strips were used so the load would be distributed along the axis of the specimen. The test setup can be seen in **Figure 3.8**.



**Figure 3.8 - Typical Splitting Tensile Test Setup**

The specimen was then loaded at a rate between 100 (45 kg) and 200 lb /min. (91 kg/min.) until failure. The load at failure was recorded as the peak load, and the tensile strength was calculated using **Eq. 3.3**.

$$T = \frac{2P}{\pi LD} \quad (3.3)$$

Where P was the peak load, L is the length of the specimen, and D is the diameter of the specimen. A post failure specimen can be seen in **Figure 3.9**.



**Figure 3.9 - Splitting Tensile Specimens Post-Test**

## 4. DURABILITY TESTS

### 4.1. INTRODUCTION

This section discusses the durability tests used to evaluate the performance of self-consolidating concrete (SCC). The durability performance of these specialized concretes is a crucial aspect in investigating the possibility of implementing these new materials into transportation-related infrastructure, such as bridges, roadways, culverts, and retaining walls. The following durability tests were included in the scope of work for this investigation:

- Resistance of Concrete to Rapid Freezing and Thawing (ASTM C 666-08)
- Electrical Indication of Concrete's Ability to Resist Chloride Ion Penetration (ASTM C 1202-10)
- Determining the Penetration of Chloride Ion into Concrete by Ponding (ASTM C 1543-10)
- Concrete Resistivity (Non-ASTM)

The outline for the durability tests is shown in **Table 4.1**. The outline identifies the number of test specimens fabricated for each test for each concrete mix. The table also includes the required curing conditions and durations, as well as the specimen age at the start of testing and the duration of the test, if applicable.

**Table 4.1 Test Matrix for Durability Performance**

Durability Property	Number of Specimens	Moist Curing Duration, days	Dry Curing Duration, days	Testing Date, days	Testing Duration, days
Freezing and Thawing	3	35	0	35	N/A <sup>1</sup>
Electrical Chloride Penetration	2 (4 disks)	28	0	28	N/A <sup>2</sup>
Ponding	3	14	14	28	120
Concrete Resistivity	3	14	21	35	168

Notes: 1. Test duration based on cycles  
2. Duration of test is 6 hours

## 4.2. RAPID FREEZING & THAWING TEST

**4.2.1. Introduction.** The rapid freeze-thaw test was one of the most critical durability tests performed in this investigation. The climate in Missouri is susceptible to multiple freeze-thaw cycles, which is a more severe environment for concrete durability than continuous freezing. The test involves subjecting specimens to multiple freeze-thaw cycles in order to measure the resistance of the material to deterioration caused by the expansion of the free water freezing inside the specimens. This resistance was measured using three parameters: the length change of the specimens, change in the fundamental transverse frequency of the specimens, and mass change of the specimens. Using these parameters the resistance to freeze-thaw can be quantified as a durability factor.

**4.2.2. Fabrication.** The specimens for the rapid freeze-thaw test were fabricated according to ASTM C 666–03, “Standard Test Method for Resistance of Concrete to Rapid Freezing and Thawing.” The molds used in the fabrication of these specimens were loaned to the project by the Construction & Materials Division of the

Missouri Department of Transportation (MoDOT) and can be seen in **Figure 4.1**. These stainless steel molds measured 3.5 in. (8.9 cm) in width, 4.5 in. (11.43 cm) in height, and 16 in. (40.64 cm) in length and conformed to ASTM C 666 requirements for specimen dimensions.



**Figure 4.1 - Freezing and Thawing Specimen Molds**

The ends of each mold contained a threaded hole to install a specialized bolt. This bolt contained a rounded end, and when the concrete specimens were de-molded, the end of this bolt protruded from both ends of the prism as shown in **Figure 4.2**. The embedded bolt provides a mechanism to measure the length change of the concrete prism as it was subjected to freezing and thawing cycles.

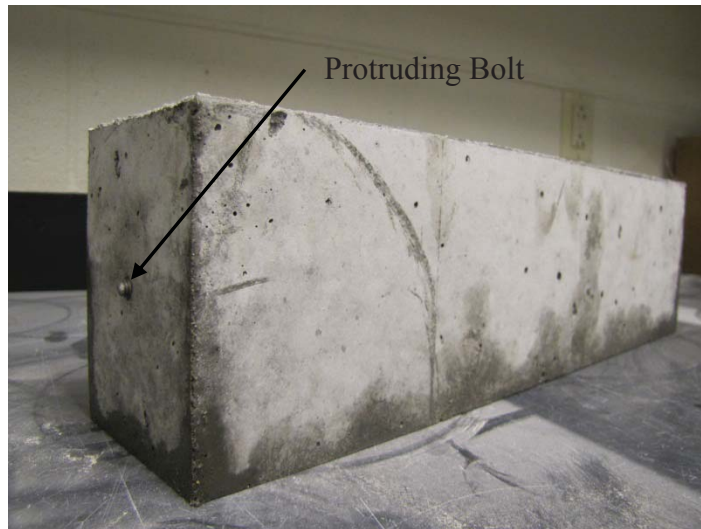


**Figure 4.2 - Freezing and Thawing Specimen with Protruding Bolt**

Once the specimens were formed and de-molded, they were placed in a temperature controlled moist curing room for 35 days prior to testing. It should be noted that this moist curing duration is a standard for MoDOT and a modification of ASTM C 666. The ASTM specifies that the prisms should be moist cured for 14 days unless otherwise specified. It should also be noted that the typical MoDOT procedure requires that specimens that will be subjected to the rapid freeze-thaw test be submersed in a lime water solution while they cure for the 35 days. However, due to space restraints in the University laboratory, the specimens were only moist cured. This change was deemed acceptable provided all specimens received the same treatment. Between 14 and 21 days, the prisms were transported from the University's moist curing chamber to the Construction & Materials testing lab of MoDOT in Jefferson City, Missouri. To be transported, the specimens were wrapped in burlap that was saturated in a 5% by weight lime water solution. The specimens were then placed into a cooler and immediately driven to the MoDOT lab and placed into the moist curing chamber to complete the 35-

day moist curing regime. All rapid freezing and thawing tests were performed by MoDOT employees of the Construction & Materials Division.

**4.2.3. Testing & Procedure.** All specimens were tested in accordance with ASTM C 666, Procedure B. When the specimens reached the appropriate age, they were brought to the target thaw temperature. The fundamental transverse frequency, mass, length, and cross section of the specimen were measured. The freeze-thaw specimens were then subjected to the appropriate freezing and thawing cycles. Each specimen was subject to 300 cycles of freezing and thawing. Every 36 cycles the specimens would be removed in the thawed state and properties of the specimen would be measured. The properties measured were fundamental transverse frequency, length change, and mass change. The specimens were then placed back into the testing apparatus and the cycles continued. The test was halted if the specimen deteriorated so extensively that the test could not continue. The relative dynamic modulus of elasticity was then calculated using **Eq. 4.1**.

$$P_c = \frac{n_1^2}{n^2} \times 100 \quad (4.1)$$

Where  $P_c$  is the relative dynamic modulus of elasticity at,  $c$ , cycles of freezing and thawing.  $N_1$  is the fundamental transverse frequency after,  $c$ , cycles of freezing and thawing and  $n$  is the fundamental transverse frequency after 0 cycles of freezing and thawing. Using the relative dynamic modulus of elasticity, the durability factor of the freezing and thawing specimen was also calculated using **Eq. 4.2**.

$$DF = \frac{PN}{M} \quad (4.2)$$

Where DF is the durability factor, P is the relative dynamic modulus of elasticity at N cycles, N is the number of cycles at which the specified value of P is reached or the specified number of cycles is reached, whichever is less, and M is the number of cycles until termination. The higher the measured durability factor, the greater resistance the concrete will have to freezing and thawing attack.

### **4.3. ELECTRICAL INDICATION TO RESIST CHLORIDE ION PENETRATION TEST**

**4.3.1. Introduction.** Chloride penetration of concrete is one of the leading durability issues facing many concrete specimens. Concrete members that are exposed to chlorides such as concrete piers in the ocean or concrete bridge decks exposed to de-icing salts all face chloride penetration. If sufficient chloride is allowed to penetrate into a concrete member, it can cause the embedded steel reinforcement to corrode and the expanding corrosion product will result in internal stresses, which in turn will cause cracking of the concrete. Over time this will cause concrete spalling and eventual failure. The electrical indication of concrete's ability to resist chloride penetration is a rapid method to determine the permeability of the concrete and its ability to withstand chloride penetration. This test is often used in correlation with the ponding test as it was in this investigation. Due to the ponding test's longer duration, this electrical test is a rapid method to estimate the durability of concrete. This test is also known as the Rapid Chloride Test (RCT).

**4.3.2. Fabrication.** The test specimens consisted of cylinders fabricated and prepared according to ASTM C 192–07, “Standard Practice for Making and Curing Concrete Test Specimens in the Laboratory.” Two 4 in. (10.16 cm) diameter x 8 in. (20.32 cm) long cylinders were used for this test for every concrete mix. These cylinders were prepared alongside the compressive strength specimens. These specimens were demolded after 24 hours and placed in the moist curing chamber for 28 days. In between 14 and 21 days after batching, these cylinders were transported to the Construction & Materials testing lab in Jefferson City to finish the curing cycle and begin testing. These specimens were wrapped in burlap that was saturated in a 5% by weight lime water solution. The specimens were then placed into a cooler and immediately driven to the Jefferson City MoDOT lab and placed into the moist curing chamber to complete the 28-day moist curing regime. All electrical chloride tests were performed by MoDOT employees of the Construction & Materials Division.

**4.3.3. Testing & Procedure.** The testing of specimens for the electrical indication of a concrete’s ability to resist chloride ion penetration is outlined in ASTM C 1202-10, “Standard Test Method for Electrical Indication of Concrete’s Ability to Resist Chloride Ion Penetration.” The test specimens consist of 4 in. (102 mm) diameter by 2 in. (51 mm) thick concrete disks. These disks were cut from specimens cast according to ASTM C 192. Two disks were cut from each concrete cylinder, with two concrete cylinders cast from each mix, which resulted in a total of 4 concrete disks for each concrete mix. One disk was cut from the top of the cylinder and the other from the middle. These disks were labeled with the mix design name and noted as either middle or

top. The specimens were allowed to surface dry for at least 1 hour before the sides of the disks were coated with a setting coating as seen in **Figure 4.3**.



**Figure 4.3 - Setting Coating Being Applied to Concrete Specimens**

After the coating dried, the specimens were placed into a vacuum desiccator and vacuumed for 3 hours. The pressure of the vacuum was at least 0.96 psi (6650 Pa). At the end of the 3 hour desiccation period, de-aerated water was poured into the water stockpot of the vacuum until the specimen was covered. The stockpot was closed and the vacuum was maintained for another hour. The vacuum was then turned off and air was allowed to enter the desiccator. The specimen was then allowed to soak in the de-aerated water for  $18 \pm 2$  hours. The specimen was then blotted dry and placed into the voltage cell. A sealant was then applied to the specimen-cell boundary. The exposed face of the specimen was then covered while the sealant was allowed to dry. Once the sealant was dry, the process was repeated to the other face of the specimen. The final specimen can be seen in **Figure 4.4**.

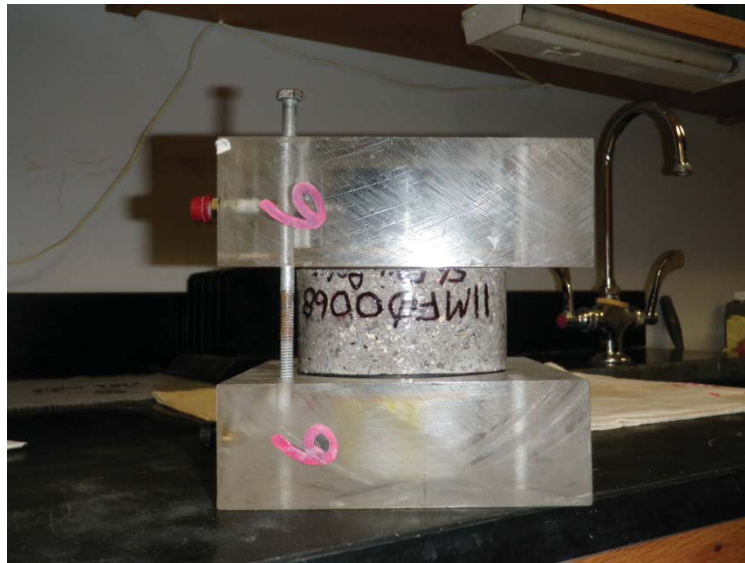


**Figure 4.4 - Typical Completed Specimen**

The side of the cell that is connected to the negative terminal is then filled with 3.0% NaCl solution while the side connected to the positive terminal is filled with 0.3 N NaOH solution. The test setup can be seen in **Figure 4.5**. The power is then turned on and the voltage is set to 60 V. The initial current is recorded and then recorded at 30 minute intervals.

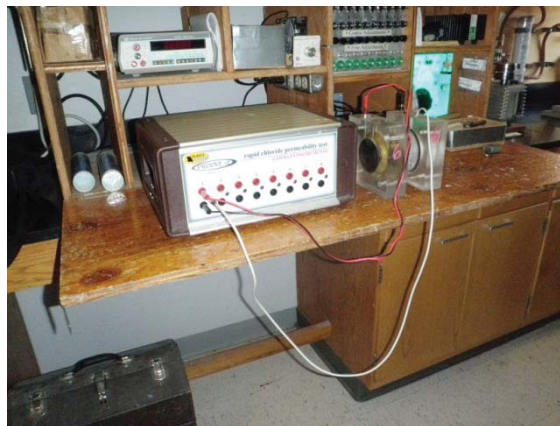


**Figure 4.5 – Typical RCT Setup**

The test is conducted for 6 hours unless the temperature in the solution exceeds 190°F. This temperature is only exceeded when the concrete is extremely permeable. The data that is recorded is then used to calculate the total charge passed through the specimen in coulombs. This is discussed further in Section 5.6.

#### **4.4. PONDING TEST**

**4.4.1. Introduction.** A serious problem facing Missouri concrete bridge decks is spalling and deterioration caused by chloride penetration and subsequent corrosion of the underlying steel. During winter months, de-icing salts are used to remove snow and ice from bridge and roadway surfaces. The chlorides contained in these de-icing salts diffuse into the concrete, eventually breaking down the passive layer of the reinforcing steel and causing corrosion. The corrosion product expands to approximately six times the original volume, resulting in internal stresses and eventually cracking. Over time, this process will lead to spalling and deterioration of the concrete. The ponding test subjects concrete specimens to a similar environment to investigate the ability of the concrete to resist chloride penetration. This test is a valuable indicator of the resistance of the concrete to chloride ingress and thus the durability of the material. Although this test requires a longer period of time compared to other methods to predict the resistance of concrete to chloride penetration, it is the most realistic test method.

**4.4.2. Fabrication.** The concrete specimens for the ponding test were fabricated according to ASTM C 1543-10, “Standard Test Method for Determining the Penetration of Chloride Ion into Concrete by Ponding.” Three specimens were made for each concrete mix. The test requires that the specimens have a surface area of at least

45.6 in<sup>2</sup> (30,000 mm<sup>2</sup>). The specimens must also be at least  $3.54 \pm 0.6$  in. ( $90 \pm 15$  mm) tall. The specimens created for the ponding test in this investigation measured 18 in. (457 mm) wide x 18 in. (457 mm) long x 4 in. (102 mm) tall. Also, the test procedure required a dike along the top of the specimen with a height of at least 0.79 in. (20 mm) high. To accomplish this, a 0.75 in.-thick (19 mm) foam panel measuring 16 in. (406 mm) x 16 in. (406 mm) in plan was placed on a sheet of plywood that would serve as the base of the mold. Walls constructed from 2 in. (51 mm) x 4 in. (102 mm) pieces of wood were then connected to the panel to arrive at the overall dimension of 18 in. (457 mm) x 18 in. (457 mm) in plan. When the concrete was placed in the mold, the foam created a void in what would become the top of the specimen. The foam formed the reservoir for the chloride solution. The concrete was placed into the formwork and consolidated as necessary. After 24 hours, the concrete specimens were de-molded and placed in a moist curing chamber at 100% relative humidity. After 14 days of moist curing, the specimens were transported to a temperature and humidity controlled environment where they would dry cure at 75°F (23.8°C) and 65% relative humidity for another 14 days. After 28 days of curing, the specimens would then begin the ponding test.

**4.4.3. Testing & Procedure.** The test procedure involved placing a 5% by weight chloride solution into the ponding specimen reservoir. The solution had to be at a depth of  $0.6 \pm 0.2$  in. ( $15 \pm 5$  mm). A typical ponded specimen can be seen in **Figure 4.6**. When the required amount of solution was poured into the reservoir, the concrete specimens were covered with plastic sheeting and the sheets were secured with elastic bands to prevent evaporation of the solution.



**Figure 4.6 - Typical Ponding Specimen**

Every two weeks the specimens were checked to ensure that the proper depth of the solution was maintained. If the reservoir was low, additional solution was added. After 60 days of ponding, the reservoir was vacuumed dry and fresh solution was added. The sheeting was replaced and the specimens were monitored every two weeks. After another 60 days, the chloride solution was vacuumed off and the specimen allowed to air dry. A few days later, a core was taken from the center of the specimen. A typical core and core location can be seen in **Figure 4.7**.



**Figure 4.7 - Concrete Core and Resulting Void in the Concrete Specimen**

The core was removed using an industry standard core driller with a medium flow of water to ensure proper blade lubrication as well as creating the proper slurry. Powder samples were then taken from the cores at specified depth intervals. The intervals were 0.25 in. (6 mm), 0.75 in. (19 mm), 1.5 in. (38 mm), and 2 in. (51 mm) from the surface of the core. A sample was also taken from the surface of the core. These depths are shown in **Figure 4.8**.

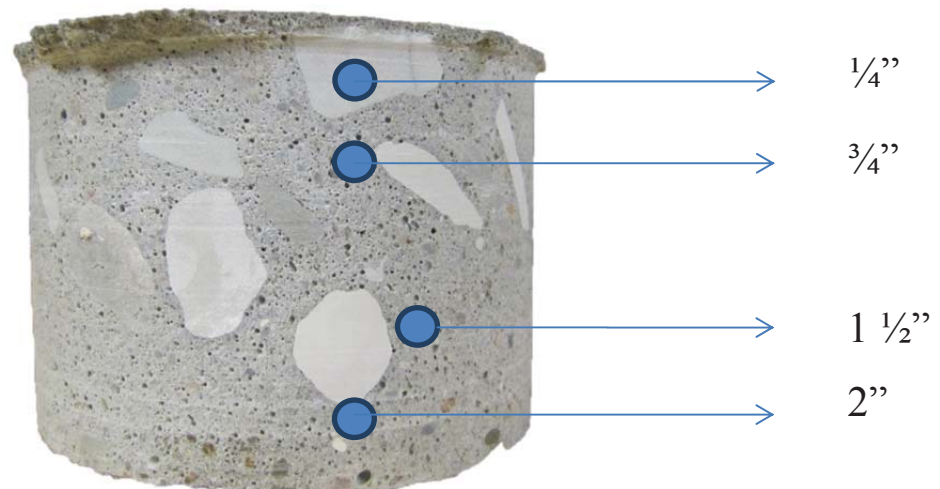


**Figure 4.8 - Depths at which Powder Samples Were Collected**  
1 in. = 2.54 cm.

The samples had to measure at least 0.053 oz. (1.5 g) to be considered sufficient. Samples were collected using a 3/8 in. (9.5 mm) drilled bit at all locations except at the 0.25 in. (6 mm) location. At this location a 3/16 in. (5 mm) drill bit was used. A paper plate was used to collect the dust and a steel plate was placed in between the core and the vise to confine the concrete and prevent spalling. A hole was cut in the paper plate and placed

over the mark to be drilled. The paper plate was then taped to the concrete specimen as to create a seal between the paper and concrete surface. This was done in order to catch the concrete dust created by drilling the hole. The drilling locations were placed on a point on the cylinder as to not drill directly into a piece of coarse aggregate unless absolutely necessary. After each hole was drilled, it was sealed using masking tape to prevent cross contamination with the other samples. Samples were also taken from the surface of the core. This was done by drilling the surface of the core to a depth of no deeper than 0.125 in. (3 mm). Samples were collected from several locations on the surface of the core to obtain the necessary sample size. A chloride analysis was then performed on the powder samples to obtain the chloride content in the concrete at the respective sample depths.

The chloride analysis of water soluble chlorides was performed using the Rapid Chloride Testing (RCT) equipment made by Germann Instruments, Inc. The 0.053 oz. (1.5 g) sample was poured into a vial containing 0.304 fl-oz. (9 mL) of the extraction liquid. The vial was shaken vigorously for 5 minutes. The extraction liquid and powder slurry were then filtered into a buffer solution by pouring the slurry through a filter paper and into a vial containing the buffer solution. While the slurry was filtering the electrode was prepared and calibrated. The preparing of the electrode began with filling it with a wetting agent. After any air bubbles were removed the wetting agent was allowed to be released in order to fully wet the circumference of the electrode tip. After the electrode had been refilled with the wetting agent, the preparation was complete. In order to calibrate the electrode and develop a scale to determine the chloride content of the specimens, the electrode was inserted into four calibration solutions of known chloride content. The four calibration liquids contained 0.005%, 0.02%, 0.05%, and 0.5% chloride

content. The electrode was inserted into each solution and the voltage was read. The four calibration liquids produced a voltage of approximately 100 mV, 72 mV, 49 mV, and -5 mV respectively. This data was used then plotted on a log chart in order to develop a scale for the rest of the testing. An example of this log chart can be seen in Appendix B. After the preparing and the calibrating the electrode was ready to use. When the filtering process was complete the electrode was inserted into the buffer solution vial which contained the buffer solution and filtered slurry and was held steady until the voltage reading stabilized. Using the recorded voltage and the developed scale, the chloride content was determined. After every use the electrode was sprayed with distilled water, blotted dry and stored in an empty vial. This data collected from each depth was used to develop a chloride profile and determine chloride penetration into the concrete.

#### **4.5. CONCRETE RESISTIVITY TEST**

**4.5.1. Introduction.** A concrete's electrical resistance may be measured in an attempt to quantify the rate at which a bare, depassivated steel bar, embedded within the concrete, corrodes. The corrosion process is dependent upon the ability of charged ions, such as hydroxyl ions  $\text{OH}^-$ , to flow from the cathode to the anode. The faster the ions can flow from the cathode to the anode, the faster the corrosion process may proceed, provided the cathode is supplied with a sufficient amount of oxygen and water. The transport of electricity through concrete closely resembles that of ionic current; therefore, it is possible to classify the rate of corrosion of a bar embedded within concrete by quantifying the electrical resistance of the surrounding concrete.

The four probe resistivity meter, also known as the Wenner probe and shown in **Figure 4.9**, is generally regarded as the most accurate method of measuring concrete resistivity. The probe contains four equally spaced electrodes that are positioned along a straight line. The two outer electrodes send an alternating current through the concrete while the inner electrodes measure the drop in potential. The resistivity is then calculated using **Eq. 4.3**.

$$\rho = \frac{2\pi sV}{I} \quad (4.3)$$

Where  $\rho$  is the resistivity ( $\Omega\text{cm}$ ) of the concrete,  $s$  is the spacing of the electrodes (cm),  $V$  is the recorded voltage (V), and  $I$  is the applied current (A).



**Figure 4.9 - Canin<sup>+</sup> Wenner Probe**

**4.5.2. Fabrication.** The concrete specimens for the resistivity test were fabricated according to ASTM C 1543–10 “Standard Test Method for Determining the Penetration of Chloride Ion into Concrete by Ponding”. The molds used to create these specimens were the same molds to create the specimens for the ponding test. The specimens were prepared the same way, using the same procedure. They were cured in the moist curing chamber for 14 days then transported to a humidity and temperature controlled environment to dry cure for an additional 21 days before testing. Testing began when the specimens reached an age of 35 days.

**4.5.3. Testing & Procedure.** One day prior to the beginning of the test, the specimens were ponded with just enough distilled water to coat the bottom of the reservoir. The specimens sat with water in them for 24 hours. The following day the water was vacuumed off using a shop vacuum cleaner. The Wernner probe was then used to take the initial resistivity measurements. The measurements were taken in a systematic manner, from left to right, then top to bottom, using the Plexiglas template shown in **Figure 4.10**. Three measurements were taken from left to right, once on the far left, once in the middle and once on the far right. Three measurements were then taken from top to bottom, once on the top, once in the middle, and once on the bottom.



**Figure 4.10 - Wenner Probe Grid**

This procedure was done in the same order, once every week. The measurements were taken weekly until the resistivity measurements became constant. However, due to time constraints the duration of the test was limited to 24 weeks.

## 5. SELF-CONSOLIDATING CONCRETE HARDENED PROPERTY AND DURABILITY RESULTS

### 5.1. COMPRESSIVE STRENGTH

The compressive strength was determined in accordance with ASTM C 39-11. A minimum of three, and many times four, replicate specimens were tested for each testing date for each experimental mix. The compressive strength was tested at 1, 7, and 28 days. The specimen strengths were averaged and reported as the compressive strength of the experimental mix. The normal strength conventional concrete (C6-58L) was compared to the normal strength self-consolidating concrete (S6-48L). A strength profile was developed in order to analyze and compare the strength gain of each mix. The individual specimen results of the normal strength mixes can be seen in **Table 5.1**.

**Table 5.1 Individual Compressive Strength Results for Normal Strength Mixes**

	Mix Design ID							
	C6-58L				S6-48L			
1 Day Compressive Strength (psi)	4,270	4,330	4,430	4,790	4,050	4,090	4,560	4,390
7 Day Compressive Strength (psi)	6,110	6,270	6,210	6,080	5,970	6,340	6,570	6,640
28 Day Compressive Strength (psi)	7,300	7,670	7,850	7,580	8,310	8,130	7,930	8,180

1 psi = 6.89 kPa

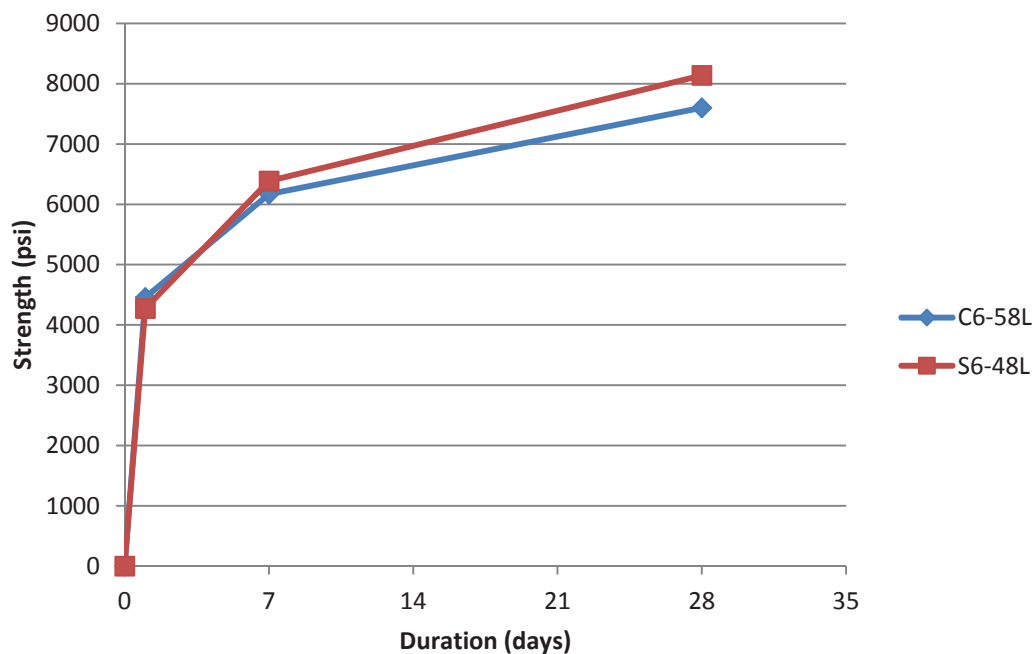
The individual results were then averaged and reported as the compressive strength of the experimental mix. The averaged values can be seen in **Table 5.2**.

**Table 5.2 Averaged Compressive Strength Results for Normal Strength Mixes**

Mix Design ID	1 Day Strength (psi)	7 Day Strength (psi)	28 Day Strength (psi)
C6-58L	4,450	6,170	7,600
S6-48L	4,270	6,390	8,140

1 psi = 6.89 kPa

These values were then plotted in order to develop a strength gain profile for the normal strength mixes, both conventional and SCC. The strength profiles for both mixes are shown in **Figure 5.1**.

**Figure 5.1 - Compressive Strength Profile for Normal Strength Mixes**

The compressive strength was also determined for the high strength experimental mixes, C10-58L and S10-48L. These tests were conducted in the same way, according to ASTM C 39. The individual specimen results can be seen in **Table 5.3**.

**Table 5.3 Individual Compressive Strength Results for  
High Strength Concrete Mixes**

	Mix Design ID							
	C10-58L				S10-48L			
1 Day Compressive Strength	5,680	5,970	4,830	4,850	7,520	7,270	7,310	7,400
7 Day Compressive Strength (psi)	8,650	8,270	9,000	8,820	10,360	10,910	11,590	11,540
28 Day Compressive Strength (psi)	11,270	10,510	10,190	11,320	13,140	13,540	13,760	-

1 psi = 6.89 kPa

The individual results were then averaged and reported as the compressive strength. The averaged compressive strength results can be found in **Table 5.4**.

**Table 5.4 Averaged Compressive Strength Results for  
High Strength Concrete Mixes**

Mix Design ID	1 Day Strength (psi)	7 Day Strength (psi)	28 Day Strength (psi)
C10-58L	5,330	8,690	10,820
S10-48L	7,380	11,100	13,480

1 psi = 6.89 kPa

From this data, the compressive strength profile was developed, with both mixes shown in **Figure 5.2**.

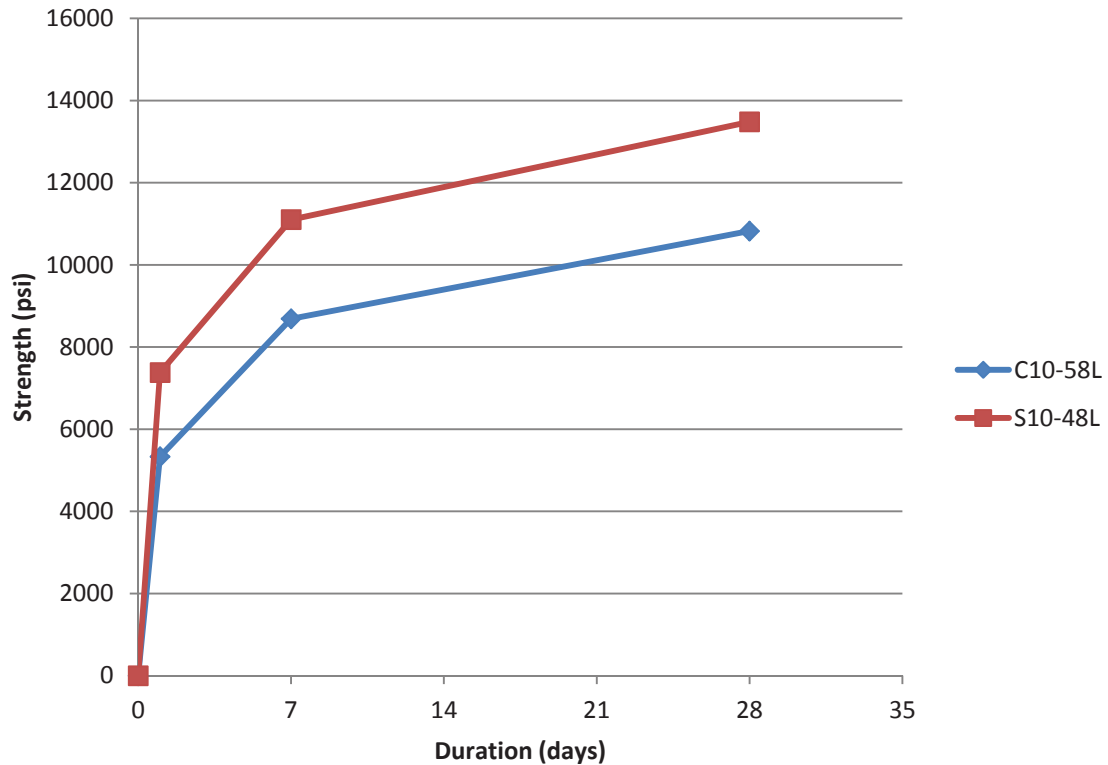


**Figure 5.2 - Compressive Strength Profile for High Strength Concrete Mixes**

From the strength profiles, the effect of the Type III cement is evident in the early strength gains for both the normal strength and high strength mixes. Both of the normal strength mixes exceeded the target strength of 6,000 psi (41.4 MPa), with the self-consolidating concrete performing slightly better than the conventional mix. The C6-58L mix also showed a more rapid strength gain than the S6-48L mix. The high strength mixes showed different behavior. The S10-48L mix gained much more strength early on than the C10-58L mix and far surpassed it in ultimate strength. However, both of these mixes surpassed the 10,000 psi (68.9 MPa) target strength.

## 5.2. MODULUS OF ELASTICITY

The modulus of elasticity was tested and calculated in accordance with ASTM C 469-10. Test specimens consisted of 4 in. (102 mm) x 8 in. (203 mm) cylinders. The specimens were tested after 28 days. During testing, both the load at  $50 \times 10^{-6}$  strain and the length change at 40% of the ultimate strength were measured. Using these values the modulus of elasticity was calculated using **Eq. 5.1**.

$$E = \frac{(S_2 - S_1)}{(\epsilon_2 - 0.000050)} \quad (5.1)$$

Where  $S_2$  is the stress at 40% of the ultimate load,  $S_1$  is the stress measured at  $50 \times 10^{-6}$  strain, and  $\epsilon_2$  is the strain at  $S_2$ . The results for the normal strength experimental mixes can be seen in **Table 5.5**.

**Table 5.5 Individual Modulus of Elasticity Results for Normal Strength Mixes**

Mix Design ID	Specimen ID	Test 1			Test 2		
		$S_2$ (psi)	$S_1$ (psi)	$\epsilon_2$ ( $\times 10^{-4}$ )	$S_2$ (psi)	$S_1$ (psi)	$\epsilon_2$ ( $\times 10^{-4}$ )
C6-58L	MOE-1	2,990	231	8.66	2990	211	8.54
	MOE-2	3,040	198	8.66	3040	198	8.66
S6-48L	MOE-1	3,290	192	10.5	3290	192	10.5
	MOE-2	3,250	190	10.2	3250	187	10.1

$$1 \text{ psi} = 6.89 \text{ kPa}$$

The values for  $S_2$  were based on results of the companion compressive strength tests. The modulus of elasticity test and compressive strength tests were performed back to back, so the values for  $S_2$  vary slightly from test to test. Using this data and **Eq. 5.1**, the modulus

of elasticity was calculated and averaged from the two tests. The averaged results can be seen in **Table 5.6**.

**Table 5.6 Average Modulus of Elasticity Results for Normal Strength Mixes**

Batch ID	Modulus of Elasticity (psi)
C6-58L	3,450,000
S6-48L	3,130,000

1 psi = 6.89 kPa

The results were also normalized using the respective measured compressive strengths. This step was performed in order to compare the coefficients with the ACI 318-08 recommended value of 57,000, as shown in **Eq. 5.2**. This equation assumes a unit weight of concrete of 145 pcf. It should be noted that while none of the concrete mixes had a unit weight of 145 pcf all were very close and it was decided that the difference would not be significant.

$$E_c = 57,000\sqrt{f'_c} \quad (5.2)$$

Where  $E_c$  is the modulus of elasticity and  $f'_c$  is the compressive strength of concrete. The measured modulus of elasticity was divided by the square root of the strength of the respective mix and then compared to the ACI coefficient. The results can be seen in **Table 5.7**.

**Table 5.7 Normalized Modulus of Elasticity for Conventional Concrete Mixes**

	C6-58L	S6-48L	ACI Coefficient
Normalized Results	39,580	34,700	57,000

$$1 \text{ psi} = 6.89 \text{ kPa}$$

The measured modulus of elasticity for the conventional concrete was also compared to the recommended AASHTO coefficient of 1,820 as shown in **Eq. 5.3**.

$$E_c = 1,820\sqrt{f'_c} \quad (5.7)$$

The measured modulus of elasticity was divided by the strength of the respective mix and the compared to the AASHTO coefficient. The results can be seen in **Table 5.8**.

**Table 5.8 Normalized AASHTO Modulus of Elasticity for Conventional Concrete Mixes**

	C6-58L	S6-48L	AASHTO Coefficient
Normalized Results	1,251	1,097	1,820

The same procedure was also performed for the high strength experimental mixes. The results of the individual tests can be seen in **Table 5.9**.

**Table 5.9 Individual Modulus of Elasticity Results for High Strength Concrete Mixes**

Mix Design ID	Specimen ID	Test 1			Test 2		
		S <sub>2</sub> (psi)	S <sub>1</sub> (psi)	$\epsilon_2$ (x10 <sup>-4</sup> )	S <sub>2</sub> (psi)	S <sub>1</sub> (psi)	$\epsilon_2$ (x10 <sup>-4</sup> )
C10-58L	MOE-1	4,360	230	11.2	4360	233	11.4
	MOE-2	4,270	227	10.6	4270	223	10.7
S10-48L	MOE-1	4,410	237	12.5	4410	248	12.5
	MOE-2	4,390	222	11.2	4390	237	11.8

1 psi = 6.89 kPa

Using this data, the average modulus of elasticity was calculated. The average modulus of elasticity for each high strength experimental mix can be found in **Table 5.10**.

**Table 5.10 Average Modulus of Elasticity Results for High Strength Concrete Mixes**

Mix Design ID	Modulus of Elasticity (psi)
C10-58L	3,900,000
S10-48L	3,630,000

1 psi = 6.89 kPa

The values for the high strength mixes were also normalized using the respective strengths. These values were then compared to the ACI coefficient of 57,000. The results can be seen in **Table 5.11**.

**Table 5.11 Normalized Modulus of Elasticity for High Strength Concrete Mixes**

	C10-58L	S10-48L	ACI Coefficient
Normalized Results	37,500	31,290	57,000

1 psi = 6.89 kPa

The same procedure was also performed on the high strength mixes and compared to the AASHTO coefficient of 1,820. The results for the high strength mixes can be seen in **Table 5.12**.

**Table 5.12 Normalized AASHTO Modulus of Elasticity for High Strength Concrete Mixes**

	C10-58L	S10-48L	AASHTO Coefficient
Normalized Results	1,186	987	1,820

### 5.3. MODULUS OF RUPTURE

The modulus of rupture test was performed in accordance with ASTM C 78-10. The modulus of rupture was calculated using the formula stated in Section 3.5.3. The values used in the equation measured for each individual test can be seen in **Table 5.13**.

**Table 5.13 Individual Modulus of Rupture Results for Normal Strength Mixes**

Mix Design ID	Specimen ID	L (in.)	Peak Load (lb.)	b <sub>1</sub> (in.)	b <sub>2</sub> (in.)	b <sub>3</sub> (in.)	b <sub>avg</sub> (in.)	d <sub>1</sub> (in.)	d <sub>2</sub> (in.)	d <sub>3</sub> (in.)	d <sub>avg</sub> (in.)
C6-58L	MOR-1	18	9,589	5.94	5.97	5.96	5.96	6.32	6.29	6.28	6.29
	MOR-2	18	8,824	6.06	6.08	6.08	6.07	5.98	5.97	5.98	5.98
	MOR-3	18	9,267	6.22	6.24	6.21	6.22	5.93	5.95	5.95	5.94
S6-48L	MOR-1	18	8,047	6.04	6.01	6.02	6.02	5.97	5.95	5.93	5.95
	MOR-2	18	8,731	6.29	6.32	6.39	6.34	5.94	5.95	5.97	5.95
	MOR-3	18	7,775	6.11	6.11	6.13	6.12	5.93	5.97	5.96	5.95

$$1 \text{ psi} = 6.89 \text{ kPa}$$

The modulus of rupture was calculated using the values in **Table 5.13** and then averaged for each concrete type. The average modulus of rupture for the normal strength mixes can be seen in **Table 5.14**.

**Table 5.14 Averaged Modulus of Rupture for Normal Strength Mixes**

Mix Design ID	Modulus of Rupture (psi)
C6-58L	740
S6-48L	670

1 psi = 6.89 kPa

The results were also normalized using the respective measured compressive strengths. This step was done in order to compare the coefficients with the ACI 318-08 recommended coefficient of 7.5, which appears in the equation to estimate the modulus of rupture, as seen in **Eq. 5.3**.

$$f_r = 7.5\sqrt{f'_c} \quad (5.3)$$

Where  $f_r$  is the modulus of rupture and  $f'_c$  is the compressive strength of concrete. ACI 318-08 states that any values between 6 and 12 are acceptable as coefficients. After the modulus was measured, the values were divided by the average measured compressive strength of the respected mix. This normalized the results, and these results were compared to the ACI coefficient of 7.5. The results of the normal strength mixes can be seen in **Table 5.15**.

**Table 5.15 Normalized Modulus of Rupture for Normal Strength Mixes**

	C6-58L	S6-48L	ACI Coefficient
Modulus of Rupture (psi)	8.5	7.4	7.5

1 psi = 6.89 kPa

The modulus of rupture was also normalized and compared to the AASHTO coefficient of 0.24 as seen in **Eq. 5.4**.

$$f_r = 0.24\sqrt{f'_c} \quad (5.4)$$

The measured modulus of rupture was divided by strength of the respective mix and then compared to the AASHTO coefficient. The results of the normal strength concrete can be seen in **Table 5.16**.

**Table 5.16 Normalized AASHTO Modulus of Rupture for Normal Strength Mixes**

	C6-58L	S6-48L	AASHTO Coefficient
Normalized Result	0.27	.23	.24

The same procedure and calculations were performed for the high strength experimental mixes. The results for the individual tests can be seen in **Table 5.17**.

The modulus of rupture was calculated from the values in **Table 5.17** and then averaged to give a measured modulus of rupture for each mix. The averaged modulus of rupture for the high strength experimental mixes can be seen in **Table 5.18**.

**Table 5.17 Individual Modulus of Rupture Results for  
High Strength Concrete Mixes**

Mix Design ID	Specimen ID	L (in.)	Peak Load (lb.)	b <sub>1</sub> (in.)	b <sub>2</sub> (in.)	b <sub>3</sub> (in.)	b <sub>avg</sub> (in.)	d <sub>1</sub> (in.)	d <sub>2</sub> (in.)	d <sub>3</sub> (in.)	d <sub>avg</sub> (in.)
C10-58L	MOR-1	18	12,791	6.18	6.14	6.13	6.15	5.92	5.96	5.95	5.94
	MOR-2	18	12,123	6.02	6.01	5.99	6.01	5.94	5.98	5.98	5.97
	MOR-3	18	12,719	6.20	6.22	6.23	6.22	5.95	5.96	5.98	5.96
S10-48L	MOR-1	18	13,808	6.01	6.01	6.06	6.03	5.96	5.93	5.92	5.94
	MOR-2	18	13,588	6.09	6.05	6.11	6.08	5.92	5.97	5.95	5.95
	MOR-3	18	12,546	6.17	6.17	6.22	6.19	5.98	5.99	5.94	5.97

1 psi = 6.89 kPa

**Table 5.18 Average Modulus of Rupture Results for High Strength Concrete Mixes**

Mix Design ID	Modulus of Rupture (psi)
C10-58L	1,040
S10-48L	1,100

1 psi = 6.89 kPa

These values were also normalized with the respective compressive strengths in order to compare to the ACI coefficient of 7.5. The normalized results can be seen in **Table 5.19**.

**Table 5.19 Normalized Modulus of Rupture Results for High Strength Concrete Mixes**

	C10-58L	S10-48L	ACI Coefficient
Normalized Results	9.98	9.52	7.5

The modulus of rupture was also normalized and compared to the AASHTO coefficient of 0.24 as seen in **Eq. 5.4**. The measured modulus of rupture was divided by strength of

the respective mix and then compared to the AASHTO coefficient. The results of the high strength concrete can be seen in **Table 5.20**.

**Table 5.20 Normalized AASHTO Modulus of Rupture for High Strength Mixes**

	C10-58L	S10-58L	AASHTO Coefficient
Normalized Result	0.32	0.30	0.24

#### 5.4. SPLITTING TENSILE

The splitting-tensile strength of the concrete mixes was tested and calculated in accordance with ASTM C 496-11. This test was performed using 6 in. (152 mm) diameter by 12 in. (305 mm) long cylindrical specimens. These specimens were loaded into the testing apparatus and loaded until failure. The splitting tensile strength was then calculated using **Eq. 5.5**.

$$T = \frac{2P}{\pi ld} \quad (5.5)$$

Where P is the maximum load applied, l is the length of the specimen, and d is the diameter. A total of 3 specimens were tested for each mix. The individual test results for the normal strength mixes are shown in **Table 5.21**.

**Table 5.21 Individual Splitting-Tensile Test Results for Normal Strength Concrete Mixes**

Mix Design ID	Specimen Number	Length (in)	Diameter (in)	Load (lb.)	Splitting Tensile Strength (psi)
C6-58L	1	12.1	6.0	37,155	326
	2	12.1	6.0	40,260	353
	3	12.1	6.0	49,575	435
S6-48L	1	12.1	6.0	40,890	359
	2	12.1	6.0	66,075	579
	3	12.1	6.0	49,620	435

1 in. = 2.54 cm.

1 lb = 0.45 kg

1 psi = 6.89 kPa

The results of the individual tests were then averaged, and the splitting tensile strength of the normal strength mixes can be seen in **Table 5.22**.

**Table 5.22 Averaged Splitting-Tensile Test Results for Normal Strength Concrete Mixes**

Mix Design ID	Splitting Tensile Strength (psi)
C6-58L	370
S6-48L	460

1 psi = 6.89 kPa

The results were also normalized using the respective measured compressive strengths. This step was done in order to compare the coefficients with the ACI coefficient of 6.7 which comes from the equation to estimate the splitting-tensile strength as seen in **Eq. 5.6**.

$$f_t = 6.7\sqrt{f'_c} \quad (5.6)$$

Where  $f_t$  is the splitting-tensile strength and  $f'_c$  is the compressive strength of concrete. After the splitting tensile strength was measured, the values were divided by the square root of the average measured strength of the respected mix. This normalized the results, and these results were compared to the ACI coefficient of 6.7. The results of the normal strength mixes can be seen in **Table 5.23**.

**Table 5.23 Normalized Splitting-Tensile Results for  
Normal Strength Concrete Mixes**

Mix Design ID	C6-58L	S6-48L	ACI Coefficient
Normalized Results	4.2	5.1	6.7

The same test was carried out on the high strength concrete mixes. The individual test results can be seen in **Table 5.24**.

**Table 5.24 Individual Splitting-Tensile Test Results for  
High Strength Concrete Mixes**

Mix Design ID	Specimen Number	Length (in.)	Diameter (in.)	Load (lb.)	Splitting Tensile Strength (psi)
C10-58L	1	12.2	6.0	66,675	580
	2	12.1	6.0	56,070	492
	3	12.1	6.0	66,090	580
S10-48L	1	12	6.0	95,100	841
	2	12.1	6.0	83,520	732
	3	12.2	6.0	81,345	708

1 in. = 2.54 cm.

1 lb = 0.45 kg

1 psi = 6.89 kPa

The results of the individual tests were then averaged, and the splitting tensile strength of the high strength mixes can be seen in **Table 5.25**.

**Table 5.25 Averaged Splitting-Tensile Test Results for High Strength Concrete Mixes**

Mix Design ID	Splitting Tensile Strength (psi)
C10-58L	550
S10-48L	760

1 psi = 6.89 kPa

These values were also normalized with the respective compressive strengths in order to compare to the ACI coefficient of 6.7. The normalized results can be seen in **Table 5.26**.

**Table 5.26 Normalized Splitting-Tensile Results for High Strength Concrete Mixes**

Mix Design ID	C10-58L	S10-48L	ACI Coefficient
Normalized Results	5.3	6.5	6.7

## 5.5. RAPID FREEZING & THAWING

The concrete's resistance to freezing and thawing was tested and calculated in accordance to ASTM C 666-08. During the freezing and thawing cycles, the relative dynamic modulus of elasticity was measured for each of the specimens using the equation stated in Section 4.2.3. Using this data, the durability factor of the specimen could be calculated using the equation stated in Section 4.2.3. The relative dynamic modulus of elasticity and durability factor of each specimen was calculated every 36 cycles. The complete data for all test specimens can be found in Appendix A. The minimum calculated durability factor was reported as the durability factor for that

specimen, and the values for the individual specimens of the normal strength mixes can be seen in **Table 5.27**.

**Table 5.27 Individual Results of Rapid Freezing and Thawing Test for Normal Strength Mixes**

Mix Design ID	Specimen ID	Initial Frequency	Terminal Frequency	Durability Factor	% Mass Change
C6-58L	FT-1	1973	1184	23.2	0.01
	FT-2	1947	1168	22.4	0.02
	FT-3	1980	1188	31.1	-0.01
S6-48L	FT-1	2013	1208	11.5	0.05
	FT-2	1979	1187	28.9	0.01
	FT-3	1902	1141	19.2	0.02

The average durability factor was reported using the three replicate specimens for each experimental mix. The higher the measured durability factor of the specimen, the better the mix will perform when exposed to cyclic freezing and thawing. The calculated durability factors for the normal strength mixes can be seen in **Table 5.28**.

**Table 5.28 Averaged Durability Factors for Normal Strength Mixes**

Mix Design ID	Durability Factor
C6-58L	25.5
S6-48L	19.9

The calculation procedure was the same for the high strength experimental mixes. The calculated durability factors for each individual specimen can be seen in **Table 5.29**.

**Table 5.29 Individual Results of Freezing and Thawing Test for High Strength Mixes**

Mix Design ID	Specimen ID	Initial Frequency	Terminal Frequency	Durability Factor	% Mass Change
C10-58L	FT-1	1990	1194	90.8	-0.01
	FT-2	1978	1187	93.1	-0.09
	FT-3	1988	1193	77.6	0
S10-48L	FT-1	2018	1211	43.4	0
	FT-2	1998	1199	61.5	-0.01
	FT-3	2041	1225	30.6	0.02

The average durability factors for the high strength experimental mixes can be seen in **Table 5.30**.

**Table 5.30 Averaged Durability Factors for High Strength Mixes**

Mix Design ID	Durability Factor
C10-58L	87.2
S10-48L	45.2

## 5.6. ELECTRICAL INDICATION TO RESIST CHLORIDE PENETRATION

The testing and calculations for this test were performed in accordance with ASTM C 1202-10. After the testing was complete, the measured current vs. time was plotted. A trend line was drawn through the graph and was integrated to calculate the area under the curve. The graphs plotted for each specimen can be found in Appendix A. An example of this graph can be seen in **Figure 5.3**.

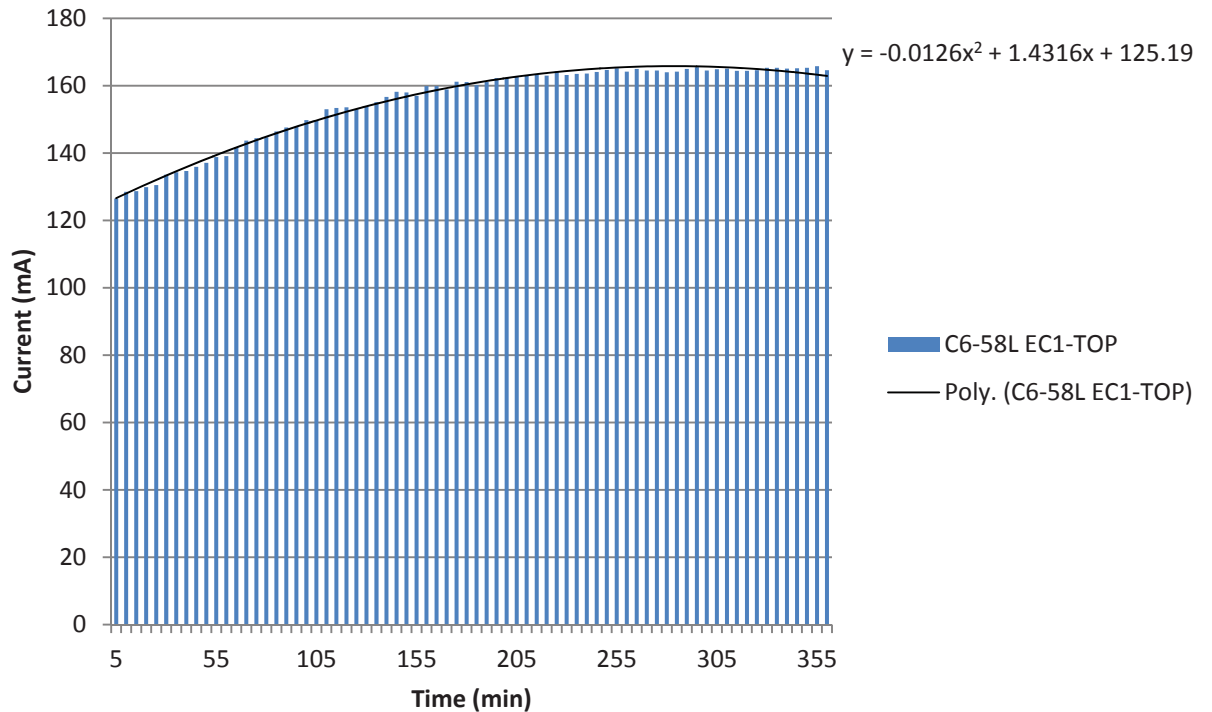


**Figure 5.3 – Example of RCT Results**

This area gives the total charge in coulombs to pass through the specimen during the 6 hour test. Since the diameter of the specimens used did not measure 3.75 in. (95 mm), the charge had to be adjusted using **Eq. 5.7**.

$$Q_s = Q_x \times \left(\frac{3.75}{x}\right)^2 \quad (5.7)$$

Where  $Q_s$  is the total charge through a 3.75 in. (95 mm) specimen,  $Q_x$  is the total charge passed through a specimen measuring  $x$  inches in diameter, and  $x$  is the diameter of the specimen that is tested. The total charge was then compared to ASTM C 1202 to assign a permeability rating, with a range from negligible (indicating the highest resistance to chloride penetration) to high (indicating the lowest resistance to chloride penetration).

The corrected results of the individual specimens for the normal strength mixes can be seen in **Table 5.31**.

**Table 5.31 Individual RCT Results for Normal Strength Mixes**

Mix Design ID	Corrected Charge Passed (Coulombs)			
	EC1-TOP	EC1-MID	EC2-TOP	EC2-MID
C6-58L	3025	3135	4050	3810
S6-48L	3990	3681	3846	3812

The average was taken of the total charge passed through all four specimens and that charge was then used to assign a permeability class. The results of the conventional mixes can be seen in **Table 5.32**.

**Table 5.32 Averaged Results of RCT and Permeability Class of Conventional Mixes**

Mix Design ID	Charge Passed (Coulombs)	Permeability Class
C6-58L	3505	Moderate
S6-48L	3832	Moderate

The ranges for the classes are as follows; 0-100 for negligible, 100-1000 for very low, 1000-2000 for low, 2000-4000 for moderate, >4000 for high. Both mixes fell into the moderate category. The same calculation process was performed on the high strength mix specimens. The individual specimen results can be seen in **Table 5.33**.

**Table 5.33 Individual Results of RCT for High Strength Mixes**

Batch ID	Corrected Charge Passed (Coulombs)			
	EC1-TOP	EC1-MID	EC2-TOP	EC2-MID
C10-58L	4314	4666	3785	4860
S10-48L	2125	2444	2391	2296

The average of the four specimens was then calculated and this value was used to assign a permeability class. The results for the high strength experimental mixes can be seen in **Table 5.34**.

**Table 5.34 Averaged Results of RCT and Permeability Class for High Strength Mixes**

Mix Design ID	Charge Passed (Coulombs)	Permeability Class
C10-58L	4406	High
S10-48L	2564	Moderate

## 5.7. PONDING TEST

The ponding test was performed in accordance with ASTM C 1543-10. After the ponding duration was complete, cores were taken from the specimens and powder samples collected at specified depths. A water soluble chloride analysis was performed on each powder sample to determine the chloride concentration. For each experimental mix, a total of 3 cores were taken from each of the three individual test specimens, with 5 powder samples taken from each core. This approach would determine an average chloride profile for each experimental mix. Using a scale set forth by Broomfield in 2007, the risk of corrosion in concrete can be determined by the amount of chloride present in concrete. The scale can be seen in **Table 5.35**.

**Table 5.35 Correlation Between Percent Chloride by Mass of Concrete and Corrosion Risk [Broomfield, 2007]**

% Chloride by mass of concrete	Corrosion Risk
<0.03	Negligible
0.03-0.06	Low
0.06-0.14	Moderate
>0.14	High

Using this scale, the concrete mixes were assigned corrosion risk based on the data collected in the chloride analysis. The averaged data for the normal strength mixes can be seen in **Table 5.36**. The complete table of data can be found in Appendix A. The data was also plotted in **Figure 5.4** with a line indicating a negligible corrosion risk.

**Table 5.36 Average Chloride Content at Specified Depths of Normal Strength Mixes**

Mix Design ID	Depth (in.)	Chloride Content (%)	Corrosion Risk
C6-58L	Surface	0.23	High
	0.25	0.07	Moderate
	0.75	0.02	Negligible
	1.5	0.009	Negligible
	2.0	0.006	Negligible
S6-48L	Surface	0.28	High
	0.25	0.09	Moderate
	0.75	0.017	Negligible
	1.5	0.011	Negligible
	2.0	0.005	Negligible

1 in. = 2.54 cm

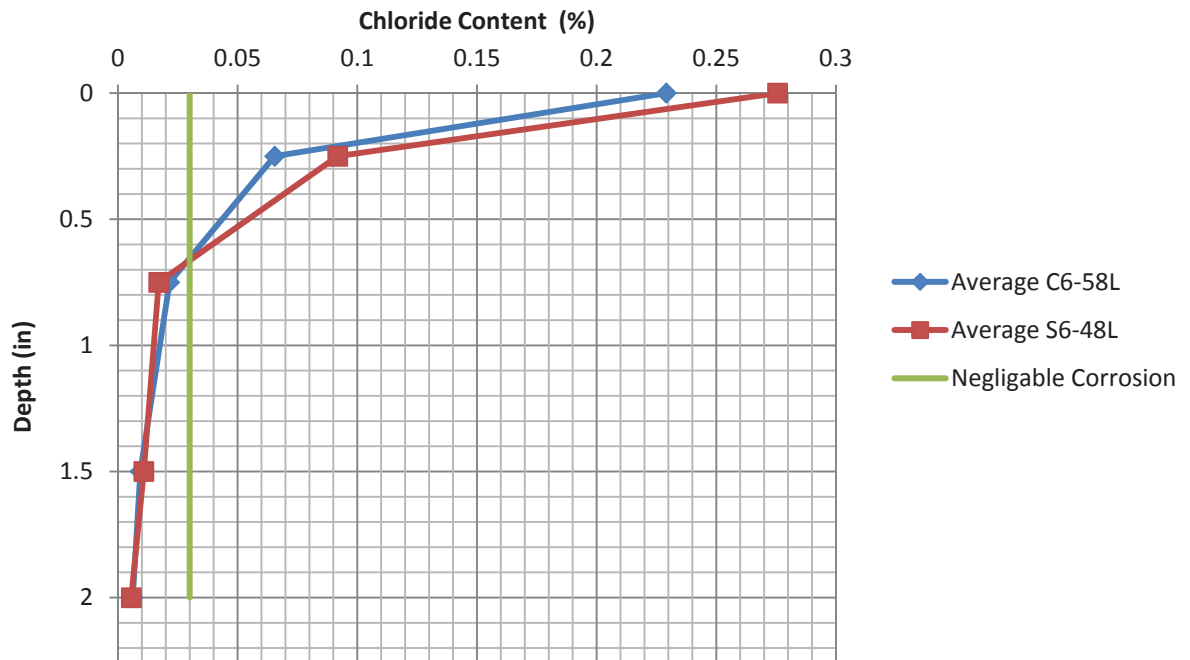


**Figure 5.4 – Average Chloride Content vs. Depth of Conventional Mixes**  
1 in. = 2.54 cm

The same process was performed on the high strength mixes. The averaged data for the high strength mixes can be seen in **Table 5.37**. The complete table of data can be seen in Appendix A. This data was also plotted in **Figure 5.5** with a line indicating a negligible corrosion risk.

**Table 5.37 Average Chloride Content at Specified Depths of High Strength Mixes**

Mix Design ID	Depth (in.)	Chloride Content (%)	Corrosion Risk
C10-58L	Surface	0.24	High
	0.25	0.095	Moderate
	0.75	0.011	Negligible
	1.5	0.0074	Negligible
	2.0	0.010	Negligible

S10-48L	Surface	0.15	High
	0.25	0.016	Negligible
	0.75	0.006	Negligible
	1.5	0.0062	Negligible
	2.0	0.0044	Negligible

1 in. = 2.54 cm.

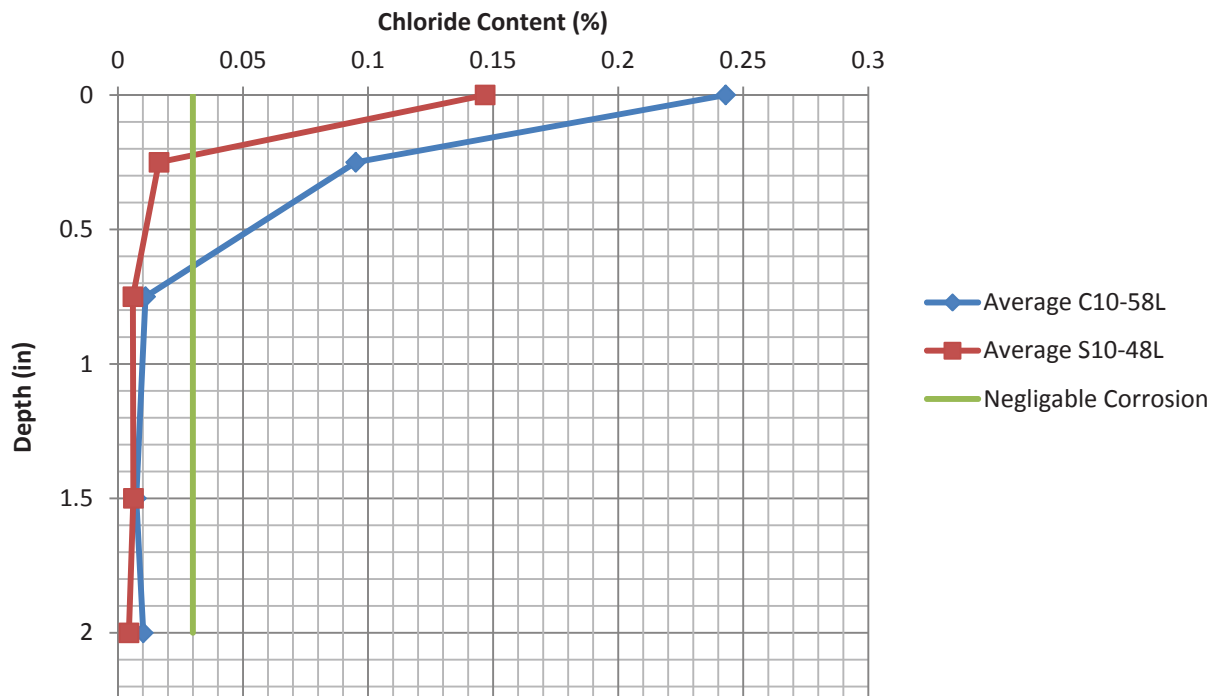


**Figure 5.5 – Average Chloride Content vs. Depth of High Strength Mixes**  
1 in. = 2.54 cm

## 5.8. CONCRETE RESISTIVITY

The concrete resistivity test was a non-ASTM test method. It is however, an industry standard, and is used quite frequently. The resistivity measurements were measured over a period of 24 weeks. These measurements can be found in Appendix A.

The test was performed on three replicate specimens with the results averaged to

determine the response of the individual concrete mix. The averages for each mix were then compared between concrete types. The individual specimen results for the conventional and SCC normal strength mixes are shown in **Figure 5.6** and **Figure 5.7**, respectively.

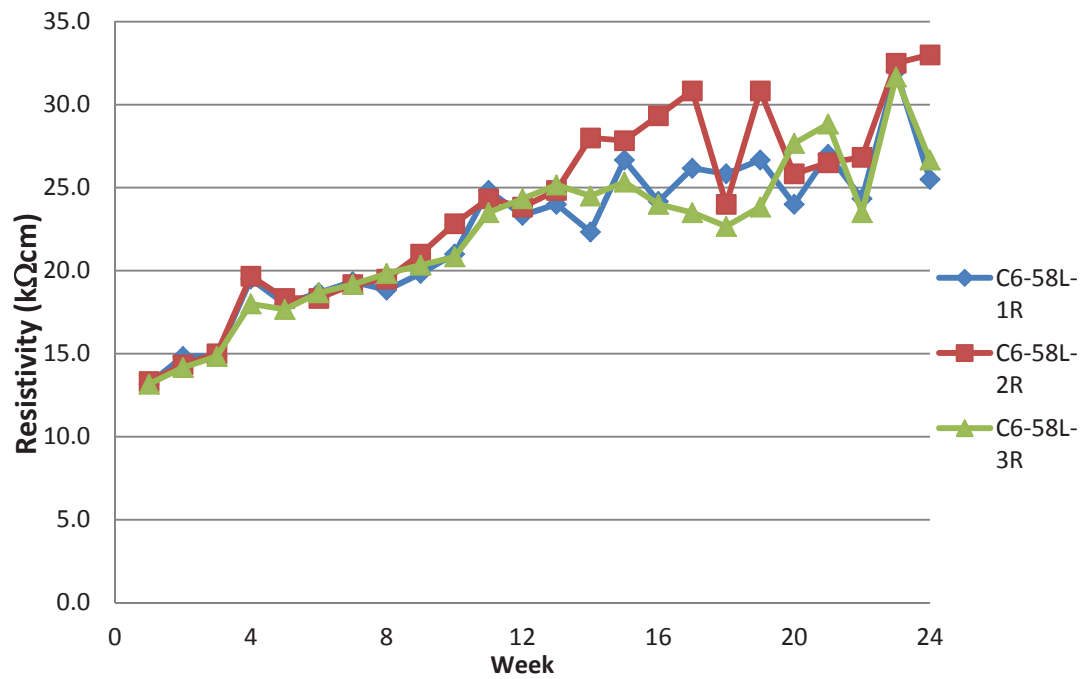


**Figure 5.6 - Individual Specimen Results for Concrete Resistivity for C6-58L Mix**

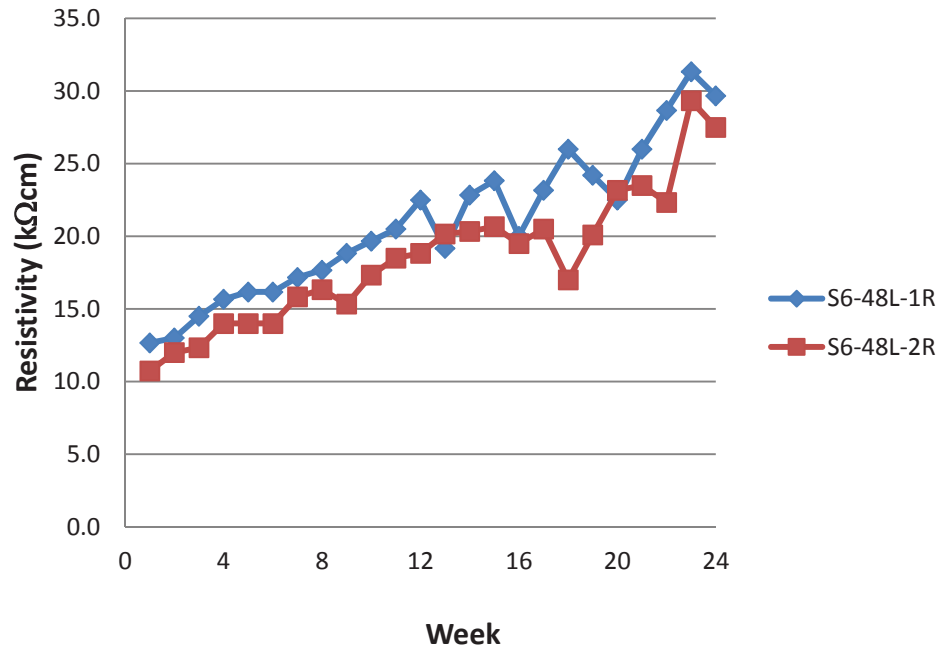


**Figure 5.7 - Individual Specimen Results for Concrete Resistivity for S6-48L Mix**

It should be noted that a specimen for the S6-48L mix was damaged during the de-molding process. The individual results were then averaged and graphed on the same plot for comparison purposes, which are shown **Figure 5.8**. A linear trend line of the results was also plotted in **Figure 5.8** in order to compare the rates at which the different mixes gained resistivity. According to Broomfield, any concrete that has a resistivity greater than 20 kΩcm is considered to have low corrosion potential. The final readings were taken at 24 weeks and can be seen in **Table 5.38**.

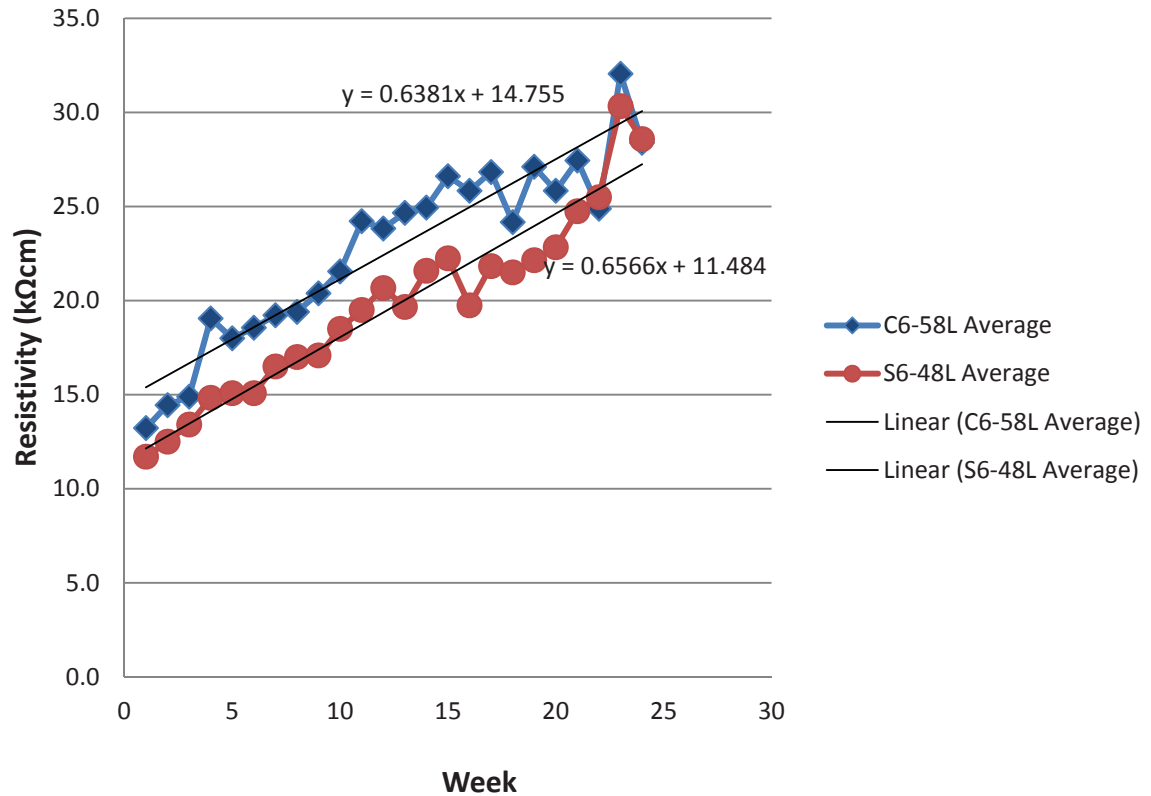


**Figure 5.8 – Averaged Results for Concrete Resistivity for Normal Strength Mixes**

**Table 5.38 Final Resistivity of Normal Strength Concrete Mixes**

Mix Design ID	Resistivity (kΩcm)
C6-58L	28.4
S6-48L	28.6

The same procedure was used for the high strength mixes. The results of the individual specimens for the C10-58L mix and the S10-48L mix can be seen in **Figure 5.9** and **Figure 5.10**, respectively.

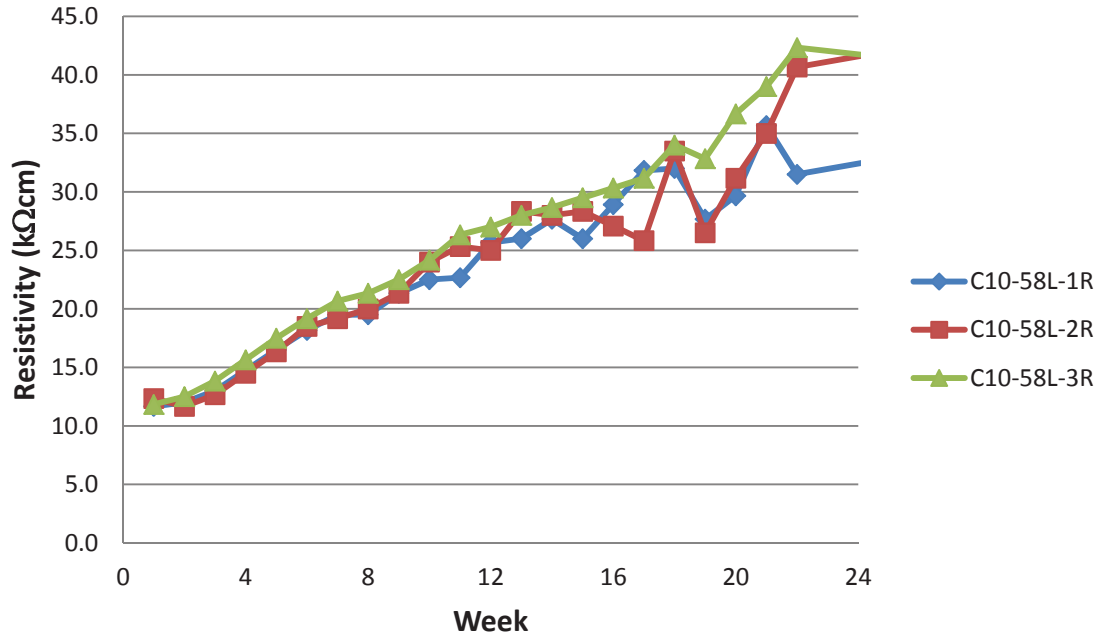


Figure 5.9 - Individual Specimen Results for Concrete Resistivity for C10-58L Mix

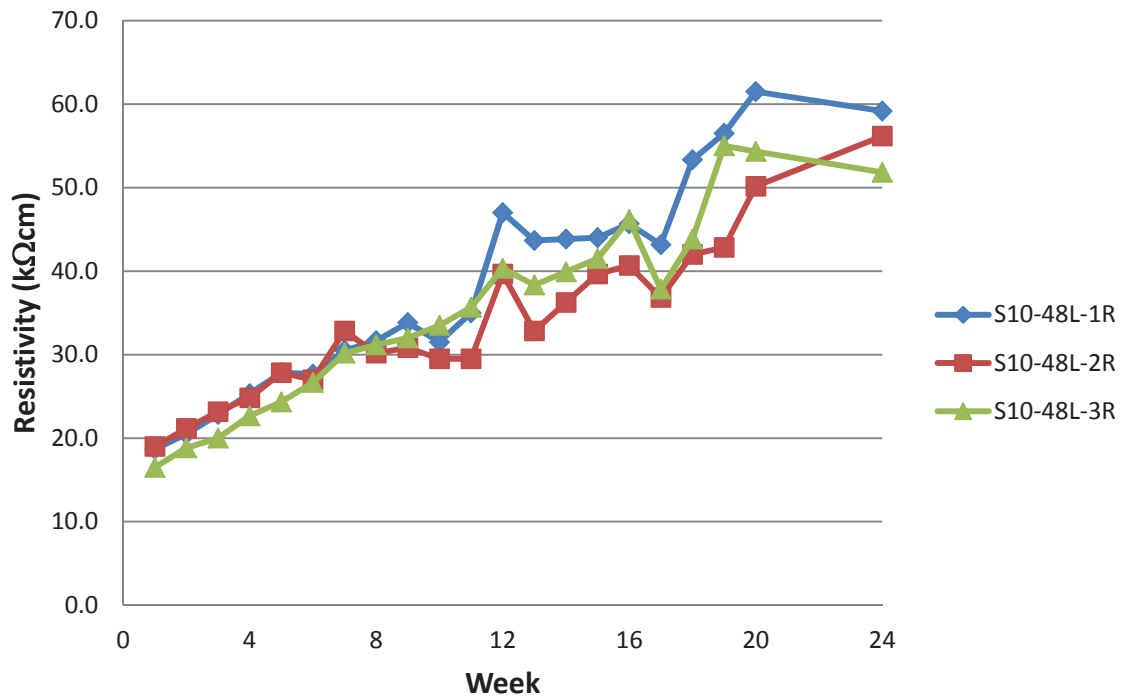
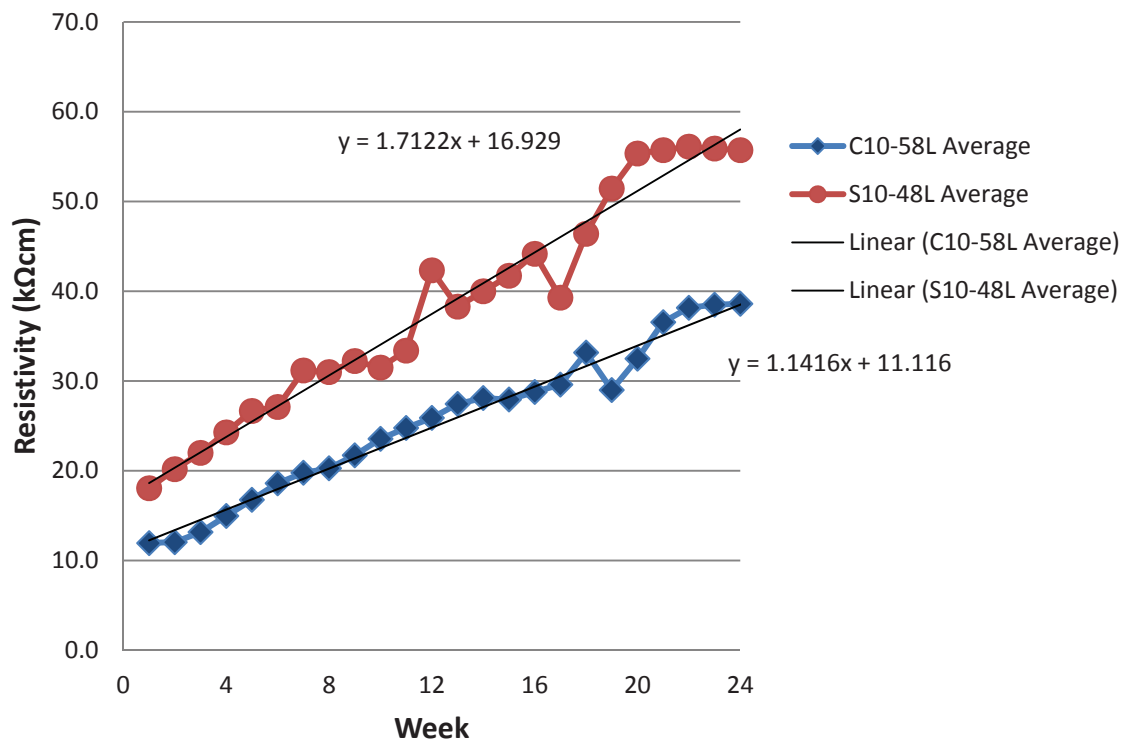


Figure 5.10 - Individual Specimen Results for Concrete Resistivity for S10-48L Mix

The measurements can be found in Appendix A. These results were then averaged and graphed on the same plot for comparison purposes, with the results for the high strength mixes shown in **Figure 5.11**. A liner trend line was plotted in order to compare the rate at which the concretes gain resistivity. The final readings were taken at 24 weeks and can be seen in **Table 5.39**.



**Figure 5.11 – Averaged Results for Concrete Resistivity for High Strength Mixes**

**Table 5.39 Final Resistivity of High Strength Concrete Mixes**

Mix Design ID	Resistivity (kΩcm)
C10-58L	38.6
S10-48L	55.7

## 6. EVALUATION OF SELF-CONSOLIDATING CONCRETE

### 6.1. NORMAL STRENGTH SCC

As stated in previous sections, both the normal strength conventional concrete mix and the normal strength SCC mix were subjected to the same mechanical property and durability tests. In this way, it was possible to evaluate the performance of the SCC relative to a benchmark – the conventional normal strength concrete mix. If the SCC mix performed as well or better than the conventional concrete, then it could be reasoned that, due to the time-saving properties of SCC, it would be beneficial to use the SCC in precast applications. The results of the mechanical property and durability tests can be found in Chapter 5. An outline of these results can be seen in **Table 6.1**. As stated in previous chapters, the C6-58L and S6-48L mix design IDs represent the conventional concrete mix and SCC mix, respectively.

**Table 6.1 Outline of Results of Normal Strength Concrete Mixes**

Test ID	Mix Design ID	
	C6-58L	S6-48L
28 Day Compressive Strength (psi)	7,600	8,140
Modulus of Elasticity (psi)	3,337,000	3,124,000
Modulus of Rupture (psi)	741	672
Splitting Tensile (psi)	371	458
Rapid Freeze – Thaw (durability factor)	25.5	19.9
RCT (coulombs)	3,505	3,832
Ponding (Depth at 0.03% Chloride Content, in)	0.65	0.65
Concrete Resistivity (kΩcm)	28.4	28.6

1 psi = 6.89 kPa

1 in. = 2.54 cm

**6.1.1. Mechanical Properties.** For compressive strength, both mixes were designed to reach 6,000 psi (41.3 MPa) at 28 days, which both mixes exceeded. However, the compressive strength for the SCC mix was slightly higher than that for the conventional mix. From the strength profiles shown in **Figure 5.1** it can be seen that the early strength development was almost identical, but the SCC mix began to exceed the conventional mix at around 3 days. This early strength development is very important to precast construction. With the resulting reduction in labor, SCC would be a good candidate for precast plants when just looking at rate of strength gain. A statistical t-test was performed on the compressive strength data in order to determine if there is any statistical difference between the two mixes. The P value of the t test between the normal

strength mixes was 0.07. Any value greater than 0.05 shows the data is statistically equal. In other words, the compressive strengths of the two mixes are essentially identical. The modulus of rupture, modulus of elasticity, and splitting-tensile strengths are typically estimated in design using equations based on previous research. These equations were mentioned in Chapter 5. The results of the modulus of rupture, modulus of elasticity, and splitting-tensile strengths were subsequently normalized using the respective compressive strengths of each mix and the resulting coefficients were then compared to recommended values within ACI standards. A summary of these results can be seen in **Table 6.2**.

**Table 6.2 Normalized Mechanical Properties Compared to  
Respective ACI Coefficients**

	C6-58L	S6-48L	ACI Coefficient
Modulus of Elasticity	38,280	34,630	57,000
Modulus of Rupture	8.5	7.4	7.5
Splitting Tensile Strength	4.2	5.1	6.7

Both mixes fell considerably short of the empirical relationships recommended for modulus of elasticity, with the SCC mix performing below the conventional mix. This result means that in the design of concrete structures constructed with these concretes, the modulus of elasticity for either mix would be overestimated. This situation can have negative effects on estimating deflection and serviceability of concrete in the field. However, with both concretes falling at about the same level, it can be stated that both C6-58L and S6-48L are comparable in this area. This fact leads to the conclusion that the low modulus of elasticity is more a function of the particular limestone coarse aggregate used in each mix. A statistical t-test was performed on the modulus of elasticity

coefficient data in order to determine if there was a statistical difference between the two mixes. The P value of the test between the two mixes was 0.1. This value is greater than 0.05 so the data is statistically equal. In other words, the modulus of elasticity of the two mixes is essentially identical. The measured modulus of elasticity for each specimen of each mix was also plotted against compressive strength for comparison with the ACI recommended relationship. This graph can be seen in **Figure 6.1**.

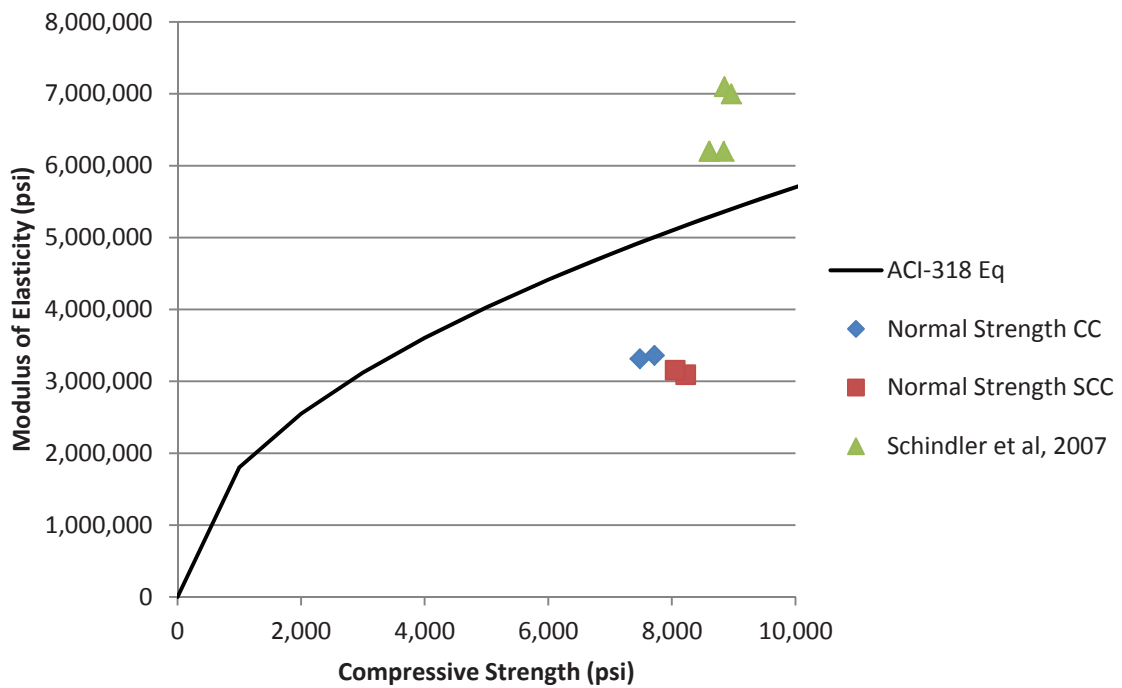


**Figure 6.1 – Compressive Strength vs. Modulus of Elasticity**

For the modulus of rupture, it can be seen that the C6-58L mix exceeded the ACI coefficient of 7.5 while the S6-48L mix barely fell short. It is important to note, however, that the modulus of rupture is highly variable as the coefficient can vary between 6 and 12 [Neville, 1997]. A statistical t-test was performed on the modulus of rupture coefficient data in order to determine if there was a statistical difference between the two

mixes. The P value of the test between the two mixes was 0.04. This value is less than 0.05 so the data is statistically different. The measured modulus of rupture for each specimen of each mix was also plotted against compressive strength for comparison with the ACI recommended relationship. Also included in the plot for comparison is data from another SCC study completed at Missouri S&T. This graph can be seen in **Figure 6.2**.

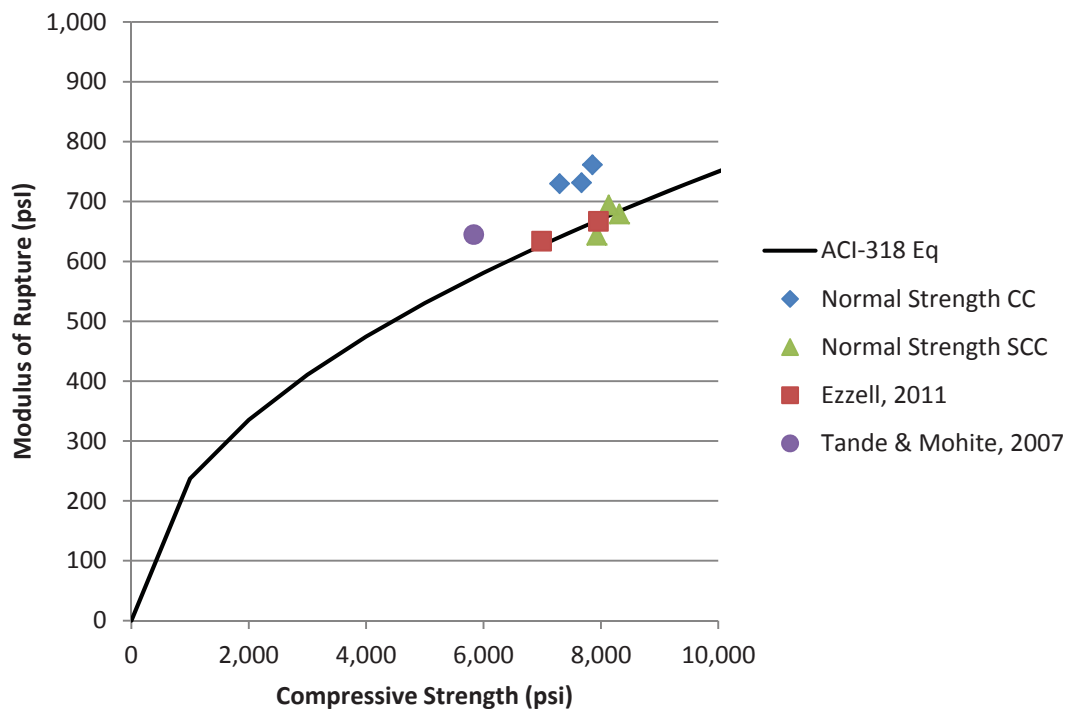


**Figure 6.2 – Compressive Strength vs. Modulus of Rupture**

For the splitting-tensile strength, the S6-48L mix showed a higher tensile strength than the C6-58L mix. However, both mixes fell short of the ACI coefficient used to estimate the splitting-tensile strength. However, splitting-tensile strength is also highly variable with values ranging from 5 to 9.5 [Oluokun, 1991]. A statistical t-test was performed on the splitting-tensile strength coefficient data in order to determine if there is

a statistical difference between the two mixes. The P value of the t-test between the normal strength mixes was 0.4. Any value greater than 0.05 shows the data is statistically equal. In other words, the splitting-tensile strengths of the two mixes are essential identical. The splitting-tensile strength of the specimens was also plotted against the compressive strength of the concrete. This graph can be seen in **Figure 6.3**.

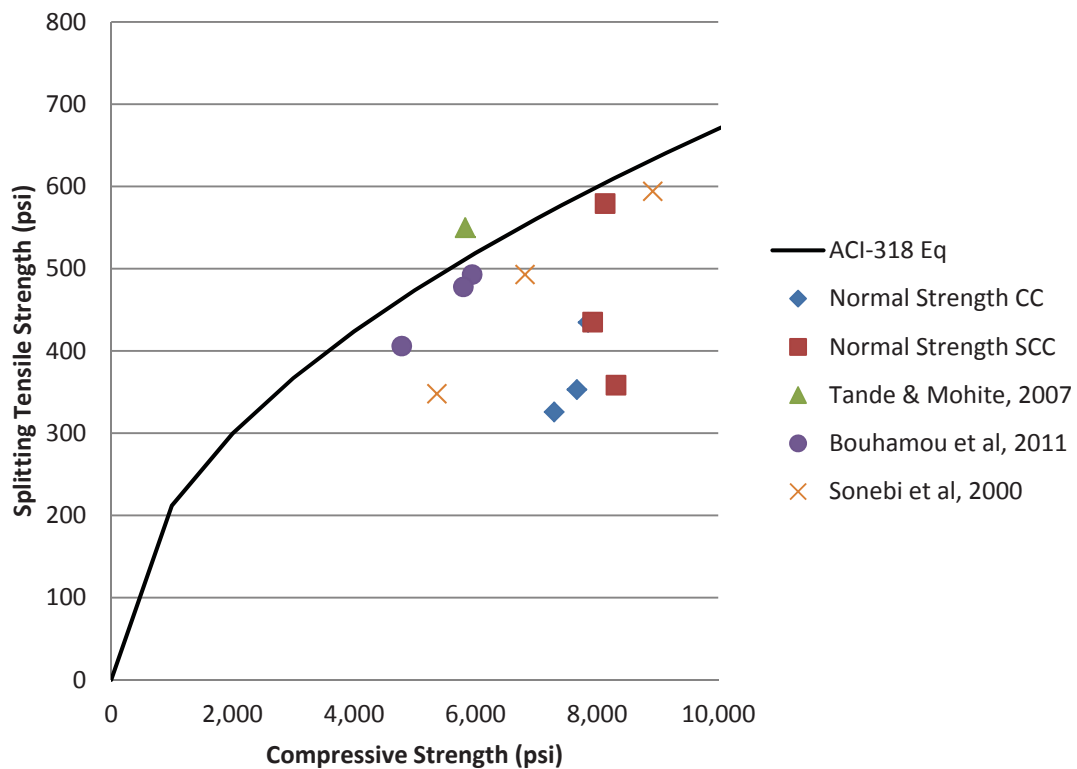


**Figure 6.3 – Compressive Strength vs. Splitting-Tensile Strength**

The measured modulus of elasticity and modulus of rupture were also compared to the AASHTO LRFD Design equations used to estimate these mechanical properties. These properties were normalized by dividing the measured values by the respective compressive strength and then compared to the AASHTO equations as mentioned in Chapter 5. A summary of these coefficients can be seen in **Table 6.3**.

**Table 6.3 Normalized Mechanical Properties Compared to  
Respective AASHTO Coefficients**

	C6-58L	S6-48L	AASHTO Coefficient
Modulus of Elasticity	1,251	1,097	1,820
Modulus of Rupture	0.27	0.23	0.24

It can be observed that these normalized results follow a very similar trend when comparing the results to the ACI coefficients. For example, the C6-58L mix showed a slightly higher coefficient than the AASHTO coefficient while the S6-48L mix showed a slightly lower coefficient than the AASHTO coefficient. This was also seen in the ACI coefficient comparison.

**6.1.2. Durability Performance.** For resistance to freezing and thawing, both the C6-58L mix and the S6-48L mix did very poorly when compared to the minimum set forth by MoDOT. MoDOT specifies a minimum durability factor of 75, while the conventional and SCC mixes recorded values of 25.5 and 19.9, respectively. Although both mixes performed poorly, the SCC was comparable to the conventional concrete, which leads to the conclusion that the poor freeze-thaw performance was more a function of the particular coarse aggregate used in the mixes (Jefferson City dolomite).

With regard to permeability, both mixes were comparable. For the Rapid Chloride Test (RCT), the lower the total charge passed, the less permeable the concrete. Both concrete mixes fell in the mid-3000 range, with the C6-58L mix being slightly less permeable. The similarity in performance continued in the concrete's resistance to chloride penetration by ponding. After the concrete was analyzed for chloride content at specified depths, it was found that the two mixes performed almost identically. Both

mixes reached the goal of 0.03% chloride content by mass, indicating negligible corrosion risk, at approximately the same depth, 0.7 in. (18 mm). The S6-48L did however show slightly higher chloride contents at the first two depths indicating a slightly higher surface permeability, which is believed to be related to the finishing of the specimens. The ponding test is a relative measure of chloride permeability, and the test indicated that the SCC is comparable to the conventional control mix. The average chloride profile of the two normal strength mixes can be seen in **Figure 6.4**.

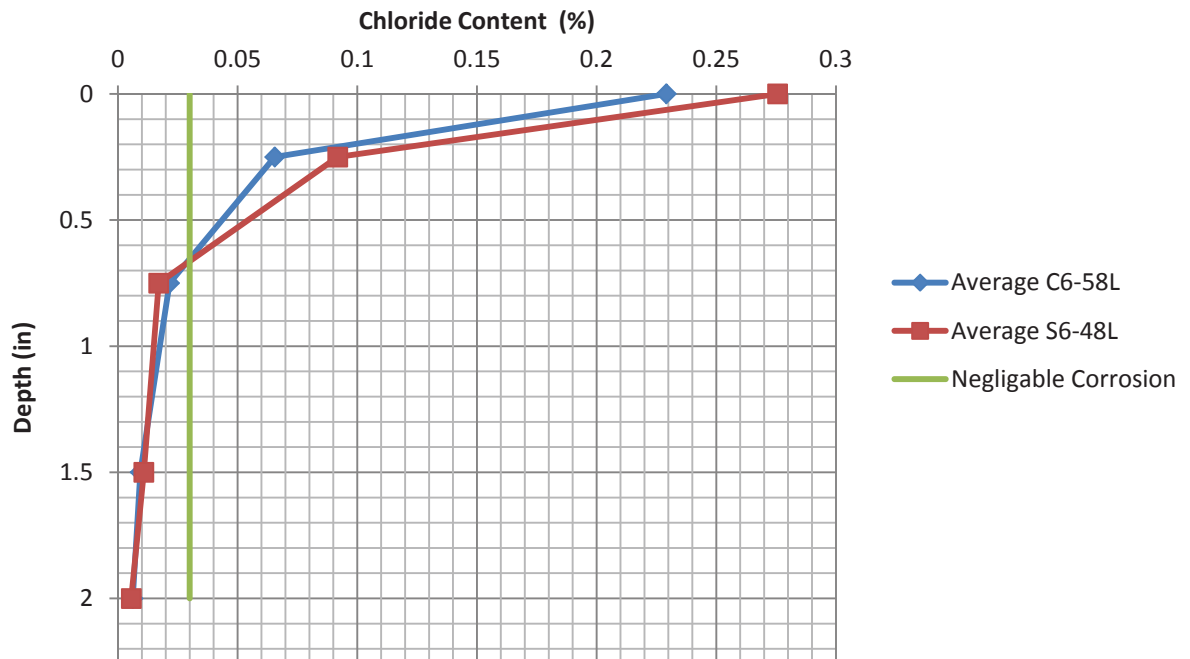


**Figure 6.4 – Average Chloride Content vs. Depth of Conventional Mixes**  
1 in. = 2.54 cm

With regard to concrete resistivity using the Wenner probe, both concrete mixes performed very similarly. The rate at which resistivity increased was almost identical. A trend line for the resistivity was plotted for each mix and the slope for the C6-58L mix

and the S6-48L mix was 0.638 and 0.656, respectively. The results of this test can be seen in **Figure 6.5**. After 24 weeks of testing, each mix reached a resistivity of approximately 28.5 kΩcm. According to Broomfield [2007], any concrete that indicates resistivity over 20 kΩcm is to be classified as having a low rate of corrosion. Both mixes exceeded this benchmark and performed very similarly.

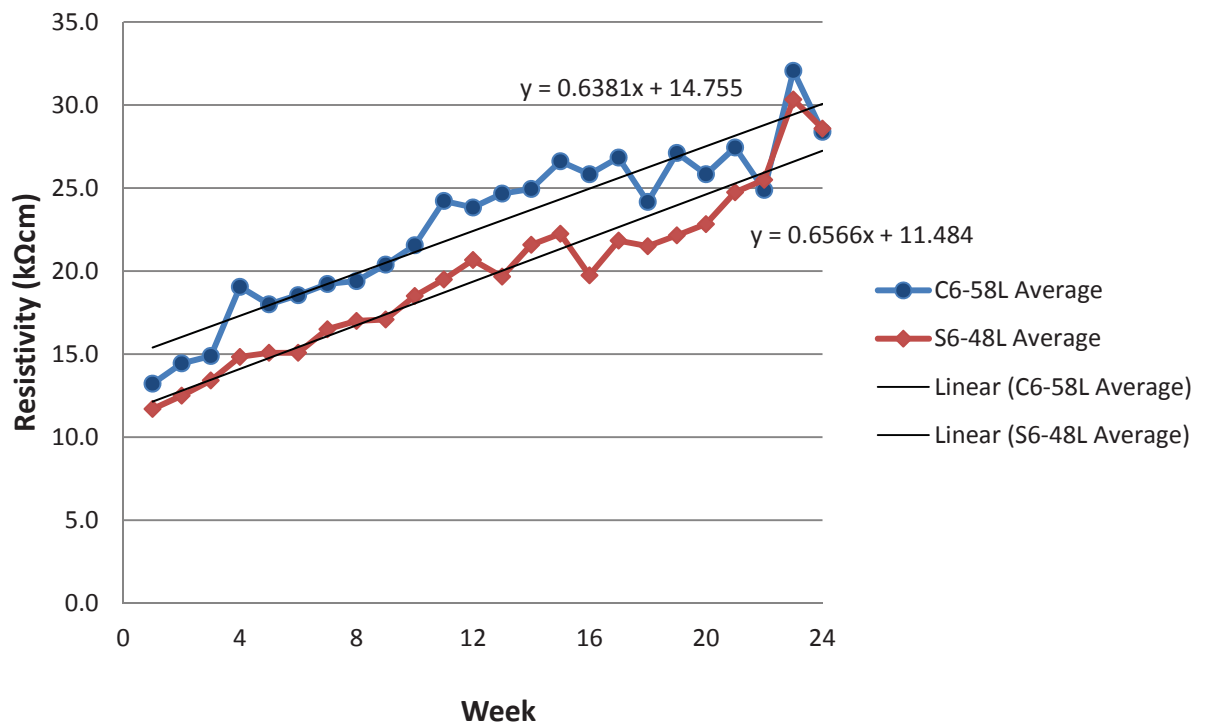


**Figure 6.5 – Average Resistivity of Normal Strength Concrete Mixes**

## 6.2. HIGH STRENGTH SCC

As stated in previous sections, both the high strength conventional concrete mix and the high strength SCC mix were subjected to the same mechanical property and durability tests. In this way, it was possible to evaluate the performance of the high strength SCC relative to a benchmark – the conventional high strength concrete mix. If

the high strength SCC mix performed as well or better than the conventional concrete, than it could be reasoned that, due to the time-saving properties of SCC, it would be beneficial to use the SCC in precast applications. The results of the mechanical property and durability tests can be found in Chapter 5. An outline of these results can be seen in **Table 6.4**. As stated in previous chapters, the C10-58L and S10-48L mix design IDs represent the high strength conventional concrete mix and high strength SCC mix, respectively.

**Table 6.4 Outline of Results of High Strength Concrete Mixes**

Test ID	Mix Design ID	
	C10-58L	S10-48L
28 Day Compressive Strength (psi)	10,823	13,482
Modulus of Elasticity (psi)	3,855,000	3,556,000
Modulus of Rupture (psi)	1,039	1,105
Splitting Tensile (psi)	550	760
Rapid Freezing – Thawing (durability factor)	87.2	45.2
RCT (coulombs)	4,406	2,564
Ponding (Depth at 0.03% Chloride Content, in)	0.2	0.65
Concrete Resistivity (k $\Omega$ cm)	38.6	55.7

1 psi = 6.89 kPa

1 in. = 2.54 cm

**6.2.1. Mechanical Properties of High Strength Mixes.** For compressive strength, both mixes were designed to reach 10,000 psi (68.9 MPa) at 28 days, which both mixes exceeded. The S10-48L exceeded this goal by a much higher margin than the C10-58L mix. The S10-48L mix also showed a much higher early strength gain, while

the later strengths for the two mixes developed at approximately the same rate. This early strength development is very important to precast construction. With the resulting reduction in labor, SCC would be a good candidate for precast plants when just looking at the rate of strength gain. A statistical t-test was performed on the compressive strength data in order to determine if there is any statistical difference between the two mixes. The P value of the t test between the high strength mixes was 0.03. Any value less than 0.05 shows the data is statistically different. In other words, the high strength SCC mix compressive strength exceeded the high strength conventional concrete mix compressive strength.

The modulus of rupture, modulus of elasticity, and splitting-tensile strengths are typically estimated in design using equations based on previous research. These equations were mentioned in Chapter 5. The results of the modulus of rupture, modulus of elasticity, and splitting-tensile strengths were subsequently normalized using the respective compressive strengths of each mix and the resulting coefficients were then compared to recommended values within ACI standards. A summary of these results can be seen in **Table 6.5**.

**Table 6.5 Normalized Mechanical Properties Compared to  
Respective ACI Coefficients**

	C10-58L	S10-48L	ACI Coefficient
Modulus of Elasticity	37,070	30,660	57,000
Modulus of Rupture	9.98	9.52	7.5
Splitting-Tensile Strength	5.3	6.5	6.7

Both high strength mixes fell considerably short of the empirical relationship recommended for modulus of elasticity, with the high strength SCC mix performing below the high strength conventional mix. This result means that in the design of concrete structures constructed with these concretes, the modulus of elasticity for either mix would be overestimated. This situation can have negative effects on estimating deflection and serviceability of concrete in the field. However, with both concretes falling at about the same level, it can be stated that both C10-58L and S10-48L are comparable in this area. This fact leads to the conclusion that the low modulus of elasticity is more a function of the particular limestone coarse aggregate used in each mix. A statistical t-test was performed on the modulus of elasticity coefficient data in order to determine if there was any statistical difference between the two mixes. The P value of the t test between the high strength mixes was 0.01. Any value less than 0.05 shows the data is statistically different, which indicates there was some additional decrease in modulus between the high strength conventional concrete and SCC separate from that caused by the aggregate. The modulus of elasticity of each specimen was also plotted against compressive strength for comparison with the ACI recommended relationship. The graph can be seen in **Figure 6.6**.

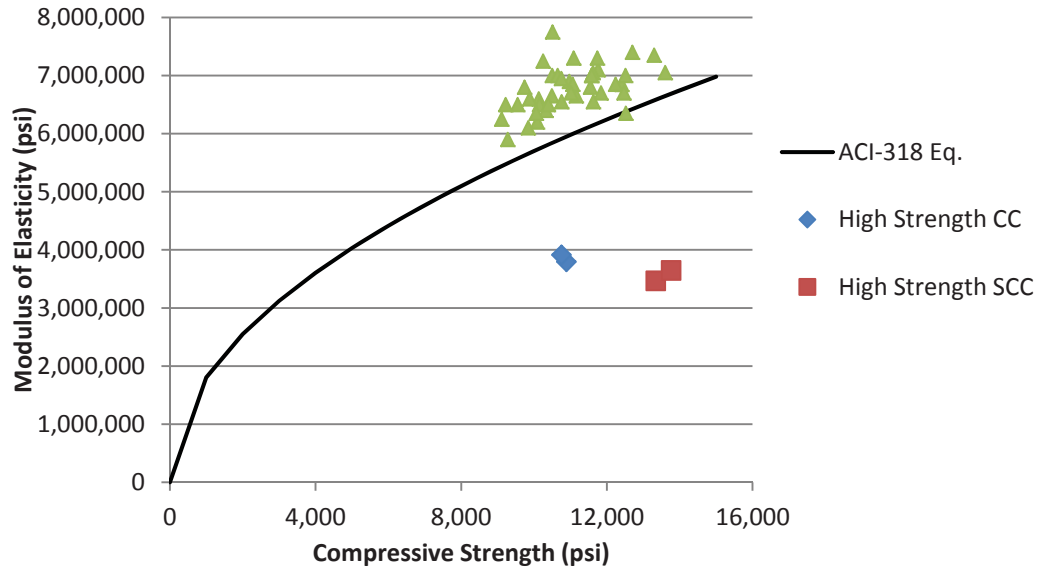


**Figure 6.6 - Compressive Strength vs. Modulus of Elasticity**

The high strength mixes were also compared to several modulus of elasticity equations found in ACI-363. The equations were developed specifically for high strength concretes. The following equations were used for comparison.

$$E_c = 38,200f_c'^{0.5} + 2,110,000 \quad (6.1)$$

$$E_c = 309,500f_c'^{0.3} \quad (6.2)$$

The results of this comparison can be seen in **Figure 6.7**.

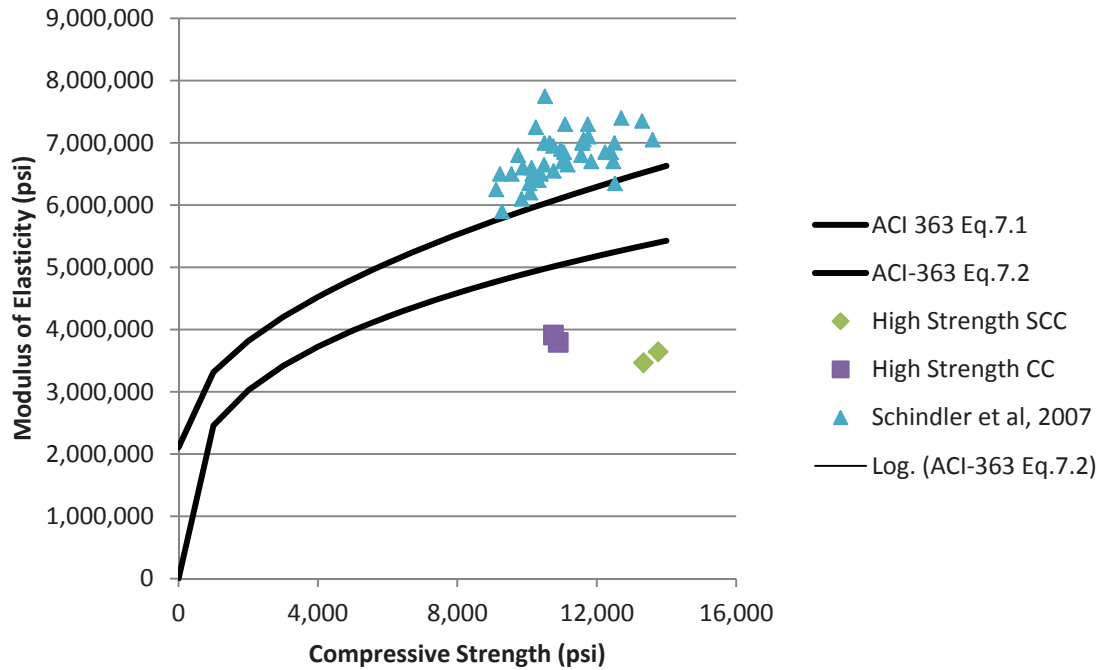


**Figure 6.7 – High Strength Mixes Compared to ACI-363 Equations**

For the modulus of rupture it can be seen that both mixes exceeded the recommended empirical relationship. It is important to note, however, that the modulus of rupture is highly variable as the coefficient can vary between 6 and 12 [Neville, 1997]. A statistical t-test was performed on the modulus of rupture coefficient data in order to determine if there was any statistical difference between the two mixes. The P value of the t test between the high strength mixes was 0.71. Any value greater than 0.05 shows the data is statistically equal. In other words, the modulus of rupture of the two mixes is essentially identical. The modulus of rupture for each specimen was plotted against the compressive strength for comparison with the ACI recommended relationship. The graph can be seen in **Figure 6.8**.

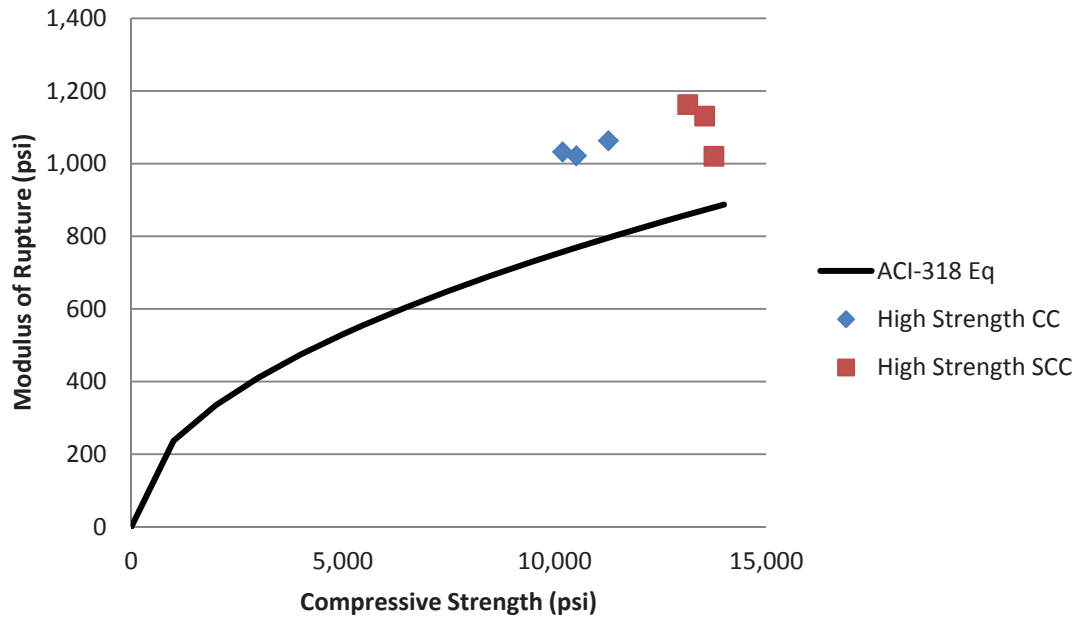


**Figure 6.8 – Compressive Strength vs. Modulus of Rupture**

For the splitting-tensile strength the S10-48L showed a higher tensile strength than the C10-58L mix. However both mixes fell short of the recommended ACI coefficient for estimating splitting-tensile strength, with the SCC falling very slightly below the recommended value (6.5 vs. 6.7). However, splitting-tensile strength is also highly variable with values ranging from 5 to 9.5 (Oluokun, 1991). A statistical t-test was performed on the splitting-tensile strength coefficient data in order to determine if there is a statistical difference between the two mixes. The P value of the t test between the high strength mixes was 0.12. Any value greater than 0.05 shows the data is statistically equal. In other words, the splitting-tensile strength of the two mixes are essential identical. The splitting-tensile strength of the specimens was also plotted against the compressive strength of concrete for comparison with the ACI recommended relationship. This graph can be seen in **Figure 6.9**.

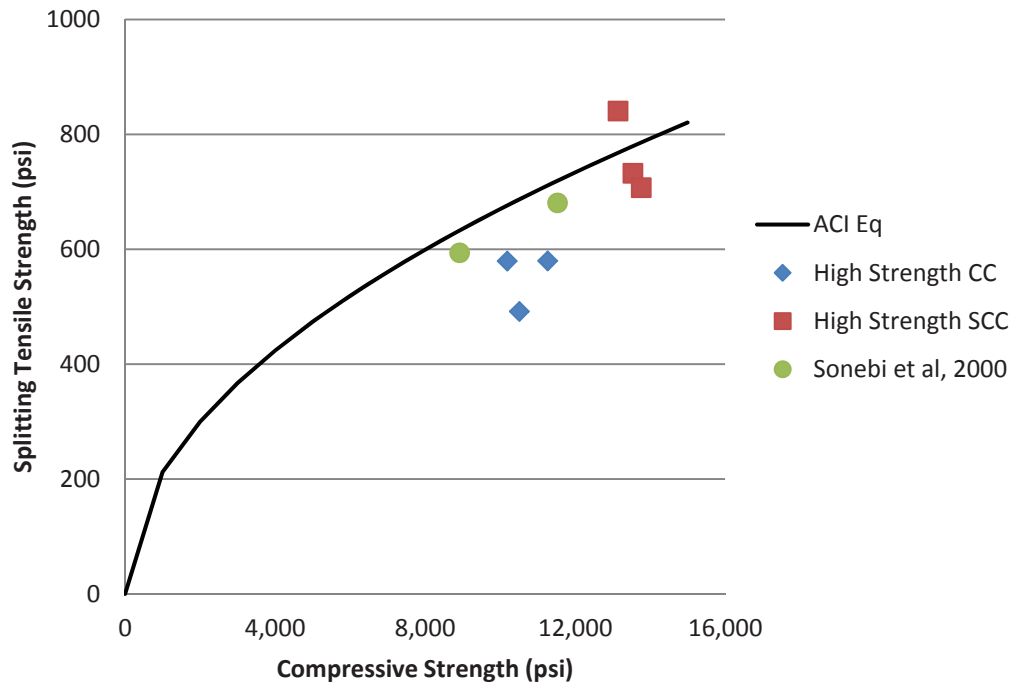


**Figure 6.9 – Compressive Strength vs. Splitting-Tensile Strength**

The measured modulus of elasticity and modulus of rupture were also compared to the AASHTO LRFD Design equations used to estimate these mechanical properties. These properties were normalized by dividing the measured values by the respective compressive strength and then compared to the AASHTO equations as mentioned in Chapter 5. A summary of these coefficients can be seen in **Table 6.6**.

**Table 6.6 Normalized Mechanical Properties Compared to Respective AASHTO Coefficients**

	C10-58L	S10-48L	AASHTO Coefficient
Modulus of Elasticity	1,186	987	1,820
Modulus of Rupture	0.32	0.30	0.24

These results also followed a very similar trend as the ACI coefficient comparison. Both the C10-58L mix and the S10-48L mix showed lower values than the AASHTO

coefficient for the modulus of elasticity while both also showed higher values for the modulus of rupture.

**6.2.2. Durability Performance of High Strength Mixes.** For resistance to freezing and thawing, only the C10-58L mix did well when compared to the minimum set forth by MoDOT. MoDOT specifies a minimum durability factor of 75, and while the high strength conventional mix recorded a value of 87.2, the high strength SCC only recorded a value of 45.2. With the high strength conventional concrete outperforming the high strength SCC it would suggest that the effect of the poor performing coarse aggregate used in this investigation (Jefferson City dolomite) is amplified when using SCC or, alternatively, that the higher paste content reduced the freeze-thaw resistance of the SCC.

With regard to permeability, the S10-48L mix showed a much better performance than the C10-58L mix. For the RCT, the high strength SCC mix was classified as moderate permeability and was close to being classified as low permeability, while the high strength conventional concrete was classified as high permeability. This indicates that the SCC is more resistive to the penetration of chloride ions. This was also observed in the performance for chloride penetration by ponding. The S10-48L mix showed not only a smaller surface chloride content but also reached the goal of 0.03% chloride content at a much shallower depth. The S10-48L mix reached the negligible corrosion level at approximately 0.2 in. (5 mm) while the C10-58L mix reached the same chloride content at approximately 0.65 in (17 mm). The ponding test is a relative measure of chloride permeability, and the test indicated that the high strength SCC performs better than the high strength conventional control mix. This resistance to chloride penetration is

likely due to the tighter microstructure caused by the higher fine aggregate content. This characteristic, along with the high dosage of HRWR, which frees water molecules to hydrate with the Portland cement, creates a denser paste in the concrete. This property is likely what makes the high strength SCC more resistive to chloride penetration. The average chloride profile of the high strength mixes can be seen in **Figure 6.10**.

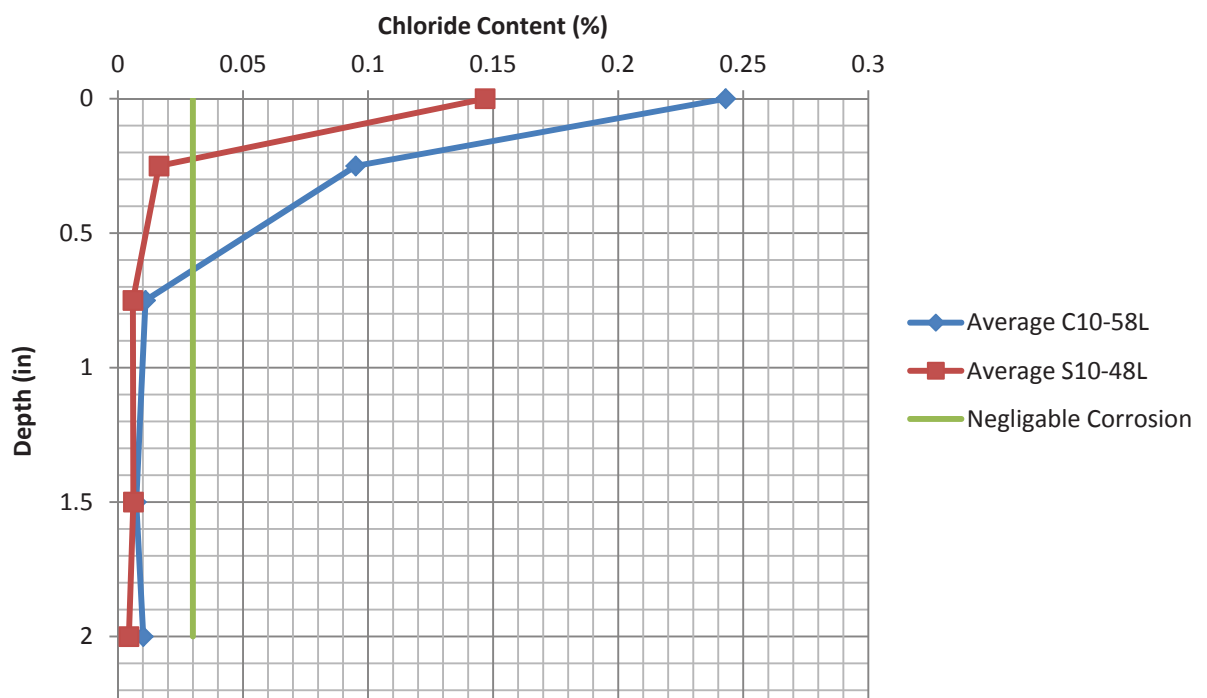


**Figure 6.10 – Average Chloride Content vs. Depth of High Strength Mixes**  
1 in. = 2.54 cm

With regard to concrete resistivity using the Wenner probe, both concrete mixes performed exceptionally well, with the S10-48L showing a higher resistivity than the C10-58L mix. The S10-48L mix showed a higher resistivity at week 1 and also an increased rate of resistivity gain than the C10-58L mix. A trend line for the resistivity

was plotted for each mix, and the slope of the C10-58L and the S10-48L mixes were 1.17 and 1.71, respectively. The results of this test can be seen in **Figure 6.11**. After 24 weeks of testing, the final resistivity for the C10-58L and S10-48L mixes was 38.6 kΩcm and 55.7 kΩcm respectively. According to Broomfield [2007], any concrete with a measured resistivity exceeding 20 kΩcm is to be classified as having a low rate of corrosion. Both concrete mixes exceeded this benchmark with the S10-48L mix far exceeding the value.

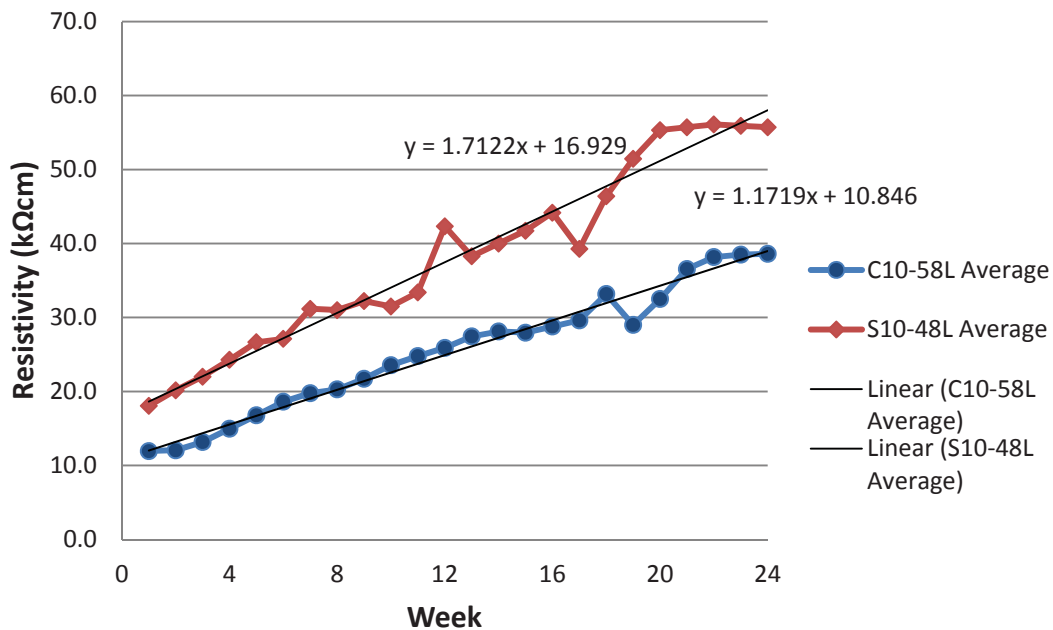


**Figure 6.11 – Average Resistivity of High Strength Concrete Mixes**

## 7. FINDINGS, CONCLUSIONS, AND RECOMMENDATIONS

### 7.1. FINDINGS AND CONCLUSIONS

**7.1.1. Normal Strength SCC.** The normal strength SCC mix in this investigation outperformed the conventional normal strength concrete in nearly every aspect tested. This finding is important for determining the plausibility of using SCC instead of conventional concrete. The S6-48L mix achieved a higher 28-day compressive strength than the C6-58L mix. With the w/cm ratio being equal, as well as the type of aggregate and cement, it is believed that the high amount of HRWR used to provide SCC with its flowable characteristics accounts for the higher strength. The HRWR allows more water to be effective in the hydration process by dispersion of cement particles. This characteristic in turn hydrates more of the Portland cement, creating a denser overall microstructure, thus improving the compressive strength of the concrete. The S6-48L mix showed a comparable modulus of elasticity to the C6-58L mix. However, both mixes fell below both the recommended ACI-318 coefficient and the AASHTO LRFD design coefficient used to estimate this property. The C6-58L mix showed a higher modulus of rupture when compared to the SCC mix and exceeded the recommended ACI coefficient used to estimate the modulus of rupture. However, in regards of the ACI-318 coefficient, the SCC mix only fell slightly below the recommended value of 7.5. These concretes also showed similar performance when compared to the AASHTO coefficient. Both concrete mixes showed comparable splitting-tensile strength, while both mixes fell below the recommended ACI-318 coefficient used to estimate the splitting-tensile strength.

The S6-48L mix showed very comparable durability behavior and even exceeded the performance of the C6-58L mix in some aspects. Both concretes performed poorly for

resistance to freeze-thaw. This result is most likely due to the aggregate source incorporated into the specimens. Jefferson City Dolomite Limestone from the Rolla quarry is known for its poor durability performance, and resistance to freeze-thaw for concrete is very dependent on the aggregate's performance. Both concrete mixes showed very similar performance with the RCT. This result was further supported by similar performance in the ponding test. While the RCT classified both concrete mixes as moderate permeability, both mixes reached negligible corrosion risk at a relatively shallow depth in the ponding test. Both mixes also performed almost identical in the area of concrete resistivity, indicating a low rate of corrosion.

**7.1.2. High Strength SCC.** The high strength SCC mix in this investigation outperformed the conventional high strength concrete in nearly every aspect tested. The S10-48L mix achieved a much higher 28-day compressive strength than the C10-58L mix. This increase in strength can most likely be attributed to the high dosage of HRWR used to produce the SCC. The HRWR disperses more cement particles to be effective in the hydration process. This characteristic in turn hydrates more of the Portland cement, creating a denser overall microstructure, thus improving the compressive strength of the concrete. This was also noted in the normal strength SCC mix but not to the degree observed in the high strength investigation. It could be concluded that the HRWR has a larger effect on strength gain at lower w/cm ratios. The HRWR creates a much denser paste. When this aspect is combined with the lower w/cm ratio necessary to achieve high strengths, it appears that SCC will achieve higher compressive strengths than an equivalent conventional concrete mix.

The S10-48L mix showed a lower modulus of elasticity than the C10-58L mix. This is attributed to the decreased amount of coarse aggregate present in the SCC mix. Both of the mixes were considerably lower than the recommended ACI coefficient used to estimate the modulus of elasticity. Both mixes showed comparable modulus of rupture and exceeded the recommended ACI coefficient. Both mixes also showed comparable splitting-tensile strength as well, while both mixes fell short of the recommended ACI coefficient used to estimate this property.

The S10-48L mix significantly outperformed the C10-58L mix in every durability test except resistance to freezing and thawing. During the freeze-thaw test, the S10-48L showed noticeably poorer performance when compared to the C10-58L mix. Neither mix contained an air entraining admixture. It is possible that the C10-58L mix entrapped more air during the mixing process than the S10-48L mix, improving its performance relative to the SCC mix. In all other durability aspects the S10-48L mix showed improved performance compared to the C10-58L mix. In both the RCT and ponding test, the S10-48L mix showed greater resistance to chloride penetration. The C10-58L mix was classified as highly permeable by the RCT while the S10-48L mix was classified as moderate. This classification was further supported by the ponding test. While both mixes performed well, the S10-48L mix achieved negligible corrosion risk at a third of the depth that the C10-58L mix achieved negligible corrosion risk. This increase in performance is most likely due to the denser microstructure achieved by SCC. The S10-48L mix also outperformed the C10-58L mix in concrete resistivity, most likely due to the denser microstructure.

## **7.2. RECOMMENDATIONS**

**7.2.1. SCC.** After thorough mechanical property and durability testing, it is recommended that SCC be implemented in precast and prestressing applications. With SCC showing comparable results for hardened mechanical properties and slightly higher performance for durability, SCC appears to be a viable option to decrease the cost of labor and time consumption during concrete placement. This performance was observed in both normal and high strength SCC, with high strength SCC performing at a slightly higher margin over high strength conventional concrete than SCC performed over conventional concrete.

APPENDIX A  
**SCC DURABILITY TEST RESULTS DATA**

**Table A.1 C6-58L-1R (Weeks 1-7)**

Date	6/23/2011	6/30/2011	7/7/2011	7/14/2011	7/21/2011	7/28/2011	8/4/2011
A1	14	15	16	21	19	20	19
A2	13	14	14	18	17	18	18
A3	13	15	15	21	18	19	19
B1	14	16	17	19	20	21	21
B2	12	14	12	18	16	16	19
B3	13	15	15	20	18	18	20
Average	13.2	14.8	14.8	19.5	18.0	18.7	19.3

**Table A.2 C6-58L-1R (Weeks 8-14)**

Date	8/18/2011	8/25/2011	9/1/2011	9/8/2011	9/15/2011	9/22/2011	9/29/2011
A1	19	21	22	24	25	20	20
A2	18	19	20	23	22	25	18
A3	19	19	19	25	19	27	27
B1	21	23	22	27	22	22	22
B2	18	17	19	24	25	23	24
B3	18	20	24	26	27	27	23
Average	18.8	19.8	21.0	24.8	23.3	24.0	22.3

**Table A.3 C6-58L-1R (Weeks 15-21)**

Date	10/6/2011	10/13/2011	10/20/2011	10/27/2011	11/3/2011	11/10/2011	11/17/2011
A1	29	36	30	33	25	25	29
A2	27	27	19	29	31	27	25
A3	26	18	29	27	29	21	24
B1	26	23	27	23	25	23	26
B2	26	17	21	22	23	23	25
B3	26	24	31	21	27	25	33
Average	26.7	24.2	26.2	25.8	26.7	24.0	27.0

**Table A.4 C6-58L-1R (Weeks 22-24)**

Date	11/24/2011	12/1/2011	12/8/2011
A1	27	35	29
A2	26	37	22
A3	25	27	25
B1	22	27	24
B2	24	24	24
B3	22	42	29
Average	24.3	32.0	25.5

**Table A.5 C6-58L-2R (Weeks 1-7)**

Date	6/23/2011	6/30/2011	7/7/2011	7/14/2011	7/21/2011	7/28/2011	8/4/2011
A1	14	15	16	19	18	20	20
A2	12	13	13	19	19	15	16
A3	14	16	17	21	20	20	21
B1	14	15	16	19	19	20	21
B2	12	12	13	19	15	16	17
B3	14	15	15	21	19	19	20
Average	13.3	14.3	15.0	19.7	18.3	18.3	19.2

**Table A.6 C6-58L-2R (Weeks 8-14)**

Date	8/18/2011	8/25/2011	9/1/2011	9/8/2011	9/15/2011	9/22/2011	9/29/2011
A1	20	23	24	25	23	29	30
A2	16	18	21	20	19	25	27
A3	25	23	24	27	29	24	31
B1	20	22	24	25	25	25	31
B2	16	19	20	22	22	24	27
B3	20	21	24	27	25	22	22
Average	19.5	21.0	22.8	24.3	23.8	24.8	28.0

**Table A.7 C6-58L-2R (Weeks 15-21)**

Date	10/6/2011	10/13/2011	10/20/2011	10/27/2011	11/3/2011	11/10/2011	11/17/2011
A1	30	30	32	24	27	28	28
A2	25	26	28	19	22	22	18
A3	31	35	38	30	42	24	40
B1	29	29	30	28	34	28	22
B2	26	26	24	21	27	24	21
B3	26	30	33	22	33	29	30
Average	27.8	29.3	30.8	24.0	30.8	25.8	26.5

**Table A.8 C6-58L-2R (Weeks 22-24)**

Date	11/24/2011	12/1/2011	12/8/2011
A1	27	34	30
A2	22	30	27
A3	26	44	46
B1	36	35	36
B2	21	25	28
B3	29	27	31
Average	26.8	32.5	33.0

**Table A.9 C6-58L-3R (Weeks 1-7)**

Date	6/23/2011	6/30/2011	7/7/2011	7/14/2011	7/21/2011	7/28/2011	8/4/2011
A1	14	15	15	19	19	20	20
A2	13	13	14	17	17	17	18
A3	13	14	16	19	18	21	21
B1	14	15	15	19	18	19	20
B2	11	12	13	16	15	16	17
B3	14	16	16	18	19	19	19
Average	13.2	14.2	14.8	18.0	17.7	18.7	19.2

**Table A.10 C6-58L-3R (Weeks 8-14)**

Date	8/18/2011	8/25/2011	9/1/2011	9/8/2011	9/15/2011	9/22/2011	9/29/2011
A1	20	22	18	26	27	29	24
A2	21	21	22	19	22	25	23
A3	22	22	24	25	22	29	22
B1	19	20	21	26	28	27	29
B2	17	19	21	22	22	17	22
B3	20	18	19	23	25	24	27
Average	19.8	20.3	20.8	23.5	24.3	25.2	24.5

**Table A.11 C6-58L-3R (Weeks 15-21)**

Date	10/6/2011	10/13/2011	10/20/2011	10/27/2011	11/3/2011	11/10/2011	11/17/2011
A1	24	24	32	25	29	30	36
A2	23	19	19	24	20	22	28
A3	31	35	28	24	30	26	26
B1	25	28	26	26	26	28	25
B2	21	19	16	16	18	23	30
B3	28	19	20	21	20	37	28
Average	25.3	24.0	23.5	22.7	23.8	27.7	28.8

**Table A.12 C6-58L-3R (Weeks 22-24)**

Date	11/24/2011	12/1/2011	12/8/2011
A1	30	33	26
A2	22	23	24
A3	22	30	28
B1	24	43	29
B2	22	27	20
B3	21	34	33
Average	23.5	31.7	26.7

**Table A.13 S6-48L-1R (Weeks 1-7)**

Date	7/6/2011	7/13/2011	7/20/2011	7/27/2011	8/3/2011	8/10/2011	8/17/2011
A1	12	12	14	15	16	16	17
A2	12	13	13	14	14	14	15
A3	14	14	16	17	18	18	20
B1	14	14	14	15	16	16	17
B2	11	11	14	15	15	15	15
B3	13	14	16	18	18	18	19
Average	12.7	13.0	14.5	15.7	16.2	16.2	17.2

**Table A.14 S6-48L-1R (Weeks 8-14)**

Date	8/24/2011	8/31/2011	9/7/2011	9/14/2011	9/21/2011	9/28/2011	10/5/2011
A1	17	18	17	19	20	13	22
A2	17	17	18	19	21	17	21
A3	16	21	21	22	27	22	28
B1	19	19	21	21	22	22	20
B2	18	18	19	19	20	16	21
B3	19	20	22	23	25	25	25
Average	17.7	18.8	19.7	20.5	22.5	19.2	22.8

**Table A.15 S6-48L-1R (Weeks 15-21)**

Date	10/12/2011	10/19/2011	10/26/2011	11/2/2011	11/9/2011	11/16/2011	11/23/2011
A1	19	23	25	24	24	27	28
A2	20	15	15	25	21	16	28
A3	28	20	24	34	29	27	27
B1	28	24	27	24	22	19	26
B2	22	17	21	21	18	19	24
B3	26	21	27	28	32	27	23
Average	23.8	20.0	23.2	26.0	24.2	22.5	26.0

**Table A.16 S6-48L-1R (Weeks 22-24)**

Date	11/30/2011	12/7/2011	12/16/2011
A1	24	32	26
A2	31	23	20
A3	40	44	44
B1	26	39	40
B2	21	24	25
B3	30	26	23
Average	28.7	31.3	26.7

**Table A.17 S6-48L-2R (Weeks 1-7)**

Date	7/6/2011	7/13/2011	7/20/2011	7/27/2011	8/3/2011	8/10/2011	8/17/2011
A1	11	12	13	14	15	15	16
A2	10	11	11	13	11	11	16
A3	12	13	14	16	16	16	17
B1	11	12	12	14	14	14	15
B2	9.4	11	11	13	14	14	15
B3	11	13	13	14	14	14	16
Average	10.7	12.0	12.3	14.0	14.0	14.0	15.8

**Table A.18 S6-48L-2R (Weeks 8-14)**

Date	8/24/2011	8/31/2011	9/7/2011	9/14/2011	9/21/2011	9/28/2011	10/5/2011
A1	16	16	17	17	18	20	20
A2	14	14	18	19	19	18	19
A3	17	17	19	21	20	22	25
B1	18	15	17	19	20	22	20
B2	16	13	16	15	17	18	18
B3	17	17	17	20	19	21	20
Average	16.3	15.3	17.3	18.5	18.8	20.2	20.3

**Table A.19 S6-48L-2R (Weeks 15-21)**

Date	10/12/2011	10/19/2011	10/26/2011	11/2/2011	11/9/2011	11/16/2011	11/23/2011
A1	20	17	20	23	26	23	26
A2	19	17	15	17	21	19	22
A3	21	21	25	14	16	25	23
B1	20	25	22	14	17	20	24
B2	20	18	16	16	19	27	20
B3	24	19	25	18	22	25	26
Average	20.7	19.5	20.5	17.0	20.1	23.2	23.5

**Table A.20 S6-48L-2R (Weeks 22-24)**

Date	11/30/2011	12/7/2011	12/16/2011
A1	22	29	28
A2	21	19	24
A3	18	34	29
B1	19	33	28
B2	29	28	25
B3	25	33	31
Average	22.3	29.3	27.5

**Table A.21 C10-58L-1R (Weeks 1-7)**

Date	7/22/2011	7/29/2011	8/5/2011	8/12/2011	8/19/2011	8/26/2011	9/2/2011
A1	12	12	12	14	16	18	20
A2	11	11	12	14	17	18	19
A3	12	13	13	14	17	19	20
B1	12	13	14	16	16	19	20
B2	11	11	14	16	16	17	18
B3	12	12	13	15	17	18	20
Average	11.7	12.0	13.0	14.8	16.5	18.2	19.5

**Table A.22 C10-58L-1R (Weeks 8-14)**

Date	9/9/2011	9/16/2011	9/23/2011	9/30/2011	10/7/2011	10/14/2011	10/21/2011
A1	20	22	23	25	26	23	23
A2	19	21	23	22	25	25	27
A3	22	23	25	26	28	27	31
B1	16	21	20	25	28	18	28
B2	19	19	18	17	23	28	28
B3	21	22	26	21	24	35	29
Average	19.5	21.3	22.5	22.67	25.7	26.0	27.7

**Table A.23 C10-58L-1R (Weeks 15-21)**

Date	10/28/2011	11/4/2011	11/11/2011	11/18/2011	11/25/2011	12/2/2011	12/9/2011
A1	30	32	34	25	32	29	34
A2	27	30	28	29	25	28	33
A3	29	31	32	31	27	33	42
B1	22	25	32	36	30	27	46
B2	23	26	28	34	22	25	32
B3	25	30	37	37	30	36	27
Average	26.0	28.9	31.8	32.0	27.7	29.7	35.7

**Table A.24 C10-58L-1R (Weeks 22-24)**

Date	12/16/2011	12/23/2011	12/30/2011
A1	33	32	32
A2	22	24	24
A3	39	41	40
B1	33	34	33
B2	35	35	36
B3	27	28	28
Average	31.5	32.3	32.2

**Table A.25 C10-58L-2R (Weeks 1-7)**

Date	7/22/2011	7/29/2011	8/5/2011	8/12/2011	8/19/2011	8/26/2011	9/2/2011
A1	12	13	13	15	17	20	18
A2	11	11	11	13	15	16	17
A3	15	12	13	15	16	18	20
B1	12	11	13	16	17	20	20
B2	11	11	12	13	15	17	18
B3	13	12	14	15	18	20	22
Average	12.3	11.7	12.7	14.5	16.3	18.5	19.2

**Table A.26 C10-58L-2R (Weeks 8-14)**

Date	9/9/2011	9/16/2011	9/23/2011	9/30/2011	10/7/2011	10/14/2011	10/21/2011
A1	21	21	26	26	27	31	30
A2	17	19	21	20	19	27	21
A3	20	23	26	28	27	32	34
B1	20	21	21	25	25	25	28
B2	19	20	24	25	23	26	25
B3	23	24	26	28	29	29	30
Average	20.0	21.3	24	25.33	25.0	28.3	28.0

**Table A.27 C10-58L-2R (Weeks 15-21)**

Date	10/28/2011	11/4/2011	11/11/2011	11/18/2011	11/25/2011	12/2/2011	12/9/2011
A1	30	29	32	36	27	34	43
A2	23	21	24	26	21	25	28
A3	32	32	29	38	28	34	37
B1	27	25	24	35	35	33	36
B2	26	25	23	25	22	28	31
B3	32	31	23	41	26	33	35
Average	28.3	27.1	25.8	33.5	26.5	31.2	35.0

**Table A.28 C10-58L-2R (Weeks 22-24)**

Date	12/16/2011	12/23/2011	12/30/2011
A1	56	56	57
A2	27	28	27
A3	48	47	48
B1	40	42	42
B2	36	37	38
B3	37	38	38
Average	40.7	41.3	41.6

**Table A.29 C10-58L-3R (Weeks 1-7)**

Date	7/22/2011	7/29/2011	8/5/2011	8/12/2011	8/19/2011	8/26/2011	9/2/2011
A1	12	12	13	15	17	18	19
A2	11	12	13	16	17	20	20
A3	12	13	15	17	17	18	21
B1	12	13	14	15	18	19	22
B2	11	12	13	15	17	19	19
B3	13	13	15	16	19	21	23
Average	11.8	12.5	13.8	15.7	17.5	19.2	20.7

**Table A.30 C10-58L-3R (Weeks 8-14)**

Date	9/9/2011	9/16/2011	9/23/2011	9/30/2011	10/7/2011	10/14/2011	10/21/2011
A1	19	22	25	26	25	27	27
A2	22	22	24	27	24	27	28
A3	22	23	26	27	30	29	31
B1	20	22	24	25	27	28	28
B2	21	21	23	25	27	26	26
B3	24	25	23	28	29	31	32
Average	21.3	22.5	24.2	26.33	27.0	28.0	28.7

**Table A.31 C10-58L-3R (Weeks 15-21)**

Date	10/28/2011	11/4/2011	11/11/2011	11/18/2011	11/25/2011	12/2/2011	12/9/2011
A1	31	31	31	34	32	30	40
A2	30	32	30	32	24	37	36
A3	31	31	30	35	29	37	42
B1	28	30	31	36	37	40	39
B2	23	26	32	33	36	34	35
B3	34	32	33	34	39	42	42
Average	29.5	30.3	31.2	34.0	32.8	36.7	39.0

**Table A.32 C10-58L-3R (Weeks 22-24)**

Date	12/16/2011	12/23/2011	12/30/2011
A1	43	44	43
A2	38	39	41
A3	46	45	46
B1	41	42	41
B2	39	41	42
B3	47	48	48
Average	42.3	43.2	43.5

**Table A.33 S10-48L-1R (Weeks 1-7)**

Date	8/5/2011	8/12/2011	8/19/2011	8/26/2011	9/2/2011	9/9/2011	9/16/2011
A1	20	23	25	28	31	32	35
A2	18	20	22	25	28	30	33
A3	19	21	24	26	30	30	28
B1	18	19	21	25	28	24	28
B2	17	18	20	21	20	27	25
B3	20	22	25	27	30	23	34
Average	18.7	20.5	22.8	25.3	27.8	27.7	30.5

**Table A.34 S10-48L-1R (Weeks 8-14)**

Date	9/23/2011	9/30/2011	10/7/2011	10/14/2011	10/21/2011	10/28/2011	11/4/2011
A1	37	41	41	44	49	45	45
A2	32	38	38	41	42	44	43
A3	28	34	36	35	50	48	48
B1	35	30	24	32	51	45	44
B2	28	26	22	27	42	38	39
B3	30	34	28	31	48	42	44
Average	31.7	33.8	31.5	35.0	47.0	43.7	43.8

**Table A.35 S10-48L-1R (Weeks 15-21)**

Date	11/11/2011	11/18/2011	11/25/2011	12/2/2011	12/9/2011	12/16/2011	12/23/2011
A1	49	60	61	56	74	69	70
A2	34	40	38	44	58	61	60
A3	41	42	47	60	46	62	63
B1	51	44	40	55	52	59	60
B2	38	42	35	45	45	48	49
B3	51	46	38	60	64	70	71
Average	44.0	45.7	43.2	53.3	56.5	61.5	62.2

**Table A.36 S10-48L-1R (Weeks 22-24)**

Date	12/30/2011	1/6/2012	1/13/2012
A1	69	68	65
A2	61	61	54
A3	61	59	69
B1	58	57	54
B2	49	49	59
B3	68	67	54
Average	61.0	60.2	59.2

**Table A.37 S10-48L-2R (Weeks 1-7)**

Date	8/5/2011	8/12/2011	8/19/2011	8/26/2011	9/2/2011	9/9/2011	9/16/2011
A1	20	22	24	20	29	32	35
A2	18	19	21	23	23	25	30
A3	22	24	27	29	32	25	35
B1	20	23	25	29	30	30	35
B2	16	18	20	22	25	21	29
B3	18	21	22	26	28	29	33
Average	19.0	21.2	23.2	24.8	27.8	27.0	32.8

**Table A.38 S10-48L-2R (Weeks 8-14)**

Date	9/23/2011	9/30/2011	10/7/2011	10/14/2011	10/21/2011	10/28/2011	11/4/2011
A1	37	29	27	29	43	30	35
A2	27	32	34	31	40	32	34
A3	32	37	36	31	41	34	38
B1	29	33	27	27	39	36	39
B2	26	27	24	27	38	29	34
B3	30	27	29	32	37	36	38
Average	30.2	30.8	29.5	29.5	39.7	32.8	36.3

**Table A.39 S10-48L-2R (Weeks 15-21)**

Date	11/11/2011	11/18/2011	11/25/2011	12/2/2011	12/9/2011	12/16/2011	12/23/2011
A1	49	42	42	44	45	50	52
A2	38	36	32	38	37	44	45
A3	46	41	37	40	43	47	49
B1	38	45	38	48	47	55	56
B2	33	35	37	36	40	47	48
B3	34	45	35	46	45	58	59
Average	39.7	40.7	36.8	42.0	42.8	50.2	51.5

**Table A.40 S10-48L-2R (Weeks 22-24)**

Date	12/30/2011	1/6/2012	1/13/2012
A1	53	57	62
A2	47	49	50
A3	48	56	72
B1	57	54	51
B2	48	50	52
B3	61	54	50
Average	52.3	53.3	56.2

**Table A.41 S10-48L-3R (Weeks 1-7)**

Date	8/5/2011	8/12/2011	8/19/2011	8/26/2011	9/2/2011	9/9/2011	9/16/2011
A1	17	20	22	24	27	29	31
A2	16	17	19	21	22	25	28
A3	18	20	21	23	26	27	29
B1	16	20	20	21	24	27	32
B2	15	16	18	22	22	24	29
B3	17	20	20	25	25	28	32
Average	16.5	18.8	20.0	22.7	24.3	26.7	30.2

**Table A.42 S10-48L-3R (Weeks 8-14)**

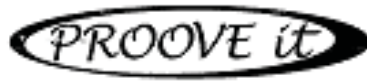
Date	9/23/2011	9/30/2011	10/7/2011	10/14/2011	10/21/2011	10/28/2011	11/4/2011
A1	34	35	36	39	42	43	44
A2	29	30	30	33	36	36	37
A3	32	33	31	36	42	34	34
B1	31	33	36	35	41	38	39
B2	28	27	31	32	37	39	40
B3	33	34	37	39	44	40	45
Average	31.2	32.0	33.5	35.7	24.3	38.3	39.9

**Table A.43 S10-48L-3R (Weeks 15-21)**

Date	11/11/2011	11/18/2011	11/25/2011	12/2/2011	12/9/2011	12/16/2011	12/30/2011
A1	49	51	49	52	52	57	58
A2	41	47	34	44	52	50	51
A3	41	40	39	39	47	58	56
B1	45	46	37	49	66	42	47
B2	36	35	33	35	53	58	54
B3	37	58	35	44	60	61	62
Average	41.5	46.2	37.8	43.8	55.0	54.3	54.6

**Table A.44 S10-48L-3R (Weeks 22-24)**

Date	12/30/2011	1/6/2012	1/13/2012
A1	56	53	51
A2	50	52	55
A3	54	52	52
B1	48	50	52
B2	52	46	44
B3	59	58	57
Average	53.2	51.8	51.8



ASTM C 1202-97



Test-compagny  
Testing street 45  
Compagny City  
Some Country

Your own logo  
Here

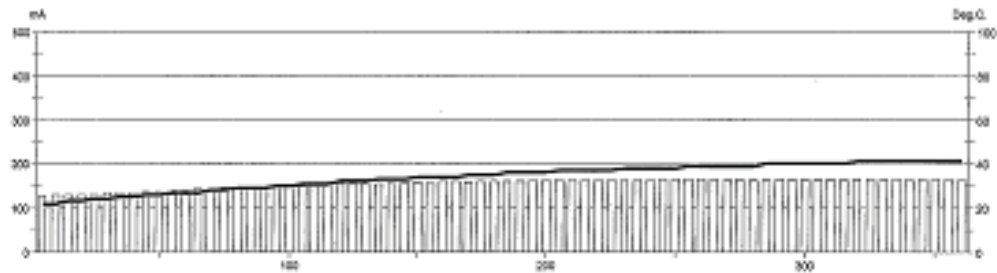


GERMANY

ASTM C 1202-97  
Prove it  
Prove it  
Prove it

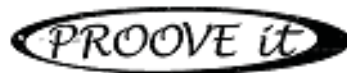
**Test report**

Voltage Used: 60  
Testing time: 06:00 hour  
Charge passed: 3352  
Adjusted Charge passed: 3025  
Permeability class: Moderate  
Instrument number: 071401  
Channel number: 1  
Report date: 8/10/2011  
Testing by: ZHLG/TP  
Reference: EC-A1-28 DAY TEST-TOP LIFT  
Sample diameter: 100  
Comment: CALLED SET A



Time	°C	mA									
00:05	22	126.5	01:35	30	147.8	03:05	36	160.2	04:35	39	164.5
00:10	22	128.5	01:40	30	149.8	03:10	36	161.1	04:40	39	164.0
00:15	23	128.7	01:45	31	149.7	03:15	36	162.3	04:45	40	164.2
00:20	23	129.9	01:50	31	153.0	03:20	36	162.3	04:50	40	165.0
00:25	24	130.5	01:55	31	153.4	03:25	37	162.7	04:55	40	165.5
00:30	24	133.6	02:00	32	153.6	03:30	37	163.0	05:00	40	164.5
00:35	25	134.3	02:05	32	153.0	03:35	37	163.3	05:05	40	164.9
00:40	25	134.7	02:10	32	153.9	03:40	37	163.0	05:10	40	165.1
00:45	26	135.9	02:15	33	155.1	03:45	37	164.3	05:15	40	164.4
00:50	26	137.1	02:20	33	156.7	03:50	38	163.2	05:20	41	164.4
00:55	27	138.8	02:25	33	158.2	03:55	38	163.5	05:25	41	164.6
01:00	27	139.1	02:30	34	158.0	04:00	38	163.6	05:30	41	165.3
01:05	27	141.8	02:35	34	157.0	04:05	38	164.1	05:35	41	165.3
01:10	28	143.7	02:40	34	159.9	04:10	38	164.7	05:40	41	165.1
01:15	28	144.4	02:45	34	159.9	04:15	39	165.2	05:45	41	165.2
01:20	29	144.7	02:50	35	158.9	04:20	39	164.2	05:50	41	165.3
01:25	29	146.4	02:55	35	161.2	04:25	39	165.0	05:55	41	165.8
01:30	29	147.6	03:00	35	161.1	04:30	39	164.5	06:00	41	164.6

Figure A.1 – C6-58L-EC1TOP RCT Data



ASTM C 1202-97



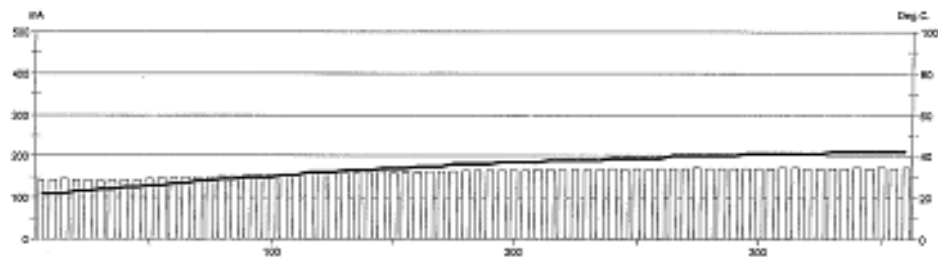
Test-company  
Testing street 45  
CompagnyCity  
Some Country



CEMEX  
BUREAU  
BUREAU  
BUREAU

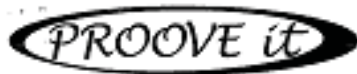
**Test report**

Voltage Used: 60  
 Testing time: 06:00 hour  
 Charge passed: 3474  
 Adjusted Charge passed: 3135  
 Permeability class: Moderate  
 Instrument number: 071401  
 Channel number: 3  
 Report date: 8/10/2011  
 Testing by: L.G./TP/ZH  
 Reference: EC-A1-28 DAY TEST-MIDDLE LIFT  
 Sample diameter: 100  
 Comment: CALLED SET A



Time	°C	mA									
00:05	22	140.7	01:35	30	153.0	03:05	36	164.1	04:35	40	171.2
00:10	22	143.5	01:40	30	154.6	03:10	36	164.5	04:40	40	170.1
00:15	22	144.5	01:45	31	155.1	03:15	37	165.1	04:45	40	170.2
00:20	23	143.8	01:50	31	156.0	03:20	37	165.7	04:50	40	169.5
00:25	23	142.1	01:55	32	156.7	03:25	37	166.0	04:55	41	169.4
00:30	24	141.1	02:00	32	157.1	03:30	37	166.3	05:00	41	170.0
00:35	24	141.9	02:05	32	158.1	03:35	38	166.9	05:05	41	170.3
00:40	25	142.7	02:10	33	158.5	03:40	38	167.0	05:10	41	171.1
00:45	25	143.3	02:15	33	159.0	03:45	38	167.6	05:15	41	171.0
00:50	26	144.5	02:20	33	160.1	03:50	38	167.5	05:20	41	170.3
00:55	26	147.0	02:25	34	162.1	03:55	38	167.3	05:25	41	170.6
01:00	27	147.8	02:30	34	161.1	04:00	39	168.6	05:30	42	170.6
01:05	27	149.2	02:35	34	160.7	04:05	39	168.3	05:35	42	170.5
01:10	28	149.4	02:40	35	161.7	04:10	39	168.8	05:40	42	172.8
01:15	28	150.6	02:45	35	162.4	04:15	39	168.5	05:45	42	170.4
01:20	29	151.7	02:50	35	162.9	04:20	39	170.6	05:50	42	171.0
01:25	29	151.9	02:55	36	163.2	04:25	40	169.7	05:55	42	170.5
01:30	30	153.4	03:00	36	164.3	04:30	40	169.3	06:00	42	171.6

Figure A.2 – C6-58L-EC1MIDDLE RCT Data



ASTM C 1202-97



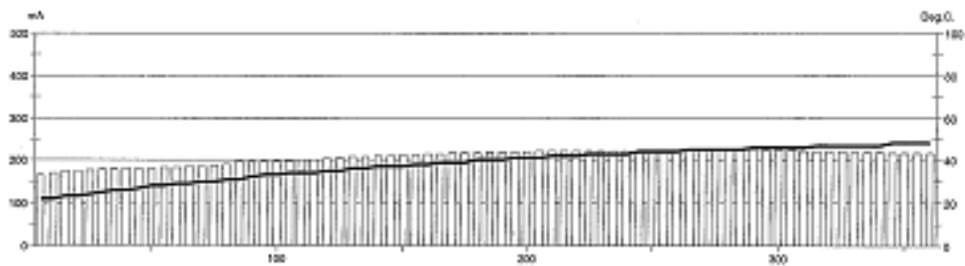
Test-company  
Testing street 45  
CompanyCity  
Some Country



CEMEX  
P.O. Box 1000  
Tel: +31 20 261 261  
Fax: +31 20 261 261  
CEMEX  
P.O. Box 1000  
Tel: +31 20 261 261  
Fax: +31 20 261 261

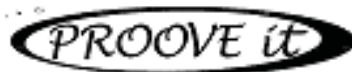
**Test report**

Voltage Used: 60  
Testing time: 06:00 hour  
Charge passed: 4488  
Adjusted Charge passed: 4050  
Permeability class: High  
Instrument number: 071401  
Channel number: 2  
Report date: 8/10/2011  
Testing by: LG/ZH/TP  
Reference: EC-A1-28 DAY TEST-TOP LIFT  
Sample diameter: 100  
Comment: THIS SET IS CALLED SET B



Time	°C	mA									
00:05	22	165.9	01:35	33	195.4	03:05	40	218.0	04:35	45	224.6
00:10	22	170.5	01:40	33	196.2	03:10	40	218.3	04:40	45	224.5
00:15	23	173.0	01:45	34	198.7	03:15	41	218.9	04:45	45	224.3
00:20	23	175.1	01:50	34	200.7	03:20	41	219.6	04:50	46	224.4
00:25	24	176.7	01:55	34	202.0	03:25	41	220.1	04:55	46	224.0
00:30	25	178.0	02:00	35	203.3	03:30	42	220.5	05:00	46	222.9
00:35	26	179.1	02:05	35	204.6	03:35	42	220.8	05:05	46	222.8
00:40	26	180.0	02:10	36	206.5	03:40	42	221.0	05:10	46	221.7
00:45	27	180.7	02:15	36	207.8	03:45	43	221.1	05:15	47	221.4
00:50	28	181.8	02:20	37	209.6	03:50	43	221.2	05:20	47	221.1
00:55	28	182.8	02:25	37	210.9	03:55	43	221.2	05:25	47	220.4
01:00	29	184.0	02:30	37	211.8	04:00	43	221.3	05:30	47	219.8
01:05	29	185.1	02:35	38	212.7	04:05	44	221.1	05:35	47	219.0
01:10	30	185.7	02:40	38	213.7	04:10	44	221.1	05:40	47	218.3
01:15	30	186.5	02:45	39	215.3	04:15	44	220.8	05:45	48	217.6
01:20	31	189.7	02:50	39	215.9	04:20	44	221.9	05:50	48	216.9
01:25	31	196.8	02:55	39	216.4	04:25	45	224.7	05:55	48	216.7
01:30	32	196.1	03:00	40	217.5	04:30	45	224.8	06:00	48	217.2

Figure A.3 – C6-58L-EC2TOP RCT Data



ASTM C 1202-97



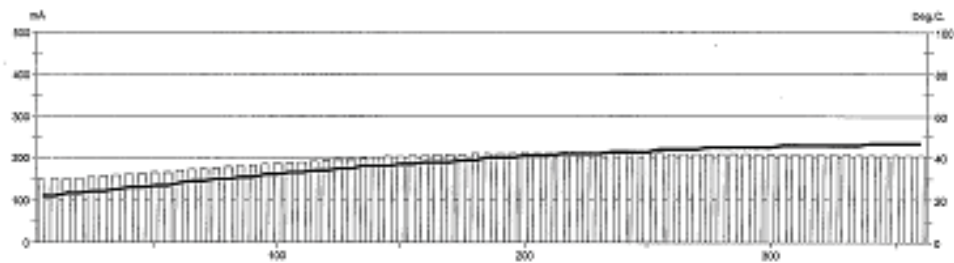
Test-compagny  
Testing street 45  
Compagny City  
Some Country



GERMAN INSTRUMENTS  
Phone: +49 201 7171  
Fax: +49 201 7171  
E-Mail: info@german-instruments.de  
www.german-instruments.de

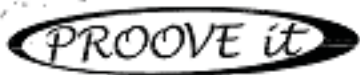
**Test report**

Voltage Used: 60  
 Testing time: 06:00 hour  
 Charge passed: 4222  
 Adjusted Charge passed: 3810  
 Permeability class: Moderate  
 Instrument number: 071401  
 Channel number: 4  
 Report date: 8/16/2011  
 Testing by: LG/ZH/TP  
 Reference: EC-A1-28 DAY TEST-MIDDLE LIFT  
 Sample diameter: 100  
 Comment: CALLED SET B



Time	°C	mA									
00:05	22	146.9	01:35	32	184.9	03:05	40	210.3	04:35	45	210.4
00:10	22	148.8	01:40	32	186.6	03:10	40	210.1	04:40	45	209.7
00:15	23	149.8	01:45	33	188.5	03:15	40	210.8	04:45	45	209.4
00:20	23	151.4	01:50	33	190.7	03:20	41	211.2	04:50	45	209.1
00:25	24	155.1	01:55	34	192.4	03:25	41	211.8	04:55	45	208.6
00:30	24	157.2	02:00	34	193.7	03:30	41	211.8	05:00	45	208.7
00:35	25	159.3	02:05	35	195.8	03:35	42	211.8	05:05	46	207.9
00:40	26	161.7	02:10	35	197.2	03:40	42	212.2	05:10	46	207.5
00:45	26	163.5	02:15	36	199.3	03:45	42	212.0	05:15	46	207.2
00:50	27	165.2	02:20	36	200.3	03:50	42	212.1	05:20	46	207.1
00:55	27	166.2	02:25	36	202.3	03:55	43	211.9	05:25	46	206.8
01:00	28	169.6	02:30	37	203.2	04:00	43	212.0	05:30	46	206.5
01:05	29	172.1	02:35	37	204.5	04:05	43	211.7	05:35	46	206.1
01:10	29	173.6	02:40	38	205.6	04:10	43	211.7	05:40	47	206.0
01:15	30	175.9	02:45	38	206.6	04:15	44	211.2	05:45	47	205.9
01:20	30	179.0	02:50	38	208.0	04:20	44	210.9	05:50	47	205.7
01:25	31	180.4	02:55	39	208.1	04:25	44	210.7	05:55	47	205.6
01:30	31	183.5	03:00	39	209.3	04:30	44	210.8	06:00	47	204.9

Figure A.4 – C6-58L-EC2MIDDLE RCT Data



ASTM C 1202-97



Test-company  
Testing street 45  
CompanyCity  
Some Country

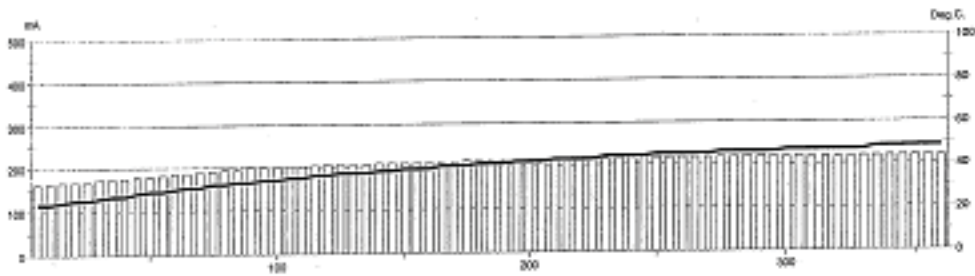
Vertical text on the right side of the TEST CO. logo.



Vertical text on the right side of the arrow logo.

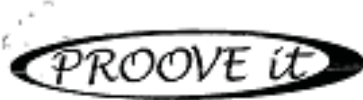
**Test report**

Voltage Used: 60  
 Testing time: 06:00 hour  
 Charge passed: 4421  
 Adjusted Charge passed: 3990  
 Permeability class: Moderate  
 Instrument number: 071401  
 Channel number: 5  
 Report date: 6/29/2011  
 Testing by: breeds  
 Reference: SCC-EC1-Top 28 day  
 Sample diameter: 100  
 Comment: UMR Study



Time	°C	mA									
00:05	23	163.2	01:35	34	198.0	03:05	41	212.2	04:35	46	217.7
00:10	23	165.5	01:40	34	200.1	03:10	41	212.1	04:40	46	217.9
00:15	24	166.5	01:45	35	201.4	03:15	42	213.1	04:45	46	217.8
00:20	25	166.7	01:50	35	202.0	03:20	42	212.9	04:50	46	218.4
00:25	25	166.9	01:55	36	203.1	03:25	42	213.9	04:55	46	217.8
00:30	26	173.2	02:00	36	204.3	03:30	43	214.0	05:00	47	217.3
00:35	27	173.2	02:05	37	205.1	03:35	43	214.8	05:05	47	217.7
00:40	27	175.8	02:10	37	206.4	03:40	43	214.5	05:10	47	216.9
00:45	28	177.8	02:15	37	206.1	03:45	43	215.1	05:15	47	217.6
00:50	29	180.4	02:20	38	207.2	03:50	44	215.4	05:20	47	217.5
00:55	29	183.1	02:25	38	207.2	03:55	44	215.7	05:25	47	217.0
01:00	30	185.0	02:30	39	207.7	04:00	44	216.4	05:30	47	218.1
01:05	31	187.8	02:35	39	208.0	04:05	44	216.7	05:35	48	218.6
01:10	31	189.6	02:40	39	208.5	04:10	45	216.6	05:40	48	218.5
01:15	32	192.6	02:45	40	209.2	04:15	45	217.3	05:45	48	218.3
01:20	32	194.0	02:50	40	209.6	04:20	45	217.0	05:50	48	217.9
01:25	33	195.1	02:55	40	211.6	04:25	45	217.2	05:55	48	218.0
01:30	33	199.5	03:00	41	211.5	04:30	45	217.3	06:00	48	218.2

Figure A.5 – S6-48L-EC1TOP RCT Data



ASTM C 1202-97



Test-compagnay  
Testing street 45  
CompagnyCity  
Some Country

Vertical logo text



Small text block with contact information

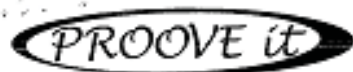
Test report

Voltage Used: 60  
 Testing time: 06:00 hour  
 Charge passed: 4079  
 Adjusted Charge passed: 3681  
 Permeability class: Moderate  
 Instrument number: 071401  
 Channel number: 6  
 Report date: 6/29/2011  
 Testing by: breeds  
 Reference: SCC-EC1-Middle 28 day  
 Sample diameter: 100  
 Comment: UMR Study



Time	°C	mA									
00:05	24	157.4	01:35	33	180.4	03:05	39	195.8	04:35	44	200.7
00:10	24	159.3	01:40	33	181.3	03:10	39	196.0	04:40	44	201.0
00:15	24	159.5	01:45	34	182.4	03:15	40	196.6	04:45	44	201.2
00:20	25	158.8	01:50	34	183.6	03:20	40	197.0	04:50	44	201.6
00:25	25	160.4	01:55	34	184.5	03:25	40	197.4	04:55	44	201.7
00:30	26	162.0	02:00	35	185.5	03:30	41	197.7	05:00	45	201.3
00:35	27	163.7	02:05	35	186.6	03:35	41	198.1	05:05	45	201.9
00:40	27	165.1	02:10	36	187.4	03:40	41	198.6	05:10	45	201.5
00:45	28	166.2	02:15	36	188.4	03:45	41	198.6	05:15	45	201.2
00:50	28	167.2	02:20	36	189.3	03:50	42	198.9	05:20	45	201.9
00:55	29	169.2	02:25	37	190.0	03:55	42	199.1	05:25	45	201.2
01:00	29	170.5	02:30	37	190.8	04:00	42	199.4	05:30	46	200.9
01:05	30	172.3	02:35	37	191.5	04:05	42	199.7	05:35	46	200.8
01:10	30	173.5	02:40	38	192.5	04:10	43	200.4	05:40	46	201.2
01:15	31	175.1	02:45	38	193.1	04:15	43	199.8	05:45	46	200.5
01:20	31	176.5	02:50	38	193.7	04:20	43	200.0	05:50	46	200.4
01:25	32	177.6	02:55	39	194.5	04:25	43	200.1	05:55	46	200.4
01:30	32	178.8	03:00	39	195.2	04:30	43	200.2	06:00	46	200.5

Figure A.6 – S6-48L-EC1MIDDLE RCT Data



ASTM C 1202-97



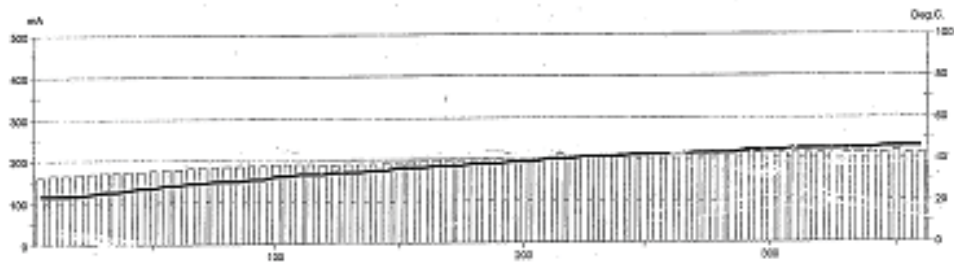
Test-company  
Testing street 45  
CompanyCity  
Some Country



STANDARD INSURANCE  
PROPERTY  
FIRE & MARINE  
INSURANCE CO. LTD.  
100  
PRINCE GEORGE  
TRADING CENTER

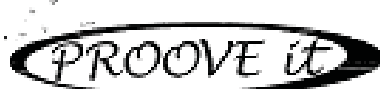
**Test report**

Voltage Used: 60  
Testing time: 05:00 hour  
Charge passed: 4262  
Adjusted Charge passed: 3846  
Permeability class: Moderate  
Instrument number: (7190)  
Channel number: 7  
Report date: 6/28/2011  
Testing by: broods  
Reference: SCC-EC2-Top 28 day  
Sample diameter: 100  
Comment: UMR Study



Time	°C	mA									
00:05	23	160.8	01:35	31	188.0	03:05	38	199.0	04:35	43	212.6
00:10	23	164.3	01:40	32	188.7	03:10	38	200.7	04:40	43	214.5
00:15	23	166.1	01:45	32	189.0	03:15	39	201.0	04:45	43	213.2
00:20	23	167.8	01:50	33	189.0	03:20	39	201.6	04:50	44	213.7
00:25	24	169.7	01:55	33	188.8	03:25	39	203.2	04:55	44	213.6
00:30	25	171.3	02:00	33	188.2	03:30	40	204.0	05:00	44	216.1
00:35	25	172.5	02:05	34	188.4	03:35	40	211.1	05:05	44	214.6
00:40	26	173.3	02:10	34	189.3	03:40	40	208.3	05:10	45	214.4
00:45	27	175.0	02:15	34	190.6	03:45	41	205.6	05:15	45	214.0
00:50	27	176.7	02:20	35	190.7	03:50	41	205.2	05:20	45	214.3
00:55	28	178.2	02:25	35	192.3	03:55	41	207.6	05:25	45	215.3
01:00	28	179.6	02:30	36	192.0	04:00	41	211.3	05:30	45	214.4
01:05	29	181.1	02:35	36	193.1	04:05	42	208.2	05:35	45	217.3
01:10	29	182.6	02:40	36	195.9	04:10	42	208.6	05:40	45	217.0
01:15	30	183.9	02:45	37	198.8	04:15	42	210.1	05:45	46	215.0
01:20	30	185.1	02:50	37	197.0	04:20	42	209.5	05:50	46	217.7
01:25	30	186.2	02:55	37	197.0	04:25	42	214.3	05:55	46	214.9
01:30	31	187.2	03:00	38	198.8	04:30	43	212.5	06:00	46	214.6

Figure A.7 – S6-48L-EC2TOP RCT Data



ASTM C 1202-97



Test-company  
Testing street 45  
Company City  
Some Country

Your contact  
department



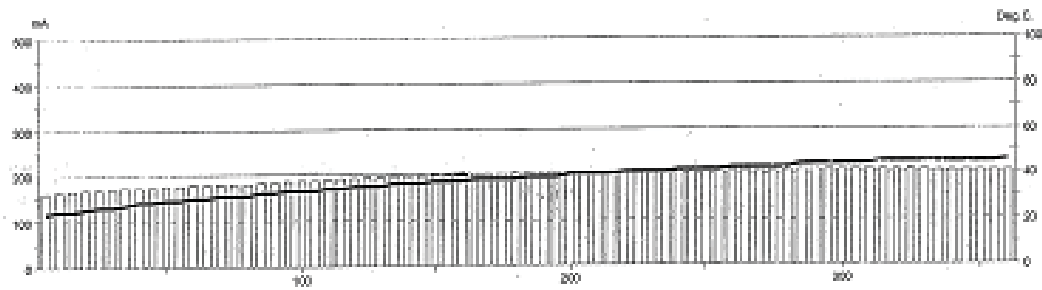
CLEARLY DEFINED

REMARKS  
Page 1 of 2 of 2  
Full document

ISO  
9001:2008  
Certified

Test report

Voltage Used: 60  
 Testing time: 06:00 hour  
 Charge passed: 4224  
 Adjusted Charge passed: 3812  
 Permeability class: Moderate  
 Instrument number: 071401  
 Channel number: 8  
 Report date: 6/29/2011  
 Testing by: broeds  
 Reference: SCC-EC2-Middle 28 day  
 Sample diameter: 100  
 Comment: UMR Study



Time	°C	mA									
00:05	23	161.1	01:35	33	186.6	03:05	39	203.6	04:35	43	207.0
00:10	24	163.9	01:40	33	188.1	03:10	39	203.8	04:40	43	207.2
00:15	24	165.3	01:45	33	188.4	03:15	39	204.2	04:45	44	207.3
00:20	25	166.8	01:50	34	190.0	03:20	40	205.2	04:50	44	207.2
00:25	26	168.3	01:55	34	191.2	03:25	40	204.7	04:55	44	207.6
00:30	26	169.8	02:00	35	192.5	03:30	40	205.1	05:00	44	207.8
00:35	27	171.3	02:05	35	194.0	03:35	40	205.6	05:05	44	208.3
00:40	28	172.5	02:10	35	194.5	03:40	41	206.0	05:10	44	208.1
00:45	28	174.1	02:15	36	196.1	03:45	41	206.1	05:15	45	207.6
00:50	29	175.7	02:20	36	196.5	03:50	41	206.9	05:20	45	207.3
00:55	29	177.1	02:25	36	197.5	03:55	41	206.6	05:25	45	206.7
01:00	30	178.4	02:30	37	199.5	04:00	42	206.1	05:30	45	206.7
01:05	30	179.6	02:35	37	199.5	04:05	42	206.3	05:35	45	206.3
01:10	31	180.4	02:40	37	199.9	04:10	42	206.5	05:40	45	205.8
01:15	31	180.9	02:45	38	200.6	04:15	42	206.5	05:45	45	205.4
01:20	31	181.7	02:50	38	201.9	04:20	43	206.6	05:50	45	205.0
01:25	32	183.6	02:55	38	201.7	04:25	43	206.8	05:55	45	204.6
01:30	32	185.0	03:00	38	202.2	04:30	43	207.0	06:00	46	204.4

Figure A.8 – S6-48L-EC2MIDDLE RCT Data



ASTM C 1202-97



Test-compagny  
Testing street 45  
CompagnyCity  
Some Country

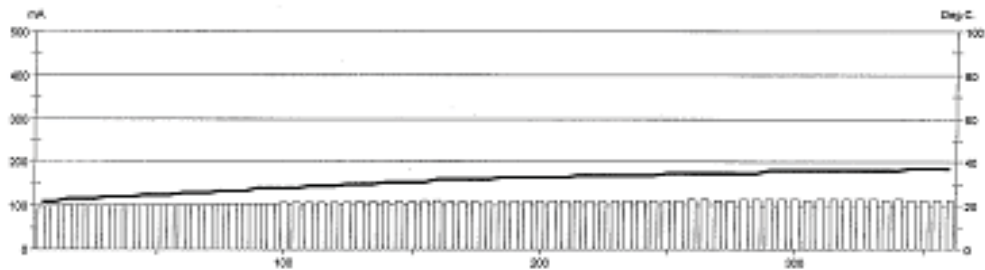
Your own logo  
diam: 100mm



CEMEX  
Pavimento 2011  
Pav. 100mm  
Pav. 100mm

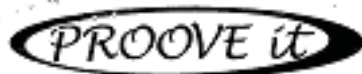
**Test report**

Voltage Used: 60  
Testing time: 06:00 hour  
Charge passed: 2355  
Adjusted Charge passed: 2125  
Permeability class: Moderate  
Instrument number: 071401  
Channel number: 1  
Report date: 7/29/2011  
Testing by: LG  
Reference: HS-SCC-1-TOP-28 DAY  
Sample diameter: 100  
Cement: ROLLA



Time	°C	mA									
00:05	22	99.1	01:35	28	105.2	03:05	33	110.4	04:35	35	112.3
00:10	22	101.2	01:40	28	106.2	03:10	33	111.1	04:40	35	113.2
00:15	23	102.0	01:45	28	106.4	03:15	33	111.6	04:45	35	114.8
00:20	23	101.6	01:50	29	107.6	03:20	33	111.6	04:50	36	113.4
00:25	23	100.8	01:55	29	107.8	03:25	33	111.2	04:55	36	113.1
00:30	24	101.5	02:00	29	107.8	03:30	33	111.1	05:00	36	113.3
00:35	24	101.8	02:05	30	107.9	03:35	34	111.2	05:05	36	112.1
00:40	24	102.1	02:10	30	108.4	03:40	34	110.7	05:10	36	113.9
00:45	25	102.4	02:15	30	109.0	03:45	34	112.2	05:15	36	113.6
00:50	25	102.7	02:20	31	108.7	03:50	34	112.7	05:20	36	113.5
00:55	25	102.7	02:25	31	108.4	03:55	34	112.6	05:25	36	113.0
01:00	26	102.9	02:30	31	108.4	04:00	34	112.7	05:30	36	113.1
01:05	26	102.9	02:35	31	110.7	04:05	34	112.6	05:35	36	112.6
01:10	26	103.5	02:40	32	110.7	04:10	35	112.6	05:40	36	112.8
01:15	27	104.0	02:45	32	110.1	04:15	35	112.4	05:45	37	112.7
01:20	27	104.1	02:50	32	110.2	04:20	35	113.3	05:50	37	112.7
01:25	27	104.8	02:55	32	110.2	04:25	35	112.9	05:55	37	112.4
01:30	28	105.1	03:00	32	110.3	04:30	35	112.7	06:00	37	111.8

Figure A.9 – C10-58L-EC1TOP RCT Data



ASTM C 1202-97



Test-compagny  
Testing street 45  
CompagnyCity  
Some Country



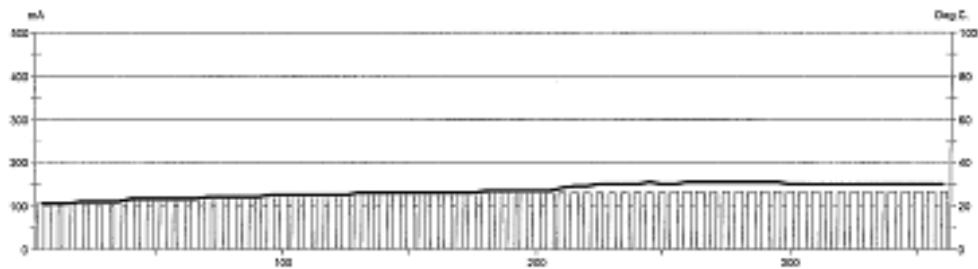
GERMAAD-DE-TRINIDADE

BOOMING  
P.O. Box 1000  
Tel: +31 (0) 20 20 20 20

www.booming.nl  
For more info

**Test report**

Voltage Used: 60  
Testing time: 06:00 hour  
Charge passed: 2708  
Adjusted Charge passed: 2444  
Permeability class: Moderate  
Instrument number: 071401  
Channel number: 2  
Report date: 7/29/2011  
Testing by: LG  
Reference: HS-SCC-MIDDLE-I-28 DAY  
Sample diameter: 100  
Comment: ROLLA



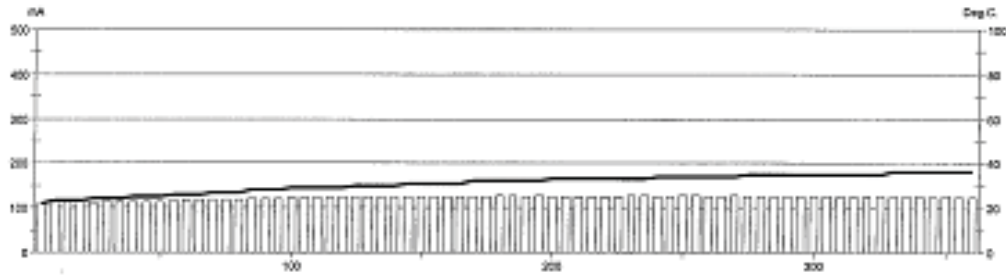
Time	°C	mA									
00:05	21	104.8	01:35	25	121.3	03:05	27	130.6	04:35	31	130.6
00:10	21	107.0	01:40	25	122.2	03:10	27	130.7	04:40	31	130.9
00:15	21	108.2	01:45	25	122.9	03:15	27	130.8	04:45	31	130.9
00:20	22	109.1	01:50	25	123.7	03:20	27	130.7	04:50	31	131.0
00:25	22	109.9	01:55	25	124.5	03:25	27	130.5	04:55	31	130.9
00:30	22	110.7	02:00	25	125.0	03:30	28	130.1	05:00	30	131.2
00:35	22	111.4	02:05	25	125.7	03:35	29	129.9	05:05	30	131.3
00:40	23	112.2	02:10	26	126.4	03:40	29	130.0	05:10	30	131.3
00:45	23	113.0	02:15	26	126.9	03:45	30	130.0	05:15	30	131.2
00:50	23	113.8	02:20	26	127.6	03:50	30	130.1	05:20	30	131.3
00:55	23	114.6	02:25	26	128.0	03:55	30	130.2	05:25	30	131.4
01:00	23	115.3	02:30	26	128.6	04:00	30	130.2	05:30	30	131.3
01:05	23	116.1	02:35	26	128.9	04:05	31	130.4	05:35	30	131.3
01:10	24	116.8	02:40	26	129.4	04:10	30	130.5	05:40	30	131.1
01:15	24	117.6	02:45	26	129.6	04:15	30	130.6	05:45	30	131.1
01:20	24	118.6	02:50	26	130.0	04:20	31	130.6	05:50	30	130.9
01:25	24	119.5	02:55	26	130.3	04:25	31	130.7	05:55	30	130.7
01:30	24	120.5	03:00	27	130.4	04:30	31	130.7	06:00	30	131.0

Figure A.10 – C10-58L-EC1MIDDLE RCT Data



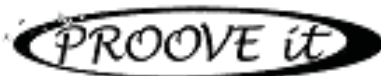
**Test report**

Voltage Used: 60  
 Testing time: 06:00 hour  
 Charge passed: 2649  
 Adjusted Charge passed: 2391  
 Permeability class: Moderate  
 Instrument number: 071401  
 Channel number: 3  
 Report date: 7/29/2011  
 Testing by: LG  
 Reference: HS-SCC-2-TOP-28 DAY  
 Sample diameter: 100  
 Comment: ROLLA



Time	°C	mA									
00:05	22	108.9	01:35	28	120.7	03:05	32	126.4	04:35	35	125.9
00:10	23	111.7	01:40	29	121.8	03:10	32	125.7	04:40	35	125.8
00:15	23	112.3	01:45	29	122.2	03:15	32	127.7	04:45	35	125.8
00:20	23	111.7	01:50	29	122.5	03:20	33	125.7	04:50	35	125.7
00:25	24	112.1	01:55	29	123.3	03:25	33	126.1	04:55	35	125.8
00:30	24	113.1	02:00	29	124.2	03:30	33	126.0	05:00	35	125.8
00:35	24	113.8	02:05	30	124.7	03:35	33	125.9	05:05	35	125.4
00:40	25	114.2	02:10	30	124.5	03:40	33	126.1	05:10	35	125.1
00:45	25	114.7	02:15	30	124.8	03:45	33	125.8	05:15	35	125.0
00:50	25	114.9	02:20	30	126.1	03:50	33	127.2	05:20	35	125.0
00:55	26	115.7	02:25	31	124.0	03:55	33	126.8	05:25	35	124.9
01:00	26	116.5	02:30	31	125.0	04:00	34	126.1	05:30	36	124.9
01:05	26	117.4	02:35	31	125.6	04:05	34	125.9	05:35	36	124.7
01:10	27	118.3	02:40	31	125.2	04:10	34	126.2	05:40	36	124.1
01:15	27	119.2	02:45	31	125.3	04:15	34	126.8	05:45	36	123.7
01:20	27	119.1	02:50	32	125.9	04:20	34	126.1	05:50	36	123.9
01:25	28	120.3	02:55	32	125.1	04:25	34	125.9	05:55	36	123.6
01:30	28	120.7	03:00	32	126.2	04:30	34	126.7	06:00	36	123.2

Figure A.11 – C10-58L-EC2TOP RCT Data



ASTM C 1202-97



Test-company  
Testing street 45  
CompagnyCity  
Some Country

Some other logo  
www.test.com  
+33 1 23 45 67 89



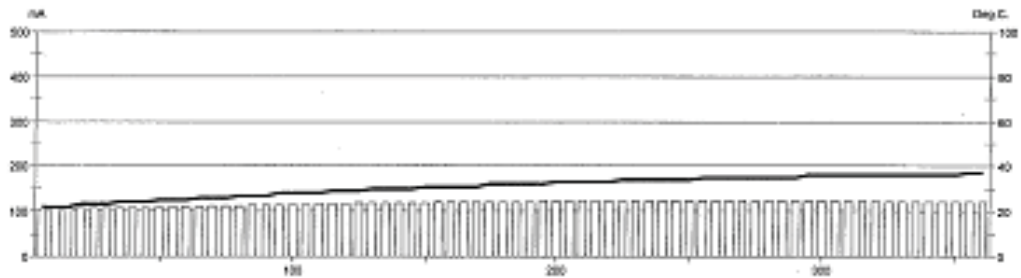
ESCALON INSTRUMENTS

ESCALON  
P.O. Box 1000  
10000

ESCALON  
P.O. Box 1000  
10000

**Test report**

Voltage Used: 60  
Testing time: 06:00 hour  
Charge passed: 2544  
Adjusted Charge passed: 2296  
Permeability class: Moderate  
Instrument number: 071401  
Channel number: 4  
Report date: 7/29/2011  
Testing by: LO  
Reference: HS-SCC-2-MIDDLE-28 DAY  
Sample diameter: 100  
Comment: ROLLA



Time	°C	mA									
00:05	22	105.3	01:35	28	113.8	03:05	32	121.4	04:35	35	123.1
00:10	22	106.8	01:40	28	114.3	03:10	32	121.4	04:40	35	123.0
00:15	22	107.3	01:45	28	114.8	03:15	32	122.1	04:45	35	122.8
00:20	23	107.3	01:50	28	115.4	03:20	33	122.1	04:50	35	122.8
00:25	23	108.5	01:55	29	115.8	03:25	33	122.3	04:55	36	122.7
00:30	23	108.5	02:00	29	116.4	03:30	33	122.4	05:00	36	122.6
00:35	24	107.2	02:05	29	117.3	03:35	33	122.9	05:05	36	122.3
00:40	24	107.9	02:10	30	117.4	03:40	33	122.5	05:10	36	122.0
00:45	24	108.2	02:15	30	117.9	03:45	34	123.0	05:15	36	122.0
00:50	25	108.7	02:20	30	118.3	03:50	34	123.1	05:20	36	121.8
00:55	25	109.3	02:25	30	118.9	03:55	34	123.0	05:25	36	121.5
01:00	25	109.7	02:30	31	119.2	04:00	34	123.0	05:30	36	121.4
01:05	26	110.0	02:35	31	119.5	04:05	34	123.2	05:35	36	120.9
01:10	26	110.7	02:40	31	120.2	04:10	34	123.3	05:40	36	120.9
01:15	26	111.4	02:45	31	120.1	04:15	35	123.3	05:45	36	120.4
01:20	27	112.1	02:50	31	120.9	04:20	35	123.1	05:50	36	120.1
01:25	27	112.9	02:55	32	120.8	04:25	35	123.3	05:55	37	119.7
01:30	27	113.3	03:00	32	121.3	04:30	35	123.2	06:00	37	119.5

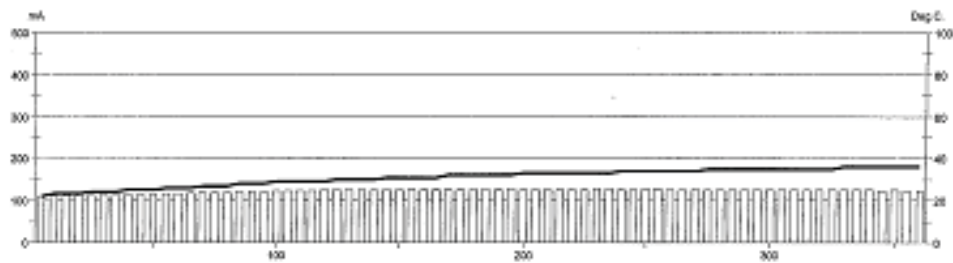
Figure A.12 – C10-58L-EC2MIDDLE RCT Data



**Test report**

Voltage Used: 60  
 Testing time: 06:00 hour  
 Charge passed: 2649  
 Adjusted Charge passed: 2191  
 Permeability class: Moderate  
 Instrument number: 071401  
 Channel number: 3  
 Report date: 7/29/2011  
 Testing by: LG  
 Reference: HS-SCC-2-TOP-28 DAY  
 Sample diameter: 100  
 Comment: ROLLA

CERAM-DETECTOR  
 MODEL  
 FROM 1980'S TO  
 THE PRESENT  
 THE  
 FROM 1980'S TO  
 THE PRESENT



Time	°C	mA									
00:05	22	108.9	01:35	28	120.7	03:05	32	126.4	04:35	35	125.9
00:10	23	111.7	01:40	29	121.8	03:10	32	125.7	04:40	35	125.8
00:15	23	112.3	01:45	29	122.2	03:15	32	127.7	04:45	35	125.8
00:20	23	111.7	01:50	29	122.5	03:20	33	125.7	04:50	35	125.7
00:25	24	112.1	01:55	29	123.3	03:25	33	126.1	04:55	35	125.8
00:30	24	113.1	02:00	29	124.2	03:30	33	126.0	05:00	35	125.8
00:35	24	113.8	02:05	30	124.7	03:35	33	125.9	05:05	35	125.4
00:40	25	114.2	02:10	30	124.5	03:40	33	126.1	05:10	35	125.1
00:45	25	114.7	02:15	30	124.8	03:45	33	125.8	05:15	35	125.0
00:50	25	114.9	02:20	30	124.1	03:50	33	127.2	05:20	35	125.0
00:55	26	115.7	02:25	31	124.0	03:55	33	126.8	05:25	35	124.9
01:00	26	116.5	02:30	31	125.0	04:00	34	126.1	05:30	36	124.9
01:05	26	117.4	02:35	31	125.6	04:05	34	125.9	05:35	36	124.7
01:10	27	118.3	02:40	31	125.2	04:10	34	126.2	05:40	36	124.1
01:15	27	119.2	02:45	31	125.3	04:15	34	126.8	05:45	36	123.7
01:20	27	119.1	02:50	32	125.9	04:20	34	126.1	05:50	36	123.9
01:25	28	120.3	02:55	32	125.1	04:25	34	125.9	05:55	36	123.6
01:30	28	120.7	03:00	32	126.2	04:30	34	126.7	06:00	36	123.2

Figure A.13 – S10-48L-EC1TOP RCT Data



Test-compagny  
Testing street 45  
Compagny City  
Some Country

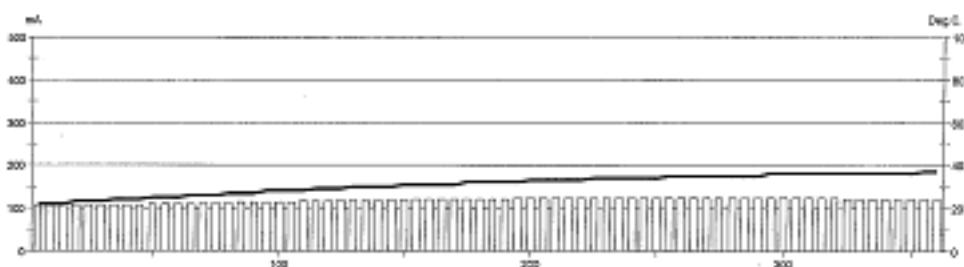
Your own logo  
here



LABORATORY  
MIDDLEBURY  
Vermont  
Phone: 802-253-1111  
Fax: 802-253-1112  
www.westco.com  
Prove it your way

**Test report**

Voltage Used: 60  
Testing time: 06:00 hour  
Charge passed: 2544  
Adjusted Charge passed: 2296  
Permeability class: Moderate  
Instrument number: 071401  
Channel number: 4  
Report date: 7/29/2011  
Testing by: LG  
Reference: HS-SCC-2-MIDDLE-28 DAY  
Sample diameter: 100  
Comment: ROLLA



Time	°C	mA									
00:05	22	105.3	01:35	28	113.8	03:05	32	121.4	04:35	35	123.1
00:10	22	106.8	01:40	28	114.3	03:10	32	121.4	04:40	35	123.0
00:15	22	107.3	01:45	28	114.8	03:15	32	122.1	04:45	35	122.8
00:20	23	107.3	01:50	28	115.4	03:20	33	122.1	04:50	35	122.8
00:25	23	106.5	01:55	29	115.8	03:25	33	122.3	04:55	36	122.7
00:30	23	106.5	02:00	29	116.4	03:30	33	122.4	05:00	36	122.6
00:35	24	107.2	02:05	29	117.3	03:35	33	122.9	05:05	36	122.3
00:40	24	107.9	02:10	30	117.4	03:40	33	122.5	05:10	36	122.0
00:45	24	108.2	02:15	30	117.9	03:45	34	123.0	05:15	36	122.0
00:50	25	108.7	02:20	30	118.5	03:50	34	123.1	05:20	36	121.8
00:55	25	109.3	02:25	30	118.9	03:55	34	123.0	05:25	36	121.5
01:00	25	109.7	02:30	31	119.2	04:00	34	123.0	05:30	36	121.4
01:05	26	110.0	02:35	31	119.5	04:05	34	123.2	05:35	36	120.9
01:10	26	110.7	02:40	31	120.2	04:10	34	123.3	05:40	36	120.9
01:15	26	111.4	02:45	31	120.1	04:15	35	123.3	05:45	36	120.4
01:20	27	112.1	02:50	31	120.9	04:20	35	123.1	05:50	36	120.1
01:25	27	112.9	02:55	32	120.8	04:25	35	123.3	05:55	37	119.7
01:30	27	113.3	03:00	32	121.3	04:30	35	123.2	06:00	37	119.5

Figure A.14 – S10-48L-EC1MIDDLE RCT Data

**Table A.45 – C6-58L Chloride Content Data**

Depth (in)	Chloride Content (%)		
	C6-58L-1P	C6-58L-2P	C6-58L-3P
0	0.29	0.23	0.23
0.25	0.05	0.09	0.07
0.75	0.02	0.03	0.02
1.5	0.01	0.01	0.01
2.0	0.01	0.01	0.01

**Table A.46 – S6-48L Chloride Content Data**

Depth (in)	Chloride Content (%)		
	S6-48L-1P	S6-48L-2P	S6-48L-3P
0	0.25	0.30	0.27
0.25	0.03	0.16	0.17
0.75	0.01	0.03	0.01
1.5	0.01	0.02	0.01
2.0	0.01	0.01	0.01

**Table A.47 – C10-58L Chloride Content Data**

Depth (in)	Chloride Content (%)		
	C10-58L-1P	C10-58L-2P	C10-58L-3P
0	0.27	0.22	0.24
0.25	0.05	0.19	0.09
0.75	0.01	0.01	0.02
1.5	0.01	0.01	0.01
2.0	0.01	0.01	0.02

**Table A.48 – S10-48L Chloride Content Data**

Depth (in)	Chloride Content (%)		
	S10-48L-1P	S10-48L-2P	S10-48L-3P
0	0.15	0.16	0.13
0.25	0.02	0.01	0.02
0.75	0.01	0.01	0.01
1.5	0.01	0.01	0.01
2.0	0.00	0.01	0.01

GM23		FREEZE & THAW LEDGER				Preliminary Testing Results @ Zero Cycles					
LAB NO:	UMR-A1	BEAM ID NO:		1	Agg. Description		Rolla				
35 Day Cure		Initial Weight in Air		9692.4	Initial bar reading		Starting Cycle Count		13153		
Initial Gage Reading		0.2495		Completion Date		Date Test Started		9/7/11			
Initial Frequency		1973		TERMINAL FREQUENCY		1184					
DATE	CYCLE # machine	Actual cycles	Weight	Ref. Bar	Gage reading	Corr. gage reading	Frqncy	RDM	Durab. Factor	% Gage Length Change	%Wght Change
9/8/11	13162	9	9693.0	0.2516	0.2509	0.2501	1911	93.81	2.81	0.0038	0.006
9/9/11	13171	18	9696.1	0.2523	0.2513	0.2498	1901	92.83	5.57	0.0019	0.038
9/12/11	13198	45	9704.4	0.2523	0.2522	0.2507	1856	88.49	13.27	0.0075	0.124
9/13/11	13207	54	9708.2	0.2523	0.2527	0.2512	1833	86.31	15.54	0.0106	0.163
9/15/11	13225	72	9718.6	0.2520	.	#VALUE!	1768	80.30	19.27	#VALUE!	0.270
9/16/11	13233	80	9722.3	0.2525	0.2558	0.2541	1741	77.87	20.76	0.0288	0.308
9/19/11	13260	107	9736.3	0.2521	0.2594	0.2581	1592	65.11	23.22	0.0538	0.453
9/21/11	13278	125	9747.4	0.2528	0.2627	0.2607	1454	54.31	22.63	0.0700	0.567
9/23/11	13296	143	9755.8	0.2522	0.2658	0.2644	1359	47.44	22.62	0.0931	0.654
9/26/11	13323	170	9764.8	0.2522	0.2705	0.2691	1217	38.05	21.56	0.1225	0.747
Totals		170						38.05	23.22	#VALUE!	0.01
Initial Measurements				Post Break Measurements							
WIDTH		DEPTH		WIDTH		DEPTH					
4.528		3.483		4.562		3.495		25.55 Avg. DF bms 1,2,3			
4.576		3.494		4.551		3.491		4.7907 Std. dev.			
4.539		3.498		4.574		3.495					
4.540		3.481									
4.546		3.489		4.562		3.494		Avg.			

Figure A.15 – C6-58L-FT1 Data

GM23		FREEZE & THAW LEDGER				Preliminary Testing Results @ Zero Cycles					
LAB NO:	UMR-A1	BEAM ID NO:		2	Agg. Description		Rolla				
35 Day Cure		Initial Weight in Air		9596.7	Initial bar reading		Starting Cycle Count		13153		
Initial Gage Reading		0.2445		Completion Date		Date Test Started		9/7/11			
Initial Frequency		1947		TERMINAL FREQUENCY		1168					
DATE	CYCLE # machine	Actual cycles	Weight	Ref. Bar	Gage reading	Corr. gage reading	Frqncy	RDM	Durab. Factor	% Gage Length Change	%Wght Change
9/8/11	13162	9	9598.7	0.2516	0.2472	0.2464	1886	93.83	2.81	0.0119	0.021
9/9/11	13171	18	9604.4	0.2523	0.2464	0.2449	1867	91.95	5.52	0.0025	0.080
9/12/11	13198	45	9616.5	0.2523	0.2491	0.2476	1819	87.28	13.09	0.0194	0.206
9/13/11	13207	54	9621.7	0.2523	0.2500	0.2485	1788	84.33	15.18	0.0250	0.261
9/15/11	13225	72	9633.9	0.252	0.2534	0.2522	1732	79.13	18.99	0.0481	0.388
9/16/11	13233	80	9638.7	0.2525	0.2560	0.2543	1702	76.42	20.38	0.0613	0.438
9/19/11	13260	107	9657.1	0.2521	0.2629	0.2616	1525	61.35	21.88	0.1069	0.629
9/21/11	13278	125	9668.1	0.2528	0.2677	0.2657	1414	52.74	21.98	0.1325	0.744
9/23/11	13296	143	9675.8	0.2522	0.2729	0.2715	1334	46.94	22.38	0.1688	0.824
9/26/11	13323	170	9683.4	0.2522	0.2800	0.2786	1177	36.54	20.71	0.2131	0.903
1/0/00	0	####		0							
1/0/00	0	####		0							
1/0/00	0	####		0							
1/0/00	0	####		0							
1/0/00	0	####		0							
1/0/00	0	####		0							
1/0/00	0	####		0							
1/0/00	0	####		0							
1/0/00	0	####		0							
1/0/00	0	####		0							
1/0/00	0	####		0							
1/0/00	0	####		0							
1/0/00	0	####		0							
Totals		170						36.54	22.38	0.21	0.02
Initial Measurements				Post Break Measurements							
WIDTH		DEPTH		WIDTH		DEPTH					
4.558		3.482		4.547		3.491					
4.557		3.509		4.567		3.489					
4.555		3.487		4.556		3.492					
4.516		3.489									
4.547		3.492		4.557		3.491		Avg.			

Figure A.16 – C6-58L-FT2 Data

GM23		FREEZE & THAW LEDGER				Preliminary Testing Results @ Zero Cycles					
LAB NO:	UMR-A1	BEAM ID NO:		3	Agg. Description		Rolla				
35 Day Cure		Initial Weight in Air		9711.3	Initial bar reading		Starting Cycle Count		13153		
Initial Gage Reading		0.2606		Completion Date		Date Test Started		9/7/11			
Initial Frequency		1980		TERMINAL FREQUENCY		1188					
DATE	CYCLE # machine	Actual cycles	Weight	Ref. Bar	Gage reading	Corr. gage reading	Frqncy	RDM	Durab. Factor	% Gage Length Change	%Wght Change
9/8/11	13162	9	9710.6	0.2516	0.2597	0.2589	1933	95.31	2.86	-0.0106	-0.007
9/9/11	13171	18	9712.2	0.2523	0.2614	0.2599	1927	94.72	5.68	-0.0044	0.009
9/12/11	13198	45	9720.0	0.2523	0.2619	0.2604	1905	92.57	13.89	-0.0012	0.090
9/13/11	13207	54	9723.4	0.2523	0.2618	0.2603	1895	91.60	16.49	-0.0019	0.125
9/15/11	13225	72	9731.3	0.252	0.2611	0.2599	1867	88.91	21.34	-0.0044	0.206
9/16/11	13233	80	9734.5	0.2525	0.2640	0.2623	1851	87.39	23.31	0.0106	0.239
9/19/11	13260	107	9751.2	0.2521	0.2664	0.2651	1746	77.76	27.73	0.0281	0.411
9/21/11	13278	125	9763.6	0.2528	0.2689	0.2669	1666	70.80	29.50	0.0394	0.539
9/23/11	13296	143	9774.8	0.2522	0.2718	0.2704	1591	64.57	30.78	0.0612	0.654
9/26/11	13323	170	9786.2	0.2522	0.2768	0.2754	1466	54.82	31.06	0.0925	0.771
1/0/00	0	####		0							
1/0/00	0	####		0							
1/0/00	0	####		0							
1/0/00	0	####		0							
1/0/00	0	####		0							
1/0/00	0	####		0							
1/0/00	0	####		0							
1/0/00	0	####		0							
1/0/00	0	####		0							
1/0/00	0	####		0							
1/0/00	0	####		0							
1/0/00	0	####		0							
1/0/00	0	####		0							
Totals		170						54.82	31.06	0.09	-0.01
Initial Measurements				Post Break Measurements							
WIDTH		DEPTH		WIDTH		DEPTH					
4.542		3.494		4.569		3.485					
4.566		3.488		4.556		3.490					
4.566		3.492		4.562		3.493					
4.560		3.512									
4.559		3.497		4.562		3.489		Avg.			

Figure A.17 – C6-58L-FT3 Data





GM23		FREEZE & THAW LEDGER				Preliminary Testing Results @ Zero Cycles					
LAB NO:	UMR-SCC	BEAM ID NO:	3	Agg. Description	0						
35 Day Moist Cure		Initial Weight in Air		9666.1	Initial bar reading		Starting Cycle Count		12593		
Initial Gage Reading		N/A (No Studs)		Completion Date		Date Test Started		7/6/11			
Initial Frequency		1902		TERMINAL FREQUENCY		1141					
DATE	CYCLE # machine	Actual cycles	Weight	Ref. Bar	Gage reading	Corr. gage reading	Frqncy	RDM	Durab. Factor	% Gage Length Change	%Wght Change
7/7/11	12602	9	9667.8	0			1851	94.71	2.84		0.018
7/11/11	12638	45	9689.4	0			1783	87.88	13.18		0.241
7/14/11	12665	72	9705.8	0			1701	79.98	19.20		0.411
7/18/11	12701	108	9733.8	0			1353	50.60	18.22		0.700
		Flexural Strength = 548 psi									
		Tangent Modulus = 0.0455 Msi									
		Maximum Strain = 0.0204 in/in									
Totals		108						50.60	19.20	0.00	0.02
Initial Measurements				Post Break Measurements							
WIDTH		DEPTH		WIDTH		DEPTH					
				4.670		3.660					
				4.563		3.559					
				4.412		3.528					
0.000		0.000		4.548		3.582		Avg.			

Figure A.20 – S6-48L-FT3 Data



GM23		FREEZE & THAW LEDGER				Preliminary Testing Results @ Zero Cycles					
LAB NO:	HSC-Rolla	BEAM ID NO:	2	Agg. Description	0						
35 Day Cure		Initial Weight in Air		9729.1	Initial bar reading		Starting Cycle Count		12736		
Initial Gage Reading		Completion Date		8/24/11	Date Test Started		7/22/11				
Initial Frequency		1978		TERMINAL FREQUENCY		1187					
DATE	CYCLE # machine	Actual cycles	Weight	Ref. Bar	Gage reading	Corr. gage reading	Frqncy	RDM	Durab. Factor	% Gage Length Change	%Wght Change
7/25/11	12763	27	9727.8	0			1957	97.89	8.81		-0.013
7/27/11	12781	45	9728.4	0			1954	97.59	14.64		-0.007
7/29/11	12799	63	9728.1	0			1954	97.59	20.49		-0.010
8/1/11	12828	92	9728.9	0			1949	97.09	29.77		-0.002
8/3/11	12844	108	9721.6	0			1946	96.79	34.84		-0.077
8/5/11	12862	126	9720.0	0			1947	96.89	40.69		-0.094
8/9/11	12897	161	9723.8	0			1937	95.90	51.46		-0.054
8/11/11	12915	179	9724.0	0			1939	96.10	57.34		-0.052
8/15/11	12951	215	9726.7	0			1927	94.91	68.02		-0.025
8/17/11	12969	233	9728.3	0			1921	94.32	73.25		-0.008
8/19/11	12984	248	9729.1	0			1920	94.22	77.89		0.000
8/22/11	13009	273	9732.3	0			1915	93.73	85.30		0.033
8/23/11	13019	283	9734.3	0			1912	93.44	88.14		0.053
8/25/11	13036	300	9735.4				1908	93.05	93.05		0.065
Totals		300						93.05	93.05	0.00	-0.09
Initial Measurements				Post Break Measurements							
WIDTH		DEPTH		WIDTH		DEPTH					
0.000		0.000		0.000		0.000		Avg.			
Flexural Strength = 836 psi											
Tangent Modulus = 0.922 MSI											
Maximum Strain 0.0098 in/in											

Figure A.22 – C10-58L-FT2 Data

GM23				FREEZE & THAW LEDGER				Preliminary Testing Results @ Zero Cycles			
LAB NO:		HSC-Rolla		BEAM ID NO:		3		Agg. Description		0	
Initial Weight in Air		10038.1		Initial bar reading		0		Starting Cycle Count		12736	
Initial Gage Reading				Completion Date		8/24/11		Date Test Started		7/22/11	
Initial Frequency		1988		TERMINAL FREQUENCY		1193					
DATE	CYCLE # machine	Actual cycles	Weight	Ref. Bar	Gage reading	Corr. gage reading	Frqncy	RDM	Durab. Factor	% Gage Length Change	%Wght Change
7/25/11	12763	27	10037.7	0			1962	97.40	8.77		-0.004
7/27/11	12781	45	10039.7	0			1956	96.81	14.52		0.016
7/29/11	12799	63	10041.9	0			1957	96.91	20.35		0.038
8/1/11	12828	92	10044.5	0			1949	96.11	29.48		0.064
8/3/11	12844	108	10047.8	0			1947	95.92	34.53		0.097
8/5/11	12862	126	10050.8	0			1940	95.23	40.00		0.127
8/9/11	12897	161	10054.4	0			1930	94.25	50.58		0.162
8/11/11	12915	179	10058.7	0			1918	93.08	55.54		0.205
8/15/11	12951	215	10067.1	0			1888	90.19	64.64		0.289
8/17/11	12969	233	10067.0	0			1865	88.01	68.35		0.288
8/19/11	12984	248	10070.5	0			1847	86.32	71.36		0.323
8/22/11	13009	273	10076.7	0			1807	82.62	75.18		0.385
8/23/11	13019	283	10080.3	0			1787	80.80	76.22		0.420
8/25/11	13036	300	10084.1				1751	77.58	77.58		0.458
Totals		300						77.58	77.58	0.00	0.00
Initial Measurements				Post Break Measurements							
WIDTH		DEPTH		WIDTH		DEPTH					
0.000		0.000		0.000		0.000		Avg.			

Figure A.23 – C10-58L-FT3 Data

GM23		FREEZE & THAW LEDGER				Preliminary Testing Results @ Zero Cycles									
LAB NO:	HS-SCC	BEAM ID NO:		1	Agg. Description		Rolla								
35 Day Cure		Initial Weight in Air		9819.9	Initial bar reading		Starting Cycle Count		12862						
Initial Gage Reading		Completion Date		9/7/11	Date Test Started		8/5/11								
Initial Frequency		2018		TERMINAL FREQUENCY		1211									
DATE	CYCLE # machine	Actual cycles	Weight	Ref. Bar	Gage reading	Corr. gage reading	Frqncy	RDM	Durab. Factor	% Gage Length Change	%Wght Change				
8/9/11	12897	35	9819.7				1982	96.46	11.25		-0.002				
8/11/11	12915	53	9821.8				1981	96.37	17.02		0.019				
8/15/11	12951	89	9832.6				1950	93.37	27.70		0.129				
8/17/11	12969	107	9841.0				1924	90.90	32.42		0.215				
8/19/11	12984	122	9847.9				1905	89.11	36.24		0.285				
8/22/11	13009	147	9862.1				1848	83.86	41.09		0.430				
8/23/11	13019	157	9869.4				1830	82.24	43.04		0.504				
8/25/11	13036	174	9882.0				1745	74.77	43.37		0.632				
8/29/11	13072	210	9917.0				1376	46.49	32.55		0.989				
Flexural Strength = 201 psi															
Tangent Modulus = 0.0292 Msi															
Maximum Strain = 0.0067 in/in															
Totals		210										46.49	43.37	0.00	0.00
Initial Measurements				Post Break Measurements											
WIDTH		DEPTH		WIDTH		DEPTH									
4.571		3.480		4.569		3.440		45.17 Avg. DF bms 1,2,3							
4.570		3.460						15.5265 Std. dev.							
0.000		0.000		4.570		3.460		Avg.							

Figure A.24 – S10-48L-FT1 Data

GM23		FREEZE & THAW LEDGER				Preliminary Testing Results @ Zero Cycles						
LAB NO:	HS-SCC	BEAM ID NO:		2	Agg. Description		Rolla					
35 Day Cure		Initial Weight in Air		9624.0	Initial bar reading		Starting Cycle Count		12862			
Initial Gage Reading		Completion Date		9/7/11	Date Test Started		8/5/11					
Initial Frequency		1998		TERMINAL FREQUENCY		1199						
DATE	CYCLE # machine	Actual cycles	Weight	Ref. Bar	Gage reading	Corr. gage reading	Frqncy	RDM	Durab. Factor	% Gage Length Change	%Wght Change	
8/9/11	12897	35	9622.7	0			1978	98.01	11.43		-0.014	
8/11/11	12915	53	9623.4	0			1982	98.40	17.38		-0.006	
8/15/11	12951	89	9626.5	0			1973	97.51	28.93		0.026	
8/17/11	12969	107	9628.6	0			1968	97.02	34.60		0.048	
8/19/11	12984	122	9631.1	0			1967	96.92	39.41		0.074	
8/22/11	13009	147	9637.7	0			1957	95.94	47.01		0.142	
8/23/11	13019	157	9642.0	0			1948	95.06	49.75		0.187	
8/25/11	13036	174	9648.0	0			1934	93.70	54.34		0.249	
8/29/11	13072	210	9669.3	0			1873	87.88	61.52		0.471	
Flexural Strength = 1081.5 psi												
Tangent Modulus = 0.1229 Msi												
Maximum Strain = 0.0101 in/in												
Totals		210							87.88	61.52	0.00	-0.01
Initial Measurements				Post Break Measurements								
WIDTH		DEPTH		WIDTH		DEPTH						
4.600		3.440		4.600		3.420						
4.600		3.420		4.610		3.400						
0.000		0.000		4.603		3.420		Avg.				

Figure A.25 – S10-48L-FT2 Data

GM23		FREEZE & THAW LEDGER				Preliminary Testing Results @ Zero Cycles					
LAB NO:	HS-SCC	BEAM ID NO:		3	Agg. Description		Rolla				
35 Day Cure		Initial Weight in Air		9132.1	Initial bar reading		Starting Cycle Count		12862		
Initial Gage Reading		Completion Date		9/7/11	Date Test Started		8/5/11				
Initial Frequency		2041		TERMINAL FREQUENCY		1225					
DATE	CYCLE # machine	Actual cycles	Weight	Ref. Bar	Gage reading	Corr. gage reading	Frqncy	RDM	Durab. Factor	% Gage Length Change	%Wght Change
8/9/11	12897	35	9133.6	0			1994	95.45	11.14		0.016
8/11/11	12915	53	9134.3	0			1983	94.40	16.68		0.024
8/15/11	12951	89	9147.1	0			1912	87.76	26.04		0.164
8/17/11	12969	107	9155.6	0			1852	82.34	29.37		0.257
8/19/11	12984	122	9163.5	0			1771	75.29	30.62		0.344
8/22/11	13009	147	9182.0	0			1516	55.17	27.03		0.546
8/23/11	13019	157	9192.5	0			1424	48.68	25.47		0.661
8/25/11	13036	174	9210.7	0			1290	39.95	23.17		0.861
8/29/11	13072	210	*	0			*	#####			#####
Flexural Strength = psi											
Tangent Modulus = Msi											
Maximum Strain = in/in											
* Beam broke into 2 pieces when pulled from the freezer											
Totals											
		210						#####	30.62	0.00	#####
Initial Measurements					Post Break Measurements						
WIDTH		DEPTH		WIDTH		DEPTH					
0.000		0.000		0.000		0.000 Avg.					

Figure A.26 – S10-48L-FT3 Data

## REFERENCES

- ASTM C 39. (2010). Standard Test Method for Compressive Strength of Cylindrical Concrete Specimens. American Society of Testing and Materials, West Conshohocken, PA.
- ASTM C 78. (2010). Standard Test Method for Flexural Strength of Concrete (Using Simple Beam with Third-Point Loading). American Society of Testing and Materials, West Conshohocken, PA.
- ASTM C 192. (2007). Standard Test Method for Making and Curing Concrete Test Specimens in the Laboratory. American Society of Testing and Materials, West Conshohocken, PA.
- ASTM C 469. (2002). Standard Test Method for Static Modulus of Elasticity and Poissons Ratio of Concrete in Compression. American Society of Testing and Materials, West Conshohocken, PA.
- ASTM C 496. (2004). Standard Test Method for Splitting Tensile Strength of Cylindrical Concrete Specimens. American Society of Testing and Materials, West Conshohocken, PA.
- ASTM C 666. (2008). Standard Test Method for Resistance of Concrete to Rapid Freezing and Thawing. American Society of Testing and Materials, West Conshohocken, PA.
- ASTM C 1202. (2010). Standard Test Method for Electrical Indication of Concrete's Ability to Resist Chloride Ion Penetration. American Society of Testing and Materials, West Conshohocken, PA.
- ASTM C 1543. (2010). Standard Test Method for Determining the Penetration of Chloride Ion into Concrete by Ponding. American Society of Testing and Materials, West Conshohocken, PA.
- ASTM C 1610. (2010). Standard Test Method for Static Segregation of Self-Consolidating Concrete Using Column Technique. American Society of Testing and Materials, West Conshohocken, PA.
- ASTM C 1611. (2010). Standard Test Method for Slump Flow of Self-Consolidating Concrete. American Society of Testing and Materials, West Conshohocken, PA.

- ASTM C 1621. (2009). Standard Test Method for Passing Ability of Self-Consolidating Concrete by J-Ring, American Society of Testing and Materials, West Conshohocken, PA.
- American Concrete Institute ACI 237 R-07. (2007). Self-Consolidating Concrete, American Concrete Institute, Farmington Hills, Michigan.
- Bennenk, W., (2002). SCC in the Daily Precast Concrete Practice, *Betonwerk and Fertigteiltechnik*, V. 34, Issue 4.
- Berke, N.S. and Hicks, M.C. (1996). Predicting Times to Corrosion from Field and Laboratory Data, Techniques to Assess the Corrosion Activity of Steel Reinforced Concrete Structures, ASTM STP 1276. Neal S. Berke, Edward Escalante, Charles K. Nmai, and David Whiting, Eds., American Society for Testing and Materials.
- Broomfield, John P. (2007). Corrosion of Steel in Concrete: Understanding, Investigation and Repair. Taylor & Francis (Second Edition).
- Coppola, L., Cerulli, T., Salvioni, D. (2005). Sustainable Development and Durability of Self-Compacting Concretes, 11<sup>th</sup> International Conference on Fracture, Proceedings, Turin, Italy.
- Khayat, K.H. (1999). Workability, Testing, and Performance of Self-Consolidating Concrete. *ACI Journal*, Proceedings May-June, Vol. 96, No. 3, pp. 346-354.
- Khayat, K.H. (2002). Optimization and Performance of Air Entrained, Self-Consolidating Concrete. *ACI Materials Journal*, Vol. 97, No. 5, pp. 526-535.
- Mansfield, F. (1981). Recording and Analysis of AC Impedance Data for Corrosion Studies. *Corrosion*, Vol. 37, No. 5, pp. 301-307.
- Mortsell, E., and Rodum, E., (2001). Mechanical and Durability Aspects of SCC for Road Structures. Proceedings of the Second International Symposium on SCC, K. Ozawa and M. Ouchi, eds., Tokyo, pp. 459-468.
- Mindess, S., Young, J.F., and Darwin, D. (2003). Concrete. Pearson Education, Inc. (Second Edition).
- Neville, A. M. (1997). Properties of Concrete. John Wiley and Sons, Inc. (Fourth Edition).
- Office of Research, Development, and Technology, Office of Safety, RDT. (1997). User Guidelines for Waste and Byproduct Materials in Pavement Construction. Report No. FHWA-RD-97-148. Federal Highway Administration, Cortest Columbus Technologies.

- Oluokun, Francis A (1991). Prediction of Concrete Tensile Strength from Its Compressive Strength: Evaluation of Existing Relations for Normal Weight Concrete. *ACI Materials Journal*, Vol. 88, No. 3, pp. 302-309.
- Persson, B., (1999). Creep, Shrinkage and Elastic Modulus of Self-Compacting Concrete. 1st International RILEM Symposium on Self-Compacting Concrete Stockholm, Sweden.
- Powers, T.C. (1975). Freezing Effects in Concrete. SP-47, American Concrete Institute, Detroit, MI, pp. 1-12.
- Sengul, O. and Gjrv, O. (2009). Effect of Embedded Steel on Electrical Resistivity Measurements on Concrete Structures. *ACI Materials Journal*, 106(1), 11-18.
- Sonebi, M., and Bartos, P. J. M. (2001). Performance of Reinforced Columns Cast with Self-Compacting Concrete. *Recent Advances in Concrete Technology, Proceedings of the Fifth CANMET/ACI International Conference*, SP-200, V. M. Malhotra, ed., American Concrete Institute, Farmington Hills, Mich., pp. 415-431.
- Whiting, D.A. and Nagi, M.A. (2003). Electrical Resistivity of Concrete - A Literature Review. R&D Serial No. 2457. Portland Cement Association, Skokie, IL.

